Title
An Improved Description of the Seismic Response of Sites with High Plasticity Soils, Organic Clays, and Deep Soft Soil Deposits

Author
Carlton, Brian

Publication Date
2014

Peer reviewed|Thesis/dissertation

An Improved Description of the Seismic Response of Sites with High Plasticity Soils, Organic Clays, and Deep Soft Soil Deposits

by

Brian Carlton

A dissertation submitted in partial satisfaction of the
requirements for the degree of
Doctor of Philosophy
in
Engineering – Civil and Environmental Engineering
in the
Graduate Division
of the
University of California, Berkeley

Committee in charge:
Professor Juan M. Pestana-Nascimento, Chair
Professor Jonathan D. Bray
Professor Douglas S. Dreger

Spring 2014

An Improved Description of the Seismic Response of Sites with High Plasticity Soils, Organic Clays, and Deep Soft Soil Deposits

by

Brian Carlton

Abstract

An Improved Description of the Seismic Response of Sites with High Plasticity Soils, Organic Clays, and Deep Soft Soil Deposits

By

Brian Carlton

Doctor of Philosophy in Civil and Environmental Engineering

University of California, Berkeley

Professor Juan M. Pestana-Nascimento, Chair

Near surface soils can greatly influence the amplitude, duration, and frequency content of ground motions. The amount of their influence depends on many factors, such as the geometry and engineering properties of the soils and underlying bedrock, as well as the earthquake source mechanism and travel path. Building codes such as the 2012 International Building Code (IBC) define six site categories for seismic design of structures, which are based on the sites defined by the National Earthquake Hazards Reduction Program (NEHRP). Site categories A, B, C, D, and E are defined by the time averaged shear wave velocity over the top 30 meters of the soil deposit. Site category F is defined as sites that include liquefiable or sensitive soils, as well as sites with more than 3 meters (10 ft) of peat or highly organic clays, more than 7.5 meters (25 ft) of soil with PI > 75, and more than 37 meters (120 ft) of soft to medium stiff clays. The IBC specifies simplified procedures to calculate design spectra for NEHRP sites A through E, and requires a site specific investigation for NEHRP F sites. However, established procedures for performing the required site specific investigations for NEHRP F sites are limited.

The objective of this research is to develop a simplified procedure to estimate design spectra for non-liquefiable NEHRP F sites, specifically sites with organic soils, highly plastic soils, and deep soft soil deposits. The results from this research will directly affect US practice by developing much needed guidelines in this area.

There is little empirical data on the seismic response of non-liquefiable NEHRP F sites. As a result, this study focused on generating data from site response analyses. To capture the variability of ground motions, this study selected five base case scenarios according to tectonic environments and representative cases encountered in common US practice. Suites of ground motions for each scenario were created by collecting ground motions from online databases. Some of the ground motions were scaled and others were spectrally matched to their respective target response spectra. Fifteen different NEHRP E and F sites were created for the site response analyses. Seven of the sites are based on actual sites from the San Francisco Bay Area, New York City, Ottawa, Canada, Guayaquil, Ecuador, and Hokkaido, Japan. The other eight sites are variations of the seven base case sites. This study conducted a total of 14,541 site response analyses using a well documented site response analysis program.

This study then developed a simplified model to estimate response spectra for non-liquefiable NEHRP F sites. The simplified model was developed in two stages. In the first stage, the results for each site were regressed separately against the ground motion intensity to estimate the effect of the ground motion scenario. In the second stage, the site specific coefficients calculated from the first stage were regressed against site properties to determine their site dependence. These two parts were then combined to form the final model. The simplified model was validated against a separate database than the one used to develop it. This validation database consisted of 24 effective stress nonlinear site response analyses for three sites and eight ground motion scenarios.

The simplified model developed in this study does not replace a site response analysis, but rather augments it. It is hoped that the results of this dissertation will help practicing engineers gain a better understanding of their site before conducting site response analyses.

To my wife Inès

Table of Contents

List of Figures

List of Tables

CHAPTER 1: INTRODUCTION

1.1 Background and Research Motivation

Near surface soils can greatly influence the amplitude, duration, and frequency content of ground motions. This has been known in a qualitative manner for quite some time.

"*MacMurdo (1824) noted that 'buildings situated on rock were not by any means so much affected ... as those whose foundations did not reach to the bottom of the soil' in the 1819 earthquake in Cutch, India*" (Kramer, 1996).

The newspaper *Alta California* reported on October 9, 1865, one day after an earthquake in San Francisco, that;

"*No house well built on hard ground has suffered, or the damage, if any, is too slight to deserve notice… In those parts of the city which were formerly part of the Bay, and have been filled in with earth, few of the foundations are firm, and there the most damage has been done*" (Huber, 1930).

After the October 21, 1868 San Francisco earthquake, the *San Francisco Bulletin* stated,

"*Where the muddy deposits of the Bay have been crusted over by filling in sand, and these lands have been built upon, the foundation has always been insecure. In some parts of this district there is a crust of from forty to sixty feet of tolerably compact earth, but underneath is a greater thickness of mud. These lands have been piled, but the entire formation is unsubstantial. It was always expected that earthquakes would seriously affect improvements on such a basis, and, in the present instance, most of the losses have occurred upon these made lands*" (Huber, 1930).

The influence of site effects was also noted after the 1906 San Francisco earthquake by the California State Earthquake Investigation Commission;

"*This investigation has clearly demonstrated that the amount of damage produced by the earthquake of April 18 in different parts of the city and county of San Francisco depended chiefly upon the geological character of the ground. Where the surface was of solid rock, the shock produced little damage; whereas upon made land great violence was manifested*" (Wood, 1908).

However, the influence of site effects was not seriously studied quantitatively until after a series of devastating earthquakes in the 1960s. These earthquakes included the 1964 Niigata, Japan earthquake, which caused widespread liquefaction, the 1964 Alaska earthquake, which caused massive landslides and widespread liquefaction, the 1967 Caracas, Venezuela earthquake, which highlighted the effect of resonance caused by sites and structures with similar natural frequencies, and the 1971 San Fernando earthquake, which caused near collapse of the lower San Fernando Dam, but also provided a wealth of new strong ground motion recordings (Seed et al., 1967; Kramer, 1996).

Duke et al. (1972) and Donovan (1973) examined the differences in earthquake accelerations on rock and soil sites using ground motion recordings from the 1971 San Fernando earthquake. Both of these studies observed that accelerations on rock sites were higher than those on soil sites for records with short source to site distances, and the opposite was true for records with long source to site distances. Following on this research, Trifunac (1976) developed an empirical model to estimate Fourier Amplitude Spectra based on magnitude, distance, and site conditions from a database of 182 records. He divided sites into three categories; basement rock, intermediate rock, and alluvium. He found that, for periods greater than about one second, spectral amplitudes recorded on alluvium sites were on average 2.5 times greater than those recorded on basement rock.

Seed et al. (1976a) examined the influence of site properties on the peak ground acceleration and peak ground velocity for 147 records from eight earthquakes with Richter magnitudes of 6 to 6.6, and source to site distances ranging from 20 to 200 km. They divided the data into four soil categories; rock, stiff soil, deep cohesionless soil, and soft to medium stiff clay and sand. Figure 1.1 shows their results. The second part of the study (Seed et al., 1976b) investigated the effect of site properties on the spectral shape of ground motions. They used a database of 104 records from 23 earthquakes with magnitudes varying from 5.25 to 7.6 and distances from 3 to 165 km. They divided the data into the same four site categories as Seed et al. (1976a), and calculated the mean response spectra for each soil category. Figure 1.2 shows their results, which clearly indicate differences in spectral shapes for different soil conditions. Mohraz (1976) found similar results.

Based on these results, the Applied Technology Council (ATC, 1978) recommended design spectra for rock, stiff soil, and soft soil sites. These were significant because in the roughly 30 years since the introduction of the response spectrum by Housner (1941) and Biot (1942), the most widely used design spectra were those proposed by Housner (1959) and later Newmark and Hall (1969), both of which were site independent. The main reason for this was that before the 1970s there were very few earthquake recordings from sites with known soil properties, and hence, no systematic quantitative investigations of the effect of near surface soils on strong ground shaking could be conducted.

After the 1985 Mexico City earthquake, the ATC added a fourth soil type for deep deposits of soft soils (Seed et al., 1988). Figure 1.3 shows the four ATC design spectra. These site factors only differentiated between soil types at long periods, and did not take into account soil nonlinearity except as a function of PGA.

In 1991 the National Center for Earthquake Engineering Research, now the Multidisciplinary Center for Earthquake Engineering Research (http://mceer.buffalo.edu/), held a workshop to improve how building codes dealt with site effects (Whitman, 1992). The workshop created a committee of nine members who studied site effects using empirical evidence from the 1989 Loma Prieta earthquake in the San Francisco Bay Area (e.g. Borcherdt 1994; Joyner et al., 1994) as well as numerical simulations using equivalent linear and nonlinear time stepping techniques (e.g. Seed et al., 1994; Dobry et al., 1994). The committee presented their research at a second workshop in 1992 (Martin, 1994). This workshop developed the site factors and site categories

that would later be integrated into the 1994 NEHRP provisions, and which are still the site factors used to this day (NEHRP, 2009).

Table 1.1 lists the NEHRP site categories. Site categories A through E were defined by the time averaged shear wave velocity of the top 30 meters (Vs_{30}). This allowed unambiguous definition of the site class. If the Vs_{30} is not available other soil properties such as the average standard penetration resistance or undrained shear strength over the top 30 meters can be used. The sixth site class, F, was defined as sites that include liquefiable or sensitive soils, as well as sites with more than 3 meters (10 ft) of peat or highly organic clays, more than 7.5 meters (25 ft) of soil with PI > 75, and more than 37 meters (120 ft) of soft to medium stiff clays.

Table 1.2 lists the site factors according to site category and ground motion intensity. The workshop recommended two site factors, one for short periods (average soil/rock amplification over a period range of 0.1-0.5 seconds (F_a)) and one for long periods (average soil/rock amplification over a period range of 0.5-2.0 seconds (F_v)). A major improvement of these site categories and factors over earlier code methods was the fact that they provided an unambiguous definition of the site class and accounted for soil nonlinearity (Dobry et al., 2000). Values of S_s and S_1 can be taken from seismic hazard maps provided by the United States Geological Survey (USGS). Using the values of S_s, S_1, and the site category, Figure 1.4 shows how to calculate the design spectrum according to the 2012 IBC (IBC, 2012) for NEHRP A through E sites. The sixth site class, F, requires a site specific investigation. However, established procedures for performing the required site specific investigations are limited.

Table 1.3 shows the site classification system proposed by Seed et al. (1997), which is based on the work of Dickenson (1994) and Chang (1996). The site classification system of Seed et al. (1997) takes into account soil stiffness, strength, and thickness, as well as ground motion intensity. It is therefore much more detailed than the code site categories, which are based on the time average shear wave velocity of the top thirty meters. The Seed et al. (1997) design spectra are calculated by estimating the PGA_{rock}, selecting the appropriate site category, and using Figure 1.5 to calculate the PGA_{soil} and design spectrum ordinates. The response spectral values of Figure 1.5 are set at mean plus one half standard deviations. To calculate the mean value, all spectral values greater than T>0 (PGA) should be divided by 1.15.

Seed et al. (1997) provide recommendations for calculating design spectra for sites with deep soft cohesive soils (E_1 and E_2) and high plasticity soils (E_3), but strongly recommend performing site specific analyses for these sites. For organic soils (F_1) and liquefiable soils (F_2), they require a site specific analysis, similar to the 2012 IBC. The Seed et al. (1997) study is one of the few comprehensive investigations that provide simplified tools to engineers for estimating the design spectrum of some non-liquefiable NEHRP F sites. Non-liquefiable NEHRP F sites are encountered in many urban areas, such as New York City (Nikolaou et al., 2001) and San Francisco, and therefore there exists a need for a simplified method to estimate non-liquefiable NEHRP F design spectra before large quantities of time and money are spent on the required site specific investigation.

1.2 Scope of Research

The objective of this research is to develop a simplified procedure to estimate design spectra for non-liquefiable NEHRP F sites, specifically sites with organic soils, highly plastic soils, and deep soft soil deposits. The results from this research will directly affect US practice by developing much needed guidelines in this area.

There is little empirical data on the seismic response of non-liquefiable NEHRP F sites. As a result, this study focused on generating data from numerical simulations called site response analyses. In general, site response analyses estimate the effect a site has on a ground motion. Mathematically, this is solved as the propagation of waves in a continuous medium. Ideally, estimation of ground shaking at a site would also include the effects of the rupture mechanism and path of the stress waves from the rupture to the site. However, these phenomena are difficult to predict and include large uncertainties. Instead, the state of the practice uses previously recorded ground motions that are representative of the design hazard recorded on 'rock' to account for source and path effects. These 'rock' ground motions are then propagated up through a soil column to estimate the response of the soil. If there are no such 'rock' ground motions, then the engineer can use simulated ground motions or existing ground motions modified through scaling or spectral matching.

Once the database of site response analyses for non-liquefiable NEHRP F sites has been calculated, a simplified model can be developed to estimate the response spectra based on ground motion and site properties. The simplified model developed for this research does not replace a site response analysis, but rather augments it. It is hoped that the results of this research will help practicing engineers gain a better understanding of their site before conducting site response analyses. This will help them focus on the important aspects of the site, which will save time and money.

1.3 Research Organization

This dissertation is divided into nine chapters. Chapter 2 describes the calculation of target ground motion measures to constrain the selection of acceleration time series that will be used as input rock motions in the site response analyses. To capture the variability of ground motions, five base case scenarios were selected according to tectonic environments and representative cases encountered in common US practice. The five base case scenarios are designated ACR1, ACR2, ACR3, SUB, and SCR. Scenarios ACR1 and ACR2 correspond to shallow crustal earthquakes in active crustal regions representing reverse earthquakes with and without pulse-like responses, scenario ACR3 represents strike-slip shallow crustal earthquakes in active crustal regions, and scenarios SUB and SCR correspond to earthquakes from subduction zones and stable continental regions, respectively.

Current practice considers the response spectrum as the most important target parameter in the selection of acceleration time series for nonlinear dynamic analyses. This study describes the selection of target response spectra for each of the base-case scenarios using ground motion prediction equations (GMPEs) that have been developed for the appropriate tectonic environment. Chapter 2 also details the selection of additional target ground motion parameters

that are considered relevant for appropriate representation of these scenarios, including peak ground acceleration (PGA), peak ground velocity (PGV), mean period (T_m), arias intensity (I_a), significant duration ($D_{5\text{-}95}$) and, for pulse-like motions, the pulse period (T_v).

Chapter 3 discusses the creation of suites of acceleration time series for each of the target scenarios created in chapter 2. First, a database of ground motions for each scenario was created by selecting pairs of measured or simulated seismic records with the same magnitude, distance, and site characteristics as well as the same tectonic environment as the target scenario. These motions are referred to as "original" ground motions. The "original" ground motions were then rotated to the direction that gave the maximum spectral acceleration at a period of 1 second. This is consistent with the specification by ASCE-7-10 of using maximum ground motions as design ground motions (ASCE, 2010). The resulting rotated motions are referred to as "seed" motions to distinguish them from the "original" ground motions. The scaled suite of "seed" ground motions that best matched the response spectrum and its standard deviation, as well as other relevant ground motion measures calculated in chapter 2, was chosen as the final suite to be used in the site response analyses. The suites for scenarios ACR1, SUB, and SCR are each composed of 11 acceleration time series, and the suites for scenarios ACR2 and ACR3 are each composed of 40 acceleration time series. In addition to scaling, the selected ground motions for scenarios ACR2 and ACR3 were also spectrally matched to their respective target response spectra. As a result, scenarios ACR2 and ACR3 each have two suites of ground motions, one scaled and one spectrally matched. Finally, to study the effect of ground motion intensity, the 40 ground motions in the scaled ACR3 suite were further scaled by factors of 0.125, 0.25, 0.5, 1, 2, and 4. This results in a total of 12 ground motion scenarios with 393 ground motions.

Chapter 4 explains the development of predictive equations to estimate the in-situ small strain shear modulus of clays, silts, sands, and gravels. The model to predict the laboratory small strain shear modulus ($G_{max,lab}$) was developed from a mixed effects regression of a database that contains 1680 tests on 331 different soils from 28 different studies. Log-likelihood ratio tests were performed to evaluate the statistical relevance of each parameter added to the model. This ensured that the model was not over-parameterized. A second database was collected to estimate the in-situ small strain shear modulus ($G_{max,in\text{-}situ}$) from $G_{max,lab}$. The two equations were then combined to create a model to estimate $G_{max,in\text{-}situ}$ directly from soil parameters. The input variables studied were the mean effective confining pressure, void ratio, overconsolidation ratio, plasticity index, fines content, coefficient of uniformity, median grain size, laboratory test type and sample type, and in-situ test type. This study then validated and compared the $G_{max,in\text{-}situ}$ model with existing models using a third collected validation database.

The first half of Chapter 5 reviews fundamental concepts related to the dynamic properties of soils, such as the small strain shear modulus (G_{max}), small strain damping (D_{min}), and how the shear modulus (G) and damping (D) change with shear strain (γ). The second half of chapter 5 highlights some published empirical models for estimating shear modulus reduction and damping curves; specifically the models of Vucetic and Dobry (1991), Darendeli (2001), and Kishida et al. (2009).

The first half of chapter 6 outlines the theory, limitations, and input parameters necessary to perform one dimensional total stress equivalent linear, total stress nonlinear, and effective stress

nonlinear site response analyses. It also discusses important aspects of site response analyses that caused confusion in the past but have recently been clarified by other researchers, such as the importance of hysteretic damping, small strain damping, layer thickness, definition of the input motion and half space, and soil strength. The second half of chapter 6 describes the development of the properties of 15 different sites used in the site response analyses. Seven sites are based on actual sites from the San Francisco Bay Area, New York City, Ottawa, Canada, Guayaquil, Ecuador, and Hokkaido, Japan. The other eight sites are variations of the seven base case sites that explore the effects of soil shear strength, plasticity index, and elastic site period on the surface response. Total stress nonlinear and effective stress nonlinear site response analyses were conducted in the program DEEPSOIL (Hashash et al., 2012) for all 15 sites and 12 ground motion scenarios, and total stress equivalent linear site response analyses were conducted in DEEPSOIL for each of the seven base case sites and all 12 ground motion scenarios. This results in a total of 14,541 site response analyses.

Chapter 7 discusses the results of the site response analyses in a qualitative manner, highlights trends noticed in the data, and compares the results with results from other studies. It investigates the effect of ground motion properties on the results of the site response analyses such as intensity, near fault pulse like motions versus near fault motions with no pulse, scaled suites versus spectrally matched suites, ground motion duration, and tectonic region. Chapter 7 also looks at the effects of different site properties on the results of the site response analyses such as soil shear strength, soil modulus reduction and damping curves, and elastic site period. In addition, chapter 7 examines the effect of different analysis types on the site response analyses (total stress equivalent linear, total stress nonlinear, and effective stress nonlinear), the standard deviation of each scenario, comparisons of the amplification factors with those implied by the PEER NGA West 2 GMPEs for NEHRP E sites, and the results of other ground motion parameters such as the peak ground acceleration (PGA), peak ground velocity (PGV), mean period (T_m), significant duration ($D_{5\text{-}95}$), and arias intensity (I_a).

Chapter 8 describes the development of a simplified model to estimate response spectra for non-liquefiable NEHRP F sites. The simplified model was developed in two stages. In the first stage, the results for each site were regressed separately against the ground motion intensity to estimate the effect of the ground motion scenario. In the second stage, the site specific coefficients calculated from the first stage were regressed against site properties to determine their site dependence. These two parts were then combined to form the final model. The simplified model was validated against a separate database than the one used to develop it. This validation database consisted of 24 nonlinear effective stress site response analyses conducted in DEEPSOIL for three sites and eight ground motion scenarios.

Chapter 9 summarizes the main findings and conclusions from the research presented in this dissertation, as well as gives suggestions for future research.

1.4 References

ASCE (2010). "Minimum design loads for buildings and other structures." ASCE/SEI 7-10, American Society of Civil Engineers; Reston, Virginia.

Applied Technology Council (ATC). (1978). ''Tentative provisions for the development of seismic regulations for buildings.'' *ATC 3-06 Report*, Redwood City, Calif.

Biot, M. A. (1942). "Analytical and experimental methods in engineering seismology." Proc. ASCE 68,49-69.

Borcherdt, R.D. (1994). "Estimates of site dependent response spectra for design (methodology and justification)." *Earthquake Spectra*, Vol. 10, p 617-653.

Chang, S.W. (1994). "Seismic response of deep stiff soil deposits." PhD dissertation, University of California, Berkeley.

Darendeli, M. B. (2001). "Development of a new family of normalized modulus reduction and material damping curves." PhD dissertation, Univ. of Texas at Austin, Austin, Texas.

Dickenson, S.E. (1994). "Dynamic response of soft and deep cohesive soils during the Loma Prieta earthquake of October 17, 1989." PhD dissertation, University of California, Berkeley.

Dobry, R., Martin, G.R., Parra, E., and Bhattacharyya, A., (1994). "Development of site dependent ratios of elastic response spectra (RRS) and site categories for building seismic codes." In *proceedings of the NCEER/SEAOC/BSSC Workshop on Site Response During Earthquakes and Seismic Code Provisions*, G.R. Margin, ed. University of Southern California, Los Angeles, November 18-20, 1992, National Center for Earthquake Engineering Research Special Publication NCEER-94-SP01, Buffalo, NY.

Dobry R., Borcherdt, R.D., Crouse, C.B., Idriss, I.M., Joyner, W.B., Martin, G.R., Power, M.S., Rinne, E.E., and Seed R.B. (2000). "New site coefficients and site classification system used in recent building seismic code provisions." *Earthquake Spectra*, 16(1), 41- 67.

Donovan, N.C. (1973). "A statistical evaluation of strong motion data including the Feb. 9, 1971 San Fernando earthquake." *Proceedings of the 5th World Conference of Earthquake Engineering*, Rome.

Duke, C.M., Johnsen, K.E., Larson, L.E., and Engman, D.C. (1972). "Effects of Site Classification and Distance on Instrumental Indices in the San Fernando Earthquake." UCLA Eng-7247, University of California, Los Angeles.

Hashash, Y.M.A, Groholski, D.R., Phillips, C. A., Park, D, Musgrove, M. (2012) "DEEPSOIL 5.1, User Manual and Tutorial." 107 p.

Housner, G. W. (1941). "An Investigation of the Effects of Earthquakes on Buildings." Ph.D. Thesis, California Institute of Technology, Pasadena, California.

Housner, G. W. (1959). "Behavior of structures during earthquakes." *J. Eng. Mech. Div.*, Proc. ASCE 85, EM4, pp. 109-129.

Huber, W.L. (1930). "The San Francisco Earthquakes of 1865 and 1868," *Bulletin of the Seismological Society of America*, Vol. 20(4), pp. 261-272.

IBC (2012). International *Building Code*, by International Code Council, Delmar Publishers.

Joyner, W.B., Fumal, T.E., and Glassmoyer, G. (1994). "Empirical spectral response ratios for strong motion data from the 1989 Loma Prieta, California, earthquake." In *proceedings of the NCEER/SEAOC/BSSC Workshop on Site Response During Earthquakes and Seismic Code Provisions*, G.R. Margin, ed. University of Southern California, Los Angeles, November 18-20, 1992, National Center for Earthquake Engineering Research Special Publication NCEER-94-SP01, Buffalo, NY.

Kishida, T., Boulanger R.W., Abrahamson N.A., Wehling T.M., Driller M.W. (2009). "Regression Models for Dynamic Properties of Highly Organic Soils." *J. of Geotech. and Geoenvir. Eng.*, ASCE, 135(4).

Kramer, Steven L. (1996). *Geotechnical Earthquake Engineering*. Prentice Hall; New Jersey.

Luco, Nicolas (2007). "Ground Motions for Design." *USGS Thailand Seismic Hazard Workshop*, January 18, 2007. <http://earthquake.usgs.gov/hazards/about/workshops/thailand/downloads/070118--Luco_on_Ground_Motions_for_Design(v8).pdf>

MacMurdo, J. (1824). "Papers relating to the earthquake which occurred in India in 1819," *Philosophical Magazine*, Vol. 63, pp. 105-177.

Martin, G.R., ed. (1994). *Proceedings of the 1992 NCEER/SEAOC/BSSC Workshop on Site Response During Earthquakes and Seismic Code Provisions*. University of Southern California, Los Angeles, November 18-20, 1992. National Center for Earthquake Engineering Research Special Publication NCEER-94-SP01, Buffalo, NY.

Mohraz, B. (1976). ''Earthquake response spectra for different geologic conditions.'' *Bulletin of the Seismological Society of America*, Vol. 66(3), 915–935.

NEHRP (2009). "NERHP recommended seismic provisions for new buildings and other structures." FEMA P-750 report prepared by the Building Seismic Safety Council of The National Institute of Building Sciences for the Federal Emergency Management Agency, Washington, D.C

Newmark, N. M., and Hall, W. J. (1969). "Seismic design criteria for nuclear reactor facilities." In *Proceedings of the 4th World Conference of Earthquake Engineering*, Santiago, Chile, B-4, 37-50.

Nikolaou, S., Mylonakas, G., and Edinger, P. (2001). "Evaluation of site factors for seismic bridge design in New York City area." *Journal of Bridge Engineering*, ASCE, Vol. 6(6), pp. 564-576.

Seed, R.B., Dickenson, S.E., Rau, G.A., White, R.K., and Mok, C.M. (1994). "Observations regarding seismic response analyses for soft and deep clay sites." In *proceedings of the NCEER/SEAOC/BSSC Workshop on Site Response During Earthquakes and Seismic Code Provisions*, G.R. Margin, ed. University of Southern California, Los Angeles, November 18-20, 1992, National Center for Earthquake Engineering Research Special Publication NCEER-94-SP01, Buffalo, NY.

Seed, H. B., Murarka, R., Lysmer, J., and Idriss, I. M. (1976a). ''Relationship between maximum acceleration, maximum velocity, distance from source and local site conditions for moderately strong earthquakes." *Bulletin of the Seismological Society of America*, Vol. 66(4), 1323–1342.

Seed, H. B., Ugas, C., and Lysmer, J. (1976b). ''Site-dependent spectra for earthquake resistant design.'' *Bulletin of the Seismological Society of America*, Vol. 66(1), 221–244.

Seed H.B., Idriss, I.M., and Dezfulian, H. (1967). "Relationships between soil conditions and building damage in the Caracas earthquake of July, 29, 1967." *Earthquake Engineering Research Center*, Report No. EERC 70-2, College of Engineering, University of California, Berkeley.

Seed H.B., Romo, M.P., Sun, J.I, Jaime, A., and Lysmer, J., (1988). "The Mexico earthquake of September 19, 1985 – Relationships between soil conditions and earthquake ground motions." *Earthquake Spectra*, Vol. 4(4), pp. 687-729.

Seed R.B., Chang S.W., Dickenson S.E., Bray J.D (1997). "Site-dependent Seismic Response Including Recent Strong Motion Data," in *Seismic Behaviour of Ground and Geotechnical Structures*, Seco e Pinto, P. S., ed., Proc. of Spec. Session on Earthquake Geotechnical Engineering, XIV International Conf. On Soil Mechanics and Foundation Engineering, Hamburg, Germany, A.A. Balkema, pp. 125-134, Sept. 6-12.

Trifunac M.D. (1976). "Preliminary empirical model for scaling Fourier Amplitude Spectra of strong ground acceleration in terms of earthquake magnitude, source-to-site distance, and recording site conditions." *Bulletin of the Seismological Society of America*, Vol. 66(4), pp. 1343-1373.

Vucetic, M. and Dobry, R. (1991). "Effect of soil plasticity on cyclic response." *Journal of Geotechnical Engineering*. ASCE, 117(1), 89–107.

Whitman, R. ed., (1992). Proceedings of the Site Effects Workshop, October 24, 1991, Report NCEER-92-0006, National Center for Earthquake Engineering Research, Buffalo, NY.

Wood, H.O. (1908). "Distribution of apparent intensity in San Francisco, in the California earthquake of April 18, 1906." *Report of the State Earthquake Investigation Commission*, Carnegie Institute of Washington, Washington DC., Vol. 1, pp. 220-245.

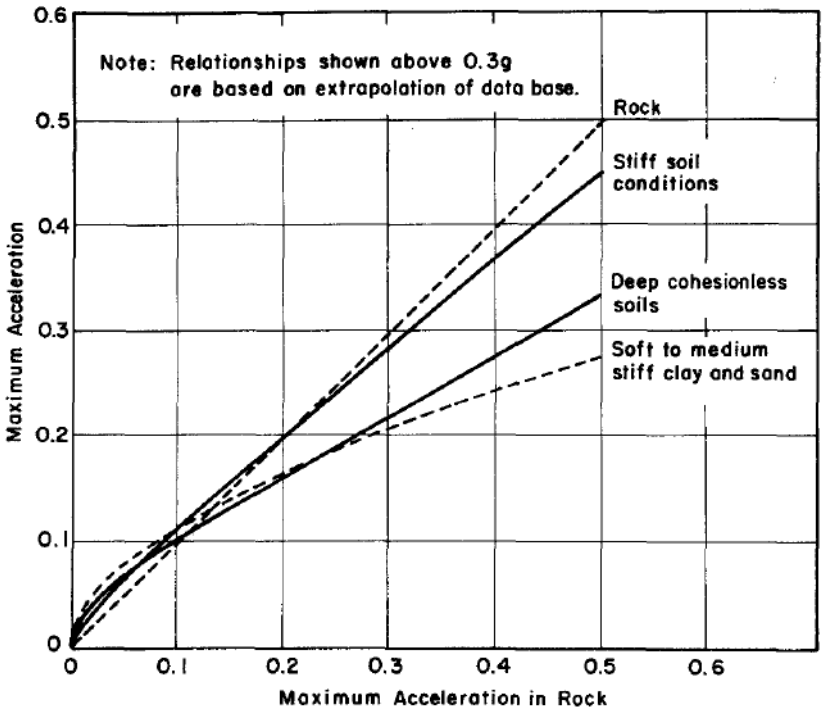

Figure 1.1: Relationship between PGA_{soil} and PGA_{rock} (From Seed et al., 1976a)

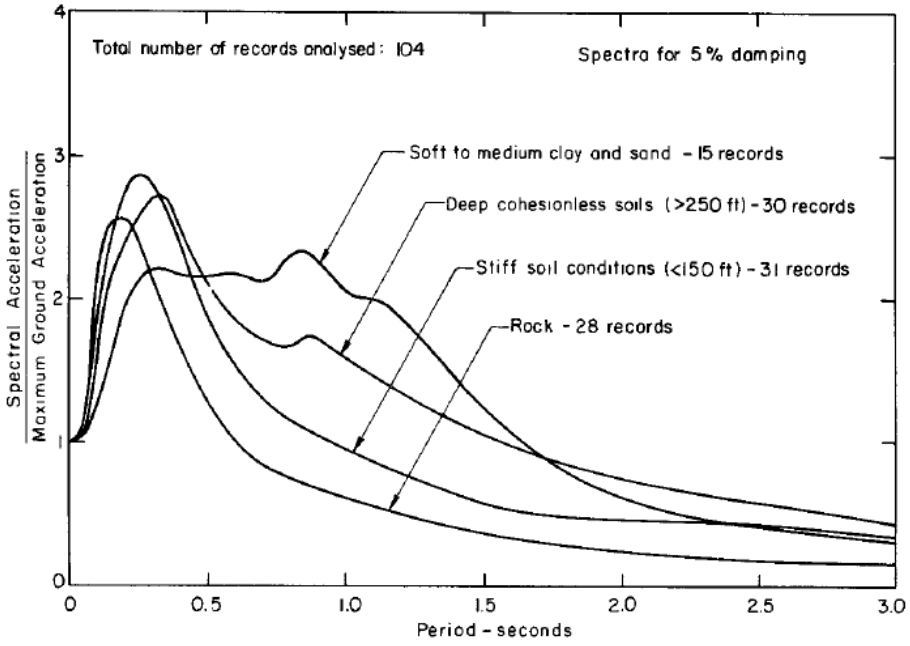

Figure 1.2: Influence of site effects on response spectrum shape (From Seed et al., 1976b)

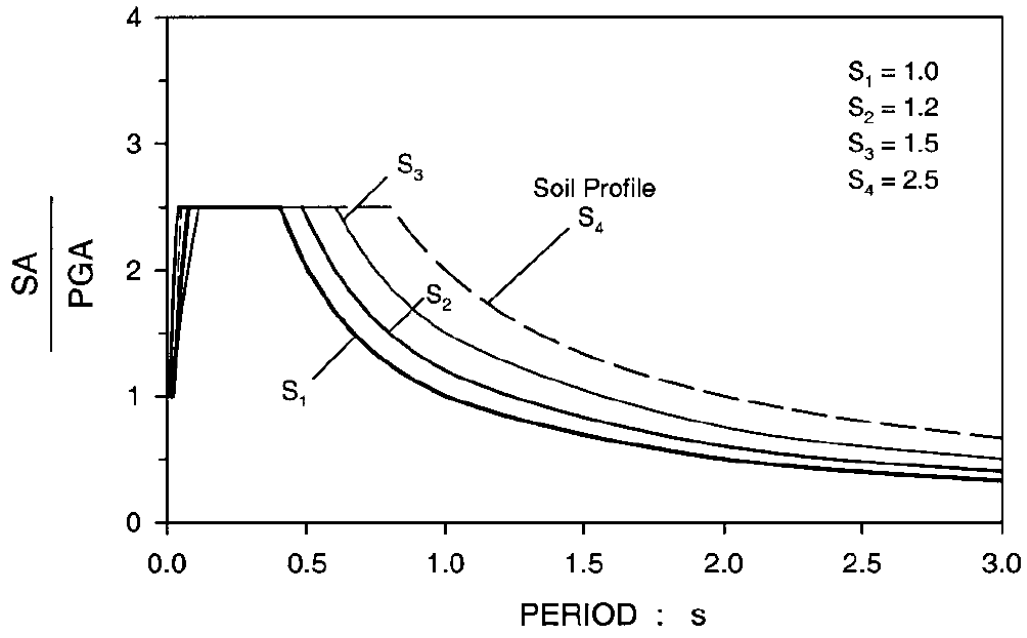

Figure 1.3: Applied Technology Council design spectra

Table 1.1: IBC site class definitions (IBC, 2012)

SITE CLASS	SOIL PROFILE NAME	AVERAGE PROPERTIES IN TOP 100 feet, SEE SECTION 1613.5.5		
		Soil shear wave velocity, $\bar{v}_s$, (ft/s)	Standard penetration resistance, $\bar{N}$	Soil undrained shear strength, $\bar{s}_u$, (psf)
A	Hard rock	$\bar{v}_s > 5{,}000$	N/A	N/A
B	Rock	$2{,}500 < \bar{v}_s \leq 5{,}000$	N/A	N/A
C	Very dense soil and soft rock	$1{,}200 < \bar{v}_s \leq 2{,}500$	$\bar{N} > 50$	$\bar{s}_u \geq 2{,}000$
D	Stiff soil profile	$600 \leq \bar{v}_s \leq 1{,}200$	$15 \leq \bar{N} \leq 50$	$1{,}000 \leq \bar{s}_u \leq 2{,}000$
E	Soft soil profile	$\bar{v}_s < 600$	$\bar{N} < 15$	$\bar{s}_u < 1{,}000$
E	—	Any profile with more than 10 feet of soil having the following characteristics: 1. Plasticity index $PI > 20$, 2. Moisture content $w \geq 40\%$, and 3. Undrained shear strength $\bar{s}_u < 500$ psf		
F	—	Any profile containing soils having one or more of the following characteristics: 1. Soils vulnerable to potential failure or collapse under seismic loading such as liquefiable soils, quick and highly sensitive clays, collapsible weakly cemented soils. 2. Peats and/or highly organic clays ($H >$ 10 feet of peat and/or highly organic clay where H = thickness of soil) 3. Very high plasticity clays ($H >$ 25 feet with plasticity index $PI > 75$) 4. Very thick soft/medium stiff clays ($H >$ 120 feet)		

Table 1.2: Site coefficient F_a (top) and F_v (bottom) (From IBC, 2012)

Site Class	Spectral Response Acceleration Parameter at Short Period				
	$S_S \le 0.25$	$S_S = 0.5$	$S_S = 0.75$	$S_S = 1.0$	$S_S \ge 1.25$
A	0.8	0.8	0.8	0.8	0.8
B	1.0	1.0	1.0	1.0	1.0
C	1.2	1.2	1.1	1.0	1.0
D	1.6	1.4	1.2	1.1	1.0
E	2.5	1.7	1.2	0.9	0.9

Site Class	Spectral Response Acceleration Parameter at 1-second Period				
	$S_1 \le 0.1$	$S_1 = 0.2$	$S_1 = 0.3$	$S_1 = 0.4$	$S_1 \ge 0.5$
A	0.8	0.8	0.8	0.8	0.8
B	1.0	1.0	1.0	1.0	1.0
C	1.7	1.6	1.5	1.4	1.3
D	2.4	2.0	1.8	1.6	1.5
E	3.5	3.2	2.8	2.4	2.4

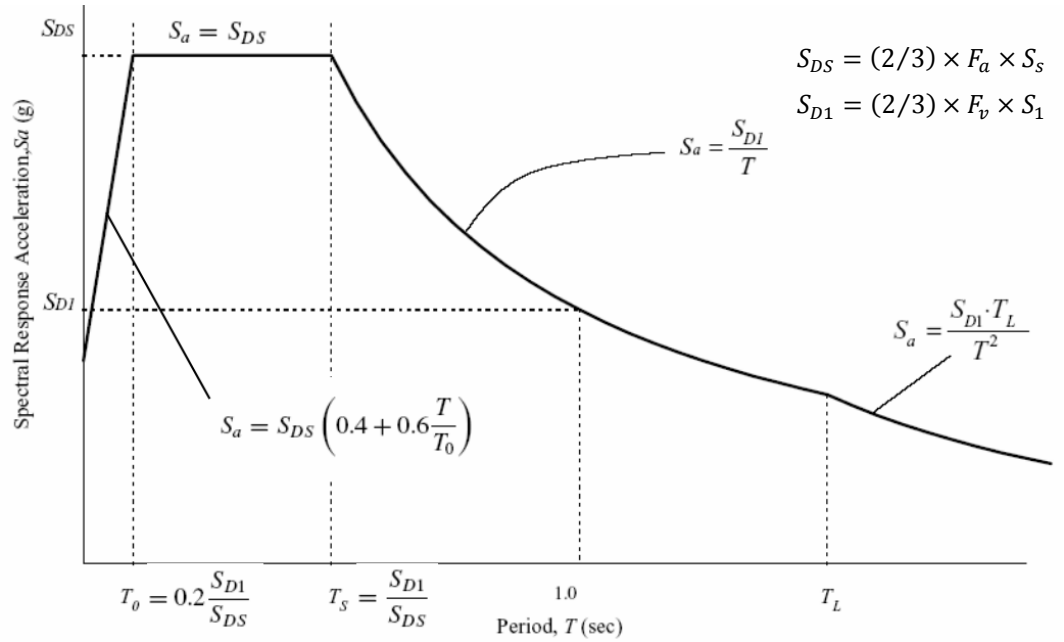

Figure 1.4: Procedure to calculate design spectrum following IBC (Modified from Luco, 2007)

Table 1.3: Site classification system proposed by Seed et al. (1997)

Site Class	Site Condition	General Description	Site Characteristics
(A_0)	A_0	Very hard rock	V_s(avg.)>5,000 ft/s in top 50 ft.
A	A_1	Competent rock with little or no soil and/or weathered rock veneer.	2,500 ft/s ≤ V_s(rock) ≤ 5,000 ft/s, and $H_{soil+weathered\ rock}$ ≤ 40 ft, with V_s > 800 ft/s (in all but the top few feet[3])
AB	AB_1	Soft, fractured and/or weathered rock.	For both AB_1 and AB_2: 40 ft ≤ $H_{soil+weathered\ rock}$ ≤ 150 ft, and V_s > 800 ft/s (in all but the top few feet[3])
	AB_2	Stiff, very shallow soil over rock and/or weathered rock.	
B	B_1	Deep, primarily cohesionless[4] soils. (H_{soil} ≤ 300 ft.)	No "soft clay" (see note 5), and $H_{cohesive\ soil}$ > 0.2 $H_{cohesionless\ soil}$
	B_2	Medium depth, stiff cohesive soils and/or mix of cohesionless with stiff cohesive soils; no "soft clay".	$H_{all\ soils}$ ≤ 200 ft, and V_s (cohesive soils) > 600 ft/s (see Note 5)
C	C_1	Medium depth, stiff cohesive soils and/or mix of cohesionless with stiff cohesive soils; thin layer(s) of soft clay.	Same as B_2 above, except 0 ft < $H_{soft\ clay}$ ≤ 10 ft. (see Note 5)
	C_2	Very deep, primarily cohesionless soils.	Same as B_1 above, except H_{soil} > 300 ft.
	C_3	Deep, stiff cohesive soils and/or mix of cohesionless with still cohesive soils; no "soft clay".	H_{soil} > 200 ft., and V_s (cohesive soils) > 600 ft/s
	C_4	Soft, cohesive soil at small to moderate levels of shaking.	10 ft < $H_{soft\ clay}$ ≤ 90 ft, and $A_{max,rock}$ ≤ 0.25 g
D	D_1	Soft, cohesive soil at medium to strong levels of shaking.	10 ft < $H_{soft\ clay}$ ≤ 90 ft, and 0.25 g < $A_{max,rock}$ ≤ 0.45 g, or (0.25 g < $A_{max,rock}$ ≤ 0.55 g and M ≤ 7-1/4)
(E)[6]	E_1	Very deep, soft cohesive soil.	$H_{soft\ clay}$ > 90 ft (see Note 5)
	E_2	Soft, cohesive soil and very strong shaking.	$H_{soft\ clay}$ > 10 ft and either: $A_{max,rock}$ > 0.55 g or $A_{max,rock}$ > 0.45 g and M > 7-1/4
	E_3	Very high plasticity clays.	H_{clay} > 30 ft with PI > 75% and V_s < 800 ft/s
(F)[7]	F_1	Highly organic and/or peaty soils.	H > 10 ft of peat and/or highly organic soils.
	F_2	Sites likely to suffer ground failure due either to significant soil liquefaction or other potential modes of ground instability.	Liquefaction and/or other types of ground failure analysis required.

Notes:

1. H = total (vertical) depth of soils of the type or types referred to.
2. V_s = seismic shear wave velocity (ft/s) at small shear strains (shear strain ~ 10^{-4}%).
3. If surface soils are cohesionless, V_s may be less than 800 ft/s in top 10 feet.
4. "Cohesionless soils" = soils with less than 30% "fines" by dry weight. "Cohesive soils" = soils with more than 30% "fines" by dry weight, and 15% ≤ PI (fines) ≤ 90%. Soils with more than 30% fines, and PI (fines) < 15% are considered "silty" soils herein, and these should be (conservatively) treated as "cohesive" soils for site classification purposes in this Table.
5. "Soft Clay" is defined as cohesive soil with: (a) Fines content ≥ 30%, (b) PI(fines) ≥ 20%, and (c) V_s ≤ 600 ft/s.
6. Site-specific geotechnical investigations and dynamic site response analyses are strongly recommended for these conditions. Response characteristics within this Class (E) of sites tends to be more highly variable than for Classes A_0 through D, and the response projections herein should be applied conservatively in the absence of (strongly recommended) site-specific studies.
7. Site-specific geotechnical investigations and dynamic site response analyses are *required* for these conditions. Potentially significant ground failure must be mitigated, and/or it must be demonstrated that the proposed structure/facility can be engineered to satisfactorily withstand such ground failure.

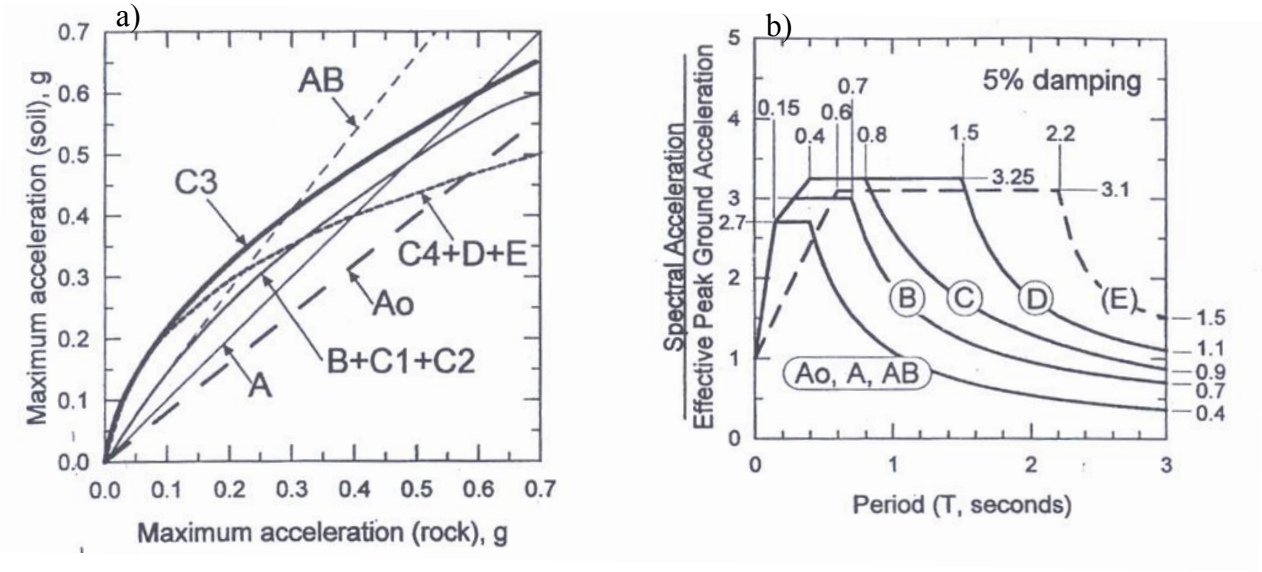

Figure 1.5: a) Site dependent relationship between PGA_{rock} and PGA_{soil} and b) site dependent response spectra (From Seed et al. 1997)

CHAPTER 2: SELECTION OF TARGET GROUND MOTION PARAMETERS

The selection of ground motions is a key component in the numerical modeling of seismic performance of structures and other engineering systems. Consistent selection of representative time series requires the determination of target ground motion parameters. This study describes the selection of target ground motion measures to constrain the selection of acceleration time series to be used as outcropping rock motions in nonlinear site response analyses. To capture the variability of ground motions, five base-case scenarios were selected according to tectonic environments and representative cases encountered in common US practice. The first three correspond to shallow crustal earthquakes in active crustal regions, representing reverse earthquakes with and without pulse-like response (ACR1, ACR2) and strike-slip earthquakes (ACR3), while the last two correspond to earthquakes from subduction zones (SUB) and stable continental regions (SCR). Current practice considers the response spectrum as the most important target parameter in the selection of acceleration time series for nonlinear dynamic analyses. This study describes the selection of target response spectra for each of the base-case scenarios using ground motion prediction equations (GMPEs) that have been developed for the appropriate tectonic environment. This study also details the selection of additional target ground motion parameters that are considered relevant for appropriate representation of these scenarios, including: peak ground acceleration (PGA), peak ground velocity (PGV), mean period (T_m), arias intensity (I_a), significant duration ($D_{5\text{-}95}$) and, for pulse-like motions, the pulse period (T_v). All target ground motion measures are assumed to be log-normally distributed and can be fully described by their mean (μ) and standard deviation (σ). For completeness, this study also briefly summarizes the models used in the determination of the various target parameters.

2.1 Introduction

The rigorous selection of ground motions is an important consideration in the seismic assessment of an engineered system as it provides the link between seismic hazard and seismic response. Consistent ground motion selection requires both the determination of a target to compare the appropriateness of different ground motions as well as an objective method for the selection, simulation, and/or modification of ground motions to match this target (Bradley, 2010). The objective of this work is to develop target ground motion parameters to constrain the selection of acceleration time series to be used as input motions in nonlinear site response analyses. These analyses are performed to develop a simplified procedure to estimate the response spectra for soil sites classified as non-liquefiable F-sites (IBC, 2012).

Current practice considers the target response spectrum as the most important target parameter in the selection of acceleration time series for nonlinear dynamic analyses. Nevertheless, the response spectrum does not capture all characteristics of seismic motions. This study considers additional target ground motions parameters for appropriate ground motion representation including: the peak ground acceleration (PGA), the peak ground velocity (PGV), the mean period (T_m), the arias intensity (I_a), and significant duration ($D_{5\text{-}95}$). To better incorporate the characteristics of near field events, this study also considered the pulse period (T_v) as an additional target ground motion parameter. All target ground motion measures are assumed to

be log-normally distributed and can be fully described by their mean (μ) and standard deviation (σ). The following sections discuss the selection of base-case scenarios representative of common US practice. This work also give full details of the methodology used for the selection of target ground motion parameters for each of the base-case scenarios. This study uses ground motion prediction equations (GMPEs) to predict the distribution properties for the various ground motion intensity measures. These GMPEs describe how the target measure changes as a function of magnitude, distance, and other parameters for different tectonic environments. The results are generally represented by mean (μ) target ground motion parameter and the one standard deviation band (μ-σ, μ+σ). These target parameters will be later used to constrain the selection and modification of ground motions to be used as input motions in nonlinear site response analyses.

2.2 Ground Motion Scenarios

To capture the variability of ground motions and their effects on the seismic response of deep soft soil deposits, five base-case scenarios were selected representing scenarios commonly encountered in US practice. The scenarios encompass: a) shallow crustal earthquakes in active crustal regions, b) earthquakes from subduction zones, and c) earthquakes in stable continental regions. Although the scenarios are constrained by using representative magnitude and distance from the fault, the study can easily be extended to other conditions with no loss of generality. Table 2.1 summarizes the selected characteristics for each scenario.

The first three scenarios (ACR1, ACR2 and ACR3) correspond to shallow crustal earthquakes in active plate margins where normal, reverse and strike slip earthquakes occur. Examples of locations where these conditions may be applicable include California, Japan, New Zealand, Italy, Greece and Turkey. The selected earthquake characteristics for scenarios ACR1 and ACR2 are a moment magnitude of 6.7 (M_w= 6.7) at a distance of 5km (R_{RUP} = 5km). The selected faulting mechanism is a dip-slip reverse type fault with surface rupture and a fault plane angle of 45 degrees. The hypothetical site was considered to be on the hanging wall which typically gives a higher seismic hazard than a site located on the foot wall (Abrahamson and Somerville, 1996). Scenario ACR1 was selected to represent ground motions with near fault characteristics and pulse type motions, while scenario ACR2 represents ground motions that do not exhibit pulse-like response. Scenario ACR3 represents a strike slip earthquake with a moment magnitude of 7.8 (M_w= 7.8) at a distance of 30km (R_{RUP} = 30km) with surface rupture and a vertical fault plane.

Subduction zone earthquakes occur at plate boundaries where one plate is subducted under another. Usually the denser ocean plate slides under the lighter continental plate and is subsumed back into the mantle. Subduction zone earthquakes tend to generate very large magnitude earthquakes because they can have rupture dimensions much greater than shallow crustal earthquakes. Examples of locations where these conditions may be applicable include Japan, Indonesia, New Zealand, Chile, Alaska and the Pacific Northwest. Subduction zone earthquakes fall into one of two categories: interface and intraslab earthquakes. Interface earthquakes, also referred to as megathrust earthquakes, are shallow angle thrust events that occur at the interface between the subducting and the overriding plates. Examples of these type of events are the 1964 M 9.2 Alaskan earthquake, 2010 M 8.8 Maule, Chile, earthquake, and the

2011 M 9.0 Tohoku, Japan, earthquake. Intraslab earthquakes occur within the subducting oceanic plate and are typically high angle normal faulting events responding to down-dip tension in the subducting plate. Examples of intraslab earthquakes are the 1949 M 7.1 and 1965 M 6.5 Puget Sound earthquakes. If the earthquake type is unknown, Youngs et al (1997) recommend that earthquakes in subduction zones with focal depths less than 50 km be considered as interface events, while events with focal depths greater than 50 km be considered as intraslab events. Similarly, Atkinson and Boore (2003) suggest that events with focal depths less than 50 km are due to thrust faulting, and earthquakes deeper than this are due to the breakup of the lower plate as it is crushed under the upper plate and absorbed back into the mantle of the earth. Scenario SUB was selected to represent an "interface" event of magnitude 9 (M_w=9) at a distance of 100 km (R_{RUP} = 100km) with a focal depth of 30 km.

Scenario SCR represents earthquakes occurring in stable continental regions. In these areas there are no defined faults and no plate boundaries yet earthquakes still occur. Examples of stable continental regions are Australia, Eastern North America and Northern Europe. The particular application of this scenario is for conditions prevalent in Central and Eastern North America (CENA). Sixteen crustal velocity models have been compiled in CENA as shown in Figure 2.1. For the purpose of ground-motion calculations for the depth, distance and frequency range of interest, 15 of the 16 crustal models predict very similar ground motions and can be grouped into one (e.g., EPRI, 1993). As a result, CENA is partitioned into two attenuation regions: the Gulf Coastal Plain (region 4) and the remaining regions, represented by the crustal velocity structure in region 12 (Midcontinent region). Scenario SCR was chosen to be representative of the Midcontinent region with a moment magnitude of 6 (M_w=6) at a distance of 17 km (R_{RUP} = 17km).

2.3 Ground Motion Prediction Equations

The three most significant characteristics to completely describe a ground motion include its intensity, duration, and frequency content. The response spectrum is generally considered as the most important target parameter in the selection of acceleration time series for nonlinear dynamic analyses, however, it only describes the intensity and frequency content. In addition to the response spectrum this study considers other ground motion measures such as the peak ground acceleration (PGA), the peak ground velocity (PGV), the mean period (T_m), the arias intensity (I_a), the significant duration (D_{5-95}) and, for pulse-like motions, the pulse period (T_v). The following sections describe the methodology used for the selection of each target ground motion parameters for each of the base-case scenarios described above.

2.3.1 Target Response Spectra for Seismic Analyses

Common linear dynamic analyses evaluate the seismic response of structures by using a target response spectrum (e.g., Chopra, 2011). This target response spectrum may be derived from a variety of sources, including: building code provisions (e.g., IBC, 2012), probabilistic seismic hazard analysis (i.e., Uniform Hazard Response Spectrum, UHS), or from GMPEs and a given earthquake scenario (e.g., Abrahamson & Silva, 2008). Generally, the target response spectrum is a pseudo-acceleration response spectrum. This spectrum represents the maxima pseudo-accelerations experienced by equivalent linear single degree of freedom systems as a function of

their natural period (typically for 5% damping). Although the pseudo-acceleration is not the same as true acceleration, for damping of 5% and periods of up to 10 seconds, the differences are negligible (e.g., Chopra, 2011). This study obtained the target response spectra for each scenario from ground motion prediction equations. Ground motion prediction equations estimate a smoothed spectral shape (Sa vs. T) as a function of magnitude, distance, and other parameters for a given event. Since the required target is for "rock," all calculations made using GMPEs specified the site conditions as "rock." The GMPEs predict not only the mean but also the standard deviation, which is typically period dependent and in some cases magnitude dependent.

Ground motions from seismic events are complex and may have significant contributions in all three directions (i.e., 2 horizontal and vertical). When only one component of the recorded ground motion is used the selection of the orientation of the ground motion can have significant effects on the response spectrum. Appendix 2A describes the different types of ground motion orientations used to develop GMPEs and also several studies that estimated factors to switch from one orientation to another. In this study all target response spectra were modified according to NERHP (2009) to predict the response spectra for the maximum demand orientation, RotD100.

2.3.1.1 Target Response Spectrum for Shallow Crustal Earthquakes in Active Tectonic Regions

In 2008, the Pacific Earthquake Engineering Research Center (PEER) concluded the "Next Generation of Ground-Motion Attenuation Models" for the western United States, commonly referred to as NGA West 1. NGA West 1 was a multidisciplinary research project coordinated by the Lifelines Program of PEER in association with the U.S. Geological Survey (USGS) and the Southern California Earthquake Center (SCEC). The program developed five GMPEs for active crustal regions based on an updated and uniformly processed ground motion database. PEER recently completed NGA West 2, an update to NGA West 1 that includes more data, especially small magnitude earthquakes. Unfortunately, these models were published after this study had been completed and were not included. However, this study compared the response spectra predicted by the NGA West 1 GMPEs with those of the NGA West 2 GMPEs and the differences for the selected scenarios were minor.

The 5% damped pseudo-acceleration target spectra for scenarios ACR1, ACR2 and ACR3 were estimated using a weighted average of the 2008 Next Generation Attenuation Ground Motion Prediction Equations (NGA GMPEs) developed by Abrahamson and Silva, 2008 (AS08), Boore and Atkinson, 2008 (BA08), Campbell and Bozorgnia, 2008 (CB08), Chiou and Youngs, 2008 (CY08), and Idriss, 2008 (I08). Each GMPE predicts the peak ground acceleration (PGA), peak ground velocity (PGV), and pseudo-acceleration response spectra from 0-10 seconds. All of the models include magnitude saturation, which leads to weaker magnitude scaling at short distances compared to magnitude scaling at larger distances. All of the models include a style of faulting factor, which differentiates between strike-slip, reverse, and normal faulting. The AS08, CB08, and CY08 models include rupture-depth and hanging-wall effects. The BA08 model includes rupture depth and hanging wall effects implicitly through R_{jb}. All of the models include period dependent standard deviations. In addition, the standard deviations for the AS08, CY08, and I08 models are magnitude dependent, and the standard deviations for the AS08, CB08, and CY08

models are also dependent on non-linear site amplification effects (Abrahamson et al, 2008). A comprehensive overview and comparison of all 2008 NGA GMPEs is available in the literature (Abrahamson et al., 2008) and Appendix 2B provides a brief summary. Detailed selection of parameters and their application is given for each scenario in the following sections.

In order to reduce the aleatory variability, the 2008 NGA ground motion prediction equations (GMPE) predict GMRotI50, referred to as GMRotI50_NGA, instead of the geometric mean of the ground motion $GM_{x,y}$. Although the GMRotI50 response spectra are systematically larger than the $GM_{x,y}$ response spectra, the difference is typically less than 3% (Boore et al., 2006).

To describe pulse like motions resulting from near fault effects, models used in practice fall into one of two categories: broadband and narrowband models. Broadband models describe the amplification of the response spectra by increasing or decreasing the spectral ordinates over a range of periods (e.g., Somerville et al., 1997). In contrast, narrowband models amplify or de-amplify the response spectra over a narrow range of periods close to the pulse period (T_v). In this study the response spectra for scenario ACR1, which is representative of pulse like motions, was modified according to Somerville et al (1997) for a dip-slip fault. The Somerville et al (1997) directivity model uses the following parameters: moment magnitude M_w, closest distance to the rupture plane R_{RUP}, the style of faulting (strike-slip or dip-slip), site classification, for strike slip the length ratio X (fraction of fault along strike that ruptures towards the site) and azimuth angle θ (angle between fault plane and ray path to the site), and for dip-slip the width ratio Y (fraction of fault up dip that ruptures towards the site) and zenith angle ϕ (angle between fault plane and ray path to the site).

2.3.1.2 Target Response Spectrum for Subduction Zones

This study used the GMPEs of Youngs et al. (1997), Atkinson and Boore (2003), Zhao et al. (2006), and Atkinson and Macias (2009) to calculate the target response spectra for scenario B, which is a large interface event. All four of these GMPEs are magnitude and distance dependent. Youngs et al (1997), Atkinson and Boore (2003), and Zhao et al (2006) also include the effects of focal depth (hypocentral depth), source type, and site factors. The Atkinson and Boore (2003) model also allows region specific coefficients (e.g., Japan or Cascadia). The Atkinson and Macias (2009) model was developed for a specific site type (NEHRP B/C boundary) and source type (interface), and therefore does not include terms for either of these conditions. This study uses a weighted average of these four attenuation models to estimate the 5% damped pseudo-acceleration target spectrum for scenario SUB. Appendix 2C provides a summary of these models and the equations used to predict the mean spectral acceleration and the peak ground acceleration (PGA) target measures as well as their respective standard deviations.

2.3.1.3 Target Response Spectrum for Stable Continental Regions

This study uses a weighted average of four GMPEs to estimate the 5% damped pseudo-acceleration target spectrum for stable continental regions representative of scenario SCR: Toro et al. (1997, 2002), Silva et al. (2002), Atkinson and Boore (2006, 2011), and Pezeshk et al (2011). Toro (2002) introduced two methods to account for magnitude saturation in the Toro et al. (1997) model. This study implements the Toro et al. (1997) model with a weight of 0.5 for both types of magnitude saturation modifications. The Silva et al. (2002) study developed five

models: single corner frequency with variable stress drop, single corner frequency with constant stress drop, single corner frequency with constant stress drop and magnitude saturation, double corner frequency model, and a double corner frequency model with magnitude saturation. This study gives equal weight to the two models that include magnitude saturation, and does not include the other three Silva et al. (2002) models. The Atkinson and Boore (2006) model uses a constant stress drop parameter fixed at 140 bars. This study uses the Atkinson and Boore 2011 update which makes the stress drop parameter magnitude dependent based on new strong motion data from Eastern North America. The Pezeshk et al (2011) model is a hybrid empirical model using the five NGA West 1 GMPEs multiplied by a modification factor to predict a GMPE for the Eastern United States.

The input parameters for all models are the moment magnitude, M_w and distance, R. The only other parameter in the Toro et al. (1997) GMPE is the region of the earthquake. This parameter is zero for earthquakes occurring in the midcontinent region and one for earthquakes occurring in the Gulf region (see Figure 2.1). This study used the coefficients for the midcontinent region. The soil parameter for the Atkinson and Boore (2006) model was chosen as S = 0 for hard rock sites (Vs_{30} = 2,000 m/s) to be consistent with the other scenario SCR models. Appendix 2D presents a summary of the equations to predict the mean spectral acceleration, the peak ground acceleration (PGA), and the peak ground velocity (PGV) as well as their respective standard deviations for each GMPE.

2.3.2 Peak Ground Acceleration (PGA) and Peak Ground Velocity (PGV)

The most direct ground motion intensity measures are the peak ground acceleration (PGA) and velocity (PGV), which are the maximum absolute value of acceleration and velocity measured from the acceleration time series and the velocity time series, respectively. These two intensity measures are commonly obtained as part of the GMPEs that estimate the response spectrum. In general, they have similar mathematical forms as those relating the pseudo-acceleration versus period. All of the GMPEs used in this study predict PGA and PGV, except the subduction zone models, which only predict PGA. There are currently no well established, widely used models to predict the PGV of subduction zone earthquakes.

Ground motions recorded at distances less than 20 km may have near fault effects, such as forward directivity, backward directivity, or fling step (NIST, 2012). Forward directivity produces ground motions with large amplitudes and short durations and can be characterized by large velocity pulses. This study uses the Bray et al (2009) model to predict the mean and standard deviation of PGV for rock sites for scenario ACR1. The Bray et al (2009) model defines rock sites as sites with no more than 20 meters of soil or weathered rock over competent rock. Appendix 2E gives details of the model.

2.3.3 Mean Period (T_m)

Site response analyses are significantly affected by the frequency content of the input ground motion. Until recently, the predominant period (T_p), the period corresponding to the maximum spectral acceleration, was the most common scalar parameter. Among several frequency measures, T_p has been found to have the largest uncertainty and, as a result, the use of this parameter is no longer recommended. Instead, this study uses the mean period, T_m, as a scalar

measure of the frequency content of the ground motion. The mean period is the period at the centroid of the Fourier amplitude spectrum and is mostly affected by low frequency content. This study uses the mean period (T_m) predicted by the Rathje et al (2004) model. The model can account for forward directivity effects. Appendix 2E describes the model in more detail.

2.3.4 Arias Intensity (I_a)

The Arias intensity (I_a) is a widely used ground motion parameter because it correlates well with commonly used demand measures of structural performance, liquefaction, and seismic slope stability (Travasarou et al, 2003). The arias intensity was defined by Arias (1970) as the square of the acceleration integrated over the entire duration of the time series. It has units of velocity and is generally reported in m/s. This study uses the average of three GMPE models to calculate the target mean and standard deviation of arias intensity: Travasarou et al (2003), Watson-Lamprey and Abrahamson (2006), and Foulser-Piggot and Stafford (2011). All models found that I_a was dependent on magnitude, rupture distance, site stiffness, and rupture mechanism. Appendix 2E provides more details of these models and their application.

2.3.5 Significant Duration ($D_{5\text{-}95}$)

Duration has a strong influence on the damage imposed by an earthquake, especially for systems that undergo cyclic degradation (Kempton and Stewart, 2006). The most common duration parameters are bracketed duration and significant duration (Stewart et al, 2001). Bracketed duration is defined as the time between when the acceleration time series first exceeds a threshold acceleration, usually 0.05g, and the last time it exceeds the threshold acceleration. The significant duration is the time between when a specified percentage of the Arias intensity occurs, usually 5-75% ($D_{5\text{-}75}$) or 5-95% ($D_{5\text{-}95}$). This study selected significant duration ($D_{5\text{-}95}$) as a target measure and uses an average of two GMPE models to predict the target mean and standard deviation. The two models selected are the Abrahamson and Silva (1996) and the Kempton and Stewart (2006) models. Appendix 2E presents a summary of the GMPEs for these models.

2.3.6 Pulse Period (T_v) for Pulse-like Ground Motions

Ground motions recorded at distances less than 20 km may exhibit near fault effects, such as forward directivity, backward directivity, or fling (NIST, 2012). These differences are best seen in the velocity time series, where forward directivity can be characterized by large velocity pulses. The period of the pulse is termed the predominant pulse period (T_v). The pulse period is related to the duration of slip at a point on the fault (rise time), and the fault dimensions, both of which are dependent on the magnitude (Somerville, 2003). The pulse period has been found to be a function of site conditions, with soil sites exhibiting a larger T_v than rock sites. This study uses two models to predict T_v: Somerville (2003) and Bray et al (2009). Appendix E presents a summary of these models. Other studies that have developed predictive equations for T_v are Alavi and Krawinkler (2000) and Shahi and Baker (2011).

2.4 Determination of Target Ground Motion Parameters

The target parameters for scenarios ACR1, ACR2, and ACR3 were the 5% damped pseudo-acceleration spectra (S_a v. T), peak ground acceleration (PGA), peak ground velocity (PGV), mean period (T_m), arias intensity (I_a), and the significant duration ($D_{5\text{-}95}$). The selection of scenario ACR1 ground motions also considered the pulse period (T_v). There are no reliable prediction equations for other parameters besides pseudo acceleration, PGA, and PGV for subduction zone and stable continental region ground motions. As a result, the selection of scenario SUB ground motions relied on the target pseudo acceleration spectrum and PGA only, while scenario SCR ground motions were chosen based on the target pseudo acceleration spectrum, PGA, and PGV. The next sections describe the selection of target ground motion parameters for all scenarios.

2.4.1 Target Ground Motion Parameters for Scenario ACR1

The 5% damped pseudo-acceleration target response spectrum for scenario ACR1 was estimated using the 2008 NGA GMPEs with equal weight given to each of the five models. The moment magnitude for scenario ACR1 was 6.7 ($M_w = 6.7$) and the faulting mechanism was a reverse type fault ($F_{RV} = 1$, $F_{NM} = 0$) with surface rupture ($Z_{TOR} = 0$) and a 45 degree fault plane ($\delta = 45$). The imaginary site was on the hanging wall ($F_{HW} = 1$), which typically has greater seismic hazard than the foot wall. Given that $R_{RUP} = 5$ and the site was located on the hanging wall of a 45 degree fault, from trigonometry $R_{JB} = 0$ and $R_x = 7$, where R_{RUP} is the closest distance to the rupture plane, R_{JB} is the closest distance to the surface projection of the rupture plane, and R_x is the horizontal distance from the top of the rupture measured perpendicular to the fault strike. Figure 2.2 gives a graphical definition of parameters R_{RUP}, R_{JB}, R_x, Z_{TOR}, and δ. The input U is an unspecified mechanism factor used in the Boore and Atkinson (2008) model, this was set to 0, for 'otherwise.' The Vs_{30} was selected as 760 m/s since the target spectra will be used to constrain time histories to be used as rock ground motions for nonlinear seismic site response analyses. For the Abrahamson and Silva (2008) and Chiou and Youngs (2008) models, the input $F_{MEASURED}$ is required and it is set as 1 when Vs_{30} is measured and 0 when Vs_{30} is inferred. This work set $F_{MEASURED}$ equal to zero since most sites that have ground motion recordings only have inferred Vs_{30} values. The parameters $Z_{1.0}$ and $Z_{2.5}$ are the depths when the shear wave velocity equals 1 km/s and 2.5 km/s respectively. For these inputs the default setting was used since for most sites these values are unknown. The fault width (W) was chosen as 17 km. Finally, the aftershock factor F_{AS} was set to 0, for 'mainshock', and the hanging wall taper (HW TAPER) had a value of 1 to use the revised taper suggested by Professor Norm Abrahamson. Table 2.2 presents a summary of the input parameters for the 2008 NGA GMPEs.

Unfortunately, the NGA West 2 GMPEs were released too late to be used as the target response spectra for scenarios ACR1, ACR2, and ACR3. However, this study compared the response spectra predicted by the NGA West 1 GMPEs with those of the NGA West 2 GMPEs and the differences for the selected scenarios were minor.

To account for near fault effects, the resulting response spectrum was modified according to Somerville et al. (1997). Assuming that the hypocenter is at the bottom of the rupture plane, and given that the fault width is 17km (W = 17), the dip angle is 45 degrees ($\delta = 45$), the depth to top the top of rupture is zero ($Z_{TOR} = 0$) and the site to rupture distance is 5km ($R_{RUP} = 5$), then *d* is

12 km and φ is 22.5 degrees, where *d* is the length along the rupture plane from the hypocenter to the closest point on the rupture to the site, and φ is the angle up from the dipping rupture to the site measured from the hypocenter (cf., Figure 2.3).

This study used the fault normal (FN) as the maximum component. Table 2.3 lists the values of the target response spectra for scenario ACR1. Figure 2.4 shows the target response spectra (5% damping) and one standard deviation band for scenario A1 for fault normal (FN) and fault parallel conditions. As can be seen from the figure, the Somerville et al. (1997) modification for near fault effects increases the base line (FP spectra) broadly for periods larger than approximately 1.0 seconds.

For scenario ACR1, the additional ground motion parameters considered were PGA, PGV, T_m, I_a, $D_{5\text{-}95}$ and the pulse period, T_v. The mean and standard deviation for the target PGA were obtained using the five 2008 NGA GMPE models with equal weights. To include near fault effects, the PGV was estimated by the method proposed by Bray et al (2009). The method was presented earlier and describes the PGV as a log normal variable that increases with the moment magnitude of the earthquake (M_w) and decreases with distance (R) from the fault for distances less than 20 km. This study used the regression established for rock sites as the ground motions will be used as rock input motions.

The mean period, T_m, was estimated with the Rathje et al. (2004) method and it included forward directivity characteristics. The proposed equation gives mean periods that increase with the magnitude of the earthquake and the distance from the fault. This study used the regression for rock sites (SC=SD=0 for V_{S30}> 760 m/s).

The target Arias intensity, I_a, was estimated using a weighted average of three models; Travasarou et al., (2003), Watson-Lamprey and Abrahamson (2006) and Foulser-Piggot and Stafford (2011), with weights of 0.4, 0.4 and 0.2, respectively. The input parameters were M_w = 6.7 and R_{rup} = 5 km. The soil parameters for Travasarou et al. (2003) were SC = SD = 0 to model Vs_{30} > 760 m/s, and F_R = 1 and F_N = 0 for a reverse fault mechanism. The other two methods both have a direct Vs_{30} input, which were set to 760 m/s for rock. Watson-Lamprey and Abrahamson (2006) requires as inputs the PGA and the pseudo spectral acceleration at T = 1 second (Sa(T=1)). These values were selected from the mean target spectrum derived earlier. The model by Foulser-Piggot and Stafford (2011) also has a mechanism term, which is F_{RV} = 1 for reverse faulting. Table 2.4 lists the input parameters used to calculate the target Arias intensity for scenario ACR1.

Significant duration, $D_{5\text{-}95}$, was estimated using the equations developed by Abrahamson and Silva (1996) and Kempton and Stewart (2006) with equal weights used for both models. For scenario ACR1, the mean duration was determined as the mean minus one standard deviation to account approximately for the concentration of energy release in the pulse motion. Table 2.5 lists the input parameters used by these models to predict the significant duration.

The pulse Period (Tv) is included for scenario ACR1 (i.e., pulse like motions) and was calculated as the weighted average of the Somerville (2003) and Bray et al. (2009) models with equal

weights for both models. The input parameters were M_w= 6.7 and a "rock site" classification. Table 2.6 lists the target ground motion parameters for scenario ACR1.

2.4.2 Target Ground Motion Parameters for Scenario ACR2

Similarly to scenario A1, the 5% damped pseudo-acceleration target response spectra for scenario ACR2 was estimated using the 2008 NGA GMPEs with equal weights for all five models. Table 2.2 lists the input parameters for the 2008 NGA GMPEs for scenario ACR2. The geometric mean component (i.e., GMRotI50_NGA) obtained from the 2008 NGA GMPEs was modified by period dependent demand factors to obtain the maximum response orientation (RotD100) as recommended by NEHRP (2009). Table 2.7 and Figure 2.5 give the target response spectrum at 5% damping for scenario ACR2.

For scenario ACR2, the additional ground motion parameters considered were PGA, PGV, T_m, I_a, and $D_{5\text{-}95}$. The mean and standard deviation for the target PGA and PGV were obtained by using the five 2008 NGA GMPE models with equal weights. The mean period, T_m, was estimated with the Rathje et al. (2004) model for no pulse effect (i.e., FD=0). The study used the regression for rock sites (SC=SD=0 for V_{S30}> 760 m/s).

The target Arias intensity, I_a, was estimated using a weighted average of the Travasarou et al., (2003), Watson-Lamprey and Abrahamson (2006) and Foulser-Piggot and Stafford (2011) models with weights of 0.4, 0.4 and 0.2, respectively. The input parameters were M_w = 6.7 and R_{rup} = 5 km. The soil parameters for Travasarou et al. (2003) were SC = SD = 0 to model Vs_{30} > 760 m/s, and F_R = 1 and F_N = 0 for a reverse fault mechanism. The other two methods both have a direct Vs_{30} input, which were set to 760 m/s for rock. Watson-Lamprey and Abrahamson (2006) requires as inputs the PGA and the pseudo spectral acceleration at T = 1 second (Sa(T=1)). These values were selected from the mean target spectra derived earlier. The model by Foulser-Piggot and Stafford (2011) also has a mechanism term, which is F_{RV} = 1 for reverse faulting. The arias intensity for scenario ACR2 and ACR1 are the same since they represent the same earthquake and amount of energy released, only the energy is delivered in a more compact manner for scenario ACR1. Table 2.4 lists the input parameters for the three models used to predict the Arias intensity.

Significant duration, $D_{5\text{-}95}$, was estimated using the equations developed by Abrahamson and Silva (1996) and Kempton and Stewart (2006) with equal weights used for both models. Table 2.5 lists the input parameters used by these models to predict the significant duration. Table 2.6 lists the target ground motion parameters for scenario ACR2.

2.4.3 Target Ground Motion Parameters for Scenario ACR3

Similarly to scenarios ACR1 and ACR2, the 5% damped pseudo-acceleration target response spectra for scenario ACR3 was estimated using the 2008 NGA GMPEs with equal weights for all five models. The input parameters were M_w = 7.8, strike slip fault mechanism (F_{RV} = 0, F_{NM} = 0) with surface rupture (Z_{TOR} = 0) and a vertical fault plane (δ = 90). There is no hanging wall in a purely strike slip motion so F_{HW} = 0 and HW TAPER = 0 (i.e., it has no effect). For a vertical strike slip event $R_{RUP} = R_{JB} = R_X$ (cf., Figure 2.2). All other input parameters were the same as for scenario A2 and they are listed in Table 2.2. The geometric mean component (i.e.,

GMRotI50_NGA) obtained from the 2008 NGA GMPEs was modified by period dependent demand factors to obtain the maximum response orientation (RotD100) as recommended by NEHRP (2009). Table 2.8 and Figure 2.6 give the pseudo-acceleration target response spectra for 5% damping and one standard deviation band for scenario ACR3.

For scenario ACR3, the additional ground motion parameters considered were PGA, PGV, T_m, I_a, and $D_{5\text{-}95}$. Similarly to scenario ACR2, the mean and standard deviation for the target PGA and PGV were obtained by using the five 2008 NGA GMPE models with equal weights. The mean period, T_m, was estimated with the Rathje et al. (2004) model for no pulse effect (i.e., FD=0). The study used the regression for rock sites (SC=SD=0 for V_{S30}> 760 m/s).

Similarly to scenarios ACR1 and ACR2, the target Arias intensity, I_a, was estimated using a weighted average of three models; Travasarou et al., (2003), Watson-Lamprey and Abrahamson (2006) and Foulser-Piggot and Stafford (2011), with weights of 0.4, 0.4 and 0.2, respectively. The input parameters were M_w = 7.8 and R_{rup} = 30 km. The soil parameters for Travasarou et al. (2003) were SC = SD = 0 to model Vs_{30} > 760 m/s, and F_R = 0 and F_N = 0 for a strike slip fault mechanism. The other two methods both have a direct Vs_{30} input, which were set to 760 m/s for rock. Watson-Lamprey and Abrahamson (2006) requires as inputs the PGA and the pseudo spectral acceleration at T = 1 second (Sa(T=1)). These values were selected from the mean target spectrum derived earlier. The model by Foulser-Piggot and Stafford (2011) also has a mechanism term, which is F_{RV} = 0 for strike-slip faulting.

Significant duration, $D_{5\text{-}95}$, was estimated using the equations developed by Abrahamson and Silva (1996) and Kempton and Stewart (2006) with equal weights used for both models. Table 2.5 lists the input parameters used by these models to predict the significant duration. Table 2.6 lists the target ground motion parameters for scenario ACR3.

2.4.4 Target Ground Motion Parameters for Scenario SUB

The 5% damped pseudo-acceleration target spectrum and its standard deviation were estimated using a weighted average of the median response spectra and standard deviation predicted by Youngs et al. (1997), Atkinson and Boore (2003, 2008), Zhao et al. (2006) and Atkinson and Macias (2009), with weights of 0.1, 0.3, 0.3 and 0.3, respectively. Scenario SUB represents an "interface" event of magnitude 9 (M_w=9) at a distance of 100 km with a focal depth of 30 km. Table 2.9 lists the input parameters for the four GMPEs. For the Atkinson and Boore (2003) and Zhao et al. (2006) models, the event magnitude was capped at M_w = 8.5. The source mechanism for all four models was interface event. The soil type parameter was 'rock' in the Youngs et al. (1997) model, and $S_C = S_D = S_E = 0$ for a NEHRP type B site with Vs_{30} equal to or greater than 760 m/s in the Atkinson and Boore (2003). The Atkinson and Macias (2009) model is only for B/C boundary (Vs_{30} = 760 m/s) sites. The soil type parameter in the Zhao et al. (2006) model was set for soils with Vs_{30} between 600 and 1100 m/s, to be consistent with the other models.

The geometric mean component obtained from the GMPEs was modified by period dependent demand factors to obtain the maximum response orientation (RotD100) as recommended by NEHRP (2009). Table 2.10 and Figure 2.7 give the pseudo-acceleration target response spectra at 5% damping and one standard deviation band for scenario SUB. The mean and standard deviation for the target PGA for this scenario were obtained by using the four GMPEs with the

same weights. No other ground motion parameters were considered in the selection of ground motions for scenario SUB. Table 2.6 lists the target ground motion parameters for scenario SUB.

2.4.5 Target Ground Motion Parameters for Scenario SCR

The 5% damped pseudo-acceleration target spectrum and its standard deviation were estimated using a weighted average of four attenuation models developed for stable continental regions: Toro el al. (1997, 2002), Silva et al. (2002), Atkinson and Boore (2006, 2011) and Pezeshk et al. (2011). This study used equal weights for all four models. The input parameters were M_w = 6.0 and R = 17for all four GMPEs. The only other parameter in the Toro et al. (1997) GMPE is the region of the earthquake. This study used the coefficients for the midcontinent region. The soil parameter for the Atkinson and Boore (2006) model was chosen as S = 0 for hard rock sites (Vs_{30} = 2,000 m/s) to be consistent with the other scenario SCR models. Table 2.11 lists the input parameters for the four attenuation relations used for scenario SCR. The geometric mean component obtained from the GMPEs was modified by the period dependent demand factors to obtain the maximum response orientation (RotD100) as recommended by Huang et al. (2010) for stable continental regions. Table 2.12 and Figure 2.8 give the pseudo-acceleration target response spectrum at 5% damping and one standard deviation band.

The target PGA and PGV as well as their corresponding standard deviations were estimated using a weighted average of the same four GMPEs used to calculate the target response spetrum. No other ground motion parameters were considered for scenario SCR. Table 2.6 lists the target ground motion parameters for scenario SCR.

2.5 Summary

This chapter described the selection of target ground motion measures to constrain the selection of acceleration time series to be used as input motions in nonlinear site response analyses. To capture the variability of ground motions, five base-case scenarios were selected according to tectonic environments and representative cases encountered in common US practice. The first three correspond to shallow crustal earthquakes in active crustal regions, representing reverse earthquakes with and without pulse-like response (ACR1, ACR2), and strike-slip earthquakes (ACR3), while the last two correspond to earthquakes from subduction zones (SUB) and stable continental regions (SCR). This study gives full details of the models used to select the target response spectra and additional target ground motions parameters, including: peak ground acceleration (PGA), peak ground velocity (PGV), mean period (T_m), arias intensity (I_a), significant duration ($D_{5\text{-}95}$) and pulse period (T_v) for pulse-like ground motions. This study uses GMPEs to predict the various ground motion intensity measures. All target ground motion measures are assumed to be log-normally distributed and can be fully described by their mean and standard deviation. The results of this study are summarized in the mean (μ) and the one standard deviation band (μ-σ, μ+σ) for each of the ground motion parameters. For completeness, the study briefly summarizes the details of the various GMPE models in the appendices.

2.6 References

Abrahamson, N.A., and Silva, W.J. (1996). "Empirical ground motion models." Report to Brookhaven National Laboratory; New York, NY, 144.

Abrahamson, N.A., and Silva, W.J. (2008). "Summary of the Abrahamson and Silva NGA Ground-Motion Relations." Earthquake Spectra 24(1), 67-97.

Abrahamson, N.A., and Somerville, P.G. (1996). "Effects of the Hanging Wall and Footwall on Ground Motions Recorded During the Northridge Earthquake." Bull. Seismol. Soc. Amer., 86(1B), S93-S99.

Abrahamson, N.A., Atkinson, G.M., Boore, D., Bozorgnia, Y., Campbell, K., Chiou, B., Idriss, I.M., Silva, W. and Youngs, R. (2008). "Comparisons of the NGA Ground-Motion Relations." Earthquake Spectra 24(1), 45-66.

Alavi, B., and Krawinkler, H. (2000) "Consideration of near-fault ground motion effects in seismic design". Proc., 12th World Conf. on Earthquake Engng, Auckland, New Zealand, paper 2665.

Arias, A. (1970). "A Measure of Earthquake Intensity," in Hansen, R. J., ed., Seismic Design for Nuclear Power Plants: MIT Press, Cambridge, Mass., 438-483.

Atkinson, G.M. and Boore, D.M. (2003). "Empirical ground-motion relations for subduction-zone earthquakes and their application to Cascadia and other regions." Bull. Seismol. Soc. Amer., (93)4, 1703-1729.

Atkinson, G.M. and Boore, D.M. (2006). "Earthquake ground-motion prediction equations for eastern North America." Bull. Seismol. Soc. Amer., (96)6, 2181-2205.

Atkinson, G.M. and Boore, D.M. (2011). "Modifications to existing ground-motion prediction equations in light of new data." Bull. Seismol. Soc. Amer., 101 (3), 1121–1135.

Atkinson, G.M., and Macias, M. (2009). "Predicted ground motions for great interface earthquakes in the Cascadia subduction zone." Bull. Seismol. Soc. Amer., 99(3) 1552-1578.

Boore, D.M., and Atkinson, G.M. (2008). "Ground-motion prediction equations for the average horizontal Component of PGA, PGV, and 5%-Damped PSA at Spectral Periods between 0.01s and 10.0s." Earthquake Spectra 24(1), 99-138.

Boore, D.M., Watson-Lamprey, J., and Abrahamson, N.A., (2006). "Orientation-independent measures of ground motion." Bull. Seismol. Soc. Amer., (96) 4A, 1502-1511.

Bradley, B. (2010) "A generalized conditional intensity measure approach and holistic ground motion selection," Earthquake Engng & Struct. Dyn., 39 (12), 1321-1342.

Bray, J., Rodriguez-Marek, A., Gillie, J. (2009). "Design ground motions near active faults," Bull. New Zealand Society for Earthquake Engineering, 42 (1), 1-8.

Campbell, K., and Bozorgnia, Y. (2008). "NGA ground motion model for the geometric mean horizontal component of PGA, PGV, PGD, and 5% damped linear elastic response spectra for periods ranging from 0.01 to 10s." Earthquake Spectra 24 (1), 139-171.

Chiou, B., and Youngs, R. (2008). "An NGA model for the average horizontal component of peak ground motion and response spectra." Earthquake Spectra 24(1), 173-215.

Chopra, A.K. (2011). Dynamics of structures: theory and applications to earthquake engineering, 4th edition, Pearson-Prentice Hall, New Jersey.

EPRI (1993)

Foulser-Piggot, R., and Stafford, P.J. (2011). "A predictive model for Arias intensity at multiple sites and consideration of spatial correlations." Earthquake Engng Struct. Dyn. (41)3, 431-451.

Huang, Y.N., Whittaker, A.S. and Luco, N. (2010). “Establishing maximum spectral demand for performance-based earthquake engineering: collaborative research with the University at Buffalo and the USGS.” USGS Technical Report: USGS Award Number 08HQGR0017, Reston, VA.

IBC 2012. International *Building Code*, by International Code Council, Delmar Publishers.

Idriss, I.M. (2008). “An NGA empirical model for estimating the horizontal spectral values generated by shallow crustal earthquakes.” Earthquake Spectra 24(1), 217-242.

Kempton, J. J., and Stewart, J. P. (2006). “Prediction equations for significant duration of earthquake ground motions considering site and near-source effects.” Earthquake Spectra (22) 4, 985-1013.

NEHRP (2009). “NERHP recommended seismic provisions for new buildings and other structures.” FEMA P-750 report prepared by the Building Seismic Safety Council of The National Institute of Building Sciences for the Federal Emergency Management Agency, Washington, D.C.

NIST (2012). “Selecting and scaling earthquake ground motions for performing response history analyses.” NIST GCR 11-917-15, prepared by the NERHP Consultants Joint Venture for the National Institute of Standards and Technology, Gaithersburg, Maryland.

Pezeshk, S., Zandieh, A., and Tavakoli, B. (2011). “Hybrid empirical ground-motion prediction equations for eastern north America using NGA models and updated seismological parameters.” Bull. Seismol. Soc. Amer., 101 (4), 1859–1870.

Rathje, E.M., Faraj, F., Russell, S. and Bray, J.D. (2004). “Empirical relationships for frequency content parameters of earthquake ground motions.” Earthquake Spectra 20(1), 119-144.

Shahi, S.K., and Baker, J.W. (2011) "An empirically calibrated framework for including the effects of near fault directivity in PSHA", Bull. Seismol. Soc. Amer., 101 (2), 742 -755.

Silva, W., Gregor, N. and Darragh, R. (2002). “Development of regional hard rock attenuation relations for central and eastern North America.” Pacific Engineering Analysis Internal Report, 27.

Somerville, P. (2003). “Magnitude scaling of the near fault rupture directivity pulse.” Physics of the Earth and Planetary Interiors 137, 201–212.

Somerville, P.G., Smith, N.F., Graves, R.W., Abrahamson, N.A. (1997). “Modification of empirical strong ground motion attenuation relations to include the amplitude and duration effects of rupture directivity.” Seismol. Res. Lett. 68(1), 199-222.

Toro, G. R., Abrahamson, N.A. and Schneider, J.F., (1997). “Model of strong ground motions from earthquakes in central and eastern North America: best estimates and uncertainties.” Seismol. Res. Lett. (68)1, 41–57.

Toro, G.R. (2002). “Modification of the Toro et al (1997) attenuation equations for large magnitudes and short distances.” Risk Engineering Inc.

Travasarou, T., Bray, J.D. and Abrahamson, N.A. (2003). “Empirical attenuation relationship for Arias intensity,” Earthquake Engng Struct. Dyn. (32) 7, 1133–1155.

Watson-Lamprey, J. and Abrahamson, N.A. (2006). “Selection of ground motion time series and

Youngs, R., Chiou, S., Silva, W. and Humphrey, J. (1997), “Strong ground motion attenuation relationships for subduction zone earthquakes.” Seismol. Res. Lett. (68)1, 58–73.

Zhao, J.X., Zhang, J., Asano, A., Ohno, Y., Oouchi, T., Takahashi, T., Ogawa, H., Irikura, K. Thio, H.K., Somerville, P.G., Fukushima, Y. and Fukushima, Y. (2006). “Attenuation relations of strong ground motion in Japan using site classification based on predominant period.” Bull. Seismol. Soc. Amer., (96)3, 898–913.

Table 2.1: Selected scenarios

ID	Mechanism	M_w	R_{rup} (km)
ACR1	Reverse (Pulse Like)	6.7	5
ACR2	Reverse (No Pulse)	6.7	5
ACR3	Strike Slip	7.8	30
SUB	Interface	9	100
SCR	Stable Continental Region	6	17

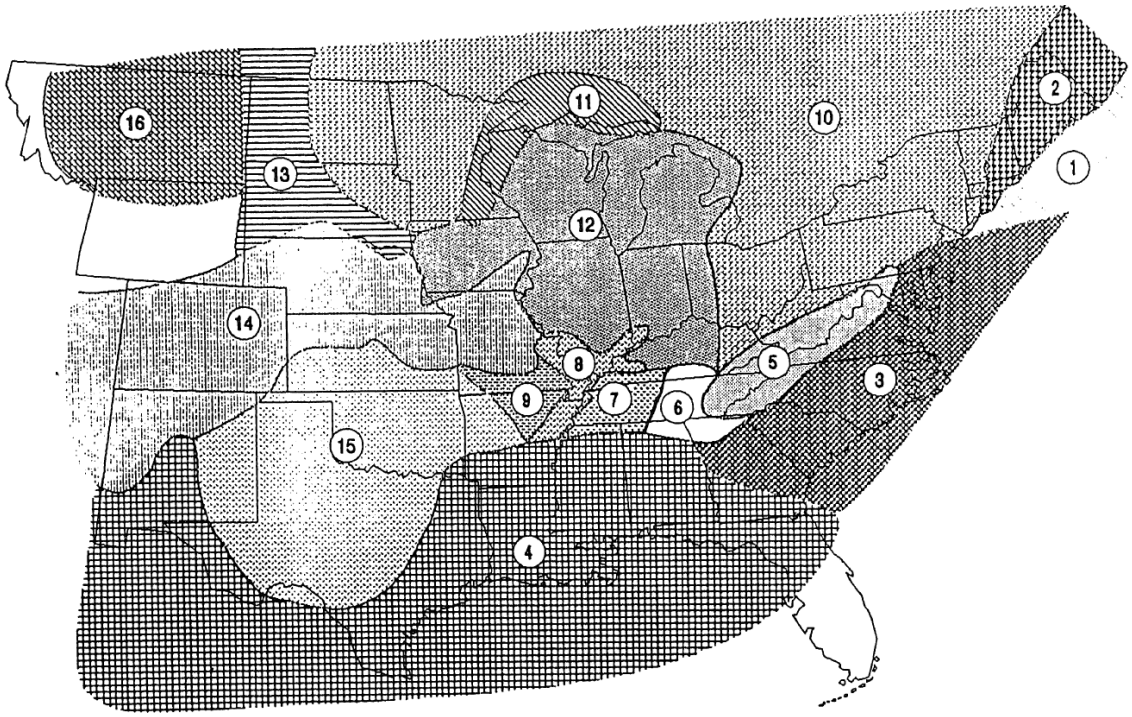

Figure 2.1: Regionalization of crustal structure for Central and Eastern North America (Toro et al., 1997)

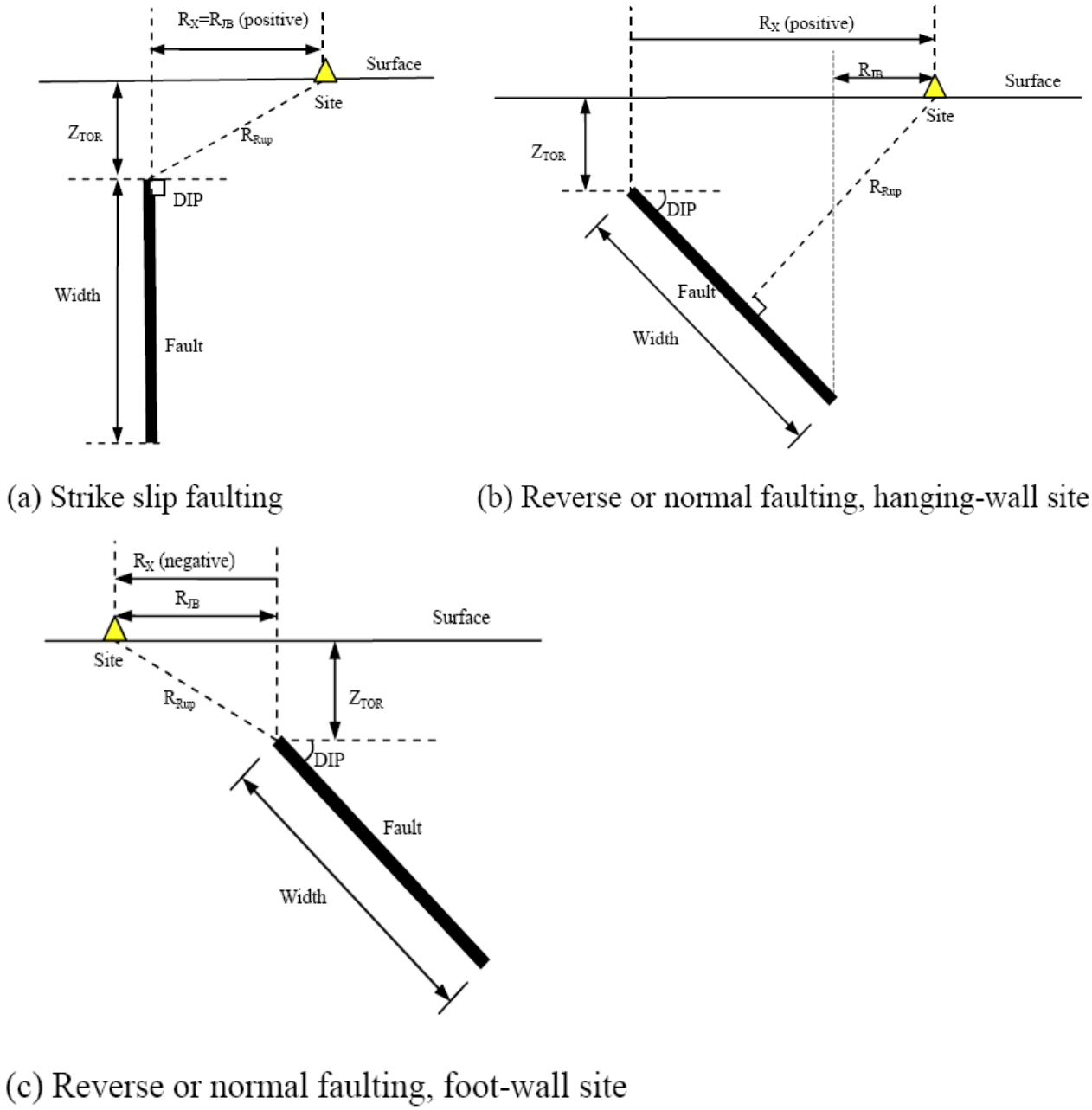

Figure 2.2: Definition of parameters R_x, R_{JB}, R_{RUP}, dip angle δ, Z_{tor}, and width for the 2008 NGA GMPEs (Courtesy of Dr. Youngs)

Table 2.2: Input parameters to the 2008 NGA GMPEs for shallow crustal earthquakes

Input Parameter	Scenarios	
	ACR1, ACR2	ACR3
M_w	6.7	7.8
R_{RUP} (km)	5.0	30.0
R_{JB} (km)	0.0	30.0
R_X (km)	7.0	30.0
U	0	0
F_{RV}	1	0
F_{NM}	0	0
F_{HW}	1	0
Z_{TOR} (km)	0	0
δ	45	90
V_{S30} (m/sec)	760	760
$F_{Measured}$	0	0
$Z_{1.0}$ (m)	DEFAULT	DEFAULT
$Z_{2.5}$ (km)	DEFAULT	DEFAULT
W (km)	17	17
F_{AS}	0	0
HW Taper	1	1

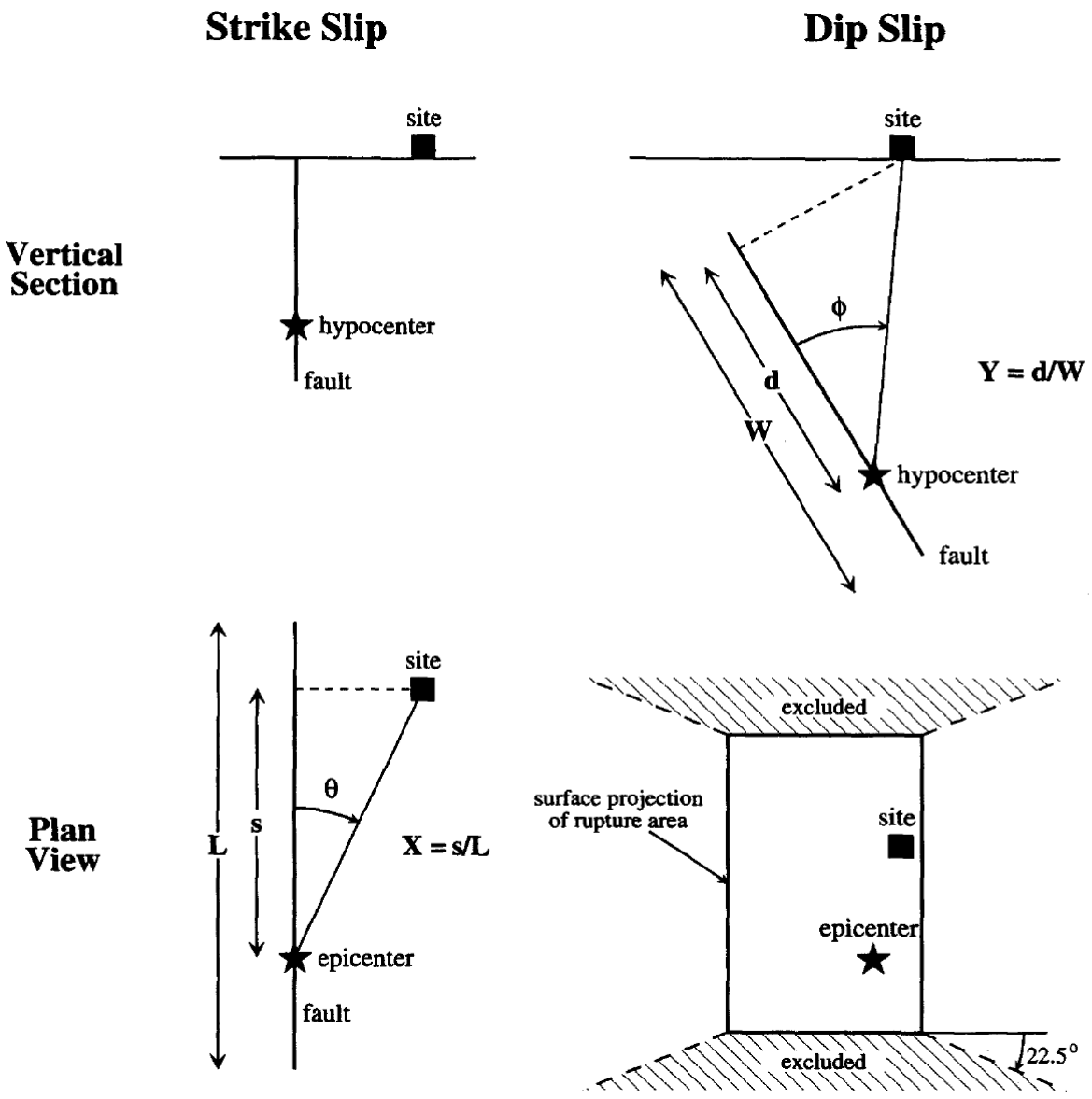

Figure 2.3: Description of geometry parameters for Somerville et al (1997)

Table 2.3: Pseudo-acceleration target spectra at 5% damping for scenario ACR1. Conditions for the no-pulse motion (i.e., fault parallel, FP) are also included

	Pulse Type Motion Fault Normal (FN)			No Pulse Motion Fault Parallel (FP)		
T (s)	μ-σ (g)	μ (g)	μ+σ (g)	μ-σ (g)	μ (g)	μ+σ (g)
0.01	0.329	0.577	1.010	0.329	0.577	1.010
0.02	0.336	0.588	1.031	0.336	0.588	1.031
0.03	0.360	0.636	1.124	0.360	0.636	1.124
0.05	0.425	0.759	1.355	0.425	0.759	1.355
0.075	0.586	1.055	1.900	0.586	1.055	1.900
0.10	0.614	1.121	2.046	0.614	1.121	2.046
0.15	0.717	1.323	2.440	0.717	1.323	2.440
0.20	0.743	1.384	2.576	0.743	1.384	2.576
0.25	0.686	1.279	2.386	0.686	1.279	2.386
0.30	0.616	1.157	2.171	0.616	1.157	2.171
0.40	0.518	0.975	1.835	0.518	0.975	1.835
0.50	0.423	0.802	1.521	0.423	0.802	1.521
0.75	0.286	0.542	1.028	0.273	0.517	0.981
1.0	0.205	0.399	0.778	0.189	0.368	0.716
1.5	0.119	0.235	0.466	0.103	0.205	0.405
2.0	0.076	0.151	0.303	0.062	0.124	0.249
3.0	0.039	0.079	0.159	0.028	0.056	0.114
4.0	0.025	0.050	0.102	0.016	0.033	0.066
5.0	0.017	0.035	0.073	0.011	0.022	0.047
7.5	0.008	0.017	0.037	0.005	0.011	0.023
10	0.004	0.009	0.020	0.003	0.006	0.013

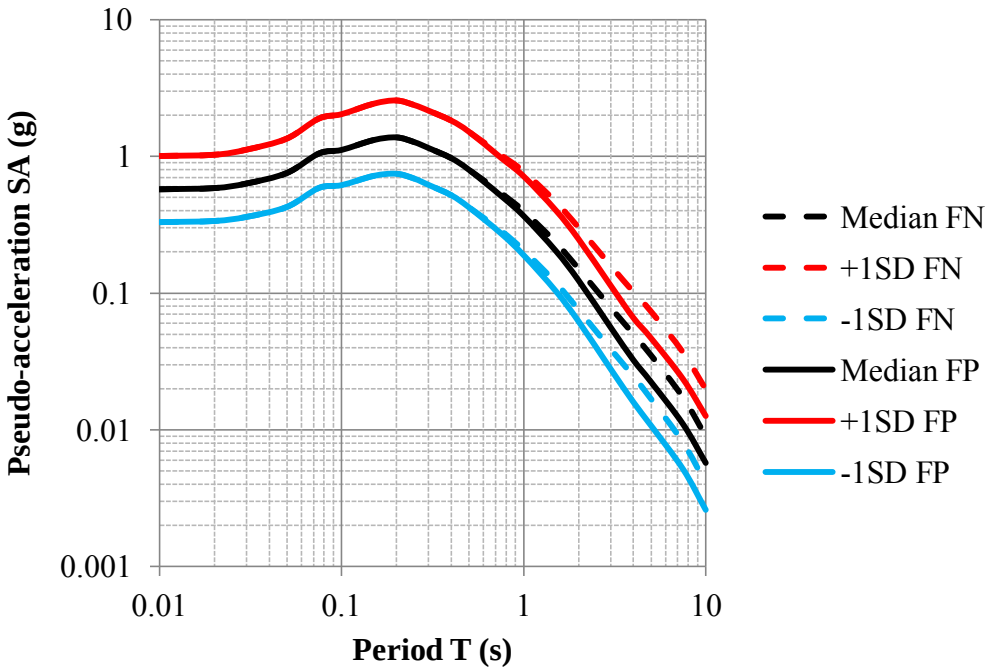

Figure 2.4: Pseudo-acceleration target spectra at 5% damping for scenario ACR1, with the mean and + and – 1 standard deviation curves for both the pulse type motion (fault normal, FN) and no pulse motion (fault parallel, FP) orientations

Table 2.4: Input parameters to determine the target I_a for scenarios ACR1, ACR2, and ACR3

Scenario	ACR1, ACR2			ACR3		
Model-Reference	T. et al 2003	WL & A 2006	FP & S 2011	T. et al 2003	WL & A 2006	FP & S 2011
M_w	6.7	6.7	6.7	7.8	7.8	7.8
R_{rup}	5	5	5	30	30	30
Site	SC = SD = 0	760 (m/s)	760 (m/s)	SC = SD = 0	760 (m/s)	760 (m/s)
Mechanism	$F_R = 1$, $F_N = 0$	na	$F_{RV} = 1$	$F_R = F_N = 0$	na	$F_{RV} = 0$
PGA (g)	na	0.56	na	na	0.15	na
Sa(T=1) (g)	na	0.37	na	na	0.14	na
Weight	0.4	0.4	0.2	0.4	0.4	0.2

Table 2.5: Input parameters to determine the target significant duration, $D_{5\text{-}95}$ for scenarios ACR1, ACR2, and ACR3

Scenario	ACR1, ACR2		ACR3	
Reference	A & S 1996	K & S 2006	A & S 1996	K & S 2006
M_w	6.7	6.7	7.8	7.8
R_{rup}	5	5	30	30
Site	Rock	760 (m/s)	Rock	760 (m/s)
$z_{1.5}$	na	2000	na	2000
Weight	0.5	0.5	0.5	0.5

Table 2.6: Mean and plus and minus one standard deviation target parameters for all five scenarios

Scenario	Percentile	PGA (g)	PGV (cm/s)	$D_{5\text{-}95}$ (s)	T_m (s)	I_a (m/s)	T_v (s)
ACR1	μ-σ	0.32	37.3	4.2	0.36	0.88	0.84
	μ	0.56	55.7	6.6	0.57	1.70	1.45
	μ+σ	0.98	83.0	10.6	0.90	3.75	2.52
ACR2	μ-σ	0.32	21.8	6.6	0.27	0.88	
	μ	0.56	37.9	10.6	0.43	1.70	
	μ+σ	0.98	65.9	16.9	0.67	3.75	
ACR3	μ-σ	0.09	9.2	20.3	0.3	0.23	
	μ	0.15	15.8	32.3	0.5	0.43	
	μ+σ	0.26	27.2	51.4	0.8	0.90	
SUB	μ-σ	0.093					
	μ	0.152					
	μ+σ	0.251					
SCR	μ-σ	0.142	2.890				
	μ	0.279	5.728				
	μ+σ	0.553	11.506				

Table 2.7: Pseudo-acceleration target spectra at 5% damping for scenario ACR2

	Geometric Mean Component GMRotI50_NGA			Maximum Rotated Component RotD100		
T (s)	μ-σ (g)	μ (g)	μ+σ (g)	μ-σ (g)	μ (g)	μ+σ (g)
0.01	0.32	0.56	0.99	0.35	0.62	1.08
0.02	0.33	0.57	1.01	0.36	0.63	1.11
0.03	0.35	0.62	1.10	0.39	0.68	1.21
0.05	0.41	0.74	1.32	0.46	0.81	1.45
0.075	0.57	1.02	1.84	0.62	1.12	2.03
0.10	0.60	1.09	1.99	0.66	1.20	2.19
0.15	0.70	1.29	2.37	0.77	1.41	2.61
0.2	0.72	1.34	2.50	0.79	1.48	2.75
0.25	0.66	1.24	2.31	0.73	1.36	2.54
0.30	0.60	1.12	2.10	0.66	1.23	2.31
0.40	0.50	0.94	1.78	0.58	1.08	2.04
0.50	0.41	0.78	1.47	0.49	0.93	1.77
0.75	0.28	0.53	1.00	0.35	0.66	1.26
1.0	0.19	0.37	0.72	0.25	0.48	0.93
1.5	0.11	0.21	0.41	0.14	0.27	0.54
2.0	0.07	0.13	0.26	0.08	0.17	0.34
3.0	0.03	0.06	0.13	0.04	0.09	0.17
4.0	0.02	0.04	0.08	0.03	0.05	0.11
5.0	0.01	0.03	0.06	0.02	0.04	0.08
7.5	0.01	0.01	0.03	0.01	0.02	0.04
10	0.00	0.01	0.01	0.00	0.01	0.02

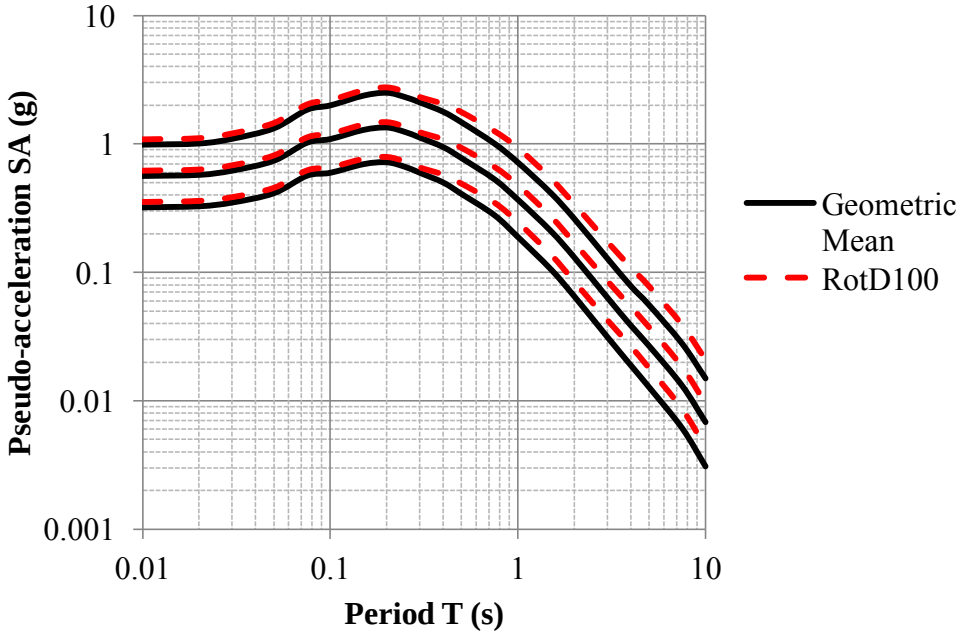

Figure 2.5: Pseudo-acceleration target spectra at 5% damping for scenario ACR2, showing the mean and + and – 1 standard deviation curves for the geometric mean (GmRotI50_NGA) and maximum (RotD100) orientations

Table 2.8: Pseudo-acceleration target spectra at 5% damping for scenario ACR3

	Geometric Mean Component GMRotI50_NGA			Maximum Rotated Component RotD100		
T (s)	μ-σ (g)	μ (g)	μ+σ (g)	μ-σ (g)	μ (g)	μ+σ (g)
0.01	0.090	0.154	0.263	0.099	0.169	0.290
0.02	0.091	0.156	0.267	0.100	0.172	0.294
0.03	0.095	0.165	0.284	0.105	0.181	0.313
0.05	0.108	0.188	0.329	0.118	0.207	0.362
0.075	0.128	0.229	0.413	0.140	0.252	0.454
0.10	0.148	0.264	0.473	0.162	0.291	0.521
0.15	0.175	0.316	0.570	0.193	0.348	0.626
0.20	0.181	0.329	0.596	0.199	0.362	0.655
0.25	0.177	0.322	0.584	0.195	0.354	0.643
0.30	0.165	0.302	0.553	0.182	0.332	0.608
0.40	0.145	0.267	0.490	0.167	0.307	0.564
0.50	0.126	0.234	0.434	0.152	0.281	0.521
0.75	0.087	0.164	0.309	0.109	0.205	0.386
1.0	0.074	0.142	0.270	0.097	0.184	0.351
1.5	0.050	0.098	0.190	0.066	0.127	0.247
2.0	0.036	0.071	0.140	0.047	0.093	0.182
3.0	0.023	0.046	0.091	0.031	0.062	0.123
4.0	0.016	0.032	0.063	0.022	0.045	0.089
5.0	0.012	0.024	0.049	0.016	0.034	0.069
7.5	0.007	0.015	0.031	0.010	0.021	0.044
10	0.004	0.009	0.019	0.006	0.012	0.026

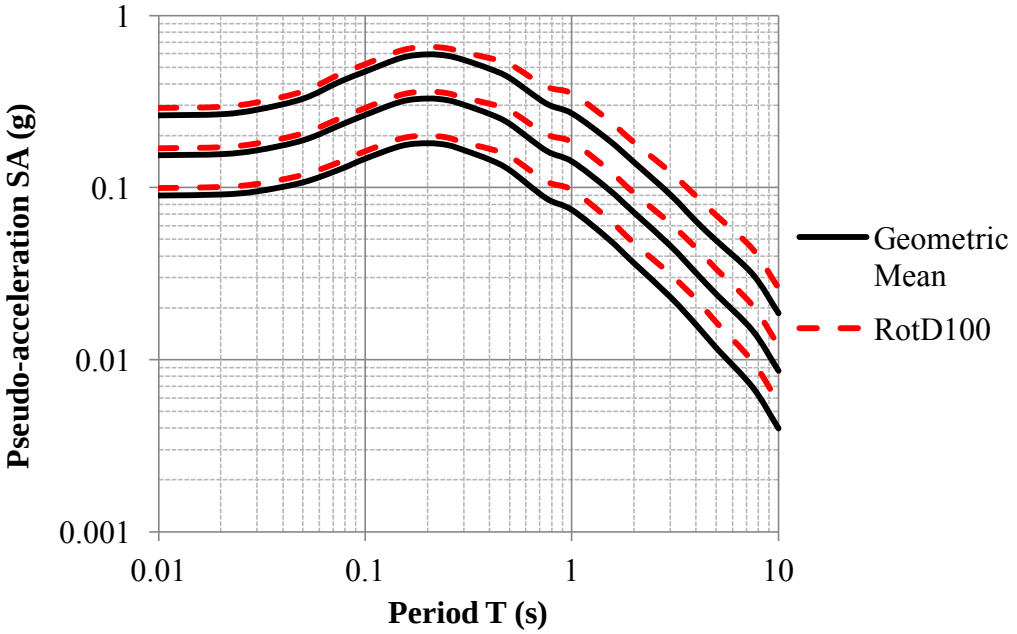

Figure 2.6: Pseudo-acceleration target spectra at 5% damping for scenario ACR3, showing the mean and + and – 1 standard deviation curves for the geometric mean (GMRotI50_NGA) and maximum (RotD100) orientations

Table 2.9: Input parameters for GMPEs for scenario SUB target spectra

Input Parameter	Youngs et al 1997	Atkinson and Boore 2003	Zhao et al 2006	Atkinson and Macias 2009
M_w	9	8.5	8.5	9
R (km)	100	100	100	100
Focal Depth (km)	30	30	30	na
Source	Interface	Interface	Interface	Interface
Site	Rock	NEHRP B	V_{s30} > 600 m/s	B/C Boundary
Weight	0.1	0.3	0.3	0.3

Table 2.10: Pseudo-acceleration target spectra at 5% damping for scenario SUB

	Geometric Mean Component GMRotI50_NGA			Maximum Rotated Component RotD100		
T (s)	μ-σ (g)	μ (g)	μ+σ (g)	μ-σ (g)	μ (g)	μ+σ (g)
0.01	0.084	0.139	0.228	0.093	0.152	0.251
0.04	0.097	0.166	0.283	0.107	0.182	0.311
0.075	0.119	0.209	0.367	0.131	0.230	0.403
0.10	0.137	0.244	0.432	0.151	0.268	0.475
0.20	0.172	0.305	0.538	0.190	0.335	0.592
0.40	0.160	0.279	0.485	0.176	0.307	0.534
0.75	0.121	0.215	0.384	0.145	0.258	0.461
1.0	0.097	0.177	0.325	0.126	0.230	0.423
1.5	0.072	0.133	0.247	0.093	0.173	0.321
2.0	0.051	0.096	0.180	0.067	0.125	0.233
3.0	0.030	0.056	0.102	0.040	0.072	0.133

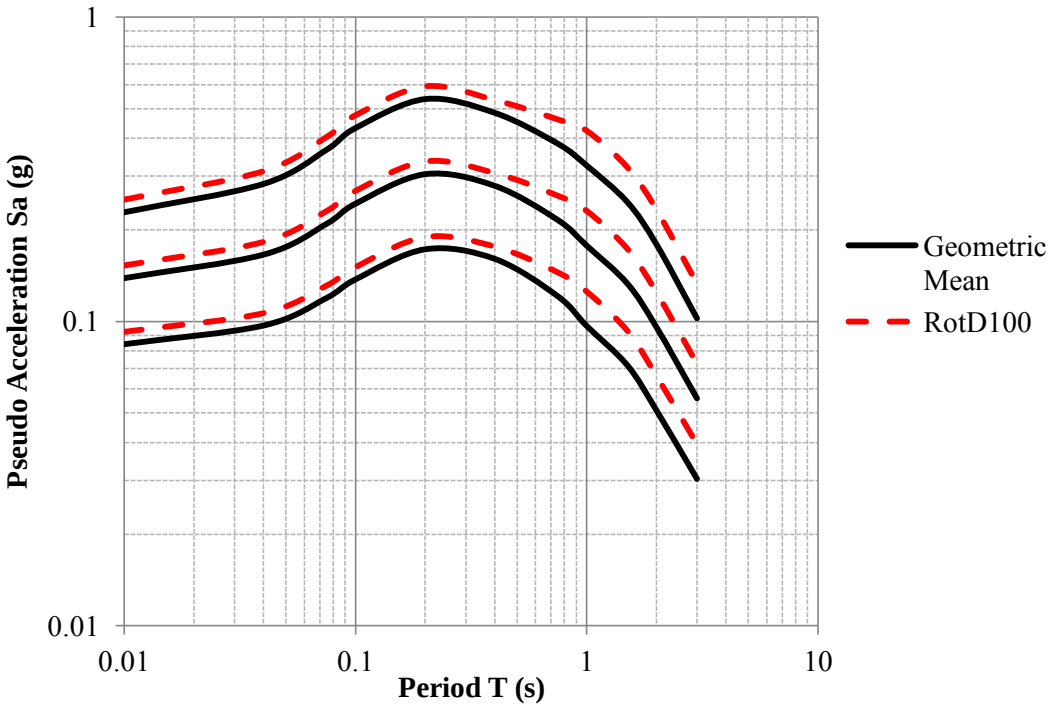

Figure 2.7: Pseudo-acceleration target spectra at 5% damping for scenario SUB, showing the mean and + and – 1 standard deviation curves for both the geometric mean and maximum (RotD100) orientations

Table 2.11: Input parameters for GMPEs for scenario SCR target spectra

Input Parameter	Atkinson & Boore 2006	Silva et al 2002	Toro et al 1997	Pezeshk et al 2011
M_w	6	6	6	6
R (km)	17	17	17	17
Site	Hard Rock	Hard Rock	Hard Rock	Hard Rock
Region	na	na	Midcontinent	na
Weight	0.25	0.25	0.25	0.25

Table 2.12: Pseudo-acceleration target spectra at 5% damping for scenario SCR

	Geometric Mean Component GMRotI50_NGA			Maximum Rotated Component RotD100		
T (s)	μ-σ (g)	μ (g)	μ+σ (g)	μ-σ (g)	μ (g)	μ+σ (g)
0.01	0.129	0.253	0.499	0.159	0.311	0.616
0.025	0.247	0.500	1.029	0.305	0.619	1.272
0.032	0.257	0.522	1.072	0.318	0.646	1.326
0.04	0.251	0.508	1.037	0.311	0.629	1.285
0.05	0.236	0.478	0.976	0.293	0.593	1.212
0.08	0.207	0.418	0.851	0.259	0.523	1.065
0.10	0.189	0.381	0.773	0.238	0.478	0.970
0.20	0.133	0.266	0.537	0.170	0.341	0.688
0.40	0.073	0.148	0.302	0.095	0.193	0.395
0.50	0.058	0.118	0.242	0.076	0.156	0.319
0.75	0.035	0.072	0.150	0.047	0.097	0.200
1.0	0.024	0.050	0.102	0.033	0.067	0.138
2.0	0.009	0.018	0.039	0.012	0.025	0.054
2.5	0.005	0.011	0.026	0.006	0.015	0.035
3.0	0.003	0.007	0.017	0.004	0.009	0.023
4.0	0.002	0.004	0.010	0.002	0.005	0.013
5.0	0.001	0.002	0.006	0.001	0.003	0.008

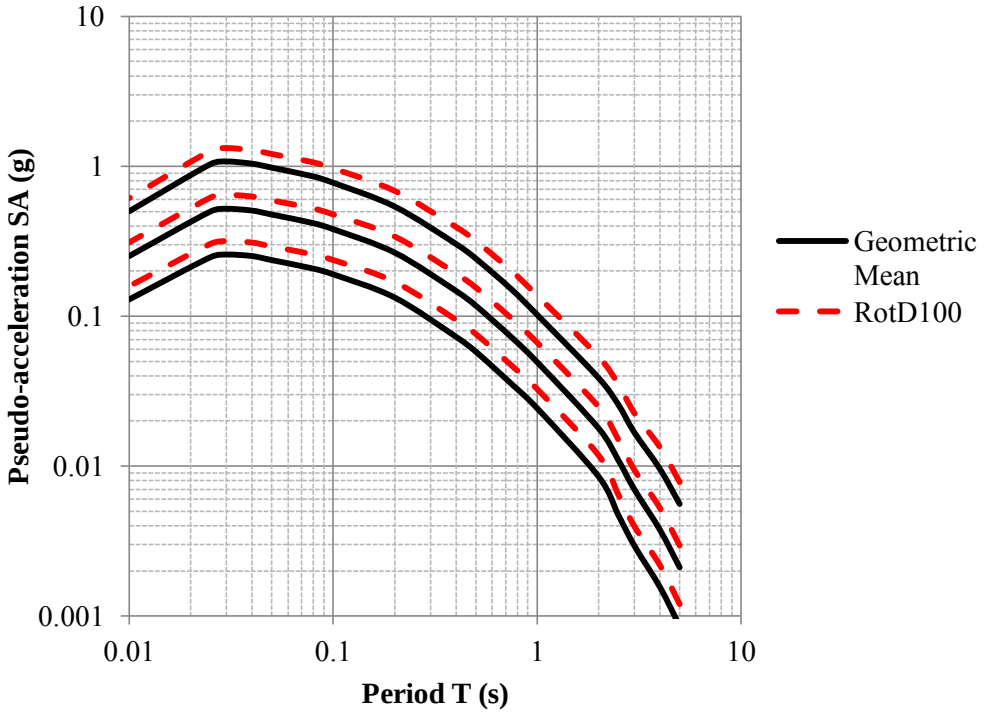

Figure 2.8: Pseudo-acceleration target spectra at 5% damping for scenario SCR, showing the mean and + and – 1 standard deviation curves for both the geometric mean and maximum (RotD100) orientation

CHAPTER 3: SELECTION OF ACCELERATION TIME SERIES FOR NONLINEAR ANALYSES

Seismic design provisions for linear analyses traditionally rely on the use of a target response spectrum, which can come from building code recommendations, attenuation relationships, or probabilistic seismic hazard assessments (PSHA). The selected target response spectrum can then be used directly in linear dynamic analyses to evaluate the seismic response of structures. For nonlinear analyses, however, the methodology requires the use of acceleration time series that conform to the prescribed target response spectrum. In Chapter 2, five base-case scenarios were selected according to tectonic environments applicable to common practice in the United States. The first three correspond to shallow crustal earthquakes in active crustal regions representing reverse earthquakes with and without pulse-like response and strike-slip earthquakes, while the last two correspond to earthquakes from subduction zones and stable continental regions. This chapter discusses the creation of suites of acceleration time series that match the mean and standard deviation of selected target ground motion parameters discussed in Chapter 2. The work initially created a database of ground motions for each scenario with similar magnitude, distance, site conditions, and tectonic environment as the target scenario. These motions were then rotated to the direction that gave the maximum spectral acceleration at a period of 1 second. For each scenario, the work selected a smaller set of scaled rotated motions that best matched the target pseudo-acceleration response spectrum and its standard deviation. Finally, these motions were filtered to match other relevant ground motion measures, such as Arias intensity and significant duration. This chapter gives full details of the methodology for selection, scaling, and spectral matching of each suite of records. The final result is five suites of acceleration time series that can be used as input rock ground motions for nonlinear site response analyses.

3.1 Introduction

Common linear dynamic analyses evaluate the seismic response of structures by directly using a target response spectrum (e.g., Chopra, 2011). This target response spectrum may be derived from a variety of sources, including building code provisions (e.g., IBC, 2012), probabilistic seismic hazard analysis (i.e., Uniform Hazard Spectrum, UHS), or ground motion prediction equations and a given deterministic scenario (e.g., Abrahamson & Silva, 2008). Generally, the target response spectrum specified is the pseudo-acceleration response spectrum. This spectrum represents the maxima pseudo-accelerations experienced by equivalent linear single degree of freedom systems as a function of their natural period (typically for 5% damping). For nonlinear analyses, the design methodology requires the use of acceleration time series. These acceleration time series are derived from measured records or simulated motions and then modified so that they individually (i.e., spectrally matched) or their average (i.e., suite of scaled motions) conform to the prescribed target response spectrum.

To capture the variability of ground motions and their effects on the seismic response of non-liquefiable NEHRP F sites, five base-case scenarios were selected according to tectonic environments applicable to common practice in the United States (cf., Table 3.1). Chapter 2 discusses in detail the creation of target response spectra and other target ground motion

parameters for each of these scenarios. Table 3.2 lists the mean and standard deviation of each target ground motion parameter for each scenario.

This chapter discusses the creation of suites of acceleration time series for each of the scenarios in Table 3.1. These suites will then be used as input "rock" ground motions in nonlinear site response analyses. The work initially created a database of ground motions for each scenario by selecting pairs of measured or simulated seismic records with the same magnitude, distance, and site characteristics as well as the same tectonic environment as the target scenario. These motions are referred to as "original" ground motions. The "original" ground motions were then rotated to the direction that gave the maximum spectral acceleration at a period of 1 second. This work is consistent with the specification by the ASCE-7-10 of using maximum ground motions as design ground motions (ASCE, 2010). The resulting rotated motions are referred to as "seed" motions to distinguish them from the "original" ground motions. The scaled suite of "seed" ground motions that best matched the response spectrum and its standard deviation, as well as other relevant ground motion measures such as Arias intensity and significant duration, was chosen as the final suite to be used in nonlinear site response analyses. The suites for scenarios ACR1, SUB, and SCR are each composed of 11 acceleration time series, and the suites for scenarios ACR2 and ACR3 are each composed of 40 acceleration time series. In addition to scaling, the selected ground motions for scenarios ACR2 and ACR3 were also spectrally matched to their respective target response spectra. As a result, scenarios ACR2 and ACR3 each had two suites of ground motions, one scaled and one spectrally matched.

3.2 Original Ground Motion Databases

Original ground motions were selected for each scenario based on several criteria. First, the recordings were from the same tectonic environment and have similar magnitude and distance characteristics as the target scenario. Second, both components of the ground motion had to have PGA > 0.03g. Finally, since the resulting time histories would eventually be used as input "rock" ground motions, the records should have Vs_{30} > 760 m/s (site classification A/B), where Vs_{30} is the time averaged shear wave velocity in the top 30m of the profile. However, not enough strong ground motion recordings met this last criteria and the site parameter was relaxed to allow recordings from sites with Vs_{30} > 400 m/s. It was not possible to screen based on fault mechanism for scenarios ACR1, ACR2 and ACR3 due to lack of sufficient ground motion recordings. The following sections describe the selection process for the different scenarios.

3.2.1 Scenario ACR1 Original Ground Motions

Scenario ACR1 represents motions from shallow crustal earthquakes in active tectonic regions that incorporate near fault effects (i.e., pulse-like response). The original ground motions for scenario ACR1 were chosen from Table C1 in the NIST GCR 11-917-15, which lists motions with pulse-like characteristics (NIST, 2012). The NIST report used motions from the PEER NGA West 1 database (Chiou et al, 2008) with M_w > 6.0 and R_{rup} < 30 km, resulting in 390 records from 35 different earthquakes. The NIST report used the following methodology to determine if a motion was "pulse-like" or not:

1. *Identify the zero crossings of the filtered velocity time series and identify the peak velocity of each "half cycle" between each pair of zero crossings. A half cycle is considered significant if its maximum value is greater than 25% of the first approximation of the PPV [peak to peak velocity]. The first approximation of the PPV is the maximum ("positive") velocity minus the minimum velocity ("negative") of the entire record.*
2. *The PPV is then calculated as the maximum difference between the peaks of adjacent significant half cycles.*
3. *The cumulative squared velocity at a given time in the velocity time series is the sum of the squared velocity of all preceding time steps. The Normalized Cumulative Squared Velocity (NCSV) at a given time is the cumulative squared velocity at that time divided by the cumulative squared velocity at the end of the record.*
4. *The NCSV at the time of the first zero crossing associated with the PPV cycle and the NCSV at the time of the last zero crossing associated with the PPV cycle is obtained. The difference between these two is referred to as the NCSV difference. The PPV cycle is always two adjacent half cycles.*
5. *The number of significant half cycles associated with the PPV cycle is calculated. A half cycle is considered to be associated with the PPV cycle if there is not a gap of time between the two half cycles greater than the difference between the two zero crossings of the adjacent half cycle associated with the PPV pulse.*

To classify motions as pulses or non-pulses, a weighting scheme was developed that considered the NCSV difference as well as the number of significant cycles. According to this system, a higher score indicates a more pulse-like motion. For each motion, a score was assigned to both of these parameters (i.e., NCSV difference and number of significant cycles). A motion scored 100% in the NCSV category if the NCSV difference was greater than 0.7. Motions that had an NCSV difference less than 0.5 scored 0%. For motions with NCSV differences between 0.7 and 0.5 the score transitioned linearly between 100% and 0%. For the number of significant cycles category, motions with 1.5 significant cycles or less scored 100%, motions with 2 cycles scored 50%, and motions with 2.5 significant cycles or more scored 0%. The total score was calculated with each of the two categories contributing 50%. Motions that scored above 60% were considered pulse-like motions.

Applying this method to the NIST GCR 11-917-15 database, 97 of the 390 records were selected as pulse-like motions. The authors visually inspected the records and added 7 motions that scored less than 60% and removed 16 motions that scored more than 60%, resulting in 88 motions classified as pulse-like. Of these, only 41 records have values of $V_{s30} > 400$ m/s. These motions were then compared with the database of near fault motions defined by Shahi and Baker (2012), and those present in both databases were selected. This left a total of 34 ground motions in the A1 original ground motion database and they are listed in Table 3A.1.

3.2.2 Scenario ACR2 Original Ground Motions

The original ground motions for scenario ACR2 were chosen from the PEER NGA West 2 database (Ancheta et al., 2013) which is an updated version of the NGA West 1 database. It has significantly more ground motions from past earthquakes, such as the 1966 Parkfield earthquake, as well as earthquakes that occurred since the development of the original database, such as the

2008 Wenchuan, China earthquake. The ground motions for the scenario ACR2 project database were selected by filtering the NGA West 2 database by values of $6.0 < M_w < 7.2$, $0 < R_{rup} < 20$km, and $V_{s30} > 400$ m/s, and excluding motions defined as pulse-like by either the NIST GCR 11-917-15 (NIST, 2012) or Shahi and Baker (2012) reports. After applying all the requirements, a total of 137 original ground motions remained in the scenario ACR2 project database and they are summarized in Table 3A.2.

3.2.3 Scenario ACR3 Original Ground Motions

Similarly to scenario A2, the original ground motions for scenario ACR3 were chosen from the PEER NGA West 2 database. The motions were selected by filtering the NGA West 2 database by values of $7.0 < M_w < 8.4$, $20 < R_{rup} < 90$km, and $V_{s30} > 400$ m/s. This process left a total of 154 original ground motions in the scenario ACR3 database and they are summarized in Table 3A.3.

3.2.4 Scenario SUB Original Ground Motions

There is no central database for earthquakes from subduction zones that is uniformly processed like the PEER databases for the western United States. As a result, the original ground motions for scenario SUB were selected from many different sources. The Tohoku and Tokachi-oki earthquake station information came from the Japanese National Research Institute for Earth Science and Disaster Prevention online database (NIED, 2012). Professor Rodriguez-Marek provided the Tohoku acceleration time series (Rodriguez-Marek, 2011), and the Tokachi-oki acceleration time series are from Professor Atkinson's website (Atkinson et al., 2013). The acceleration time series for the Maule, Chile, and the South of Peru earthquakes (except the Moquegua site) are from the University of Chile's National Network of Accelerographs (RENADIC) and the Center for Engineering Strong Motion Data (CESMD) websites (RENADIC, 2012; CESMD, 2012). The acceleration time series for the South of Peru earthquake at the Moquegua site are from the Peru-Japan Center for Seismic Investigation (CISMID) online database (CISMID, 2012). Professors Montalva and Boroschek provided the site information for the Maule, Chile earthquake (Montalva, 2012; Boroschek et al., 2012). Professors Montalva and Rodriguez-Marek provided the site information for the South of Peru earthquake (Montalva, 2012, Rodriguez-Marek et al., 2010). The Michoacán acceleration time series are from the National Oceanic and Atmospheric Administration (NOAA) National Geophysical Data Center (NOAA, 2012). Two large magnitude synthetic subduction zone events for western Canada are from Atkinson (2009), and four large magnitude synthetic subduction zone events for Victoria, British Columbia, and Seattle, Washington, are from Atkinson and Macias (2009). The resulting original ground motion database for scenario SUB has a total of 36 records and they are summarized in Table 3A.4.

3.2.5 Scenario SCR Original Ground Motions

Similarly to scenario SUB, the original ground motions for scenario SCR were gathered from several different sources. The 1976 Gazli, Uzbekistan, 1978 Tabas, Iran, and the 1985 Nahanni, Canada, motions are from the PEER NGA West 1 database. In their 1998 study of Eastern North American earthquakes, Atkinson and Boore (1998) justified the inclusion of the 1985 Nahanni earthquake based on the work by Wetmiller et al. (1989). Wetmiller and coworkers concluded

that the high shear wave velocity of the bedrock, thrust mechanisms, regional stress regime, and shallow focal depth of the 1985 Nahanni earthquake are similar enough to earthquakes in stable continental regions to justify its inclusion in a database for these regions. Atkinson and Boore (1998) also included the rock records from the 1976 Gazli, Uzbekistan, and 1978 Tabas, Iran earthquakes since "they are from large intraplate earthquakes and improve the magnitude-distance distribution of the database significantly at large magnitudes." The Nahanni 0, 2, and 3, as well as the Miramichi, NB, ground motions are all from the Consortium of Organizations for Strong-Motion Observation Systems (COSMOS) Virtual Data Center (COSMOS, 2012). La Malbaie, Riviere du Loup, Val des Bois and the synthetic eastern Canada earthquakes are from Professor Atkinson's website (Atkinson et al., 2013). The Mineral Virginia earthquake and its aftershock are from the CESMD website (CESMD, 2012). The Arcadia, OK, Greenbrier, AR, Guy, AR, Mount Carmel, IL, Saguenay, QC, and Sparks, OK earthquakes are from an early version of the NGA East database (Goulet, 2012). The original ground motion database for scenario SCR has a total of 46 records and they are summarized in Table 3A.5.

3.3 Determination of "Seed" Ground Motions

This study rotated the original ground motions to the direction that gave the maximum spectral acceleration at a period of one second. This direction is referred to as the Maximum direction, and the orthogonal component is the Minimum direction. Rotated ground motions are referred to as "seed" motions to distinguish them from original ground motions. The work is consistent with the ASCE/SEI 7-10 specification of maximum ground motions as design ground motions (ASCE, 2010). The scenario ACR1 ground motions were rotated to the azimuth that the NIST GCR team found gave the maximum PPV. In addition to rotating the ground motions, some of the scenario SUB and scenario SCR motions were baseline corrected. All ground motions from the PEER NGA databases are already baseline corrected. The following sections describe the methodology for scaling or spectrally matching the "seed" ground motions to conform to the corresponding target response spectra.

3.3.1 Scaled "Seed" Ground Motions

This section describes the methodology used to select a suite of scaled ground motions that match both the median and standard deviation of the target response spectrum for each of the five scenarios. This study used the computer code SigmaSpectra to make an initial selection of the best suite of ground motions from a larger pool of possible ground motions (i.e., seed motions), and to scale each time series to simultaneously match the mean and the standard deviation of the target acceleration response spectrum (Kottke and Rathje, 2008). These motions are referred to as the scaled seed motions, to differentiate them from the unscaled seed motions.

SigmaSpectra uses a semi-automated procedure to select and scale a specified number of ground motions to fit a target acceleration response spectrum and its standard deviation. The software assigns scale factors to each individual motion from a population of possible motions to find the suite that best matches the mean and the standard deviation of the target response spectrum. The scaling process involves multiplying the initial time series by a scalar, thus changing the amplitude of the motion while preserving the original frequency content. To quantify the

goodness of fit of a suite of response spectra to the mean target spectrum, SigmaSpectra uses the Root Mean Squared Error (RMSE), given by:

$$RMSE = \sqrt{\frac{1}{n_p}\sum_{i=1}^{n_p}\left(lnSa_{avg,i}^{scaled} - lnSa_{target,i}\right)^2} \tag{3.1}$$

where n_p is the number of periods in the response spectra to be targeted, and $Sa_{target,i}$ and $Sa_{avg,i}^{scaled}$ are the target spectral acceleration and the mean spectral acceleration of the suite of scaled ground motions for the i-th period, respectively. The spectral values are assumed to be log-normal distributed.

SigmaSpectra first finds a suite of motions that best batches the mean target response spectrum by minimizing the RMSE. The program then scales each individual time series in the suite to match the target standard deviation, but keeps the average scaling factor the same. This method ensures that the RMSE (i.e., matching of the mean) remains the same. SigmaSpectra uses the Centroid Method to determine the best scaling factors to use for each time series as described by Kottke and Rathje (2008). The root mean squared error is also used to evaluate the goodness of fit of the standard deviation of the scaled suite, σ_{ln}RMSE, and it is given by:

$$\sigma_{ln}RMSE = \sqrt{\frac{1}{n_p}\sum_{i=1}^{n_p}\left(\sigma_{ln,i}^{suite} - \sigma_{ln,i}^{target}\right)^2} \tag{3.2}$$

where $\sigma_{ln,i}^{suite}$ and $\sigma_{ln,i}^{target}$ are the standard deviation for the suite and the target standard deviation for the i-th period, respectively.

Instead of cycling through every possible combination of motions and then selecting the suite with the lowest RMSE, the program uses a reduced set of seed motions, n_{seed}, to conduct a smaller number of trials. The "seed" notation used in this work, meaning maximum rotated motions, has no relation with the one used by Kottke and Rathje (2008). The user provides the total number of motions in the database (n_{total}) and specifies the number of seed motions (n_{seed}) and the desired number of motions in a suite (n_m), where $n_{seed} < n_m$. SigmaSpectra then creates every possible combination of n_{seed} motions from the database with N_{seed} being the number of rigorous combinations of size n_{seed} given by:

$$N_{seed} = \frac{n_{total}!}{n_{seed}!\,(n_{total} - n_{seed})!} \tag{3.3}$$

The program then selects one motion from the remaining set that gives the lowest RMSE and adds it to the suite, and repeats this process until n_m motions are reached. The number of trials for this iterative procedure, N_{trials}, is given by:

$$N_{trials} = N_{seed} \times \left[\sum_{j=n_{seed}}^{n_m - 1} (n_{total} - j) \right] \quad (3.4)$$

This procedure significantly reduces computation time while still ensuring an RMSE close to the one found using all possible combinations (Kottke and Rathje, 2008). Table 3.4 lists n_{total}, n_{seed}, and n_m, for each scenario used in this work.

3.3.2 Spectrally Matched Ground Motions for Scenarios ACR2 and ACR3

The selected motions for scenarios ACR2 and ACR3 from the previous procedure were also spectrally matched to their respective target spectrum. This work used the program RspMatch 2009 (Al-Atik and Abrahamson, 2010) and the methodology is described in the following paragraphs. The spectrally matched motions are referred to as Matched motions.

Abrahamson (1992) developed the program RspMatch using the formal optimization procedure proposed by Lilhanand and Tseng (1988), which adjusted the time series in the time domain by adding wavelets. The advantage of the procedure in the time domain over the other two spectral matching methods, frequency domain and frequency domain with random vibration theory, is that it preserves the non-stationary characteristics of the time series and has better convergence properties. Nevertheless, the original program had the shortcoming that it did not integrate to zero end velocity or displacement, which caused drift and required subsequent baseline correction. Hancock et al. (2006) revised the program by modifying the adjustment wavelets which removed the need for baseline correction. However, the revised program, RspMatch 2005, had the shortcoming of reduced computational speed and overall efficiency and the modified wavelets did not converge in all cases. Al Atik and Abrahamson (2010) produced a revised version, referred to as RspMatch 2009, by introducing a new adjustment function consisting of a cosine function tapered with a Gaussian function that integrates to zero end velocity and displacement. The new formulation provides a stable and computationally efficient solution, and ensures convergence.

Table 3.5 summarizes the input parameters used in RspMatch 2009 as well as their interpretation. The RspMatch 2009 manual recommends performing spectral matching in multiple passes, starting with higher frequencies and matching lower frequencies progressively in subsequent passes. Since high frequency spectral accelerations are influenced by low frequency wavelets, the non-stationary characteristics of the initial times series are better preserved by successively incorporating lower frequencies. This study used three passes to spectrally match the ground motions. Pass one performed spectral matching over frequency ranges of 1-10 Hz, pass two from 0.5-10 Hz, and pass three from 0.33-10 Hz. Many of the spectrally matched response spectra showed large spikes in the periods outside the range of 0.33-10 Hz. For these motions the spectral matching range was increased until these spikes were removed, giving a smooth response spectra.

A frequency range of 0.33-10 Hz translates to a period range of 0.1 to 3 seconds, which is the period range of most structures and the period range of interest for this study. ASCE 7-10 recommends a period range of $0.2T_i - 1.5T_i$ for selecting and scaling ground motions, where T_i is

the fundamental period of the structure. The PEER GMSM Method 300 (PEER GMSM, 2009) and the Eurocode 8 (Comité Européen de Normalisation, 2004) both recommend a period range of $0.2T_i - 2.0T_i$. According to the above mentioned codes, the use of the proposed matched ground motions (period range of 0.1 to 3 seconds) would be appropriate for determining the response of structures with fundamental periods between 0.5 and 1.5 seconds.

The target response spectra for scenarios ACR2 and ACR3 were linearly interpolated to determine 40 values per order of magnitude on a log period scale as suggested by Hancock et al. (2006). This resulted in a total of 55 spectral ordinates in the matched period range of 0.1-3 seconds, and a total of 120 spectral ordinates over the entire range of periods (0.01-10 seconds). The program linearly scaled the seed motion to the spectral acceleration of the target spectra at T = 1 second only before the first iteration. This was done because the original motions were rotated to the direction where Sa(T=1 sec) was maximized. The group size was lowered from the default value of 30 to 15 spectral ordinates. All other parameters were left as the default values suggested in the RspMatch 2009 manual.

3.4 Selected Suites of Ground Motions

The following paragraphs describe the selected scaled ground motions for each scenario. Appendix 3B contains a one page summary for each ground motion selected in this study containing the acceleration, velocity and displacement time series, Husid plot, the pseudo-acceleration response spectra and other details. Table 3.3 summarizes the statistics for magnitude, distance and shear velocity parameter, V_{s30}, for the five suites of selected ground motions.

3.4.1 Selected Ground Motions for Scenario ACR1

Although this study considered all the target parameters in the final selection, the most important parameters for scenario ACR1 were the period of the pulse, T_v, the peak ground velocity, PGV, and target response spectrum. Table 3.6 summarizes the selected 11 ground motions for scenario ACR1, along with their scaling factor, intensity measures (i.e., PGA, PGV, I_a), duration (D_{5-95}), and frequency parameters (T_v and T_m). Parameters in cells highlighted red are more than one standard deviation above the median target value for that parameter. If the cell is shaded yellow, then the value is less than one standard deviation below the target value. Figure 3.1 shows the response spectra of the 11 selected ground motions and compares the suite's median and median +/- one standard deviation versus the target spectrum and one standard deviation band. The graph shows excellent agreement for both the target median and standard deviation of the response spectra giving confidence in the methodology described earlier. Individual plots for each selected ground motion can be found in Appendix 3B.

3.4.2 Selected Ground Motions for Scenarios ACR2 and ACR3

A first screening of the seed ground motions was done with SigmaSpectra for scenarios ACR2 and ACR3. The seven suites with the lowest RMSE from the SigmaSpectra analyses were saved. For scenario ACR2 this procedure gave 65 different ground motions, and for scenario ACR3 60 ground motions. The seed motions from this reduced set of motions were then spectrally matched with RspMatch 2009 to their respective target spectra. There is little

guidance available as to what is an acceptable level of modification to an initial ground motion. Following the recommendations of Hancock et al. (2006), this study conducted a visual inspection of the acceleration, velocity, and displacement time series, as well as the Husid plot (Husid, 1973), which shows the growth of the normalized arias intensity over time, for each Matched motion to determine whether the non-stationary characteristics were retained, and whether or not they still looked like 'realistic' time series. A maximum of 10 Chi Chi acceleration time series was allowed for scenario ACR3 to prevent this event from dominating the suite. Forty scaled and matched motions for scenarios ACR2 and ACR3 were selected based on the relevant target parameter and the previously described criteria. These 40 motions were analyzed with SigmaSpectra again to determine the scaling parameter for each motion based on the final suite, since the final suite of motions was different than any of the initial seven suites.

Table 3.7 and Table 3.8 summarize the selected ground motions for scenarios ACR2 and ACR3, respectively. The tables provide each motion with their scaling factor, intensity measures (i.e., PGA, PGV, and I_a), duration ($D_{5\text{-}95}$), and frequency parameter (T_m). Cells highlighted red are more than one standard deviation above the median target value for that parameter, and cells highlighted yellow are less than one standard deviation below the target value. Figure 3.2 shows the response spectra of the forty selected scaled ground motions for scenario ACR2 and compares the suite's median and median +/- one standard deviation against the target response spectrum and one standard deviation band. The graph shows excellent agreement for both the target median and standard deviation of the response spectra. Figure 3.3 shows the response spectra of the matched ground motions and compares them with the target response spectra. The figure shows excellent agreement between the individual spectrum and the target spectra over the range of periods of interest (e.g., 0.1 to 3 seconds). For periods outside the matched range the response is typically within the one standard deviation band. Individual plots for each selected ground motion can be found in Appendix 3B.

Figure 3.4 shows the response spectra of the forty selected scaled ground motions for scenario ACR3 and compares the suite's median and median +/- one standard deviation against the target response spectrum and one standard deviation band. Similarly to scenario ACR2, the graph shows excellent agreement of the suite for both the target median and standard deviation of the response spectra. Figure 3.5 shows the response spectra of the spectrally matched ground motions and compares them with the target response spectra. The figure shows excellent agreement between the individual spectrum and the target spectra over the range of periods of interest (e.g., 0.1 to 3 seconds). For periods outside the matched range the response is generally within the one standard deviation band, except for periods larger than 5 seconds. Individual plots for each selected ground motion can be found in Appendix 3B.

3.4.3 Selected Ground Motions for Scenarios SUB and SCR

SigmaSpectra was used to find seven suites of 11 ground motions each with the lowest RMSE for scenarios SUB and SCR. This initial screening process reduced the number of possible ground motions from 36 to 20 for scenario SUB, and from 46 to 21 for scenario SCR. The final 11 scaled acceleration time series were chosen from these reduced sets based on a visual inspection of how well each individual response spectrum matched the target spectrum shape. In addition, no more than three synthetic motions were allowed to be in the final suite of 11 motions for either scenario. Table 3.9 and Table 3.10 summarize the selected 11 ground motions for

scenarios SUB and SCR, along with their scaling factor, intensity measures (i.e., PGA, PGV, and I_a), duration (D_{5-95}), and frequency parameters (T_m). Figure 3.6 and Figure 3.7 show the response spectra of the eleven selected scaled ground motions for scenarios SUB and SCR, respectively. The figures compare each suite's median and median +/- one standard deviation against the target response spectrum and one standard deviation band. Both graphs show good agreement for both the target median and standard deviation of the response spectra. Individual plots for each selected ground motion can be found in Appendix 3B.

3.5 Summary

This chapter summarizes the creation of suites of acceleration time series to be used as input "rock" motions in nonlinear site response analyses for five scenarios representative of common US practice. The work initially selected pairs of measured or simulated seismic records, referred to as "original" ground motions with similar characteristics as those selected for each base-case scenario. This process yielded 34, 137, 154, 36 and 46 motions for scenarios ACR1, ACR2, ACR3, SUB and SCR, respectively. These motions were then rotated to the direction that gave the maximum spectral acceleration at a period of 1 second to obtain maximum ground motions and they are referred to as "seed" motions. The work selected a smaller suite of scaled ground motions from the entire population of seed motions that best fit the mean and standard deviation of the target response spectra. The resulting suites were also filtered to best match the mean of other relevant ground motion parameters, such as PGA, PGV, Arias Intensity (I_a), duration (D_{5-95}), mean period, T_m, and pulse period, T_v. Additional constraints were added such that no single earthquake, such as the Chi Chi earthquake, or synthetic motions, dominated the suite. The final result is five suites of scaled ground motions with eleven ground motions for scenarios ACR1, SUB, and SCR, and 40 ground motions for scenarios ACR2 and ACR3. For each suite of motions, the mean and standard deviation of the response spectra is in excellent agreement with target values, which gives confidence on the methodology selected. The average PGA and PGV are in good agreement with target values, and other parameters are within the one standard deviation band. This reflects the difficulty of simultaneously matching all ground motion parameters. Table 3.11 presents a summary of the average ground motion parameters for each suite. For scenarios ACR2 and ACR3, two additional suites were constructed by spectrally matching the selected motions to the target response spectra in the range of 0.1 to 3 seconds. These two suites are referred to as matched ground motions (ACR2M and ACR3M).

3.6 References

Abrahamson, N.A. (1992). “Non-stationary spectral matching,” Seismol. Res. Lett. (63)1, 30.

Abrahamson, N.A., and Silva, W.J. (2008). “Summary of the Abrahamson and Silva NGA Ground-Motion Relations.” Earthquake Spectra 24(1), 67-97.

Al Atik, L., and Abrahamson, N.A. (2010). “An Improved Method for Nonstationary Spectral Matching.” Earthquake Spectra, 26(3), 601-617.

Ancheta, T.D., Darragh, R.B., Stewart, J.P., Seyhan, E., Silva, W.J., Chiou, B.S.J., Wooddell, K.E., Graves, R.W., Kottke, A.R., Boore, D.M., Kishida, T. and Donahue, J.L. (2013). PEER NGA West2 Database, PEER Report 2013/03, PEER, University of California, Berkeley, California.

ASCE (2010). “Minimum design loads for buildings and other structures.” ASCE/SEI 7-10, American Society of Civil Engineers; Reston, Virginia.

Atkinson, G.M. (2009). “Earthquake time histories compatible with the 2005 National Building Code of Canada Uniform Hazard Spectrum.” Can. J. Civil Engng. (36)6, 991-1000.

Atkinson, G.M. and Boore, D.M. (1998). “Evaluation of models for earthquake source spectra in eastern North America.” Bull. Seismol. Soc. Amer., (88)4, 917-934.

Atkinson, G.M., and Macias, M. (2009). “Predicted ground motions for great interface earthquakes in the Cascadia subduction zone.” Bull. Seismol. Soc. Amer., 99(3) 1552-1578.

Atkinson, G.M., Assatourians, K. and Dunn, B. (2013). “Seismotoolbox,” University of Western Ontario, Canada. http://www.seismotoolbox.ca/ (last accessed Oct 22, 2013)

Boore, D.M., Watson-Lamprey, J., and Abrahamson, N.A., (2006). “Orientation-independent measures of ground motion.” Bull. Seismol. Soc. Amer., (96) 4A, 1502-1511.

Boroschek, R., Yáñez, F., Bejarano, I., Molnar, S., Torres A. (2012). “Summary of the geotechnical characterization of the university of Chile strong motion accelerograph stations.” Universidad de Chile, Facultad de Ciencias Físicas y Matemáticas.

CESMD (2012). Center for Engineering Strong Motion Data online database, http://strongmotioncenter.org/, accessed October 2012.

Chiou, B., Darragh, R., Gregor, N., and Silva, W. (2008). “NGA project strong-motion database,” Earthquake Spectra, (24) 1, 23-44.

Chopra, A.K. (2011). Dynamics of structures: theory and applications to earthquake engineering, 4th edition, Pearson-Prentice Hall, New Jersey.

CISMID (2012) Centro Peruano Japonés de Investigaciones Sísmicas y Mitigación de Desastres. online database. http://www.cismid-uni.org/

Comité Européen de Normalisation (2004) "Eurocode 8: Design of structures for earthquake resistance—Part 1: General rules, seismic actions and rules for buildings." EN 1 (1998): 2004.

COSMOS (2012). Consortium of Organizations for Strong-Motion Observation Systems Virtual Data Center, http://db.cosmos-eq.org/scripts/earthquakes.plx, accessed October 2012.

Goulet, C. (2012), NGA East Project Coordinator, personal communication.

Hancock, J., Watson-Lamprey, J., Abrahamson, N. A., Bommer, J. J., Markatis, A., McCoy, E., and Mendis, R., (2006). “An improved method of matching response spectra of recorded earthquake ground motion using wavelets.” J. Earthquake Engng, (10)1, 67–89.

Husid, R., (1973). “Terremotos: análisis espectral y características de acelerogramas como base del diseño sísmico.” Universidad Católica Andrés Bello, Santiago, Chile.

IBC (2012). International Building Code, by International Code Council, Delmar Publishers.

Kottke, A., and Rathje, E. (2008). “A semi-automated procedure for selecting and scaling recorded earthquake motions for dynamic analysis.” Earthquake Spectra, 24(4), 911-932.

Lilhanand, K., and Tseng, W.S., (1988). “Development and application of realistic earthquake time histories compatible with multiple damping response spectra.” Ninth World Conference on Earthquake Engineering; Tokyo, Japan, (2), 819–824.

Montalva, G. (2012). Universidad de Concepción, Chile. Personal communication, April 5 2012.

NEHRP (2009). “NERHP recommended seismic provisions for new buildings and other structures.” FEMA P-750 report prepared by the Building Seismic Safety Council of The National Institute of Building Sciences for the Federal Emergency Management Agency, Washington, D.C.

NIST (2012). “Selecting and scaling earthquake ground motions for performing response history analyses.” NIST GCR 11-917-15, prepared by the NERHP Consultants Joint Venture for the National Institute of Standards and Technology, Gaithersburg, Maryland.

NIED (2012). Japanese National Research Institute for Earth Science and Disaster Prevention online database, http://www.k-net.bosai.go.jp/. Last accessed October 2012.

NOAA (2012). National Oceanic & Atmospheric Administration, National Geophysical Data Center, http://www.ngdc.noaa.gov/hazard/data/cdroms/EQ_StrongMotion_v3/data/mex03/ . Last accessed October 2012.

PEER GMSM (2009). Evaluation of Ground Motion Selection and Modification Methods: Predicting Median Interstory Drift Response of Buildings, PEER Report 2009, Haselton, C.B., Editor, PEER, University of California, Berkeley, California.

RENADIC (2012). Red de Cobertura Nacional de Acelerografos, University of Chile website http://terremotos.ing.uchile.cl/. Accessed October 2012.

Rodriguez-Marek, A. (2011). Personal communication, October 17 2011.

Rodriguez-Marek, A., Bay, J.A., Park, K., Montalva, G.A., Cortez-Flores, A., Wartman, J. and Boroschek, R. (2010). “Engineering analysis of ground motion records from the 2001 Mw 8.4 southern Peru earthquake.” Earthquake Spectra, (26)2, 499-524.

Shahi, S.K., and Baker, J.W. (2012). “Directionality models for the NGA West 2 project.” PEER Report 2012/03.

Wetmiller, R.B., Horner, R.B., Hasegawa, H.S., North, R.G., Lamontagne, M., Weichert, D.H., and Evans, S.G., (1989). “An analysis of the 1985 Nahanni earthquakes.” Bull. Seismol. Soc. Amer., (78), 590-616.

Table 3.1: Selected scenarios

Scenario	Mechanism	M_w	R_{rup} (km)
ACR1	Reverse (Pulse Like)	6.7	5
ACR2	Reverse (No Pulse)	6.7	5
ACR3	Strike Slip	7.8	30
SUB	Interface- Subduction Zone	9	100
SCR	Stable Continental Region	6	17

Table 3.2: Mean (μ) +/- one standard deviation (σ) target ground motion parameters

Scenario	Target	PGA (g)	PGV (cm/s)	D_{5-95} (s)	T_m (s)	I_a (m/s)	T_v (s)
ACR1	μ-σ	0.32	37.3	4.2	0.36	0.88	0.84
	μ	0.56	55.7	6.6	0.57	1.70	1.45
	μ+σ	0.98	83.0	10.6	0.90	3.75	2.52
ACR2	μ-σ	0.32	21.8	6.6	0.27	0.88	
	μ	0.56	37.9	10.6	0.43	1.70	
	μ+σ	0.98	65.9	16.9	0.67	3.75	
ACR3	μ-σ	0.09	9.2	20.3	0.3	0.23	
	μ	0.15	15.8	32.3	0.5	0.43	
	μ+σ	0.26	27.2	51.4	0.8	0.90	
SUB	μ-σ	0.093					
	μ	0.152					
	μ+σ	0.251					
SCR	μ-σ	0.142	2.890				
	μ	0.279	5.728				
	μ+σ	0.553	11.506				

Table 3.3: Mean (μ) and standard deviation (σ) of M_w, R_{rup}, and V_{s30} characteristics

Scenario	Statistic	Original/ Seed Motions			Suite of Selected Motions		
		M_w	R_{rup} or R_{epi} (km)	V_{s30} (m/s)	M_w	R_{rup} or R_{epi} (km)	V_{s30} (m/s)
ACR1	Target	6.7	5	>760	6.7	5	>760
	μ	7.16	8.0	742	6.95	8.7	1099
	σ	0.51	6.3	454	0.39	4.5	653
	Max	7.62	28.1	2016	7.62	16.7	2016
	Min	6.19	0.3	438	6.30	1.8	443
ACR2	Target	6.7	5	>760	6.7	5	>760
	μ	6.42	11.4	564	6.56	12.0	564
	σ	0.39	5.4	191	0.37	5.2	133
	Max	7.14	20.0	1428	7.14	19.1	1000
	Min	5.99	0.2	401	5.99	3.3	401
ACR3	Target	7.8	30	>760	7.8	30	>760
	μ	7.53	57.1	531	7.47	48.9	572
	σ	0.23	19.6	99	0.30	17.1	143
	Max	7.90	90.0	964	7.90	90.0	964
	Min	7.00	21.9	412	7.00	21.9	412
SUB	Target	9	100	>760	9	100	>760
	μ	8.61	121.1	704	8.64	119.6	517
	σ	0.34	34.3	309	0.37	32.5	56
	Max	9.00	192.0	1500	9.00	190.0	611
	Min	8.10	71.0	389	8.10	77.4	430
SCR	Target	6	17	>760	6	17	>760
	μ	5.48	32.1	976	5.93	28.4	1217
	σ	0.92	36.7	571	1.05	27.7	716
	Max	7.35	194.8	2000	7.35	91.4	2000
	Min	4.10	1.2	475	4.40	2.0	660

Table 3.4: Input parameters used for SigmaSpectra (after Kottke & Rathje, 2008)

Scenario	n_{total}	n_{seed}	n_m
ACR1	34	3	11
ACR2	137	3	40
ACR3	154	3	40
SUB	36	3	11
SCR	46	3	11

Table 3.5: Input variables for RSPMatch 2009 (Al Atik & Abrahamson, 2010)

Variable	Explanation
nPass	Number of adjustment passes.
*.inp	Name of the first run file.
MaxIter	Maximum number of iterations for spectral matching. This value is typically set between 5 and 20 depending on how close the initial response spectrum is to the target spectrum.
Tol	Tolerance for maximum mismatch in fraction of target. This value is typically set to 0.05 for 5% maximum deviation from the target spectrum.
Gamma	Convergence damping. This factor specifies the fraction of adjustment made to the acceleration time series at each iteration. This parameter is usually set to 1.
iModel	Flag indicating the adjustment model to be used in spectral matching. 1 = Reverse acceleration impulse response function based on Lilhanand and Tseng (1988). 6 = Tapered cosine function, 7 = Improved tapered cosine function.
a1, a2, f1, f2	Parameters that describe the frequency dependence of the taper for adjustment model 6. If model 7 is selected, the user can enter any default values for these taper parameters as they will not affect the results.
Scale, Per	Flag to linearly scale the acceleration time series and the response spectrum to match the target spectrum at the specified period, Per. The scaling flag can take the following values: 0 = No scaling is applied, 1 = Scaling the acceleration time series before and after each iteration, 2 = Scaling the initial time series to match the target spectrum at the specified period only before the first iteration
dtflag	Interpolation factor (integer greater than or equal to 1) used to interpolate the acceleration time series to 1/dtflag of the input time step.
evmin	Minimum normalized eigenvalue used in the singular value decomposition (SVD). The recommended value for this parameter is 1.0e-4.
Groupsize	Number of spectral values to use in matching one subgroup (Typically set to 30).
MaxFreq	Maximum frequency (Hz) up to which spectral matching is performed.
f1, f2, npole	Parameters used to set the frequency band and the number of poles for the bandpass filter to be applied to the initial acceleration time series. The use of this filter is not recommended as it might introduce drift to the velocity and displacement time series.
iModPGA	Peak ground modification flag. This parameter should be set to 1 for modifying PGA or 0 otherwise. If Model 7 is selected, this parameter is not used in the code and a default value can be entered.
iSeed, RanFactor	Parameters used to randomize the target response spectrum by introducing random variations about the mean target spectrum. iSeed is the seed number for the random number generator, while RanFactor sets the amplitude of variation. The use of target randomization is not recommended and these parameters are typically set to zero.
freqMatch1, freqMatch2	Frequency range for spectral matching. Spectral matching for a certain pass is performed for all frequencies between freqMatch1 and freqMatch2. Since short period spectral accelerations are influenced by long period wavelets, it is recommended to do spectral matching in multiple passes. The first pass is typically performed for a frequency range of 1 to 100Hz. Longer periods are matched progressively in subsequent passes.
Baseline Cor Flag	Baseline correction flag. 1= applies baseline correction to the acceleration time series following each iteration. 0= no baseline correction is applied. For Model 7, baseline correction is not active regardless of the value of this flag.
Scale Factor	Scale factor used to scale the initial acceleration time series prior to spectral matching.

Table 3.6: Ground motion parameters of selected acceleration time series of scenario ACR1

NGA #	M_w	R_{rup} (km)	V_{s30} (m/s)	Scaling Factor	PGA (g)	PGV (cm/s)	D_{5-95} (s)	T_m (s)	I_a (m/s)	T_v (s)
77	6.6	1.81	2016.1	0.69	0.89	82.54	7.05	0.50	5.11	1.20
285	6.9	8.18	1000	2.05	0.36	80.24	14.31	0.96	1.92	1.30
292	6.9	10.84	1000	1.19	0.43	62.19	14.98	0.86	2.06	3.00
763	6.9	9.96	729.7	1.31	0.57	33.43	4.78	0.36	1.63	1.40
825	7.0	6.96	513.7	0.75	1.13	93.33	6.02	0.37	3.41	4.00
879	7.3	2.19	1369	1.01	0.73	145.53	13.06	0.30	6.96	4.30
1050	6.7	7.01	2016.1	1.31	0.66	60.09	3.78	0.49	2.15	3.20
1051	6.7	7.01	2016.1	1.06	1.48	113.32	5.96	0.44	11.65	0.80
1148	7.5	13.49	523	2.02	0.33	74.47	9.86	0.52	1.00	6.00
1486	7.6	16.74	465.6	1.97	0.21	43.05	18.65	0.56	1.22	6.00
3473	6.3	11.52	443	1.26	0.49	43.93	4.83	0.39	1.59	0.80

Intensity, duration, and frequency parameters are for the scaled motions. Red highlighted values are more than one standard deviation above the target mean and yellow highlighted values are more than one standard deviation below the target mean value.

Table 3.7: Ground motion parameters of selected acceleration time series of scenario ACR2

NGA #	M_w	R_{rup} (km)	V_{s30} (m/s)	Scaling Factor	PGA (g)	PGV (cm/s)	$D_{5\text{-}95}$ (s)	T_m (s)	I_a (m/s)
28	6.2	17.64	408.9	3.53	0.68	40.46	22.45	0.49	4.13
33	6.2	15.96	527.9	2.13	0.50	45.06	5.13	0.44	2.13
125	6.5	15.8	424.8	2.24	0.58	37.02	4.32	0.45	1.98
164	6.5	15.2	659.6	2.19	0.44	30.15	32.27	0.49	5.44
265	6.3	14.4	659.6	2.63	0.48	40.06	6.28	0.45	2.24
284	6.9	9.6	1000	3.50	0.58	45.47	18.15	0.42	4.05
448	6.2	3.26	488.8	2.23	0.47	33.64	7.20	0.42	3.04
587	6.6	16.1	424.8	2.15	0.63	49.73	5.34	0.42	2.51
690	6.0	15.2	401.4	2.22	0.52	41.41	5.09	0.42	2.35
753	6.9	3.9	462.2	2.32	0.46	41.33	7.69	0.47	2.46
769	6.9	18.3	663.3	2.42	0.45	54.31	10.15	0.45	2.54
801	6.9	14.7	671.8	1.91	0.50	46.79	10.18	0.38	3.43
809	6.9	18.5	714	2.30	0.52	38.56	10.16	0.31	5.31
952	6.7	18.4	545.7	2.24	0.59	39.40	8.17	0.37	3.66
957	6.7	16.9	821.7	2.74	0.75	47.36	11.95	0.39	4.51
1012	6.7	19.1	706.2	2.04	0.53	46.45	10.08	0.34	4.39
1078	6.7	16.7	715.1	2.30	0.56	41.79	7.88	0.36	4.04
1111	6.9	7.1	609	2.28	0.60	34.83	10.35	0.44	3.26
1612	7.1	4.17	424.8	2.72	0.54	48.77	15.07	0.34	5.14
1618	7.1	8	659.6	2.70	0.53	53.92	14.84	0.44	4.23
1787	7.1	10.3	684.9	2.31	0.49	30.15	9.61	0.46	2.97
2622	6.2	16.46	624.9	2.48	0.51	40.82	9.72	0.37	3.32
2703	6.2	17.7	542.6	2.64	0.45	38.25	12.29	0.36	3.92
3470	6.3	13	468.1	3.28	0.46	48.82	8.71	0.41	2.90
3746	7.0	15.29	497	3.69	0.61	39.57	8.30	0.43	2.25
3943	6.6	9.12	616.5	2.38	0.44	44.39	4.52	0.40	2.07
3966	6.6	8.83	420.2	2.47	0.54	51.66	15.44	0.27	5.88
4031	6.5	6.22	497	2.39	0.53	47.72	8.59	0.44	3.25
4096	6.0	4.32	424.8	2.73	0.64	51.63	9.60	0.41	3.24
4106	6.0	15.83	408.9	3.45	0.71	57.40	14.75	0.52	2.79
4132	6.0	4.46	712.8	2.11	0.44	45.35	6.62	0.40	2.86
4137	6.0	13.7	438.3	2.97	0.49	38.86	8.19	0.38	3.25
4229	6.6	10.72	564.3	2.18	0.50	40.73	9.42	0.34	5.00
4456	7.1	8.01	424.8	2.19	0.46	34.04	11.18	0.45	2.84
4457	7.1	4.35	659.6	1.98	0.59	46.32	10.29	0.48	2.54
4477	6.3	6.4	488	2.65	0.60	37.03	10.36	0.32	4.97
4480	6.3	6.27	475	2.91	0.56	56.46	7.13	0.31	3.26
4482	6.3	6.55	552	2.24	0.58	47.13	6.29	0.36	2.89
4489	6.3	15.77	515	3.02	0.62	36.78	12.76	0.42	3.31
5478	6.9	16.96	556	2.17	0.52	32.02	9.16	0.34	4.38

Intensity, duration, and frequency parameters are for the scaled motions. Red highlighted values are more than one standard deviation above the target mean and yellow highlighted values are more than one standard deviation below the target mean value.

Table 3.8: Ground motion parameters of selected acceleration time series of scenario ACR3

NGA #	M_w	R_{rup} (km)	V_{s30} (m/s)	Scaling Factor	PGA (g)	PGV (cm/s)	$D_{5\text{-}95}$ (s)	T_m (s)	I_a (m/s)
572	7.3	51.38	659.6	1.76	0.15	13.35	11.99	0.54	0.37
891	7.3	50.85	684.9	2.79	0.15	17.80	33.24	0.39	1.23
897	7.3	41.43	684.9	2.56	0.16	18.59	36.78	0.31	1.74
1162	7.5	31.74	424.8	1.81	0.15	15.96	10.97	0.54	0.24
1163	7.5	60.05	424.8	2.23	0.15	14.05	21.95	0.81	0.20
1164	7.5	51.95	424.8	2.72	0.14	14.79	32.79	0.60	0.32
1169	7.5	55.3	659.6	2.84	0.14	25.17	38.16	0.45	0.57
1170	7.5	53.43	424.8	2.54	0.16	27.06	14.62	0.50	0.40
1190	7.6	50.53	473.9	2.21	0.13	15.68	36.35	0.58	0.67
1191	7.6	64.15	473.9	2.46	0.14	19.29	43.78	0.52	1.10
1214	7.6	56.93	411.5	2.56	0.11	16.88	35.64	0.61	0.60
1218	7.6	58.75	473.9	2.70	0.13	17.16	40.88	0.56	0.80
1230	7.6	47.53	473.9	2.62	0.13	16.21	30.41	0.59	0.45
1272	7.6	51.15	553.4	2.86	0.14	22.62	18.26	0.55	0.37
1284	7.6	48.35	473.9	2.31	0.14	17.49	23.05	0.56	0.52
1377	7.6	40.49	553.4	2.49	0.15	18.88	33.56	0.57	0.49
1474	7.6	52.98	553.4	2.05	0.17	29.50	16.64	0.59	0.41
1594	7.6	36.7	553.4	2.26	0.14	19.56	37.30	0.50	0.79
1616	7.1	23.41	517	2.68	0.21	18.36	14.32	0.72	0.25
1626	7.7	34.61	659.6	2.28	0.13	33.98	27.88	0.43	0.71
1763	7.1	89.98	724.9	2.63	0.16	21.41	19.40	0.49	0.40
1786	7.1	61.21	684.9	2.32	0.12	37.09	19.38	0.46	0.58
1795	7.1	50.42	684.9	2.47	0.14	18.78	16.72	0.54	0.36
1836	7.1	42.06	684.9	2.40	0.16	20.61	17.06	0.44	0.34
2107	7.9	50.94	963.9	2.29	0.13	18.87	17.34	0.55	0.33
2111	7.9	43	963.9	2.21	0.20	18.54	19.12	0.65	0.31
4716	7.9	30.49	418.2	1.75	0.12	14.25	85.03	0.58	0.61
4740	7.9	22.31	760	1.15	0.15	18.06	60.71	0.33	1.58
4742	7.9	21.85	430	1.52	0.14	18.39	72.08	0.34	1.52
4758	7.9	42.14	508.5	1.60	0.15	15.33	82.33	0.35	0.56
4781	7.9	27.23	430.5	1.29	0.13	15.10	44.34	0.55	0.55
4787	7.9	22.63	474.6	1.03	0.15	15.52	78.28	0.31	1.17
5826	7.2	80.95	659.6	2.76	0.16	14.99	34.60	0.34	1.19
5834	7.2	89.93	424.8	2.55	0.13	14.28	35.16	0.46	0.70
5842	7.2	57.95	659.6	2.69	0.12	23.65	38.16	0.67	0.43
6891	7.0	43.6	659.6	2.14	0.13	10.30	29.02	0.63	0.41
6928	7.0	25.67	659.6	1.33	0.16	22.45	12.21	0.53	0.31
6949	7.0	53.75	424.8	2.18	0.13	13.82	20.87	0.46	0.65
6992	7.0	79.53	424.8	2.10	0.17	16.53	19.61	0.62	0.32
8163	7.2	57.49	659.6	5.00	0.16	18.30	35.86	0.41	1.01

Intensity, duration, and frequency parameters are for the scaled motions. Red highlighted values are more than one standard deviation above the target mean and yellow highlighted values are more than one standard deviation below the target mean value.

.

Table 3.9: Ground motion parameters of selected acceleration time series of scenario SUB

ID#	M_w	R_{rup} (km)	V_{s30} (m/s)	Scaling Factor	PGA (g)	PGV (cm/s)	$D_{5\text{-}95}$ (s)	T_m (s)	I_a (m/s)
SUB32	8.1	147	Rock	1.70	0.106	13.54	18.3	0.75	0.19
SUB35	8.1	190	Rock	1.84	0.087	16.27	17.0	0.81	0.15
SUB40	8.8	77.4	540	0.92	0.294	39.35	38.1	0.60	2.14
SUB42	8.8	96.1	540	1.33	0.215	21.28	40.5	0.45	2.36
SUB52	8.4	158	511	0.96	0.178	17.27	18.1	0.61	0.35
SUB53	9.0	120.5	505	1.92	0.114	16.39	121.8	1.00	0.79
SUB54	9.0	105.3	430	1.65	0.141	13.98	97.1	0.53	1.39
SUB58	9.0	101.9	482	1.11	0.279	25.25	49.7	0.61	1.85
SUB62	8.5	102.78	B/C	1.29	0.266	35.73	52.0	0.80	0.84
SUB64	9.0	112.29	B/C	1.37	0.147	32.28	95.8	0.94	1.20
SUB65	8.3	104.85	611	1.49	0.072	14.37	35.7	0.63	0.16

Intensity, duration, and frequency parameters are for the scaled motions.

Table 3.10: Ground motion parameters of selected acceleration time series of scenario SCR

ID #	M_w	R_{epi} (km)	V_{s30} (m/s)	Scaling Factor	PGA (g)	PGV (cm/s)	$D_{5\text{-}95}$ (s)	T_m (s)	I_a (m/s)
SCR2	7.0	19.6	A	0.32	0.203	9.43	5.7	0.27	0.22
SCR3	7.0	17.0	A	0.32	0.249	7.64	7.0	0.22	0.42
SCR5	6.0	17.0	A	0.66	0.329	7.67	1.5	0.18	0.23
SCR14	5.7	57.5	B	1.49	0.198	10.50	18.1	0.47	0.29
SCR15	5.7	53.5	A	5.71	0.547	6.00	31.7	0.08	4.92
SCR23	4.4	6.1	659.6	2.03	0.755	12.10	0.5	0.18	0.31
SCR25	6.9	6.1	659.6	0.49	0.179	16.04	7.2	0.46	0.23
SCR30	4.6	27.7	2000	6.13	0.384	7.99	12.2	0.10	0.41
SCR31	4.6	14.8	2000	13.95	0.421	9.04	22.5	0.10	0.93
SCR38	5.9	91.4	A	2.88	0.387	10.36	8.4	0.18	0.75
SCR44	7.4	2.0	767	0.20	0.161	17.51	15.3	0.47	0.40

Intensity, duration, and frequency parameters are for the scaled motions.

Table 3.11: Average ground motion parameters for selected suites

Scenario	PGA (g)	PGV (cm/s)	$D_{5\text{-}95}$ (s)	T_m (s)	I_a (m/s)	T_v (s)
ACR1	0.66	75.65	9.39	0.52	3.52	2.91
ACR2	0.68	55.23	10.62	0.46	6.29	
ACR3	0.19	21.52	31.99	0.51	1.52	
SUB	0.17	22.34	53.1	0.7	1.04	
SCR	0.35	10.39	11.83	0.25	0.83	

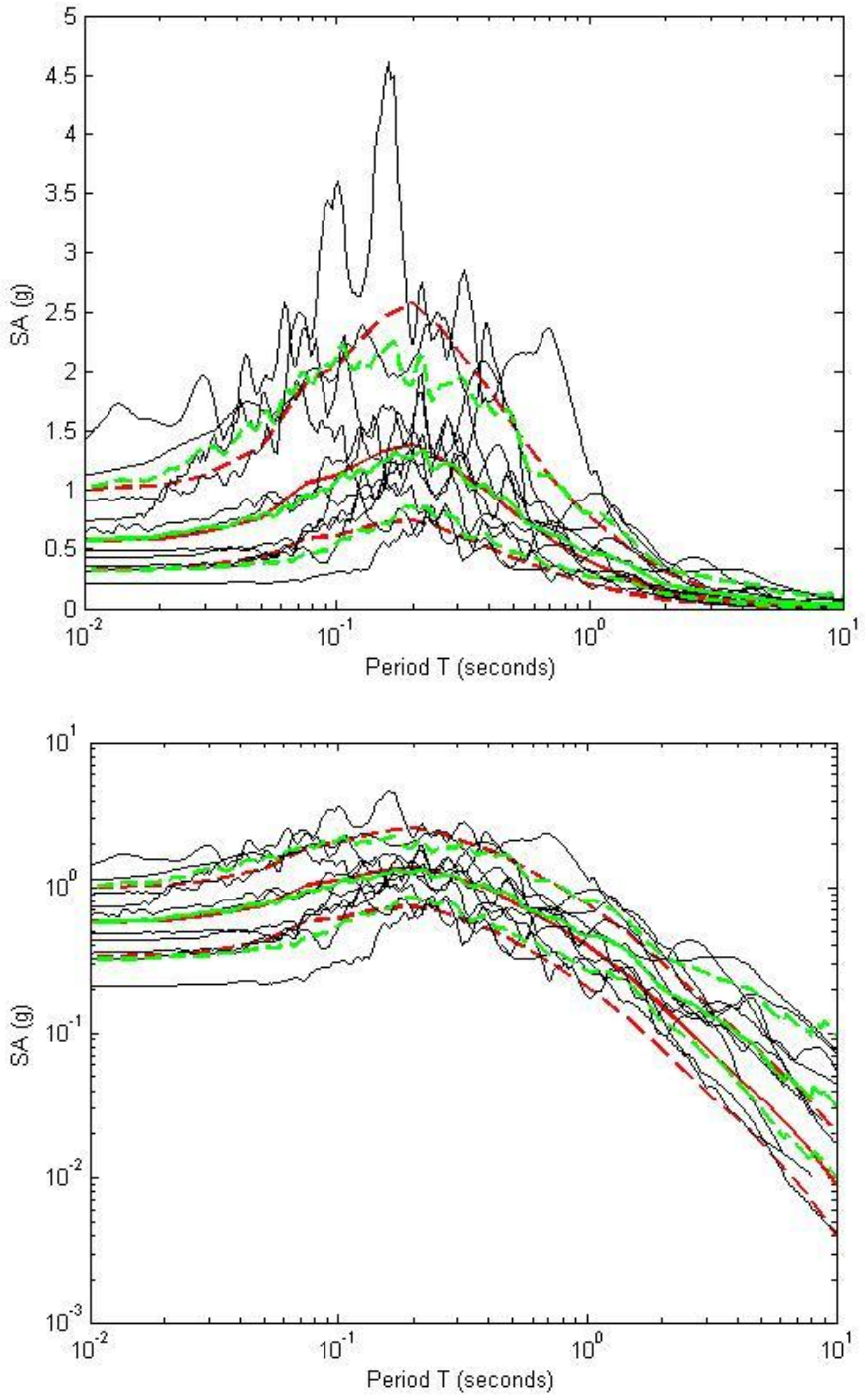

Figure 3.1: Summary of response spectra for scenario ACR1 suite of motions (black lines) with their mean and plus and minus one standard deviation spectra (green) and the target spectra (red lines) shown in a) semi-log and b) log-log plots.

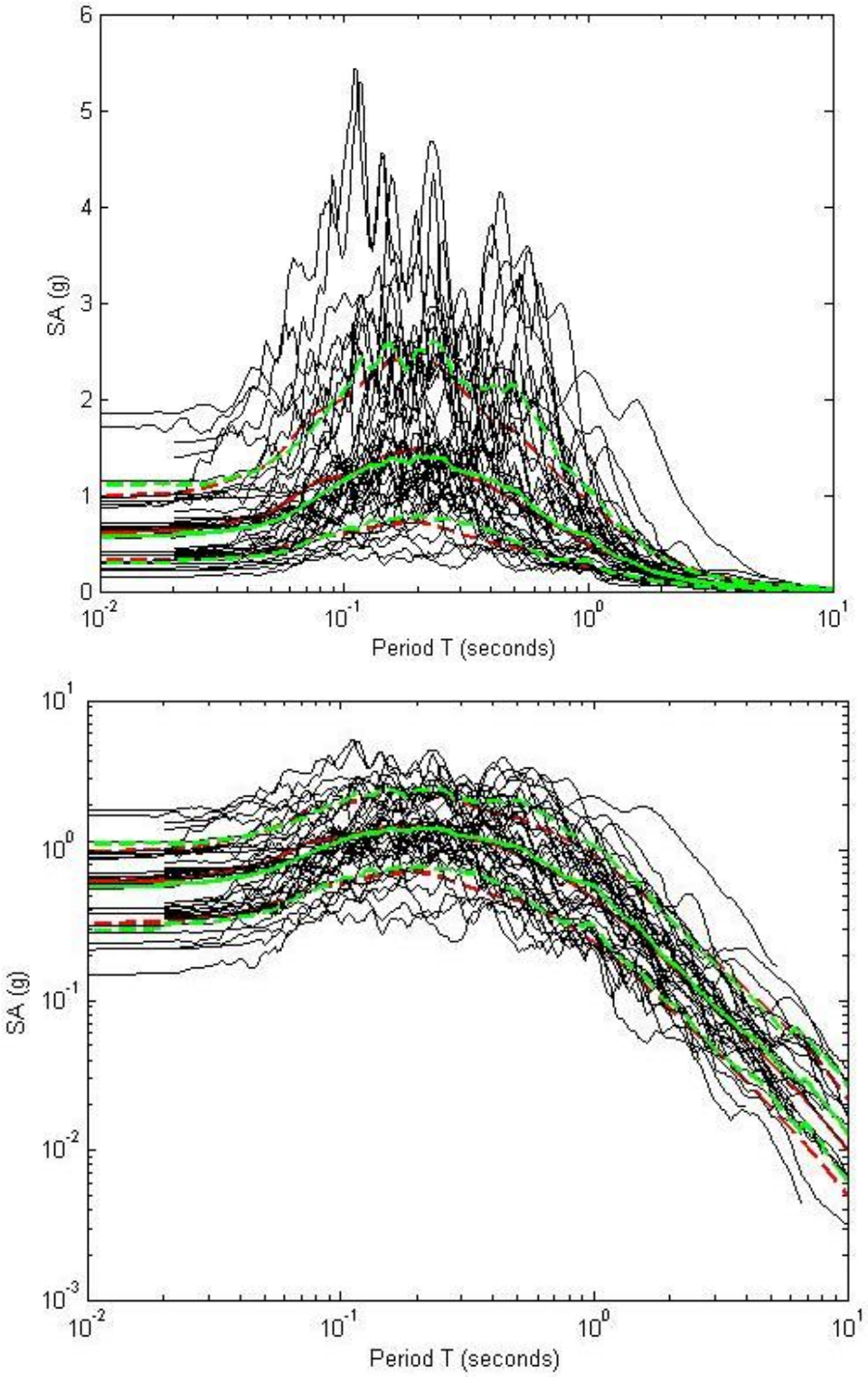

Figure 3.2: Summary of response spectra of selected ground motions for scenario ACR2 motions (black lines) with their mean and plus and minus one standard deviation spectra (green) and the target spectra (red lines) shown in a) semi-log and b) log log plots.

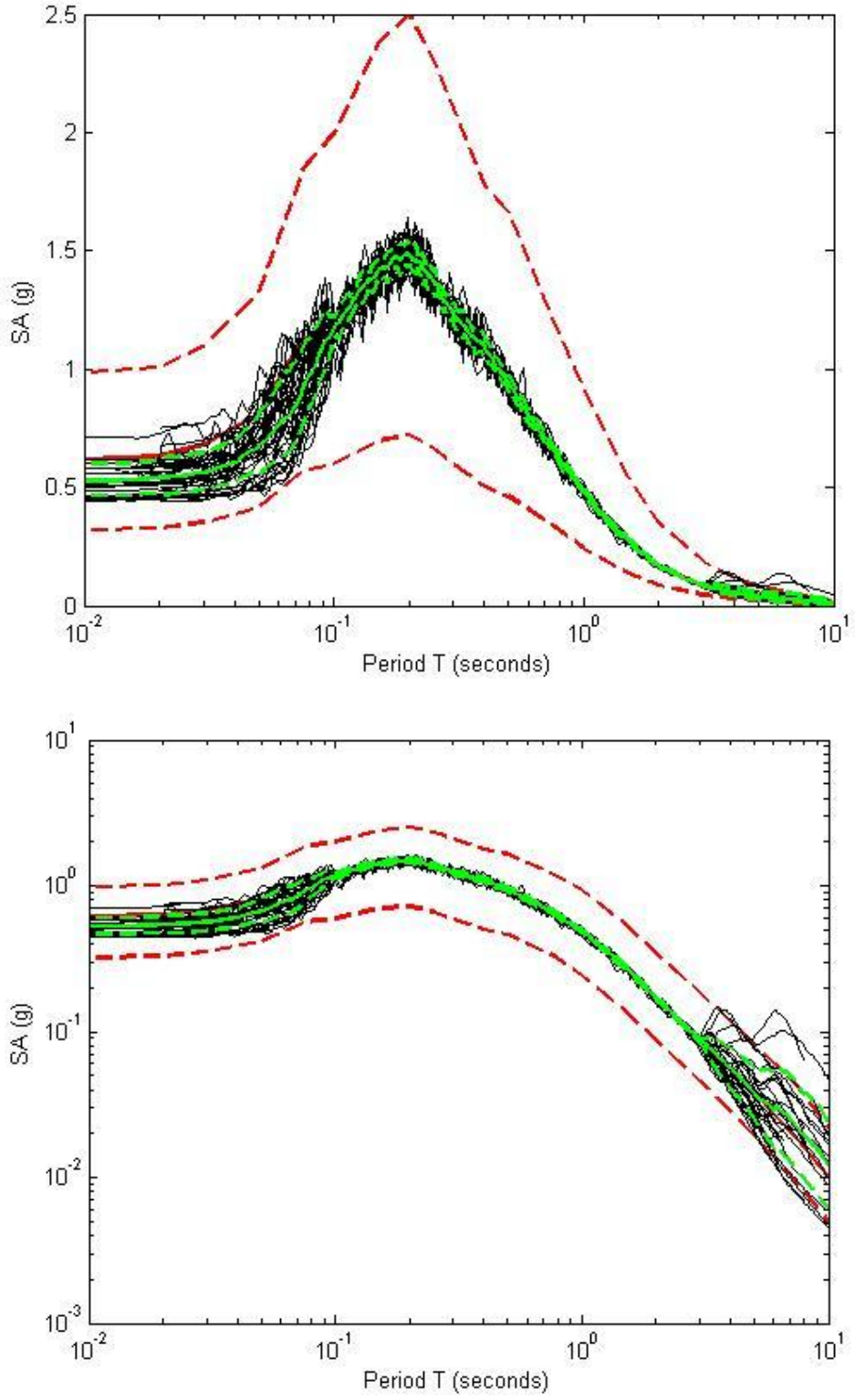

Figure 3.3: Summary of response spectra of selected matched ground motions for scenario ACR2M motions (black lines) with their mean and plus and minus one standard deviation spectra (green) and the target spectra (red lines) shown in a) semi-log and b) log-log plots.

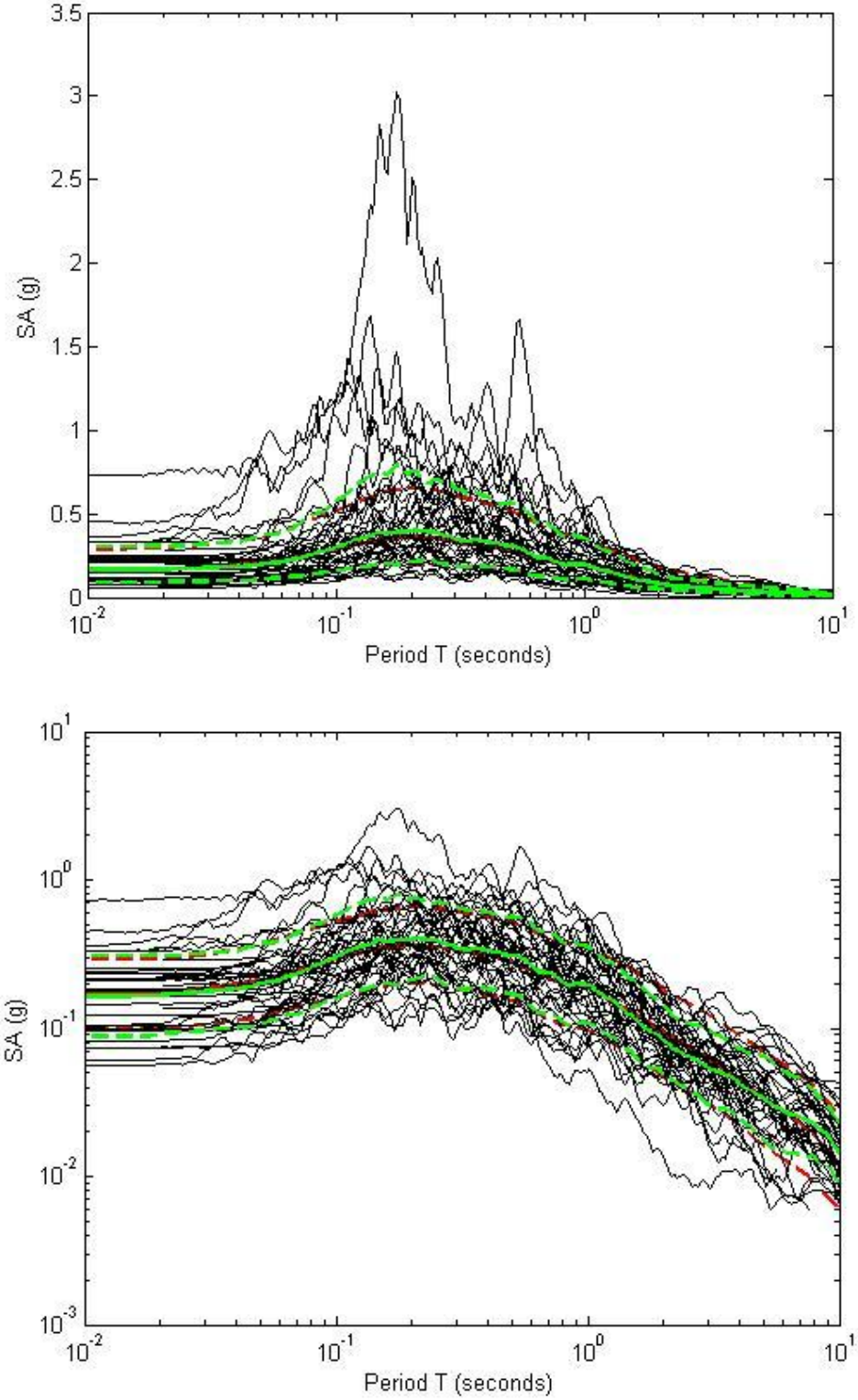

Figure 3.4: Response spectra of final 40 selected scaled scenario ACR3 motions (black lines) with their mean and plus and minus one standard deviation spectra (green) and the target spectra (red lines) shown in A) semi-log and B) log log plots.

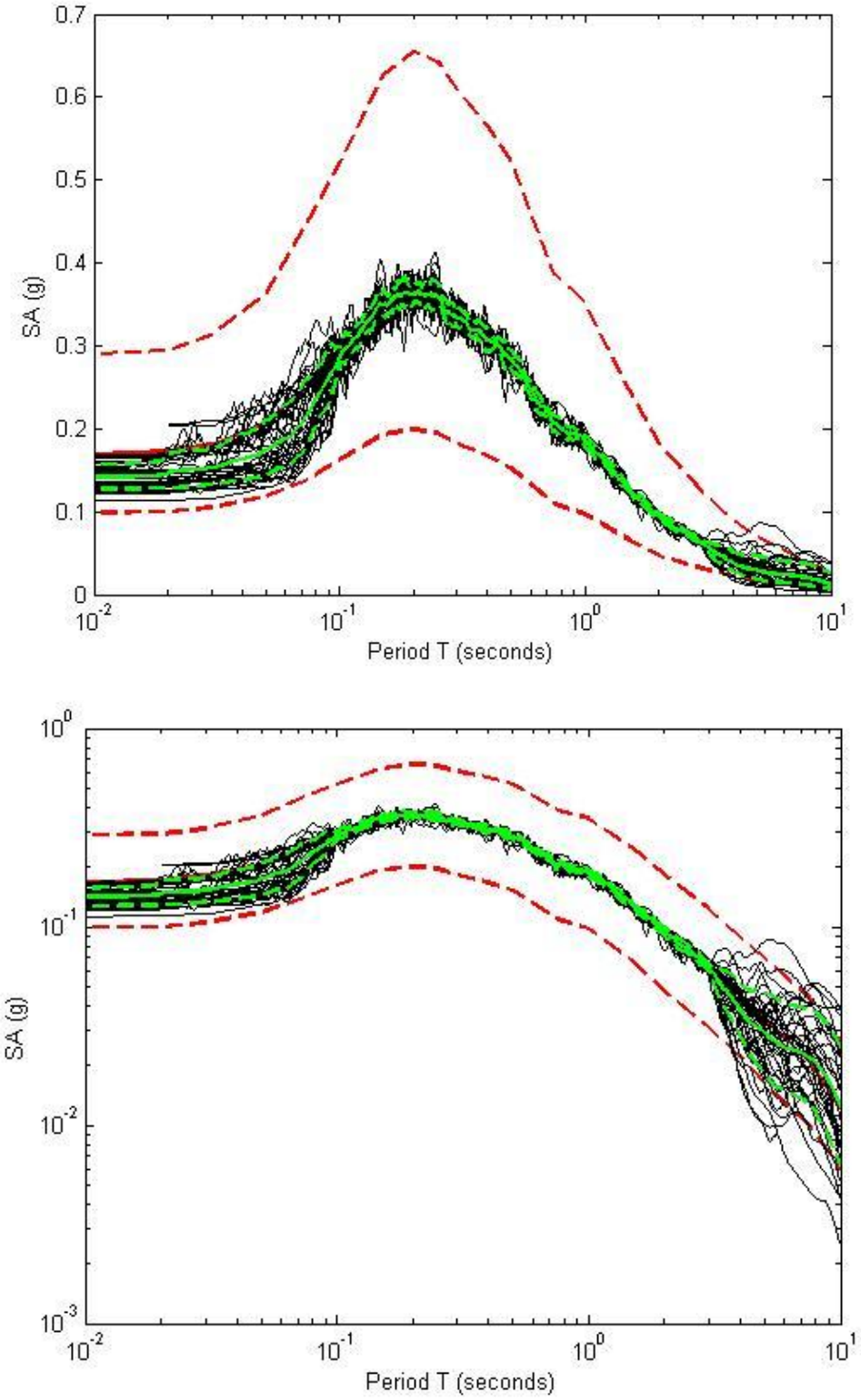

Figure 3.5: Summary of response spectra of selected matched ground motions for scenario ACR3M (black lines) with their mean and plus and minus one standard deviation spectra (green) and the target spectra (red lines) shown in a) semi-log and b) log-log plots.

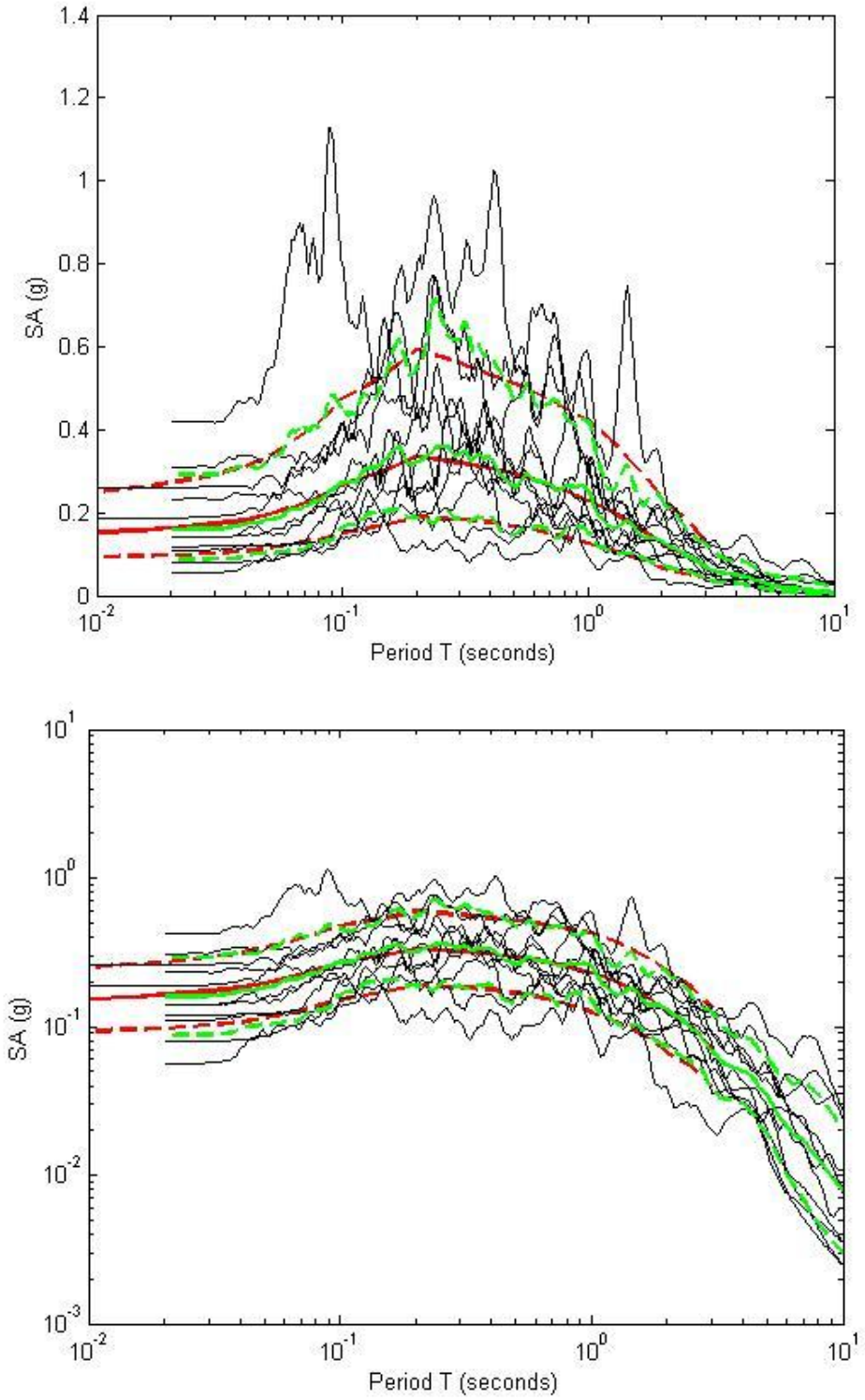

Figure 3.6: Summary of response spectra of selected matched ground motions for scenario SUB (black lines) with their mean and plus and minus one standard deviation spectra (green) and the target spectra (red lines) shown in a) semi-log and b) log-log plots.

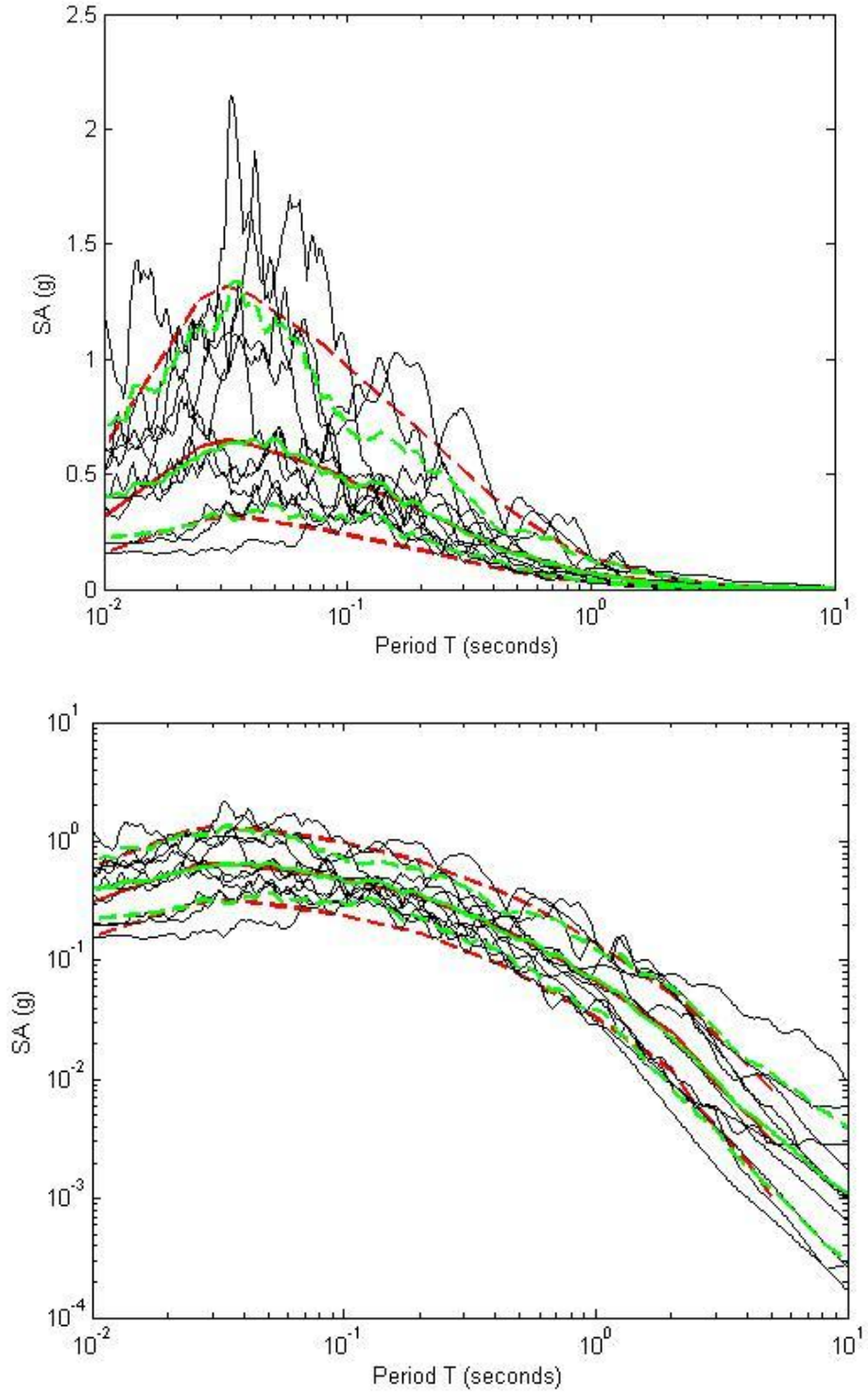

Figure 3.7: Summary of response spectra of selected matched ground motions for scenario SCR (black lines) with their mean and plus and minus one standard deviation spectra (green) and the target spectra (red lines) shown in a) semi-log and b) log-log plots.

CHAPTER 4: A UNIFIED MODEL FOR ESTIMATING THE IN-SITU SMALL STRAIN SHEAR MODULUS OF CLAYS, SILTS, SANDS, AND GRAVELS

This chapter presents a model to estimate the in-situ small strain shear modulus of clays, silts, sands, and gravels. First, a model to predict the laboratory small strain shear modulus ($G_{max,lab}$) is developed from a mixed effects regression of a collected database that contains 1680 tests on 331 different soils from 28 studies. Second, a separate database was collected to estimate the in-situ small strain shear modulus ($G_{max,in\text{-}situ}$) from $G_{max,lab}$. The two models were then combined to create a model to estimate $G_{max,in\text{-}situ}$ directly from soil parameters. This study investigated the influence of the mean effective confining pressure, void ratio, overconsolidation ratio, plasticity index, fines content, coefficient of uniformity, median grain size, laboratory test type and sample type, and in-situ test type on the small strain shear modulus. Finally, the unified model was validated and compared with existing models using a third database. The residuals of the proposed model had a smaller standard deviation and less biased results for the validation database than the comparison models. The proposed model is dependent on the mean effective confining pressure, void ratio, overconsolidation ratio, plasticity index, fines content, and coefficient of uniformity. The standard deviation was also estimated so the uncertainty of the small strain shear modulus can be included in probabilistic studies. This study found the standard deviation to be independent of the parameters investigated.

4.1 Introduction

The small strain shear modulus (G_{max}) of soils is an essential element in many aspects of geotechnical engineering. For example, G_{max} is necessary to estimate the deformations of excavations, tunnels, and foundations under repetitive and rapidly applied loads such as dynamic compaction, machine vibration, and ocean waves. The small strain shear modulus is also a fundamental component of many seismic analyses, including hazard analysis, seismic site response analysis, and soil–structure interaction.

The small strain shear modulus is defined as the shear stress divided by the shear strain at strains smaller than the linear cyclic threshold shear strain, γ_{tl} (Vucetic, 1994). At strains smaller than γ_{tl} soils exhibit linear elastic behavior and the shear modulus is a constant maximum value, G_{max}. The small strain shear modulus is related to the shear wave velocity V_s of the soil through equation (4.1):

$$G_{max} = \rho \times V_s^2 \tag{4.1}$$

where ρ is the mass of the soil. Using equation (4.1), G_{max} can be estimated from in-situ seismic measurements of V_s. However, in-situ tests are often costly and time consuming compared with simple laboratory tests performed on borehole cuttings that measure soil characteristics such as plasticity index, coefficient of uniformity, water content, etc. In addition, in-situ tests measure an average V_s value for large volumes of soil and can miss variations in V_s due to thin layers.

Instead of performing in-situ seismic measurements, previous researchers (e.g. Hardin, 1978; Jamiolkowski et al., 1991; Menq, 2003) developed empirical relations to estimate G_{max}. These models are based on results from dynamic laboratory tests. Results from laboratory tests consistently give smaller values of G_{max} than in-situ tests due to sample disturbance, cementation, and confinement time (Lefebvre et al., 1993; Darendeli 2001). It is common practice to adjust the results from empirical models developed from laboratory results with a constant factor (e.g. Chiara and Stokoe, 2006) or a time dependent factor (e.g. Anderson and Stokoe, 1978) to account for the discrepancy between in-situ and laboratory values of G_{max}.

Most existing models are based on small databases that lack a broad range of soil types and parameters. These models are often only accurate for certain soils or within a narrow range of soil parameters. In addition, few models give the uncertainty of the prediction of G_{max}. This chapter presents a unified model for estimating the in-situ small strain shear modulus of clays, silts, sands, and gravels that also tracks the uncertainty of the prediction.

The unified model was developed in two steps. First, a model to predict the laboratory small strain shear modulus ($G_{max,lab}$) was developed from a mixed effects regression of a collected database that contains 1680 tests on 331 different soils from 28 studies. Second, a separate database was collected to estimate the in-situ small strain shear modulus ($G_{max,in\text{-}situ}$) from $G_{max,lab}$. This study chose this approach rather than creating a model for $G_{max,insitu}$ directly for several reasons. In laboratory tests of G_{max} parameters such as the confining pressure, void ratio, coefficient of uniformity, etc., are known exactly and their effect on G_{max} can be isolated and tested. For example, the effect of confining pressure on G_{max} can be examined directly in the laboratory by conducting tests at different confining pressures while keeping all other parameters the same. In addition, the new $G_{max,lab}$ model can be compared to existing models for $G_{max,lab}$.

4.2 Review of Previous Studies

Previous studies have investigated the effect of numerous different parameters on the small strain shear modulus. Hardin (1978) suggested that the small strain shear modulus could be expressed as:

$$G_{max}/p_a = A \times OCR^k \times f(e) \times (\sigma'_m/p_a)^n \qquad (4.2)$$

where A and n are constants, OCR is the overconsolidation ratio, k is a function of plasticity index (PI), f(e) is a function of the void ratio e, σ'_m is the mean effective confining pressure, and p_a is atmospheric pressure in the same units as G_{max} and σ'_m. Other parameters studied by different researchers include confinement time (t_g), excitation frequency (f), number of loading cycles (N), fines content (FC, defined as the percent weight of soil with grain size < 0.075mm), the median grain size (D_{50}), and the coefficient of uniformity (Cu). This section summarizes the effect of each of the above parameters on G_{max} as determined in previous studies.

Chung et al. (1984), Alarcon-Guzman et al. (1989), and Saxena and Reddy (1989) found that as the mean effective confining pressure of clean sands increases, the small strain shear modulus increases, and as the void ratio increases, the small strain shear modulus decreases. Kim and

Novack (1981), Kokusho et al. (1982), and Kallioglou et al. (2008) found the same for cohesive soils. All of the models for G_{max} reviewed in this study use a power law to describe the relationship between G_{max} and the mean effective confining pressure, as shown in equation (4.2). Hardin (1978) and the ROSRINE study (Nigbor, 2012) found that for cohesive and cohesionless soils the average value of n is about 0.5.

The effect of the void ratio on G_{max} is not as uniformly described. Hardin (1978) proposed that $f(e) = 1/(0.3 + 0.7e^2)$ and Jamiolkowski et al. (1991) suggested that $f(e) = 1/(e^{1.3})$. Both models give roughly the same response from $0.5 < e < 1.5$ and converge when $e = 1$. However, at values of the void ratio outside this range the models diverge by more than 10%.

Hardin (1978), Vucetic and Dobry (1991), and Darendeli (2001) argued that as OCR increases G_{max} increases for cohesive soils. Hardin (1978) also suggested that the effect of OCR increases with plasticity index. Kokusho (1982) found that the effect of OCR cannot be explained by void ratio alone, and that as OCR increases G_{max} increases by a constant rate, independent of plasticity index. Alarcon-Guzman et al. (1989) and Lo Presti et al. (1993) found that OCR has no effect on G_{max} for cohesionless soils. This is consistent with the model proposed by Hardin (1978), where k decreases to zero for non-plastic soils.

In addition to the effect of plasticity index on the effect of OCR, Kagawa (1992) and Kallioglou et al. (2008) reported that as the plasticity index increases G_{max} decreases. Kagawa (1992) tested soft marine clays with PI between 25 and 64, and Kallioglou et al. (2008) tested soils from Greece with PI between 5 and 66. Okur and Ansal (2007) measured the small strain shear modulus of cohesive soils from Turkey with PI values between 9 and 40 and found that plasticity index has no effect on G_{max}.

Anderson and Stokoe (1978), EPRI (1993), and the ROSRINE study (Nigbor, 2012), found that as the confinement time increases the small strain shear modulus increases for cohesive soils and cohesionless soils. Schmertmann (1991) reported that the percent change in the small strain shear modulus per log cycle of time is 1 to 3% for sands, 3 to 6% for silts, and 6 to 40% for clays. Kokusho (1982) found that as the plasticity index increases the effect of the confinement time on G_{max} increases, and that as D_{50} increases the effect of confinement time on G_{max} decreases. This is consistent with the findings that confinement time has a greater effect on cohesive soils than cohesionless soils. Kim and Novack (1981) postulated that the effect of ageing was due to strengthening of particle bonding in clayey soils. Anderson and Stokoe (1978) and Athanasopoulos (1993) also noted that as the OCR increases the effect of confinement time on G_{max} decreases.

Darendeli (2001) reported that for every order of magnitude increase in the excitation frequency, the small strain shear modulus increases by about 10% for cohesive soils. Shibuya et al. (1995) found that for cohesive soils the excitation frequency has a negligible effect on G_{max} when it is varied between 0.005 and 0.1 Hz. Lo Presti et al. (1993, 1997), and Yasuda and Matsumoto (1993) found that the excitation frequency has no effect on sands. Menq (2003) also found that the excitation frequency had no effect on the G_{max} of dry sands, however, for saturated sands, he found that G_{max} measured at $f = 400$ Hz with a resonant column device was about 20% higher than G_{max} measured when $f = 1$ Hz using a torsional shear device.

Darendeli (2001) and Lanzo (2009) found that the number of loading cycles has a negligible effect on the small strain shear modulus of cohesive soils. Alarcon-Guzman et al. (1989) and Lo Presti et al. (1993, 1997) found that the number of loading cycles has no effect on the small strain shear modulus of cohesionless soils either.

Yamada et al. (2008) measured the G_{max} of soils with fines content between 25.3% and 100%. They found that as the fines content increases, G_{max} decreases. Iwasaki and Tatsuoka (1977) measured the G_{max} of sands with fines content between 0% and 33%. They also found that as the fines content increases, G_{max} decreases.

Ishihara (1996) found that the G_{max} of cohesionless soils increases as D_{50} increases. Seed et al. (1984) and Yasuda and Matsumoto (1993) found that in general, gravels have greater G_{max} than sands, and that this discrepancy is due to particle size, which can be related to D_{50}. Menq (2003) found that as D_{50} increases the effect of void ratio on the G_{max} of cohesionless soils increases. In other words, the void ratio function f(e) is dependent on D_{50}, and as D_{50} increases the absolute value of f(e) increases.

Iwasaki and Tatsuoka (1977), Ishihara (1996), and Menq (2003) found that as the coefficient of uniformity increases, the small strain shear modulus decreases independent of void ratio for cohesionless soils. In addition, Menq (2003) observed that as Cu increases the effect of the mean effective confining pressure on G_{max} increases for cohesionless soils.

Table 4.1 lists the parameters outlined above and their effects on the small strain shear modulus for cohesive and cohesionless soils. An upward facing arrow indicates that as the parameter in the column marked 'controlling parameter' increases, G_{max} increases. A downward facing arrow specifies that as the 'controlling parameter' increases, G_{max} decreases. A blank cell means that this investigation is not aware of any study measuring the given relationship. The cells under the column 'cross correlations' indicate that as the 'controlling parameter' increases, the effect of the parameter under 'cross correlations' on G_{max} either increases (upward facing arrow), or decreases (downward facing arrow). For example, as the plasticity index increases, the effects of t_g and OCR on G_{max} increase, and as D_{50} increases, the effect of t_g on G_{max} decreases and the effect of e on G_{max} increases for cohesionless soils.

4.3 Collected Database for Laboratory Small Strain Shear Modulus

This investigation collected data from 1680 tests on 331 different soils from 28 studies that measured G_{max} in the laboratory. Table 4.2 lists the references of the studies from where the data were collected, as well as the test, sample, and soil type. Figure 4.1a shows the distribution of soil types in the $G_{max,lab}$ database according to their USCS classification and whether the soil was an 'undisturbed' sample or reconstituted in the laboratory. Figure 4.1b shows the distribution of the number of tests according to soil type.

Figure 4.2 shows the distribution of the grain size and plasticity characteristics of the collected soils and Figure 4.3 shows the data collected for each individual test. The collected values of $G_{max,lab}$ were measured using six different testing devices; resonant column (RC), torsional shear

(TS), cyclic triaxial (CT), direct simple shear (DSS), bender element (BE), and flat plate dilatometer (DMT). The majority of the measured $G_{max,lab}$ values are from resonant column devices. Figure 4.4 shows scatter plots of the void ratio versus confining pressure and plasticity index versus liquid limit.

The plasticity index and USCS designation was known for each of the 331 soils, however, the value of the fines content was known for only 212 soils. When no fines content was known for a soil the average value of the USCS designation was used. Specifically, for soils with USCS designations of SW, SP, GW, and GP, the fines content was estimated as 2.5%, for coarse grained soils with dual classification (i.e. SP-SM, SW-SM etc) fines content was estimated as 8.5%, for soils with USCS designations of SM, SC, GM, and GC, fines content was estimated as 31%, and for soils with USCS designations of ML, MH, CL, and CH, fines content was estimated as 75%.

The coefficient of uniformity was known only for soils with $FC < 50\%$, and only 102 of the 331 soils reported D_{50} values. There was not enough data regarding the excitation frequency, number of loading cycles, or confinement time to estimate their effects on the small strain shear modulus. However, as mentioned in the previous section, several studies have shown that the number of loading cycles has a negligible effect on the small strain shear modulus and that the effect of the excitation frequency is small (10% change or less in G_{max} for every order of magnitude change in the excitation frequency). The effect of confining time was assumed to be negligible for the $G_{max,lab}$ database because a majority of the tests were either conducted at confining pressures greater than in-situ pressures or were from reconstituted samples.

4.4 Short Explanation of Mixed Effects Regression

Previous studies derived models for $G_{max,lab}$ using least squares regression, which gives equal weight to each test. This method of analysis is correct when regression is done on a single soil or when there are an equal number of tests per soil. In the collected $G_{max,lab}$ database, however, there are soils with more than 100 tests, and many soils with only one recorded test. Therefore, it is incorrect to analyze the data with a least squares regression because it would give an incorrect weight to each soil. Instead, a mixed effects model (Pinheiro and Bates, 2000) is used to determine regression coefficients for the $G_{max,lab}$ model.

Mixed effects regression is a maximum likelihood method that accounts for correlations in the data within specified groups. These models account for both fixed and random effects. The random effects account for correlations within groups that the modeler wants to consider but that they do not want to model explicitly. The fixed effects are parameters in the statistical model that are estimated explicitly. Fixed effects should be fixed for the entire population and not dependent on any given group whereas the random effects are group dependent. Researchers that develop ground motion prediction equations (GMPEs) commonly use mixed effects regression. The groups for the development of GMPEs are individual earthquakes; for the $G_{max,lab}$ model the data is grouped by soil, which gave a total of 331 groups. All mixed effects regression were performed in the program MATLAB (MATLAB, 2012), which has a built in mixed effects regression sub routine.

In mixed effects models, the error is divided into within group and between group terms. The within group residual (ε) represents the difference between any single data point and the median prediction for that group, while the between group residual (η) represents the difference between the median prediction for a single group and the median prediction based on the entire database. The within group and between group error terms are assumed to be independent normally distributed with standard deviation ϕ and τ respectively. The total standard deviation for the model is computed as $\sigma = \sqrt{\phi^2 + \tau^2}$.

The mixed effects model was applied to the $G_{max,lab}$ database as shown in equation (4.3):

$$ln\left[G_{max,lab,i,j}\right] = ln\left[f\left(\psi_i, \theta_{i,j}\right)\right] + \eta_i + \varepsilon_{i,j} \quad (4.3)$$

where $G_{max,lab,i,j}$ is the measured $G_{max,lab}$ of the i^{th} soil and j^{th} test, $f(\psi_i, \theta_{i,j})$ is the predictive model for $G_{max,lab}$ with soil parameters ψ_i and test parameters $\theta_{i,j}$, η_i is the between soil residual for the i^{th} soil and $\varepsilon_{i,j}$ is the within soil residual for the i^{th} soil and j^{th} test. Soil parameters ψ_i include plasticity index, fines content, median grain size, coefficient of uniformity, and sample type (reconstituted or 'undisturbed'). Test parameters $\theta_{i,j}$ include mean effective confining pressure, void ratio, overconsolidation ratio, and test type (resonant column, torsional shear etc.).

The natural logarithm of the small strain shear modulus was used because the natural logs of the within and between soil residuals were found to be normally distributed per the χ^2 test at a significance level of 95%. All of the residuals and standard deviations are therefore in natural log units.

4.5 Development of the Model to Estimate $G_{max,lab}$

The relationship between the small strain shear modulus and void ratio was analyzed first by performing a mixed effects regression for tests with OCR = 1 and mean effective confining pressure = 1 atmosphere. This study determined coefficients for both the Hardin (1978) void ratio model (equation (4.4)) and the model proposed by Jamiolkowski et al. (1991) (equation (4.5)) shown below, where a_1, a_2, a_3, and c_1 and c_2 are constants.

$$ln\left(G_{max,lab,i,j}\right) = ln\left[a_1/\left(a_2 + e_{i,j}^{a_3}\right)\right] + +\eta_i + \varepsilon_{i,j} \quad (4.4)$$

$$ln\left(G_{max,lab,i,j}/p_a\right) = ln\left[c_1 \times e_{i,j}^{c_2}\right] + \eta_i + \varepsilon_{i,j} \quad (4.5)$$

The power model proposed by Jamiolkowski et al. (1991) gave a slightly smaller (0.414) within soil standard error than the Hardin (1978) model (0.432). This study conducted the remaining analyses with both models and found that the Jamiolkowski et al. (1991) void ratio model also gave a smaller standard deviation for the final model than the void ratio formulation proposed by Hardin (1978). The rest of the paper uses the Jamiolkowski et al. (1991) formulation for the void ratio and the coefficients listed were derived for this model.

Table 4.3 lists the value of c_2 and its standard error. The coefficient is similar to that proposed in the original formulation by Jamiolkowski et al. (1991). Figure 4.5 shows the data for OCR = 1 and mean effective confining pressure = 1 atmosphere with equation (4.5).

Menq (2003) reported that the value of c_2 is dependent on D_{50} for cohesionless soils. To study the influence of soil parameters such as D_{50} on c_2, this study separated the data into different bins according to the soil parameter and conducted mixed effects regression separately for each bin. Figure 4.6 shows coefficient c_2 determined for each bin according to PI, FC, D_{50}, and Cu. The circle is the median value of c_2 and the error bars are the standard error. The values are placed in the center of their respective bins on the x-axis. Figure 4.6 shows that coefficient c_2 has no clear trend with PI, FC, D_{50}, or Cu for the soils investigated in this study.

Figure 4.7 shows the within soil residuals found from subtracting the $\ln(G_{max,lab})$ predicted with equation (4.5) from the measured $\ln(G_{max,lab})$ for all soils with OCR = 1. As expected based on previous studies, the within soil residuals show an increasing trend with mean effective confining pressure. Menq (2003) found that the influence of σ'_m on $G_{max,lab}$ was dependent on Cu. To quantify the effect of σ'_m on $G_{max,lab}$ and examine the cross correlation with soil parameters PI, FC, D_{50}, and Cu, this study separated the data into different bins according to the soil parameter and conducted mixed effects regression separately for each bin, using equation (4.6) for all tests in the database with OCR = 1. The value of coefficient c_2 was kept fixed at the value listed in Table 4.3. Figure 4.8 shows the results.

$$ln\left(G_{max,lab,i,j}/p_a\right) = ln\left[c_1 \times e_{i,j}^{c_2} \times \left(\sigma'_{m,i,j}/p_a\right)^n\right] + \eta_i + \varepsilon_{i,j} \qquad (4.6)$$

Figure 4.8d shows that the value of n has a clear increasing trend with Cu. In addition, Figure 4.8d shows that when soils with FC $\geq$ 30% are given a dummy value of Cu = 1 they fit the trend described by the other soils. To model this trend equation (4.7) was substituted for n in equation (4.6) and a mixed effects regression was conducted for all tests with OCR = 1, keeping c_2 fixed at the value listed in Table 4.3, and giving soils with FC $\geq$ 30% a dummy value of Cu = 1.

$$n = c_3 \times {Cu_i}^{c_4} \qquad (4.7)$$

Table 4.3 lists the values of c_3 and c_4 found with mixed effects regression and their standard errors. Figure 4.8d shows that equation (4.7) and the model derived for n by Menq (2003) for cohesionless soils are similar.

The effect of OCR on $G_{max,lab}$ was examined next. This investigation performed a mixed effects regression using equation (4.8) for all tests in the database, keeping the values of c_2, c_3, and c_4 fixed at the values listed in Table 4.3. This study examined the effects of PI, FC, D_{50}, and Cu on the value of coefficient k in the same manner as for coefficient c_2 and n. The results, shown in Figure 4.9, indicate that the value of k has a clear increasing trend with PI.

$$ln\left(G_{max,lab,i,j}/p_a\right) = ln\left[c_1 \times e_{i,j}^{c_2} \times \left(\sigma'_{m,i,j}/p_a\right)^n \times OCR_{i,j}^k\right] + \eta_i + \varepsilon_{i,j} \qquad (4.8)$$

To model the effect of PI on the value of coefficient k, a power relation similar to that proposed by Hardin (1978) was chosen as shown below:

$$k = c_5 \times \left(\frac{PI_i}{100}\right)^{c_6} \leq 0.5 \tag{4.9}$$

Equation (4.9) was substituted into equation (4.8) and a mixed effects regression was conducted for all tests in the database, keeping the values of c_2, c_3, and c_4 fixed at the values listed in Table 4.3. Table 4.3 lists the values of c_5 and c_6 and their standard errors.

Figure 4.9d shows the relation for k derived in this study and from Hardin (1978). This study found that as PI increases k increases but at a different rate than that given by Hardin (1978). The value of k was capped at 0.5, which is the same as in the relation proposed by Hardin (1978), because the trend appears to level off and the data do not support a continuation of the curve.

Figure 4.10 shows the between soil residuals for equation (4.8) plotted versus plasticity index, fines content, median grain size, and coefficient of uniformity. There is a slight decreasing trend with plasticity index, fines content, and coefficient of uniformity, which agrees with the results of the studies done by Kagawa (1992) and Kallioglou et al. (2008); Yamada et al. (2007); and Iwasaki and Tatsuoka (1977) and Menq (2003), respectively. There appears to be no trend with D_{50}, which contradicts the findings of Seed et al. (1984) and Ishihara (1996).

To quantify the effects of the between soil parameters this study separated the between soil residuals into different bins according to fines content. When the between soil residuals are distributed in this manner there is no trend with PI for bins with FC < 30%, and no trend with Cu for soils with FC > 30%. Other than this break at FC = 30%, the trends for PI and Cu do not show dependence on fines content. Based on this analysis, this study developed equation (4.10) and equation (4.11) as shown below:

$$A = (FC_i + 1)^{c_7} \times \left[Cu_i^{c_8} \times B + (PI_i + 1)^{c_9} \times (1 - B)\right] \tag{4.10}$$

$$B = \begin{cases} 1 & for\ FC < 30\% \\ 0 & for\ FC \geq 30\% \end{cases} \tag{4.11}$$

where FC is in percent. To calculate the effect of FC, PI, and Cu on $G_{max,lab}$, this study substituted equation (4.10) into equation (4.8) to give equation (4.12), then performed a mixed effects regression using equation (4.12) for all tests in the database. The values of c_2, c_3, c_4, c_5, and c_6 were kept fixed at the values listed in Table 4.3.

$$\begin{aligned} ln\left(G_{max,lab,i,j}/p_a\right) \\ = ln\Big[c_1 \times e_{i,j}^{c_2} \times \left(\sigma'_{m,i,j}/p_a\right)^n \times OCR_{i,j}^k \times (FC_i + 1)^{c_7} \\ \times \left[Cu_i^{c_8} \times B + (PI_i + 1)^{c_9} \times (1 - B)\right]\Big] + \eta_i + \varepsilon_{i,j} \end{aligned} \tag{4.12}$$

The mixed effects regression calculated a value of the PI coefficient c_9 = -0.012, with a standard error of .021. Because the standard error of c_9 is greater than the actual value of coefficient c_9,

this indicates that PI is not a good predictor of $G_{max,lab}$ in the context of equation (4.12). As a result, equation (4.12) was modified to the equation given below:

$$\begin{aligned} ln\left(G_{max,lab,i,j}/p_a\right) \\ = ln\Big[c_1 \times e_{i,j}^{c_2} \times \left(\sigma'_{m,i,j}/p_a\right)^n \times OCR_{i,j}^k \times (FC_i + 1)^{c_7} \\ \times \left[Cu_i^{c_8} \times B + (1 - B)\right]\Big] + \eta_i + \varepsilon_{i,j} \end{aligned} \tag{4.13}$$

which is the same as equation (4.12) except without the PI term. This study then performed a mixed effects regression using equation (4.13) and all tests in the database. The values of c_2, c_3, c_4, c_5, and c_6 were kept fixed at the values listed in Table 4.3. Figure 4.11 shows the between soil residuals for equation (4.13). It shows that there is no trend with PI, FC, D_{50} or Cu, which further supports the decision to drop the PI term from equation (4.12). Section 4.6 discusses the appropriateness of each parameter in detail. Table 4.3 lists the values and standard errors of c_7 and c_8.

This investigation allowed coefficient c_1 to vary with each model. Table 4.4 lists the different values of c_1 for each equation. It is important to remember that equation (4.5) was derived for tests with $\sigma'_m = 1$ atmosphere and OCR = 1, equation (4.6) for tests with OCR = 1, and equations (4.8) and (4.13) for all tests in the database.

To determine whether to distinguish between reconstituted and 'undisturbed' samples, this study performed a one way analysis of variance (ANOVA) test. An ANOVA test compares the means of different sets of data and uses their variances to determine whether the means are significantly different. The output is a p-value, which is the probability that data taken from the same population could result in the differences between the observed means of the datasets. A small p-value indicates that the two datasets are statistically different, whereas a large p-value means they are not. Typical standards for small p-values are 0.01 to 0.05 (1 to 5%). The ANOVA test of the between soil residuals for reconstituted and 'undisturbed' samples yielded a p-value of 0.7545, or 75%. This means equation (4.12)(4.13) predicts equally well $G_{max,lab}$ for reconstituted and undisturbed soil samples, and that the data do not support distinguishing between them when estimating $G_{max,lab}$.

This study also conducted a one way ANOVA test of the within soil residuals for each test type (resonant column, torsional shear, etc.), to see if test type made a statistically significant difference in the value of $G_{max,lab}$. The ANOVA test gave a p-value of 1 (100%), which means equation (4.13) predicts equally well $G_{max,lab}$ for all laboratory test types and that the data do not support distinguishing between them when estimating $G_{max,lab}$.

Figure 4.12 shows box plots of the between soil residuals for sample type and within soil residuals for test type. The lines in the boxes are the median values, the edges of the boxes are the 25^{th} and 75^{th} percentiles, and the whiskers extend to the most extreme data points not considered outliers. Outliers are shown as red crosses and are defined as more than ± 2.7 standard deviations away from the median. Figure 4.12 shows that there is little variation in the between or within soil standard deviations due to sample type or test type, respectively.

4.6 Evaluation of the $G_{max,lab}$ Model

The more parameters added to a model the better the model will be able to fit the data. However, the uncertainty from adding another parameter can outweigh the improvement in the quality of the fit. In addition, it is not desirable to create a model that fits only the collected data but one that fits the entire population of $G_{max,lab}$ values. In other words, it is important to avoid over parameterization. One way to measure whether the change in the quality of the fit is sufficient to justify the greater complexity of the model is through a log-likelihood ratio test. The likelihood is a measure of how likely the data is given the specific model. It is the product of the probability of observing the individual data points. The log-likelihood is the logarithm of this number.

The log-likelihood ratio test compares the log-likelihoods of two models, where one model is a special case of the other. This is achieved by constraining one or more of the parameters in the more complex model to be fixed values in the simpler model. The criterion for comparing the models is the difference in their deviances, where deviance is -2 times the log-likelihood. The log-likelihood ratio test uses a χ^2 distribution where the degrees of freedom of the test are the number of constrained parameters in the simpler model. The output is a p-value, which in this case is the probability of seeing a difference in the model fits that could be explained by randomness in the dataset. A small p-value for a test indicates there is a small chance that the better fit of the more complex model is due to randomness in the data. A large p-value indicates a non-negligible probability that the difference between the fits of the models is due to randomness. In other words, a small p-value signifies that the more complex model is appropriate, and a large p-value means it is not.

To test the appropriateness of adding additional parameters to the $G_{max,lab}$ model, this study conducted log-likelihood ratio tests between equations (4.5) and (4.6), (4.6) and (4.8), (4.8) and (4.12), and (4.8) and (4.13). Table 4.5 shows the p-values for each equation compared to the previous one. Table 4.5 also lists the within soil, between soil, and total standard deviation computed for each equation from all of the data. The small p-values shown in Table 4.5 for equations (4.6) and (4.8) indicate that there is a significant dependence of $G_{max,lab}$ on the proposed formulations for mean effective confining pressure and OCR. The decrease in the total standard deviation from equations (4.5) to (4.6) and from equations (4.6) to (4.8) confirms this finding. The p-value for equation (4.12), which adds the effect of PI, FC, and Cu, is greater than 0.05, which indicates that not all of the input variables are necessary, whereas the p-value for equation (4.13), which only adds the effect of FC and Cu to equation (4.8), is less than 0.05. In addition, the standard deviations of equations (4.12) and (4.13) are the same. This further supports the decision to remove the PI term from the model. It also shows that while the addition of the FC and Cu term to the model are validated by the log-likelihood ratio tests and the removal of bias from the residuals, the reduction in the standard deviation between equations (4.8) and (4.13) is negligible.

Figure 4.13 shows the variability of the between soil standard deviation with fines content and the variability of the within soil standard deviation with the mean effective confining pressure. There is no obvious trend of the standard deviation with either parameter. This indicates that the model predicts equally well values of $G_{max,lab}$ for tests conducted at low or high mean effective

confining pressures, and for soils with low or high fines contents. The standard deviation was found to be independent of e, OCR, PI, D_{50}, and Cu as well.

4.7 Model for Estimating $G_{max,in\text{-}situ}$ from the measured value of $G_{max,lab}$

Equation (4.12) estimates the mean value of the small strain shear modulus based on laboratory data. However, values of $G_{max,lab}$ are different from values of $G_{max,in\text{-}situ}$ due to sample disturbance, cementation, and confinement time (t_g). This section describes the development of a model to determine $G_{max,in\text{-}situ}$ from measured values of $G_{max,lab}$.

This study collected data from 70 soils where G_{max} was measured in-situ and in the laboratory at the same mean effective confining pressure. All of the soils in the in-situ database are from Holocene deposits or beneath newly placed embankments. Table 4.6 lists the references of the studies from where the data was collected, as well as the tested soil and the in-situ and laboratory test type. Figure 4.14a shows the distribution of soils in the $G_{max,lab}$ database according to their USCS classification, and Figure 4.15 shows the distribution of void ratio with the mean effective confining pressure σ'_m, and the plasticity index PI with the liquid limit LL.

This study examined the correlation between the measured values of $G_{max,lab}$ and $G_{max,in\text{-}situ}$ by performing least squares regression on the data using linear, logarithmic, power, polynomial, and exponential equation forms. The power formulation, shown in equation (4.14), gave the best fit to the data ($R^2 = 0.91$):

$$ln\left(G_{max,in-situ}\right) = ln\left(0.78 \times {G_{max,lab}}^{1.10}\right) + \omega \qquad (4.14)$$

where ω is the in-situ residual with standard deviation κ. Figure 4.16a shows equation (4.14) versus the data, and Figure 4.16b shows the residuals. The in-situ residuals (ω) from equation (4.14) were then plotted versus the e, σ'_m, OCR, PI, FC, D_{50}, and Cu values of the collected data. As an example, Figure 4.17 shows the in-situ residuals versus the mean effective confining pressure and the plasticity index. These plots as well as those for the other parameters revealed no significant trends with the in-situ residuals.

In addition, a one way ANOVA test of the in-situ residuals on the in-situ field test type (downhole, crosshole, etc.) was conducted. The ANOVA test gave a p-value of 0.81 (81%), which means the in-situ test type has no statistically significant effect on the $G_{max,in\text{-}situ}$ of the collected data. Figure 4.18 shows the results of the one-way ANOVA test.

The results of this section are similar to the results found by Chiara and Stokoe (2006). They found a negligible effect of σ'_m, PI, and depth on the trend between $G_{max,in\text{-}situ}$ and $G_{max,lab}$, and that this trend is best described by a power law. They also found that $G_{max,lab}$ tends to be larger than $G_{max,in\text{-}situ}$ at small values of $G_{max,in\text{-}situ}$, whereas for large values of $G_{max,in\text{-}situ}$ the opposite is observed. This is because soils with small values of $G_{max,in\text{-}situ}$ are generally loose and uncemented, and they become denser due to sampling. Stiffer soils, on the other hand, tend to have larger in-situ than laboratory G_{max} values because sampling can break bonds created by cementation and can cause a rearrangement of soil particles that destroys the 'structure' of the sample.

To create one model to estimate the in-situ small strain shear from soil and test parameters, this study combined equations (4.13) and (4.14) into equation (4.15). The total standard deviation (σ_{Total}) was determined for equation (4.15) with equation (4.16), where the in-situ standard deviation κ is 0.36 and Table 4.5 lists the within (ϕ) and between (τ) soil standard deviations.

$$ln\left(G_{max,in-situ,i,j}/p_a\right) = ln\left[0.78 \times \left(c_1 \times e_{i,j}^{c_2} \times \left(\sigma'_{m,i,j}/p_a\right)^n \times OCR_{i,j}^k \times (FC_i + 1)^{c_7} \times A\right)^{1.10}\right] + \eta_i + \varepsilon_{i,j} + \omega \quad (4.15)$$

$$\sigma_{Total} = \sqrt{\phi^2 + \tau^2 + \kappa^2} \quad (4.16)$$

The value of σ_{Total} for equation (4.15) is 0.58 natural log units, which is comparable to the value found by Chiara and Stokoe (2006). It is also similar to the total standard deviation found for equations to predict pseudo-acceleration response spectra (about 0.5 to 0.8 natural log units). This study found κ to be independent of e, σ'_m, OCR, PI, FC, D_{50}, and Cu.

4.8 Model Validation and Comparison

This investigation validated and compared equation (4.15) against existing models using a third database. The validation database consists of 344 samples of 259 different soils from 7 studies. The validation database consists of data from studies and projects that conducted in-situ seismic tests and also collected samples to determine soil properties at the same locations as the data from the seismic tests. Therefore, the validation database includes $G_{max,in-situ}$ and parameters such as e, σ'_m, PI, etc., but does not include values of $G_{max,lab}$. Table 4.7 lists the references of the studies from which the database was collected, as well as the in-situ seismic test and soil type. Figure 4.19a shows the number of different soils in the validation database according to their USCS classification, and Figure 4.19b shows the number of tests according to their general soil type. Figure 4.20 shows the distribution of void ratio with σ'_m, and PI with LL.

This study compared equation (4.15) with the models proposed by Jamiolkowsi et al. (1991) and Hardin (1978) for the entire validation database, and for subsets of the validation database where FC < 30% and another subset where FC ≥ 30%. In addition, equation (4.15) was compared with the models proposed by Kokusho et al. (1982) and Kallioglou et al. (2008) for the subset of soils with FC ≥ 30%. This study used equation (4.14) to estimate $G_{max,in-situ}$ from $G_{max,lab}$ for all four of the comparison models to be consistent with equation (4.15). Equation (4.14) to predict $G_{max,in-situ}$ from $G_{max,lab}$ was developed independently from the equation to predict $G_{max,lab}$, and therefore was not biased to this results of this study. Figure 4.21 and Table 4.8 show the results for the entire database, results for soils in the validation database with FC < 30%, and results for soils in the validation database with FC ≥ 30%.

Table 4.8 lists the mean, median, and standard deviation of the total residuals for each model. When the mean and median are close to zero the model on average predicts accurately the value

of $G_{max,in\text{-}situ}$, whereas if the mean and median are positive the model tends to under-predict, and if they are negative the model tends to over-predict. The mean and median values of the total residuals for equation (4.15) are the closest to zero of all the considered models and datasets. The Jamiolkowski et al. (1991) and Hardin (1978) models have similar mean values as equation (4.15) for soils with FC < 30%, but for soils with FC ≥ 30% they tend to over-predict the value of $G_{max,in\text{-}situ}$. The Kokusho et al. (1982) and Kallioglou et al. (2008) models tend to under-predict the value of $G_{max,in\text{-}situ}$ for soils with FC ≥ 30%. Equation (4.15) also has the smallest standard deviation of all the considered models for each dataset. The Jamiolkowski et al. (1991) and Hardin (1978) models have similar values of standard deviation as each other for each subset of the validation data, and smaller standard deviation values than the Kokusho et al. (1982) and Kallioglou et al. (2008) models for soils with FC ≥ 30%.

4.9 Summary and Conclusion

This chapter studied the effects of the mean effective confining pressure, void ratio, overconsolidation ratio, plasticity index, fines content, coefficient of uniformity, median grain size, laboratory test type, and sample type on $G_{max,lab}$ by means of a mixed effects regression. Equation (4.13) presents the model to estimate $G_{max,lab}$ from soil and test parameters. This study performed log-likelihood ratio tests to evaluate the statistical relevance of each parameter added to the model. This ensured that the model was not over-parameterized. Table 4.5 lists the results of the log-likelihood tests.

This study then used a second set of data to develop a model to predict $G_{max,in\text{-}situ}$ from $G_{max,lab}$. Equation (4.14) shows the model for $G_{max,in\text{-}situ}$. Equations (4.13) and (4.14) were then combined to produce a model to estimate $G_{max,in\text{-}situ}$ from soil and test parameters. This model is reproduced below in equation (4.17) through equation (4.20). Table 4.3 lists coefficients c_2 through c_8, and Table 4.4 lists the value of c_1:

$$G_{max,in-situ}/p_a = 0.78 \times [c_1 \times e^{c_2} \times (\sigma'_m/p_a)^n \times OCR^k \times (FC+1)^{c_7} \times [Cu^{c_8} \times B + (1-B)]\,]^{1.10} \quad (4.17)$$

$$n = c_3 \times Cu^{B \cdot c_4} \quad (4.18)$$

$$k = c_5 \times \left(\frac{PI}{100}\right)^{c_6} \leq 0.5 \quad (4.19)$$

$$B = \begin{cases} 1 & for\ FC < 30\% \\ 0 & for\ FC \geq 30\% \end{cases} \quad (4.20)$$

where $\sigma_{Total} = 0.58$.

This study found the same value for c_2 as Jamiolkowski et al. (1991), similar values for c_3, c_4, and c_8 as Menq (2003), similar values for c_5 and c_6 as Hardin (1978), and a similar model to estimate $G_{max,in\text{-}situ}$ from $G_{max,lab}$ as Chiara and Stokoe (2006). The model is unique from other models in that it includes a fines content dependent term for Cu and a separate term for fines

content, which allows a smooth transition from clean sands and gravels to silts and clays. Finally, a third database was collected to validate and compare the model to other existing models. The model was compared with models by Jamiolkowski et al. (1991), Hardin (1978), Kokusho et al. (1982), and Kallioglou et al. (2008). Table 4.8 and Figure 4.21 present the results. The residuals of the model developed in this chapter had a mean and median closer to zero and a smaller standard deviation than the other four models considered. This demonstrates that the model is robust and can be used to estimate the in-situ small strain shear modulus of clays, silts, sands, and gravels.

Equation (4.17) through equation (4.20) give the median predicted value of $G_{max,in\text{-}situ}$. To determine the predicted plus or minus one standard deviation values of $G_{max,in\text{-}situ}$, add or subtract the value predicted with equation (4.17) through equation (4.20) by $\exp(\pm\sigma_{total})$. The estimates of the standard deviation allow the uncertainty of the small strain shear modulus to be included in probabilistic studies.

This study found no significant effect of D_{50}, sample type, or laboratory test type on $G_{max,lab}$, and that the function to relate $G_{max,lab}$ to $G_{max,in\text{-}situ}$ was not dependent on e, σ'_m, OCR, PI, FC, D_{50}, Cu or the in-situ test type. In addition, this study found the within soil (ϕ), between soil (τ), and in-situ standard (κ) deviations to be independent of e, σ'_m, OCR, PI, FC, D_{50}, and Cu.

4.10 References

Alarcon-Guzman, A., Chameau, J. L., Leonards, G. A., and Frost, J. D. (1989). "Shear modulus and cyclic undrained behavior of sands." *Soils Found*., 29(4), 105–119.

Athanasopoulos, G.A. (1993). "Effects of ageing and overconsolidtaion on the elastic stiffness of a remoulded clay." *Geotechnical and Geological Engineering*, Vol 11, 51-65.

Anderson, D.G., Stokoe II, K.H. (1978). "Shear Modulus: A Time-Dependent Soil Property." *Dynamic Geotechnical Testing*. ASTM STP 654, ASTM, 66 – 90.

Bellotti, R., Benoit, J., Fretti, C., and Jamiolkowski, M. (1997). "Stiffness of Toyoura sand from dilatometer tests." *J. Geotech. Geoenviron. Eng*., 123(9), 836–846.

Borden, R. H., Shao, L., and Gupta, A. (1996). "Dynamic properties of Piedmont residual soils." *J. Geotech. Geoenviron. Eng*, 122(10) 813–821.

Cavallaro, A., Lo Presti, D.C.F., and Maugeri, M. (2000). "Dynamic geotechnical characterization of soils subjected to umbria and marches earthquake." *Earthquake Engineering 12th World Conference*, Auckland, New Zealand.

Chiara, Nicola and K. Stokoe (2006). "Sample disturbance in resonant column test measurement of small strain shear wave velocity." *Proceedings of Soil Stress-Strain Behavior: Measurement, Modeling and Analysis*, Rome, Italy, March 16-17.

Chung, R. M., Yokel, F. Y., and Drnevich, V. P. (1984). "Evaluation of dynamic properties of sands by resonant column testing." *Geotech. Test. J*., 7(2), 60–69.

Darendeli, M. B. (2001). "Development of a new family of normalized modulus reduction and material damping curves." PhD dissertation, Univ. of Texas at Austin, Austin, Texas.

Doroudian, M., Vucetic, M., (1995). "A Direct Simple Shear Device for Measuring Small-Strain Behavior." *Geotechnical Testing Journal*, 18(1), 69-85.

EPRI (1993). "Guidelines for Determining Design Basis Ground Motions." *Electric Power and Research Institute*, Project, Report Vols. I-IV.

Hardin, B. (1978).''The nature of stress-strain behavior of soils,'' *Proc. of Geotechnical Division Specialty Conference on Earthquakes Engineering & Soil Dynamics*, ASCE, Pasadena, CA, Vol.1, pp. 3–90.

Ishihara K. (1996). "Soil Behavior in Earthquake Geotechnics." *Oxford Science Publications* 350p.

Iwasaki, T., and Tatsuoka, F. (1977). "Effects of grain size and grading on dynamic shear moduli of sands." *Soils Found.*, 17 (3), 19–35.

Jamiolkowski, M., Leroueil, S., and D.C.F. Lo Presti. (1991). "Design Parameters from Theory to Practice." *Theme Lecture, Proc. Geo-Coast 91*, Yokohama, Vol 2, 877-917.

Jovicic, V., and Coop, M. R. (1997). "Stiffness of coarse grained soils at small strains." *Geotechnique*, 47(3), 545–561.

Kagawa, T. (1992). "Moduli and damping factors of soft marine clays." *Journal of Geotechnical Engineering*. ASCE, 118(9),1360–1375.

Kallioglou, P., Tika, Th. and Pitilakis, K. (2008). "Shear Modulus and Damping Ratio of Cohesive Soils." *Journal of Earthquake Engineering*. 12(6), 879 – 913.

Kim, T. and Novak, M. (1981). "Dynamic properties of some cohesive soils of Ontario." *Canadian Geotechnical Journal*. Vol 18, 371–389.

Kokusho, T., Yoshida, Y. and Esashi, Y. (1982). "Dynamic properties of soft clay for a wide strain range." *Japanese Society of Soil Mechanics and Foundations*. Vol 22, 1–18.

Kokusho, T. (1980). "Cyclic triaxial test of dynamic soil properties for wide strain range." *Soils Found.*, 20(2), 45–60.

Lanzo, G., A. Pagliaroli, Tommasi, P., and Chiocci F.L. (2009). "Simple shear testing of sensitive, very soft offshore clay for wide strain range." *Canadian Geotechnical Journal*. Vol 46, 1277 – 1288.

Lanzo, G., and Pagliaroli, A. (2006). "Stiffness of natural and reconstituted Augusta clay at small to medium strains." *Soil Stress-Strain Behavior: Measurement, Modelling and Analysis*, eds. Hoe I. Ling et al.; Springer, 323-331.

Lefebvre, Guy, Denis Leboeuf, Mushin E. Rahhal, Alain Lacroix, Joseph Warde, and Kenneth Stokoe (1994). "Laboratory and field determinations of small-strain shear modulus for a structured Champlain clay." Can. Geotech. J. 31, 61-70.

Lo Presti, D.C.F., Jamiolkowski, M., Pallara, O., Cavallaro, A. & Pedroni, S. (1997). "Shear modulus and damping of soils." *Géotechnique*, 47(3), 603–617.

LoPresti, D. C. F., Pallara, O., Lancellotta, R., and Maniscalco, R. (1993). "Monotonic and cyclic loading behavior of two sands at small strains." *Geotech. Test. J.*, 16(4), 409–424.

MATLAB and Statistics Toolbox Release 2012b (2012). The MathWorks, Inc., Natick, Massachusetts, United States.

Menq, Farn-Yuh (2003). "Dynamic Properties of Sandy and Gravelly Soils." PhD dissertation, Univ. of Texas at Austin, Austin, Texas.

Nikolaou, Sissy. "Deep soft soil sites in the greater NYC metropolitan area." Personal communication, April 26, 2012.

Nigbor, Robert. "Resolution of Site Response Issues in the Northridge Earthquake (ROSRINE)." Personal communication, October 24, 2012.

Okur, D.V., Ansal, A. (2007). "Stiffness degradation of natural fine grained soils during cyclic loading." *Soil Dynamics and Earthquake Engineering*. Vol 27, 843 – 854.

Pass, Daniel G. (1994). "Soil Characterization of the Deep Accelerometer Site at Treasure Island, San Francisco, California." Masters thesis, University of New Hampshire, Durham, New Hampshire.

Pinheiro, J.C., and Bates, D.M., (2000). *Mixed Effects Models in S and S-PLUS*. Springer-Verlag, New York.

S&ME Inc. (1998). "Second report of seismic analysis—Daniel Island terminal, Charleston, South Carolina." Project Rep. No. 1131-97-741, Mount Pleasant, S.C.

S&ME Inc. (1993). "Seismic soil pile interaction analyses—Mark Clark expressway/Stono River crossings, Charleston, South Carolina." Project Rep. No. 1131-92-162, Mount Pleasant, S.C.

Saxena, S., and Reddy, K. (1989). "Dynamic moduli and damping ratios for Monterey No. 0 sand by resonant column tests." *Soils Found.*, 29(2), 37–51.

Schmertmann, J.H. (1991). "The mechanical ageing of soils." *Journal of Geotechnical and Geoenvironemtnal Engineering*, ASCE 117, 1288-330.

Schneider, J.A., Hoyos, L., Jr., Mayne, P.W., Macari, E.J., and Rix, G.J. (1999). "Field and laboratory measurements of dynamic shear modulus of Piedmont residual soils." *Behavioral Characteristics of Residual Soils, GSP 92*, ASCE, Reston, VA, pp. 12-25.

Seed, H. B., Wong, R. T., Idriss, I. M., and Tokimatsu, K. (1984). "Moduli and damping factors for dynamic analyses of cohesionless soils." Rep.. UBC/EERC 84-14, Univ. of California, Berkeley,Calif.

Shibuya, S., and H. Tanaka (1996). "Estimate of elastic shear modulus in Holocene soil deposits." *Soils and Foundations*, 36(4), 45-55.

Shibuya, S., Toshiyuki, T., Fukuda, F., and Degoshi, T. (1995). "Strain rate effects on shear modulus and damping of normally consolidated clays." *Geotechnical Testing Journal*, ASTM, 18(3), 365-375.

Tika, Th., Kallioglou, P., Koninis, G., Michaelidis, P., Efthimiou, M., Pitilakis, K., (2010). "Dynamic properties of cemented soils from Cyprus." *Bulletin of Engineering Geology and the Environment*, Vol 69, 295-307.

Vucetic, M. (1994). "Cyclic Threshold Shear Strains in Soils." *Journal of Geotechnical Engineering*, ASCE, 120(12), 2208-2228.

Vucetic, M., and Dobry, R. (1991). "Effect of soil plasticity on cyclic response." *Journal of Geotechnical Engineering*, ASCE, 117(1), 89-107.

Yamada, S., Hyodo, M., Orense, R., and Dinesh, S. V. (2008). "Initial shear modulus of remolded sand-clay mixtures." *J. Geotech. Geoenviron. Eng*. ASCE, 134(7), 960–971.

Yasuda, N., and Matsumoto, N. (1993). "Dynamic deformation characteristics of sands and rockfill materials." *Can. Geotech. J.*, 30(5), 747–757.

Yasuda, N., Ohta, N., and Nakamura, A. (1996). "Dynamic deformation characteristics of undisturbed riverbed gravels." *Can. Geotech. J*., 33(2), 237–247.

Table 4.1: Parameters studied by other researchers and their effect on G_{max}

Controlling Parameter	G_{max} Cohesive	G_{max} Cohesionless	Cross Correlations			
			t_g	*OCR*	σ'_m	*e*
σ'_m	↑	↑				
e	↓	↓				
t_g	↑	↑				
OCR	↑	NE[a]	↓			
f	NE[a]	NE[a]				
N	NE[a]	NE[a]				
PI	↓		↑	↑		
FC	↓	↓				
D_{50}		↑	↓			↑[b]
Cu		↓			↑[b]	

a = negligible effect; b = only for cohesionless soils

Table 4.2: Laboratory data collected to develop $G_{max,lab}$ model

Reference	Test Type[a]	Sample Type[b]	Soil(s) Tested
Alarcon-Guzman et al. 1989	RC	R	Ottawa 20-30, 50-70 Sand
Athanasapoulos 1993	RC	R	Kaolinite
Bellotti et al. 1997	DMT	R	Toyoura Sand
Borden et al. 1996	TS, RC	U	Soils from North Carolina
Cavallaro et al. 2000	RC	U	Fabriano Clay
Chung et al. 1984	RC	R	Monterey Sand
Doroudian and Vucetic 1995	DSS	R	Kaolinite
EPRI 1994	RC	U, R	Soils from California and Taiwan
Iwasaki and Tatsuoka 1977	RC	R	Toyoura and Iruma Sand
Jovicic and Coop 1997	BE	R	Ham River and Dog's Bay Sand
Kallioglou et al. 2008	RC	U, R	Soils from Greece and Cyprus
Kokusho et al. 1982	CT	U	Soils from Chiba, Japan
Kokusho 1980	CT	R	Toyoura Sand
Lanzo and Pagliaroli 2006	DSS	U, R	Augusta Clay
Lanzo et al. 2009	DSS	U	Vasto Clay
Lo Presti et al. 1997	RC	R	Toyoura and Quiou Sand
Lo Presti et al. 1993	RC	R	Ticino and Quiou Sand
Okur and Ansal 2007	CT	U	Soils from Turkey
Nigbor 2012 (ROSRINE)	RC, DSS	U, R	Soils from California
S&ME Inc 1993, 1998	TS, RC	U	Soils from Charleston, SC
Saxena and Reddy 1989	RC	R	Monterey Sand
Schneider et al. 1999	RC	U	Piedmont Residual Soils
Seed et al. 1984	CT	R	Oroville, Pyramid, Venado, and Livermore Gravel
Shibuya et al. 1995	TS	R	Kiyohoro Clay and Kaolinite
Tika et al. 2010	RC	U	Soils from Cyprus
Yamada et al. 2008	TS	U, R	Japanese Clays
Yasuda and Matsumoto 1993	TS	R	Toyoura Sand, Rockfill
Yasuda et al. 1996	CT	R	Riverbed Gravel

[a]RC = resonant column; TS = torsional shear; CT = cyclic triaxial; DSS = direct simple shear; BE = bender element; DMT = flat plate dilatometer

[b]R = reconstituted; U = 'undisturbed'

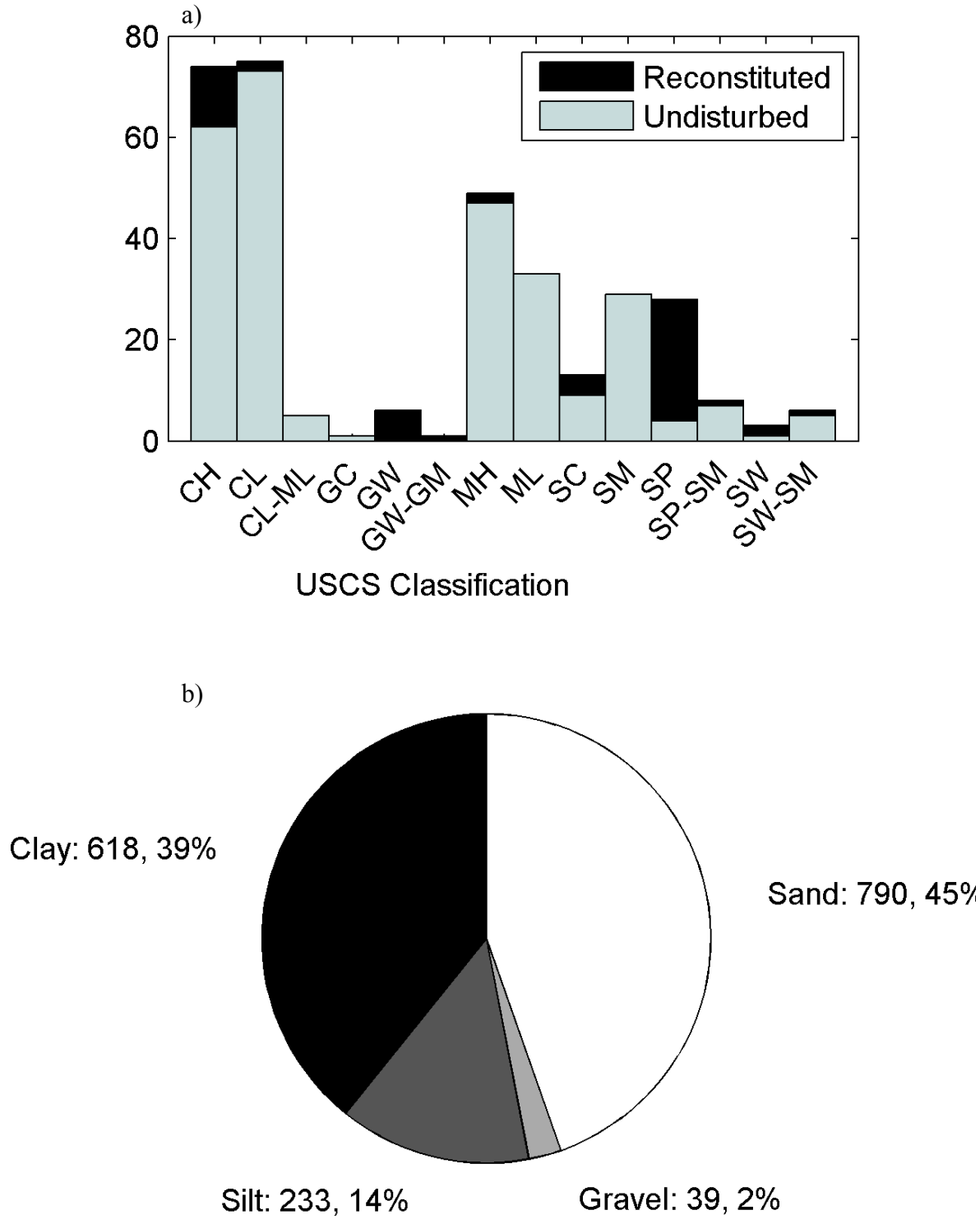

Figure 4.1: $G_{max,lab}$ a) USCS designation and sample type, and b) number and percentage of tests for each general soil type

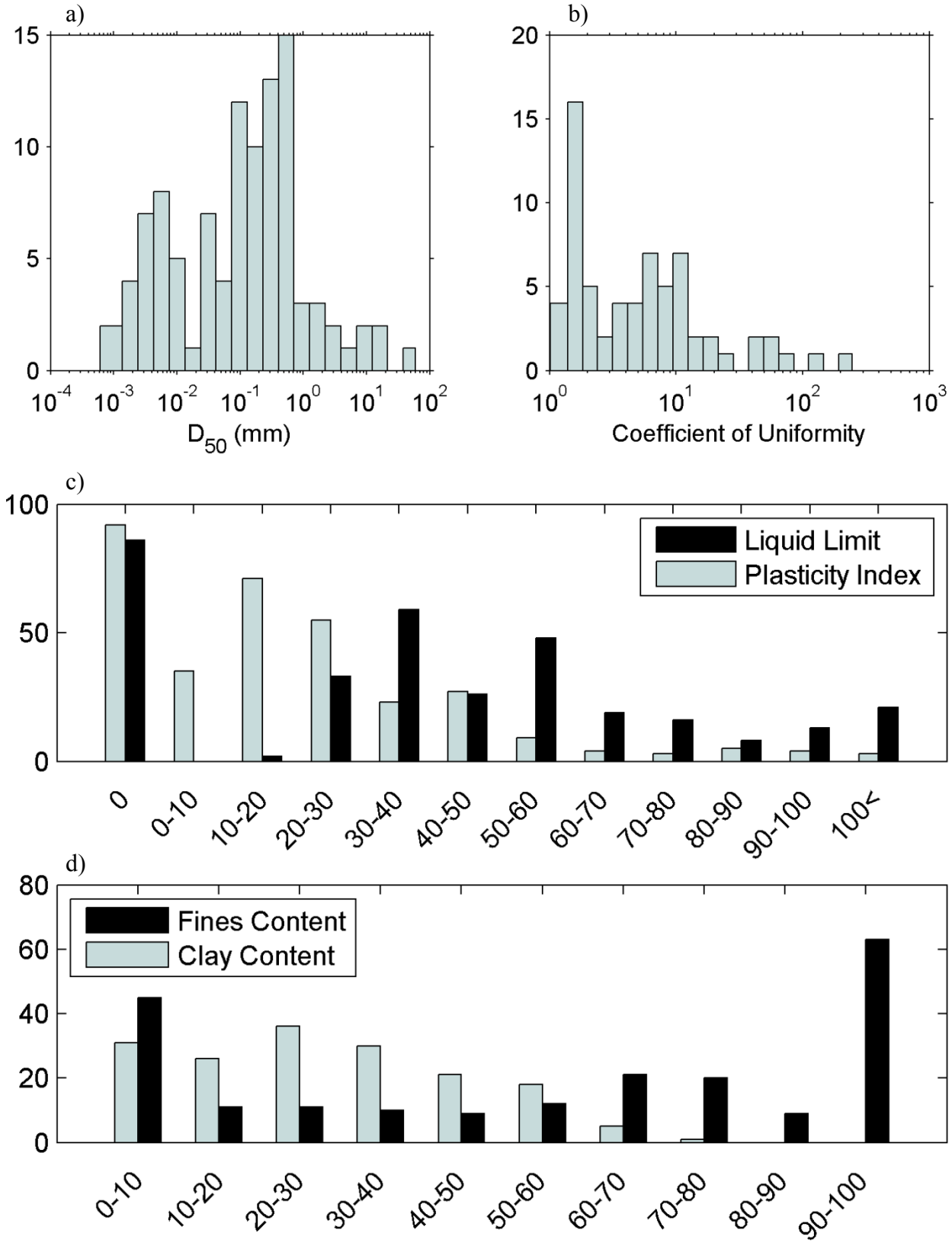

Figure 4.2: Histograms showing distribution of a) median grain size (D_{50}), b) coefficient of uniformity (Cu), c) liquid limit (LL) and plasticity index (PI), d) fines content (FC) and clay content of the $G_{max,lab}$ database

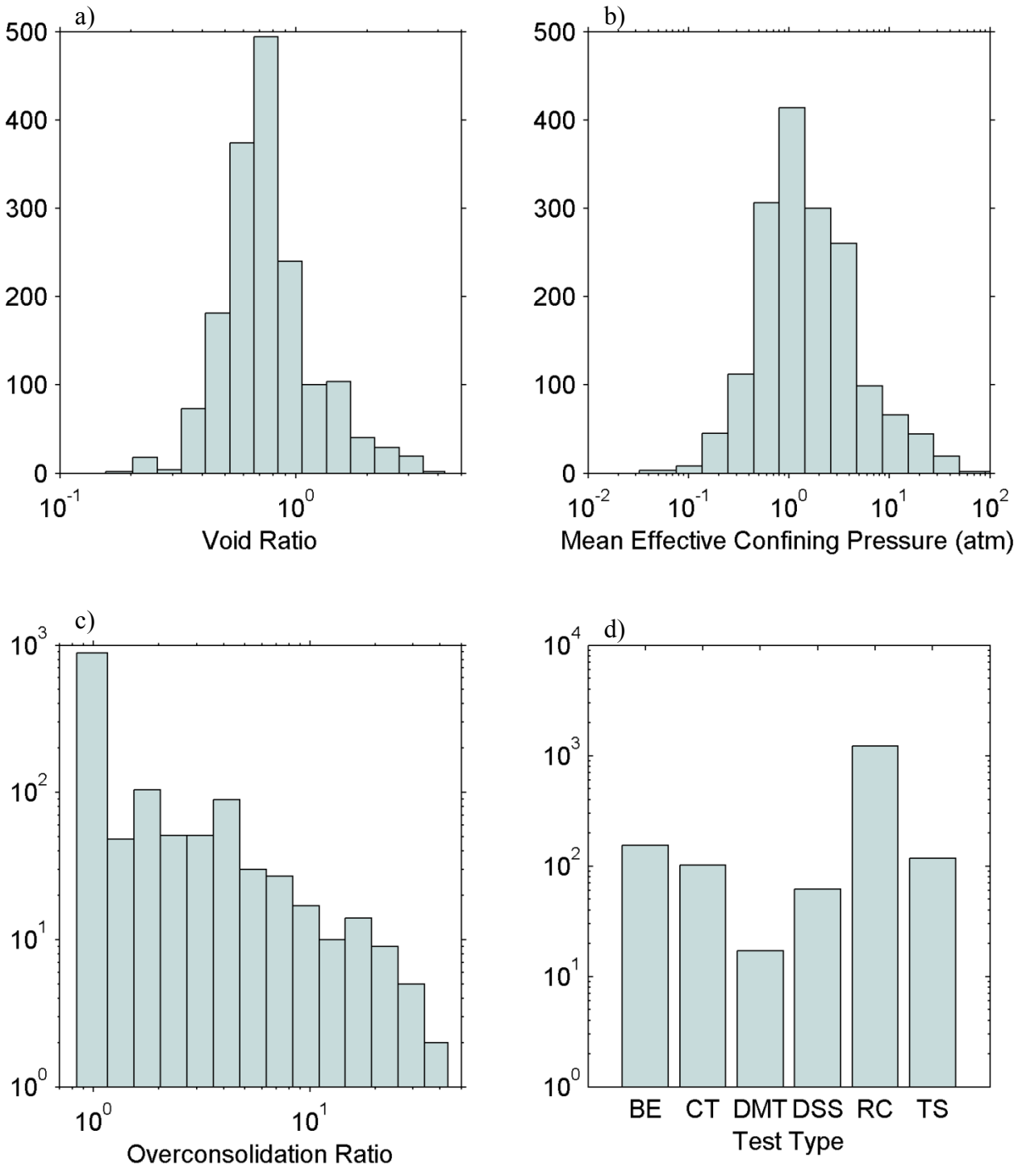

Figure 4.3: Histograms showing distribution of a) void ratio (e), b) mean effective confining pressure (σ'_m), c) overconsolidation ratio (OCR), and d) test type of the $G_{max,lab}$ database

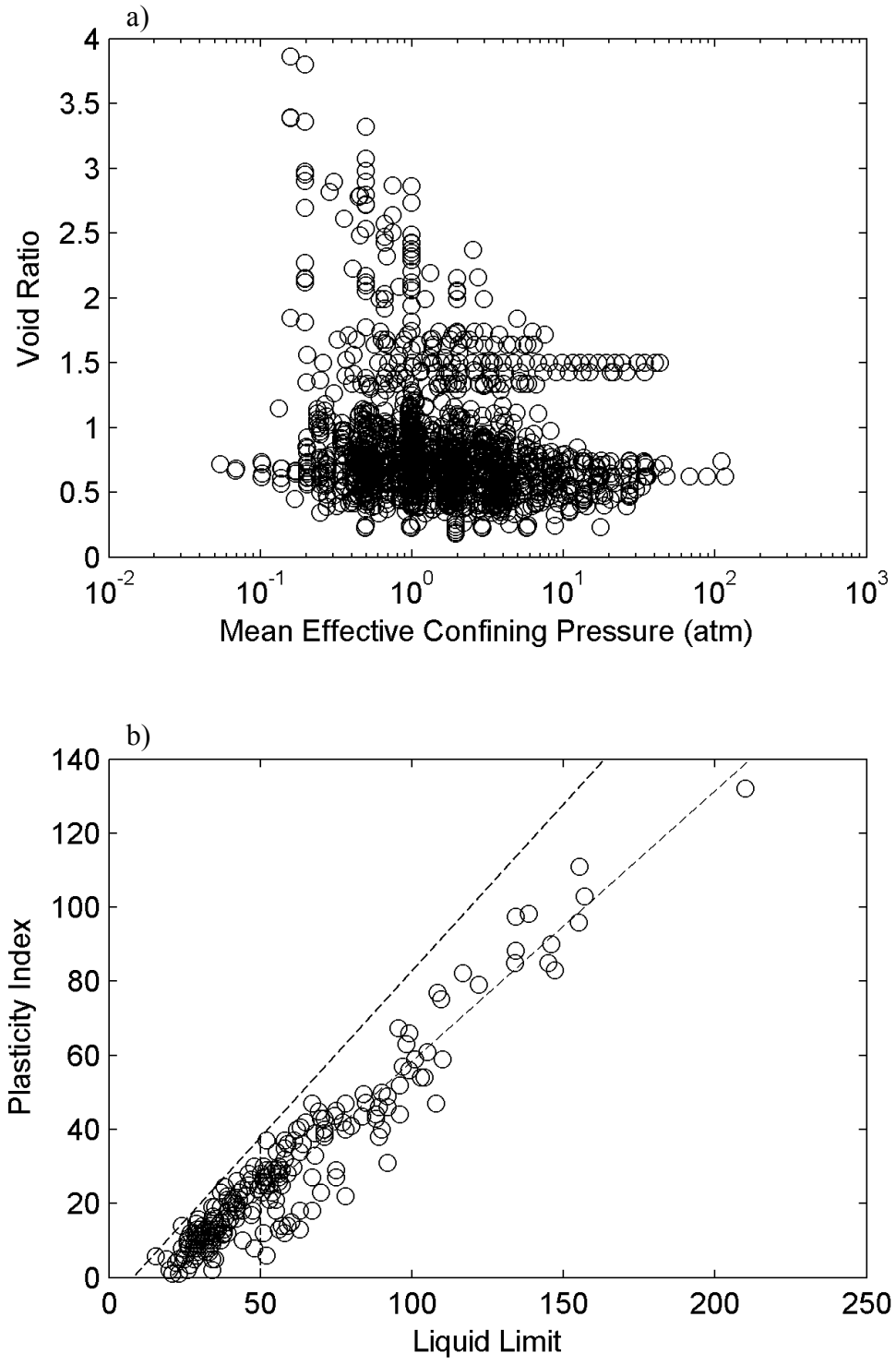

Figure 4.4: Scatter plots of combinations of Gmax,lab database parameters

Table 4.3: Regression coefficients for the $G_{max,lab}$ model

Coefficient	Value	Standard Error
c_2	-1.309	0.0817
c_3	0.465	0.0138
c_4	0.106	0.0102
c_5	2.022	0.0463
c_6	1.933	0.0231
c_7	-0.124	0.0161
c_8	-0.170	0.0308

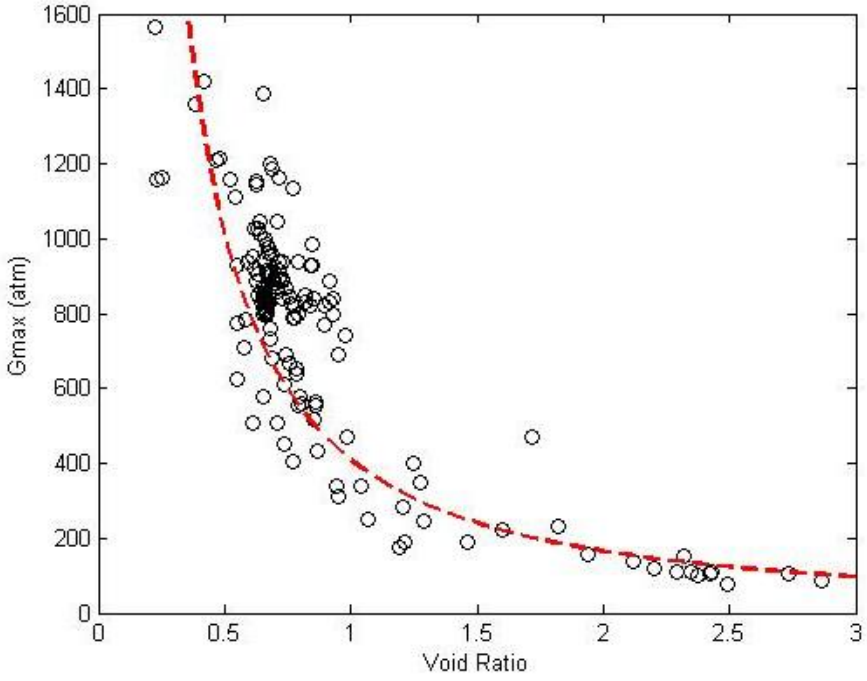

Figure 4.5: Tests with OCR = 1 and σ'_m = 1 atmosphere. Trend line is for equation (4.5).

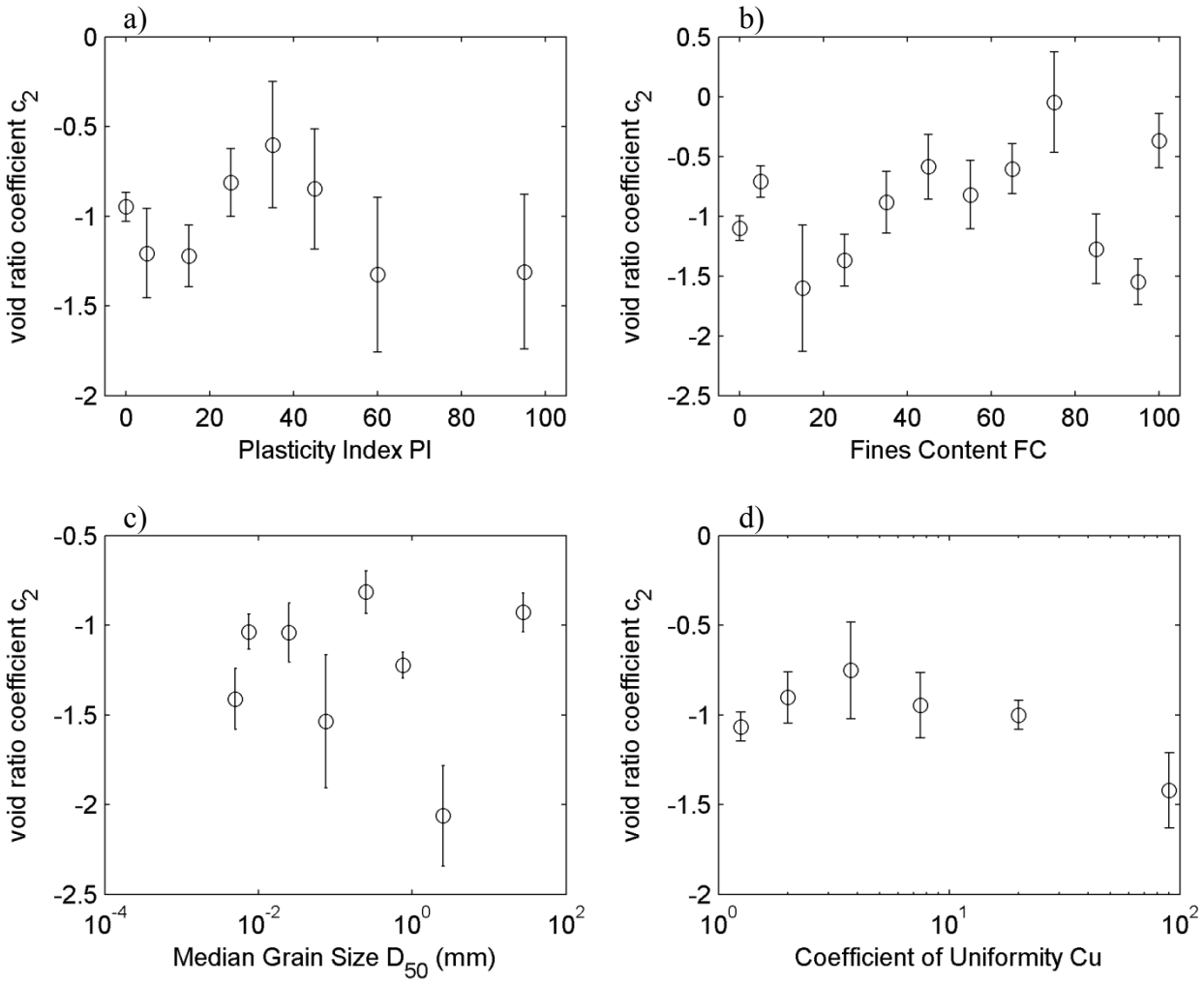

Figure 4.6: Void ratio coefficient c_2 for tests with OCR = 1 and σ'_m = 1 atmosphere regressed for different bins of a) PI, b) FC, c) D_{50}, and d) Cu. Error bars are the standard errors of the predicted value of c_2.

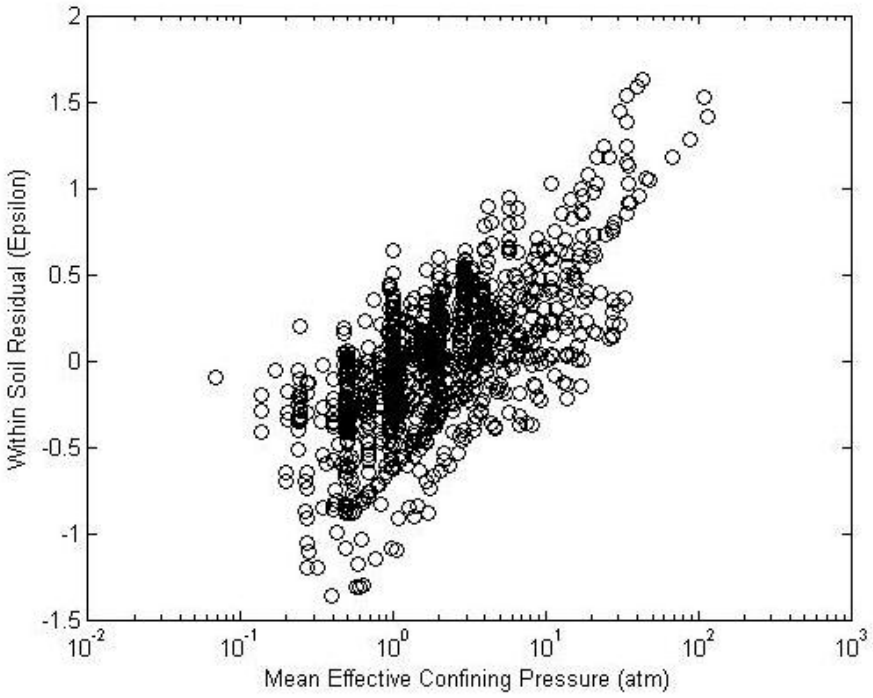

Figure 4.7: Within soil residuals ε for equation (4.5) for all tests with OCR = 1

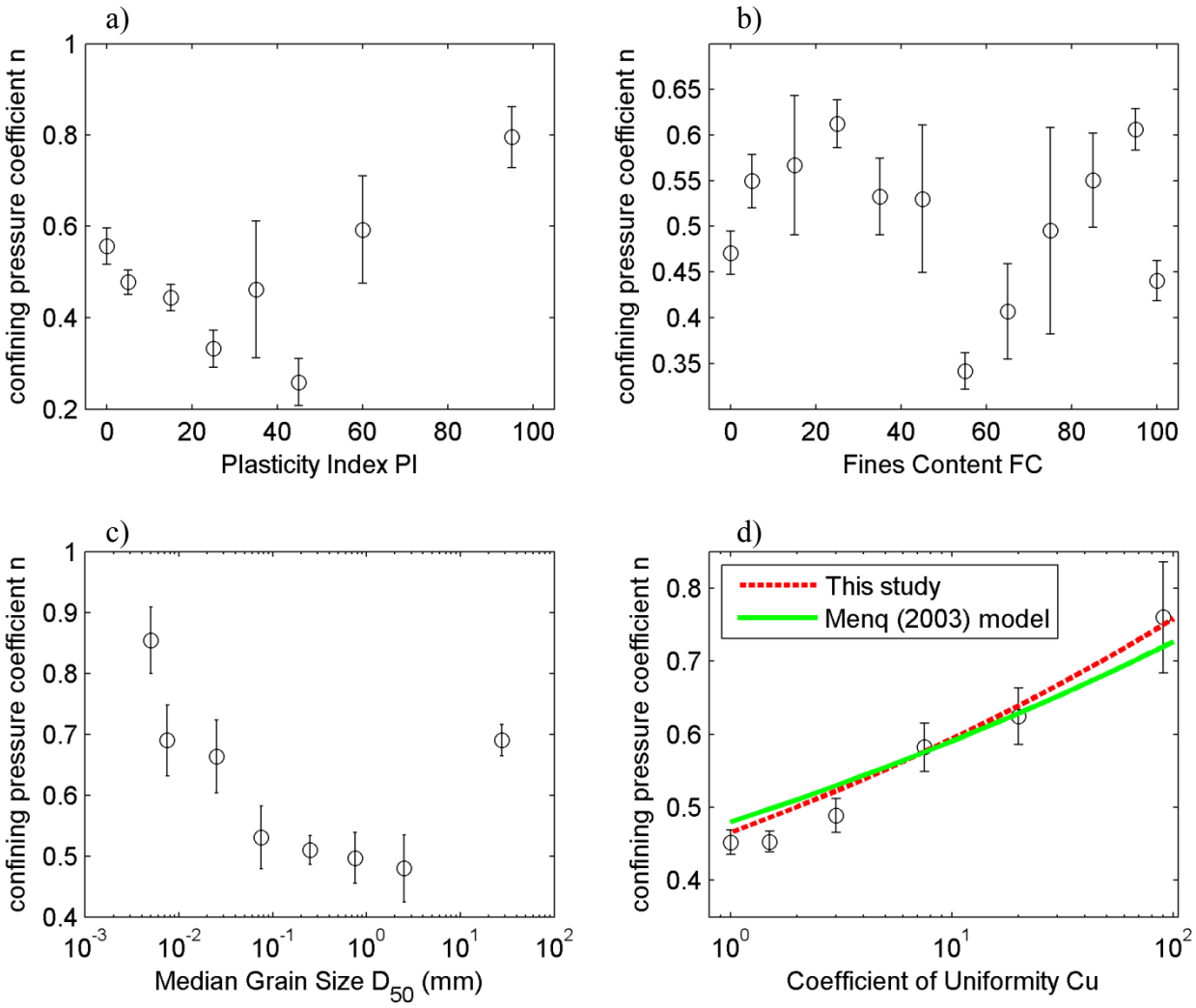

Figure 4.8: Coefficient n for tests with OCR = 1 regressed for different bins of a) PI, b) FC, c) D_{50}, and d) Cu, where the Cu = 1 bin is soils with FC > 30 %. Error bars are the standard errors of the predicted value of n.

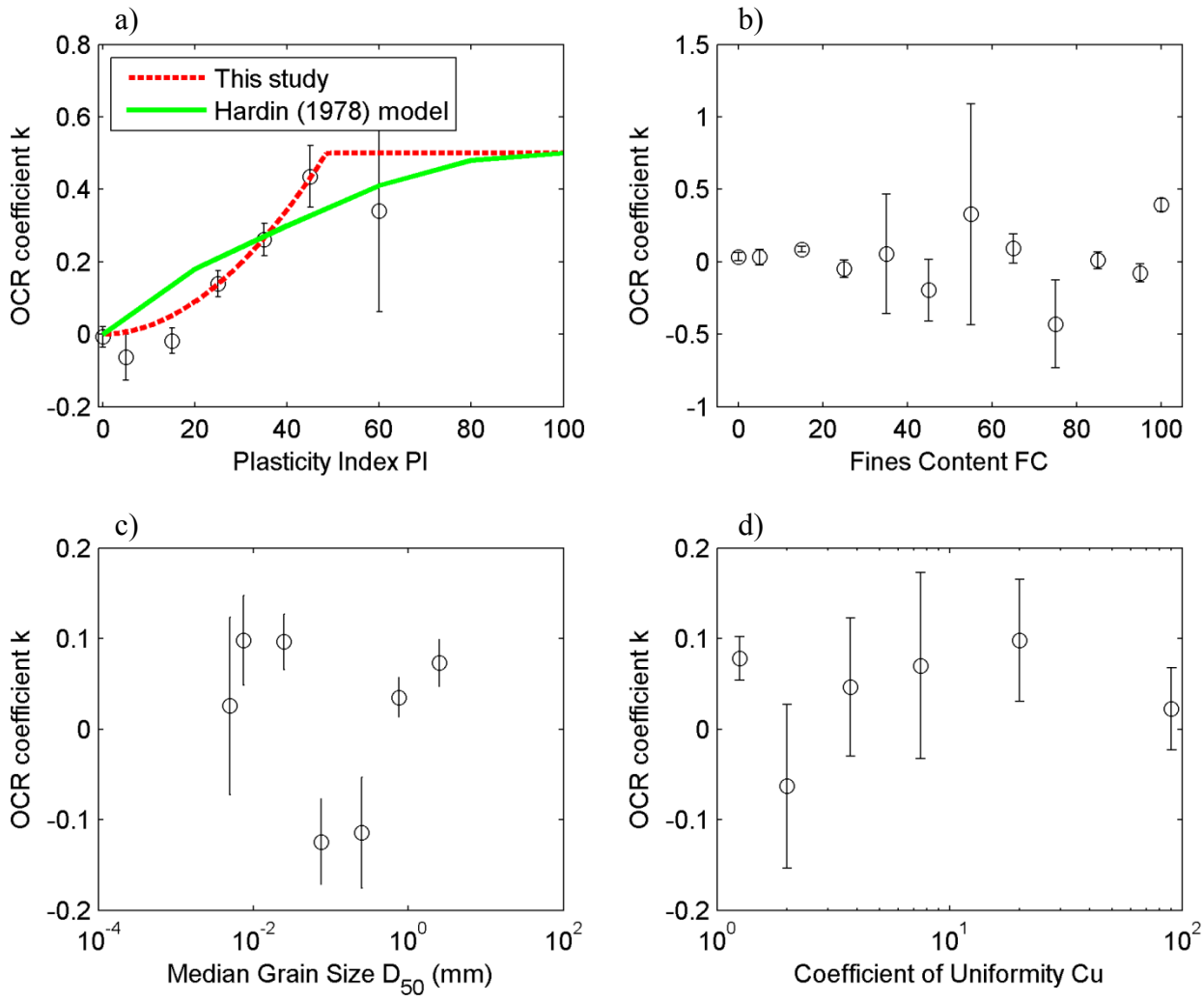

Figure 4.9: Coefficient k for all tests regressed against different bins of a) PI, b) FC, c) D_{50}, and d) Cu. Error bars are the standard errors of the predicted value of k. The point at PI = 60 is for soils with PI > 50.

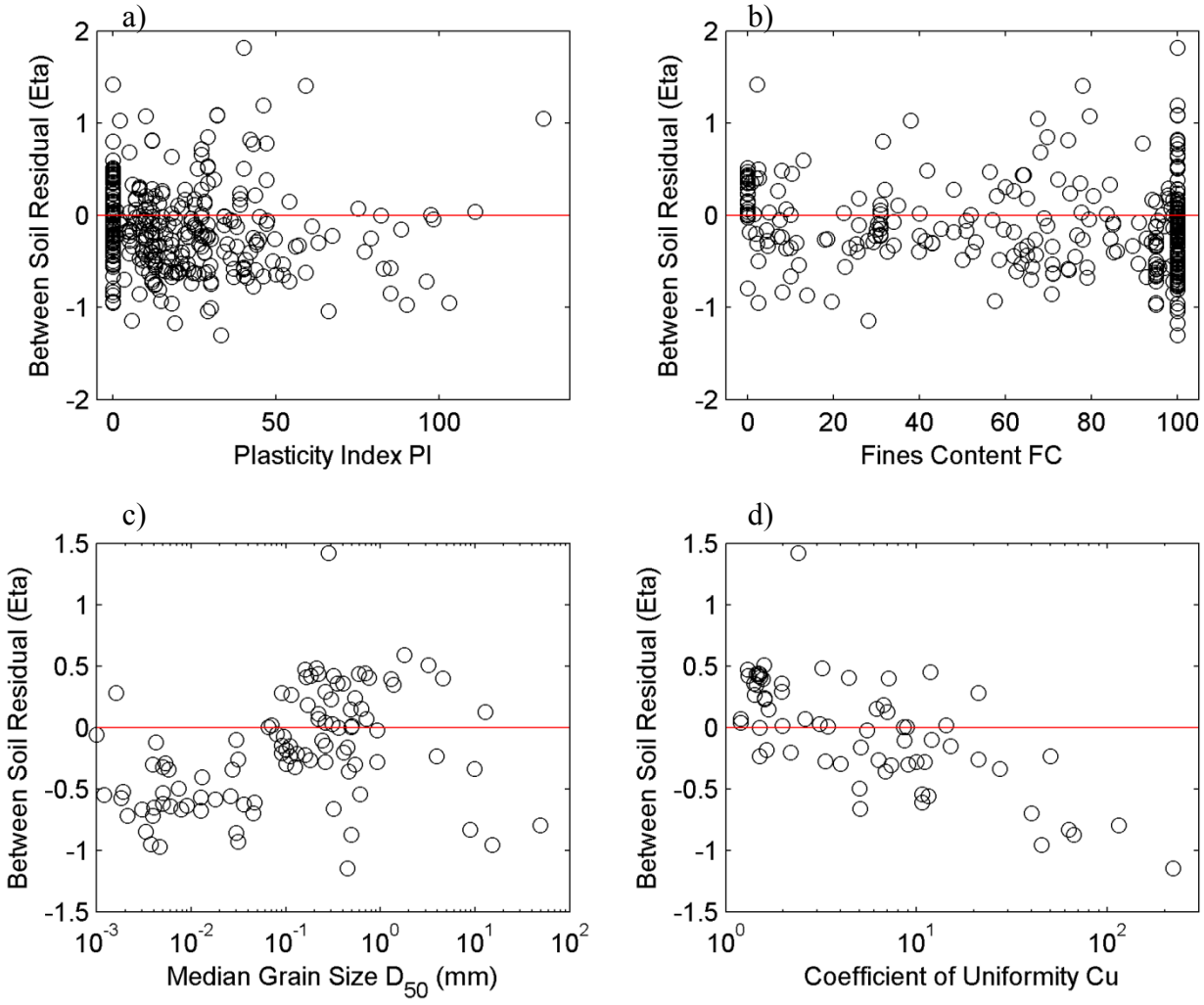

Figure 4.10: Between soil residuals η for equation (4.8) versus a) PI, b) FC, c) D_{50}, and d) Cu

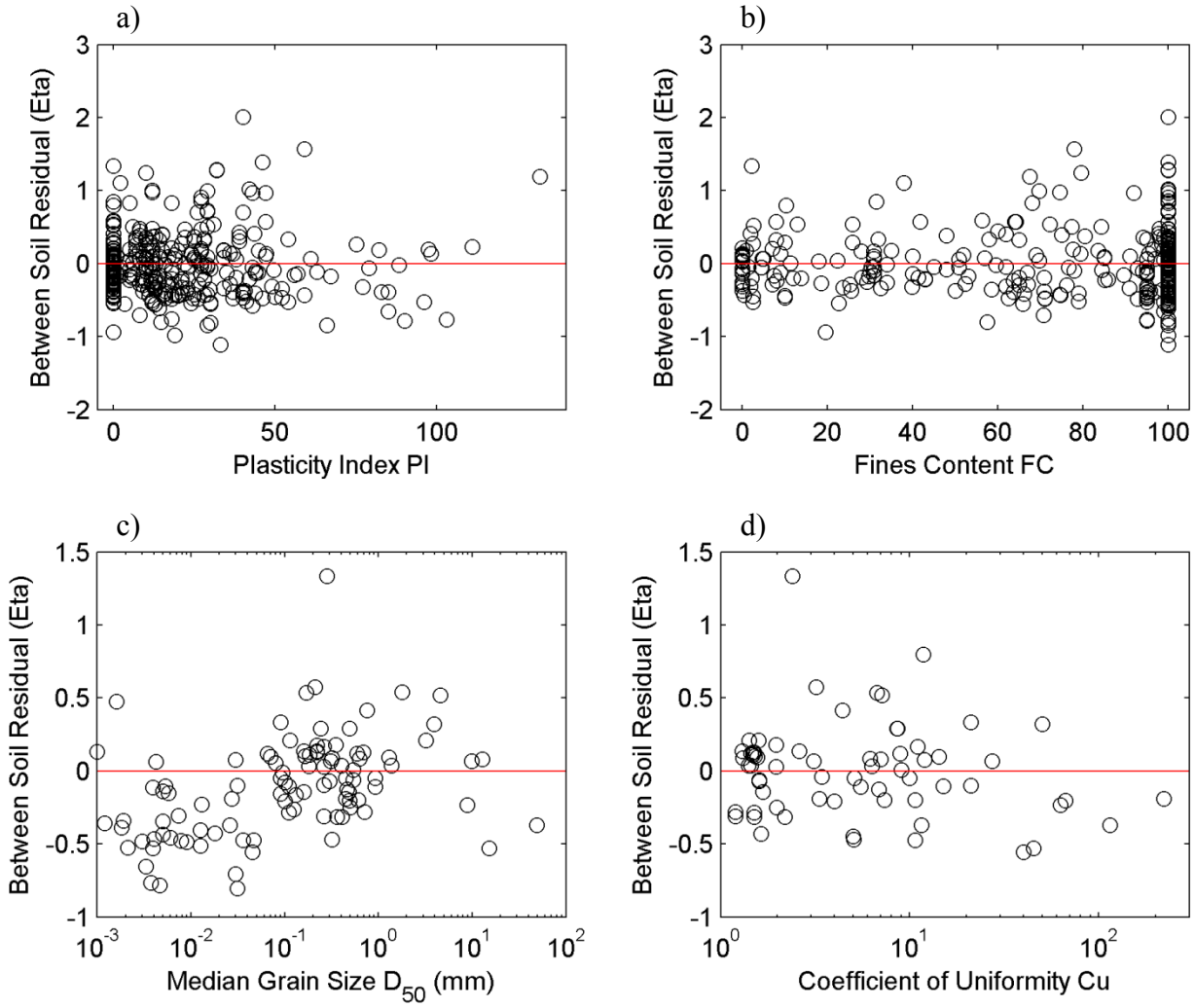

Figure 4.11: Between soil residuals η for equation (4.13) versus a) PI, b) FC, c) D_{50}, and d) Cu

Table 4.4: Value of coefficient c_1 regressed for equation (4.5) (only for soils with σ'_m = 1 atmosphere and OCR = 1); equation (4.6) (only for tests with OCR = 1), and equations (4.8) and (4.13) (all tests in the database)

Equation #	Value	Standard Error
4.5	408.6	20.19
4.6	444.9	13.89
4.8	457.1	15.85
4.13	790.2	41.8

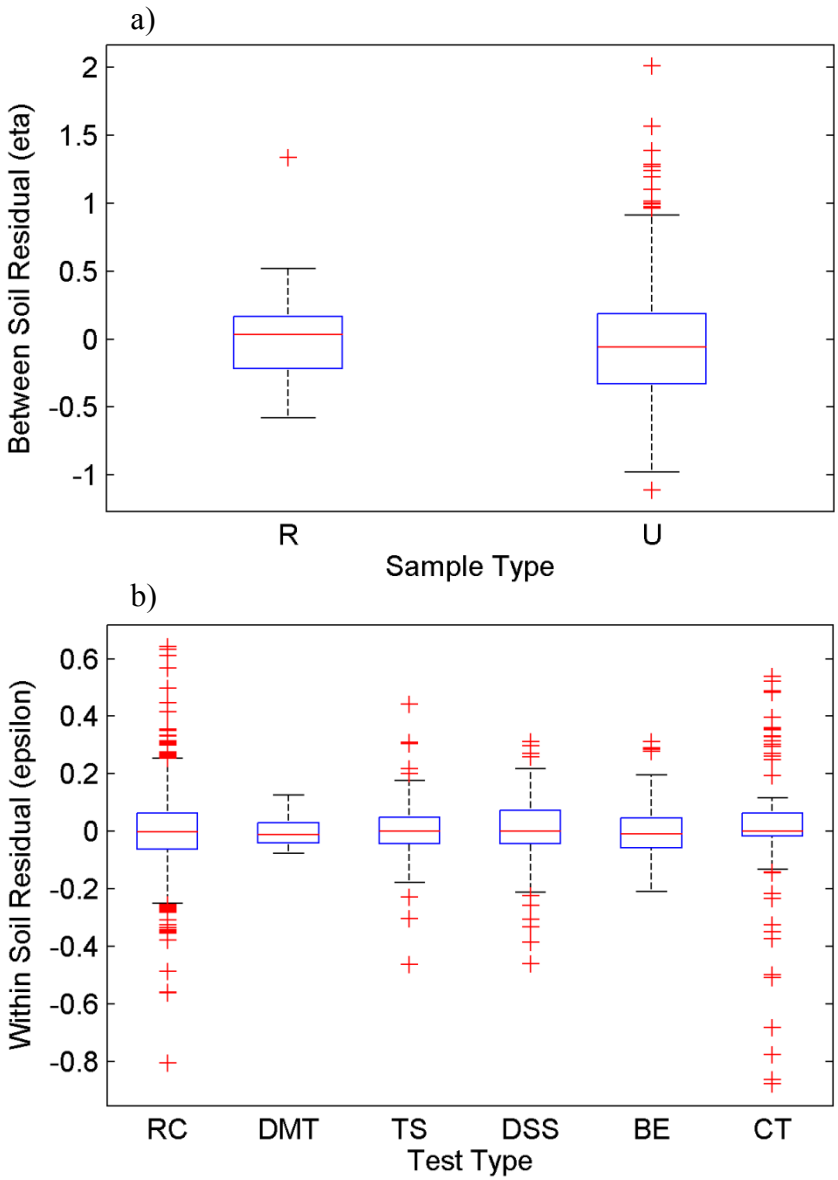

Figure 4.12: One-way ANOVA test results for a) between soil residuals η versus sample type (r = reconstituted; u = 'undistrurbed'), p-value = 0.75, and b) within soil residuals ε versus test type (RC = resonant column; DMT = flat plate dilatometer; TS = torsional shear; DSS = direct simple shear; BE = bender element; CT = cyclic triaxial), p-value = 1.0

Table 4.5: Evaluation of the different $G_{max,lab}$ models (for all soils in the database)

Equation #	σ	τ	σ_{total}	p
4.5	0.414	0.638	0.761	
4.6	0.135	0.516	0.534	< 0.001
4.8	0.130	0.456	0.474	< 0.001
4.12	0.130	0.438	0.457	0.93
4.13	0.130	0.438	0.457	0.004

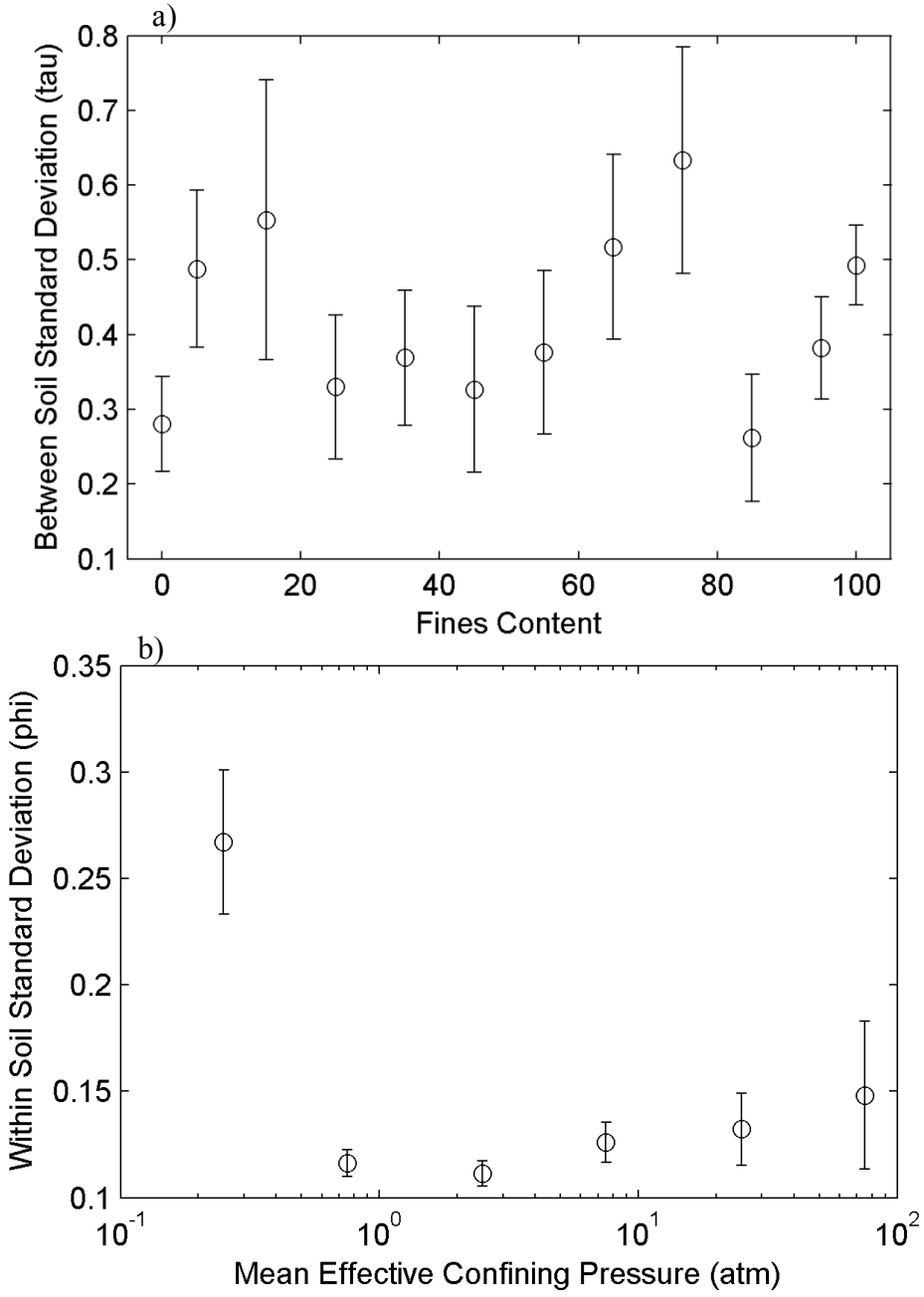

Figure 4.13: Between soil standard deviation τ versus fines content and within soil standard deviation ϕ versus σ'_m for equation (4.13), error bars are 95% confidence intervals.

Table 4.6: Data collected to develop $G_{max,insitu}$ model

Reference	Lab Test[a]	Field Test[b]	Soil(s) Tested
Cavallaro et al. 2000	RC, TS	DH	Fabriano Clay
EPRI 1994	RC	CH,DH,SL	Soils from California and Taiwan
Lefebvre et al. 1994	RC	SASW	Champlain Clay
Nigbor 2012 (ROSRINE)	RC	SL	Soils from California
Schneider et al. 1999	RC	SASW	Piedmont Residual Soils

[a]RC = resonant column; TS = torsional shear

[b]CH = crosshole; DH = downhole; SASW = spectral analysis of surface waves; SL = suspension logger

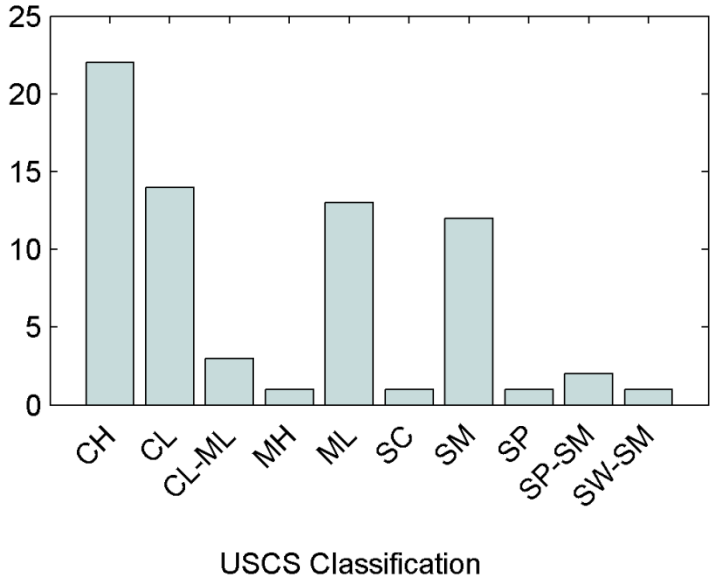

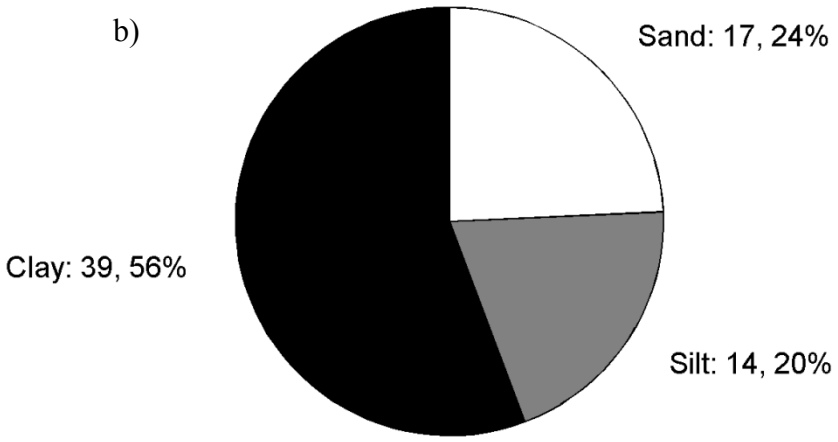

Figure 4.14: In-situ soil database; a) USCS designation for each soil b) number and percentage of tests for each general soil type

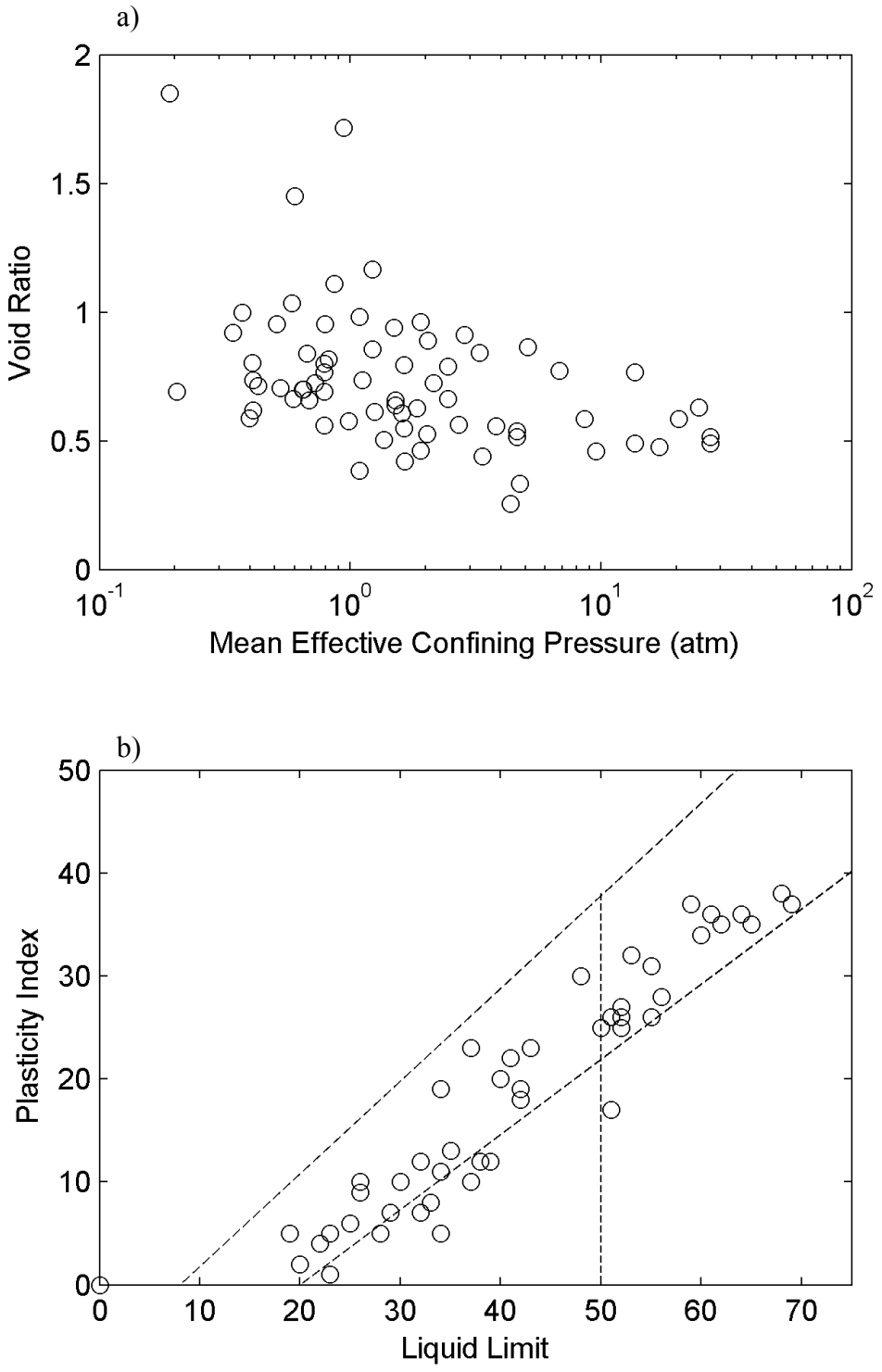

Figure 4.15: In-situ soil database; a) distribution of void ratio and σ'_m; b) plasticity characteristics of collected soils

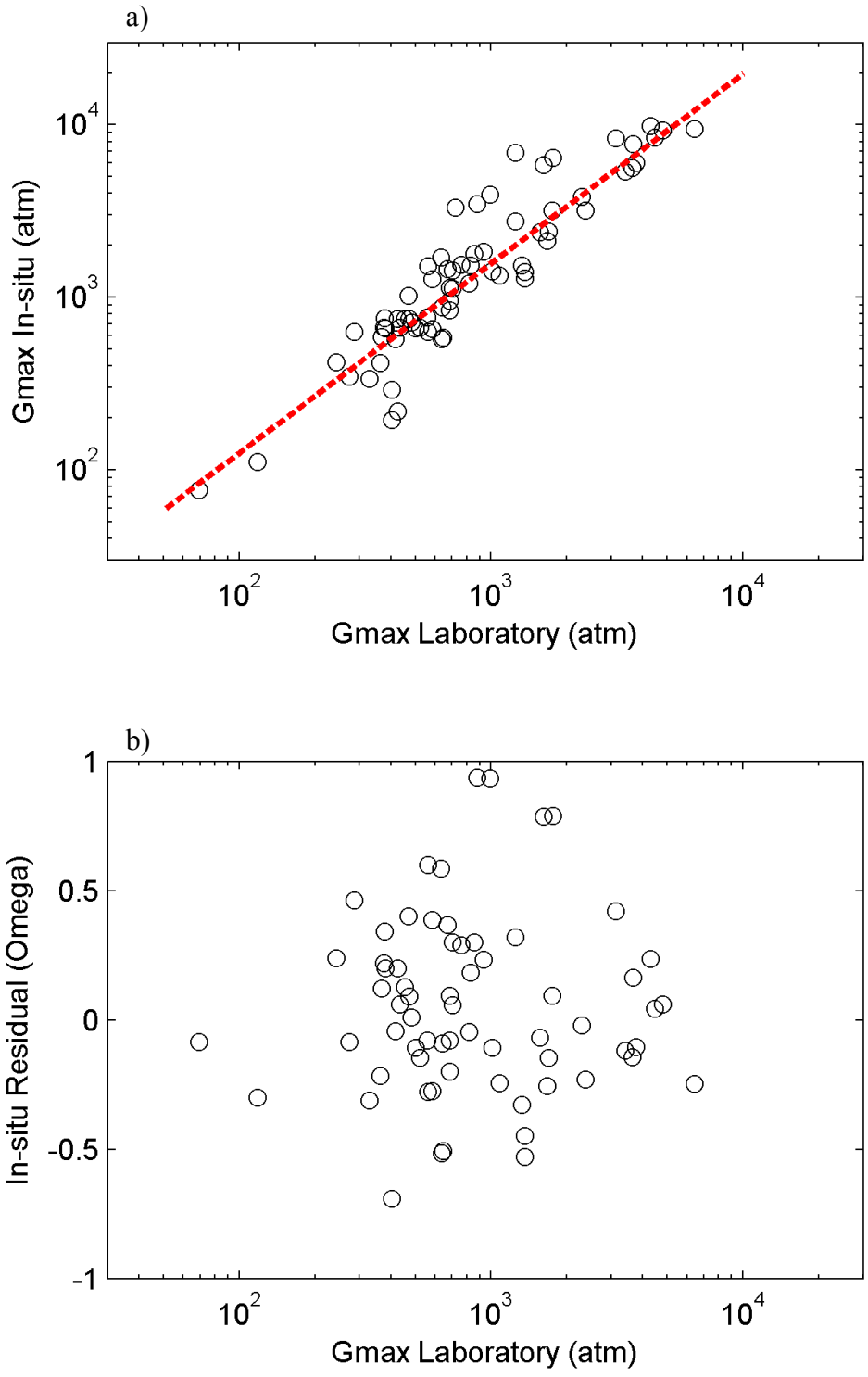

Figure 4.16: Comparison of $G_{max,lab}$ vs $G_{max,in-situ}$ (R^2 = 0.91) and residuals

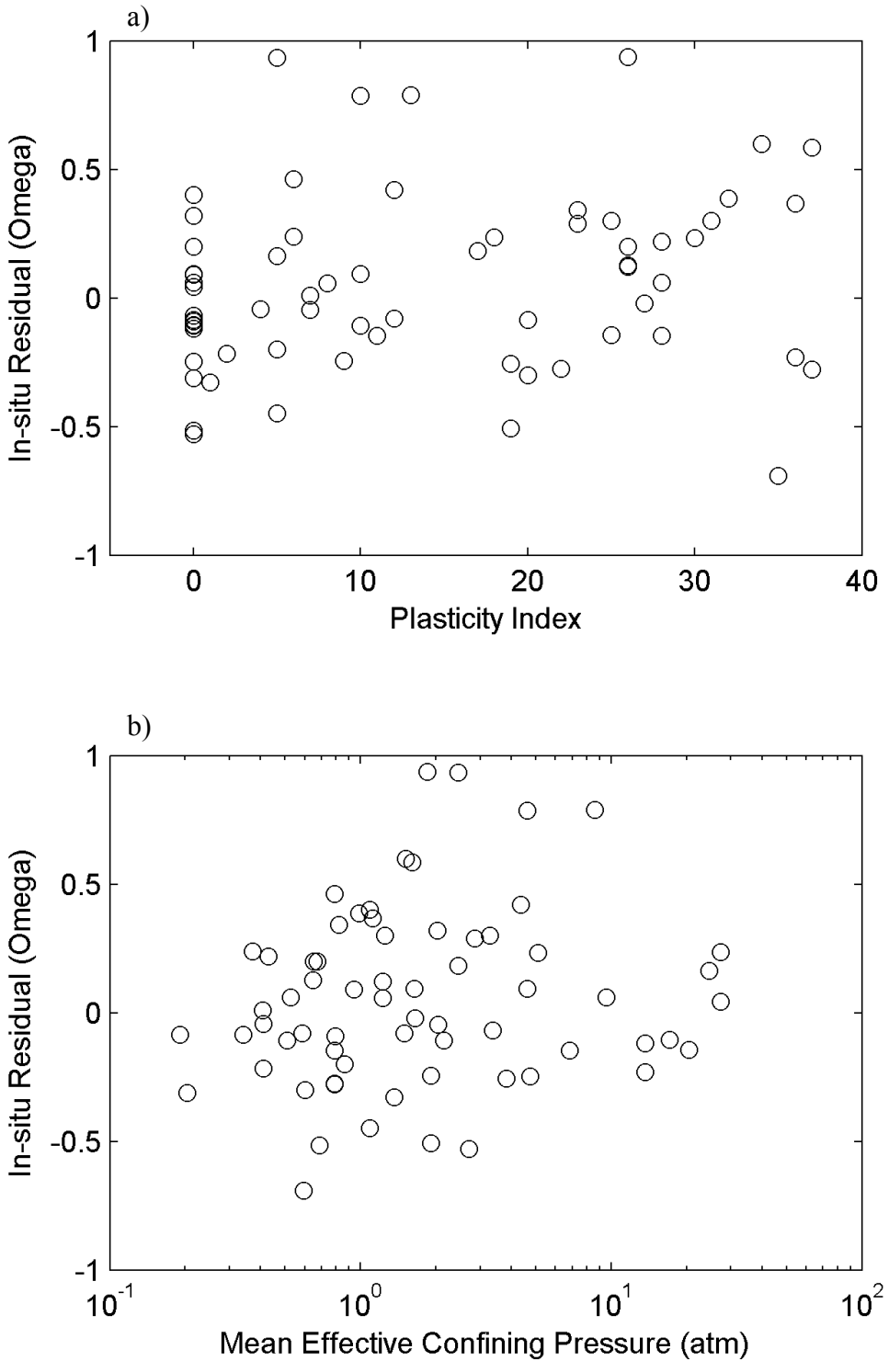

Figure 4.17: In-situ residuals ω versus a) PI and b) σ'_m

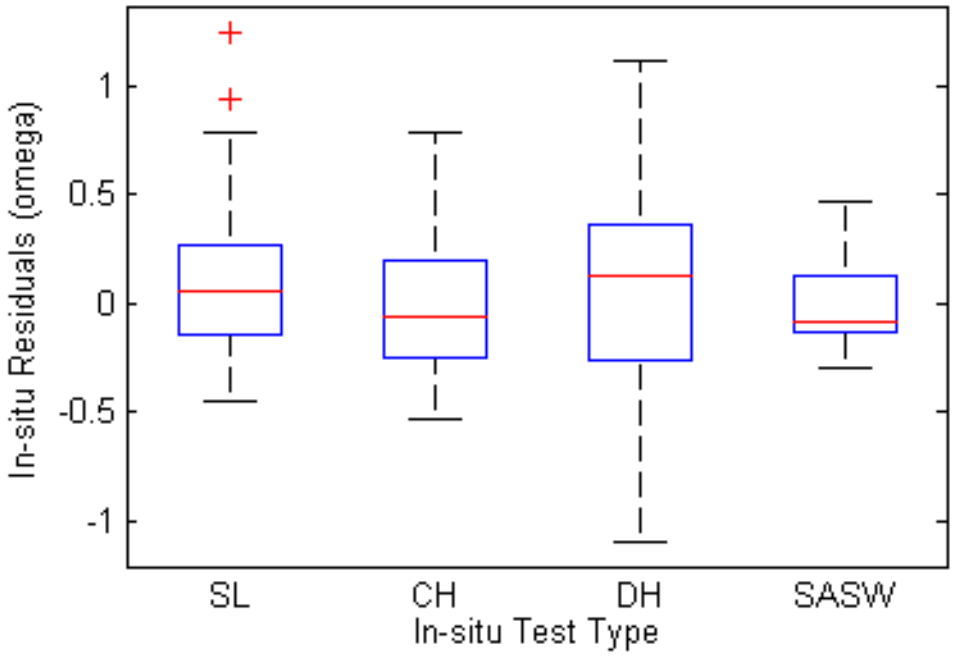

Figure 4.18: One-way ANOVA test results for in-situ residuals ω versus in-situ test type (SL = suspension logger; CH = crosshole; DH = downhole; SASW = spectral analysis of surface waves); p-value = 0.81

Table 4.7: Data collected to validate $G_{max,insitu}$ model

Reference	Field Test[a]	Soil(s) Tested
EPRI 1994	CH,DH,SL	Soils from California and Taiwan
Lefebvre et al. 1994	SASW	Champlain Clay
Nikolaou 2012	CH	Soils from New York City
Nigbor 2012 (ROSRINE)	SL	Soils from California
Pass 1991	CH	Soils from Treasure Island, CA
Schneider et al. 1999	SASW	Piedmont Residual Soils
Shibuya and Tanaka 1996	SCPT	Various Japanese Clays

[a]CH = crosshole; DH = downhole; SASW = spectral analysis of surface waves; SL = suspension logger; SCPT = seismic cone penetration test

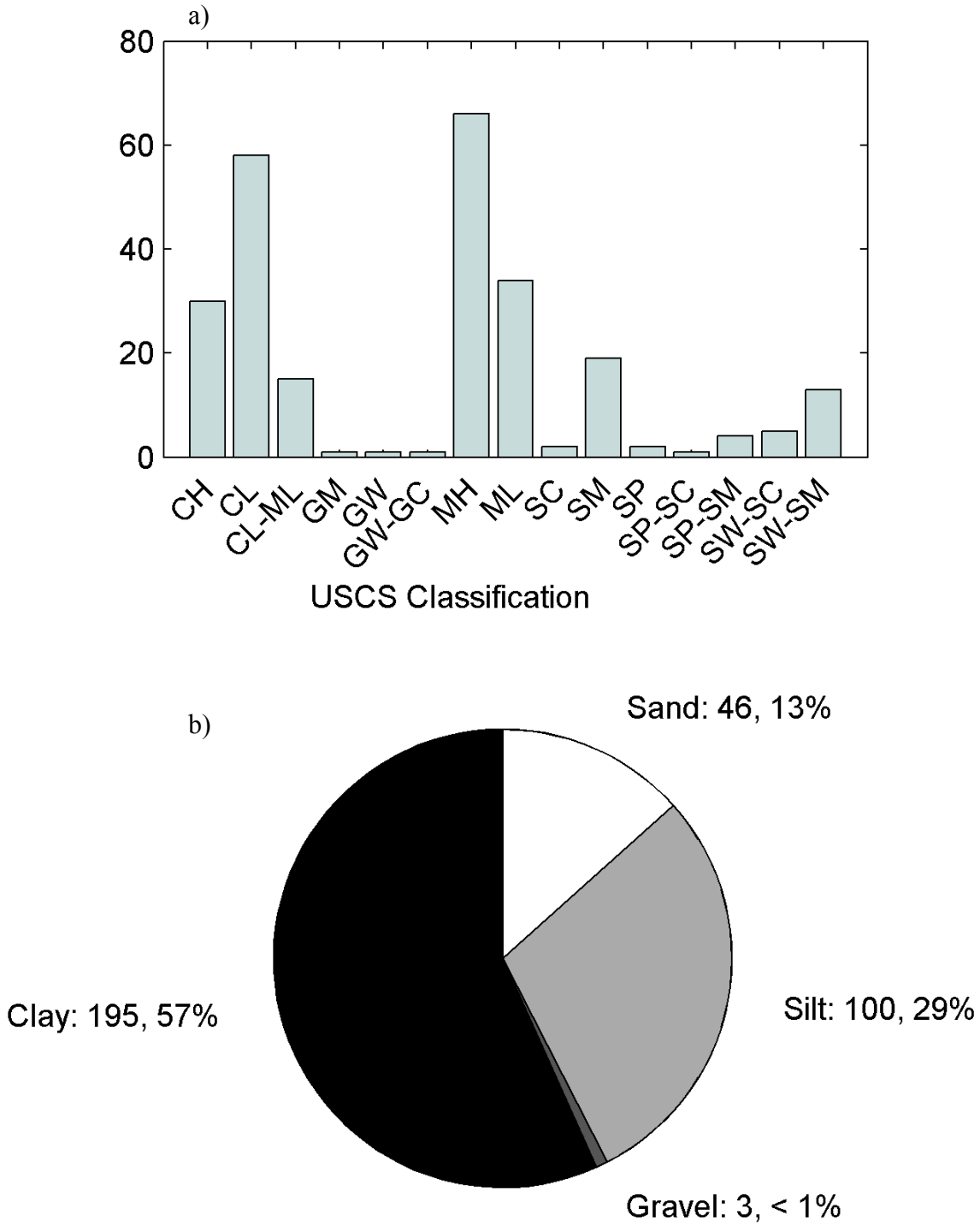

Figure 4.19: Model validation database; a) USCS designation for each soil and b) number and percentage of tests for each general soil type

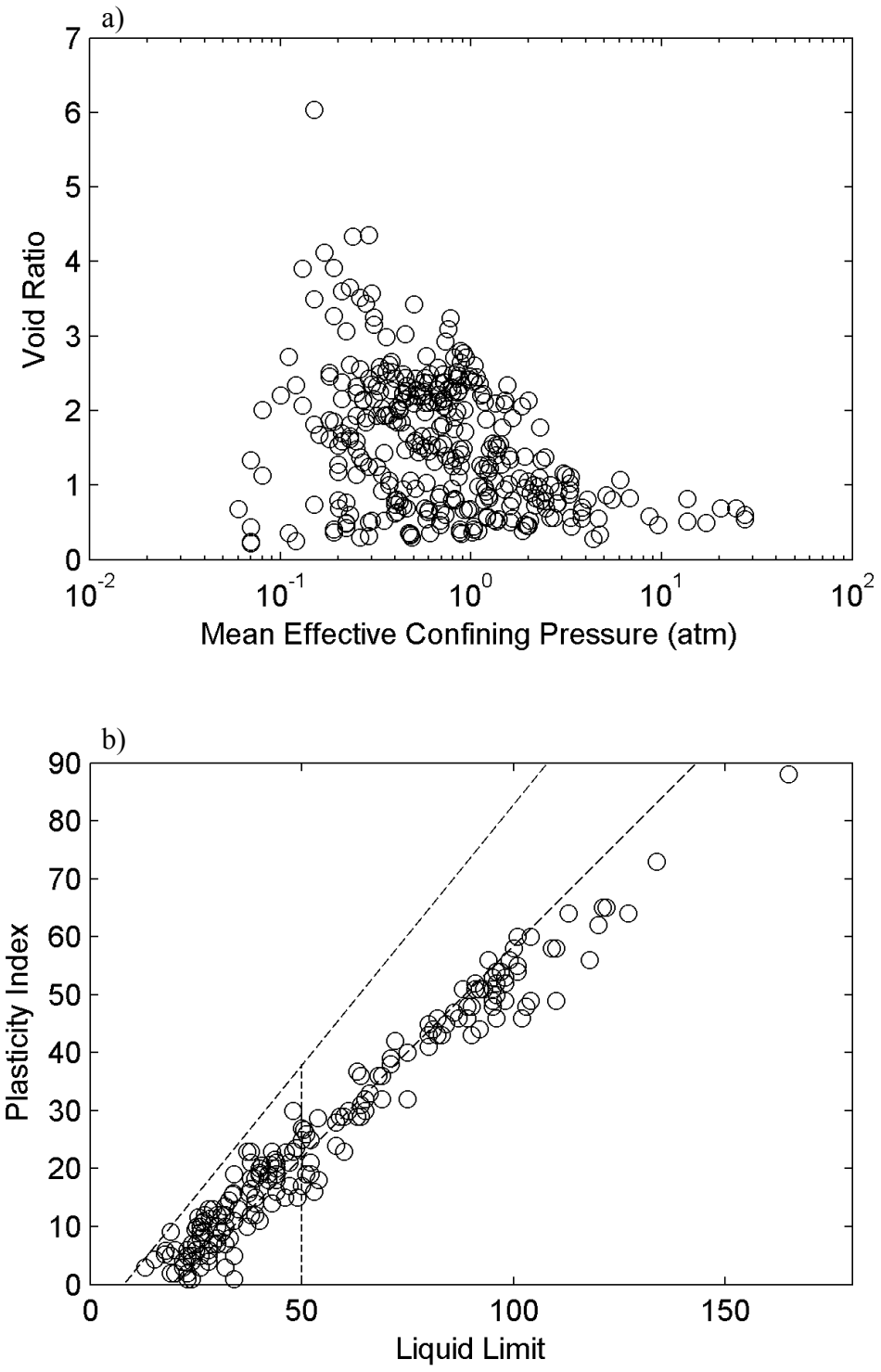

Figure 4.20: Model validation database; a) distribution of void ratio and σ'_m; b) plasticity characteristics

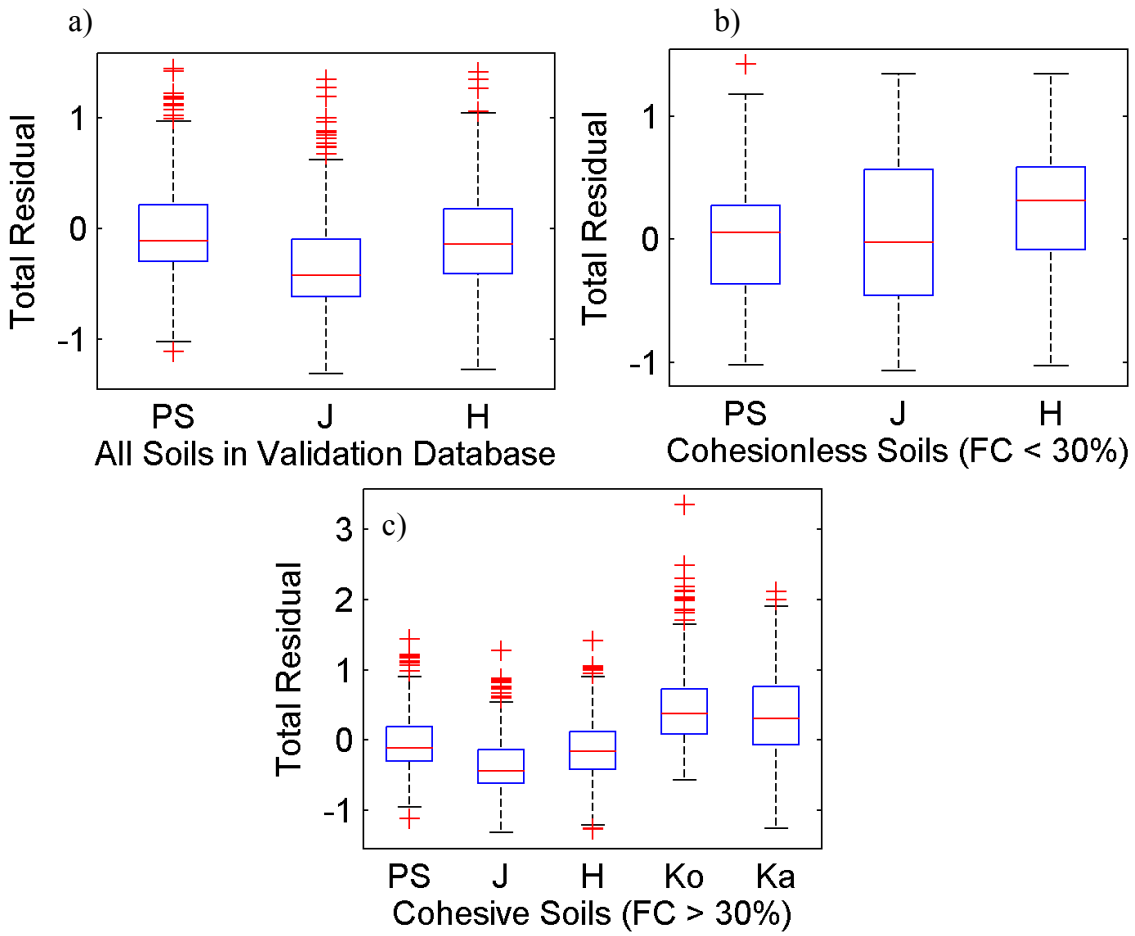

Figure 4.21: $G_{max,in\text{-}situ}$ model comparison for a) all soils in the validation database, b) soils with FC < 30%, and c) soils with FC > 30%; PS = present study; J = Jamiolkowski et al (1991); H = Hardin (1978); Ko = Kokusho et al. (1982); Ka = Kallioglou et al. (2008)

Table 4.8: Comparison of models

		Present Study	Jamiolkowski et al. (1991)	Hardin (1978)	Kokusho et al. (1982)	Kallioglou et al. (2008)
All Soils	Mean	-0.03	-0.33	-0.11		
	Median	-0.12	-0.43	-0.15		
	σ_{total}	0.43	0.46	0.47		
FC < 30%	Mean	0.03	0.00	0.26		
	Median	0.06	-0.02	0.31		
	σ_{total}	0.63	0.68	0.63		
FC > 30%	Mean	-0.04	-0.35	-0.13	0.51	0.34
	Median	-0.12	-0.44	-0.16	0.38	0.30
	σ_{total}	0.41	0.43	0.44	0.60	0.60

CHAPTER 5: SHEAR MODULUS REDUCTION AND DAMPING CURVES

5.1 Introduction

Many researchers have devoted considerable effort towards developing analytical techniques for evaluating the seismic response of soils. However, the accuracy and reliability of seismic response analyses are highly dependent on the characterization of the dynamic properties of the soil, such as the small strain shear modulus (G_{max}), small strain damping (D_{min}), and how the shear modulus (G) and damping (D) change with shear strain (γ). The first half of this chapter reviews past research and observed trends between different soil or testing parameters and the dynamic properties of soils. The second half of this chapter describes the empirical models for estimating shear modulus reduction and damping curves developed by Vucetic and Dobry (1991), Darendeli (2001), and Kishida et al. (2009). The models of Darendeli (2001) and Kishida et al. (2009) are used to model the dynamic properties of soils in the site response analyses when no dynamic tests were conducted for a particular soil.

In site response analyses the stiffness and damping are the most important soil properties (Kramer, 1996). Figure 5.1 shows a hysteresis loop exhibited by a soil subjected to cyclic loading, as during an earthquake for example. The shear modulus is defined as the shear stress divided by the shear strain. The tangent shear modulus is the slope of the hysteresis loop at any given point along the curve. The secant shear modulus is the slope of the line that passes through the origin and the tip of the hysteresis loop. Shear modulus reduction curves are given as the secant shear modulus divided by the small strain shear modulus (G_{sec}/G_{max}) versus shear strain (γ). The equivalent viscous damping (D) is proportional to the energy loss from a single cycle of shear deformation. It is estimated from the width and inclination of the hysteresis loop, as shown in Figure 5.1, where A_{loop} is the area of the hysteresis loop. Figure 5.2 shows the backbone curve, which is the curve corresponding to the tips of the hysteresis loops at different shear strains. The backbone curve asymptotically approaches the shear strength of the soil τ_{ff}, at large strains, and the slope of the backbone curve at small strains is the small strain shear modulus (G_{max}). Figure 5.3 shows a shear modulus reduction curve, and Figure 5.4 shows a damping curve. As the shear strain increases the normalized shear modulus decreases and the damping increases.

Figure 5.3 and Figure 5.4 also show how Vucetic (1994) divided the shear modulus reduction and damping curves into three regions separated by two shear strain values. Vucetic (1994) called these shear strains the linear cyclic threshold shear strain (γ_{tl}) and the volumetric cyclic threshold shear strain (γ_{tv}). Darendeli (2001) referred to these shear strain values as the elastic threshold shear strain (γ_t^e) and the cyclic threshold shear strain (γ_t^c). At shear strains smaller than γ_{tl} soils exhibit linear elastic behavior, the shear modulus is a constant maximum value, G_{max}, and the damping is a constant minimum value, D_{min}. At shear strains between γ_{tl} and γ_{tv} soils exhibit nonlinear elastic behavior. The shear modulus degrades and damping increases, but the amount of plastic deformation and pore pressure generation is negligible so that deformations are

recoverable upon unloading. At shear strains greater than γ_{tv}, soils exhibit nonlinear plastic behavior and volume change and pore pressure generation are observed.

5.2 Observed Trends

Chapter 4 presented a detailed analysis of the small strain shear modulus and proposed a new unified model to estimate G_{max} for clays, silts, sands, and gravels. The following section describes the observed trends found by other researchers for normalized shear modulus reduction curves, as well as the damping at small and medium/large shear strains.

5.2.1 Shear Modulus Reduction Curves

Many researchers have found that soil type, and especially plasticity index (PI) as the soil type index, is the most influential parameter in regards to shear modulus reduction curves of cohesive soils. As PI increases, the G/G_{max} curves shift to the right, and the volumetric cyclic threshold shear strain (γ_{tv}) increases (Kokusho et al., 1982; Sun et al., 1988; Vucetic and Dobry, 1991; Ishibashi and Zhang, 1993; Darendeli, 2001; Zhang et al., 2005; Okur and Ansal, 2007).

As the mean effective confining pressure increases the G/G_{max} curves shift to the right as well for both cohesive and cohesionless soils, but this effect decreases with increasing PI (Kokusho, 1980; Sun et al., 1988; Kagawa, 1992; Menq, 2003; Zhang et al., 2005). Menq (2003) also found that as the coefficient of uniformity increases the effect of the mean effective confining pressure (σ'_m) on G/G_{max} decreases.

Sun et al. (1988), Vucetic and Dobry (1991), and Kallioglou et al. (2008) found that as the initial void ratio (e) increases the shear modulus reduction curves also shift to the right. However, Vucetic and Dobry (1991) concluded that plasticity index (PI) has a stronger influence than void ratio (e) because it is less susceptible to disturbance.

Anderson and Stokoe (1978) and Zhang et al. (2005) found that as the confinement time (t_g) increases the shear modulus ratio at medium and large shear strains increases for cohesive soils.

Vucetic and Dobry (1991), Kagawa (1992), and Lanzo et al. (2009) observed that as the number of shearing cycles (N) increases the shear modulus ratio decreases, and as the shear strain increases the effect of N increases. In other words, at larger shear strains the effect of the number of shearing cycles is greater. Alarcon-Guzman et al. (1989) and Lo Presti et al. (1997) found that as N increases the value of G/G_{max} of cohesionless soils increases, which is the opposite found for cohesive soils.

The effect of excitation frequency (f), however, is negligible at medium and large shear strains for both cohesive and cohesionless soils (Sun et al., 1988; Lo Presti et al., 1997; Darendeli, 2001; Yamada et al., 2008).

Darendeli (2001) found that as the overconsolidation ratio (OCR) increases, G/G_{max} increases slightly for cohesive soils but not for cohesionless soils. Kokusho et al. (1982), Sun et al. (1988),

Vucetic and Dobry (1991), and Kallioglou et al. (2008) found that OCR has a negligible effect on G/G_{max} of cohesive soils.

Seed et al. (1984), Yasuda and Matsumoto (1993), and Yasuda et al (1996) found that the G/G_{max} of gravels was usually greater than that for sands for a given shear strain. This can loosely be interpreted as the fact that when D_{50} increases the value of G/G_{max} increases.

Menq (2003) and Iwasaki and Tatsuoka (1977) observed that as Cu increased the shear modulus ratio decreased.

Table 5.1 lists the effects on the shear modulus reduction curve described above in a compact form. An upward facing arrow indicates that as the parameter in the 'controlling parameter' column increases, the value of G/G_{max} increases for a given shear strain. In other words, for an upward facing arrow the G/G_{max} curve shifts to the right. The cells under the column 'cross correlations' indicate that as the 'controlling parameter' increases, the effect of the parameter under 'cross correlations' on G/G_{max} either increases (upward facing arrow), or decreases (downward facing arrow). For example, as PI increases the effect of confining pressure on G/G_{max} decreases.

5.2.2 Damping at Small Strains

The majority of small strain damping ratio values for cohesive soils are between 0.5% and 5% (Seed and Idriss, 1970; Sun et al, 1988; Vucetic and Dobry, 1991; Darendeli, 2001). For cohesionless soils D_{min} ranges between 0.2% and 2% (Menq 2003). Within such a small range, and due to the limitation of testing apparatus, it is difficult to determine D_{min} and the parameters that influence it. As a result, there is no consensus on which parameters influence D_{min} the most. The following section outlines the effects of some parameters on the value of small strain damping in soils as found by previous studies.

Kim and Novack (1981), Kokusho et al. (1982), Vucetic et al. (1998), and Darendeli (2001) found that as the mean effective confining pressure increases the value of D_{min} for cohesive soils decreases. Chung et al. (1984), Saxena and Reddy (1989), and Menq (2003) found the same for cohesionless soils.

Kallioglou et al. (2008) and Tika et al. (2010) observed that as the void ratio (e) increases the value of D_{min} for cohesive soils decreases. Laird (1994) found the same for cohesionless soils. Kim and Novack (1981), Kokusho (1992), EPRI (1993), the ROSRINE study (Nigbor, 2012), and Darendeli (2001) found that as the confining time (t_g) increases D_{min} decreases for cohesive soils. EPRI (1993), the ROSRINE study (Nigbor, 2012), and Darendeli (2001) also observed this same effect for cohesionless soils, but to a lesser extent than cohesive soils.

Vucetic et al. (1998) and Darendeli (2001) found that for cohesive soils as OCR increases, D_{min} decreases. Menq (2003) found a negligible effect of OCR on D_{min} for cohesionless soils.

Shibuya et al. (1995) hypothesized that D_{min} had a U shaped variation with excitation frequency (f). At frequencies less than 0.1 Hz, Shibuya found that D_{min} decreased with increasing f,

between 0.1 and 10 Hz D_{min} was unaffected by changes in f, and above 10 Hz D_{min} increased with increasing f. However, Vucetic et al. (1998) found that f had no effect on D_{min} for frequencies between 0.01 and 0.1 Hz for cohesive or cohesionless soils. Darendeli (2001) determined that frequency has a negligible effect on D_{min} below 1 Hz, but that above 1 Hz D_{min} increases by about 100% over a log-cycle increase in excitation frequency for both cohesive and cohesionless soils. He also noticed that the effect of frequency increased with increasing plasticity index (PI). Cavallaro et al. (2000) found that small strain damping values for cohesive soils determined using cyclic torsional shear tests at 0.1 Hz excitation frequency were always lower than damping values determined with resonant column tests, which are conducted at much higher frequencies.

Lo Presti et al. (1997), and Darendeli (2001), found the effect of the number of loading cycles (N) on the value of damping (D) to be negligible at shear strains below the volumetric cyclic threshold shear strain (γ_{tv}) for cohesive and cohesionless soils. Lanzo et al. (2009) found the same for very soft clays taken from offshore Italy.

Pyke derived analytically that the effect of PI on damping ratio for cohesive soils changes based on shear strain (EPRI 1993). For strains smaller than about 0.005%, as PI increases D increases, whereas for strains larger than about 0.005% D decreases as PI increases. Stokoe et al. (1994), Vucetic et al. (1998), and Darendeli (2001) later confirmed this experimentally. Darendeli (2001) explains the reason for this switch is due to the change in the predominant type of damping occurring in the soil. At medium and large strains the soil nonlinearity greatly affects the stress-strain curve of the soil. The more nonlinear a soil behaves the larger the area under the hysteresis loop becomes, which in turn means greater damping. As PI increases soil nonlinearity decreases, therefore, as PI increases damping decreases at large shear strains. At small strains, however, soils behave more linearly, and the effect of the viscosity of the soil skeleton (also called creep or relaxation) is more dominant (Vucetic et al. 1998).

Menq (2003) found that as D_{50} increased D_{min} decreased, and as the coefficient of uniformity (Cu) increased D_{min} increased.

Table 5.2 lists the effects of the parameters described above on the small strain damping. The format is the same as for Table 5.1.

5.2.3 Damping at Medium and Large Strains

Vucetic and Dobry (1991), Darendeli (2001), Okur and Ansal (2007), and Yamada et al. (2008) found that for medium and large shear strains, as plasticity index (PI) increases damping (D) decreases for cohesive soils. As mentioned earlier, for strains smaller than about 0.005% the opposite is true.

Kokusho (1980), Saxena and Reddy (1989), and Lo Presti et al. (1997) found that as the mean effective confining pressure (σ'_m) increases the damping ratio (D) decreases for cohesionless soils. Kagawa (1992), Darendeli (2001), and Zhang (2005) found the same for cohesive soils. They also found that as PI increases the magnitude of the effect of σ'_m decreases.

Vucetic and Dobry (1991) and Kallioglou et al. (2008) determined that as void ratio (e) increases damping (D) decreases for cohesive soils. However, as stated earlier for G/G_{max}, Vucetic and Dobry (1991) concluded that plasticity index has a stronger influence than void ratio (e) on damping because it is less susceptible to disturbance.

Koutsoftas and Fischer (1980), Kokusho et al. (1982) and Vucetic and Dobry (1991) determined that OCR has no effect on damping for cohesive soils at medium and large strains. Darendeli (2001), on the other hand, found that OCR has a small decreasing effect on damping for cohesive soils.

There is little to no effect of confinement time (t_g) on damping at medium and large strains once the effect of confinement time at small strains has been accounted for (Darendeli 2001). As confinement time increases D_{min} decreases, which shifts the entire damping curve down at every strain level.

At strains larger than the volumetric cyclic threshold shear strain (γ_{tv}) the damping ratio (D) decreases as the number of shearing cycles (N) increases for cohesive soils (Lo Presti et al., 1997; Darendeli, 2001; Lanzo et al., 2009). Menq (2003) observed that for cohesionless soils as N increases D decreases, however, Lo Presti et al (1997) found that D increased, which is the same as they found for G/G_{max} for cohesionless soils.

Lo Presti et al. (1997) found that excitation frequency (f) has a negligible effect on the damping ratio at medium to large shear strains for cohesionless soils. Darendeli (2001) and Menq (2003) concluded that there is little to no effect of excitation frequency on damping at medium and large strains once the effect of excitation frequency has been accounted for at small strains.

Darendeli (2001) found that the effect of excitation frequency (f) and number of shearing cycles (N) increases with increasing strain, and that as the plasticity index (PI) increases the effect of f increases but the effect of N decreases for cohesive soils.

Yasuda and Matsumoto (1993) found that as the median grain size (D_{50}) increases, the damping ratio (D) increases for cohesionless soils.

Table 5.3 lists the effects of the parameters described above on damping at medium and large shear strains. The format is the same as for Table 5.1 and Table 5.2. Many of the parameters that influence the shear modulus reduction curves of cohesive soils have the opposite effect on damping curves.

5.3 Published Models

There are many published models to predict shear modulus reduction and damping curves. Models that have been widely used in research and practice include the models developed by Seed and Idriss (1970), Seed et al (1984), Vucetic and Dobry (1991), Ishibashi and Zhang (1993), EPRI (1993), Darendeli (2001), Menq (2003), Zhang et al (2005), and Kishida et al (2009). The next few sections explain in detail the models by Vucetic and Dobry (1991), Darendeli (2001), and Kishida et al (2009), followed by a brief comparison of the different

models. This study used the Darendeli (2001) model for soils when no measured shear modulus reduction and damping curves were available, except for organic soils, where the model of Kishida et al (2009) was used. Chapter 6 discusses the selection of the soil and site parameters in detail.

5.3.1 Vucetic and Dobry (1991)

Vucetic and Dobry (1991) derived their model from the experimental results of 17 different publications (Table 5.4) that included clays with OCR from 1 to 15 and some sands. Their analysis showed that; (1) the plasticity index (PI) was the most influential parameter with regards to the shear modulus reduction and damping curves, (2) as PI increases the shear modulus reduction curve shifts to the right, the volumetric cyclic threshold shear strain (γ_{tv}) increases, and the damping curve decreases for a given shear strain, (3) as PI increases the rate of degradation of the shear modulus (G) with loading cycles (N) decreases for normally consolidated soils.

Vucetic and Dobry (1991) found that more consistent trends were obtained with PI than void ratio (e). They hypothesized that this was because PI depends only on the composition of the soil (size, shape, and mineralogy of the soil particles, chemistry of the pore water, etc.), whereas the void ratio depends both on the composition of the soil and on the consolidation stresses and OCR. Therefore, plasticity index is a better indicator than void ratio because it is less susceptible to sample disturbance and more representative of the soil composition.

Figure 5.5 and Figure 5.6 show the recommended shear modulus reduction and damping curves of Vucetic and Dobry (1991), respectively. They provide no equations for the curves. Vucetic and Dobry (1991) cautioned that their model should not be used for soils with a very sensitive structure, such as quick clays, and that damping at small strains was not well defined and required more investigation.

5.3.2 Darendeli (2001)

Darendeli (2001) developed a model to predict shear modulus reduction and damping curves from a database of 110 soil samples from 20 sites using a First-order, Second-Moment Bayesian Method (FSBM). The soil samples were tested in a combined resonant column and torsional shear device (RCTS) at the University of Texas at Austin (UTA) over a period of ten years. Professor Ken Stokoe and his graduate students developed the RCTS equipment to measure the dynamic properties of soils at both small and large shear strains. Detailed information regarding the equipment, testing method, theory, and calibration is presented in Darendeli and Stokoe (1997).

Table 5.5 lists the sites, regions, number of samples, and references of the data that Dareneli (2001) used to develop his model. The majority of the soil samples were from California and were funded as part of two large research projects conducted by the Electric Power Research Institute (EPRI, 1993), and the Resolution of Site Response Issues in the 1994 Northridge Earthquake (ROSRINE), (Nigbor, 2012). Figure 5.7 shows the distribution of the soils in the database used by Darendeli (2001) according to the mean effective confining pressure (σ'_m), Unified Soil Classification System (USCS) designation, and plasticity index (PI).

Darendeli (2001) based his model on the hyperbolic model proposed by Hardin and Drnevich (1972), but added a curvature coefficient, a, as shown in equation (5.1). The curvature coefficient, as the name implies, has an impact on the curvature of the normalized shear modulus reduction curve.

$$\frac{G}{G_{max}} = \frac{1}{1 + \left(\frac{\gamma}{\gamma_r}\right)^a} \tag{5.1}$$

$$a = \phi_5 \tag{5.2}$$

Where ϕ_5 is a coefficient determined from regression analyses. The reference strain, γ_r, is the shear strain in percent when G/G_{max} equals 0.5. The reference strain is a function of plasticity index (PI), overconsolidation ratio (OCR), and mean effective confining pressure (σ'_m) in atmospheres, as shown in equation (5.3):

$$\gamma_r = \left(\phi_1 + \phi_2 \times PI \times OCR^{\phi_3}\right) \times \sigma'^{\phi_4}_m \tag{5.3}$$

where ϕ_1 through ϕ_4 are coefficients. Darendeli (2001) divided damping into two parts; small strain damping (D_{min}) due to friction and/or viscous losses at the contact surfaces between particles, and damping due to soil nonlinearity or hysteresis (DMasing). These two values of damping are estimated separately and then added together to predict the total equivalent damping of the soil, as shown in equation (5.4):

$$D = F \times D_{Masing} + D_{min} \tag{5.4}$$

where D is damping in percent, and F is a reduction factor described later. D_{Masing} is calculated from the ratio of the dissipated energy to stored strain energy in one complete cycle of motion (see Figure 5.1). Assuming Masing behavior, the dissipated energy (area inside the hysteresis loop, A_{Loop}) can be calculated by integrating the backbone curve over one loading cycle. D_{Masing} can then be written as:

$$D_{Masing,a=1} = \frac{100}{\pi} \times \left[4 \times \frac{\gamma - \gamma_r \times \left(\frac{\gamma + \gamma_r}{\gamma_r}\right)}{\frac{\gamma^2}{\gamma + \gamma_r}} - 2\right] \tag{5.5}$$

assuming a = 1, and γ is the shear strain in percent. For values of a other than 1 the integral cannot be solved in a closed form solution. Darendeli (2001) used the trapezoid rule to determine numerically the value of D_{Masing} for other values of a. He then fit a polynomial to calculate D_{Masing} from $D_{Masing,a=1}$ as:

$$D_{Masing} = c_1 \times D_{Masing,a=1} + c_2 \times {D_{Masing,a=1}}^2 + c_3 \times {D_{Masing,a=1}}^3 \tag{5.6}$$

$$c_1 = -1.1143 \times a^2 + 1.8618 \times a + 0.2523 \tag{5.7}$$

$$c_2 = -0.0805 \times a^2 - 0.0710 \times a - 0.0095 \quad (5.8)$$

$$c_3 = -0.0005 \times a^2 + 0.0002 \times a + 0.0003 \quad (5.9)$$

Darendeli (2001) found that damping calculated only as a function of Masing behavior over predicted damping at large shear strains. To match the measured test data, Darendeli (2001) introduced a reduction factor F.

$$F = b \times \left(\frac{G}{G_{max}}\right)^{0.1} \quad (5.10)$$

$$b = \phi_{11} + \phi_{12} \times ln(N) \quad (5.11)$$

where ϕ_{11} and ϕ_{12} are coefficients. The scaling coefficient b and the normalized modulus reduction curves are used to scale the damping curve estimated from Masing behavior to fit the experimental observations.

Darendeli (2001) found that small strain damping was dependent on the plasticity index (PI), overconsolidation ratio (OCR), mean effective confining pressure (σ'_m), and loading frequency (f) as shown in equation (5.12).

$$D_{min} = \left(\phi_6 + \phi_7 \times PI \times OCR^{\phi_8}\right) \times \sigma'^{\phi_9}_m \times [1 + \phi_{10} \times ln(f)] \quad (5.12)$$

where ϕ_6 through ϕ_9 are coefficients. The Darendeli (2001) model requires five input parameters; plasticity index (PI), overconsolidation ratio (OCR), mean effective confining pressure in atmospheres (σ'_m), loading frequency (f) in Hz, and number of loading cycles (N). However, the effects of OCR, loading frequency, and number of loading cycles on dynamic soil behavior are minor, with the two most important input parameters being the plasticity index and mean effective confining pressure. Darendeli (2001) recommends not to extrapolate the curves to shear strains higher than 1%.

Table 5.6 lists the coefficients for the Darendeli (2001) model. Figure 5.8 and Figure 5.9 show the dependence of the predicted shear modulus reduction and damping curves on confining pressure, and Figure 5.10 and Figure 5.11 show the predicted dependence on plasticity index.

5.3.3 Kishida et al (2009)

The model for shear modulus reduction and damping curves of Kishida et al (2009) is for organic soils. Their database consisted of 37 samples of highly fibrous peat to amorphous organic clays with organic contents (OC) ranging from 14-81%, water contents from 88-495%, total densities of 10.35-14.21 kN/m^3, and vertical effective stresses from 11-135 kPa. Table 5.7 lists the references and properties of each test. Six of the soils were tested in the combined resonant column torsional shear (RC/TS) device developed by Ken Stokoe and coworkers mentioned above (Darendeli and Stokoe, 1997), and 31 were tested in cyclic triaxial tests (TX).

Kishida et al (2009) developed their model in a sequence of trials that assessed the most efficient predictor variables, variable transformations, and functional forms. The final model for the secant shear modulus is given below:

$$\begin{aligned} ln(G) = b_0 + b_1 \times X_1 + b_2 \times X_2 + b_3 \times X_3 + b_4 \times X_4 \\ + b_5 \times (X_2 - 4) \times (X_3 - 0.5) + b_6 \times (X_1 + 2.5) \times (X_3 - 0.5) \\ + b_7 \times (X_2 - 4) \times (X_3 - 0.5) + b_8 \times (X_1 + 2.5) \times (X_2 - 4) \times (X_3 - 0.5) \end{aligned} \quad (5.13)$$

where G is the secant shear modulus in kPa, and the variables X_1, X_2, X_3, and X_4 are transformed predictor variables of shear strain γ (%), vertical effective stress σ'_v (kPa), organic content OC (%), and the laboratory consolidation ratio (LCR), respectively. The LCR is defined as the in-situ vertical effective stress divided by the vertical effective stress in the laboratory. Thus, for samples tested at in-situ stresses the LCR = 1. The transformed predictor variables are defined as:

$$X_1 = ln(\gamma + \gamma_r) \quad (5.14)$$

$$X_2 = ln(\sigma'_v) \quad (5.15)$$

$$X_3 = \frac{2}{\left[1 + exp\left(\frac{OC}{23}\right)\right]} \quad (5.16)$$

$$X_4 = ln(LCR) \quad (5.17)$$

$$\gamma_r = exp[b_9 + b_{10} \times (X_3 - 0.5)] \quad (5.18)$$

The coefficients b_2, b_4, b_5, b_6, b_7, and b_8 are calculated as follows:

$$b_2 = 1 - 0.185 \times \left[1 + \frac{ln(\gamma_r) + 2.5}{ln\left(\frac{1+\gamma}{\gamma_r}\right)}\right] \quad (5.19)$$

$$b_4 = 0.8 - 0.4 \times X_3 \quad (5.20)$$

$$b_5 = \frac{0.185}{ln\left(\frac{1+\gamma}{\gamma_r}\right)} \quad (5.21)$$

$$b_7 = -0.37 \times \left[1 + \frac{ln(\gamma_r) + 2.5}{ln\left(\frac{1+\gamma}{\gamma_r}\right)}\right] \quad (5.22)$$

$$b_8 = \frac{0.37}{ln\left(\frac{1+\gamma}{\gamma_r}\right)} \tag{5.23}$$

The function for damping is:

$$D = c_0 + c_1 \times X_5 + c_2 \times X_2 + c_3 \times X_3 + c_4 \times (X_5 + 1) \times (X_2 - 4) + c_5 \times (X_2 - 4) \times (X_3 - 0.5) \tag{5.24}$$

Where D is the damping in percent, X_2 and X_3 are as defined above, and:

$$X_5 = ln\left[ln\left(\frac{G_{max}}{G}\right) + 0.103\right] \tag{5.25}$$

Table 5.8 lists the coefficients b_0, b_1, b_3, b_6, b_9, b_{10}, and c_0 through c_5 for the Kishida et al (2009) model. Figure 5.12 and Figure 5.13 show the shear modulus reduction and damping curves for different confining pressures using the Kishida et al (2009) model. Figure 5.14 and Figure 5.15 show the shear modulus reduction and damping curves for different organic contents (OC) using the Kishida et al (2009) model.

5.3.4 Comparison

Figure 5.16 and Figure 5.17 compare the shear modulus reduction and damping curves predicted by Vucetic and Dobry (1991) and Darendeli (2001) for different values of plasticity index. These figures show that in general the curves predicted by Vucetic and Dobry (1991) have greater volumetric cyclic threshold shear strains (γ_{tv}) than the curves predicted by Darendeli (2001). In other words, the model of Vucetic and Dobry (2001) predicts greater shear modulus reduction curve values and lower damping ratio values for a given shear strain and plasticity index for than the model of Darendeli (2001). Theoretically this means that site response analyses that use Vucetic and Dobry (1991) as the soil shear modulus reduction and damping curves (MRD) will predict greater intensity ground motions at the surface than site response analyses that model soil dynamic properties with the model of Darendeli (2001), everything else being equal. This is because the shear modulus will degrade less and the damping will be less for the same shear strain, allowing more energy to propagate up to the surface. However, the damping curves of Darendeli (2001) are steeper in shape, so at low values of PI and moderate values of shear strain, the Darendeli (2001) curves fall below the corresponding Vucetic and Dobry (1991) curve.

Figure 5.16 and Figure 5.17 also show the difference between the two sets of curves is greater at larger values of PI than at smaller values, which means differences in site response analyses between using the two models will be greater for site profiles with deposits of high plasticity soils. However, the model of Vucetic and Dobry (1991) is not confining pressure dependent, whereas the model of Darendeli (2001) is. The Darendeli (2001) curves plotted in Figure 5.16 and Figure 5.17 are for a mean effective confining pressure of one atmosphere. Therefore, at pressures less than one atmosphere the difference between the curves will increase, whereas for confining pressures greater than one atmosphere the difference will decrease. At large confining

pressures the shear modulus reduction and damping curves (MRD) predicted by the Darendeli (2001) model may have larger values of volumetric cyclic threshold shear strains (γ_{tv}) than those predicted by the Vucetic and Dobry (1991) model.

Figure 5.18 and Figure 5.19 compare the shear modulus reduction and damping curves of Vucetic and Dobry (1991), Darendeli (2001), and Kishida et al (2009) for one atmosphere of confining pressure. The Kishida et al (2009) model is not PI dependent, so a true comparison cannot be made. However, Figure 5.18 and Figure 5.19 show that even for low levels of organic content (OC = 10%), the model of Kishida et al (2009) predicts larger values of volumetric cyclic threshold shear strains (γ_{tv}) than the model of Darendeli (2001) for PI = 200 at the same confining pressure. The shear modulus reduction curve of Vucetic and Dobry (1991) for PI = 200 falls between the curves of Kishida et al (2009) for OC = 10% and OC = 70%, however the damping curve of Vucetic and Dobry (1991) is lower than either curve of the two Kishida et al (2009) curves shown in the figure.

5.4 Summary

Dynamic properties of soils are very important for seismic site response analyses. This chapter reviewed the fundamental relationships between stiffness and damping in soil. It then presented an overview of past research regarding the dynamic properties of soils, and outlined how different parameters affect the shear modulus reduction and damping curves of cohesive and cohesionless soils. The models of Vucetic and Dobry (1991), Darendeli (2001), and Kishida et al (2009) were explained and compared. These comparisons demonstrated the importance of the selection of the shear modulus reduction and damping curves in seismic site response analyses.

Another important aspect of seismic site response analyses that must be considered when selecting shear modulus reduction and damping curves is the implied soil shear strength. At large shear strains the implied shear strength of the soil can greatly influence the results of the site response analyses. However, most laboratory investigations of the dynamic properties of soils do not measure shear strains larger than 0.1-0.5% (e.g. Darendeli 2001; Zhang et al, 2005). When shear modulus reduction and damping curves are extrapolated to shear strains of 1-10% there is no guarantee that they will match the shear strength of the soil, which can lead to erroneous results. Chapter 6 discusses this issue in detail.

Chapter 6 also describes the theory, limitations, and input parameters necessary to perform site response analyses, as well as the selection of site properties of each soil profile used in this project.

5.5 References

Alarcon-Guzman, A., Chameau, J. L., Leonards, G. A., and Frost, J. D. (1989). "Shear modulus and cyclic undrained behavior of sands." *Soils Found*., 29(4), 105–119.

Andersen, K. H. (1983). "Strength and deformation properties of clay subjected to cyclic loading." Report No. 52412-8, Norwegian Geotechnical Institute, Oslo, Norway.

Anderson, D. G., Phukunhaphan, A., Douglas, B. J., and Martin, G. R. (1983). "Cyclic behavior of six marine clays." Proc, Evaluation of Seafloor Soil Properties under Cyclic Loads, ASCE, 1-27.

Anderson, D. G., and Richart, F. E., Jr. (1976). "Effects of straining on shear modulus of clays." *J. Geotech. Engrg. Div.*, ASCE, 102(9), 975-987.

Anderson, D.G., and Stokoe II, K.H. (1978). "Shear Modulus: A Time-Dependent Soil Property." *Dynamic Geotechnical Testing*. ASTM STP 654, ASTM, 66 – 90.

Andreasson, B. A. (1981). "Dynamic deformation characteristics of a soft clay." *Proc. Int. Conf. on Recent Advances in Geotechnical Earthquake Engineering and Soil Dynamics*, Vol. 1, 65-70.

Arulnathan, R. (2000). "Dynamic properties and site response of organic soils." Ph.D. thesis, Dept. of Civil and Environmental Engineering, Univ. of California, Davis, Calif.

Cavallaro, A., Lo Presti, D.C.F., and Maugeri, M. (2000). "Dynamic geotechnical characterization of soils subjected to umbria and marches earthquake." *Earthquake Engineering 12th World Conference*, Auckland, New Zealand.

Chung, R. M., Yokel, F. Y., and Drnevich, V. P. (1984). "Evaluation of dynamic properties of sands by resonant column testing." *Geotech. Test. J.*, 7(2), 60–69.

Darendeli, M. B. (2001). "Development of a new family of normalized modulus reduction and material damping curves." PhD dissertation, Univ. of Texas at Austin, Austin, Texas.

Darendeli, M.B. and Stokoe, K.H., II (1997). "Dynamic Properties of Soils Subjected to the 1994 Northridge Earthquake," Geotechnical Engineering Report GR97-5, Civil Engineering Department, The University of Texas at Austin, Austin, TX, December.

Darendeli, M.B. (1997). "Dynamic Properties of Soils Subjected to 1994 Northridge Earthquake," M.S. Thesis, University of Texas at Austin, 609 pp.

EPRI (1993). "Guidelines for Determining Design Basis Ground Motions." *Electric Power and Research Institute*, Project, Report Vols. I-V.

Hardin, B. O. and Drnevich, V.P. (1972). "Shear Modulus and Damping in Soils: Design Equations and Curves," *Journal of Soil Mechanics and Foundation Engineering Div*., ASCE, Vol. 98 No. SM7, p 667-692.

Hwang, S.K. and Stokoe, K.H., II (1993a). "Dynamic Properties of Undisturbed Soil Samples from Lotung, Taiwan," *Geotechnical Engineering Report GR93-3*, Civil Engineering Department, The University of Texas at Austin, Austin, TX, March.

Hwang, S.K. and Stokoe, K.H., II (1993b). "Dynamic Properties of Undisturbed Soil Samples from Treasure Island, California." *Geotechnical Engineering Report GR93-4*, Civil Engineering Department, The University of Texas at Austin, Austin, TX, March.

Hwang, S. K. (1997). "Investigation of the Dynamic Properties of Natural Soils," Ph.D. Dissertation, University of Texas at Austin, 394 pp.

Ishibashi, I. and Zhang, X. (1993). ''Unified dynamic shear moduli and damping ratios of sand and clay.'' *Japanese Society of Soil Mechanics and Foundations*, 33(1), 182–191.

Iwasaki, T., and Tatsuoka, F. (1977). "Effects of grain size and grading on dynamic shear moduli of sands." *Soils Found.*, 17 (3), 19–35.

Kagawa, T. (1992). “Moduli and damping factors of soft marine clays.” *Journal of Geotechnical Engineering*. ASCE, 118(9),1360–1375.
Kallioglou, P., Tika, Th. and Pitilakis, K. (2008). “Shear Modulus and Damping Ratio of Cohesive Soils.” *Journal of Earthquake Engineering*. 12(6), 879 – 913.
Kim, T. and Novak, M. (1981). “Dynamic properties of some cohesive soils of Ontario.” *Canadian Geotechnical Journal*. Vol 18, 371–389.
Kishida, T., Boulanger R.W., Abrahamson N.A., Wehling T.M., Driller M.W. (2009). “Regression Models for Dynamic Properties of Highly Organic Soils.” *J. of Geotech. and Geoenvir. Eng.*, ASCE, 135(4).
Kokusho, T., Yoshida, Y. and Esashi, Y. (1982). “Dynamic properties of soft clay for a wide strain range.” *Japanese Society of Soil Mechanics and Foundations*. Vol 22, 1–18.
Kokusho, T. (1980). “Cyclic triaxial test of dynamic soil properties for wide strain range.” *Soils Found.*, 20(2), 45–60.
Koutsoftas, D.C., and Fischer, J.A. (1980). “Dynamic properties of two marine clays.” Journal of Geotechnical Engineering, ASCE. 106(6), 645-657.
Kramer, Steven L. (1996). *Geotechnical Earthquake Engineering*. Prentice Hall; New Jersey.
Laird, J. P. (1994). “Linear and Nonlinear Dynamic Properties of Soil at High Confining Pressures,” M.S. Thesis, University of Texas at Austin.
Lanzo, G., A. Pagliaroli, Tommasi, P., and Chiocci F.L. (2009). “Simple shear testing of sensitive, very soft offshore clay for wide strain range.” *Canadian Geotechnical Journal*. Vol 46, 1277 – 1288.
Leon, J. L., Jaime, A., and Rabago, A. (1974). “Dynamic properties of soils: Preliminary study." *Internal Report*, Institute de Ingenieria, UNAM, Mexico City, Mexico (in Spanish).
Lodde, P. F., and Stokoe, K. H., II. (1982). “Dynamic response of San Francisco Bay mud.” *Geotechnical Engineering Report GT-82-2*, Univ. of Texas at Austin, Austin, Tex.
Lo Presti, D.C.F., Jamiolkowski, M., Pallara, O., Cavallaro, A. & Pedroni, S. (1997). “Shear modulus and damping of soils.” *Géotechnique*, 47(3), 603–617.
Menq, Farn-Yuh (2003). “Dynamic Properties of Sandy and Gravelly Soils.” PhD dissertation, Univ. of Texas at Austin, Austin, Texas.
Nigbor, Robert. “Resolution of Site Response Issues in the Northridge Earthquake (ROSRINE).” Personal communication, October 24, 2012.
Nishigaki, Y. (1971). “Young's modulus change of clay due to strain level.” *Proc. 26th Convention of the JSCE*, Part 3, 93-95 (in Japanese).
Okur, D.V., Ansal, A. (2007). “Stiffness degradation of natural fine grained soils during cyclic loading.” *Soil Dynamics and Earthquake Engineering*. Vol 27, 843 – 854.
Romo, M. P., and Jaime, A. (1986). “Dynamic characteristics of some clays of the Mexico Valley and seismic response of the ground.” *Technical Report*, Apr., Institute de Ingenieria, Mexico City, Mexico (in Spanish).
Romo, M. P., Jaime, A., and Resendiz, D. (1988). "The Mexico earthquake of September 19, 1985: General soil conditions and clay properties in the Valley of Mexico." *Earthquake Spectra*, 4(4), 731-752.
Saxena, S., and Reddy, K. (1989). “Dynamic moduli and damping ratios for Monterey No. 0 sand by resonant column tests.” *Soils Found.*, 29(2), 37–51.
Seed, H. B., Wong, R. T., Idriss, I. M., and Tokimatsu, K. (1984). “Moduli and damping factors for dynamic analyses of cohesionless soils.” Rep. UBC/EERC 84-14, Univ. of California, Berkeley,Calif.

Seed, H. B., Wong, R. T., Idriss, I. M., and Tokimatsu, K. (1986). "Moduli and damping factors for dynamic analyses of cohesionless soils." *J. Geotech. Engrg.*, ASCE, 112(11), 1016-1032.
Seed, H.B., and Idriss, I.M. (1970). "Soil moduli and damping factors for dynamic response analyses." Report No. EERC 70-10, University of California, Berkeley, California.
Shibuya, S., Toshiyuki, T., Fukuda, F., and Degoshi, T. (1995). "Strain rate effects on shear modulus and damping of normally consolidated clays." *Geotechnical Testing Journal*, ASTM, 18(3), 365-375.
Stokoe, K. H., Bay, J. A., Rosenbald, B. L., Hwang, S. K., and Twede, M. R. (1994). "In situ seismic and dynamic laboratory measurements of geotechnical materials at Queensboro Bridge and Roosevelt Island." *Geotechnical Engineering Rep. No. GR94-5*, Civil Engineering Dept., Univ. of Texas at Austin, Austin, Tex.
Stokoe, K. H., Hwang, S. K., Lee, J. N.-K., and Andrus, R.D. (1994). "Effects of Various Parameters on the Stiffness and Damping of Soils at Small to Medium Strains," Proceedings, *International Symposium on Prefailure Deformation Characteristics of Geomaterials*, Vol 2, 785-816.
Stokoe, K.H., II and Darendeli, M.B. (1998). "Laboratory Evaluation of the Dynamic Properties of Intact Soil Specimens: Garner Valley, California," *Geotechnical Engineering Report GR98-3*, Civil Engineering Department, The University of Texas at Austin, Austin, TX, March.
Stokoe, K.H., II, Hwang, S.K., Darendeli, M.B. and Lee, N.-K.J. (1998a). "Correlation Study of Nonlinear Dynamic Soil Properties; Savannah River Site, Aiken, South Carolina," *Geotechnical Engineering Report GR98-4*, Civil Engineering Department, The University of Texas at Austin, Austin, TX, January.
Stokoe, K.H., II, Moulin, B.S. and Darendeli, M.B. (1998b). "Laboratory Evaluation of the Dynamic Properties of Intact Soil Specimens from Daniel Island Terminal, South Carolina," *Geotechnical Engineering Report GR98-2*, Civil Engineering Department, The University of Texas at Austin, Austin, TX, February.
Stokoe, K.H., II, Darendeli, M.B. and Menq, F.-Y. (1998d). "Laboratory Evaluation of the Dynamic Properties of Intact Soil Specimens: San-Francisco-Oakland Bay Bridge, East-Span Seismic Safety Project, Phase I – Site Characterization," *Geotechnical Engineering Report GR98-8*, Civil Engineering Department, The University of Texas at Austin, Austin, TX, July.
Stokoe, K.H., II, Darendeli, M.B. and Menq, F.-Y. (1998e). "Summary Laboratory Test Results," *ROSRINE Data Dissemination Workshop*, University of Southern California, Los Angeles, CA, December 15th, 129 pp.
Stokoe, K.H., II, Valle, C. and Darendeli, M.B. (2001). "Laboratory Evaluation of the Dynamic Properties of Coarse Grained Specimens from Various Sites in California," *Geotechnical Engineering Report GR01-2*, Civil Engineering Department, The University of Texas at Austin, Austin, TX.
Sun, J., Golesorkhi R., and Seed, H. (1988), ''Dynamic moduli and damping ratio for cohesive soils,'' Report No. UCB/EERC-88/15. University of California Berkeley, Earthquake Engineering Research Center.
Tan, K. Y., and Vucetic, M. (1989). "Behavior of medium and low plasticity clays under cyclic simple shear conditions." *Proc. Fourth Int. Conf. on Soil Dynamics and Earthquake Engineering, Soil dynamics and liquefaction*, 131-141.

Tika, Th., Kallioglou, P., Koninis, G., Michaelidis, P., Efthimiou, M., Pitilakis, K., (2010). "Dynamic properties of cemented soils from Cyprus." *Bulletin of Engineering Geology and the Environment*, Vol 69, 295-307.

Vucetic, M., G. Lanzo, and M. Doroudian (1998). "Damping at small strains in cyclic simple shear test." *Journal of Geotechnical Engineering*, ASCE, 124(7).

Vucetic, M. (1994). "Cyclic Threshold Shear Strains in Soils." *Journal of Geotechnical Engineering*, ASCE, 120(12), 2208-2228.

Vucetic, M., and Dobry, R. (1986). "Cyclic degradation of normally and overconsolidated clays under simple shear loading conditions." *Report No. CE-86-01*, Civil Engineering Department, Rensselaer Polytechnic Institute, Troy, N.Y.

Vucetic, M., and Dobry, R. (1991). "Effect of soil plasticity on cyclic response." *Journal of Geotechnical Engineering*, ASCE, 117(1), 89-107.

Wehling, T. M., Boulanger, R. W., Arulnathan, R., Harder, L. F., and Driller, M. W. (2003). "Nonlinear dynamic properties of a fibrous organic soil." *J. Geotech. Geoenviron. Eng.*, 129(10), 929–939.

Wehling, T. M., Boulanger, R. W., Harder, L. F., Jr., and Driller, M. W. (2001). "Dynamic properties of Sherman Island peat: Phase II study." *Rep. No. UCD/CGM-01/01*, Center for Geotechnical Modeling, Univ. of California, Davis, Calif.

Yamada, S., Hyodo, M., Orense, R., and Dinesh, S. V. (2008). "Initial shear modulus of remolded sand-clay mixtures." *J. Geotech. Geoenviron. Eng*. ASCE, 134(7), 960–971.

Yasuda, N., and Matsumoto, N. (1993). "Dynamic deformation characteristics of sands and rockfill materials." *Can. Geotech. J.*, 30(5), 747–757.

Yasuda, N., Ohta, N., and Nakamura, A. (1996). "Dynamic deformation characteristics of undisturbed riverbed gravels." *Can. Geotech. J*., 33(2), 237–247.

Zen, K., Umehara, Y., and Hamada, K. (1978). "Laboratory tests and in situ seismic survey on vibratory shear modulus of clayey soils with various plasticities." *Proc. Fifth Japanese Earthquake Engineering Symp.*, 721-728.

Zhang, J., Andrus, R.D., and Juang, C.H. (2005). "Normalized Shear Modulus and Material Damping Ratio Relationships." *Journal of Geotechnical and Geoenvironmental Engineering*. ASCE, 131(4), 453 – 464.

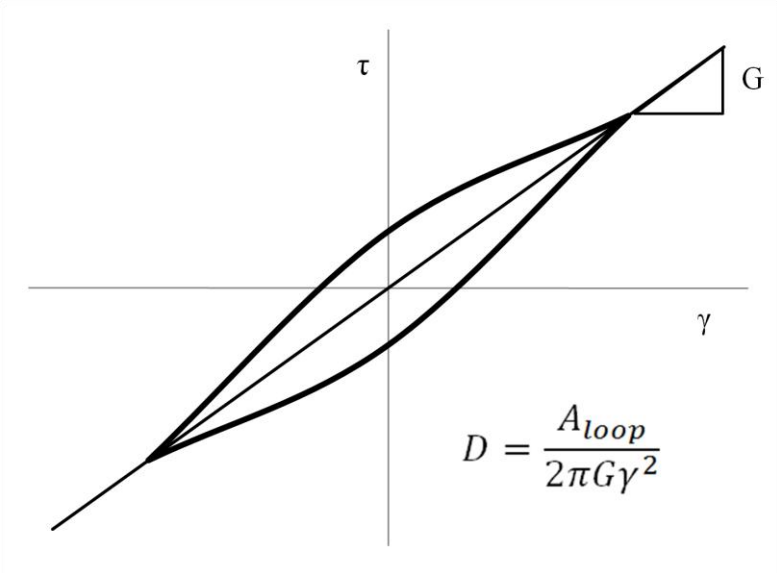

Figure 5.1: Hysteresis loop of soil showing G and D, where A_{loop} is the area of the hysteresis loop

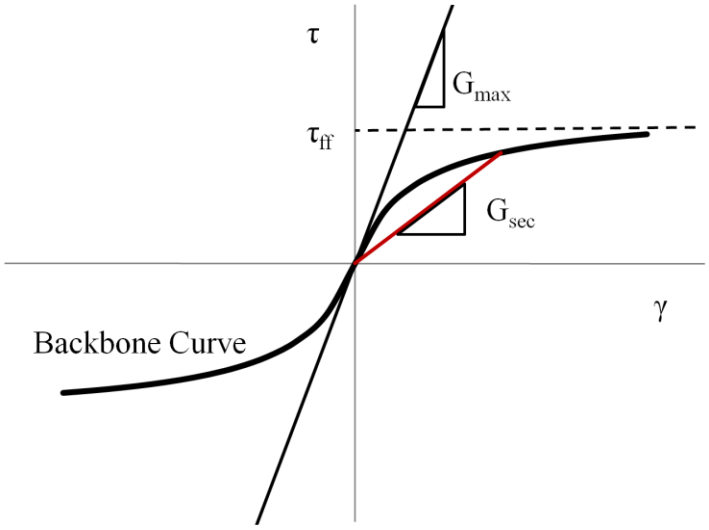

Figure 5.2: Backbone curve showing the reduction of G from G_{max}

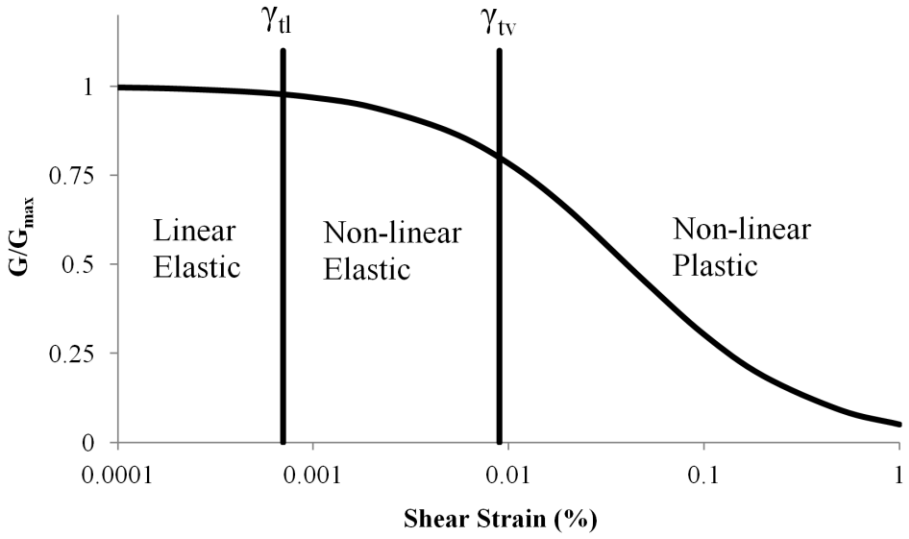

Figure 5.3: Shear modulus reduction curve showing the linear (γ_{tl}) and volumetric cyclic threshold shear strains (γ_{tv})

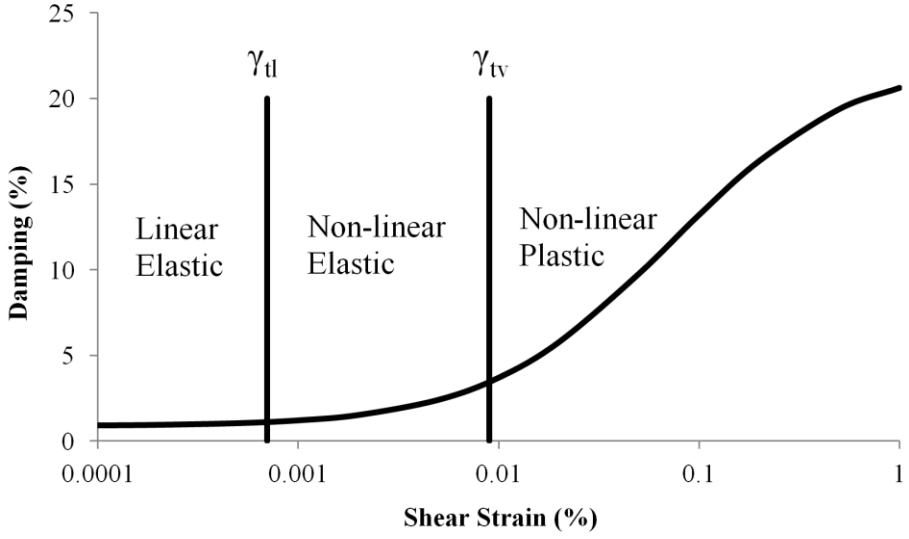

Figure 5.4: Damping curve showing the linear (γ_{tl}) and volumetric cyclic threshold shear strains (γ_{tv})

Table 5.1: Parameters studied by other researchers and their effect on G/G_{max} for a given shear strain

Controlling Parameter	G/G_{max} Cohesive	G/G_{max} Cohesionless	Cross Correlations
			σ'_m
σ'_m	↑	↑	
e	↑		
t_g	↑		
OCR	NE[a]	NE[a]	
f	NE[a]	NE[a]	
N	↓	↑	
PI	↑		↓[b]
FC			
D_{50}		↑	
Cu		↓	↓[c]

a = negligible effect; b = only for cohesive soils: c = only for cohesionless soils

Table 5.2: Parameters studied by other researchers and their effect on D_{min}

Increasing Parameter	D_{min} Cohesive	D_{min} Cohesionless	Cross Correlations
			f
σ'_m	↓	↓	
e	↓	↓	
t_g	↓	↓	
OCR	↓	NE[a]	
f	↑	↑	
N	NE[a]	NE[a]	
PI	↑		↑[b]
FC			
D50		↓	
Cu		↑	

a = negligible effect; b = only for cohesive soils

Table 5.3: Parameters studied by other researchers and their effect on *D* for a given shear strain

Controlling Parameter	*D* Cohesive	*D* Cohesionless	Cross Correlations	
			f	N
σ'_m	↓	↓		
e	↓			
t_g	NE[a]	NE[a]		
OCR	NE[a]	NE[a]		
f	↓	NE[a]		
N	↓	↓		
PI	↓		↑[b]	↓[b]
FC				
D50		↑		
Cu				

a = negligible effect; b = only for cohesive soils

Table 5.4: References used in Vucetic and Dobry (1991)

Reference
Andersen (1983)
Anderson and Richart (1976)
Anderson et al (1983)
Andreasson (1981)
Kim and Novak (1981)
Kokusho et al (1982)
Koutsoftas and Fischer (1980)
Leon et al. (1974)
Lodde and Stokoe (1982)
Nishigaki (1971)
Romo and Jaime (1986)
Romo et al (1988)
Seed and Idriss (1970)
Seed et al (1986)
Tan and Vucetic (1989)
Vucetic and Dobry (1986)
Zen et al (1978)

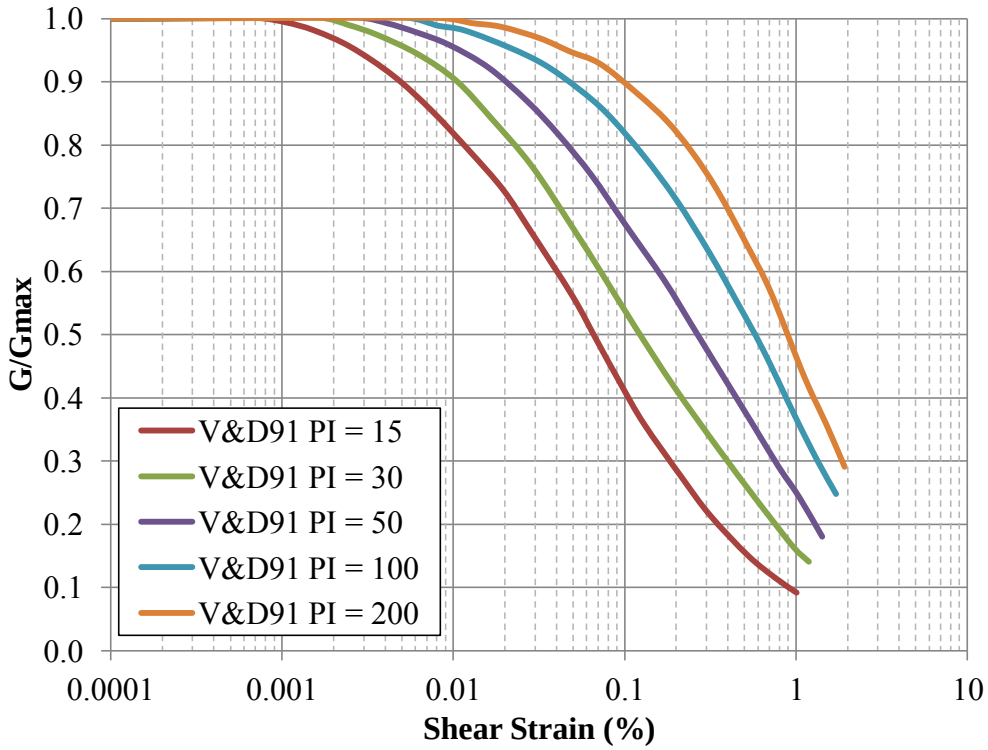

Figure 5.5: Shear modulus reduction curves from Vucetic and Dobry (1991) for cohesive soils

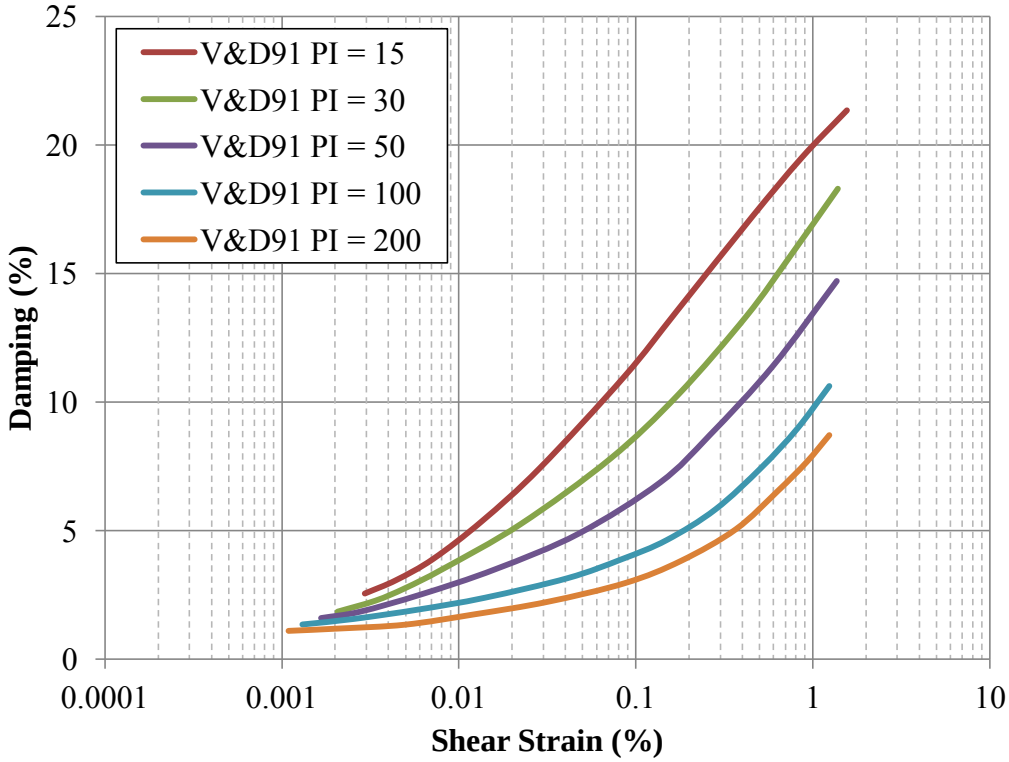

Figure 5.6: Damping curves from Vucetic and Dobry (1991) for cohesive soils

Table 5.5: Darendeli (2001) database

Site	Region	# of Samples	Reference
Treasure Island	Northern California	8	Hwang and Stokoe, 1993b; Hwang, 1997
Garner Valley	Northern California	4	Stokoe and Darendeli, 1998
Bay Bridge	Northern California	4	Stokoe et al, 1998d
San Francisco Airport	Northern California	2	Hwang, 1997
Oakland Outer Harbor	Northern California	5	Hwang, 1997
Gilroy	Northern California	12	Hwang and Stokoe, 1993b; Hwang, 1997; Stokoe et al, 2001
Corralitos	Northern California	2	Stokoe et al, 2001
North Palm Springs	Southern California	1	Stokoe et al, 2001
Borrego	Southern California	4	Hwang, 1997
Imperial Valley College	Southern California	2	Stokoe et al, 2001
Potrero Canyon	Southern California	4	Stokoe et al, 1998e
Newhall	Southern California	2	Darendeli and Stokoe, 1997; Darendeli, 1997
Rinaldi Receiving Station	Southern California	4	Stokoe et al, 1998e
Kagel	Southern California	4	Darendeli and Stokoe, 1997; Darendeli, 1997
Sepulveda VA Hospital	Southern California	8	Darendeli and Stokoe, 1997; Darendeli, 1997
Arleta	Southern California	2	Darendeli and Stokoe, 1997; Darendeli, 1997
La Cienaga	Southern California	16	Darendeli and Stokoe, 1997; Darendeli, 1997; Stokoe et al, 1998e
Savannah River Site	South Carolina	15	Hwang, 1997; Stokoe et al, 1998a
Daniel Island	South Carolina	3	Stokoe et al, 1998b
Lotung	Taiwan	8	Hwang and Stokoe, 1993a; Hwang, 1997

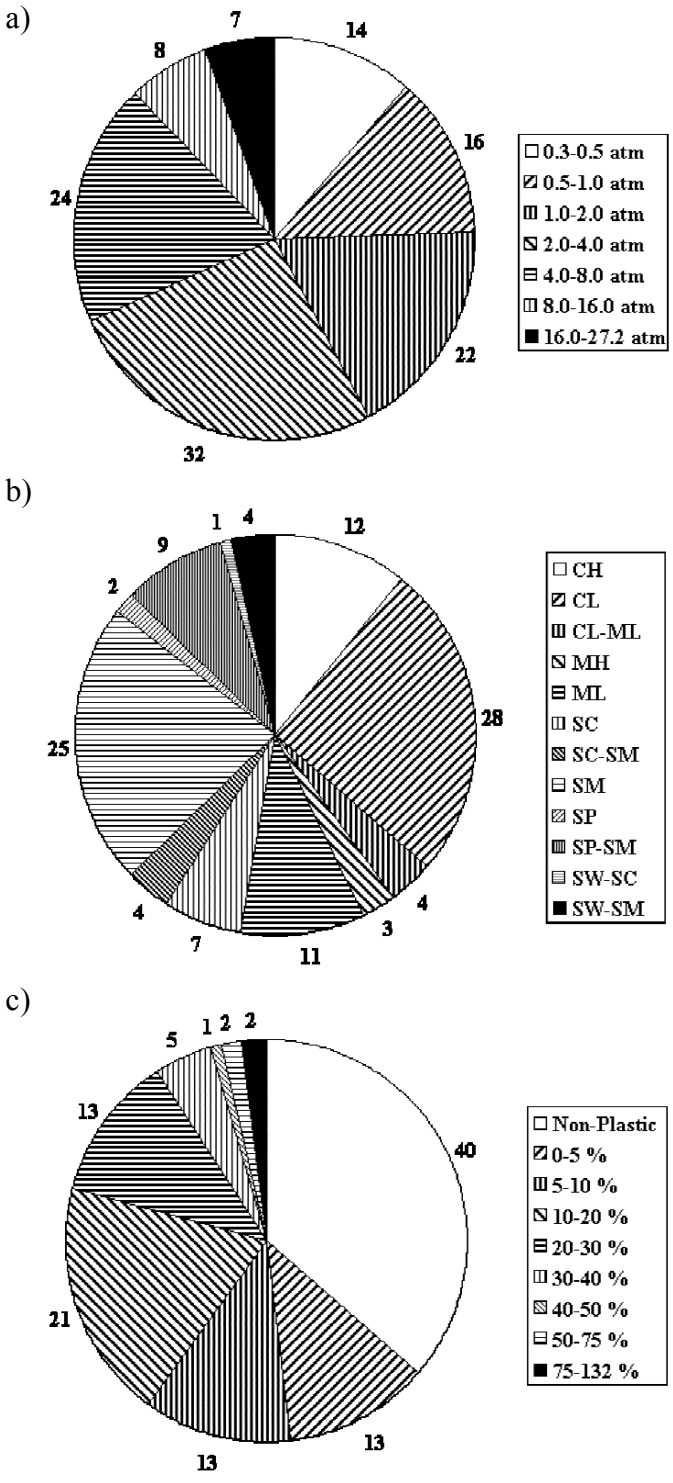

Figure 5.7: Distribution of Darendeli (2001) database according to a) mean effective confining pressure in atmospheres, b) USCS designation, and c) plasticity index (PI) (From Darendeli, 2001)

Table 5.6: Coefficients for the Darendeli (2001) model

ϕ_1	0.0352
ϕ_2	0.0010
ϕ_3	0.3246
ϕ_4	0.3483
ϕ_5	0.9190
ϕ_6	0.8005
ϕ_7	0.0129
ϕ_8	-0.1069
ϕ_9	-0.2889
ϕ_{10}	0.2919
ϕ_{11}	0.6329
ϕ_{12}	-0.0057

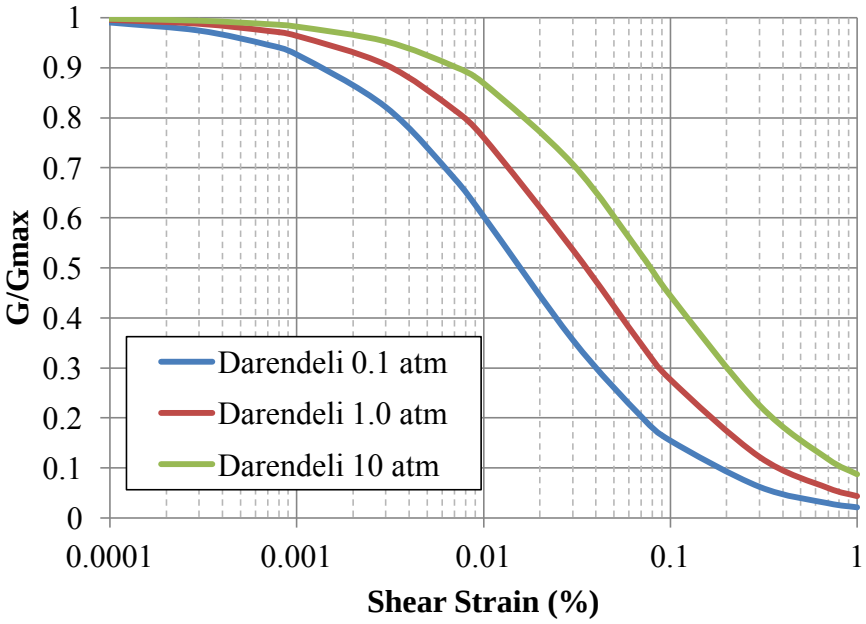

Figure 5.8: Shear modulus reduction curves for sands at different confining pressures (PI = 0, OCR = 1, f = 1 Hz, N = 10), for Darendeli (2001)

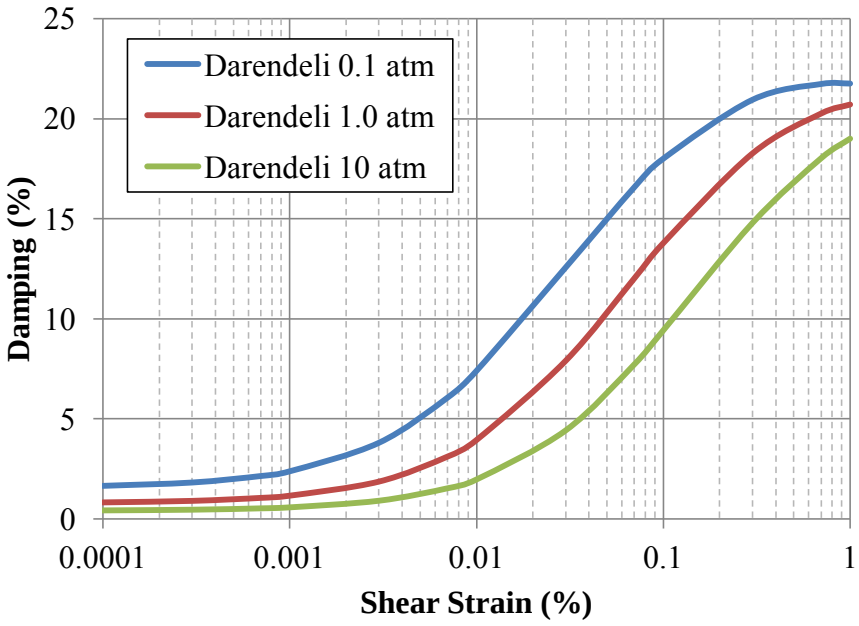

Figure 5.9: Damping curves for sands at different confining pressures (PI = 0, OCR = 1, f = 1 Hz, N = 10), for Darendeli (2001)

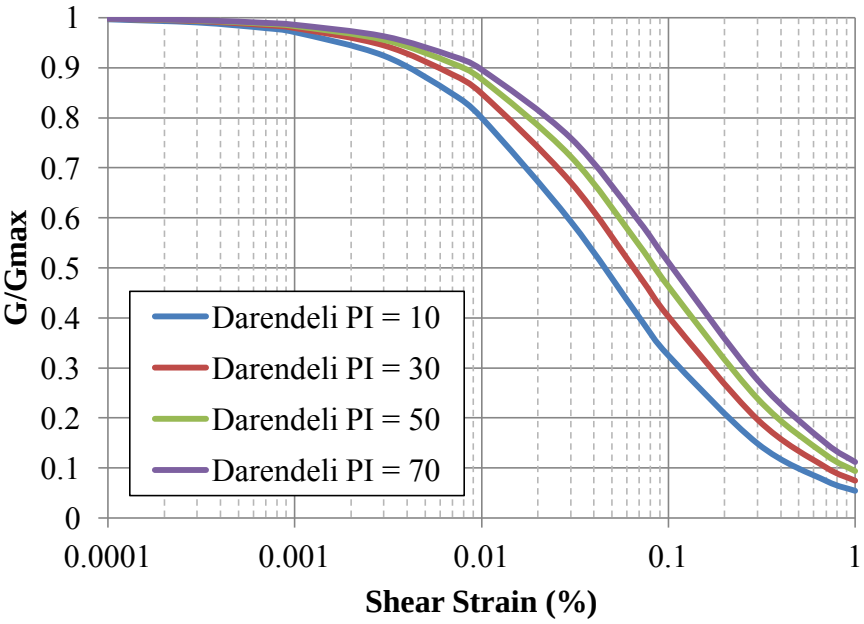

Figure 5.10: Shear modulus reduction curves for soils at different values of PI (σ'_m = 1 atn, OCR = 1, f = 1 Hz, N = 10), for Darendeli (2001)

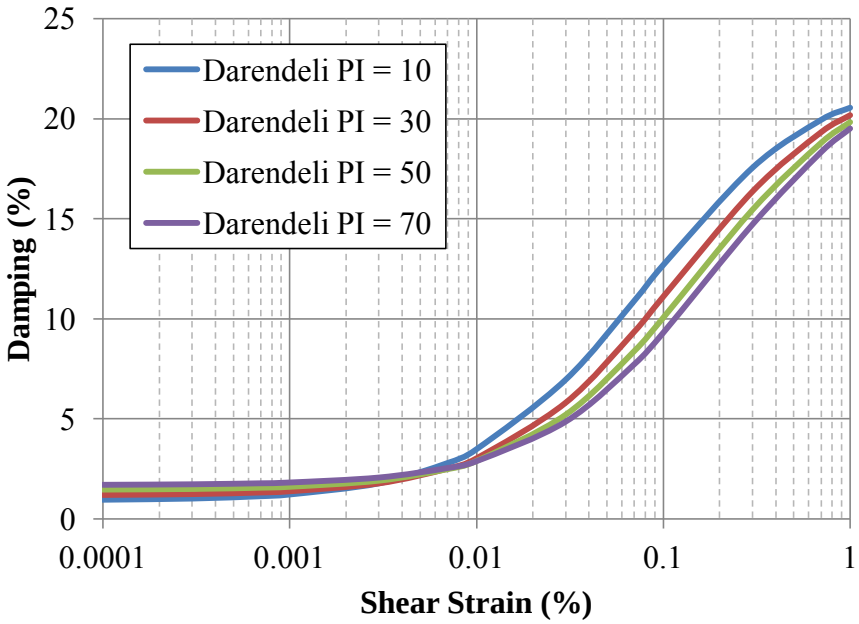

Figure 5.11: Damping curves for soils at different values of PI (σ'_m = 1 atn, OCR = 1, f = 1 Hz, N = 10), for Darendeli (2001)

Table 5.7: Summary of database used to develop Kishida et al (2009) model (from Kishida et al, 2009)

Boring location	Reference	Number of samples	Test type	Sample depth (m)	Initial water content (%)[a]	Organic content (%)[b]	Initial density (Mg/m^3)	In situ σ'_{vo} (kPa)	In lab σ'_{vc} (kPa)
Sherman Island	Wehling et al. (2003)	11	TX	2.7–12.0	165–495	31–52	1.062–1.236	10–78	10–86
Sherman Island	Arulnathan et al. (2000)	10	TX	12.8–13.7	169–240	44–65	1.131–1.182	128–136	66–200
Montezuma Slough	Wehling et al., draft (2003)	6	TX	3.3–6.6	115–492	15–61	1.056–1.327	16–67	16–67
Clifton Court	Wehling et al., draft (2003)	4	TX	18.6–20.6	113–180	17–34	1.196–1.365	68–69	68–69
Clifton Court	Stokoe (2003, personal communication)	4	RC/TS	18.8–20.5	88–241	14–35	1.188–1.450	68–69	55–69
Queensboro Bridge	Stokoe et al. (1994)	2	RC/TS	9.1–9.7	210–285	35–63	1.090–1.130	114	76

[a]Water content determined by oven drying at 90°C as recommended by Landva et al. (1983).

[b]Organic contents (100%-ash contents) determined from igniting at 440°C corresponding to method C of ASTM (2005a,b) D 2974–00 standard.

Table 5.8: Coefficients for the Kishida et al (2009) model

b_0	5.110
b_1	-0.729
b_3	-0.693
b_6	0.000
b_9	-1.410
b_{10}	-0.950
c_0	2.860
c_1	0.571
c_2	-0.103
c_3	-0.141
c_4	0.042
c_5	-0.240

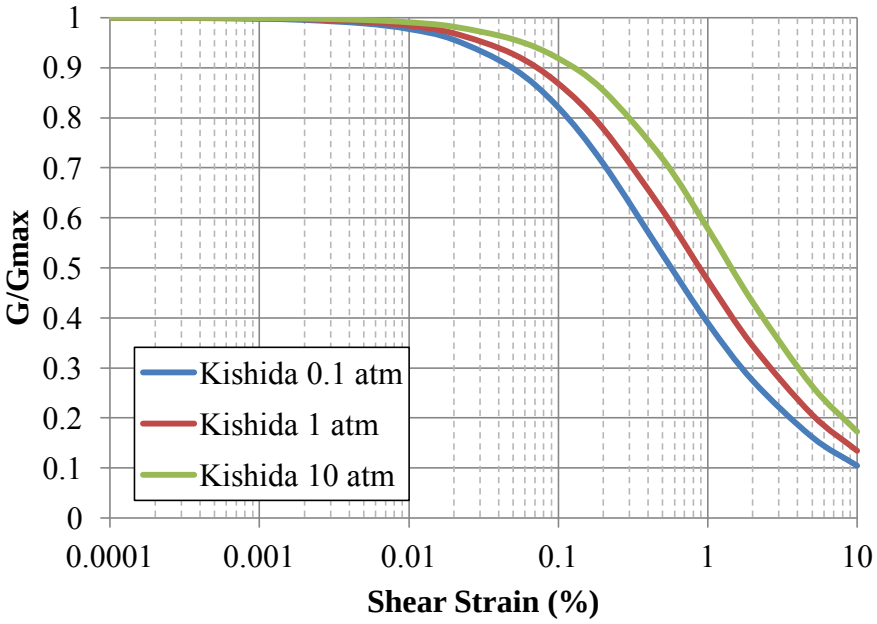

Figure 5.12: Shear modulus reduction curves at different confining pressures (OC = 40%, LCR = 1) for Kishida et al (2009)

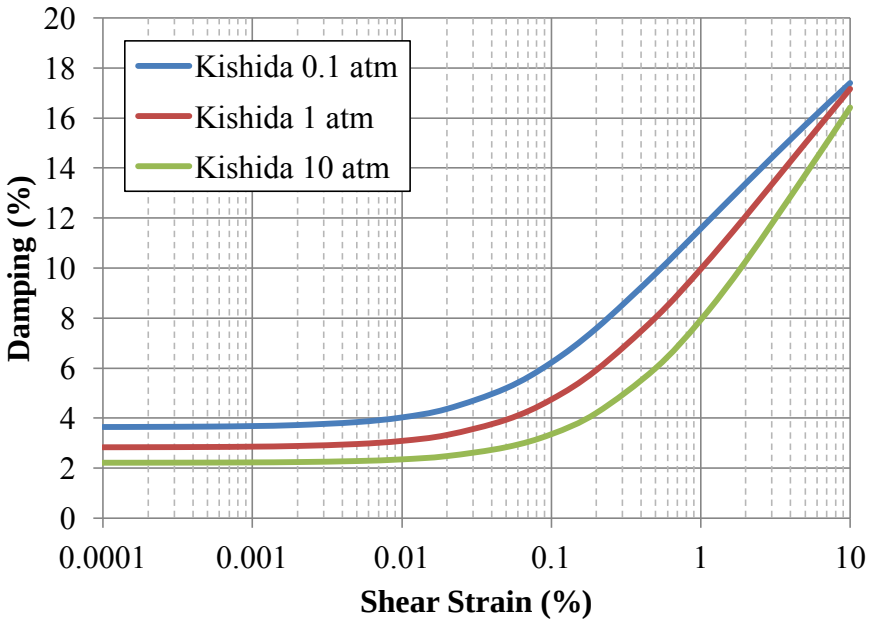

Figure 5.13: Damping curves at different confining pressures (OC = 40%, LCR = 1) for Kishida et al (2009)

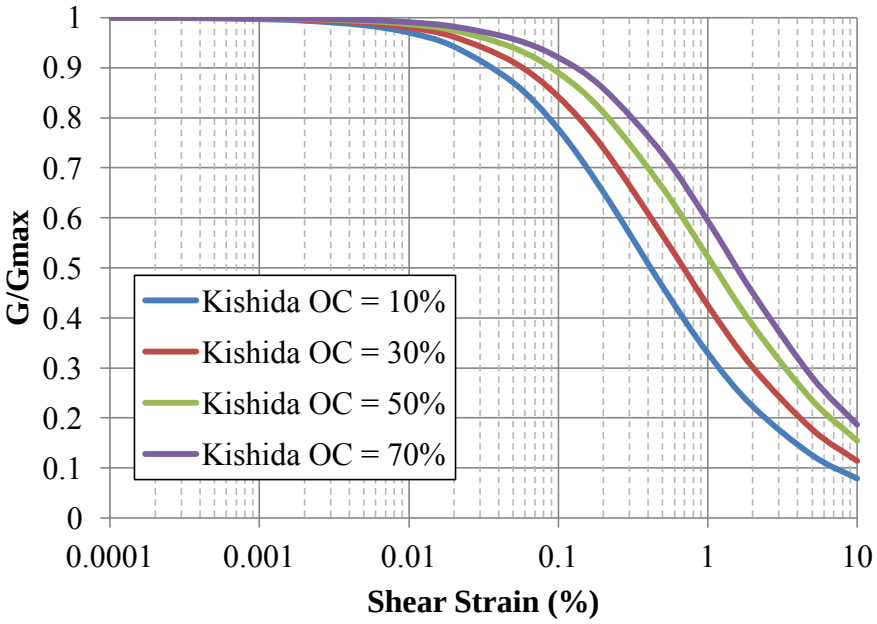

Figure 5.14: Shear modulus reduction curves for different organic contents (σ'_v = 1 atm, LCR = 1) for Kishida et al (2009)

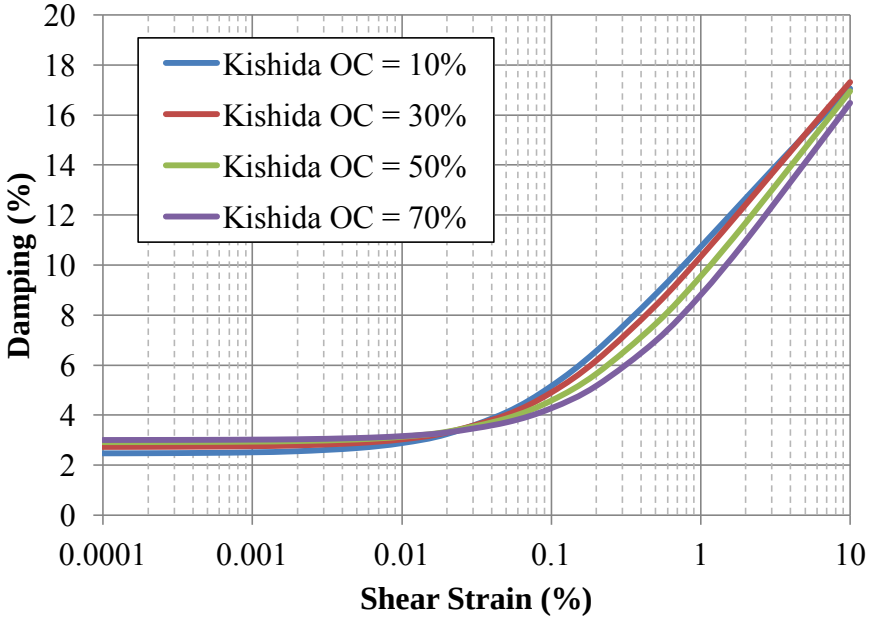

Figure 5.15: Damping curves for different organic contents (σ'_v = 1 atm, LCR = 1) for Kishida et al (2009)

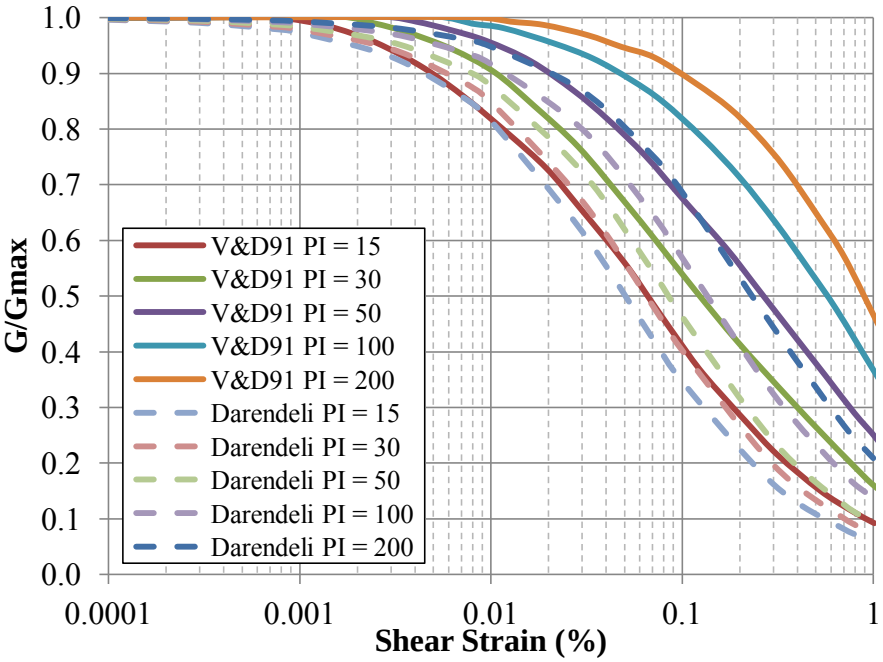

Figure 5.16: Comparison of the shear modulus reduction curves predicted by Darendeli (2001) and Vucetic and Dobry (1991) for different values of PI (σ'_m =1 atm, OCR = 1, f = 1 Hz, N = 10).

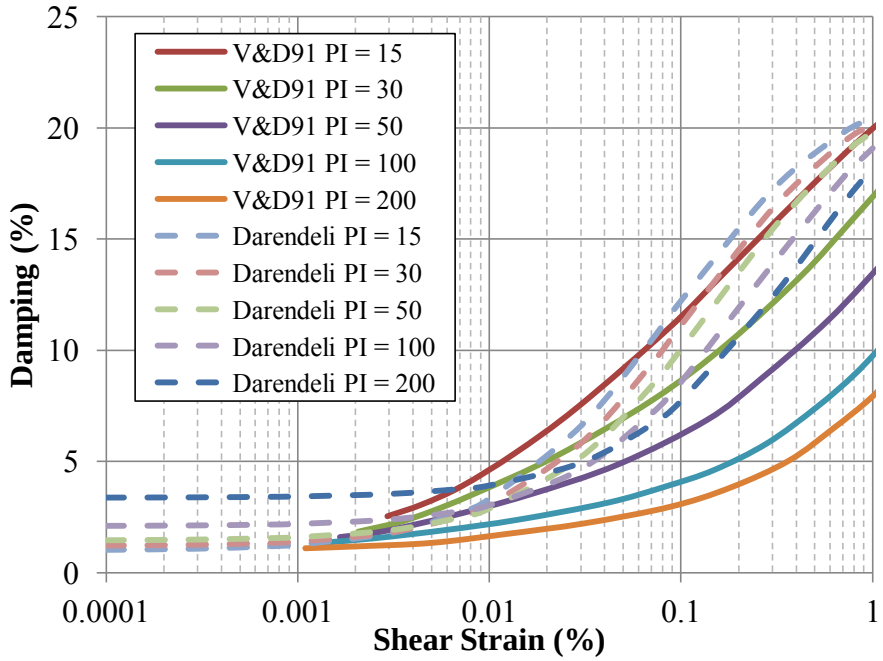

Figure 5.17: Comparison of the damping curves predicted by Darendeli (2001) and Vucetic and Dobry (1991) for different values of PI (σ'_m =1 atm, OCR = 1, f = 1 Hz, N = 10).

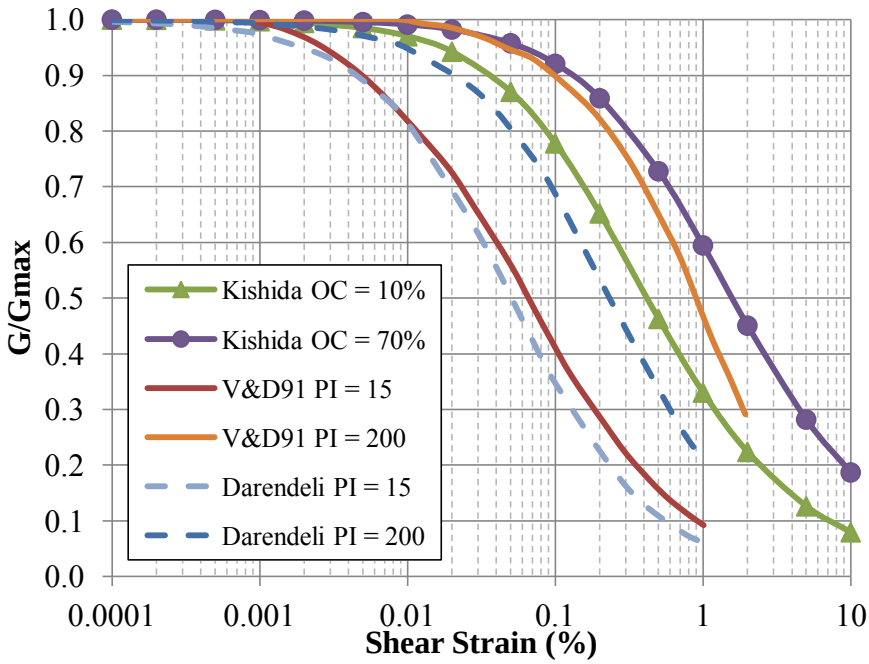

Figure 5.18: Comparison of the shear modulus reduction curves predicted by Darendeli (2001), Vucetic and Dobry (1991), and Kishida et al (2009) for different values of PI and organic content (OC) (σ'_m =1 atm, OCR & LCR = 1, f = 1 Hz, N = 10).

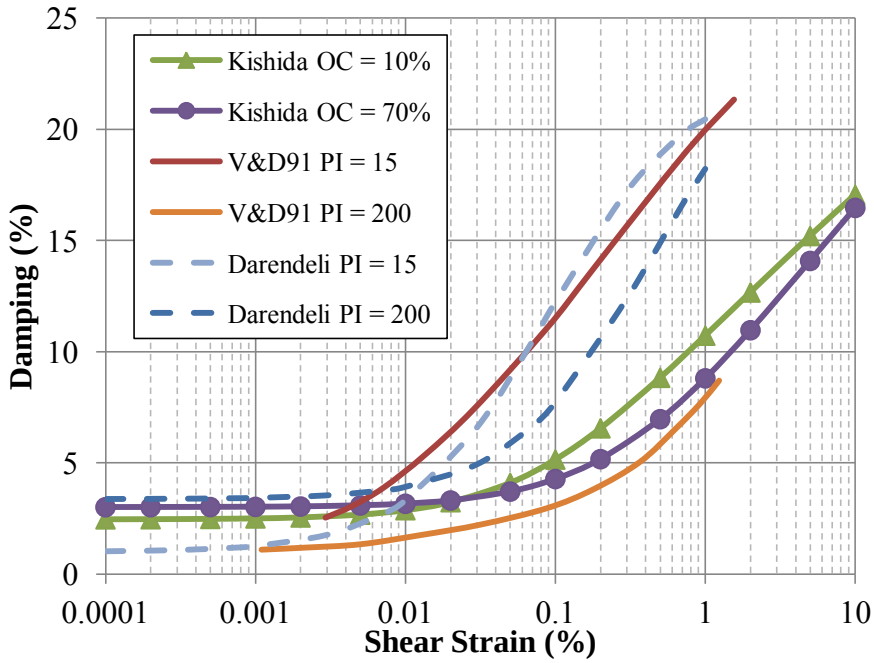

Figure 5.19: Comparison of the damping curves predicted by Darendeli (2001), Vucetic and Dobry (1991), and Kishida et al (2009) for different values of PI and organic content (OC) (σ'_m =1 atm, OCR & LCR = 1, f = 1 Hz, N = 10).

CHAPTER 6: SITE RESPONSE ANALYSES

6.1 Introduction

The primary objective of this study was to estimate the seismic response of soil deposits with high plasticity soils, organic clays, and deep soft soil deposits. Because there is little empirical data on the seismic response of these types of sites, this study focused on generating data from numerical simulations called site response analyses. In general, site response analyses estimate the effect a site has on a ground motion. Mathematically, this is solved as the propagation of waves in a continuous medium. Ideally, estimation of ground shaking at a site would also include the effects of the rupture mechanism and path of the stress waves from the rupture to the site. However, these phenomena are difficult to predict and include large uncertainties. Instead, the state of the practice uses previously recorded ground motions that are representative of the design hazard recorded on 'rock' to account for source and path effects. These 'rock' ground motions are then propagated up through a soil column to estimate the response of the soil, as shown in Figure 6.1. If there are no such 'rock' ground motions, then the engineer can use simulated ground motions or existing ground motions modified through scaling or spectral matching, as was done in chapter 3.

There are three broad categories of soil models used in site response analyses; equivalent linear, nonlinear, and advanced constitutive models (Kramer 1996). In addition, site response analyses can be solved in one, two, or three dimensions, and using total or effective stresses, depending on the problem being investigated. Total stress equivalent linear models are the simplest type of model but also have the most limitations. Advanced constitutive models are able to capture many important aspects of soil behavior but are often complex and difficult to calibrate. Research and practice commonly use one dimensional total stress equivalent linear or total stress nonlinear site response analyses. One dimensional site response analyses assume that the soil profile is composed of horizontal soil layers and that the ground shaking is entirely due to vertically propagating horizontal shear waves.

There are many different computer programs that incorporate one dimensional total stress equivalent linear and/or nonlinear site response analyses models. The most widely used total stress equivalent linear program is SHAKE (Schnabel et al., 1972), or one of its derivatives such as SHAKE90 (Idriss and Sun, 1992), SHAKE 2000 (Ordóñez, 2012), or SHAKE04 (Youngs, 2004). Computer codes that implement nonlinear site response methods include SUMDES (Li et al. 1992), TESS (Pyke 2000), D-MOD2000 (Matasovic and Ordóñez, 2012), and DEEPSOIL (Hashash et al 2012). This study performed one dimensional total stress equivalent linear, total stress nonlinear, and effective stress nonlinear site response analyses in the program DEEPSOIL to investigate the seismic response of non-liquefiable NEHRP F sites.

Sections 6.2, 6.3, and 6.4 outline the theory, limitations, and input parameters necessary to perform one dimensional total stress equivalent linear, total stress nonlinear, and effective stress nonlinear site response analyses, respectively. Section 6.5 then discusses important aspects of site response analyses that caused confusion in the past but have recently been clarified by other researchers. Section 6.6 describes the selection of site parameters common to all sites, while

section 6.7 focuses specifically on the properties of each soil profile used in this project. It is very important to understand the inputs and processes of any analysis before looking at the results, because, in the words of early IBM instructor George Fuechsel, "garbage in, garbage out."

6.2 Equivalent Linear Analysis

Engineers use equivalent linear models for their robustness, simplicity, flexibility, and low computational requirements (Hashash et al., 2010). Linear and equivalent linear models are faster than nonlinear models because they can be computed in the frequency domain due to the principal of superposition.

To understand equivalent linear models it is important to first understand how linear models calculate site response. Linear models take an acceleration time series in the time domain and convert it to the frequency domain using a Fast Fourier Transform (FFT). The FFT determines the amplitude of harmonic waves at many different frequencies whose summation would be the acceleration time series. The Fourier series is then multiplied by a transfer function that determines how each frequency in the input motion is either amplified or deamplified to produce the Fourier series of the output motion. The Fourier series of the output motion is then transformed back to the time domain using the inverse FFT. Transfer functions are solutions to the wave equation of a vertically propagating horizontal shear wave. They are dependent on frequency and the stiffness, damping, and density properties of the soil profile (Kramer 1996).

In equivalent linear models the response of the soil profile is first calculated using the small strain stiffness and damping as outlined above for linear methods. From this initial estimate, shear strain histories for each layer are computed. Then, for each layer, the effective shear strain is calculated as some fraction of the maximum shear strain, usually 0.65. The values of stiffness and damping at the effective shear strain are then determined from shear modulus reduction and damping curves. The process is repeated until the difference between the stiffness and damping properties in two consecutive iterations falls below a set tolerance level.

The equivalent linear method uses the same stiffness and damping properties for the entire duration of the acceleration time series. This results in several drawbacks. First, this leads to an under prediction of the stiffness and an over prediction of the damping when the peak shear strain is much larger than the shear strains at other time intervals, and to an over prediction of the stiffness and under prediction of the damping when the shear strain is nearly uniform with time. This limitation can be partly accounted for by adjusting the ratio of the effective shear strain to the peak shear strain. Second, because the stiffness and damping do not change with time, equivalent linear analyses can predict high levels of amplification near the natural frequencies of the soil profile. These large resonances at the natural site frequencies are not seen in empirical data because the stiffness and damping of actual soil deposits change with time during strong ground shaking (Kramer 1996).

Other limitations of equivalent linear analyses include the fact that they are formulated in terms of total stress, and therefore cannot predict pore pressure generation and cyclic degradation that could significantly reduce the stiffness and stress of soils layers, resulting in failure for cohesive

soils and liquefaction for cohesionless soils. Finally, equivalent linear analyses cannot predict accurately the response of soils at large shear strains because soil response at large strains is highly nonlinear and the dynamic properties change significantly over the duration of the shaking.

Despite these limitations, the most common site response analysis method continues to be the equivalent linear method. This is due to the qualities listed above; robustness, simplicity, flexibility, and low computational requirements. In addition, the input parameters for equivalent linear programs such as SHAKE are physical parameters that are readily understood, in contrast to nonlinear or advanced constitutive models that might have curve fitting parameters with no physical meaning. Input parameters for equivalent linear analyses include the shear wave velocity, soil unit weight, shear modulus reduction and damping curves, and their variation with depth and stratigraphy.

This project conducted a corresponding total stress equivalent linear analysis for all of the nonlinear analyses performed for seven of the 15 sites. All total stress equivalent linear analyses were conducted in DEEPSOIL using an effective to maximum shear stress ratio of 0.65.

6.3 Total Stress Nonlinear Analysis

In one dimensional nonlinear site response analyses the soil column is idealized either as a continuous medium divided into finite elements with distributed mass or as a multiple degree of freedom lumped mass system. The program DEEPSOIL uses the lumped mass system. In the lumped mass system, each soil layer is represented by a corresponding mass, nonlinear spring, and dashpot, as shown in Figure 6.2. In contrast to equivalent linear models that are solved in the frequency domain, nonlinear models are solved in the time domain by direct numerical integration of the dynamic equation of motion for each time step. In this way, nonlinear models follow the stress-strain path of the soil throughout the duration of the seismic shaking. The dynamic equation of motion for each node of the system is combined into the global equation of motion:

$$M \times \ddot{u} + C \times \dot{u} + K \times u = -M \times I \times \ddot{u}_g \qquad (6.1)$$

where M is the mass matrix, C is the viscous damping matrix, K is the stiffness matrix, ü is the vector of nodal relative accelerations, u̇ is the vector of nodal relative velocities, u is the vector of nodal relative displacements, I is the unit vector, and $\ddot{u}_g$ is the acceleration at the base of the soil column (the input time series). Equation (6.1) is solved for each time increment using a time integration method such as the Newmark β method (Newmark, 1959). The mass matrix M is formed by lumping half of the mass from two adjacent layers at their common boundary. The stiffness matrix K is recalculated at each time increment to account for soil nonlinearity. With this method the appropriate shear modulus and damping for the given shear strain are used at each time step.

The calculation process for a nonlinear model is as follows (Kramer 1996): The input acceleration time series is used to determine the motion at the base of the soil profile. Then, the motion at each layer boundary is calculated moving from the bottom of the soil profile to the top.

Using the displacements at each layer boundary the shear strain in each layer is calculated. The shear stress for each layer is estimated from the shear strain using a specified constitutive model. This process is repeated for the next time step until the end of shaking.

The constitutive model in nonlinear models generally has a backbone curve that describes the stress strain relationship for monotonic loading, a set of rules governing the unloading and reloading behavior of the soil, and a pore water pressure generation model. An example of a backbone curve is the modified hyperbolic model developed by Matasovic and Vucetic (1993) given below, which is based on the hyperbolic model of Konder and Zelasko (1963).

$$\tau = \frac{G_{max} \times \gamma}{1 + \beta \times \left(\frac{\gamma}{\gamma_r}\right)^a} \tag{6.2}$$

Where τ = shear stress, G_{max} = initial shear modulus, γ = shear strain, and β, a, and γ_r are model parameters.

Many nonlinear site response models use the extended Masing rules to control the unloading and reloading characteristics of soils. The extended Masing rules state (Masing, 1926; Pyke, 1979):

1) The stress strain curve follows the backbone curve for initial loading.
2) The unloading and reloading curves have the same shape as the backbone curve, but enlarged by a factor of 2 with the origin shifted to the reversal point (γ_{rev},τ_{rev}).
3) When the unloading or reloading curve exceeds the maximum past strain (γ_m) and intersects the backbone curve, the stress strain path follows that of the backbone curve until the next reversal point.
4) When the unloading or reloading curve intersects the curve from the previous cycle, then the stress-strain curve follows the path of the previous cycle.

Figure 6.3 shows the above four rules graphically. The modified hyperbolic model developed by Matasovic and Vucetic (1993) gives the following equation for the unload-reload curves when implementing the extended Masing rules;

$$\tau = \frac{2 \times G_{max} \times \left(\frac{\gamma - \gamma_{rev}}{2}\right)}{1 + \beta \times \left(\frac{\gamma - \gamma_{rev}}{2 \times \gamma_r}\right)^a} + \tau_{rev} \tag{6.3}$$

where γ_{rev} and τ_{rev} are the shear strain and shear stress at the last reversal point, respectively.

The model used in DEEPSOIL for all of the nonlinear site response analyses was the MRDF model. This model is a pressure dependent hyperbolic model based on the modified hyperbolic model developed by Matasovic and Vucetic (1993) given in Equations (6.2) and (6.3). There are several differences between the model of Matasovic and Vucetic (1993) and the MRDF model implemented in DEEPSOIL. The MRDF model couples the confining pressure and shear stress by making γ_r pressure dependent:

$$\gamma_r = \gamma_{ref} \times \left(\frac{\sigma'_v}{\sigma_{ref}}\right)^b \tag{6.4}$$

where σ'_v is the effective vertical stress, σ_{ref} is the vertical effective stress at which $\gamma_r = \gamma_{ref}$, and b is a curve fitting parameter. The MRDF model also includes depth dependent small strain damping:

$$\xi = D_{min} \times \left(\frac{1}{\sigma'_v}\right)^d \tag{6.5}$$

where D_{min} is the small strain damping when $\sigma'_v = 1$, and d is a curve fitting parameter to adjust for pressure dependency.

Finally, the MRDF model includes a reduction factor $F(\gamma_m)$ to match better the measured values of damping at large strains than the values predicted when using the extended Masing rules with the MKZ model. The reduction factor $F(\gamma_m)$ is explained further in a later section. Equations (6.6) and (6.7) give the relation between stress and strain for the backbone curve and the unloading-reloading curves in the MRDF model, respectively.

$$\tau = \frac{G_{max} \times \gamma}{1 + \beta \times \left(\frac{\gamma}{\gamma_r}\right)^a} \tag{6.6}$$

$$\tau = F(\gamma_m) \times \left[\frac{2 \times G_{max} \times \left(\frac{\gamma - \gamma_{rev}}{2}\right)}{1 + \beta \times \left(\frac{\gamma - \gamma_{rev}}{2 \cdot \gamma_r}\right)^a} - \frac{G_{max} \times (\gamma - \gamma_{rev})}{1 + \beta \times \left(\frac{\gamma_m}{\gamma_r}\right)^a}\right] + \frac{G_{max} \times (\gamma - \gamma_{rev})}{1 + \beta \times \left(\frac{\gamma_m}{\gamma_r}\right)^a} + \tau_{rev} \tag{6.7}$$

The input parameters for the MRDF model in DEEPSOIL for total stress nonlinear analysis are the shear wave velocity (Vs), unit weight, and D_{min}, γ_{ref}, σ_{ref}, β, a, b, d, P_1, P_2, P_3 for each layer. Parameters P_1, P_2, and P_3 are used to determine the reduction factor $F(\gamma_m)$ and are discussed later. All of the parameters except the shear wave velocity and unit weight can be estimated from user defined target shear modulus reduction and damping curves. DEEPSOIL has a built in optimization scheme to determine the model parameters that best fit the target shear modulus reduction and damping curves. Therefore, the input parameters for a total stress nonlinear analysis using the MRDF model in DEEPSOIL are the same as for a total stress equivalent linear analysis.

6.4 Effective Stress Nonlinear Analysis

One of the advantages of effective stress site response models over total stress models is their ability to predict the change in pore water pressure and soil degradation due to cyclic loading.

Cyclic shearing of fully saturated soils causes plastic deformations due to the progressive collapse of the soil skeleton. As the soil skeleton collapses residual excess pore water pressures are generated, which decrease the effective stress. Because the stiffness and strength of soils are dependent on the effective confining pressure, as the effective stress decreases the stiffness and strength also decrease. As a result, the generation and redistribution of excess pore water pressure within a soil deposit can significantly affect the seismic response of a site (Matasovic 1993).

There are three categories of pore pressure generation models; stress based, strain based, and energy based. The first pore pressure generation models, such as the Seed et al. (1975) model, were stress based models. However, stress based models are difficult to implement in practice because they require that the input ground motion be converted to an equivalent number of uniform cycles. In addition, stress based pore pressure generation models cannot be used in conjunction with strain based backbone curve models such as the MKZ model outlined above.

DEEPSOIL allows implementation of the strain based pore pressure generation models of Matasovic and Vucetic (1993) for sands and Matasovic and Vucetic (1995) for clays, and the energy based model GMP of Green et al. (2000) for sands. The two strain based pore pressure generation models of Matasovic and Vucetic (1993; 1995) are based on the model developed by Dobry et al. (1985) for saturated sands.

Dobry et al. (1985) derived their model from the theoretical effective stress pore pressure generation model of Martin et al. (1975), and validated it using the results of seven series of cyclic direct simple shear, cyclic triaxial, and cyclic torsional shear tests. Figure 6.4 summarizes the results of Dobry et al (1985), and shows that the residual excess pore pressure ratio ($r_u = u_N^* = u_N/\sigma'_v$) increases as the number of applied shearing cycles N and shear strain γ increase. Vucetic and Dobry (1988a) formalized the model as:

$$r_u = \frac{u_N}{\sigma'_v} = \frac{p \times f \times F \times N \times (\gamma - \gamma_{tv})^k}{1 + f \times F \times N \times (\gamma - \gamma_{tv})^k} \qquad (6.8)$$

where r_u is the residual excess pore pressure ratio, u_N is the residual excess pore pressure after N cycles, σ'_v is the initial vertical effective stress before shearing, γ_{tv} is the volumetric threshold shear strain, f is 1 for one dimensional analyses and 2 for two dimensional analyses, and p, F, and k are curve fitting parameters. The volumetric threshold shear strain γ_{tv} is "the cyclic strain amplitude above which a significant permanent volume change or a permanent pore-water pressure change may occur in the soil, while below it the soil microstructure remains practically unchanged and consequently volume and pore-water pressure changes are negligible" (Vucetic, 1994).

Figure 6.5 shows the effect of cyclic degradation on the backbone curve of a fully saturated soil. As the number of cycles increases for a given shear strain, the corresponding shear stress and the small strain shear modulus decrease. The excess pore pressure of sands is linked to the degradation of stiffness and strength through the modulus (δ_G) and stress (δ_τ) degradation index factors (Matasovic and Vucetic, 1993):

$$\delta_G = \sqrt{1 - r_u} \tag{6.9}$$

$$\delta_\tau = 1 - (r_u)^v \tag{6.10}$$

where *v* is a curve fitting parameter introduced by Matasovic and Vucetic (1993).

To quantify the cyclic degradation in clays, Idriss et al (1978) defined the degradation index δ as the ordinate of the backbone curve for N cycles divided by the ordinate of the initial backbone curve at the same shear strain value. The degradation index δ for clays is therefore:

$$\delta = \frac{G_{s,N}}{G_{s,1}} = \frac{\tau_N/\gamma}{\tau_1/\gamma} = \frac{\tau_N}{\tau_1} \tag{6.11}$$

where $G_{s,N}$ and τ_N are the secant shear modulus and shear stress at N cycles and shear strain γ, respectively, and $G_{s,1}$ and τ_1 are the secant shear modulus and shear stress of the initial backbone curve at shear strain γ, respectively. Idriss et al (1978) found that the rate of degradation was constant for a given shear strain, and proposed the following equation:

$$\delta = N^{-t} \tag{6.12}$$

where N is the number of cycles and t is the degradation parameter (the rate of degradation).

Matasovic and Vucetic (1995) developed a cyclic degradation and pore pressure generation model for clays based on the model of Dobry et al (1985) and the degradation index δ and degradation parameter *t* concepts of Idriss et al. (1978). They modified the hyperbolic model of Pyke and Beikae (1993) to account for the volumetric threshold shear strain as such:

$$t = s \times (\gamma - \gamma_{tv})^r \tag{6.13}$$

where s and r are curve fitting parameters.

The Matasovic and Vucetic (1995) model for clays first estimates the degradation index parameter δ as shown in equations (6.12) and (6.13), and then calculates the pore pressure generation from δ. This is the opposite of their model for sands, which estimates the excess pore pressure generated for a given shear strain and then calculates the degradation index parameters using equations (6.9) and (6.10).

Figure 6.6 shows the reason why δ for clays is not calculated from the excess pore pressure like it is for sands. Matasovic and Vucetic (1995) found that in overconsolidated clays negative pore pressures develop at the beginning of cyclic loading at the same time that the soil stiffness and strength decrease. As a result, for a given negative value of excess pore pressure, there are two different values of degradation. This is contradictory to the effective stress principle because stiffness and strength decrease as the apparent effective stress increases. Matasovic and Vucetic (1995) hypothesize that cyclic degradation and cyclic pore water pressure generation in clays is due to "distortion and consequent deterioration of clay microstructure caused by the breakage of clay particle bonds." Therefore, excess pore pressure in clays cannot uniquely define cyclic

degradation in a direct way as in sands, because in clays the generation of excess pore pressure is not the only factor affecting degradation.

Matasovic and Vucetic (1995) found that a polynomial fit the curves in Figure 6.6 the best, and proposed the following equation to calculate the excess pore pressure ratio from the cyclic degradation:

$$r_u = \frac{u_N}{\sigma'_v} = A \times \delta^3 + B \times \delta^2 + C \times \delta + D \tag{6.14}$$

where A, B, C, and D are curve fitting parameters dependent on OCR. Table 6.1 lists the values of A, B, C, and D for different values of OCR.

Energy based models are empirical models that relate the generation of residual excess pore pressure to the amount of energy dissipated per unit volume of soil. The GMP model of Green et al. (2000) is a special case of the more general equation proposed by Berrill and Davis (1985), and is based on approximately 150 cyclic triaxial tests on sands with varying fines contents from 0% to 100% non-plastic silt. The equations of the GMP model are:

$$r_u = \sqrt{\frac{W_s}{PEC}} \leq 1 \tag{6.15}$$

$$W_s = \frac{1}{2 \times \sigma'_v} \sum_{i=1}^{n-1} (\tau_{i+1} + \tau_i) \times (\gamma_{i+1} - \gamma_i) \tag{6.16}$$

$$PEC = \frac{W_{s,r_u=0.65}}{0.4225} \tag{6.17}$$

where W_s is the dissipated energy per unit volume of soil divided by σ'_v, PEC is the pseudo energy capacity, n is the total number of points in the acceleration time series, τ_i and γ_i are the shear stress and shear strain at time i, respectively, and τ_{i+1} and γ_{i+1} are the shear stress and shear strain at time i+1, respectively. Figure 6.7 shows how the dissipated energy W_s is calculated for a given increment of time from the stress strain curve. Polito et al. (2008) developed Equation (6.18) to estimate PEC from fines content FC and relative density D_r.

$$ln(PEC) = \begin{cases} FC < 35\% : exp(c_3 \times D_r) + c_4 \\ FC \geq 35\% : c_1 \times FC^{c_2} + exp(c_3 \times D_r) + c_4 \end{cases} \tag{6.18}$$

where c_1 = -0.597, c_2 = 0.312, c_3 = 0.0139, and c_4 = -1.021. The GMP model is implemented in DEEPSOIL using the degradation parameters listed in equations (6.9) and (6.10).

The equations for all three pore pressure generation models available in DEEPSOIL are given below for reference.

For cohesionless soils:

$$\delta_G = \sqrt{1 - r_u} \tag{6.19}$$

$$\delta_\tau = 1 - (r_u)^v \tag{6.20}$$

Matasovic and Vucetic (1993)

$$r_u = \frac{p \times f \times F \times N \times (\gamma - \gamma_{tv})^k}{1 + f \times F \times N \times (\gamma - \gamma_{tv})^k} \tag{6.21}$$

Green et al. (2000), Polito et al. (2008):

$$r_u = \sqrt{\frac{W_s}{PEC}} \leq 1 \tag{6.22}$$

$$W_s = \frac{1}{2 \times \sigma'_v} \sum_{i=1}^{n-1} (\tau_{i+1} + \tau_i) \times (\gamma_{i+1} - \gamma_i) \tag{6.23}$$

$$ln(PEC) = \begin{cases} FC < 35\% : exp(c_3 \times D_r) + c_4 \\ FC \geq 35\% : c_1 \times FC^{c_2} + exp(c_3 \times D_r) + c_4 \end{cases} \tag{6.24}$$

For cohesive soils:

$$\delta_G = \delta_\tau = N^{-t} \tag{6.25}$$

Matasovic and Vucetic (1995):

$$t = s \times (\gamma - \gamma_{tv})^r \tag{6.26}$$

$$r_u = A \times N^{-3 \cdot t} + B \times N^{-2 \cdot t} + C \times N^{-t} + D \tag{6.27}$$

Where r_u is the residual excess pore pressure ratio, σ'_v is the initial vertical effective stress, γ_{tv} is the volumetric threshold shear strain, f is 1 for one dimensional analyses and 2 for two dimensional analyses, v, p, F, and k are curve fitting parameters for the Matasovic and Vucetic (1993) sand model, and s, r, A, B, C, and D are curve fitting parameters for the Matasovic and Vucetic (1995) clay model, W_s is the dissipated energy per unit volume of soil divided by σ'_v, PEC is the pseudo energy capacity, D_r = relative density, FC = fines content, c_1 = -0.597, c_2 = 0.312, c_3 = 0.0139, and c_4 = -1.021. The above equations show that the most important parameters controlling the pore pressure generation for the strain based models are the amplitude of the cyclic shear strain γ, the number of cycles N of cyclic straining, and the volumetric threshold shear strain γ_{tv} of the soil.

To include the pore pressure generation models mentioned above in the MRDF model of DEEPSOIL, Moreno-Torres et al. (2010) incorporated the degradation index parameters with the backbone curve and the unloading-reloading curves of equations (6.6) and (6.7) as shown below:

$$\tau = \frac{G_{max} \times \gamma \times \delta_G}{1 + \beta \times \left(\frac{\delta_G}{\delta_\tau}\right)^a \times \left(\frac{\gamma}{\gamma_r}\right)^a} \tag{6.28}$$

$$\tau = F(\gamma_m) \times \left[\frac{2 \times G_{max} \times \delta_G \times \left(\frac{\gamma - \gamma_{rev}}{2}\right)}{1 + \beta \times \left(\frac{\delta_G}{\delta_\tau}\right)^a \times \left(\frac{\gamma - \gamma_{rev}}{2 \cdot \gamma_r}\right)^a} - \frac{G_{max} \times \delta_G \times (\gamma - \gamma_{rev})}{1 + \beta \times \left(\frac{\delta_G}{\delta_\tau}\right)^a \times \left(\frac{\gamma_m}{\gamma_r}\right)^a}\right] + \frac{G_{max} \cdot \delta_G \cdot (\gamma - \gamma_{rev})}{1 + \beta \cdot \left(\frac{\delta_G}{\delta_\tau}\right)^a \cdot \left(\frac{\gamma_m}{\gamma_r}\right)^a} + \tau_{rev} \tag{6.29}$$

For a total stress analysis, $\delta_G = \delta_\tau = 1$ and equations (6.44) and (6.45) reduce to equations (6.6) and (6.7).

DEEPSOIL models the dissipation and redistribution of residual excess pore pressures using a form of Terzaghi's one dimensional theory of consolidation as shown below:

$$\frac{\delta u}{\delta t} = C_v \left(\frac{\delta^2 u}{\delta z^2}\right)_{st} + \left(\frac{\delta u}{\delta t}\right)_{C_v} \tag{6.30}$$

To include this feature the coefficient of consolidation C_v must be specified for each soil layer, as well as whether the bottom boundary is permeable or impermeable. This study set the boundary layer to be impermeable for all effective stress nonlinear site response analyses.

6.5 Important Aspects of Site Response Analyses

6.5.1 Hysteretic Damping

One shortcoming when using the extended Masing rules for nonlinear site response analyses is that it can lead to overestimation of damping at moderate and large shear strains, which leads to an underestimation of the shear strains in the soil layer and potentially an underestimation of the intensity of the ground motion at the surface. Because damping is a function of the area contained within cyclic stress strain loops, this means that the hysteresis loops calculated with the extended Masing rules are too wide at moderate and large shear strains (see Figure 6.8).

There are four methods of dealing with this; optimize the fit of the modulus reduction curve and accept the misfit of the damping curve, optimize the fit of the damping curve and accept the misfit of the modulus reduction curve, optimize the fit of both the modulus reduction and damping curves at the same time and accept the lesser fit of both curves, or include an additional model parameter (Stewart et al 2008). Pyke (1979) suggested modifying the second Masing rule so that the unloading-reloading curve can be scaled by a factor (n) different than two to match laboratory measurements of damping at moderate and large shear strains. Lo Presti et al (2006) implemented this idea in their cyclic nonlinear site response analysis code ONDA. They found

that they could model cyclic hardening by increasing the value of n and cyclic degradation by decreasing the value of n. Darendeli (2001) proposed modifying the damping calculated from the extended Masing rules by a reduction factor based on the shear modulus reduction curve (G/G_{max}) and the number of applied cycles N. The equation for the reduction factor employed by Darendeli (2001) is:

$$F(\gamma_m) = [0.6329 - 0.0057 \times ln(N)] \times \left(\frac{G(\gamma_m)}{G_0}\right)^{0.1} \tag{6.31}$$

where $G(\gamma_m)$ is the secant shear modulus for the maximum shear strain level γ_m. Phillips and Hashash (2009) built on the idea of Darendeli (2001) and proposed the following equation for the reduction factor:

$$F(\gamma_m) = P_1 - P_2 \times \left(1 - \frac{G(\gamma_m)}{G_{max}}\right)^{P_3} \tag{6.32}$$

where P_1, P_2, and P_3 are curve fitting parameters. As mentioned previously, DEEPSOIL has a built in optimization procedure to determine the best parameters to fit a set of user defined shear modulus reduction and damping curves.

6.5.2 Small Strain Damping

Cyclic nonlinear models using the extended Masing rules predict near zero levels of damping for small strains, which is in contradiction to field and laboratory measurements. To correct this, code designers incorporate velocity proportional viscous damping through the use of Rayleigh damping (Rayleigh and Lindsay, 1945). Rayleigh damping is proportional to the mass and stiffness matrix as:

$$C = a_0 \times M + a_1 \times K \tag{6.33}$$

where a_0 and a_1 are scalar coefficients calibrated to obtain the correct damping at the target frequencies. Stewart et al (2008) recommend the target frequencies be the natural frequencies at the first and third modes of the soil profile, which are calculated as (Kramer 1996):

$$f_n = (2 \times n - 1) \times \left(\frac{\overline{V_s}}{4 \times H}\right) \tag{6.34}$$

where f_n is the natural frequency of mode n, $\overline{V_s}$ is the time averaged shear wave velocity of the site, and H is the thickness of the site. Values of a_0 and a_1 for natural frequencies of modes i and j are then computed as:

$$\begin{bmatrix}\xi_i \\ \xi_j\end{bmatrix} = \frac{1}{4 \times \pi}\begin{bmatrix}\frac{1}{f_i} & f_i \\ \frac{1}{f_j} & f_j\end{bmatrix}\begin{bmatrix}a_0 \\ a_1\end{bmatrix} \tag{6.35}$$

where ξ_i and ξ_j are the damping ratios for frequencies f_i and f_j. Stewart et al (2008) recommend that the target damping ratios ξ_i and ξ_j be set equal to the small strain damping ratio. This formulation is known as full Rayleigh damping.

Park and Hashash (2004) devised extended Rayleigh damping, which uses four target modes. They used the orthogonality conditions of the mass and stiffness matrices to show that the damping matrix can consist of any combination of these matrices:

$$C = M \times \sum_{b=0}^{n-1} a_b \times (M^{-1} \times K)^b \tag{6.36}$$

where n is the number of modes used to construct the damping matrix C, and the scalar coefficient a_b is given by:

$$\xi_n = \frac{1}{4 \times \pi \times f_n} \times \sum_{b=0}^{n-1} a_b \times (2 \times \pi \times f_n)^{2 \cdot b} \tag{6.37}$$

Equations (6.36) and (6.37) show that, theoretically, any number of modes could be included in the damping matrix formulation. However, they recommend using four modes because more modes could lead to a singular matrix, which renders the problem unsolvable or drastically increases the computation time.

One drawback of Rayleigh damping is that it is frequency dependent. Figure 6.9 shows how this can lead to over or under predicting the damping at frequencies away from the target frequencies. In the past it also lead to confusion in practice about what target damping ratios and frequencies to use.

In answer to this problem, Phillips and Hashash (2009) devised a frequency independent viscous damping formulation and implemented it in DEEPSOIL. They used the work of Liu and Gorman (1995), which provides solutions for negative and rational indexed series, to reduce equations (6.36) and (6.37) for when b = 0.5, to the following equations:

$$C = M \times \sum_{b=0}^{n-1} a_b \times \Phi \times \omega^{2 \cdot b} \times \Phi^{-1} = M a_{0.5} \times \Phi \times \omega \times \Phi^{-1} \tag{6.38}$$

$$\xi_n = \frac{1}{4 \times \pi \times f_n} \times (a_{0.5} \times 2 \times \pi \times f_n) = 0.5 \times a_{0.5} \tag{6.39}$$

where ω is a diagonal matrix of the natural frequencies and Φ is the real modal matrix of the system. Equations (6.38) and (6.39) show that the viscous damping ratio is not frequency dependent for b = 0.5. Use of the frequency independent damping formulation is more computationally expensive than full Rayleigh damping because it must calculate ω and Φ, which in turn require calculating the eigenvalues and eigenvectors of $M^{-1} \cdot K$ (Phillips and Hashash,

2009). However, the increase in computation time is insignificant on a modern computer. In addition, Phillips and Hashash (2009) show that the frequency independent formulation predicts the site response better than when using full Rayleigh damping, and that it is easier to implement in practice.

This study used the frequency independent damping formulation proposed by Phillips and Hashash (2009) for all nonlinear site response analyses conducted in DEEPSOIL.

6.5.3 Layer Thickness

In time domain analyses, the minimum period (maximum frequency) that can be propagated through a soil layer is given by:

$$T_{min,i} = \frac{4 \times H_i}{V_{s,i}} \tag{6.40}$$

where $T_{min,i}$ is the minimum period that layer i can propagate, $V_{s,i}$ is the shear wave velocity of layer i, and H_i is the height of layer i. The minimum period corresponds to the fundamental period of the soil layer. Periods smaller than T_{min} will not be propagated though the soil layer. Stewart et al (2008) show that for periods smaller than T_{min}, nonlinear site response analyses under predict the pseudo acceleration response spectral values. Response spectra at periods below T_{min} tend to be flat and equal to the PGA because all of the high frequency waves are filtered out. Therefore, T_{min} should be chosen consistent with the frequency content of the input motion and the period band of interest for the project.

The DEEPSOIL manual recommends that the minimum period be between 0.02 and 0.04 seconds (25-50Hz) (Hashash et al, 2012). In addition, when conducting time domain analyses, DEEPSOIL automatically calculates T_{min} for each layer and displays the output to the user. This provides a useful check on the input soil profile parameters.

This study adjusted the soil layer thicknesses so that the highest T_{min} for all profile layers was 0.04 seconds (25Hz). In addition, copies of all soil profiles were created that were exactly the same except the soil layers were half as thick, giving a T_{min} value of 0.02 seconds (50Hz). The T_{min} = 0.02 seconds soil profiles were only used in the analyses of the SCR ground motions (stable continental region) because the frequency range of interest for these motions is higher than for the other ground motions.

6.5.4 Definition of Input Motion and Half Space (Base)

Another area of confusion when conducting site response analyses has been the specification of the input time series as a within motion or an outcropping motion, and whether the half space at the base of the soil profile should be modeled as rigid or elastic. Outcropping motions are ground motions recorded at the ground surface, or at outcrops of rock. Within motions are motions recorded from within a soil profile. Within and outcropping motions are not the same due to site effects and boundary conditions and cannot be used interchangeably. Even for hard rock sites where site effects are small, outcropping motions are different from within motions because free surface motions are twice the amplitude of the incident seismic wave due to full

reflection, whereas within motions are the sum of upward and downward propagating waves reflected from overlying layers (Kramer 1996).

Site response analyses predict the effect of a ground motion propagating up through a soil layer to the surface. The input motion at the base of the soil layer should therefore be a within motion. However, there are many more surface outcrop recordings than downhole within recordings. As a result, it has been the state of the practice for many years to take an outcropping motion and convert it to a within motion through the process of deconvolution. Because the equivalent linear method uses linear analysis, the input ground motion may be specified at any layer, and the response at any layer can be related to the response at any other layer. During deconvolution, the outcropping motion is specified at the surface and the response at the top of the within rock layer (half space) is predicted. This motion is then used as the within motion at the base of the soil profile for the site response analysis.

The next step is the specification of the half-space as rigid or elastic. Rigid bases are fixed and therefore completely reflect any descending waves back up through the soil profile. Elastic bases, or compliant bases, require specification of the rock stiffness and damping, and only partially reflect descending waves back up through the soil profile. Some of the elastic wave energy is dissipated into the bedrock, which reduces the ground motion intensity at the surface.

To clarify when to use within or outcropping motions, rigid or elastic bases, as well as what combination of the two, Stewart et al (2008) compared the response of time domain analyses with elastic material properties to frequency domain analyses, which provide an exact solution for linear material properties. They looked at all four parameter combinations; within motion and rigid base, within motion and elastic base, outcropping motion and rigid base, and outcropping motion with an elastic base.

Figure 6.10 shows that when using within motions with an elastic base the response at the surface is under predicted, when using outcropping motions with a rigid base the surface response is over predicted, and the other two cases match the solution from the frequency domain analysis. Based on these results, Stewart et al (2008) recommend that when the input motion is an outcropping motion, the time series should be applied without modification using an elastic base, and if the input motion is a within motion taken from a vertical array or a down-hole recording, then the within motion should be used without modification using a rigid base.

All of the motions used in this study are surface recordings. Therefore, this study used the ground motions outlined in the previous chapter without modification in conjunction with an elastic base. The rock properties are specified along with the soil properties for each site in the following sections.

6.5.5 Implied Strength

Site response analyses that predict large levels of shear strain must take into account the shear strength (τ_{ff}) of the soil in addition to the stiffness and damping. At large shear strains the implied shear strength of the soil can greatly influence the results of the site response analyses. If the shear strength of a soil is overestimated this could lead to predictions of shear stress greater than the shear strength, which means the soil in that layer has failed and the results are incorrect.

If the shear strength is underestimated then the predicted surface ground motion intensity could be much lower than reality, which could lead to an unconservative design.

Most laboratory investigations of the dynamic properties of soils do not measure shear strains larger than 0.1-0.5% (e.g. Darendeli 2001; Zhang et al, 2005). When they are extrapolated to shear strains of 1-10% there is no guarantee that they will match the shear strength. Stewart et al (2008) compared the implied shear strength from the shear modulus degradation curves given by Darendeli (2001) to the empirical relations for ratios of G_{max} to shear strength given by Weiler (1988). They found that the implied shear strength from Darendeli (2001) underestimated the shear strength at confining pressures of 100 kPa, but gave similar results to Weiler (1988) for confining pressures of 500 kPa. Hashash et al (2010) note that while sometimes an empirical shear modulus reduction curve will underestimate the soil's shear strength, other times it may overestimate the shear strength.

Stewart et al (2008) and later Yee et al (2013) proposed a method to adjust the soil backbone curve so that it follows cyclic test results or correlation relationships up to a given strain level γ_1, and at strains larger than γ_1 it asymptotically approaches the shear strength (τ_{ff}). This procedure essentially takes two curves and splices them together at the specified strain γ_1 to form a hybrid curve that matches both small and large strain behavior of soils. Yee et al (2013) give the following procedure to create the hybrid curve:

1) Estimate the shear modulus reduction curve from cyclic test results or correlation relationships
2) Determine γ_1 such that $\gamma_1 < 0.3$-0.5% and
    a. For values of $\alpha < 1.0$, choose γ_1 such that $\tau_1 \leq 0.3 \times \tau_{ff}$, where

$$\tau_1 = \frac{G_{max}\gamma_1}{1 + \left(\frac{\gamma_1}{\gamma_r}\right)^{\alpha}} \tag{6.41}$$

    b. For values of $\alpha \geq 1.0$, choose γ_1 such that $\gamma_1 \approx \gamma_r$
3) Calculate G_{y1}, the tangent modulus of the first curve at γ_1, using equation (6.42). This ensures a smooth transition between the two curves.

$$\frac{G_{\gamma_1}}{G_{max}} = \frac{1 + (1-\alpha) \times \left(\frac{\gamma_1}{\gamma_r}\right)^{\alpha}}{\left[1 + \left(\frac{\gamma_1}{\gamma_r}\right)^{\alpha}\right]^2} \tag{6.42}$$

4) Estimate γ'_{ref}, the reference stress shifted by τ_1

$$\gamma'_{ref} = \frac{\left(\tau_{ff} - \tau_1\right)}{G_{\gamma_1}} \tag{6.43}$$

5) Finally, calculate G/G_{max} for $\gamma > \gamma_1$

$$\gamma' = \gamma - \gamma_1 \tag{6.44}$$

$$\frac{G}{G_{max}} = \frac{\frac{\gamma_1}{1 + (\gamma_1/\gamma_r)^{\alpha}} + \frac{\left(G_{\gamma_1}/G_{max}\right) \times \gamma'}{1 + \left(\gamma'/\gamma'_{ref}\right)}}{\gamma} \tag{6.45}$$

The procedure outlined above ensures that the shear modulus reduction curve matches test data for small and medium strains, matches shear strength data for large shear strains, and that the transition between the two curves is smooth with no noticeable kink. Professor Stewart (personal communication, October 15, 2013) recommends calculating the damping curves from the backbone curve generated by the hybrid shear modulus reduction curve outlined above. This study estimated the hybrid backbone curve using the hybrid shear modulus reduction curve, extended Masing rules, and the reduction factor predicted by Darendeli (2001). Figure 6.11 shows an example hybrid curve compared to the shear modulus reduction and damping curves estimated using Darendeli (2001) and the 'strength' curve (i.e., the curve generated using $\gamma_r = (Su/G_{max})$ and $\alpha = 1$). The hybrid curve matches the Darendeli (2001) curve at small strains and the 'strength' curve at large strains.

The MRDF model in DEEPSOIL predicts a single hyperbole and therefore cannot match perfectly the strength adjusted hybrid curves outlined above. Professor Hashash (personal communication, October 23, 2013) currently has a student working on creating a cyclic nonlinear soil model that can accommodate a hybrid curve. However, this model was not available at the time this research was undertaken. Until the new model is ready, Hashash et al (2010) recommend the following procedure when using DEEPSOIL to best approximate the hybrid curve:

1) Calculate the strength adjusted hybrid curve
2) Use the internal optimization program in DEEPSOIL to obtain the nonlinear parameters that best approximate the target hybrid curve
3) DEEPSOIL then computes the implied shear strength of the soil as the maximum shear stress value calculated using the equations below for all points on the shear modulus reduction curve.

   For cohesive soils:

$$\tau_{ff} = G_{max} \times \left(\frac{G}{G_{max}}\right) \times \gamma \tag{6.46}$$

   For cohesionless soils:

$$\phi = tan^{-1}\left(\frac{\tau_{max}}{\sigma'_v}\right) \tag{6.47}$$

4) Compare the implied shear strength estimated by DEEPSOIL with the desired target shear strength
5) If the implied shear strength is less than the desired target shear strength, manually increase the shear modulus reduction curve for shear strains larger than γ_1. If the implied shear strength is greater than the desired target shear strength, manually decrease the shear modulus reduction curve for shear strains larger than γ_1.

6) Repeat steps 2-5 until the implied shear strength and desired target shear strengths are reasonably close.

This study followed the procedure of Yee et al (2013) for creating the hybrid shear modulus reduction and damping curves, and the procedure given by Hashash et al (2010) for estimating the cyclic nonlinear parameters of the MRDF model. All of the implied soil strengths for the soil profiles used in this study were within 5% of the target shear strengths for dynamic shear strengths greater than 20 kPa, and 1 kPa of the target shear strengths for soil layers with dynamic shear strengths less than 20 kPa.

6.6 Selection of General Site Parameters

This study performed site response analyses for 15 sites, all of which are categorized as NEHRP site classes E or F. Seven of the sites, called the base case sites, are based on actual soil profiles. The other eight sites are variations on the seven base case sites that explore the effects of strength, plasticity index (PI), and elastic site period (Ts) on the surface response.

The data used to create the seven base case sites was gathered from reports in the literature and site investigations performed by private companies. If data for a given site existed, that data was used to construct the input parameters for the site response analyses. If data was available for some layers but not all layers, then general correlation relationships were calibrated to the measured data and the calibrated correlation was used to estimate the parameters for other layers. The method of calibration and the general correlation selected are described in more detail for each specific site later in the chapter. The following section describes the procedures used to estimate site properties when no data was available.

6.6.1 Estimation of Strength Parameters

When no strength data was available, the shear strength of the cohesive soils was estimated using the SHANSEP method proposed by Ladd and Foott (1974):

$$\tau_{ff} = Su = \sigma_v' \times \left(\frac{Su}{\sigma_v'}\right)_{NC} \times OCR^m \tag{6.48}$$

where Su is the undrained shear strength, $(\mathrm{Su}/\sigma_\mathrm{v}')_\mathrm{NC}$ is the shear strength ratio for normally consolidated soils, and m is a constant. For cohesive soils $(\mathrm{Su}/\sigma_\mathrm{v}')_\mathrm{NC}$ was fixed at 0.25 to represent direct simple shear and m = 0.8.

For cohesionless soils the shear strength was determined using Mohr Coulomb failure criteria assuming zero cohesion:

$$\tau_{ff} = \sigma_v' \times tan(\phi) \tag{6.49}$$

where ϕ is the internal friction angle. The internal friction angle was determined from SPT blow counts, where available, using the relations given by Peck et al. (1974) and Meyerhoff (1956). When no SPT blow counts were available, the internal friction angle was estimated from the

general description of density given on the boring log (e.g. “loose”, “dense”, or “very dense”) with the relations given by Peck et al (1974).

The static shear strengths were multiplied by 1.1 to adjust for rate effects, cyclic softening, and progressive failure. Cohesive soils that are sheared at earthquake strain rates can have shear strength values 1.1 to 1.5 times the static shear strength (Sheahan et al, 1996; Biscontin and Pestana, 1999). In contrast, cyclic softening decreases the shear strength due to an increase in excess pore pressure with cycles, and because cyclic shearing is much more damaging to soil than unidirectional shearing. Progressive failure also decreases the estimated values of shear strength and represents the fact that not all parts of the soil fail at the same time.

6.6.2 Shear Modulus Reduction and Damping Curves

Some of the soils for the sites listed below had data on the shear modulus reduction and damping curves. When this data was available it was used, or it was used to calibrate the Darendeli (2001) model for other layers of the same soil but with different PI, OCR, or confining pressure. The method of calibration is described for each site where this was done. For layers where there was no data, the Darendeli (2001) model was used to estimate the shear modulus reduction and damping curves for the given PI, OCR, and confining pressure. The value of frequency and number of cycles was 1 Hz and 10 cycles, respectively, for all soils.

The model derived by Darendeli (2001) does not account for ageing effects. To account for the effect of ageing, the PI of Pleistocene soils was increased to represent shear modulus reduction and damping curves with greater volumetric threshold shear strains γ_{tv}. The PI ADJ column in the site tables listed in Appendix 6A is the adjusted PI that accounts for the effect of ageing. Holocene soils were not adjusted for age effects.

6.6.3 Half Space Parameters

The unit weight and shear wave velocity for the underlying rock half-space was 23 kN/m^3 and 760 m/s for all profiles and scenarios except scenario SCR. The unit weight and shear wave velocity for the underlying rock half-space for scenario SCR was 25 kN/m^3 and 2000 m/s. The shear wave velocity values were taken to be consistent with the shear wave velocities used to create the target response spectra, and the unit weights are representative of soft rock and hard rock conditions (Nikolaou, 2004).

6.6.4 Pore Pressure Generation and Cyclic Degradation Parameters

The pore pressure generation models of Matasovic and Vucetic (1993) for sands and Matasovic and Vucetic (1995) for clays were used for all effective stress nonlinear analyses. The clay model has seven parameters; the cyclic volumetric threshold shear strain γ_{tv}, and curve fitting parameters s, r, A, B, C, and D. The sand model has six parameters; the cyclic volumetric threshold shear strain γ_{tv}, and curve fitting parameters v, p, f, F, and k. The best database of reported values for the Matasovic and Vucetic (1993; 1995) pore pressure generation and cyclic degradation models is the site response analysis program D-MOD2000 manual (Matasovic and Ordóñez, 2012). Table 6.1, Table 6.2, and Table 6.3 list the recommended values of the Matasovic and Vucetic (1993; 1995) models given in the D-MOD2000 manual for clays, low

plasticity silts, and sands, respectively, as well as the values reported for low plasticity silt given in Anderson et al (2011).

The values in Table 6.1 for the clay model are from Matasovic and Vucetic (1995) and are based on strain controlled cyclic DSS testing of five clays taken from two sites offshore of Venezuela. Figure 6.12 shows the Atterberg limits of the tested clays. They plot around the A line and range in PI from 20 to 60 and in LL from 45 to 100. The soils were tested at vertical effective stresses of 89 kPa to 1,382 kPa, OCR from 1 to 4, and shear strains from 0.2% to 5.09%.

There is very little guidance in the literature on how to estimate the curve fitting parameters of the clay model when no test data are available, especially when dealing with soils that are different than the five soils tested by Matasovic and Vucetic (1995). In addition, there are very few reported values of the curve fitting parameters with which to compare measured values. However, it would be incorrect to apply the values of Table 6.1 to all cohesive soils in a seismic site response analysis. Figure 6.13 shows two figures from Vucetic and Dobry (1988b) and Tan and Vucetic (1989), who found that as PI and OCR increase, the degradation parameter t decreases. Figure 6.14 shows the combined effect of PI and OCR on t (Vucetic, 1992; Matasovic, 1993). Therefore, to take into account the effect of PI and OCR on the cyclic degradation and pore pressure generation of cohesive soils, simple correlations based on Figure 6.14 and the data in Table 6.1 were created for this project. These correlations were developed to capture the trend of t with PI and OCR, and provide a smooth interpolation between the given values, rather than applying the same parameters to all cohesive soils and ignoring the effects of PI and OCR.

The correlations developed in this study to calculate the curve fitting parameters of the Matasovic and Vucetic (1995) clay model are:

$$s = 1.6374 \times PI^{-0.802} \times OCR^{-0.417} \tag{6.50}$$

$$r = 0.7911 \times PI^{-0.113} \times OCR^{-0.147} \tag{6.51}$$

$$A = \begin{cases} 7.6451 & for\ OCR\ < 1.1 \\ 15.641 \times OCR^{-0.242} & for\ OCR\ \geq 1.1 \end{cases} \tag{6.52}$$

$$B = \begin{cases} -14.714 & for\ OCR\ < 1.1 \\ -33.691 \times OCR^{-0.33} & for\ OCR\ \geq 1.1 \end{cases} \tag{6.53}$$

$$C = \begin{cases} 6.38 & for\ OCR\ < 1.1 \\ 21.45 \times OCR^{-0.468} & for\ OCR\ \geq 1.1 \end{cases} \tag{6.54}$$

$$D = \begin{cases} 0.6922 & for\ OCR\ < 1.1 \\ -3.4708 \times OCR^{-0.857} & for\ OCR\ \geq 1.1 \end{cases} \tag{6.55}$$

These models were developed using a trial and error process of several different functional forms and nonlinear least squares regression. The above equations represent the best fit for each equation. Figure 6.15 shows that Equations (6.50) and (6.51) match the predicted effect of PI

and OCR on t for a given shear strain as shown in Figure 6.14. Figure 6.16 shows that Equations (6.52), (6.53), (6.54), and (6.55) match the values of A, B, C, and D given in Table 6.1, and provide reasonable values when extrapolated to OCR of 5. These correlations are used from OCR = 1 to 5, and PI = 15 to 200.

Mortezaie and Vucetic (2013) conducted 16 cyclic DSS tests on a Kaolinite clay with PI = 28 for different combinations of loading frequency f (0.1 Hz, 0.01 Hz, and 0.001 Hz) and vertical effective stress σ'_v (220 kPa and 680 kPa) at three values of shear strain (0.1%, 0.25%, and 0.5%). They found that as frequency increased by a factor of 10, the cyclic degradation parameter t increased by about 20-50%, and as σ'_v increased from 220 kPa to 680 kPa, t decreased by about 20-38%. They also found that r_u decreased as f and σ'_v increased. These trends were not included in the correlation equations used to estimate the curve fitting parameters for the Matasovic and Vucetic (1995) model because the interactions between PI, OCR, f, and σ'_v are not known. In addition, on a practical level, there is not enough data to construct simple correlation equations. However, the trends found in Mortezaie and Vucetic (2013) should be kept in mind during the interpretation of the site response analyses.

The volumetric threshold shear strain has received considerably more attention than the other parameters in the Matasovic and Vucetic (1993, 1995) models. Vucetic (1994) synthesized available published laboratory data and found that γ_{tv} depends on soil type and is correlated to plasticity index. He found that the average value of γ_{tv} was about the same shear strain as when G/G_{max} = 0.65, as shown in Figure 6.17. Hsu and Vucetic (2006) conducted five cyclic DSS tests on two silts (PI = 14 and 20, LL = 50 and 53) and one clay (PI = 30, LL = 50). They confirmed that γ_{tv} is greater in cohesive soils than in cohesionless soils and that it tends to increase as PI increases. They also found very little change in the value of γ_{tv} when the initial vertical effective stress was changed from 108 to 220 kPa for the PI = 20 silt and when it was changed from 222 to 666 kPa for the clay with PI = 30.

This study chose the volumetric cyclic threshold shear strain as the strain when G/G_{max} = 0.65. This is consistent with the work of Vucetic (1994) and Hsu and Vucetic (2006), as well as with the shear modulus reduction and damping curves used in the study.

Similar to the clay model, the only guidance in the literature on how to estimate the curve fitting parameters without specific test data for the Matasovic and Vucetic (1993) sand model is in the D-MOD2000 Manual (Matasovic and Ordóñez, 2012). Table 6.2 and Table 6.3 list the values given by the D-MOD2000 Manual for the Matasovic and Vucetic (1993) pore pressure generation model for two low plasticity silts and eight non-plastic sands and silts, respectively. Figure 6.19 shows the grain size distribution curves for the soils listed in Table 6.3.

This study chose v = f = p = 1 for all cohesionless soils and low plasticity silts. The values of v in Table 6.2 and Table 6.3 are all equal to one except for Santa Monica Beach Sand, and the values of p are all within $\pm$ 7.1% of 1. Therefore, the decision was made to choose v = p = 1 for simplicity. The value of f is 1 for one dimensional analysis and 2 to simulate pore pressure generation in two dimensions. Because the clay model only takes into account pore pressure generation in one dimension, f =1 was chosen to be consistent with the clay model.

Simple correlations for the curve fitting parameters *F* and *s* were developed to capture trends and provide smooth transitions from one soil layer to the next; similar to what was done for the clay model. Figure 6.20 and Figure 6.21 show the values of F and s plotted against the values of shear wave velocity (V_s) and fines content (FC) reported in Table 6.2 and Table 6.3. Figure 6.20 shows that as the shear wave velocity increases F decreases, and Figure 6.21 shows that as fines content increases s increases. As F decreases and s increases the amount of excess pore pressure generated for a given shear strain and number of loading cycles decreases. This makes intuitive sense because as the soil becomes stiffer and has more fines it is less likely to liquefy. Equations (6.56) and (6.57) give the correlations developed in this study to calculate the curve fitting parameters F and s of the Matasovic and Vucetic (1993) sand model.

$$F = 3810 \times V_s^{-1.55} \tag{6.56}$$

$$s = (FC + 1)^{0.1252} \tag{6.57}$$

Where V_s is in m/s and FC is in percent. Equations (6.56) and (6.57) were used for soils with V_s between 150 m/s and 624 m/s and fines contents between 0% and 100%. These models were developed using a trial and error process of several different functional forms and nonlinear least squares regression. The above equations represent the best fit for each equation.

This study chose the volumetric threshold shear strain of the sand layers as the strain when G/G_{max} = 0.65 to be consistent with the clay model and the chosen shear modulus reduction curves used in the site response analyses.

The values of all the pore pressure generation and cyclic degradation parameters for each site are listed in Appendix 6B along with the other DEEPSOIL input parameters for each site.

6.6.5 Pore Pressure Dissipation Parameters

The input parameters required for the DEEPSOIL dissipation model are the coefficient of consolidation (C_v) for each layer, and whether the base is permeable or impermeable. Every analysis conducted in this study had an impermeable base. When no data was available the coefficient of consolidation for cohesive soils was selected based on the liquid limit using the following correlation from NAVFAC 7.01 (1986), and shown in Figure 6.22:

$$C_v = 0.79861 \times LL^{-2.7905} \tag{6.58}$$

where C_v is in m^2/s.

The values of the coefficient of consolidation for cohesionless soils were based on Table 6.4, Table 6.5, and Table 6.6, which were taken from Pestana et al (1997). An average value of m_v = $5*10^{-5}$ m^2/kN from Table 6.6 was chosen for the volumetric compressibility for all cohesionless soils. Based on Table 6.4, values of hydraulic conductivity k were chosen for each cohesionless soil layer according to their USCS fines content designation as follows: k = $3*10^{-5}$ m/s for soils with FC between 12% and 50 % (e.g. SC, SM); k = $8*10^{-5}$ m/s for soils with FC between 5% and 12% (e.g. SP-SC); k = $5*10^{-4}$ m/s for sands with FC < 5% (e.g. SP or SW); and k = $5*10^{-2}$ m/s

for gravels with FC < 5% (e.g. GP or GW). The coefficient of consolidation was then estimated using Equation (6.59);

$$C_v = \frac{k}{m_v \times \gamma_w} \tag{6.59}$$

where C_v is in m^2/s.

This study set the groundwater table at one meter below the ground surface for all sites.

6.7 Selected Sites for Site Response Analyses

As mentioned earlier, this study performed site response analyses for 15 sites, all of which are categorized as NEHRP site classes E or F. The following sections describe in detail the parameters chosen for each of the sites. Seven of the sites, called the base case sites, are based on actual soil profiles, and their parameters were chosen based on measured field data and laboratory testing. The other eight sites are variations on the seven base case sites that explore the effects of strength, plasticity index (PI), and elastic site period (Ts) on the surface response.

6.7.1 San Francisco Bay Area Sites

Two of the base case sites are from the San Francisco Bay Area. The first Bay Area site is modeled after the deep soft soil deposit located under the APEEL #1 recording station in Redwood Shores, CA. The APEEL #1 station (CGS - CSMIP Station 58375) was located at 37.545 N, 122.231W, at the south-east edge of San Francisco Bay on reclaimed marsh land. The Bay Area site profile is composed of approximately 2 meters of fill at the top, followed by 20 meters of Young Bay Mud, 42 meters of stiff clay (Old Bay Clay), 20 meters of silty sand, 81 more meters of Old Bay Clay, and 25 meters of gravelly sand over Franciscan Formation bedrock at a depth of 185 meters.

The soil type and shear wave velocity profile for Bay Area are based on those of APEEL#1 given by Gibbs et al (1993). The unit weights, OCR, PI, shear strengths, and age for the Young Bay Mud, Old Bay Clay, and Posey Sands are taken from Bonaparte and Mitchell (1979), Pass (1994), Rau (1999), and Biscontin (2001), who conducted tests on these same soils taken from different locations in the San Francisco Bay. The unit weights for the gravel and sand layers at the bottom of the profile are estimated from NAVFAC 7.01 (1986). Figure 6.23 shows the soil properties versus depth for site Bay Area.

The site Bay Area F is a variation on site Bay Area. It is the same as Bay Area except that the thickness of the Young Bay Mud deposit is extended from 20 meters to 37 meters, making it a NEHRP F site. In addition, the upper deposit of Old Bay Clay was reduced from 42 meters to 30 meters. This ensured that the elastic site period was roughly the same for Bay Area and Bay Area F. Figure 6.24 shows the soil properties versus depth for site Bay Area F.

The second San Francisco Bay Area site (Bay Area II) is based on a soil profile of a marshland at the edge of the San Francisco Bay. Due to the sensitive nature of the data, however, the exact

location and the company that conducted the site investigation cannot be reported at this time. The site is composed of about one meter of fill, followed by ten meters of high plasticity organic clay, six meters of Young Bay Mud, and 15 meters of Old Bay Clay over bedrock at a depth of 32 meters. The site is an F site due to the thick layer (> 3 meters) of organic clay.

All of the data are based on measured values except the shear modulus reduction and damping curves. As mentioned previously, the shear modulus reduction and damping curves for all of the soil layers with no measured curves are based on the curves by Darendeli (2001) using the measured values of PI, OCR, and confining stress. However, the database used to develop the Darendeli (2001) model did not include any organic soils, and the highest PI soil was PI = 132, whereas some layers of the organic clay have PI values of 200. Therefore, a second site (Bay Area II K) was constructed that is exactly the same as Bay Area II except that the shear modulus reduction and damping curves of the organic clay layers are based on the model developed by Kishida et al (2009), which is specifically for organic clays and peats. The strength of the soil was kept the same, so the only difference was in the shear modulus reduction and damping curves at small and moderate strains. At large strains the curves are the same because they are modified for the same strength. Figure 6.23 shows soil properties versus depth for site Bay Area II and Bay Area II K.

The effect of soil shear strength on the surface response was investigated by creating two sites based on Bay Area II K, but with different shear strengths. Sites Bay Area II K S2 and Bay Area II K S4 are the same as Bay Area II K except that the shear strength of the soil at all layers is twice as large and four times as large, respectively. Figure 6.26 and Figure 6.27 show the soil properties versus depth for sites Bay Area II K S2 and Bay Area II K S4, respectively.

6.7.2 Guayaquil, Ecuador, Site HAGP

The HAGP profile is based on a site investigation of a hospital in Guayaquil, Ecuador. Xavier Vera Grunauer, CEO of GeoEstudios, a geotechnical firm located in Guayaquil, Ecuador, provided all of the data for the site. Information provided by Mr. Grunauer includes site descriptions, boring logs, SPT data, CPT data, shear wave velocity profiles from the Refraction Microtremor technique (ReMi), and the results of laboratory strength, consolidation, and dynamic tests.

HAGP consists of two meters of fill, followed by 37 meters of high plasticity soft clay (Guayaquil Clay), and 11 meters of dense sand over bedrock at a depth of 50 meters. The HAGP soil profile follows the data provided by Mr. Grunauer for the soil profile of the hospital in Guayaquil with two exceptions. The thickness of the high plasticity soft clay was extended from 34 meters to 37 meters so that it classifies as a NEHRP F site. Second, SPT and CPT data provided by Mr. Grunauer only extend to a depth of 38 meters, which is two meters into the dense sand, and no data exists on the soils below this or the depth to bedrock. However, based on the seismic microzonation study conducted by Mr. Grunauer and GeoEstudios for the city of Guayaquil, they estimate that the elastic site period of the soil profile beneath the hospital is between 1.2 and 1.4 seconds. Therefore, the properties of the top two meters of the sand layer were extrapolated to a depth of 50 meters, which gives an elastic site period of 1.23 seconds. Figure 6.28 shows the soil properties versus depth for site HAGP.

Mr. Grunauer provided two shear modulus reduction and damping curves measured from the Guayaquil Clay. The Darendeli (2001) curves were calibrated for these two measured curves and then extrapolated for other PI, OCR, and confining pressures. The Darendeli (2001) curves were calibrated by changing the value of a from 0.919 to 0.75, the frequency to 3.5 Hz, and by replacing the damping reduction factor of Darendeli (2001) with that of Phillips and Hashash (2009) with parameters $P_1 = 0.85$, $P_2 = 0.3$, and $P_3 = -0.4$. The Darendeli (2001) curves without modification were used for the shear modulus reduction and damping curves for the fill and dense sand layers.

6.7.3 Ottawa, Canada Site JSSS

The JSSS profile is based on information collected by Medioli et al (2012) for a deep sediment site located at 45.3832 N, 76.1546 W, near Ottawa, Canada. Their investigation included geophysical, geochemical, and geotechnical measurements, as well as a 97 meter continuously cored borehole. The borehole is in close proximity with the strong motion station JSSS, located at 45.3859 N, 76.1562 W.

The JSSS site profile consists of two meters of sandy clay at the top, followed by a crust of three meters of highly overconsolidated Leda Clay, three meters of slightly overconsolidated Leda Clay, 11 meters of interbedded silty clay and clayey silt, 74 meters of Leda clay, and 19 meters of Pleistocene gravel overlying bedrock at a depth of 115 meters. All of the layer thicknesses, as well as the shear wave velocity, unit weight and shear strength for the layers down to the gravel are from Medioli et al (2012). The shear wave velocity for the gravel layer at the bottom of the soil profile is the average velocity from all sites within Ottawa encountering that unit (James Hunter, personal communication, June 20, 2013). Values of plasticity index are from Rasmussen (2012). Overconsolidation ratios are calculated from the SHANSEP method (Ladd and Foott, 1974) using the shear strengths given in Medioli et al (2012). Figure 6.28 shows the soil properties versus depth for site JSSS.

6.7.4 Hokkaido, Japan, KiK-NET Sites

The KIKNET sites are based on the soil profile of KiK-NET station TKCH07 located at 42.6450 N, 143.5242 E, near the eastern shore of Hokkaido, Japan. Naoki Sakai of the National Research Institute for Earth Science and Disaster Prevention translated the TKCH07 profile from Japanese to English.

The KIKNET profiles consists of 14 meters of high plasticity clay with a highly overconsolidated crust, followed by 14 meters of very silty sand with moderate plasticity, 10 meters of well graded silty sand with low plasticity, and 55 meters of silt over bedrock at a depth of 103 meters. The TKCH07 profile provided the shear wave velocities, layer thicknesses, and soil types. The other parameters were defined based on general soil characteristics for the given soil type and shear wave velocity.

To capture the effect of plasticity index, the PI of the upper clay deposit was varied from 40 to 160. Site KIKNET40 had a PI of 40, KIKNET a PI of 80, and KIKNET160 a PI in the upper clay deposit of 160. Sites KIKNET and KIKNET160 classify as NERHP F sites, whereas KIKNET40 is a NERHP E site. The three sites are the same except for the PI value of the upper

clay deposit. Figure 6.30, Figure 6.31, and Figure 6.32 show the soil properties versus depth for sites KIKNET40, KIKNET, and KIKNET160, respectively.

In addition, the strength of every layer of KIKNET80 was multiplied by two and four to evaluate the effect of strength. KIKNET S2 has double the strength of KIKNET, and KIKNET S4 has four times the strength, otherwise they are the same. Figure 6.33 and Figure 34Figure 6.28 show soil properties versus depth for sites KIKNET S2 and KIKNET S4, respectively.

6.7.5 Mueser Rutledge Consulting Engineers Sites MRCE1 and MRCE2

MRCE1 and MRCE2 are based on site investigations conducted by Mueser Rutledge Consulting Engineers (MRCE) in New York City. Dr. Sissy Nikolaou provided the information, which included site descriptions, cross sections, boring logs, shear wave velocity profiles, and the results of laboratory strength, consolidation, and dynamic tests (Nikolaou, personal communication, April 26, 2012).

The MRCE1 profile consists of three meters of silty sand fill, followed by 16 meters of high plasticity organic clay with an overconsolidated crust, three meters of silty sand (Upper Outwash), 28 meters of varved silt and clay, 10 meters of silty sand (Lower Outwash), 18 meters of clay (Raritan Formation), and 12 meters of sand (Lloyd Formation) over bedrock at 90 meters. The shear wave velocity, unit weight, OCR, PI, age, and shear strength down to 60 meters were taken from the measured data supplied by MRCE. The age, relative depth, and soil types below 60 meters (Raritan and Lloyd Formations) were based on general background geology given in the site descriptions by MRCE. Shear wave velocities for the Raritan and Lloyd Formations were calculated with the model for G_{max} derived in chapter 4 and unit weights estimated from general unit weights for similar soil types given in NAVFAC 7.01 (1986). Figure 6.35 shows soil properties versus depth for site MRCE1.

Rutgers University conducted five resonant column tests on samples of the high plasticity organic clay to determine characteristic shear modulus reduction and damping curves for the MRCE site investigations. These five tests matched the shear modulus reduction curves predicted by Darendeli (2001) for their given PI, OCR, and confining pressures. However, the damping ratio with shear strain predicted by the Darendeli (2001) curves overestimated the measured values. To match the measured damping curves, parameter b was set equal to 0.5 and frequency to 0.1 Hz in the Darendeli (2001) formulation. These adjustments adequately reduced the predicted damping to match the measured damping. The curves predicted by Darendeli (2001) matched the measured curves much better than those predicted using the model provided by Kishida et al (2009) for highly organic soils.

The MRCE2 soil profile is based on a shallow soft soil site in New York City near the Hudson River. It consists of four meters of silty sand fill, followed by 18 meters of high plasticity organic clay with an overconsolidated crust, and 8 meters of dense Pleistocene sand over bedrock at 30 meters. The shear wave velocity profile for the entire depth as well as all of the properties for the high plasticity organic clay were taken directly from the data provided by MRCE. The data for the sand layers is based on the sand layers in MRCE1 for the same depth intervals. Figure 6.36 shows the soil properties versus depth for site MRCE2.

6.8 Summary

This chapter outlined the theory, limitations, and input parameters necessary to perform one dimensional total stress equivalent linear, total stress nonlinear, and effective stress nonlinear site response analyses in the program DEEPSOIL. It also discussed several important points that must be addressed when conducting site response analyses, such as the matching of both the shear modulus reduction and damping curves, small strain damping, the implied soil shear strength, layer thickness, and specification of the input ground motion and half space.

The second half of this chapter summarized the specific soil properties and model parameters used in the site response analyses. This study performed site response analyses for 15 sites, all of which are categorized as NEHRP site classes E or F. Table 6.7 summarizes relevant site properties for each site. It lists the NEHRP site category, Vs_{30}, depth to bedrock, elastic site period (T_s), the total thickness of the special soil layers (Th), the mean shear wave velocity of the special soil layers (Vs_{mean}), the minimum value of the cyclic resistance ratio (CRR_{min}) of the special soil layers, where CRR is the dynamic shear strength of the soil divided by the vertical effective confining pressure, and the mean value of the shear strain when $G/G_{max} = 0.5$ of the special soil layers ($\gamma_{0.5,mean}$). The "special" soil layers are the soil layers that classify a site as a non-liquefiable NEHRP F site, such as peat or highly organic clays, soils with PI > 75, and soft to medium stiff clays. These parameters are explained in greater detail in chapter 8.

Seven of the sites are based on actual soil profiles. The other eight sites are variations on the first seven sites that explore the effects of strength, plasticity index (PI), and elastic site period (Ts) on the surface response. Appendix 6A lists the site properties such as unit weight, Vs, PI, OCR, USCS designation, etc. of each site by layer. Appendix 6B contains tables with all of the DEEPSOIL input parameters used to conduct the site response analyses. The next two chapters discuss the results of the site response analyses.

6.9 References

Anderson, D.G., Shin, S., and Kramer, S.L. (2011). "Observations from Nonlinear, Effective-Stress Ground Motion Response Analyses following the AASHTO Guide Specifications for LRFD Seismic Bridge Design." Transportation Research Board Annual Meeting.

Berrill, J.B. and Davis, R.O. (1985). "Energy Dissipation and Seismic Liquefaction of Sands: Revised Model." *JSSMFE Soils and Foundations*, 25(2), pp. 106-118.

Biscontin, G. (2001). "Modeling the dynamic behavior of lightly overconsolidated soil deposits on submerged slopes." Ph.D. Dissertation, Univ. of California, Berkeley.

Biscontin, G. and Pestana, J.M. (1999). "Influence of peripheral velocity on undrained shear strength and deformability characteristics of a bentonite-kaolinite mixture," Geotechnical Engng Report No. UCB/GT/99-19, Dep. of Civil & Environ. Eng., University of California, Berkeley.

Bonaparte R., Mitchell J.K. (1979). "The properties of San Francisco Bay Mud at Hamilton Air Force Base," University of California, Berkeley, Dept. of Civil Eng. Geotech. Eng. Report.

Darendeli, M. (2001). "Development of a new family of normalized modulus reduction and material damping curves." Ph.D. Thesis, Dept. of Civil Eng., Univ. of Texas, Austin.

Dickenson, S. (2008). "Nonlinear Effective-Stress Modeling of Dynamic Soil Response, Proposed Oregon LNG Facility, Warrenton, Oregon." Technical Memorandum, Stephen Dickenson, Corvallis, Oregon.

Dobry, R., Pierce, W. G., Dyvik, R., Thomas, G. E., and Ladd, R. S. (1985a). "Pore pressure model for cyclic straining of sand." Rensselaer Polytechnic Institute, Troy, New York.

Gibbs, J.F., Fumal, T.E., Powers, T.J. (1993). "Seismic Velocities and geologic logs from borehole measurements at eight strong motion stations that recorded the 1989 Loma Prieta, California, Earthquake." *USGS Open File Report* 93-376.

Green, R.A., Mitchell, J.K. and Polito, C.P. (2000). "An Energy-Based Pore Pressure Generation Model for Cohesionless Soils," *Proceedings: John Booker Memorial Symposium*, Melbourne, Australia, November 16-17, 2000.

Hashash, Y.M.A., Groholski, D.R. Phillips, C.A., (2010). "Recent advances in non-linear site response analysis." In proceedings of *Fifth International Conference on Recent Advances in Geotechnical Earthquake Engineering and Soil Dynamics*, May 24-29, San Diego, CA.

Hashash, Y.M.A, Groholski, D.R., Phillips, C. A., Park, D, Musgrove, M. (2012) "DEEPSOIL 5.1, User Manual and Tutorial." 107 p.

Hsu, C. and Vucetic, M. (2006). "Threshold shear strain for cyclic pore-water pressure in cohesive soils." *Journal of the Geotechnical and Geoenviromental Engineering*, ASCE, 132 (10), 1325-1335.

Idriss, I. M. and Sun, J. I. (1992) "User's Manual for SHAKE91, A Computer Program for Conducting Equivalent Linear Seismic Response Analyses of Horizontally Layered Soil Deposits."

Idriss, I. M., Dobry, R., and Singh, R. D. (1978). "Nonlinear behavior of soft clays during cyclic loading." *J. Geotech. Engrg. Div.*, ASCE, 104(GT12), 1427-1447.

KiK-NET site TKCH07 (in Japanese), translated by Dr. Naoki Sakai, *National Research Institute for Earth Science and Disaster Prevention*, Japan. http://www.kyoshin.bosai.go.jp/, accessed May 12, 2013.

Kishida, T., Boulanger R.W., Abrahamson N.A., Wehling T.M., Driller M.W. (2009). "Regression Models for Dynamic Properties of Highly Organic Soils." *J. of Geotech. and Geoenvir. Eng.*, ASCE, 135(4).

Kondner, R. L., and J.S. Zelasko (1963). "A hyperbolic stress-strain formulation of sands," *Proc. of 2nd Pan American Conference on Soil Mechanics and Foundation Engineering*, Sao Paulo, Brasil, 289–324.

Kramer, Steven L. (1996). *Geotechnical Earthquake Engineering*. Prentice Hall; New Jersey.

Ladd, C. C., and Foott, R. (1974). "A New design procedure for stability of soft clays." *Journal of the Geotechnical Engineering Division*, ASCE,100(GT7), pp. 763-786.

Li, X.S., Z.L. Wang and C.K. Shen (1992). *SUMDES: A nonlinear procedure for response analysis of horizontally-layered sites subjected to multi-directional earthquake loading*, Dept. of Civil Eng., Univ. of Calif., Davis.

Liu M., and Gorman D.G. (1995). "Formulation of Rayleigh damping and its extensions." *Computers and Structures*, 57(2), pp. 277–85.

Lo Presti, D.C.F., Lai, C.G. and I. Puci (2006). "ONDA: Computer code for nonlinear seismic response analyses of soil deposits." *J. of Geotech. and Geoenvir. Eng.*, ASCE, 132(2), 223–236.

Martin, G.R., Finn, W.D.L. and Seed, H.B. "Fundamentals of Liquefaction under Cyclic Loading," *Journal of the Geotechnical Engineering Division*, ASCE, 101(GTS), p 423-438.

Masing, G. (1926). "Eigenspannungen and verfertigung beim messing." *Proc. 2nd Int. Congress on Applied Mech.*, Zurich, Switzerland, pp. 332–335.

Matasovic, N. (1993). "Seismic response of composite horizontally-layered soil deposits," Ph.D. Thesis, University of California, Los Angeles.

Matasovic, N. and Ordóñez, G.A. (2012). "D-MOD2000 – A Computer Program for Seismic Site Response Analysis of Horizontally Layered Soil Deposits, Earthfill Dams, and Solid Waste Landfills." GeoMotions, LLC; Lacey, Washington, USA.

Matasovic, Neven, and M. Vucetic (1995) "Generalized Cyclic Degradation-Pore Pressure Generation Model for Clays," *Journal of Geotechnical and Geoenvironmental Engineering*, ASCE, Vol. 121, No. 1, pp 33-42.

Matasovic, Neven, and M. Vucetic (1993). "Cyclic Characterization of Liquefiable Sands," *Journal of Geotechnical and Geoenvironmental Engineering*, ASCE, Vol. 119, No. 11, pp 1805-1822.

Medioli, B.E., S. Alpay, H.L. Crow, D.I. Cummings, M.J. Hinton, R.D. Knight, C. Logan, A.J.M. Pugin, H.A.J. Russell, and D.R. Sharpe (2012). "Integrated data sets form a buried valley borehole, Champlain Sea basin, Kinburn, Ontario." Geological Survey of Canada, Current Research 2012-2013.

Meyerhof, G.G. (1956). "Penetration tests and bearing capacity of cohesionless soil," *Journal of the Soil Mechanics and Foundation Division,* ASCE, 82(SM1), 1-19.

Moreno-Torres, O., Hashash, Y. M. A., and Olson, S. M. (2010). "A simplified coupled soil-pore water pressure generation for use in site response analysis." *GeoFlorida: Advances in Analysis, Modeling & Design*, West Palm Beach, Florida.

Mortezaie, A. and Vucetic, M. (2013). "Effect of Frequency and Vertical Stress on Cyclic Degradation and Pore Water Pressure in Clay in the NGI Simple Shear Device." *J. Geotech. Geoenviron. Eng.*, ASCE, 139(10), 1727–1737.

NAVFAC DM 7.01 (1986). "Soil Mechanics." Design Manual 7.01, United States Department of the Navy, Naval Facilities Engineering Command, Alexandria, VA, 348p.

Newmark, Nathan M. (1959) "A method of computation for structural dynamics," *Journal of the Engineering Mechanics Division*, Vol. EM 3, pp 67-94.

Nikolaou, S. (2004). "Local Geology of New York City and its Effect on Seismic Ground Motions." In *Proceedings: Fifth International Conference on Case Histories in Geotechnical Engineering*, New York, April 13-17.

Nikolaou, S., Go, J., Beyzaei, C., Moss, C., and Deming, P. (2012). "Geo-Seismic Design in the Eastern United States: State of Practice." *Geotechnical Engineering State of the Art and Practice: Keynote Lectures from GeoCongress 2012*, ASCE, March 25 – 29, Oakland, CA, pp. 828-854.

Ordóñez, G.A. (2012). "SHAKE2000 – A Computer Program for the 1-D Analysis of Geotechnical Earthquake Engineering Problems." Geomotions L.L.C., Lacey, Washington, USA.

Park, D. and Y.M.A. Hashash (2004). "Soil damping formulation in nonlinear time domain site response analysis," *J. of Earthquake Eng.*, 8(2), 249-274.

Pass, D.G. (1994). "Soil Characterization of the Deep Accelerometer Site at Treasure Island, San Francisco, California." Masters thesis, University of New Hampshire, Durham, New Hampshire.

Peck, R.B., Hanson, W.E., Thornburn, T.H. (1974). *Foundation Engineering*. John Wiley and Sons; New York.

Pestana, J.M., Hunt, C.H., Goughnour, R.R. (1997). "FEQDRAIN: a finite element computer program for the analysis of the earthquake generation and dissipation of pore water pressure in layered sand deposits with vertical drains," UCB/EERC-97/15, Earthquake Engineering Research Center, University of California, Berkeley, 88 pages.

Phillips, C., Hashash, Y.M.A., (2009). "Damping formulation for nonlinear 1D site response analyses." *Soil Dynamics and Earthquake Engineering*, 29, 1143–1158.

Polito, C. P., Green, R. A., and Lee, J. H. (2008). "Pore pressure generation models for sands and silty soils subjected to cyclic loading." *Journal of Geotechnical and Geoenvironmental Engineering*, 134(10), 1490-1500.

Port and Harbour Research Institute (PHRI), Eds. (1997). "Handbook on liquefaction remediation of reclaimed land." Balkema, Rotterdam.

Pyke, R.M. (1979). "Nonlinear soil models for irregular cyclic loadings," *J. Geotech. Eng.*, ASCE, 105(GT6), 715-726.

Pyke, R.M. (2000). *TESS: A computer program for nonlinear ground response analyses*. Taga Engineering Systems & Software, Lafayette, Calif.

Pyke. R.. and Beikae. M. (1993). *TESS – A computer program for nonlinear ground response analyses: User's manual*. Taga Engineering Software Services, Berkeley, California.

Rasmussen, K.K., (2012). "An Investigation of Monotonic and Cyclic Behaviour of Leda Clay" (2012). Ph.D. Dissertation, University of Western Ontario - Electronic Thesis and Dissertation Repository. Paper 629.

Rau, G.A. (1999). "Evaluation of strength degradation in seismic loading of Holocene Bay Mud from Marin County, California." Ph.D. Dissertation, Univ. of California, Berkeley.

Rayleigh J.W.S, Lindsay R.B. "The theory of sound." Vol.2 (1). New York: Dover Publications; 1945.

Schnabel, P.B, J. Lysmer and H.B. Seed (1972). "SHAKE: A computer program for earthquake response analysis of horizontally layered site,." *Report no. UCB/EERC-72/12*, Earthquake Engrg. Research Center, Univ. of Calif., Berkeley, California, 102p

Seed, H.B., Martin, P.P. & Lysmer, J. (1975). "The Generation and Dissipation of Pore Water Pressures During Soil Liquefaction." Report No. UCB/EERC/75-26, Earthquake Engineering Research Center, University of California, Berkeley, California.

Sheahan, T.C., C.C. Ladd, and J.T. Germaine (1996) "Rate-dependent undrained shear behavior of saturated clay," *J. Geotech. Engr.*, ASCE, 122 (2), 99-108.

Stewart, J.P., Kwok, A.O., Hashash, Y.M.A, Matasovic, N., Pyke, R., Wang, Z., Yang, Z. (2008). "Benchmarking of Nonlinear Geotechnical Ground Response Analysis Procedures." Pacific Earthquake Engineering Research Center Report 2008/04.

Tan, K., and Vucetic, M. (1989). "Behavior of medium and low plasticity clays under cyclic simple shear conditions." *Proc., 4th Int. Conf. on Soil Dynamics and Earthquake Engineering, Soil Dynamics and Liquefaction Volume*, A. S. Cakmak and I. Herrera, eds. Computational Mechanics Publications, Boston, 131–142.

Terzaghi, K. and Peck, P.B. (1948). "Soil mechanics in engineering practice." John Wiley and Sons.

Thilakaratne, V., and Vucetic, M. (1987). " 'Class A' Prediction of accelerations and seismic pore pressures at the Owi Island Site during October, 4, 1985earthquake in Tokyo Bay." Report No. 87-3, Department of Civil and Environmental Engineering, Clarkson University, Potsdam, New York, 92p.

Tsuchida, H. (1970). "Prediction and countermeasure against the liquefaction in sand deposits." Abstract of the Seminar in the Port and Harbor Research Institute, 3.1-3.33 (in Japanese).

Vucetic, M. (1990). "Normalized behavior of clay under irregular cyclic loading." *Canadian Geotech. J.*, 27, 29-46.

Vucetic, M. (1992). "Soil Properties and Seismic Response." In *Proceedings of 10th World Conference of Earthquake Engineering*, July 19 – 24, Madrid, Spain, 1199 – 1204.

Vucetic, M. (1994). "Cyclic Threshold Shear Strains in Soils," *Journal of Geotechnical Engineering*, ASCE, 120(12) pp. 2208-2228.

Vucetic, M. and Dobry, R. (1988a) "Cyclic Triaxial Strain-Controlled Testing of Liquefiable Sands," *American Society for Testing and Materials Special Technical Publication 977*, Advanced Triaxial Testing of Soil and Rock, pp. 475-485.

Vucetic, M., and Dobry, R. (1988b). "Degradation of marine clays under cyclic loading." *J. Geotech. Engrg.,* ASCE, 114(2), 133-149.

Weiler, W.A. (1988). "Small strain shear modulus of clay," *Proc. of ASCE Conference on Earthquake Engineering and Soil Dynamics II: Recent Advances in Ground Motion Evaluation*, Geotechnical Special Publication 20, ASCE, New York, 331-345.

Yee, E., Stewart J.P., Tokimatsu K. (2013). "Elastic and Large-Strain Nonlinear Seismic Site Response from Analysis of Vertical Array Recordings." *J. Geotech. Geoenviron. Eng.* 139(10).

Youngs, R.R. (2004). *Software validation report for SHAKE04*, Geomatrix Consultants.

Zhang, J., R.D. Andrus and C.H. Juang (2005). "Normalized shear modulus and material damping ratio relationships," *J. Geotech. Geoenviron. Eng.*, ASCE, 131(4), 453-464.

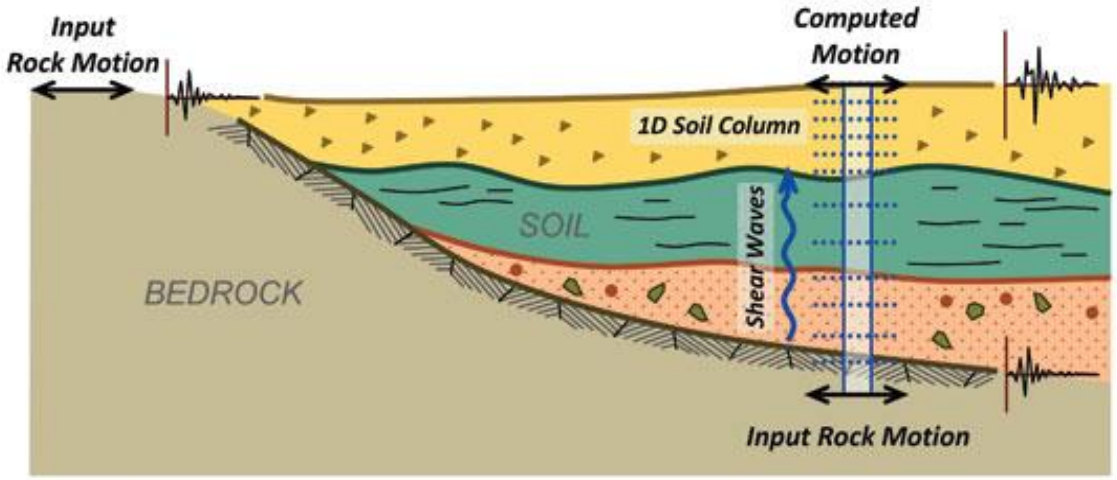

Figure 6.1: Graphical description of one dimensional site response analysis (From Nikolaou et al., 2012)

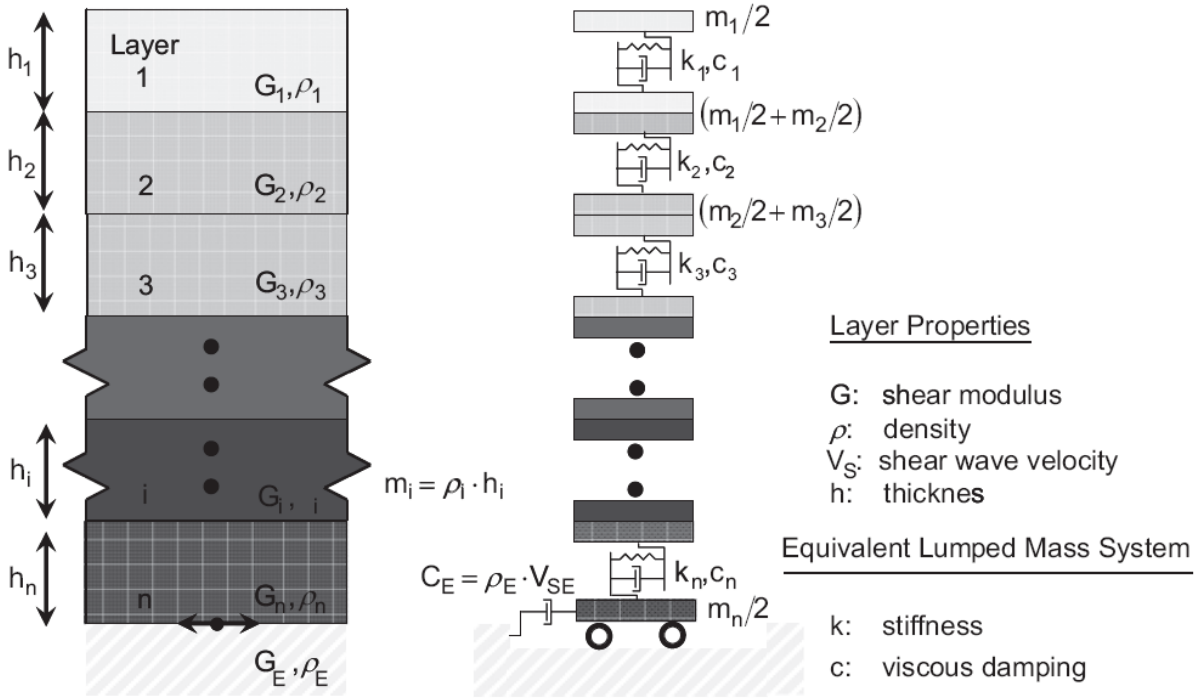

Figure 6.2: Graphical representation of a lumped mass system (From Phillips and Hashash, 2009)

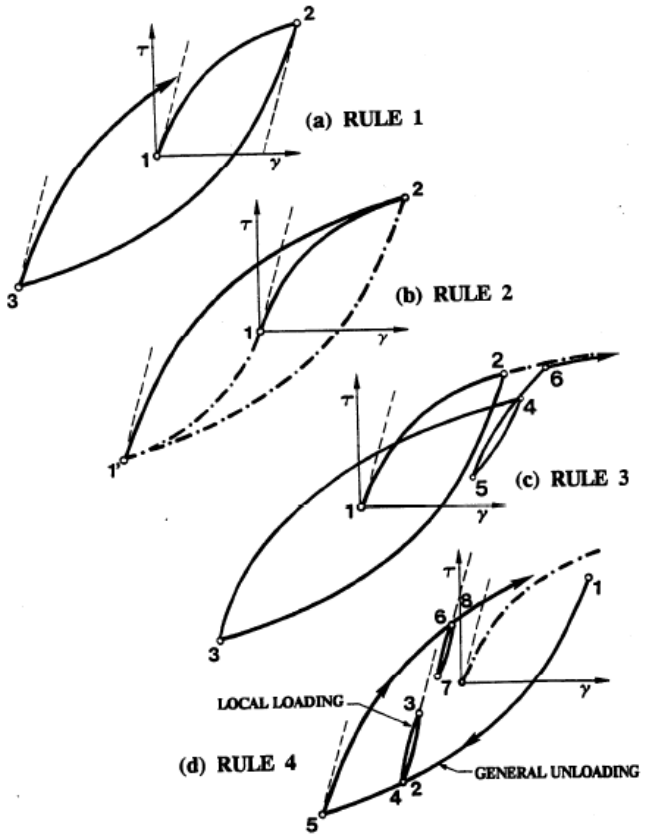

Figure 6.3: Extended Masing rules (From Vucetic, 1990)

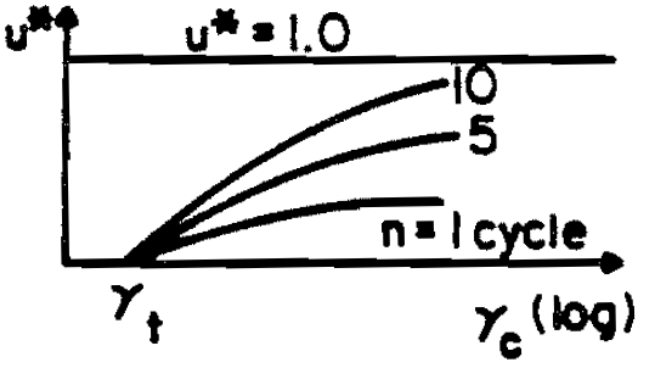

Figure 6.4: Model developed by Dobry et al (1985); the pore pressure ratio u* increases as shear strain (γ_c) increases, and the rate of increase is greater for a larger number of cycles (n), and the pore pressure ratio is zero below the volumetric threshold shear strain γ_t (From Dobry et al., 1985).

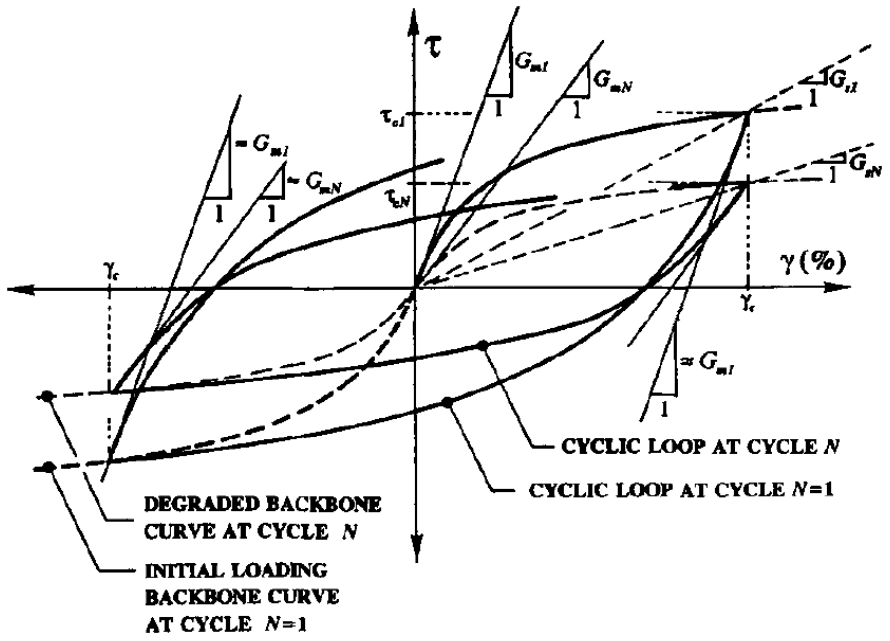

Figure 6.5: Effect of cyclic degradation on the backbone curve of a fully saturated soil. As the number of cycles increases for a given shear strain, the corresponding shear stress and the small strain shear modulus decrease (From Matasovic and Vucetic, 1995)

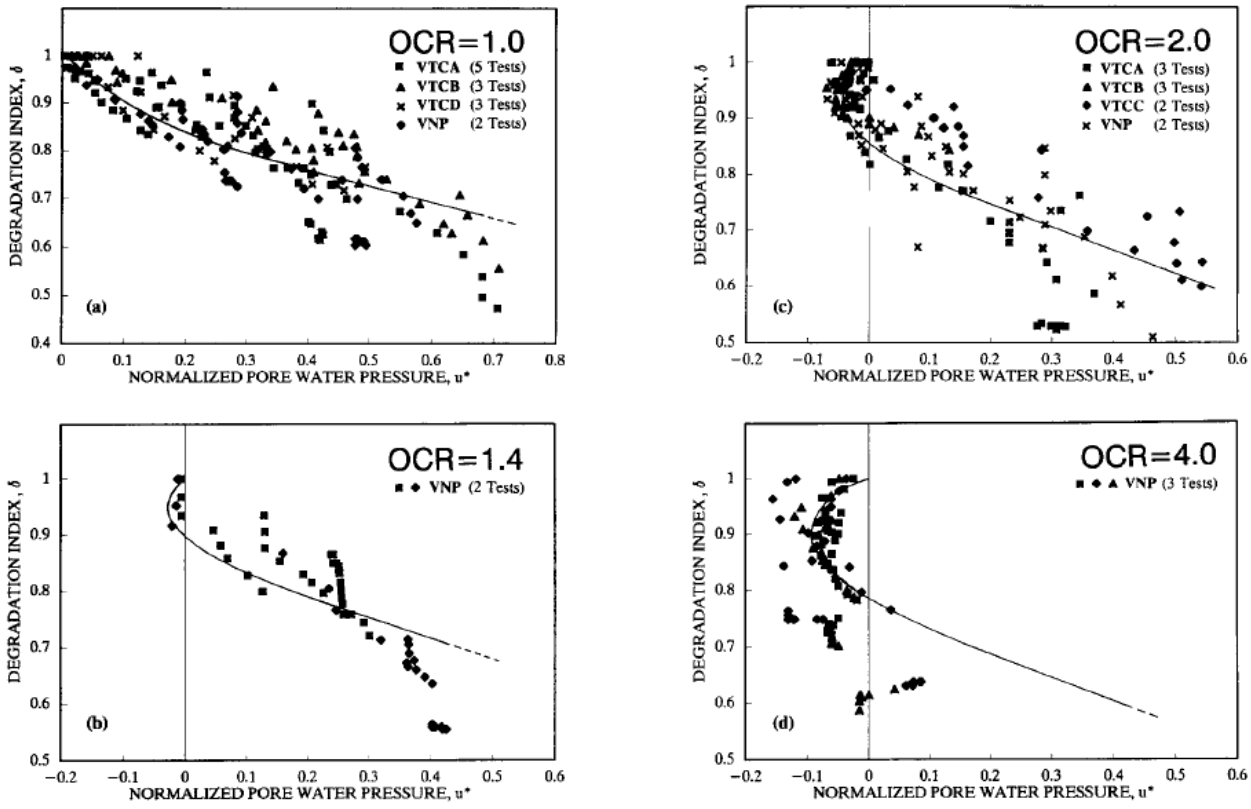

Figure 6.6: Results of several clays in cyclic simple shear and the model proposed by Matasovic and Vucetic (1995) (From Matasovic and Vucetic, 1995)

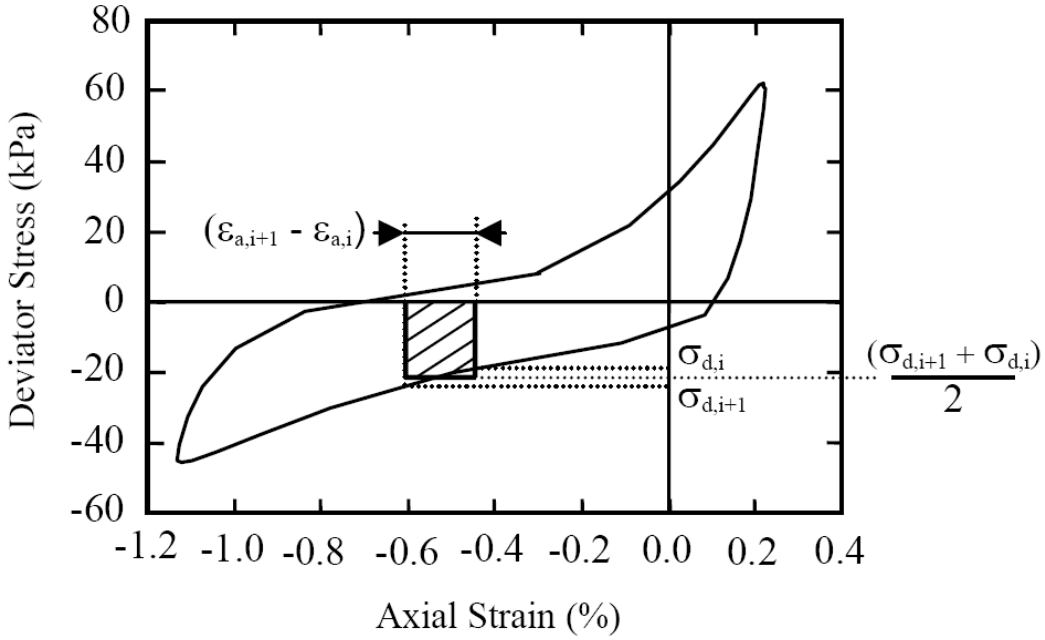

Figure 6.7: Graphical representation of Ws calculated using equation (6.16), where Ws is the dissipated energy per unit volume for a soil sample in cyclic loading (From Green et al., 2000)

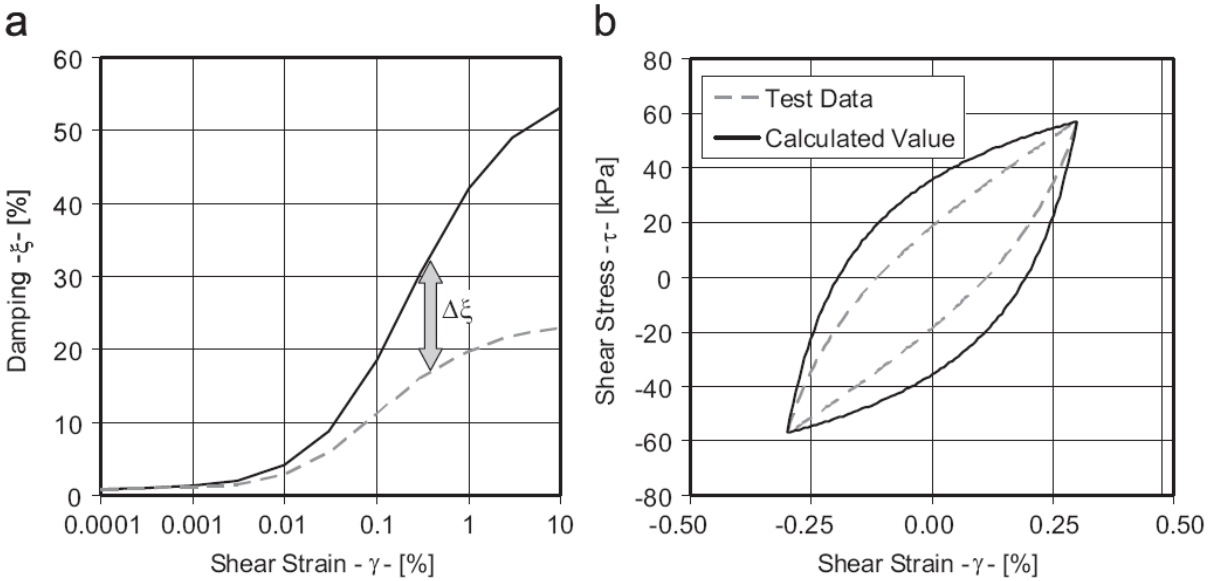

Figure 6.8: Example of misfit between calculated damping using extended Masing rules and measured damping for (a) damping versus shear strain curve and (b) shear stress versus shear strain (From Phillips and Hashash, 2009)

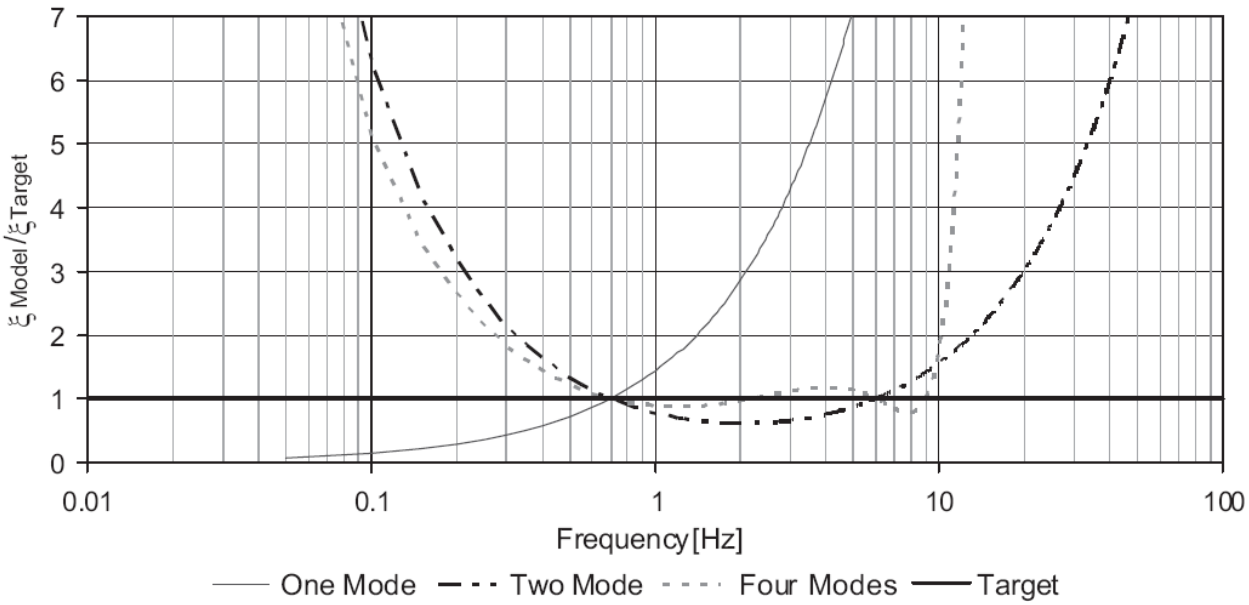

Figure 6.9: Effect of number of modes on Rayleigh damping (From Phillips and Hashash, 2009)

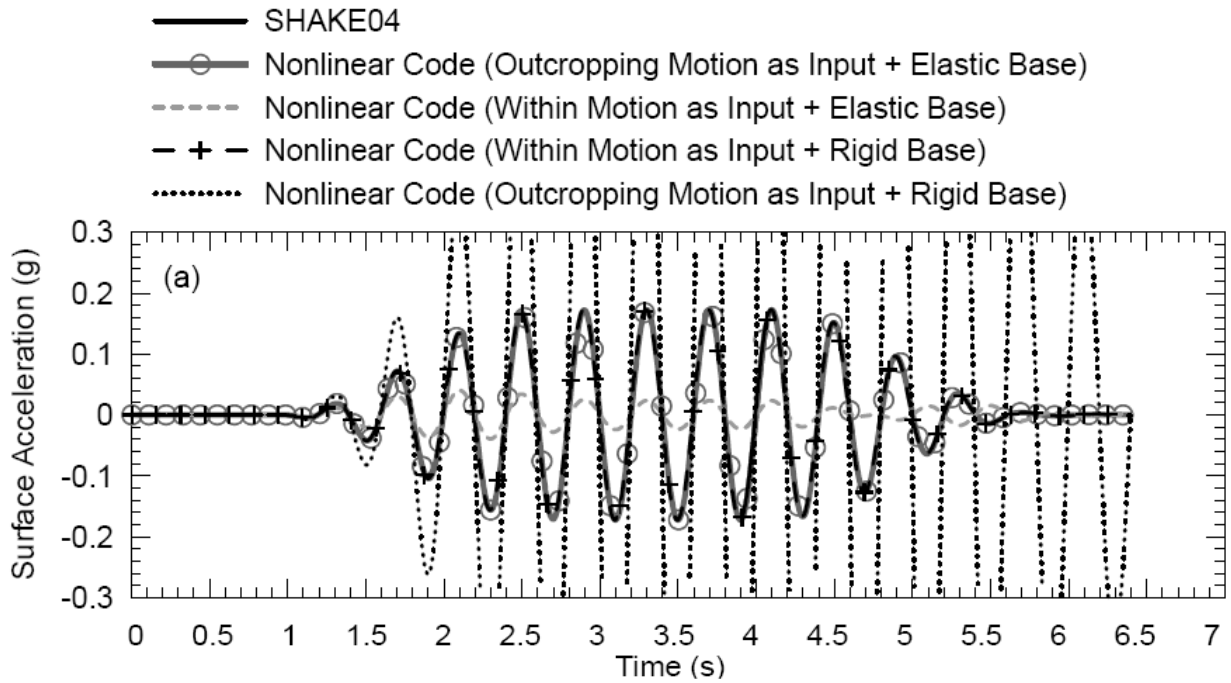

Figure 6.10: Effect of base definition and motion type on surface response of ground motions (From Stewart et al, 2008)

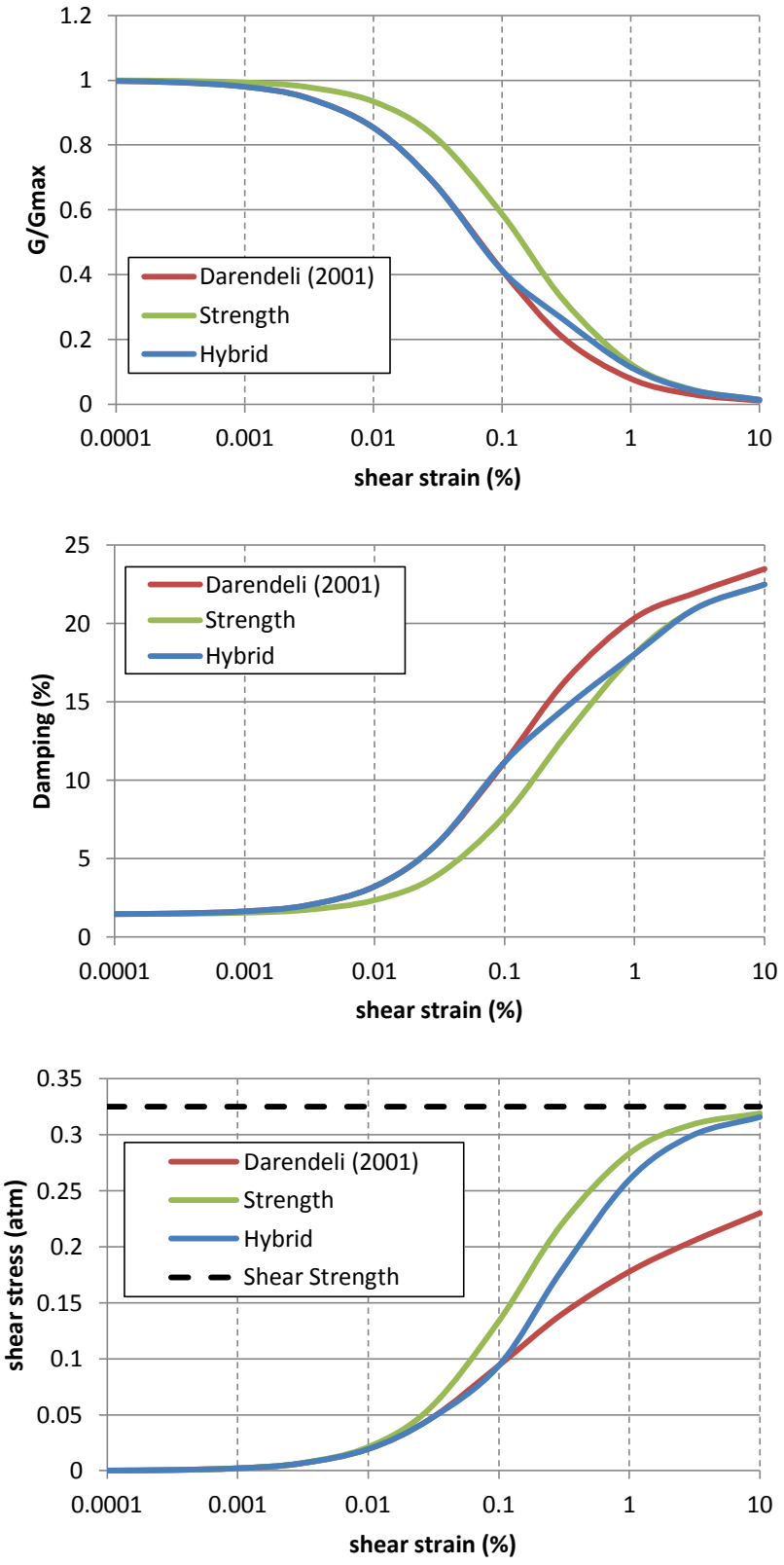

Figure 6.11: Example of hybrid curve using the procedure described by Yee et al. (2013)

Table 6.1: Material parameters for the Matasovic and Vucetic (1995) clay pore pressure generation model (From Matasovic and Ordóñez, 2012)

Material	Reference	γ_{tv} (%)	Pore Water Pressure and Degradation Model Parameters					
			s_t	r	A	B	C	D
Marine Clay (OCR = 1.0)	Matasovic and Vucetic (1995)	0.1	0.075	0.495	7.6451	-14.7174	6.3800	0.6922
Marine Clay (OCR = 1.4)	Matasovic and Vucetic (1995)	0.1	0.064	0.520	14.6202	-30.5124	18.4265	-2.5343
Marine Clay (OCR = 2.0)	Matasovic and Vucetic (1995)	0.1	0.054	0.480	12.9495	-26.3287	15.3736	-1.9944
Marine Clay (OCR = 4.0)	Matasovic and Vucetic (1995)	0.1	0.042	0.423	11.2634	-21.4595	11.2404	-1.0443

Table 6.2: Material parameters for low plasticity silts for the Matasovic and Vucetic (1993) pore pressure generation model (From Matasovic and Ordóñez, 2012; Anderson et al., 2010)

Material	Reference	k (ft/s)	Degradation Model	Pore Water Pressure Model				γ_{tv}
			v	*f*	*p*	*F*	*s*	(%)
Warrenton, Oregon Silt recovered from 130 to 248 ft b.g.s; 73% < fines < 99%; 32.9% < water content <37.3%; 86.3 < γ_{dry} < 88.9 pcf; 822 < Vs < 1086 fps; OCR = 1.0; PI = 10, LL = 37	Dickenson (2008)	not reported	1	1	1	0.493	1.761	0.06
Stillaguamish River Silt, Washington; recovered from 30 to 95 ft b.g.s; 60% < fines < 90%; 600 ft < Vs < 900 ft/s; PI = 8-10; LL = 31-32	Anderson et al. (2010)	not reported	not reported	2	1.05	0.3	1.5	0.02

Table 6.3: Material parameters for the Matasovic and Vucetic (1993) sand pore pressure generation model (From Matasovic and Ordóñez, 2012)

Material	Reference	k (ft/s)	Degradation Model	Pore Water Pressure Model				γ_{tv} (%)
			ν	f	p	F	s	
Banding Sand (BS); poorly-graded commercially available sand; D_r= 40%; D_{50}=0.19; Cc=0.9; C_u=1.4; $\gamma_{d,min}$ = 90 pcf; $\gamma_{d,max}$ = 106 pcf	Dobry et al. (1985)	5.5×10^{-4}	1.0	1.0	1.00	10.9	1.00	0.017
Wildlife Site Sand A (WSA); void ratio 0.84 to 0.85; 37 % fines; N ≈ 5; V_s ≈ 350 ft/s	Vucetic and Dobry (1988)	9.8×10^{-4}	1.0	2.0	1.04	2.6	1.70	0.020
Wildlife Site Sand B (WSB); void ratio 0.74 to 0.76; 25 % fines; N ≈ 6 to 13; V_s ≈ 450 to 500 ft/s	Vucetic and Dobry (1988)	6.6×10^{-3}	1.0	2.0	1.04	2.6	1.70	0.020
Heber Road Site Sand PB; void ratio 0.70; 15 % fines; V_s ≈ 500 to 600 ft/s	Vucetic and Dobry (1988)	1.4×10^{-4}	1.0	2.0	1.05	1.706	1.09	0.024
Heber Road Site Sand CF; void ratio 0.70; 22 % fines; V_s ≈ 400 to 466 ft/s	Vucetic and Dobry (1988)	3.9×10^{-5}	1.0	1.0	1.071	1.333	1.08	0.022
Santa Monica Beach Sand (SMB); clean uniform beach sand similar to Monterey No. 0; void ratio = 0.56; zero fines; dense; V_s ≈ 867 ft/s	Matasovic (1993)	3.3×10^{-1}	3.8	1.0	1.00	0.73	1.00	0.020
Owi Island *Sand* at depths from 6 to 14 m b.g.s.; silty fine sand placed as hydraulic fill; 18 % < fines < 35 %	Thilakaratne and Vucetic (1987)	6.6×10^{-3}	1.0	2.0	1.005	3.0	1.80	0.025
Owi Island *Silt* at depth of 6 m; placed as hydraulic fill; 50 % < fines < 85 %	Thilakaratne and Vucetic (1987)	9.8×10^{-4}	1.0	2.0	0.95	2.5	1.60	0.015

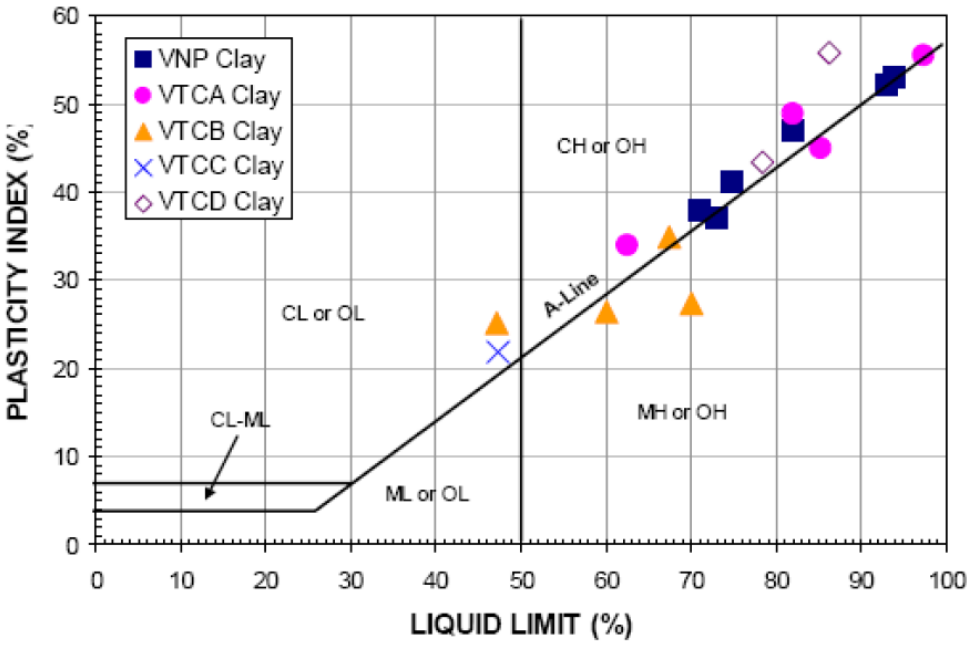

Figure 6.12: Atterberg limits of soils tested in Matasovic and Vucetic (1995) and used to find the parameters listed in Table 6.1 (From Matasovic and Ordóñez, 2012)

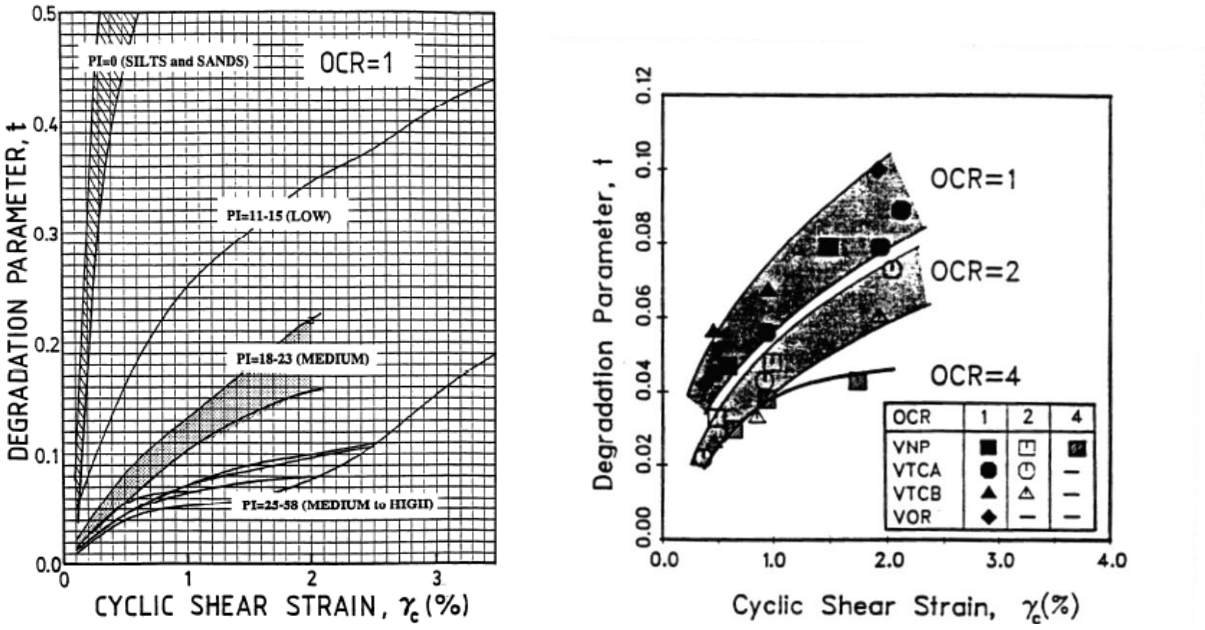

Figure 6.13: Effect of a) PI (Tan and Vucetic, 1989) and b) OCR on the degradation parameter t (Vucetic and Dobry , 1988b)

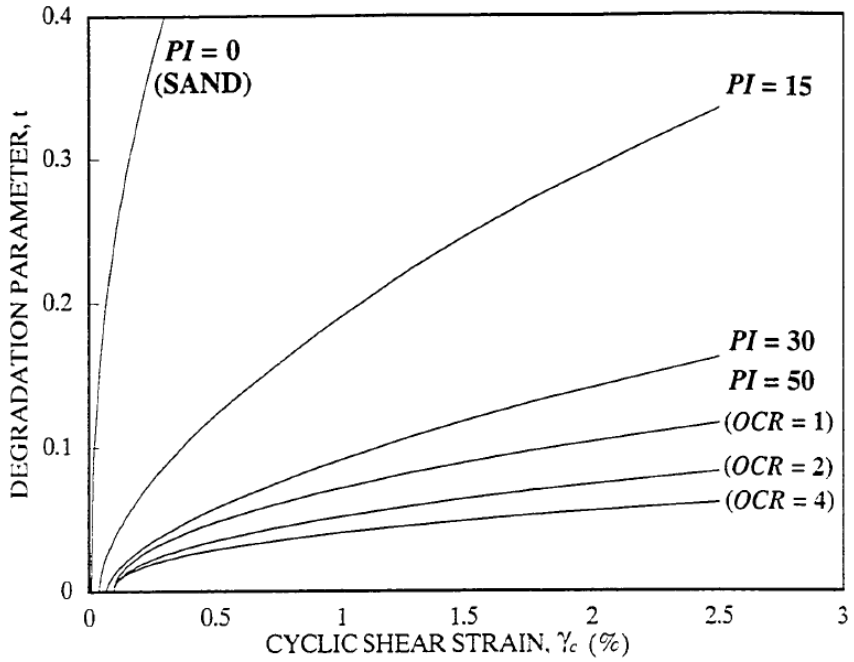

Figure 6.14: Effect of PI and OCR on the degradation parameter t (Vucetic, 1992; Matasovic, 1993)

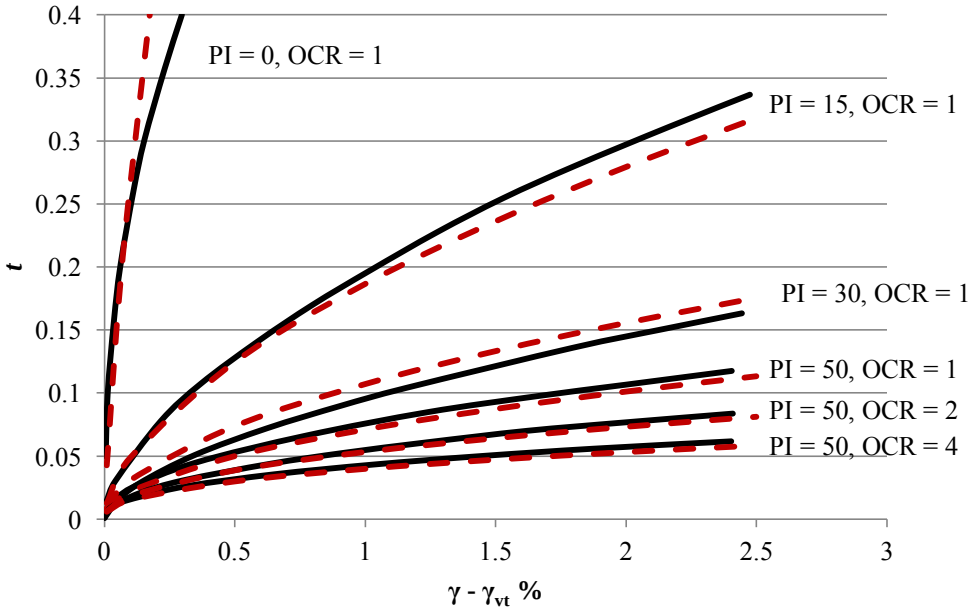

Figure 6.15: Comparison of the curves given by Matasovic (1993) and Vucetic (1992) (solid black lines) for t for different values of PI and OCR and the correlations presented in this work (dotted red lines).

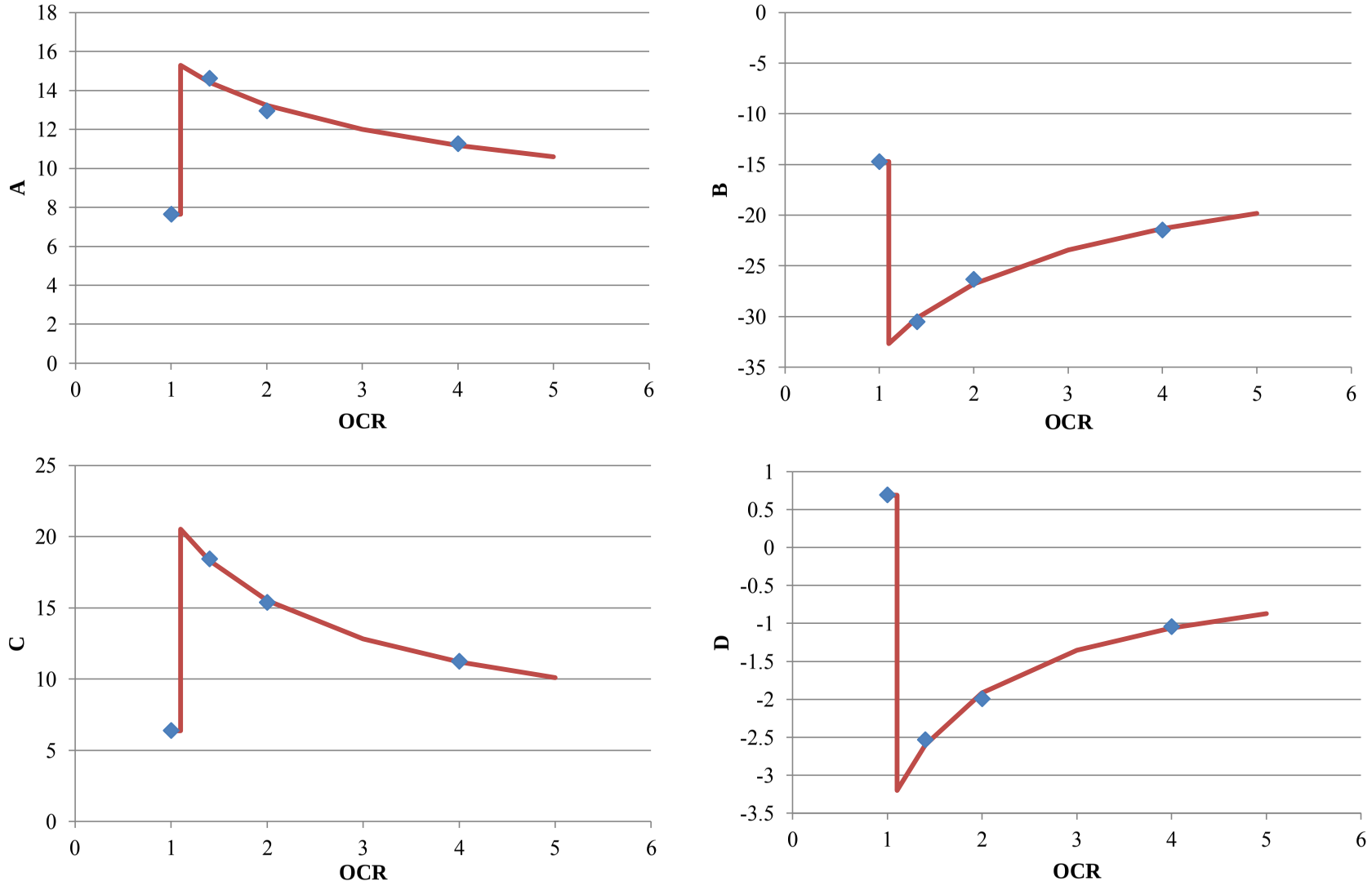

Figure 6.16: Comparison of given curve fitting parameters in Matasovic and Vucetic (1995) (blue dots) and correlations presented in this work (red lines)

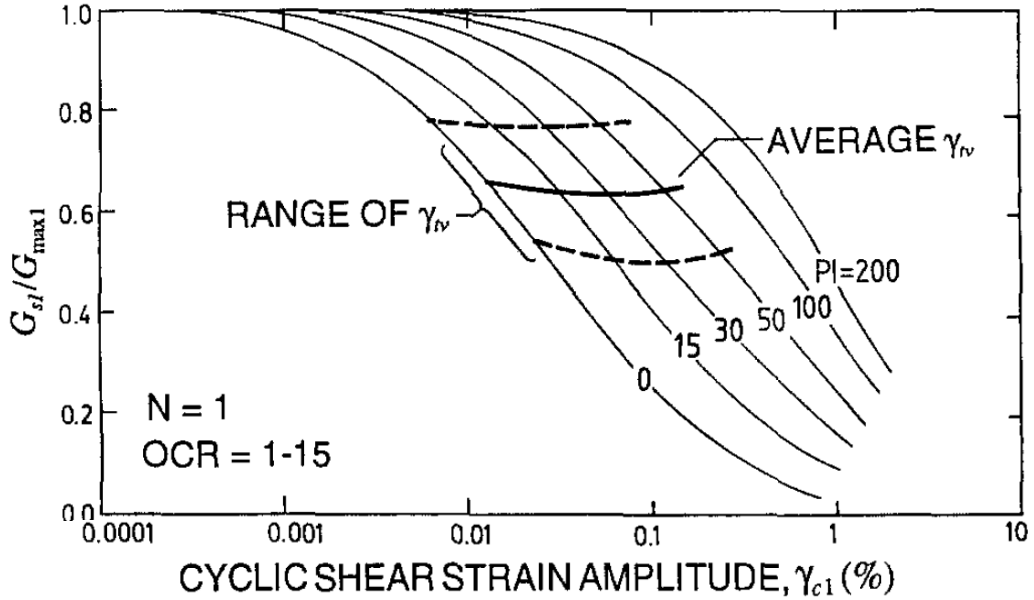

Figure 6.17: Relation between the volumetric cyclic threshold shear strain γ_{tv} and shear modulus reduction curves (From Vucetic, 1994)

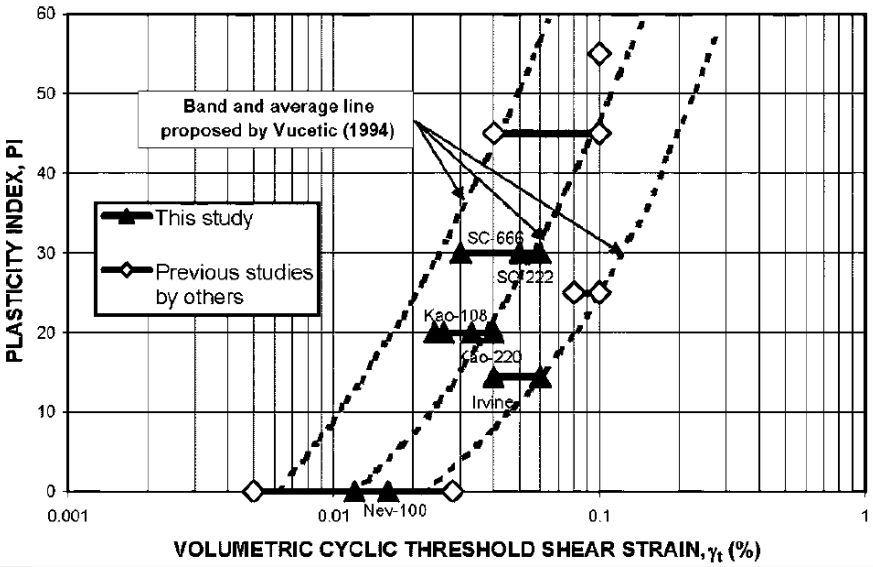

Figure 6.18: Effect of PI on the volumetric cyclic threshold shear strain for fully saturated soils, the bars represent a range (From Hsu and Vucetic, 2006)

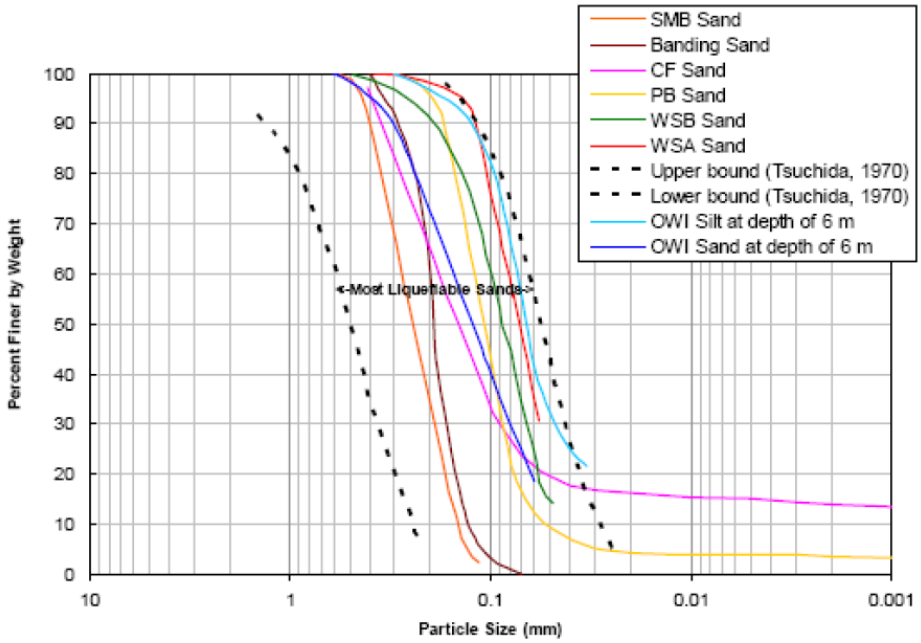

Figure 6.19: Grain size distribution of sands listed in Table 6.3 (From Matasovic and Ordóñez, 2012)

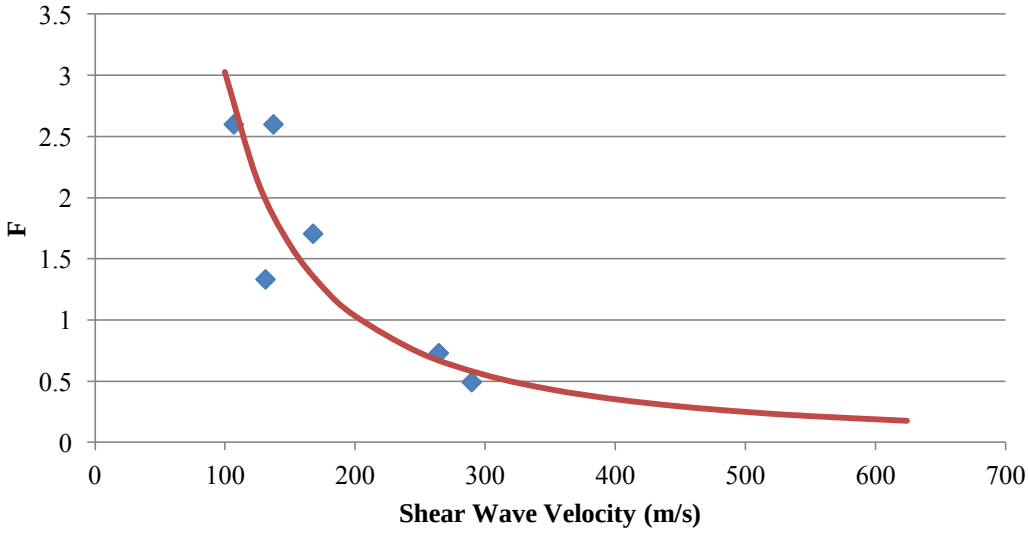

Figure 6.20: Comparison of given values of F in Matasovic and Ordóñez (2012) (blue dots) and the correlation used in this project (red line).

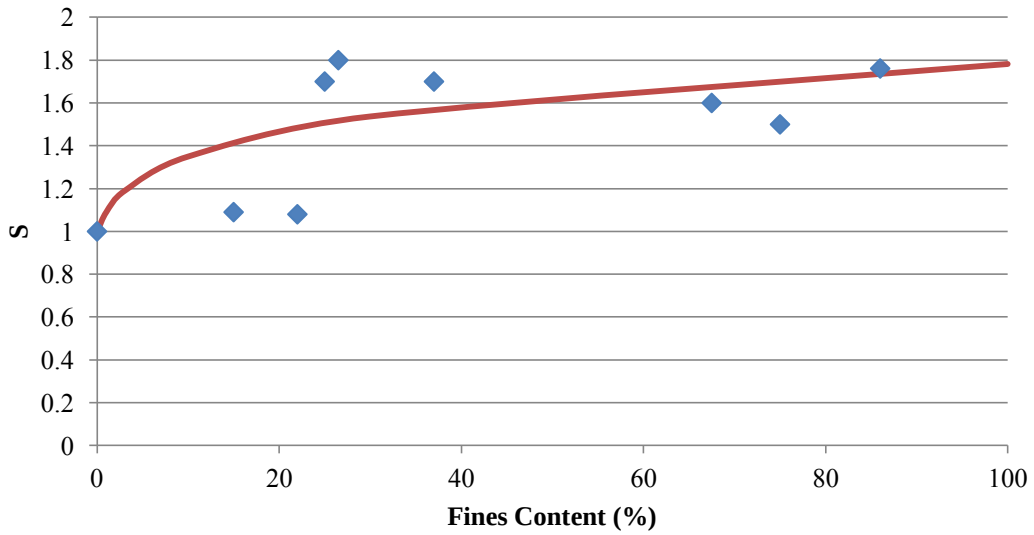

Figure 6.21: Comparison of given values of s in Matasovic and Ordóñez (2012) (blue dots) and Anderson et al (2010) and the correlation used in this project (red line).

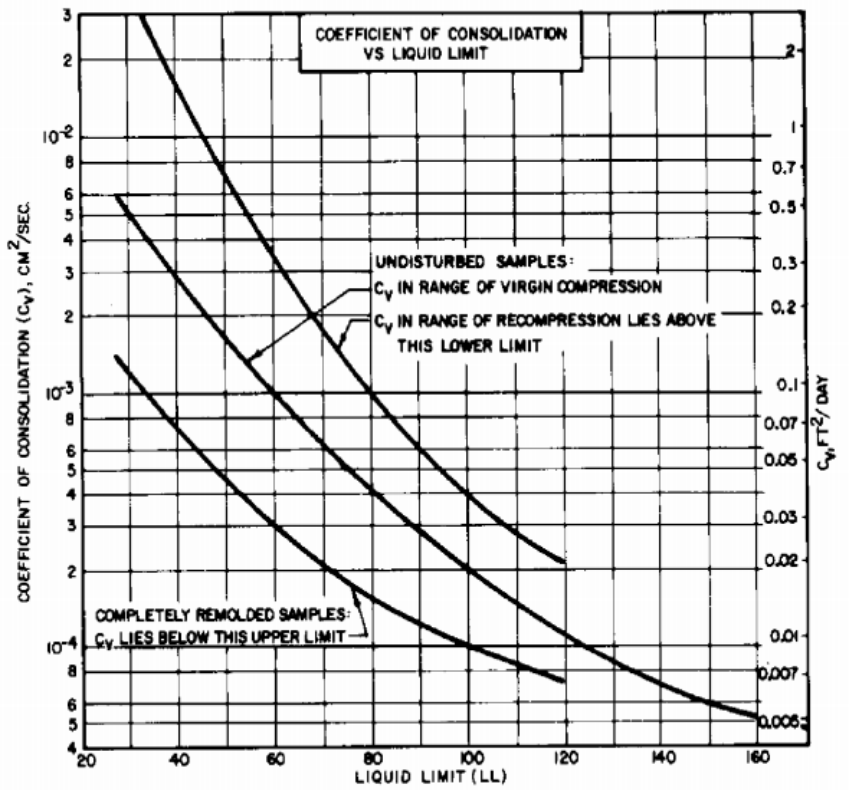

Figure 6.22: Approximate correlation between liquid limit (LL) and coefficient of consolidation (C_v) for silts and clays (From NAVFAC 7.1, 1986)

Table 6.4: Coefficient of hydraulic conductivity for granular soils (after Terzaghi and Peck, 1948) (From Pestana et al., 1997)

Soil type	Particle size (mm)	Coefficient of hydraulic conductivity (cm/s)
Very fine sand	0.05~0.10	0.001~0.005
Fine sand	0.10~0.25	0.005~0.01
Medium sand	0.25~0.50	0.01~0.1
Coarse sand	0.50~1.00	0.1~1.0
Small pebbles	1.00~5.00	1.0~5.0

Table 6.5: Typical Values of k_h/k_v for sand deposits (From Pestana et al., 1997)

Description	k_h/k_v
Uniform (clean sands)	1.5~2
Moderately anisotropic (silt seams)	4~5
Highly anisotropic	10~100

Table 6.6: Typical values of volumetric compressibility of sand (modified from PHRI, 1997) (From Pestana et al., 1997)

Type of sand	Coefficient of volumetric compressibility		Mean particle size, D_{50} (mm)
	(ft^2/lb)*	(m^2/kN)*	
Sacramento River Sand	1×10^{-6}	2×10^{-5}	~0.2
El Monte Sand (D)	1×10^{-6}	2×10^{-5}	~0.22
El Monte Sand (E)	1×10^{-6}	2×10^{-5}	~0.1
Akita Port Sand	$1.5 \sim 2 \times 10^{-6}$	$3 \sim 4 \times 10^{-5}$	0.15
El Monte Sand (C)	2×10^{-6}	4×10^{-5}	0.65
Monterey Sand	2×10^{-6}	4×10^{-5}	0.6
Fuji River Sand	3×10^{-6}	6×10^{-5}	0.4
El Monte Sand (B)	4×10^{-6}	8×10^{-5}	3.0
Ogishima Sand	5×10^{-6}	10×10^{-5}	0.32
* Measured at $u/\sigma_c' < 0.5$, $\sigma_c' = 2048$ $ft^2/lb = 98.1$ kN/m^2			

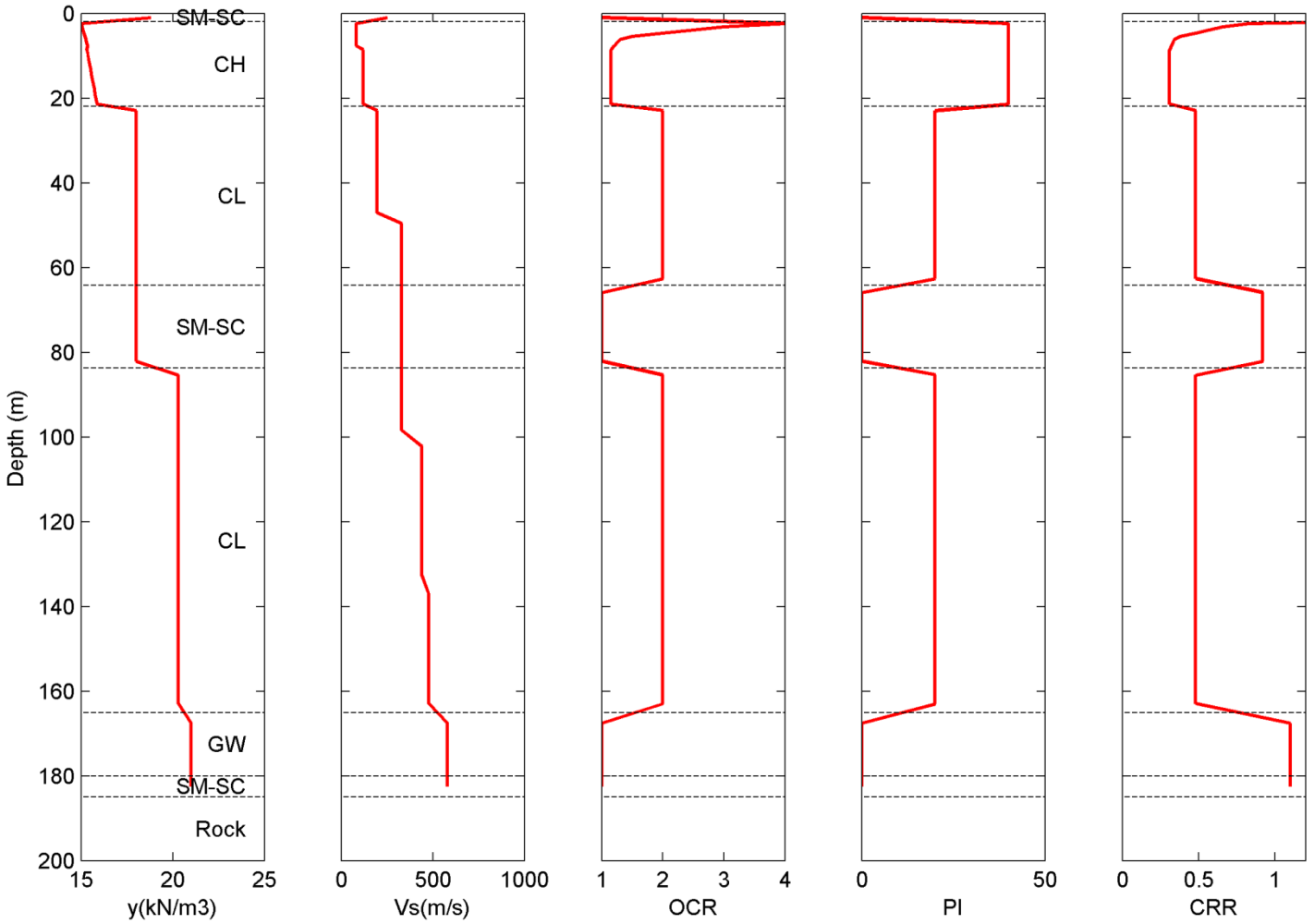

Figure 6.23: Site properties for San Francisco site Bay Area

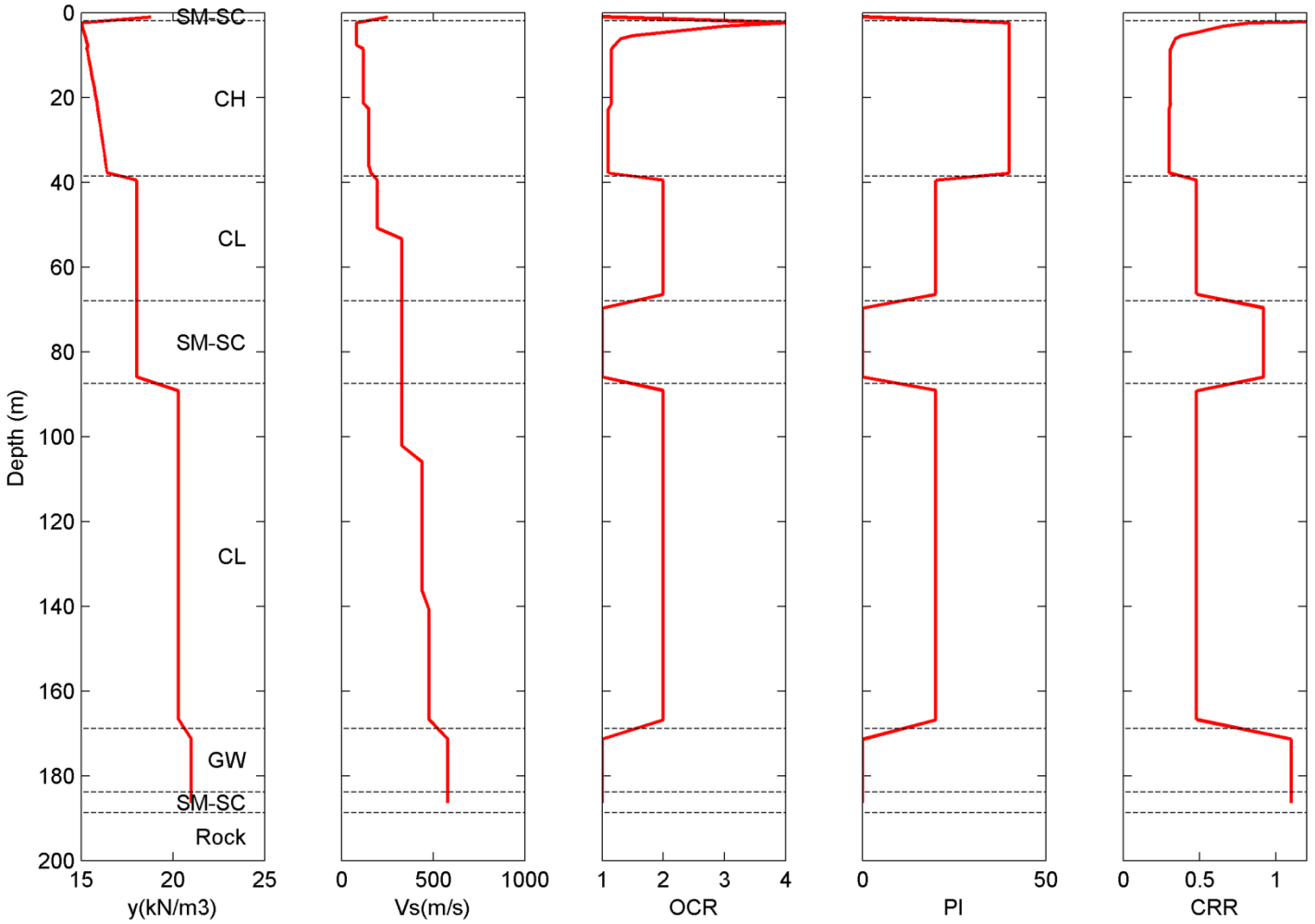

Figure 6.24: Site properties for San Francisco site Bay Area F

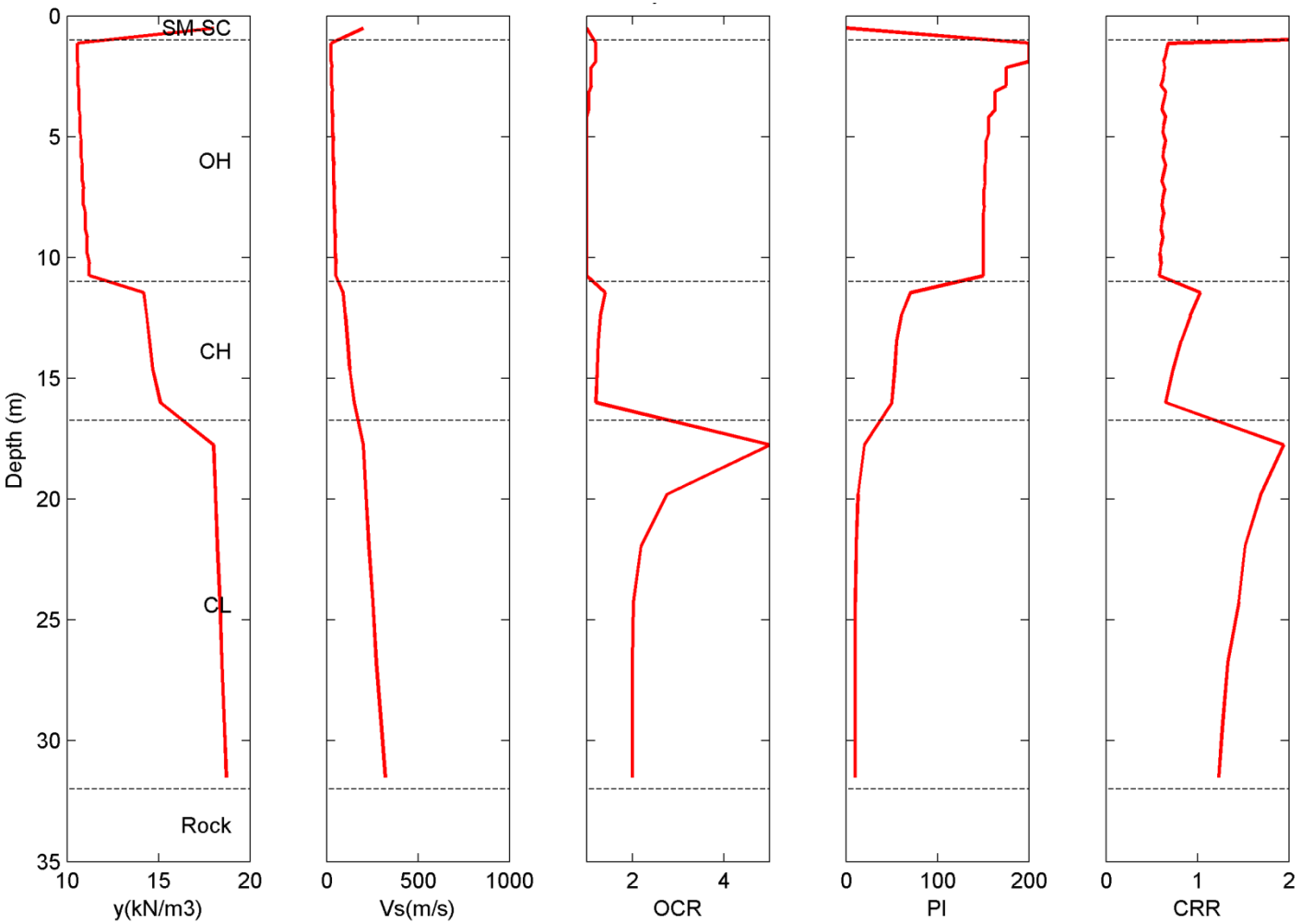

Figure 6.25: Site properties for San Francisco site Bay Area II and Bay Area II K

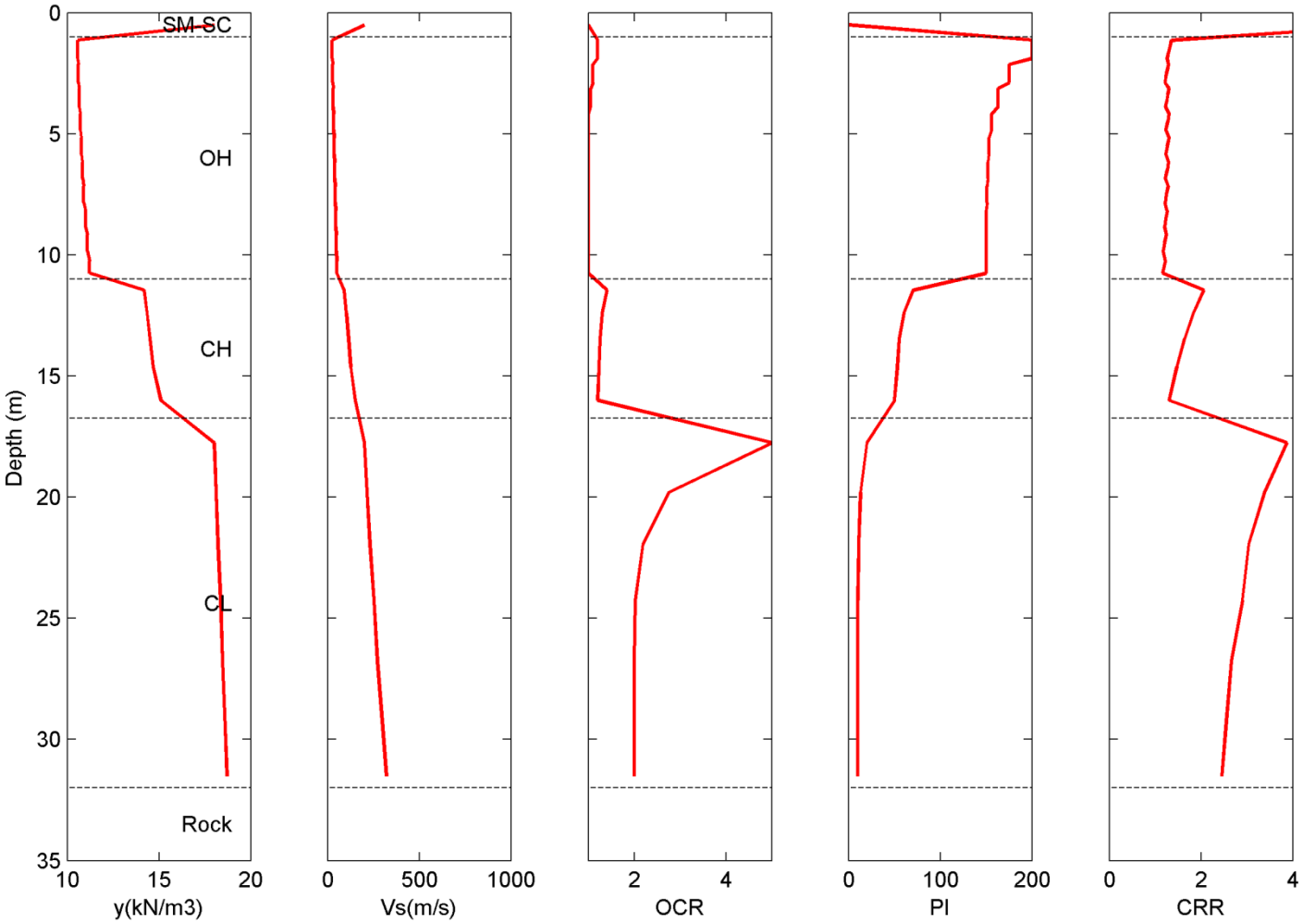

Figure 6.26: Site properties for site Bay Area II K S2

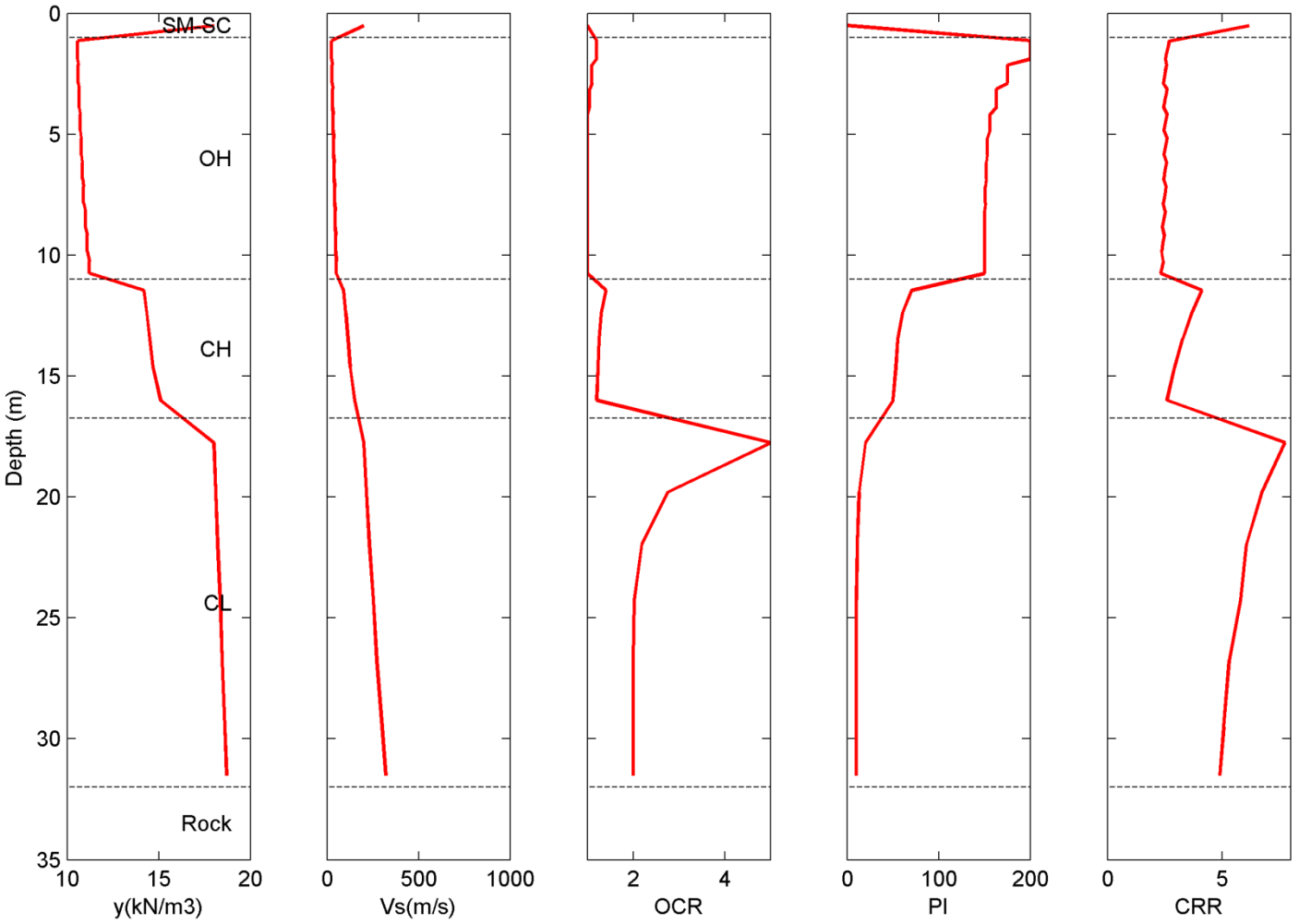

Figure 6.27: Site properties for site Bay Area II K S4

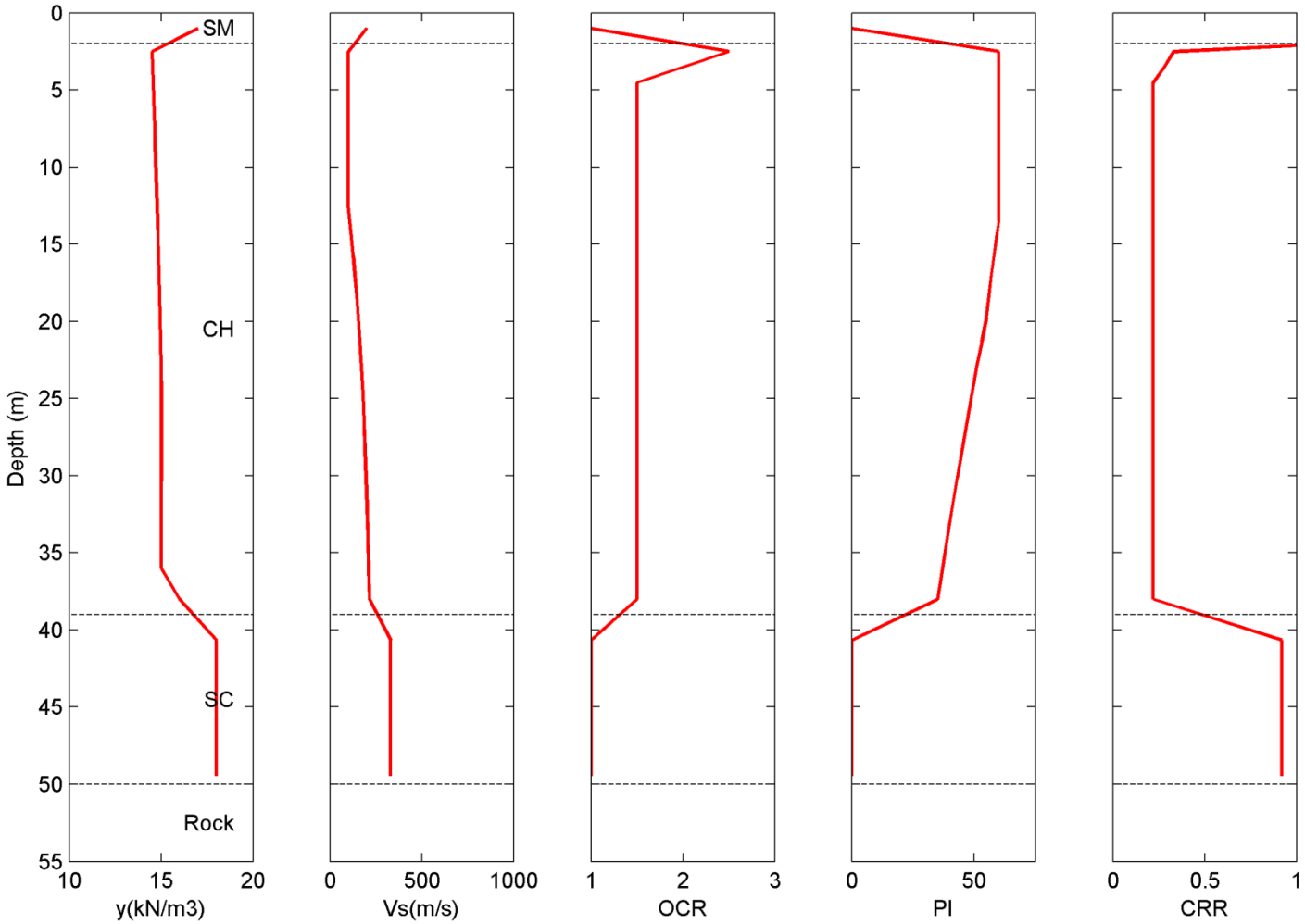

Figure 6.28: Site properties for Guayaquil, Ecuador site HAGP

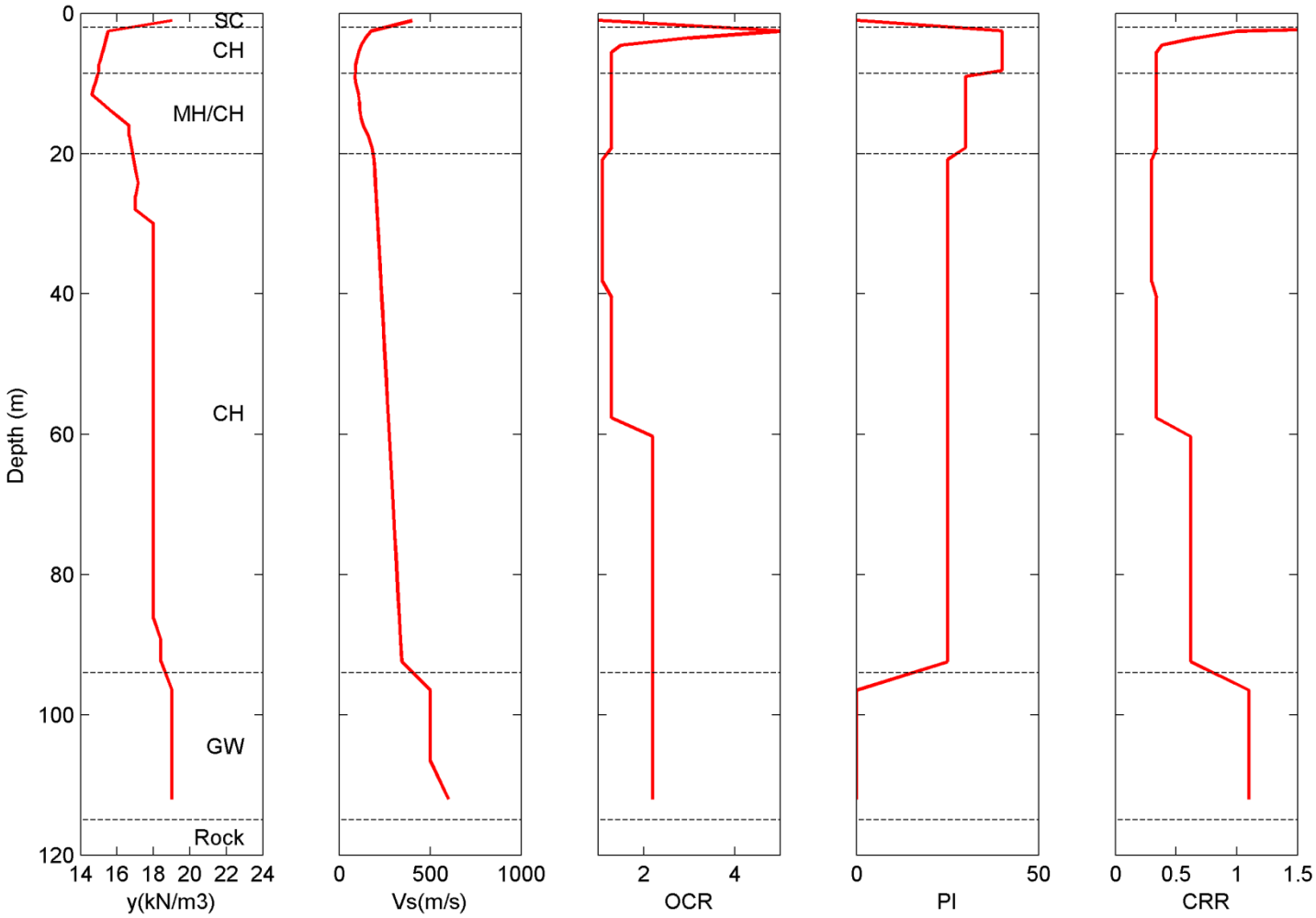

Figure 6.29: Site properties of Ottawa, Canada site JSSS

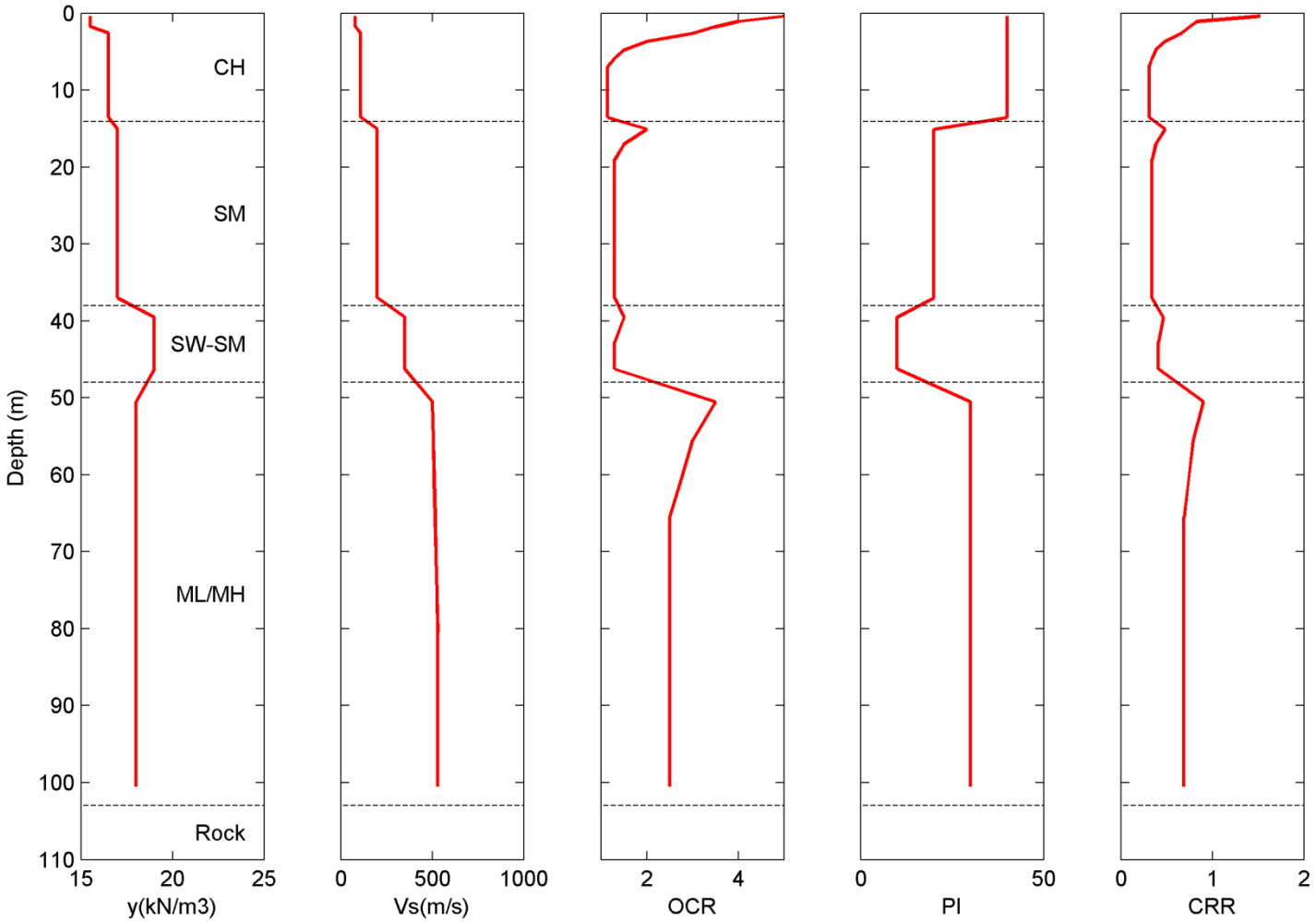

Figure 6.30: Site properties for Hokkaido, Japan site KIKNET40

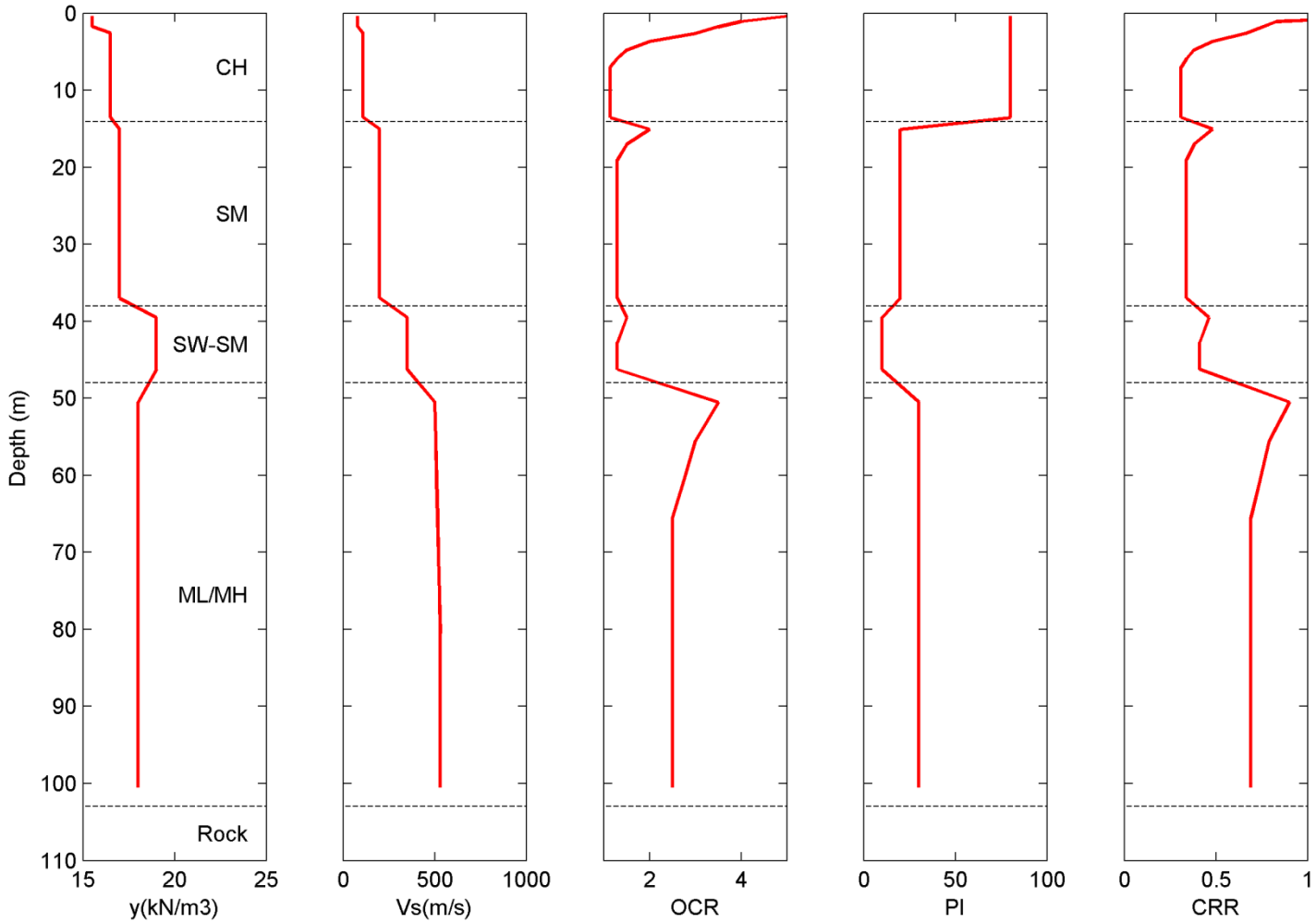

Figure 6.31: Site properties for Hokkaido, Japan site KIKNET

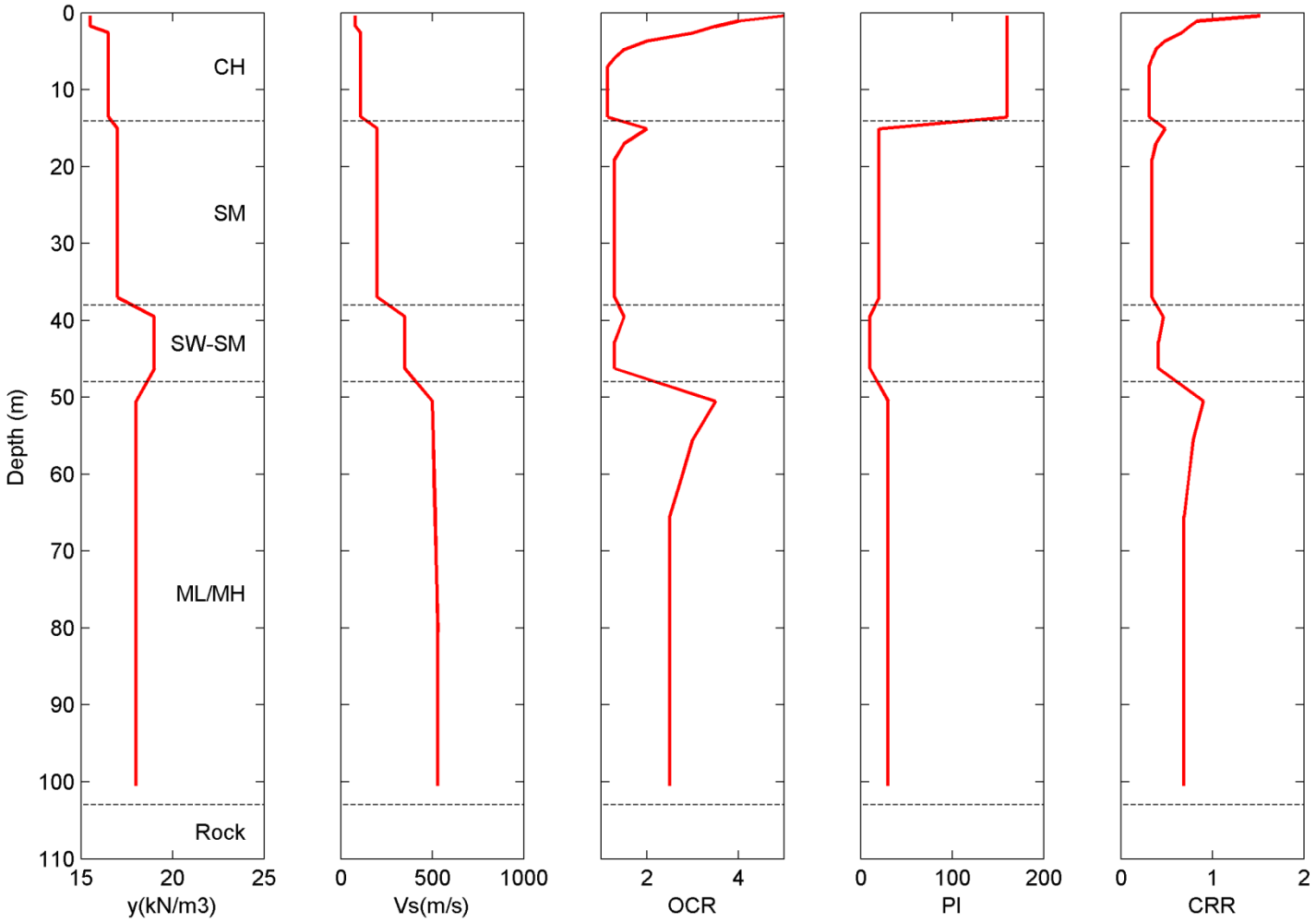

Figure 6.32: Site properties for Hokkaido, Japan site KIKNET160

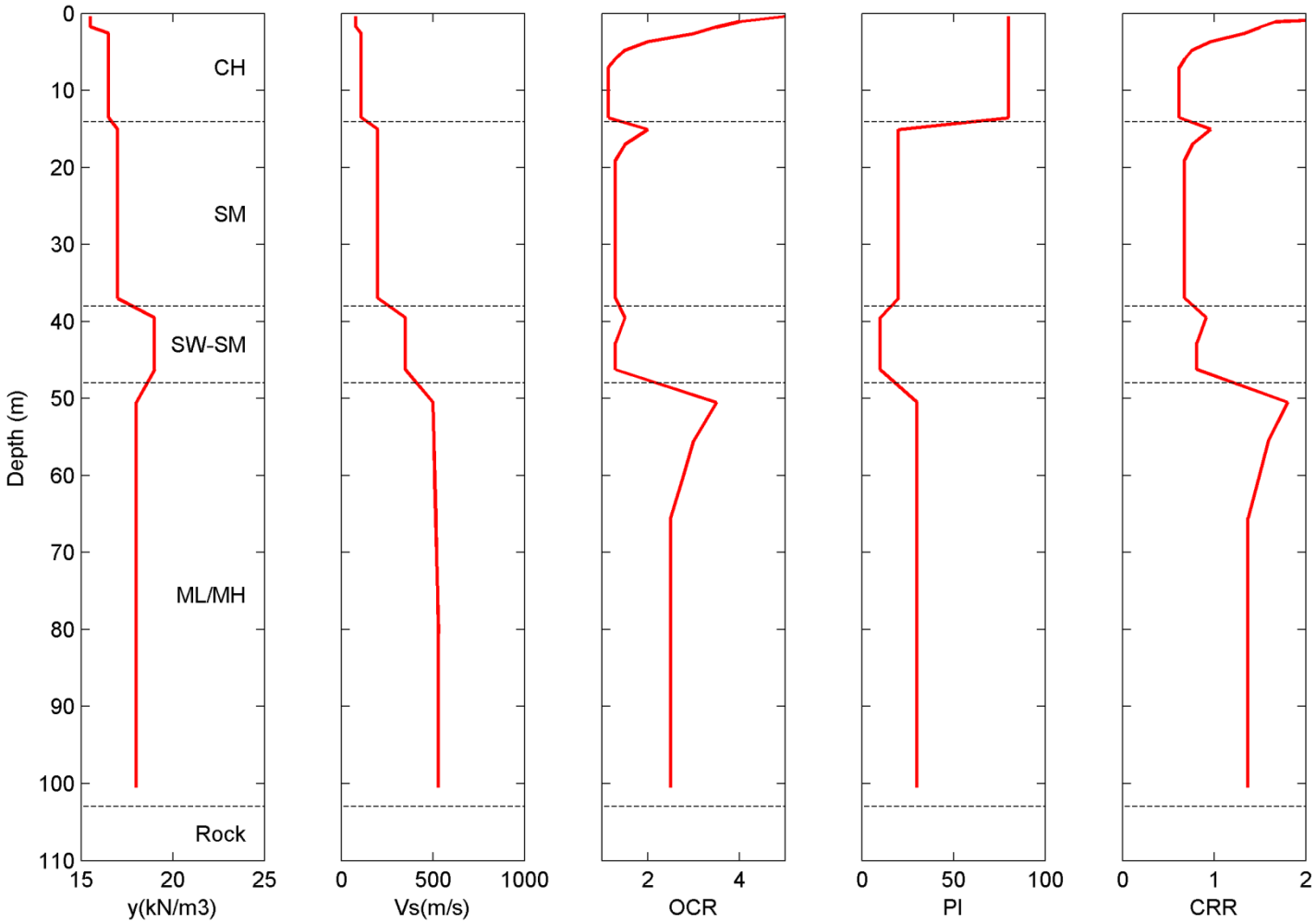

Figure 6.33: Site properties for Hokkaido, Japan site KIKNET S2

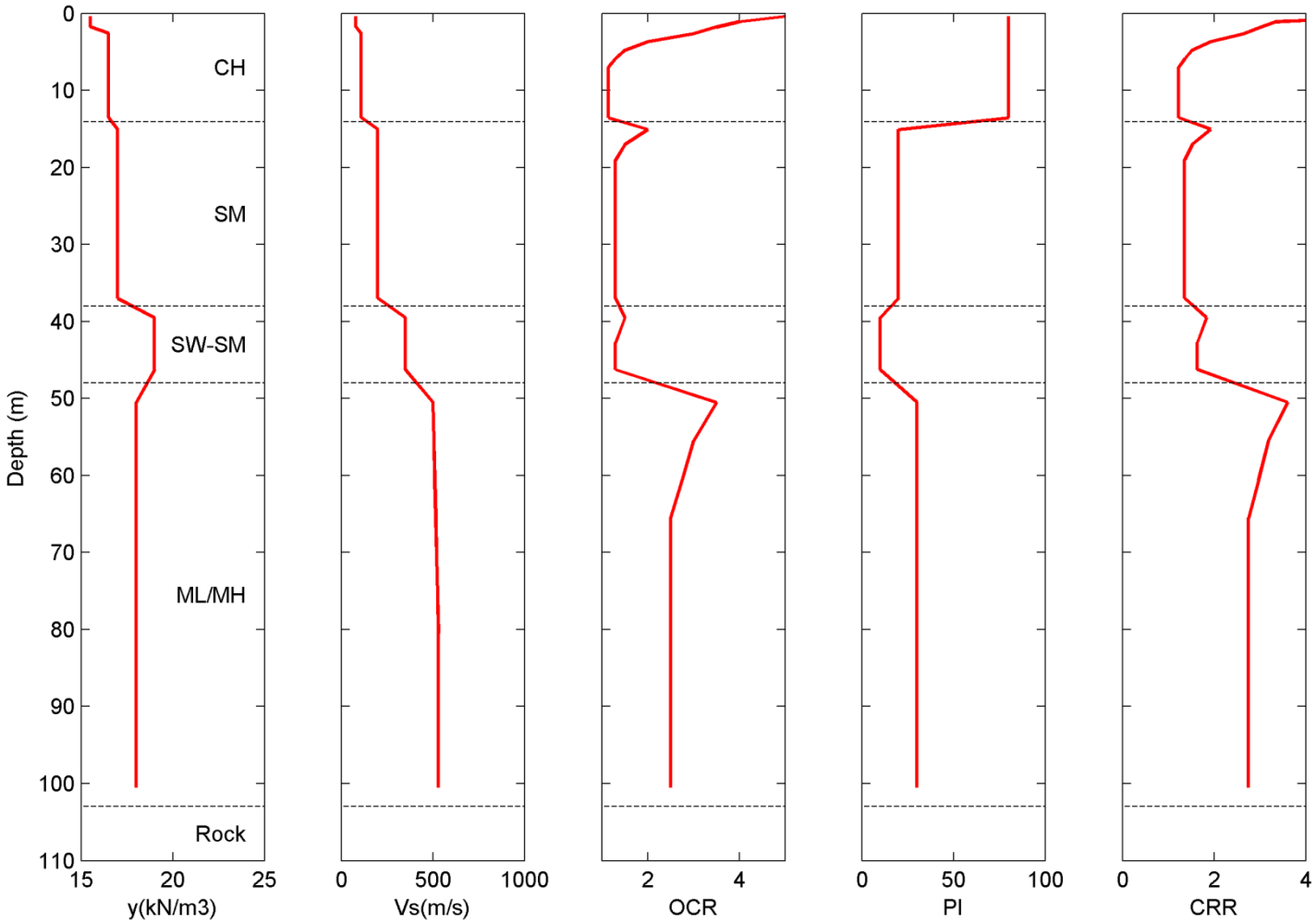

Figure 34: Site properties for Hokkaido, Japan site KIKNET S4

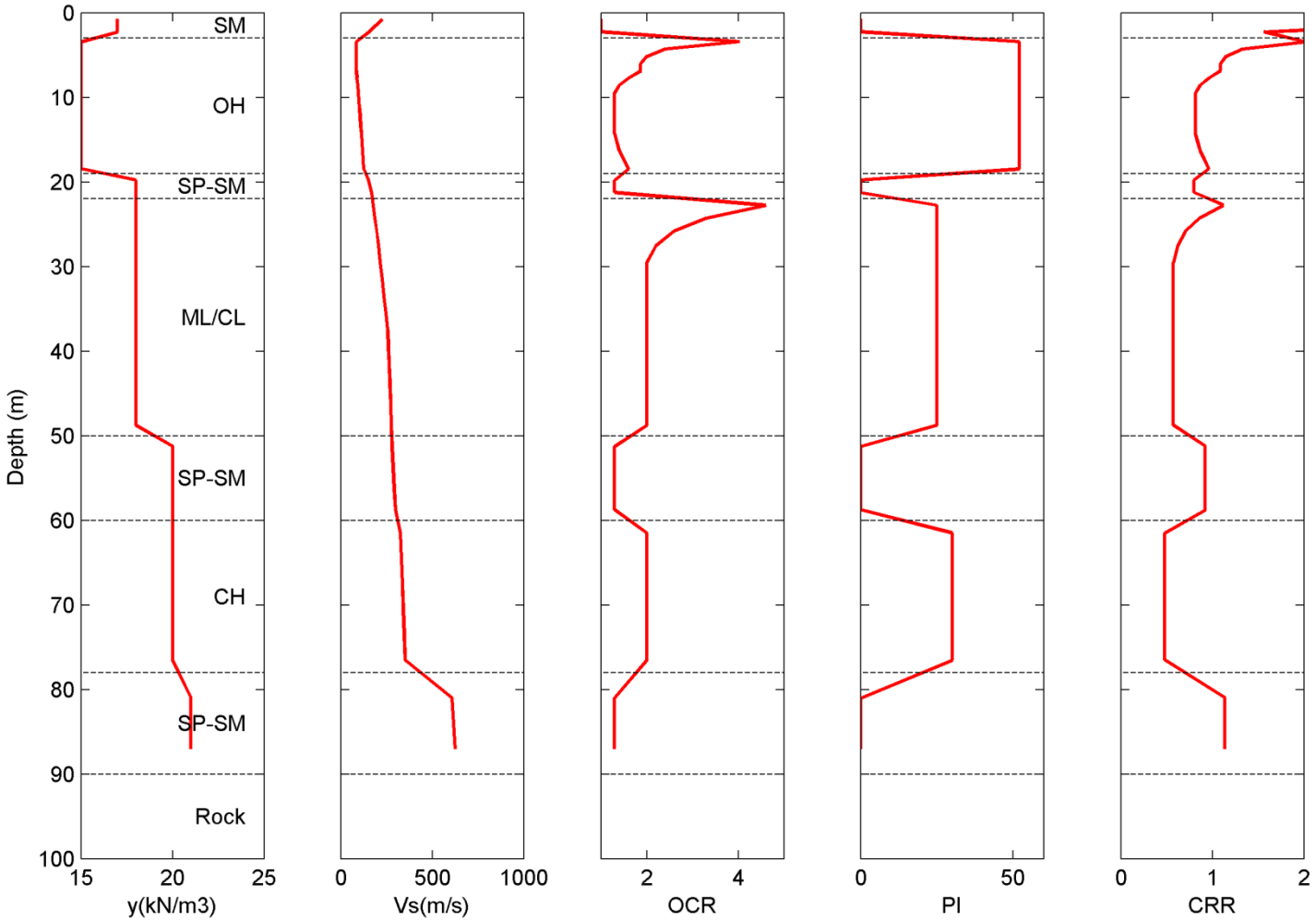

Figure 6.35: Site properties for New York City site MRCE1

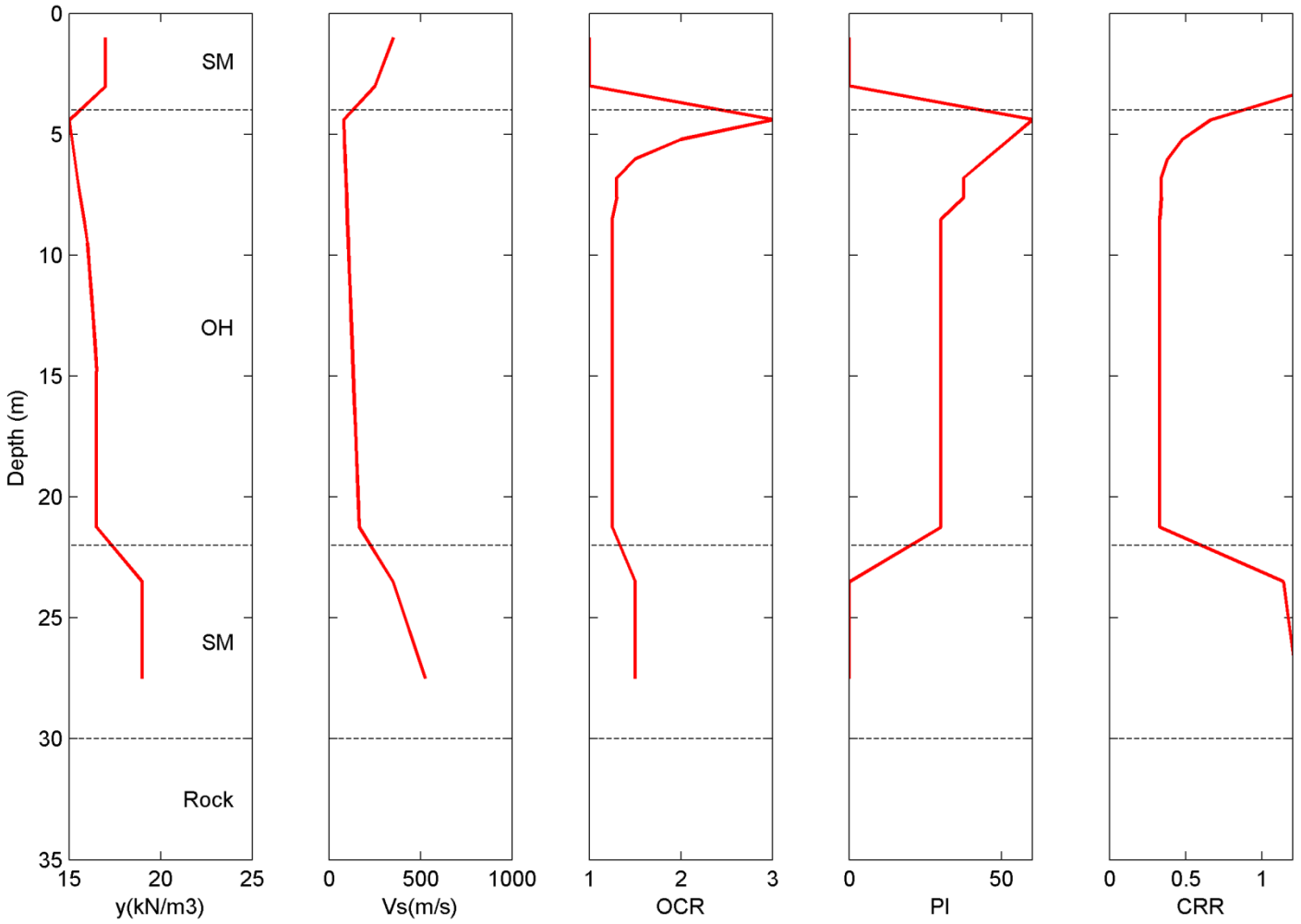

Figure 6.36: Site properties for New York City site MRCE2

Table 6.7: Summary of 15 sites used in site response analyses

ID	Approximate Location	NEHRP	Vs_{30} (m/s)	Depth (m)	T_s (s)	Th (m)	Vs_{mean} (m/s)	$\gamma_{0.5,mean}$ (%)	CRR_{min}
Bay Area	SF Bay Area	E	125	185	2.66	19.25	101.4	0.0580	0.30
Bay Area F	SF Bay Area	F	119	189	2.84	36.85	119.6	0.0699	0.29
Bay Area II	SF Bay Area	F	79	32	1.58	9.75	34.8	0.1216	0.61
Bay Area II K	SF Bay Area	F	79	32	1.58	9.75	34.8	0.7238	0.58
Bay Area II K S2	SF Bay Area	F	79	32	1.58	9.75	34.8	0.9831	1.15
Bay Area II K S4	SF Bay Area	F	79	32	1.58	9.75	34.8	1.8661	2.35
HAGP	Guayaquil, Ecuador	F	127	50	1.23	37.00	136.3	0.0733	0.22
JSSS	Ottawa, Canada	F	143	115	1.93	56.00	173.1	0.0597	0.29
KIKNET40	Hokkaido, Japan	E	140	103	1.56	13.40	99.0	0.0483	0.30
KIKNET	Hokkaido, Japan	F	140	103	1.56	13.40	99.0	0.0707	0.30
KIKNET160	Hokkaido, Japan	F	140	103	1.56	13.40	99.0	0.1026	0.30
KIKNET S2	Hokkaido, Japan	F	140	103	1.56	13.40	99.0	0.0781	0.61
KIKNET S4	Hokkaido, Japan	F	140	103	1.56	13.40	99.0	0.0912	1.22
MRCE1	New York City	F	128	90	1.69	15.15	94.3	0.0886	0.80
MRCE2	New York City	F	162	30	0.74	17.20	112.0	0.0582	0.33

CHAPTER 7: RESULTS OF SITE RESPONSE ANALYSES

7.1 Introduction

There is little data on the seismic response of soil deposits with high plasticity soils, organic clays, and deep soft soil deposits. Therefore, this study focused on site response analyses to develop a better understanding of the effect of these types of soils on site response. Chapter 2 outlined the development of five base-case scenarios and their target parameters. The base case scenarios were selected according to tectonic environments applicable to common practice in the United States and are designated scenarios ACR1, ACR2, ACR3, SUB, and SCR. Scenario ACR1 and ACR2 correspond to shallow crustal earthquakes in active plate margins representing reverse earthquakes with and without pulse-like responses, scenario ACR3 represents strike-slip shallow crustal earthquakes in active plate margins, and scenarios SUB and SCR correspond to earthquakes from subduction zones and stable continental regions, respectively.

Chapter 3 described the selection and modification of input rock ground motions for each of the scenarios. A total of eleven ground motions for scenarios ACR1, SUB, and SCR, and 40 ground motions for scenarios ACR2 and ACR3 were selected and scaled to match their target response spectra. The 40 selected ground motions for scenarios ACR2 and ACR3 were also spectrally matched over the period range of 0.1-3 seconds. In addition, to investigate the effect of ground motion intensity, the scenario ACR3 ground motions were further scaled by factors of 0.125, 0.25, 0.5, 1, 2, and 4. In other words, the 40 ground motions in scenario ACR3 were first scaled so that their average response spectrum matched the target response spectrum, then they were all scaled again by the same factor to either increase or decrease the overall intensity of the ground motions. This results in a total of 12 ground motion scenarios with 393 ground motions. Table 7.1 lists the identification, number of ground motions per scenario, and tectonic region of each of the 12 ground motion scenarios used in the site response analyses.

Chapter 6 described the development of the properties of 15 different sites used in the site response analyses. Table 7.2 lists the site properties for each of the 15 sites. It lists the NEHRP site category, Vs_{30}, depth to bedrock, elastic site period (T_s), the total thickness of the special soil layers (Th), the mean shear wave velocity of the special soil layers (Vs_{mean}), the minimum value of the cyclic resistance ratio (CRR_{min}) of the special soil layers, where CRR is the dynamic shear strength of the soil divided by the vertical effective confining pressure, and the mean value of the shear strain when $G/G_{max} = 0.5$ of the special soil layers ($\gamma_{0.5,mean}$). The "special" soil layers are the soil layers that classify a site as a non-liquefiable NEHRP F site, such as peat or highly organic clays, soils with PI > 75, and soft to medium stiff clays. These parameters are explained in greater detail in chapter 8. Seven sites are based on actual sites, while the other eight sites are variations of the seven base case sites that explore the effects of strength, plasticity index (PI), and elastic site period (Ts) on the surface response. This study conducted total stress nonlinear and effective stress nonlinear site response analyses for all 15 sites and 12 ground motion scenarios, and total stress equivalent linear site response analyses for each of the seven base case sites and all 12 ground motion scenarios. This results in a total of 14,541 site response analyses.

This chapter discusses the results of the site response analyses, highlights trends noticed in the data, and compares the results with results from other studies. Section 7.2 discusses the effect of ground motion properties on the site response analyses. It shows plots of different scenarios for a given site to investigate the effects of ground motion intensity (scenarios 12ACR3, 25ACR3, 50ACR3, 100ACR3, 200ACR3, and 400ACR3), near fault pulse like motions versus near fault motions with no pulse (scenario ACR1 versus ACR2), scaled suites versus spectrally matched suites (scenarios ACR2 versus ACR2M and 100ACR3 versus ACR3M), duration (scenario 100ACR3 versus SUB), and tectonic region (scenarios 100ACR3, SUB, and SCR). Section 7.3 analyzes the effect of different site properties on the site response analyses. It shows plots for a given scenario and different sites investigating the effects of soil strength (sites Bay Area II K, Bay Area II K S2, and Bay Area II K S4, and sites KIKNET, KIKNET S2, KIKNET S4), soil shear modulus reduction and damping curves (sites Bay Area II and Bay Area II K, and sites KIKNET40, KIKNET, and KIKNET160), and site elastic period (sites MRCE2, HAGP, KIKNET, Bay Area II K, MRCE1, JSSS, Bay Area, and Bay Area F). Section 7.4 investigates the effect of different analysis types on the site response analyses. Total stress equivalent linear site response analyses were conducted only for the seven base case sites, so only the results from those sites are compared. Section 7.5 looks at the standard deviation of each scenario and the effect of site, scenario, and analysis type on the standard deviation. Section 7.6 compares the amplification factors calculated in this study with those implied by the NGA West 2 GMPEs for NERHP E sites. Finally, section 7.7 looks at the results of the site response analyses in terms of other ground motion parameters such as PGA, PGV, T_m, $D_{5\text{-}95}$, and I_a.

All response spectra in this chapter are shown only from their lowest to their highest useable periods. All the acceleration time series used in this study had Nyquist frequencies of 50 Hz or 100 Hz, therefore, the lowest useable period was controlled by the layer properties as discussed in Chapter 6. For scenario SCR the lowest useable period was 0.2 seconds (50 Hz), and for all other scenarios it was 0.4 seconds (25 Hz). The highest useable period for each suite was determined as the longest period where at least 63 % of the ground motions in that suite had highest useable periods equal to or greater than that period, which corresponds to 25 ground motions for suites with 40 motions, and 7 ground motions for suites with 11 motions. Table 7.1 lists the highest and lowest useable periods for each scenario.

7.2 Effect of Ground Motion: Comparing Scenarios for a Given Site

Figure 7.1 through Figure 7.3 show plots comparing the results of the effective stress site response analyses for site Bay Area. Figure 7.1 compares scenarios 12ACR3, 25ACR3, 50ACR3, 100ACR3, 200ACR3, and 400ACR3, Figure 7.2 compares scenarios ACR1, ACR2, ACR2M, 100ACR3, and ACR3M, and Figure 7.3 compares scenarios 100ACR3, SUB, and SCR. The scenarios were grouped in this fashion to investigate the effect of ground motion intensity, near fault effects and scaling versus spectral matching, and the effect of tectonic region, respectively. All curves are the mean values of the parameter for the given scenario and site for effective stress analyses. For example, the curves for scenario ACR1 in Figure 7.2 are the mean values of the results of the effective stress site response analyses using the 11 ground motions in scenario ACR1 and the site profile Bay Area.

Each figure contains six plots. The top left plot is the calculated response spectra for each scenario at the surface of the given site. The top right plot gives the spectral amplification ratio Amp(T) versus period, where Amp(T) is the calculated surface response spectra divided by the input rock response spectra at each period. The bottom four plots on each page show, from left to right, the maximum shear strain, shear stress ratio, pore pressure ratio, and PGA with depth, where the shear stress ratio and pore pressure ratio are the shear stress and pore pressure divided by the vertical effective stress. The dotted horizontal lines in the bottom four plots define the boundary between different soil types. The USCS soil designation for each layer is given in the plot with shear strain. This makes it easier to visualize the soil column while interpreting the results. The red dotted line in the maximum shear stress ratio plot is the shear strength ratio of the soil profile, where the shear strength ratio is the shear strength divided by the vertical effective stress. Appendix 7A shows similar figures for all 15 sites.

Figure 7.1 shows that as the intensity of the input ground motion increases, the calculated response spectra at the soil surface increases at all periods, and the peaks of the response spectra shift to longer periods. This is consistent with the work of Roblee et al. (1996) who found that as the intensity of the input ground motion increased, the resonance of the surface response spectrum shifted to longer periods for soft soils. In addition, Figure 7.1 shows that as the intensity of the input ground motion increases, the amplification decreases for periods less than the peak period, but increases for periods longer than the peak period, which agrees with the results of Bazzurro and Cornell (2004) and Kamai et al. (2013). Bazzurro and Cornell (2004) also found that as the input ground motion intensity increases the peak amplification diminishes, and the period of the peak amplification shifts to longer periods. This study found the same results for all sites analyzed. The period where the smallest amplification occurs increases slightly as the ground motion intensity increases.

When the intensity of the input ground motion increases, the maximum shear strain, shear stress ratio, pore pressure ratio, and PGA of the soil profile increase for all depths. As the soil reaches its maximum shear strength ratio (dotted red line in the figures), the rate of increase of the maximum shear stress ratio with intensity and the rate of increase of the PGA with intensity decrease. Because the shear modulus reduction curves are calibrated to asymptotically approach the shear strength of the soil at large shear strains, the shear stress ratio also asymptotically approaches the shear strength ratio, and therefore the rate of increase of the shear stress ratio decreases as it approaches the shear strength ratio.

Figure 7.2 shows that the values for scenarios ACR2 and ACR2M are very similar, and the values for scenarios 100ACR3 and ACR3M are also similar. These results indicate that scaling and spectral matching give the same average response. Scenario ACR1 is similar to scenarios ACR2 and ACR2M except for the calculated response spectra at the surface, which has greater spectral values at long periods than scenarios ACR2 and ACR2M. However, the amplification at long periods is similar for scenarios ACR1, ACR2, and ACR2M, which shows that the difference in the surface response spectra is caused by the difference in the input motion. Scenario ACR1 also has greater pore pressure ratios and shear strains than scenarios ACR2 and ACR2M for sites Bay Area, Bay Area F, Bay Area II, Bay Area II K, HAGP, JSSS, and MRCE2 (Appendix 7A shows results for all of the sites).

Figure 7.3 shows that scenario SUB has slightly greater values of maximum shear strain, shear stress ratio, and pore pressure ratio than scenario 100ACR3. This is probably due to the longer duration of scenario SUB ground motions than scenario 100ACR3 ground motions. However, their response spectra, amplification, and max PGA with depth are very similar. This is in contradiction to the results of Dickenson (1994), who stated that increased input ground motion magnitude (i.e. duration of shaking), led to increased amplification. Scenario SCR has less amplification at short periods and more amplification at long periods than scenarios 100ACR3 and SUB. This is most likely due to the fact that there is more energy in the input motion at short periods and less at long periods in the scenario SCR ground motions.

In general, the maximum shear strain, shear stress ratio, and PGA tend to increase as the shear wave velocity decreases. However, for greater intensity input ground motions and soft soil layers (i.e., low shear wave velocity), the PGA decreases due to the higher levels of shear strain that result in greater soil damping.

Figure 7.4 compares the spectral ratio (Sa(T) / PGA) calculated at the surface for site Bay Area. The plots in the top row show scenarios 12ACR3, 25ACR3, 50ACR3, 100ACR3, 200ACR3, and 400ACR3, the plots in the middle row show scenarios ACR1, ACR2, ACR2M, 100ACR3, and ACR3M, and the plots in the bottom row show scenarios 100ACR3, SUB, and SCR. The left column is plotted in semi-log space and the right column is plotted arithmetically. Both plots also show the median spectral ratios given by Seed et al (1997) for their soil class E, which is analogous to NEHRP F sites. Specifically, the Seed et al. (1997) E site is defined as very deep, soft cohesive soil; soft cohesive soil and very strong shaking; and very high plasticity clays. The Seed et al (1997) median spectral ratios are calculated by dividing the values given in the paper by 1.15. Appendix 7A shows similar figures for all 15 sites.

Figure 7.4 shows that as the intensity of the input ground motion increases, the peak spectral ratio decreases and the period of the peak spectral ratio increases. The spectral shape also becomes wider and shifts to the right, so that spectral ratios for higher intensity input ground motions have lower values at short periods and greater values at long periods than low intensity input ground motions, which agree with the results of Seed et al (1997), and Kamai et al (2013).

The spectral shapes for scenarios ACR2 and ACR2M and scenarios 100ACR3 and ACR3M are roughly the same, which is expected because their response spectra are about the same. The spectral ratio values for scenario ACR1 are generally lower than those for ACR2 and ACR2M for short and medium periods, but greater than those for ACR2 and ACR2M for long periods. The spectral shapes for scenarios 100ACR3 and SUB are similar for all periods, and the spectral shape of scenario SCR peaks sooner than the spectral shapes of scenarios 100ACR3 and SUB. Finally, Figure 7.4 shows that the Seed et al (1997) soil class E spectral shape is roughly the same as scenario 100ACR3 and ACR3M for site Bay Area.

7.3 Effect of Site: Comparing Sites for a Given Ground Motion Scenario

Figure 7.5 compares amplification factors of sites with different soil shear strengths. It shows results of effective stress analyses for sites Bay Area II K, Bay Area II K S2, Bay Area II K S4, KIKNET, KIKNET S2, and KIKNET S4, and for scenarios 12ACR3, 25ACR3, 50ACR3,

100ACR3, 200ACR3, and 400ACR3. The results of these sites are shown because the only difference between the three Bay Area II sites are their soil shear strengths, and similarly the only difference between the three KIKNET sites are their soil shear strengths. In other words, only the shear modulus reduction and damping curves at large strains are changed, all of the other parameters such as shear wave velocity, unit weight, soil types etc. remain the same. The S2 and S4 in a site name stand for double shear strength and quadruple shear strength, respectively. For example, site Bay Area II K S2 has soil shear strengths twice as large as site Bay Area II K, site Bay Area II K S4 has soil shear strengths four times as large as site Bay Area II K, and similarly for the KIKNET sites. Figure 7.5 shows that as the strength of the soil profile increases the amplification increases for periods less than the peak amplification period. For periods greater than the peak amplification period there is a cross-over and sites with larger strengths have smaller amplification. In addition, as the strength increases the peak amplification increases, peak amplification period decreases, and the period at which the amplification is a minimum increases. The effect of the soil profile strength is more pronounced as the intensity of the input ground motion increases. The soil profile strength has no effect on the calculated surface response spectra for scenario 12ACR3, but for scenario 400ACR3 there is a significant difference.

Figure 7.6 compares amplification factors of sites with different shear modulus reduction and damping curves (MRD curves). It shows results of effective stress analyses for sites Bay Area II, Bay Area II K, KIKNET40, KIKNET, and KIKNET160, and for scenarios 12ACR3, 25ACR3, 50ACR3, 100ACR3, 200ACR3, and 400ACR3. The results of these sites are shown because the only difference between the two Bay Area II sites are their MRD curves at small and medium strains, and similarly the only difference between the three KIKNET sites are their MRD curves at small and medium strains. All of the other parameters such as shear wave velocity, unit weight, soil strength etc. remain the same. Figure 7.6 shows that as the MRD curves shift to the right (increase in the volumetric threshold shear strain γ_{tv}), the amplification increases for periods less than the peak amplification period. This is similar to the results of Rodriguez-Marek et al. (2001), who found that clay sites and Pleistocene sites had greater amplification ratios than sand sites and Holocene sites because the clay and Pleistocene soils had greater volumetric threshold shear strain γ_{tv} values. However, for periods greater than the peak amplification period, sites with greater γ_{tv} have smaller amplification factors. In addition, as γ_{tv} increases, the periods at which the amplification is maximum and minimum both decrease. Figure 7.7 shows the results of Nikolaou et al. (2001), who also found that when the soil plasticity increased (i.e. as γ_{tv} increased), the response spectrum increased for short periods, decreased for long periods, and the peak period of the response spectrum decreased. These trends are the same as those observed for differences in soil strength.

The amplification values for site Bay Area II K are significantly greater than those for site Bay Area II for periods less than the period of the peak amplification. Figure 7.8 shows that the Bay Area II K curves have much greater γ_{tv} values and smaller damping values than those for site Bay Area II. For small intensity motions such as the scenario 12ACR3 ground motions, the difference is most likely due to the difference in small strain damping. Site Bay Area II has small strain damping values between 5% and 7.5% for the organic clay layers, whereas site Bay Area II K has small strain damping values between 3.35% and 3.5%. The difference between KIKNET40, KIKNET, and KIKNET160 is negligible for scenario 12ACR3 ground motions but

increases as the intensity of the input ground motion increases up to about scenario 100ACR3. The difference between the three KIKNET sites remains the same for scenarios 100ACR3, 200ACR3, and 400ACR3, and it is never as large as the difference between the response of sites Bay Area II and Bay Area II K. The KIKNET sites never have as great a difference in amplification as sites Bay Area II and Bay Area II K because the differences in their MRD curves are not as great as the differences in the MRD curves of sites Bay Area II and Bay Area II K. The difference between the Bay Area II and Bay Area II K sites remains about the same for all levels of intensity of the input ground motions.

Figure 7.9 compares amplification factors of sites with different elastic site periods (T_s). It shows results of nonlinear effective stress analyses for sites MRCE2, HAGP, KIKNET, Bay Area II K, MRCE1, JSSS, Bay Area, and Bay Area F, for scenarios 12ACR3, 25ACR3, 50ACR3, 100ACR3, 200ACR3, and 400ACR3. Unlike the sites shown to investigate the effects of soil strength and shear modulus reduction curves, these sites do not have all other parameters in common. Each site has different soil shear strengths, different shear wave velocity profiles etc., in addition to having different elastic site periods. Appendix 7B contains figures comparing results of the effective stress site response analyses by strength, MRD curves, and elastic site period for response spectrum and amplification ratios, with layouts similar to Figure 7.5, Figure 7.6, and Figure 7.9.

The peak amplification periods for the eight sites shown in Figure 7.9 correspond roughly to their elastic site periods (T_s). The sites are arranged in the legend from shortest to longest elastic site period, where site MRCE2 has the shortest elastic site period (0.74 seconds) and site Bay Area F (2.84 seconds) has the longest elastic site period. As the elastic site period increases the peak amplification period shifts to greater periods. Kamai et al. (2013) found this same trend for soil depth, and Chapman et al. (1996) noted that thicker deposits of soil produced larger responses for long periods, and thinner deposits produced larger responses at short periods. In particular, Kamai et al. (2013) looked at the effect of varying parameter z_1, the depth to a shear wave velocity of 1,000 m/s, and found that as z_1 increased the peak amplification period increased. Figure 7.10 shows their results, which are similar to the results of Figure 7.9 comparing site elastic period for the analyses conducted in this study. Kamai et al. (2013) also found that the effect of soil depth is greatest for soils with low Vs_{30} values and sites with z_1 values between 8 to 300 meters. For z_1 depths greater than 300 meters, they found that soil scaling becomes increasingly weak, a phenomena that they attribute to the limitations of modeling deep soil profiles with a 1D soil column.

For periods greater than the peak amplification period, all the site amplification curves follow roughly the same shape. This is because long period seismic waves sample deeper and generally stiffer layers of a site profile, and therefore long period seismic waves are not as affected by shallow soft soil layers that typically experience the greatest nonlinear effects (Kaklamanos et al., 2013). For periods less than the peak amplification period, the amplification curves are more varied due to the response of the site's higher modes. The variation between the amplification of the sites decreases as the intensity of the input ground motion increases. The minimum amplification values occur at about the same period as the peak period of the average input ground motion scenario response spectrum, which is 0.2 seconds for all scenarios except scenario SCR, where it is 0.04 seconds. Figure 7.11 shows the amplification for the effective

stress analyses of scenario SCR. Figure 7.11 shows that for all 15 sites the minimum amplification period for scenario SCR is about 0.04 seconds, supporting the idea that the minimum amplification period is dependent on the peak period of the input ground motion.

Figure 7.12 contains six plots showing the effect of site strength and soil MRD curves on the spectral ratio (Sa(T) / PGA) and the max shear strain, shear stress ratio, pore pressure ratio, and PGA with depth for scenario ACR2 and the Bay Area II sites, and Figure 7.13 shows similar plots for the KIKNET sites. The upper right plot in each figure shows the spectral ratio in semi-log space, and the upper left plot shows the spectral ratio in arithmetic space. Both plots also show the median (values given in the paper divided by 1.15) response spectral shape given by Seed et al. (1997) for their soil class E. The bottom four plots of each figure have similar layouts as Figure 7.1 through Figure 7.3, and show, from left to right, the maximum shear strain, shear stress ratio, pore pressure ratio, and PGA with depth. Appendix 7B contains figures similar to Figure 7.12 and Figure 7.13 comparing results of effective stress site response analyses by strength, soil MRD curves, and elastic site period for spectral ratio and maximum shear strain, shear stress ratio, pore pressure ratio, and PGA with depth for different scenarios.

Figure 7.12 and Figure 7.13 show that, in general, as the strength increases the spectral shape decreases for all periods. This effect is more pronounced as the intensity of the input ground motion increases (see Appendix 7B). As the γ_{tv} increases, the spectral shape of the calculated surface response spectra shifts to the left and up. In other words, it shifts to smaller periods and larger spectral ratios. Kamai et al. (2013) also found that soils with greater values of γ_{tv} had spectral shapes shifted to shorter periods.

Figure 7.12 and Figure 7.13 show that, as the soil strength and γ_{tv} increase, the maximum shear stress ratio and maximum PGA with depth increase. This effect is more pronounced for larger intensity input motions (see Appendix 7B). The effect of soil strength and MRD curves on the maximum shear strain and pore pressure ratio with depth is more complicated. As soil strength and γ_{tv} increase, the value of G/G_{max} increases for a given shear strain, and the damping decreases. Increased soil stiffness will cause the soil shear strains for a given ground motion to decrease, but decreased damping will dissipate less energy, which can cause the soil shear strains to increase. The pore pressure generation models used in this study by Matasovic and Vucetic (1993) for sands and Matasovic and Vucetic (1995) for clays are highly dependent on the volumetric threshold shear strain (γ_{tv}). Therefore, as the soil strength and γ_{tv} increase, the shear strains and pore pressure ratios may either increase or decrease, depending on the combined change in stiffness and damping. It is also interesting to note that the soil MRD curves in Figure 7.12 and Figure 7.13 were changed only in the soil layers labeled OH and CH, respectively, and yet the soil layers immediately beneath these two layers were also affected, even though they had the exact same soil MRD curves. These differences in layers with the same soil properties are due to reflections of seismic waves from the upper layers, where the soil properties are different. The soil strength was changed for all soil layers, but the effect of soil strength is more pronounced for layers with lower shear wave velocities because these layers experience higher shear strains.

Figure 7.14 investigates the effect of elastic site period on the spectral shape for effective stress analyses of scenario 100ACR3. Figure 7.14 shows that no clear correlation between elastic site

period and spectral shape can be made for these sites, because there are too many other factors that are different as well. Figure 7.12, Figure 7.13, and Figure 7.14 show that the spectral shape predicted by Seed et al. (1997) for their category E soil profile has peak amplitudes about the same as the predicted spectral shapes found in this study. However, the period range over which those peak amplitudes occur is fixed at 0.6 seconds to 2.2 seconds. The procedure of Seed et al. (1997) does not allow changes in the spectral shape for a given site class due to ground motion properties such as intensity, or site properties such as strength. This section and the previous section showed that, even within a site class, the width of the spectral shape is dependent on the input ground motion and site properties.

7.4 Effect of Analysis Type: Comparing Total Stress Equivalent Linear, Total Stress Nonlinear, and Effective Stress Nonlinear Analyses

Rathje and Kottke (2011) compared results of total stress equivalent linear analyses using the program Strata (Kottke and Rathje, 2008) with the results of total stress nonlinear analyses performed using DEEPSOIL. They conducted tests for two sites, the Sylmar County Hospital (SCH) in the San Fernando Valley of Southern California and the Calvert Cliffs (CC) site in Maryland on the coast of Chesapeake Bay. They used a suite of 15 input ground motions that were spectrally matched to a target response spectrum for an earthquake with M_w = 6.5 and R = 20 km. They scaled the suite to different PGA levels to examine the effect of ground motion intensity.

Rathje and Kottke (2011) found that for input PGA greater than 0.05 g, the total stress nonlinear site response analyses predicted less amplification than the total stress equivalent linear analyses for periods less than 0.04 seconds, greater amplification for periods between 0.04 and 0.2 seconds, and less amplification at the natural period of the site. Figure 7.15 shows the relative difference between the two analysis methods for different input ground motion PGA levels, frequencies, and both sites. Rathje and Kottke (2011) define the relative difference δ_{SR} as:

$$\delta_{SR}(\%) = \frac{Amp_{NL} - Amp_{EQL}}{Amp_{EQL}} \times 100\% \qquad (7.1)$$

where Amp_{NL} is the amplification of the total stress nonlinear analyses and Amp_{EQL} is the amplification ratio of the total stress equivalent linear analyses.

Rathje and Kottke (2011) state that the total stress nonlinear method predicts less amplification than the total stress equivalent linear method for periods less than 0.04 seconds due to incoherence in the frequency phasing caused by the changing of the stiffness and damping properties with time. This in turn creates destructive interference, which reduces the amplitude of the ground motion for periods less than 0.04 seconds. Total stress nonlinear analyses predict greater amplification than total stress equivalent linear analyses for periods between 0.04 and 0.2 seconds due to the instantaneous change in stiffness after a stress reversal in the total stress nonlinear analyses, which amplifies low period (high frequency) energy because the tangent shear modulus is usually greater than the secant shear modulus, and over-damping of low periods (high frequencies) in the total stress equivalent linear analyses due to the constant stiffness and

damping properties selected based on a fraction of the peak strain. If the peak strain for a soil layer is much larger than the rest of the strains predicted for the duration of the earthquake the response will be over-damped, if the strains are uniform then the response will be under-damped. High frequency (low period) energy generally produces small shear strains, and therefore is most often over-damped by total stress equivalent linear analyses. Stewart et al. (2008) and Kaklamanos et al. (2013) also found that total stress equivalent linear analyses under-predict the response spectrum at short periods. Finally, Rathje and Kottke (2011) believe that the total stress nonlinear method predicts smaller amplification than the total stress equivalent linear method for periods near the site period because the continuously changing material properties modeled in total stress nonlinear analyses do not cause as much resonance as the constant material properties used in total stress equivalent linear analyses.

Site response analyses were conducted in this study using total stress equivalent linear, total stress nonlinear and effective stress nonlinear analyses for the seven base case sites. Figure 7.16 compares the amplification calculated using total stress equivalent linear, total stress nonlinear, and effective stress nonlinear site response analyses for site Bay Area. Figure 7.16 contains 12 plots, where each plot corresponds to a scenario. All curves are the mean amplification values for site Bay Area and the specified scenario and analysis type. Appendix 7C contains similar figures for all seven of the base case sites, as well as plots showing the corresponding response spectra and spectral shapes.

Figure 7.16 shows that total stress equivalent linear, total stress nonlinear and effective stress nonlinear analyses predict the same amplification for scenarios 12ACR3 and 25ACR3. For all other scenarios, however, the total stress equivalent linear method predicts greater amplification than the total and effective stress nonlinear methods for periods less than the peak amplification period. For periods greater than the peak amplification period the total stress equivalent linear analyses predict similar amplification as the total stress nonlinear analyses, but less than the effective stress nonlinear analyses, which predict the greatest amplification. The effective stress nonlinear analyses predict the same amplification as the total stress nonlinear analyses for periods less than the peak period except for scenarios 200ACR3, 400ACR3, and SUB, where the effective stress nonlinear analyses predict less than the total stress nonlinear analyses. In general, however, the effective stress nonlinear analyses are not much different than the total stress nonlinear analyses for the soil profiles tested in this study. This is because the sites used in this study contain soils with high volumetric threshold shear strain values, below which no degradation or pore water pressure generation takes place. In addition, the soils tested are extremely weak soils, and once they pass the volumetric threshold shear strain they quickly fail, at which point the soil has already degraded to a level that the effect of cyclic degradation and pore pressure generation on the results are negligible.

Figure 7.17 contains five plots showing the site response predictions using different analysis types for site Bay Area and scenario 400ACR3. The plot in the upper left corner shows the response spectra, the plot in the upper right corner displays the spectral ratio (Sa(T) / PGA) in semi-log space, and the bottom three plots show, from left to right, the maximum shear strain, shear stress ratio, and PGA with depth.

Figure 7.17 shows that total stress equivalent linear analyses predict the largest values of shear stress ratio and PGA with depth, followed by total stress nonlinear analyses, and then effective stress nonlinear analyses predicting the smallest values. The differences between the total and effective stress nonlinear analyses are small. In general, effective stress nonlinear analyses predict the largest shear strains, followed by total stress nonlinear analyses, and then total stress equivalent linear analyses. These trends are more pronounced for greater intensity ground motions and softer soils. For low intensity ground motions and stiffer soils, all three methods predict the same response.

7.5 Standard Deviation of Calculated Response

It is important to know the standard deviation of site response analyses to better understand the accuracy and reliability of the results. It is also important for engineers and hazard analysts to know what parameters influence the standard deviation the most, as this allows them to better allocate time and resources to define the parameters that matter the most when conducting site response analyses. Several studies that investigated the standard deviation of site response analyses are Roblee et al. (1996), Stewart et al. (2008), and Li and Assimaki (2010). Roblee et al. (1996) used a stochastic finite fault model and random vibration theory equivalent linear approach to study the effect of source, path, and site variation on the standard deviation of ground motions. They found that the most significant parameters controlling ground motion variability are the site profile, ground motion intensity, and period range of interest. Figure 7.18 shows that for softer soil sites and greater intensity ground motions the reduction in standard deviation for knowing the exact site properties (i.e. shear wave velocity profile and soil MRD curves) is greatest. In other words, uncertainty in site properties has the greatest effect on the total standard deviation for soft soil sites and large intensity ground motions.

Stewart et al. (2008) compared calculated results from nonlinear total stress analyses with measured values from four vertical arrays. They investigated the effect of the variation of shear wave velocity profile, MRD curves, and nonlinear model on the overall response standard deviation. They estimated standard deviation due to using five different models as:

$$\sigma_m = \sqrt{\frac{\sum_i \left[ln\left(Sa(T)\right)_i - ln\left(\overline{Sa}(T)\right)\right]^2}{N-1}} \tag{7.2}$$

where $Sa(T)_i$ is the spectral acceleration of model *i* at period T, and $\overline{Sa}(T)$ is the median spectral acceleration of all five models at period T, and N = 5. They estimated the overall response standard deviation due to shear wave velocity variation based on the First Order Second Moment (FOSM) method (Baker and Cornell 2003; Melchers 1999). This method calculates standard deviation from only three shear wave velocity profiles, one at the median value μ, and the other two at plus and minus $\sqrt{3}$ standard deviations of the shear wave velocity (σ_{Vs}). The overall response standard deviation due to shear wave velocity variability ($\sigma_{RS,Vs}$) is then calculated as:

$$\sigma_{RS,V} = \sum_{i=1}^{3} w_i \times \left[ln\left(Sa(T)\right)_i - ln\left(\widehat{Sa}(T)\right)\right]^2 \tag{7.3}$$

where

$$Sa(T)_1 = Sa(T)_\mu$$

$$Sa(T)_2 = Sa(T)_{\mu+\sqrt{3}\times\sigma_{Vs}}$$

$$Sa(T)_2 = Sa(T)_{\mu-\sqrt{3}\times\sigma_{Vs}}$$

$$ln\left(\widehat{Sa}(T)\right) = \sum_{i=1}^{3} w_i \times ln\left(Sa(T)\right)_i$$

$$w_1 = 2/3\,;\; w_2 = w_3 = 1/6$$

The overall response standard deviation due to the variability in the soil MRD curves ($\sigma_{RS,G}$) is calculated in a similar way. Figure 7.19 shows the results of Stewart et al. (2008). They found that changing the soil MRD curves most affected the total standard deviation for periods less than 0.5 seconds, and that the range of periods affected was not dependent on the elastic site period. They also found that material curve uncertainty is not significant for shallow soil sites (e.g. Turkey Flat site in Figure 7.19).

Li and Assimaki (2010) investigated the uncertainty of site response analyses for three sites in the Los Angeles Basin using a dataset of synthetic ground motions and nonlinear site response analyses. Figure 7.20 shows that the variability of the MRD curves is the dominate source of the overall response standard deviation for short periods (less than 1.5 seconds), for intermediate periods (1.5 < 3 seconds) the variability of the MRD curves and the shear wave velocity contribute equally to the overall response standard deviation, and for long periods (T > 3 seconds), the overall response standard deviation is independent of the MRD curve and shear wave velocity uncertainties. This is consistent with the findings of Stewart et al. (2008). Li and Assimaki (2010) explain that the overall response standard deviation dependency on MRD curve and shear wave velocity uncertainties decreases for longer periods because the seismic wavelengths in the long period range are longer than the thickness of soft soil layers near the surface. The overall response standard deviations at long periods are controlled by the uncertainties in the source and path effects (Roblee et al., 1996).

Comparing Figure 7.20a with Figure 7.20b shows that as the intensity of the ground motion increases, the overall response standard deviation increases. In addition, the intensity of the ground motion affects not only the magnitude of the overall response standard deviation caused by the uncertainty in the soil properties, but also the period range where it is most influential, especially for soft soil sites. Soft soil sites will have greater uncertainty at longer periods than stiff soil sites due to their resonant characteristics. Li and Assimaki (2010) also found that the range of periods affected by changing the soil MRD curves is independent of shear wave velocity, and that uncertainties in the shear wave velocity are more sensitive to shear wave velocity discontinuities in the near surface that control the amplification potential of the site.

This section focuses on the standard deviation of the site response results. The standard deviations shown are for a given scenario, site, and analysis type. Each curve represents the standard deviation of the ground motions and how the analysis type or site affected it. They do not represent the standard deviation due to uncertainties in the shear wave velocity profile or soil MRD curves. Figure 7.21 compares the standard deviation of effective stress analyses calculated for site Bay Area for different scenarios. The plots in the left hand column show the standard deviation in natural log units for the response spectra (σ_{RS}) calculated at the ground surface, and the right hand column contains plots showing the standard deviation in natural log units of the amplification ratios (σ_{AMP}). The top row compares scenarios 12ACR3, 25ACR3, 50ACR3, 100ACR3, 200ACR3, and 400ACR3, the middle row compares scenarios ACR1, ACR2, ACR2M, 100ACR3, and ACR3M, and the bottom row compares scenarios 100ACR3, SUB, and SCR. Appendix 7D contains similar figures for all sites. All of the trends described below for site Bay Area are similar for the other sites.

Figure 7.21 shows that as the period increases, the response spectra standard deviations σ_{RS} increase for all scenarios. Smaller intensity ground motions have greater σ_{RS}, but the standard deviations increase less with period, so that at long periods (about 7 seconds), the σ_{RS} for all intensity levels are the same (about 0.6 for site Bay Area). The opposite trends occur for the amplification standard deviations σ_{AMP}. The σ_{AMP} decrease as period increases, and larger intensity ground motions have greater σ_{AMP}. However, the amplification standard deviations σ_{AMP} do not converge at long periods, as the response spectra standard deviations σ_{RS} do. Bazzurro and Cornell (2004) also found that the standard deviations for amplification ratios were greater at short periods and decreased as period increased.

The response spectra standard deviations σ_{RS} for scenarios ACR1, ACR2, ACR2M, 100ACR3, and ACR3M increase as the period increases. In general, the σ_{RS} of matched scenarios ACR2M and ACR3M are less than their respective scaled scenarios, ACR2 and 100ACR3. The σ_{RS} for scenario ACR1 are roughly similar to those for scenario ACR2, although the σ_{RS} of scenario ACR1 show a consistent drop over the period range of 1.5 to 3 seconds for all sites. The amplification standard deviation σ_{AMP} of scenarios ACR2M and ACR3M show no trend with period, and are consistently lower than the σ_{AMP} for scenarios ACR2 and 100ACR3. In contrast, the σ_{AMP} of scenarios ACR1 and ACR2 decrease as period increases, and have similar values.

As period increases, the response spectra standard deviation σ_{RS} for scenarios SUB and SCR increase and the amplification standard deviation σ_{AMP} decrease. Scenario SUB has similar or slightly smaller σ_{RS} than scenario 100ACR3. Scenarios 100ACR3, SUB, and SCR have similar amplification standard deviations σ_{AMP} except at long periods ($T > 5$ seconds), where the σ_{AMP} for scenario SCR increase and are greater than those for scenarios 100ACR3 and SUB.

Figure 7.22 through Figure 7.24 show the effect of site properties on the amplification standard deviations for effective stress analyses. All three figures contain six plots, with each plot showing results for one of the scenarios 12ACR3, 25ACR3, 50ACR3, 100ACR3, 200ACR3, or 400ACR3. Figure 7.22 examines the effect of soil strength, and displays results from sites Bay Area II K, Bay Area II K S2, Bay Area II K S4, KIKNET, KIKNET S2, and KIKNET S4. Figure 7.23 investigates the effect of soil MRD curves, and shows the results of sites Bay Area II, Bay Area II K, KIKNET40, KIKNET, and KIKNET160. Figure 7.24 looks at the effect of

site elastic period, and gives the results of sites MRCE2, HAGP, MRCE1, JSSS, Bay Area, and Bay Area F. Appendix 7D contains similar figures for the other six scenarios, as well as plots of the response spectra standard deviation.

Figure 7.22 shows that as the intensity of the input ground motion increases, the effect of the strength of the soil increases, and as the strength of the soil increases, the amplification standard deviations σ_{AMP} decrease. In addition, the period range affected by changes in the soil strength also changes with intensity level. For example, the period range affected by soil strength for scenario 25ACR3 is about 0.1 to 1 seconds, for scenarios 50ACR3 and 100ACR3 about 0.04 to 2 seconds, for scenario 200ACR3 about 0.2 to 10 seconds, and for scenario 400ACR3 periods from 0.4 to 10 seconds. These results show that, as the intensity level of the ground motion increases, the period range where the amplification standard deviations σ_{AMP} are affected by the soil strength increases. This is most likely due to the affect of the degraded site period shifting to larger periods as the intensity level increases.

Figure 7.23 shows that as the soil plasticity index (PI) increases for the KIKNET sites, the amplification standard deviations σ_{AMP} decrease. However, this trend is greatest for scenarios 25ACR3, 50ACR3, and 100ACR3. This is because small intensity input ground motions (e.g. scenario 12ACR3) induce small shear strains, so the difference in MRD curves is not great, and large intensity motions (e.g. scenarios 200ACR3 and 400ACR3) induce large shear stains, and at large shear strains the strength of the soil dominates. Therefore, the difference is greatest for moderate strain levels. For scenarios 200ACR3 and 400ACR3, site Bay Area II K, which has soils with greater values of γ_{tv} than site Bay Area II, has greater amplification standard deviations σ_{AMP} at all periods, which is contrary to the trends described above for the KIKNET sites. In addition, for lower intensity scenarios at long periods, the Bay Area II K amplification standard deviations σ_{AMP} are greater than those for site Bay Area II. The two curves cross over around a period of two seconds.

Figure 7.24 shows that there is no discernible trend in amplification standard deviation σ_{AMP} with elastic site period. There is also no noticeable trend with site depth, which is contrary to what Kamai et al. (2013) found, however this could be due to the effect of other site parameters obscuring the effect of the elastic site period. Figure 7.25 shows the results of Kamai et al. (2013) for the σ_{AMP} of sites with different soil depths for an input PGA of 0.01g. They found that the amplification standard deviation σ_{AMP} decreases with depth for periods less than one second and increases with depth for periods greater than one second.

Figure 7.26 compares the effect of analysis type on the amplification standard deviation σ_{AMP} for site Bay Area. There are 12 plots, with each plot showing the results of one scenario and all three analysis types versus period. Appendix 7D contains similar figures for all base case sites as well as for the response spectra standard deviation σ_{RS}.

Figure 7.26 shows that total stress equivalent linear analyses predict smaller amplification standard deviations σ_{AMP} than total or effective stress nonlinear analyses for mid-range periods. As the intensity of the input ground motion increases, the difference between the results of the total stress equivalent linear analyses and the total and effective stress nonlinear analyses increases, as well as the period band over which the results are different. Effective stress

nonlinear analyses predict larger values of σ_{AMP} than those predicted by total stress nonlinear analyses for long periods, and this trend increases as the intensity of the scenario increases.

7.6 Comparison with Implied NGA West 2 Site Amplification Factors Fa and Fv for NEHRP E sites

This section compares site amplification factors Fa and Fv calculated from the nonlinear effective stress site response analyses conducted in this investigation and those implied by the NGA West 2 GMPEs for NEHRP E sites as calculated by Stewart and Seyhan (2013). These comparisons are only for illustrative purposes because the implied NGA West 2 GMPE site factors calculated by Stewart and Seyhan (2013) are for NEHRP E sites, whereas this study investigated mainly NEHRP F sites. The amplification factor Fa is the average amplification for periods between 0.1 to 0.5 seconds, and Fv is the average amplification for periods between 0.4 to 2.0 seconds (Dobry et al., 2000).

Amplification factors for use in site response modeling can be calculated either empirically from recorded data or theoretically through seismic site response analyses. Empirical site amplification factors are calculated in two ways; either through a reference site approach where the measured response spectrum from a site is divided by the measured response spectrum from a nearby reference rock site, or through a non-reference site approach where the measured response spectrum from a site is divided by the median value of the response spectrum predicted by a GMPE for reference rock site conditions (Stewart and Seyhan; 2013).

The NGA West 2 GMPE site amplification models are based on a combination of theoretical and non-reference site empirical analyses. Abrahamson et al. (2013), Boore et al (2013), and Campbell and Bozorgnia (2013) derived coefficients for site response empirically, and constrained the nonlinearity (i.e. the slope of the site amplification ratio with respect to the ground motion intensity) based on simulations by Kamai et al (2013). Chiou and Youngs (2013) determined coefficients for both the linear and nonlinear terms of their site amplification model from non-reference site empirical analyses. All four models derived their empirical coefficients using the NGA West 2 database (Ancheta et al., 2013). The input variables for the four models, ignoring basin effects, are Vs_{30} and an intensity measure at a reference Vs_{30}. For Boore et al. (2013) and Campbell and Bozorgnia (2013) the intensity measure is PGA at Vs_{30} = 760 m/s and Vs_{30} = 1100 m/s, respectively, and for Abrahamson et al. (2013) and Chiou and Youngs (2013) the intensity measure is Sa(T) at Vs_{30} = 1100 m/s and Vs_{30} = 1130 m/s, respectively.

The main objective of Kamai et al. (2013) was to provide the NGA West 2 GMPE developers more information to constrain the nonlinear scaling of their site response models. Kamai et al. (2013) developed a site amplification model based on the results of random vibration theory equivalent linear analyses conducted with the computer program RASCALS (Silva and Lee; 1987). They ran simulations for 53 different base soil profiles that included ten Vs_{30} values, eight soil depths, and four MRD models. The surface response was computed for 11 values of input rock PGA, ranging from 0.01 g to 1.5 g, for three different magnitudes. The shear wave velocity and layer thicknesses of the 53 base soil profiles were randomized according to the correlation models of Silva et al. (1997), and the MRD curves were randomized using a standard

deviation of 0.35 natural log units at a cyclic shear strain of 0.03% and truncated at two standard deviations. Using these randomizations, thirty simulations for each base case soil profile, input motion level, and magnitude were completed. Kamai et al. (2013) is an update of Walling et al. (2008), with two main differences. Kamai et al (2013) included a larger simulation database with additional magnitudes and soil profiles and it investigated the differences between using PGA and Sa(T) as a predictor variable for site amplification.

Figure 7.27 and Figure 7.28 compare amplification factors Fa and Fv calculated from the nonlinear effective stress site response analyses conducted in this investigation for mainly NEHRP F sites, and those implied by the NGA West 2 GMPEs for NEHRP E sites as calculated by Stewart and Seyhan (2013). The NGA West 2 GMPEs did not calculate values of Fa or Fv, the values compared here are the Fa and Fv values calculated by Stewart and Seyhan (2013) using the NGA West 2 GMPEs. To calculate the implied values of Fa and Fv, Stewart and Seyhan (2013) normalized all of the amplification ratios of the NGA West 2 GMPEs to a reference rock shear wave velocity of 760 m/s and calculated the PGA as Sa(T=0.2) = 2.3*PGA and Sa(T=1.0) = 0.7*PGA for the Abrahamson et al (2013) and Chiou and Youngs (2013) models, which use Sa(T) as the intensity measure. The values of 2.3 and 0.7 were determined based on Sa(T)/PGA ratios calculated from the median predicted values for rock site conditions with $6 < M_w < 8$ and $R_{rup} < 30$ km. Huang et al. (2010) used a similar procedure for the same purpose.

Figure 7.27 and Figure 7.28 show Fa and Fv, respectively, for scenarios 12ACR3, 25ACR3, 50ACR3, 100ACR3, 200ACR3, and 400ACR3. There are six plots per figure, where the top left plot in each figure compares the results from sites Bay Area II K, Bay Area II K S2, and Bay Area II K S4 (soil strength), the top right plot compares the sites KIKNET, KIKNET S2, and KIKNET S4 (soil strength), the middle left plot compares sites Bay Area II and Bay Area II K (soil MRD curves), the middle right plot compares sites KIKNET40, KIKNET, and KIKNET160 (soil MRD curves), the bottom left plot compares sites MRCE2, HAGP, KIKNET, and Bay Area II K (elastic site period), and the bottom right plot compares sites MRCE1, JSSS, Bay Area, and Bay Area F (elastic site period). The individual points show the results of one ground motion for effective stress nonlinear analysis and the given site, scenario, and amplification factor.

Both figures show that as the PGA of the input motion (PGA rock) increases, the value of Fa and Fv decrease, regardless of site or scenario. In addition, the top two plots show that as strength increases Fa and Fv increase, but only at intermediate and large values of PGA rock. At low values of PGA rock the strength of the soil has no effect on Fa or Fv. This is logical because strength only affects the large strain portion of the MRD curves. The soil strength appears to have a greater effect on the value of Fv than Fa.

The middle plots of Figure 7.27 and Figure 7.28 show that as γ_{tv} increases, Fa and Fv increase, except for large values of PGA rock, where the soil strength dominates the response and the values of Fa and Fv are the same for MRD curves that predict the same strength. This is seen in the difference between the amplification factors for sites Bay Area II and Bay Area II K. Site Bay Area II K has soil with greater values of γ_{tv} than site Bay Area II, however, the curves converge at large shear strains due to similar shear strengths. The plot of the KIKNET sites with different plasticity index PI values is more complicated. For sites KIKNET40, KIKNET, and

KIKNET160, as PI increases Fa and Fv decrease for low values of PGA rock, increase for moderate values of *PGA* rock, and remain the same for large values of PGA rock. This complicated response reflects the effect of PI on the damping curves as estimated by Darendeli (2001), which are the MRD curves used to model the three sites. Higher PI values in the Darendeli (2001) model have greater D_{min} values, so sites with larger PI values will have lower amplification factors for small values of PGA rock. At moderate shear strain values the Darendeli (2001) model predicts that higher values of PI have greater G/G_{max} values and lower damping values for a given shear strain, which means sites with higher PI values will have larger amplification factors at moderate values of PGA rock. The sites predict the same amplification factors for large values of PGA rock because they have the same shear strength, and shear strength dominates the response at large shear strains.

The bottom two plots of Figure 7.27 and Figure 7.28 show no evidence that Fa or Fv are affected by the elastic site period for the sites investigated in this study.

All of the KIKNET and all of the Bay Area II K sites have similar values of Fa as the values predicted by the NGA West 2 GMPEs for NEHRP E sites. All of the Bay Area II K sites have similar Fv values as the NGA West 2 GMPEs for low values of PGA rock, but only Bay Area II K S4 and KIKNET S4 have similar values of Fv at moderate and large values of PGA rock. All of the other sites fall below the implied NGA West 2 GMPE Fa and Fv values for NEHRP E sites for all levels of PGA rock. However, the site amplification factors show similar shapes as a function of PGA rock. In addition, it must be remembered that the implied NGA West 2 GMPE Fa and Fv values are for NEHRP E sites, whereas most of the sites investigated in this study are NEHRP F sites.

Comparing Figure 7.27 to Figure 7.28, one can see that the values of Fv are more spread out than the values of Fa. In other words, for a given PGA rock, there is more variation of the value of Fv than the value of Fa. In addition, as PGA rock increases, Fa decreases more rapidly than Fv for both the values calculated in this study and those implied by the NGA West 2 GMPEs. The reason for this is that soil nonlinearity has a greater effect on high frequency ground motions than low frequency ground motions, because high frequency ground motions have a greater fraction of their wavelengths in soft soil layers where there is high damping than low frequency ground motions (Stewart and Seyhan, 2013).

Appendix 7E contains figures showing similar plots to Figure 7.27 and Figure 7.28, but for scenarios ACR1, ACR2, ACR2M, ACR3M, SUB, and SCR. These plots show that scenarios ACR2 and ACR2M, and scenarios 100ACR3 and ACR3M have similar amplification values. The main difference is that the matched scenarios (ACR2M and ACR3M) have a much smaller distribution of PGA rock values than the scaled motions. However, for the same values of PGA rock, the amplification values are the same. Scenarios ACR1 and ACR2, and scenarios 100ACR3 and SUB also have similar values of Fa and Fv. Calculated amplification factors for scenario SCR are greater than the other scenarios and the NGA West 2 GMPE predicted amplification factors for all sites. This could be due to higher frequency content and impedance ratios for scenario SCR ground motions, which represent stable continental region earthquakes, while the NGA West 2 GMPEs were derived for active crustal regions (Nikolaou et al., 2012).

As the PGA rock increases from 0.2 to 0.7 g, the estimated value of Fa for scenario SCR remains the same, whereas the value of Fv increases.

Figure 7.29 and Figure 7.30 compare analysis type and show the calculated amplification factors for total stress equivalent linear, and total and effective stress nonlinear analyses for scenarios 12ACR3, 25ACR3, 50ACR3, 100ACR3, 200ACR3, and 400ACR3 and six sites. The total stress equivalent linear method computes larger Fa and Fv values than the total or effective stress nonlinear methods for all levels of PGA rock. The total stress nonlinear method predicts larger Fa and Fv values than the effective stress nonlinear method only for moderate levels of PGA rock. At small levels of PGA rock the volumetric threshold shear strain γ_{tv} is not reached and no pore pressure generation or soil degradation occurs. At large levels of PGA rock the soil is near failure and highly degraded due to large shear strains, therefore degradation due to pore pressure generation or loading cycles has a minimum effect. Analysis type has a greater effect on the values of Fv than Fa.

7.7 Results of Other Ground Motion Parameters

Figure 7.31 through Figure 7.33 compare amplification ratios of PGA, PGV, T_m, $D_{5\text{-}95}$, and I_a versus the input ground motoin PGA. There are six plots per figure, with one parameter per plot. The plot in the upper left of each page shows the amplification of PGA, the plot in the upper right shows PGV amplification, the middle left plot shows PGD amplification, the middle right shows $D_{5\text{-}95}$ amplification, the lower left plot presents T_m amplification, and the lower right plot in each figure shows the amplification of I_a versus PGA rock. Each plot in all three figures shows results from scenarios 12ACR3, 25ACR3, 50ACR3, 100ACR3, 200ACR3, and 400ACR3. Figure 7.31 shows the effect of soil strength by comparing sites Bay Area II K, Bay Area II K S2, Bay Area II K S4, KIKNET, KIKNET S2, and KIKNET S4, Figure 7.32 shows the effect of soil MRD curves by comparing sites Bay Area II, Bay Area II K, KIKNET40, KIKNET, and KIKNET160, and Figure 7.33 shows the effect of elastic site period by comparing sites MRCE2, HAGP, MRCE1, JSSS, Bay Area, and Bay Area F. Appendix 7F contains similar figures for the other scenarios.

Figure 7.31 through Figure 7.33 show that as PGA rock increases, the PGA, PGV and I_a amplification decrease, the PGD amplification remains the same, and the T_m and $D_{5\text{-}95}$ amplification increase up to a certain threshold PGA rock level and then decrease and become much more spread out. This PGA rock level is around 0.2 g for the KIKNET sites and about 1.0 g for the Bay Area II K sites. The effect of duration (scenario 100ACR3 compared with scenario SUB) and the effect of scaling as opposed to spectral matching (scenarios ACR2 and ACR2M, and 100ACR3 and ACR3M) have a negligible effect on the calculated response (see Appendix 7F).

Figure 7.31 shows that as the shear strength of the soil increases, the PGA, PGV and I_a amplification increase, PGD amplification remain the same, and the T_m and $D_{5\text{-}95}$ amplification decrease up to a threshold PGA rock level and then the trend switches, where sites with greater shear strength have higher T_m and $D_{5\text{-}95}$ amplification. The switch and greater variability in the response of the T_m and $D_{5\text{-}95}$ amplification at greater values of PGA rock is due to soil degradation and pore water pressure buildup in the soil modeled by the effective stress nonlinear

analyses. As will be shown later, the decrease in T_m and D_{5-95} amplification at large PGA rock levels is only observed in the nonlinear effective stress site response analyses and does not occur in the total stress equivalent linear and total stress nonlinear analyses. The soil profile shear strength has no effect on the site response at low levels of PGA rock.

Figure 7.32 shows that as γ_{tv} increases, the PGA, PGV and I_a amplification increase, the PGD amplification remains the same, and the T_m and D_{5-95} amplification decrease. The PGA, PGV and I_a amplification of sites Bay Area II and Bay Area II K converge at large PGA rock values, whereas the values of the KIKNET sites appear to converge at small values of PGA rock. Kamai et al. (2013) also found that soils with greater values of γ_{tv} gave increased PGA amplification values for PGA rock values from 0.01g to 1.5g.

Figure 7.33 shows that there is no discernible difference in the amplification ratios of PGA, PGV, PGD, I_a, T_m, or D_{5-95} based on elastic site period.

Figure 7.34 compares the effect of analysis type on the PGA, PGV, PGD, I_a, T_m, or D_{5-95}versus the input rock PGA, with one plot per ground motion parameter as described above. Each plot presents the results from scenarios 12ACR3, 25ACR3, 50ACR3, 100ACR3, 200ACR3, and 400ACR3 for site Bay Area and the specified ground motion parameter and analysis type. Appendix 7F contains similar figures for other sites.

Figure 7.34 shows that all three analyses types predict similar amplification ratios for all six parameters for small levels of PGA rock. As the level of PGA rock increases, however, total stress equivalent linear analyses predict larger PGA, PGV, I_a, and T_m amplification than total and effective stress nonlinear analyses. All three analyses types predict similar amplification ratios for PGD except for two ground motions where the total stress equivalent linear analyses predict significantly larger amplification ratios. As PGA rock increases, the total stress equivalent linear analyses predict smaller values of D_{5-95} amplification than the total and effective stress nonlinear analyses. However, around 0.8 g PGA rock, the effective stress nonlinear analyses predict decreasing D_{5-95} amplification ratios whereas amplification ratios predicted with total stress nonlinear analyses continue to increase. As mentioned earlier, this difference is thought to be due to soil degradation and pore water pressure buildup in the soil modeled by the effective stress nonlinear analyses, which is not present in the total stress analyses. This difference also causes the effective stress nonlinear analyses to predict smaller amplification ratios for PGV, I_a, and T_m than total stress nonlinear analyses at large values of PGA rock.

7.8 Comparison with Seed et al (1997) PGA 'Bend-over' Curves

Figure 7.35 compares PGA_{soil} vesus PGA_{rock} values, also called 'bend-over' curves, for the effective stress nonlinear site response analyses conducted in this investigation with those given by Seed et al. (1997) for their site E. Figure 7.36 compares the bend-over curves for the three different analyses types used in this investigation (total stress nonlinear, effective stress nonlinear, and total stress equivalent linear) with those given by Seed et al. (1997) for their site E. Seed et al. (1997) E sites are analogous to non-liquefiable and non-organic NEHRP F sites, and are defined as very deep, soft cohesive soil; soft cohesive soil and very strong shaking; and

very high plasticity clays. Each figure shows results for scenarios 12ACR3, 25ACR3, 50ACR3, 100ACR3, 200ACR3, and 400ACR3.

All of the bend-over curves calculated in this study fall below the curves given by Seed et al. (1997), except those for sites Bay Area II K S4 and KIKNET S4 for effective stress nonlinear analyses (Figure 7.35), and sites KIKNET and MRCE1 for total stress equivalent linear analyses (Figure 7.36). Figure 7.35 shows that the bend-over curves for all sites flatten out and appear to have a maximum PGA_{soil} value, which remains constant above a certain threshold PGA_{rock} value. The maximum PGA_{soil} value for a given PGA_{rock} value increases as the shear strength and volumetric threshold shear strain of the soil increase. Figure 7.36 shows that effective stress nonlinear site response analyses predict the smallest values of PGA_{soil} for a given value of PGA_{rock}, followed by total stress nonlinear analyses, and then total stress equivalent linear analysis predicting the greatest values.

7.9 Summary

This study conducted total stress equivalent linear site response analyses for seven base case sites and total and nonlinear effective stress nonlinear site response analyses for 15 sites using 12 ground motion scenarios for a total of 14,541 site response analyses. Chapter 2 described the selection of the scenario target parameters, chapter 3 outlined the selection of the acceleration time series, and chapter 6 explained the selection of the site properties. This chapter discussed the results of the site response analyses, highlighted trends noticed in the data, and compared the results with results from other studies.

Table 7.3 lists the notation used to describe Table 7.4 and Table 7.5. Table 7.4 and Table 7.5 summarize all of the trends noticed in this chapter pertaining to site response analyses in a concise format. Table 7.4 describes how the parameter in each row changes (↑ increase, ↓ decrease) as the ground motion intensity increases, the soil shear strength increases, the soil MRD curves shift to the right (i.e. γ_{tv} increases), or the site elastic period (Ts) increases. Table 7.5 compares parameters predicted for two different scenarios or two analysis types. The cells under these columns describe which of these two is greater than the other for the given parameter (> or <), or whether they are equal (=). For example, the > in the cell in the first column and second row of Table 7.5 signifies that the response spectrum values of scenario ACR1 are greater than the response spectrum values of scenario ACR2 for periods greater than the peak period. As an additional example, the > in the cell in the sixth column and fourth row of Table 7.5 signifies that total stress equivalent linear analyses predict larger amplification for periods less than the peak amplification period than total stress nonlinear analyses. A D in a cell of Table 7.4 or Table 7.5 means that the parameter increases for some sites and decreases for other sites, and that the trend depends on other factors, an NE in a cell means that no trend was found in this study between the specified parameters (negligible effect), and NA means that the comparison is not applicable.

The results of this chapter show that the intensity of the input ground motion and the strength and MRD curves of the soil are very important for site response analyses of non-liquefiable NEHRP F site soils. This is because non-liquefiable NEHRP F sites consist of soft soils and their behavior is very nonlinear. As the intensity of the ground motion increases, the effect of

the soil strength on the site response results increases. The results of this chapter also indicate that scaling and spectral matching give the same average response values, and that there is little difference between pulse-like and no pulse motions, and between long duration and short duration motions, other than the differences in the input ground motions. Finally, this chapter showed that total stress equivalent linear analyses give significantly different results than nonlinear analyses. This is due to soil nonlinearity, which the total stress equivalent linear analyses cannot capture as well as the nonlinear analyses. However, there was not a significant difference between total and effective stress nonlinear analyses methods. The lack of difference between these two methods is because the sites used in this study contain soils with high volumetric threshold shear strain values, below which no degradation or pore water pressure generation takes place. In addition, the soils tested are extremely weak soils, and once they pass the volumetric threshold shear strain they quickly fail, at which point the soil has already degraded to a level where the effect of cyclic degradation and pore pressure generation on the results are negligible.

This chapter analyzed the results of the site response analyses in a qualitative manner. The following chapter discusses the development of a simplified procedure to estimate the response spectra for non-liquefiable NEHRP F sites using the data generated by the site response analyses.

7.10 References

Abrahamson, N.A., Silva, W.J., and Kamai, R. "Update of the AS08 Ground-Motion Prediction Equations Based on the NGA-West2 Data Set." PEER Report 2013/04, *Pacific Earthquake Engineering Research Center*, University of California, Berkeley, CA.

Ancheta T.D., Darragh R.B., Stewart J.P., Seyhan E., Silva W.J., Chiou B.S.-J., Wooddell K.E., Graves R.W., Kottke A.R., Boore D.M., Kishida T., Donahue J.L., (2013). "PEER NGA-West 2 database," PEER Report 2013/03, *Pacific Earthquake Engineering Research Center*, University of California, Berkeley, CA.

Baker, J.W., and Cornell, C.A., (2003). "Uncertainty specification and propagation for loss estimation using FOSM methods." Proceedings, *9th International Conference on Applications of Statistics and Probability in Civil Engineering* (ICASP9), San Francisco, California, July 6-9.

Bazzurro, P., and Cornell, C.A. (2004). "Ground-Motion Amplification in Nonlinear Soil Sites with Uncertain Properties." *Bulletin of the Seismological Society of America*, 94(6), pp. 2090–2109.

Boore, D.M., Stewart, J.P., Seyhan, E., Atkinson, G.M., (2013). "NGA-West2 Equations for Predicting Response Spectral Accelerations for Shallow Crustal Earthquakes." PEER Report 2013/05, *Pacific Earthquake Engineering Research Center*, University of California, Berkeley, CA.

Campbell, K.W., and Yousef Bozorgnia, (2013). "NGA-West2 Campbell-Bozorgnia Ground Motion Model for the Horizontal Components of PGA, PGV, and 5%-Damped Elastic Pseudo-Acceleration Response Spectra for Periods Ranging from 0.01 to 10 sec." PEER Report 2013/06, *Pacific Earthquake Engineering Research Center*, University of California, Berkeley, CA.

Chapman, M.C., Martin, J.R., Olgun, C.G., and Beale, J.N. (2006). "Site-Response Models for Charleston, South Carolina, and Vicinity Developed from Shallow Geotechnical Investigations." *Bulletin of the Seismological Society of America*, 96(2), pp. 467–489.

Chiou, B.S.J., and Robert R. Youngs, (2013). "Update of the Chiou and Youngs NGA Ground Motion Model for Average Horizontal Component of Peak Ground Motion and Response Spectra." PEER Report 2013/07, *Pacific Earthquake Engineering Research Center*, University of California, Berkeley, CA.

Darendeli, M. B. (2001). "Development of a new family of normalized modulus reduction and material damping curves." PhD dissertation, Univ. of Texas at Austin, Austin, Texas.

Dickenson, S.E. (1994). "Dynamic Response of Soft and Deep Cohesive Soils During the Loma Prieta Earthquake of October 17, 1989." PhD dissertation, University of California, Berkeley.

Dobry R., Borcherdt, R.D., Crouse, C.B., Idriss, I.M., Joyner, W.B., Martin, G.R., Power, M.S., Rinne, E.E., and Seed R.B. (2000). "New site coefficients and site classification system used in recent building seismic code provisions." *Earthquake Spectra*, 16(1), 41- 67.

Huang, Y.N., Whittaker, A.S., Luco, N. (2010). "NEHRP site amplification factors and the NGA relationships." Earthquake Spectra, 26(2) 583–593.

Kaklamanos, J., Bradely, B.A., Thompson, E.M., and Baise, L.G. (2013). "Critical Parameters Affecting Bias and Variability in Site-Response Analyses Using KiK-net Downhole Array Data." *Bulletin of the Seismological Society of America*, 103(3), pp. 1733–1749.

Kamai, R, Abrahamson, N.A., and Silva, W.J.,."Nonlinear Horizontal Site Response for the NGA-West2 Project." PEER Report 2013/12, *Pacific Earthquake Engineering Research Center*, University of California, Berkeley, CA.

Kishida, T., Boulanger R.W., Abrahamson N.A., Wehling T.M., Driller M.W. (2009). "Regression Models for Dynamic Properties of Highly Organic Soils." *J. of Geotech. and Geoenvir. Eng.*, ASCE, 135(4).

Kottke, A.R. and Rathje, E.M. (2008). "Technical manual for Strata." PEER Report 2008/10, *Pacific Earthquake Engineering Research Center*, University of California, Berkeley, CA.

Li, W. and Assimaki, D. (2010). "Site- and Motion-Dependent Parametric Uncertainty of Site-Response Analyses in Earthquake Simulations." *Bulletin of the Seismological Society of America,* 100(3), pp. 954–968.

Matasovic, Neven, and M. Vucetic (1995) "Generalized Cyclic Degradation-Pore Pressure Generation Model for Clays," *Journal of Geotechnical and Geoenvironmental Engineering*, ASCE, Vol. 121, No. 1, pp 33-42.

Matasovic, Neven, and M. Vucetic (1993). "Cyclic Characterization of Liquefiable Sands," *Journal of Geotechnical and Geoenvironmental Engineering*, ASCE, Vol. 119, No. 11, pp 1805-1822.

Melchers, R.E. (1999). *Structural Reliability Analysis and Prediction*. John Wiley and Sons, Chichester, UK.

Nikolaou, S., Mylonakis, G., and Edinger, P.(2001). "Evaluation of Site Factors for Seismic Bridge Design in the New York City Area." *Journal of Bridge Engineering*, ASCE, Vol. 6, pp. 564-576.

Nikolaou, S., Go, J., Beyzaei, C., Moss, C., and Deming, P. (2012). "Geo-Seismic Design in the Eastern United States: State of Practice." *Geotechnical Engineering State of the Art and Practice: Keynote Lectures from GeoCongress 2012*, ASCE, March 25 – 29, Oakland, CA, pp. 828-854.

Rathje, E.M., and Kottke, A.R., (2011). "Relative Differences Between Equivalent Linear and Nonlinear Site Response Methods." In Proceedings of *5th International Conference on Earthquake Geotechnical Engineering*, Santiago, Chile, January 10-13.

Roblee, C.J., Silva, W.J., Toro, G.R., and Abrahamson, N. (1996). "Variability in Site-Specific Seismic Ground-Motion Design Predictions." In *Uncertainty in the Geologic Environment: From Theory to Practice*, C. D. Shakelford and P. P. Nelson (Editors), ASCE Geotech Special Publication No. 58, Madison Wisconsin, 31 July–3 August 1996.

Rodriguez-Marek, A., Bray, J.D., and Abrahamson, N.A., (2001). "An Empirical Geotechnical Site Response Procedure." *Earthquake Spectra*, 17(1), pp. 65-87.

Seed R.B., Chang S.W., Dickenson S.E., Bray J.D. (1997). "Site-dependent Seismic Response Including Recent Strong Motion Data," in *Seismic Behaviour of Ground and Geotechnical Structures*, Seco e Pinto, P. S., ed., Proc. of Spec. Session on Earthquake Geotechnical Engineering, XIV International Conf. On Soil Mechanics and Foundation Engineering, Hamburg, Germany, A.A. Balkema, pp. 125-134, Sept. 6-12.

Silva, W. J, Abrahamson, N.A., Toro, G., Costantino C. (1997). "Description and validation of the stochastic ground motion model." *Pacific Engineering and Analysis Report*, available at www.pacificengineering.org/rpts_page1.shtml

Silva, W.J., Lee, K. (1987). "WES RASCAL code for synthesizing earthquake ground motions." *State-of-the-Art for Assessing Earthquake Hazards in the United States*, Report 24, U.S. Army Engineers Waterways Experiment Station, Miscellaneous Paper S-73-1.

Stewart, J.P., and Seyhan, E. (2013). “Semi-Empirical Nonlinear Site Amplification and its Application in NEHRP Site Factors.” PEER Report 2013/13, *Pacific Earthquake Engineering Research Center*, University of California, Berkeley, CA.

Stewart, J.P., Kwok, A.O., Hashash, Y.M.A, Matasovic, N., Pyke, R., Wang, Z., Yang, Z. (2008). “Benchmarking of Nonlinear Geotechnical Ground Response Analysis Procedures.” Pacific Earthquake Engineering Research Center Report 2008/04.

Walling, M., Silva, W.J., Abrahamson, N.A (2008). “Nonlinear site amplification factors for constraining the NGA models.” Earthquake Spectra, 24(1) 243–255.

Table 7.1: Ground motion scenarios used in the site response analyses

ID	# of GM	LUP (s)	HUP (s)	Region	Notes
12ACR3	40	0.04	13.33	ACR	Scenario ACR3 scaled motions multiplied by 0.125
25ACR3	40	0.04	13.33	ACR	Scenario ACR3 scaled motions multiplied by 0.25
50ACR3	40	0.04	13.33	ACR	Scenario ACR3 scaled motions multiplied by 0.50
100ACR3	40	0.04	13.33	ACR	Scenario ACR3 scaled motions
200ACR3	40	0.04	13.33	ACR	Scenario ACR3 scaled motions multiplied by 2
400ACR3	40	0.04	13.33	ACR	Scenario ACR3 scaled motions multiplied by 4
ACR3M	40	0.04	13.33	ACR	Scenario ACR3 matched motions
ACR1	11	0.04	8.85	ACR	
ACR2	40	0.04	6.15	ACR	Scenario ACR2 scaled motions
ACR2M	40	0.04	6.15	ACR	Scenario ACR2 matched motions
SUB	11	0.04	5	SUB	
SCR	11	0.02	10	SCR	

LUP = lowest useable period, HUP = highest useable period

ACR = active crustal region, SUB = subduction zone, SCR = stable continental region

Table 7.2: Properties of sites used in site response analyses

ID	Approximate Location	NEHRP	Vs_{30} (m/s)	Depth (m)	T_s (s)	Th (m)	Vs_{mean} (m/s)	$\gamma_{0.5,mean}$ (%)	CRR_{min}
Bay Area	SF Bay Area	E	125	185	2.66	19.25	101.4	0.0580	0.30
Bay Area F	SF Bay Area	F	119	189	2.84	36.85	119.6	0.0699	0.29
Bay Area II	SF Bay Area	F	79	32	1.58	9.75	34.8	0.1216	0.61
Bay Area II K	SF Bay Area	F	79	32	1.58	9.75	34.8	0.7238	0.58
Bay Area II K S2	SF Bay Area	F	79	32	1.58	9.75	34.8	0.9831	1.15
Bay Area II K S4	SF Bay Area	F	79	32	1.58	9.75	34.8	1.8661	2.35
HAGP	Guayaquil, Ecuador	F	127	50	1.23	37.00	136.3	0.0733	0.22
JSSS	Ottawa, Canada	F	143	115	1.93	56.00	173.1	0.0597	0.29
KIKNET40	Hokkaido, Japan	E	140	103	1.56	13.40	99.0	0.0483	0.30
KIKNET	Hokkaido, Japan	F	140	103	1.56	13.40	99.0	0.0707	0.30
KIKNET160	Hokkaido, Japan	F	140	103	1.56	13.40	99.0	0.1026	0.30
KIKNET S2	Hokkaido, Japan	F	140	103	1.56	13.40	99.0	0.0781	0.61
KIKNET S4	Hokkaido, Japan	F	140	103	1.56	13.40	99.0	0.0912	1.22
MRCE1	New York City	F	128	90	1.69	15.15	94.3	0.0886	0.80
MRCE2	New York City	F	162	30	0.74	17.20	112.0	0.0582	0.33

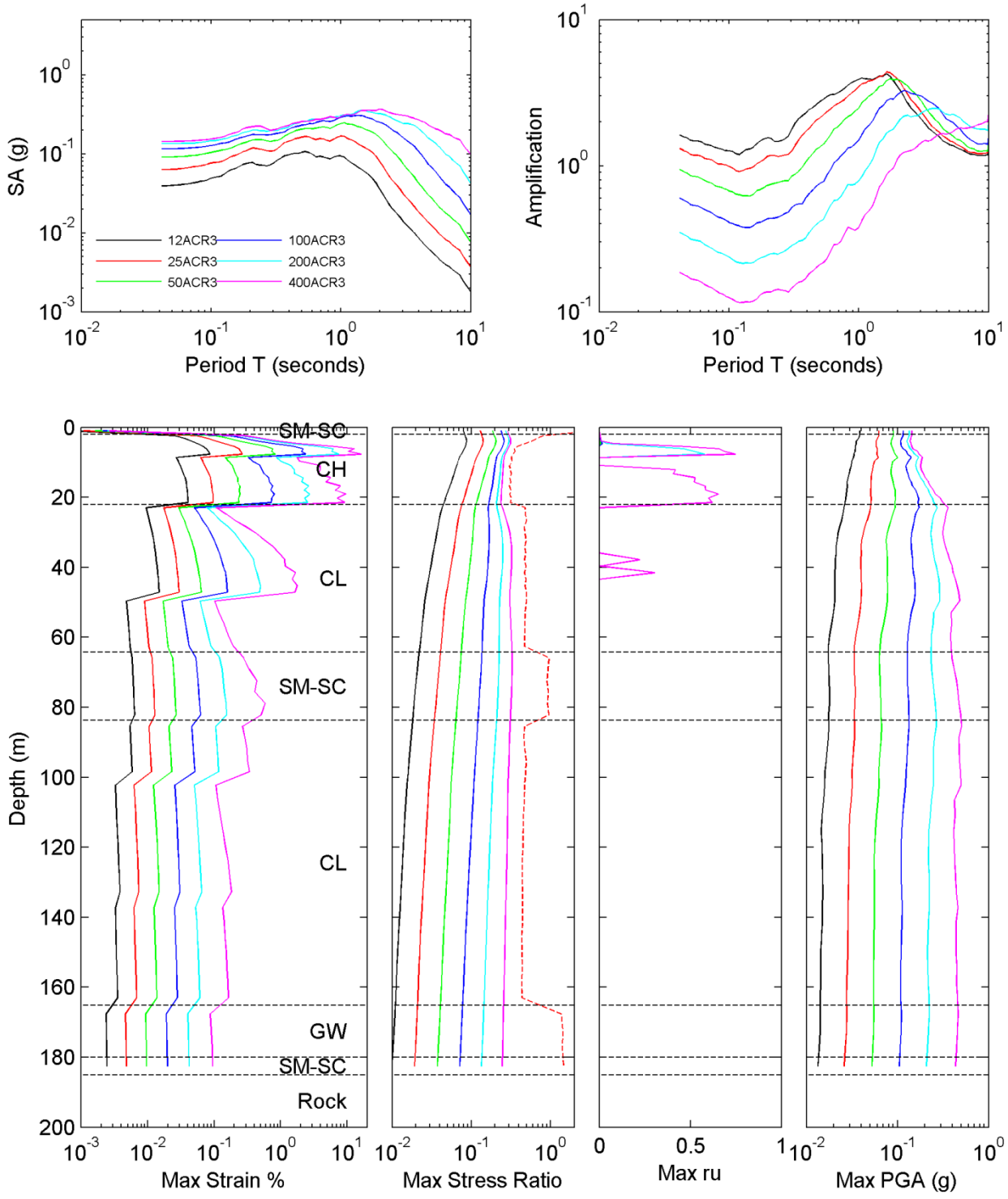

Figure 7.1: Effective stress nonlinear site response analyses for site Bay Area and scenarios 12ACR3, 25ACR3, 50ACAR3, 100ACR3, 200ACR3, and 400ACR3. Horizontal dotted black lines represent soil type boundaries, where soil types are defined by USCS designation, and the vertical dotted red line is the shear strength ratio (Su/σ'_v).

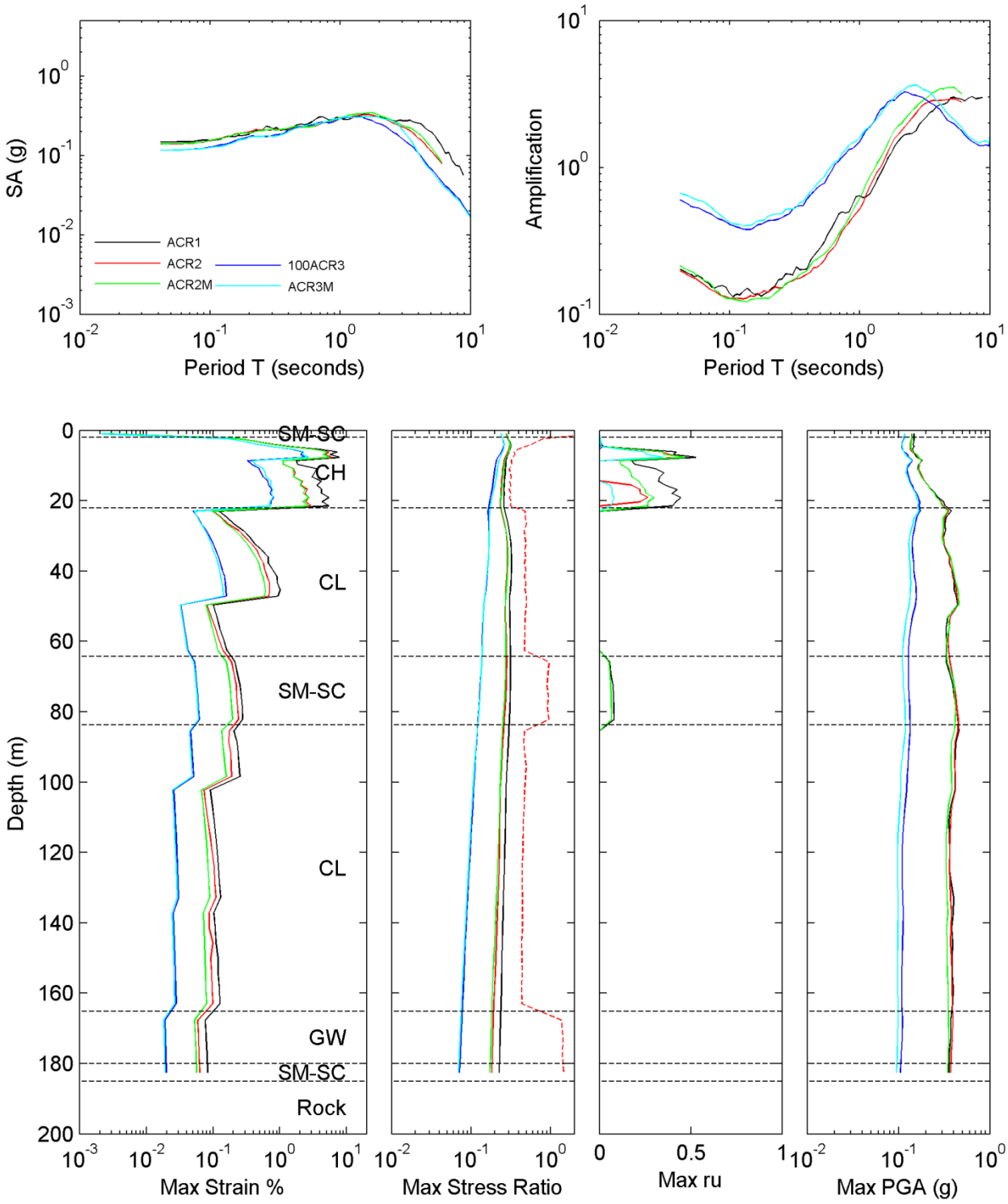

Figure 7.2: Effective stress nonlinear site response analyses for site Bay Area and scenarios ACR1, ACR2, ACR2M, 100ACR3, and ACR3M. Horizontal dotted black lines represent soil type boundaries, where soil types are defined by USCS designation, and the vertical dotted red line is the shear strength ratio (Su/σ'_v).

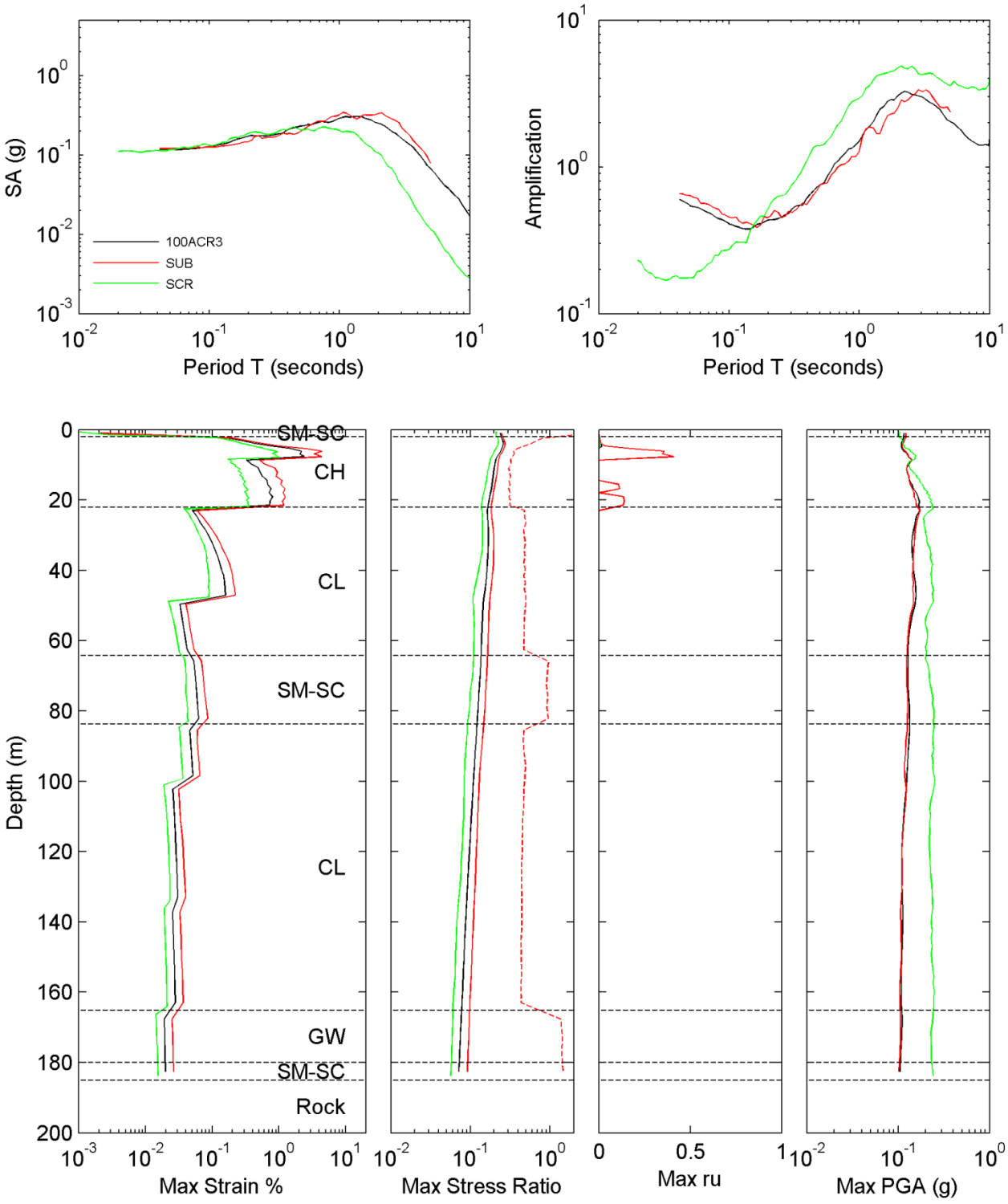

Figure 7.3: Effective stress nonlinear site response analyses for site Bay Area and scenarios 100ACR3, SUB, and SCR. Horizontal dotted black lines represent soil type boundaries, where soil types are defined by USCS designation, and the vertical dotted red line is the shear strength ratio (Su/σ'_v).

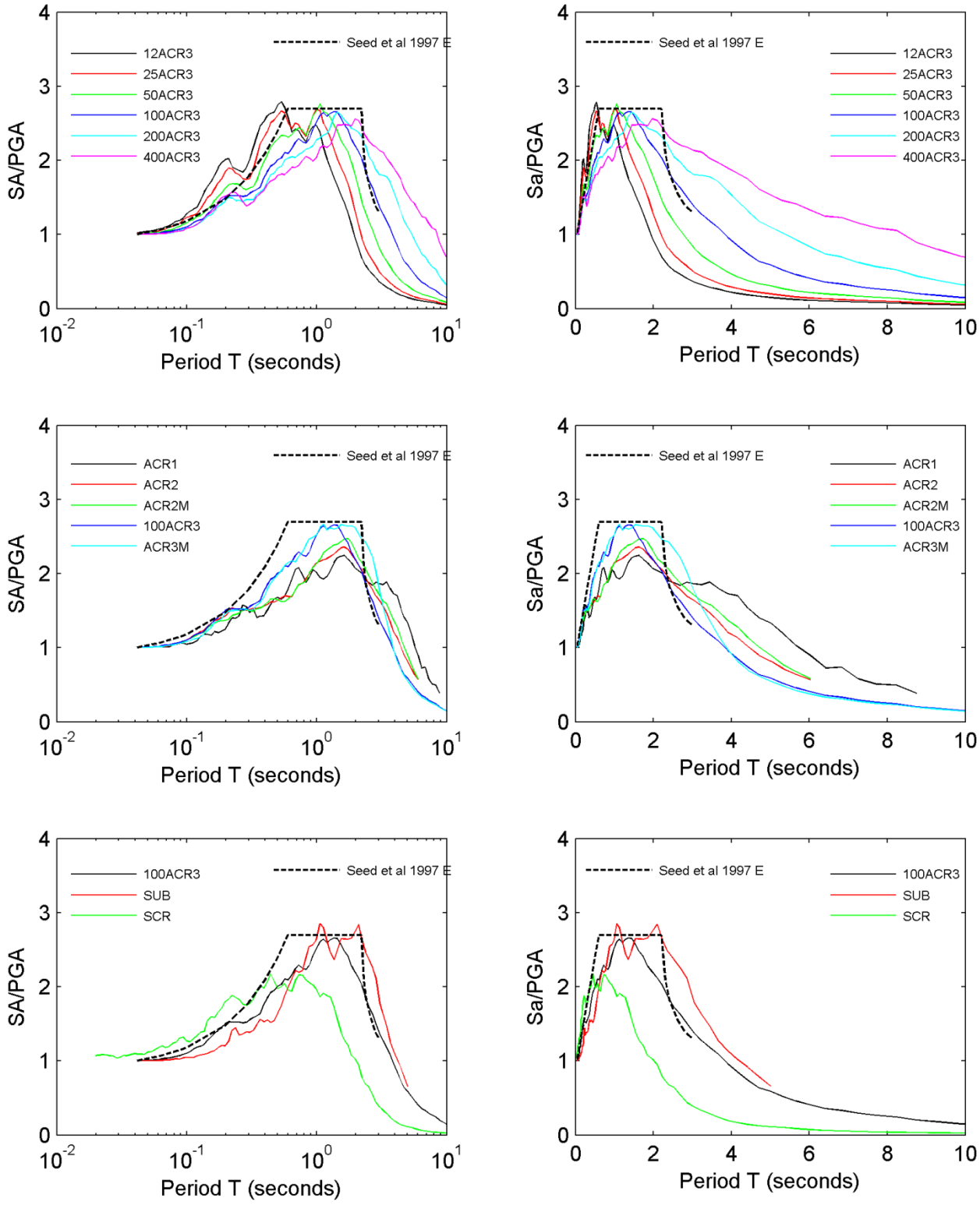

Figure 7.4: Effective stress nonlinear site response analyses for site Bay Area, plots in the left column are in semi-log space and plots in the right column are in arithmetic space

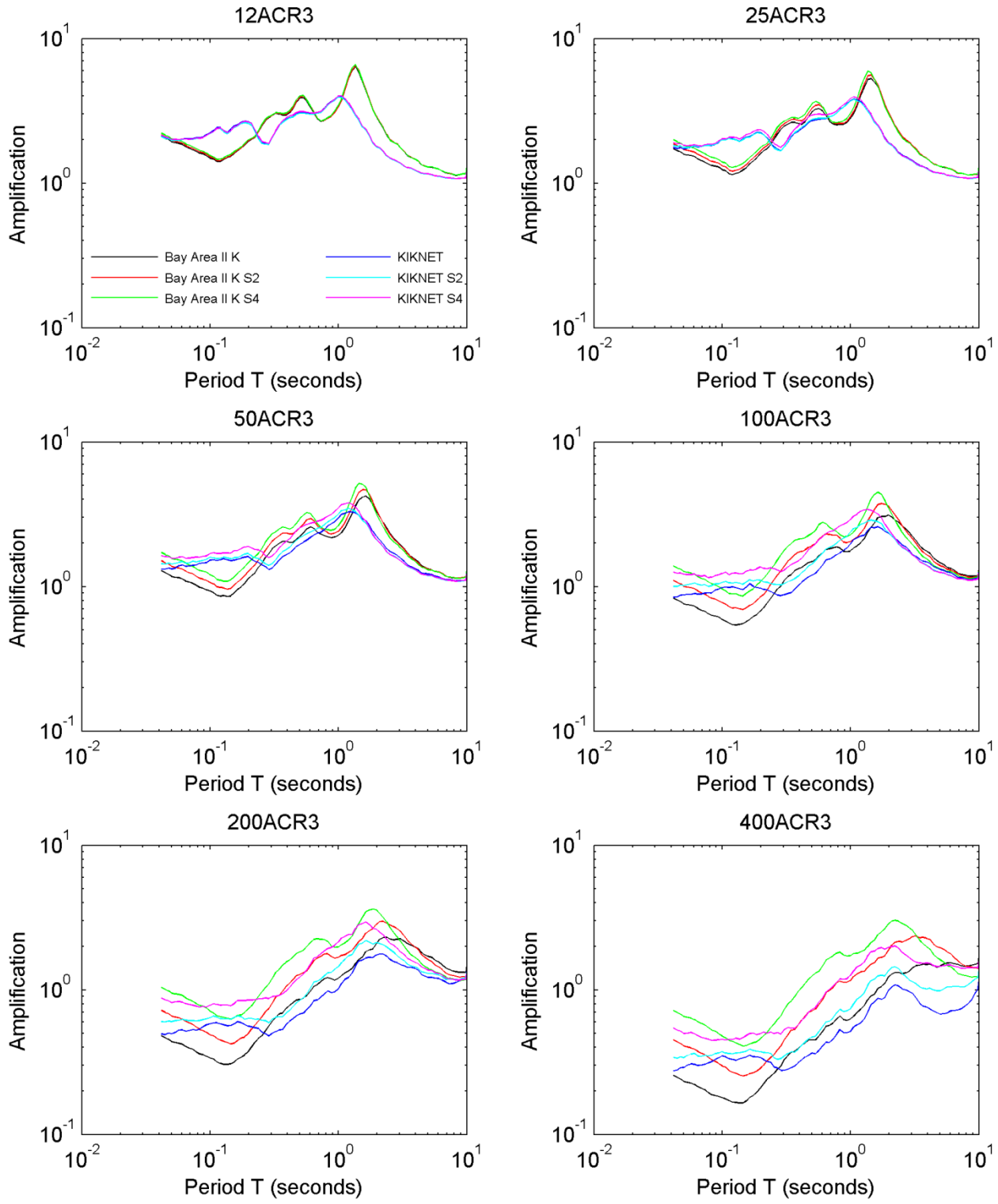

Figure 7.5: Comparison of the effect of site profile strength on the amplification of effective stress nonlinear analyses for scenarios 12ACR3, 25ACR3, 50ACR3, 100ACR3, 200ACR3, and 400ACR3

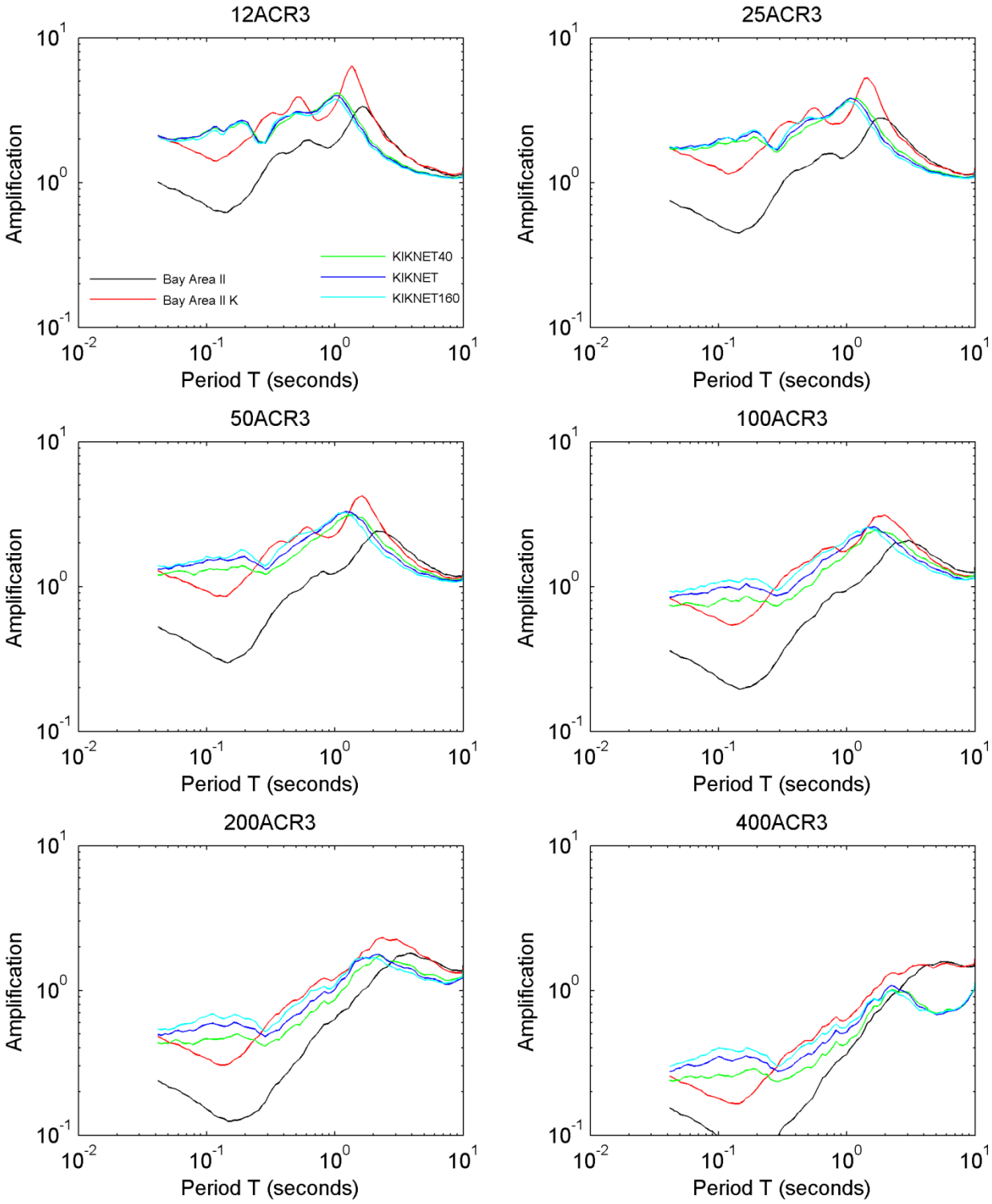

Figure 7.6: Comparison of the effect of site profile MRD curves on the amplification of effective stress nonlinear analyses for scenarios 12ACR3, 25ACR3, 50ACR3, 100ACR3, 200ACR3, and 400ACR3

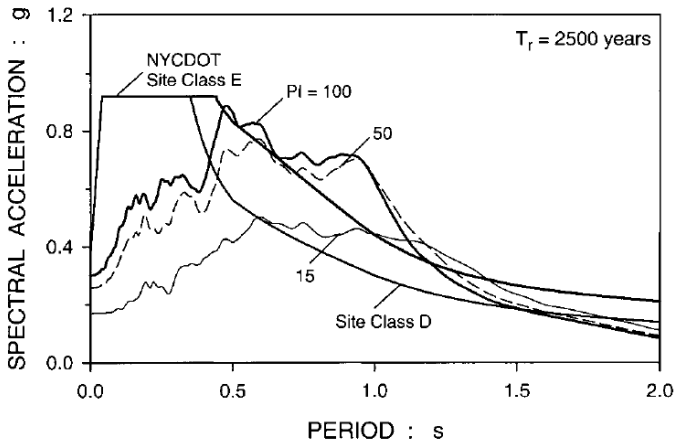

Figure 7.7: Effect of MRD curves on response spectra (from Nikolaou et al. 2001)

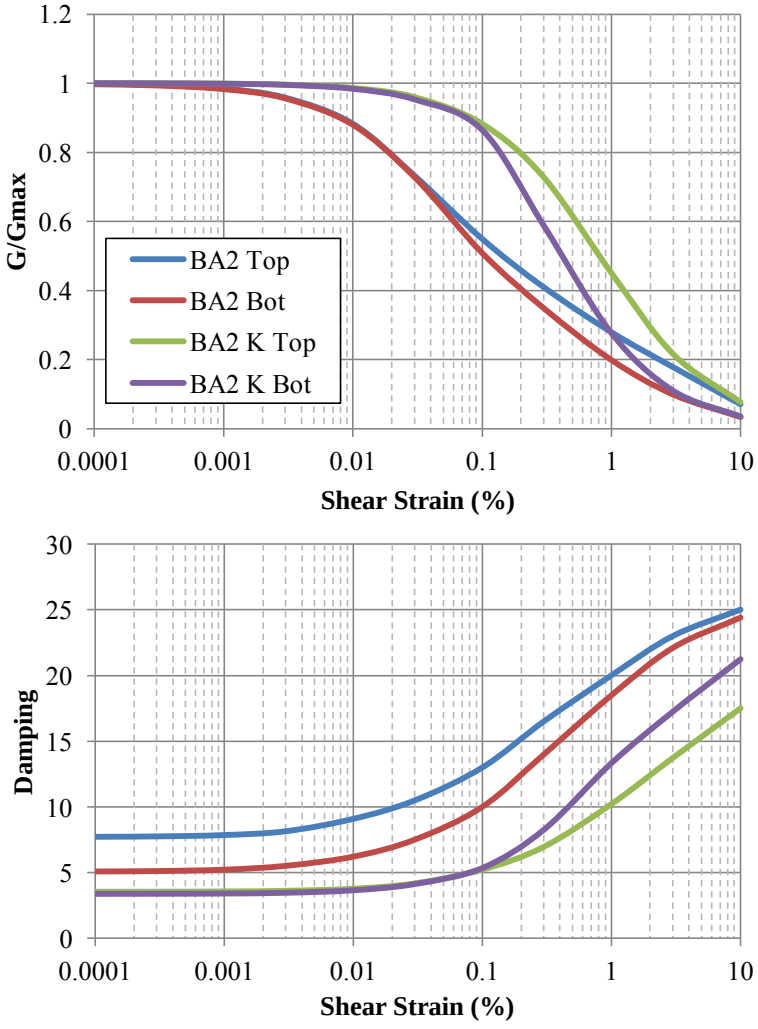

Figure 7.8: Comparison of the MRD curves for the top (Top) and bottom (Bot) layers of the OH soil deposit for site Bay Area II and Bay Area II K

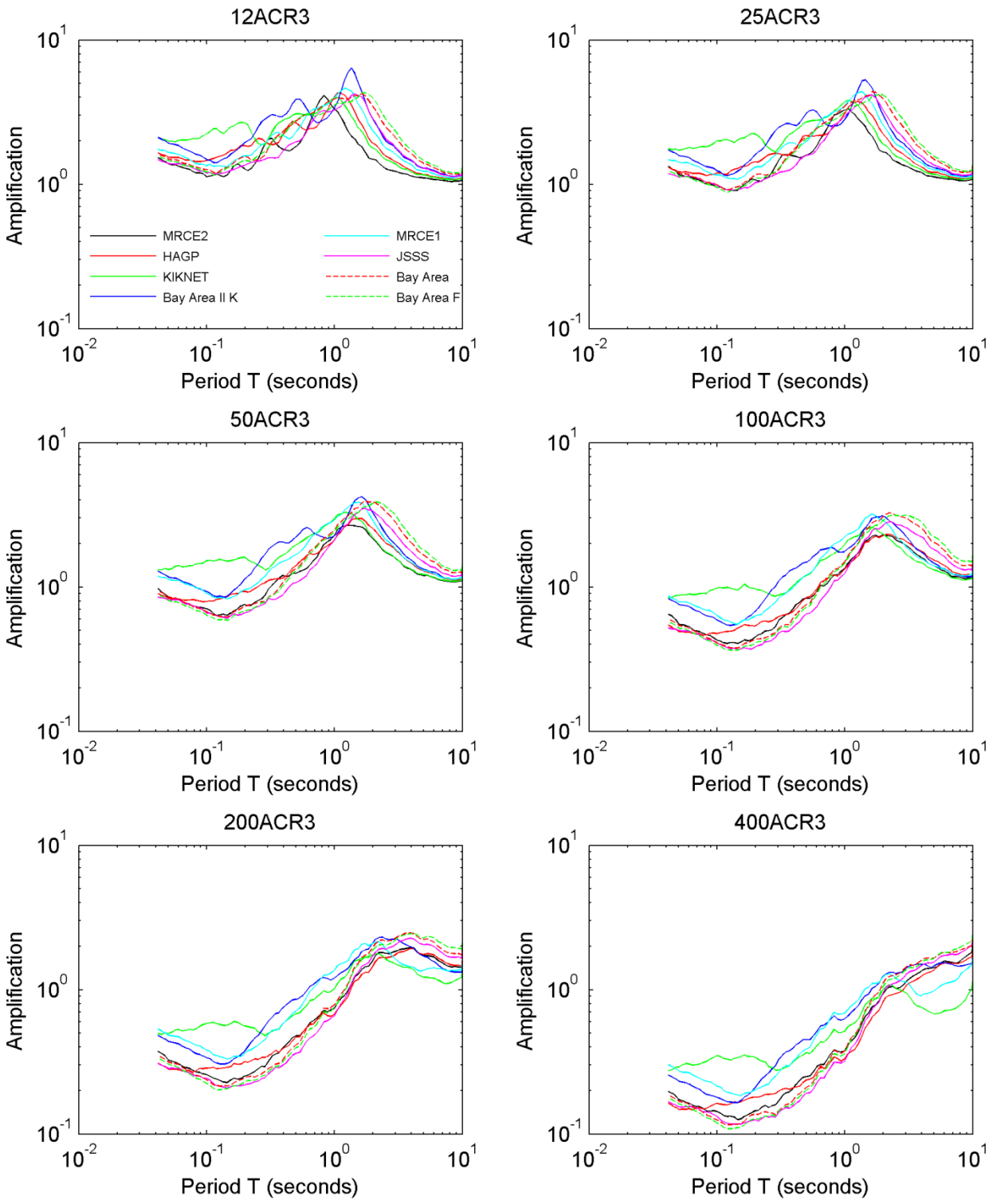

Figure 7.9: Comparison of the effect of the elastic site period on the amplification of effective stress nonlinear analyses for scenarios 12ACR3, 25ACR3, 50ACR3, 100ACR3, 200ACR3, and 400ACR3

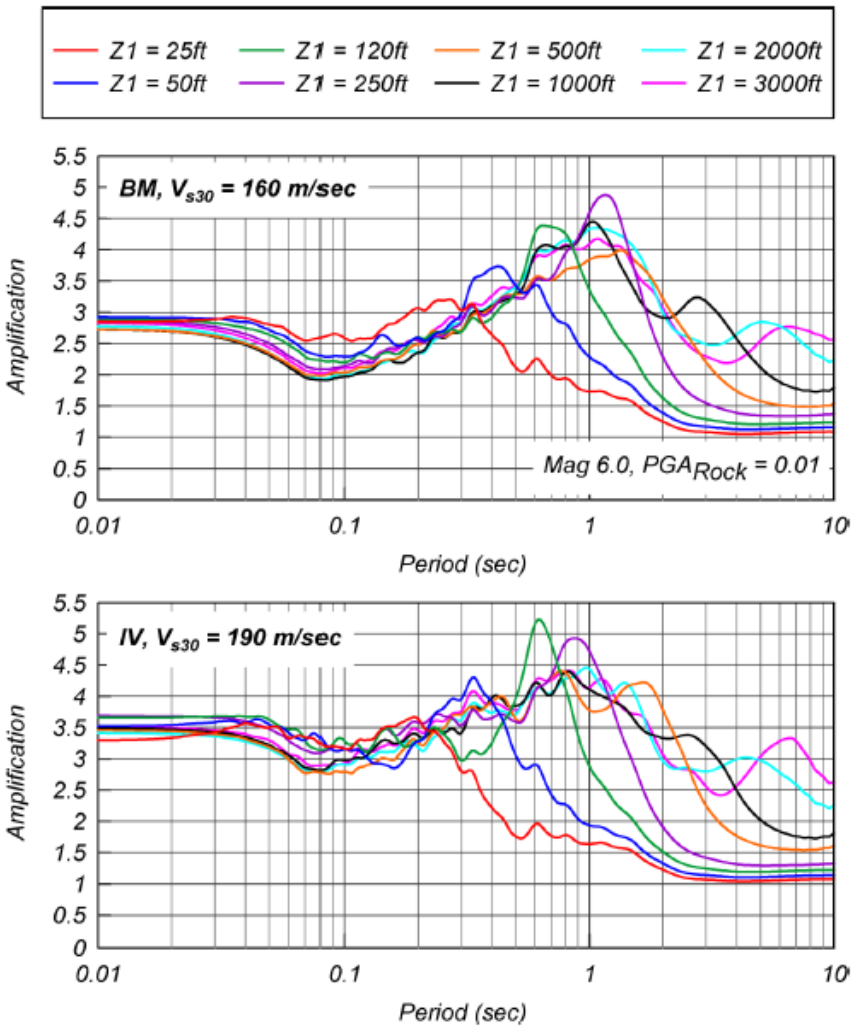

Figure 7.10: Amplification factors for various depths and for sites with Vs_{30} = 160 m/s using the Bay Mud MRD curves, and for sites with Vs_{30} = 190 m/s using the Imperial Valley MRD curves. Input ground motions with PGA = 0.01 g (from Kamai et al., 2013).

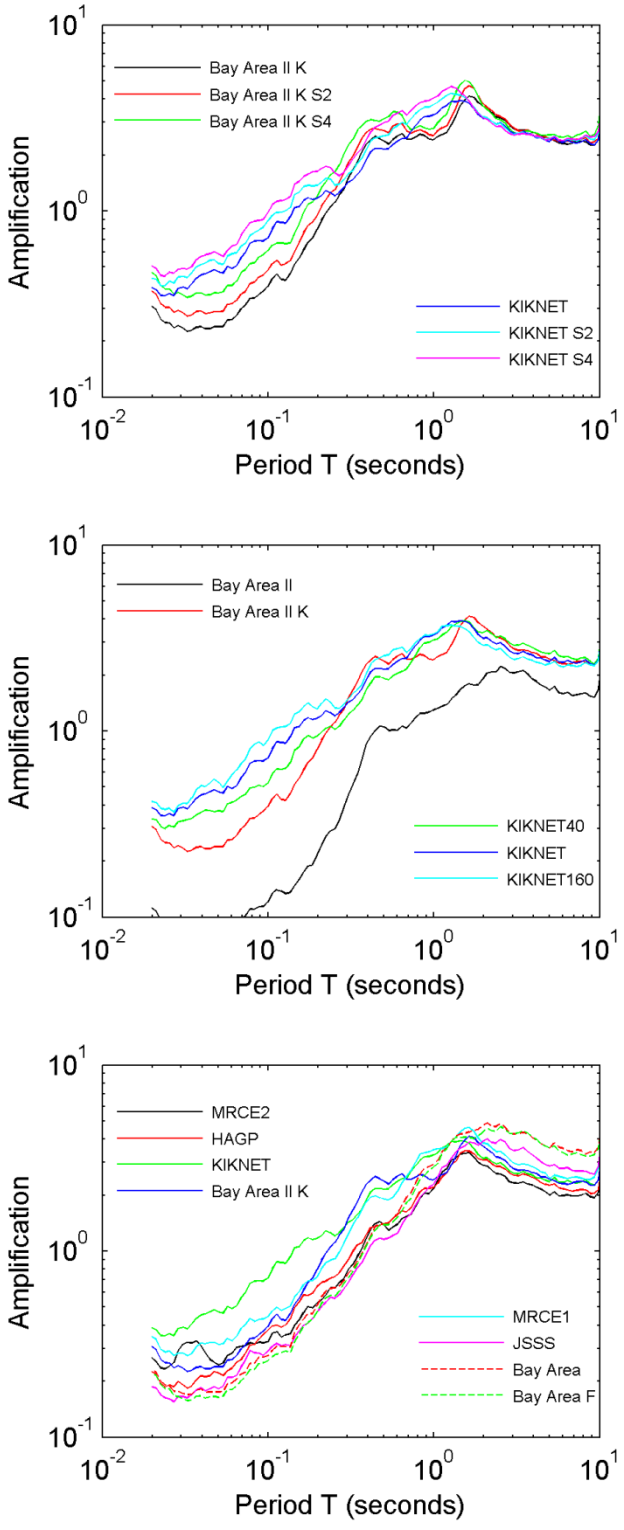

Figure 7.11: Comparison of amplification for effective stress nonlinear analyses of scenario SCR

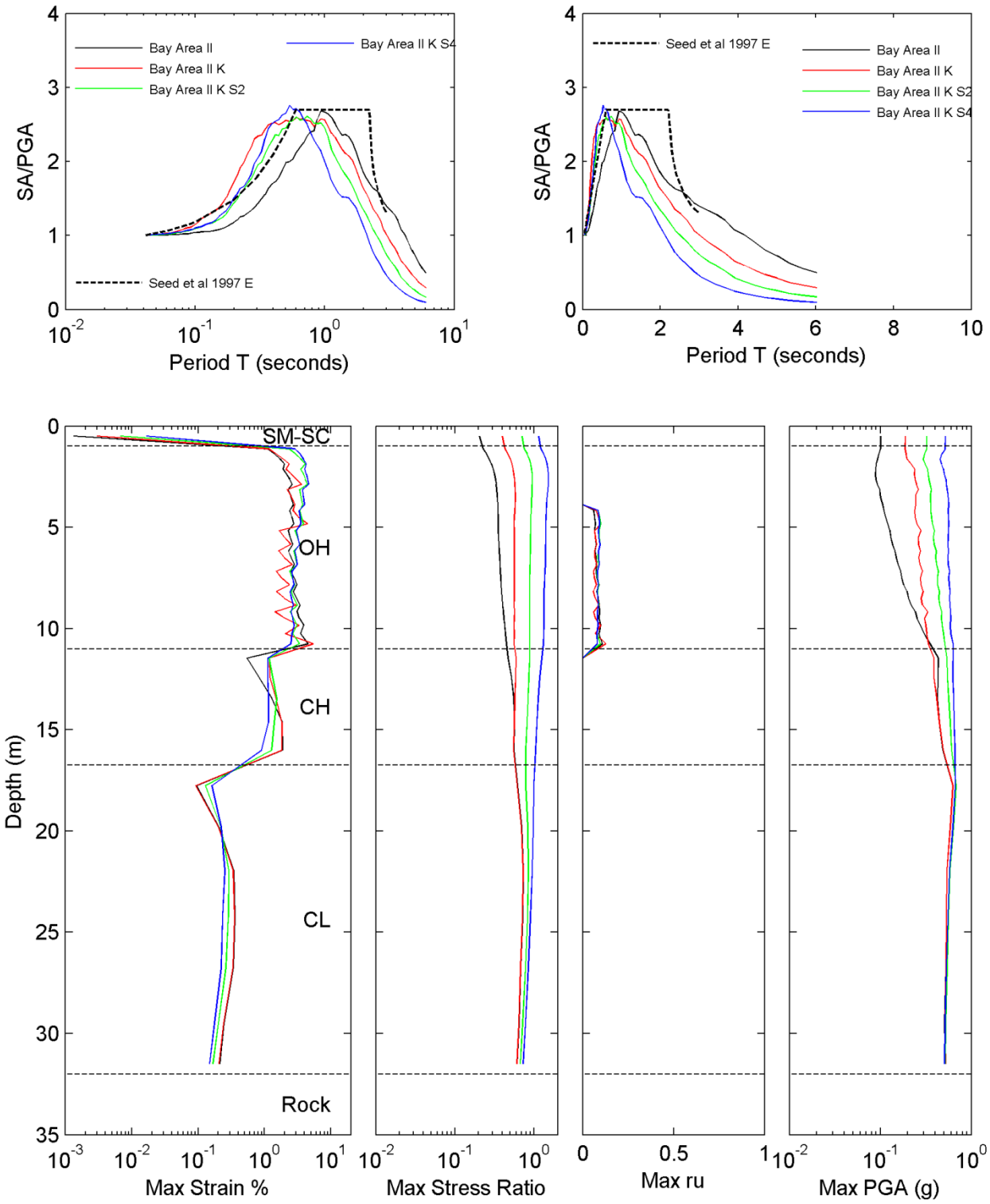

Figure 7.12: Comparison of the effect of site strength and MRD curves on spectral shape and maximum shear strain, shear stress ratio, pore pressure ratio (r_u), and PGA with depth for Bay Area II sites, scenario ACR2, and effective stress nonlinear analyses

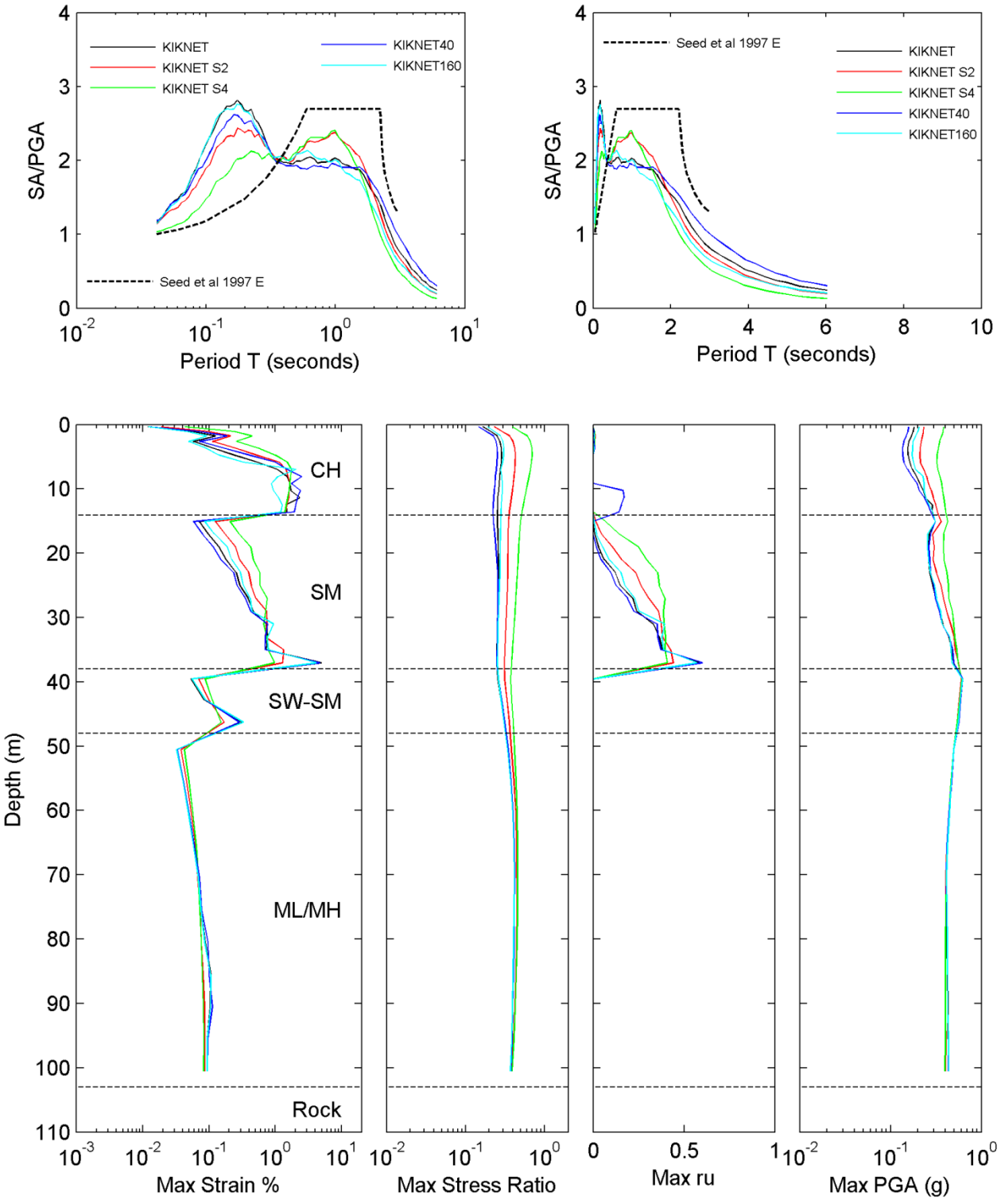

Figure 7.13: Comparison of the effect of site strength and MRD curves on spectral shape and maximum shear strain, shear stress ratio, pore pressure ratio (r_u), and PGA with depth for KIKNET sites, scenario ACR2, and effective stress nonlinear analyses

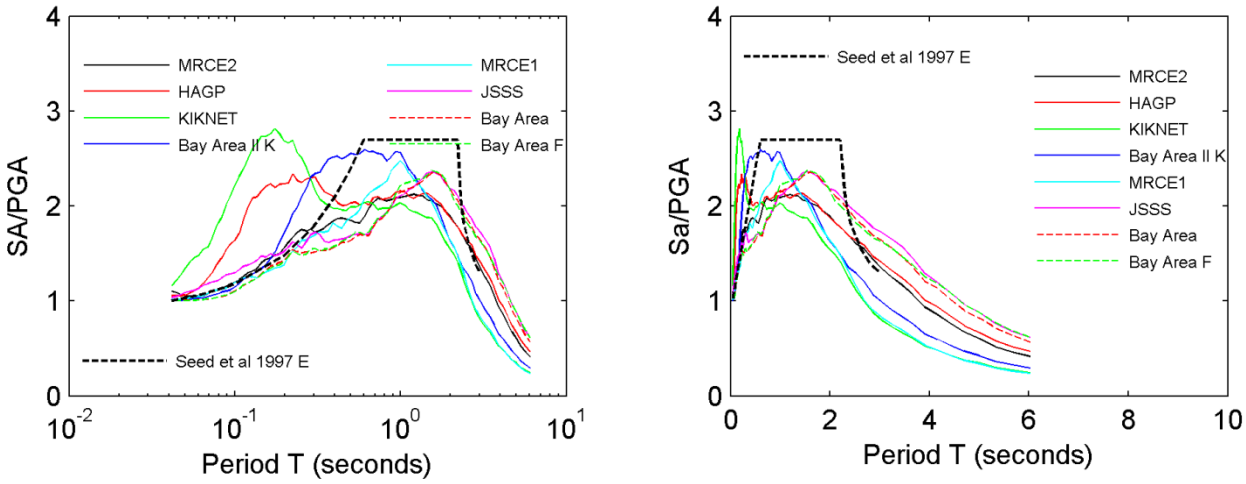

Figure 7.14: Comparison of the effect of elastic site period on the spectral shape for effective stress nonlinear analyses of scenario 100ACR3 and various sites

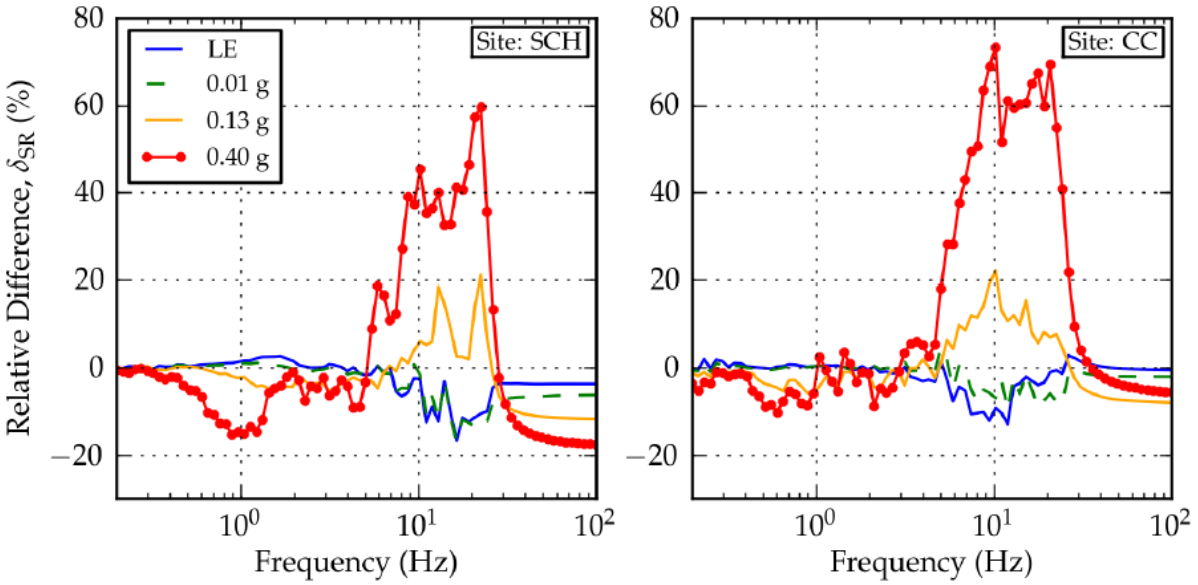

Figure 7.15: Relative difference between analysis types for linear elastic site properties (LE), and for three different input ground motion PGA levels, where δ_{SR} = (Amp_{NL} – Amp_{EQL})/Amp_{EQL}*100%, Amp_{NL} is the amplification of the total stress nonlinear analyses, and Amp_{EQL} is the amplification of the total stress equivalent linear analyses (from Rathje and Kottke, 2011)

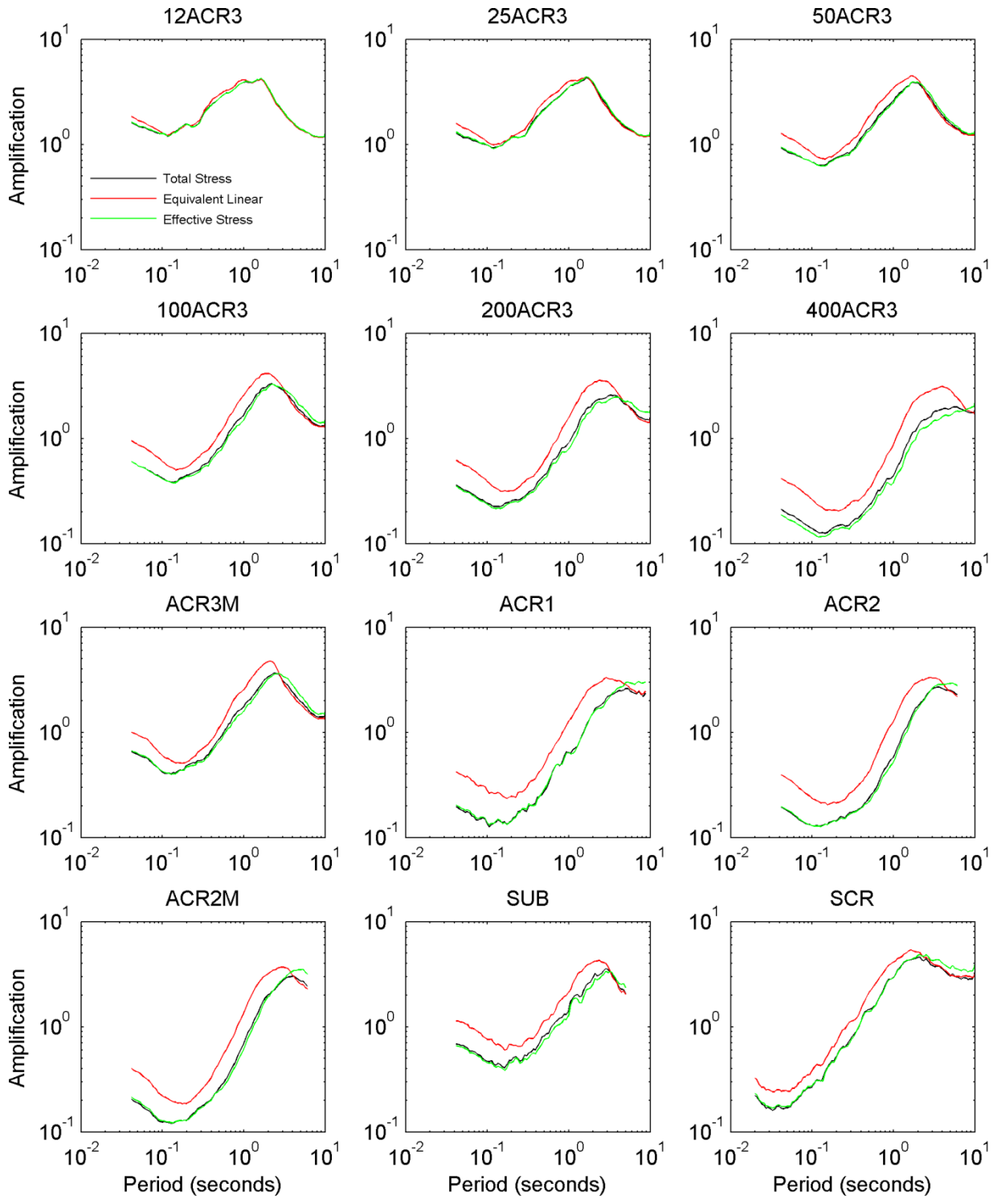

Figure 7.16: Comparison of analysis type (total stress nonlinear, total stress equivalent linear, and effective stress nonlinear) for site Bay Area

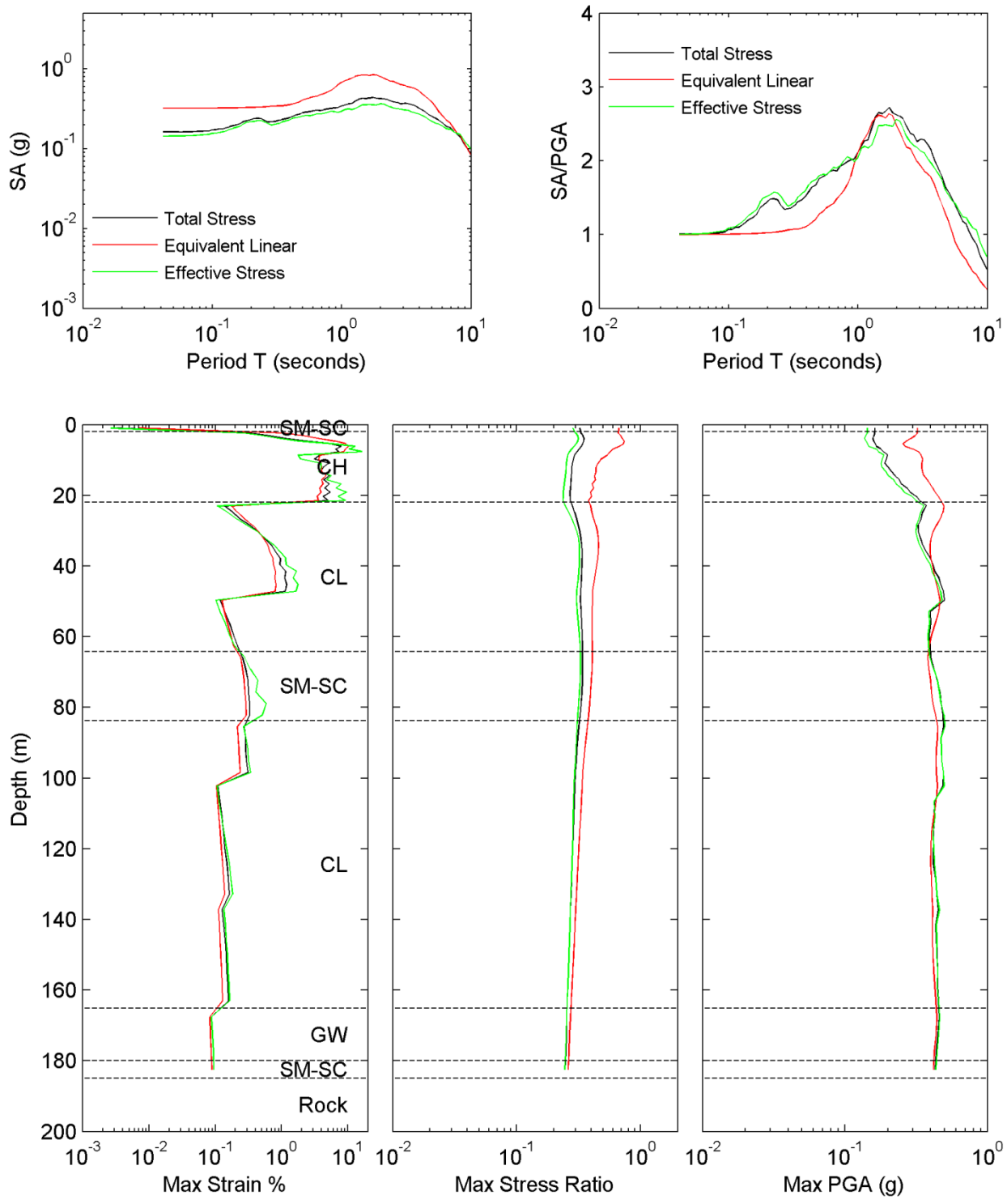

Figure 7.17: Comparison of analysis type (total stress nonlinear, total stress equivalent linear, and effective stress nonlinear) for site Bay Area and scenario 400ACR3

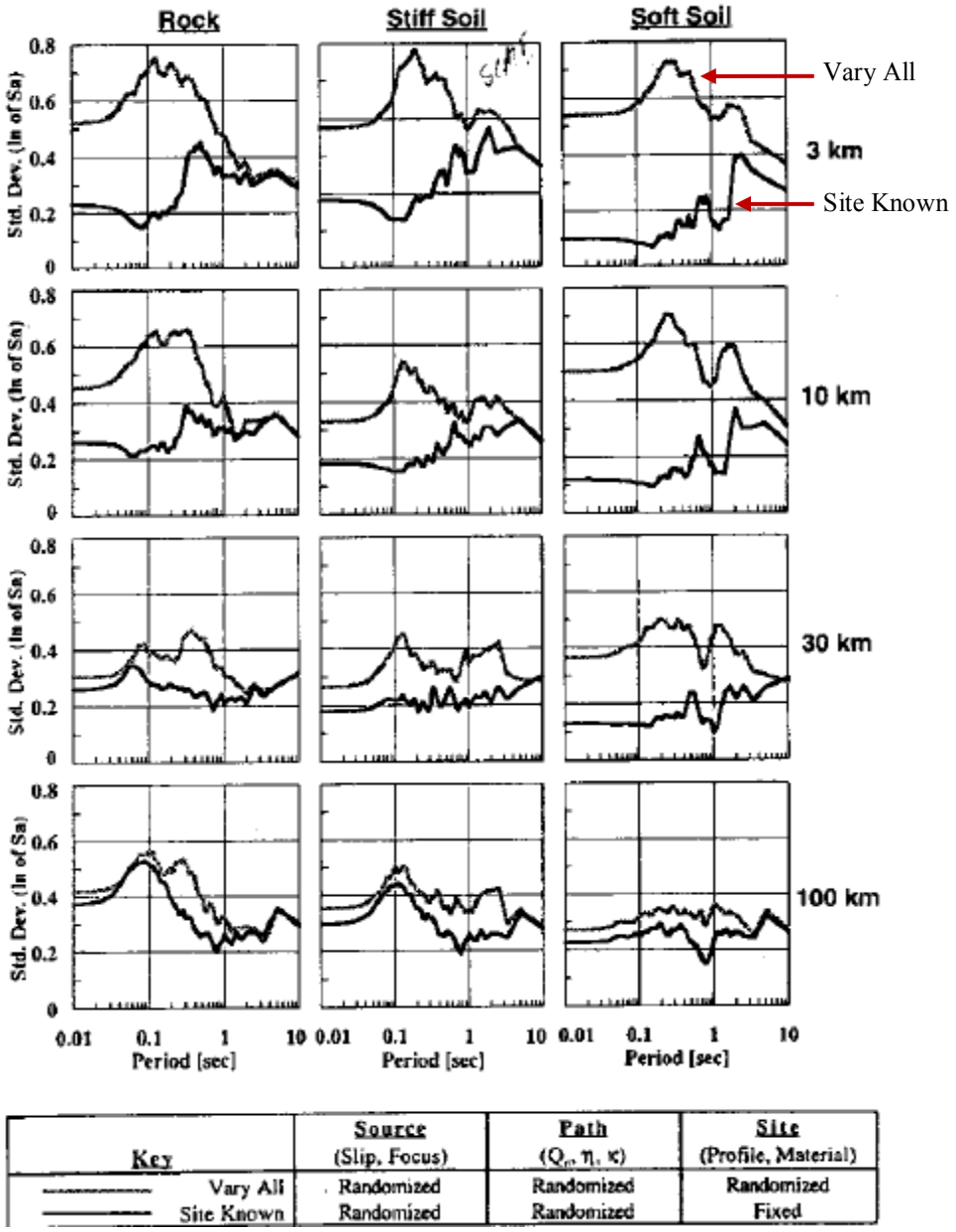

Key	Source (Slip, Focus)	Path (Q_o, η, κ)	Site (Profile, Material)
Vary All	Randomized	Randomized	Randomized
Site Known	Randomized	Randomized	Fixed

Figure 7.18: Comparison of standard deviation for surface response spectra when site properties are known or not known for different sites, ground motion intensity (distance), and periods (From Roblee et al., 1996)

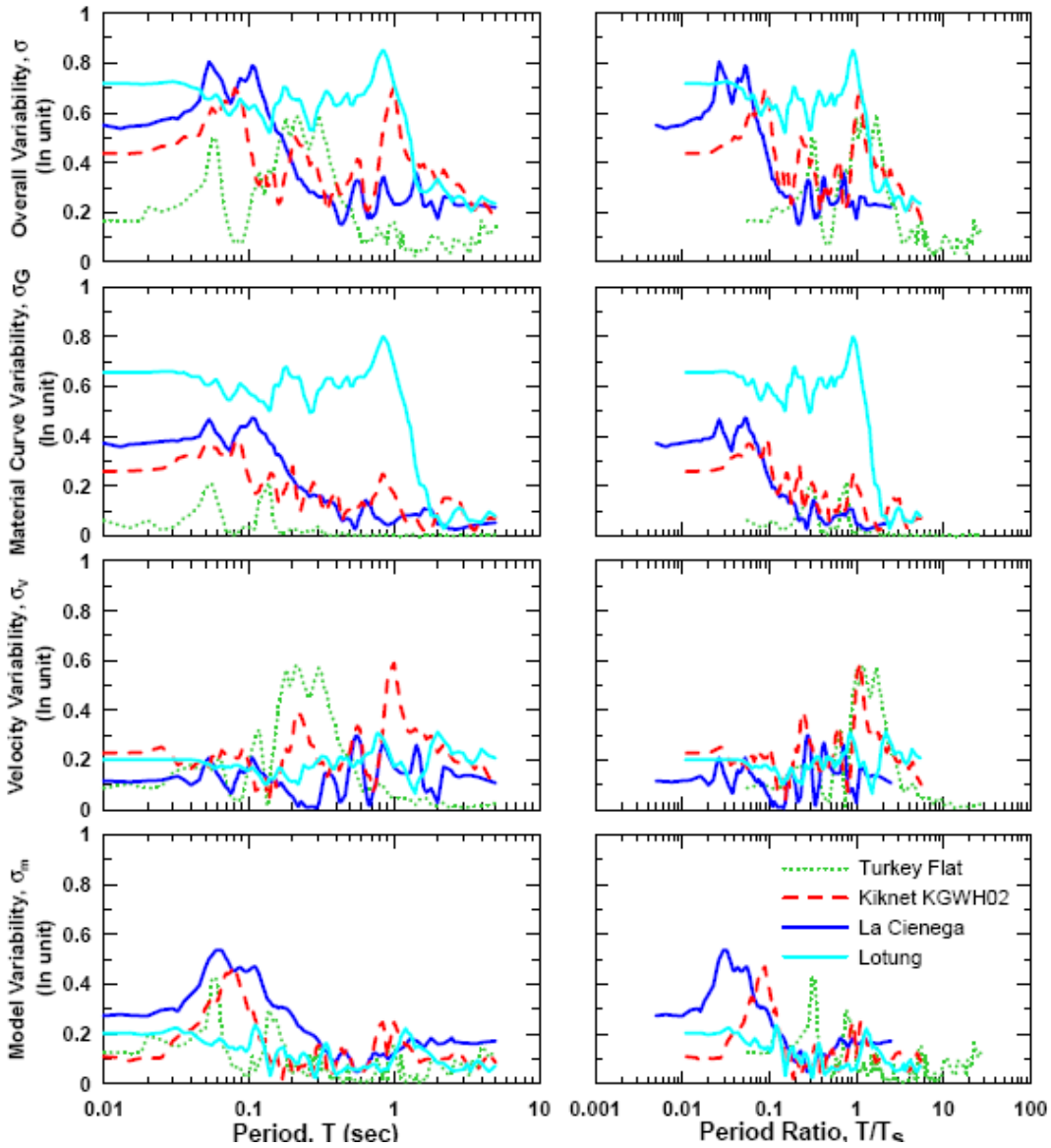

Figure 7.19: Comparison of standard deviations due to various sources for four vertical array sites (From Stewart et al., 2008)

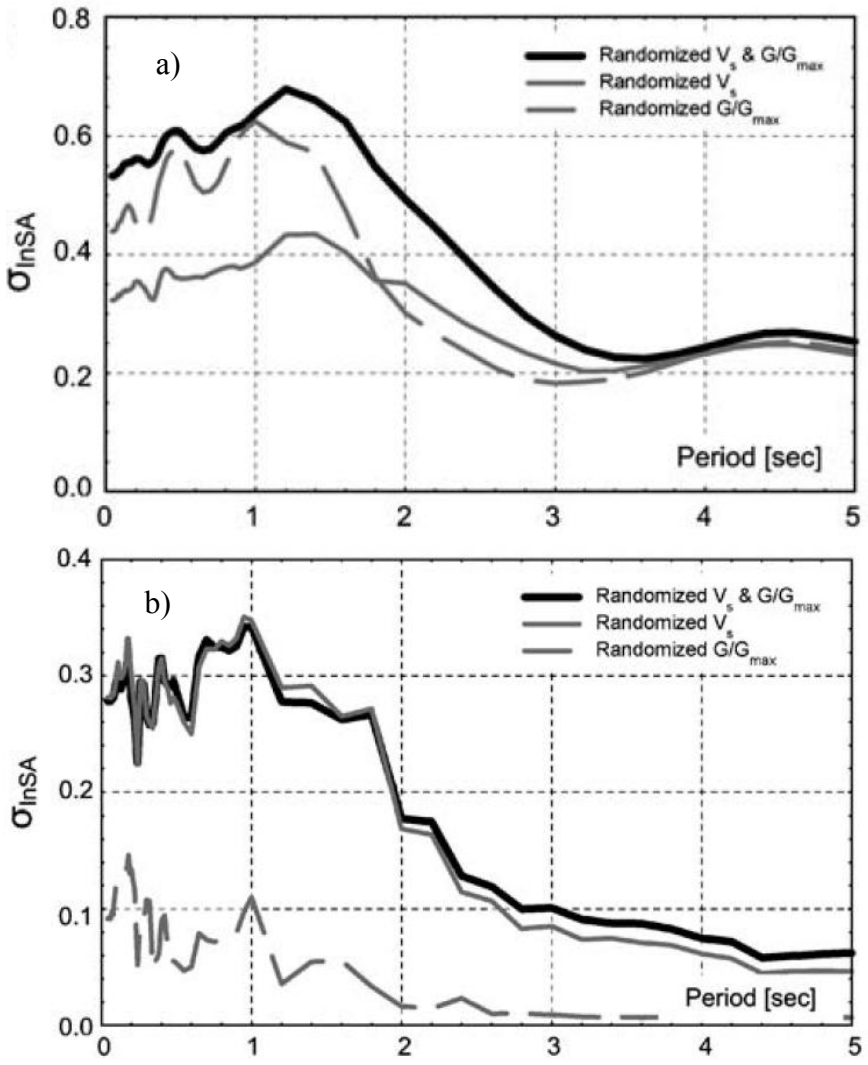

Figure 7.20: Comparison of standard deviations due to randomization of Vs profile and soil MRD curves for a) strong input ground motions and b) weak input ground motions (From Li and Assimaki, 2010)

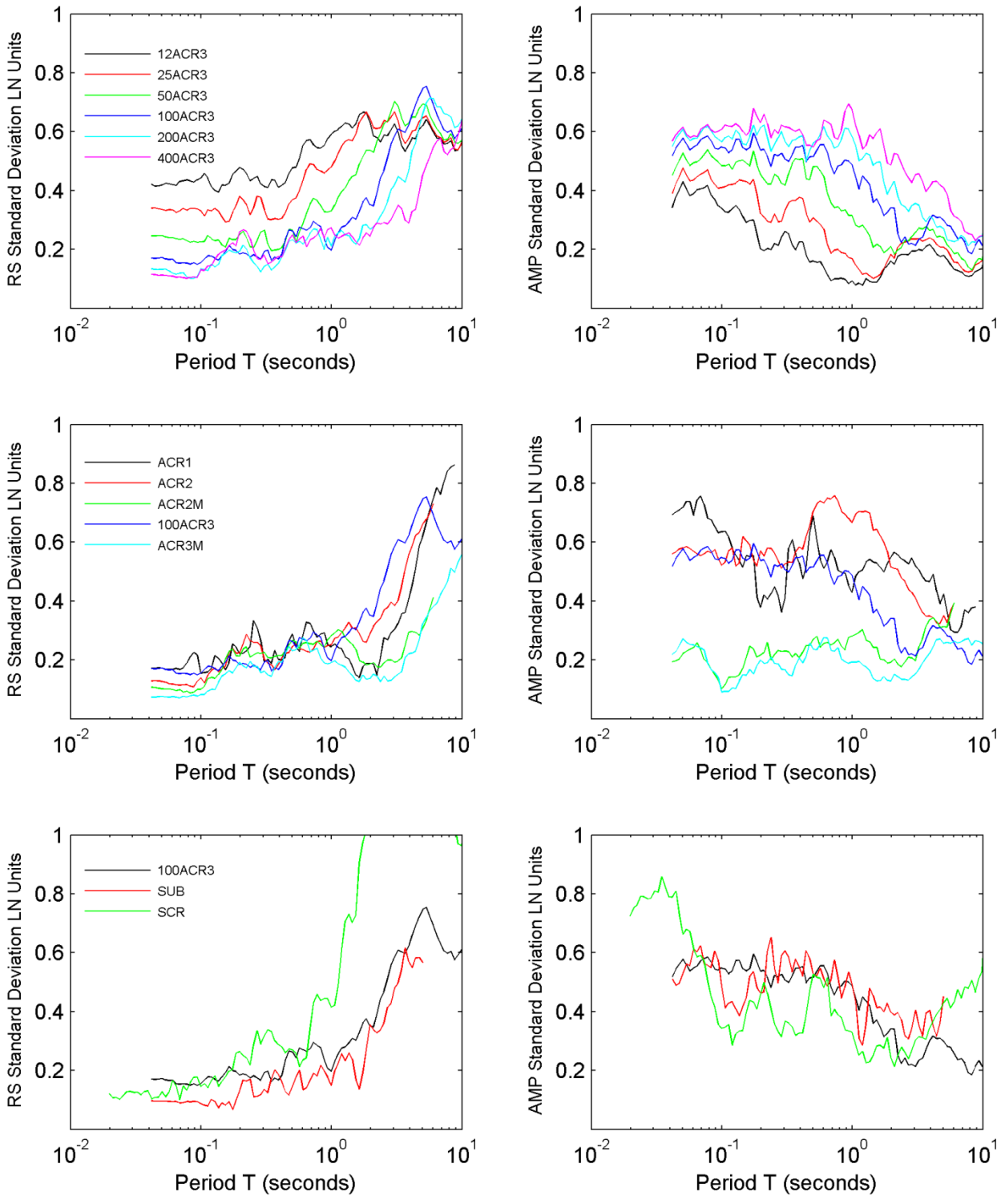

Figure 7.21: Comparison of the response spectra and amplification standard deviations for site Bay Area

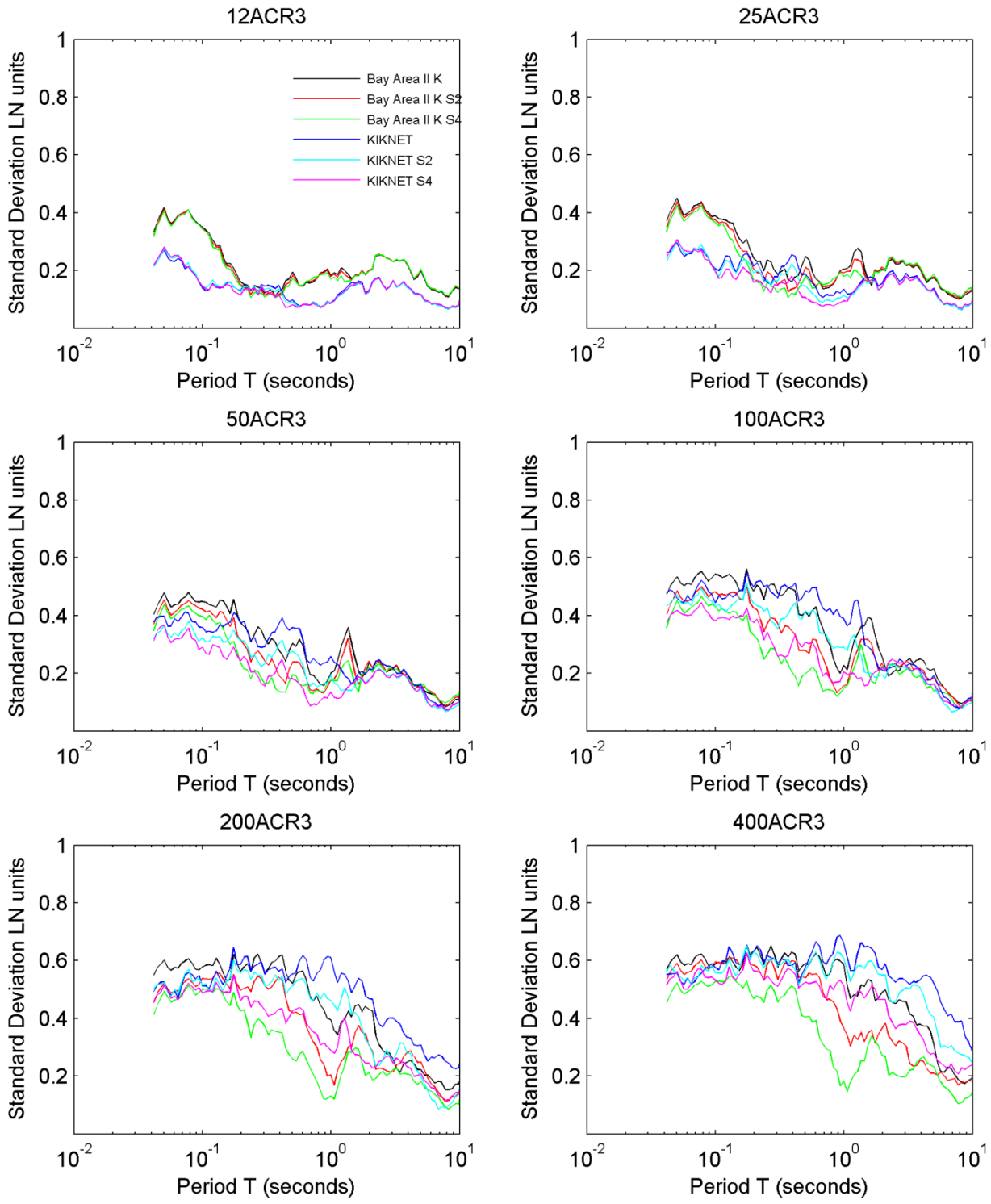

Figure 7.22: Comparison of the effect of soil strength on the standard deviation of amplification of effective stress nonlinear analyses for scenarios 12ACR3, 25ACR3, 50ACR3, 100ACR3, 200ACR3, and 400ACR3

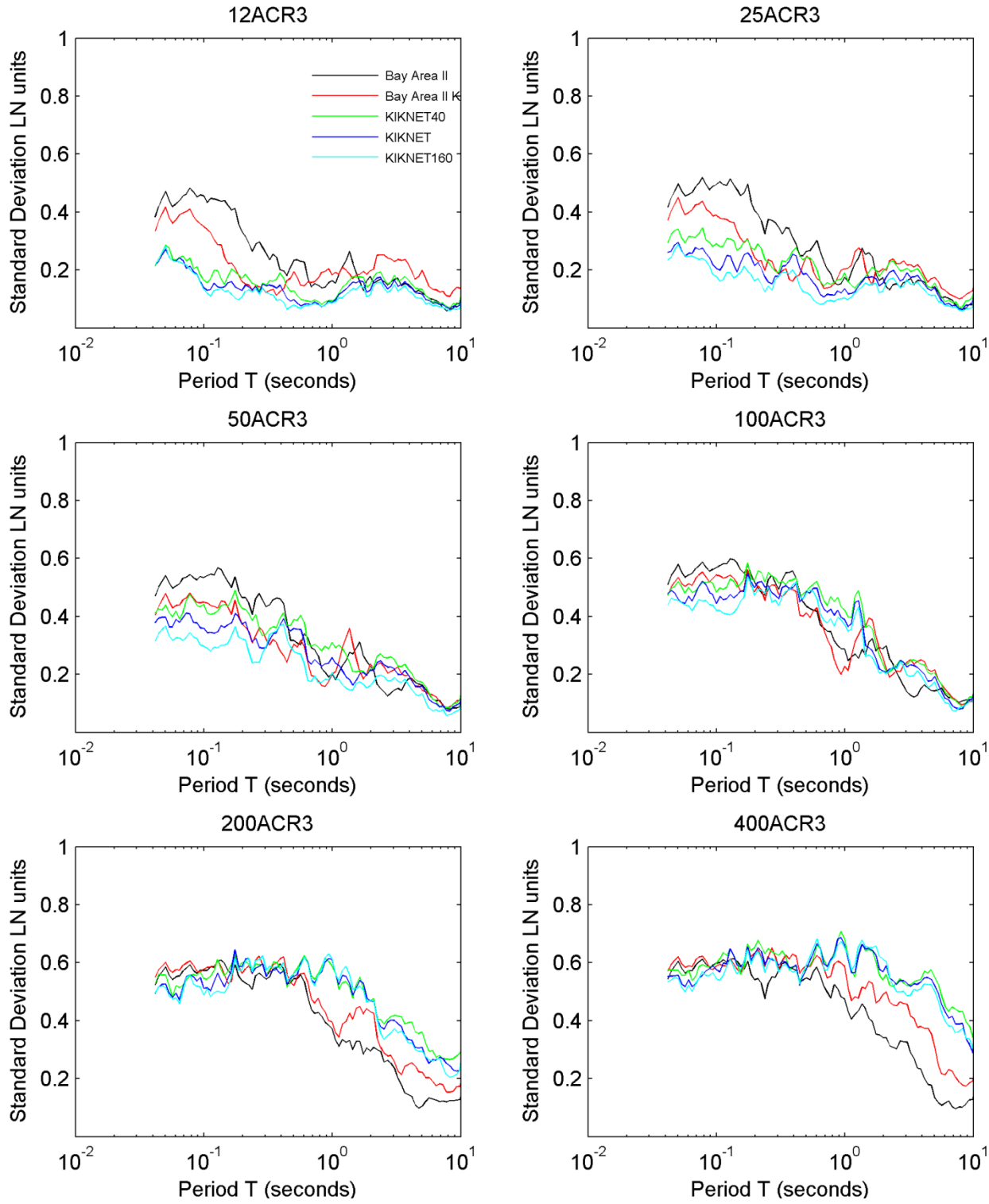

Figure 7.23: Comparison of the effect of soil MRD curves on the standard deviation of spectral amplification of effective stress nonlinear analyses for scenarios 12ACR3, 25ACR3, 50ACR3, 100ACR3, 200ACR3, and 400ACR3

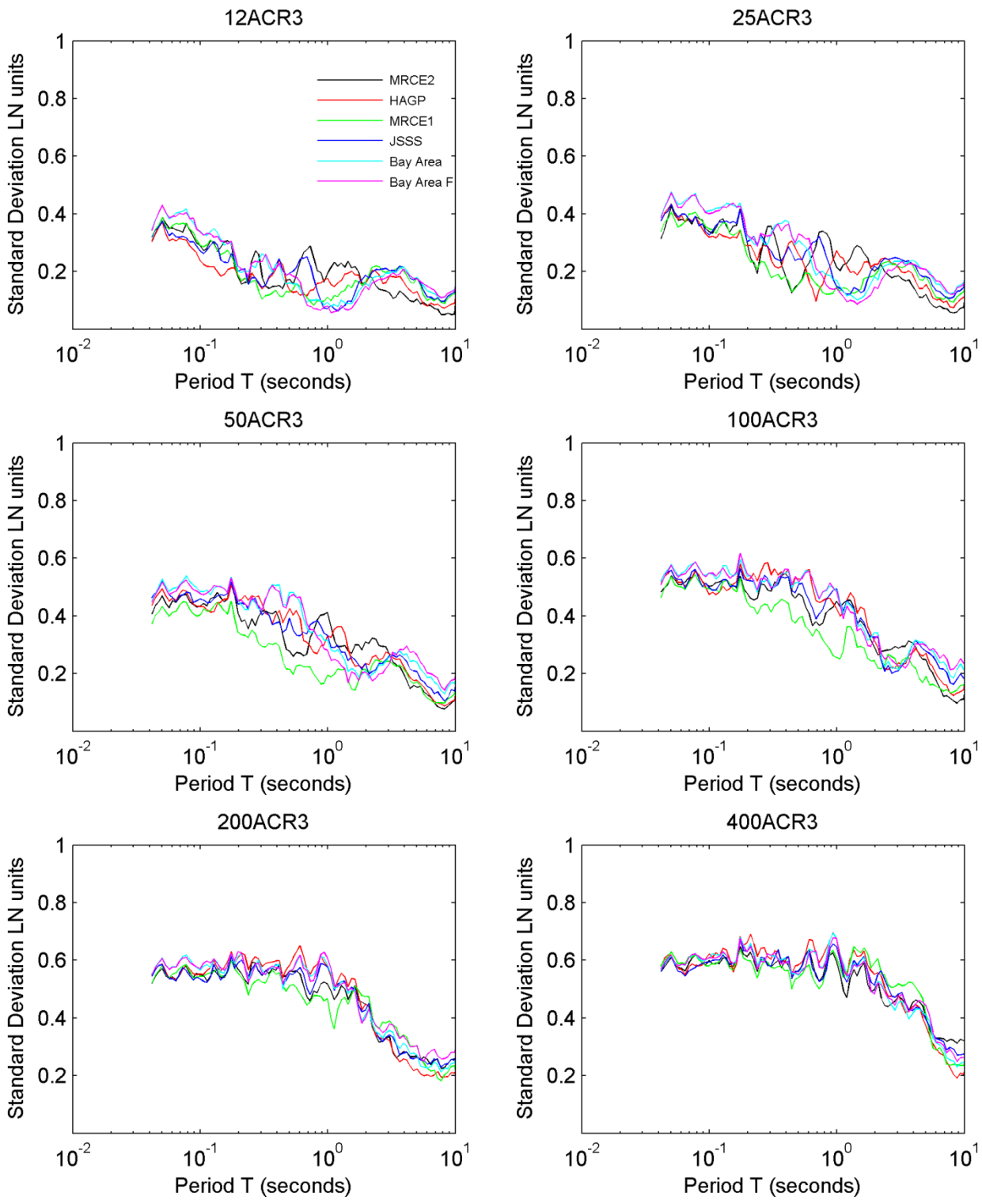

Figure 7.24: Comparison of the effect of the elastic site period on the amplification of effective stress nonlinear analyses for scenarios 12ACR3, 25ACR3, 50ACR3, 100ACR3, 200ACR3, and 400ACR3

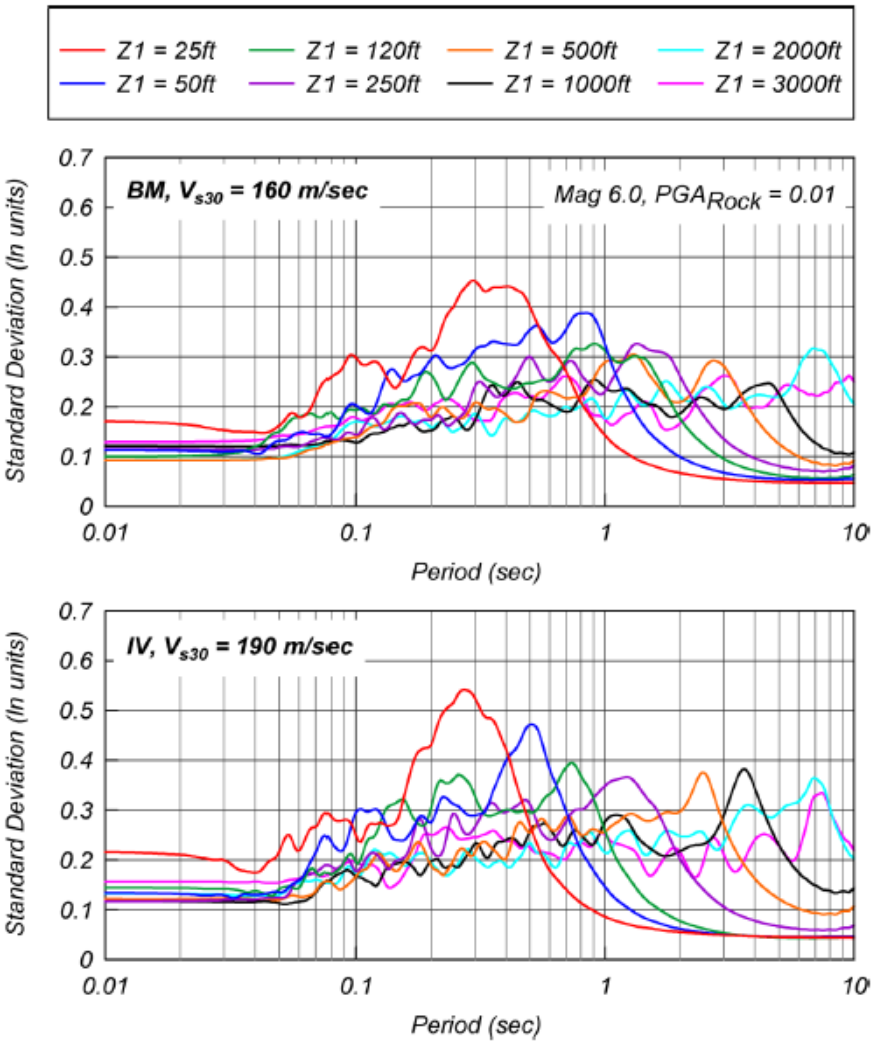

Figure 7.25: Standard deviation of amplification for sites with varying depths, where z_1 is the depth to when Vs = 1000 m/s, and the input ground motion PGA = 0.01g (From Kamai et al., 2013)

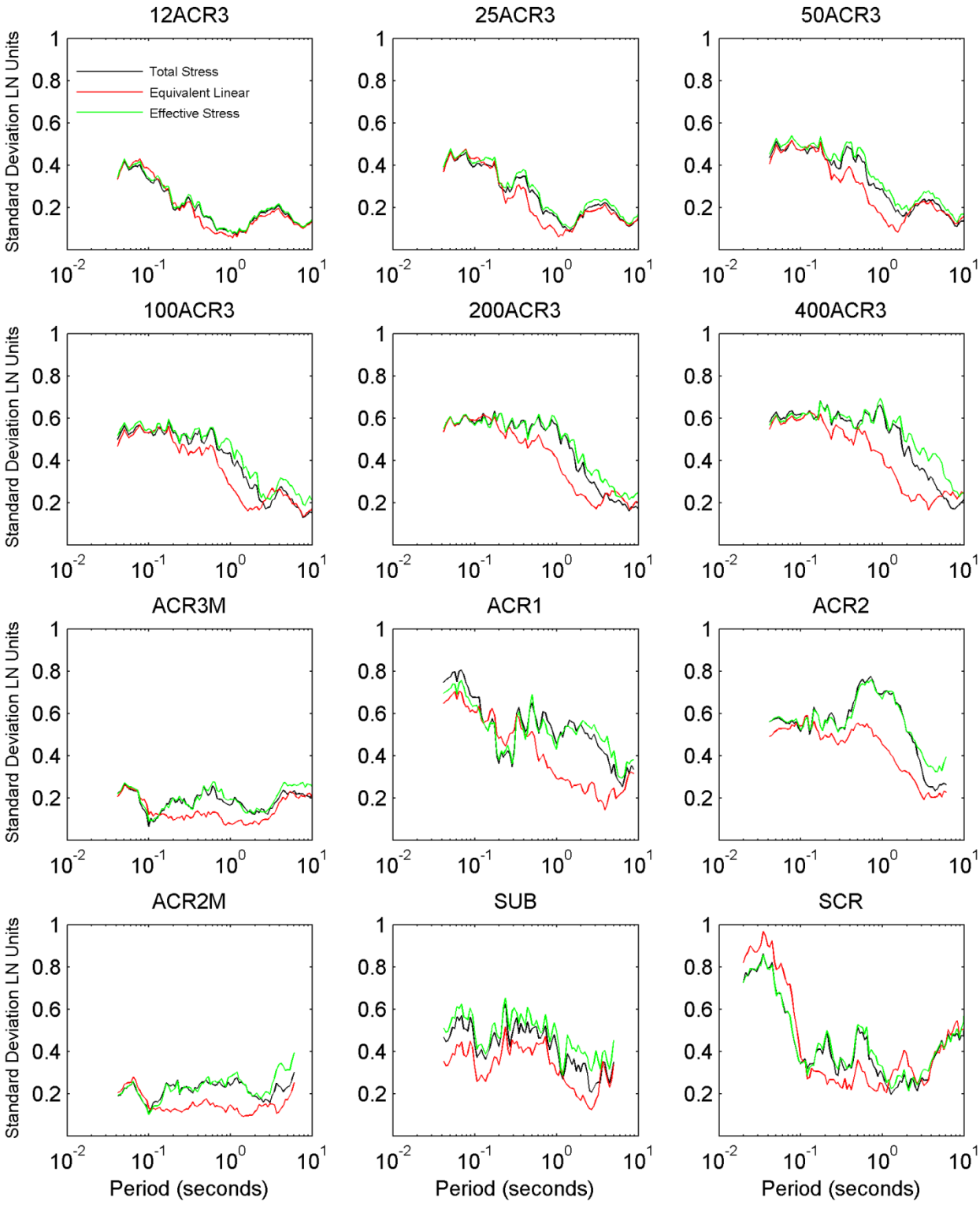

Figure 7.26: Comparison of analysis type (total stress nonlinear, total stress equivalent linear, and effective stress nonlinear) for standard deviation of amplification for site Bay Area

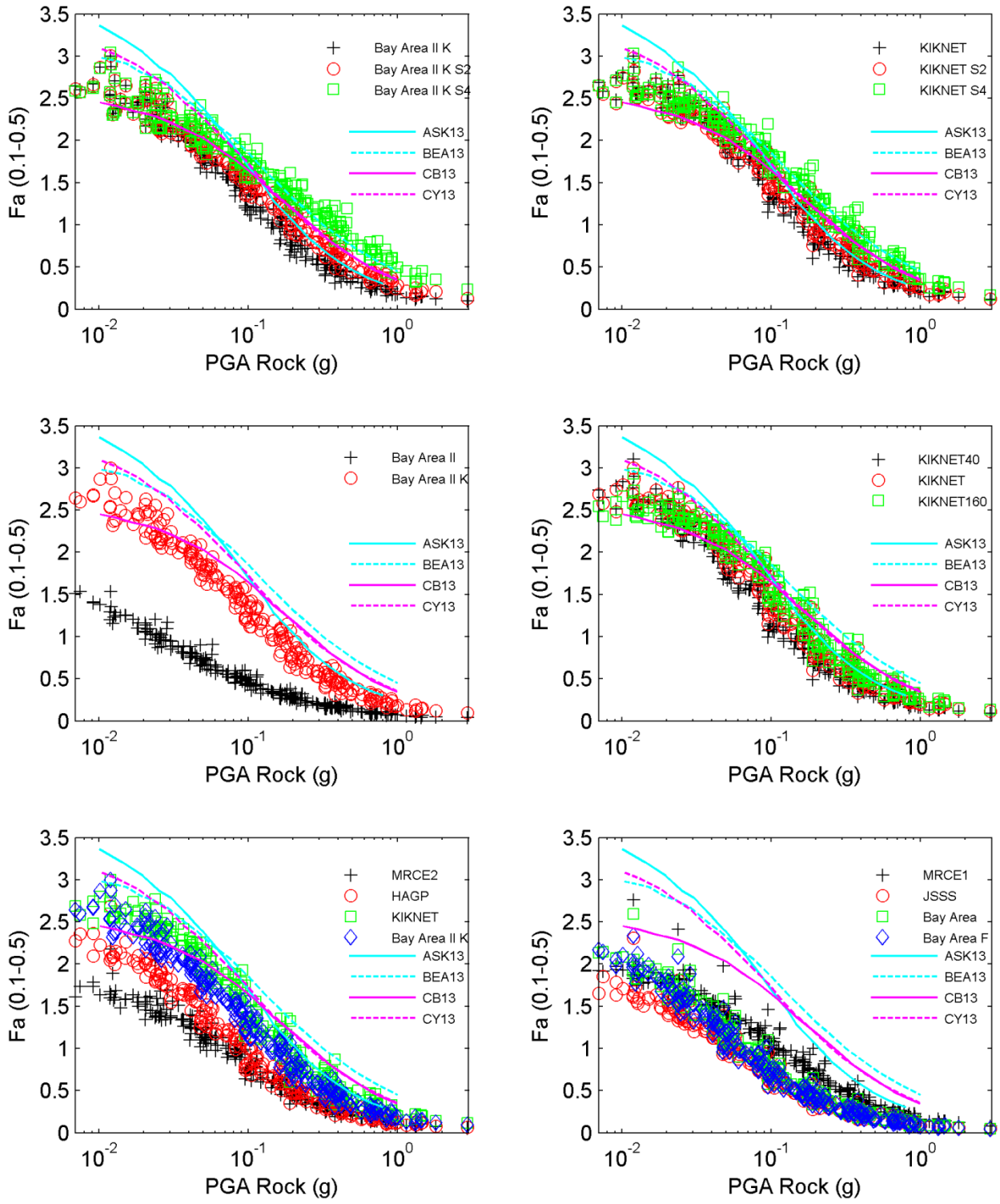

Figure 7.27: Amplification factor Fa for scenarios 12ACR3, 25ACR3, 50ACR3, 100ACR3, 200ACR3, and 400ACR3 calculated in this study for effective stress nonlinear analyses compared with Fa calculated by Seyhan and Stewart (2013) for NGA West 2 GMPEs

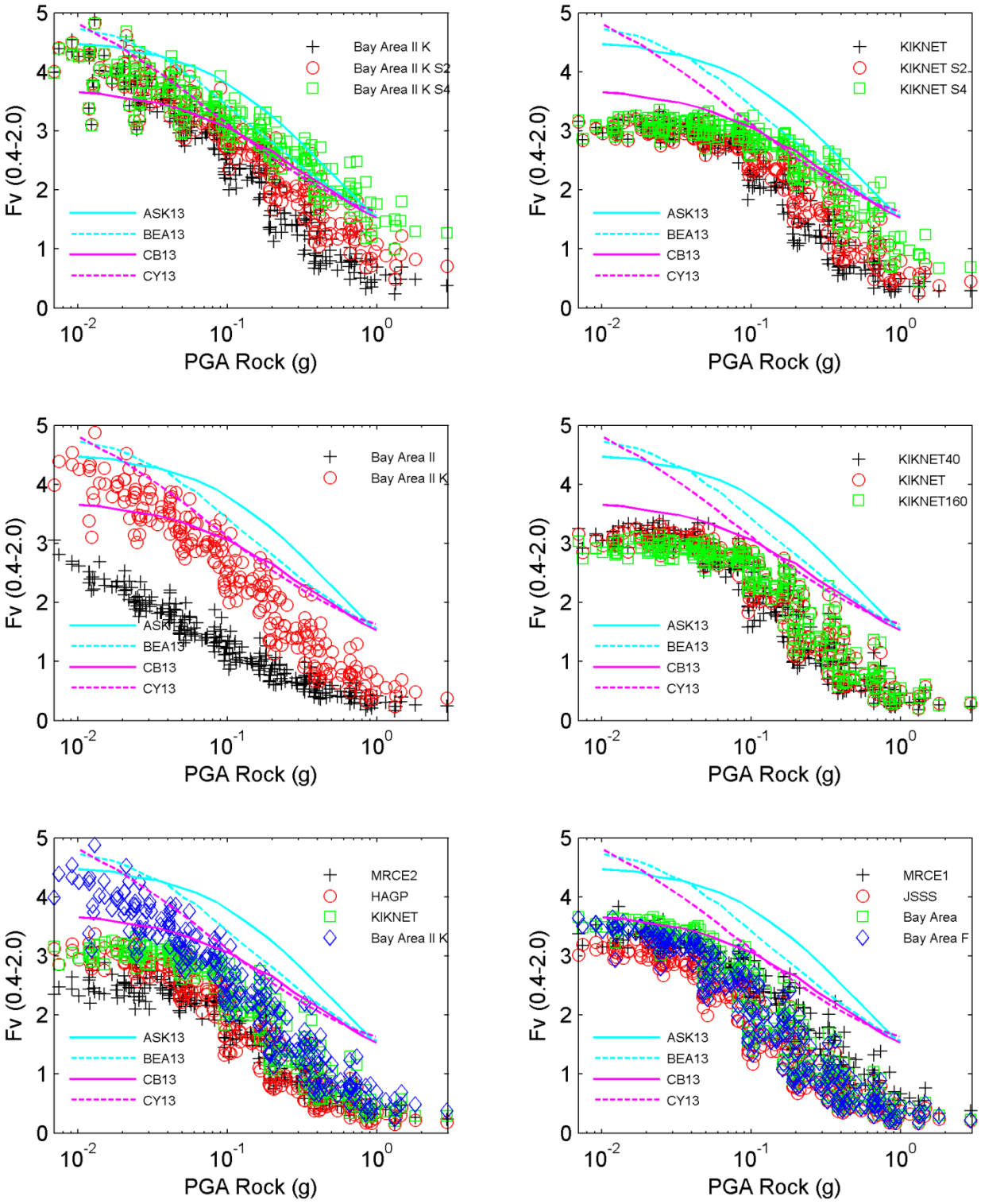

Figure 7.28: Amplification factor Fv for scenarios 12ACR3, 25ACR3, 50ACR3, 100ACR3, 200ACR3, and 400ACR3 calculated in this study for effective stress nonlinear analyses compared with Fv calculated by Seyhan and Stewart (2013) for NGA West 2 GMPEs

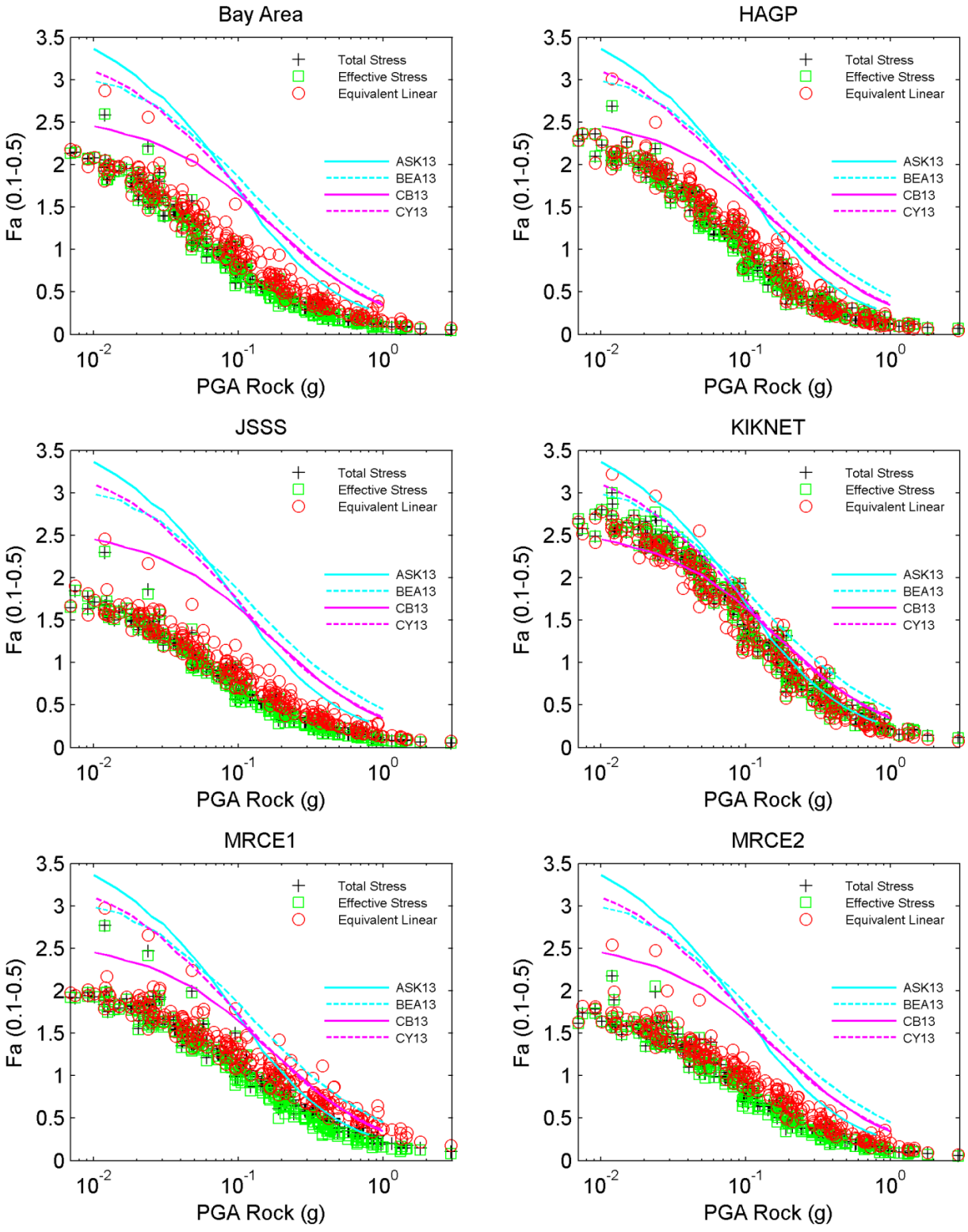

Figure 7.29: Comparison of amplification factor Fa for scenarios 12ACR3, 25ACR3, 50ACR3, 100ACR3, 200ACR3, and 400ACR3 and different analysis types (total stress nonlinear, total stress equivalent linear, and effective stress nonlinear), also plotted are Fa values implied by the NGA West 2 GMPEs calculated by Seyhan and Stewart (2013) for NEHRP E sites

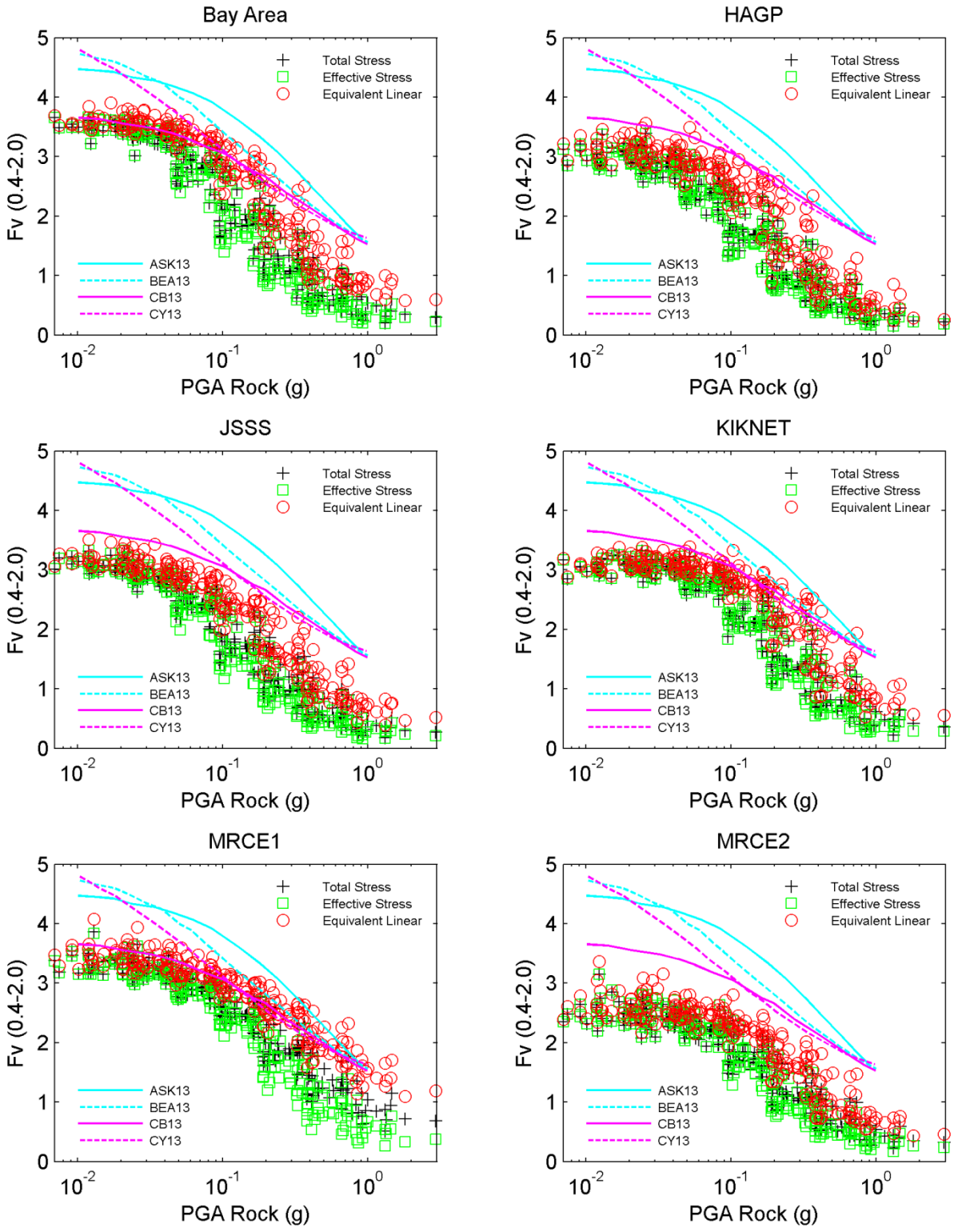

Figure 7.30: Comparison of amplification factor Fv for scenarios 12ACR3, 25ACR3, 50ACR3, 100ACR3, 200ACR3, and 400ACR3 and different analysis types (total stress nonlinear, total stress equivalent linear, and effective stress nonlinear), also plotted are Fv implied by the NGA West 2 GMPEs calculated by Seyhan and Stewart (2013) for NEHRP E sites

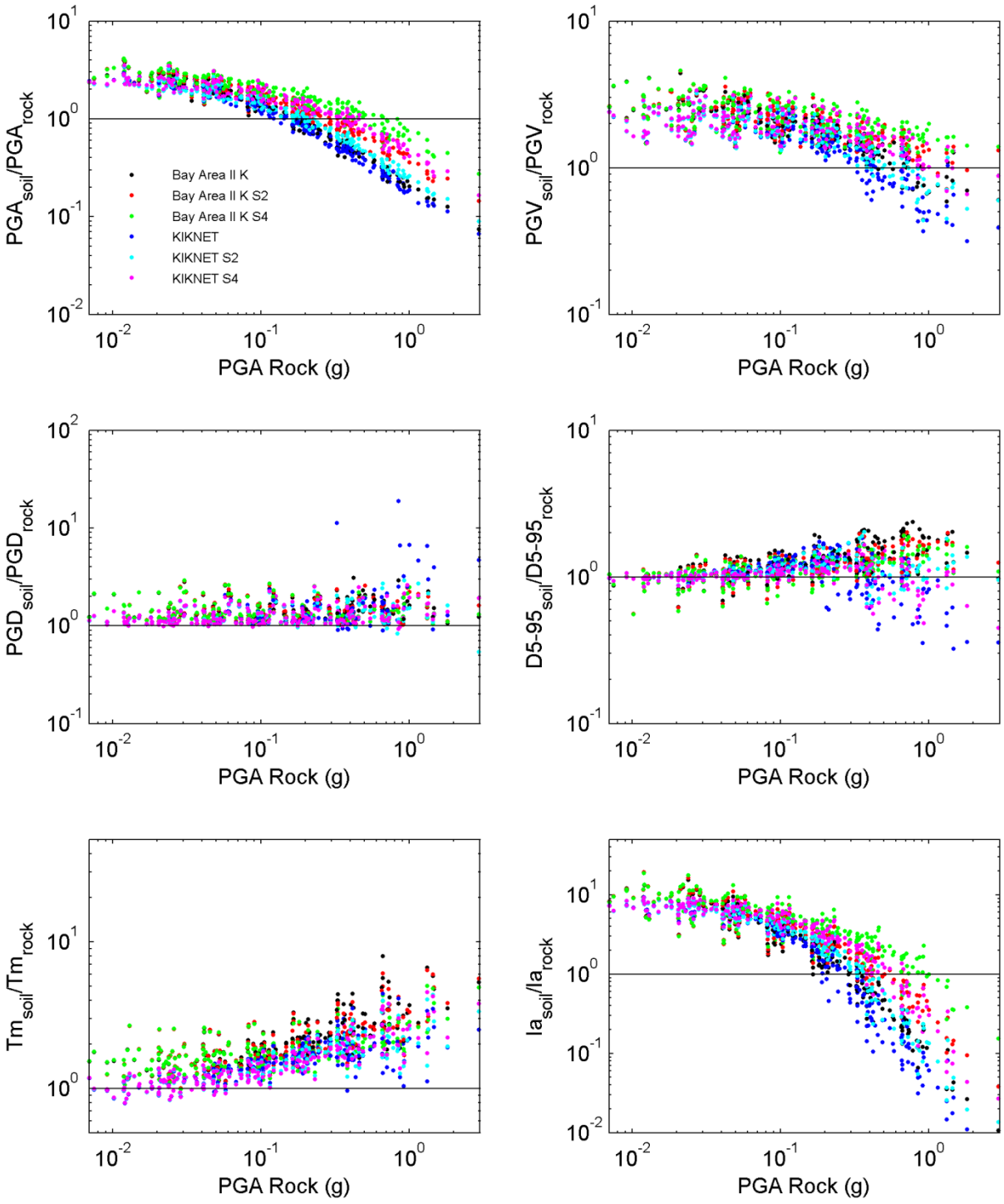

Figure 7.31: Comparison of the effect of site profile strength on the amplification of PGA, PGV, PGD, $D_{5\text{-}95}$, T_m, and I_a, for scenarios 12ACR3, 25ACR3, 50ACR3, 100ACR3, 200ACR3, and 400ACR3 versus PGA rock for effective stress nonlinear analyses.

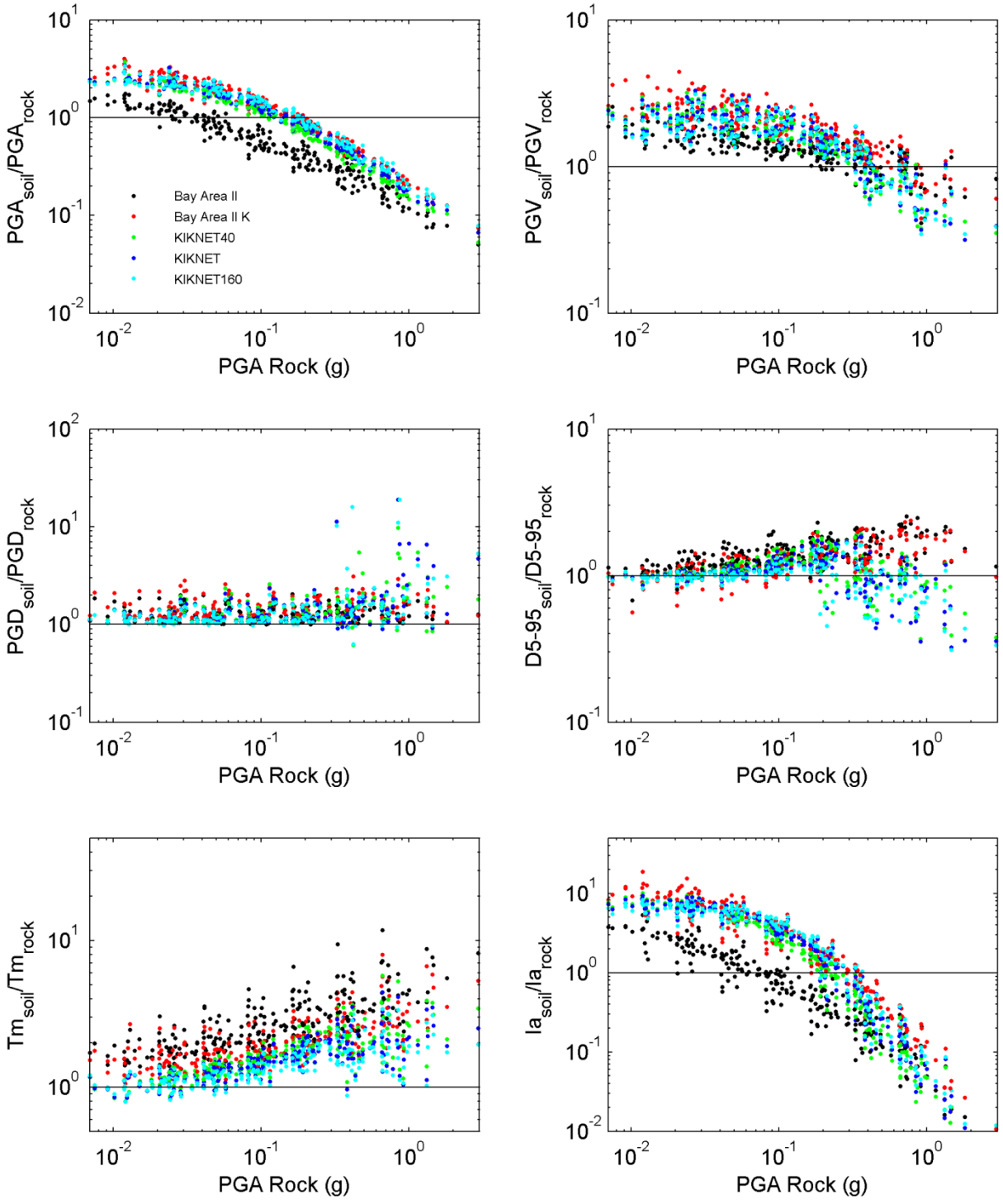

Figure 7.32: Comparison of the effect of soil MRD curves on the amplification of PGA, PGV, PGD, $D_{5\text{-}95}$, T_m, and I_a, for scenarios 12ACR3, 25ACR3, 50ACR3, 100ACR3, 200ACR3, and 400ACR3 versus PGA rock for effective stress nonlinear analyses.

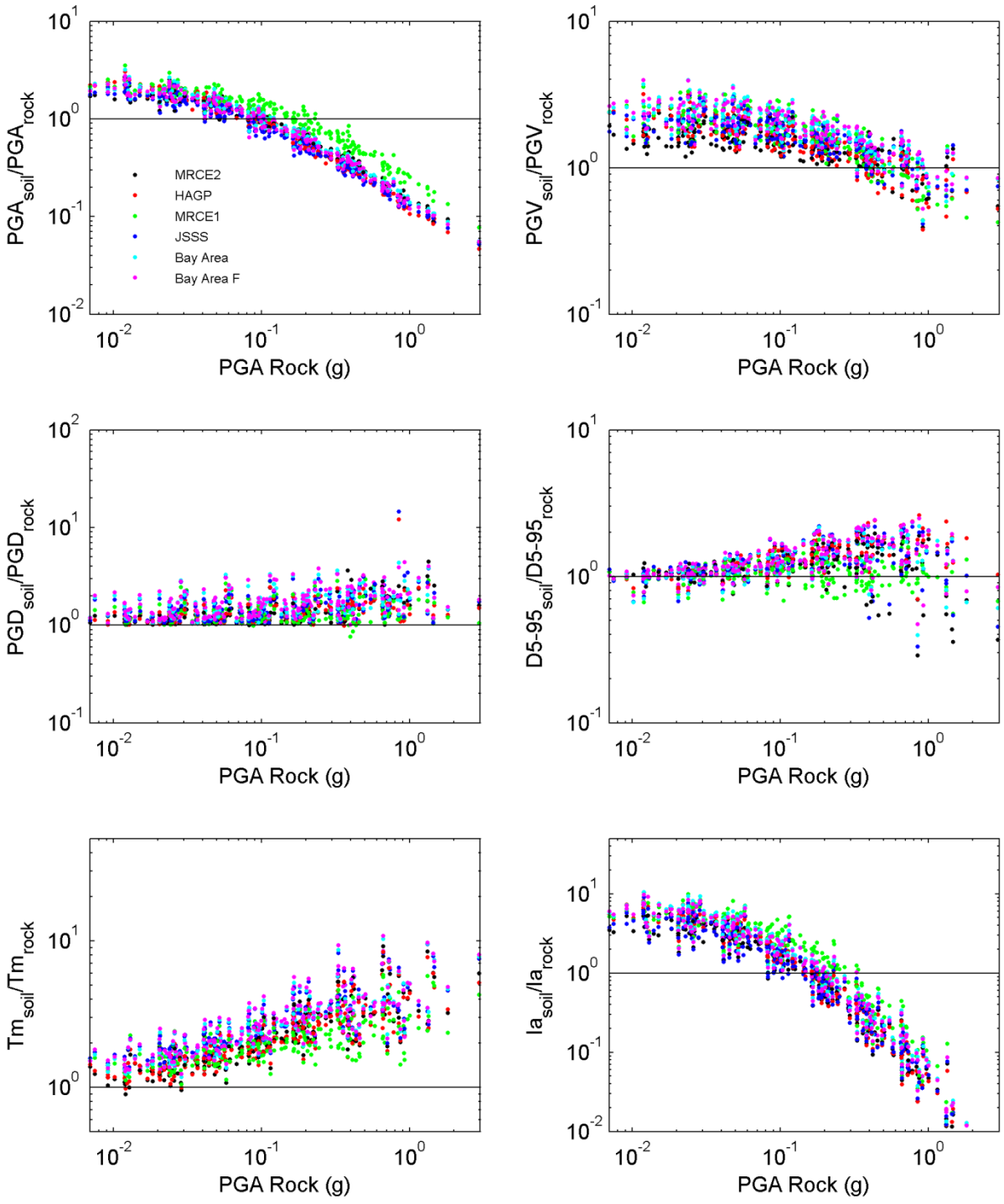

Figure 7.33: Comparison of the effect of elastic site period on the amplification of PGA, PGV, PGD, $D_{5\text{-}95}$, T_m, and I_a, for scenarios 12ACR3, 25ACR3, 50ACR3, 100ACR3, 200ACR3, and 400ACR3 versus PGA rock for effective stress nonlinear analyses

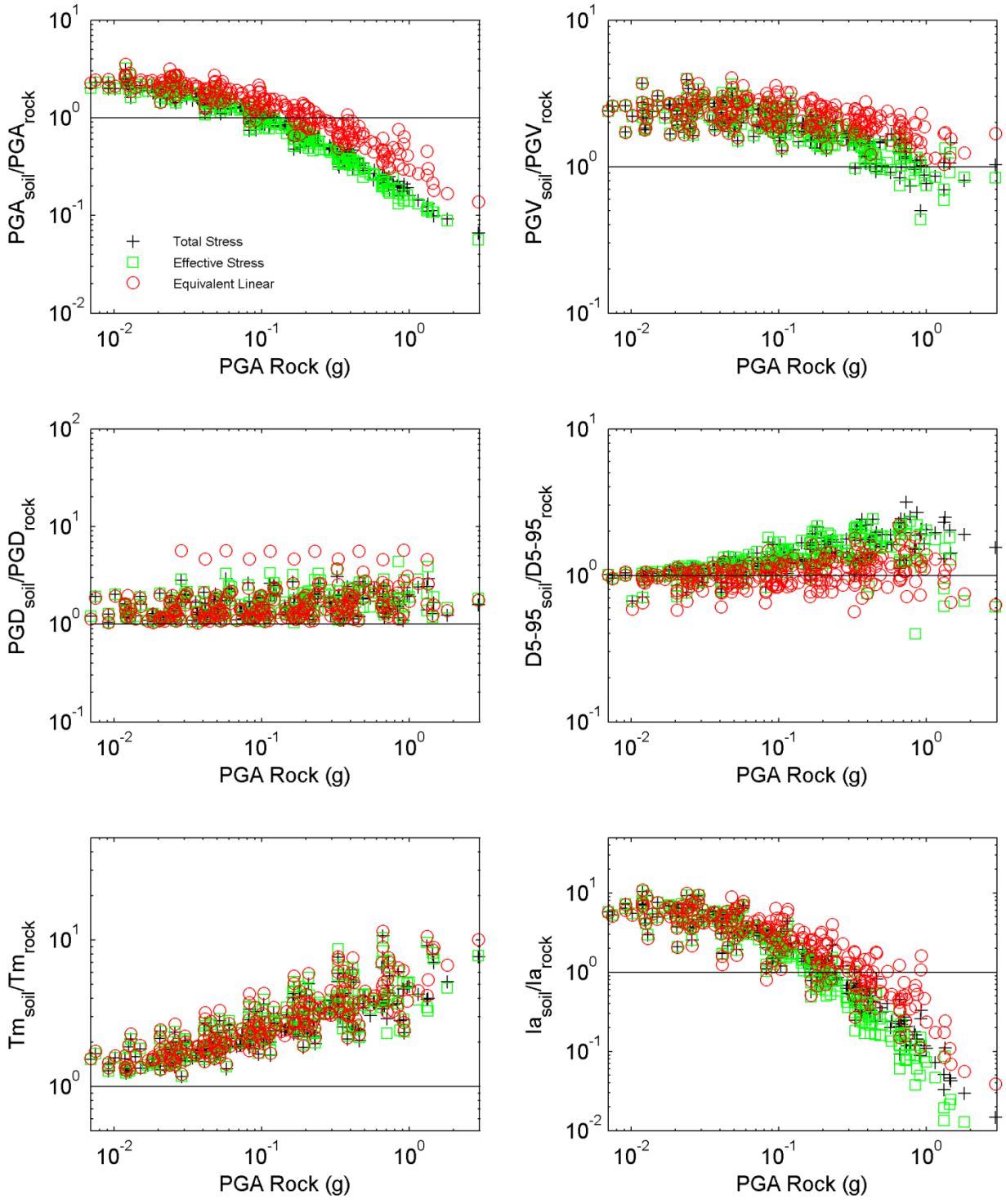

Figure 7.34: Comparison of the effect of analysis type (total stress nonlinear, effective stress nonlinear, total stress equivalent linear) on the amplification of PGA, PGV, PGD, $D_{5\text{-}95}$, T_m, and I_a, for scenarios 12ACR3, 25ACR3, 50ACR3, 100ACR3, 200ACR3, and 400ACR3 versus PGA rock for site Bay Area

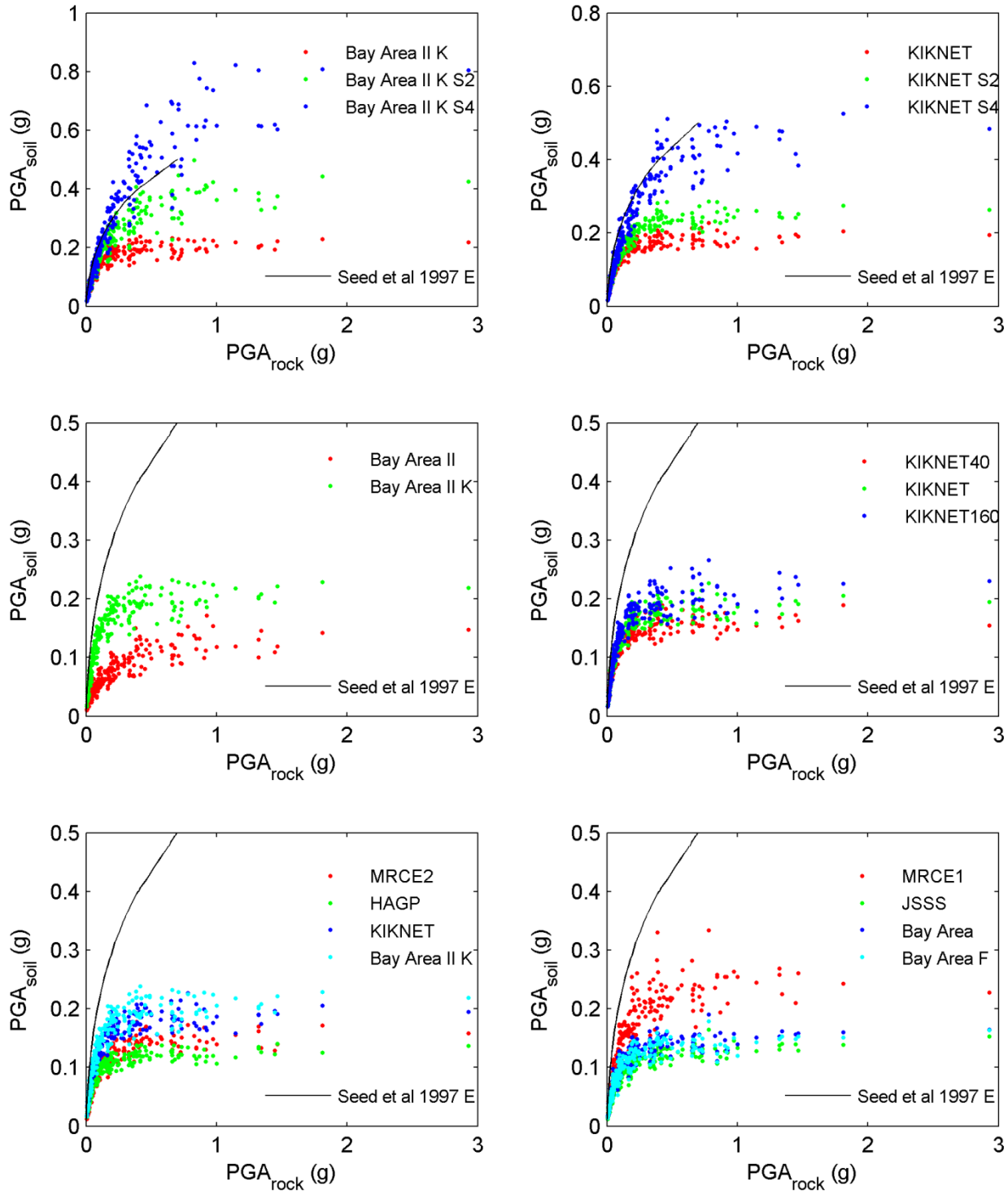

Figure 7.35: Comparison of PGA_{soil} versus PGA_{rock} for sites investigated in this study with effective stress nonlinear site response analyses, and the given by Seed et al. (1997) for their E sites

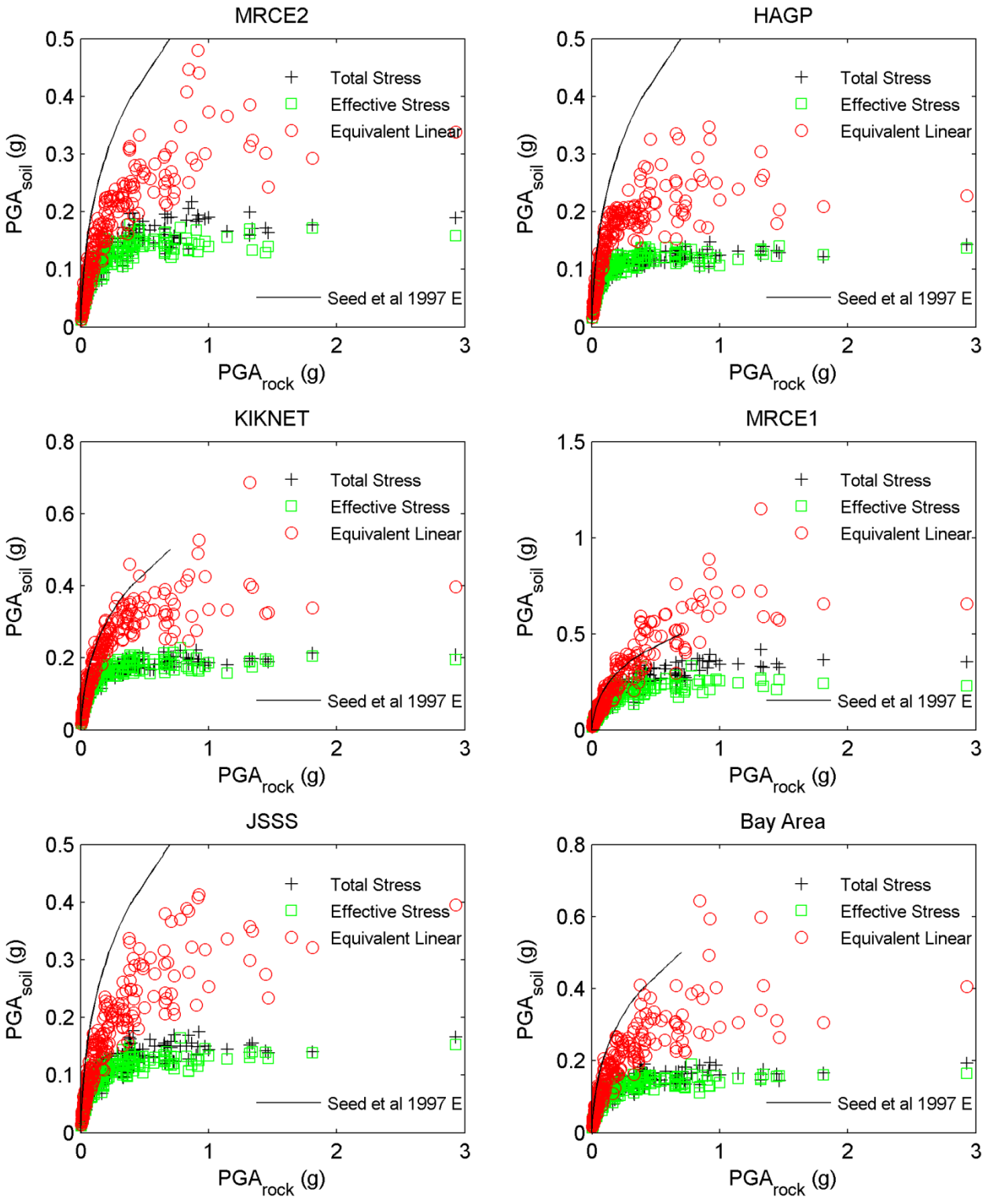

Figure 7.36: Comparison of analysis type (total stress nonlinear, effective stress nonlinear, total stress equivalent linear) for PGA_{soil} versus PGA_{rock} of sites investigated in this study, and the curve of Seed et al. (1997) for their E sites

Table 7.3: Definition of notation used in Table 7.4 and Table 7.5

Parameter	Definition
$Sa(T<T_{p,Sa})$	Psuedo-spectral acceleration values for periods less than $T_{p,Sa}$
$Sa(T>T_{p,Sa})$	Psuedo-spectral acceleration values for periods greater than $T_{p,Sa}$
$T_{p,Sa}$	Period of the peak psuedo-spectral accleration value
$Amp(T < T_{p,amp})$	Amplification values for periods less than $T_{p,amp}$
$Amp(T > T_{p,amp})$	Amplification values for periods greater than $T_{p,amp}$
Amp_p	Peak amplification value
$T_{p,amp}$	Period of the peak amplification value
$T_{min,amp}$	Period of the minimum amplification value
$\gamma_{max}(D)$	Maximum shear strain with depth (D)
$CRR_{max}(D)$	Maximum shear stress ratio with depth (D)
$r_{u,max}(D)$	Maximum pore pressure ratio with depth (D)
$PGA_{max}(D)$	Maximum PGA with depth (D)
SR_p	Peak spectral ratio (Sa(T) / PGA) value
T_{pSR}	Period of the peak spectral ratio
Shape	Spectral shape (Sa(T) / PGA) (SR for all periods)
σ_{RS}	Response spectra standard deviation
σ_{AMP}	Amplification standard deviation
Fa	Short period amplificatoin factor (0.1-0.5 s)
Fv	Mid period amplification factor (0.4-2 s)
A_{PGA}	Amplificaiton of PGA (PGA_{soil}/PGA_{rock})
A_{PGV}	Amplificaiton of PGV (PGV_{soil}/PGV_{rock})
A_{PGD}	Amplificaiton of PGD (PGD_{soil}/PGD_{rock})
A_{Tm}	Amplificaiton of Tm (Tm_{soil}/Tm_{rock})
A_{D5-95}	Amplificaiton of D_{5-95} ($D_{5-95,soil}/D_{5-95}$,rock)
A_{Ia}	Amplificaiton of Ia (Ia_{soil}/Ia_{rock})
EQL	Total stress equivalent linear analysis
TSN	Total stress nonlinear analysis
ESN	Effective stress nonlinear analysis

Table 7.4: Summary of the effects of ground motion intensity and site characteristics on the results of the site response analyses reviewed in this chapter

	Intensity ↑	Strength ↑	MRD →	Ts ↑
$Sa(T<T_p)$	↑	↑	↑	NE
$Sa(T>T_p)$	↑	↑ [3]	NE	NE
T_p	↑	NE	NE	NE
$Amp(T < T_p)$	↓	↑	↑	NE
$Amp(T > T_p)$	↑	↓	↓	↑
Amp_p	↓	↑	↑	↑
$T_{p,amp}$	↑	↓	↓	↑
$T_{min,amp}$	↑	↑	↓	NE
$\gamma_{max}(D)$	↑	D	D	NE
$CRR_{max}(D)$	↑	↑	↑	NE
$r_{u,max}(D)$	↑	D	D	NE
$PGA_{max}(D)$	↑	↑	↑	NE
SR_p	↓	↓	↑	NE
T_{pSR}	↑	NE	↓	NE
Shape	→	↓	←	NE
σ_{RS}	↓	↑	↑	NE
σ_{AMP}	↑	↓	↓	NE
Fa	↓	↑ [2,3]	↑ [1,2]	NE
Fv	↓	↑ [2,3]	↑ [1,2]	NE
A_{PGA}	↓	↑	↑	NE
A_{PGV}	↓	↑	↑	NE
A_{PGD}	NE	NE	NE	NE
A_{Tm}	↑ [1,2]	↓ [1,2]	↓	NE
A_{D5-95}	↑ [1,2]	↓ [1,2]	↓	NE
A_{Ia}	↓	↑	↑	NE

[1] For small values of PGA rock; [2] For moderate values of PGA rock; [3] For large values of PGA rock; D = may increase or decrease, depends on other factors; NE = negligible effect

Table 7.5: Summary of the effects of scenario and analysis type on the results of the site response analyses reviewed in this chapter

	ACR1:ACR2	ACR2:ACR2M	100ACR3:ACR3M	100ACR3:SUB	100ACR3:SCR	EQL:TSN	EQL:ESN	TSN:ESN
$Sa(T<T_p)$	=	=	=	=	< or =	>	>	=
$Sa(T>T_p)$	>	=	=	=	>	=	< [2,3]	< [2,3]
T_p	=	=	=	=	>	< [3]	< [3]	=
$Amp(T < T_p)$	=	=	=	=	>	>	>	=
$Amp(T > T_p)$	=	=	=	=	<	=	<	<
Amp_p	=	=	=	=	<	>	>	=
$T_{p,amp}$	=	=	=	=	> or =	<	<	<
$T_{min,amp}$	=	=	=	=	>	>	>	>
$\gamma_{max}(D)$	>	=	=	>	>	D	D	D
$CRR_{max}(D)$	=	=	=	>	>	>	>	>
$r_{u,max}(D)$	>	=	=	>	> or =	NA	NA	NA
$PGA_{max}(D)$	=	=	=	=	<	>	>	>
SR_p	=	=	=	=	> or =	<	> [2,3]	> [2,3]
T_{pSR}	=	=	=	=	>	< [3]	< [3]	=
Shape	ACR1 →	=	=	=	← SCR	↓ EQL	↓ EQL	=
σ_{RS}	=	>	>	=	= [4]	>	> [2]	= [4]
σ_{AMP}	=	>	>	=	= [4]	<	<	= [4]
Fa	=	=	=	=	<	>	>	> [2]
Fv	=	=	=	=	<	>	>	> [2]
A_{PGA}	=	=	=	=	>	>	>	=
A_{PGV}	=	=	=	=	=	>	>	=
A_{PGD}	=	=	=	=	<	>	>	=
A_{Tm}	=	=	=	=	=	=	=	> [3]
A_{D5-95}	=	=	=	=	<	>	>	> [3]
A_{Ia}	=	=	=	=	=	>	>	=

[1] For small values of PGA rock; [2] For moderate values of PGA rock; [3] For large values of PGA rock; [4] < for long T; D = may increase or decrease, depends on other factors; NA = not applicable

CHAPTER 8: DEVELOPMENT OF A SIMPLIFIED MODEL TO ESTIMATE NON-LIQUEFIABLE NEHRP F SITE DESIGN SPECTRA

8.1 Introduction

Chapter 7 examined the results of the site response analyses in a qualitative manner. It highlighted trends and explored the influence of different parameters on the results. This chapter examines the results of the site response analyses in a quantitative manner, and discusses the development of a simplified model to estimate non-liquefiable NERHP F site design spectra. Section 8.2 briefly outlines previous research on site amplification models to place the present model in context. Section 8.3 discusses the model development and regression analyses. Section 8.4 presents a sensitivity analysis that illustrates the effect of each input parameter on the calculated amplification. Section 8.5 describes how to calculate each of the input parameters and lists some resources for estimating them. Section 8.6 explains the creation of a validation data set to test the results of the regression analyses. Section 8.7 is compares the simplified model with the results that would be obtained using 80% of the NERHP E site design spectra at the appropriate intensity levels.

The simplified model presented in this chapter does not replace a site response analysis, but rather augments it. It is hoped that the results of this chapter as well as the previous chapter will help practicing engineers gain a better understanding of their site before conducting site response analyses. This will help them to focus on the important aspects of the site, which will allow them to save time and money.

8.2 Background

Researchers and practitioners in earthquake engineering have long known that near surface soils have a strong influence on ground motions. Building codes such as the 2012 IBC (IBC, 2012) account for the influence of site effects through the use of site factors, which are the average amplification over a period range. The design spectrum is then constructed using these amplification factors and a set of equations that relate them to the spectral acceleration at other periods. Ground motion prediction equations (GMPEs) incorporate site effects at each period directly, and therefore can model changes in spectral shape due to site effects more flexibly than code based site factors.

8.2.1 Site Amplification Factors

Professor Harry Seed and his colleagues conducted one of the first comprehensive studies of the effect of near surface soils on ground motions in 1976 (Seed et al., 1976a,b). Based on these and similar results from other researchers, the Applied Technology Council (ATC, 1978) recommended design spectra for rock, stiff soil, and soft soil sites. After the 1985 Mexico City earthquake, the ATC added a fourth soil type for deep deposits of soft soils. These site factors only differentiated between soil types at long periods, and did not take into account soil nonlinearity.

In 1991 the National Center for Earthquake Engineering Research, now the Multidisciplinary Center for Earthquake Engineering Research (http://mceer.buffalo.edu/), held a workshop to improve how building codes dealt with site effects (Whitman, 1992). The workshop created a committee of nine members who studied site effects using empirical evidence from the 1989 Loma Prieta earthquake in the San Francisco Bay Area, as well as numerical simulations using equivalent linear and nonlinear time stepping techniques (e.g. Seed et al., 1994; Dobry et al., 1994). The committee presented their research at a second workshop in 1992 (Martin, 1994). This workshop developed the site factors and site categories that would later be integrated into the 1994 NEHRP provisions, and which are still the basis for the NEHRP provisions to this day. The workshop recommended two site factors, one for short periods (average soil/rock amplification over a period range of 0.1-0.5 seconds (F_a)) and one for long periods (average soil/rock amplification over a period range of 0.5-2.0 seconds (F_v)). Table 8.1 lists the NEHRP site categories, and Table 8.2 lists the site factors according to site category and ground motion intensity. A major improvement of these site factors over earlier site factors is the fact that they account for soil nonlinearity (Dobry et al., 2000). Values of S_s and S_1 can be taken from seismic hazard maps provided by the USGS. Using the values of S_s and S_1 and the site category, Figure 8.1 shows how to calculate the design spectrum from F_a and F_v according to the 2012 IBC.

8.2.2 Site Amplification Models for Use with GMPEs

Another approach to account for site effects is to include them directly in a ground motion prediction equation (GMPE) that calculates the response spectrum over a range of periods. Researchers working on a report for the Electric Power Research Institute's (EPRI) 1993 study of design ground motions for Eastern North America included nonlinear site effects into their GMPEs using equation (8.1) shown below (EPRI, 1993, Volume 2 Appendix C):

$$f_{site} = a + b \times ln(PGA_{rock}) \tag{8.1}$$

where a and b are period dependent coefficients and PGA_{rock} is the peak ground acceleration on rock. They did regression analyses of a and b for three different site classifications; rock, deep soil, and shallow stiff soil. The Abrahamson and Silva (1997) GMPE has two site types; rock and shallow soil, and deep soil. They used a similar site amplification model as the EPRI 1993 model, but added coefficient c as shown below:

$$f_{site} = a + b \times ln(PGA_{rock} + c) \tag{8.2}$$

The GMPE developed by Boore et al. (1997) was one of the first to incorporate a continuous function for site response based on Vs_{30} rather than using discreet site categories. The functional form used related linear site amplification to Vs_{30} as:

$$f_{site} = a \times ln\left(\frac{Vs_{30}}{Vs_{ref}}\right) \tag{8.3}$$

where a and Vs_{ref} are period dependent coefficients. The Boore et al. (1997) GMPE did not, however, include nonlinear site effects.

Choi and Stewart (2005) developed a unified model that included both linear and nonlinear site effects, as shown in equation (8.4) below:

$$ln(Amp) = ln(Amp_L) + ln(Amp_{NL}) \quad (8.4)$$

where Amp is the total amplification defined as the ratio of the surface Sa(T) on a soil site divided by the Sa(T) that would be expected on a rock site, Amp_L is the portion of the amplification due to linear site effects, and Amp_{NL} is the nonlinear amplification. They conducted a mixed effects regression using a database of 919 records from 59 earthquakes and 209 sites. Equation (8.5) gives the final model developed by Choi and Stewart (2005), which is a continuous function of Vs_{30} similar to the Boore et al. (1997) GMPE, but also includes a nonlinear site term:

$$ln(Amp) = a \times ln\left(\frac{Vs_{30}}{Vs_{ref}}\right) + b \times ln\left(\frac{PGA_{Rock}}{0.1}\right) \quad (8.5)$$

where a, b, and Vs_{ref} are period dependent coefficients.

As part of the PEER NGA West 1 project, Walling et al. (2008) developed a database of site response analyses to help the NGA developers constrain the nonlinear scaling of the site amplification models within their GMPEs. They conducted site response analyses using the computer program RASCALS (Silva and Lee, 1987). The RASCALS program defines the source and path effects using the stochastic point-source model and the site effects with a one dimensional random vibration theory based equivalent linear method. The site response analyses conducted included sites with average Vs_{30} values from 270 to 900 m/ s, soil depths from 15 to 914 m, and PGA_{rock} values from 0.01 g to 1.5 g. Walling et al. (2008) used four sets of shear modulus reduction and damping curves; EPRI, Peninsular Range, Imperial Valley, and Bay Mud. They developed separate site amplification models for the EPRI and Peninsular Range shear modulus reduction curves that are functions of Vs_{30} and PGA_{rock}.

Kamai et al. (2013) was an update of Walling et al. (2008) for the PEER NGA West 2 project. They used the RASCALS computer program to expand the database developed by Walling et al. (2008), as well as investigated using PGA_{rock} or $Sa(T)_{rock}$ as a predictor variable for site amplification. Kamai et al. (2013) ran simulations for three magnitudes (Mw = 5, 6, and 7) instead of only one (Mw = 6.5), and added a soil profile with Vs_{30} = 190 m/s. The simulations of Walling et al. (2008) included a soil site with Vs_{30} = 160 m/s, however neither they nor Kamai et al. (2013) included these results in their regression analyses. Kamai et al. (2013) used the same functional form for their site amplification model as Walling et al. (2008), which is similar to the Choi and Stewart (2005) model:

$$ln(Amp) = \begin{cases} a \times \ln\left(\frac{Vs_{30}^*}{V_{Lin}}\right) - b \times ln(GM_{Rock} + c) \\ +b \times ln\left(GM_{Rock} + c \times \left(\frac{Vs_{30}^*}{V_{Lin}}\right)^n\right) + d & for\ Vs_{30} < V_{Lin} \\ (a + b \times n) \times ln\left(\frac{Vs_{30}^*}{V_{Lin}}\right) + d & for\ Vs_{30} \geq V_{Lin} \end{cases} \quad (8.6)$$

where:

$$Vs_{30}^* = \begin{cases} Vs_{30} & for\ Vs_{30} < V_1 \\ V_1 & for\ Vs_{30} \geq V_1 \end{cases} \quad (8.7)$$

The variable V_1 is the value of Vs_{30} above which the soil amplification no longer scales linearly with respect to Vs_{30} (Abrahamson and Silva, 2008), GM_{rock} is PGA_{rock} in the Walling et al. (2008) model, and is PGA_{rock} or $Sa(T)_{rock}$ in the Kamai et al. (2013) model, b and V_{Lin} are period dependent coefficients, and a, c, n, and d are period independent coefficients.

The NGA GMPEs developed by Abrahamson and Silva (2008) and Campbell and Bozorgnia (2008, 2013) use the Peninsular Range and PGA_{rock} based soil amplification model from Walling et al. (2008), and Abrahamson et al. (2013) uses the Peninsular Range model with $Sa(T)_{rock}$ as the ground motion intensity variable from Kamai et al (2013). Chiou and Youngs (2008, 2013) use a functional form constrained by Walling et al. (2008) for their soil amplification model, but calculated the amount of nonlinearity based on empirical regression of the NGA databases (Chiou et al., 2008; Ancheta et al., 2013). Boore and Atkinson (2008) used the functional form of Choi and Stewart (2005) for their soil amplification model, but also constrained the results based on empirical data from the NGA 2008 database (Chiou et al., 2008). The Boore et al. (2014) GMPE utilizes a soil amplification model developed by Stewart and Seyhan (2013) that uses both the simulation data developed by Kamai et al. (2013) and empirical data from the NGA West 2 database (Ancheta et al., 2013). The site amplification model of Stewart and Seyhan (2013) is:

$$ln(Amp_L) = \begin{cases} c \times ln\left(\frac{Vs_{30}}{V_{ref}}\right) & for\ Vs_{30} \leq V_c \\ c \times ln\left(\frac{V_c}{V_{ref}}\right) & for\ Vs_{30} > V_c \end{cases} \quad (8.8)$$

$$ln(Amp_{NL}) = f_1 + f_2 \times ln\left(\frac{PGA_{Rock} + f_3}{f_3}\right) \quad (8.9)$$

where:

$$f_2 = f_4 \times \left[e^{f_5 \times (min[Vs_{30},760] - 360)} - e^{f_5 \times (760 - 360)}\right] \quad (8.10)$$

and V_c is the velocity above which ground motions do not scale with Vs_{30}, V_{ref} is the Vs_{30} where the amplification is one (taken as 760 m/sec), and c and f_1 through f_5 are period dependent coefficients. Stewart and Seyhan (2013) fixed the value of f_1 equal to 0 so that the nonlinear portion goes to zero for $PGA_{rock} << f_3$. They also fixed coefficient f_3 at 0.1 g because the values

of f_2 and f_3 cannot be reliably computed simultaneously. They chose f_3 = 0.1g by conducting regression analyses using equation (8.9) on the NGA West 2 database and choosing the value that gave the least dispersion in the data for Vs_{30} bins of Vs_{30} < 200 m/s and 200 < Vs_{30} < 310 m/s. Figure 8.2 shows the values of f_3 calculated by Stewart and Seyhan (2013) from the NGA West 2 database and values they calculated from the site response analyses conducted by Kamai et al. (2013) for different Vs_{30} values and shear modulus reduction and damping curves.

8.3 Model Development

To develop a simplified model to estimate the response spectra of non-liquefiable NEHRP F sites, this study conducted least squares regression on the average amplification ratio from the effective stress nonlinear site response analyses for each site and scenario combination, as defined below:

$$ln\left(Amp(T)_{i,j}\right) = \frac{1}{n}\sum_{i=1}^{n} ln\left(\frac{Sa(T)_{soil}}{Sa(T)_{rock}}\right)_{i,j} \tag{8.11}$$

where $Amp(T)_{i,j}$ is the mean amplification for the i^{th} scenario and j^{th} site at period T, and n is the number of ground motions in the i^{th} scenario. The average amplification ratio for each site and scenario combination was used rather than the amplification of each individual site response analysis for two reasons. First, taking the mean amplification ratio for each site and scenario combination allows the standard deviation due to ground motion variability to be easily tracked and kept separate from the standard deviation due to the misfit of the simplified model to the site response analyses results. Second, using the mean amplification for each site and scenario combination allows the use of least squares regression, which gives equal weight to each data point, since there are an equal number of sites per scenario.

Table 8.3 lists the ground motion scenarios and Table 8.4 the sites used in the effective stress nonlinear site response analyses. All of the sites and all of the scenarios except the matched scenarios, ACR2M and ACR3M, were used in the regression analyses. The matched scenarios were not used in the regression analyses because they have about the same mean amplification ratios as the scaled scenarios. Using the matched scenarios would essentially give scenario ACR2 and scenario 100ACR3 double weight. As a result, there were 150 amplification ratios per period (10 scenarios each for 15 sites). The regression analyses were only performed for periods between the lowest and highest useable periods listed in Table 8.3 for each scenario.

The simplified model was developed in two stages. In the first stage, the results for each site were regressed separately against the ground motion intensity to estimate the effect of the ground motion scenario. In the second stage, the site specific coefficients calculated from the first stage were regressed against site properties to determine their site dependence. These two parts were then combined to form the final model.

8.3.1 Model Development: Stage 1

Equation (8.12) gives the functional form of the first stage model:

$$ln(Amp) = f_1 + f_2 \times ln\left(\frac{GM_{Rock} + f_3}{f_3}\right) \quad (8.12)$$

where GM_{rock} is either PGA_{rock} or $Sa(T)_{rock}$, and f_1, f_2, and f_3 are period and site dependent coefficients. Equation (8.12) is essentially the Stewart and Seyhan (2013) model. This functional form was chosen because the coefficients f_1 and f_2 have clear physical meanings, as shown in Figure 8.3. When GM_{rock} is << f_3, the nonlinear term goes to zero and ln(Amp) = f_1. Therefore, f_1 represents the maximum linear site amplification when the ground motion intensity is small. Coefficient f_2 controls the slope of the amplification curve versus ground motion intensity. In other words, f_2 controls the nonlinearity of the response. Figure 8.3 shows that when $f_2 > 0$ amplification increases as ground motion intensity increases, when $f_2 < 0$ amplification decreases as ground motion intensity increases, and the greater the absolute value of f_2 the faster the amplification increases or decreases with ground motion intensity.

Coefficients f_2 and f_3 are highly correlated and therefore both do not need to be period dependent. The value of f_3 was fixed at 0.1 g, similar to Stewart and Seyhan (2013). This value was calculated by conducting regression analyses for each site and period using equation (8.12) with different fixed values of f_3 ranging from .01 to 1 g, and selecting the value of f_3 that gave the lowest root mean squared error (RMSE) over all sites and periods, where:

$$RMSE = \sqrt{\frac{1}{n}\sum_{i=1}^{n}\left(ln(Amp)_i - ln\left(Amp_{eq8.12}\right)_i\right)^2} \quad (8.13)$$

Amp is the amplification calculated with the site response analyses, $Amp_{eq8.12}$ is the amplification calculated with equation (8.12), and n is the number of data points.

For every fixed value of f_3, the ground motion intensity parameter GM_{rock} was also alternated between PGA_{rock}, and $Sa(T)_{rock}$. The RMSE taken over all periods and sites was considerably smaller for models that used $Sa(T)_{rock}$ as the intensity parameter than for models that used PGA_{rock}. Figure 8.4 plots the RMSE of each period taken over all sites using equation (8.12) when f_3 = 0.1 g. Figure 8.4 shows that models that used $Sa(T)_{rock}$ have lower RMSE values than models that used PGA_{rock} for all periods less than about 3.5 seconds. This result agrees with the results of Bazzurro and Cornell (2004). Bazzurro and Cornell (2004) conducted site response analyses with 78 acceleration time series from 28 earthquakes through two soil profiles, one primarily sandy and the other primarily clayey, using the nonlinear program SUMDES (Li et al., 1992). They tested seven different functional forms and found that $Sa(T)_{rock}$ is the single parameter with the best predictive power. Kamai et al. (2013) found that there was no statistically significant difference between using PGA_{rock}, and $Sa(T)_{rock}$. However, they note that in their study they did not use actual acceleration time series, but random vibration theory, which has a unique spectral shape and therefore a strong correlation between PGA and Sa(T) (Kamai et al. 2013). This study used acceleration time series with several different spectral shapes, which is why it agrees better with the results of Bazzurro and Cornell (2004).

Based on these two findings, equation (8.12) was modified to equation (8.14) given below, and regressions were performed for each site and period.

$$ln(Amp(T)) = f_1(T) + f_2(T) \times ln\left(\frac{Sa(T)_{Rock} + 0.1}{0.1}\right) \qquad (8.14)$$

Figure 8.5 shows the calculated values of f_1 and f_2 versus period for each site using equation (8.14). Scenario SCR is the only scenario with $Sa(T)_{rock}$ values from T = 0.02 to 0.04 seconds. As a result, to calculate the values of f_1 and f_2 for T = 0.02 to 0.04 seconds, the values of $Sa(T)_{rock}$ for the other scenarios were calculated by linearly interpolating between the values of $Sa(T=0.04)_{rock}$ and $PGA_{rock} = Sa(T=0.01)_{rock}$ for each scenario. Values of $Sa(T)_{rock}$ for periods greater than the highest useable period of each scenario were not used in the regression analyses. For example, for T = 10 seconds, values of f_1 and f_2 were calculated based on regression of $Sa(T)_{rock}$ values from scenarios 12ACR3, 25ACR3, 50ACR3, 100ACR3, 200ACR3, 400ACR3, and SCR only, and not scenarios ACR1, ACR2, and SUB.

Figure 8.5a shows that f_1 is positive for all periods except for one site, which means that at very small ground motion intensities the site amplifies the response at the surface for all periods. The exception is site Bay Area II, which has negative f_1 values (i.e. deamplification) around 0.1 seconds. The value of f_1 peaks for all sites from periods of 1 to 2 seconds, which is about the same as the elastic site periods of the sites tested in this project. Figure 8.5b shows that f_2 ranges from -0.5 to -1.5 at short and mid periods, but then increases and becomes positive for some sites at long periods. Positive values of f_2 mean that the amplification increases as the ground motion intensity increases. This occurs because the site period degrades to longer periods as the intensity increases, which increases the amplification at those periods.

The effect of site period degradation on amplification is better understood by examining Figure 8.6. Figure 8.6 contains plots of the amplification of the Bay Area II sites (Bay Area II, Bay Area II K, Bay Area II K S2, and Bay Area II K S4) verses the spectral acceleration at 12 different periods. The data for short periods all decrease as the ground motion intensity increases (i.e. negative values of f_2). However, around one second they begin to flatten out. For periods of 1.8 and 3.0 seconds the data has a humped shape. In other words, as the ground motion intensity increases, the amplification increases up to a point, and then decreases again for larger intensity motions. At periods of 5 and 10 seconds the data flatten out and approach zero, or no amplification. Figure 8.7 shows similar results from Kamai et al. (2013), where at longer periods the amplification factors show a humped shape as ground motion intensity increases.

Comparing Figure 8.3 with Figure 8.6 one can see that equation (8.14) cannot capture the humped shape caused by site period degradation; it can only capture increasing or decreasing behavior. However, as will be shown later, the residuals due to the model's inability to capture site period degradation are comparable and within the same range as residuals for other periods. As a result, the ability of the model to predict a humped shape was not considered worth the additional complexity that would need to be added to the model.

Figure 8.8a compares the values of f_1 from this study with those from the model proposed by Stewart and Seyhan (2013) for Vs_{30} = 150 m/s and Vs_{30} = 180 m/s. Both curves fall about in the

middle of the f_1 values calculated in this study up to a period of 2 seconds. For periods greater than 2 seconds, the f_1 values from this study fall off more sharply than those for the Stewart and Seyhan (2013) model. The Stewart and Seyhan (2013) model also dips around 0.06 seconds, which is slightly earlier than the dip at 0.1 seconds for f_1 values calculated in this study. The value of f_1 in the Stewart and Seyhan (2013) model is a function of Vs_{30} only (see equation (8.8)), and is applicable down to Vs_{30} = 150 m/s. The values of Vs_{30} for this study range from 80 to 160 m/s.

Figure 8.8b compares the calculated values of f_2 for this study with the values from Stewart and Seyhan (2013), the values inferred from the Kamai et al. (2013) model, and the mean empirical values calculated from the NGA West 2 database by Stewart and Seyhan (2013) for NEHRP E sites. The f_2 values of the NGA West 2 database fall about in the middle of the f_2 values calculated in this study. Values of f_2 from the other studies are greater than those from the NGA West 2 database, but still within the spread of f_2 values from this study. The Stewart and Seyhan (2013) and Kamai et al. (2013) models predict that the value of f_2 increases as Vs_{30} increases, which is not the case for the sites in this study. Figure 8.5b shows that for the period range of 0.01 to about 1 second, site Bay Area II K S4 with Vs_{30} = 79 m/s has the greatest values of f_2, and site HAGP with Vs_{30} = 127 m/s has the lowest. Figure 8.5 and Figure 8.8 show that more than just Vs_{30} is necessary to describe the seismic response of non-liquefiable NEHRP F sites.

8.3.2 Model Development: Stage 2

The second stage of the regression calculated the dependence of f_1 and f_2 on site properties. This study investigated 12 different site properties. The 12 site properties investigated were chosen based on the findings of chapter 7. They are mostly features of the "special" soil layers that classify the site as a NEHRP F site rather than properties for the entire site or properties averaged over the top 30 meters of the site. The "special" soil layers that classify sites as non-liquefiable NEHRP F sites are peat and organic soil layers, soil layers with PI > 75, or thick deposits of soft soil. The 12 site properties investigated were the thickness of the special soil layers (Th), the elastic site period (Ts), the minimum and mean shear wave velocity of the special soil layers (Vs_{min}, Vs_{mean}), the minimum and mean values of the cyclic resistance ratio (CRR_{min}, CRR_{mean}) of the special soil layers, where CRR is the dynamic shear strength of the soil divided by the vertical effective confining pressure, the minimum and mean value of the dynamic shear strength of the special soil layers (τ_{min}, τ_{mean}), the minimum and mean value of the shear strain when G/G_{max} = 0.5 of the special soil layers ($\gamma_{0.5,min}$, $\gamma_{0.5,mean}$), and the minimum and mean value of the small strain damping of the special soil layers ($Dmin_{min}$, $Dmin_{mean}$). Table 8.5 lists the values of the 12 site properties described above for each of the 15 sites used in this study.

Figure 8.9 plots the coefficient of determination (R^2) using equation (8.15) to predict the value of f_1 at each period using a different site property as the independent variable X:

$$f_1(T) = c_1(T) + c_2(T) \times ln(X) \tag{8.15}$$

Figure 8.9 shows that no one parameter can predict f_1 well over all periods. For periods greater than about two seconds the elastic site period (Ts) has R^2 values of 0.6 to 0.8, and for periods between 0.7 seconds and one second the min and mean shear wave velocity of the special soil layers (Vs_{min}, Vs_{mean}) have R^2 values of 0.6 to 0.7. Figure 8.10 plots the coefficient of

determination (R^2) using equation (8.15) but for f_2 instead of f_1. The CRR_{min} and CRR_{mean} have the greatest predictive power of the site properties investigated for estimating f_2, with R^2 values from 0.8 to 0.9 for periods less than one second, R^2 = 0.4 to 0.6 for periods between one and three seconds, and R^2 = 0 for periods greater than three seconds. None of the investigated site properties can predict f_2 well for periods greater than three seconds. This is most likely because equation (8.14) cannot predict a humped amplification curve due to the degradation of the elastic site period, as shown in Figure 8.6.

Figure 8.9 and Figure 8.10 show regression analyses for only one site property at a time and one functional form. However, the effect of a particular site on a ground motion is complex and most likely a function of several variables. Therefore, this study conducted regression analyses on f_1 and f_2 for many different combinations of site properties using equations (8.16), (8.17), and (8.18):

$$f(T) = c_1(T) + \sum_{i=1}^{k} c_{i+1}(T) \times ln(X_i) \tag{8.16}$$

$$f(T) = c_1(T) + \sum_{i=1}^{k} c_{i+1}(T) \times X_i \tag{8.17}$$

$$f(T) = c_1(T) + \sum_{i=1}^{k} c_{i+1}(T) \times X_i^{d_i(T)} \tag{8.18}$$

where f is either f_1 or f_2, k is the number of variables in the model, c_1 through c_{k+1} and d_1 through d_k are coefficients, and X_i is the i^{th} site property in the model. Regression analyses were performed for all possible combinations of the site properties using models with k = 1-6, with the restrictions that minimum site properties were not allowed in the same model with mean site properties, and only one strength property was used per model (i.e. only one of CRR_{min}, CRR_{mean}, τ_{min}, τ_{mean}). These restrictions were used because these properties are highly correlated and are not independent predictors. This regression method lead to a total of 1,617 different trial models for f_1 and f_2.

Figure 8.11 shows the combination of site properties that gave the smallest RMSE for each number of variables allowed in the model. Figure 8.11a shows that the single best predictor of f_1 over all periods is Vs_{min}. However, for a model with three variables, the three best predictors of f_1 are Vs_{mean}, γ_{mean}, and Th. Figure 8.11b shows that the single best predictor of f_2 over all periods is CRR_{min}. The site property CRR_{min} remains in the model for all number of variables, which indicates that it is a strong predictor of f_2.

8.3.3 Model Development: Final Model

The final model combines equation (8.14) with models to predict f_1 and f_2. To determine the pair of models for f_1 and f_2 to use in the final model, this study compared the $RMSE_{adj}$ of the final model for all 36 pair-wise combinations of the 12 f_1 and f_2 models that gave the lowest RMSE

when predicting f_1 or f_2, as shown in Figure 8.11. The adjusted RMSE ($RMSE_{adj}$) and adjusted coefficient of multiple determination (R^2_{adj}) were calculated as shown below:

$$RMSE_{adj} = \sqrt{\frac{1}{(n-p-1)}\sum_{i=1}^{n}\left(Amp - Amp_{pred}\right)_i^2} \tag{8.19}$$

$$R^2_{adj} = [(n-1) \times R^2 - p]/(n-p-1) \tag{8.20}$$

where Amp is the amplification calculated with the site response analyses, Amp_{pred} is the amplification predicted with the final model, n is the total number of data points taken over all periods and intensity levels, and p is the number of coefficients used in the model. The adjusted RMSE and the adjusted coefficient of multiple determination were used as goodness of fit criteria because they account for the addition of more variables by a reduction factor based on the number of coefficients used in the model.

This study ranked the models according to their $RMSE_{adj}$ values, where rank = 1 is the final model with the lowest $RMSE_{adj}$, and rank = 36 is the final model with the f_1 and f_2 model pair that gave the largest $RMSE_{adj}$ according to equation (8.19). Figure 8.12 and Table 8.6 give the results. Figure 8.12c and Figure 8.12d show that as the number of variables included in the final model increases, $RMSE_{adj}$ decreases and R^2_{adj} increases. However, a model with 12 input site properties is not practical. Instead, this study chose the model indicated by the red star with rank = 24. The model with rank = 24 was chosen because it occurs at a break in the slope where the addition of more model parameters has less of an effect on the goodness of fit than before the break in the slope. This is clearly seen in Table 8.6, where adding eight variables to the model with four variables only increases R^2_{adj} by 0.029 (0.968- 0.939), whereas adding two variables to the model with two variables increases R^2_{adj} by 0.073 (0.939- 0.865). A model with fewer variables is desired because it is easier to implement in practice and there is less chance of the model being over-parameterized and bias toward the dataset used to develop it. Table 8.6 also lists the number of variables used to predict f_1 and f_2 for each of the final models. The site properties for each of the f_1 and f_2 models correspond to the site properties shown in Figure 8.11 for the same number of variables.

Equations (8.21) and (8.22) show the models of f_1 and f_2 for the final model with rank = 24:

$$\begin{aligned} f_1(T) = c_1(T) + c_2(T) \times ln(Th) + c_3(T) \times ln(Vs_{mean}) \\ + c_4(T) \times ln\left(\gamma_{0.5,mean}\right) \end{aligned} \tag{8.21}$$

$$f_2(T) = c_5(T) + c_6(T) \times ln(CRR_{min}) \tag{8.22}$$

where c_1 through c_6 are period dependent coefficients. Figure 8.13 and Table 8.7 give the values of c_1 through c_6 by period.

The final selected simplified model to predict the surface response spectrum of a non-liquefiable NEHRP F site consists of equations (8.14), (8.21), and (8.22), and is dependent on the site,

ground motion scenario, and period. Figure 8.14a shows the predicted amplification values versus the amplification values calculated from the nonlinear site response analyses in ln units. Figure 8.14b shows the residuals versus the values predicted with the simplified model, where the residuals are defined as the site response amplification values minus the simplified amplification values. These two plots show that there is no bias in the results and that there is an even distribution of the error for all predicted values. The R^2 value is 0.94 and the RMSE is 0.21. These are different from the $RMSE_{adj}$ and R^2_{adj} values given above because they are the absolute values, not the adjusted values. Figure 8.14c shows the residuals versus period and Figure 8.14d shows the standard deviation versus period. These two plots demonstrate that even though the functional form of equation (8.14) cannot follow the humped curve of the amplification versus ground motion intensity, the misfit due to this deficiency is comparable to the misfit at other periods. Based on these results, the ability of the model to predict a humped shape was not considered worth the additional complexity that would need to be added to the model.

Figure 8.15 displays the residuals by site and scenario versus period. While not much can be seen for points near the zero residuals line, these plots help to identify the sites, scenarios, and periods of outliers. For example, Figure 8.15 shows the simplified model over predicts the spectral response value of scenario SCR for the Bay Area II sites at short periods, but that it under predicts the response for the KIKNET sites at short periods. Figure 8.15 also shows that the simplified model under predicts the response of scenario SCR for sites Bay Area and Bay Area F at long periods, and over predicts the response of scenarios 400ACR3 and ACR2 for the KIKNET sites and site Bay Area II at long periods. Besides these outliers, almost all of the residuals are less than plus or minus 0.4 ln units, which is a little less than two standard deviations (see Figure 8.14).

Figure 8.16 compares the response spectra calculated from the site response analyses with the response spectra predicted from the simplified method for all scenarios and site Bay Area. It also plots the residuals versus period. Figure 8.16 shows that the simplified model is able to capture the trend and magnitude of the response spectra calculated from the site response analyses for all scenarios, regardless of the scenario intensity, tectonic region, magnitude, or distance. The plots of the residuals show that for site Bay Area, the simplified model over predicts the short periods and under predicts the long periods. Appendix 8A contains similar figures for all of the sites investigated in this study.

8.3.4 Standard Deviation

It is important to know the standard deviation of site response analyses to understand better the accuracy and reliability of the results. This study tracked two types of standard deviation; the standard deviation of the residuals of the simplified model fit (σ_{res}), and the standard deviation of the response spectra of the individual ground motions for a given site and scenario (σ_{RS}). Figure 8.14 shows σ_{res} versus period. Chapter 7.5 analyzed qualitatively the values of σ_{RS} for each site and scenario. Because this study developed the simplified model described above by regressing on the average spectral amplification ratio for each site and scenario (see equation (8.11)), the two standard deviations were kept separate. To estimate the total standard deviation (σ_{total}) the two standard deviations can be combined using equation (8.23):

$$\sigma(T)_{total} = \sqrt{\sigma(T)_{res}^2 + \bar{\sigma}(T)_{RS}^2} \quad (8.23)$$

where $\bar{\sigma}(T)_{RS}$ is the mean standard deviation of all the site and scenario σ_{RS}.

Figure 8.17a compares σ_{res} calculated in this study to σ_{res} calculated by Kamai et al. (2013) for sites with Vs_{30} = 190 m/s and using the Peninsula and Range MRD curves and Sa(T) as the ground motion intensity measure. Figure 8.17b compares σ_{total} for each study. Figure 8.17a shows that this study has greater values of σ_{res} than those of the Kamai et al. (2013) model for all periods. Figure 8.17b shows that both studies have comparable values of σ_{total} for periods less than three seconds, but for periods greater than three seconds the values of σ_{total} for this study continue to increase whereas the values of σ_{total} for the Kamai et al. (2013) model decrease. Comparing Figure 8.17a with Figure 8.17b shows that the difference at long periods in σ_{total} is mainly due to σ_{RS}. This agrees with the results of Roblee et al. (1996), who found that for long periods the overall response standard deviation is controlled by uncertainties in the source and path effects. Table 8.8 lists the values of σ_{res}, σ_{RS}, and σ_{total} by period.

8.4 Sensitivity Analysis of the Input Parameters

The following section presents a sensitivity analysis of the input parameters for the simplified model. Sensitivity analyses allow researchers and practitioners to understand better the effect of each input parameter on the predicted response. The five input parameters for the simplified model are the thickness of the special soil layers (Th), the mean shear wave velocity of the special soil layers (Vs_{mean}), the minimum value of the cyclic resistance ratio (CRR_{min}) of the special soil layers, where CRR is the dynamic shear strength of the soil divided by the vertical effective confining pressure, the mean value of the shear strain when $G/G_{max} = 0.5$ of the special soil layers ($\gamma_{0.5,mean}$), and the spectral acceleration expected on a rock site for the period range of interest ($Sa(T)_{rock}$). This study performed the sensitivity analysis by selecting representative values of standard deviations of the input variables and then calculating the predicted amplification for when one input variable is varied by $\pm$ 2 standard deviations and all other input variables are kept at their baseline values. This process was repeated for all 5 variables.

The sensitivity analysis assumed all input variables were log normally distributed and chose representative values of the standard deviations of the input variables from relevant sources in the literature. Kishida et al. (2009) give a standard deviation of the shear wave velocity of peats and organic clays of $\sigma_{Vs,mean} = 0.331$ in ln units. Wills and Clayhan found that $\sigma_{Vs,mean} = 0.243$ for intertidal mud around the San Francisco Bay and Sacramento/San Joaquin delta. This study used the value calculated by Kishida et al. (2009) for the standard deviation of the shear wave velocity of the special soil layers.

The standard deviation of CRR_{min} was calculated from Ladd (1991), who found that the mean value of $(Su/\sigma_v')_{NC}$ in equation (8.24) was 0.25 for soft and organic clays and had a standard deviation of 0.05, which equates to 0.182 ln units. As a result, this study used $\sigma_{CRR,min} = 0.182$ for the sensitivity analysis.

$$\tau_{ff} = Su = \sigma_v' \times \left(\frac{Su}{\sigma_v'}\right)_{NC} \times OCR^m \tag{8.24}$$

This study calculated the standard deviation of $\gamma_{0.5,mean}$ from the shear modulus reduction curves derived by Darendeli (2001). Darendeli (2001) gives the following equation for the standard deviation of shear modulus reduction curves:

$$\sigma_{G/Gmax} = exp(\phi_{13}) + \sqrt{\frac{0.25}{exp(\phi_{14})} - \frac{(G/G_{max} - 0.5)^2}{exp(\phi_{14})}} \tag{8.25}$$

where G/G_{max} is the value of the normalized shear modulus reduction curve, and ϕ_{13} andϕ_{14} are coefficients. Equation (8.25) gives the standard deviation of the shear modulus reduction curves, not the shear strain when $G/G_{max} = 0.5$. To calculate the standard deviation of $\gamma_{0.5,mean}$, this study used equation (8.25) to calculate $\sigma_{G/Gmax}$, then rearranged equation (8.29) to solve for $\gamma/\gamma_{0.5}$ for when $G/G_{max} = 0.5 \pm \sigma_{G/Gmax}$:

$$\frac{G}{G_{max}} = \frac{1}{1 + \left(\frac{\gamma}{\gamma_{0.5}}\right)^{0.919}} \tag{8.26}$$

where equation (8.26) is the equation for G/G_{max} given by Darendeli (2001). The resulting value of the standard deviation of $\gamma_{0.5,mean}$ used in the sensitivity analysis was $\sigma_{\gamma 0.5,mean} = 0.425$.

This study found no correlations for the thickness of non-liquefiable NEHRP F site special soil layers. Therefore, this investigation used a value of $\sigma_{Th} = 0.3$ for the sensitivity analysis, which is similar to the standard deviation of the shear wave velocity.

The standard deviation of $Sa(T)_{rock}$ was taken as the standard deviation given by the five NGA West 1 GMPEs used to develop the target response spectrum for scenario 100ACR3 (see chapter 2).

Figure 8.18 shows the results of the sensitivity analysis for each of the five input parameters at all periods for site Bay Area and scenario 100ACR3. The dotted line in each plot is the baseline amplification calculated for when all input variables are set at their baseline values. The solid lines are the amplification values calculated when the given input variable is set to $\pm$ 2 standard deviations and all other input variables are kept at their baseline values. Figure 8.18 shows that the calculated amplification is sensitive to all five input variables for periods less than about two seconds. However, for periods greater than two seconds, the amplification is not sensitive to $\gamma_{0.5,mean}$, for periods greater than four seconds the amplification is not sensitive to CRR_{min} and $Sa(T)_{rock}$, and for periods greater than seven seconds the amplification is not sensitive to the input values of Th and Vs_{mean} tested in this study.

Figure 8.19a shows the amplification value calculated when a given parameter is increased by two standard deviations minus the baseline amplification values. Figure 8.19a shows that when Th and $Sa(T)_{rock}$ are increased by +2 standard deviations, the calculated amplification for short

periods will be less than the baseline amplification, while the opposite is true for Vs_{mean}, CRR_{min}, and $\gamma_{0.5,mean}$. Figure 8.19b is the same as Figure 8.19a except that it plots the absolute value of the difference between the calculated amplification when a given input variable is increased by two standard deviations compared with the baseline amplification. This makes a comparison of the relative magnitude of the effect of each input variable on the amplification easier. Figure 8.19b shows that the calculated amplification is most sensitive to the Vs_{mean} of the special soil layers for almost all periods, but especially for periods around 0.1 seconds. The calculated amplification is also sensitive to $Sa(T)_{rock}$ for periods less than about four seconds, and is least sensitive to CRR_{min}, and $\gamma_{0.5,mean}$.

8.5 Estimating Properties for Use in the Simplified Model

The simplified model requires the spectral acceleration on rock $Sa(T)_{rock}$ over the period range of interest as well as four site properties; the total thickness of the special soil layers (Th), the mean shear wave velocity of the special soil layers (Vs_{mean}), the minimum value of the cyclic resistance ratio (CRR_{min}) of the special soil layers, where CRR is the dynamic shear strength of the soil divided by the vertical effective confining pressure, and the mean value of the shear strain when $G/G_{max} = 0.5$ of the special soil layers ($\gamma_{0.5,mean}$). The "special" soil layers are the soil layers that classify a site as a non-liquefiable NEHRP F site, such as peat or highly organic clays, soils with PI > 75, and soft to medium stiff clays. The following section describes how to calculate each of the input parameters for the simplified model, as well as lists a few of the techniques, methods, and correlations available in the literature to estimate the necessary parameters.

The thickness (Th) of the special soil layers can be estimated from boring logs, shear wave velocity profiles, and soil samples retrieved at various depths. Soil samples are necessary to determine if there are organic soil layers or cohesive soils with PI > 75. The organic content of soil samples can be estimated according to ASTM D2974 (ASTM, 2014a), and the plasticity index of soil samples can be estimated by performing Atterberg limit tests according to ASTM D4318 (ASTM, 2014b). The thickness of soft to medium stiff clay layers can be estimated from boring logs to see if the soil is clay, and the shear wave velocity profile to estimate the stiffness.

The shear wave velocity (Vs) of the special soil layers can be determined from in-situ seismic tests such as the down hole or cross hole seismic tests, spectral analysis of surface waves test (SASW), or the seismic cone test. In addition, empirical models to estimate G_{max} such as the model presented in chapter 4 can also be used to estimate Vs. Once the value of Vs is known for each layer of the special soils, the value of Vs_{mean} is calculated as:

$$Vs_{mean} = \frac{Th}{\sum_{i=1}^{n} \frac{h_i}{Vs_i}} \tag{8.27}$$

where h_i is the thickness of special soil layer i, Vs_i is the shear wave velocity of special soil layer i, and n is the number of special soil layers.

The shear strength of the special soil layers can be estimated from field tests such as the vane shear test or the cone penetration test (CPT), from laboratory tests such as the triaxial

compression test or direct simple shear test, or from soil properties using the SHANSEP method (Ladd and Foott, 1974) or other relevant soil strength models. To adjust the static shear strength for rate effects, relationships given by Sheahan et al. (1996) or Biscontin and Pestana (1999) may be used. Once the dynamic shear strengths of all the special soil layers are known, the value of CRR_{min} is calculated as the minimum value of the dynamic shear strength of each special soil layer divided by its vertical effective confining pressure:

$$CRR_{min} = min\left[\frac{\tau_i}{\sigma'_{v,i}}, \frac{\tau_{i+1}}{\sigma'_{v,i+1}}, \ldots, \frac{\tau_n}{\sigma'_{v,i}}\right] \quad (8.28)$$

where τ_i is the dynamic shear strength of special soil layer i, $\sigma'_{v,i}$ is the vertical effective stress of special soil layer i, and n is the number of special soil layers.

The shear modulus reduction and damping curves of the special soil layers can be estimated from laboratory tests such as the resonant column test, cyclic triaxial test, or the cyclic direct simple shear test. In addition, they can be estimated from appropriate models found in the literature. Once the shear modulus reduction curves of all the special soil layers are known, $\gamma_{0.5}$ of each special soil layer is defined as the shear strain value in percent where $G/G_{max} = 0.5$. Using the values of $\gamma_{0.5}$ for the special soil layers, the value of $\gamma_{0.5,mean}$ is calculated as:

$$\gamma_{0.5,mean} = \frac{1}{Th} \times \sum_{i=1}^{n} h_i \times \gamma_{0.5} \quad (8.29)$$

When no dynamic test data are available for a specific soil, this study recommends the model developed by Darendeli (2001) to estimate the shear strain when $G/G_{max} = 0.5$ ($\gamma_{0.5}$) for a given soil layer:

$$\gamma_{0.5} = (0.0352 + 0.001 \times PI \times OCR^{0.3246}) \times \sigma'^{0.3483}_m \quad (8.30)$$

where $\gamma_{0.5}$ is in percent, PI is the plasticity index, OCR is the overconsolidation ratio, and σ'_m is the mean effective confining pressure in atmospheres. This study recommends the model by Kishida et al. (2009) for peats and organic soil layers.

Other models that can be used to estimate $\gamma_{0.5}$ directly are those by Vucetic and Dobry (1991) and Zhang et al. (2005). The following equation for $\gamma_{0.5}$ is inferred from the curves of Vucetic and Dobry (1991) for cohesive soils:

$$\gamma_{0.5} = -0.2106 \times \left(\frac{PI}{100}\right)^3 + 0.5116 \times \left(\frac{PI}{100}\right)^2 + 0.2669 \times \left(\frac{PI}{100}\right) + 0.0226 \quad (8.31)$$

This equation should not be used for PI > 200.

Zhang et al. (2005) proposed the following equation for $\gamma_{0.5}$ for cohesive soils:

$$\gamma_{0.5} = \gamma_{r1}\left(\frac{\sigma'_m}{P_a}\right)^k \tag{8.32}$$

where

$$k = \begin{cases} 0.42 \times e^{-.0456 \times PI} & \text{for residual/saprolite soil} \\ 0.316 \times e^{-.0142 \times PI} & \text{for Quaternary soil} \\ 0.316 \times e^{-.011 \times PI} & \text{for Tertiary and older soil} \end{cases} \tag{8.33}$$

$$\gamma_{r1} = \begin{cases} 0.0009 \times PI + 0.0385 & \text{for residual/saprolite soil} \\ 0.0011 \times PI + 0.0749 & \text{for Quaternary soil} \\ 0.0004 \times PI + 0.0311 & \text{for Tertiary and older soil} \end{cases} \tag{8.34}$$

To estimate $Sa(T)_{rock}$, any applicable ground motion prediction equation may be used. For active crustal regions the $Sa(T)_{rock}$ can be estimated used the five NGA West 1 GMPEs (Abrahamson and Silva, 2008; Boore and Atkinson, 2008; Campbell and Bozorgnia, 2008; Chiou and Youngs, 2008; and Idriss, 2008) or the new NGA West 2 GMPEs (Abrahamson et al., 2013; Campbell and Bozorgnia, 2013; Chiou and Youngs, 2013; Boore et al., 2013; and Idriss, 2013). The models by Youngs et al. (1997), Atkinson and Boore (2003), Zhao et al. (2006), and Atkinson and Macias (2009) may be used for subduction zones, and the models by Toro et al. (1997, 2002), Silva et al. (2002), Atkinson and Boore (2006, 2011), and Pezeshk et al (2011) for stable continental regions.

8.6 Validation of the Simplified Model

To test the robustness of the simplified model, a second, smaller database of effective stress nonlinear site response analyses was compiled. The simplified method was then used to predict the response of the validation database and its goodness of fit evaluated. This validation was necessary since there exists very little empirical data on the site response of non-liquefiable NEHRP F sites with which to validate the model.

The validation database consists of three sites and eight ground motion scenarios. Table 8.9 lists the target values of the ground motion scenarios and Figure 8.20 shows the target response spectrum for each scenario. The validation scenarios were chosen to give different spectral shapes and ground motion intensities than the scenarios of the main database. The target response spectrum for each scenario was calculated in the same way as the target response spectra of the main database outlined in Chapter 2; the four ground motions for active crustal regions were calculated using the five NGA West 1 GMPEs (Abrahamson and Silva, 2008; Boore and Atkinson, 2008; Campbell and Bozorgnia, 2008; Chiou and Youngs, 2008; and Idriss, 2008), the two subduction zone scenario response spectra were calculated with the Youngs et al. (1997), Atkinson and Boore (2003), Zhao et al. (2006), and Atkinson and Macias (2009) GMPEs, and the two response spectra for the stable continental region scenarios were calculated with the Toro et al. (1997, 2002), Silva et al. (2002), Atkinson and Boore (2006, 2011), and Pezeshk et al (2011) GMPEs. Table 8.10 lists the ground motions selected for each scenario.

The ground motions listed in Table 8.10 were spectrally matched to their respective target response spectrum over the period range of 0.06 to 5 seconds using the program RspMatch 2009 (Al-Atik and Abrahamson, 2010). The ground motions were spectrally matched because the simplified procedure was developed to estimate the average ground motion from a suite of ground motions, which is a smoothed response spectrum, not from an individual motion that has peaks and troughs. Spectrally matching one motion to the target response spectrum gives a rough estimate of the average value for the scenario. Ideally, more ground motions would be used for each scenario, as was done with the main database. Appendix 8B contains plots comparing the original ground motions to the spectrally matched ground motions used in the validation site response analyses.

Table 8.11 lists the site properties of the special soil layers and Figure 8.21, Figure 8.22, and Figure 8.23 show site properties versus depth for the three validation sites. This study chose the validation site properties so that each site was a non-liquefiable NEHRP F site and had different values of the input site parameters (Th, Vs_{mean}, $\gamma_{0.5,mean}$, and CRR_{min}) for the simplified model than the original sites. Validation sites 1 and 3 are NEHRP F sites because they have 37 meters or more of soft to medium stiff clays, and validation site 2 is a NEHRP F site because it has more than 3 meters of peat or organic clay. The values of Th for validation sites 1 and 2 are the thicknesses of the special soil layers, which are the CH layer for validation site 1 shown in Figure 8.21, and the OH layer for validation site 2 shown in Figure 8.22. The value of Th for validation site 3 is the combined thicknesses of all the CH layers and MH/CH layer, ignoring the clayey sand seams (SC) that separate them. The values of Vs_{mean}, CRR_{min}, and $\gamma_{0.5,mean}$ for each validation site were calculated using equations (8.27), (8.28), and (8.29).

Effective stress nonlinear site response analyses were conducted in the program DEEPSOIL (Hashash et al., 2012) for each site and scenario combination, giving a total of 24 site response analyses. Appendix 8B contains tables listing the input parameters for each site in DEEPSOIL. The surface response spectrum for each of the 24 validation cases was predicted using the simplified model and compared to the results of the validation site response analyses. The values of $Sa(T)_{rock}$ used in the simplified model were the spectral values of the input ground motions used in the validation site response analyses.

Figure 8.24a shows the predicted amplification values versus the amplification values calculated from the validation nonlinear site response analyses in ln units. Figure 8.24b shows the residuals versus the values predicted with the simplified model, where the residuals are defined as the validation site response amplification values minus the simplified amplification values. These two plots show that there is no bias in the results and that there is an even distribution of the error for all predicted values. This is significant because the validation data was not used in the development of the simplified model. The R^2 value of the validation site response analyses amplification ratios to the amplification predicted with the simplified model is 0.87, and the RMSE is 0.34. Figure 8.24c shows the residuals versus period and Figure 8.24d shows the standard deviation versus period. The standard deviation varies between 0.2 to 0.25 with three spikes to values of 0.45 at periods of 0.1, 2, and 10 seconds.

Figure 8.25 displays the residuals by site and scenario versus period. Figure 8.25a shows that for validation sites 1 and 3 there is an even distribution of the residuals with period. For validation

site 2 however, the simplified model over predicts the amplification at short periods, and under predicts the amplification at long periods. Figure 8.25b shows that there is an even distribution of residuals for all scenarios, except for the stable continental region scenarios at short periods, where the simplified model over predicts the response.

Figure 8.26 compares the response spectra calculated from site response analyses with the response spectra predicted from the simplified method for all scenarios and validation site 1. It also plots the residuals versus period. The response spectra from the site response analyses are not as smooth as those from the main database because only one input ground motion was used. Figure 8.26 shows that the simplified model is able to capture the trend and magnitude of the response spectra calculated from the site response analyses for all scenarios, regardless of the scenario intensity, tectonic region, magnitude, or distance. The plots of the residuals for validation site 1 show no bias with period, however the scatter about the zero residuals line is greater than for most of the sites tested in the main database. Appendix 8B contains similar figures for all of the validation sites.

8.7 Comparison with 80% of IBC Specified NEHRP E Site Design Spectra

The 2012 International Building Code (IBC, 2012) requires site specific studies for NEHRP F sites. The 2012 IBC also requires that design spectra calculated from site specific studies be no less than 80% of the code design spectra for the particular site conditions. This section compares the response spectra calculated with the effective stress nonlinear site response analyses conducted in this study with design spectra calculated following the method of the 2012 IBC for NEHRP E sites multiplied by 0.80. The purpose of this section is to examine how reasonable the 80% design spectrum floor is for non-liquefiable NEHRP F sites, and also to demonstrate the variability of NEHRP F sites and reemphasize the need for a simplified procedure.

Section 8.2.1 outlines the development of the code design factors, and Figure 8.1 shows how to use the site factors to calculate the design spectrum according to the 2012 IBC. Instead of using the factors given in the 2012 IBC for E sites, however, the new 2015 NEHRP site factors derived by Stewart and Seyhan (2013) and approved by the Provisions Update Committee of the Building Seismic Safety Council Section were used. Table 8.12 lists the new 2015 NEHRP site factors as well as the current site factors. Figure 8.27 plots the calculated design spectrum for each of the scenarios used in this study multiplied by 0.80.

Figure 8.28a shows the predicted code amplification values versus the amplification values calculated from the nonlinear site response analyses in ln units. Figure 8.28b shows the residuals versus the values predicted with the code. Figure 8.28c shows the residuals versus period and Figure 8.28d shows the standard deviation versus period. The R^2 value is 0.56, the RMSE is 0.57, and the standard deviation varies with period from 0.4 to 0.6. These goodness of fit measures are much worse than those for the simplified method, however, this is expected because the code procedure is for NEHRP E sites and is based on Vs_{30}, whereas the simplified method was developed for non-liquefiable NEHRP F sites, and takes into account the effects of the shear strength, thickness, and shear modulus reduction curves of the "special" soil layers.

Figure 8.29 compares the response spectra calculated from site response analyses with the response spectra predicted from the code for all scenarios and site Bay Area. Figure 8.29 shows that the code method, which is 80% of the NEHRP E design spectra for each scenario, over predicts the response spectra for periods less than about one second and under predicts the period of the peak spectral values for all scenarios except 12ACR3 and 25ACR3.

Figure 8.28 and Figure 8.29 show the importance of a site specific study for NEHRP F sites and the necessity for a simplified method to estimate their design spectra. Figure 8.28 and Figure 8.29 also show that the 80% floor of response spectral values required by the 2012 IBC method is consistently greater than the response spectral values predicted in this study, for all scenarios except 12ACR3 and 25ACR3. This demonstrates that NEHRP F sites may lead to design spectra that are less than 80% of NEHRP E site design spectra for moderate to large levels of shaking intensity.

8.8 Conclusion

This chapter examined results of effective stress nonlinear site response analyses conducted in the program DEEPSOIL (Hashash et al., 2012) for all combinations of 15 sites and 10 ground motion scenarios. Section 8.2 briefly outlined previous research on site amplification models, and section 8.3 described the development of a simplified model based on the results of the site response analyses to estimate the response spectrum at the surface of a non-liquefiable NEHRP F site. The simplified model was developed in two stages. In the first stage, the results for each site were regressed separately against the ground motion intensity to estimate the effect of the ground motion scenario. In the second stage, the site specific coefficients calculated from the first stage were regressed against site properties to determine their site dependence. These two parts were then combined to form the final model given below:

$$ln(Amp(T)) = f_1(T) + f_2(T) \times ln\left(\frac{Sa(T)_{Rock} + 0.1}{0.1}\right) \tag{8.35}$$

$$f_1(T) = c_1(T) + c_2(T) \times ln(Th) + c_3(T) \times ln(Vs_{mean}) + c_4(T) \times ln\left(\gamma_{0.5,mean}\right) \tag{8.36}$$

$$f_2(T) = c_5(T) + c_6(T) \times ln(CRR_{min}) \tag{8.37}$$

where Amp(T) is the amplification defined as the ratio of the surface spectral acceleration at period T divided by the spectral acceleration that would be expected on a rock site for the same period T, $Sa(T)_{rock}$ is the spectral acceleration on rock at period T, Th is the total thickness in meters of the special soil layers, Vs_{mean} is the mean shear wave velocity of the special soil layers in m/s, $\gamma_{0.5,\ mean}$ is the mean shear strain when G/Gmax = 0.5 of the special soil layers in percent, CRR_{min} is the minimum value of the cyclic resistance ratio of the special soil layers, where CRR is the dynamic shear strength of the soil divided by the vertical effective confining pressure, and c_1 through c_6 are period dependent coefficients listed in Table 8.7. The "special" soil layers are defined as the soil layers that classify the site as a NEHRP F site, such as peat and organic soil layers, soil layers with PI > 75, or thick deposits of soft soil.

The thickness (Th) of the special soil layers can be estimated from boring logs, shear wave velocity profiles, and soil samples retrieved at various depths. The special soil layers do not necessarily have to be contiguous. The other site parameters are calculated as:

$$Vs_{mean} = \frac{Th}{\sum_{i=1}^{n} \frac{h_i}{Vs_i}} \tag{8.38}$$

$$CRR_{min} = min\left[\frac{\tau_i}{\sigma'_{v,i}}, \frac{\tau_{i+1}}{\sigma'_{v,i+1}}, \ldots, \frac{\tau_n}{\sigma'_{v,i}}\right] \tag{8.39}$$

$$\gamma_{0.5,mean} = \frac{1}{Th} \times \sum_{i=1}^{n} h_i \times \gamma_{0.5,i} \tag{8.40}$$

where h_i is the thickness, Vs_i is the shear wave velocity, τ_i is the dynamic shear strength, $\sigma'_{v,i}$ is the vertical effective stress, and $\gamma_{0.5,i}$ is the shear strain where $G/G_{max} = 0.5$ for special soil layer i, and n is the number of special soil layers. The values of $Sa(T)_{rock}$ can be estimated using any applicable ground motion prediction equation (e.g. Abrahamson et al. (2013) for active crustal regions).

The standard deviation for the model can be taken as either the standard deviation of the residuals due to the misfit of the simplified model to the site response analyses (σ_{res}), or the total standard deviation (σ_{total}), which includes both σ_{res} and the standard deviation of the response spectra of the individual ground motions for a given site and scenario (σ_{RS}). Table 8.8 lists the values of σ_{res}, σ_{RS}, and σ_{total} by period. The value of σ_{res} varies between 0.15 and 0.25.

The simplified model was validated against a separate database than the one used to develop it. This validation database consisted of three sites and eight ground motion scenarios. The validation of the model is important because it prevents over-parameterization. The model performed well ($R^2 = 0.89$, RMSE = 0.34) and showed no bias.

The simplified model presented in this chapter does not replace a site response analysis, but rather augments it. It is hoped that the results of this chapter as well as the previous chapter will help practicing engineers gain a better understanding of their site before conducting site response analyses. This will help them to focus on the important aspects of the site, which will save time and money.

8.9 References

Abrahamson, N. A., and Silva, W. J., (1997). "Empirical response spectral attenuation relations for shallow crustal earthquakes, *Seismological Research Letters*, Vol 68, pp. 94–127.

Abrahamson, N.A., and Silva, W.J. (2008). "Summary of the Abrahamson and Silva NGA Ground-Motion Relations." *Earthquake Spectra* 24(1), 67-97.

Abrahamson, N.A., Silva, W.J., and Kamai, R. (2013). "Update of the AS08 Ground-Motion Prediction Equations Based on the NGA-West2 Data Set." PEER Report 2013/04, *Pacific Earthquake Engineering Research Center*, University of California, Berkeley, CA.

Al Atik, L., and Abrahamson, N.A. (2010). "An Improved Method for Nonstationary Spectral Matching." Earthquake Spectra, 26(3), 601-617.

Ancheta, T.D., Darragh, R.B., Stewart, J.P., Seyhan, E., Silva, W.J., Chiou, B.S.J., Wooddell, K.E., Graves, R.W., Kottke, A.R., Boore, D.M., Kishida, T. and Donahue, J.L. (2013). "PEER NGA West2 Database." *PEER Report 2013/03*, PEER, University of California, Berkeley, California.

Applied Technology Council (ATC). (1978). ''Tentative provisions for the development of seismic regulations for buildings.'' ATC 3-06 Rep., Redwood City, Calif.

ASTM Standard D2974 (2014a). "Standard Test Methods for Moisture, Ash, and Organic Matter of Peat and Other Organic Soils." *ASTM International*, West Conshohocken, PA, < http://www.astm.org/>

ASTM Standard D4318 (2014b). "Standard Test Methods for Liquid Limit, Plastic Limit, and Plasticity Index of Soils." *ASTM International*, West Conshohocken, PA, < http://www.astm.org/>

Bazzurro, P., and Cornell, C.A. (2004). "Ground-Motion Amplification in Nonlinear Soil Sites with Uncertain Properties." *Bulletin of the Seismological Society of America*, 94(6), pp. 2090–2109.

Biscontin, G. and Pestana, J.M. (1999). "Influence of peripheral velocity on undrained shear strength and deformability characteristics of a bentonite-kaolinite mixture," Geotechnical Engng Report No. UCB/GT/99-19, Dep. of Civil & Environ. Eng., University of California, Berkeley.

Boore, D.M., and Atkinson, G.M. (2008). "Ground-motion prediction equations for the average horizontal Component of PGA, PGV, and 5%-Damped PSA at Spectral Periods between 0.01s and 10.0s." *Earthquake Spectra* 24(1), 99-138.

Boore, D. M., Joyner, W. B., and Fumal, T. E., (1997). "Equations for estimating horizontal response spectra and peak acceleration from western North American earthquakes: A summary of recent work." *Seismological Research Letters*, Vol 68, pp. 128–153.

Boore, D.M., Stewart, J.P., Seyhan, E., Atkinson, G.M., (2013). "NGA-West2 Equations for Predicting Response Spectral Accelerations for Shallow Crustal Earthquakes." PEER Report 2013/05, *Pacific Earthquake Engineering Research Center*, University of California, Berkeley, CA.

Campbell, K., and Bozorgnia, Y. (2008). "NGA ground motion model for the geometric mean horizontal component of PGA, PGV, PGD, and 5% damped linear elastic response spectra for periods ranging from 0.01 to 10s." *Earthquake Spectra* 24 (1), 139-171.

Campbell, K.W., and Yousef Bozorgnia, (2013). "NGA-West2 Campbell-Bozorgnia Ground Motion Model for the Horizontal Components of PGA, PGV, and 5%-Damped Elastic Pseudo-Acceleration Response Spectra for Periods Ranging from 0.01 to 10 sec." PEER

Report 2013/06, *Pacific Earthquake Engineering Research Center*, University of California, Berkeley, CA.
Chiou, B., Darragh, R., Gregor, N., and Silva, W. (2008). "NGA project strong-motion database," *Earthquake Spectra*, (24) 1, 23-44.
Chiou, B., and Youngs, R. (2008). "An NGA model for the average horizontal component of peak ground motion and response spectra." *Earthquake Spectra* 24(1), 173-215.
Chiou, B.S.J., and Robert R. Youngs, (2013). "Update of the Chiou and Youngs NGA Ground Motion Model for Average Horizontal Component of Peak Ground Motion and Response Spectra." PEER Report 2013/07, *Pacific Earthquake Engineering Research Center*, University of California, Berkeley, CA.
Choi, Y., and Stewart, J. P. (2005). "Nonlinear Site Amplification as Function of 30 m Shear Wave Velocity." *Earthquake Spectra*, Vol 21, pp. 1–30.
Darendeli, M. B. (2001). "Development of a new family of normalized modulus reduction and material damping curves." PhD dissertation, Univ. of Texas at Austin, Austin, Texas.
Dobry R., Borcherdt, R.D., Crouse, C.B., Idriss, I.M., Joyner, W.B., Martin, G.R., Power, M.S., Rinne, E.E., and Seed R.B. (2000). "New site coefficients and site classification system used in recent building seismic code provisions." *Earthquake Spectra*, 16(1), 41- 67.
Dobry, R., Martin, G.R., Parra, E., and Bhattacharyya, A., (1994). "Development of site dependent ratios of elastic response spectra (RRS) and site categories for building seismic codes." In *proceedings of the NCEER/SEAOC/BSSC Workshop on Site Response During Earthquakes and Seismic Code Provisions*, G.R. Margin, ed. University of Southern California, Los Angeles, November 18-20, 1992, National Center for Earthquake Engineering Research Special Publication NCEER-94-SP01, Buffalo, NY.
Electric Power Research Institute (EPRI), (1993). *Guidelines for Determining Design Basis Ground Motions*. Palo Alto, CA: Electric Power Research Institute, vol. 1–5, TR 102293.
Hashash, Y.M.A, Groholski, D.R., Phillips, C. A., Park, D, Musgrove, M. (2012) "DEEPSOIL 5.1, User Manual and Tutorial." 107 p.
IBC (2012). International *Building Code*, by International Code Council, Delmar Publishers.
Idriss, I.M. (2008). "An NGA empirical model for estimating the horizontal spectral values generated by shallow crustal earthquakes." Earthquake Spectra 24(1), 217-242.
Idriss, I.M. (2013). "NGA-West2 Model for Estimating Average Horizontal Values of Pseudo-Absolute Spectral Accelerations Generated by Crustal Earthquakes." PEER Report 2013/08, *Pacific Earthquake Engineering Research Center*, University of California, Berkeley, CA.
Kishida, T., Boulanger R.W., Abrahamson N.A., Wehling T.M., Driller M.W. (2009). "Regression Models for Dynamic Properties of Highly Organic Soils." *J. of Geotech. and Geoenvir. Eng.*, ASCE, 135(4).
Ladd, C. C. (1991). "Stability evaluation during staged construction." *Journal of Geotechnical Engineering*, ASCE, 117(4), 540-615.
Ladd, C. C., and Foott, R. (1974). "A New design procedure for stability of soft clays." *Journal of the Geotechnical Engineering Division*, ASCE,100(GT7), pp. 763-786.
Li, X.S., Z.L. Wang and C.K. Shen (1992). *SUMDES: A nonlinear procedure for response analysis of horizontally-layered sites subjected to multi-directional earthquake loading*, Dept. of Civil Eng., Univ. of Calif., Davis.
Luco, Nicolas (2007). "Ground Motions for Design." *USGS Thailand Seismic Hazard Workshop*, January 18, 2007.

<http://earthquake.usgs.gov/hazards/about/workshops/thailand/downloads/070118--Luco_on_Ground_Motions_for_Design(v8).pdf>

Martin, G.R., ed. (1994). *Proceedings of the 1992 NCEER/SEAOC/BSSC Workshop on Site Response During Earthquakes and Seismic Code Provisions*. University of Southern California, Los Angeles, November 18-20, 1992. National Center for Earthquake Engineering Research Special Publication NCEER-94-SP01, Buffalo, NY.

Roblee, C.J., Silva, W.J., Toro, G.R., and Abrahamson, N. (1996). "Variability in Site-Specific Seismic Ground-Motion Design Predictions." In *Uncertainty in the Geologic Environment: From Theory to Practice*, C. D. Shakelford and P. P. Nelson (Editors), ASCE Geotech Special Publication No. 58, Madison Wisconsin, 31 July–3 August 1996.

Seed, R.B., Dickenson, S.E., Rau, G.A., White, R.K., and Mok, C.M. (1994). "Observations regarding seismic response analyses for soft and deep clay sites." In *proceedings of the NCEER/SEAOC/BSSC Workshop on Site Response During Earthquakes and Seismic Code Provisions*, G.R. Margin, ed. University of Southern California, Los Angeles, November 18-20, 1992, National Center for Earthquake Engineering Research Special Publication NCEER-94-SP01, Buffalo, NY.

Seed, H. B., Murarka, R., Lysmer, J., and Idriss, I. M. (1976a). ''Relationship between maximum acceleration, maximum velocity, distance from source and local site conditions for moderately strong earthquakes.'' *Bulletin of the Seismological Society of America*, Vol 66, pp. 1323–1342.

Seed, H. B., Ugas, C., and Lysmer, J. (1976b). ''Site-dependent spectra for earthquake resistant design.'' *Bulletin of the Seismological Society of America*, Vol 66, pp. 221–244.

Sheahan, T.C., C.C. Ladd, and J.T. Germaine (1996) "Rate-dependent undrained shear behavior of saturated clay," *J. Geotech. Engr.*, ASCE, 122 (2), 99-108.

Silva, W.J., Lee, K. (1987). "WES RASCAL code for synthesizing earthquake ground motions." *State-of-the-Art for Assessing Earthquake Hazards in the United States*, Report 24, U.S. Army Engineers Waterways Experiment Station, Miscellaneous Paper S-73-1.

Stewart, J.P., and Seyhan, E. (2013). "Semi-Empirical Nonlinear Site Amplification and its Application in NEHRP Site Factors." PEER Report 2013/13, *Pacific Earthquake Engineering Research Center*, University of California, Berkeley, CA.

Walling, M., Silva, W.J., Abrahamson, N.A (2008). "Nonlinear site amplification factors for constraining the NGA models." *Earthquake Spectra*, 24(1) 243–255.

Whitman, R. ed., (1992). Proceedings of the Site Effects Workshop, October 24, 1991, Report NCEER-92-0006, National Center for Earthquake Engineering Research, Buffalo, NY.

Wills, CJ, and KB Clahan (2006). "Developing a map of geologically defined site-condition categories for California." *Bull. Seismo. Soc. Am.*, 96(4A), 1483–1501.

Vucetic, M. and Dobry, R. (1991). "Effect of soil plasticity on cyclic response." *Journal of Geotechnical Engineering*. ASCE, 117(1), 89–107.

Zhang, J., Andrus, R.D., and Juang, C.H. (2005). "Normalized Shear Modulus and Material Damping Ratio Relationships." *Journal of Geotechnical and Geoenvironmental Engineering*. ASCE, 131(4), 453 – 464.

Table 8.1: IBC site class definitions (IBC, 2012)

SITE CLASS	SOIL PROFILE NAME	AVERAGE PROPERTIES IN TOP 100 feet, SEE SECTION 1613.5.5		
		Soil shear wave velocity, $\bar{v}_s$, (ft/s)	Standard penetration resistance, $\bar{N}$	Soil undrained shear strength, $\bar{s}_u$, (psf)
A	Hard rock	$\bar{v}_s > 5{,}000$	N/A	N/A
B	Rock	$2{,}500 < \bar{v}_s \leq 5{,}000$	N/A	N/A
C	Very dense soil and soft rock	$1{,}200 < \bar{v}_s \leq 2{,}500$	$\bar{N} > 50$	$\bar{s}_u \geq 2{,}000$
D	Stiff soil profile	$600 \leq \bar{v}_s \leq 1{,}200$	$15 \leq \bar{N} \leq 50$	$1{,}000 \leq \bar{s}_u \leq 2{,}000$
E	Soft soil profile	$\bar{v}_s < 600$	$\bar{N} < 15$	$\bar{s}_u < 1{,}000$
E	—	Any profile with more than 10 feet of soil having the following characteristics: 1. Plasticity index $PI > 20$, 2. Moisture content $w \geq 40\%$, and 3. Undrained shear strength $\bar{s}_u < 500$ psf		
F	—	Any profile containing soils having one or more of the following characteristics: 1. Soils vulnerable to potential failure or collapse under seismic loading such as liquefiable soils, quick and highly sensitive clays, collapsible weakly cemented soils. 2. Peats and/or highly organic clays ($H > 10$ feet of peat and/or highly organic clay where H = thickness of soil) 3. Very high plasticity clays ($H > 25$ feet with plasticity index $PI > 75$) 4. Very thick soft/medium stiff clays ($H > 120$ feet)		

Table 8.2: Site coefficient F_a (top) and F_v (bottom) (From IBC, 2012)

Site Class	Spectral Response Acceleration Parameter at Short Period				
	$S_S \leq 0.25$	$S_S = 0.5$	$S_S = 0.75$	$S_S = 1.0$	$S_S \geq 1.25$
A	0.8	0.8	0.8	0.8	0.8
B	1.0	1.0	1.0	1.0	1.0
C	1.2	1.2	1.1	1.0	1.0
D	1.6	1.4	1.2	1.1	1.0
E	2.5	1.7	1.2	0.9	0.9
Site Class	**Spectral Response Acceleration Parameter at 1-second Period**				
	$S_1 \leq 0.1$	$S_1 = 0.2$	$S_1 = 0.3$	$S_1 = 0.4$	$S_1 \geq 0.5$
A	0.8	0.8	0.8	0.8	0.8
B	1.0	1.0	1.0	1.0	1.0
C	1.7	1.6	1.5	1.4	1.3
D	2.4	2.0	1.8	1.6	1.5
E	3.5	3.2	2.8	2.4	2.4

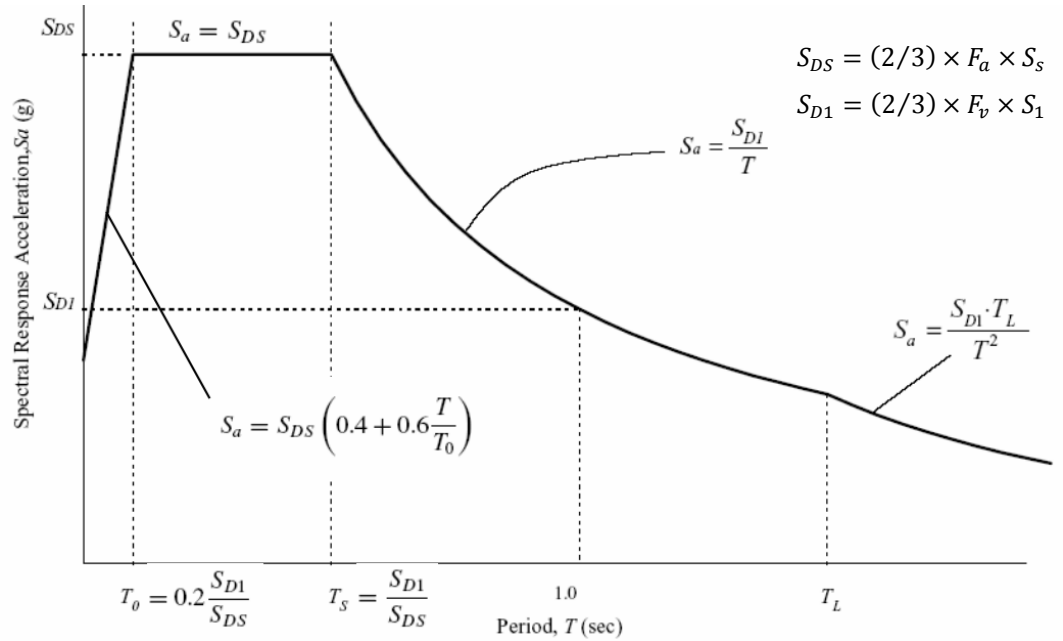

Figure 8.1: Procedure to calculate design spectrum following IBC (Modified from Luco, 2007)

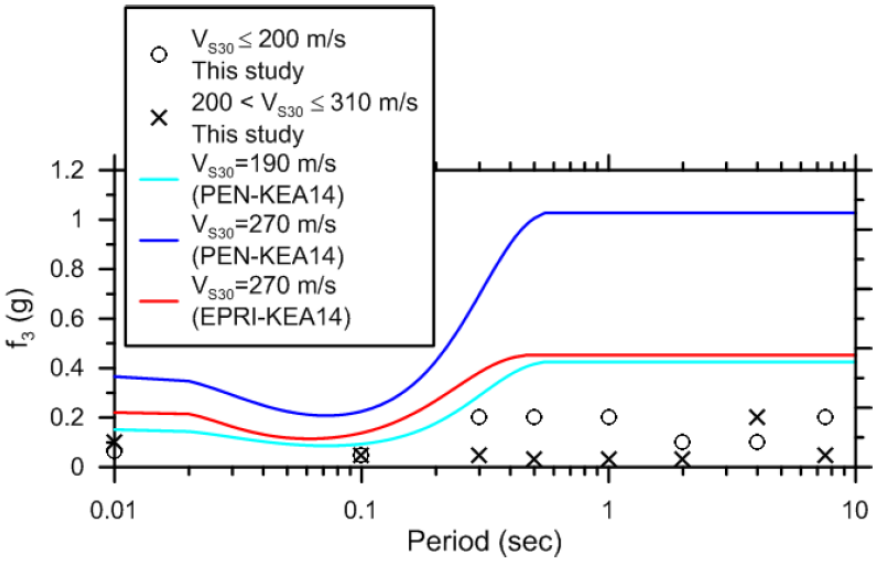

Figure 8.2: Comparison of coefficient f_3 from different studies (From Stewart and Seyhan, 2013)

Table 8.3: Ground motion scenarios used in the site response analyses

ID	# of GM	LUP (s)	HUP (s)	Region	Notes
12ACR3	40	0.04	13.33	ACR	Scenario ACR3 scaled motions multiplied by 0.125
25ACR3	40	0.04	13.33	ACR	Scenario ACR3 scaled motions multiplied by 0.25
50ACR3	40	0.04	13.33	ACR	Scenario ACR3 scaled motions multiplied by 0.50
100ACR3	40	0.04	13.33	ACR	Scenario ACR3 scaled motions
200ACR3	40	0.04	13.33	ACR	Scenario ACR3 scaled motions multiplied by 2
400ACR3	40	0.04	13.33	ACR	Scenario ACR3 scaled motions multiplied by 4
ACR3M	40	0.04	13.33	ACR	Scenario ACR3 matched motions
ACR1	11	0.04	8.85	ACR	
ACR2	40	0.04	6.15	ACR	Scenario ACR2 scaled motions
ACR2M	40	0.04	6.15	ACR	Scenario ACR2 matched motions
SUB	11	0.04	5	SUB	
SCR	11	0.02	10	SCR	

LUP = lowest useable period, HUP = highest useable period

ACR = active crustal region, SUB = subduction zone, SCR = stable continental region

Table 8.4: Properties of sites used in site response analyses

ID	Approximate Location	NEHRP	Vs_{30} (m/s)	Depth (m)	T_s (s)	Th (m)	Vs_{mean} (m/s)	$\gamma_{0.5,mean}$ (%)	CRR_{min}
Bay Area	SF Bay Area	E	125	185	2.66	19.25	101.4	0.0580	0.30
Bay Area F	SF Bay Area	F	119	189	2.84	36.85	119.6	0.0699	0.29
Bay Area II	SF Bay Area	F	79	32	1.58	9.75	34.8	0.1216	0.61
Bay Area II K	SF Bay Area	F	79	32	1.58	9.75	34.8	0.7238	0.58
Bay Area II K S2	SF Bay Area	F	79	32	1.58	9.75	34.8	0.9831	1.15
Bay Area II K S4	SF Bay Area	F	79	32	1.58	9.75	34.8	1.8661	2.35
HAGP	Guayaquil, Ecuador	F	127	50	1.23	37.00	136.3	0.0733	0.22
JSSS	Ottawa, Canada	F	143	115	1.93	56.00	173.1	0.0597	0.29
KIKNET40	Hokkaido, Japan	E	140	103	1.56	13.40	99.0	0.0483	0.30
KIKNET	Hokkaido, Japan	F	140	103	1.56	13.40	99.0	0.0707	0.30
KIKNET160	Hokkaido, Japan	F	140	103	1.56	13.40	99.0	0.1026	0.30
KIKNET S2	Hokkaido, Japan	F	140	103	1.56	13.40	99.0	0.0781	0.61
KIKNET S4	Hokkaido, Japan	F	140	103	1.56	13.40	99.0	0.0912	1.22
MRCE1	New York City	F	128	90	1.69	15.15	94.3	0.0886	0.80
MRCE2	New York City	F	162	30	0.74	17.20	112.0	0.0582	0.33

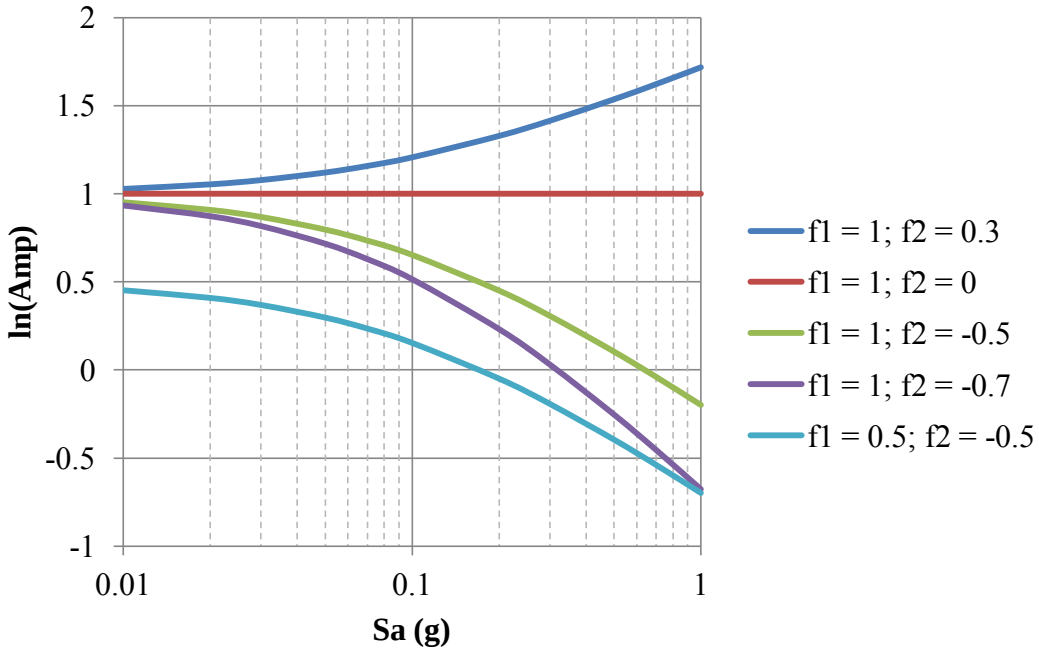

Figure 8.3: Effect of f_1 and f_2 on the fit line for ln(Amp) versus Sa (g), when f_3 = 0.1 g

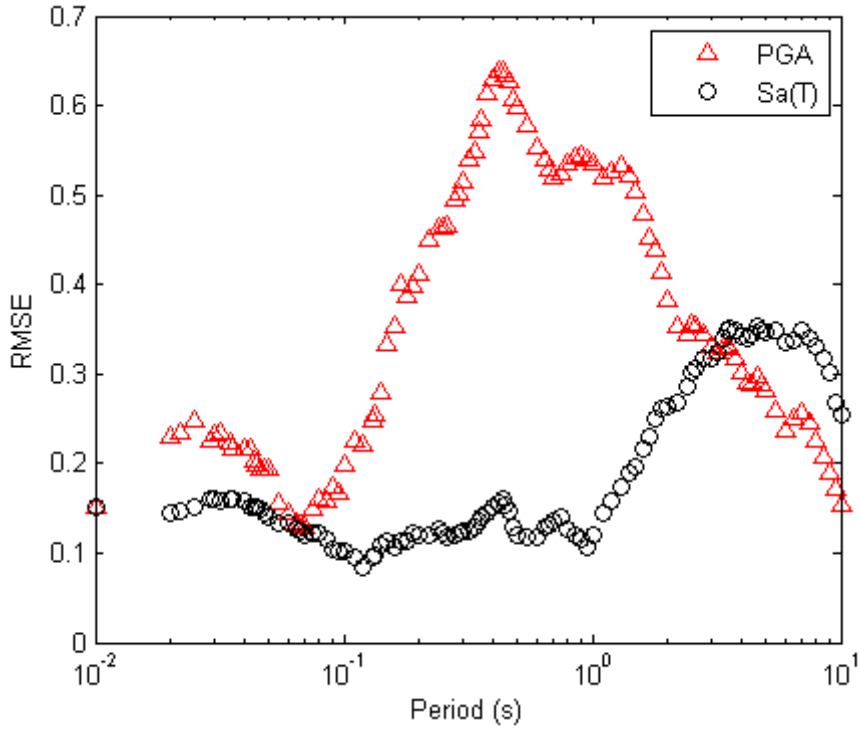

Figure 8.4: Comparison of the root mean squared error (RMSE) of models using PGA or Sa(T) as the ground motion intensity measure versus period, f_3 = 0.1 g

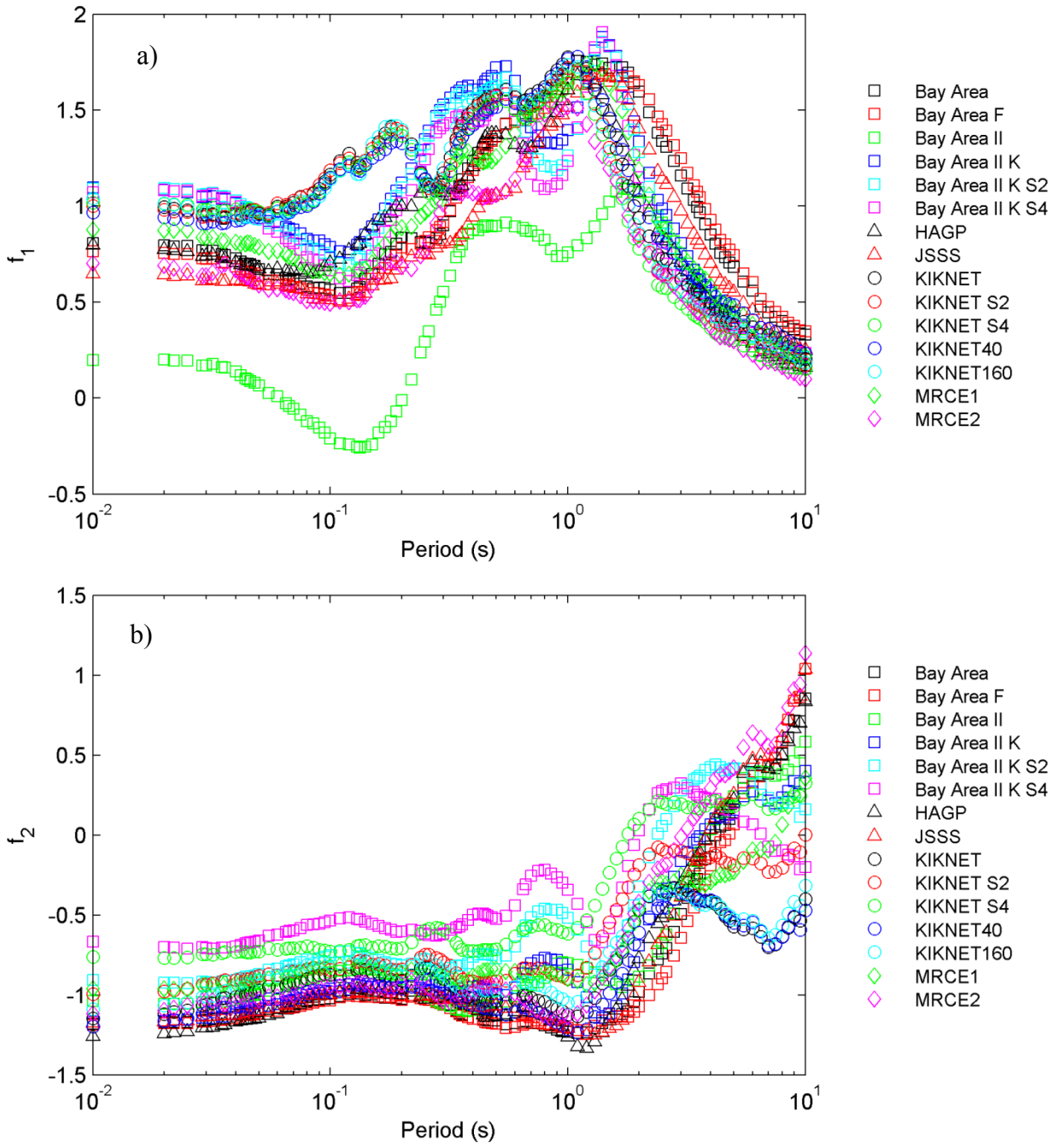

Figure 8.5: Calculated values of a) f_1 and b) f_2 by period for each site using equation (8.14)

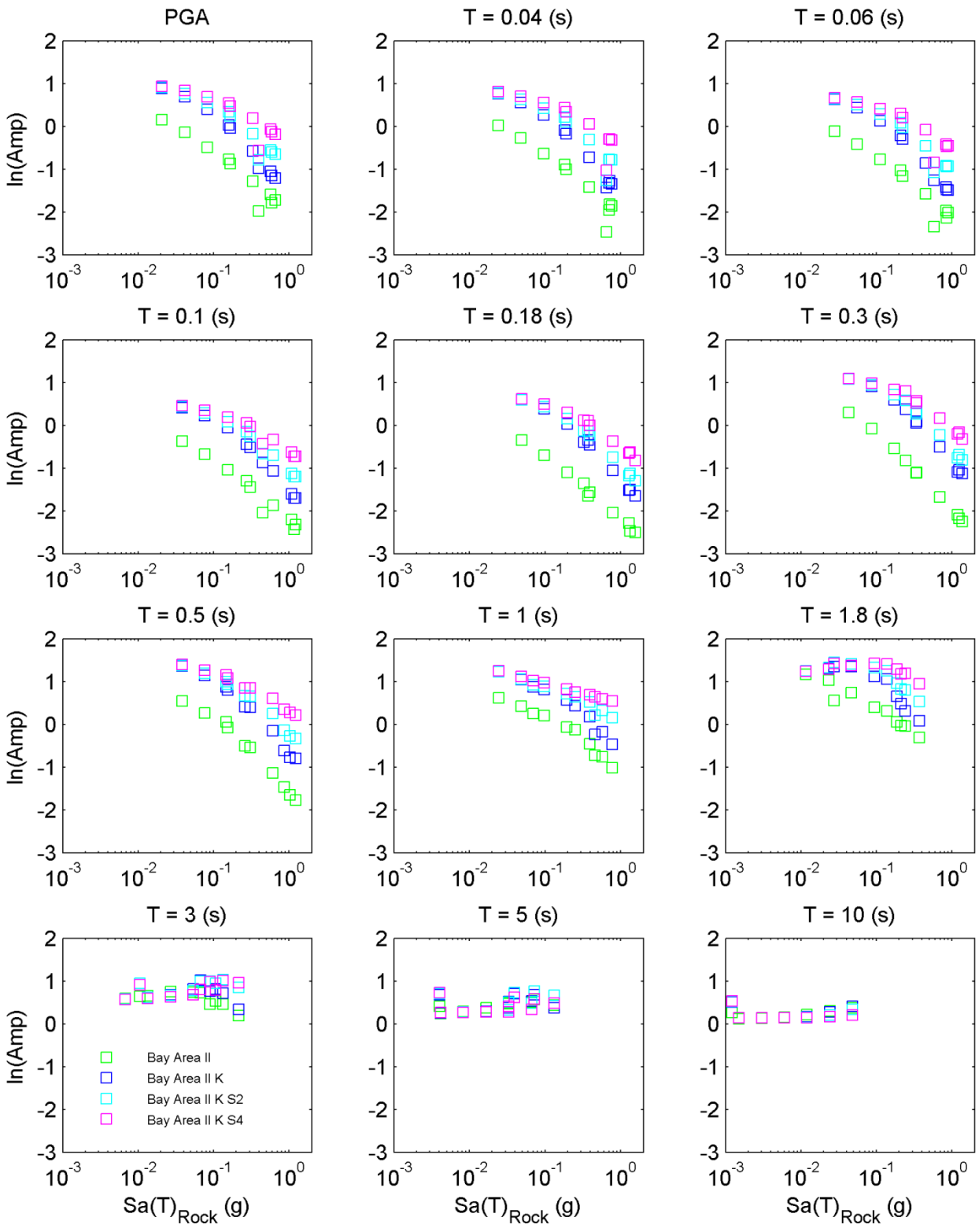

Figure 8.6: Amplification versus $Sa(T)_{Rock}$ for Bay Area II sites at different periods

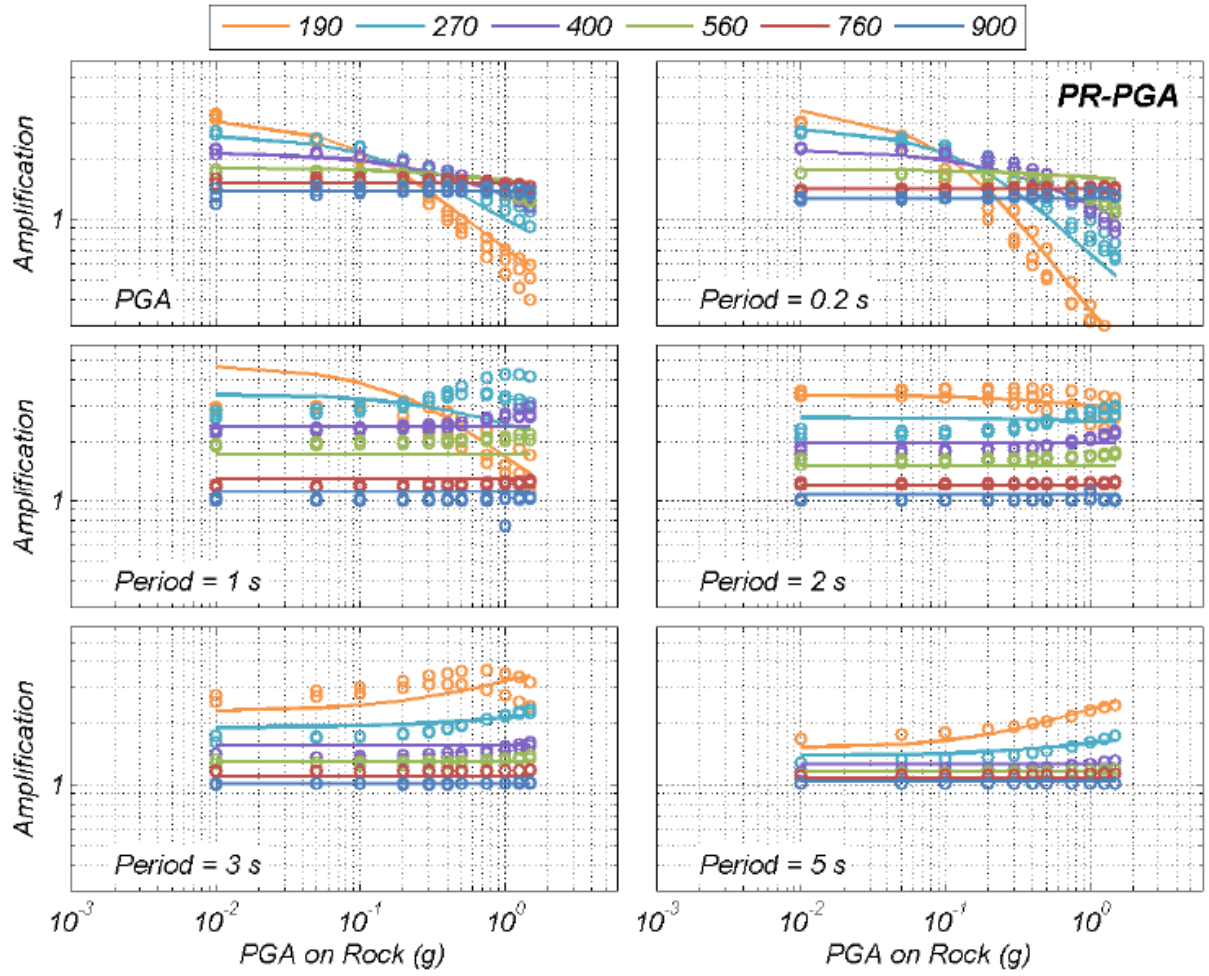

Figure 8.7: Amplification verses PGA_{rock} for six different periods, colored lines correspond to the Kamai et al. (2013) model for different Vs_{30} (m/s) values and the dots are results of their site response analyses (From Kamai et al., 2013)

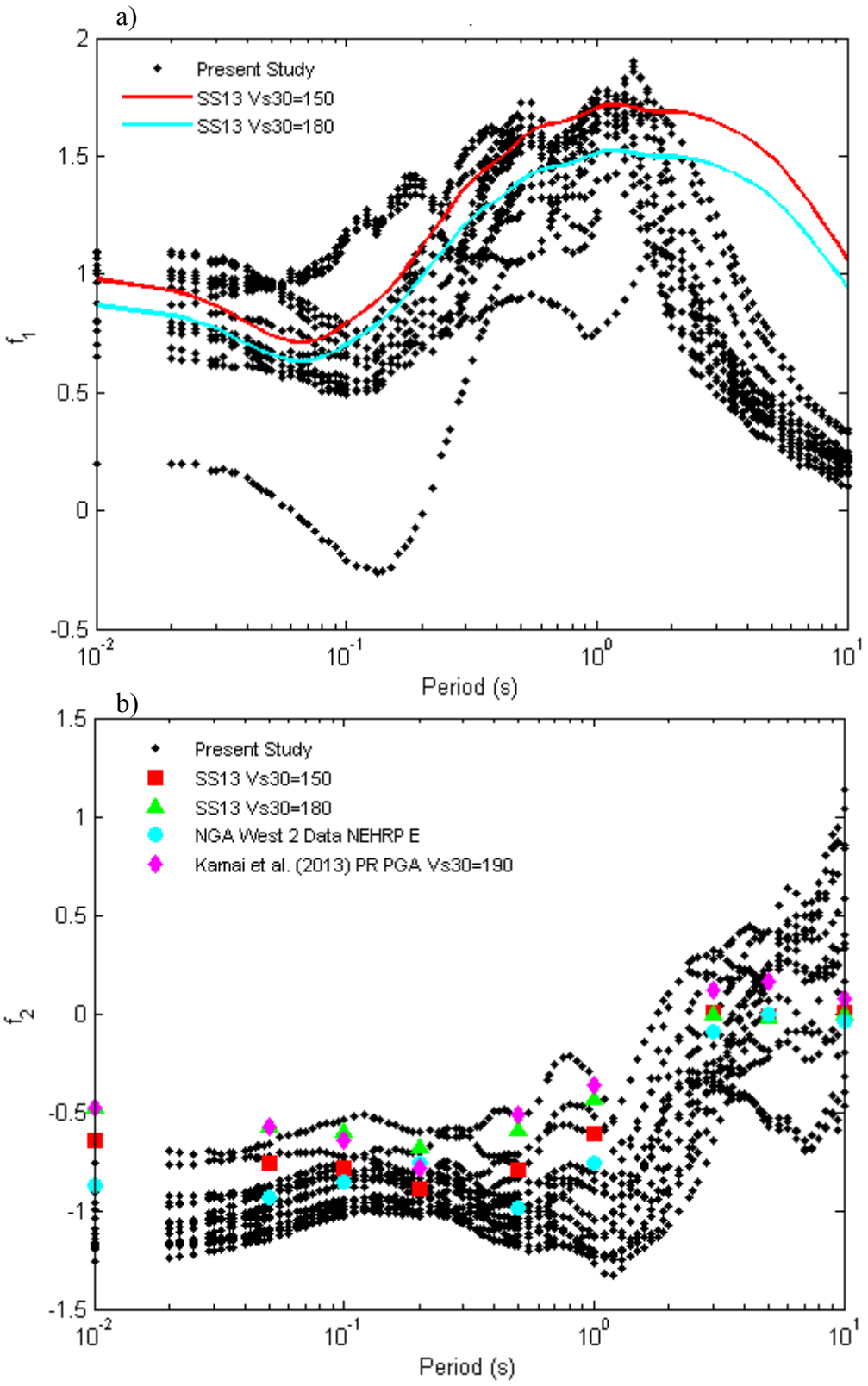

Figure 8.8: Comparison of calculated values of a) f_1 and b) f_2 using equation (8.12) with those from other studies, where SS13 is Stewart and Seyhan (2013)

Table 8.5: Site properties tested in regression analyses

Site	Th (m)	Ts (s)	Vs_{mean} (m/s)	CRR_{mean}	τ_{mean} (kPa)	$\gamma_{0.5,mean}$ (%)	$Dmin_{mean}$ (%)	Vs_{min} (m/s)	CRR_{min}	τ_{min} (kPa)	$\gamma_{0.5,min}$ (%)	$Dmin_{min}$ (%)
Bay Area	19.25	2.66	101.4	0.32	19.7	0.0580	1.68	82	0.30	13.8	0.0530	1.35
Bay Area F	35.85	2.84	119.6	0.31	30.2	0.0699	1.46	82	0.29	13.8	0.0530	1.14
Bay Area II	9.75	1.58	34.8	0.64	7.8	0.1216	5.65	25	0.61	5.8	0.1145	5.04
Bay Area II K	9.75	1.58	34.8	0.63	7.8	0.7238	3.47	25	0.58	5.8	0.5403	3.38
Bay Area II K S2	9.75	1.58	34.8	1.28	15.7	0.9831	3.46	25	1.15	11.3	0.7116	3.38
Bay Area II K S4	9.75	1.58	34.8	2.58	31.4	1.8661	3.46	25	2.35	22.3	1.1232	3.38
HAGP	36.00	1.23	136.3	0.23	18.2	0.0733	2.30	100	0.22	6.5	0.0473	1.44
JSSS	56.00	1.93	173.1	0.34	40.5	0.0597	1.17	87	0.29	12.2	0.0456	0.83
KIKNET	13.40	1.56	99.0	0.34	13.5	0.0707	2.65	80	0.29	4.6	0.0367	2.11
KIKNET S2	13.40	1.56	99.0	0.65	26.5	0.0781	2.64	80	0.61	6.7	0.0384	2.09
KIKNET S4	13.40	1.56	99.0	1.30	52.7	0.0912	2.60	80	1.22	12.9	0.0421	2.04
KIKNET40	13.40	1.56	99.0	0.34	13.7	0.0483	1.90	80	0.30	3.9	0.0228	1.50
KIKNET160	13.40	1.56	99.0	0.33	13.1	0.1026	4.14	80	0.30	2.9	0.0484	3.31
MRCE1	15.15	1.69	94.3	0.91	50.6	0.0886	1.81	85	0.80	34.5	0.0766	1.53
MRCE2	17.20	0.74	112.0	0.34	25.2	0.0582	0.45	80	0.33	14.8	0.0502	0.38

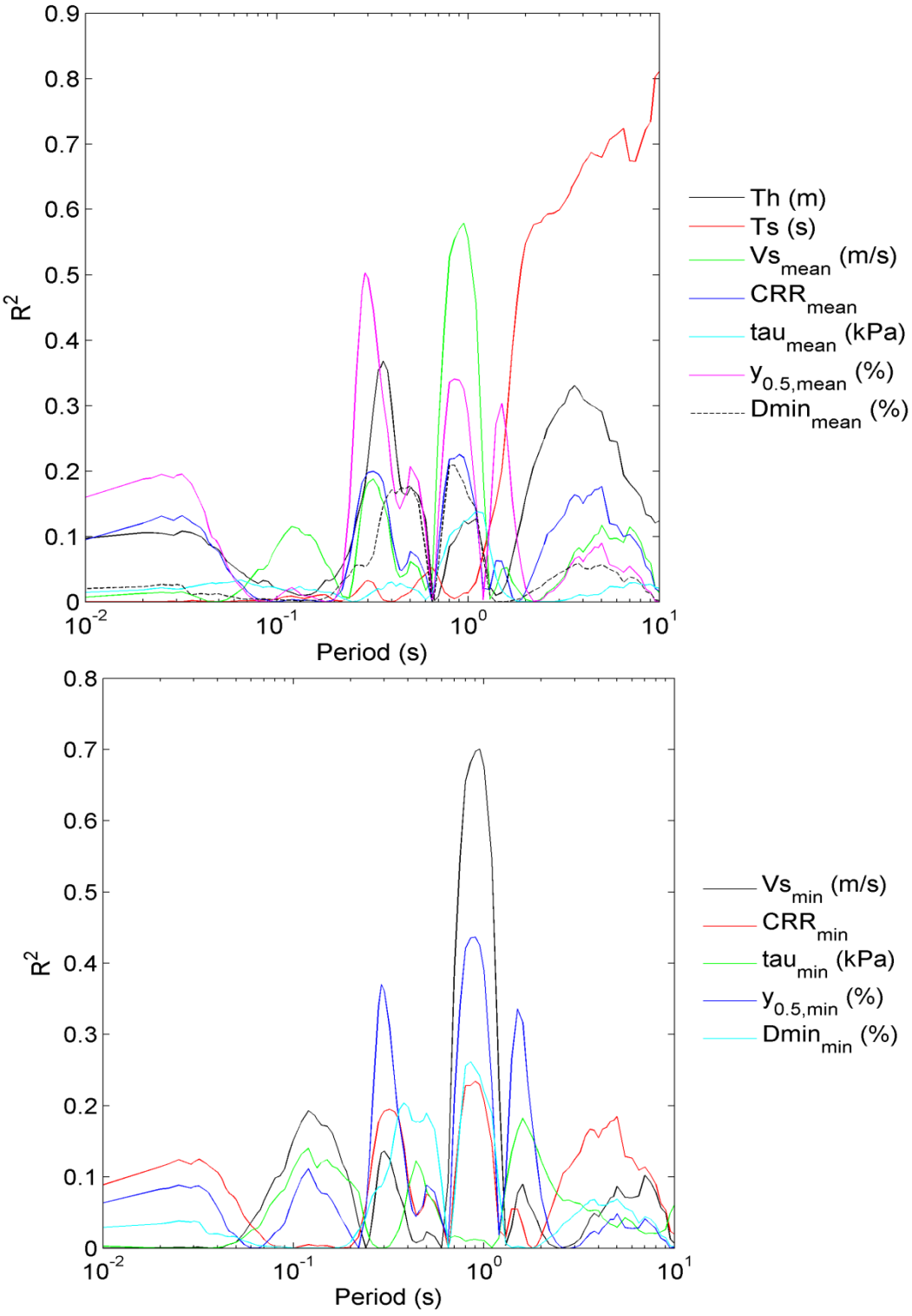

Figure 8.9: Coefficient of determination R^2 for f_1, for all 12 site properties versus period

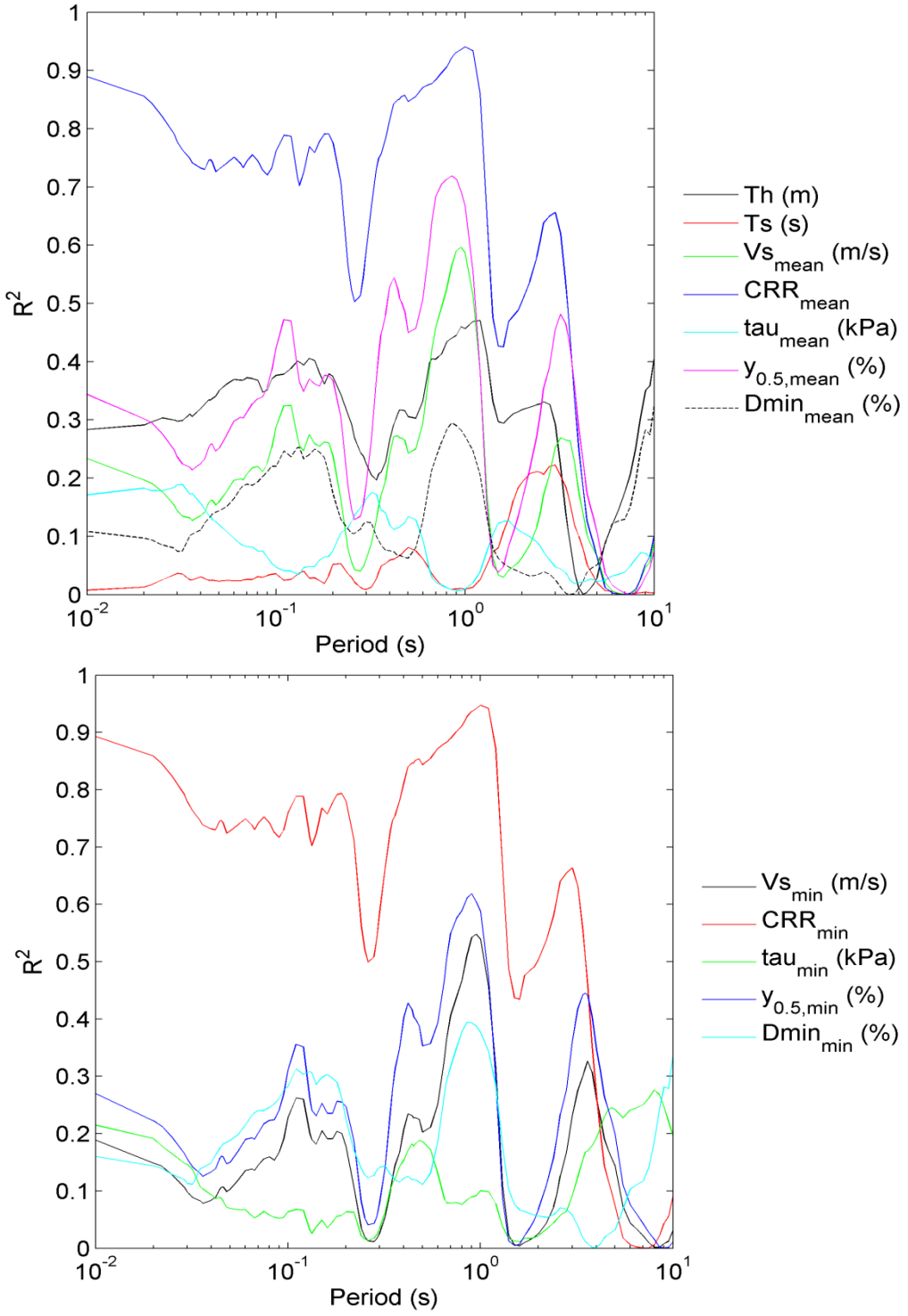

Figure 8.10: Coefficient of determination R^2 for f_2, for all 12 site properties versus period

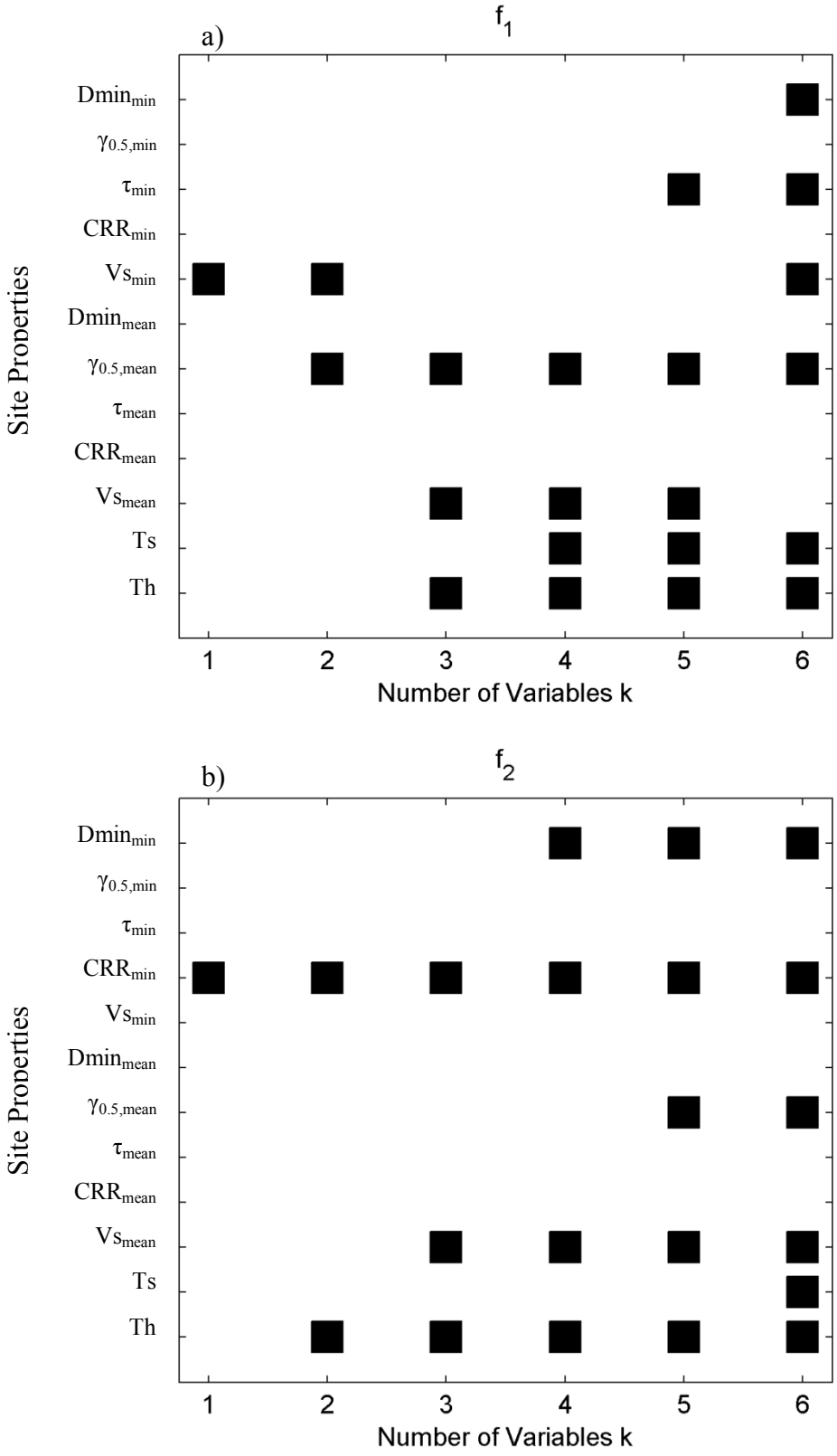

Figure 8.11: Combination of site properties for a given number of variables k allowed in the model that gave the best fit (smallest RMSE) for a) f_1 and b) f_2

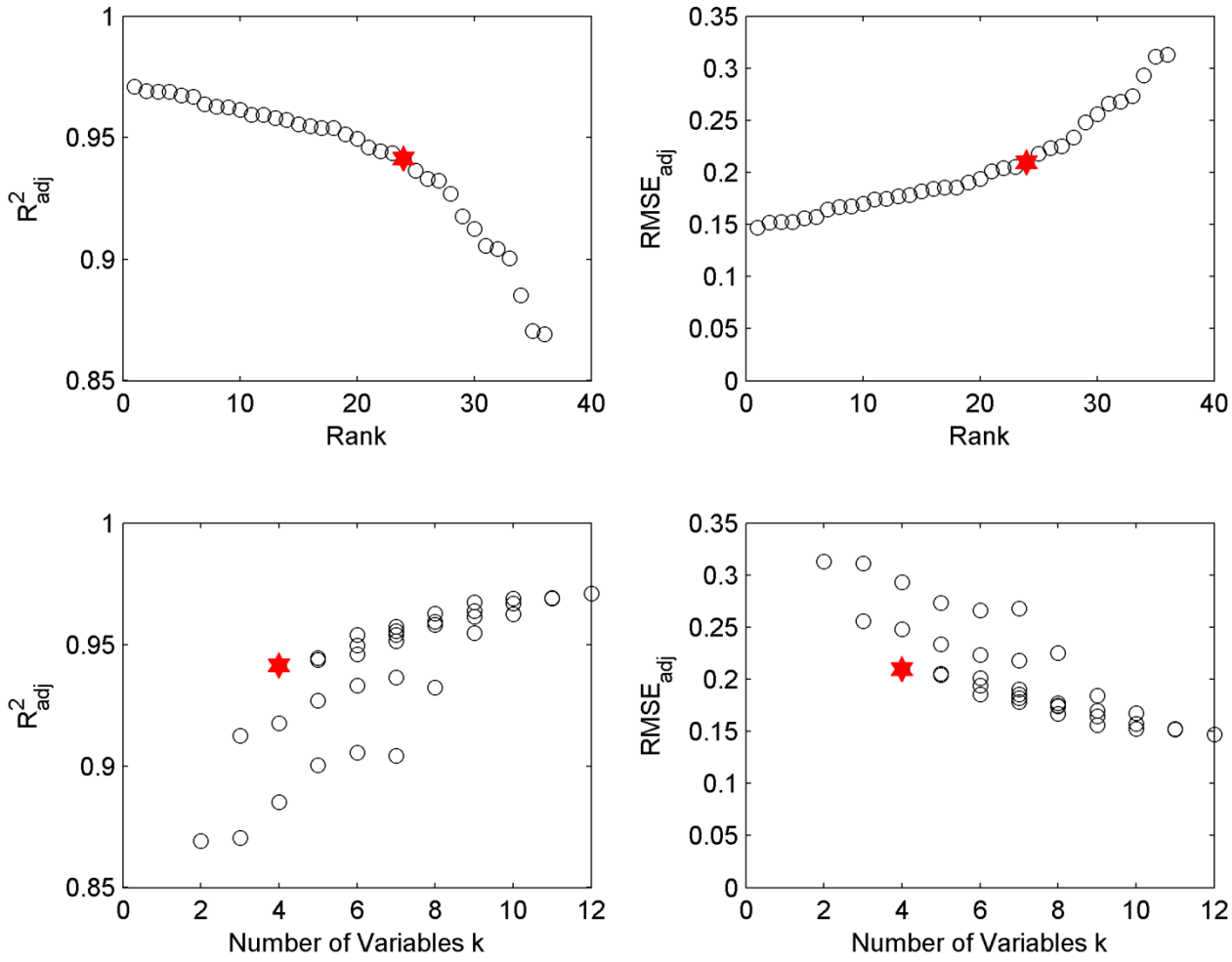

Figure 8.12: Comparison of the goodness of fit of different models, the red star indicates the selected final model

Table 8.6: Comparison of the goodness of fit of different models, this study chose model with rank = 24

Rank	f_1 # of Variables	f_2 # of Variables	R^2_{adj}	$RMSE_{adj}$
1	6	6	0.968	0.1545
2	5	6	0.966	0.1588
3	6	5	0.966	0.1594
4	5	5	0.966	0.1589
5	5	4	0.965	0.1623
6	6	4	0.964	0.1642
7	6	3	0.961	0.1712
8	5	3	0.960	0.1728
9	4	6	0.959	0.1749
10	4	5	0.958	0.1764
11	3	5	0.956	0.1805
12	6	2	0.956	0.1807
13	4	4	0.955	0.1836
14	5	2	0.955	0.1843
15	3	4	0.953	0.1880
16	3	6	0.951	0.1915
17	6	1	0.951	0.1916
18	5	1	0.951	0.1910
19	4	3	0.948	0.1966
20	3	3	0.947	0.1997
21	4	2	0.943	0.2066
22	3	2	0.942	0.2090
23	4	1	0.941	0.2105
24	3	1	0.939	0.2138
25	2	5	0.932	0.2252
26	2	4	0.929	0.2299
27	2	6	0.927	0.2331
28	2	3	0.923	0.2395
29	2	2	0.914	0.2534
30	2	1	0.909	0.2604
31	1	5	0.900	0.2734
32	1	6	0.898	0.2763
33	1	4	0.895	0.2798
34	1	3	0.880	0.2993
35	1	2	0.866	0.3168
36	1	1	0.865	0.3172

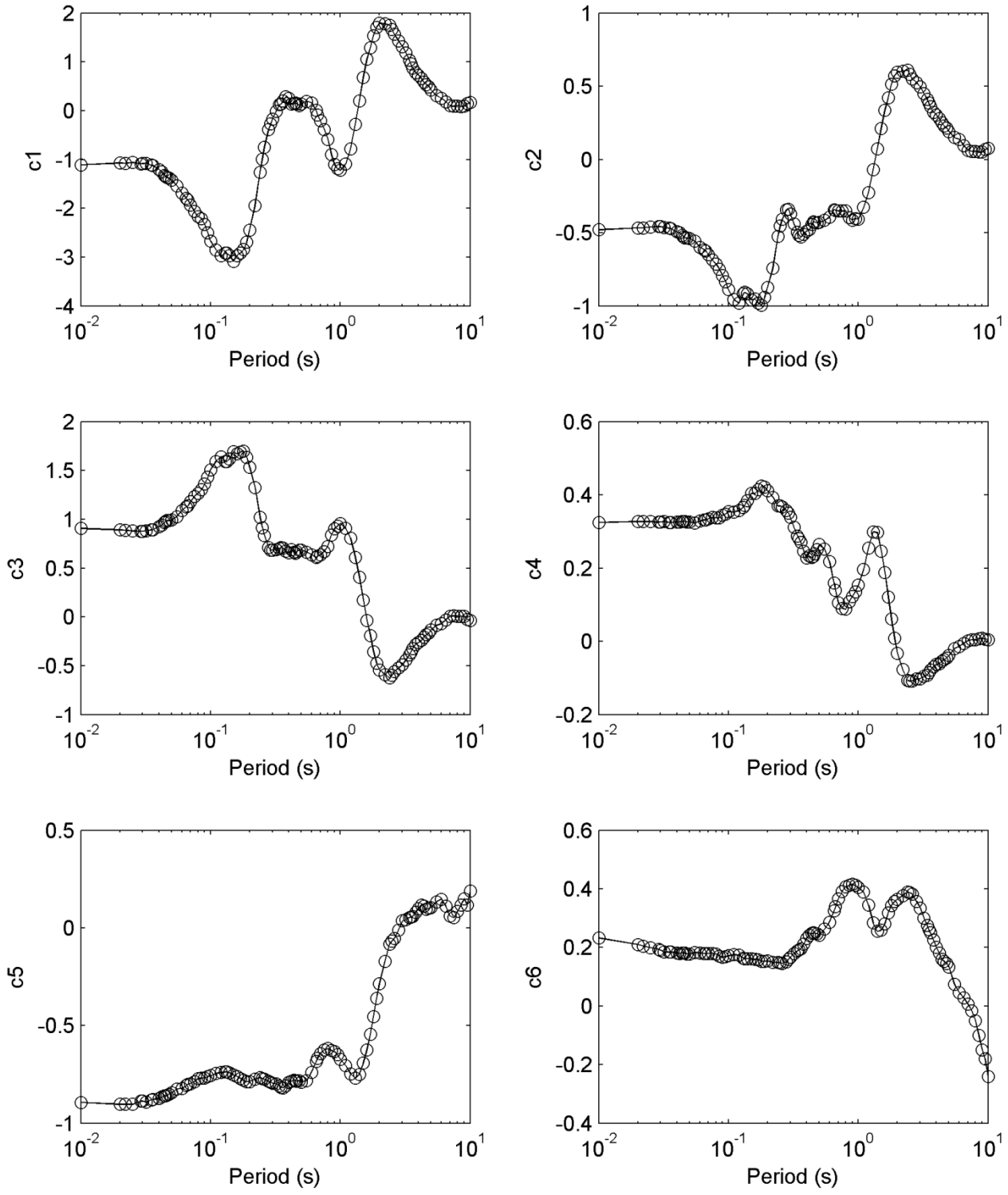

Figure 8.13: Period dependent coefficients c_1 through c_6

Table 8.7: Period dependent coefficients c_1 through c_6 for the simplified model

T (s)	c_1	c_2	c_3	c_4	c_5	c_6
PGA	-1.1073	-0.4789	0.9070	0.3252	-0.8938	0.2324
0.02	-1.0703	-0.4673	0.8897	0.3270	-0.9034	0.2103
0.022	-1.0753	-0.4664	0.8889	0.3274	-0.9028	0.2048
0.025	-1.0635	-0.4598	0.8814	0.3272	-0.9033	0.1989
0.029	-1.0880	-0.4574	0.8787	0.3253	-0.8868	0.1932
0.03	-1.0832	-0.4581	0.8784	0.3260	-0.8875	0.1904
0.032	-1.0796	-0.4635	0.8827	0.3268	-0.8908	0.1853
0.035	-1.1154	-0.4695	0.8913	0.3249	-0.8811	0.1842
0.036	-1.1244	-0.4721	0.8945	0.3246	-0.8784	0.1838
0.04	-1.2053	-0.4946	0.9262	0.3263	-0.8733	0.1801
0.042	-1.2530	-0.5016	0.9385	0.3261	-0.8660	0.1797
0.044	-1.3243	-0.5196	0.9657	0.3270	-0.8606	0.1812
0.045	-1.3473	-0.5294	0.9776	0.3272	-0.8601	0.1804
0.046	-1.3712	-0.5349	0.9858	0.3275	-0.8570	0.1801
0.048	-1.3823	-0.5368	0.9873	0.3263	-0.8516	0.1782
0.05	-1.4211	-0.5408	0.9959	0.3262	-0.8450	0.1774
0.055	-1.5398	-0.5553	1.0262	0.3236	-0.8244	0.1820
0.06	-1.6841	-0.5991	1.0919	0.3287	-0.8218	0.1814
0.065	-1.7981	-0.6176	1.1271	0.3311	-0.8075	0.1794
0.067	-1.8323	-0.6253	1.1383	0.3314	-0.8012	0.1791
0.07	-1.9324	-0.6509	1.1801	0.3349	-0.7982	0.1796
0.075	-2.0674	-0.6858	1.2334	0.3387	-0.7873	0.1795
0.08	-2.1677	-0.7118	1.2685	0.3375	-0.7719	0.1778
0.085	-2.2105	-0.7484	1.3012	0.3378	-0.7695	0.1704
0.09	-2.3329	-0.7915	1.3618	0.3447	-0.7679	0.1661
0.095	-2.5025	-0.8360	1.4320	0.3478	-0.7617	0.1684
0.1	-2.6712	-0.8890	1.5083	0.3543	-0.7568	0.1716
0.11	-2.8548	-0.9569	1.5940	0.3534	-0.7454	0.1755
0.12	-2.9734	-0.9812	1.6405	0.3567	-0.7405	0.1733
0.13	-2.9201	-0.9151	1.5917	0.3659	-0.7379	0.1636
0.133	-2.9206	-0.9070	1.5894	0.3714	-0.7370	0.1612
0.14	-2.9660	-0.9169	1.6196	0.3850	-0.7421	0.1615
0.15	-3.0855	-0.9578	1.6920	0.4038	-0.7538	0.1611
0.16	-2.9648	-0.9530	1.6709	0.4036	-0.7607	0.1589
0.17	-2.9129	-0.9800	1.6898	0.4140	-0.7708	0.1578
0.18	-2.8463	-0.9957	1.6963	0.4237	-0.7803	0.1533
0.19	-2.6951	-0.9423	1.6333	0.4214	-0.7869	0.1533
0.2	-2.4509	-0.8744	1.5327	0.4111	-0.7868	0.1538
0.22	-1.9419	-0.7427	1.3247	0.3935	-0.7735	0.1498
0.24	-1.2607	-0.5258	1.0208	0.3701	-0.7676	0.1485
0.25	-0.9899	-0.4543	0.9153	0.3700	-0.7716	0.1477
0.26	-0.7541	-0.4067	0.8322	0.3676	-0.7757	0.1460
0.28	-0.3823	-0.3426	0.7104	0.3569	-0.7859	0.1514
0.29	-0.2661	-0.3401	0.6837	0.3497	-0.7899	0.1591
0.3	-0.1770	-0.3728	0.6866	0.3388	-0.7960	0.1663
0.32	-0.0118	-0.4384	0.6902	0.3119	-0.7982	0.1791
0.34	0.1219	-0.4981	0.7011	0.2875	-0.8089	0.1877
0.35	0.1400	-0.5174	0.7127	0.2811	-0.8159	0.1917
0.36	0.2024	-0.5301	0.7072	0.2703	-0.8185	0.1960
0.38	0.2835	-0.5121	0.6729	0.2465	-0.8103	0.2113
0.4	0.2557	-0.4891	0.6592	0.2283	-0.7913	0.2314

0.42	0.1333	-0.4800	0.6887	0.2328	-0.7846	0.2408
0.44	0.1466	-0.4414	0.6633	0.2289	-0.7795	0.2481
0.45	0.1601	-0.4246	0.6543	0.2315	-0.7820	0.2497
0.46	0.1384	-0.4285	0.6679	0.2394	-0.7842	0.2492
0.48	0.1102	-0.4317	0.6840	0.2509	-0.7837	0.2469
0.5	0.1393	-0.4296	0.6860	0.2641	-0.7902	0.2409
0.55	0.1934	-0.4160	0.6643	0.2517	-0.7815	0.2624
0.6	0.1585	-0.3938	0.6377	0.2185	-0.7394	0.2863
0.65	0.0070	-0.3427	0.6077	0.1599	-0.6836	0.3250
0.667	-0.0914	-0.3469	0.6218	0.1398	-0.6667	0.3388
0.7	-0.2044	-0.3514	0.6352	0.1054	-0.6432	0.3656
0.75	-0.3845	-0.3517	0.6707	0.0902	-0.6244	0.3906
0.8	-0.5936	-0.3509	0.7207	0.0882	-0.6179	0.4072
0.85	-0.8978	-0.3982	0.8364	0.1086	-0.6285	0.4121
0.9	-1.0987	-0.4130	0.9019	0.1221	-0.6335	0.4155
0.95	-1.1902	-0.4030	0.9293	0.1358	-0.6492	0.4115
1	-1.2212	-0.4069	0.9568	0.1544	-0.6741	0.4044
1.1	-1.0903	-0.3270	0.9075	0.1970	-0.7057	0.3886
1.2	-0.7858	-0.2246	0.8047	0.2554	-0.7471	0.3449
1.3	-0.2810	-0.0703	0.6107	0.2985	-0.7699	0.2841
1.4	0.1991	0.0737	0.4047	0.2974	-0.7492	0.2549
1.5	0.6763	0.2130	0.1691	0.2463	-0.6906	0.2584
1.6	1.0540	0.3367	-0.0351	0.1873	-0.6262	0.2814
1.7	1.2929	0.4205	-0.1904	0.1204	-0.5443	0.3173
1.8	1.5396	0.5147	-0.3546	0.0616	-0.4550	0.3435
1.9	1.7080	0.5721	-0.4750	0.0089	-0.3610	0.3564
2	1.7911	0.5960	-0.5430	-0.0329	-0.2853	0.3651
2.2	1.7798	0.6043	-0.5911	-0.0771	-0.1712	0.3766
2.4	1.7510	0.6087	-0.6263	-0.1071	-0.0825	0.3899
2.5	1.6591	0.5808	-0.5953	-0.1084	-0.0669	0.3869
2.6	1.5696	0.5499	-0.5593	-0.1081	-0.0538	0.3828
2.8	1.4317	0.5260	-0.5238	-0.1026	-0.0112	0.3574
3	1.3139	0.4959	-0.4913	-0.1020	0.0364	0.3346
3.2	1.1827	0.4499	-0.4401	-0.0961	0.0430	0.2995
3.4	1.0381	0.4120	-0.3913	-0.0918	0.0536	0.2756
3.5	0.9600	0.3874	-0.3600	-0.0859	0.0551	0.2612
3.6	0.8775	0.3625	-0.3256	-0.0789	0.0581	0.2510
3.8	0.7770	0.3219	-0.2806	-0.0694	0.0798	0.2249
4	0.7250	0.3040	-0.2627	-0.0629	0.0992	0.2006
4.2	0.6627	0.2804	-0.2417	-0.0618	0.1175	0.1815
4.4	0.5809	0.2504	-0.2075	-0.0545	0.1112	0.1590
4.6	0.5351	0.2283	-0.1830	-0.0503	0.0944	0.1521
4.8	0.4937	0.2143	-0.1660	-0.0455	0.1000	0.1445
5	0.4246	0.1909	-0.1350	-0.0389	0.1039	0.1334
5.5	0.3089	0.1502	-0.0849	-0.0193	0.1332	0.0742
6	0.2540	0.1374	-0.0691	-0.0140	0.1469	0.0452
6.5	0.1793	0.0936	-0.0311	-0.0056	0.1113	0.0277
7	0.1015	0.0623	0.0069	0.0020	0.0609	0.0059
7.5	0.0915	0.0567	0.0108	0.0045	0.0519	-0.0167
8	0.0956	0.0563	0.0054	0.0042	0.0852	-0.0501
8.5	0.0850	0.0511	0.0081	0.0077	0.1174	-0.1010
9	0.0898	0.0504	0.0056	0.0081	0.1496	-0.1502
9.5	0.1461	0.0686	-0.0244	0.0062	0.1165	-0.1800
10	0.1684	0.0777	-0.0376	0.0044	0.1886	-0.2402

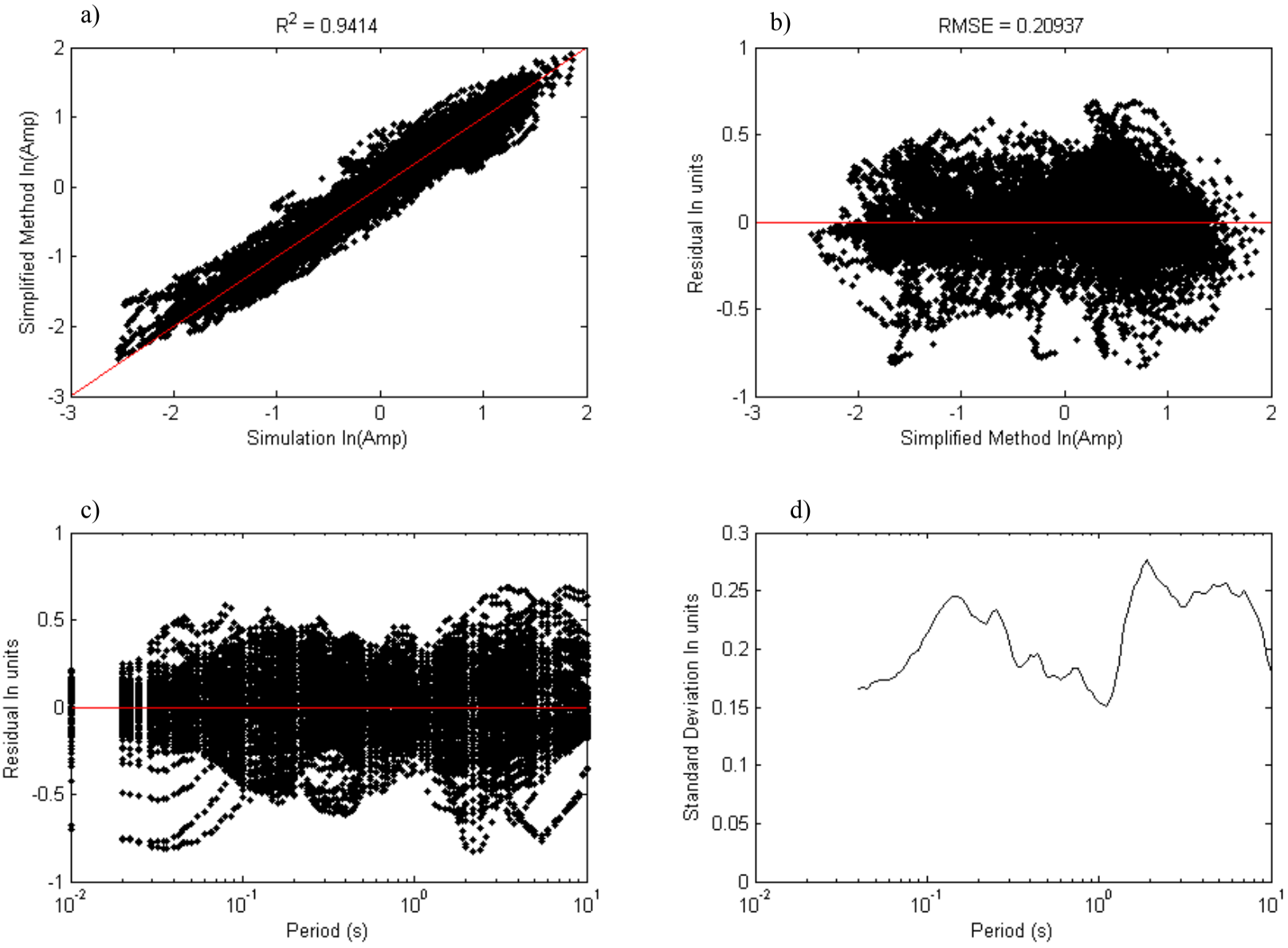

Figure 8.14: Results of the simplified model

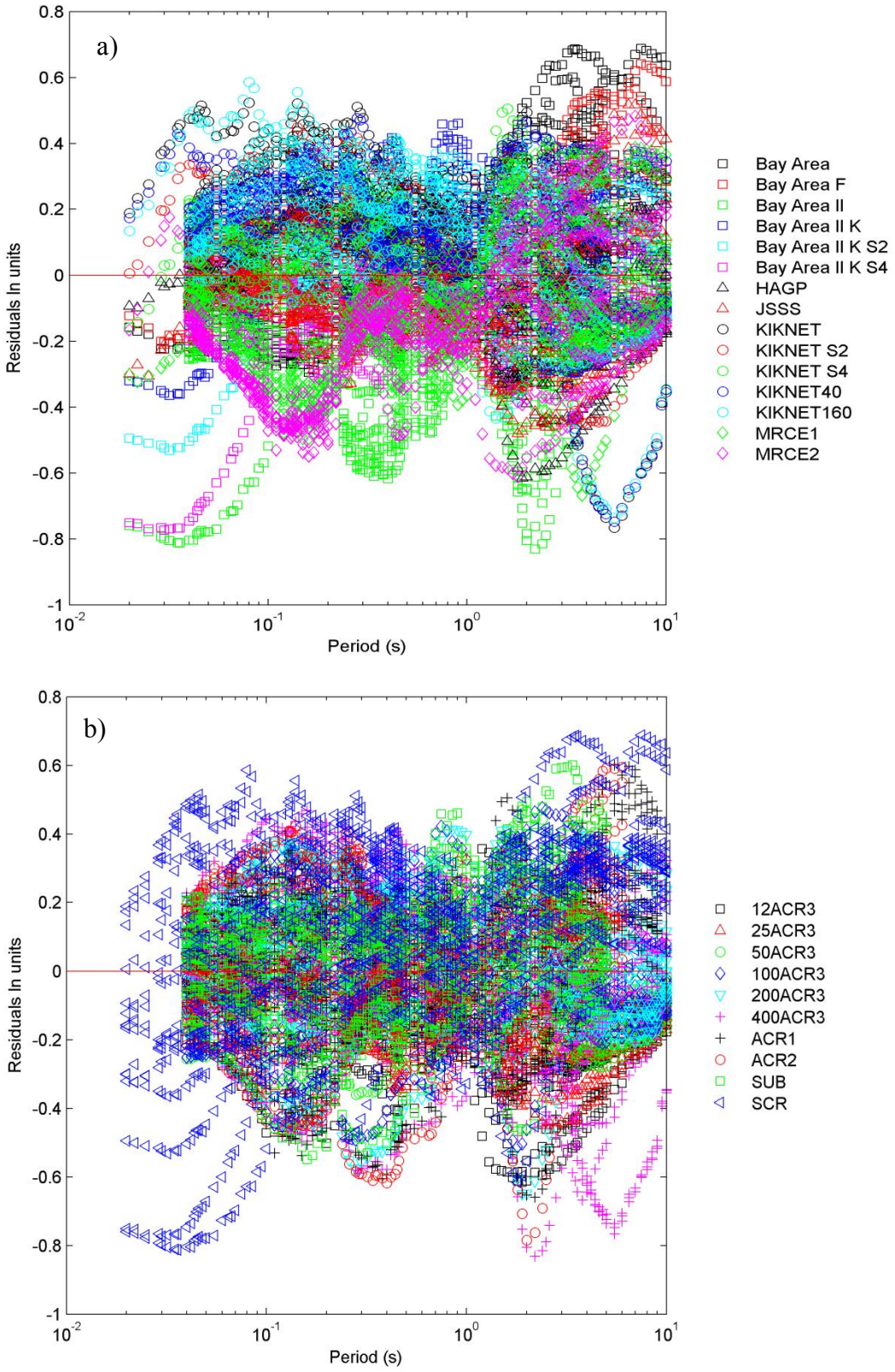

Figure 8.15: Residuals versus period for a) sites and b) scenarios

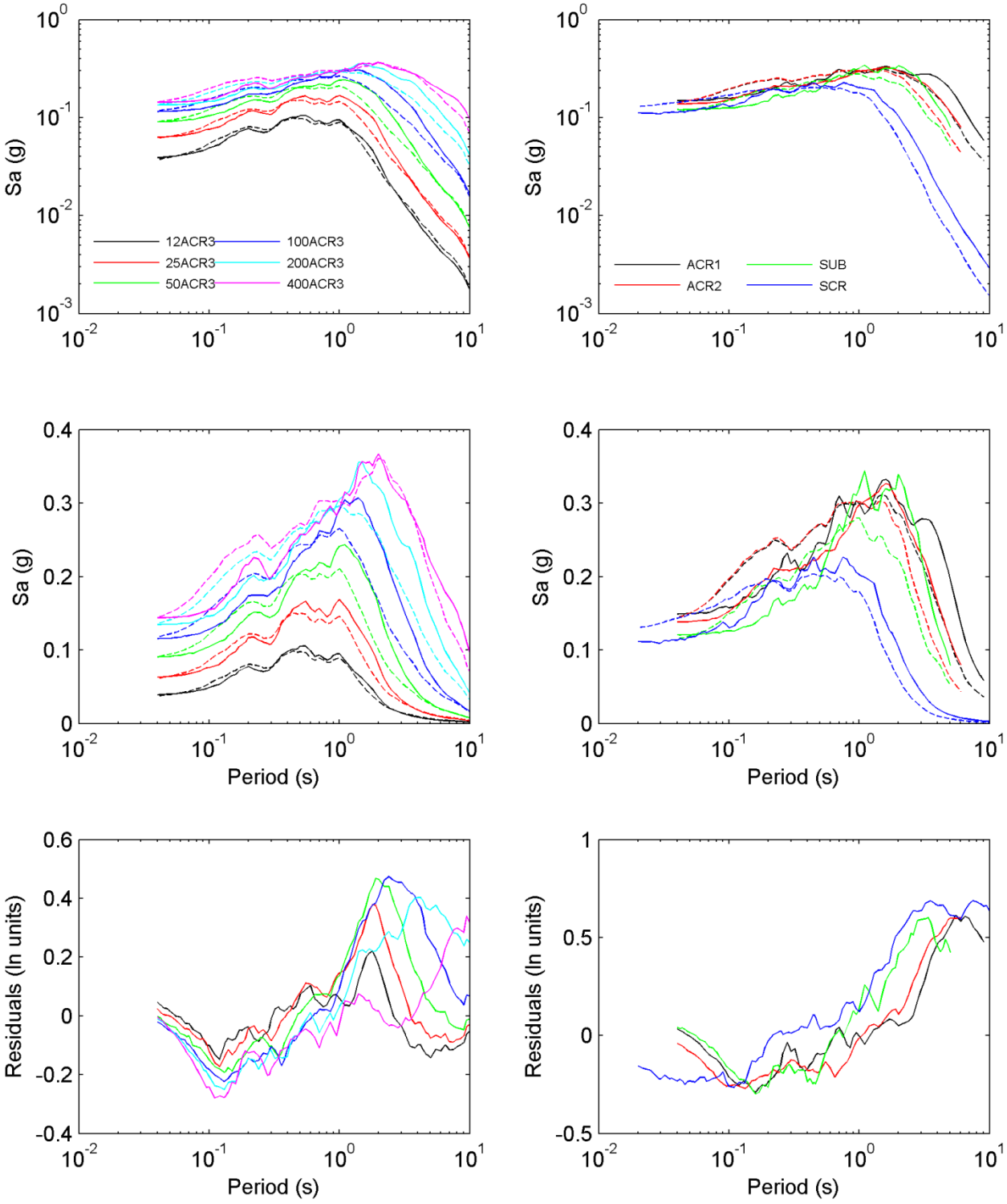

Figure 8.16: Comparison of response spectra calculated from effective stress nonlinear site response analyses (solid lines) and simplified method (dashed lines) for site Bay Area and all scenarios

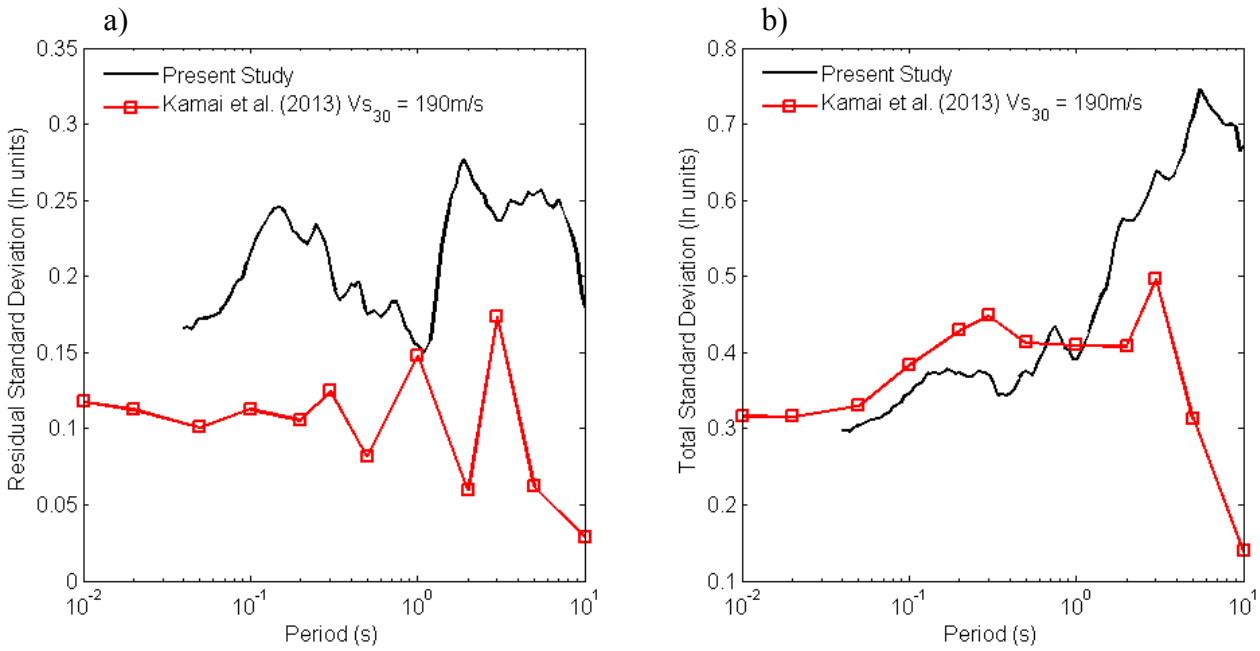

Figure 8.17: Comparison of the a) residual standard deviations σ_{res} and b) the total standard deviations σ_{total} from the present study and Kamai et al. (2013)

Table 8.8: Standard deviation values for the simplified model

Period	σ_{res}	$\overline{\sigma}_{RS}$	σ_{total}	Period	σ_{res}	$\overline{\sigma}_{RS}$	σ_{total}	Period	σ_{res}	$\overline{\sigma}_{RS}$	σ_{total}
0.040	0.1658	0.2467	0.2972	0.26	0.2299	0.2962	0.3749	1.6	0.2537	0.4433	0.5108
0.042	0.1667	0.2465	0.2976	0.28	0.2217	0.3012	0.3740	1.7	0.2589	0.4742	0.5402
0.044	0.1655	0.2462	0.2967	0.29	0.2156	0.3028	0.3717	1.8	0.2721	0.4944	0.5644
0.045	0.1659	0.2466	0.2972	0.30	0.2057	0.3083	0.3706	1.9	0.2765	0.5041	0.5749
0.046	0.1672	0.2481	0.2992	0.32	0.1911	0.3063	0.3610	2.0	0.2720	0.5045	0.5731
0.048	0.1714	0.2500	0.3031	0.34	0.1850	0.2908	0.3447	2.2	0.2607	0.5106	0.5733
0.050	0.1721	0.2505	0.3040	0.35	0.1851	0.2908	0.3447	2.4	0.2546	0.5265	0.5848
0.055	0.1727	0.2552	0.3081	0.36	0.1863	0.2913	0.3458	2.5	0.2533	0.5368	0.5936
0.060	0.1738	0.2586	0.3115	0.38	0.1895	0.2870	0.3439	2.6	0.2464	0.5462	0.5992
0.065	0.1756	0.2591	0.3130	0.40	0.1947	0.2857	0.3458	2.8	0.2423	0.5672	0.6168
0.067	0.1784	0.2583	0.3139	0.42	0.1933	0.2916	0.3498	3.0	0.2367	0.5927	0.6383
0.070	0.1809	0.2606	0.3173	0.44	0.1963	0.2992	0.3578	3.2	0.2368	0.5884	0.6343
0.075	0.1862	0.2611	0.3207	0.45	0.1946	0.3072	0.3637	3.4	0.2440	0.5795	0.6288
0.080	0.1935	0.2644	0.3276	0.46	0.1898	0.3151	0.3679	3.5	0.2477	0.5770	0.6279
0.085	0.1973	0.2667	0.3317	0.48	0.1802	0.3276	0.3738	3.6	0.2495	0.5746	0.6264
0.090	0.1990	0.2691	0.3347	0.50	0.1753	0.3314	0.3749	3.8	0.2489	0.5802	0.6313
0.095	0.2086	0.2725	0.3432	0.55	0.1772	0.3242	0.3695	4.0	0.2472	0.5940	0.6434
0.10	0.2139	0.2712	0.3454	0.60	0.1732	0.3508	0.3912	4.2	0.2474	0.6045	0.6532
0.11	0.2261	0.2743	0.3555	0.65	0.1770	0.3616	0.4025	4.4	0.2513	0.6157	0.6650
0.12	0.2337	0.2751	0.3610	0.67	0.1785	0.3714	0.4121	4.6	0.2551	0.6341	0.6835
0.13	0.2406	0.2843	0.3724	0.70	0.1834	0.3845	0.4260	4.8	0.2536	0.6534	0.7009
0.13	0.2416	0.2828	0.3720	0.75	0.1832	0.3937	0.4342	5.0	0.2535	0.6633	0.7101
0.14	0.2448	0.2832	0.3743	0.80	0.1747	0.3829	0.4208	5.5	0.2568	0.6996	0.7453
0.15	0.2454	0.2796	0.3721	0.85	0.1660	0.3709	0.4064	6.0	0.2478	0.6885	0.7317
0.16	0.2425	0.2843	0.3737	0.90	0.1631	0.3698	0.4042	6.5	0.2449	0.6750	0.7181
0.17	0.2370	0.2943	0.3779	0.95	0.1564	0.3590	0.3916	7.0	0.2499	0.6660	0.7113
0.18	0.2293	0.2971	0.3753	1.0	0.1545	0.3596	0.3913	7.5	0.2416	0.6576	0.7006
0.19	0.2278	0.2944	0.3722	1.1	0.1503	0.3799	0.4085	8.0	0.2340	0.6587	0.6990
0.20	0.2245	0.2983	0.3733	1.2	0.1589	0.3975	0.4280	8.5	0.2249	0.6629	0.7000
0.22	0.2213	0.2946	0.3684	1.3	0.1881	0.4123	0.4532	9.0	0.2132	0.6634	0.6968
0.24	0.2307	0.2873	0.3685	1.4	0.2198	0.4185	0.4727	9.5	0.1909	0.6362	0.6642
0.25	0.2338	0.2906	0.3730	1.5	0.2380	0.4201	0.4829	10.0	0.1801	0.6462	0.6709

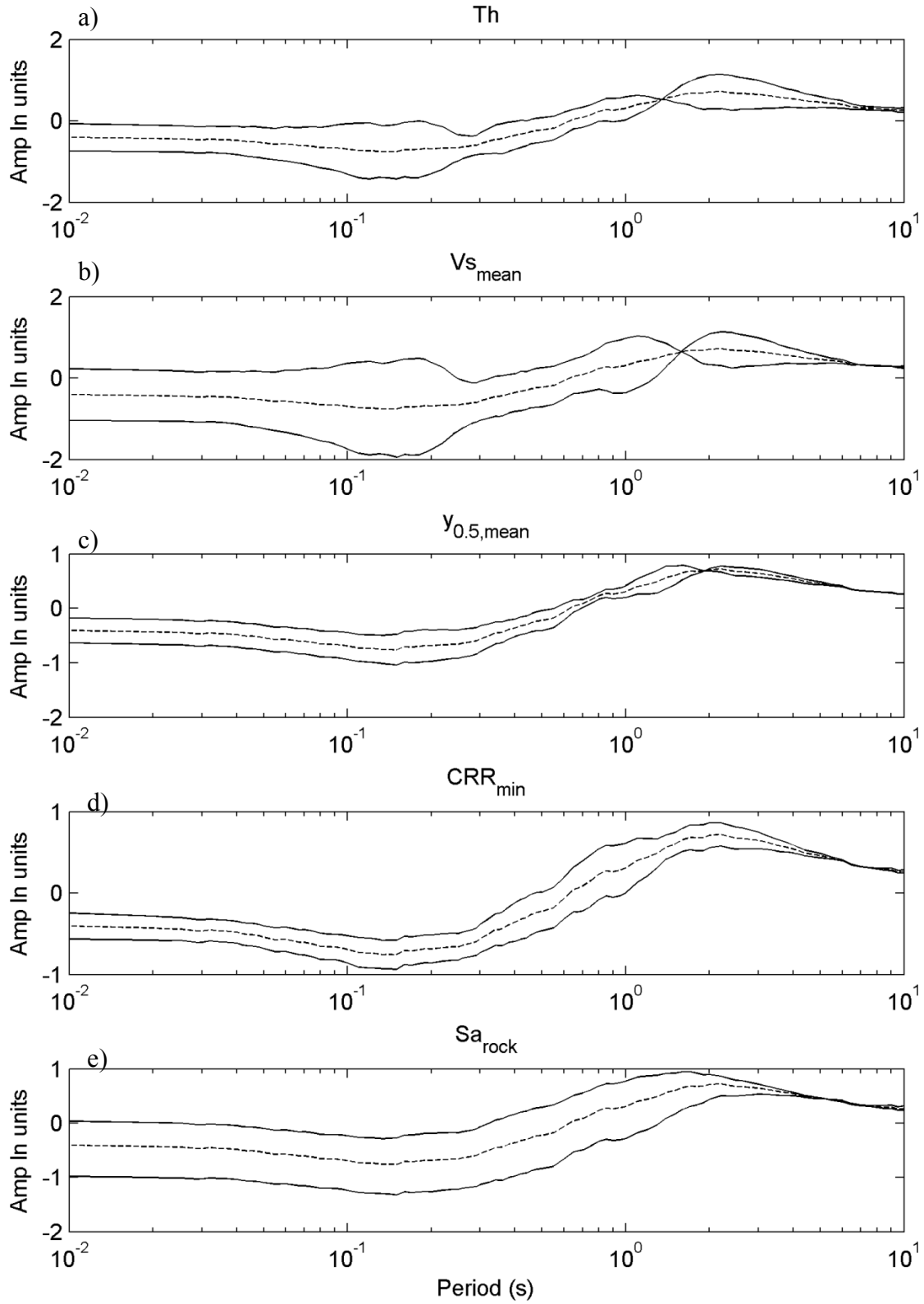

Figure 8.18: Results of the sensitivity analysis for site Bay Area and scenario 100ACR3, the dotted line in each plot is the baseline amplification and the solid lines are the amplification values calculated when the given input variable is set to $\pm$ 2 standard deviations and all other variables are kept at baseline values.

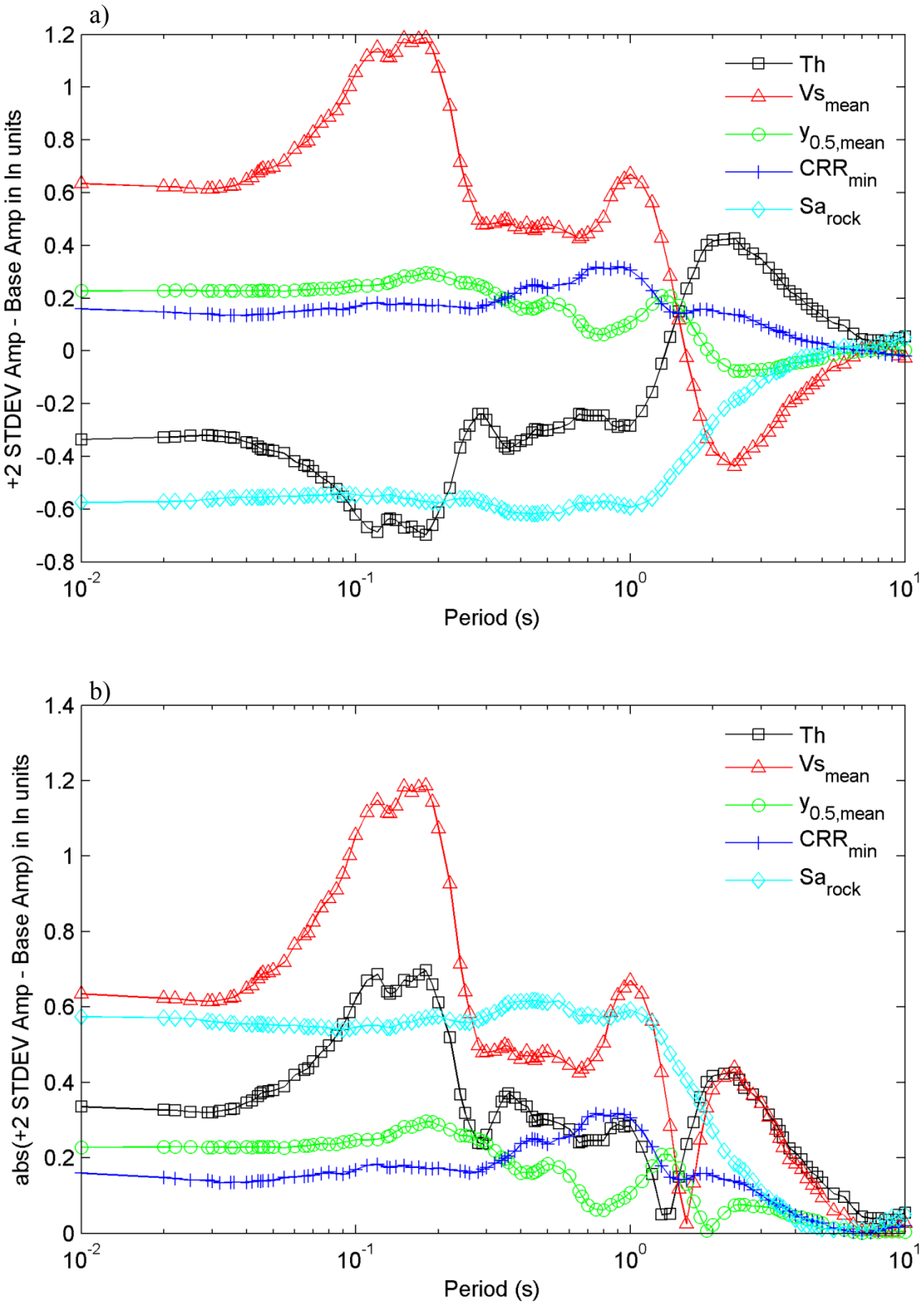

Figure 8.19: Results of the sensitivity analysis for site Bay Area and scenario 100ACR3 showing the difference in the amplification value calculated when each parameter is changed by two standard deviations and the baseline amplification values

Table 8.9: Validation dataset target scenarios

Scenario	M_w	R_{rup} (km)	Vs_{30} (m/s)	Region	$D_{5\text{-}95}$ (s)
V1	6.5	20	760	ACR	12
V2	7.5	20	760	ACR	24.5
V3	7.8	5	760	ACR	26
V4	5.5	2	760	ACR	4.1
V5	8.2	50	760	SUB	
V6	9.2	50	760	SUB	
V7	5.5	25	2000	SCR	
V8	6.5	10	2000	SCR	

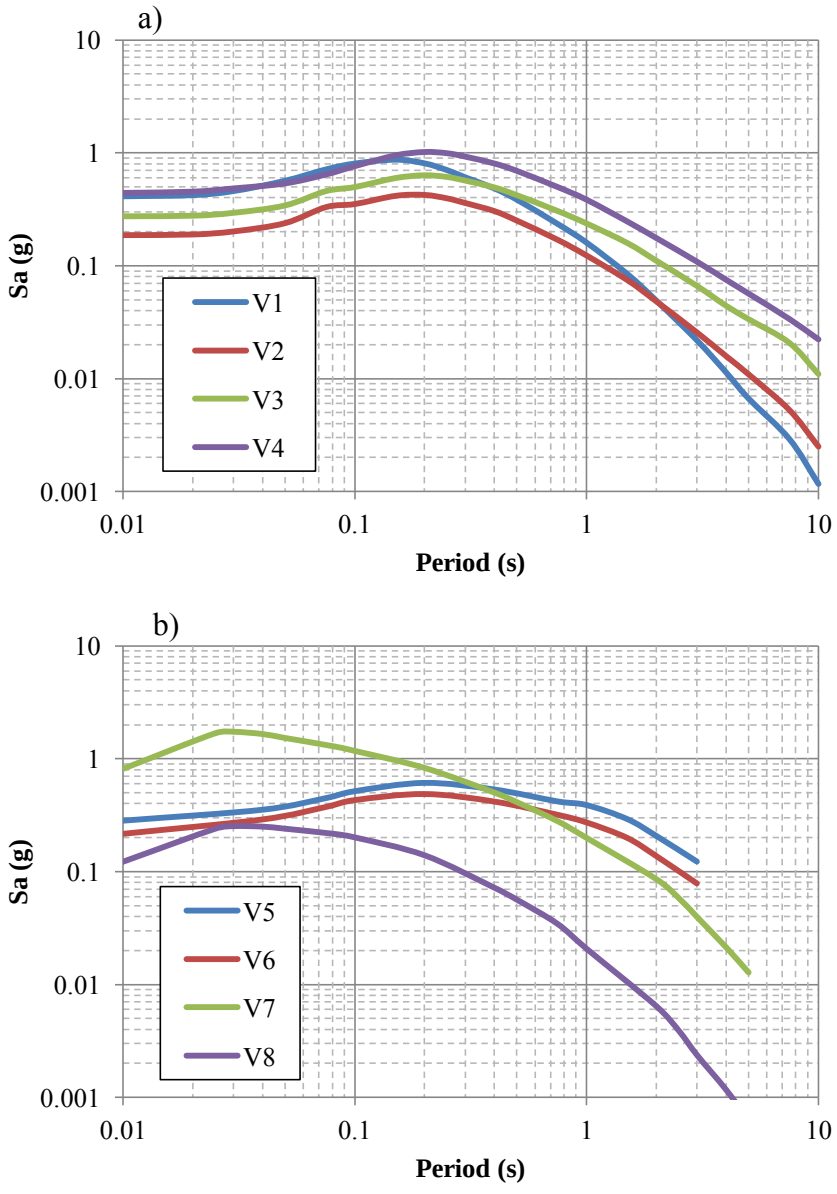

Figure 8.20: Target response spectra for the validation database

Table 8.10: Selected ground motions for the validation database

Scenario	ID	Event	Year	Station	Tectonic Region
V1	NGA 1070	Northridge 1	1994	San Gabriel E Grand Ave	ACR
V2	NGA 1184	Chi-Chi, Taiwan	1999	CHY010	ACR
V3	NGA 1521	Chi-Chi, Taiwan	1999	TCU089	ACR
V4	NGA 2150	Big Bear City	2003	7 Oaks Dam R Abut.	ACR
V5	SUB39	Maule, Chile	2010	Santiago Puente Alto	Subduction
V6	SUB59	Tohoku	2011	Ogawa	Subduction
V7	SCR21	Mt Carmel IL	2008	OLIL	SCR
V8	SCR26	Nahanni 1	1985	Site 3	SCR

Scenario	Mechanism	M_w	R_{rup} (km)	Vs_{30} (m/s)	$D_{5\text{-}95}$ (s)	LUP (s)	HUP (s)
V1	Reverse	6.69	39.3	401	13.9	0.04	6.25
V2	Reverse-Oblique	7.62	20	550	28.7	0.04	25.00
V3	Reverse-Oblique	7.62	8.9	680	26.1	0.04	11.11
V4	Strike Slip	4.92	32.5	660	9.1	0.04	5.88
V5	Interface	8.8	75	540	39.6	0.04	6.67
V6	Interface	9	94	465	79.6	0.04	5.00
V7		5.3	36.4	475	41.0	0.02	20.00
V8		6.8	5.3	660	11.6	0.02	8.33

LUP = lowest useable period; HUP = highest useable period

Table 8.11: Validation site properties

Site	Th (m)	Ts (s)	Vs_{mean} (m/s)	CRR_{mean}	τ_{mean} (kPa)	$\gamma_{0.5,mean}$ (%)
Val1	37.00	1.82	119.6	0.31	30.2	0.0699
Val2	6.95	1.26	78.9	1.04	43.3	0.0855
Val3	76.80	2.03	201.8	0.34	49.2	0.0567

Site	$Dmin_{mean}$ (%)	Vs_{min} (m/s)	CRR_{min}	τ_{min} (kPa)	$\gamma_{0.5,min}$ (%)	$Dmin_{min}$ (%)
Val1	1.46	82	0.29	13.8	0.0530	1.14
Val2	1.95	85	0.84	34.5	0.0766	1.81
Val3	1.20	87	0.29	12.2	0.0283	0.86

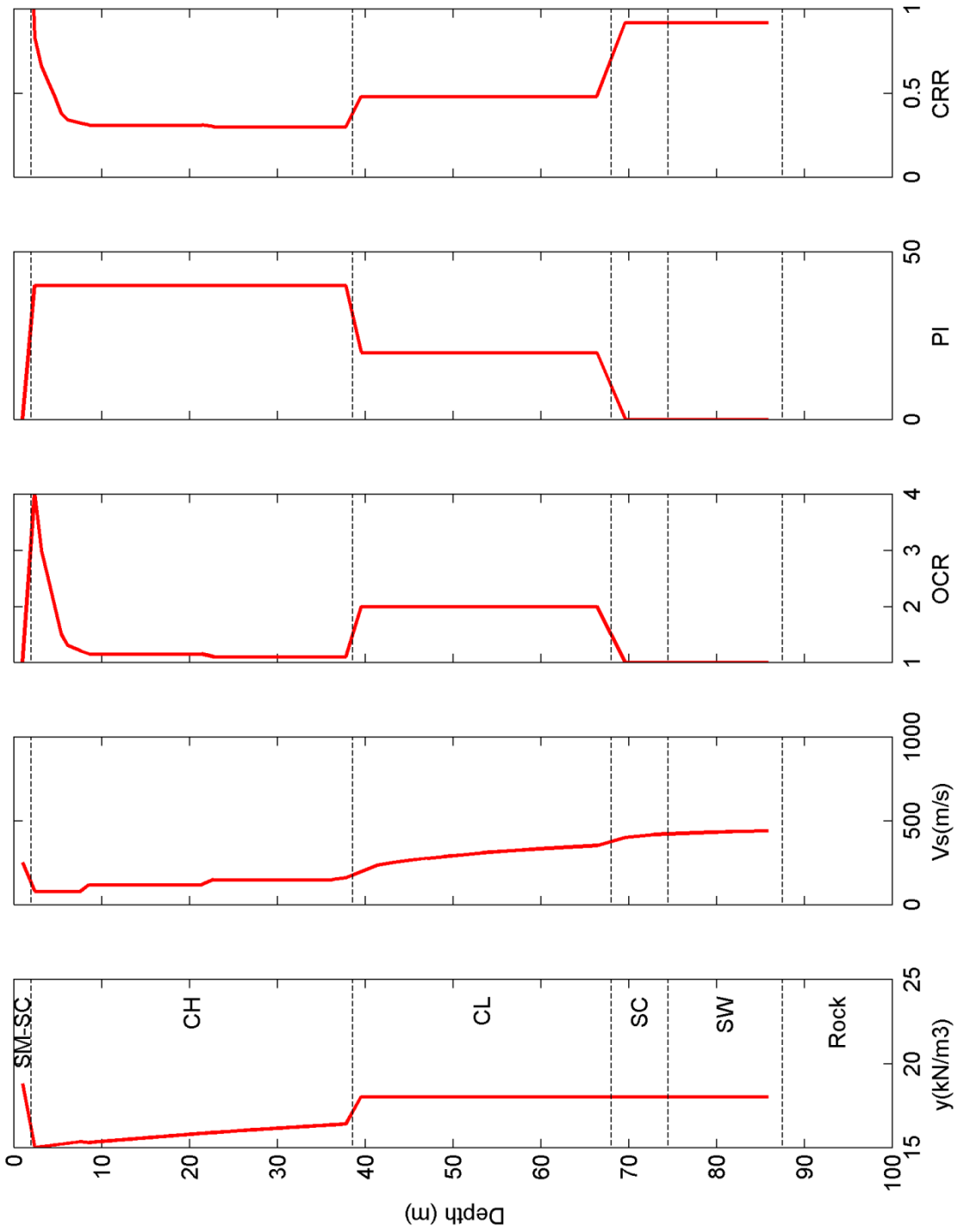

Figure 8.21: Site properties for validation site 1

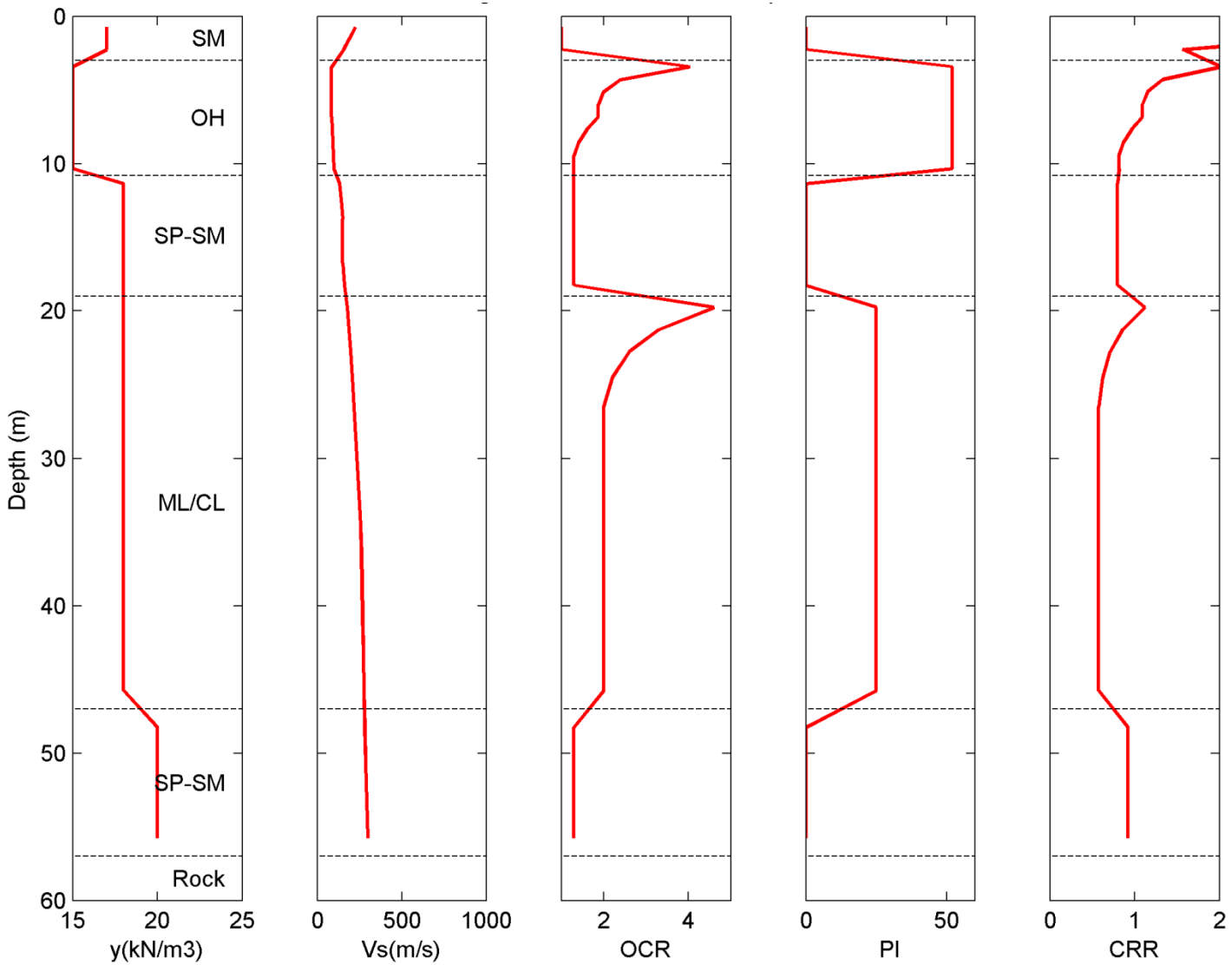

Figure 8.22: Site properties for validation site 2

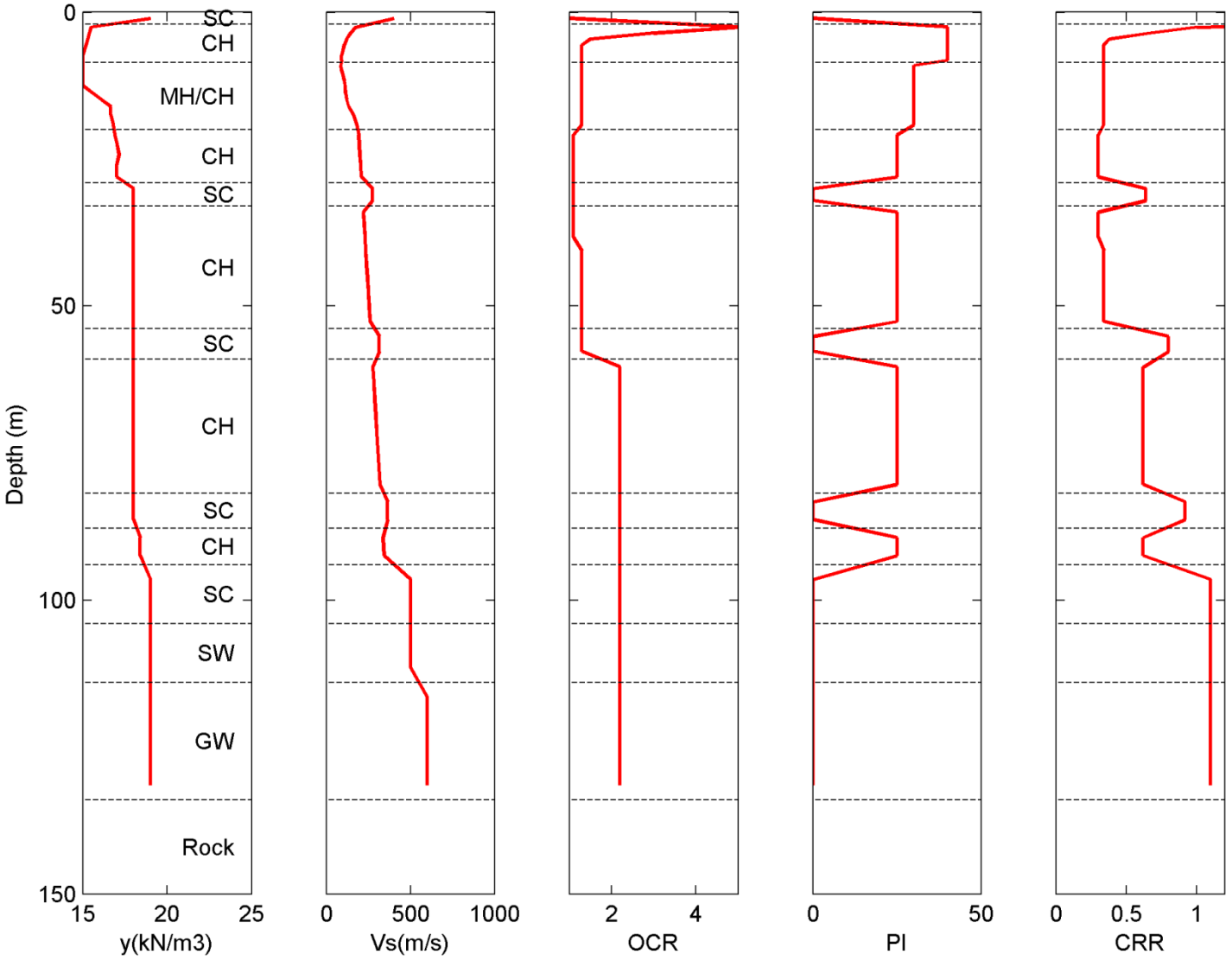

Figure 8.23: Site properties for validation site 3

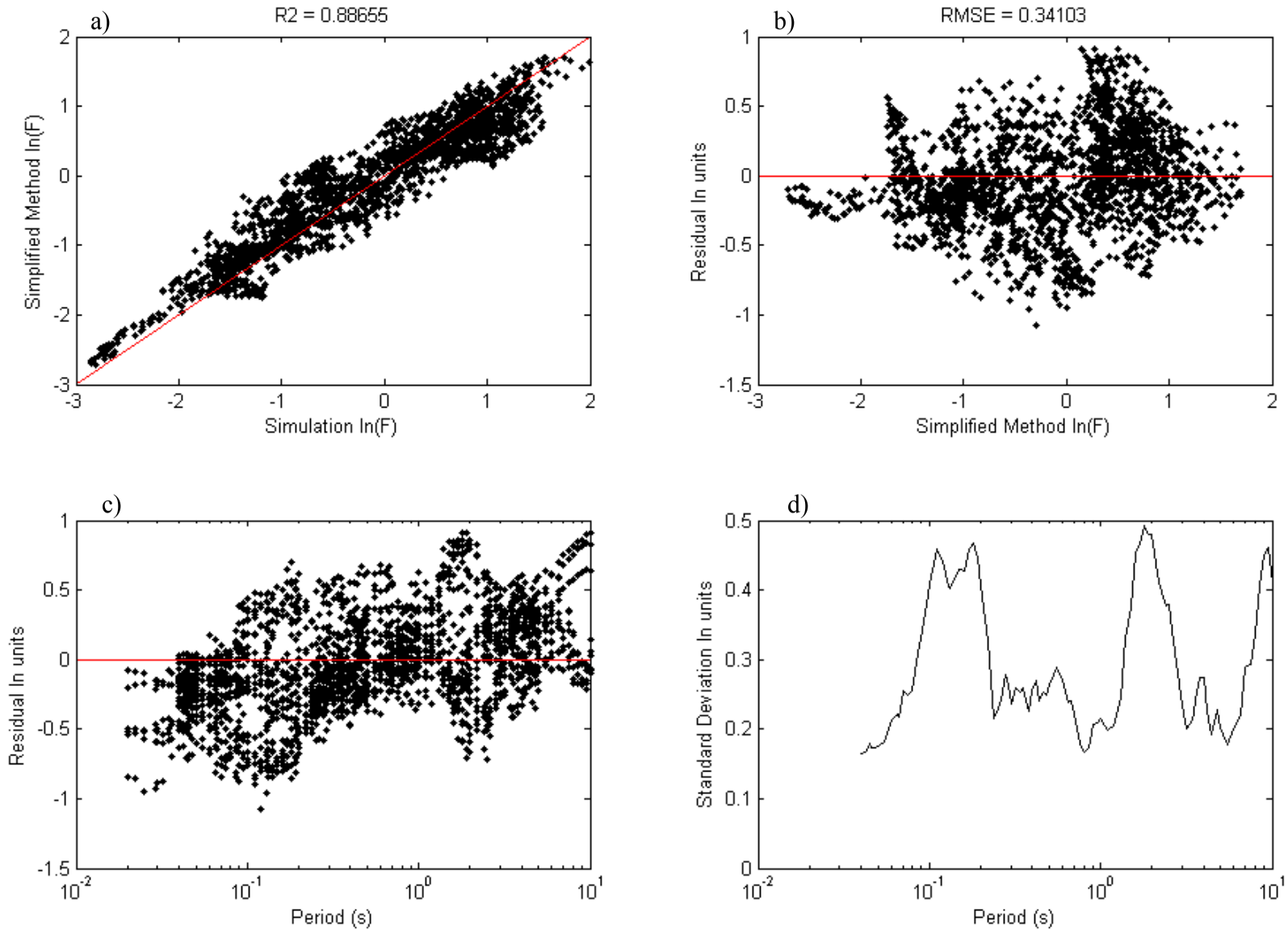

Figure 8.24: Validation results

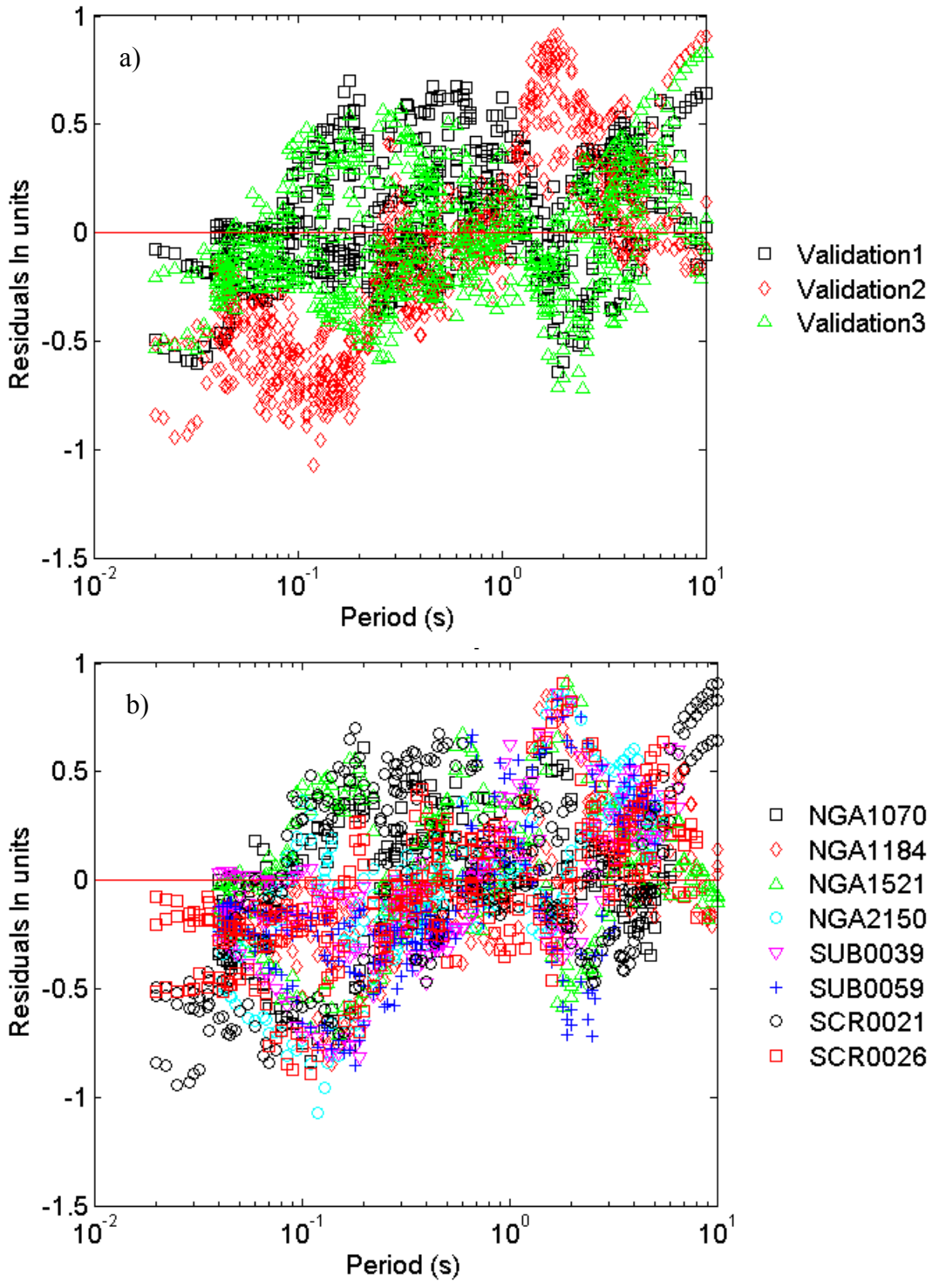

Figure 8.25: Validation residuals by a) site and b) scenario

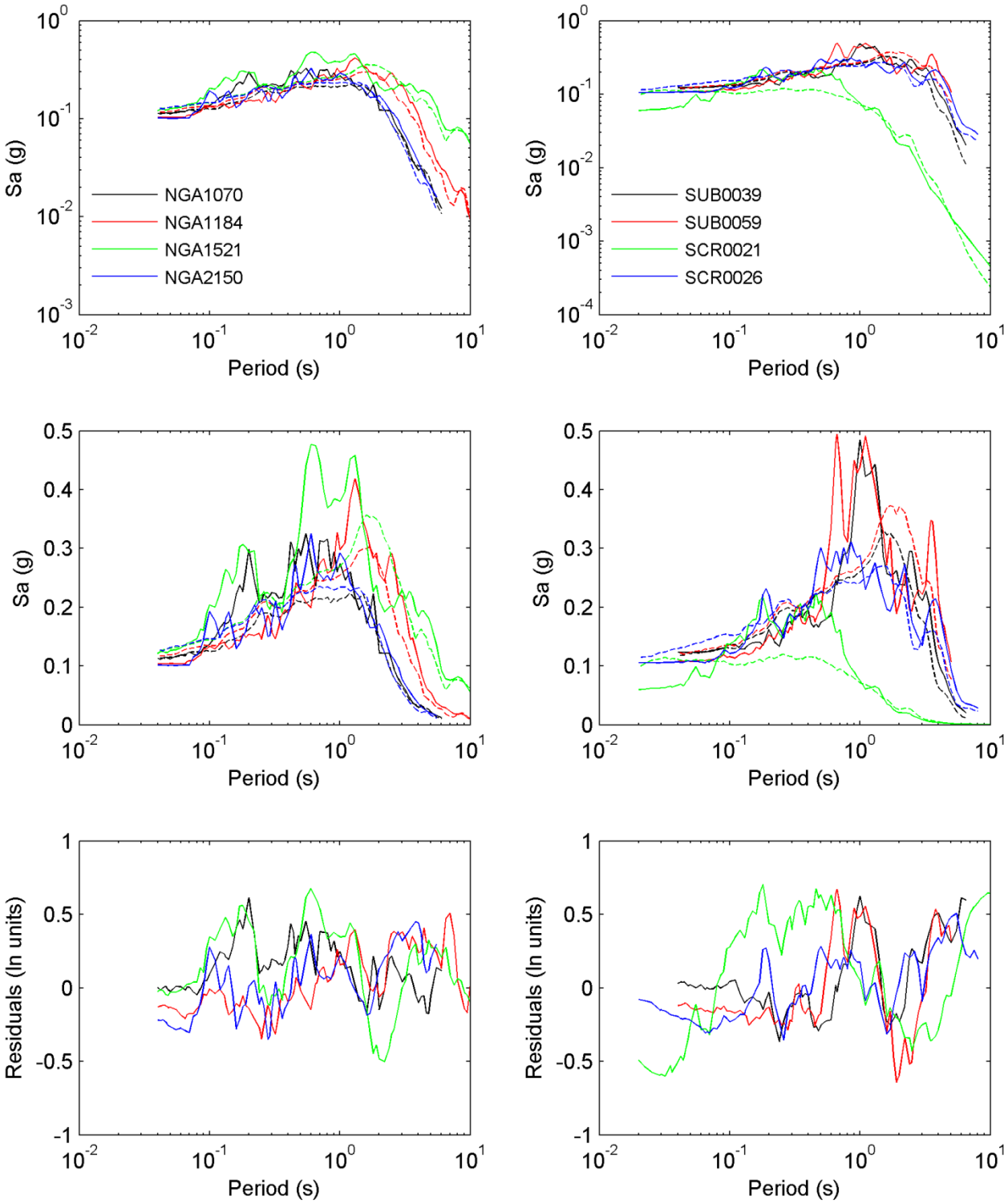

Figure 8.26: Comparison of response spectra calculated from the effective stress nonlinear validation site response analyses (solid lines) and simplified method (dashed lines) for validation site 1 and all validation scenarios

Table 8.12: Current NEHRP, ASCE, and IBC site factors (ASCE), and the proposed NEHRP 2015 site factors (PEER) (From Stewart and Seyhan, 2013)

F_a

Site	$S_s < 0.25$		$S_s = 0.5$		$S_s = 0.75$		$S_s = 1.0$		$S_s = 1.25$		$S_s > 1.5$	
Class	PEER	ASCE	PEER	ASCE	PEER	ASCE	PEER	ASCE	PEER	ASCE	PEER	ASCE
A	0.8	**0.8**	0.8	**0.8**	0.8	**0.8**	0.8	**0.8**	0.8	**0.8**	0.8	na
B	0.9	**1.0**	0.9	**1.0**	0.9	**1.0**	0.9	**1.0**	0.9	**1.0**	0.9	na
C	1.3	**1.2**	1.3	**1.2**	1.2	**1.1**	1.2	**1.0**	1.2	**1.0**	1.2	na
D	1.6	**1.6**	1.4	**1.4**	1.2	**1.2**	1.1	**1.1**	1.0	**1.0**	1.0	na
E	2.4	**2.5**	1.7	**1.7**	1.3	**1.2**	1.1	**0.9**	0.9	**0.9**	0.8	na

F_v

Site	$S_1 < 0.1$		$S_1 = 0.2$		$S_1 = 0.3$		$S_1 = 0.4$		$S_1 = 0.5$		$S_1 > 0.6$	
Class	PEER	ASCE	PEER	ASCE	PEER	ASCE	PEER	ASCE	PEER	ASCE	PEER	ASCE
A	0.8	**0.8**	0.8	**0.8**	0.8	**0.8**	0.8	**0.8**	0.8	**0.8**	0.8	na
B	0.8	**1.0**	0.8	**1.0**	0.8	**1.0**	0.8	**1.0**	0.8	**1.0**	0.8	na
C	1.5	**1.7**	1.5	**1.6**	1.5	**1.5**	1.5	**1.4**	1.5	**1.3**	1.4	na
D	2.4	**2.4**	2.2	**2.0**	2.0	**1.8**	1.9	**1.6**	1.8	**1.5**	1.7	na
E	4.2	**3.5**	3.3	**3.2**	2.8	**2.8**	2.4	**2.4**	2.2	**2.4**	2.0	na

F_{PGA}

Site	$PGA < 0.1$		$PGA = 0.2$		$PGA = 0.3$		$PGA = 0.4$		$PGA = 0.5$		$PGA > 0.6$	
Class	PEER	ASCE	PEER	ASCE	PEER	ASCE	PEER	ASCE	PEER	ASCE	PEER	ASCE
A	0.8	**0.8**	0.8	**0.8**	0.8	**0.8**	0.8	**0.8**	0.8	**0.8**	0.8	na
B	0.9	**1.0**	0.9	**1.0**	0.9	**1.0**	0.9	**1.0**	0.9	**1.0**	0.9	na
C	1.3	**1.2**	1.2	**1.2**	1.2	**1.1**	1.2	**1.0**	1.2	**1.0**	1.2	na
D	1.6	**1.6**	1.4	**1.4**	1.3	**1.2**	1.2	**1.1**	1.1	**1.0**	1.1	na
E	2.4	**2.5**	1.9	**1.7**	1.6	**1.2**	1.4	**0.9**	1.2	**0.9**	1.1	na

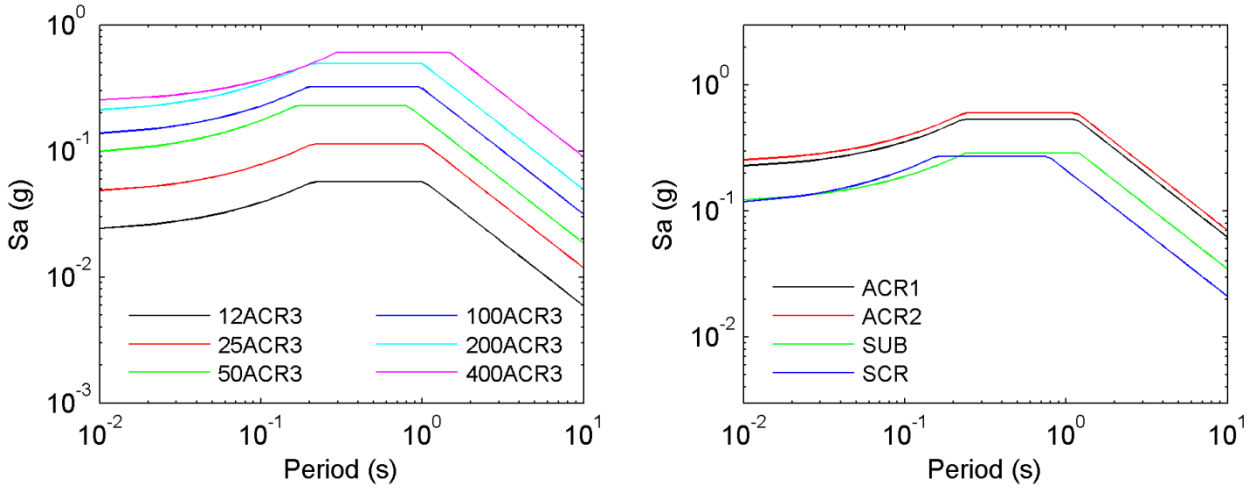

Figure 8.27: Design spectra for all scenarios based on 2012 IBC method multiplied by 0.8 and using 2015 NEHRP E site factors

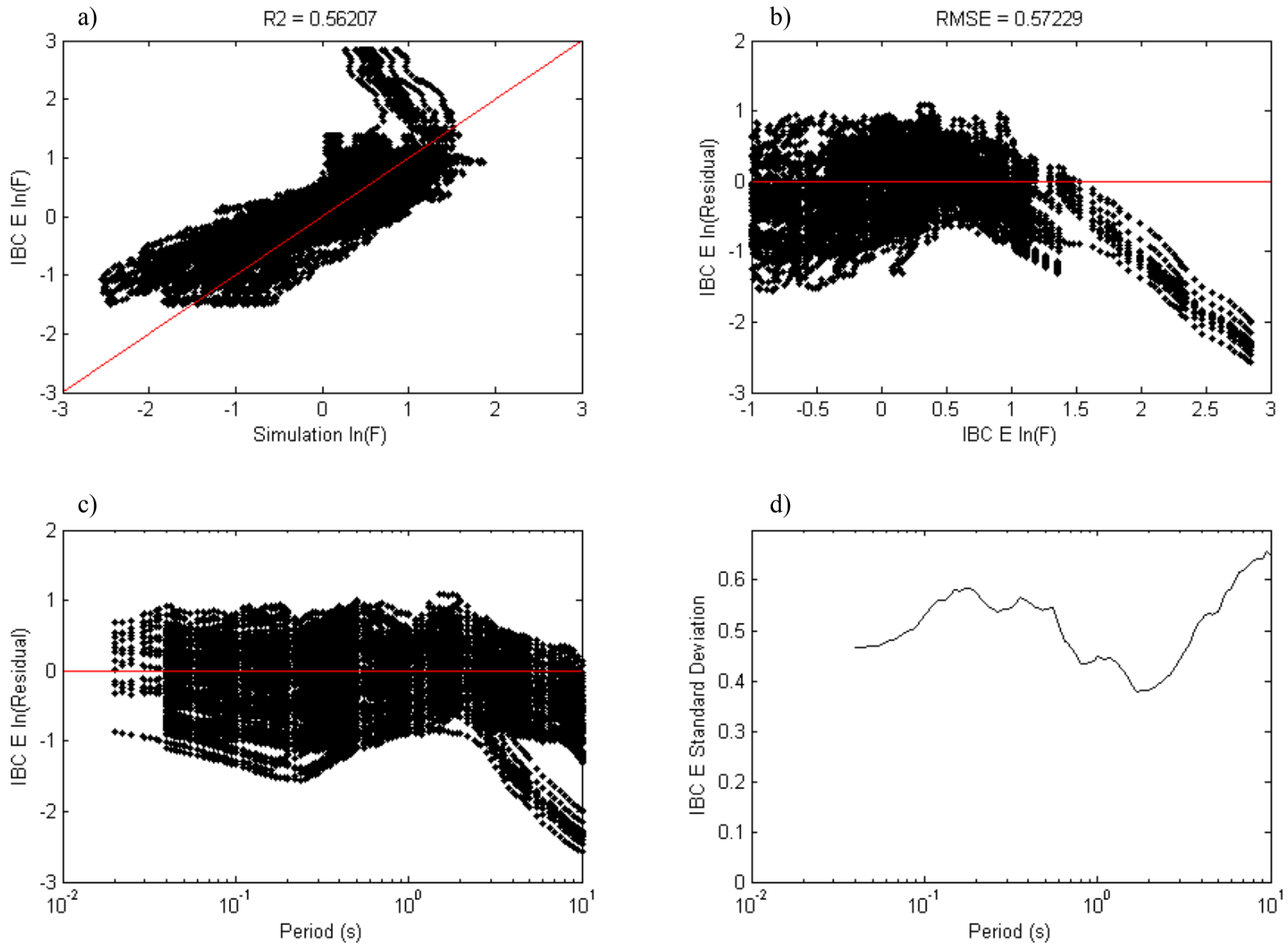

Figure 8.28: Results from 2012 IBC method multiplied by 0.8 and using 2015 NEHRP E site factors

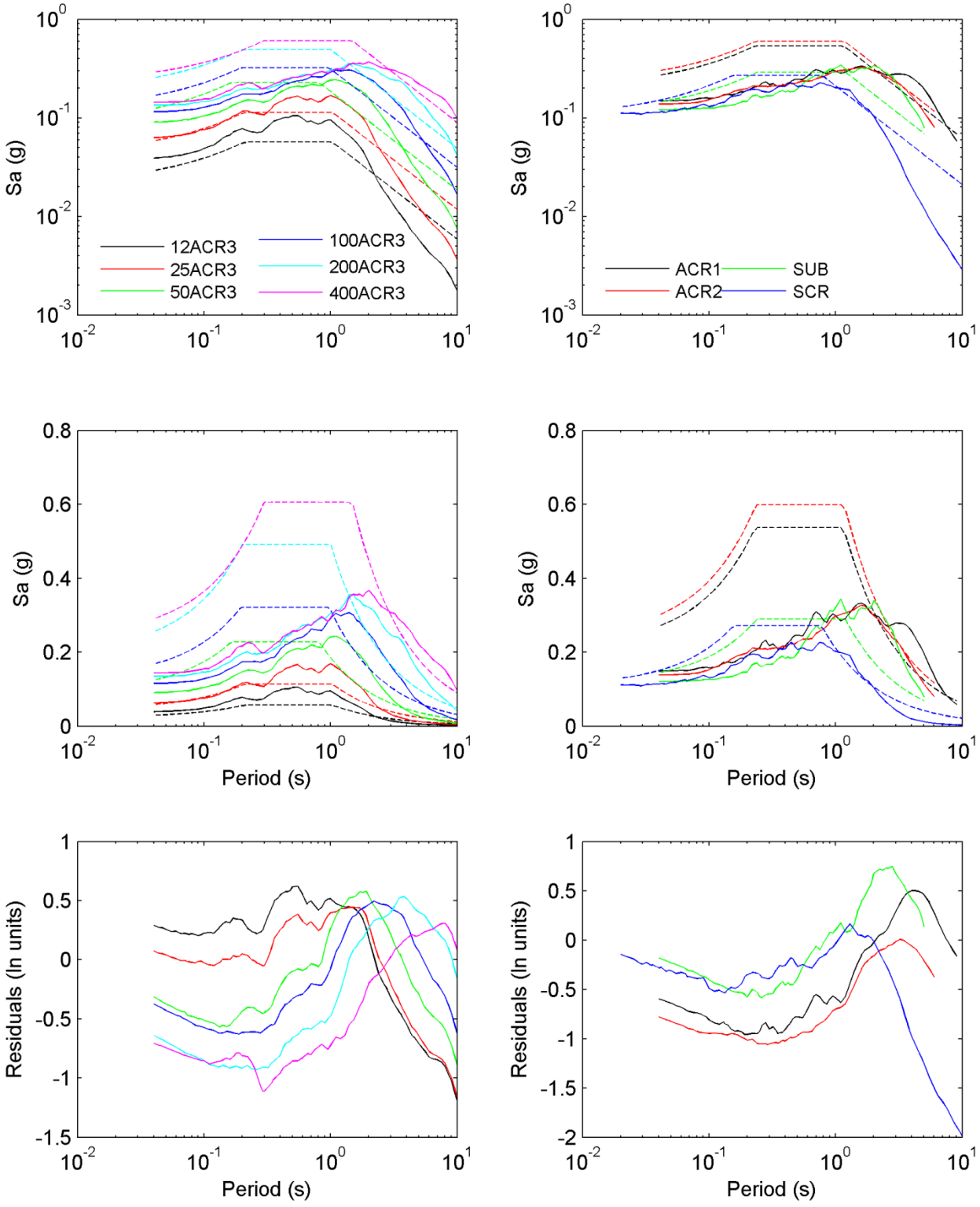

Figure 8.29: Comparison of response spectra calculated from the effective stress nonlinear site response analyses (solid lines) and 2012 IBC method multiplied by 0.8 using 2015 NEHRP site E factors (dashed lines) for site Bay Area and all scenarios

CHAPTER 9: CONCLUSION

9.1 Summary

There is little data on the seismic response of soil deposits with high plasticity soils, organic clays, and deep soft soil deposits. Therefore, this study focused on site response analyses to develop a better understanding of the effect of these types of soils on site response. Chapter 2 outlined the development of five base-case scenarios and their target parameters. The base case scenarios were selected according to tectonic environments applicable to common practice in the United States and are designated scenarios ACR1, ACR2, ACR3, SUB, and SCR. Scenario ACR1 and ACR2 correspond to shallow crustal earthquakes in active crustal regions representing reverse earthquakes with and without pulse-like responses, scenario ACR3 represents strike-slip shallow crustal earthquakes in active crustal regions, and scenarios SUB and SCR correspond to earthquakes from subduction zones and stable continental regions, respectively. Table 9.1 lists the magnitude, distance, and faulting mechanism of each of the target scenarios, and Table 9.2 lists the target ground motion parameters for each scenario.

Chapter 3 described the selection and modification of input rock ground motions for each of the scenarios. A total of eleven ground motions for scenarios ACR1, SUB, and SCR, and 40 ground motions for scenarios ACR2 and ACR3 were selected and scaled to match their target response spectra. The 40 selected ground motions for scenarios ACR2 and ACR3 were also spectrally matched over the period range of 0.1-3 seconds. In addition, to investigate the effect of ground motion intensity, the scenario ACR3 ground motions were further scaled by factors of 0.125, 0.25, 0.5, 1, 2, and 4. In other words, the 40 ground motions in scenario ACR3 were first scaled so that their average response spectrum matched the target response spectrum, then they were all scaled again by the same factor to either increase or decrease the overall intensity of the ground motions. This results in a total of 12 ground motion scenarios with 393 ground motions. Table 9.3 lists the identification, number of ground motions per scenario, and tectonic region of each of the 12 ground motion scenarios used in the site response analyses, and Figure 9.1 shows the response spectrum of each scenario.

Chapter 4 developed predictive equations to estimate the in-situ small strain shear modulus of clays, silts, sands, and gravels. This study developed the model to predict the laboratory small strain shear modulus ($G_{max,lab}$) from a mixed effects regression of a database that contains 1680 tests on 331 different soils from 28 different studies. Log-likelihood ratio tests were performed to evaluate the statistical relevance of each parameter added to the model. This ensured that the model was not over-parameterized. A second database was collected to estimate the in-situ small strain shear modulus ($G_{max,in\text{-}situ}$) from $G_{max,lab}$. The two equations were then combined to create a model to estimate $G_{max,in\text{-}situ}$ directly from soil parameters. The input variables studied were the mean effective confining pressure, void ratio, overconsolidation ratio, plasticity index, fines content, coefficient of uniformity, median grain size, laboratory test type and sample type, and in-situ test type.

This study then validated and compared the resulting model with existing models using a third collected validation database. Figure 9.2 shows the total residuals of the proposed model and the

Jamiolkowski et al. (1991), Hardin (1978), Kokusho et al. (1982), and Kallioglou et al. (2008) models for the validation database. The red lines in the boxes are the median values, the edges of the boxes are the 25^{th} and 75^{th} percentiles, and the whiskers extend to the most extreme data points not considered outliers. Outliers are shown as crosses and are defined as more than $\pm$ 2.7 standard deviations away from the median. Figure 9.2 shows that the residuals of the proposed model had a smaller standard deviation and less biased results for the validation database than the models of Jamiolkowski et al. (1991), Hardin (1978), Kokusho et al. (1982), and Kallioglou et al. (2008).

The first half of Chapter 5 reviewed fundamental concepts related to the dynamic properties of soils, such as the small strain shear modulus (G_{max}), small strain damping (D_{min}), and how the shear modulus (G) and damping (D) change with shear strain (γ). Table 9.4 through Table 9.7 describe the effect of the mean effective confining pressure ($\sigma'_{m,}$), void ratio (e), confinement time (t_g), overconsolidation ratio (OCR), excitation frequency (f), number of shearing cycles (N), plasticity index (PI), fines content (FC), median grain size (D_{50}), and coefficient of uniformity (Cu), on the dynamic properties of soils. An upward facing arrow indicates that as the parameter in the 'controlling parameter' column increases, the value of the dynamic property increases for a given shear strain. A blank cell means that this investigation is not aware of any study measuring the given relationship. The cells under the column 'cross correlations' indicate that as the 'controlling parameter' increases, the effect of the parameter under 'cross correlations' on the dynamic property either increases (upward facing arrow), or decreases (downward facing arrow). For example, Table 9.5 shows that as PI increases the effect of confining pressure on G/G_{max} decreases. The second half of chapter 5 highlighted some published empirical models for estimating shear modulus reduction and damping curves; specifically the models of Vucetic and Dobry (1991), Darendeli (2001), and Kishida et al. (2009).

The first half of chapter 6 outlined the theory, limitations, and input parameters necessary to perform one dimensional total stress equivalent linear, total stress nonlinear, and effective stress nonlinear site response analyses. It also discussed important aspects of site response analyses that caused confusion in the past but have recently been clarified by other researchers (e.g. Stewart et al., 2008; Hashash et al., 2010), such as the importance of hysteretic damping, small strain damping, layer thickness, definition of the half space, and soil strength. The second half of chapter 6 described the development of the properties of 15 different sites used in the site response analyses. Table 9.8 lists the site properties for each of the 15 sites. Seven sites are based on actual sites from the San Francisco Bay Area, New York City, Ottawa, Canada, Guayaquil, Ecuador, and Hokkaido, Japan. The other eight sites are variations of the seven base case sites that explore the effects of strength, plasticity index (PI), and elastic site period (Ts) on the surface response. Table 9.8 lists the NEHRP site category, Vs_{30}, depth to bedrock, elastic site period (T_s), the total thickness of the special soil layers (Th), the mean shear wave velocity of the special soil layers (Vs_{mean}), the minimum value of the cyclic resistance ratio (CRR_{min}) of the special soil layers, where CRR is the dynamic shear strength of the soil divided by the vertical effective confining pressure, and the mean value of the shear strain when $G/G_{max} = 0.5$ of the special soil layers ($\gamma_{0.5,mean}$). The "special" soil layers are the soil layers that classify a site as a non-liquefiable NEHRP F site, such as peat or highly organic clays, soils with PI > 75, and soft to medium stiff clays. This study conducted total and effective stress nonlinear site response analyses in the program DEEPSOIL (Hashash et al., 2012) for all 15 sites and 12 ground motion

scenarios, and total stress equivalent linear site response analyses in DEEPSOIL for each of the seven base case sites and all 12 ground motion scenarios. This resulted in a total of 14,541 site response analyses.

Chapter 7 discussed the results of the site response analyses in a qualitative manner, highlighted trends noticed in the data, and compared the results with results from other studies. It investigated the effect of ground motion properties on the results of the site response analyses such as intensity (scenarios 12ACR3, 25ACR3, 50ACR3, 100ACR3, 200ACR3, and 400ACR3), near fault pulse like motions versus near fault motions with no pulse (scenario ACR1 versus ACR2), scaled suites versus spectrally matched suites (scenarios ACR2 versus ACR2M and 100ACR3 versus ACR3M), duration (scenario 100ACR3 versus SUB), and tectonic region (scenarios 100ACR3, SUB, and SCR). Chapter 7 also looked at the effects of different site properties on the results of the site response analyses such as soil strength (sites Bay Area II K, Bay Area II K S2, and Bay Area II K S4, and sites KIKNET, KIKNET S2, and KIKNET S4), soil modulus reduction and damping curves (sites Bay Area II and Bay Area II K, and sites KIKNET40, KIKNET, and KIKNET160), and elastic site period. In addition, chapter 7 examined the effect of different analysis types on the site response analyses (total stress equivalent linear, total stress nonlinear, and effective stress nonlinear), the standard deviation of each scenario, comparisons of the amplification factors with those implied by the PEER NGA West 2 GMPEs for NERHP E sites, and the results of other ground motion parameters such as the peak ground acceleration (PGA), peak ground velocity (PGV), mean period (T_m), significant duration ($D_{5\text{-}95}$), and arias intensity (I_a).

Table 9.9 and Table 9.10 summarize all of the trends described in chapter 7 pertaining to site response analyses. In Table 9.9 the cells under the columns titled Intensity, Strength, MRD, and T_s describe what happens to the parameter in the corresponding row (↑ increase, ↓ decrease) as the ground motion intensity increases, the soil shear strength increases, the soil MRD curves shift to the right, or the elastic site period increases, respectively. Table 9.10 compares two variables of the site response analyses against each other, where the two variables are separated by a colon in the top row. The cells under these columns describe which of these two names is greater than the other for the given parameter (> or <), or whether they are equal (=). For example, the > in the cell in the first column and second row of Table 9.10 signifies that the spectral values of scenario ACR1 are greater than the spectral values of scenario ACR2 for periods greater than the peak period ($Sa(T>T_p)$). As an additional example, the > in the cell in the sixth column and fourth row signifies that total stress equivalent linear analyses predict larger spectral amplification ratios for periods less than the peak amplification period than total stress nonlinear analyses. A D in a cell means that the parameter increases for some sites and decreases for other sites, and that the trend depends on other factors. A NE in a cell means that no trend was found in this study between the specified parameters (negligible effect), and NA means that the comparison is not applicable. Table 9.11 lists the definitions of each of the parameters used in tables Table 9.9 and Table 9.10.

Chapter 8 developed a simplified model to estimate response spectra for non-liquefiable NEHRP F sites. The simplified model was developed in two stages. In the first stage, the results for each site were regressed separately against the ground motion intensity to estimate the effect of the ground motion scenario. This study found that the spectral acceleration at period T was a better

predictor of the amplification at period T than the PGA. In the second stage, the site specific coefficients calculated from the first stage were regressed against site properties to determine their site dependence. These two parts were then combined to form the final model.

Figure 9.3a shows the predicted amplification values versus the amplification values calculated from the nonlinear site response analyses in ln units. Figure 9.3b shows the residuals versus the values predicted with the simplified model, where the residuals are defined as the site response amplification values minus the amplification values predicted with the simplified model. These two plots show that the simplified model predicts well the amplification values calculated from the site response analyses (R^2 = 0.94 and RMSE = 0.21), that there is no bias in the results, and that there is an even distribution of the error for all predicted values. Figure 9.3c shows the residuals versus period and Figure 9.3d shows the standard deviation versus period. These two plots show that there is no bias in the model for period. Figure 9.4 compares the response spectra calculated from the effective stress nonlinear site response analyses with the response spectra predicted from the simplified method for all scenarios and site Bay Area. It also plots the residuals versus period. Figure 9.4 shows that the simplified model is able to capture the trend and magnitude of the response spectra calculated from the site response analyses for all scenarios, regardless of the scenario intensity, tectonic region, magnitude, or distance.

The model was regressed on the mean amplification value for a given site and scenario, therefore, the standard deviation for the model can be taken as either the standard deviation of the residuals due to the misfit of the simplified model to the site response analyses (σ_{res}), or the total standard deviation (σ_{total}), which includes both σ_{res} and the standard deviation of the response spectra of the individual ground motions for a given site and scenario (σ_{RS}).

The simplified model was validated against a separate database than the one used to develop it. This validation database consisted of 24 nonlinear effective stress site response analyses conducted in DEEPSOIL for three sites and eight ground motion scenarios. The model performed well against the validation database and showed no bias.

The simplified model presented in chapter 8 does not replace a seismic site response analysis; instead it augments it. It is hoped that the results of chapters 7 and 8 will help practicing engineers gain a better understanding of their site before conducting site response analyses.

9.2 Recommendations

This study developed two tools to aid geotechnical engineers performing site response analyses. The first tool is a model to estimate the in-situ small strain shear modulus of clays, silts, sands, and gravels, and the second is a model to estimate the response spectra of non-liquefiable NEHRP F sites. The model to estimate the in-situ small strain shear modulus is reproduced below:

$$G_{max,in-situ}/p_a = 0.78 \times [c_1 \times e^{c_2} \times (\sigma'_m/p_a)^n \times OCR^k \times (FC+1)^{c_7} \times [Cu^{c_8} \times B + (1-B)]\,]^{1.10} \quad (9.1)$$

$$n = c_3 \times Cu^{B \cdot c_4} \tag{9.2}$$

$$k = c_5 \times \left(\frac{PI}{100}\right)^{c_6} \leq 0.5 \tag{9.3}$$

$$B = \begin{cases} 1 & for\ FC < 30\% \\ 0 & for\ FC \geq 30\% \end{cases} \tag{9.4}$$

where $G_{max,in\text{-}situ}$ is the in-situ small strain shear modulus, p_a is atmospheric pressure in the same units as $G_{max,in\text{-}situ}$ and σ'_m, e is the void ratio, σ'_m is the mean effective confining pressure, OCR is the overconsolidation ratio, FC is the fines content defined as the percent weight of soil with grain size < 0.075mm, Cu is the coefficient of uniformity, PI is plasticity index, and c_1 through c_8 are coefficients listed in Table 9.12. The standard deviation for the full model is 0.58 ln units.

This study found the same value for c_2 as Jamiolkowski et al. (1991), similar values for c_3, c_4, and c_8 as Menq (2003), similar values for c_5 and c_6 as Hardin (1978), and a similar model to estimate $G_{max,in\text{-}situ}$ from $G_{max,lab}$ as Chiara and Stokoe (2006). The model is unique from other models in that it includes a fines content dependent term for Cu and a separate term for fines content, which allows a smooth transition from clean sands and gravels to silts and clays.

The model to estimate the surface pseudo-acceleration response spectra of non-liquefiable NEHRP F sites is reproduced below:

$$ln(Amp(T)) = f_1(T) + f_2(T) \times ln\left(\frac{Sa(T)_{Rock} + 0.1}{0.1}\right) \tag{9.5}$$

$$\begin{gathered} f_1(T) = c_1(T) + c_2(T) \times ln(Th) + c_3(T) \times ln(Vs_{mean}) \\ + c_4(T) \times ln(\gamma_{0.5,mean}) \end{gathered} \tag{9.6}$$

$$f_2(T) = c_5(T) + c_6(T) \times ln(CRR_{min}) \tag{9.7}$$

where Amp(T) is the amplification defined as the ratio of the surface spectral acceleration at period T divided by the spectral acceleration that would be expected on a rock site for the same period T, $Sa(T)_{rock}$ is the spectral acceleration on rock at period T, Th is the total thickness in meters of the special soil layers, Vs_{mean} is the mean shear wave velocity of the special soil layers in m/s, $\gamma_{0.5,mean}$ is the mean shear strain when $G/G_{max} = 0.5$ of the special soil layers in percent, CRR_{min} is the minimum value of the cyclic resistance ratio of the special soil layers, where CRR is the dynamic shear strength of the soil divided by the vertical effective confining pressure, and c_1 through c_6 are period dependent coefficients listed in Table 9.13. The "special" soil layers are defined as the soil layers that classify the site as a NEHRP F type site, such as peat layers, soil layers with PI > 75, or thick deposits of soft soil.

Section 8.4 gives recommendations on how to estimate the input parameters Th, Vs_{mean}, $\gamma_{0.5,mean}$, CRR_{min}, and $Sa(T)_{rock}$ of the simplified model. The thickness (Th) of the special soil layers can be estimated from boring logs, shear wave velocity profiles, and soil samples retrieved at various

depths. The special soil layers do not necessarily have to be contiguous. The other site parameters are calculated as:

$$Vs_{mean} = \frac{Th}{\sum_{i=1}^{n} \frac{h_i}{Vs_i}} \tag{9.8}$$

$$CRR_{min} = min\left[\frac{\tau_i}{\sigma'_{v,i}}, \frac{\tau_{i+1}}{\sigma'_{v,i+1}}, \ldots, \frac{\tau_n}{\sigma'_{v,i}}\right] \tag{9.9}$$

$$\gamma_{0.5,mean} = \frac{1}{Th} \times \sum_{i=1}^{n} h_i \times \gamma_{0.5,i} \tag{9.10}$$

where h_i is the thickness, Vs_i is the shear wave velocity, τ_i is the dynamic shear strength, $\sigma'_{v,i}$ is the vertical effective stress, and $\gamma_{0.5,i}$ is the shear strain where $G/G_{max} = 0.5$ for special soil layer i, and n is the number of special soil layers. The values of $Sa(T)_{rock}$ can be estimated using any applicable ground motion prediction equation.

Table 9.14 lists the values of the standard deviation of the residuals due to the misfit of the simplified model to the site response analyses (σ_{res}), the average standard deviation of the response of the individual ground motions for a given site and scenario ($\overline{\sigma}_{RS}$), and the total standard deviation (σ_{total}) by period.

9.3 Future Research

There is a wide variety of future research that could build on the results found in this study. The model to estimate in-situ small strain shear modulus requires many different parameters as input variables. This can be prohibitive, especially for a simplified model where the objective is to estimate the desired parameter without having to perform numerous in-situ and/or laboratory tests. One avenue of future research would be to develop equations to estimate the in-situ small strain shear modulus based on subsets of the parameters included in the full model. For example, instead of six input variables, a model for only the mean effective confining stress and void ratio could be developed, along with the appropriate standard deviation and coefficients. This would allow engineers flexibility to use the data they have to estimate the in-situ small strain shear modulus. In addition, they could clearly see how knowing an additional input variable would reduce the standard deviation, and then make an informed decision about whether to spend time and money determining that variable.

Another area of future research would be to validate the simplified model for estimating response spectra of non-liquefiable NEHRP F sites against recorded ground motions. Validation against empirical evidence is crucial for any model, however, very few ground motions recorded on NEHRP F sites are currently available. To solve this problem, a future line of research could instrument NEHRP F sites with downhole arrays. This would allow direct comparison of the simplified model to empirical data because the input rock ground motion would be known.

Placing instruments at sites and waiting for an earthquake can be expensive, however, so another approach would be to conduct centrifuge tests on NEHRP F sites. The exact properties of both the site and the input ground motions would be known. In addition, different sites and scenarios could be tested to examine certain aspects of the site such as the strength, plasticity index, or site period, and aspects of the ground motion such as intensity, duration, or tectonic region, as was done in this study.

Other methods to validate the model, or increase the database to create a new model, would be to conduct 2D and/or 3D site response analyses in programs such as FLAC or PLAXIS. Two and three-dimensional analyses could investigate basin effects, or the effect of surface waves, which cannot be adequately modeled in one-dimensional analyses.

Finally, the database created from the site response analyses contains more information than just pseudo-acceleration response spectra. Using the already created database, future research could develop models for other ground motion parameters such as the peak ground velocity (PGV), the significant duration ($D_{5\text{-}75}$ or $D_{5\text{-}95}$), the mean period (T_m), and the arias intensity (I_a). In addition, guidelines of when it is appropriate to use total stress equivalent linear analyses, total stress nonlinear analyses, and effective stress nonlinear analyses could be developed.

9.4 References

Biscontin, G. and Pestana, J.M. (1999). "Influence of peripheral velocity on undrained shear strength and deformability characteristics of a bentonite-kaolinite mixture," Geotechnical Engng Report No. UCB/GT/99-19, Dep. of Civil & Environ. Eng., University of California, Berkeley.

Chiara, Nicola and K. Stokoe (2006). "Sample disturbance in resonant column test measurement of small strain shear wave velocity." *Proceedings of Soil Stress-Strain Behavior: Measurement, Modeling and Analysis*, Rome, Italy, March 16-17.

Darendeli, M. B. (2001). "Development of a new family of normalized modulus reduction and material damping curves." PhD dissertation, Univ. of Texas at Austin, Austin, Texas.

Hardin, B. (1978).''The nature of stress-strain behavior of soils,'' *Proc. of Geotechnical Division Specialty Conference on Earthquakes Engineering & Soil Dynamics*, ASCE, Pasadena, CA, Vol.1, pp. 3–90.

Hashash, Y.M.A, Groholski, D.R., Phillips, C. A., Park, D, Musgrove, M. (2012). "DEEPSOIL 5.1, User Manual and Tutorial." 107 p.

Hashash, Y.M.A., Groholski, D.R. Phillips, C.A., (2010). "Recent advances in non-linear site response analysis." In proceedings of *Fifth International Conference on Recent Advances in Geotechnical Earthquake Engineering and Soil Dynamics*, May 24-29, San Diego, CA.

Jamiolkowski, M., Leroueil, S., and D.C.F. Lo Presti. (1991). "Design Parameters from Theory to Practice." *Theme Lecture, Proc. Geo-Coast 91*, Yokohama, Vol 2, 877-917.

Kallioglou, P., Tika, Th. and Pitilakis, K. (2008). "Shear Modulus and Damping Ratio of Cohesive Soils." *Journal of Earthquake Engineering*. 12(6), 879 – 913.

Kishida, T., Boulanger R.W., Abrahamson N.A., Wehling T.M., Driller M.W. (2009). "Regression Models for Dynamic Properties of Highly Organic Soils." *J. of Geotech. and Geoenvir. Eng.*, ASCE, 135(4).

Kokusho, T., Yoshida, Y. and Esashi, Y. (1982). "Dynamic properties of soft clay for a wide strain range." *Japanese Society of Soil Mechanics and Foundations*. Vol 22, 1–18.

Ladd, C. C., and Foott, R. (1974). "A New design procedure for stability of soft clays." *Journal of the Geotechnical Engineering Division*, ASCE,100(GT7), pp. 763-786.

Menq, Farn-Yuh (2003). "Dynamic Properties of Sandy and Gravelly Soils." PhD dissertation, Univ. of Texas at Austin, Austin, Texas.

Sheahan, T.C., C.C. Ladd, and J.T. Germaine (1996) "Rate-dependent undrained shear behavior of saturated clay," *J. Geotech. Engr.*, ASCE, 122 (2), 99-108.

Stewart, J.P., Kwok, A.O., Hashash, Y.M.A, Matasovic, N., Pyke, R., Wang, Z., Yang, Z. (2008). "Benchmarking of Nonlinear Geotechnical Ground Response Analysis Procedures." Pacific Earthquake Engineering Research Center Report 2008/04.

Vucetic, M., and Dobry, R. (1991). "Effect of soil plasticity on cyclic response." *Journal of Geotechnical Engineering*, ASCE, 117(1), 89-107.

Table 9.1: Target scenarios

ID	Mechanism	M_w	R_{rup} (km)
ACR1	Reverse (Pulse Like)	6.7	5
ACR2	Reverse (No Pulse)	6.7	5
ACR3	Strike Slip	7.8	30
SUB	Interface	9	100
SCR	Stable Continental Region	6	17

Table 9.2: Mean and plus and minus one standard deviation target parameters for all five scenarios

Scenario	Percentile	PGA (g)	PGV (cm/s)	D_{5-95} (s)	T_m (s)	I_a (m/s)	T_v (s)
ACR1	μ-σ	0.32	37.3	4.2	0.36	0.88	0.84
	μ	0.56	55.7	6.6	0.57	1.70	1.45
	μ+σ	0.98	83.0	10.6	0.90	3.75	2.52
ACR2	μ-σ	0.32	21.8	6.6	0.27	0.88	
	μ	0.56	37.9	10.6	0.43	1.70	
	μ+σ	0.98	65.9	16.9	0.67	3.75	
ACR3	μ-σ	0.09	9.2	20.3	0.3	0.23	
	μ	0.15	15.8	32.3	0.5	0.43	
	μ+σ	0.26	27.2	51.4	0.8	0.90	
SUB	μ-σ	0.093					
	μ	0.152					
	μ+σ	0.251					
SCR	μ-σ	0.142	2.89				
	μ	0.279	5.73				
	μ+σ	0.553	11.51				

Table 9.3: Ground motion scenarios used in the site response analyses

ID	# of GM	LUP (s)	HUP (s)	Region	Notes
12ACR3	40	0.04	13.33	ACR	Scenario ACR3 scaled motions multiplied by 0.125
25ACR3	40	0.04	13.33	ACR	Scenario ACR3 scaled motions multiplied by 0.25
50ACR3	40	0.04	13.33	ACR	Scenario ACR3 scaled motions multiplied by 0.50
100ACR3	40	0.04	13.33	ACR	Scenario ACR3 scaled motions
200ACR3	40	0.04	13.33	ACR	Scenario ACR3 scaled motions multiplied by 2
400ACR3	40	0.04	13.33	ACR	Scenario ACR3 scaled motions multiplied by 4
ACR3M	40	0.04	13.33	ACR	Scenario ACR3 matched motions
ACR1	11	0.04	8.85	ACR	
ACR2	40	0.04	6.15	ACR	Scenario ACR2 scaled motions
ACR2M	40	0.04	6.15	ACR	Scenario ACR2 matched motions
SUB	11	0.04	5	SUB	
SCR	11	0.02	10	SCR	

LUP = lowest useable period, HUP = highest useable period

ACR = active crustal region, SUB = subduction zone, SCR = stable continental region

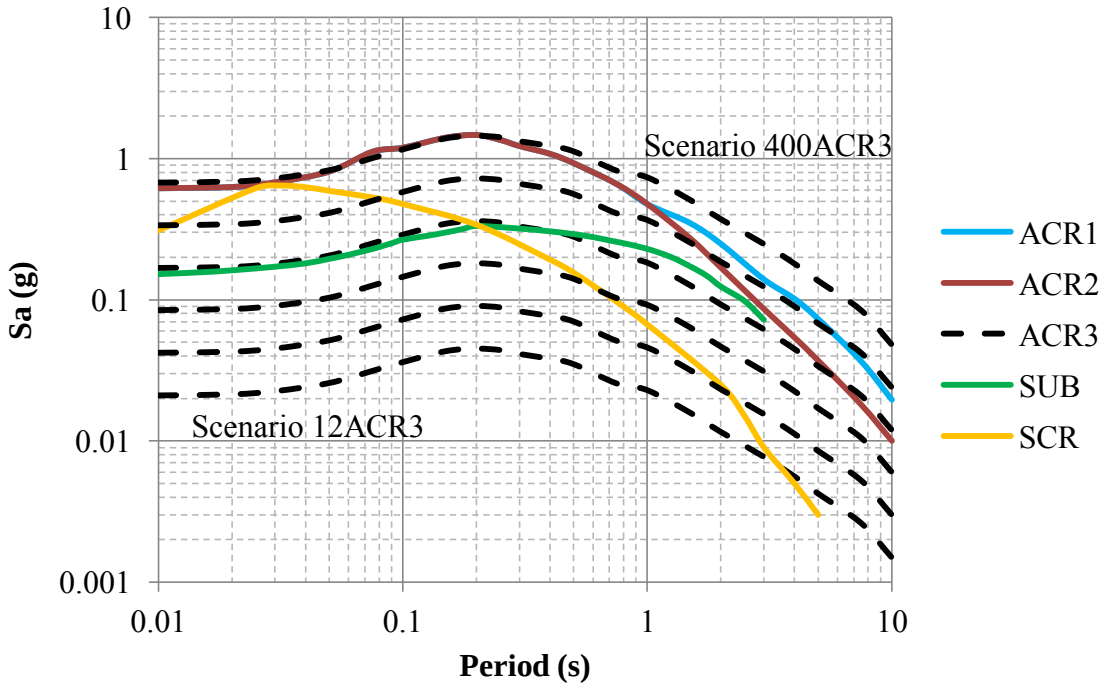

Figure 9.1: Scenario response spectra used in site response analyses; scenario ACR3 was scaled up and down to give a range of ground motion intensity

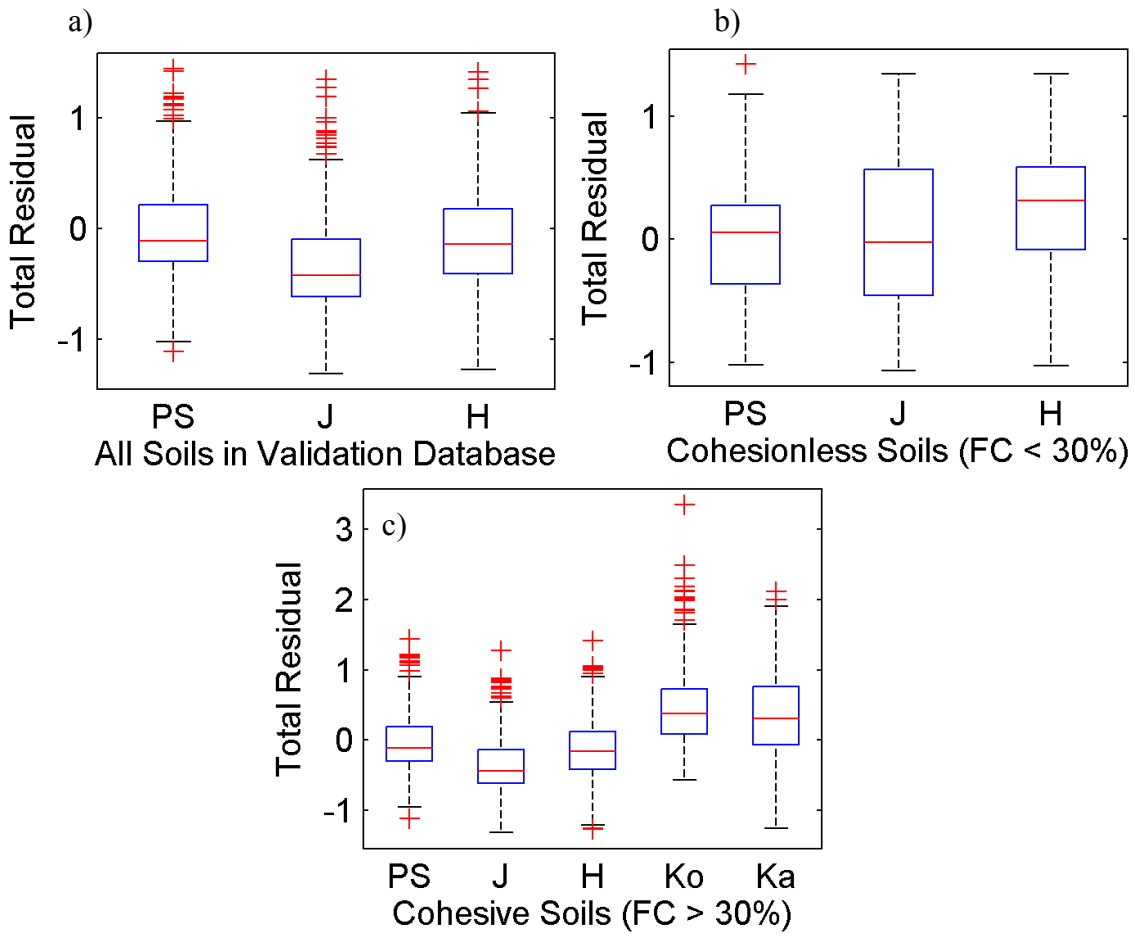

Figure 9.2: $G_{max,in\text{-}situ}$ model comparison for a) all soils in the validation database, b) soils with FC < 30%, and c) soils with FC > 30%; PS = present study; J = Jamiolkowski et al (1991); H = Hardin (1978); Ko = Kokusho et al. (1982); Ka = Kallioglou et al. (2008)

Table 9.4: Parameters studied by other researchers and their effect on G_{max}

Controlling Parameter	G_{max} Cohesive	G_{max} Cohesionless	Cross Correlations			
			t_g	*OCR*	σ'_m	*e*
σ'_m	↑	↑				
e	↓	↓				
t_g	↑	↑				
OCR	↑	NE[a]	↓			
f	NE[a]	NE[a]				
N	NE[a]	NE[a]				
PI	↓		↑	↑		
FC	↓	↓				
D50		↑	↓			↑[b]
Cu		↓			↑[b]	

a = negligible effect; b = only for cohesionless soils

Table 9.5: Parameters studied by other researchers and their effect on G/G_{max} for a given shear strain

Controlling Parameter	G/G_{max} Cohesive	G/G_{max} Cohesionless	Cross Correlations
			σ_m'
σ'_m	↑	↑	
e	↑		
t_g	↑		
OCR	NE[a]	NE[a]	
f	NE[a]	NE[a]	
N	↓	↑	
PI	↑		↓[b]
FC			
D50		↑	
Cu		↓	↓[c]

a = negligible effect; b = only for cohesive soils: c = only for cohesionless soils

Table 9.6: Parameters studied by other researchers and their effect on D_{min}

Increasing Parameter	D_{min} Cohesive	D_{min} Cohesionless	Cross Correlations
			f
σ'_m	↓	↓	
e	↓	↓	
t_g	↓	↓	
OCR	↓	NE[a]	
f	↑	↑	
N	NE[a]	NE[a]	
PI	↑		↑[b]
FC			
$D50$		↓	
Cu		↑	

a = negligible effect; b = only for cohesive soils

Table 9.7: Parameters studied by other researchers and their effect on D for a given shear strain

Controlling Parameter	D Cohesive	D Cohesionless	Cross Correlations	
			f	N
σ'_m	↓	↓		
e	↓			
t_g	NE[a]	NE[a]		
OCR	NE[a]	NE[a]		
f	↓	NE[a]		
N	↓	↓		
PI	↓		↑[b]	↓[b]
FC				
$D50$		↑		
Cu				

a = negligible effect; b = only for cohesive soils

Table 9.8: Properties of sites used in site response analyses

ID	Approximate Location	NEHRP	Vs_{30} (m/s)	Depth (m)	T_s (s)	Th (m)	Vs_{mean} (m/s)	$\gamma_{0.5,mean}$ (%)	CRR_{min}
Bay Area	SF Bay Area	E	125	185	2.66	19.25	101.4	0.0580	0.30
Bay Area F	SF Bay Area	F	119	189	2.84	36.85	119.6	0.0699	0.29
Bay Area II	SF Bay Area	F	79	32	1.58	9.75	34.8	0.1216	0.61
Bay Area II K	SF Bay Area	F	79	32	1.58	9.75	34.8	0.7238	0.58
Bay Area II K S2	SF Bay Area	F	79	32	1.58	9.75	34.8	0.9831	1.15
Bay Area II K S4	SF Bay Area	F	79	32	1.58	9.75	34.8	1.8661	2.35
HAGP	Guayaquil, Ecuador	F	127	50	1.23	37.00	136.3	0.0733	0.22
JSSS	Ottawa, Canada	F	143	115	1.93	56.00	173.1	0.0597	0.29
KIKNET40	Hokkaido, Japan	E	140	103	1.56	13.40	99.0	0.0483	0.30
KIKNET	Hokkaido, Japan	F	140	103	1.56	13.40	99.0	0.0707	0.30
KIKNET160	Hokkaido, Japan	F	140	103	1.56	13.40	99.0	0.1026	0.30
KIKNET S2	Hokkaido, Japan	F	140	103	1.56	13.40	99.0	0.0781	0.61
KIKNET S4	Hokkaido, Japan	F	140	103	1.56	13.40	99.0	0.0912	1.22
MRCE1	New York City	F	128	90	1.69	15.15	94.3	0.0886	0.80
MRCE2	New York City	F	162	30	0.74	17.20	112.0	0.0582	0.33

Table 9.9: Summary of the effects of ground motion intensity and site characteristics on the results of the site response analyses reviewed in this chapter

	Intensity ↑	Strength ↑	MRD →	Ts ↑
$Sa(T<T_p)$	↑	↑	↑	NE
$Sa(T>T_p)$	↑	↑ [3]	NE	NE
T_p	↑	NE	NE	NE
$Amp(T < T_p)$	↓	↑	↑	NE
$Amp(T > T_p)$	↑	↓	↓	↑
Amp_p	↓	↑	↑	↑
$T_{p,amp}$	↑	↓	↓	↑
$T_{min,amp}$	↑	↑	↓	NE
$\gamma_{max}(D)$	↑	D	D	NE
$CRR_{max}(D)$	↑	↑	↑	NE
$r_{u,max}(D)$	↑	D	D	NE
$PGA_{max}(D)$	↑	↑	↑	NE
SR_p	↓	↓	↑	NE
T_{pSR}	↑	NE	↓	NE
Shape	→	↓	←	NE
σ_{RS}	↓	↑	↑	NE
σ_{AMP}	↑	↓	↓	NE
Fa	↓	↑ [2,3]	↑ [1,2]	NE
Fv	↓	↑ [2,3]	↑ [1,2]	NE
A_{PGA}	↓	↑	↑	NE
A_{PGV}	↓	↑	↑	NE
A_{PGD}	NE	NE	NE	NE
A_{Tm}	↑ [1,2]	↓ [1,2]	↓	NE
$A_{D5\text{-}95}$	↑ [1,2]	↓ [1,2]	↓	NE
A_{Ia}	↓	↑	↑	NE

[1] For small values of PGA rock; [2] For moderate values of PGA rock; [3] For large values of PGA rock; D = may increase or decrease, depends on other factors; NE = negligible effect

Table 9.10: Summary of the effects of scenario and analysis type on the results of the site response analyses reviewed in this chapter

	ACR1:ACR2	ACR2:ACR2M	100ACR3:ACR3M	100ACR3:SUB	100ACR3:SCR	EQL:TSN	EQL:ESN	TSN:ESN
$Sa(T<T_p)$	=	=	=	=	< or =	>	>	=
$Sa(T>T_p)$	>	=	=	=	>	=	< [2,3]	< [2,3]
T_p	=	=	=	=	>	< [3]	< [3]	=
$Amp(T < T_p)$	=	=	=	=	>	>	>	=
$Amp(T > T_p)$	=	=	=	=	<	=	<	<
Amp_p	=	=	=	=	<	>	>	=
$T_{p,amp}$	=	=	=	=	> or =	<	<	<
$T_{min,amp}$	=	=	=	=	>	>	>	>
$\gamma_{max}(D)$	>	=	=	>	>	D	D	D
$CRR_{max}(D)$	=	=	=	>	>	>	>	>
$r_{u,max}(D)$	>	=	=	>	> or =	NA	NA	NA
$PGA_{max}(D)$	=	=	=	=	<	>	>	>
SR_p	=	=	=	=	> or =	<	> [2,3]	> [2,3]
T_{pSR}	=	=	=	=	>	< [3]	< [3]	=
Shape	ACR1 →	=	=	=	← SCR	↓ EQL	↓ EQL	=
σ_{RS}	=	>	>	=	= [4]	>	> [2]	= [4]
σ_{AMP}	=	>	>	=	= [4]	<	<	= [4]
Fa	=	=	=	=	<	>	>	> [2]
Fv	=	=	=	=	<	>	>	> [2]
A_{PGA}	=	=	=	=	>	>	>	=
A_{PGV}	=	=	=	=	=	>	>	=
A_{PGD}	=	=	=	=	<	>	>	=
A_{Tm}	=	=	=	=	=	=	=	> [3]
A_{D5-95}	=	=	=	=	<	>	>	> [3]
A_{Ia}	=	=	=	=	=	>	>	=

[1] For small values of PGA rock; [2] For moderate values of PGA rock; [3] For large values of PGA rock; [4] < for long T; D = may increase or decrease, depends on other factors; NA = not applicable

Table 9.11: Definition of terms used in Table 9.9 and Table 9.10

Parameter	Definition
$Sa(T<T_{p,Sa})$	Psuedo-spectral acceleration values for periods less than $T_{p,Sa}$
$Sa(T>T_{p,Sa})$	Psuedo-spectral acceleration values for periods greater than $T_{p,Sa}$
$T_{p,Sa}$	Period of the peak psuedo-spectral accleration value
$Amp(T < T_{p,amp})$	Amplification values for periods less than $T_{p,amp}$
$Amp(T > T_{p,amp})$	Amplification values for periods greater than $T_{p,amp}$
Amp_p	Peak amplification value
$T_{p,amp}$	Period of the peak amplification value
$T_{min,amp}$	Period of the minimum amplification value
$\gamma_{max}(D)$	Maximum shear strain with depth (D)
$CRR_{max}(D)$	Maximum shear stress ratio with depth (D)
$r_{u,max}(D)$	Maximum pore pressure ratio with depth (D)
$PGA_{max}(D)$	Maximum PGA with depth (D)
SR_p	Peak spectral ratio (Sa(T) / PGA) value
T_{pSR}	Period of the peak spectral ratio
Shape	Spectral shape (Sa(T) / PGA) (SR for all periods)
σ_{RS}	Response spectra standard deviation
σ_{AMP}	Amplification standard deviation
Fa	Short period amplificatoin factor (0.1-0.5 s)
Fv	Mid period amplification factor (0.4-2 s)
A_{PGA}	Amplificaiton of PGA (PGA_{soil}/PGA_{rock})
A_{PGV}	Amplificaiton of PGV (PGV_{soil}/PGV_{rock})
A_{PGD}	Amplificaiton of PGD (PGD_{soil}/PGD_{rock})
A_{Tm}	Amplificaiton of Tm (Tm_{soil}/Tm_{rock})
A_{D5-95}	Amplificaiton of D_{5-95} ($D_{5-95,soil}/D_{5-95}$,rock)
A_{Ia}	Amplificaiton of Ia (Ia_{soil}/Ia_{rock})
EQL	Total stress equivalent linear analysis
TSN	Total stress nonlinear analysis
ESN	Effective stress nonlinear analysis

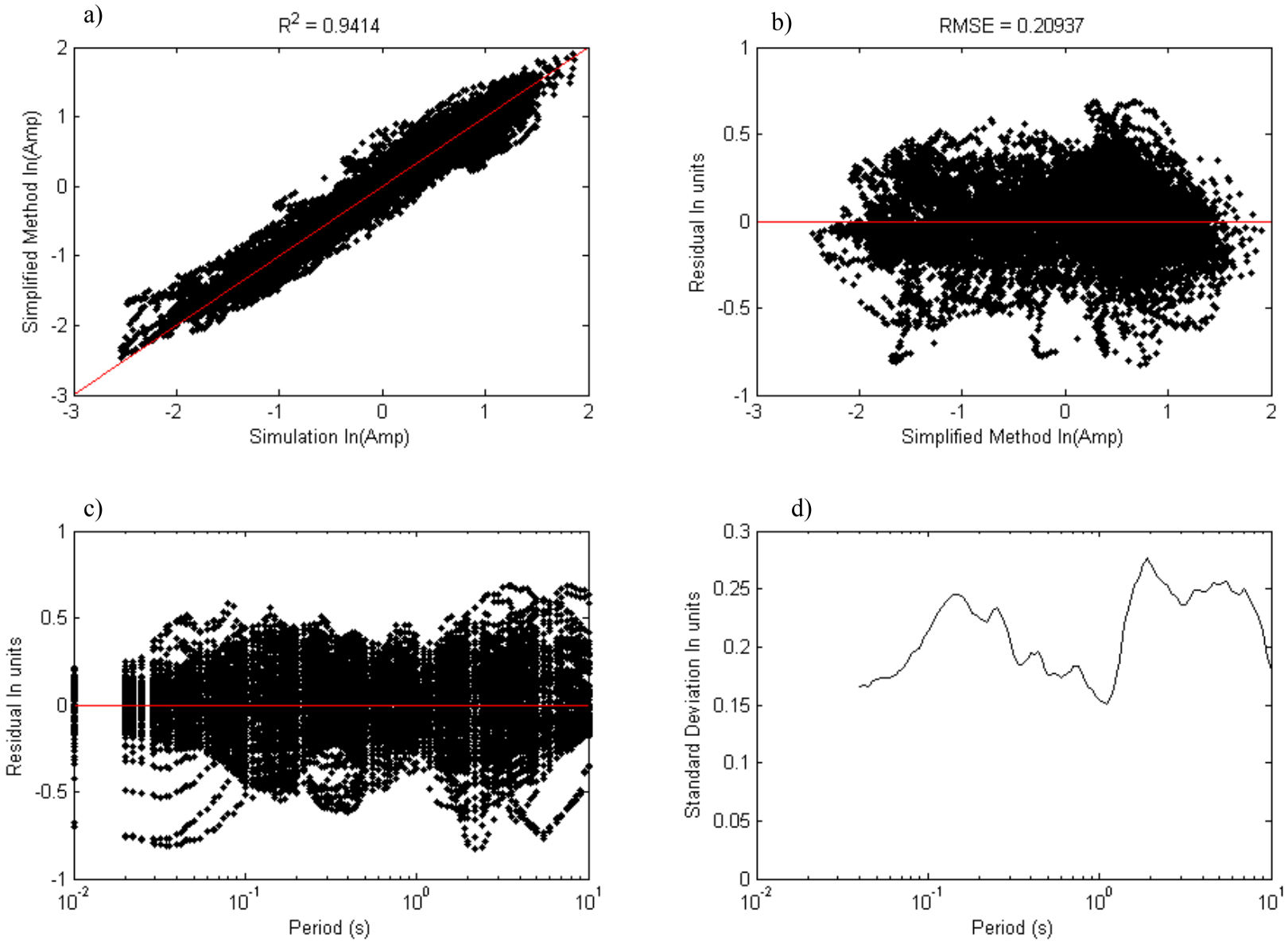

Figure 9.3: Results of the simplified model

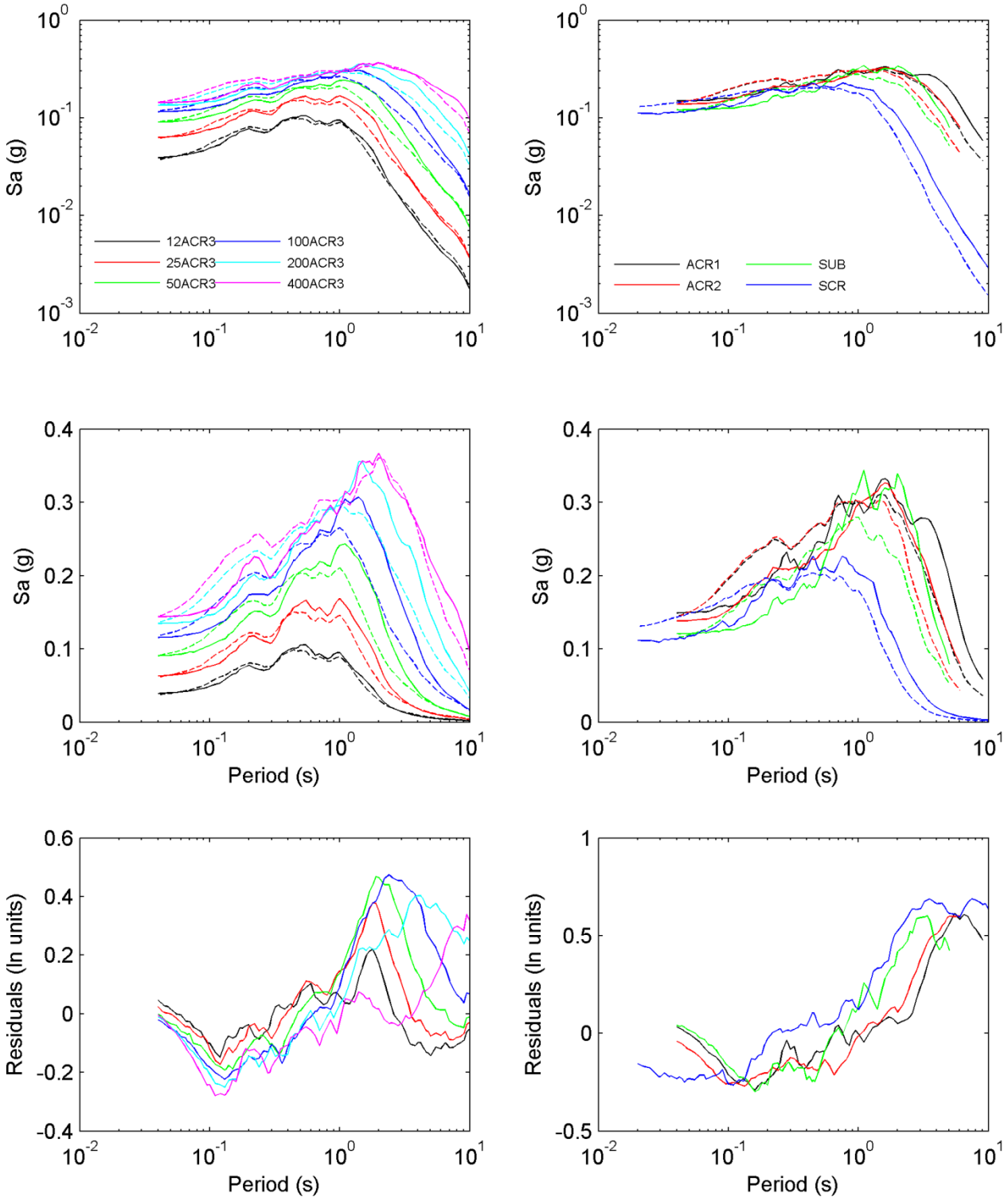

Figure 9.4: Comparison of response spectra calculated from effective stress nonlinear site response analyses (solid lines) and simplified method (dashed lines) for site Bay Area and all scenarios

Table 9.12: Regression coefficients for the $G_{max,in\text{-}situ}$ model

Coefficient	Value	Standard Error
c_1	790.2	41.8
c_2	-1.309	0.0817
c_3	0.465	0.0138
c_4	0.106	0.0102
c_5	2.022	0.0463
c_6	1.933	0.0231
c_7	-0.124	0.0161
c_8	-0.170	0.0308

Table 9.13: Period dependent coefficients for the simplified NEHRP F site model

T (s)	c_1	c_2	c_3	c_4	c_5	c_6
PGA	-1.1073	-0.4789	0.9070	0.3252	-0.8938	0.2324
0.02	-1.0703	-0.4673	0.8897	0.3270	-0.9034	0.2103
0.022	-1.0753	-0.4664	0.8889	0.3274	-0.9028	0.2048
0.025	-1.0635	-0.4598	0.8814	0.3272	-0.9033	0.1989
0.029	-1.0880	-0.4574	0.8787	0.3253	-0.8868	0.1932
0.03	-1.0832	-0.4581	0.8784	0.3260	-0.8875	0.1904
0.032	-1.0796	-0.4635	0.8827	0.3268	-0.8908	0.1853
0.035	-1.1154	-0.4695	0.8913	0.3249	-0.8811	0.1842
0.036	-1.1244	-0.4721	0.8945	0.3246	-0.8784	0.1838
0.04	-1.2053	-0.4946	0.9262	0.3263	-0.8733	0.1801
0.042	-1.2530	-0.5016	0.9385	0.3261	-0.8660	0.1797
0.044	-1.3243	-0.5196	0.9657	0.3270	-0.8606	0.1812
0.045	-1.3473	-0.5294	0.9776	0.3272	-0.8601	0.1804
0.046	-1.3712	-0.5349	0.9858	0.3275	-0.8570	0.1801
0.048	-1.3823	-0.5368	0.9873	0.3263	-0.8516	0.1782
0.05	-1.4211	-0.5408	0.9959	0.3262	-0.8450	0.1774
0.055	-1.5398	-0.5553	1.0262	0.3236	-0.8244	0.1820
0.06	-1.6841	-0.5991	1.0919	0.3287	-0.8218	0.1814
0.065	-1.7981	-0.6176	1.1271	0.3311	-0.8075	0.1794
0.067	-1.8323	-0.6253	1.1383	0.3314	-0.8012	0.1791
0.07	-1.9324	-0.6509	1.1801	0.3349	-0.7982	0.1796
0.075	-2.0674	-0.6858	1.2334	0.3387	-0.7873	0.1795
0.08	-2.1677	-0.7118	1.2685	0.3375	-0.7719	0.1778
0.085	-2.2105	-0.7484	1.3012	0.3378	-0.7695	0.1704

0.09	-2.3329	-0.7915	1.3618	0.3447	-0.7679	0.1661
0.095	-2.5025	-0.8360	1.4320	0.3478	-0.7617	0.1684
0.1	-2.6712	-0.8890	1.5083	0.3543	-0.7568	0.1716
0.11	-2.8548	-0.9569	1.5940	0.3534	-0.7454	0.1755
0.12	-2.9734	-0.9812	1.6405	0.3567	-0.7405	0.1733
0.13	-2.9201	-0.9151	1.5917	0.3659	-0.7379	0.1636
0.133	-2.9206	-0.9070	1.5894	0.3714	-0.7370	0.1612
0.14	-2.9660	-0.9169	1.6196	0.3850	-0.7421	0.1615
0.15	-3.0855	-0.9578	1.6920	0.4038	-0.7538	0.1611
0.16	-2.9648	-0.9530	1.6709	0.4036	-0.7607	0.1589
0.17	-2.9129	-0.9800	1.6898	0.4140	-0.7708	0.1578
0.18	-2.8463	-0.9957	1.6963	0.4237	-0.7803	0.1533
0.19	-2.6951	-0.9423	1.6333	0.4214	-0.7869	0.1533
0.2	-2.4509	-0.8744	1.5327	0.4111	-0.7868	0.1538
0.22	-1.9419	-0.7427	1.3247	0.3935	-0.7735	0.1498
0.24	-1.2607	-0.5258	1.0208	0.3701	-0.7676	0.1485
0.25	-0.9899	-0.4543	0.9153	0.3700	-0.7716	0.1477
0.26	-0.7541	-0.4067	0.8322	0.3676	-0.7757	0.1460
0.28	-0.3823	-0.3426	0.7104	0.3569	-0.7859	0.1514
0.29	-0.2661	-0.3401	0.6837	0.3497	-0.7899	0.1591
0.3	-0.1770	-0.3728	0.6866	0.3388	-0.7960	0.1663
0.32	-0.0118	-0.4384	0.6902	0.3119	-0.7982	0.1791
0.34	0.1219	-0.4981	0.7011	0.2875	-0.8089	0.1877
0.35	0.1400	-0.5174	0.7127	0.2811	-0.8159	0.1917
0.36	0.2024	-0.5301	0.7072	0.2703	-0.8185	0.1960
0.38	0.2835	-0.5121	0.6729	0.2465	-0.8103	0.2113
0.4	0.2557	-0.4891	0.6592	0.2283	-0.7913	0.2314
0.42	0.1333	-0.4800	0.6887	0.2328	-0.7846	0.2408
0.44	0.1466	-0.4414	0.6633	0.2289	-0.7795	0.2481
0.45	0.1601	-0.4246	0.6543	0.2315	-0.7820	0.2497
0.46	0.1384	-0.4285	0.6679	0.2394	-0.7842	0.2492
0.48	0.1102	-0.4317	0.6840	0.2509	-0.7837	0.2469
0.5	0.1393	-0.4296	0.6860	0.2641	-0.7902	0.2409
0.55	0.1934	-0.4160	0.6643	0.2517	-0.7815	0.2624
0.6	0.1585	-0.3938	0.6377	0.2185	-0.7394	0.2863
0.65	0.0070	-0.3427	0.6077	0.1599	-0.6836	0.3250
0.667	-0.0914	-0.3469	0.6218	0.1398	-0.6667	0.3388
0.7	-0.2044	-0.3514	0.6352	0.1054	-0.6432	0.3656
0.75	-0.3845	-0.3517	0.6707	0.0902	-0.6244	0.3906
0.8	-0.5936	-0.3509	0.7207	0.0882	-0.6179	0.4072
0.85	-0.8978	-0.3982	0.8364	0.1086	-0.6285	0.4121
0.9	-1.0987	-0.4130	0.9019	0.1221	-0.6335	0.4155
0.95	-1.1902	-0.4030	0.9293	0.1358	-0.6492	0.4115

1	-1.2212	-0.4069	0.9568	0.1544	-0.6741	0.4044
1.1	-1.0903	-0.3270	0.9075	0.1970	-0.7057	0.3886
1.2	-0.7858	-0.2246	0.8047	0.2554	-0.7471	0.3449
1.3	-0.2810	-0.0703	0.6107	0.2985	-0.7699	0.2841
1.4	0.1991	0.0737	0.4047	0.2974	-0.7492	0.2549
1.5	0.6763	0.2130	0.1691	0.2463	-0.6906	0.2584
1.6	1.0540	0.3367	-0.0351	0.1873	-0.6262	0.2814
1.7	1.2929	0.4205	-0.1904	0.1204	-0.5443	0.3173
1.8	1.5396	0.5147	-0.3546	0.0616	-0.4550	0.3435
1.9	1.7080	0.5721	-0.4750	0.0089	-0.3610	0.3564
2	1.7911	0.5960	-0.5430	-0.0329	-0.2853	0.3651
2.2	1.7798	0.6043	-0.5911	-0.0771	-0.1712	0.3766
2.4	1.7510	0.6087	-0.6263	-0.1071	-0.0825	0.3899
2.5	1.6591	0.5808	-0.5953	-0.1084	-0.0669	0.3869
2.6	1.5696	0.5499	-0.5593	-0.1081	-0.0538	0.3828
2.8	1.4317	0.5260	-0.5238	-0.1026	-0.0112	0.3574
3	1.3139	0.4959	-0.4913	-0.1020	0.0364	0.3346
3.2	1.1827	0.4499	-0.4401	-0.0961	0.0430	0.2995
3.4	1.0381	0.4120	-0.3913	-0.0918	0.0536	0.2756
3.5	0.9600	0.3874	-0.3600	-0.0859	0.0551	0.2612
3.6	0.8775	0.3625	-0.3256	-0.0789	0.0581	0.2510
3.8	0.7770	0.3219	-0.2806	-0.0694	0.0798	0.2249
4	0.7250	0.3040	-0.2627	-0.0629	0.0992	0.2006
4.2	0.6627	0.2804	-0.2417	-0.0618	0.1175	0.1815
4.4	0.5809	0.2504	-0.2075	-0.0545	0.1112	0.1590
4.6	0.5351	0.2283	-0.1830	-0.0503	0.0944	0.1521
4.8	0.4937	0.2143	-0.1660	-0.0455	0.1000	0.1445
5	0.4246	0.1909	-0.1350	-0.0389	0.1039	0.1334
5.5	0.3089	0.1502	-0.0849	-0.0193	0.1332	0.0742
6	0.2540	0.1374	-0.0691	-0.0140	0.1469	0.0452
6.5	0.1793	0.0936	-0.0311	-0.0056	0.1113	0.0277
7	0.1015	0.0623	0.0069	0.0020	0.0609	0.0059
7.5	0.0915	0.0567	0.0108	0.0045	0.0519	-0.0167
8	0.0956	0.0563	0.0054	0.0042	0.0852	-0.0501
8.5	0.0850	0.0511	0.0081	0.0077	0.1174	-0.1010
9	0.0898	0.0504	0.0056	0.0081	0.1496	-0.1502
9.5	0.1461	0.0686	-0.0244	0.0062	0.1165	-0.1800
10	0.1684	0.0777	-0.0376	0.0044	0.1886	-0.2402

Table 9.14: Standard deviation values for the simplified NEHRP F site model

Period	σ_{res}	$\bar{\sigma}_{RS}$	σ_{total}	Period	σ_{res}	$\bar{\sigma}_{RS}$	σ_{total}	Period	σ_{res}	$\bar{\sigma}_{RS}$	σ_{total}
0.040	0.1658	0.2467	0.2972	0.26	0.2299	0.2962	0.3749	1.6	0.2537	0.4433	0.5108
0.042	0.1667	0.2465	0.2976	0.28	0.2217	0.3012	0.3740	1.7	0.2589	0.4742	0.5402
0.044	0.1655	0.2462	0.2967	0.29	0.2156	0.3028	0.3717	1.8	0.2721	0.4944	0.5644
0.045	0.1659	0.2466	0.2972	0.30	0.2057	0.3083	0.3706	1.9	0.2765	0.5041	0.5749
0.046	0.1672	0.2481	0.2992	0.32	0.1911	0.3063	0.3610	2.0	0.2720	0.5045	0.5731
0.048	0.1714	0.2500	0.3031	0.34	0.1850	0.2908	0.3447	2.2	0.2607	0.5106	0.5733
0.050	0.1721	0.2505	0.3040	0.35	0.1851	0.2908	0.3447	2.4	0.2546	0.5265	0.5848
0.055	0.1727	0.2552	0.3081	0.36	0.1863	0.2913	0.3458	2.5	0.2533	0.5368	0.5936
0.060	0.1738	0.2586	0.3115	0.38	0.1895	0.2870	0.3439	2.6	0.2464	0.5462	0.5992
0.065	0.1756	0.2591	0.3130	0.40	0.1947	0.2857	0.3458	2.8	0.2423	0.5672	0.6168
0.067	0.1784	0.2583	0.3139	0.42	0.1933	0.2916	0.3498	3.0	0.2367	0.5927	0.6383
0.070	0.1809	0.2606	0.3173	0.44	0.1963	0.2992	0.3578	3.2	0.2368	0.5884	0.6343
0.075	0.1862	0.2611	0.3207	0.45	0.1946	0.3072	0.3637	3.4	0.2440	0.5795	0.6288
0.080	0.1935	0.2644	0.3276	0.46	0.1898	0.3151	0.3679	3.5	0.2477	0.5770	0.6279
0.085	0.1973	0.2667	0.3317	0.48	0.1802	0.3276	0.3738	3.6	0.2495	0.5746	0.6264
0.090	0.1990	0.2691	0.3347	0.50	0.1753	0.3314	0.3749	3.8	0.2489	0.5802	0.6313
0.095	0.2086	0.2725	0.3432	0.55	0.1772	0.3242	0.3695	4.0	0.2472	0.5940	0.6434
0.10	0.2139	0.2712	0.3454	0.60	0.1732	0.3508	0.3912	4.2	0.2474	0.6045	0.6532
0.11	0.2261	0.2743	0.3555	0.65	0.1770	0.3616	0.4025	4.4	0.2513	0.6157	0.6650
0.12	0.2337	0.2751	0.3610	0.67	0.1785	0.3714	0.4121	4.6	0.2551	0.6341	0.6835
0.13	0.2406	0.2843	0.3724	0.70	0.1834	0.3845	0.4260	4.8	0.2536	0.6534	0.7009
0.13	0.2416	0.2828	0.3720	0.75	0.1832	0.3937	0.4342	5.0	0.2535	0.6633	0.7101
0.14	0.2448	0.2832	0.3743	0.80	0.1747	0.3829	0.4208	5.5	0.2568	0.6996	0.7453
0.15	0.2454	0.2796	0.3721	0.85	0.1660	0.3709	0.4064	6.0	0.2478	0.6885	0.7317
0.16	0.2425	0.2843	0.3737	0.90	0.1631	0.3698	0.4042	6.5	0.2449	0.6750	0.7181
0.17	0.2370	0.2943	0.3779	0.95	0.1564	0.3590	0.3916	7.0	0.2499	0.6660	0.7113
0.18	0.2293	0.2971	0.3753	1.0	0.1545	0.3596	0.3913	7.5	0.2416	0.6576	0.7006
0.19	0.2278	0.2944	0.3722	1.1	0.1503	0.3799	0.4085	8.0	0.2340	0.6587	0.6990
0.20	0.2245	0.2983	0.3733	1.2	0.1589	0.3975	0.4280	8.5	0.2249	0.6629	0.7000
0.22	0.2213	0.2946	0.3684	1.3	0.1881	0.4123	0.4532	9.0	0.2132	0.6634	0.6968
0.24	0.2307	0.2873	0.3685	1.4	0.2198	0.4185	0.4727	9.5	0.1909	0.6362	0.6642
0.25	0.2338	0.2906	0.3730	1.5	0.2380	0.4201	0.4829	10.0	0.1801	0.6462	0.6709

APPENDIX 2A: RESPONSE SPECTRA MAXIMUM DEMAND FACTORS

2A.1 Introduction

Ground motions from seismic events are complex and they may have significant contributions in all three directions (i.e., 2 horizontal and vertical). Recently, some engineering and research projects have used both horizontal components of the ground motion for site response analyses with a small fraction of these projects also using the vertical component. The State-of-the-Practice, however, still relies on performing site response analyses using only one horizontal component of the input ground motion. As a result, the question arises of which horizontal component is the most appropriate to use in analyses. One option is to use the ground motion that gives the largest response spectral values of the two orientations that were recorded in the field (e.g., x, y). Such analyses give results that are dependent on the direction in which the sensors were installed in the field, and therefore, they do not represent a consistent measure of earthquake intensity. A second option is to use the geometric mean (GMx,y) of the response spectra determined from the as recorded ground motion components. This approach appears to give an unbiased result but it is still dependent on the orientation of the sensors. A third option is to rotate the recordings to fault normal (FN) and fault parallel (FP) directions and use one of those (i.e., typically the one producing the highest demand). Unfortunately, fault characteristics may be undefined for many earthquakes, especially those resulting from subduction zones or stable continental regions.

2A.2 Maximum Demand Ground Motion

Boore et al. (2006) introduced two new measures of ground motion intensity that are independent of the orientation of the recorded ground motion. The first parameter is GMRotDpp, which is the ground motion at the orientation that gives the "pp" percentile of the geometric mean of the response spectra values at a given period, with the geometric mean values calculated from the two orthogonal components rotated at a specified angle. For example, GMRotD100 is the ground motion at the orientation that gives the maximum geometric mean response spectral value (i.e., 100 percentile) for a given period. A second measure, GMRotIpp, is similar to GMRotDpp except it is less period dependent. GMRotIpp is the ground motion at the orientation that produces the least variation from the desired percentile of the rotation dependent $GM_{x,y}$ normalized by GMRotDpp for the period range of interest.

In ASCE/SEI 7-05 and all previous editions, the direction of the design ground motion was not specified (ASCE, 2005). More recently, the ASCE/SEI 7-10 specifies the maximum ground motion, RotD100 as the design ground motion (ASCE, 2010). The reason for this change can be found in the National Earthquake Hazards Reduction Program commentary to chapter 21 modifications (NEHRP, 2009):

> *"Many engineers find the maximum direction to be a more meaningful parameter for structural design. The basic concept is that a structure is designed to resist the ground motion at its site; the prediction of ground motion is inherently statistical, and the basis for the statistical estimate of the ground motion is rooted in the probability that a structure will actually fail. In general, structures will not have the same resistance in all directions; however, for those structures in which seismic resistance is a significant economic factor, there is a tendency to design to the level required by building codes,*

with the result that the resistance of the structure is relatively insensitive to the direction of the motion. When one considers such structures subjected to two simultaneous components of ground motion, these structures characteristically fail in the direction of the stronger of the two components. Failure rates of simple buildings in one recent study (low-rise wood buildings in Applied Technology Council, 2008) show this effect: the overall failure rate for three-dimensional analyses was higher than those for two-dimensional analyses for the same set of structures analyzed for the same 22 pairs of ground motions. The specification of maximum direction ground motions reduces the probability of structural failure based upon equivalent static two-dimensional design compared to the use of the geomean based demand, but this reduction has not been quantified at this time. For consistency, revisions have been made to both probabilistic and deterministic ground motion criteria to reflect required use of maximum direction ground motions."

2A.3 Determination of Maximum Demand Factors

In order to reduce the aleatory variability, the 2008 NGA GMPEs predict GMRotI50, referred to as GMRotI50_NGA, instead of the geometric mean of the ground motion $GM_{x,y}$. Although the GMRotI50 response spectra are systematically larger than the $GM_{x,y}$ response spectra, the difference is typically less than 3% (Boore et al., 2006). Maximum demand factors are period dependent scalars used to convert GMRotI50 or GMRotI50_NGA to RotD100. Huang et al. (2008) determined maximum demand factors, RotD100/GMRotI50 and RotD100/ GMRotI50_NGA for near field earthquakes in active tectonic regions. The work used 147 records from 19 earthquakes taken from the NGA West 1 database with moment magnitudes ranging from 6.5 to 7.9 and distances less than 15 km and was the basis for the values adopted by NEHRP (2009) for the design response spectra of active tectonic regions. Huang et al. (2010) recomputed factors using the same database as in the previous work giving slightly different values. Table 2A.1 lists the maximum demand factors obtained by Huang et al. (2008, 2010) as well as those adopted by NEHRP (2009). NEHRP (2009) recommends using a minimum maximum design factor of 1.1 for small periods ($T < 0.3$ sec), a variable factor for periods between 0.3 and 4 sec, and a maximum value of 1.4 for periods larger than 4 seconds as shown in Figure 2A.1.

Several other researchers have proposed maximum demand factors for shallow crustal earthquakes in active tectonic regions (e.g., Beyer and Bommer, 2006; Watson-Lamprey and Boore, 2007; Huang et al. 2010; Shahi and Baker, 2012). Beyer and Bommer (2006) used 949 records from 103 earthquakes taken from the PEER NGA database. The work included earthquakes with moment magnitudes between 4.2 and 7.9 and hypocentral distances between 5 and 200 km while excluding any records from the Chi Chi earthquake to avoid bias. The researchers proposed maximum demand factors ranging from 1.2 at short periods to 1.3 at long periods. Watson-Lamprey and Boore (2007) used 3397 records from 175 earthquakes, using almost the entire PEER NGA West 1 database. Their work suggested that the maximum demand factors had a slight dependence on distance, magnitude and radiation pattern. Nevertheless, these dependencies were small enough to be considered negligible for most engineering purposes. Huang et al. (2010) computed factors for far field earthquakes, consisting of 165

records from 19 earthquakes taken from the PEER NGA West 1 database, with $M_w > 6.5$ and closest site to fault distances between 30 and 50 km. Shahi and Baker's (2012) database included 3000 ground motions collected from the NGA West 2 database. They used a mixed-effects model that prevents well-recorded earthquakes such as the Chi Chi earthquake from disproportionately influencing the results. The researchers reported a slight dependence with distance, stating that for distances less than 3km the factors are about 2% larger than the average factors for the whole dataset.

Table 2A.2 summarizes the ratio of RotD100/GMRotI50 (not the NGA GMPE predicted values) for the different researchers. The ratios reported for Huang et al (2010) correspond to Bin 1, which includes all of the earthquakes they selected for analysis. Figure 2A.2 shows that the Huang et al. far field factors for RotD100/GMRotI50 match nicely with those from Watson-Lamprey and Boore (2007) and Shahi and Baker (2012), while Beyer and Bommer (2006) factors match well with the Huang et al. (2010) near field factors.

Table 2A.3 lists the factors obtained by Huang et al. (2010) for stable continental regions while Figure 2A.3 compares them with the NEHRP 2009 factors. The database for the Central and Eastern US (CEUS) ground motions included 63 pairs of ground motions recorded from 19 earthquakes that occurred mostly in Eastern North America between 1976 and 2010. Figure 2A.3 shows that the maximum demand factors for stable continental regions are consistently higher than the adopted values in NEHRP 2009 for periods less than 3 seconds. For periods larger than 3 seconds, Huang et al (2010) predict nearly identical values as those for shallow crustal earthquakes in active tectonic regions.

2A.4 References

ASCE (2005). "Minimum design loads for buildings and other structures." ASCE/SEI 7-05, American Society of Civil Engineers; Reston, Virginia.

ASCE (2010). "Minimum design loads for buildings and other structures." ASCE/SEI 7-10, American Society of Civil Engineers; Reston, Virginia.

Beyer, K., and Bommer, J.J. (2006). "Relationships between median values and between aleatory variabilities for different definitions of the horizontal component of motion." Bull. Seismol. Soc. Amer., 96(4A), 1512-1522.

Boore, D.M., Watson-Lamprey, J., and Abrahamson, N.A., (2006). "Orientation-independent measures of ground motion." Bull. Seismol. Soc. Amer., (96) 4A, 1502-1511.

Huang, Y.N., Whittaker, A.S. and Luco, N. (2008). "Maximum spectral demands in the near-fault region." Earthquake Spectra, (24)1, 319–341.

Huang, Y.N., Whittaker, A.S. and Luco, N. (2010). "Establishing maximum spectral demand for performance-based earthquake engineering: collaborative research with the University at Buffalo and the USGS." USGS Technical Report: USGS Award Number 08HQGR0017, Reston, VA.

NEHRP (2009). "NERHP recommended seismic provisions for new buildings and other structures." FEMA P-750 report prepared by the Building Seismic Safety Council of The National Institute of Building Sciences for the Federal Emergency Management Agency, Washington, D.C.

Shahi, S.K., and Baker, J.W. (2012). "Directionality models for the NGA West 2 project." PEER Report 2012/03.

Watson-Lamprey, J., and Boore, D.M. (2007). "Beyond SaGMRotI: Conversion to SaArb, SaSN, and SaMaxRot." Bull. Seismol. Soc. Amer., 97(5), 1511-1524.

Table 2A.1: Maximum Demand Factors for modifying GMPE_NGA spectral shape for near fault earthquakes in active tectonic regions

	Maximum Demand Factors for Near Fault Earthquakes in Active Tectonic Regions, RotD100/GMRotI50_NGA		
Period (s)	Huang et al 2008	Huang et al 2010	NEHRP 2009
PGA	1.0	1.01	1.1
0.05	1.0	-	-
0.1	0.9	-	1.1
0.2	0.9	0.91	1.1
0.3	1.0	-	1.1
0.5	1.2	1.13	1.2
1	1.3	1.29	1.3
2	1.3	1.33	1.3
3	1.4	1.45	-
4	1.4	1.49	1.4

Empty cells imply that no value was specified by the author

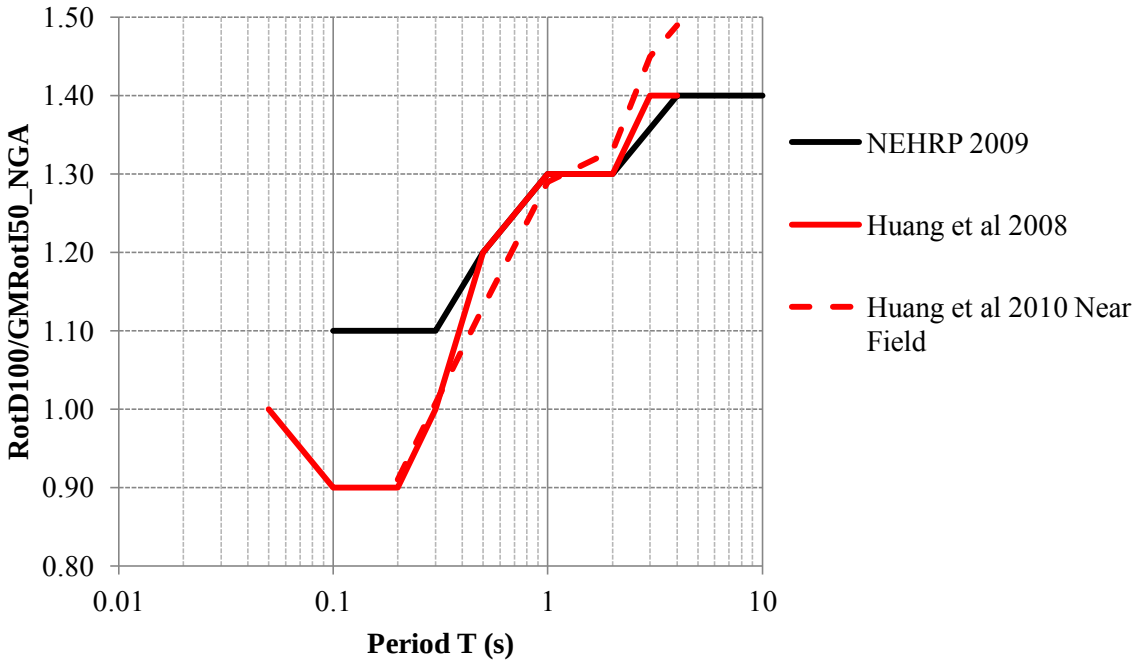

Figure 2A.1: Maximum Demand Factors, RotD100/GMRotI50_NGA, for shallow crustal earthquakes in active tectonic regions.

Table 2A.2: Maximum Demand Factors for rotated geometric mean spectral response, RotD100/GMRotI50

	Maximum Demand Factors for Shallow Crustal Earthquakes in Active Tectonic Regions, RotD100/GMRotI50				
Period (s)	Beyer & Bommer 2006	Watson-Lamprey & Boore 2007	Huang et al 2010 Near Field	Huang et al 2010 Far Field	Shahi & Baker 2012
PGA	1.20	1.20	1.21	1.18	1.19
0.02					1.19
0.05					1.19
0.1	1.20	1.19			1.19
0.15	1.20	1.21			
0.2	1.22	1.22	1.22	1.2	1.21
0.3	1.24	1.24			1.24
0.4	1.26	1.24			
0.5	1.27	1.25	1.29	1.23	1.25
0.7	1.30	1.25			
1.0	1.30	1.27	1.31	1.27	1.26
1.5	1.30	1.27			
2.0	1.30	1.27	1.31	1.27	1.28
3.0	1.30	1.28	1.31	1.27	1.29
4.0	1.30	1.29	1.37	1.31	1.31
5.0	1.30	1.31			1.31
7.5					1.34
10.0					1.36

Empty cells imply that no value was specified by the author

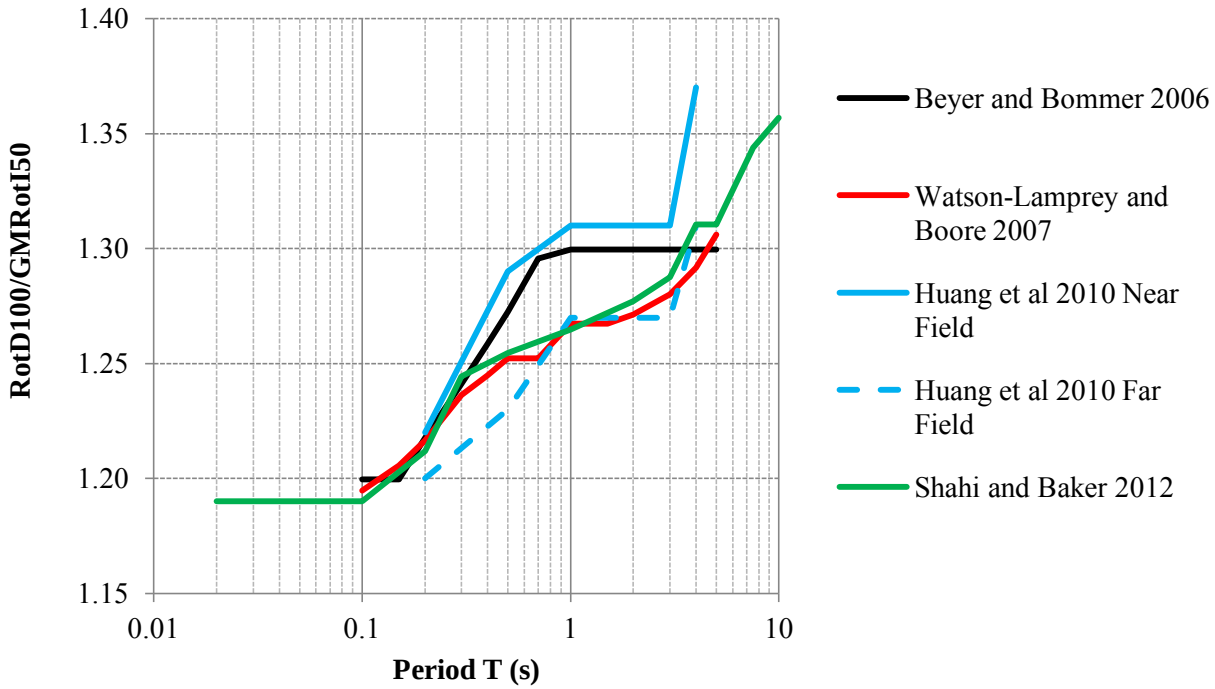

Figure 2A.2: Maximum Demand Factors, RotD100/GMRotI50, for shallow crustal earthquakes in active tectonic regions.

Table 2A.3: Maximum Demand Factors for rotated geometric mean spectral response, RotD100/GMRotI50 for Stable Continental regions (after Huang et al., 2010)

Period (s)	PGA	0.2	0.5	1.0	2.0	3.0	4.0
Maximum Demand Factor RotD100/GMRotI50	1.23	1.28	1.32	1.35	1.39	1.35	1.40

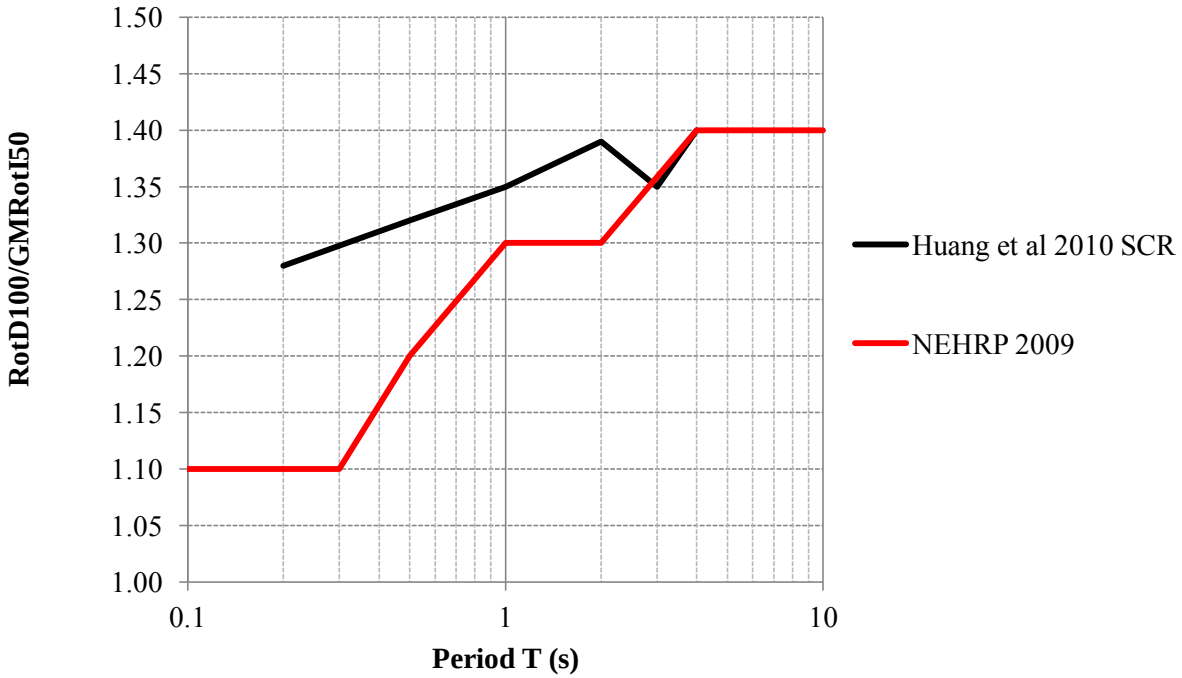

Figure 2A.3: Comparison of Maximum Demand Factors for Stable Continental Regions and the NERHP 2009 factors for active tectonic regions.

APPENDIX 2B: GMPEs FOR EARTHQUAKES IN ACTIVE CRUSTAL REGIONS

2B.1 GMPEs for Crustal Earthquakes in Tectonically Active Regions

In 2008 the Pacific Earthquake Engineering Research Center (PEER) concluded the "Next Generation of Ground-Motion Attenuation Models" for the western United States, commonly referred to as NGA West 1. NGA West 1 was a multidisciplinary research project coordinated by the Lifelines Program of PEER in association with the U.S. Geological Survey (USGS) and the Southern California Earthquake Center (SCEC). The program developed five GMPEs for active crustal regions based on an updated and uniformly processed ground motion database. The GMPE models are Abrahamson and Silva, 2008 (AS08), Boore and Atkinson, 2008 (BA08), Campbell and Bozorgnia, 2008 (CB08), Chiou and Youngs, 2008 (CY08), and Idriss, 2008 (I08). Each GMPE predicts the peak ground acceleration (PGA), peak ground velocity (PGV), and pseudo-acceleration response spectra from 0.01-10 seconds. A comprehensive overview and comparison of all 2008 NGA GMPEs is available in the literature (Abrahamson et al., 2008) and only a brief summary is included here.

The NGA developers started with the same database of 3551 recordings from 173 earthquakes. However, each group of developers used a different subset of the data. Table 2B.1 lists the number of earthquakes and records used by each group of developers. The AS08, CY08, and I08 datasets include aftershocks, whereas the other two do not. The I08 dataset only includes sites with 450 m/s< Vs_{30} < 900 m/s (Abrahamson et al, 2008). Another reason for differences between the models is that PEER required the developers to extrapolate their models outside the range of data that is well constrained. Therefore, each model reflects the scientific and engineering judgment of its developers.

Table 2B.2 summarizes the main features included in each model. All of the models include magnitude saturation, which leads to weaker magnitude scaling at short distances compared to magnitude scaling at larger distances. All of the models include a style of faulting factor, which differentiates between strike-slip, reverse, and normal faulting. The AS08, CB08, and CY08 models include rupture-depth and hanging-wall effects. The BA08 model includes rupture depth and hanging wall effects implicitly through R_{jb}. The AS08, BA08, and CB08 models constrain non-linear soil amplification with analytical model results (Walling et al, 2008) or other published non-linear amplification factors (Choi and Stewart, 2005). The CY08 model derived the non-linear soil amplification relationship directly from empirical data. The I08 model is applicable only for rock sites. The AS08, CB08, and CY08 models included a soil depth effect. The AS08 model constrained the shallow soil depth scaling using analytical results from 1-D site amplification (Silva, 2005), and AS08 and CY08 constrained the deep soil depth scaling using analytical results from 3-D basin amplification (Day et al, 2005). The CY08 model derived the soil scaling from the data.

All of the models include period dependent standard deviations. In addition, the standard deviations for the AS08, CY08, and I08 models are magnitude dependent, and the standard deviations for the AS08, CB08, and CY08 models are also dependent on non-linear site amplification effects (Abrahamson et al, 2008).

The functional form of each model is a linear combination of functions in natural log space. Equation 2B.1 shows the functional form for the median ground motion for the AS08 model. The other four GMPEs have similar functional forms.

$$ln[Sa(T)] = f_1(M, R_{rup}) + a_{12} \times F_{RV} + a_{13} \times F_{NM} + a_{15} \times F_{AS} + f_5(PGA_{1100}, Vs_{30}) + F_{HW} \cdot f_4(R_{jb}, R_{rup}, R_x, W, \delta, Z_{TOR}, M) + f_6(Z_{TOR}) + f_8(R_{rup}, M) + f_{10}(Z_{1.0}, Vs_{30}) \quad (2B.1)$$

where Sa(T) is the 5% damped spectral acceleration at period T in g, f_1 is the base model for magnitude and distance, f_5 is the site response model, f_4 is the hanging wall model, f_6 is the depth to top of rupture model, f_8 is the large distance model, f_{10} is the soil depth model, a_{12}, a_{13}, and a_{15} are coefficients, and the rest of the parameters are defined in Table 2B.3. Figure 2.2 gives a graphical definition of parameters R_x, R_{jb}, R_{rup}, δ, Z_{TOR}, and W.

The NGA West 1 models have median values within a factor of 1.5 for vertical strike-slip faults with magnitudes between 5.5 and 7.5. The greatest differences are for small magnitudes (M = 5), very large magnitudes (M = 8), and sites over the hanging wall. Standard deviations are similar for M > 6.5. The greatest differences in the standard deviations are for small magnitudes due to the different treatments of aftershocks by the different developers, and for soft soil sites at short distances due to the inclusion or exclusion of non-linear soil effects on the standard deviation (Abrahamson et al, 2008).

PEER recently completed NGA West 2, an update to NGA West 1 that includes more data, especially small magnitude earthquakes. In addition, NGA West 2 includes modeling of directivity and directionality, scaling of GMPEs for different levels of damping, GMPEs for vertical ground motion, a more thorough treatment of epistemic uncertainty, and evaluation of soil amplification factors in NGA models versus NEHRP site factors (http://peer.berkeley.edu/ngawest2/). Unfortunately, these models were published too late to be used in the current project.

2B.2 References

Abrahamson, N.A., Atkinson, G.M., Boore, D., Bozorgnia, Y., Campbell, K., Chiou, B., Idriss, I.M., Silva, W. and Youngs, R. (2008). "Comparisons of the NGA Ground-Motion Relations." Earthquake Spectra 24(1), 45-66.

Abrahamson, N.A., and Silva, W.J. (2008). "Summary of the Abrahamson and Silva NGA Ground-Motion Relations." Earthquake Spectra 24(1), 67-97.

Boore, D.M., and Atkinson, G.M. (2008). "Ground-motion prediction equations for the average horizontal Component of PGA, PGV, and 5%-Damped PSA at Spectral Periods between 0.01s and 10.0s." Earthquake Spectra 24(1), 99-138.

Campbell, K., and Bozorgnia, Y. (2008). "NGA ground motion model for the geometric mean horizontal component of PGA, PGV, PGD, and 5% damped linear elastic response spectra for periods ranging from 0.01 to 10s." Earthquake Spectra 24 (1), 139-171.

Chiou, B., and Youngs, R. (2008). "An NGA model for the average horizontal component of peak ground motion and response spectra." Earthquake Spectra 24(1), 173-215.

Choi, Y. and J. P. Stewart (2005). Nonlinear site amplification as function of 30 m shear-wave velocity, Earthquake Spectra, 21, 1-30.

Day, S. M., J. Bielak, D. Dreger, R. Graves, S. Larsen, K. Olsen, A. Pitarka (2005). 3D ground motion simulations in basins, Final report prepared for the Pacific Earthquake Engineering Research Center, Project 1A03.

Idriss, I.M. (2008). "An NGA empirical model for estimating the horizontal spectral values generated by shallow crustal earthquakes." Earthquake Spectra 24(1), 217-242.

Silva, W. J. (2005) Site response simulations for the NGA project. Report prepared for the Pacific Earthquake Engineering Research Center.

Walling, M., Silva, W. and Abrahamson, N. (*2008*) Nonlinear Site Amplification Factors for Constraining the NGA Models. Earthquake Spectra: February 2008, 24 (1) 243-255.

Table 2B.1: Datasets used by different NGA developers (from Abrahamson et al, 2008)

	AS08	BA08	CB08	CY08	I08
Number of Earthquakes	135	58	64	125	72
Number of Recordings	2754	1574	1561	1950	942

Table 2B.2: Main features included in NGA West 1 models (from Abrahamson et al, 2008)

Features	AS08	BA08	CB08	CY08	I08
Saturation at short distances	X	X	X	X	X
Style-of-Faulting Factor	X	X	X	X	X
Rupture Depth Factor	X	Implicit through R_{JB}	X (RV only)	X	
Hanging Wall Factor	X	Implicit through R_{JB}	X	X	
Nonlinear site Amplification	X Constrained	X Constrained	X Constrained	X	
Soil/Sediment Depth Factor	X Constrained		X Constrained	X	
Magnitude dependent standard deviation	X			X	X
Nonlinear effects on standard deviation	Intra-event & inter-event terms		Intra-event term only	Intra-event & inter-event term	

Table 2B.3: Parameters and terminology used for NGA West 1 models (adapted from Abrahamson et al, 2008)

Parameter	AS08	BA08	CB08	CY08	I08
Moment Magnitude	M	M	M	M	M
Depth-to-top-of-rupture (km)	Z_{TOR}		Z_{TOR}	Z_{TOR}	
Reverse style-of-faulting flag	F_{RV}	RS	F_{RV}	F_{RV}	F
Normal style-of-faulting flag	F_{NM}	NS	F_{NM}	F_{NM}	
Strike-slip style-of-faulting flag		SS			
Unspecified style-of-faulting flag		US			
Aftershock flag	F_{AS}			AS	
Average dip of rupture plane (degrees)	δ*		δ*	δ*	
Down-dip rupture width (km)	W*				
Closest distance to rupture plane (km)	R_{rup}		R_{rup}	R_{rup}	R_{rup}
Horizontal distance to the surface projection of the rupture (km)	R_{jb}*	R_{jb}	R_{jb}*	R_{jb}*	R_{jb}*
Horizontal distance to the top edge of rupture measured perpendicular to strike (km)	R_x*			R_x*	
Hanging Wall Flag	F_{HW}			F_{HW}	
Average Shear Wave Velocity in the top 30 m (m/s)	Vs_{30}	Vs_{30}	Vs_{30}	Vs_{30}	
Depth to Vs = 1 km/s (km)	$Z_{1.0}$			$Z_{1.0}$	
Depth to Vs = 2.5 km/s (km)			$Z_{2.5}$		
Rock Motion PGA for nonlinear site response	PGA_{1100}	pga4nl	A_{1100}		
Rock Motion Sa for nonlinear site response				$y_{ref}(T)$	
Vs_{30} of rock motion used for nonlinear site response	1100	760	110	1130	
Flag for Vs_{30} measured or inferred	$F_{measured}$			$F_{measured}$	

*Used for hanging wall scaling only

APPENDIX 2C: GMPEs FOR SUBDUCTION ZONES

2C.1 Introduction

Although there has been no major collective effort for subduction zone earthquakes similar to NGA West or NGA East yet (PEER has plans for an NGA Subduction zone project), there are several widely used subduction zone GMPEs. Four commonly used subduction zone GMPEs, and the ones used in this study to calculate the target response spectrum and PGA for scenario SUB, are Youngs et al. (1997), Atkinson and Boore (2003), Zhao et al. (2006), and Atkinson and Macias (2009). The following paragraphs briefly describe each of the four GMPEs.

All four of these GMPEs are magnitude and distance dependent. Youngs et al (1997), Atkinson and Boore (2003), and Zhao et al (2006) also include the effects of focal depth (hypocentral depth), source type, and site factors. In addition, the Atkinson and Boore (2003) model allows region specific coefficients (e.g., Japan or Cascadia). The Atkinson and Macias (2009) model was developed for a specific site type (NEHRP B/C boundary) and source type (interface), and therefore does not include terms for either of these conditions.

2C.2 Youngs et al (1997) Subduction Zone Model

Youngs et al. (1997) performed mixed effects regression on a database of 64 Japanese earthquakes with 204 records, and 99 other earthquakes with 274 records. Equations (2C. 1) and **Error! Reference source not found.** give the Youngs et al (1997) GMPE for rock and soil respectively while equation **Error! Reference source not found.** describes the period independent standard deviation. Rock sites are those with at most a few feet of soil over weathered rock.

$$\begin{aligned} ln[Sa(T)] = {} & 0.2418 + 1.414 \times M + c_1 + c_2 \times (10 - M)^3 \\ & + c_3 \times ln\left(R_{rup} + 1.7818 \times e^{0.554 \cdot M}\right) \\ & + 0.00607 \times H + 0.3846 \times Z_T \end{aligned} \qquad \text{(2C. 1)}$$

$$\begin{aligned} ln[Sa(T)] = {} & -0.6687 + 1.438 \times M + c_1 + c_2 \times (10 - M)^3 \\ & + c_3 \times ln\left(R_{rup} + 1.097 \times e^{0.617 \cdot M}\right) \\ & + 0.00648 \times H + 0.3643 \times Z_T \end{aligned} \qquad \text{(2C. 2)}$$

$$\sigma = c_4 + c_5 \times M \qquad \text{(2C. 3)}$$

where Sa(T) is the 5% damped spectral acceleration at period T in g, M is moment magnitude, R_{rup} is the rupture distance (km), H is the focal depth (km), Z_T = 0 for interface and 1 for intraslab earthquakes, and c_1 through c_5 are site dependent coefficients that are summarized in Table 2C.1. For M > 8, the magnitude used to calculate the total standard deviation is capped at 8. The Youngs et al (1997) GMPE is valid for $10 < R_{rup} < 500$ km and $M_w > 5.0$.

Youngs et al (1997) found that intraslab earthquakes produced peak motions that were on average 50 percent higher than those for interface earthquakes for the same magnitude and distance. Soil and rock response spectra were similar for small magnitude events, but diverged for larger magnitudes, with soil having more intense long period motions. They also found that for large magnitude events at large distances, subduction zone earthquakes were greater than shallow crustal earthquakes. The difference between these predictions increased as magnitude

increased. Finally, Youngs et al (1997) noted that their model was poorly constrained at rupture distances less than 50 km, and that the scatter of peak ground acceleration about the median value decreased with increasing magnitude.

2C.3 Atkinson and Boore (2003) Subduction Zone Model

Atkinson and Boore (2003) performed a mixed effects regression on a data set of 40 Japanese earthquakes with 613 records and 40 other earthquakes with 542 records. Their GMPE is described by:

$$log[Sa(T)] = c_1 + c_2 \times M + c_3 \times H + c_4 \times R - g \cdot log(R) + c_5 \times sl \times S_c + c_6 \times sl \times S_D + c_7 \times S_E \quad \text{(2C. 4)}$$

$$R = \sqrt{R_{rup}^2 + (0.00724 \times 10^{0.507 \cdot M})^2} \quad \text{(2C. 5)}$$

where Sa(T) is the 5% damped spectral acceleration at period T in g, M is moment magnitude, R_{rup} is the rupture distance (km), H is the focal depth (km), g is a geometrical spreading coefficient that is different for intraslab and interface earthquakes, *sl* is a parameter that accounts for soil nonlinearity, S_C, S_D, and S_E equal 1 for NEHRP site class C, D, and E sites respectively, and 0 otherwise, and c_1 through c_7 are coefficients dependent on earthquake type (intraslab or interface) and shown in Table 2C.2. In addition, the coefficient c_1 can be refined to better model the Japan or the Cascadia region. An error in the original database for interface events caused the pseudo-acceleration at a period of 0.2 seconds to be too high and at 0.4 seconds to be too low. The Atkinson and Boore erratum (2008) gives the correction factor and it is also provided for completeness in Table 2C.2. The coefficients for both intraslab and interface are presented. Similarly to the Youngs et al (1997) model, Atkinson and Boore (2003) also found lower variability for larger magnitudes and for higher frequencies.

2C.4 Zhao et al. (2006) Subduction Zone Model

Zhao et al. (2006) created a GMPE for Japan that has magnitude dependent coefficients for crustal, interface, and intraslab events. The database included 1481 records from crustal earthquakes, 1520 records from interface earthquakes, and 1725 records from intraslab earthquakes. The Zhao et al (2006) GMPE is given by:

$$log[Sa(T)] = a \times M + b \times R - log(r) + e \times (H - h_c) \times \delta_h + S_R + S_I + S_S + S_{SL} \times log(R) + C_k \quad \text{(2C. 6)}$$

$$r = R + c \times \exp(d \times M) \quad \text{(2C. 7)}$$

where Sa(T) is the 5% damped spectral acceleration at period T in g, M is moment magnitude, R is the rupture distance or hypocentral distance depending on which is available (km), H is the focal depth (km), h_c is a depth correction factor, δ_h is zero for when $H < h_c$ and 1 for when $H > h_c$, S_R, S_I, and S_S are source terms that only apply for reverse, interface, and intraslab events respectively, S_{SL} is a path term that only applies for intraslab events, C_K is the site class term, and a, b, c, d, and e are coefficients. The Zhao et al (2006) GMPE is valid for scenarios with

magnitudes between 5 and 8.5, focal depths between 0 and 125 km, and R < 300 km. Table 2C.3 lists the coefficients for the Zhao et al (2006) GMPE.

2C.5 Atkinson and Macias (2009) Subduction Zone Model

Atkinson and Macias (2009) used a stochastic finite fault model to simulate acceleration time series for interface earthquakes in the Cascadia subduction zone with magnitudes between 7.5 and 9.0. They validated the model using data from more than 300 time series at distances of 40 to 500 km recorded during the M = 8.1 2003 Tokachi-Oki, Japan, earthquake and four of its aftershocks. The GMPE provides response spectra for NEHRP B/C boundary conditions in Seattle, Vancouver, and Victoria. The standard deviations are taken from Campbell and Bozorgnia (2008). The Atkinson and Macias (2009) subduction zone GMPE is:

$$log[Sa(T)] = c_0 + c_3 \times (M-8) + c_4 \times (M-8)^2 + c_1 \times log(R) + c_2 \times R \quad \text{(2C. 8)}$$

$$R = \sqrt{R_{rup}^2 + (M^2 - 3.1 \times M - 14.55)^2} \quad \text{(2C. 9)}$$

where Sa(T) is the 5% damped spectral acceleration at period T in g, M is moment magnitude, R_{rup} is the rupture distance (km), and c_0 through c_4 are period dependent coefficients that are summarized in Table 2C.4.

2C.6 References

Atkinson, G.M. and Boore, D.M. (2003). "Empirical ground-motion relations for subduction-zone earthquakes and their application to Cascadia and other regions." Bull. Seismol. Soc. Amer., (93)4, 1703-1729.

Atkinson, G.M. and Boore, D.M. (2008). "Erratum to: Empirical ground-motion relations for subduction-zone earthquakes and their application to Cascadia and other regions." Bull. Seismol. Soc. Amer., (98)5, 2567-2569.

Atkinson, G.M., and Macias, M. (2009). "Predicted ground motions for great interface earthquakes in the Cascadia subduction zone." Bull. Seismol. Soc. Amer., 99(3) 1552-1578.

Campbell, K., and Bozorgnia, Y. (2008). "NGA ground motion model for the geometric mean horizontal component of PGA, PGV, PGD, and 5% damped linear elastic response spectra for periods ranging from 0.01 to 10s." Earthquake Spectra 24 (1), 139-171.

Youngs, R., Chiou, S., Silva, W. and Humphrey, J. (1997), "Strong ground motion attenuation relationships for subduction zone earthquakes." Seismol. Res. Lett. (68)1, 58–73.

Zhao, J.X., Zhang, J., Asano, A., Ohno, Y., Oouchi, T., Takahashi, T., Ogawa, H., Irikura, K. Thio, H.K., Somerville, P.G., Fukushima, Y. and Fukushima, Y. (2006). "Attenuation relations of strong ground motion in Japan using site classification based on predominant period." Bull. Seismol. Soc. Amer., (96)3, 898–913.

Table 2C.1: GMPE Coefficients for the Youngs et al (1997) Subduction model

Rock sites

Period, T (s)	Coefficients				
	c_1	c_2	c_3	c_4	c_5
PGA	0	0	-2.552	1.45	-0.1
0.075	1.275	0	-2.707	1.45	-0.1
0.1	1.188	-0.0011	-2.655	1.45	-0.1
0.2	0.722	-0.0027	-2.528	1.45	-0.1
0.3	0.246	-0.0036	-2.454	1.45	-0.1
0.4	-0.115	-0.0043	-2.401	1.45	-0.1
0.5	-0.4	-0.0048	-2.36	1.45	-0.1
0.75	-1.149	-0.0057	-2.286	1.45	-0.1
1.0	-1.736	-0.0064	-2.234	1.45	-0.1
1.5	-2.634	-0.0073	-2.16	1.5	-0.1
2.0	-3.328	-0.008	-2.107	1.55	-0.1
3.0	-4.511	-0.0089	-2.033	1.65	-0.1

Soil Sites

Period, T (s)	Coefficients				
	c_1	c_2	c_3	c_4	c_5
PGA	0	0	-2.329	1.45	-0.1
0.075	2.4	-0.0019	-2.697	1.45	-0.1
0.1	2.516	-0.0019	-2.697	1.45	-0.1
0.2	1.549	-0.0019	-2.464	1.45	-0.1
0.3	0.793	-0.002	-2.327	1.45	-0.1
0.4	0.144	-0.002	-2.23	1.45	-0.1
0.5	-0.438	-0.0035	-2.14	1.45	-0.1
0.75	-1.704	-0.0048	-1.952	1.45	-0.1
1.0	-2.87	-0.0066	-1.785	1.45	-0.1
1.5	-5.101	-0.0114	-1.47	1.5	-0.1
2.0	-6.433	-0.0164	-1.29	1.55	-0.1
3.0	-6.672	-0.0221	-1.347	1.65	-0.1
4.0	-7.618	-0.0235	-1.272	1.65	-0.1

Table 2C.2: GMPE Coefficients for the Atkinson and Boore (2003) Subduction model

Interface Events

Period, T (s)	Coefficients							Total	Intra	Inter
	c_1	c_2	c_3	c_4	c_5	c_6	c_7	σ_t	σ_1	σ_2
0.01	2.99100	0.03525	0.00759	-0.00206	0.190	0.240	0.290	0.230	0.200	0.110
0.04	2.87530	0.07052	0.01004	-0.00278	0.150	0.200	0.200	0.260	0.220	0.140
0.10	2.77890	0.09841	0.00974	-0.00287	0.150	0.230	0.200	0.270	0.250	0.100
0.20	2.66380	0.12386	0.00884	-0.00280	0.150	0.270	0.250	0.280	0.250	0.130
0.40	2.52490	0.14770	0.00728	-0.00235	0.130	0.370	0.380	0.290	0.250	0.150
1.00	2.14420	0.13450	0.00521	-0.00110	0.100	0.300	0.550	0.340	0.280	0.190
2.00	2.19070	0.07148	0.00224	0.00000	0.100	0.250	0.400	0.340	0.290	0.180
3.00	2.30100	0.02237	0.00012	0.00000	0.100	0.250	0.360	0.360	0.310	0.180

Intraslab events

Period, T (s)	Coefficients							Total	Intra	Inter
	c_1	c_2	c_3	c_4	c_5	c_6	c_7	σ_t	σ_1	σ_2
0.01	-0.04713	0.69090	0.01130	-0.00202	0.190	0.240	0.290	0.270	0.230	0.140
0.04	0.50697	0.63273	0.01275	-0.00234	0.150	0.200	0.200	0.250	0.240	0.070
0.10	0.43928	0.66675	0.01080	-0.00219	0.150	0.230	0.200	0.280	0.270	0.070
0.20	0.51589	0.69186	0.00572	-0.00192	0.150	0.270	0.250	0.280	0.260	0.100
0.40	0.00545	0.77270	0.00173	-0.00178	0.130	0.370	0.380	0.280	0.260	0.100
1.00	-1.02133	0.87890	0.00130	-0.00173	0.100	0.300	0.550	0.290	0.270	0.110
2.00	-2.39234	0.99640	0.00364	-0.00118	0.100	0.250	0.400	0.300	0.280	0.110
3.00	-3.70012	1.11690	0.00615	-0.00045	0.100	0.250	0.360	0.300	0.290	0.080

Table 2C.2: GMPE Coefficients for the Atkinson and Boore (2003) Subduction model (continued)

Region specific coefficient c_1

	Interface Events		Intraslab Events	
Period, T (s)	Cascadia	Japan	Cascadia	Japan
0.01	2.79	3.14	-0.25	0.1
0.04	2.6	3.05	0.23	0.68
0.10	2.5	2.95	0.16	0.61
0.20	2.54	2.84	0.4	0.7
0.40	2.5	2.58	-0.01	0.07
1.00	2.18	2.18	-0.98	-0.98
2.00	2.33	2.14	-2.25	-2.44
3.00	2.36	2.27	-3.64	-3.73

Coefficients g, and sl

$g = 10^{(1.2-0.18M)}$ for interface events,

$g = 10^{(0.301-0.01M)}$ for in-slab events

$sl = 1.$

for $PGA_{rx} \leq 100$ cm/sec^2 or frequencies ≤ 1 Hz

$sl = 1. - (f - 1)\ (PGA_{rx} - 100.)/400.$

for $100 < PGA_{rx} < 500$ cm/sec^2 (1 Hz $< f < 2$ Hz)

$sl = 1. - (f - 1)$

for $PGA_{rx} \geq 500$ cm/sec^2 (1 Hz $< f < 2$ Hz)

$sl = 1. - (PGA_{rx} - 100.)/400.$

for $100 < PGA_{rx} < 500$ cm/sec^2 ($f \geq 2$ Hz and PGA)

$sl = 0.$

for $PGA_{rx} \geq 500$ cm/sec^2 ($f \geq 2$ Hz and PGA);

Erratum (2008)- Correction for the 0.2 and 0.4 s spectral amplitudes.

$$\log \mathrm{PSA}(2.5\ \mathrm{Hz})_{\mathrm{corrected}} = 0.333 \log[\mathrm{PSA}(2.5\ \mathrm{Hz})]_{\mathrm{AB\ 03}} + 0.667 \log[\mathrm{PSA}(5\ \mathrm{Hz})]_{\mathrm{AB\ 03}},$$

$$\log \mathrm{PSA}(5\ \mathrm{Hz})_{\mathrm{corrected}} = 0.333 \log[\mathrm{PSA}(5\ \mathrm{Hz})]_{\mathrm{AB\ 03}} + 0.667 \log[\mathrm{PSA}(2.5\ \mathrm{Hz})]_{\mathrm{AB\ 03}},$$

Table 2C.3: GMPE Coefficients for the Zhao et al (2006) Subduction model

Period, T (s)	Coefficients					Source Terms			Path term
	a	b	c	d	e	S_R	S_I	S_S	S_{SL}
PGA	1.101	-0.0056	0.0055	1.08	0.01412	0.251	0	2.607	-0.528
0.05	1.076	-0.0067	0.0075	1.06	0.01463	0.251	0	2.764	-0.551
0.1	1.118	-0.0079	0.009	1.083	0.01423	0.24	0	2.156	-0.42
0.15	1.134	-0.0072	0.01	1.053	0.01509	0.251	0	2.161	-0.431
0.2	1.147	-0.0066	0.012	1.014	0.01462	0.26	0	1.901	-0.372
0.25	1.149	-0.0059	0.014	0.966	0.01459	0.269	0	1.814	-0.36
0.3	1.163	-0.0052	0.015	0.934	0.01458	0.259	0	2.181	-0.45
0.4	1.2	-0.0042	0.01	0.959	0.01257	0.248	-0.041	2.432	-0.506
0.5	1.25	-0.0034	0.006	1.008	0.01114	0.247	-0.053	2.629	-0.554
0.6	1.293	-0.0028	0.003	1.088	0.01019	0.233	-0.103	2.702	-0.575
0.7	1.336	-0.0026	0.0025	1.084	0.00979	0.22	-0.146	2.654	-0.572
0.8	1.386	-0.0024	0.0022	1.088	0.00944	0.232	-0.164	2.48	-0.54
0.9	1.433	-0.0023	0.002	1.109	0.00972	0.22	-0.206	2.332	-0.522
1.0	1.479	-0.0022	0.002	1.115	0.01005	0.211	-0.239	2.233	-0.509
1.25	1.551	-0.0021	0.002	1.083	0.01003	0.251	-0.256	2.029	-0.469
1.5	1.621	-0.0022	0.002	1.091	0.00928	0.248	-0.306	1.589	-0.379
2.0	1.694	-0.002	0.0025	1.055	0.00833	0.263	-0.321	0.966	-0.248
2.5	1.748	-0.0019	0.0028	1.052	0.00776	0.262	-0.337	0.789	-0.221
3.0	1.759	-0.0015	0.0032	1.025	0.00644	0.307	-0.331	1.037	-0.263
4.0	1.826	-0.002	0.004	1.044	0.0059	0.353	-0.39	0.561	-0.169
5.0	1.825	-0.0024	0.005	1.065	0.0051	0.248	-0.498	0.225	-0.12

Table 2C.3: GMPE Coefficients for the Zhao et al (2006) Subduction model - Continued

	Site Terms					Prediction Error		
Period	C_H	C_1	C_2	C_3	C_4	σ	τ	σ_t
PGA	0.293	1.111	1.344	1.355	1.42	0.604	0.398	0.723
0.05	0.939	1.684	1.793	1.747	1.814	0.64	0.444	0.779
0.1	1.499	2.061	2.135	2.031	2.082	0.694	0.49	0.849
0.15	1.462	1.916	2.168	2.052	2.113	0.702	0.46	0.839
0.2	1.28	1.669	2.085	2.001	2.03	0.692	0.423	0.811
0.25	1.121	1.468	1.942	1.941	1.937	0.682	0.391	0.786
0.3	0.852	1.172	1.683	1.808	1.77	0.67	0.379	0.77
0.4	0.365	0.655	1.127	1.482	1.397	0.659	0.39	0.766
0.5	-0.207	0.071	0.515	0.934	0.955	0.653	0.389	0.76
0.6	-0.705	-0.429	-0.003	0.394	0.559	0.653	0.401	0.766
0.7	-1.144	-0.866	-0.449	-0.111	0.188	0.652	0.408	0.769
0.8	-1.609	-1.325	-0.928	-0.62	-0.246	0.647	0.418	0.77
0.9	-2.023	-1.732	-1.349	-1.066	-0.643	0.653	0.411	0.771
1.0	-2.451	-2.152	-1.776	-1.523	-1.084	0.657	0.41	0.775
1.25	-3.243	-2.923	-2.542	-2.327	-1.936	0.66	0.402	0.773
1.5	-3.888	-3.548	-3.169	-2.979	-2.661	0.664	0.408	0.779
2.0	-4.783	-4.41	-4.039	-3.871	-3.64	0.669	0.414	0.787
2.5	-5.444	-5.049	-4.698	-4.496	-4.341	0.671	0.411	0.786
3.0	-5.839	-5.431	-5.089	-4.893	-4.758	0.667	0.396	0.776
4.0	-6.598	-6.181	-5.882	-5.698	-5.588	0.647	0.382	0.751
5.0	-6.752	-6.347	-6.051	-5.873	-5.798	0.643	0.377	0.745

Site Class Definitions Used in the Present Study and the Approximately Corresponding NEHRP Site Classes

Site Class	Description	Natural Period	V_{30} Calculated from Site Period	NEHRP Site Classes
Hard rock			$V_{30} > 1100$	A
SC I	Rock	$T < 0.2$ sec	$V_{30} > 600$	A + B
SC II	Hard soil	$0.2 = T < 0.4$ sec	$300 < V_{30} = 600$	C
SC III	Medium soil	$0.4 = T < 0.6$ sec	$200 < V_{30} = 300$	D
SC IV	Soft soil	$T = 0.6$ sec	$V_{30} = 200$	E + F

Table 2C.4: GMPE Coefficients for the Atkinson and Macias (2009) Subduction model

Period, T (s)	Coefficients					Standard deviation
	c_0	c_1	c_2	c_3	c_4	σ_{total}
PGA	5.006	-1.5573	-0.00034	0.1774	0.0827	0.24
0.050	5.843	-1.9391	0.00000	0.1813	0.0199	0.26
0.063	5.823	-1.8889	-0.00022	0.1845	0.0160	0.26
0.079	5.676	-1.7633	-0.00071	0.1784	0.0245	0.27
0.100	5.490	-1.6257	-0.00115	0.1736	0.0261	0.27
0.125	5.209	-1.4404	-0.00163	0.1788	0.0151	0.27
0.159	4.930	-1.2671	-0.00204	0.1645	0.0301	0.27
0.200	4.746	-1.1691	-0.00212	0.1593	0.0432	0.27
0.250	4.472	-1.0133	-0.00234	0.1713	0.0255	0.27
0.316	4.303	-0.9322	-0.00231	0.1713	0.0270	0.27
0.400	4.167	-0.8854	-0.00211	0.1802	0.0258	0.27
0.500	3.999	-0.8211	-0.00195	0.1870	0.0271	0.27
0.633	3.859	-0.7746	-0.00179	0.2010	0.0153	0.28
0.794	3.733	-0.7473	-0.00159	0.2035	0.0292	0.28
1.000	3.621	-0.7376	-0.00128	0.2116	0.0328	0.29
1.266	3.453	-0.6885	-0.00119	0.2417	0.0125	0.29
1.587	3.393	-0.7101	-0.00089	0.2483	0.0103	0.29
2.000	3.241	-0.6741	-0.00081	0.2696	-0.0064	0.30
2.500	3.104	-0.6585	-0.00063	0.2990	-0.0074	0.30
3.125	2.978	-0.6431	-0.00057	0.3258	-0.0103	0.30
4.000	2.814	-0.6108	-0.00046	0.3490	-0.0299	0.30
5.000	2.671	-0.5942	-0.00040	0.3822	-0.0417	0.32
6.250	2.569	-0.6048	-0.00024	0.4324	-0.0641	0.34
7.692	2.489	-0.6412	-0.00003	0.4760	-0.0629	0.35
10.000	2.338	-0.6311	0.00000	0.5357	-0.0737	0.38

APPENDIX 2D: GMPEs FOR STABLE CONTINENTAL REGIONS

2D.1 Introduction

The following paragraphs briefly describe the four GMPEs used to predict the target response spectrum, PGA, and PGV for scenario SCR, corresponding to stable continental regions (SCR). The four GMPEs used in this study were Toro et al. (1997) (modified by Toro 2002), Silva et al. (2002), Atkinson and Boore (2006) (modified by Atkinson and Boore 2011) and Pezeshk et al. (2011). PEER is currently working on NGA East, a project similar to NGA West except for stable continental regions (such as the Eastern United States). Unfortunately, the NGA East models were not published by the time this study was completed.

2D.2 Toro et al. (1997) SCR Model

Toro et al. (1997) created a database of ground motions using a stochastic point source model with source excitation characterized by Brune's ω^2 model. They performed regression analyses on this database to calculate the coefficients of the model. Since point sources models may over predict the ground motion at sites near the rupture plane of a large earthquake, Toro et al. (1997) advised that the results for distances shorter than one or two source dimensions should be used with caution. They state, however, that this is rarely a problem in Central and Eastern United States. Toro (2002) introduced two methods to account for magnitude saturation in the 1997 model, one using an empirically derived formulation from Atkinson and Silva (1997), and the other one from simulations. The Toro et al (1997) GMPE for stable continental regions, as modified by Toro (2002), is:

$$ln[Sa(T)] = c_1 + c_2 \times (M-6) + c_3 \times (M-6)^2 - c_4 \times ln(R_m) - (c_5 - c_4) \times max\left[ln\left(\frac{R_m}{100}\right), 0\right] - c_6 \times R_m \quad \text{(2D. 1)}$$

$$R_m = W_1 \times \sqrt{{R_{jb}}^2 + c_7^2 \times [exp(-1.25 + 0.227 \times M)]^2} + W_2\left[R_{rup} + 0.089 \times exp(0.6 \times M)\right] \quad \text{(2D. 2)}$$

where Sa(T) is the 5% damped spectral acceleration at period T in g, M is moment magnitude, R_{jb} is the closest horizontal distance to the rupture plane, R_{rup} is the rupture distance (km), W_1 and W_2 are weight factors specified by the user, and c_1 through c_7 are period and region dependent coefficients and they are summarized in Table 2D.1 for the midcontinent region and the Gulf plain region. The Toro et al. (1997) model is valid for $0.1 < T < 2$ seconds, $5 < M < 8$, $0 < R_{JB} < 500$ km, and hard rock sites.

2D.3 Silva et al. (2002) SCR Model

The Silva et al. (2002) study used 5 stochastic point source models to generate the data. The different models are: single corner frequency with variable stress drop, single corner frequency with constant stress drop, single corner frequency with constant stress drop and magnitude saturation, double corner frequency model, and a double corner frequency model with magnitude saturation. The simulations reflected the variability of source depth, path, and site parameters found in the Central and Eastern United States. They ran 300 simulations for each M and R pair,

using distances of 1, 5, 10, 20, 50, 75, 100, 200, and 400 km, and magnitudes of 4.5, 5.5, 6.5, 7.5, and 8.5. The equation for the Silva et al (2002) stable continental region GMPE is:

$$ln[Sa(T)] = c_1 + c_2 \times M + (c_6 + c_7 \times M) \times ln\left(R_{jb} + exp(c_4)\right) + c_{10} \times (M - 6)^2 \quad \text{(2D.3)}$$

where Sa(T) is the 5% damped spectral acceleration at period T in g, M is moment magnitude, R_{jb} is the closest horizontal distance to the surface projection of the rupture surface, and c_1 through c_{10} are coefficients specific to the type of stochastic point source models chosen and they are summarized in Table 2D.2 (one table for each of the five models).

2D.4 Atkinson and Boore (2006) SCR Model

The Atkinson and Boore (2006) equations were derived from a simulated ground-motion database using a seismological model of source, path, and site parameters. The seismological model parameters were obtained using empirical data from small to moderate Eastern North American earthquakes. Ground motions from 10 earthquakes with moment magnitudes from 3.5 to 8.0 were simulated, in 0.5 magnitude unit increments, at 24 values of fault distances ranging from 1 to 1000 km. They defined eight lines at equally spaced azimuths spreading out from a point above the center of the top of the fault plane to capture the average effects of directivity. Atkinson and Boore (2006) performed 20 random trials for each magnitude and observation point. They simulated 38,400 horizontal-component ground-motion records for hard rock sites in total. In the 2006 model the stress drop parameter was fixed at 140 bars. In their 2011 update, Atkinson and Boore (2011) made the stress drop parameter magnitude dependent based on new strong motion data from Eastern North America. The GMPE for Atkinson and Boore (2006) for stable continental regions, as modified by Atkinson and Boore (2011), is:

$$log[Sa(T)] = c_1 + c_2 \times M + c_3 \times M^2 + (c_4 + c_5 \times M) \times f_1 + (c_6 + c_7 \times M) \times f_2 + (c_8 + c_9 \times M) \times f_0 + c_{10} \times R_{rup} + S \quad \text{(2D.4)}$$

$$f_0 = max\left(log\left({}^{10}/_{R_{rup}}\right), 0\right) \quad \text{(2D.5)}$$

$$f_1 = min\left(log\left(R_{rup}\right), log(70)\right) \quad \text{(2D.6)}$$

$$f_2 = max\left(log\left({}^{R_{rup}}/_{140}\right), 0\right) \quad \text{(2D.7)}$$

where Sa(T) is the 5% damped spectral acceleration at period T in g, M is moment magnitude, R_{rup} is the rupture distance (km), S is the nonlinear site term (S=0 for hard rock sites), and c_1 through c_{10} are regression coefficients which are summarized in Table 2D.3.

2D.5 Pezeshk et al (2011) SCR Model

The Pezeshk et al (2011) model is a hybrid empirical model using the five NGA West 1 GMPEs multiplied by a modification factor to predict a GMPE for the Eastern United States. The modification factor is the ratio of stochastic simulations of ground motions for the two regions. The adjustment factors reflect the regional differences in source, path, and site. They developed the model to predict the 5% damped response spectra for GMRotI50 motions on hard rock sites (Vs_{30} = 2000 m/s), with moment magnitude from 5 to 8, and R_{rup} 0-1000 km. The resulting equation for the Pezeshk et al (2011) stable continental region GMPE is very similar to the model of Atkinson and Boore (2006):

$$log[Sa(T)] = c_1 + c_2 \times M + c_3 \times M^2 + (c_4 + c_5 \times M) \times f_1 + (c_6 + c_7 \times M) \times f_2 + (c_8 + c_9 \times M) \times f_0 + c_{10} \times R \quad (2D.8)$$

$$R = \sqrt{R_{rup}^2 + c_{11}^2} \quad (2D.9)$$

$$f_0 = max\left(log\left({}^{R}/_{140}\right), 0\right) \quad (2D.10)$$

$$f_1 = min\left(log(R), log(70)\right) \quad (2D.11)$$

$$f_2 = max\left[min\left\{log\left({}^{R}/_{70}\right), log\left({}^{140}/_{70}\right)\right\}, 0\right] \quad (2D.12)$$

where Sa(T) is the 5% damped spectral acceleration at period T in g, M is moment magnitude, R_{rup} is the rupture distance (km), and c_1 through c_{11} are regression coefficients which are summarized in Table 2D.4.

2D.6 References

Atkinson, G.M. and Boore, D.M. (2006). "Earthquake ground-motion prediction equations for eastern North America." Bull. Seismol. Soc. Amer., (96)6, 2181-2205.

Atkinson, G.M. and Boore, D.M. (2011). "Modifications to existing ground-motion prediction equations in light of new data." Bull. Seismol. Soc. Amer., 101 (3), 1121–1135.

Atkinson, G.M., and Silva, W. (1997). "An empirical study of earthquake source spectra for California earthquakes." *Bull. Seism. Soc. Am.*, 87, 97-113.

Pezeshk, S., Zandieh, A., and Tavakoli, B. (2011). "Hybrid empirical ground-motion prediction equations for eastern north America using NGA models and updated seismological parameters." Bull. Seismol. Soc. Amer., 101 (4), 1859–1870.

Silva, W., Gregor, N. and Darragh, R. (2002). "Development of regional hard rock attenuation relations for central and eastern North America." Pacific Engineering Analysis Internal Report, 27.

Toro, G. R., Abrahamson, N.A. and Schneider, J.F., (1997). "Model of strong ground motions from earthquakes in central and eastern North America: best estimates and uncertainties." Seismol. Res. Lett. (68)1, 41–57.

Toro, G.R. (2002). "Modification of the Toro et al (1997) attenuation equations for large magnitudes and short distances." Risk Engineering Inc.

Table 2D.1: GMPE Coefficients for the Toro et al (1997) SCR model

Midcontinent Region

Period, T (s)	c_1	c_2	c_3	c_4	c_5	c_6	c_7
0.01	2.2	0.81	0	1.27	1.16	0.0021	9.3
0.029	4	0.79	0	1.57	1.83	0.0008	11.1
0.04	3.68	0.8	0	1.46	1.77	0.0013	10.5
0.1	2.37	0.81	0	1.1	1.02	0.004	8.3
0.2	1.73	0.84	0	0.98	0.66	0.0042	7.5
0.4	1.07	1.05	-0.1	0.93	0.56	0.0033	7.1
1.0	0.09	1.42	-0.2	0.9	0.49	0.0023	6.8
2.0	-0.74	1.86	-0.31	0.92	0.46	0.0017	6.9

Gulf Plain Region

Period, T (s)	c_1	c_2	c_3	c_4	c_5	c_6	c_7
0.01	2.91	0.92	0	1.49	1.61	0.0014	10.9
0.029	4.81	0.91	0	1.89	1.8	0.0008	11.9
0.04	5.19	0.91	0	1.96	1.96	0.0004	12.9
0.1	5.08	1	0	1.87	2.52	0.0002	14.1
0.2	3.1	0.92	0	1.34	1.95	0.0017	11.4
0.4	1.64	1.06	-0.08	0.99	1.27	0.0036	8.9
1.0	0.24	1.31	-0.15	0.79	0.82	0.0034	7.2
2.0	-0.81	1.72	-0.26	0.74	0.71	0.0025	6.6

Table 2D.2: GMPE Coefficients for the Silva el at (2002) SCR model

Single Corner Model with Variable Stress Drop

Period, T (s)	c_1	c_2	c_4	c_5	c_6	c_7	c_8	c_{10}	$\sigma_{parametric}$	σ_{total}
PGV	3.39476	0.62991	2.4	0	-2.7626	0.20554	0	-0.13908	0.5582	------
PGA	4.19301	0.07506	2.7	0	-3.0041	0.20195	0	-0.08927	0.6912	0.84
0.010	4.395	0.06737	2.7	0	-3.0202	0.20242	0	-0.08804	0.6994	0.8468
0.020	6.21252	0.0022	2.9	0	-3.213	0.20863	0	-0.0808	0.7561	0.8939
0.025	6.17831	0.01178	2.9	0	-3.1903	0.2066	0	-0.08055	0.7534	0.8902
0.032	5.53534	0.05373	2.8	0	-3.0748	0.19936	0	-0.08092	0.7462	0.8869
0.040	5.37048	0.06513	2.8	0	-3.0485	0.19764	0	-0.08164	0.7339	0.8795
0.050	5.20282	0.07947	2.8	0	-3.0192	0.19552	0	-0.08262	0.7165	0.8675
0.055	5.13193	0.08668	2.8	0	-3.0057	0.19447	0	-0.08317	0.7106	0.8604
0.060	5.06492	0.09382	2.8	0	-2.9931	0.19346	0	-0.08376	0.7058	0.8602
0.070	4.49895	0.13453	2.7	0	-2.8925	0.18688	0	-0.08509	0.6982	0.8521
0.080	4.36936	0.14791	2.7	0	-2.8719	0.1852	0	-0.08661	0.6923	0.8476
0.100	4.09661	0.17267	2.7	0	-2.8374	0.18244	0	-0.09012	0.6837	0.8468
0.120	3.82611	0.19671	2.7	0	-2.8077	0.18	0	-0.09412	0.6717	0.8485
0.150	3.42429	0.23007	2.7	0	-2.7722	0.17711	0	-0.10076	0.6587	0.8339
0.160	3.29848	0.24288	2.7	0	-2.7593	0.17594	0	-0.10319	0.6535	0.829
0.200	2.43129	0.31603	2.6	0	-2.6448	0.16751	0	-0.11332	0.6412	0.826
0.240	1.94719	0.36067	2.6	0	-2.6123	0.16463	0	-0.12422	0.6326	0.8272
0.300	1.2763	0.43069	2.6	0	-2.5637	0.15989	0	-0.14085	0.6231	0.8358
0.400	0.27922	0.55253	2.6	0	-2.4805	0.15109	0	-0.16795	0.611	0.832
0.500	-0.7007	0.66331	2.6	0	-2.4223	0.14517	0	-0.19572	0.6016	0.8426
0.750	-2.6689	0.90369	2.6	0	-2.2886	0.13067	0	-0.24886	0.5844	0.8815
1.000	-4.3594	1.10344	2.6	0	-2.1956	0.12077	0	-0.29213	0.5697	0.8739
1.600	-7.4395	1.47547	2.5	0	-1.9718	0.09962	0	-0.35266	0.5388	0.945
2.000	-8.8267	1.63766	2.5	0	-1.8997	0.09204	0	-0.37384	0.5217	1.0095
3.000	-11.666	1.92782	2.4	0	-1.7379	0.07805	0	-0.3956	0.4887	1.0871
5.0	-14.965	2.23977	2.3	0	-1.5873	0.0661	0	-0.38601	0.4529	1.2228
10.0	-18.884	2.53845	2.1	0	-1.4418	0.05839	0	-0.30968	0.4199	1.3429

Table 2D.2: GMPE Coefficients for the Silva el at (2002) SCR model (continued)

Single Corner Model with Constant Stress Drop

Period, T (s)	c_1	c_2	c_4	c_5	c_6	c_7	c_8	c_{10}	$\sigma_{parametric}$	σ_{total}
PGV	2.51086	0.76168	2.4	0	-2.726	0.20021	0	-0.10368	0.555	------
PGA	3.16202	0.22938	2.7	0	-2.9715	0.19714	0	-0.0562	0.6886	0.8379
0.010	3.36079	0.22218	2.7	0	-2.9876	0.19761	0	-0.05509	0.6969	0.8447
0.020	5.16438	0.15928	2.9	0	-3.1808	0.20386	0	-0.04851	0.7537	0.8918
0.025	5.1346	0.16824	2.9	0	-3.1591	0.20195	0	-0.04828	0.7511	0.8883
0.032	4.50147	0.20875	2.8	0	-3.0451	0.19494	0	-0.04861	0.7439	0.8849
0.040	4.34191	0.21938	2.8	0	-3.0195	0.19332	0	-0.04924	0.7316	0.8776
0.050	4.18102	0.23274	2.8	0	-2.9911	0.19131	0	-0.05011	0.7143	0.8657
0.055	4.11372	0.23943	2.8	0	-2.9781	0.19032	0	-0.05058	0.7084	0.8586
0.060	4.05039	0.24603	2.8	0	-2.9658	0.18937	0	-0.0511	0.7036	0.8584
0.070	3.92488	0.25884	2.8	0	-2.9434	0.18762	0	-0.05225	0.6961	0.8503
0.080	3.37375	0.29732	2.7	0	-2.847	0.18144	0	-0.05357	0.6902	0.8459
0.100	3.11592	0.31985	2.7	0	-2.8138	0.17885	0	-0.05663	0.6817	0.8452
0.120	2.86034	0.34166	2.7	0	-2.7852	0.17656	0	-0.0601	0.6698	0.847
0.150	2.47996	0.37179	2.7	0	-2.7511	0.17386	0	-0.06588	0.6568	0.8324
0.160	2.36181	0.38344	2.7	0	-2.7386	0.17274	0	-0.06802	0.6516	0.8275
0.200	1.52694	0.45169	2.6	0	-2.6263	0.16462	0	-0.07695	0.6393	0.8246
0.240	1.06963	0.49226	2.6	0	-2.5947	0.16186	0	-0.08664	0.6304	0.8255
0.300	0.43668	0.55655	2.6	0	-2.5475	0.15729	0	-0.10162	0.6204	0.8338
0.400	-0.5047	0.67008	2.6	0	-2.4662	0.14872	0	-0.12648	0.6075	0.8295
0.500	-1.4355	0.77358	2.6	0	-2.4093	0.14297	0	-0.15233	0.5971	0.8394
0.750	-3.3221	1.00226	2.6	0	-2.2782	0.1288	0	-0.20311	0.5787	0.8777
1.000	-4.965	1.19548	2.6	0	-2.1858	0.119	0	-0.24566	0.5639	0.8701
1.600	-7.9741	1.55786	2.5	0	-1.9642	0.0982	0	-0.30626	0.534	0.9423
2.000	-9.3359	1.71687	2.5	0	-1.8934	0.0908	0	-0.32809	0.5177	1.0074
3.000	-12.146	2.00333	2.4	0	-1.7322	0.07698	0	-0.35126	0.4854	1.0857
5.0	-15.417	2.31029	2.3	0	-1.5826	0.06531	0	-0.34272	0.4483	1.2211
10.0	-19.289	2.59965	2.1	0	-1.4387	0.05802	0	-0.26815	0.4106	1.34

Table 2D.2: GMPE Coefficients for the Silva el at (2002) SCR model (continued)

Single Corner Model with Constant Stress Drop and Magnitude Saturation

Period, T (s)	c_1	c_2	c_4	c_5	c_6	c_7	c_8	c_{10}	$\sigma_{parametric}$	σ_{total}
PGV	4.60099	0.44166	2.6	0	-3.1301	0.2635	0	-0.11559	0.5648	--------
PGA	5.53459	-0.1169	2.9	0	-3.4217	0.26461	0	-0.0681	0.6998	0.8471
0.010	5.73885	-0.1242	2.9	0	-3.4389	0.2651	0	-0.06699	0.7079	0.8538
0.020	7.17445	-0.1681	3	0	-3.5651	0.26786	0	-0.06041	0.7643	0.9008
0.025	7.14087	-0.1588	3	0	-3.5427	0.26589	0	-0.06019	0.7619	0.8974
0.032	6.97878	-0.1471	3	0	-3.5123	0.26392	0	-0.06051	0.755	0.8943
0.040	6.81012	-0.1359	3	0	-3.485	0.2622	0	-0.06115	0.7429	0.887
0.050	6.63937	-0.1219	3	0	-3.4548	0.26008	0	-0.06201	0.7259	0.8753
0.055	6.56761	-0.1149	3	0	-3.441	0.25904	0	-0.06249	0.72	0.8682
0.060	5.96397	-0.0697	2.9	0	-3.3341	0.25145	0	-0.063	0.7152	0.868
0.070	5.83477	-0.0566	2.9	0	-3.311	0.24965	0	-0.06416	0.7077	0.8599
0.080	5.70631	-0.0439	2.9	0	-3.2901	0.24799	0	-0.06548	0.7017	0.8553
0.100	5.43782	-0.0206	2.9	0	-3.255	0.24527	0	-0.06853	0.6933	0.8546
0.120	5.1732	0.00188	2.9	0	-3.2248	0.24286	0	-0.072	0.6814	0.8562
0.150	4.30417	0.06695	2.8	0	-3.1045	0.23411	0	-0.07779	0.6685	0.8417
0.160	4.18416	0.07875	2.8	0	-3.0916	0.23297	0	-0.07992	0.6633	0.8368
0.200	3.71953	0.1249	2.8	0	-3.0459	0.22877	0	-0.08886	0.6511	0.8338
0.240	3.25319	0.16616	2.8	0	-3.0127	0.22589	0	-0.09854	0.6423	0.8346
0.300	2.60689	0.23165	2.8	0	-2.9632	0.22112	0	-0.11352	0.6325	0.8428
0.400	1.64228	0.34751	2.8	0	-2.8777	0.21215	0	-0.13838	0.6199	0.8386
0.500	0.69539	0.45254	2.8	0	-2.818	0.20613	0	-0.16423	0.6097	0.8484
0.750	-1.2293	0.68518	2.8	0	-2.6802	0.19127	0	-0.21501	0.5914	0.8861
1.000	-2.8991	0.88116	2.8	0	-2.583	0.18098	0	-0.25757	0.5767	0.8785
1.600	-6.0369	1.25821	2.7	0	-2.3393	0.15765	0	-0.31816	0.5472	0.9498
2.000	-7.4205	1.41946	2.7	0	-2.2643	0.14984	0	-0.33999	0.5309	1.0142
3.000	-10.333	1.71755	2.6	0	-2.0856	0.13401	0	-0.36316	0.4981	1.0914
5.0	-13.697	2.03488	2.5	0	-1.9197	0.12052	0	-0.35463	0.4597	1.2253
10.0	-17.698	2.33877	2.3	0	-1.7536	0.11071	0	-0.28005	0.4204	1.3431

Table 2D.2: GMPE Coefficients for the Silva el at (2002) SCR model (continued)

Double Corner Model

Period, T (s)	c_1	c_2	c_4	c_5	c_6	c_7	c_8	c_{10}	$\sigma_{parametric}$	σ_{total}
PGV	4.06989	0.46794	2.5	0	-2.7481	0.19743	0	-0.0761	0.5582	--------
PGA	3.54103	0.18904	2.7	0	-2.9742	0.19819	0	-0.0581	0.6912	0.84
0.010	3.74623	0.18152	2.7	0	-2.9887	0.19854	0	-0.0573	0.6994	0.8468
0.020	5.06834	0.14806	2.8	0	-3.0841	0.19935	0	-0.0536	0.7561	0.8939
0.025	5.03119	0.15779	2.8	0	-3.0613	0.19746	0	-0.0538	0.7534	0.8902
0.032	4.86717	0.17018	2.8	0	-3.0325	0.1956	0	-0.0543	0.7462	0.8869
0.040	4.69293	0.18262	2.8	0	-3.0067	0.19396	0	-0.0552	0.7339	0.8795
0.050	4.0767	0.22547	2.7	0	-2.9004	0.1872	0	-0.0565	0.7165	0.8675
0.055	3.99907	0.23357	2.7	0	-2.8873	0.18619	0	-0.0572	0.7106	0.8604
0.060	3.92454	0.24169	2.7	0	-2.875	0.18521	0	-0.0579	0.7058	0.8602
0.070	3.7751	0.25773	2.7	0	-2.8523	0.18339	0	-0.0595	0.6982	0.8521
0.080	3.624	0.27369	2.7	0	-2.8316	0.1817	0	-0.0613	0.6923	0.8476
0.100	3.30684	0.30373	2.7	0	-2.7975	0.17893	0	-0.0651	0.6837	0.8468
0.120	2.60454	0.35667	2.6	0	-2.6993	0.17238	0	-0.0693	0.6717	0.8485
0.150	2.14018	0.39715	2.6	0	-2.6668	0.16973	0	-0.0757	0.6587	0.8339
0.160	1.99361	0.41219	2.6	0	-2.6551	0.16868	0	-0.078	0.6535	0.829
0.200	1.42831	0.46988	2.6	0	-2.6138	0.16486	0	-0.0867	0.6412	0.826
0.240	0.86777	0.52085	2.6	0	-2.5851	0.16235	0	-0.0948	0.6326	0.8272
0.300	0.1092	0.59537	2.6	0	-2.5412	0.15808	0	-0.1051	0.6231	0.8358
0.400	-0.9687	0.7137	2.6	0	-2.465	0.15003	0	-0.1175	0.611	0.832
0.500	-1.9597	0.8081	2.6	0	-2.4113	0.14449	0	-0.1253	0.6016	0.8426
0.750	-3.7736	0.98718	2.6	0	-2.2811	0.13007	0	-0.1332	0.5844	0.8815
1.000	-5.4702	1.1259	2.5	0	-2.1347	0.1171	0	-0.1383	0.5697	0.8739
1.600	-7.683	1.34978	2.5	0	-1.9457	0.09603	0	-0.1613	0.5388	0.945
2.000	-8.7688	1.452	2.5	0	-1.8649	0.08722	0	-0.1813	0.5217	1.0095
3.000	-11.048	1.64665	2.4	0	-1.7001	0.07272	0	-0.2294	0.4887	1.0871
5.0	-13.889	1.89859	2.3	0	-1.5477	0.06068	0	-0.2896	0.4529	1.2228
10.0	-17.745	2.22485	2.1	0	-1.4008	0.05305	0	-0.3164	0.4199	1.3429

Table 2D.2: GMPE Coefficients for the Silva el at (2002) SCR model (continued)

Double Corner Model with Magnitude Saturation

Period, T (s)	c_1	c_2	c_4	c_5	c_6	c_7	c_8	c_{10}	$\sigma_{parametric}$	σ_{total}
PGV	5.79531	0.17529	2.6	0	-3.1122	0.25573	0	-0.088	0.5582	--------
PGA	5.91196	-0.1573	2.9	0	-3.424	0.26564	0	-0.07	0.6912	0.84
0.010	6.12213	-0.1649	2.9	0	-3.4394	0.26601	0	-0.0693	0.6994	0.8468
0.020	7.55648	-0.209	3	0	-3.5531	0.26853	0	-0.0655	0.7561	0.8939
0.025	7.51145	-0.1986	3	0	-3.5289	0.26652	0	-0.0657	0.7534	0.8902
0.032	7.33736	-0.1856	3	0	-3.4982	0.26456	0	-0.0663	0.7462	0.8869
0.040	6.61204	-0.1337	2.9	0	-3.3759	0.25613	0	-0.0671	0.7339	0.8795
0.050	6.42423	-0.1173	2.9	0	-3.346	0.25401	0	-0.0684	0.7165	0.8675
0.055	6.34238	-0.1089	2.9	0	-3.3322	0.25295	0	-0.0691	0.7106	0.8604
0.060	6.26384	-0.1004	2.9	0	-3.3191	0.25192	0	-0.0698	0.7058	0.8602
0.070	6.10708	-0.0839	2.9	0	-3.2951	0.25	0	-0.0714	0.6982	0.8521
0.080	5.94942	-0.0674	2.9	0	-3.2733	0.24822	0	-0.0732	0.6923	0.8476
0.100	5.13706	-0.0017	2.8	0	-3.1519	0.23929	0	-0.077	0.6837	0.8468
0.120	4.81663	0.02793	2.8	0	-3.1222	0.23686	0	-0.0812	0.6717	0.8485
0.150	4.34277	0.06911	2.8	0	-3.0881	0.23409	0	-0.0876	0.6587	0.8339
0.160	4.19281	0.08441	2.8	0	-3.0758	0.233	0	-0.0899	0.6535	0.829
0.200	3.61568	0.14311	2.8	0	-3.0324	0.229	0	-0.0986	0.6412	0.826
0.240	3.04705	0.19471	2.8	0	-3.0022	0.22639	0	-0.1068	0.6326	0.8272
0.300	2.27626	0.27031	2.8	0	-2.9562	0.22193	0	-0.117	0.6231	0.8358
0.400	1.17695	0.39078	2.8	0	-2.8763	0.21352	0	-0.1294	0.611	0.832
0.500	0.17104	0.48663	2.8	0	-2.82	0.20773	0	-0.1372	0.6016	0.8426
0.750	-1.6801	0.66971	2.8	0	-2.6832	0.19261	0	-0.1451	0.5844	0.8815
1.000	-3.1084	0.79561	2.8	0	-2.5856	0.18195	0	-0.1502	0.5697	0.8739
1.600	-5.7502	1.05061	2.7	0	-2.32	0.1554	0	-0.1732	0.5388	0.945
2.000	-6.8605	1.15548	2.7	0	-2.2347	0.1461	0	-0.1932	0.5217	1.0095
3.000	-9.2435	1.36201	2.6	0	-2.0519	0.12954	0	-0.2413	0.4887	1.0871
5.0	-12.179	1.62451	2.5	0	-1.8829	0.11564	0	-0.3015	0.4529	1.2228
10.0	-16.163	1.96535	2.3	0	-1.7137	0.10547	0	-0.3283	0.4199	1.3429

Table 2D.3: GMPE Coefficients for the Atkinson and Boore (2006) SCR model
Hard Rock Sites (Vs_{30} = 2000 m/s)

Period, T (s)	c_1	c_2	c_3	c_4	c_5	c_6	c_7	c_8	c_9	c_{10}
PGV	-1.442	0.9909	-0.05848	-2.701	0.2155	-2.436	0.2659	0.08479	-0.06927	-3.73E-04
PGA	0.9069	0.983	-0.06595	-2.698	0.1594	-2.795	0.212	-0.3011	-0.06532	-4.48E-04
0.025	1.522	0.9597	-0.06351	-2.813	0.1458	-3.654	0.2362	-0.6544	-0.055	-4.85E-05
0.031	1.436	0.9592	-0.06276	-2.714	0.14	-3.728	0.2343	-0.543	-0.06448	-3.23E-05
0.040	1.264	0.968	-0.06232	-2.581	0.1317	-3.644	0.2276	-0.3506	-0.08126	-1.23E-04
0.050	1.105	0.9719	-0.06197	-2.466	0.1276	-3.39	0.2144	-0.1391	-0.09839	-3.17E-04
0.063	0.9109	0.9802	-0.06208	-2.36	0.1263	-2.972	0.191	0.1069	-0.1173	-5.79E-04
0.079	0.6906	0.9974	-0.06276	-2.262	0.1246	-2.487	0.1636	0.2139	-0.1207	-8.47E-04
0.100	0.4797	1.017	-0.06404	-2.201	0.127	-2.007	0.1326	0.3371	-0.1266	-1.05E-03
0.125	0.2144	1.054	-0.06664	-2.154	0.1295	-1.608	0.1046	0.4273	-0.1303	-1.15E-03
0.158	-0.1455	1.123	-0.07143	-2.116	0.1302	-1.303	0.08311	0.5617	-0.1438	-1.18E-03
0.199	-0.6153	1.227	-0.07886	-2.087	0.1312	-1.12	0.06788	0.6055	-0.1459	-1.13E-03
0.251	-1.121	1.342	-0.08722	-2.082	0.1349	-0.9714	0.05628	0.614	-0.1432	-1.06E-03
0.315	-1.721	1.483	-0.09739	-2.08	0.1382	-0.8893	0.04869	0.6101	-0.1389	-9.54E-04
0.397	-2.437	1.649	-0.1084	-2.051	0.1363	-0.8426	0.04483	0.7386	-0.1557	-8.51E-04
0.500	-3.216	1.826	-0.1201	-2.018	0.1344	-0.8134	0.04437	0.8839	-0.1751	-7.70E-04
0.629	-3.917	1.987	-0.1314	-2.045	0.1419	-0.7818	0.04297	0.7878	-0.159	-6.95E-04
0.794	-4.604	2.132	-0.1406	-2.062	0.1468	-0.7974	0.04345	0.7748	-0.1558	-5.79E-04
1.000	-5.272	2.264	-0.1483	-2.069	0.1497	-0.8132	0.04666	0.8262	-0.1622	-4.86E-04
1.250	-5.724	2.324	-0.1505	-2.104	0.1565	-0.8202	0.05186	0.8563	-0.1661	-4.33E-04
1.587	-6.043	2.342	-0.1496	-2.157	0.1662	-0.8704	0.06047	0.9207	-0.1734	-3.75E-04
2.000	-6.183	2.302	-0.1442	-2.223	0.177	-0.937	0.07067	0.9518	-0.1768	-3.22E-04
2.500	-6.169	2.211	-0.1348	-2.299	0.1898	-0.986	0.0786	0.9683	-0.1765	-2.82E-04
3.125	-6.038	2.08	-0.1221	-2.367	0.2002	-1.073	0.0895	1.002	-0.1803	-2.31E-04
4.000	-5.791	1.916	-0.1071	-2.441	0.2113	-1.162	0.1018	1.012	-0.1824	-2.01E-04
5.000	-5.408	1.714	-0.09012	-2.537	0.2267	-1.268	0.1162	0.9792	-0.1767	-1.76E-04

Table 2D.4: GMPE Coefficients for the Pezeshk et al (2011) SCR model

Period, T (s)	c_1	c_2	c_3	c_4	c_5	c_6	c_7
PGA	1.5828	0.2298	-0.0385	-3.8325	0.3535	0.3321	-0.0917
0.01	2.0434	0.1987	-0.0384	-4.0521	0.3688	0.1995	-0.0892
0.02	2.305	0.1877	-0.037	-4.0443	0.3616	-0.1222	-0.0916
0.03	1.9848	0.2203	-0.0362	-3.8032	0.3384	0.07814	-0.1126
0.04	1.6854	0.2404	-0.0358	-3.6129	0.3247	0.2956	-0.118
0.05	1.4517	0.2414	-0.0347	-3.4683	0.3177	0.5224	-0.1296
0.075	1.0698	0.2989	-0.039	-3.377	0.318	0.7422	-0.1215
0.1	0.9314	0.3088	-0.0384	-3.2926	0.3063	0.7064	-0.0952
0.15	0.3964	0.4317	-0.0458	-3.2112	0.2937	0.6084	-0.0673
0.2	-0.4883	0.6278	-0.0565	-3.0304	0.2673	0.5422	-0.0535
0.25	-1.0098	0.7401	-0.0631	-2.9959	0.2623	0.4421	-0.0363
0.3	-1.68	0.886	-0.0716	-2.8894	0.2481	0.4869	-0.0432
0.4	-2.3106	1.022	-0.0797	-2.9265	0.2515	0.4716	-0.0404
0.5	-3.1365	1.201	-0.0904	-2.8823	0.2456	0.3333	-0.0211
0.75	-4.5494	1.508	-0.1087	-2.8614	0.2424	0.4023	-0.0309
1	-5.4113	1.69	-0.1196	-2.8998	0.2465	0.3766	-0.0293
1.5	-6.4806	1.867	-0.1282	-2.9338	0.2525	0.2633	-0.0144
2	-6.934	1.907	-0.1287	-3.0128	0.2639	0.3172	-0.0215
3	-7.4264	1.881	-0.1205	-2.9742	0.2576	0.2585	-0.0152
4	-7.8064	1.895	-0.1183	-3.005	0.2588	0.3069	-0.0255
5	-8.2704	1.938	-0.118	-2.9501	0.2503	0.3296	-0.0302
7.5	-8.3376	1.806	-0.1042	-2.9839	0.2542	0.2879	-0.0225
10	-9.1046	1.899	-0.1076	-2.8611	0.2395	0.2868	-0.0229

Table 2D.4: GMPE Coefficients for the Pezeshk et al (2011) SCR model (continued)

Period, T (s)	c_8	c_9	c_{10}	c_{11}	c_{12}	c_{13}	c_{14}
PGA	-2.5517	0.1831	-4.224E-04	6.6521	-0.0211	0.3778	0.2791
0.01	-2.5948	0.1847	-3.965E-04	7.0645	-0.0197	0.3688	0.2792
0.02	-2.9998	0.1941	-1.707E-04	7.3314	-0.0197	0.3691	0.2796
0.03	-3.3125	0.2017	-5.322E-05	7.1183	-0.0209	0.3817	0.2838
0.04	-3.332	0.1977	-1.113E-04	6.8113	-0.0218	0.3914	0.2874
0.05	-3.2109	0.1956	-2.669E-04	6.3705	-0.0224	0.399	0.2905
0.075	-2.6889	0.1723	-6.659E-04	6.0817	-0.0231	0.4108	0.2976
0.1	-2.209	0.1472	-9.254E-04	6.1621	-0.0226	0.4102	0.3007
0.15	-1.6121	0.1072	-1.077E-03	6.2667	-0.0219	0.4066	0.3023
0.2	-1.3516	0.08784	-1.045E-03	6.1905	-0.0205	0.3979	0.3033
0.25	-1.2309	0.07733	-9.648E-04	6.0635	-0.0193	0.3908	0.3041
0.3	-1.149	0.07056	-9.049E-04	5.9891	-0.0184	0.3867	0.3068
0.4	-1.0923	0.06554	-7.853E-04	6.0263	-0.0168	0.3774	0.3082
0.5	-1.0022	0.05519	-7.069E-04	5.9117	-0.0156	0.3722	0.3119
0.75	-0.975	0.05536	-5.685E-04	5.9835	-0.0134	0.3654	0.3203
1	-0.947	0.05249	-4.563E-04	6.1234	-0.0118	0.3588	0.3249
1.5	-0.9007	0.04974	-3.540E-04	5.9875	-0.0104	0.3569	0.3327
2	-0.8749	0.04774	-3.025E-04	6.1355	-0.0094	0.3561	0.3387
3	-0.8821	0.05376	-2.641E-04	6.0598	-0.0085	0.354	0.3431
4	-0.8808	0.05703	-2.423E-04	6.2536	-0.0079	0.3527	0.3463
5	-1.0125	0.07332	-2.002E-04	6.3423	-0.0069	0.3577	0.358
7.5	-1.1817	0.09598	-1.624E-04	6.5181	-0.0072	0.373	0.371
10	-1.3786	0.1222	-1.268E-04	6.5384	-0.0075	0.3848	0.381

Appendix 2E: Additional Ground Motion Parameters

2E1. Introduction

The most common target ground motion parameter for selection of ground motions for nonlinear analysis is the pseudo acceleration response spectrum. This appendix gives details on the models used to estimate additional ground motion parameters that are considered important in the selection of time histories. These parameters include the peak ground acceleration (PGA) and peak ground velocity (PGV), frequency content parameters such as the mean period (T_m), predominant period (T_p), smoothed spectral predominant period (T_o), the average period (T_{avg}), and the pulse period (T_v), the arias intensity (I_a), and duration parameters such as the bracketed duration and the significant duration.

2E.2 Peak Ground Acceleration (PGA) and Peak Ground Velocity (PGV)

The most direct intensity measures are the peak ground acceleration (PGA) and velocity (PGV), which are the maximum absolute value of acceleration and velocity measured from the acceleration time series and the velocity time series, respectively. PGA and PGV are widely used in geotechnical as well as structural earthquake engineering in simplified methods for estimation of structural response. Integration from acceleration to velocity and velocity to displacement tends to dilute the high frequency components of a record and augment the low frequency components (Stewart et al, 2001). Therefore, PGA is most affected by high frequency energy and PGV is most sensitive to mid-range frequencies. Many GMPEs that predict the response spectrum also predict PGA and PGV. In general, they have similar mathematical forms as those relating the pseudo-acceleration versus period as a function of magnitude and distance as well as other relevant event and site properties. All of the GMPEs presented earlier predict PGA and PGV, except the subduction zone models, which only predict PGA. There are currently no well established, widely used models to predict the PGV of subduction zone earthquakes.

Ground motions recorded at distances less than 20 km may have near fault effects, such as forward directivity, backward directivity, or fling step (NIST, 2012). Forward and backward directivity can greatly alter the intensity, duration, and frequency content of a ground motion. In particular, forward directivity produces ground motions with large amplitudes and short durations, and backward directivity produces ground motions with small amplitudes and large durations. These differences are best seen in the velocity time series, where forward directivity is characterized by large velocity pulses.

Bray et al (2009) proposed an equation to predict PGV based on a mixed effects regression of an empirical database of near fault records. Their database was a subset of the PEER dataset and included 68 records from 17 earthquakes with $M_w > 6$ and $R_{rup} < 20$ km. Bray et al (2009) found that PGV of near fault motions increases with increasing magnitude and decreasing rupture distance. They also found that soil sites had larger values of PGV than rock sites. The predictive equation developed by Bray et al (2009) for PGV is:

$$ln(PGV) = a + b \times M + c \times ln\left(R_{rup}^2 + d^2\right) \qquad (2E.1)$$

where PGV is the peak ground velocity in units of cm/s, M is the moment magnitude, R_{rup} is the rupture distance in km, and a, b, c, and d are regression coefficients. Table 2E.1 lists the

coefficients and the total standard deviation in natural log units for soil and rock site conditions. Bray et al (2009) define rock sites as sites with no more than 20 meters of soil or weathered rock over competent rock.

2E.3 Frequency Content Parameters

Site response analyses are significantly affected by the frequency content of the input ground motion. Although the response spectrum completely characterizes the frequency content of a ground motion, a scalar frequency content parameter is easier to compare to the natural frequency of a site to evaluate if resonance is likely to occur. In addition, scalar frequency content parameters make it easier to compare different ground motions when selecting ground motions for site response analyses.

Rathje et al (1998, 2004) investigated four simplified frequency content parameters: mean period (T_m), predominant period (T_p), smoothed spectral predominant period (T_o), and the average period (T_{avg}). They found that these parameters increase as magnitude and distance increase, for sites with forward directivity, and as the NEHRP site class decreases. Rathje et al (2004) also found that T_m and T_{avg} are most affected by low frequency content of ground motions, while T_o and T_p are mostly affected by the high frequency content.

The mean period is the period at the centroid of the Fourier amplitude spectrum and it is computed as:

$$T_m = \frac{\sum_i C_i^2 \times \left(\frac{1}{f_i}\right)}{\sum_i C_i^2} \text{ for } 0.25\ Hz \leq f_i \leq 20\ Hz \qquad \text{(2E.2)}$$

where C_i are the Fourier amplitudes of the accelerogram and f_i are the discrete fast Fourier transform frequencies, with frequency intervals used in the fast Fourier transform less than or equal to 0.05 Hz.

The frequency content parameters T_p, T_o, and T_{avg} are based on the 5% damped acceleration response spectrum. The predominant period (T_p) is the period corresponding to the maximum spectral acceleration. Rathje et al (1998) found that T_p had the largest uncertainty and that previous prediction equations were inconsistent with their data set. Rathje et al (2004) recommend not using T_p, and instead propose the parameter T_o. The smoothed predominant period (T_o) is the period corresponding to the maximum spectral acceleration for a smoothed response spectra. In this way, T_o is similar to T_p, but has smaller uncertainty. Rathje et al (2004) define the smoothed predominant period (T_o) as:

$$T_o = \frac{\sum_i T_i \times ln\left(\frac{S_a(T_i)}{PGA}\right)}{\sum_i ln\left(\frac{S_a(T_i)}{PGA}\right)} \text{ for } T_i \text{ with } \geq 1.2, \Delta \log T_i \leq 0.02 \qquad \text{(2E.3)}$$

where T_i are the acceleration response spectrum periods equally spaced on a log axis, and $Sa(T_i)$ are the spectral accelerations at T_i . The smoothed predominant period is computed using only periods with Sa > 1.2*PGA.

The average period (T_{avg}) is similar to T_m except that it is computed using spectral accelerations instead of the Fourier amplitudes and the periods are equally spaced on an arithmetic scale. The average period is calculated as:

$$T_{avg} = \frac{\sum_i T_i \times \left(\frac{S_a(T_i)}{PGA}\right)^2}{\sum_i \left(\frac{S_a(T_i)}{PGA}\right)^2} \text{ for } 0.05 \text{ s} \leq T_i \leq 4 \text{ s}, \Delta T_i \leq 0.05 \text{ s} \quad \text{(2E.4)}$$

Rathje et al (2004) used theoretical source models to establish the functional form of their predictive equations. They then performed mixed effects regression analyses on a dataset consisting of 1208 records from 71 earthquakes with magnitudes between 4.7 and 7.6 to determine the coefficients. Rathje et al (2004) proposed the following functional form:

$$ln(T) = c_1 + c_2 \times (M_w - 6) + c_3 \times R + c_4 \times S_C + c_5 \times S_D + c_6 \times (1 - R/20) \times FD \quad \text{(2E.5)}$$

for $5.0 \leq M_w \leq 7.25$ for T_m and for $4.7 \leq M_w \leq 7.6$ for T_{avg} and T_o

$$ln(T) = c_1 + c_2 \times (7.25 - 6) + c_3 \times R + c_4 \times S_C + c_5 \times S_D + c_6 \times (1 - R/20) \times FD \quad \text{(2E.6)}$$

for $M_w > 7.25$ for T_m

where T is the frequency content parameter (T_m , T_o, or T_{avg} in seconds), c_1 through c_6 are regression coefficients corresponding to each frequency content parameter, M_w is moment magnitude, R is the closest distance to the fault rupture plane in km, SC and SD designate NERHP site class (SC = SD = 0 for Site Class B, SC = 1 and SD = 0 for Site Class C, SC = 0 and SD = 1 for Site Class D), and FD designates forward directivity conditions (FD = 1 for sites with M_w > 6.0, R < 20.0 km, azimuth angle <30°, and rupture length ratio > 0.5, FD = 0 otherwise). Table 2E.2 lists the coefficients c_1 through c_6 for each frequency content parameter and Table 2E.3 lists the total standard error term by NEHRP site class and frequency content parameter.

2E.4 Pulse Period (T_v) for Near Fault Ground Motions.

Ground motions recorded at distances less than 20 km may exhibit near fault effects, such as forward directivity, backward directivity, or fling (NIST, 2012). These differences are best seen in the velocity time series, where forward directivity can be characterized by large velocity pulses. The period of the pulse is termed the predominant pulse period (T_v).

Somerville (2003) and Bray et al (2009) found that T_v increased with magnitude. This dependence is expected because the pulse period is related to the duration of slip at a point on the fault (rise time), and the fault dimensions, both of which are dependent on the magnitude

(Somerville, 2003). They also found that T_v was a function of site conditions, with soil sites exhibiting a larger T_v than rock sites. However, due to nonlinear site effects, the amount of increase is dependent on the intensity of the ground motion and the dynamic properties of the soil layer (Somerville, 2003).

Somerville (2003) developed predictive equation for T_v on rock sites from 15 recordings of eight earthquakes, and the predictive equation for T_v on soil sites from 12 recordings from six earthquakes. The relationships are:

$$log(T_v) = -3.7 + 0.5 \times M_w \quad \text{for Rock sites} \qquad \text{(2E.7)}$$

$$log(T_v) = -2.02 + 0.346 \times M_w \quad \text{for Soil sites} \qquad \text{(2E.8)}$$

Bray et al (2009) developed their model from a database of 68 records from 17 earthquakes using a mixed effects regression. The relationships for rock and soil sites are given below, along with the total standard deviation for each soil type.

$$ln(T_v) = -6.37 + M_w \;\; ; \;\; \sigma_{total} = 0.55, \qquad \text{for Rock sites} \qquad \text{(2E.9)}$$

$$ln(T_v) = -3.71 + 0.65 \cdot M_w \;\; ; \;\; \sigma_{total} = 0.51, \qquad \text{for Soil sites} \qquad \text{(2E.10)}$$

Other studies that have developed predictive equations for T_v are Alavi and Krawinkler (2000) and Shahi and Baker (2011).

2E.5 Arias Intensity (I_a)

The Arias intensity (I_a) is a widely used ground motion parameter because it correlates well with commonly used demand measures of structural performance, liquefaction, and seismic slope stability (Travasarou et al, 2003). Travasarou et al. (2003) and Watson-Lamprey and Abrahamson (2006) showed that I_a is the most important parameter when predicting Newmark displacement with only one variable. The arias intensity was defined by Arias (1970) as the square of the acceleration integrated over the entire duration of the time series. It is calculated as:

$$I_a = \frac{\pi}{2g} \times \int_0^\infty a(t)^2 \, dt \qquad \text{(2E.11)}$$

where I_a is in m/s, a(t) is the acceleration time history in units of g, and g is the acceleration of gravity. Travasarou et al (2003), Watson-Lamprey and Abrahamson (2006), and Foulser-Piggot and Stafford (2011) found that I_a was dependent on magnitude, rupture distance, site stiffness, and rupture mechanism.

2E.5.1 Travasarou et al. (2003) Model

Travasarou et al. (2003) developed an empirical prediction equation for I_a based on a theoretical functional form by performing mixed effects regression on a database of 1208 records from 75

earthquakes. Their model is limited to active crustal earthquakes with magnitudes between 4.7 and 7.6. The following equation gives the median I_a predicted by Travasarou et al (2003):

$$\begin{aligned} ln(I_a) &= c_1 + c_2 \times (M-6) + c_3 \times ln\left({}^{M}/_{6}\right) \\ &+ c_4 \times ln\left(\sqrt{R_{rup}^2 + h^2}\right) + \left(s_{11} + s_{12} \times (M-6)\right) \times S_C \\ &+ \left(s_{21} + s_{22} \times (M-6)\right) \times S_D + f_1 \times F_N + f_2 \times F_R \end{aligned} \quad \text{(2E.12)}$$

where I_a is the Arias intensity in m/s, M is the moment magnitude, R_{rup} is the rupture distance, SC and SD are the site terms according to Bray and Rodriguez-Marek (1997) (SC = SD = 0 for B, SC = 1 and SD = 0 for C, and SC = 0 and SD = 1 for D), FN and FR are fault mechanism terms (FN = FR = 0 for strike slip, FN = 1 and FR = 0 for normal, and FN = 0 and FR = 1 for reverse faults), and c, h, s, and f are site terms listed in Table 2E.4. The standard deviation is given as:

$$\sigma_{total} = \sqrt{\tau^2 + \sigma^2} \quad \text{(2E.13)}$$

$$\tau = \begin{cases} 0.611 & \text{for M} \leq 4.7 \\ 0.611 - 0.0466 \times (M - 4.7) & \text{for } 4.7 < M < 7.6 \\ 0.476 & \text{for M} \geq 7.6 \end{cases} \quad \text{(2E.14)}$$

$$\sigma = \begin{cases} \sigma_1 & \text{for } I_a \leq 0.0132 \\ \sigma_1 - 0.1064 \times \left(ln(I_a) - ln(0.0132)\right) & \text{for } 0.0132 < I_a < 0.1245 \\ \sigma_2 & \text{for } I_a \geq 0.1245 \end{cases} \quad \text{(2E.15)}$$

The coefficients σ_1 and σ_2 are site dependent and they are listed in Table 2E.5.

2E.5.2 Watson-Lamprey and Abrahamson (2006) Model

Watson-Lamprey and Abrahamson (2006) developed their model from a database of 6158 records from 150 earthquakes with magnitudes between 4.5 and 7.9 and distances of 0 to 300 km. This database was a subset of the PEER dataset available at the time. The equation for arias intensity is:

$$\begin{aligned} ln(I_a/9.81) &= -1.991 + 0.497 \times M - 0.355 \times ln(Vs_{30}) \\ &- 0.081\left(ln\left(R_{rup}\right) - 3.4\right) \\ &-0.018 \times \left(ln\left(R_{rup}\right) - 3.4\right)^2 + 1.296 \times \ln(\text{PGA}) \\ &+0.328 \times \ln(\text{Sa}_{\text{T=1}}) \end{aligned} \quad \text{(2E.16)}$$

where I_a is the arias intensity in m/s, M is moment magnitude, Vs_{30} is the time averaged shear wave velocity in the top 30 meters of the site, R_{rup} is the rupture distance in km, PGA is the peak ground acceleration in g, and $Sa_{T=1}$ is the 5% damped spectral acceleration at T = 1 second. The

standard deviation is 0.34 natural log units. The standard deviation for this model is much less than for Travasarou et al. (2003) because it includes the values of PGA and $Sa_{T=1}$.

2E.5.3 Foulser-Piggot and Stafford (2011) Model

Foulser-Piggot and Stafford (2011) developed a model for I_a from a database of 2406 recordings from 114 earthquakes with magnitudes between 4.79 to 7.9, R_{rup} < 100 km, Vs_{30} values between 116 to 2017 m/s, and depth to top of rupture < 15 km. Of the 114 earthquakes used in the dataset, 56 had strike-slip, 35 had reverse or reverse-oblique, and 23 had normal or normal-oblique mechanisms. This database was a subset of the PEER dataset available at the time. The predictive equation developed by Foulser-Piggot and Stafford (2011) for arias intensity is:

$$ln\left(I_a^{ref}\right) = c_1 + c_2 \times (8.5 - M_w)^2 + (c_3 + c_4 \times M_w) \times ln\left(\sqrt{R_{rup}^2 + c_5^2}\right) + c_6 \times F_{RV} \quad \text{(2E.17)}$$

$$ln(I_a) = ln\left(I_a^{ref}\right) + f_{site} \quad \text{(2E.18)}$$

$$f_{site} = v_1 \times ln(Vs_{30}/1100) + v_2 \times b \times ln\left(\frac{I_a^{ref} + v_4}{v_4}\right) \quad \text{(2E.19)}$$

$$b = v_2 \times \left[e^{v_3 \times (Vs_{30} - 280)} - e^{v_3 \times 820}\right] \quad \text{(2E.20)}$$

where I_a is the arias intensity in m/s, M is moment magnitude, Vs_{30} is the time averaged shear wave velocity in the top 30 meters of the site, R_{rup} is the rupture distance in km, FRV = 1 for reverse and reverse-oblique mechanisms and 0 otherwise, and c and v are coefficients listed in Table 2E.6. The standard deviation is computed as:

$$\sigma_{total} = \sqrt{\sigma_E^2 + \sigma_A^2 \times max(M_w, 5)^{2 \cdot \delta_1} \times (\delta_2 + |1 + NL|^{\delta_3})^2} \quad \text{(2E.21)}$$

$$NL = b \times \left(\frac{I_a^{ref}}{I_a^{ref} + v_4}\right) \quad \text{(2E.22)}$$

where σ_{total} is the total standard deviation in natural log units, and σ and δ are coefficients listed in Table 2E.7. Foulser-Piggot and Stafford (2011) recommend that their model is useable for magnitudes between 5 and 8, R_{rup} < 100 km, and Vs_{30} values between 200 and 1000 m/s.

2E.6 Duration Parameters

Duration has a strong influence on the damage imposed by an earthquake, especially for systems that undergo cyclic degradation (Kempton and Stewart, 2006). The most common duration parameters are bracketed duration and significant duration (Stewart et al, 2001). Bracketed duration is defined as the time between when the acceleration time series first exceeds a threshold acceleration, usually 0.05g, and the last time it exceeds the threshold acceleration. The

significant duration is the time between when a specified percentage of the Arias intensity occurs, usually 5-75% ($D_{5\text{-}75}$) or 5-95% ($D_{5\text{-}95}$).

The duration of strong ground shaking is related to the time necessary for rupture to spread across the fault surface. Larger rupture zones will produce larger durations of strong ground shaking. Therefore, because the size of the rupture area is closely correlated to magnitude, duration is dependent on magnitude (Stewart et al, 2001).

2E.6.1 Abrahamson and Silva (1996) Model

Abrahamson and Silva (1996) developed a model for estimating $D_{5\text{-}75}$ and $D_{5\text{-}95}$ with strong ground motion data up through the 1994 Northridge earthquake near Los Angeles, CA. They found that duration is a function of magnitude, distance, and site effects:

$$ln(D) = ln\left[\frac{(\Delta\sigma/10^{1.5\times M+16.05})^{-1/3}}{4.9\times 10^{6}\times\beta} + S\times c_1 + c_2\times\left(R_{rup}-R_c\right)\right] + D_{rat} \quad \text{for } R_{rup}\geq R_c \quad (2E.23)$$

$$ln(D) = ln\left[\frac{(\Delta\sigma/10^{1.5\times M+16.05})^{-1/3}}{4.9\times 10^{6}\times\beta} + S\times c_1\right] + D_{rat} \quad \text{for } R_{rup} < R_c \quad (2E.24)$$

$$\Delta\sigma = exp\left(b_1 + b_2\times(M-6)\right) \quad (2E.25)$$

where D is $D_{5\text{-}75}$ or $D_{5\text{-}95}$, M is moment magnitude, R_{rup} is the rupture distance in km, S = 0 for rock sites and 1 for soil sites, and β, b_1, b_2, c_1, c_2, D_{rat}, and R_c are regression coefficients listed in Table 2E.8. Table 2E.8 also lists the total standard deviation in natural log units.

2E.6.2 Kempton and Stewart (2006) model

Kempton and Stewart (2006) found empirically that significant duration increases with magnitude and distance, and that it decreases with increasing Vs_{30}. They also found that duration decreases with depth when the seismic source is located beneath the basin of the site, and duration increases with depth when the source is located outside the site basin. In addition, their regression analyses showed statistical differences between the results for strike-slip versus dip-slip earthquakes and for forward versus backward directivity for $D_{5\text{-}75}$, but not for $D_{5\text{-}95}$.

Kempton and Stewart (2006) developed their model from a database with 1559 records from 73 shallow crustal earthquakes with magnitudes between 4.4 and 7.6, and R_{rup} < 300 km. This database was a subset of the PEER database available at the time. The predictive equation developed by Kempton and Stewart (2006) for significant duration is:

$$ln(D) = ln\left[\frac{(\Delta\sigma/10^{1.5\times M+16.05})^{-1/3}}{4.9\cdot 10^{6}\cdot\beta} + R\times c_2 + (c_4 + c_5\times Vs_{30}) + (c_6 + c_7\cdot z_{1.5})\right] + \varepsilon \quad \text{(2E.26)}$$

$$\varepsilon = c_{10}\times(R-20) \quad \text{for R} < 20 \text{ km}$$
$$\varepsilon = 0 \quad \text{for R} > 20 \text{ km}$$

where D is either $D_{5\text{-}75}$ or $D_{5\text{-}95}$, M is the moment magnitude, R is the closest site to source distance in km, Vs_{30} is the time averaged shear wave velocity in the top 30 meters of the site in m/s, $z_{1.5}$ is the depth to a shear wave velocity equal to 1.5 km/s, $\Delta\sigma$ is the same as for the Abrahamson and Silva (1996) and b, c, and β are coefficients listed in Table 2E.9. Kempton and Stewart (2006) state that their model should only be used for magnitudes between 5 and 7.6 and R < 200 km. They also recommend assuming $z_{1.5}$ = 2000 meters when unknown and state that this assumption is not critical.

2E.7 References

Abrahamson, N.A., and Silva, W.J. (1996). "Empirical ground motion models." Report to Brookhaven National Laboratory; New York, NY, 144.

Alavi, B., and Krawinkler, H. (2000) "Consideration of near-fault ground motion effects in seismic design." Proc., 12th World Conf. on Earthquake Engng, Auckland, New Zealand, paper 2665.

Arias, A. (1970). "A Measure of Earthquake Intensity," in Hansen, R. J., ed., Seismic Design for Nuclear Power Plants: MIT Press, Cambridge, Mass., 438-483.

Bray, J. D., and Rodriguez-Marek, A. (1997). "Geotechnical Site Categories." Proceedings. First PEER, PG&E Workshop on Seismic Reliability of Utility Lifelines, San Francisco, CA, 1997.

Bray, J., Rodriguez-Marek, A., Gillie, J. (2009). "Design ground motions near active faults," *Bull. New Zealand Society for Earthquake Engineering*, 42 (1), 1-8.

Foulser-Piggot, R., and Stafford, P.J. (2011). "A predictive model for Arias intensity at multiple sites and consideration of spatial correlations." Earthquake Engng Struct. Dyn. (41)3, 431-451.

Kempton, J. J., and Stewart, J. P. (2006). "Prediction equations for significant duration of earthquake ground motions considering site and near-source effects." Earthquake Spectra (22) 4, 985-1013.

NIST (2012). "Selecting and scaling earthquake ground motions for performing response history analyses." NIST GCR 11-917-15, prepared by the NERHP Consultants Joint Venture for the National Institute of Standards and Technology, Gaithersburg, Maryland.

Rathje, E.M., Abrahamson, N.A., Bray, J.D. (1998). "Simplified frequency content estimates of earthquake ground motions." *J. Geotech. Geoenviron. Eng.,* ASCE, 124, p150-159.

Rathje, E.M., Faraj, F., Russell, S. and Bray, J.D. (2004). "Empirical relationships for frequency content parameters of earthquake ground motions." Earthquake Spectra 20(1), 119-144.

Shahi, S.K., and Baker, J.W. (2011) "An empirically calibrated framework for including the effects of near fault directivity in PSHA", Bull. Seismol. Soc. Amer., 101 (2), 742 -755.

Somerville, P. (2003). "Magnitude scaling of the near fault rupture directivity pulse." Physics of the Earth and Planetary Interiors 137, 201–212.
Stewart, J.P., Chiou, S., Bray, J.D., Graves, R.W., Somerville, P.G., Abrahamson, N.A. (2001). "Ground Motion Evaluation Procedures for Performance-Based Design." PEER Report 2001/09 Pacific Earthquake Engineering Research Center, University of California, Berkeley, California.
Travasarou, T., Bray, J.D. and Abrahamson, N.A. (2003). "Empirical attenuation relationship for Arias intensity," Earthquake Engng Struct. Dyn. (32) 7, 1133–1155.
Watson-Lamprey, J. and Abrahamson, N.A. (2006). "Selection of ground motion time series and limits on scaling," Soil Dynamics & Earthquake Engineering (26)5, 477-482.

Table 2E.1: Coefficients for the Bray et al. (2009) PGV model

	Soil sites	Rock-sites
a	2.11	1.86
b	0.55	0.55
c	-0.39	-0.39
d	5.00	5.00
σ_{total}	0.44	0.40

Table 2E.2: Coefficients for the Rathje et al. (2004) model of frequency content parameters

	T_m	T_o	T_{avg}
c_1	-1	-0.89	-1.78
c_2	0.18	0.29	0.3
c_3	0.0038	0.003	0.0045
c_4	0.078	0.07	0.15
c_5	0.27	0.25	0.33
c_6	0.4	0.37	0.24

Table 2E.3: Total standard error terms by NEHRP site class (after Rathje et al., 2004)

Site	T_m	T_o	T_{avg}
B	0.45	0.40	0.44
C	0.42	0.38	0.40
D	0.35	0.32	0.38

Table 2E.4: Coefficients of Travasarou et al. (2003) arias intensity model

c_1	c_2	c_3	c_4	h	s_{11}	s_{12}	s_{21}	s_{22}	f_1	f_2
2.799	-1.981	20.724	-1.703	8.775	0.454	0.101	0.479	0.334	-0.166	0.512

Table 2E.5: Parameters for calculation of σ for the Travasarou et al. (2003) I_a model

	B	C	D
σ_1	1.181	1.166	0.965
σ_2	0.942	0.972	0.726

Table 2E.6: Coefficients of Foulser-Piggot and Stafford (2011) arias intensity model

c_1	c_2	c_3	c_4	c_5	c_6	v_1	v_2	v_3	v_4
4.9862	-0.1939	-4.0332	0.2887	6.3049	0.3507	-1.1576	-0.4576	-0.0029	0.0818

Table 2E.7: Standard deviation coefficients for the Foulser-Piggot and Stafford (2011) arias intensity model

δ_1	δ_2	δ_3	σ_E	σ_A
-0.5921	3.8311	4.0762	0.6556	0.5978

Table 2E.8: Coefficients for the Abrahamson and Silva (1996) duration model

	β	b_1	b_2	c_1	c_2	D_{rat}	R_c	σ_{tot}
D_{5-75}	3.2	5.204	0.851	0.805	0.063	0	10	0.55
D_{5-95}	3.2	5.204	0.851	0.805	0.063	0.845	10	0.49

Table 2E.9: Coefficients for the Kempton and Stewart (2006) duration model

(SS = strike slip, DS = dip slip, BD = backward directivity, FD = forward directivity)

									c_{10}			
	b_1	b_2	β	c_2	c_4	c_5	c_6	c_7	SS (BD)	SS (FD)	DS	σ_{tot}
D_{5-75}	6.02	n/a	3.2	0.07	0.82	-0.0013	0.4	0.00005	0	0.016	0.02	0.53
D_{5-95}	2.79	0.82	3.2	0.15	3	-0.0041	-0.44	0.0012	0.015	0.015	0.015	0.44

APPENDIX 3A: GROUND MOTION DATABASES

Appendix 3A: Ground Motion Databases

Table 3A.1 through Table 3A.5 contain the "original" ground motions for scenarios ACR1, ACR2, ACR3, SUB and SCR with the corresponding values of moment magnitude and distance as well as the average shear wave velocity in the top 30 m of the deposit.

Table 3A.6 through Table 3A.10 contain the selected ground motions for scenarios ACR1, ACR2, ACR3, SUB and SCR after scaling and applying other constraints to match relevant ground motion measures (i.e., mean target response spectra and standard deviation, PGV, PGA among others).

Table 3A.1: Scenario ACR1 "original" ground motion database

NGA#	Event	Year	Station	M_w	R_{rup} (km)	V_{s30} (m/s)
77	San Fernando	1971	Pacoima Dam (upper left abut)	6.61	1.81	2016
285	Irpinia, Italy-01	1980	Bagnoli Irpinio	6.90	8.18	1000
292	Irpinia, Italy-01	1980	Sturno	6.90	10.84	1000
451	Morgan Hill	1984	Coyote Lake Dam (SW Abut)	6.19	0.53	597
459	Morgan Hill	1984	Gilroy Array #6	6.19	9.86	663
763	Loma Prieta	1989	Gilroy - Gavilan Coll.	6.93	9.96	729.7
779	Loma Prieta	1989	LGPC	6.93	3.88	477.7
825	Cape Mendocino	1992	Cape Mendocino	7.01	6.96	513.7
828	Cape Mendocino	1992	Petrolia	7.01	8.18	712.8
879	Landers	1992	Lucerne	7.28	2.19	1369
1013	Northridge-01	1994	LA Dam	6.69	5.92	629
1050	Northridge-01	1994	Pacoima Dam (downstr)	6.69	7.01	2016.1
1051	Northridge-01	1994	Pacoima Dam (upper left)	6.69	7.01	2016.1
1086	Northridge-01	1994	Sylmar - Olive View Med FF	6.69	5.3	440.5
1148	Kocaeli, Turkey	1999	Arcelik	7.51	13.49	523
1182	Chi-Chi, Taiwan	1999	CHY006	7.62	9.77	438.2
1476	Chi-Chi, Taiwan	1999	TCU029	7.62	28.05	473.9
1485	Chi-Chi, Taiwan	1999	TCU045	7.62	26	704.6
1486	Chi-Chi, Taiwan	1999	TCU046	7.62	16.74	465.6
1489	Chi-Chi, Taiwan	1999	TCU049	7.62	3.78	487.3
1493	Chi-Chi, Taiwan	1999	TCU053	7.62	5.97	454.6
1494	Chi-Chi, Taiwan	1999	TCU054	7.62	5.3	460.7
1505	Chi-Chi, Taiwan	1999	TCU068	7.62	0.32	487.3
1510	Chi-Chi, Taiwan	1999	TCU075	7.62	0.91	573
1511	Chi-Chi, Taiwan	1999	TCU076	7.62	2.76	615
1515	Chi-Chi, Taiwan	1999	TCU082	7.62	5.18	472.8
1519	Chi-Chi, Taiwan	1999	TCU087	7.62	7	473.9
1529	Chi-Chi, Taiwan	1999	TCU102	7.62	1.51	714.3
1530	Chi-Chi, Taiwan	1999	TCU103	7.62	6.1	494.1
1548	Chi-Chi, Taiwan	1999	TCU128	7.62	13.15	599.6
1550	Chi-Chi, Taiwan	1999	TCU136	7.62	8.29	473.9
2627	Chi-Chi, Taiwan-03	1999	TCU076	6.20	14.66	615
3473	Chi-Chi, Taiwan-06	1999	TCU078	6.30	11.52	443
3548	Loma Prieta	1989	Los Gatos - Lexington Dam	6.93	5.02	1070.3

Table 3A.2: Scenario ACR2 "original" ground motion database

NGA #	Earthquake	Year	Station	M_w	R_{rup} (km)	V_{s30} (m/s)
1	Helena, Montana-01	1935	Carroll College	6.0	2.86	659.6
2	Helena, Montana-02	1935	Helena Fed Bldg	6.0	2.92	659.6
28	Parkfield	1966	Cholame - Shandon Array #12	6.2	17.64	408.9
33	Parkfield	1966	Temblor pre-1969	6.2	15.96	527.9
71	San Fernando	1971	Lake Hughes #12	6.6	19.3	602.1
125	Friuli, Italy-01	1976	Tolmezzo	6.5	15.8	424.8
164	Imperial Valley-06	1979	Cerro Prieto	6.5	15.2	659.6
265	Victoria, Mexico	1990	Cerro Prieto	6.3	14.4	659.6
284	Irpinia, Italy-01	1980	Auletta	6.9	9.6	1000
289	Irpinia, Italy-01	1980	Calitri	6.9	17.6	600
296	Irpinia, Italy-02	1980	Bagnoli Irpinio	6.2	19.56	1000
297	Irpinia, Italy-02	1980	Bisaccia	6.2	14.4	659.6
300	Irpinia, Italy-02	1980	Calitri	6.2	8.8	600
448	Morgan Hill	1984	Anderson Dam (Downstream)	6.2	3.26	488.8
454	Morgan Hill	1984	Gilroy - Gavilan Coll.	6.2	14.84	729.7
455	Morgan Hill	1984	Gilroy Array #1	6.2	14.91	1428
495	Nahanni, Canada	1985	Site 1	6.8	9.6	659.6
497	Nahanni, Canada	1985	Site 3	6.8	5.32	659.6
537	N. Palm Springs	1986	Silent Valley - Poppet Flat	6.1	17.03	684.9
587	New Zealand-02	1987	Matahina Dam	6.6	16.1	424.8
589	Whittier Narrows-01	1987	Alhambra - Fremont School	6.0	14.66	550
594	Whittier Narrows-01	1987	Baldwin Park - N Holly	6.0	16.72	544.7
619	Whittier Narrows-01	1987	Garvey Res. - Control Bldg	6.0	14.5	468.2
632	Whittier Narrows-01	1987	LA - Cypress Ave	6.0	16.97	446
634	Whittier Narrows-01	1987	LA - Fletcher Dr	6.0	18.86	446
637	Whittier Narrows-01	1987	LA - N Figueroa St	6.0	16.53	405.2
675	Whittier Narrows-01	1987	Pasadena - CIT Athenaeum	6.0	17.24	415.1
680	Whittier Narrows-01	1987	Pasadena - CIT Kresge Lab	6.0	18.12	969.1
683	Whittier Narrows-01	1987	Pasadena - Old House Rd	6.0	19.17	455.4
690	Whittier Narrows-01	1987	San Gabriel - E Grand Ave	6.0	15.2	401.4
753	Loma Prieta	1989	Corralitos	6.9	3.9	462.2
765	Loma Prieta	1989	Gilroy Array #1	6.9	9.64	1428
769	Loma Prieta	1989	Gilroy Array #6	6.9	18.3	663.3
779	Loma Prieta	1989	LGPC	6.9	3.88	477.7
801	Loma Prieta	1989	San Jose - Santa Teresa Hills	6.9	14.7	671.8
809	Loma Prieta	1989	UCSC	6.9	18.5	714
810	Loma Prieta	1989	UCSC Lick Observatory	6.9	18.4	714

Table 3A.2: Scenario ACR2 "original" ground motion database (continued)

NGA #	Earthquake	Year	Station	M_w	R_{rup} (km)	V_{s30} (m/s)
825	Cape Mendocino	1992	Cape Mendocino	7.0	6.96	513.7
827	Cape Mendocino	1992	Fortuna-Fortuna Blvd	7.0	19.9	457.1
952	Northridge-01	1994	Beverly Hills - 12520 Mulhol	6.7	18.4	545.7
954	Northridge-01	1994	Big Tujunga, Angeles	6.7	19.7	446
957	Northridge-01	1994	Burbank - Howard Rd	6.7	16.9	821.7
983	Northridge-01	1994	Jensen Filter Plant Generator	6.7	5.43	525.8
1012	Northridge-01	1994	LA 00	6.7	19.1	706.2
1016	Northridge-01	1994	La Crescenta-New York	6.7	18.5	446
1042	Northridge-01	1994	N Hollywood - Coldwater	6.7	12.5	446
1052	Northridge-01	1994	Pacoima Kagel Canyon	6.7	7.3	508.1
1078	Northridge-01	1994	Santa Susan Ground	6.7	16.7	715.1
1080	Northridge-01	1994	Simi Valley - Katherine Rd	6.7	13.4	557.4
1083	Northridge-01	1994	Sunland-Mt Gleason Ave	6.7	13.3	446
1108	Kobe, Japan	1995	Kobe University	6.9	0.92	1043
1111	Kobe, Japan	1995	Nish-Akashi	6.9	7.1	609
1126	Kozani, Greece-01	1995	Kozani	6.4	19.54	659.6
1611	Duzce, Turkey	1999	Lamont 1058	7.1	0.21	424.8
1612	Duzce, Turkey	1999	Lamont 1059	7.1	4.17	424.8
1614	Duzce, Turkey	1999	Lamont 1061	7.1	11.5	481
1617	Duzce, Turkey	1999	Lamont 375	7.1	3.93	424.8
1618	Duzce, Turkey	1999	Lamont 531	7.1	8	659.6
1666	Northridge-02	1994	Pacoima Kagel Canyon	6.1	10.91	508.1
1787	Hector Mine	1999	Hector	7.1	10.3	684.9
2457	Chi-Chi, Taiwan-03	1999	CHY024	6.2	19.65	427.7
2622	Chi-Chi, Taiwan-03	1999	TCU071	6.2	16.46	624.9
2625	Chi-Chi, Taiwan-03	1999	TCU074	6.2	16.63	549.4
2626	Chi-Chi, Taiwan-03	1999	TCU075	6.2	19.65	573
2628	Chi-Chi, Taiwan-03	1999	TCU078	6.2	7.62	443
2632	Chi-Chi, Taiwan-03	1999	TCU084	6.2	9.3	680
2635	Chi-Chi, Taiwan-03	1999	TCU089	6.2	9.8	680
2655	Chi-Chi, Taiwan-03	1999	TCU122	6.2	19.3	475.5
2658	Chi-Chi, Taiwan-03	1999	TCU129	6.2	12.8	664
2699	Chi-Chi, Taiwan-04	1999	CHY024	6.2	19.73	427.7
2703	Chi-Chi, Taiwan-04	1999	CHY028	6.2	17.7	542.6
2734	Chi-Chi, Taiwan-04	1999	CHY074	6.2	6.2	553
2739	Chi-Chi, Taiwan-04	1999	CHY080	6.2	12.5	680
3470	Chi-Chi, Taiwan-06	1999	TCU072	6.3	13	468.1

Table 3A.2: Scenario ACR2 "original" ground motion database (continued)

NGA #	Earthquake	Year	Station	M_w	R_{rup} (km)	V_{s30} (m/s)
3744	Cape Mendocino	1992	Bunker Hill FAA	7.0	10.05	477.7
3746	Cape Mendocino	1992	Centerville Beach, Naval Fac	7.0	15.29	497
3907	Tottori, Japan	2000	OKY004	6.6	19.72	475.8
3925	Tottori, Japan	2000	OKYH07	6.6	15.23	940.2
3943	Tottori, Japan	2000	SMN015	6.6	9.12	616.5
3947	Tottori, Japan	2000	SMNH01	6.6	5.86	446.3
3954	Tottori, Japan	2000	SMNH10	6.6	15.59	424.8
3964	Tottori, Japan	2000	TTR007	6.6	11.29	469.8
3966	Tottori, Japan	2000	TTR009	6.6	8.83	420.2
4031	San Simeon, CA	2003	Templeton - 1-story Hospital	6.5	6.22	497
4040	Bam, Iran	2003	Bam	6.6	1.7	487.4
4067	Parkfield-02, CA	2004	Parkfield - GOLD HILL	6.0	3.43	424.8
4069	Parkfield-02, CA	2004	Parkfield - JACK CANYON	6.0	9.46	521.9
4075	Parkfield-02, CA	2004	Parkfield - WORK RANCH	6.0	10.77	424.8
4083	Parkfield-02, CA	2004	Parkfield - TURKEY FLAT #1 (0M)	6.0	5.29	1276
4084	Parkfield-02, CA	2004	Parkfield - 1-STORY SCHOOL BLDG	6.0	2.67	424.8
4096	Parkfield-02, CA	2004	BEAR VALLEY RANCH	6.0	4.32	424.8
4097	Parkfield-02, CA	2004	Slack Canyon	6.0	2.99	684.9
4103	Parkfield-02, CA	2004	Parkfield - Cholame 4W	6.0	4.23	438.3
4106	Parkfield-02, CA	2004	Parkfield - Cholame 12W	6.0	15.83	408.9
4110	Parkfield-02, CA	2004	Parkfield - Fault Zone 6	6.0	2.7	438.3
4113	Parkfield-02, CA	2004	Parkfield - Fault Zone 9	6.0	2.85	438.3
4122	Parkfield-02, CA	2004	Parkfield - Gold Hill 3W	6.0	5.41	438.3
4123	Parkfield-02, CA	2004	Parkfield - Gold Hill 4W	6.0	8.27	438.3
4124	Parkfield-02, CA	2004	Parkfield - Gold Hill 5W	6.0	11.52	438.3
4125	Parkfield-02, CA	2004	Parkfield - Gold Hill 6W	6.0	15.79	438.3
4129	Parkfield-02, CA	2004	Parkfield - TEMBLOR	6.0	12.54	424.8
4132	Parkfield-02, CA	2004	Parkfield - Vineyard Cany 2E	6.0	4.46	712.8
4137	Parkfield-02, CA	2004	Parkfield - Vineyard Cany 6W	6.0	13.7	438.3
4138	Parkfield-02, CA	2004	Parkfield - UPSAR 01	6.0	10.08	424.8
4139	Parkfield-02, CA	2004	Parkfield - UPSAR 02	6.0	9.95	424.8
4140	Parkfield-02, CA	2004	Parkfield - UPSAR 03	6.0	9.95	424.8
4141	Parkfield-02, CA	2004	Parkfield - UPSAR 05	6.0	9.61	424.8
4142	Parkfield-02, CA	2004	Parkfield - UPSAR 06	6.0	9.61	424.8
4143	Parkfield-02, CA	2004	Parkfield - UPSAR 07	6.0	9.61	424.8
4144	Parkfield-02, CA	2004	Parkfield - UPSAR 08	6.0	9.41	424.8

Table 3A.2: Scenario ACR2 "original" ground motion database (continued)

NGA #	Earthquake	Year	Station	M_w	R_{rup} (km)	V_{s30} (m/s)
4145	Parkfield-02, CA	2004	Parkfield - UPSAR 09	6.0	9.34	424.8
4146	Parkfield-02, CA	2004	Parkfield - UPSAR 10	6.0	9.14	424.8
4147	Parkfield-02, CA	2004	Parkfield - UPSAR 11	6.0	9.41	424.8
4148	Parkfield-02, CA	2004	Parkfield - UPSAR 12	6.0	9.47	424.8
4149	Parkfield-02, CA	2004	Parkfield - UPSAR 13	6.0	9.47	424.8
4211	Niigata, Japan	2004	NIG021	6.6	11.26	418.5
4229	Niigata, Japan	2004	NIGH12	6.6	10.72	564.3
4451	Montenegro, Yugo.	1979	Bar-Skupstina Opstine	7.1	6.98	424.8
4456	Montenegro, Yugo.	1979	Petrovac - Hotel Olivia	7.1	8.01	424.8
4457	Montenegro, Yugo.	1979	Ulcinj - Hotel Albatros	7.1	4.35	659.6
4458	Montenegro, Yugo.	1979	Ulcinj - Hotel Olimpic	7.1	5.76	424.8
4477	L'Aquila, Italy	2009	GRAN SASSO (Assergi)	6.3	6.4	488
4478	L'Aquila, Italy	2009	GRAN SASSO (Lab. INFN galleria)	6.3	11.15	1000
4480	L'Aquila, Italy	2009	L'Aquila - V. Aterno - Centro Valle	6.3	6.27	475
4481	L'Aquila, Italy	2009	L'Aquila - V. Aterno -Colle Grilli	6.3	6.81	685
4482	L'Aquila, Italy	2009	L'Aquila - V. Aterno -F. Aterno	6.3	6.55	552
4483	L'Aquila, Italy	2009	L'Aquila - Parking	6.3	5.38	717
4484	L'Aquila, Italy	2009	L'Aquila - V. Aterno - Il Moro	6.3	5.93	1000
4489	L'Aquila, Italy	2009	Montereale	6.3	15.77	515
4867	Chuetsu-oki	2007	Teradomari Uedamachi Nagaoka	6.8	15.19	523.1
4874	Chuetsu-oki	2007	Oguni Nagaoka	6.8	20	407.4
4876	Chuetsu-oki	2007	Kashiwazaki Nishiyamacho Ikeura	6.8	12.63	500
5478	Iwate	2008	AKT023	6.9	16.96	556
5482	Iwate	2008	AKTH04	6.9	17.94	458.7
5618	Iwate	2008	IWT010	6.9	16.27	825.8
5656	Iwate	2008	IWTH24	6.9	5.18	486.4
5657	Iwate	2008	IWTH25	6.9	4.8	506.4

Table 3A.3: Scenario ACR3 "original" ground motion database.

NGA #	Event	Year	Station	M_w	R_{rup} (km)	V_{s30} (m/s)
14	Kern County	1952	Santa Barbara Courthouse	7.4	82.19	515
572	Taiwan SMART1(45)	1986	SMART1 E02	7.3	51.38	659.6
830	Cape Mendocino	1992	Shelter Cove Airport	7.0	28.78	513.7
891	Landers	1992	Silent Valley - Poppet Flat	7.3	50.85	684.9
897	Landers	1992	Twentynine Palms	7.3	41.43	684.9
1154	Kocaeli, Turkey	1999	Bursa Sivil	7.5	65.53	659.6
1162	Kocaeli, Turkey	1999	Goynuk	7.5	31.74	424.8
1163	Kocaeli, Turkey	1999	Hava Alani	7.5	60.05	424.8
1164	Kocaeli, Turkey	1999	Istanbul	7.5	51.95	424.8
1169	Kocaeli, Turkey	1999	Maslak	7.5	55.3	659.6
1170	Kocaeli, Turkey	1999	Mecidiyekoy	7.5	53.43	424.8
1186	Chi-Chi, Taiwan	1999	CHY014	7.6	34.18	473.9
1190	Chi-Chi, Taiwan	1999	CHY019	7.6	50.53	473.9
1191	Chi-Chi, Taiwan	1999	CHY022	7.6	64.15	473.9
1206	Chi-Chi, Taiwan	1999	CHY042	7.6	28.17	553.4
1208	Chi-Chi, Taiwan	1999	CHY046	7.6	24.11	473.9
1210	Chi-Chi, Taiwan	1999	CHY050	7.6	44.76	473.9
1211	Chi-Chi, Taiwan	1999	CHY052	7.6	39.02	473.9
1214	Chi-Chi, Taiwan	1999	CHY057	7.6	56.93	411.5
1218	Chi-Chi, Taiwan	1999	CHY061	7.6	58.75	473.9
1230	Chi-Chi, Taiwan	1999	CHY079	7.6	47.53	473.9
1232	Chi-Chi, Taiwan	1999	CHY081	7.6	41.67	473.9
1234	Chi-Chi, Taiwan	1999	CHY086	7.6	28.42	553.4
1235	Chi-Chi, Taiwan	1999	CHY087	7.6	28.91	417.6
1245	Chi-Chi, Taiwan	1999	CHY102	7.6	37.72	553.4
1248	Chi-Chi, Taiwan	1999	CHY109	7.6	41.03	473.9
1249	Chi-Chi, Taiwan	1999	CHY110	7.6	41.03	473.9
1251	Chi-Chi, Taiwan	1999	ENA	7.6	66.88	553.4
1252	Chi-Chi, Taiwan	1999	ESL	7.6	44.54	553.4
1256	Chi-Chi, Taiwan	1999	HWA002	7.6	56.93	473.9
1257	Chi-Chi, Taiwan	1999	HWA003	7.6	56.14	473.9
1271	Chi-Chi, Taiwan	1999	HWA022	7.6	62.07	473.9
1272	Chi-Chi, Taiwan	1999	HWA023	7.6	51.15	553.4
1273	Chi-Chi, Taiwan	1999	HWA024	7.6	43.15	553.4
1274	Chi-Chi, Taiwan	1999	HWA025	7.6	53.79	473.9
1275	Chi-Chi, Taiwan	1999	HWA026	7.6	51.96	457.5
1280	Chi-Chi, Taiwan	1999	HWA031	7.6	51.46	473.9
1281	Chi-Chi, Taiwan	1999	HWA032	7.6	47.16	473.9

Table 3A.3: Scenario ACR3 "original" ground motion database (continued)

NGA #	Event	Year	Station	M_w	R_{rup} (km)	V_{s30} (m/s)
1284	Chi-Chi, Taiwan	1999	HWA035	7.6	48.35	473.9
1287	Chi-Chi, Taiwan	1999	HWA038	7.6	42.54	473.9
1291	Chi-Chi, Taiwan	1999	HWA044	7.6	58.22	473.9
1293	Chi-Chi, Taiwan	1999	HWA046	7.6	51.8	553.4
1301	Chi-Chi, Taiwan	1999	HWA056	7.6	41.1	511.3
1302	Chi-Chi, Taiwan	1999	HWA057	7.6	50.6	553.4
1303	Chi-Chi, Taiwan	1999	HWA058	7.6	45.77	553.4
1304	Chi-Chi, Taiwan	1999	HWA059	7.6	49.15	473.9
1305	Chi-Chi, Taiwan	1999	HWA060	7.6	57.51	473.9
1313	Chi-Chi, Taiwan	1999	ILA007	7.6	84.07	473.9
1315	Chi-Chi, Taiwan	1999	ILA010	7.6	80.18	473.9
1319	Chi-Chi, Taiwan	1999	ILA015	7.6	85.4	553.4
1321	Chi-Chi, Taiwan	1999	ILA021	7.6	76.9	473.9
1322	Chi-Chi, Taiwan	1999	ILA024	7.6	67.81	553.4
1325	Chi-Chi, Taiwan	1999	ILA031	7.6	83.31	649.3
1333	Chi-Chi, Taiwan	1999	ILA043	7.6	77.17	473.9
1338	Chi-Chi, Taiwan	1999	ILA050	7.6	66.88	473.9
1339	Chi-Chi, Taiwan	1999	ILA051	7.6	79.03	473.9
1340	Chi-Chi, Taiwan	1999	ILA052	7.6	85.13	553.4
1347	Chi-Chi, Taiwan	1999	ILA063	7.6	61.06	553.4
1350	Chi-Chi, Taiwan	1999	ILA067	7.6	38.82	553.4
1351	Chi-Chi, Taiwan	1999	KAU001	7.6	44.93	473.9
1358	Chi-Chi, Taiwan	1999	KAU012	7.6	84.61	473.9
1360	Chi-Chi, Taiwan	1999	KAU018	7.6	78.41	473.9
1375	Chi-Chi, Taiwan	1999	KAU047	7.6	54.95	473.9
1377	Chi-Chi, Taiwan	1999	KAU050	7.6	40.49	553.4
1380	Chi-Chi, Taiwan	1999	KAU054	7.6	30.85	473.9
1387	Chi-Chi, Taiwan	1999	KAU069	7.6	70.71	473.9
1391	Chi-Chi, Taiwan	1999	KAU077	7.6	82.96	553.4
1392	Chi-Chi, Taiwan	1999	KAU078	7.6	88.99	473.9
1400	Chi-Chi, Taiwan	1999	NCU	7.6	80.44	473.9
1401	Chi-Chi, Taiwan	1999	NSK	7.6	58.09	553.4
1406	Chi-Chi, Taiwan	1999	SSD	7.6	85.75	473.9
1407	Chi-Chi, Taiwan	1999	STY	7.6	40.49	553.4
1427	Chi-Chi, Taiwan	1999	TAP035	7.6	89.91	438.1
1428	Chi-Chi, Taiwan	1999	TAP036	7.6	88.45	553.4
1463	Chi-Chi, Taiwan	1999	TCU003	7.6	86.57	517.3
1464	Chi-Chi, Taiwan	1999	TCU006	7.6	72.61	473.9

Table 3A.3: Scenario ACR3 "original" ground motion database (continued)

NGA #	Event	Year	Station	M_w	R_{rup} (km)	V_{s30} (m/s)
1465	Chi-Chi, Taiwan	1999	TCU007	7.6	88.2	473.9
1466	Chi-Chi, Taiwan	1999	TCU008	7.6	85.09	473.9
1467	Chi-Chi, Taiwan	1999	TCU009	7.6	81.08	460.1
1468	Chi-Chi, Taiwan	1999	TCU010	7.6	82.27	473.9
1471	Chi-Chi, Taiwan	1999	TCU015	7.6	49.81	473.9
1472	Chi-Chi, Taiwan	1999	TCU017	7.6	54.28	558.8
1473	Chi-Chi, Taiwan	1999	TCU018	7.6	66.25	473.9
1474	Chi-Chi, Taiwan	1999	TCU025	7.6	52.98	553.4
1475	Chi-Chi, Taiwan	1999	TCU026	7.6	56.12	473.9
1476	Chi-Chi, Taiwan	1999	TCU029	7.6	28.05	473.9
1477	Chi-Chi, Taiwan	1999	TCU031	7.6	30.18	473.9
1478	Chi-Chi, Taiwan	1999	TCU033	7.6	40.89	423.4
1479	Chi-Chi, Taiwan	1999	TCU034	7.6	35.69	473.9
1485	Chi-Chi, Taiwan	1999	TCU045	7.6	26	704.6
1487	Chi-Chi, Taiwan	1999	TCU047	7.6	35	520.4
1516	Chi-Chi, Taiwan	1999	TCU083	7.6	80.32	473.9
1518	Chi-Chi, Taiwan	1999	TCU085	7.6	58.09	553.4
1522	Chi-Chi, Taiwan	1999	TCU092	7.6	88.07	473.9
1523	Chi-Chi, Taiwan	1999	TCU094	7.6	54.53	589.9
1524	Chi-Chi, Taiwan	1999	TCU095	7.6	45.18	446.6
1525	Chi-Chi, Taiwan	1999	TCU096	7.6	54.46	473.9
1555	Chi-Chi, Taiwan	1999	TCU147	7.6	71.27	537.9
1558	Chi-Chi, Taiwan	1999	TTN002	7.6	68.71	473.9
1561	Chi-Chi, Taiwan	1999	TTN005	7.6	82.84	473.9
1572	Chi-Chi, Taiwan	1999	TTN018	7.6	74.45	473.9
1576	Chi-Chi, Taiwan	1999	TTN024	7.6	60.01	553.4
1577	Chi-Chi, Taiwan	1999	TTN025	7.6	65.79	473.9
1578	Chi-Chi, Taiwan	1999	TTN026	7.6	70.33	473.9
1580	Chi-Chi, Taiwan	1999	TTN028	7.6	78.48	473.9
1582	Chi-Chi, Taiwan	1999	TTN032	7.6	57.65	473.9
1584	Chi-Chi, Taiwan	1999	TTN036	7.6	80	473.9
1585	Chi-Chi, Taiwan	1999	TTN040	7.6	48.33	473.9
1586	Chi-Chi, Taiwan	1999	TTN041	7.6	45.35	418.2
1587	Chi-Chi, Taiwan	1999	TTN042	7.6	65.25	473.9
1588	Chi-Chi, Taiwan	1999	TTN044	7.6	58.97	473.9
1590	Chi-Chi, Taiwan	1999	TTN046	7.6	65.9	473.9
1591	Chi-Chi, Taiwan	1999	TTN047	7.6	74	473.9
1593	Chi-Chi, Taiwan	1999	TTN050	7.6	89.28	473.9

Table 3A.3: Scenario ACR3 "original" ground motion database (continued)

NGA #	Event	Year	Station	M_w	R_{rup} (km)	V_{s30} (m/s)
1594	Chi-Chi, Taiwan	1999	TTN051	7.6	36.7	553.4
1613	Duzce, Turkey	1999	Lamont 1060	7.1	25.88	782
1616	Duzce, Turkey	1999	Lamont 362	7.1	23.41	517
1619	Duzce, Turkey	1999	Mudurnu	7.1	34.3	659.6
1620	Duzce, Turkey	1999	Sakarya	7.1	45.16	471
1626	Sitka, Alaska	1972	Sitka Observatory	7.7	34.61	659.6
1763	Hector Mine	1999	Anza - Pinyon Flat	7.1	89.98	724.9
1767	Hector Mine	1999	Banning - Twin Pines Road	7.1	83.43	684.9
1786	Hector Mine	1999	Heart Bar State Park	7.1	61.21	684.9
1795	Hector Mine	1999	Joshua Tree N.M. - Keys View	7.1	50.42	684.9
1832	Hector Mine	1999	Seven Oaks Dam Project Office	7.1	87.2	659.6
1836	Hector Mine	1999	Twentynine Palms	7.1	42.06	684.9
2107	Denali, Alaska	2002	Carlo (temp)	7.9	50.94	963.9
2111	Denali, Alaska	2002	R109 (temp)	7.9	43	963.9
3745	Cape Mendocino	1992	Butler Valley Station 2	7.0	43.15	477.7
3750	Cape Mendocino	1992	Loleta Fire Station	7.0	23.74	455
4453	Montenegro, Yugo.	1979	Dubrovnik - Pomorska Skola	7.1	66.67	659.6
4455	Montenegro, Yugo.	1979	Herceg Novi - O.S.D. Paviviv	7.1	25.55	659.6
4716	Wenchuan, China	2008	Deyangbaima	7.9	30.49	418.2
4740	Wenchuan, China	2008	Maoxiandiban	7.9	22.31	760
4742	Wenchuan, China	2008	Maoxiannanxin	7.9	21.85	430
4758	Wenchuan, China	2008	Qionglaiyouzha	7.9	42.14	508.5
4781	Wenchuan, China	2008	Jiangyouchonghua	7.9	27.23	430.5
4787	Wenchuan, China	2008	Jiangyoudizhentai	7.9	22.63	474.6
4792	Wenchuan, China	2008	Lushan	7.9	82.75	587.2
4793	Wenchuan, China	2008	Mingshan	7.9	83.79	600.4
4802	Wenchuan, China	2008	Baoxingdizhenju	7.9	71.01	760
5826	El Mayor-Cucapah	2010	Heroes Of The Revolution	7.2	80.95	659.6
5828	El Mayor-Cucapah	2010	Rancho Agua Caliente	7.2	82.26	659.6
5830	El Mayor-Cucapah	2010	Rancho San Luis	7.2	45.47	659.6
5834	El Mayor-Cucapah	2010	Valle de la Trinidad	7.2	89.93	424.8
5842	El Mayor-Cucapah	2010	Anza Borrego S.P. - Tierra Blan	7.2	57.95	659.6
6891	Darfield, New Zealand	2010	CSHS	7.0	43.6	659.6
6928	Darfield, New Zealand	2010	LPCC	7.0	25.67	659.6
6931	Darfield, New Zealand	2010	LTZ	7.0	89.18	659.6
6949	Darfield, New Zealand	2010	PEEC	7.0	53.75	424.8
6963	Darfield, New Zealand	2010	RPZ	7.0	57.65	659.6
6980	Darfield, New Zealand	2010	WAKC	7.0	72.5	424.8
6992	Darfield, New Zealand	2010	LSRC	7.0	79.53	424.8
8163	El Mayor-Cucapah	2010	SANTA ISABEL VIEJO	7.2	57.49	659.6

Table 3A.4: Scenario SUB "original" ground motion database.

ID	Event	Year	Station	M_w	R_{rup} (km)	V_{s30} (m/s)
SUB8	West Canada 9	Synth	N/A	9.0	112.4	A
SUB24	West Canada 9	Synth	N/A	9.0	156.7	A
SUB30	Michoacán, Mexico	1985	Papanoa	8.1	86	Rock
SUB31	Michoacán, Mexico	1985	El Suchil	8.1	130	Rock
SUB32	Michoacán, Mexico	1985	Atoyac	8.1	147	Rock
SUB34	Michoacán, Mexico	1985	El Cayaco	8.1	171	Rock
SUB35	Michoacán, Mexico	1985	Coyuca	8.1	190	Rock
SUB39	Maule, Chile	2010	Santiago Puente Alto	8.8	75	540
SUB40	Maule, Chile	2010	Cerro Santa Lucia	8.8	77.4	540
SUB41	Maule, Chile	2010	Los Vilos (Punta de Chungos)	8.8	177.9	1122
SUB42	Maule, Chile	2010	Santiago La Florida	8.8	96.1	540
SUB43	Maule, Chile	2010	Papudo	8.8	116.2	517
SUB44	Maule, Chile	2010	Recinto d. SHOA, Cerro El Roble	8.8	92.7	540
SUB45	Maule, Chile	2010	Municip. San Jose de Maipo	8.8	87.3	449.7
SUB47	South Peru	2001	Arica	8.4	139	432
SUB48	South Peru	2001	Arica Costanera	8.4	138	389
SUB49	South Peru	2001	Cuya	8.4	192	540
SUB50	South Peru	2001	Moquegua	8.4	71	573
SUB51	South Peru	2001	Putre	8.4	191	1050
SUB52	South Peru	2001	Poconchile	8.4	158	511
SUB53	Tohoku	2011	Yokote	9.0	120.5	505
SUB54	Tohoku	2011	Tsubakidai	9.0	105.3	430
SUB55	Tohoku	2011	Yanagawa	9.0	84.6	468
SUB56	Tohoku	2011	Shimogoh	9.0	124.7	546
SUB57	Tohoku	2011	Shimodate	9	105	511
SUB58	Tohoku	2011	Kuroiso	9	102	482
SUB59	Tohoku	2011	Ogawa	9	94	465
SUB61	Cascadia 4	Synth	Seattle	8.5	157	B/C
SUB62	Cascadia 3	Synth	Victoria	8.5	103	B/C
SUB63	Cascadia 2	Synth	Seattle	9	130	B/C
SUB64	Cascadia 1	Synth	Victoria	9	112	B/C
SUB65	Tokachi-oki	2003	Tomuraushi	8.3	105	611
SUB66	Tokachi-oki	2003	Yuni	8.3	112	470
SUB67	Tokachi-oki	2003	Minamifurano	8.3	100	504
SUB68	Tokachi-oki	2003	Rikubetsu	8.3	98	442
SUB69	Tokachi-oki	2003	Yuhbari	8.3	102	627

ID numbers were chosen by the author. Synth motions are synthetic motions. Letter values in V_{s30} column are for estimated NERHP soil types.

Table 3A.5: Scenario SCR "Original" ground motion database.

ID	Event	Year	Station	M_w	R_{epi} (km)	V_{s30} (m/s)
SCR1	Arcadia OK	2010	OK005	4.2	5.9	unk
SCR2	East Canada 7a	synth	synth	7.0	19.6	A
SCR3	East Canada 7b	synth	synth	7.0	17.0	A
SCR4	East Canada 6a	synth	synth	6.0	17.0	A
SCR5	East Canada 6b	synth	synth	6.0	17.0	A
SCR6	East Canada 6c	synth	synth	6.0	17.0	A
SCR7	Gazli, USSR	1976	Karakyr	6.8	12.8	660
SCR8	Greenbrier AR	2011	WHAR	4.7	5.2	unk
SCR9	Greenbrier AR	2011	X201	4.7	3.2	unk
SCR10	Greenbrier AR	2011	X301	4.7	6.5	unk
SCR11	Guy AR	2010	X201	4.4	1.2	unk
SCR12	Guy AR	2010	WHAR	4.2	3.5	unk
SCR13	La Malbaie QC	1997	Sainte Mathilde	4.3	14.5	2000
SCR14	Mineral VA	2011	VA Corbin(Fredricksberg Obs)	5.7	57.5	B
SCR15	Mineral VA	2011	VA Charlottesville	5.7	53.5	A
SCR16	Mineral VA	2011	VA Reston Fire St 25	5.7	121.6	unk
SCR17	Mineral VA	2011	11809	5.7	52.1	unk
SCR18	Mineral VA	2011	NANPP	5.7	18.6	unk
SCR19	Mineral VA Aftershock	2011	Hadensville - Fire Dept	4.5	13.9	unk
SCR20	Miramichi, NB	1982	Mitchell Lake Rd	4.1	6.3	unk
SCR21	Mt Carmel IL	2008	OLIL	5.3	36.4	475
SCR22	Mt Carmel IL	2008	WVIL	5.3	9.7	670
SCR23	Nahanni 0	1985	Site 2	4.4	6.1	660
SCR24	Nahanni 1	1985	Site 1	6.9	6.9	660
SCR25	Nahanni 1	1985	Site 2	6.9	6.1	660
SCR26	Nahanni 1	1985	Site 3	6.9	22.4	660
SCR27	Nahanni 2	1985	Site 1	5.4	6.9	660
SCR28	Nahanni 3	1985	Site 3	5.7	22.4	660
SCR29	Riviere du Loup QC	2005	Saint Andre	4.6	5.9	2000
SCR30	Riviere du Loup QC	2005	Sainte Mathilde	4.6	27.7	2000
SCR31	Riviere du Loup QC	2005	Saint Simeon	4.6	14.8	2000
SCR32	Riviere du Loup QC	2005	RDLQ	4.6	17.2	unk
SCR33	Riviere du Loup QC	2005	STPQ	4.6	25.5	unk
SCR34	Riviere du Loup QC	2005	KAMO	4.6	32.4	unk

ID numbers were chosen by the author. Synth motions are synthetic motions. Letter values in V_{s30} column are for estimated NERHP soil types, unk = unknown

Table 3A.5: Scenario SCR "Original" ground motion database (continued)

ID	Event	Year	Station	M_w	R_{epi} (km)	V_{s30} (m/s)
SCR36	Saguenay QC	1988	CHIQ	5.9	50.5	Unk
SCR37	Saguenay QC	1988	LMBQ	5.9	95.5	Unk
SCR38	Saguenay QC	1988	LMQ	5.9	91.4	A
SCR39	Saguenay QC	1988	SANQ	5.9	60.5	unk
SCR40	Saguenay QC	1988	Dickey	5.9	194.8	unk
SCR41	Sparks OK	2011	OK002	5.6	40.8	unk
SCR42	Sparks OK	2011	OK010	5.6	44.3	unk
SCR43	Tabas, Iran	1978	Dayhook	7.4	13.9	660
SCR44	Tabas, Iran	1978	Tabas	7.4	2.0	767
SCR45	Val des Bois QC	2010	OT004	5.0	63.3	898
SCR46	Val des Bois QC	2010	OT006	5.0	53.6	900
SCR47	Val des Bois QC	2010	OT008	5.0	62.2	580

ID numbers were chosen by the author. Synth motions are synthetic motions. Letter values in V_{s30} column are for estimated NERHP soil types, unk = uknown.

Table 3A.6: Scenario ACR1 selected ground motion database (11 records)

NGA#	Event	Year	Station	M_w	R_{rup} (km)	V_{s30} (m/s)
77	San Fernando	1971	Pacoima Dam (upper left abut)	6.61	1.81	2016
285	Irpinia, Italy-01	1980	Bagnoli Irpinio	6.90	8.18	1000
292	Irpinia, Italy-01	1980	Sturno	6.90	10.84	1000
763	Loma Prieta	1989	Gilroy - Gavilan Coll.	6.93	9.96	729.7
825	Cape Mendocino	1992	Cape Mendocino	7.01	6.96	513.7
879	Landers	1992	Lucerne	7.28	2.19	1369
1050	Northridge-01	1994	Pacoima Dam (downstr)	6.69	7.01	2016.1
1051	Northridge-01	1994	Pacoima Dam (upper left)	6.69	7.01	2016.1
1148	Kocaeli, Turkey	1999	Arcelik	7.51	13.49	523
1486	Chi-Chi, Taiwan	1999	TCU046	7.62	16.74	465.6
3473	Chi-Chi, Taiwan-06	1999	TCU078	6.30	11.52	443

Table 3A.7: Scenario ACR2 selected ground motion database (40 records)

NGA #	Earthquake	Year	Station	M_w	R_{rup} (km)	V_{s30} (m/s)
28	Parkfield	1966	Cholame - Shandon Array #12	6.2	17.64	408.9
33	Parkfield	1966	Temblor pre-1969	6.2	15.96	527.9
125	Friuli, Italy-01	1976	Tolmezzo	6.5	15.8	424.8
164	Imperial Valley-06	1979	Cerro Prieto	6.5	15.2	659.6
265	Victoria, Mexico	1990	Cerro Prieto	6.3	14.4	659.6
284	Irpinia, Italy-01	1980	Auletta	6.9	9.6	1000
448	Morgan Hill	1984	Anderson Dam (Downstream)	6.2	3.26	488.8
587	New Zealand-02	1987	Matahina Dam	6.6	16.1	424.8
690	Whittier Narrows-01	1987	San Gabriel - E Grand Ave	6.0	15.2	401.4
753	Loma Prieta	1989	Corralitos	6.9	3.9	462.2
769	Loma Prieta	1989	Gilroy Array #6	6.9	18.3	663.3
801	Loma Prieta	1989	San Jose - Santa Teresa Hills	6.9	14.7	671.8
809	Loma Prieta	1989	UCSC	6.9	18.5	714
952	Northridge-01	1994	Beverly Hills - 12520 Mulhol	6.7	18.4	545.7
957	Northridge-01	1994	Burbank - Howard Rd	6.7	16.9	821.7
1012	Northridge-01	1994	LA 00	6.7	19.1	706.2
1078	Northridge-01	1994	Santa Susan Ground	6.7	16.7	715.1
1111	Kobe, Japan	1995	Nish-Akashi	6.9	7.1	609
1612	Duzce, Turkey	1999	Lamont 1059	7.1	4.17	424.8
1618	Duzce, Turkey	1999	Lamont 531	7.1	8	659.6
1787	Hector Mine	1999	Hector	7.1	10.3	684.9
2622	Chi-Chi, Taiwan-03	1999	TCU071	6.2	16.46	624.9
2703	Chi-Chi, Taiwan-04	1999	CHY028	6.2	17.7	542.6
3470	Chi-Chi, Taiwan-06	1999	TCU072	6.3	13	468.1
3746	Cape Mendocino	1992	Centerville Beach, Naval Fac	7.0	15.29	497
3943	Tottori, Japan	2000	SMN015	6.6	9.12	616.5
3966	Tottori, Japan	2000	TTR009	6.6	8.83	420.2
4031	San Simeon, CA	2003	Templeton - 1-story Hospital	6.5	6.22	497
4096	Parkfield-02, CA	2004	BEAR VALLEY RANCH	6.0	4.32	424.8
4106	Parkfield-02, CA	2004	Parkfield - Cholame 12W	6.0	15.83	408.9
4132	Parkfield-02, CA	2004	Parkfield - Vineyard Cany 2E	6.0	4.46	712.8
4137	Parkfield-02, CA	2004	Parkfield - Vineyard Cany 6W	6.0	13.7	438.3
4229	Niigata, Japan	2004	NIGH12	6.6	10.72	564.3
4456	Montenegro, Yugo.	1979	Petrovac - Hotel Olivia	7.1	8.01	424.8
4457	Montenegro, Yugo.	1979	Ulcinj - Hotel Albatros	7.1	4.35	659.6
4477	L'Aquila, Italy	2009	GRAN SASSO (Assergi)	6.3	6.4	488
4480	L'Aquila, Italy	2009	L'Aquila - V. Aterno - Centro Valle	6.3	6.27	475
4482	L'Aquila, Italy	2009	L'Aquila - V. Aterno -F. Aterno	6.3	6.55	552
4489	L'Aquila, Italy	2009	Montereale	6.3	15.77	515
5478	Iwate	2008	AKT023	6.9	16.96	556

Table 3A.8: Scenario ACR3 selected ground motion database (40 records)

NGA #	Event	Year	Station	M_w	R_{rup} (km)	V_{s30} (m/s)
572	Taiwan SMART1(45)	1986	SMART1 E02	7.3	51.38	659.6
891	Landers	1992	Silent Valley - Poppet Flat	7.3	50.85	684.9
897	Landers	1992	Twentynine Palms	7.3	41.43	684.9
1162	Kocaeli, Turkey	1999	Goynuk	7.5	31.74	424.8
1163	Kocaeli, Turkey	1999	Hava Alani	7.5	60.05	424.8
1164	Kocaeli, Turkey	1999	Istanbul	7.5	51.95	424.8
1169	Kocaeli, Turkey	1999	Maslak	7.5	55.3	659.6
1170	Kocaeli, Turkey	1999	Mecidiyekoy	7.5	53.43	424.8
1190	Chi-Chi, Taiwan	1999	CHY019	7.6	50.53	473.9
1191	Chi-Chi, Taiwan	1999	CHY022	7.6	64.15	473.9
1214	Chi-Chi, Taiwan	1999	CHY057	7.6	56.93	411.5
1218	Chi-Chi, Taiwan	1999	CHY061	7.6	58.75	473.9
1230	Chi-Chi, Taiwan	1999	CHY079	7.6	47.53	473.9
1272	Chi-Chi, Taiwan	1999	HWA023	7.6	51.15	553.4
1284	Chi-Chi, Taiwan	1999	HWA035	7.6	48.35	473.9
1377	Chi-Chi, Taiwan	1999	KAU050	7.6	40.49	553.4
1474	Chi-Chi, Taiwan	1999	TCU025	7.6	52.98	553.4
1594	Chi-Chi, Taiwan	1999	TTN051	7.6	36.7	553.4
1616	Duzce, Turkey	1999	Lamont 362	7.1	23.41	517
1626	Sitka, Alaska	1972	Sitka Observatory	7.7	34.61	659.6
1763	Hector Mine	1999	Anza - Pinyon Flat	7.1	89.98	724.9
1786	Hector Mine	1999	Heart Bar State Park	7.1	61.21	684.9
1795	Hector Mine	1999	Joshua Tree N.M. - Keys View	7.1	50.42	684.9
1836	Hector Mine	1999	Twentynine Palms	7.1	42.06	684.9
2107	Denali, Alaska	2002	Carlo (temp)	7.9	50.94	963.9
2111	Denali, Alaska	2002	R109 (temp)	7.9	43	963.9
4716	Wenchuan, China	2008	Deyangbaima	7.9	30.49	418.2
4740	Wenchuan, China	2008	Maoxiandiban	7.9	22.31	760
4742	Wenchuan, China	2008	Maoxiannanxin	7.9	21.85	430
4758	Wenchuan, China	2008	Qionglaiyouzha	7.9	42.14	508.5
4781	Wenchuan, China	2008	Jiangyouchonghua	7.9	27.23	430.5
4787	Wenchuan, China	2008	Jiangyoudizhentai	7.9	22.63	474.6
5826	El Mayor-Cucapah	2010	Heroes Of The Revolution	7.2	80.95	659.6
5834	El Mayor-Cucapah	2010	Valle de la Trinidad	7.2	89.93	424.8
5842	El Mayor-Cucapah	2010	Anza Borrego S.P. - Tierra Blan	7.2	57.95	659.6
6891	Darfield, New Zealand	2010	CSHS	7.0	43.6	659.6
6928	Darfield, New Zealand	2010	LPCC	7.0	25.67	659.6
6949	Darfield, New Zealand	2010	PEEC	7.0	53.75	424.8
6992	Darfield, New Zealand	2010	LSRC	7.0	79.53	424.8
8163	El Mayor-Cucapah	2010	SANTA ISABEL VIEJO	7.2	57.49	659.6

Table 3A.9: Scenario SUB selected ground motion database (11 records)

ID	Event	Year	Station	M_w	R_{rup} (km)	V_{s30} (m/s)
SUB32	Michoacan, Mexico	1985	Atoyac	8.1	147	Rock
SUB35	Michoacan, Mexico	1985	Coyuca	8.1	190	Rock
SUB40	Maule, Chile	2010	Cerro Santa Lucia	8.8	77.4	540
SUB42	Maule, Chile	2010	Santiago La Florida	8.8	96.1	540
SUB52	South Peru	2001	Poconchile	8.4	158	511
SUB53	Tohoku	2011	Yokote	9.0	120.5	505
SUB54	Tohoku	2011	Tsubakidai	9.0	105.3	430
SUB58	Tohoku	2011	Kuroiso	9	102	482
SUB62	Cascadia 3	Synth	Victoria	8.5	103	B/C
SUB64	Cascadia 1	Synth	Victoria	9	112	B/C
SUB65	Tokachi-oki	2003	Tomuraushi	8.3	105	611

ID numbers were chosen by the author. Synth motions are synthetic motions. Letter values in V_{s30} column are for estimated NERHP soil types.

Table 3A.10: Scenario SCR selected ground motion database (11 records)

ID	Event	Year	Station	M_w	R_{epi} (km)	V_{s30} (m/s)
SCR2	East Canada 7a	synth	synth	7.0	19.6	A
SCR3	East Canada 7b	synth	synth	7.0	17.0	A
SCR5	East Canada 6b	synth	synth	6.0	17.0	A
SCR14	Mineral VA	2011	VA Corbin(Fredricksberg Obs)	5.7	57.5	B
SCR15	Mineral VA	2011	VA Charlottesville	5.7	53.5	A
SCR23	Nahanni 0	1985	Site 2	4.4	6.1	660
SCR25	Nahanni 1	1985	Site 2	6.9	6.1	660
SCR26	Nahanni 1	1985	Site 3	6.9	22.4	660
SCR30	Riviere du Loup QC	2005	Sainte Mathilde	4.6	27.7	2000
SCR31	Riviere du Loup QC	2005	Saint Simeon	4.6	14.8	2000
SCR38	Saguenay QC	1988	LMQ	5.9	91.4	A
SCR44	Tabas, Iran	1978	Tabas	7.4	2.0	767

ID numbers were chosen by the author. Synth motions are synthetic motions. Letter values in V_{s30} column are for estimated NERHP soil types.

APPENDIX 3B: SCENARIO ACR1 GROUND MOTION DATA

Appendix 3B-F: Properties of Selected Acceleration Time Series

Appendices 3B to 3F contain one page summaries for each selected ground motion in scenarios ACR1, ACR2, ACR3, SUB, and SCR, respectively. Each summary shows the scaled acceleration, velocity and displacement time series, the Husid plot describing the build-up of the Arias intensity versus time, and the scaled response spectrum compared with the target mean and mean plus and minus one standard deviation response spectra for each ground motion. The summary also contains a table listing the PGA, PGV, PGD, I_a, T_m and $D_{5\text{-}95}$ (and T_v for scenario ACR1) for the rotated (i.e., maximum direction motion) and the scaled motion.

For scenarios ACR2 and ACR3 (appendices 3C and 3D), the summary page contains both the scaled motion and the spectrally matched motion. The summary table contains a listing of the PGA, PGV, PGD, I_a, T_m and $D_{5\text{-}95}$ for the rotated, scaled, and spectrally matched motion.

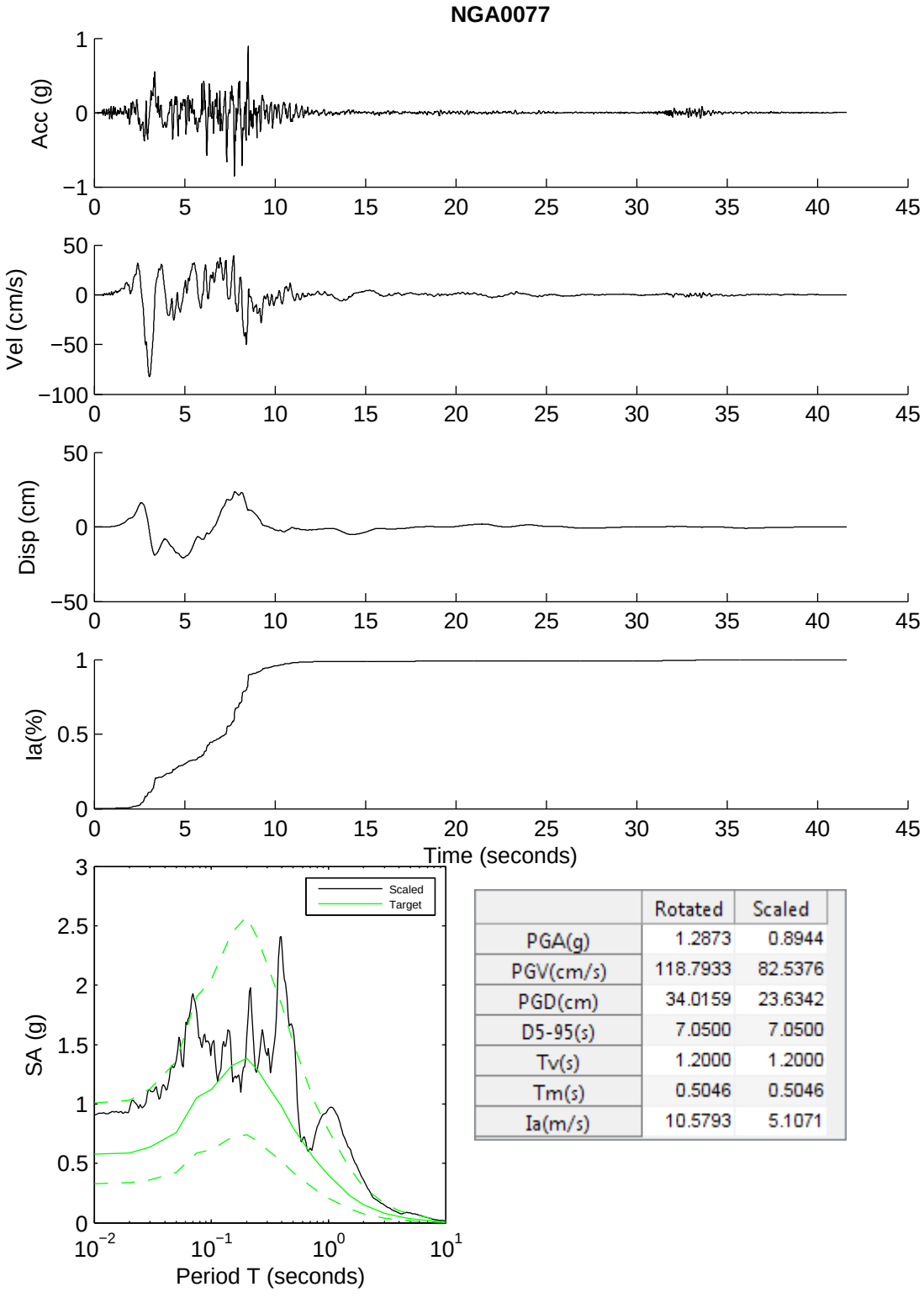

	Rotated	Scaled
PGA(g)	1.2873	0.8944
PGV(cm/s)	118.7933	82.5376
PGD(cm)	34.0159	23.6342
D5-95(s)	7.0500	7.0500
Tv(s)	1.2000	1.2000
Tm(s)	0.5046	0.5046
Ia(m/s)	10.5793	5.1071

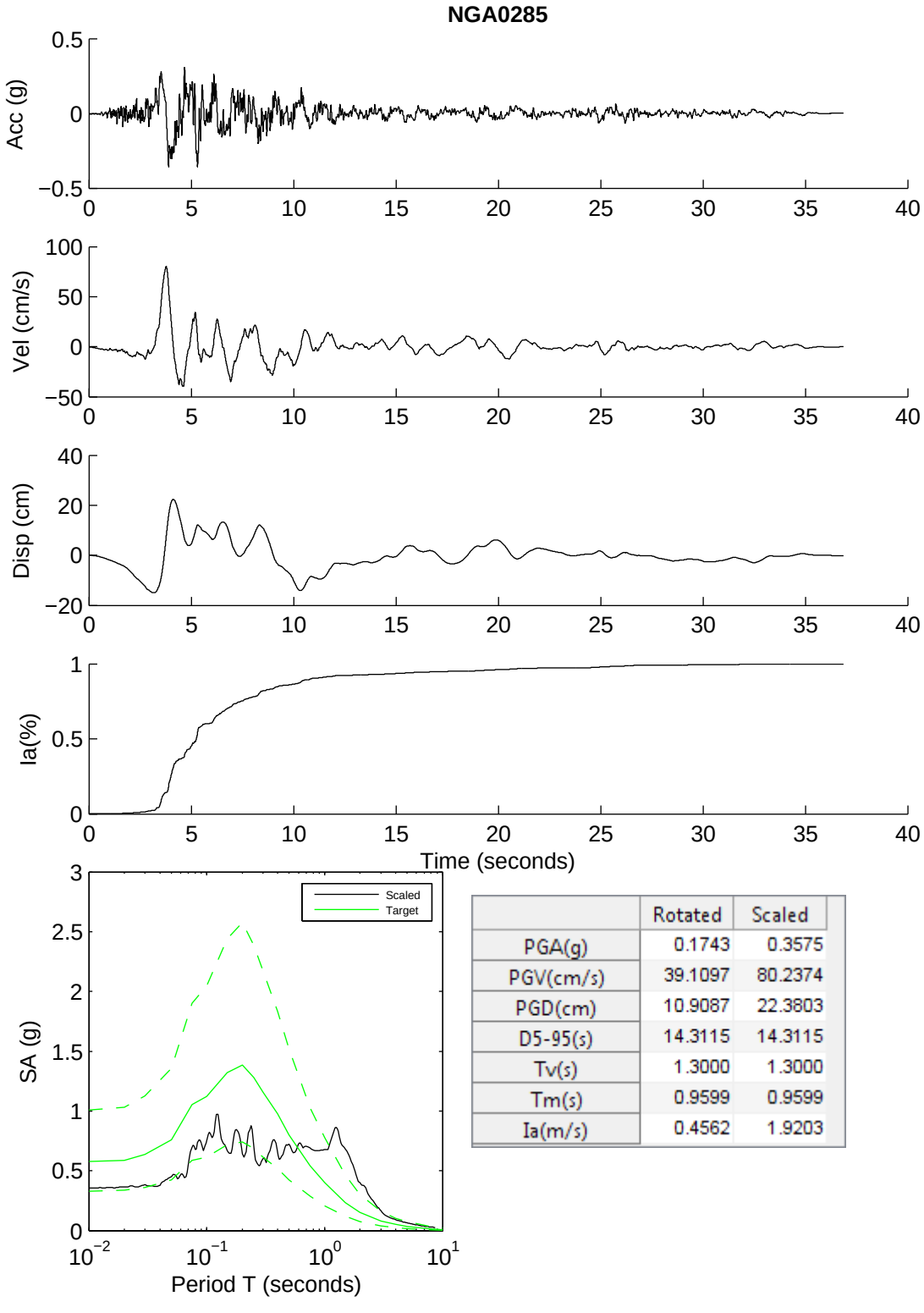

	Rotated	Scaled
PGA(g)	0.1743	0.3575
PGV(cm/s)	39.1097	80.2374
PGD(cm)	10.9087	22.3803
D5-95(s)	14.3115	14.3115
Tv(s)	1.3000	1.3000
Tm(s)	0.9599	0.9599
Ia(m/s)	0.4562	1.9203

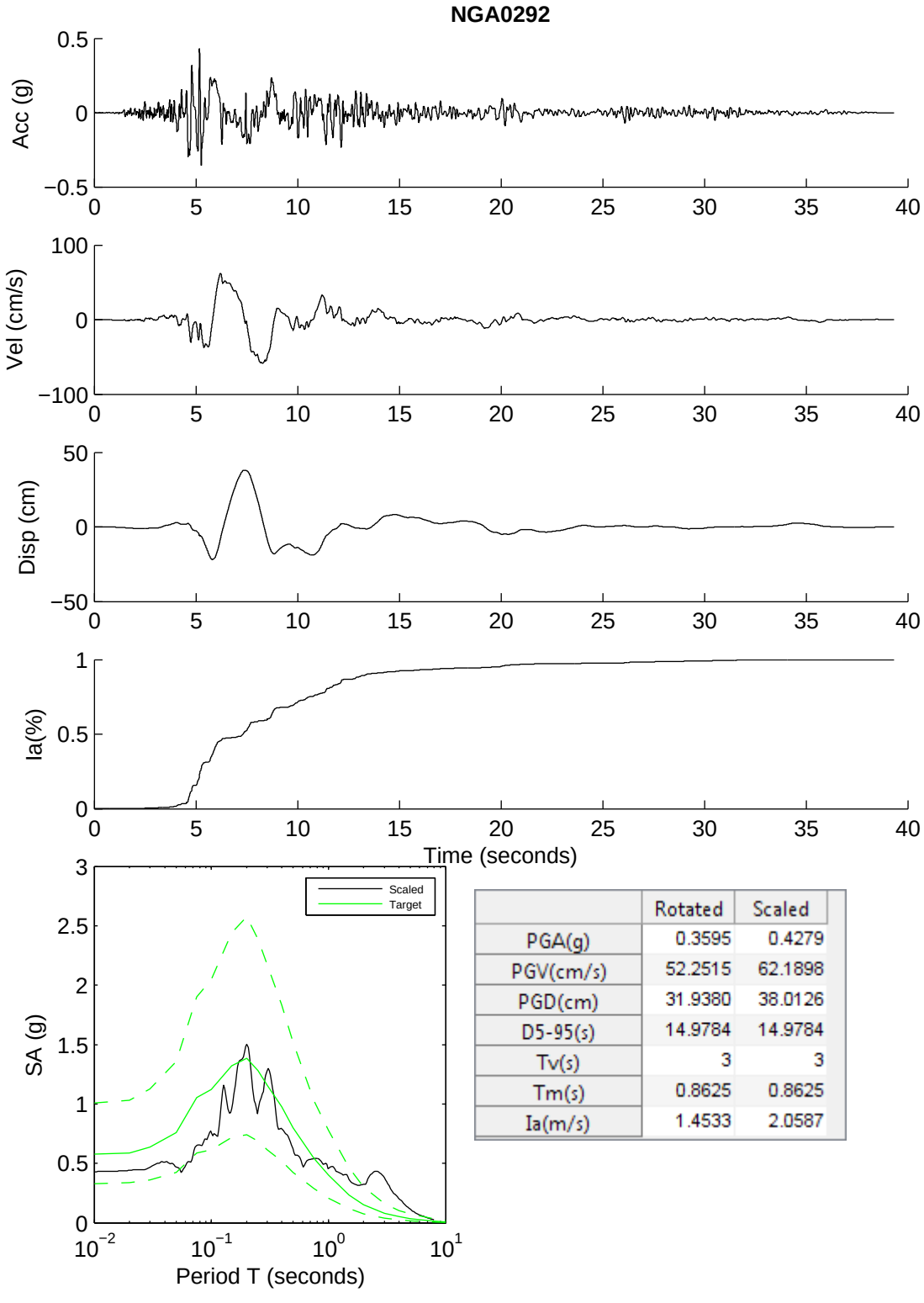

	Rotated	Scaled
PGA(g)	0.3595	0.4279
PGV(cm/s)	52.2515	62.1898
PGD(cm)	31.9380	38.0126
D5-95(s)	14.9784	14.9784
Tv(s)	3	3
Tm(s)	0.8625	0.8625
Ia(m/s)	1.4533	2.0587

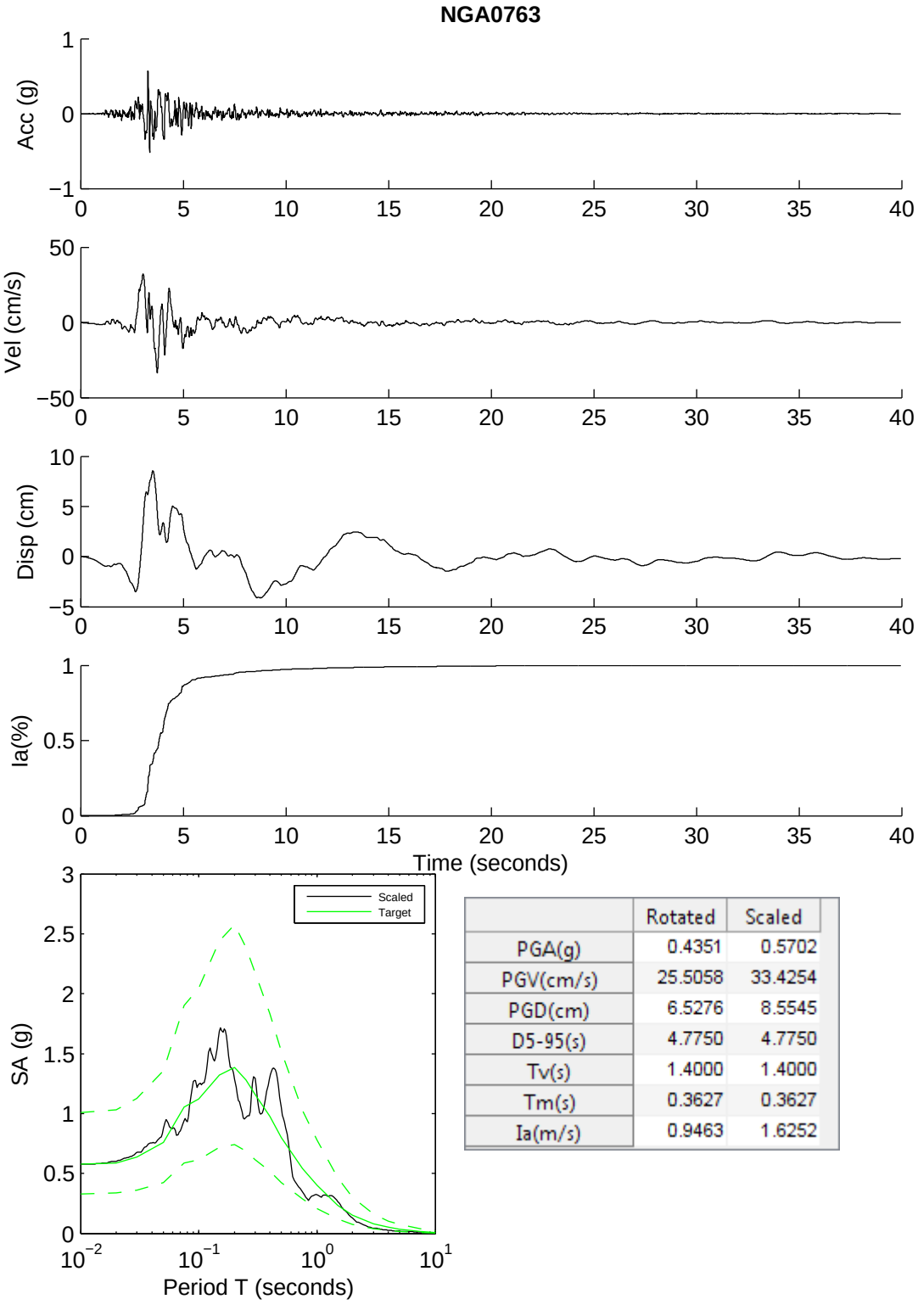

	Rotated	Scaled
PGA(g)	0.4351	0.5702
PGV(cm/s)	25.5058	33.4254
PGD(cm)	6.5276	8.5545
D5-95(s)	4.7750	4.7750
Tv(s)	1.4000	1.4000
Tm(s)	0.3627	0.3627
Ia(m/s)	0.9463	1.6252

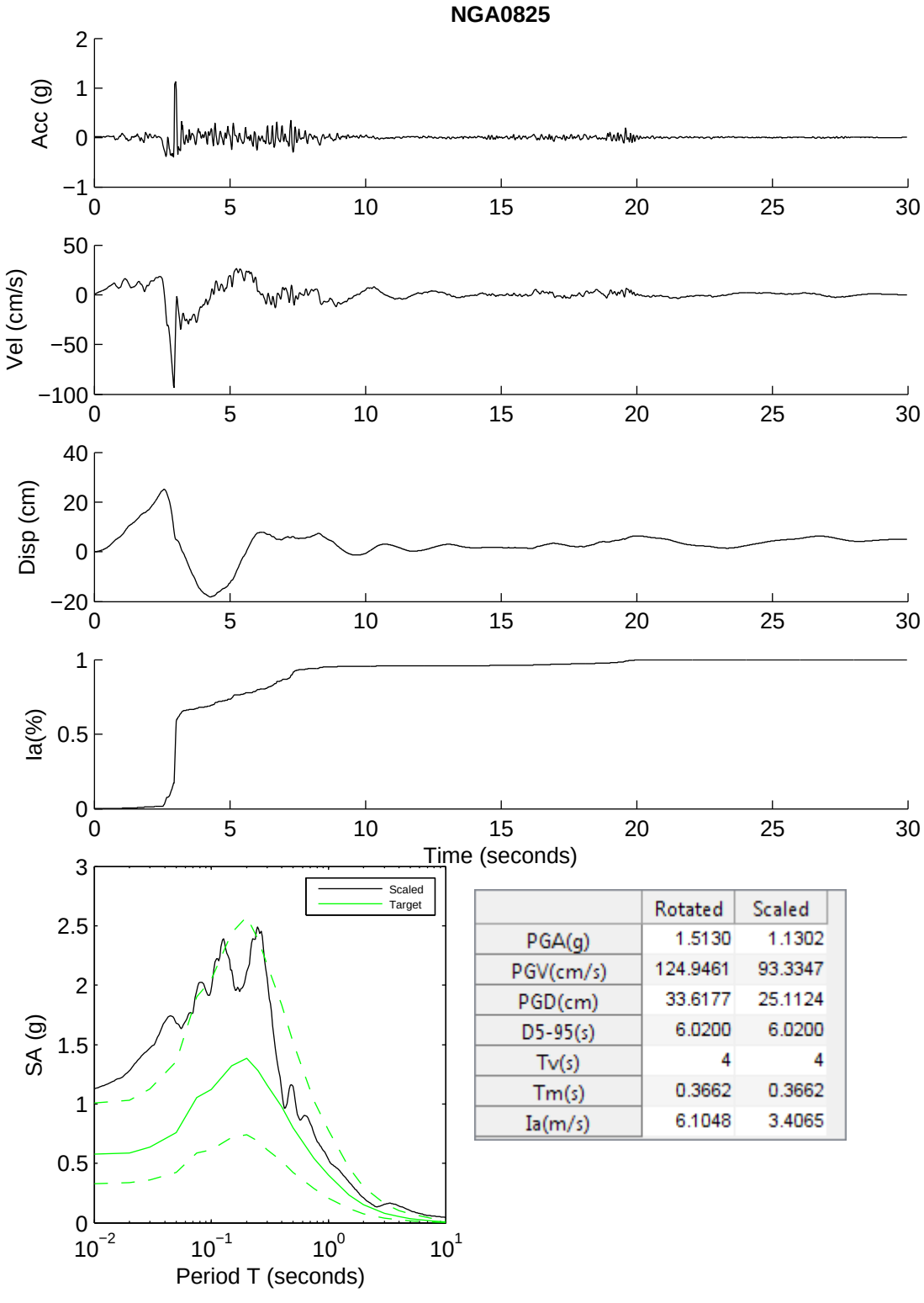

	Rotated	Scaled
PGA(g)	1.5130	1.1302
PGV(cm/s)	124.9461	93.3347
PGD(cm)	33.6177	25.1124
D5-95(s)	6.0200	6.0200
Tv(s)	4	4
Tm(s)	0.3662	0.3662
Ia(m/s)	6.1048	3.4065

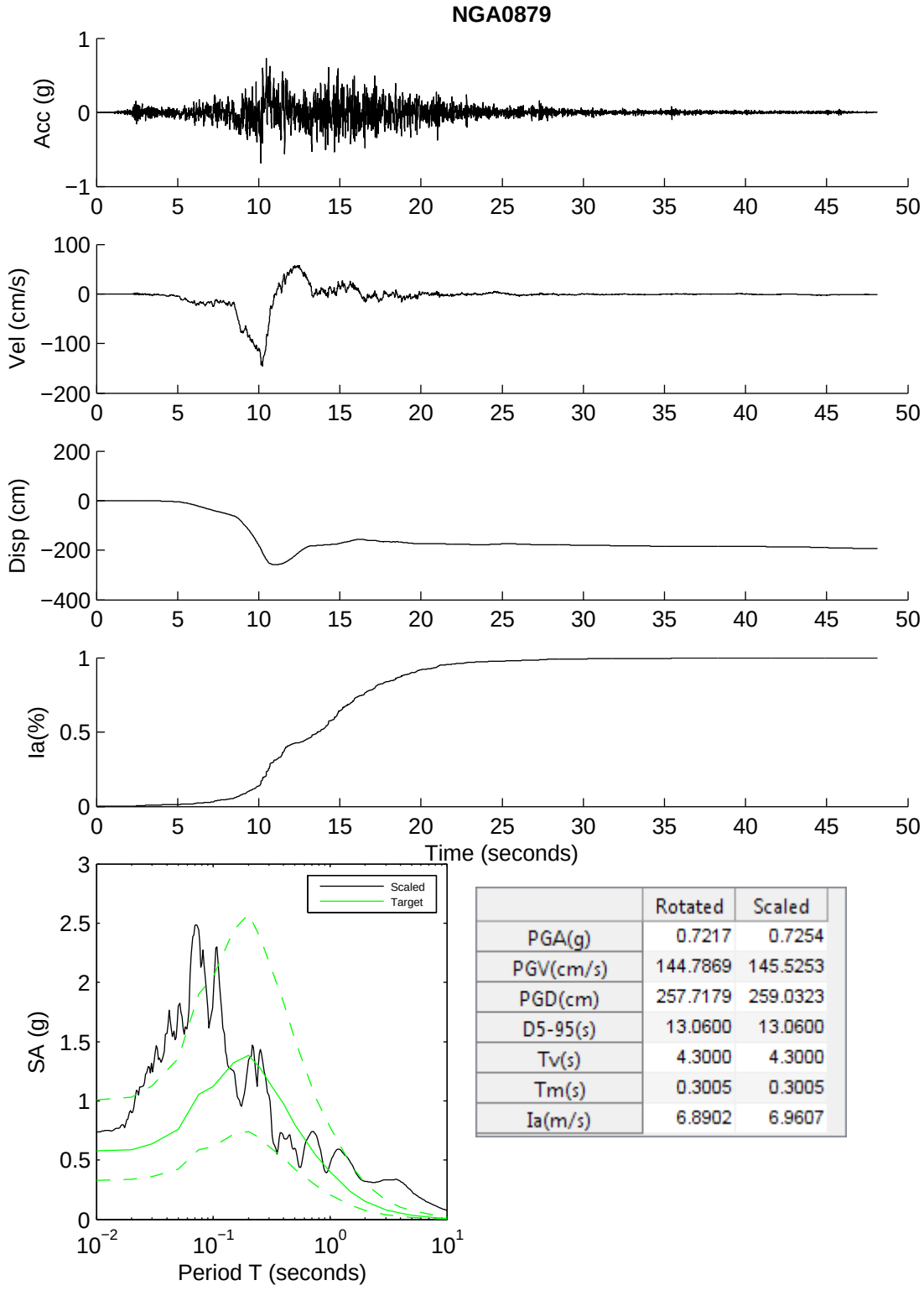

	Rotated	Scaled
PGA(g)	0.7217	0.7254
PGV(cm/s)	144.7869	145.5253
PGD(cm)	257.7179	259.0323
D5-95(s)	13.0600	13.0600
Tv(s)	4.3000	4.3000
Tm(s)	0.3005	0.3005
Ia(m/s)	6.8902	6.9607

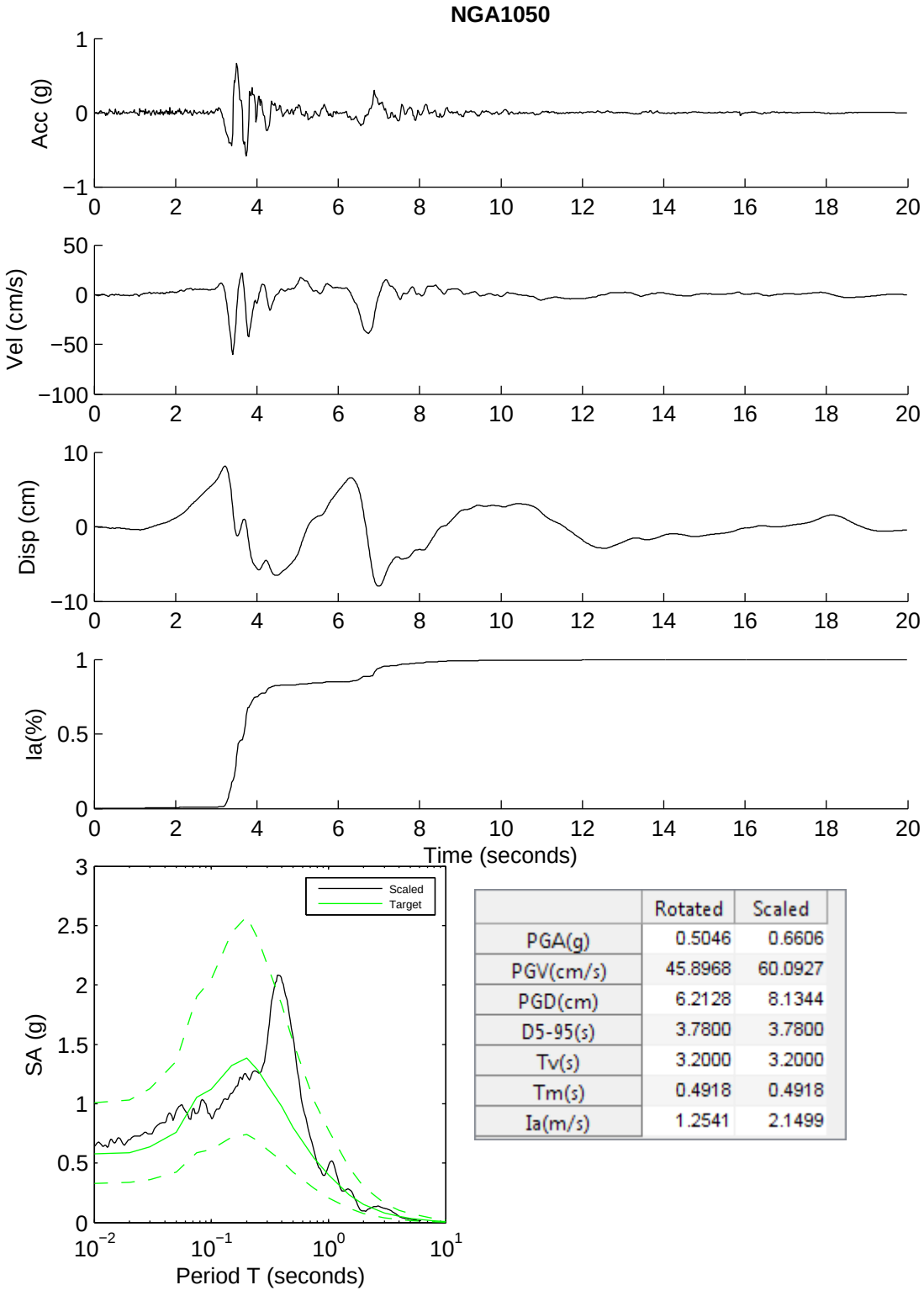

	Rotated	Scaled
PGA(g)	0.5046	0.6606
PGV(cm/s)	45.8968	60.0927
PGD(cm)	6.2128	8.1344
D5-95(s)	3.7800	3.7800
Tv(s)	3.2000	3.2000
Tm(s)	0.4918	0.4918
Ia(m/s)	1.2541	2.1499

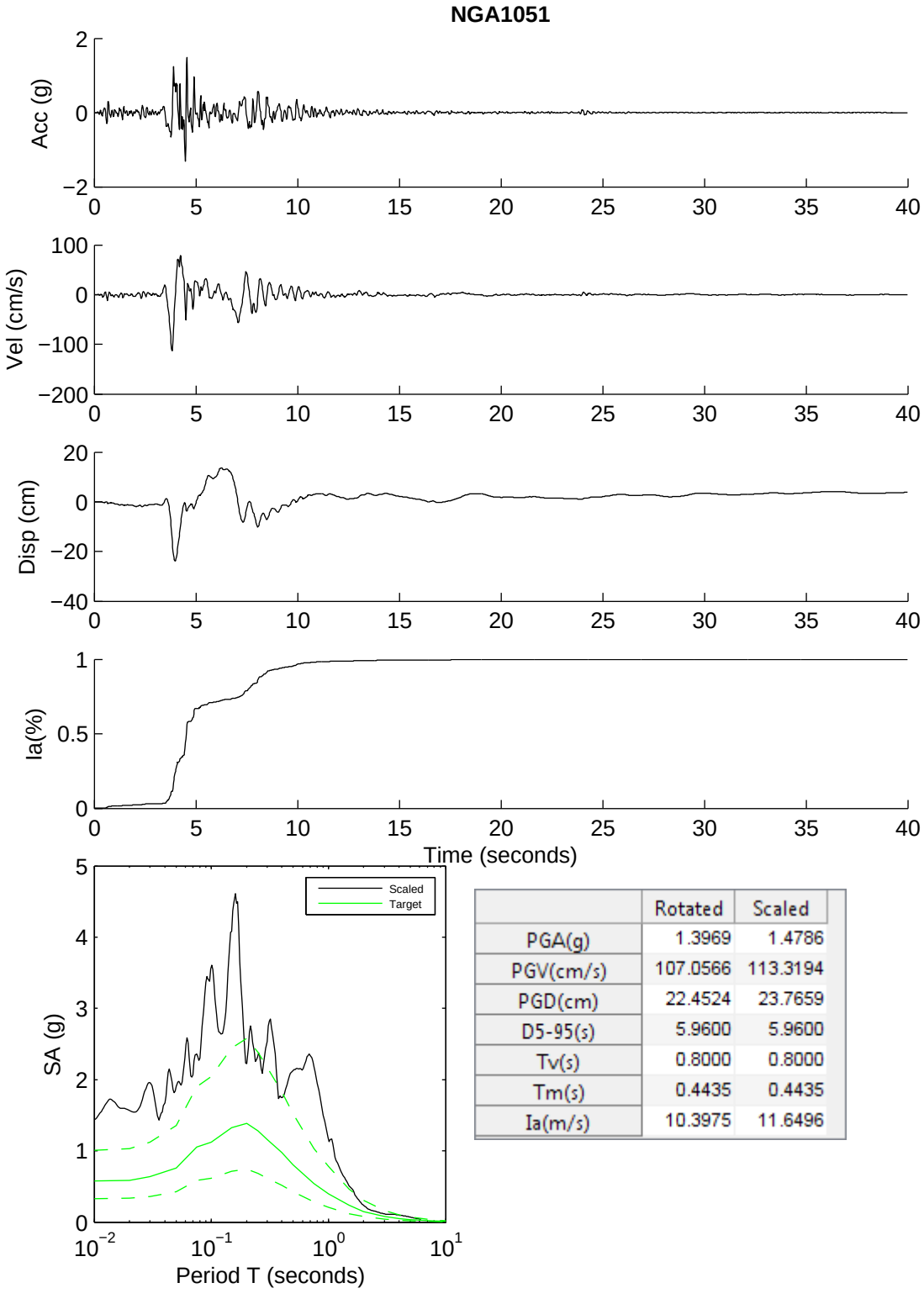

	Rotated	Scaled
PGA(g)	1.3969	1.4786
PGV(cm/s)	107.0566	113.3194
PGD(cm)	22.4524	23.7659
D5-95(s)	5.9600	5.9600
Tv(s)	0.8000	0.8000
Tm(s)	0.4435	0.4435
Ia(m/s)	10.3975	11.6496

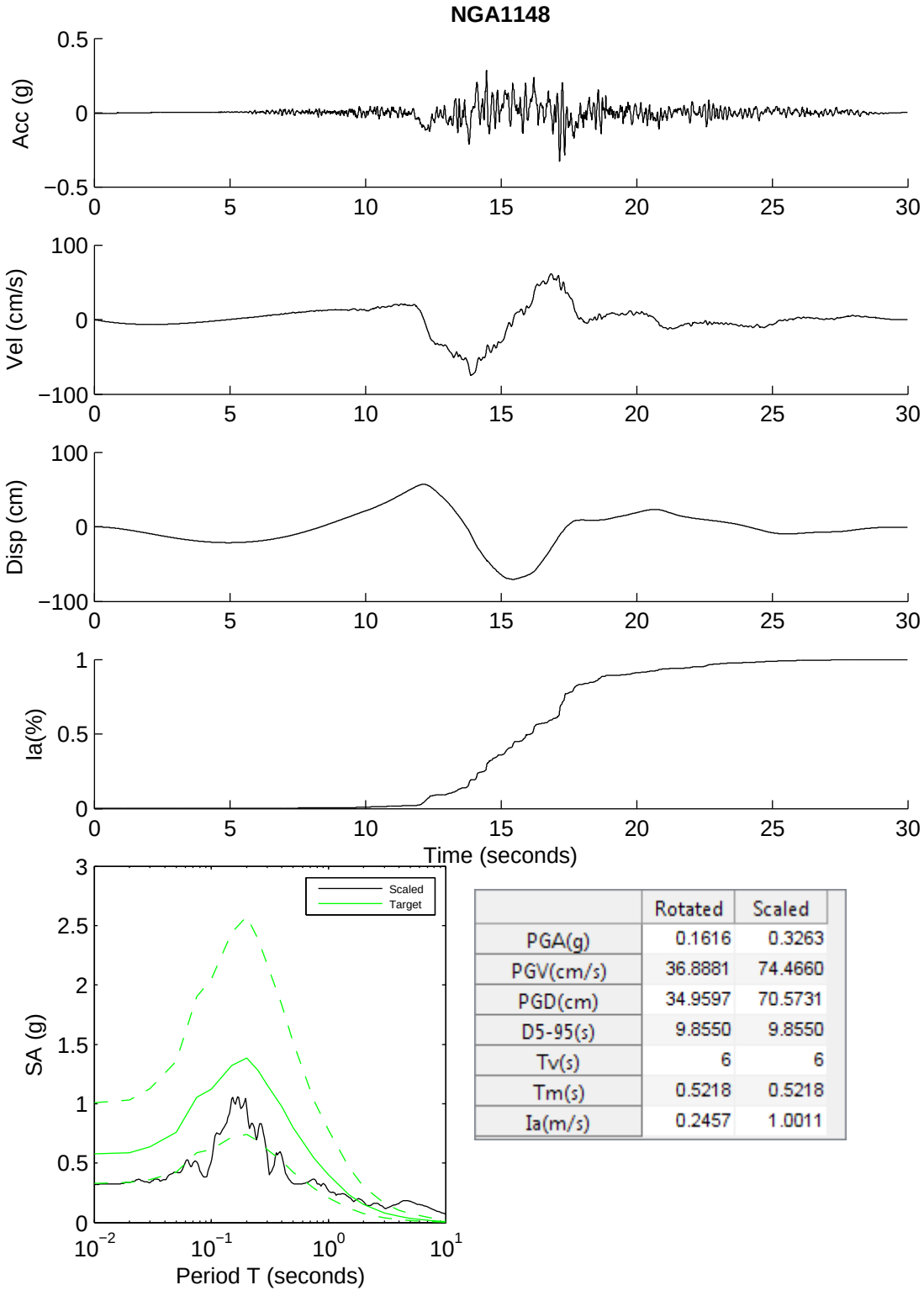

	Rotated	Scaled
PGA(g)	0.1616	0.3263
PGV(cm/s)	36.8881	74.4660
PGD(cm)	34.9597	70.5731
D5-95(s)	9.8550	9.8550
Tv(s)	6	6
Tm(s)	0.5218	0.5218
Ia(m/s)	0.2457	1.0011

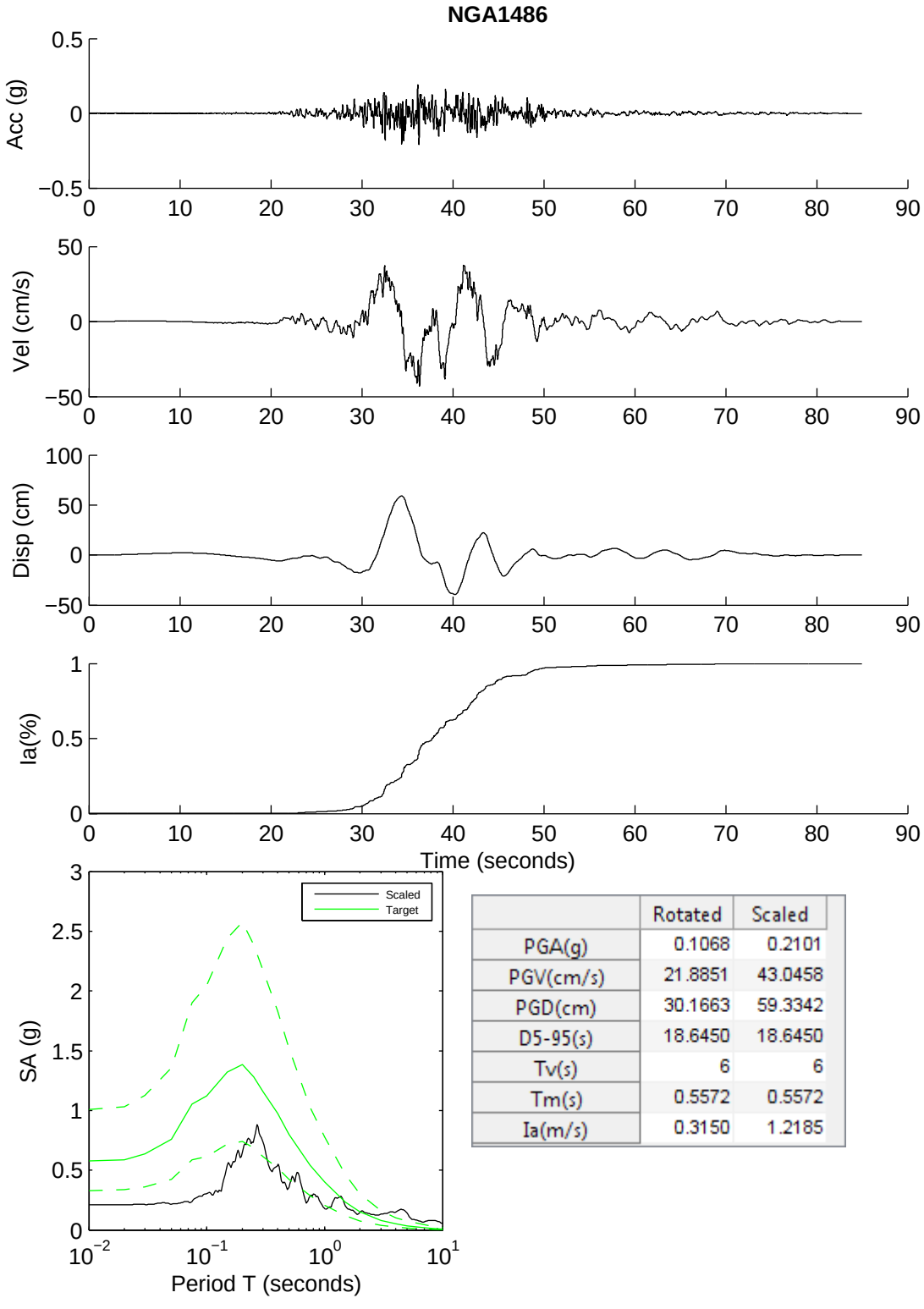

	Rotated	Scaled
PGA(g)	0.1068	0.2101
PGV(cm/s)	21.8851	43.0458
PGD(cm)	30.1663	59.3342
D5-95(s)	18.6450	18.6450
Tv(s)	6	6
Tm(s)	0.5572	0.5572
Ia(m/s)	0.3150	1.2185

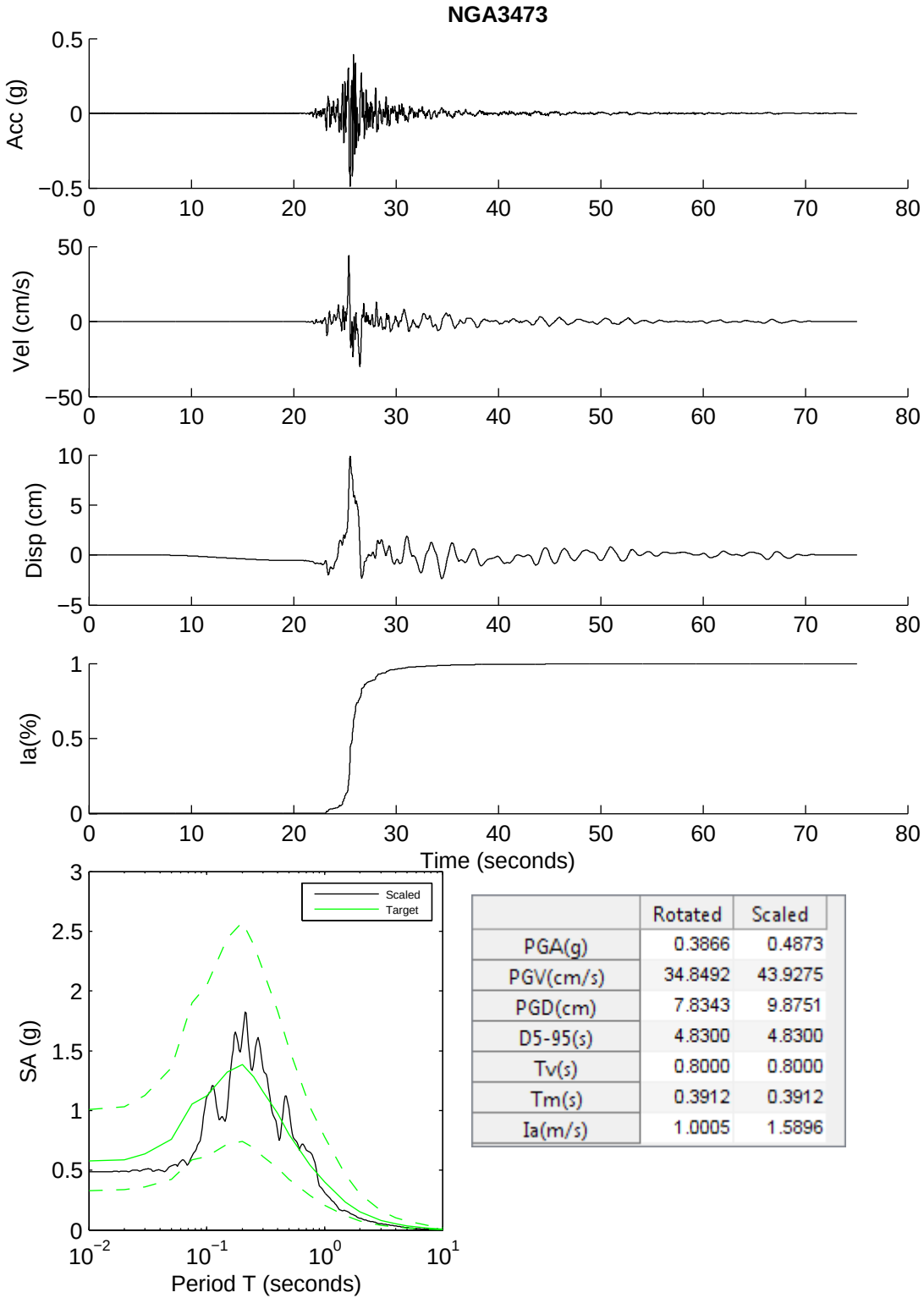

	Rotated	Scaled
PGA(g)	0.3866	0.4873
PGV(cm/s)	34.8492	43.9275
PGD(cm)	7.8343	9.8751
D5-95(s)	4.8300	4.8300
Tv(s)	0.8000	0.8000
Tm(s)	0.3912	0.3912
Ia(m/s)	1.0005	1.5896

APPENDIX 3C: SCENARIO ACR2 GROUND MOTION DATA

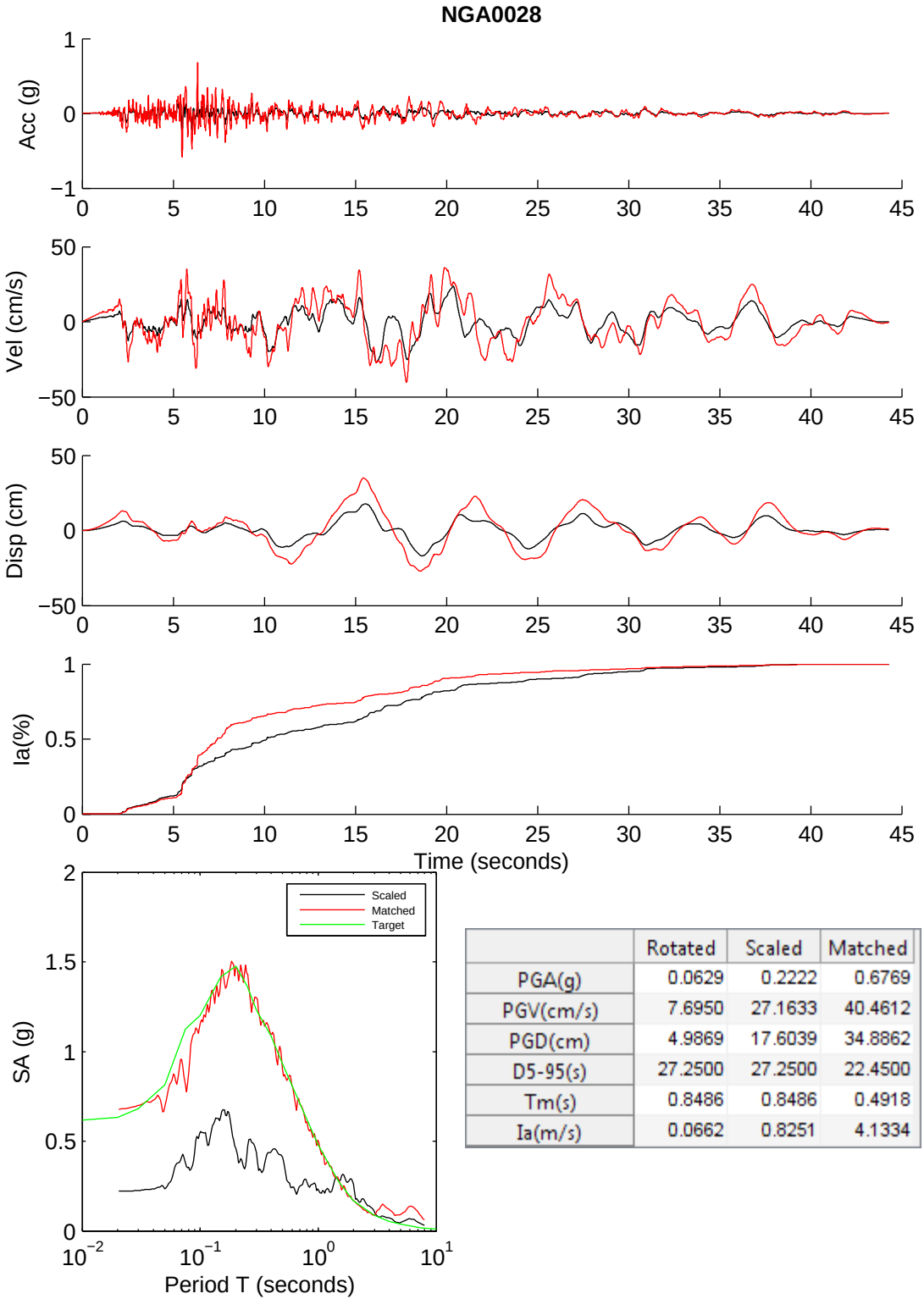

	Rotated	Scaled	Matched
PGA(g)	0.0629	0.2222	0.6769
PGV(cm/s)	7.6950	27.1633	40.4612
PGD(cm)	4.9869	17.6039	34.8862
D5-95(s)	27.2500	27.2500	22.4500
Tm(s)	0.8486	0.8486	0.4918
Ia(m/s)	0.0662	0.8251	4.1334

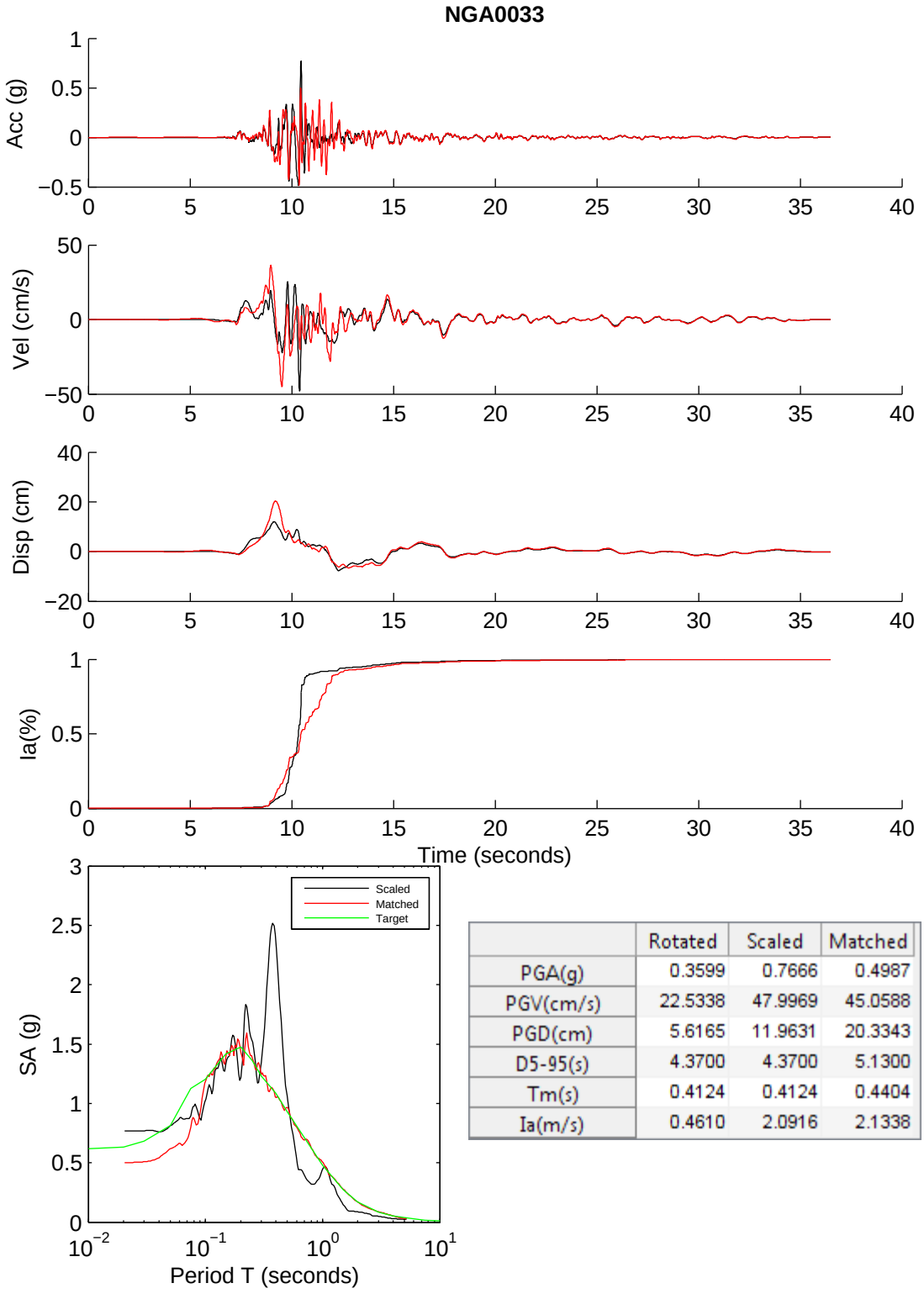

	Rotated	Scaled	Matched
PGA(g)	0.3599	0.7666	0.4987
PGV(cm/s)	22.5338	47.9969	45.0588
PGD(cm)	5.6165	11.9631	20.3343
D5-95(s)	4.3700	4.3700	5.1300
Tm(s)	0.4124	0.4124	0.4404
Ia(m/s)	0.4610	2.0916	2.1338

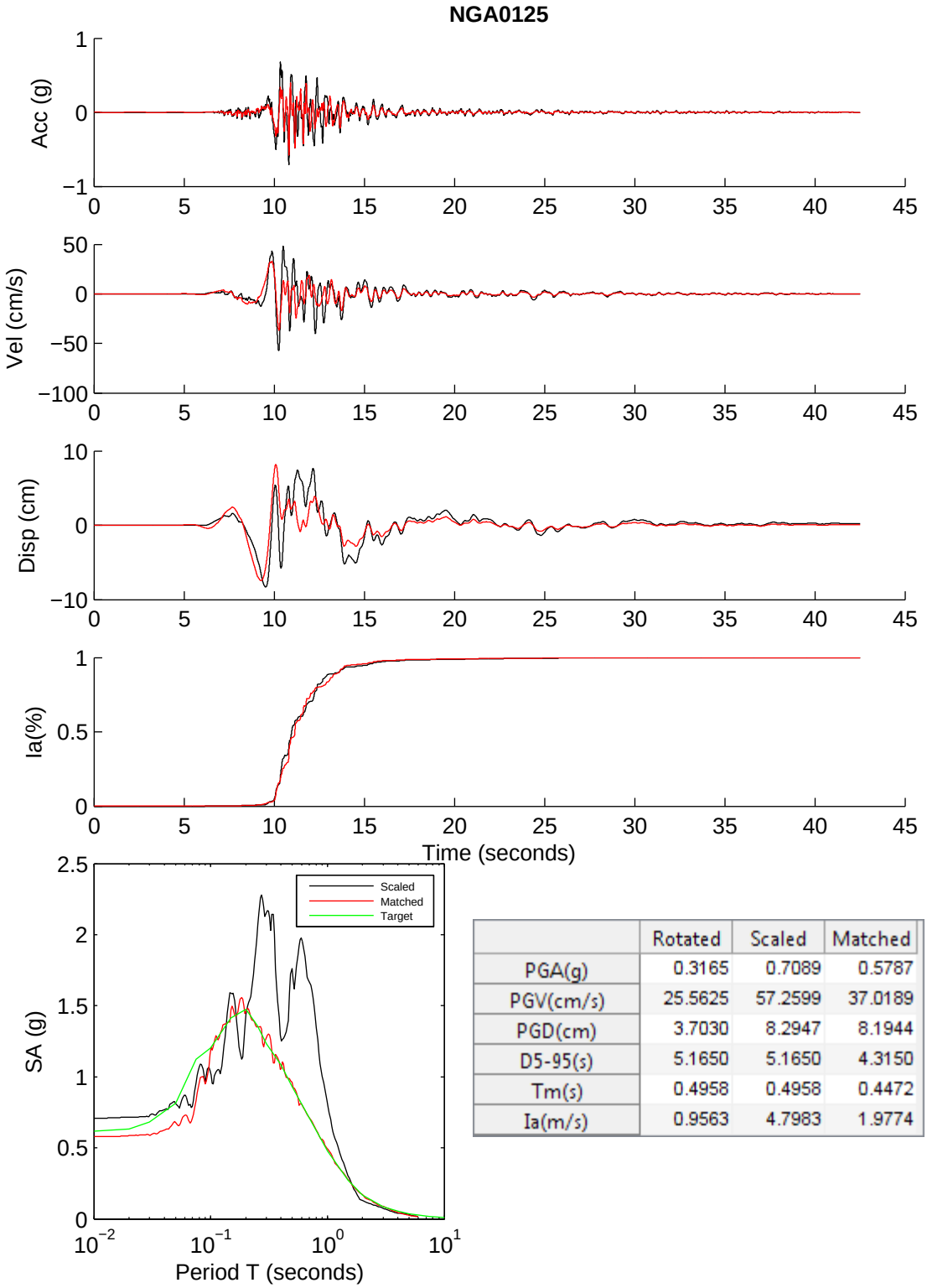

	Rotated	Scaled	Matched
PGA(g)	0.3165	0.7089	0.5787
PGV(cm/s)	25.5625	57.2599	37.0189
PGD(cm)	3.7030	8.2947	8.1944
D5-95(s)	5.1650	5.1650	4.3150
Tm(s)	0.4958	0.4958	0.4472
Ia(m/s)	0.9563	4.7983	1.9774

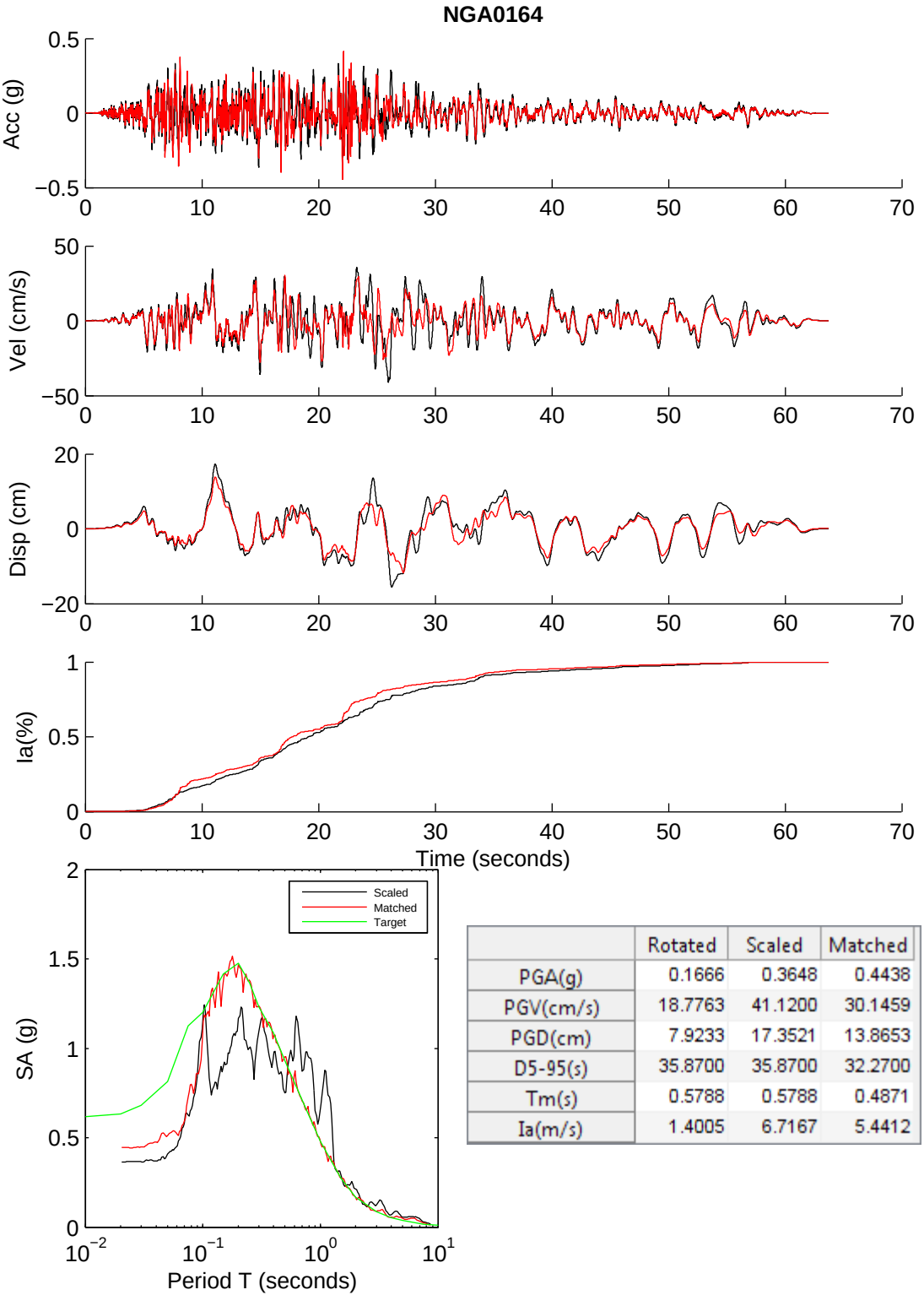

	Rotated	Scaled	Matched
PGA(g)	0.1666	0.3648	0.4438
PGV(cm/s)	18.7763	41.1200	30.1459
PGD(cm)	7.9233	17.3521	13.8653
D5-95(s)	35.8700	35.8700	32.2700
Tm(s)	0.5788	0.5788	0.4871
Ia(m/s)	1.4005	6.7167	5.4412

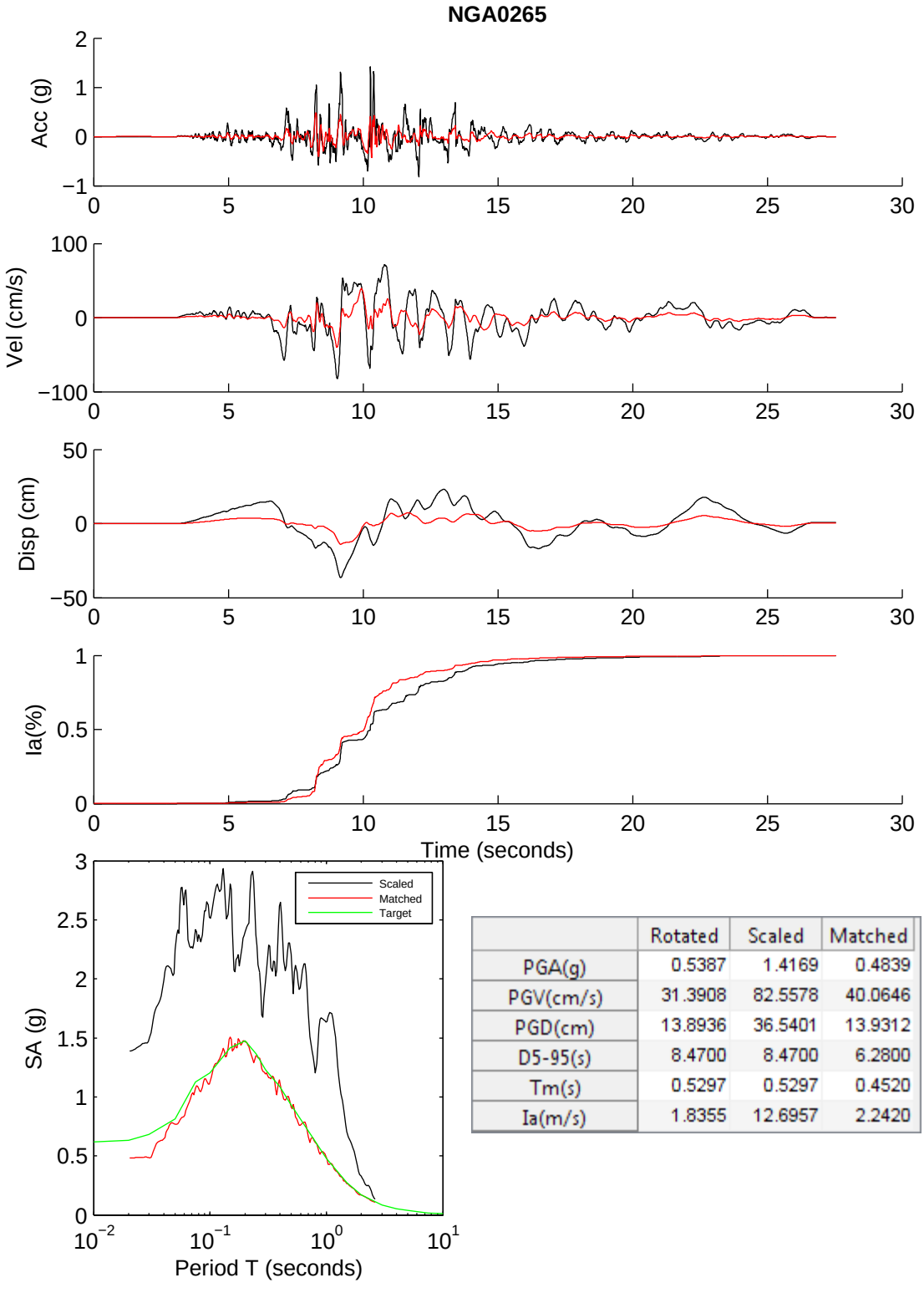

	Rotated	Scaled	Matched
PGA(g)	0.5387	1.4169	0.4839
PGV(cm/s)	31.3908	82.5578	40.0646
PGD(cm)	13.8936	36.5401	13.9312
D5-95(s)	8.4700	8.4700	6.2800
Tm(s)	0.5297	0.5297	0.4520
Ia(m/s)	1.8355	12.6957	2.2420

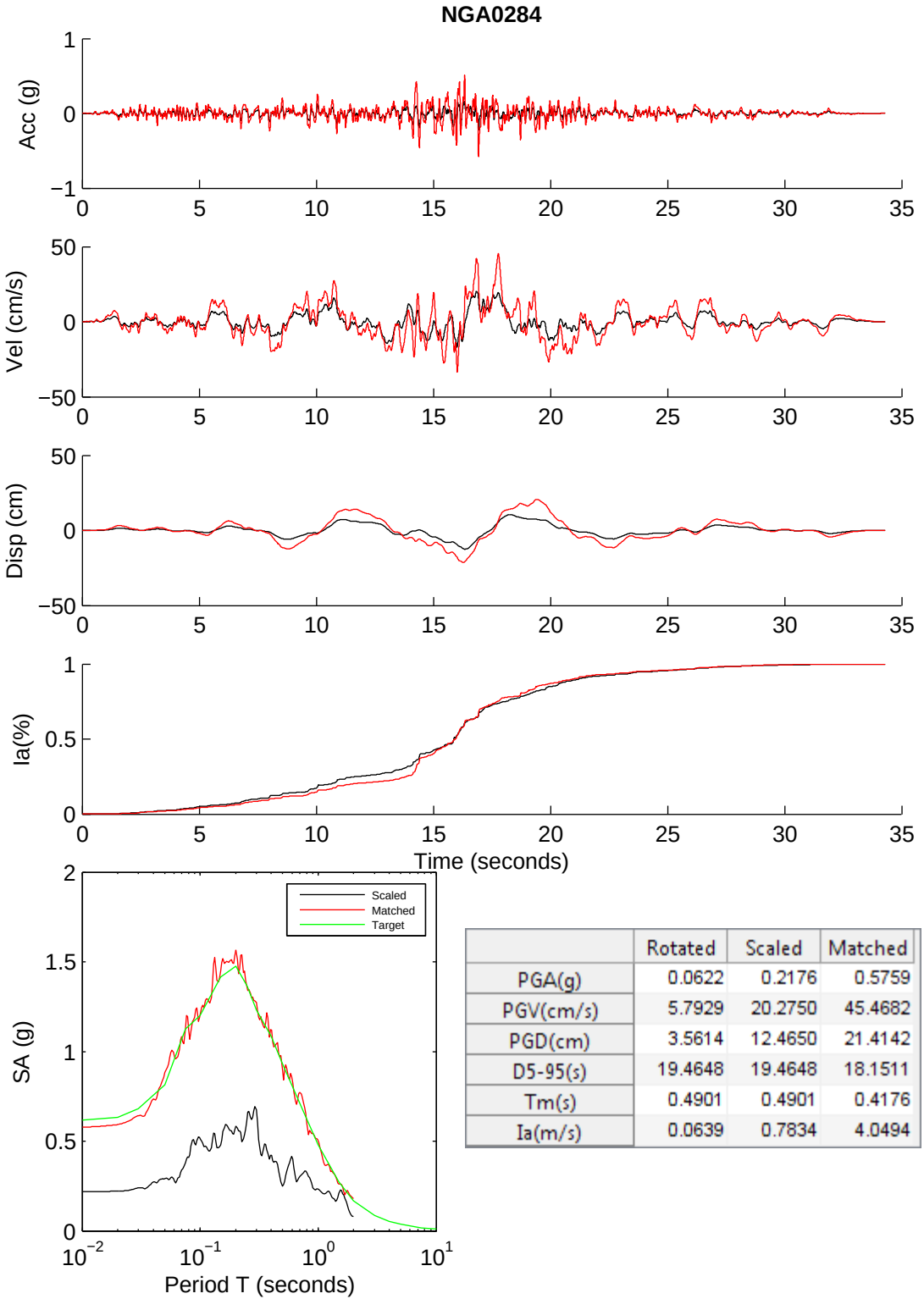

	Rotated	Scaled	Matched
PGA(g)	0.0622	0.2176	0.5759
PGV(cm/s)	5.7929	20.2750	45.4682
PGD(cm)	3.5614	12.4650	21.4142
D5-95(s)	19.4648	19.4648	18.1511
Tm(s)	0.4901	0.4901	0.4176
Ia(m/s)	0.0639	0.7834	4.0494

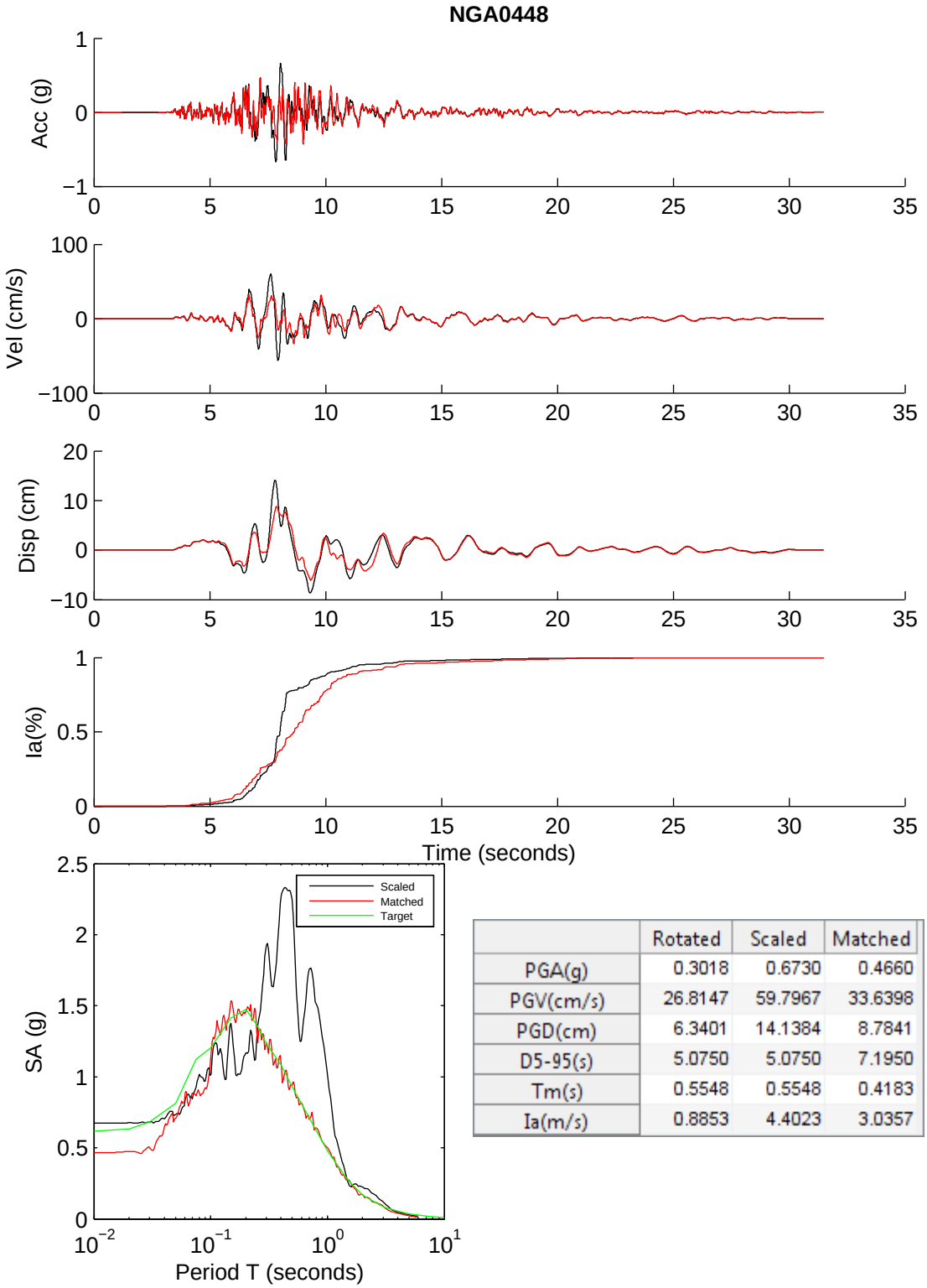

	Rotated	Scaled	Matched
PGA(g)	0.3018	0.6730	0.4660
PGV(cm/s)	26.8147	59.7967	33.6398
PGD(cm)	6.3401	14.1384	8.7841
D5-95(s)	5.0750	5.0750	7.1950
Tm(s)	0.5548	0.5548	0.4183
Ia(m/s)	0.8853	4.4023	3.0357

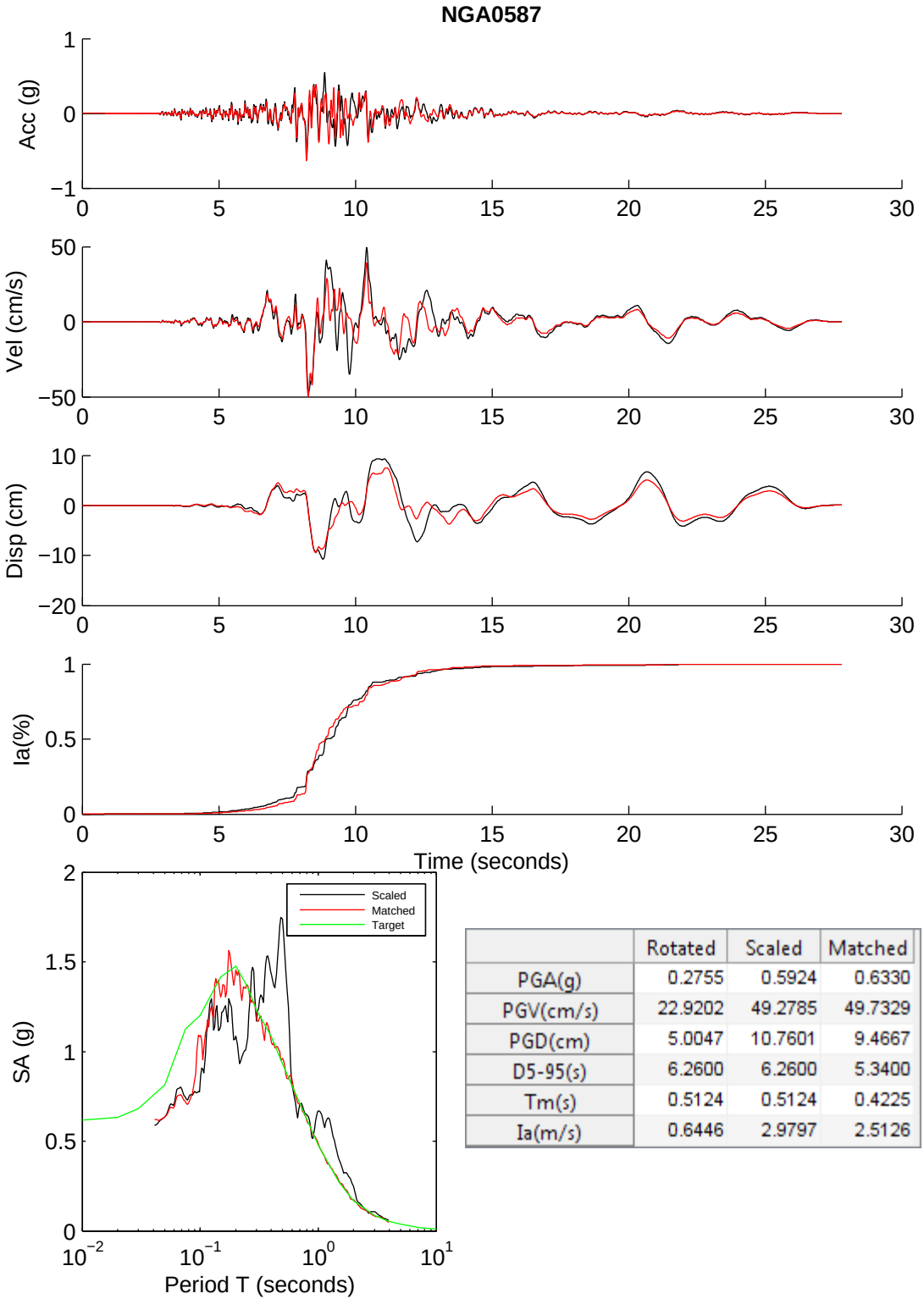

	Rotated	Scaled	Matched
PGA(g)	0.2755	0.5924	0.6330
PGV(cm/s)	22.9202	49.2785	49.7329
PGD(cm)	5.0047	10.7601	9.4667
D5-95(s)	6.2600	6.2600	5.3400
Tm(s)	0.5124	0.5124	0.4225
Ia(m/s)	0.6446	2.9797	2.5126

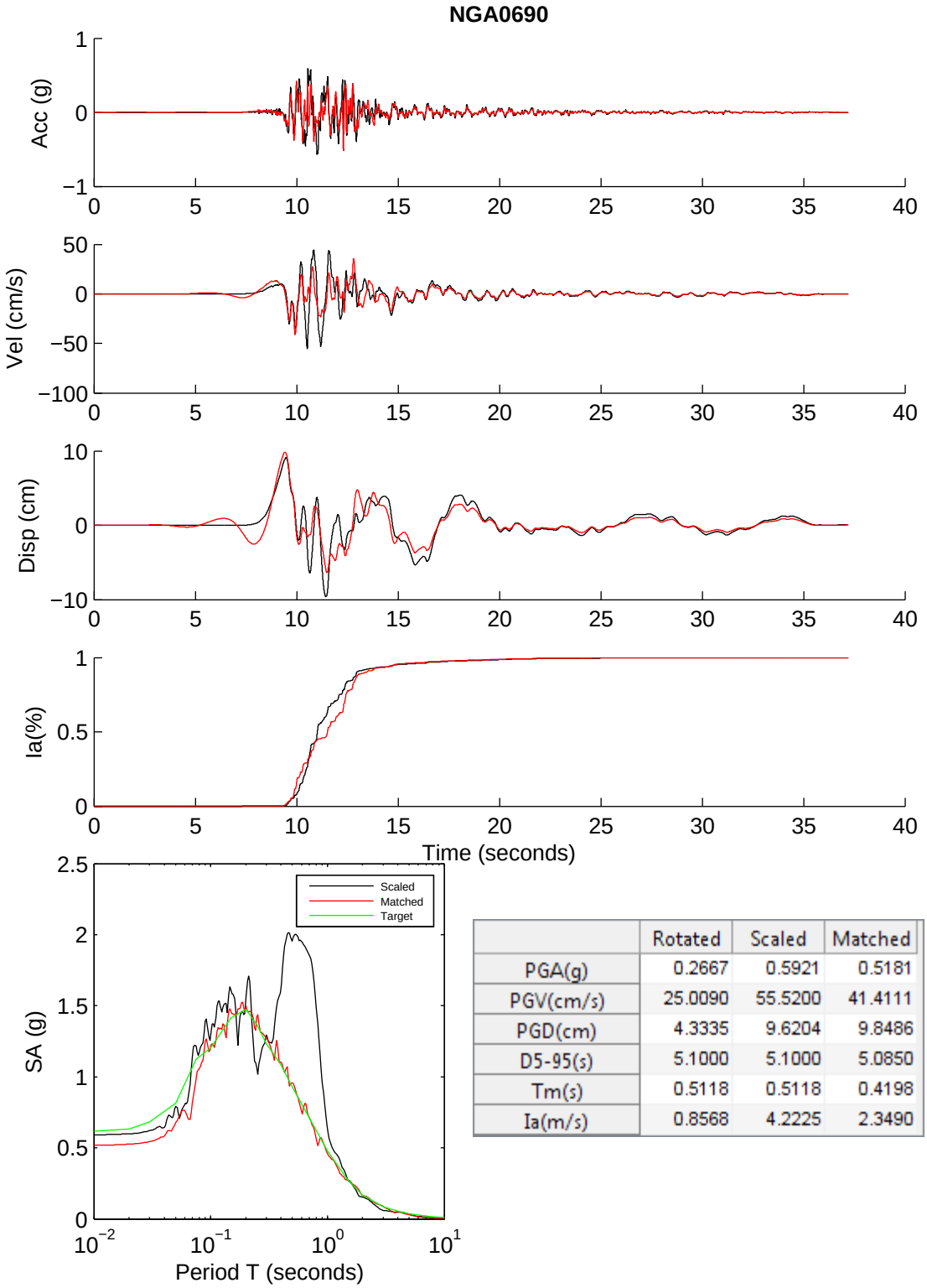

	Rotated	Scaled	Matched
PGA(g)	0.2667	0.5921	0.5181
PGV(cm/s)	25.0090	55.5200	41.4111
PGD(cm)	4.3335	9.6204	9.8486
D5-95(s)	5.1000	5.1000	5.0850
Tm(s)	0.5118	0.5118	0.4198
Ia(m/s)	0.8568	4.2225	2.3490

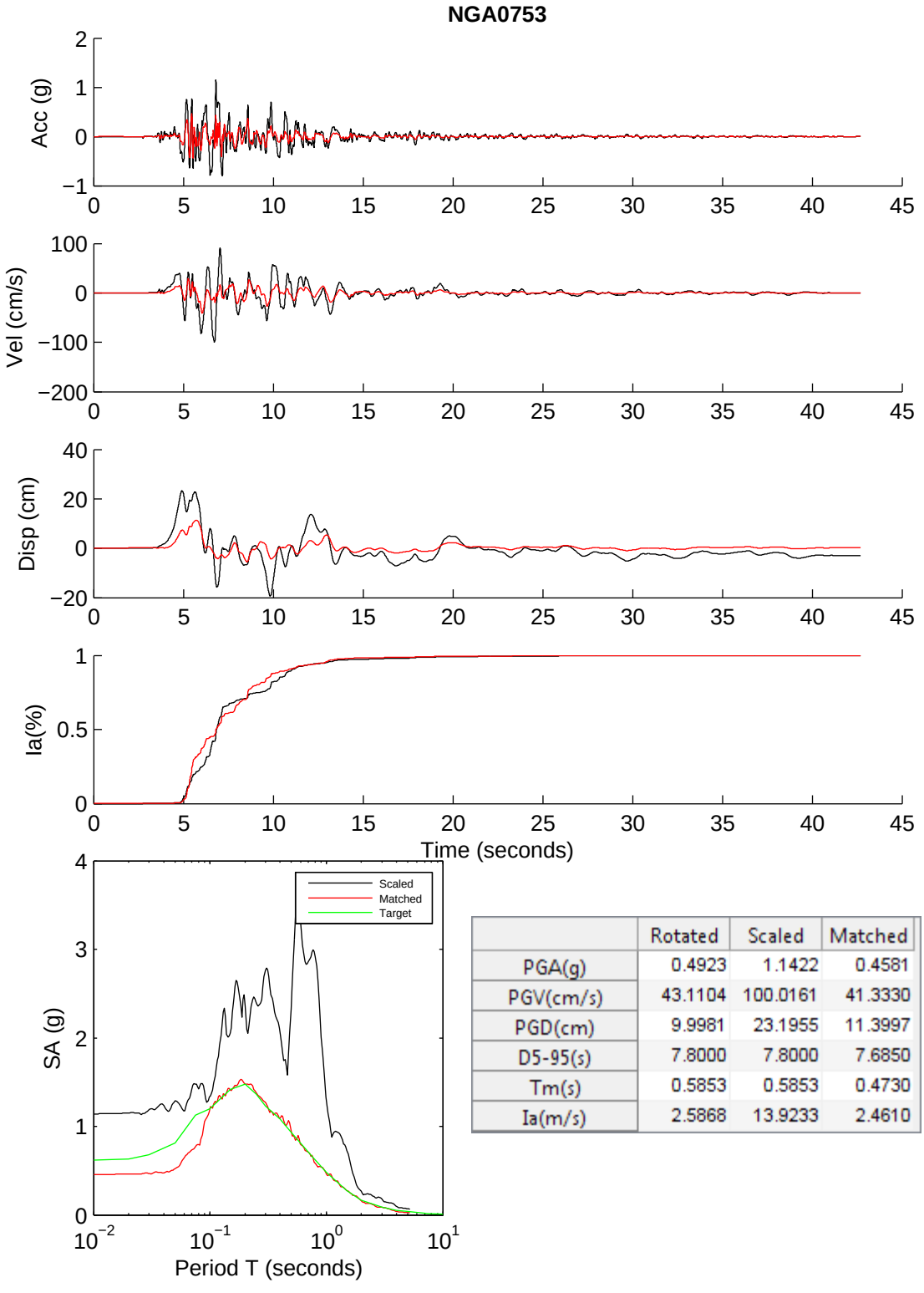

	Rotated	Scaled	Matched
PGA(g)	0.4923	1.1422	0.4581
PGV(cm/s)	43.1104	100.0161	41.3330
PGD(cm)	9.9981	23.1955	11.3997
D5-95(s)	7.8000	7.8000	7.6850
Tm(s)	0.5853	0.5853	0.4730
Ia(m/s)	2.5868	13.9233	2.4610

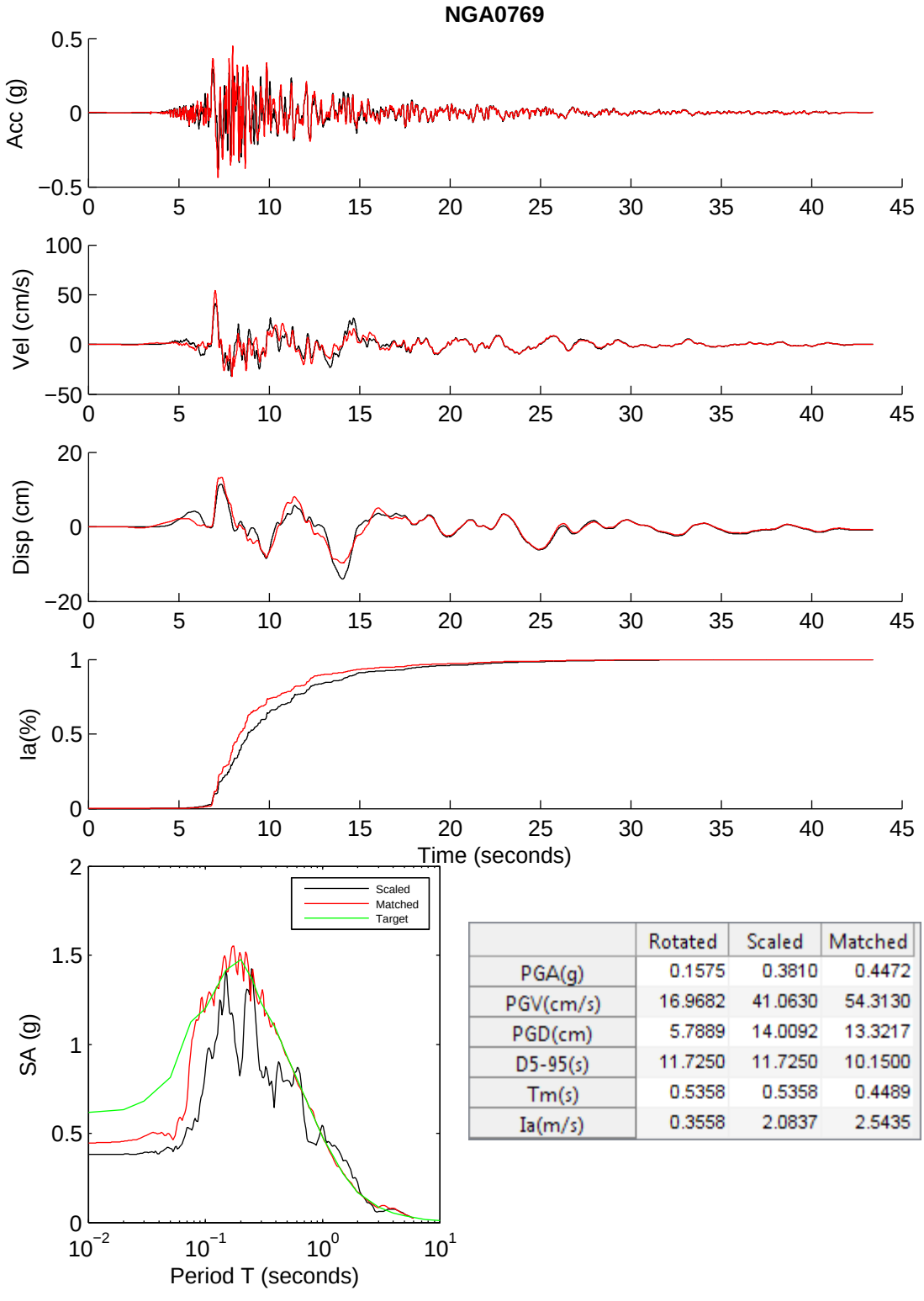

	Rotated	Scaled	Matched
PGA(g)	0.1575	0.3810	0.4472
PGV(cm/s)	16.9682	41.0630	54.3130
PGD(cm)	5.7889	14.0092	13.3217
D5-95(s)	11.7250	11.7250	10.1500
Tm(s)	0.5358	0.5358	0.4489
Ia(m/s)	0.3558	2.0837	2.5435

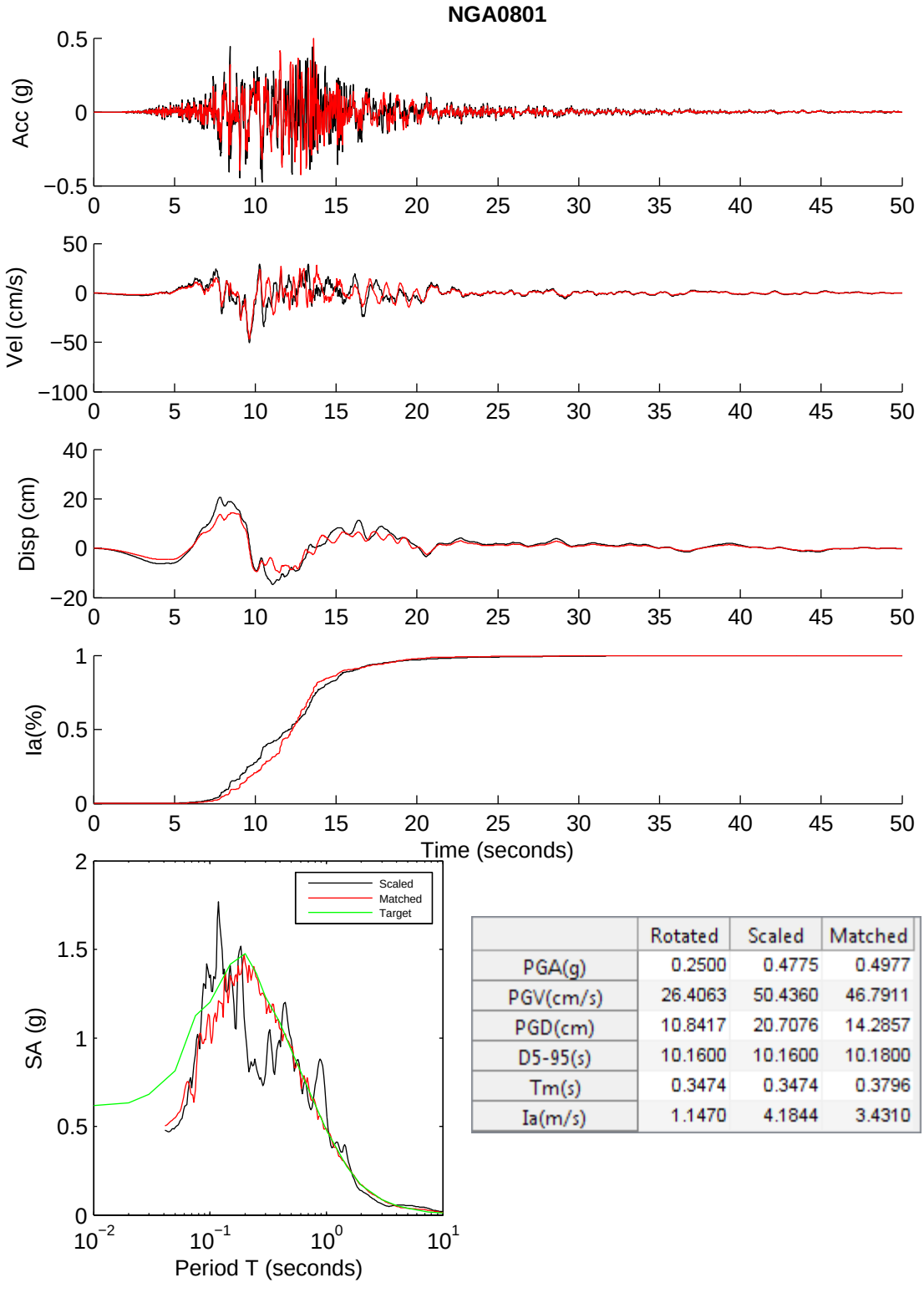

	Rotated	Scaled	Matched
PGA(g)	0.2500	0.4775	0.4977
PGV(cm/s)	26.4063	50.4360	46.7911
PGD(cm)	10.8417	20.7076	14.2857
D5-95(s)	10.1600	10.1600	10.1800
Tm(s)	0.3474	0.3474	0.3796
Ia(m/s)	1.1470	4.1844	3.4310

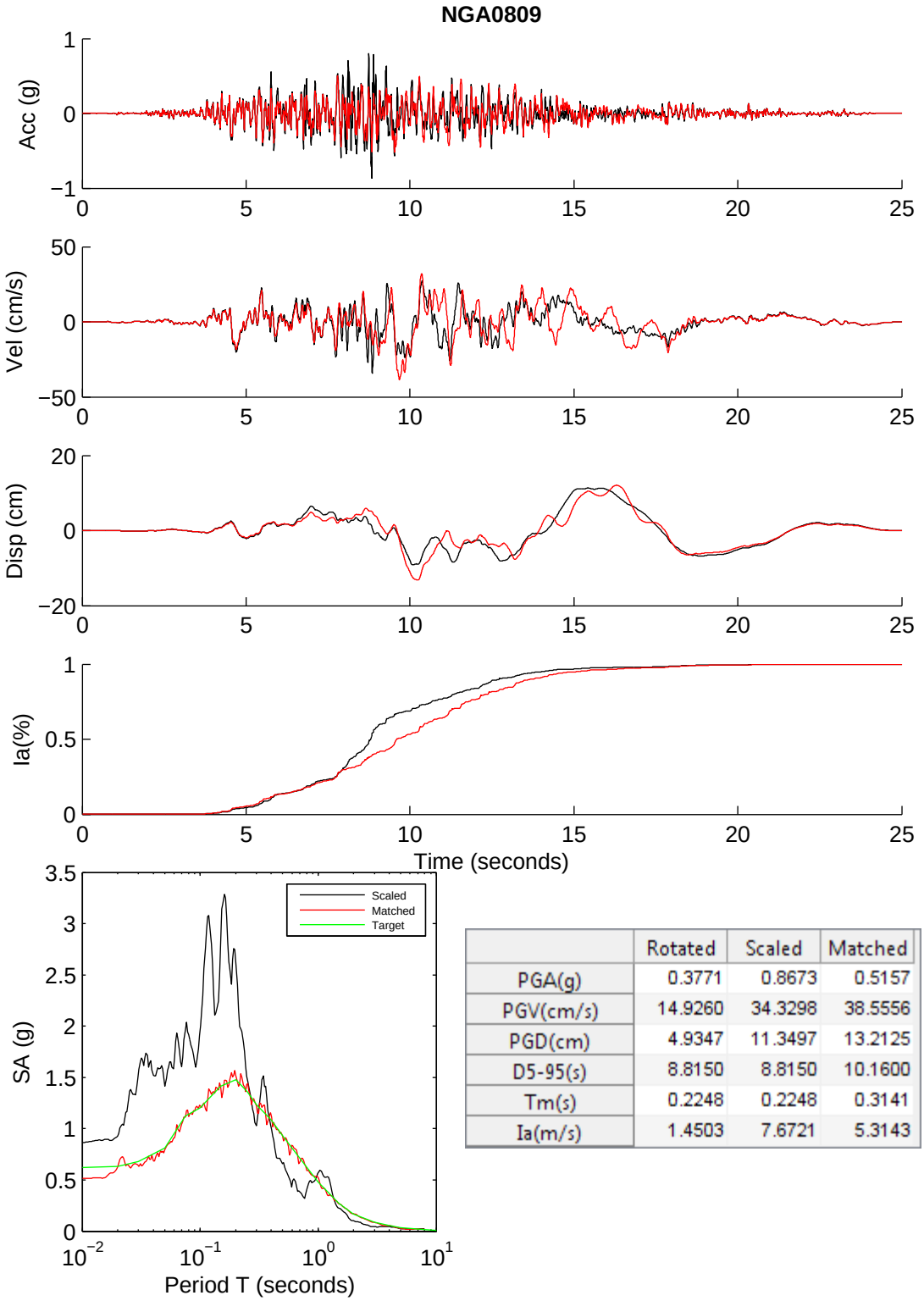

	Rotated	Scaled	Matched
PGA(g)	0.3771	0.8673	0.5157
PGV(cm/s)	14.9260	34.3298	38.5556
PGD(cm)	4.9347	11.3497	13.2125
D5-95(s)	8.8150	8.8150	10.1600
Tm(s)	0.2248	0.2248	0.3141
Ia(m/s)	1.4503	7.6721	5.3143

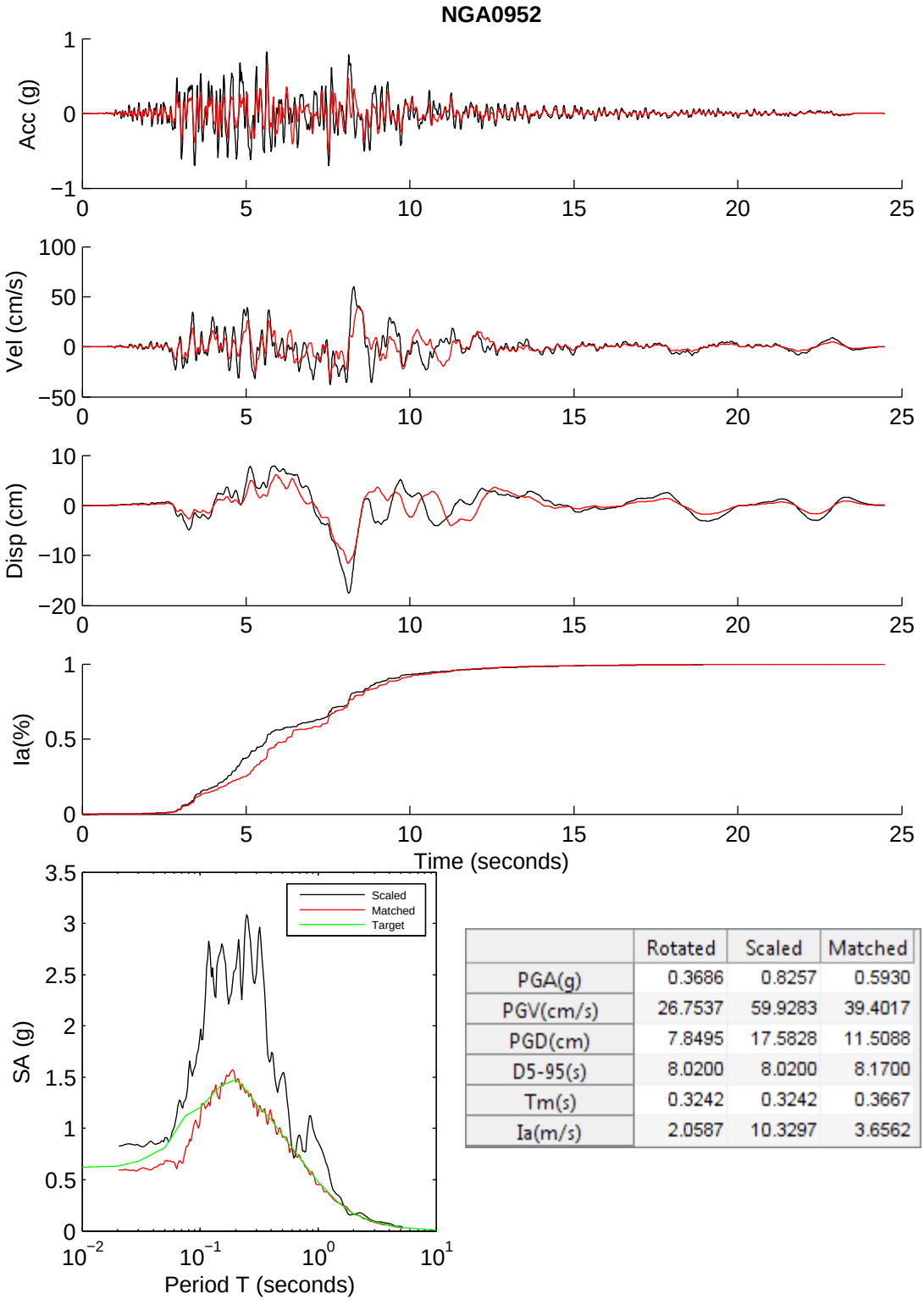

	Rotated	Scaled	Matched
PGA(g)	0.3686	0.8257	0.5930
PGV(cm/s)	26.7537	59.9283	39.4017
PGD(cm)	7.8495	17.5828	11.5088
D5-95(s)	8.0200	8.0200	8.1700
Tm(s)	0.3242	0.3242	0.3667
Ia(m/s)	2.0587	10.3297	3.6562

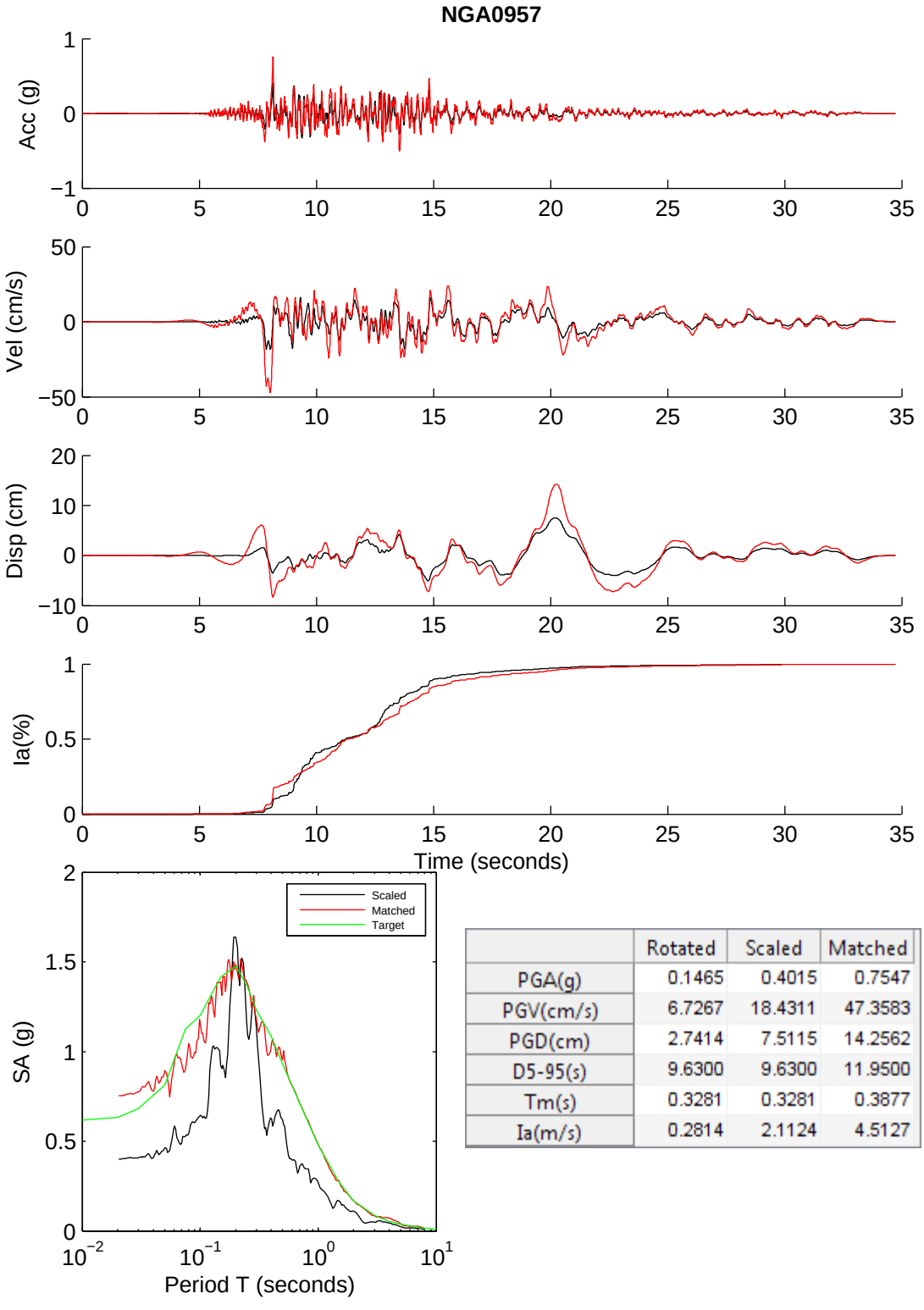

	Rotated	Scaled	Matched
PGA(g)	0.1465	0.4015	0.7547
PGV(cm/s)	6.7267	18.4311	47.3583
PGD(cm)	2.7414	7.5115	14.2562
D5-95(s)	9.6300	9.6300	11.9500
Tm(s)	0.3281	0.3281	0.3877
Ia(m/s)	0.2814	2.1124	4.5127

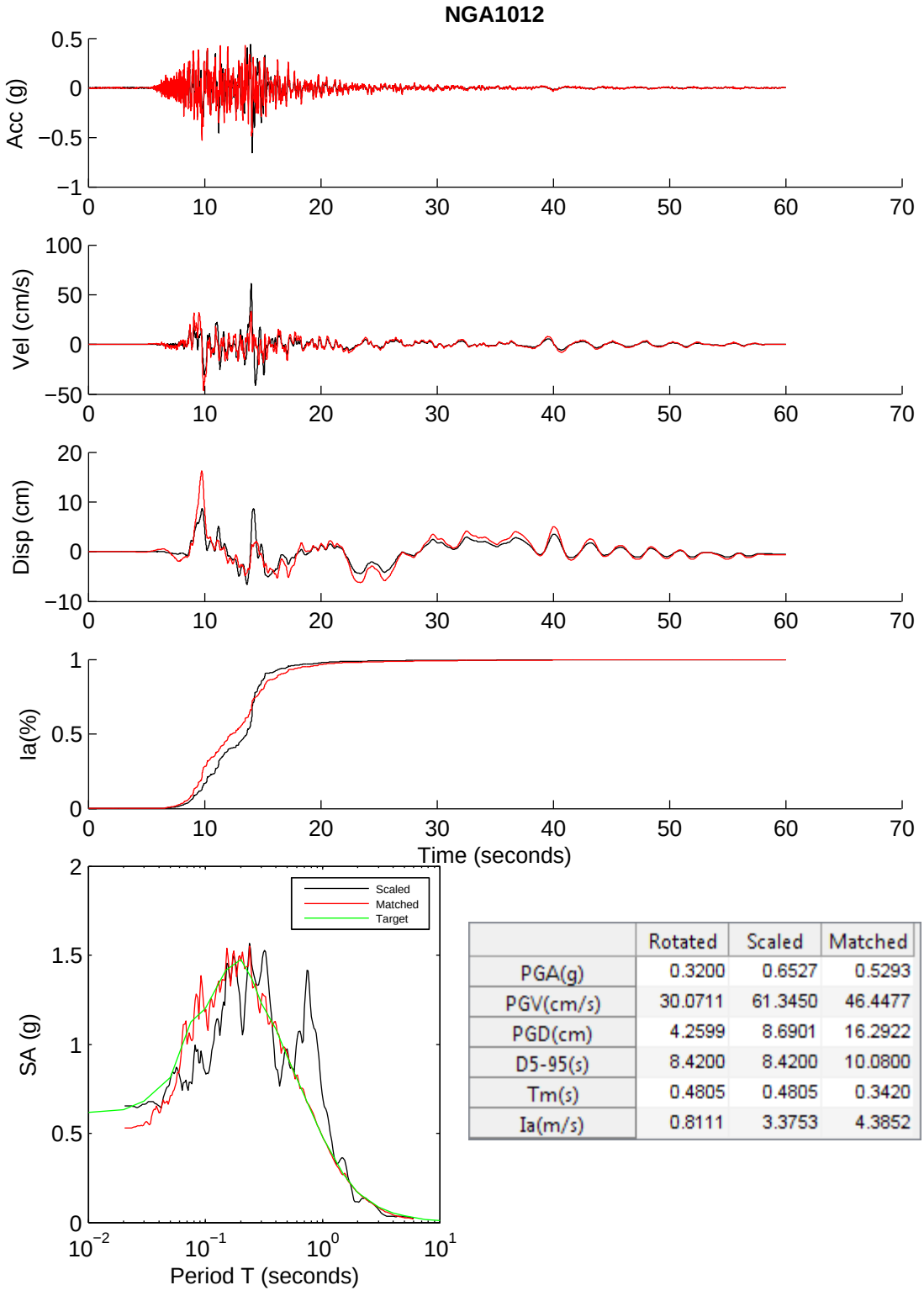

	Rotated	Scaled	Matched
PGA(g)	0.3200	0.6527	0.5293
PGV(cm/s)	30.0711	61.3450	46.4477
PGD(cm)	4.2599	8.6901	16.2922
D5-95(s)	8.4200	8.4200	10.0800
Tm(s)	0.4805	0.4805	0.3420
Ia(m/s)	0.8111	3.3753	4.3852

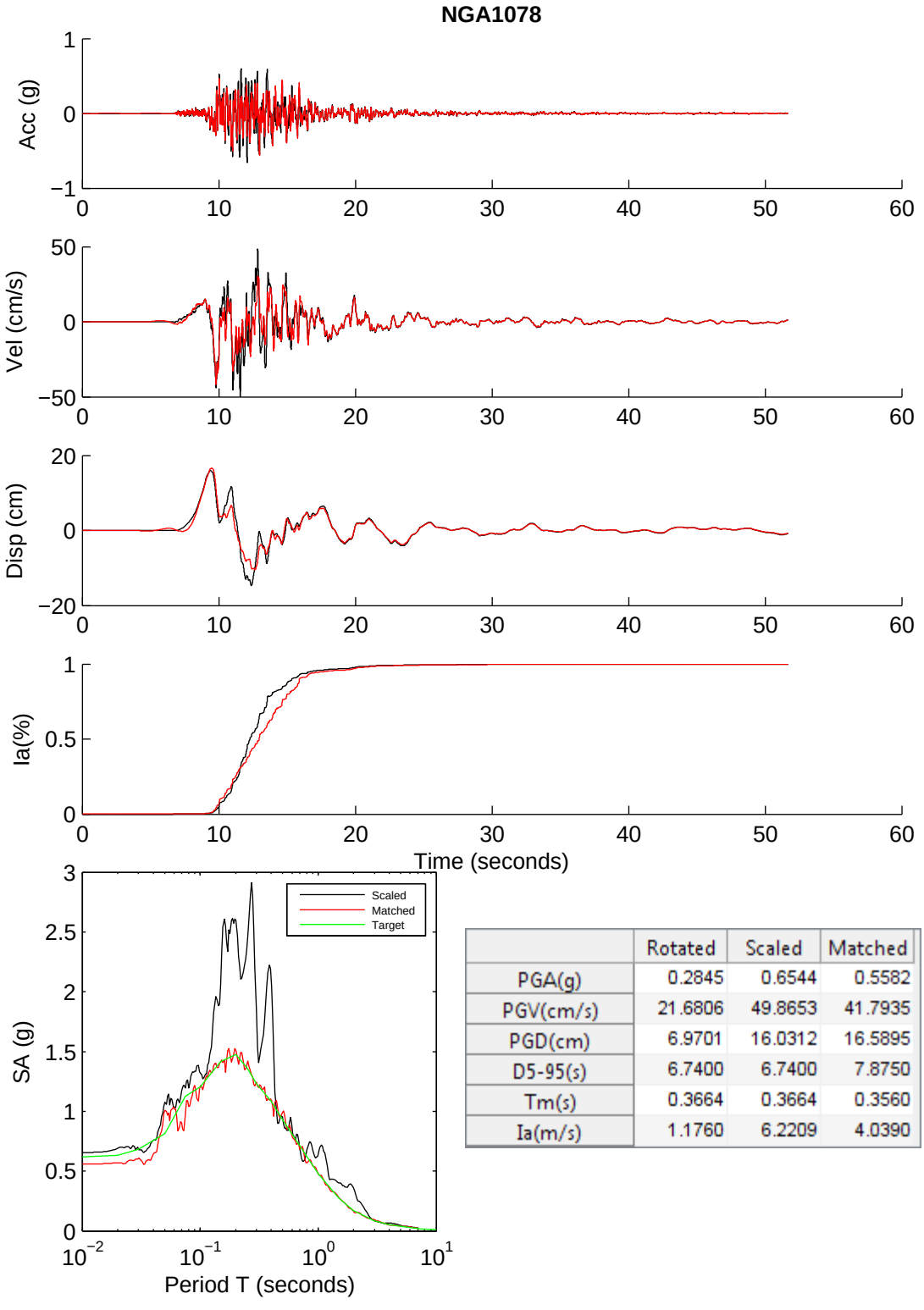

	Rotated	Scaled	Matched
PGA(g)	0.2845	0.6544	0.5582
PGV(cm/s)	21.6806	49.8653	41.7935
PGD(cm)	6.9701	16.0312	16.5895
D5-95(s)	6.7400	6.7400	7.8750
Tm(s)	0.3664	0.3664	0.3560
Ia(m/s)	1.1760	6.2209	4.0390

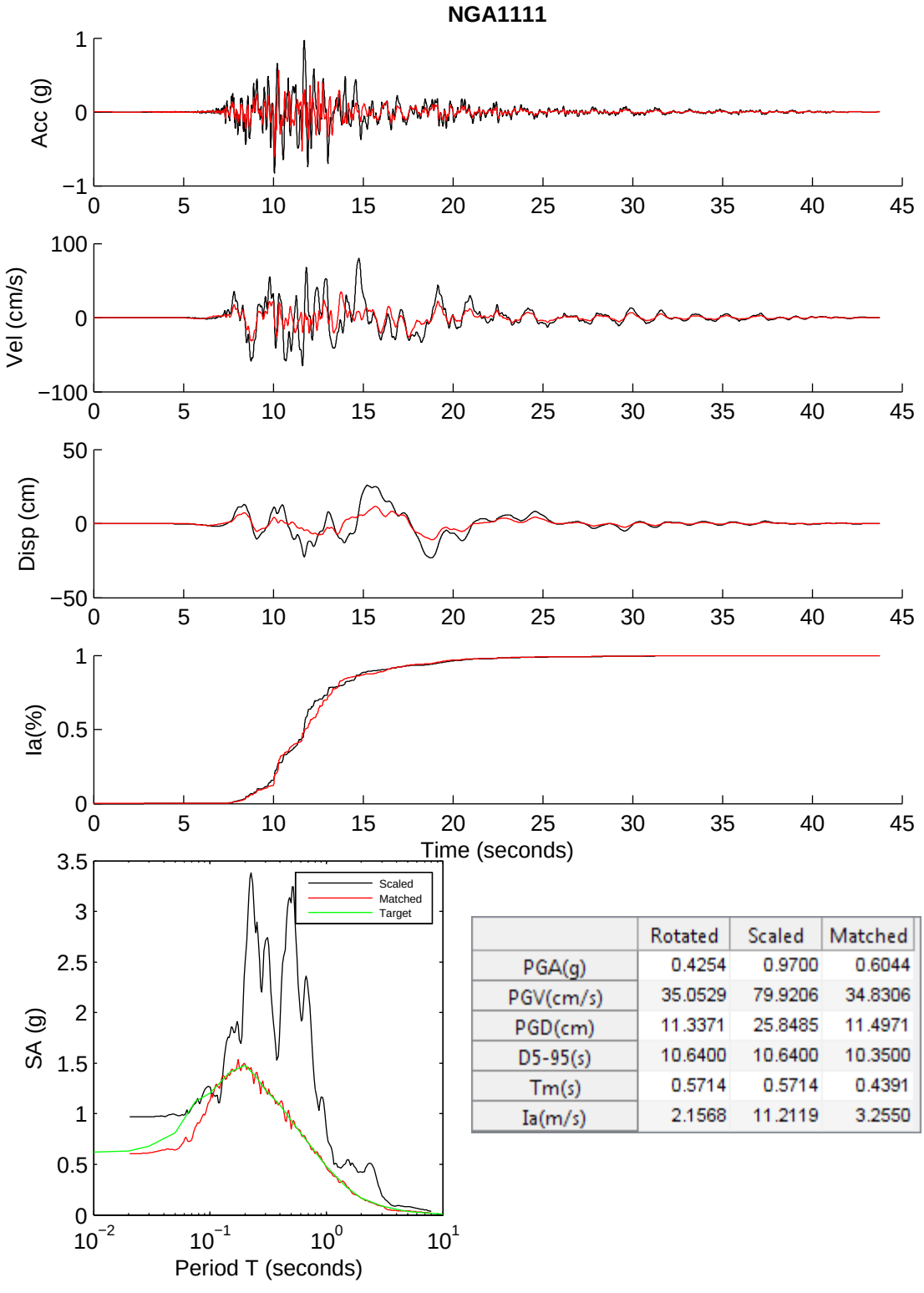

	Rotated	Scaled	Matched
PGA(g)	0.4254	0.9700	0.6044
PGV(cm/s)	35.0529	79.9206	34.8306
PGD(cm)	11.3371	25.8485	11.4971
D5-95(s)	10.6400	10.6400	10.3500
Tm(s)	0.5714	0.5714	0.4391
Ia(m/s)	2.1568	11.2119	3.2550

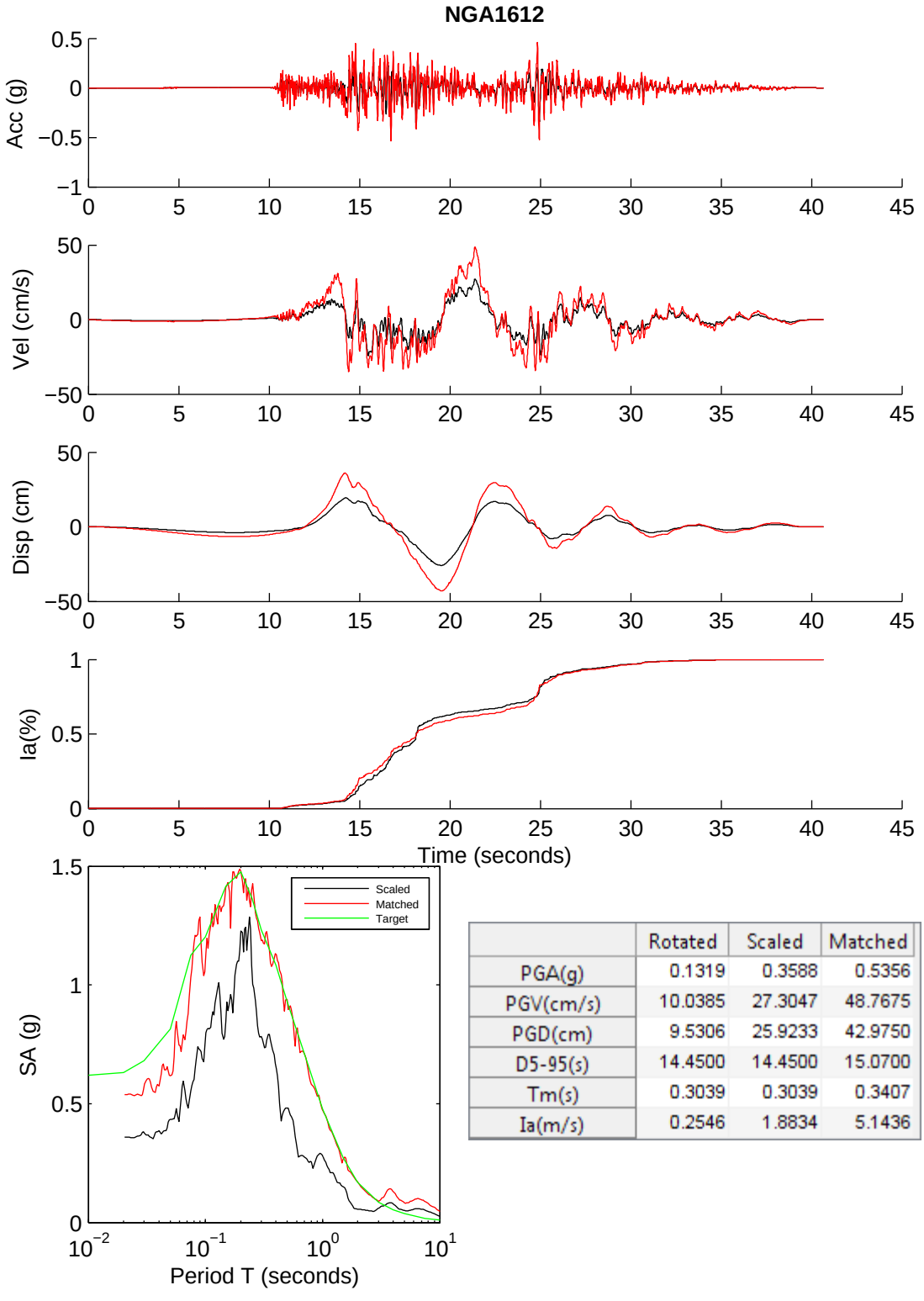

	Rotated	Scaled	Matched
PGA(g)	0.1319	0.3588	0.5356
PGV(cm/s)	10.0385	27.3047	48.7675
PGD(cm)	9.5306	25.9233	42.9750
D5-95(s)	14.4500	14.4500	15.0700
Tm(s)	0.3039	0.3039	0.3407
Ia(m/s)	0.2546	1.8834	5.1436

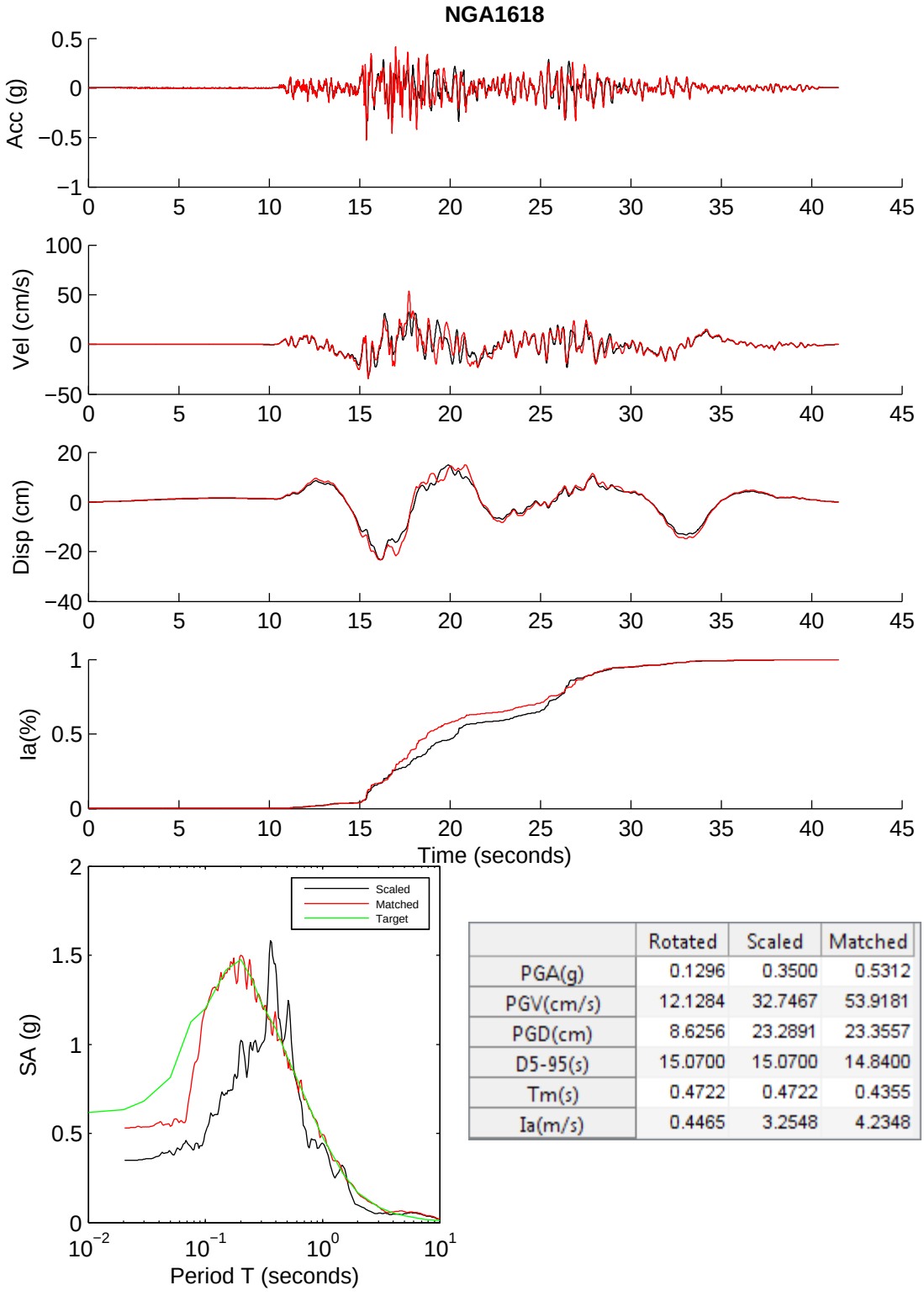

	Rotated	Scaled	Matched
PGA(g)	0.1296	0.3500	0.5312
PGV(cm/s)	12.1284	32.7467	53.9181
PGD(cm)	8.6256	23.2891	23.3557
D5-95(s)	15.0700	15.0700	14.8400
Tm(s)	0.4722	0.4722	0.4355
Ia(m/s)	0.4465	3.2548	4.2348

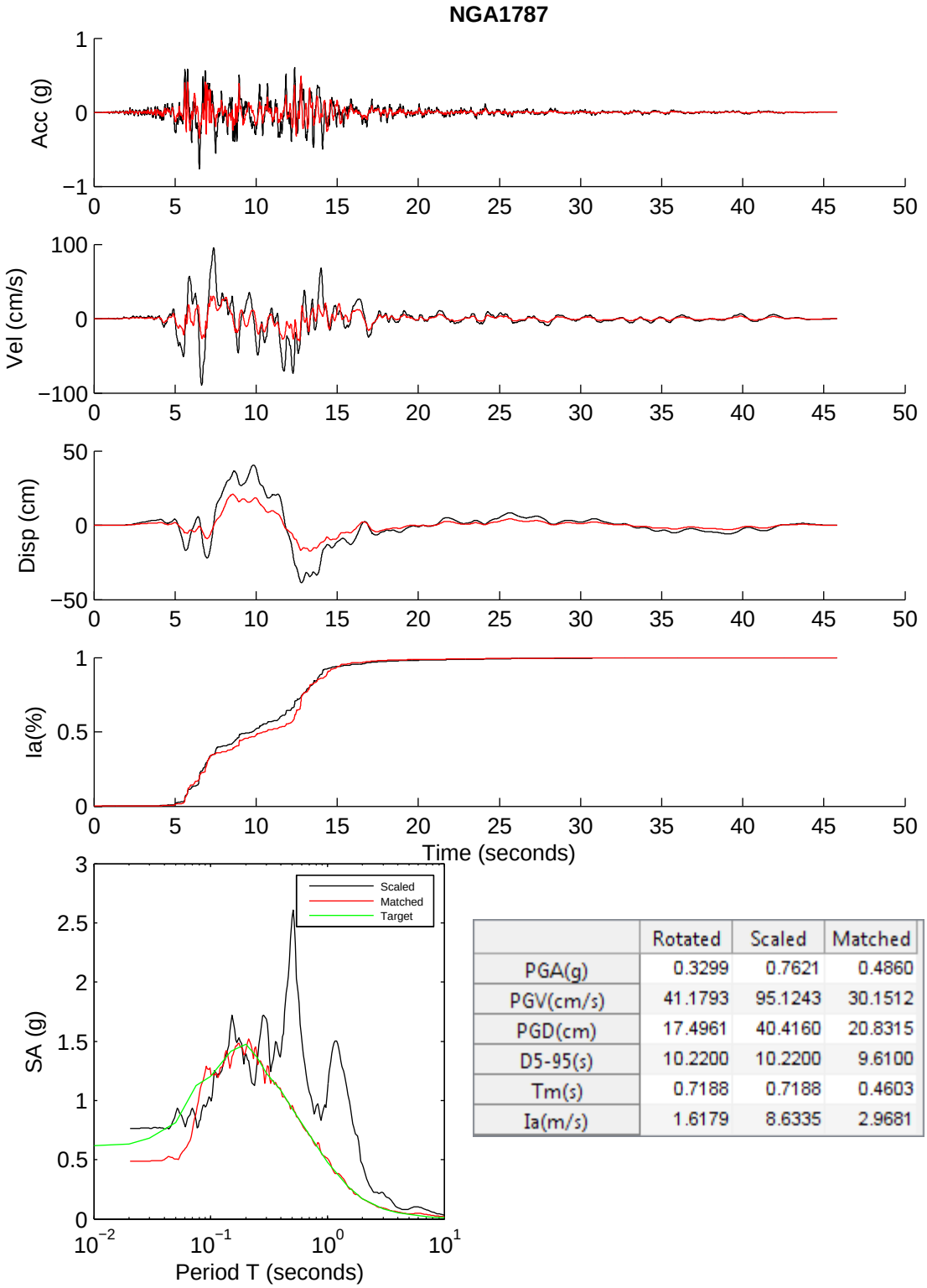

	Rotated	Scaled	Matched
PGA(g)	0.3299	0.7621	0.4860
PGV(cm/s)	41.1793	95.1243	30.1512
PGD(cm)	17.4961	40.4160	20.8315
D5-95(s)	10.2200	10.2200	9.6100
Tm(s)	0.7188	0.7188	0.4603
Ia(m/s)	1.6179	8.6335	2.9681

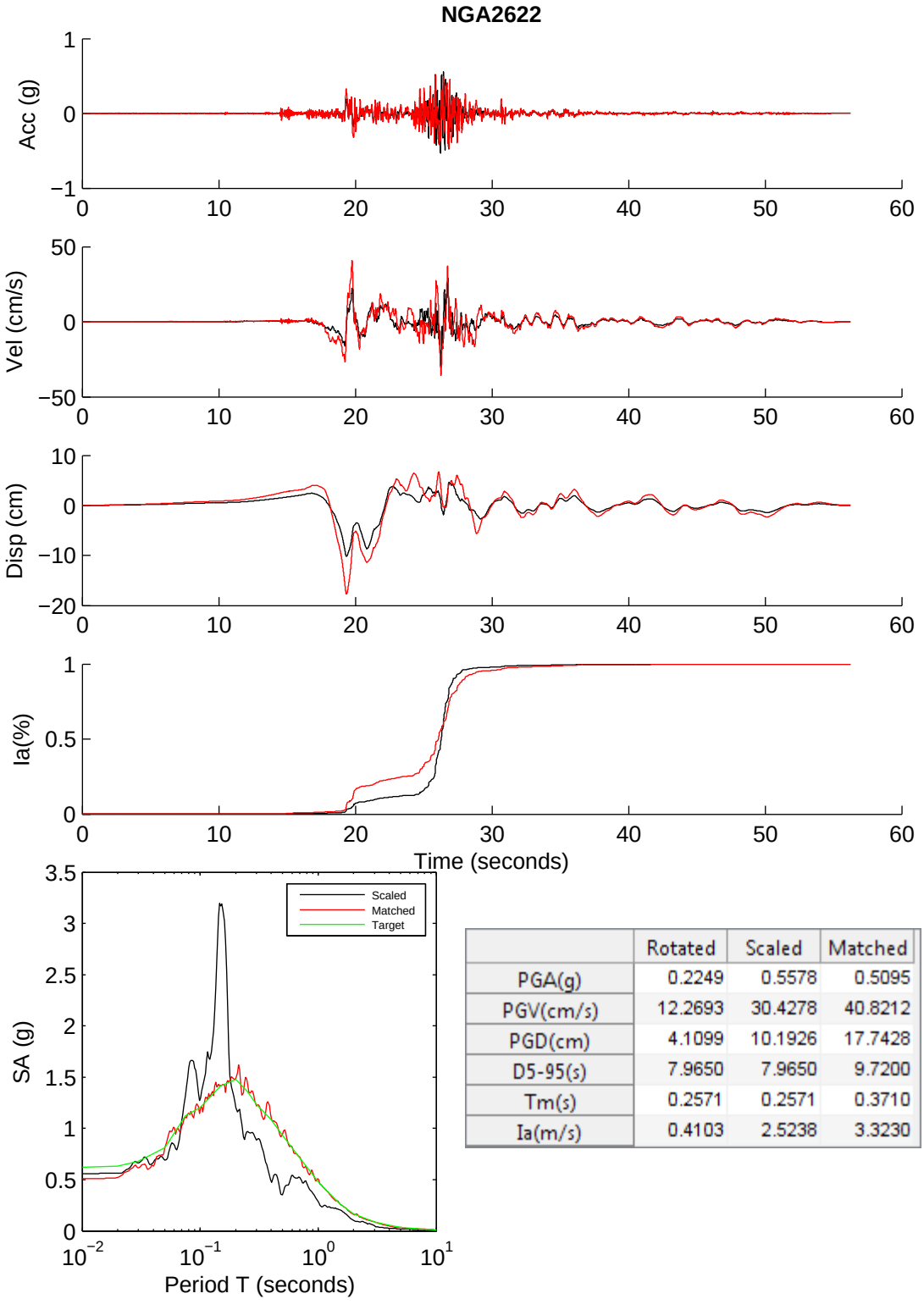

	Rotated	Scaled	Matched
PGA(g)	0.2249	0.5578	0.5095
PGV(cm/s)	12.2693	30.4278	40.8212
PGD(cm)	4.1099	10.1926	17.7428
D5-95(s)	7.9650	7.9650	9.7200
Tm(s)	0.2571	0.2571	0.3710
Ia(m/s)	0.4103	2.5238	3.3230

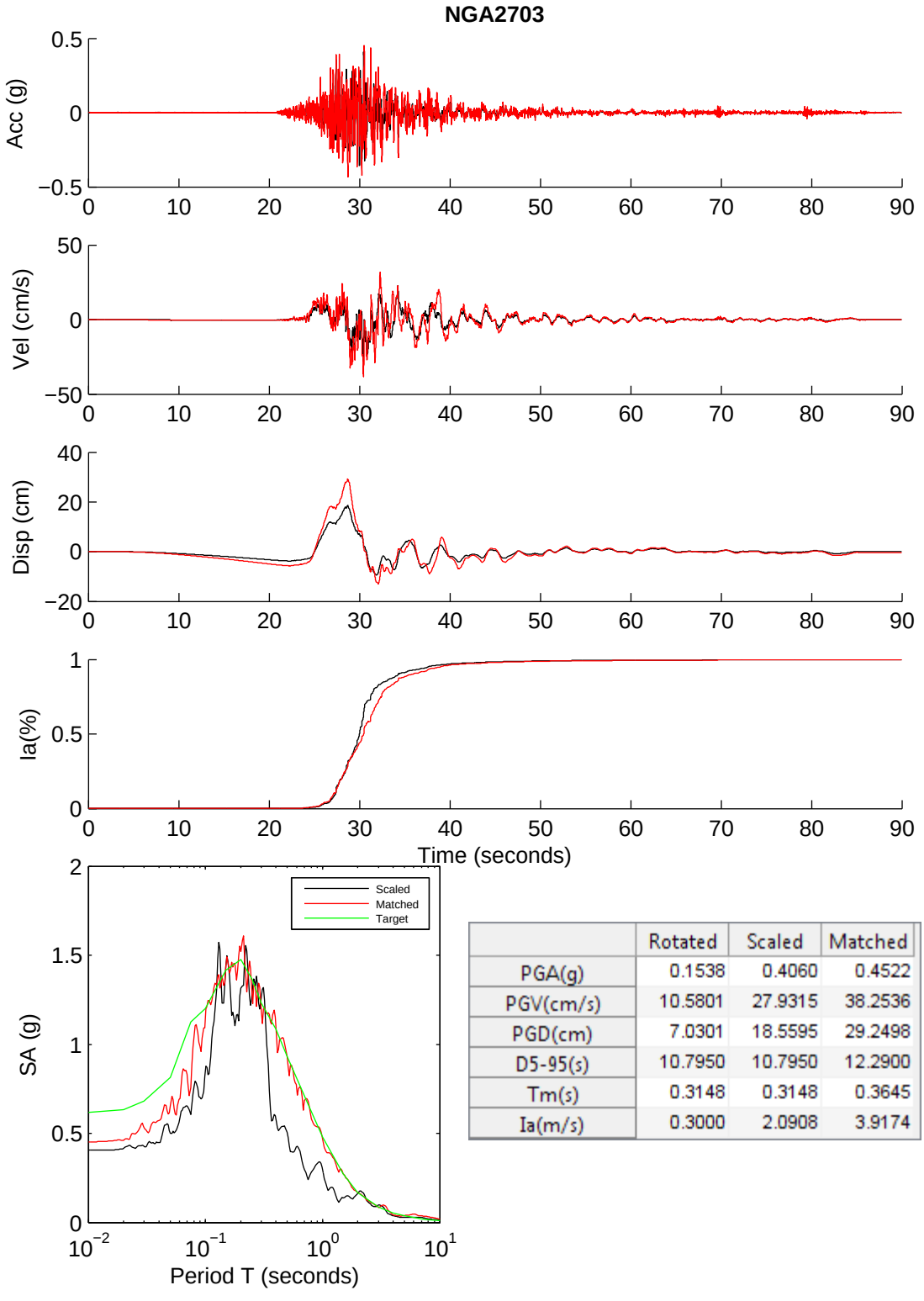

	Rotated	Scaled	Matched
PGA(g)	0.1538	0.4060	0.4522
PGV(cm/s)	10.5801	27.9315	38.2536
PGD(cm)	7.0301	18.5595	29.2498
D5-95(s)	10.7950	10.7950	12.2900
Tm(s)	0.3148	0.3148	0.3645
Ia(m/s)	0.3000	2.0908	3.9174

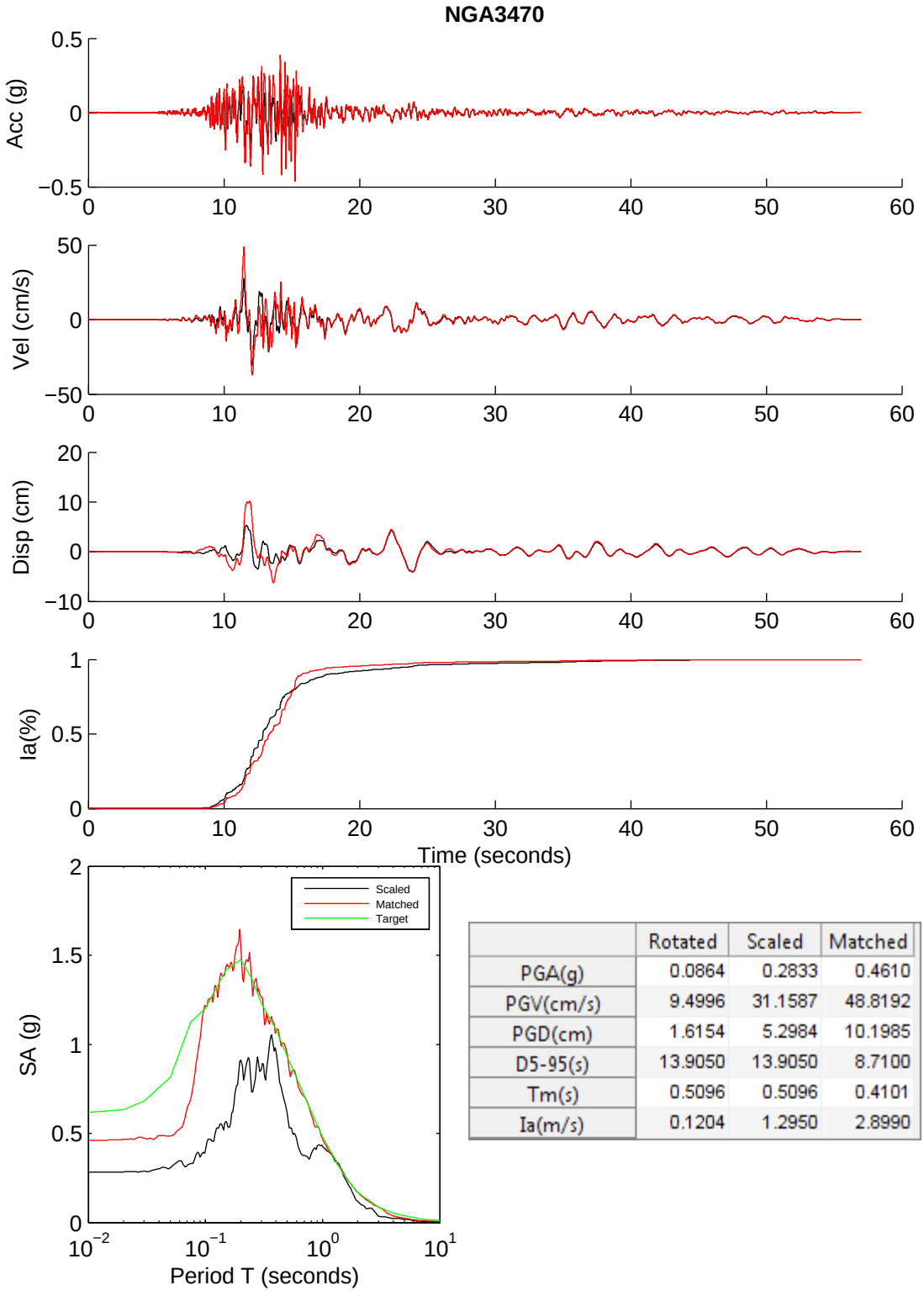

	Rotated	Scaled	Matched
PGA(g)	0.0864	0.2833	0.4610
PGV(cm/s)	9.4996	31.1587	48.8192
PGD(cm)	1.6154	5.2984	10.1985
D5-95(s)	13.9050	13.9050	8.7100
Tm(s)	0.5096	0.5096	0.4101
Ia(m/s)	0.1204	1.2950	2.8990

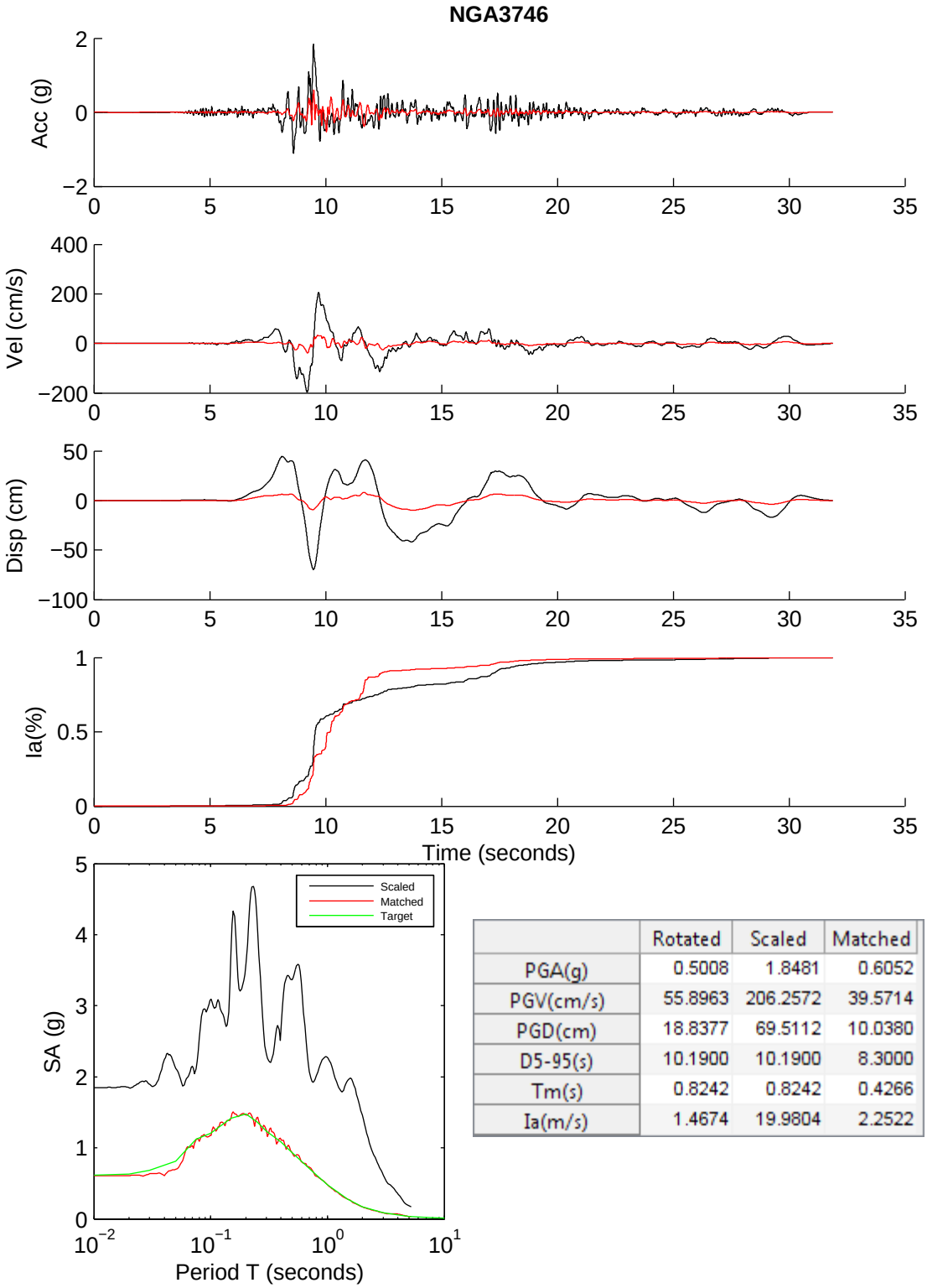

	Rotated	Scaled	Matched
PGA(g)	0.5008	1.8481	0.6052
PGV(cm/s)	55.8963	206.2572	39.5714
PGD(cm)	18.8377	69.5112	10.0380
D5-95(s)	10.1900	10.1900	8.3000
Tm(s)	0.8242	0.8242	0.4266
Ia(m/s)	1.4674	19.9804	2.2522

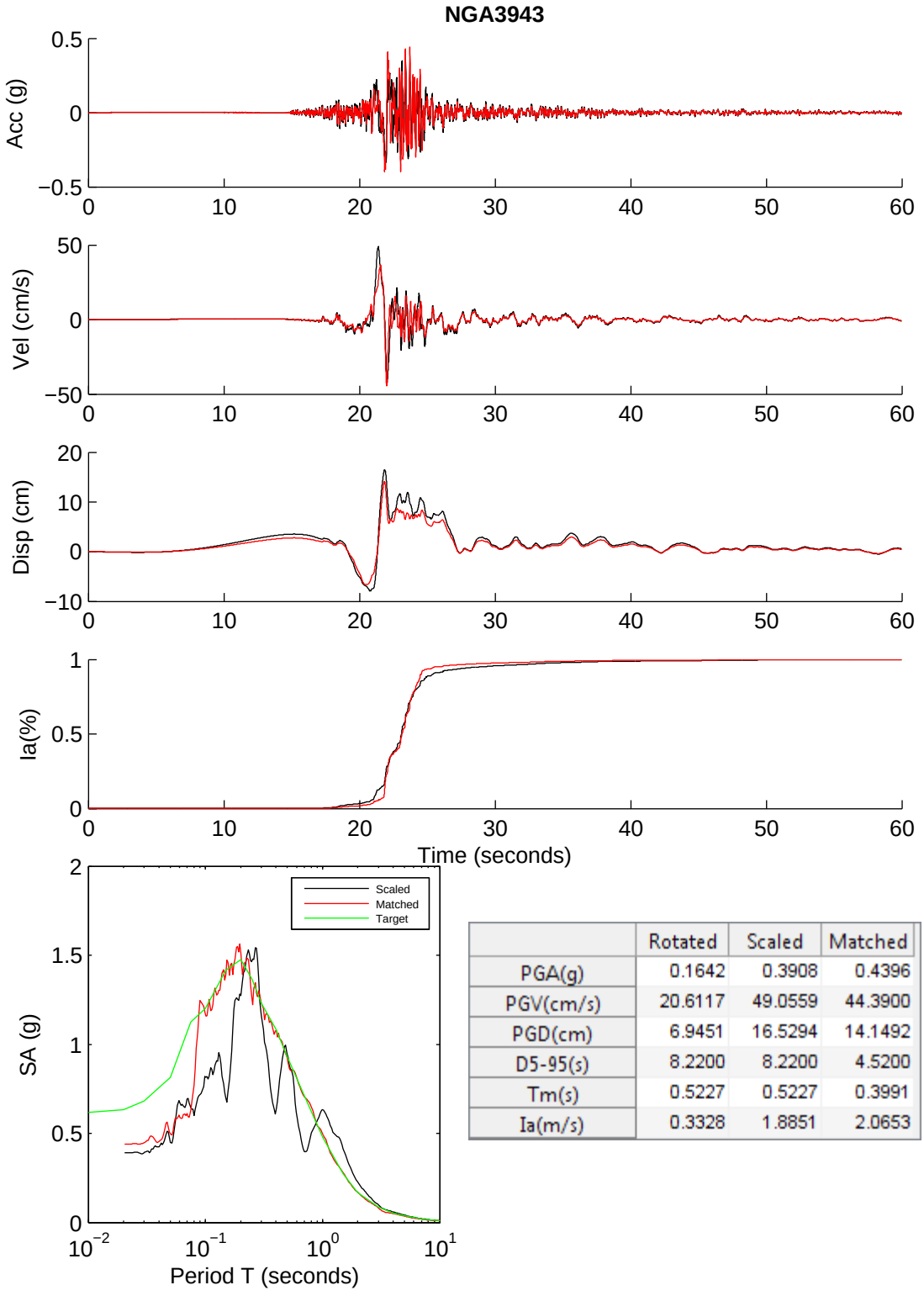

	Rotated	Scaled	Matched
PGA(g)	0.1642	0.3908	0.4396
PGV(cm/s)	20.6117	49.0559	44.3900
PGD(cm)	6.9451	16.5294	14.1492
D5-95(s)	8.2200	8.2200	4.5200
Tm(s)	0.5227	0.5227	0.3991
Ia(m/s)	0.3328	1.8851	2.0653

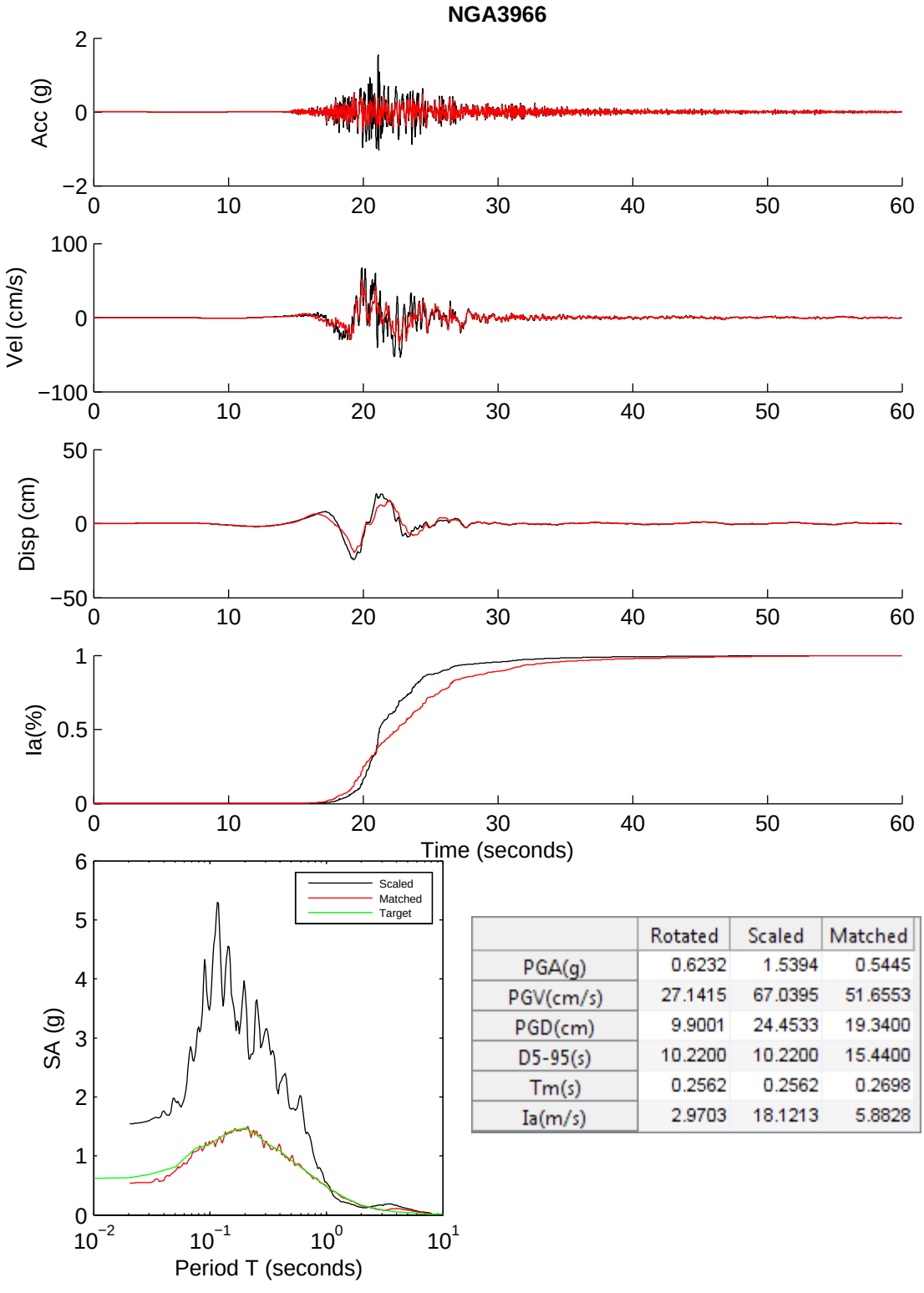

	Rotated	Scaled	Matched
PGA(g)	0.6232	1.5394	0.5445
PGV(cm/s)	27.1415	67.0395	51.6553
PGD(cm)	9.9001	24.4533	19.3400
D5-95(s)	10.2200	10.2200	15.4400
Tm(s)	0.2562	0.2562	0.2698
Ia(m/s)	2.9703	18.1213	5.8828

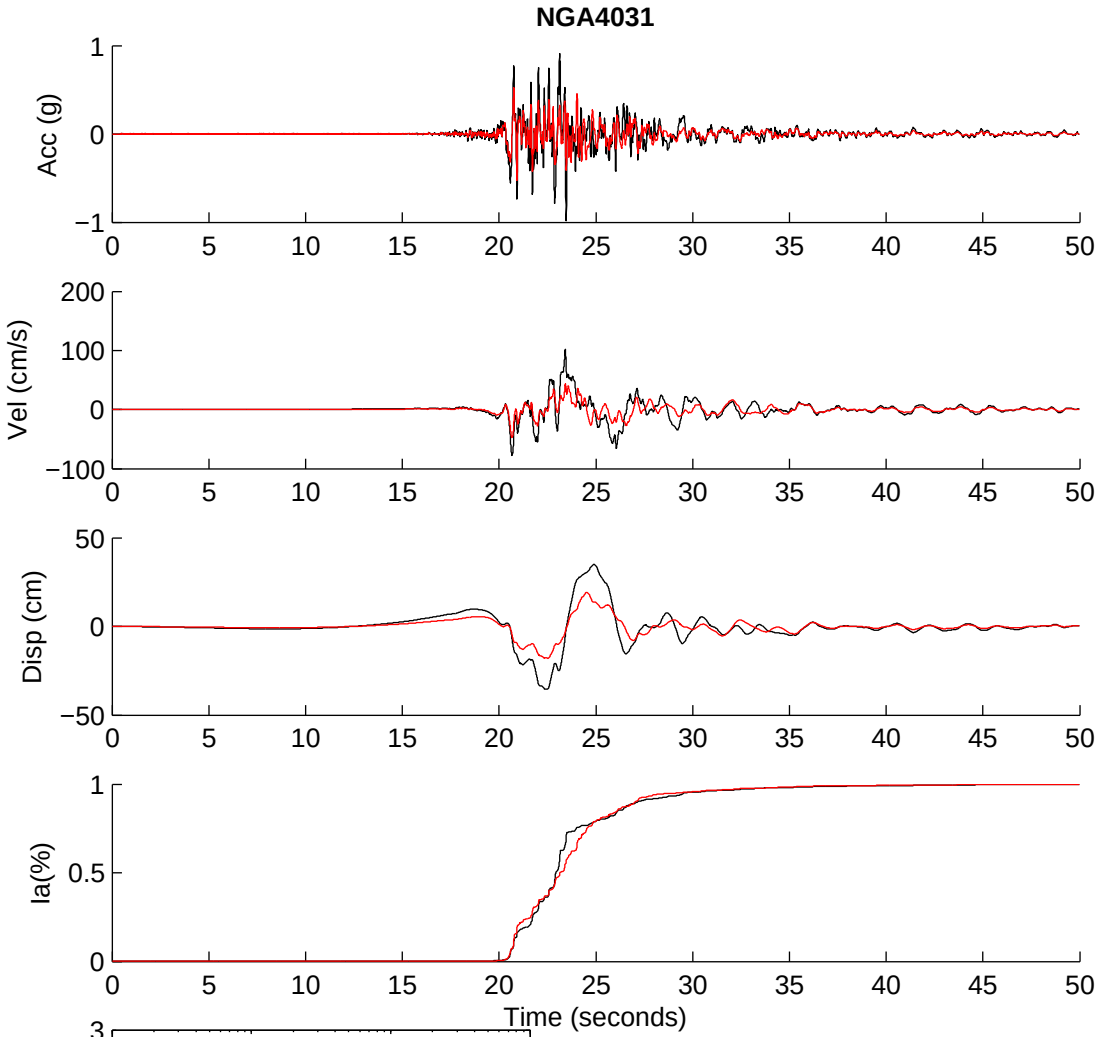

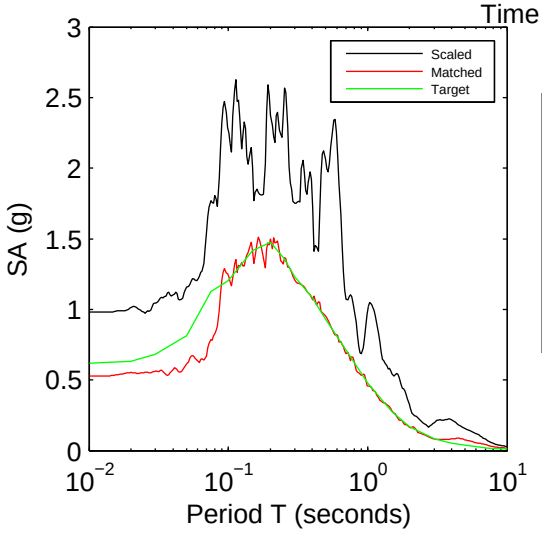

	Rotated	Scaled	Matched
PGA(g)	0.4100	0.9799	0.5269
PGV(cm/s)	42.7933	102.2761	47.7189
PGD(cm)	14.8524	35.4973	19.2875
D5-95(s)	8.9700	8.9700	8.5850
Tm(s)	0.4931	0.4931	0.4396
Ia(m/s)	1.4696	8.3946	3.2493

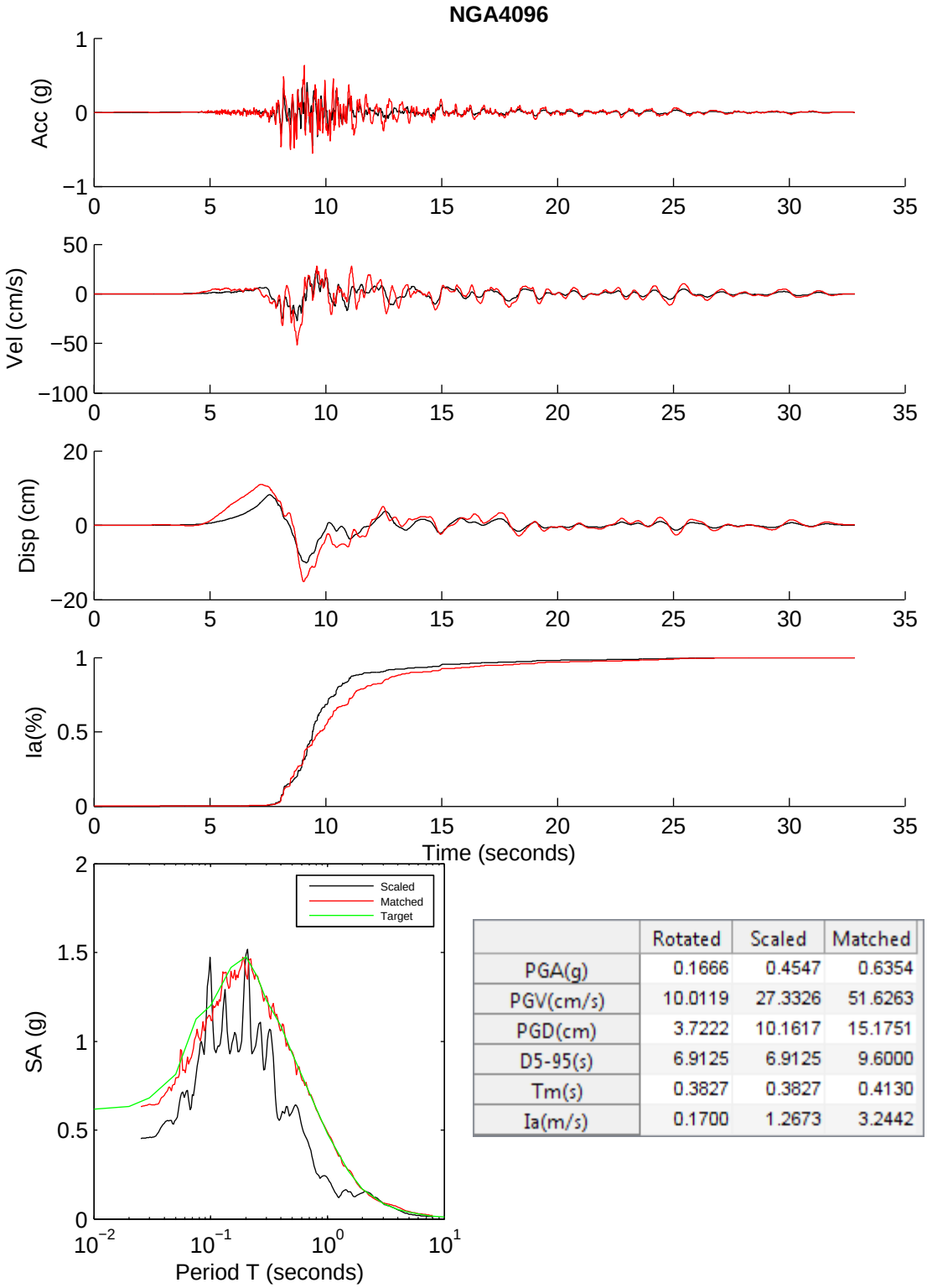

	Rotated	Scaled	Matched
PGA(g)	0.1666	0.4547	0.6354
PGV(cm/s)	10.0119	27.3326	51.6263
PGD(cm)	3.7222	10.1617	15.1751
D5-95(s)	6.9125	6.9125	9.6000
Tm(s)	0.3827	0.3827	0.4130
Ia(m/s)	0.1700	1.2673	3.2442

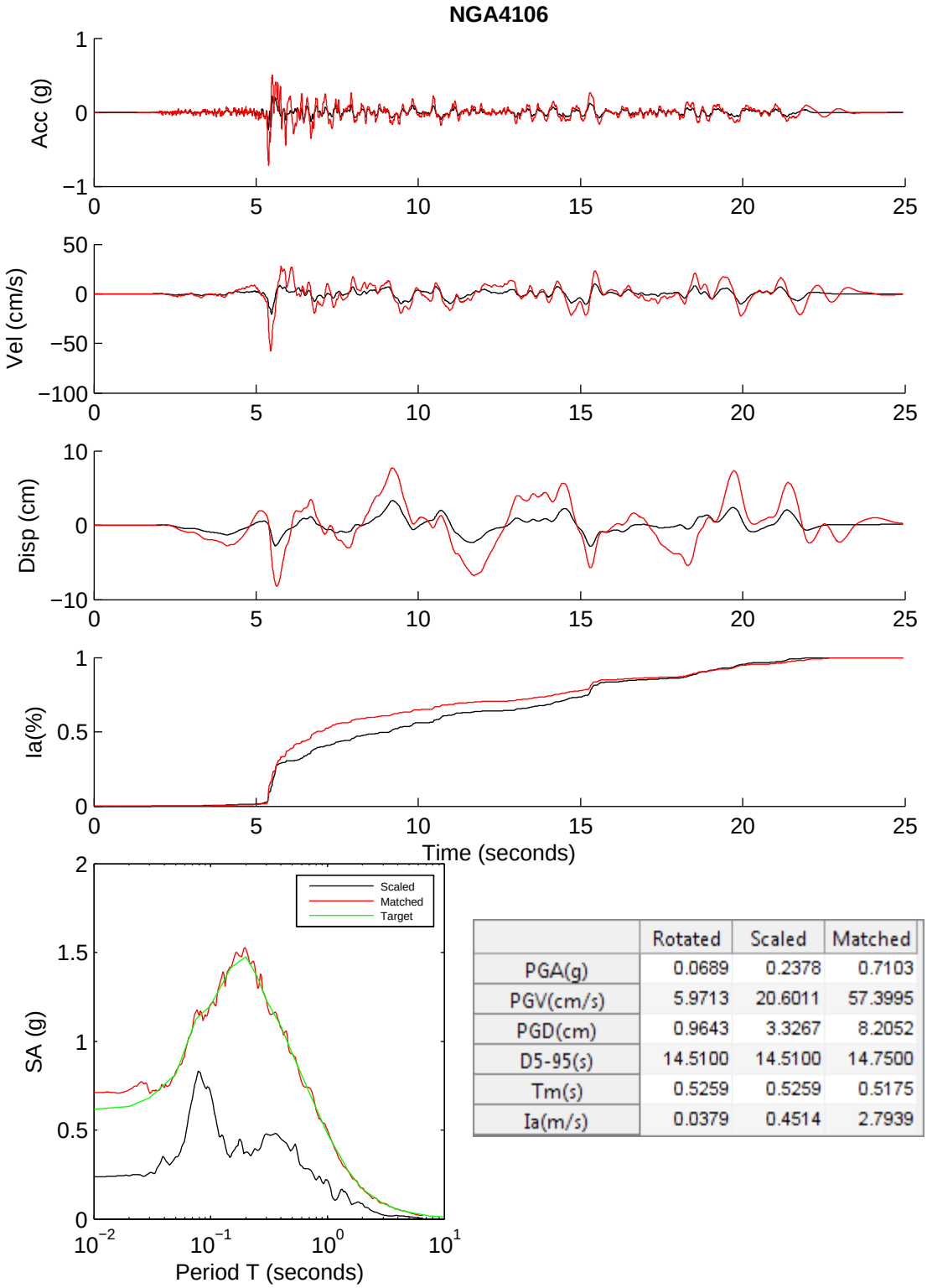

	Rotated	Scaled	Matched
PGA(g)	0.0689	0.2378	0.7103
PGV(cm/s)	5.9713	20.6011	57.3995
PGD(cm)	0.9643	3.3267	8.2052
D5-95(s)	14.5100	14.5100	14.7500
Tm(s)	0.5259	0.5259	0.5175
Ia(m/s)	0.0379	0.4514	2.7939

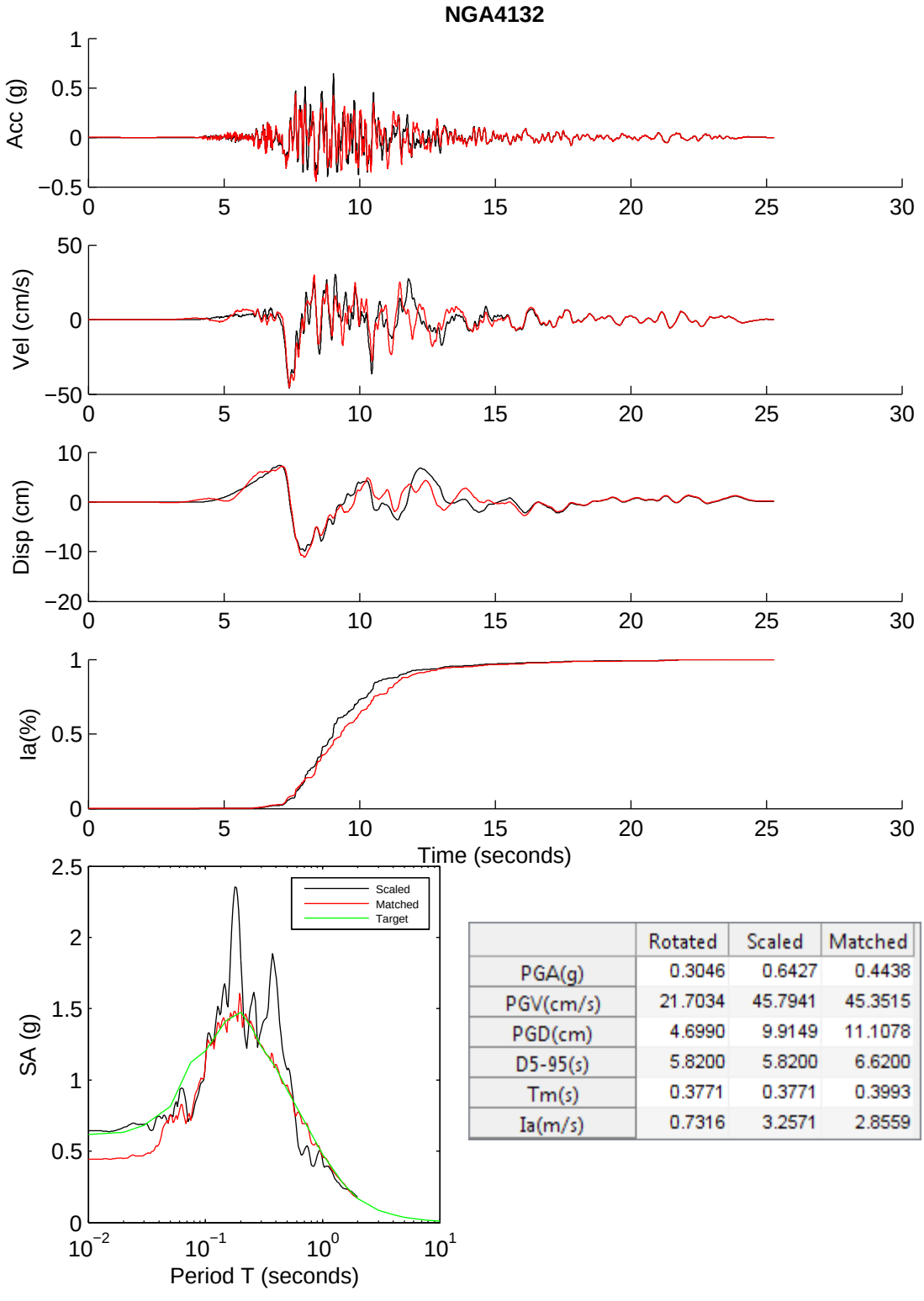

	Rotated	Scaled	Matched
PGA(g)	0.3046	0.6427	0.4438
PGV(cm/s)	21.7034	45.7941	45.3515
PGD(cm)	4.6990	9.9149	11.1078
D5-95(s)	5.8200	5.8200	6.6200
Tm(s)	0.3771	0.3771	0.3993
Ia(m/s)	0.7316	3.2571	2.8559

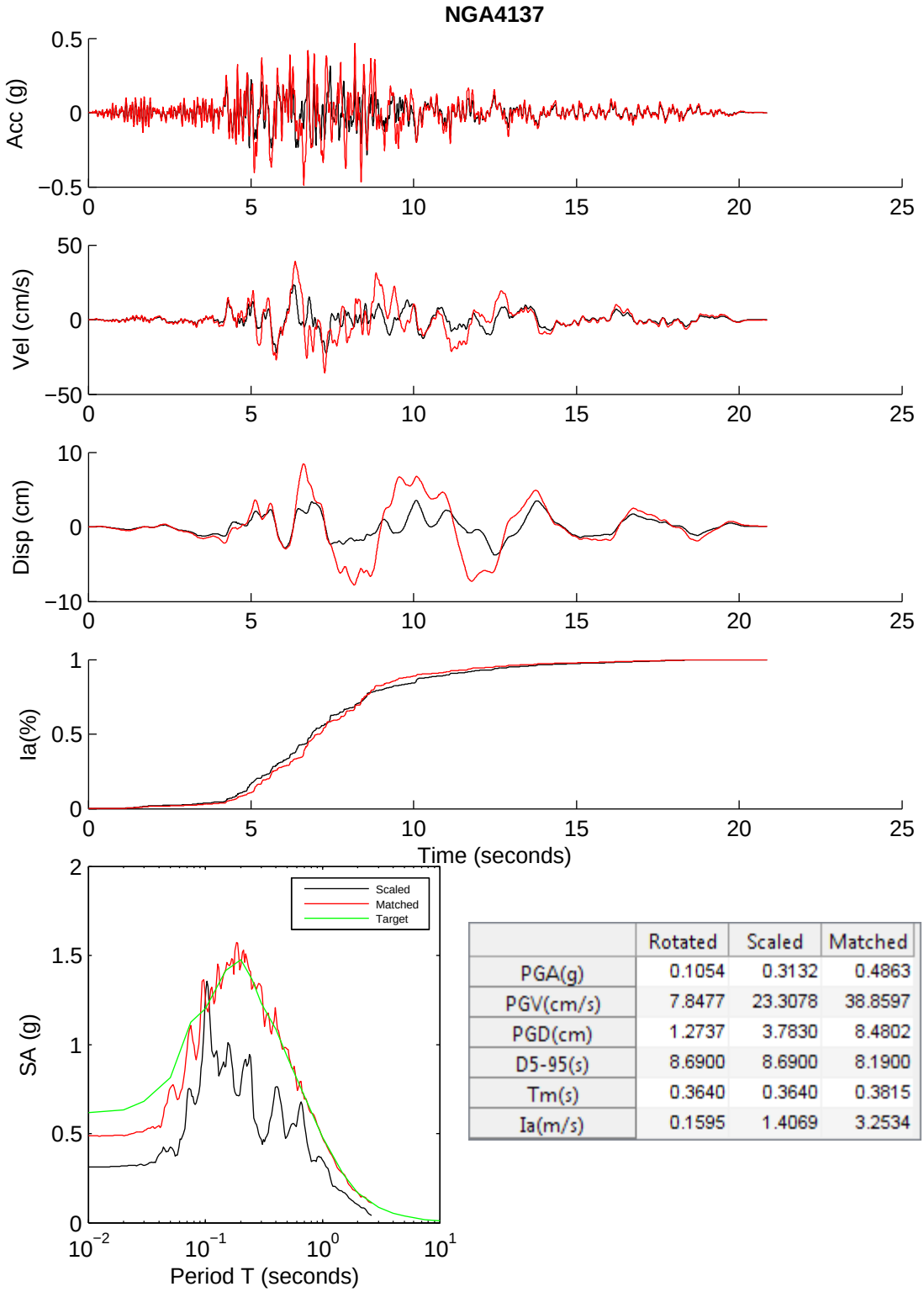

	Rotated	Scaled	Matched
PGA(g)	0.1054	0.3132	0.4863
PGV(cm/s)	7.8477	23.3078	38.8597
PGD(cm)	1.2737	3.7830	8.4802
D5-95(s)	8.6900	8.6900	8.1900
Tm(s)	0.3640	0.3640	0.3815
Ia(m/s)	0.1595	1.4069	3.2534

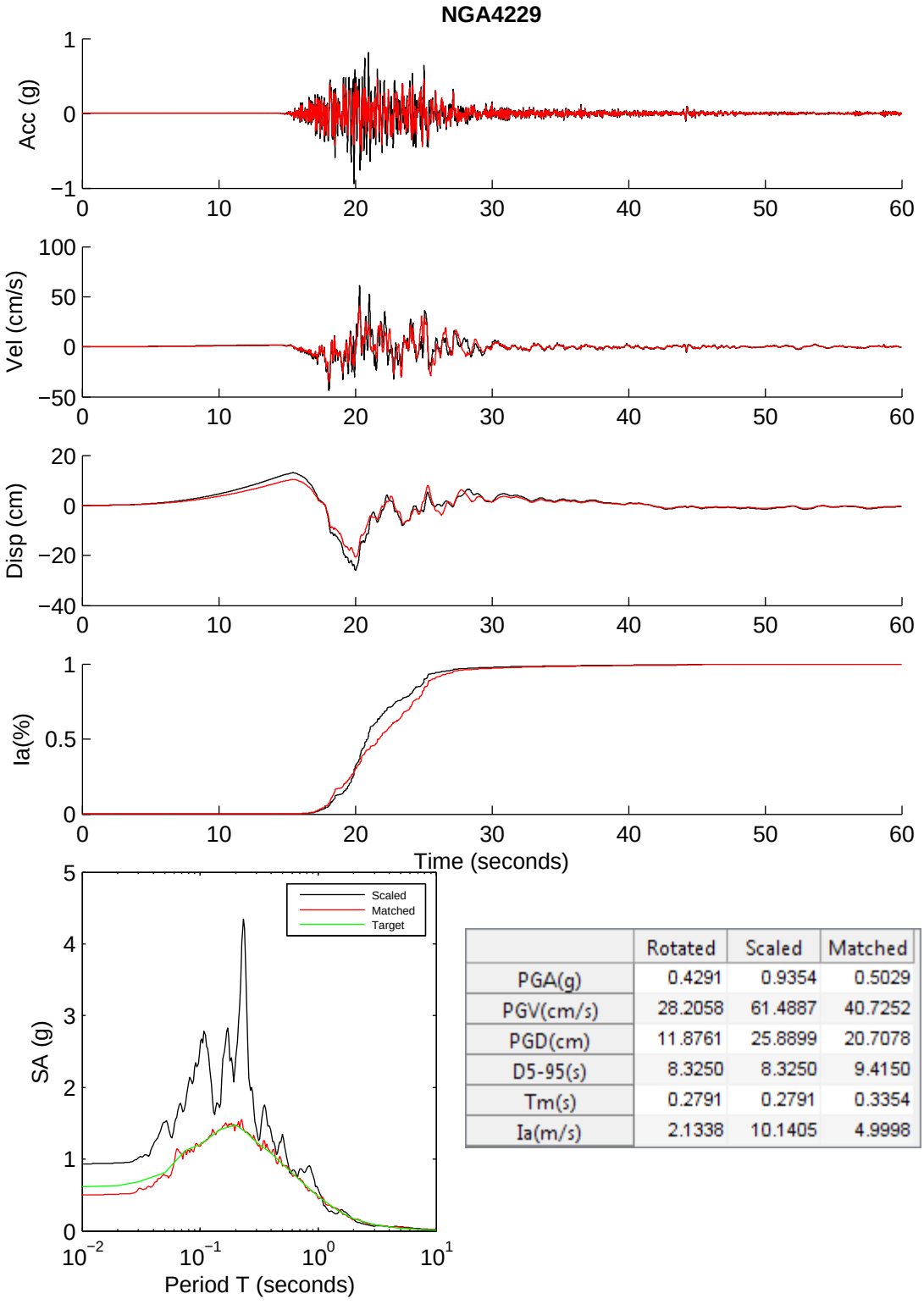

	Rotated	Scaled	Matched
PGA(g)	0.4291	0.9354	0.5029
PGV(cm/s)	28.2058	61.4887	40.7252
PGD(cm)	11.8761	25.8899	20.7078
D5-95(s)	8.3250	8.3250	9.4150
Tm(s)	0.2791	0.2791	0.3354
Ia(m/s)	2.1338	10.1405	4.9998

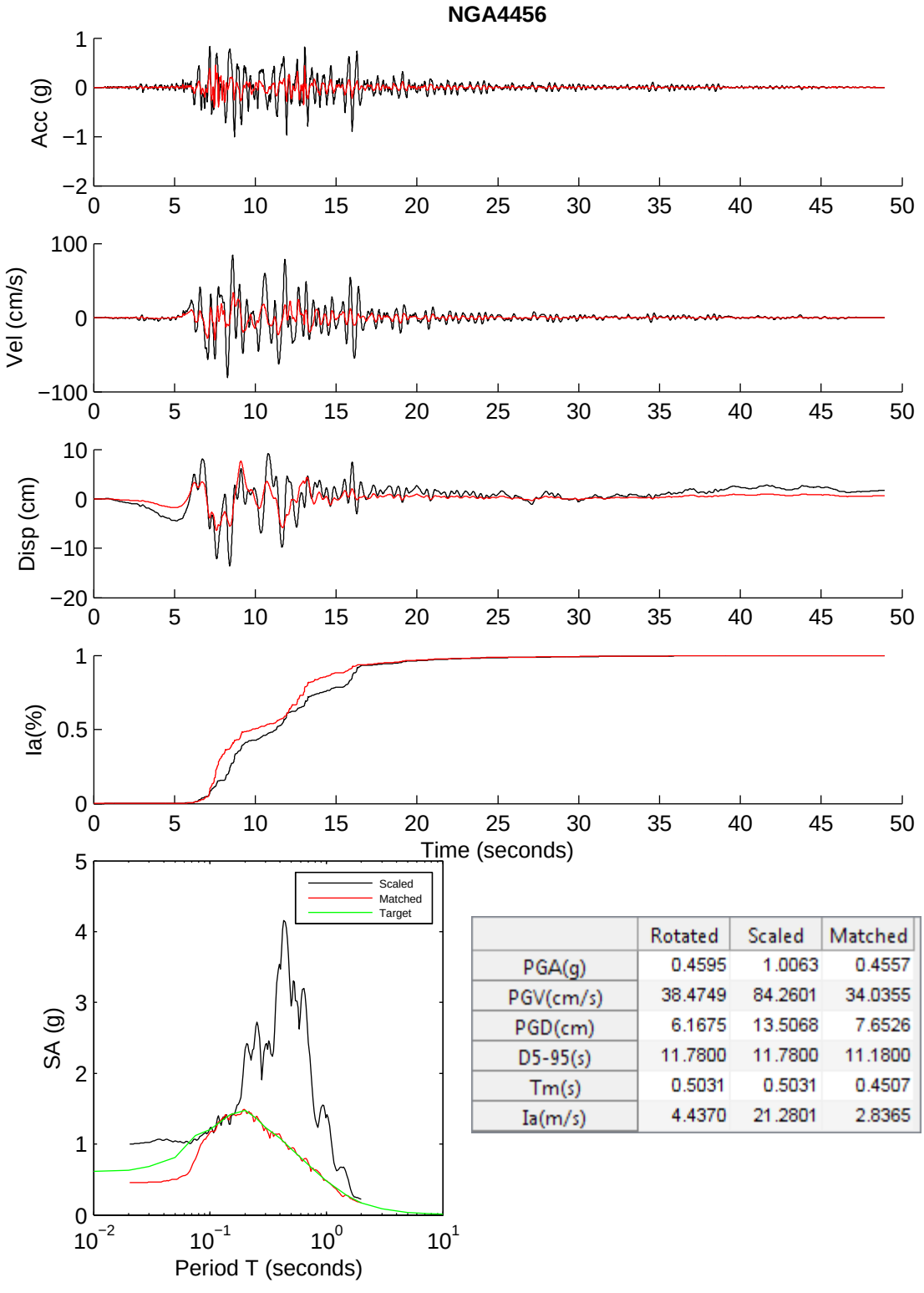

	Rotated	Scaled	Matched
PGA(g)	0.4595	1.0063	0.4557
PGV(cm/s)	38.4749	84.2601	34.0355
PGD(cm)	6.1675	13.5068	7.6526
D5-95(s)	11.7800	11.7800	11.1800
Tm(s)	0.5031	0.5031	0.4507
Ia(m/s)	4.4370	21.2801	2.8365

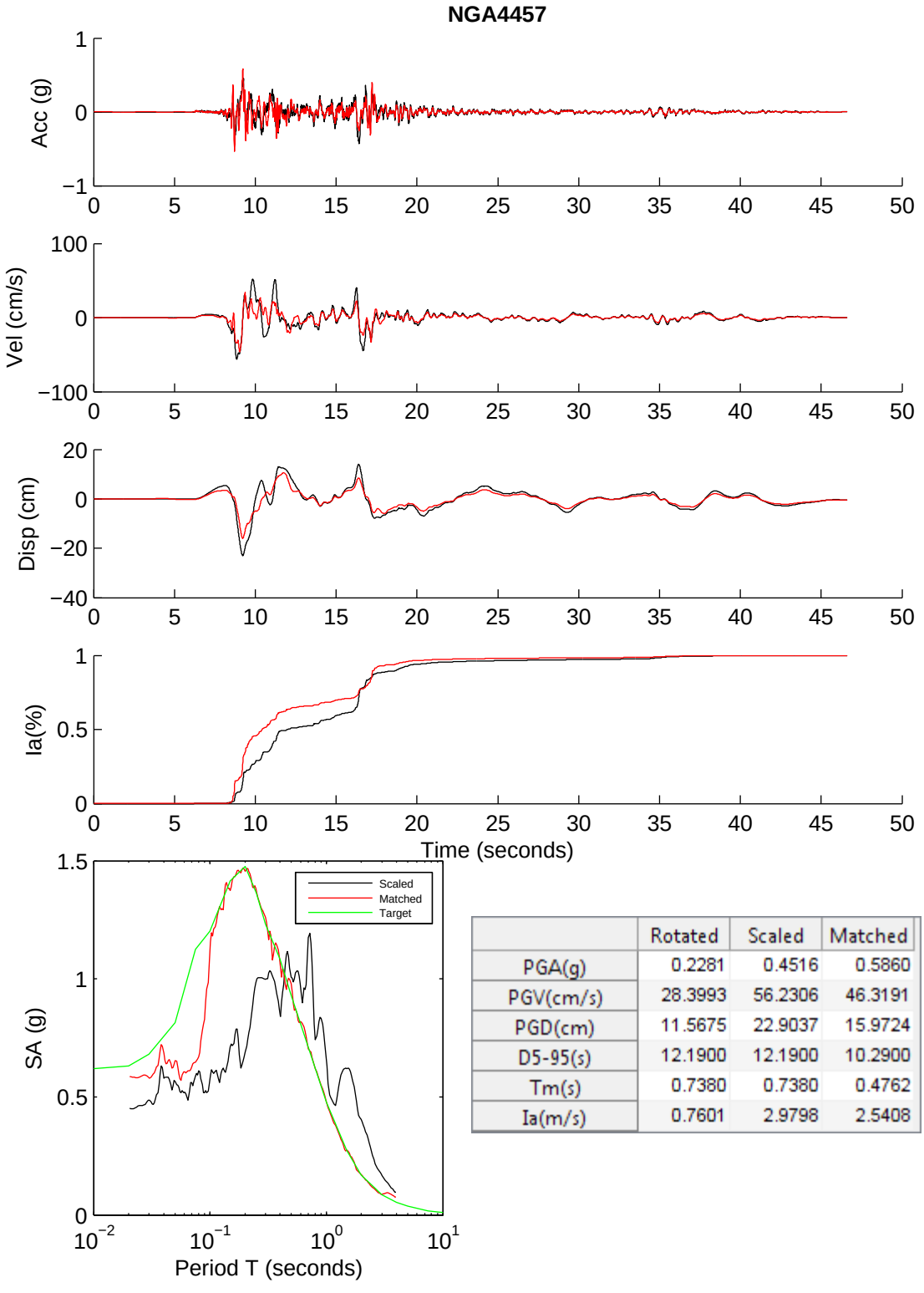

	Rotated	Scaled	Matched
PGA(g)	0.2281	0.4516	0.5860
PGV(cm/s)	28.3993	56.2306	46.3191
PGD(cm)	11.5675	22.9037	15.9724
D5-95(s)	12.1900	12.1900	10.2900
Tm(s)	0.7380	0.7380	0.4762
Ia(m/s)	0.7601	2.9798	2.5408

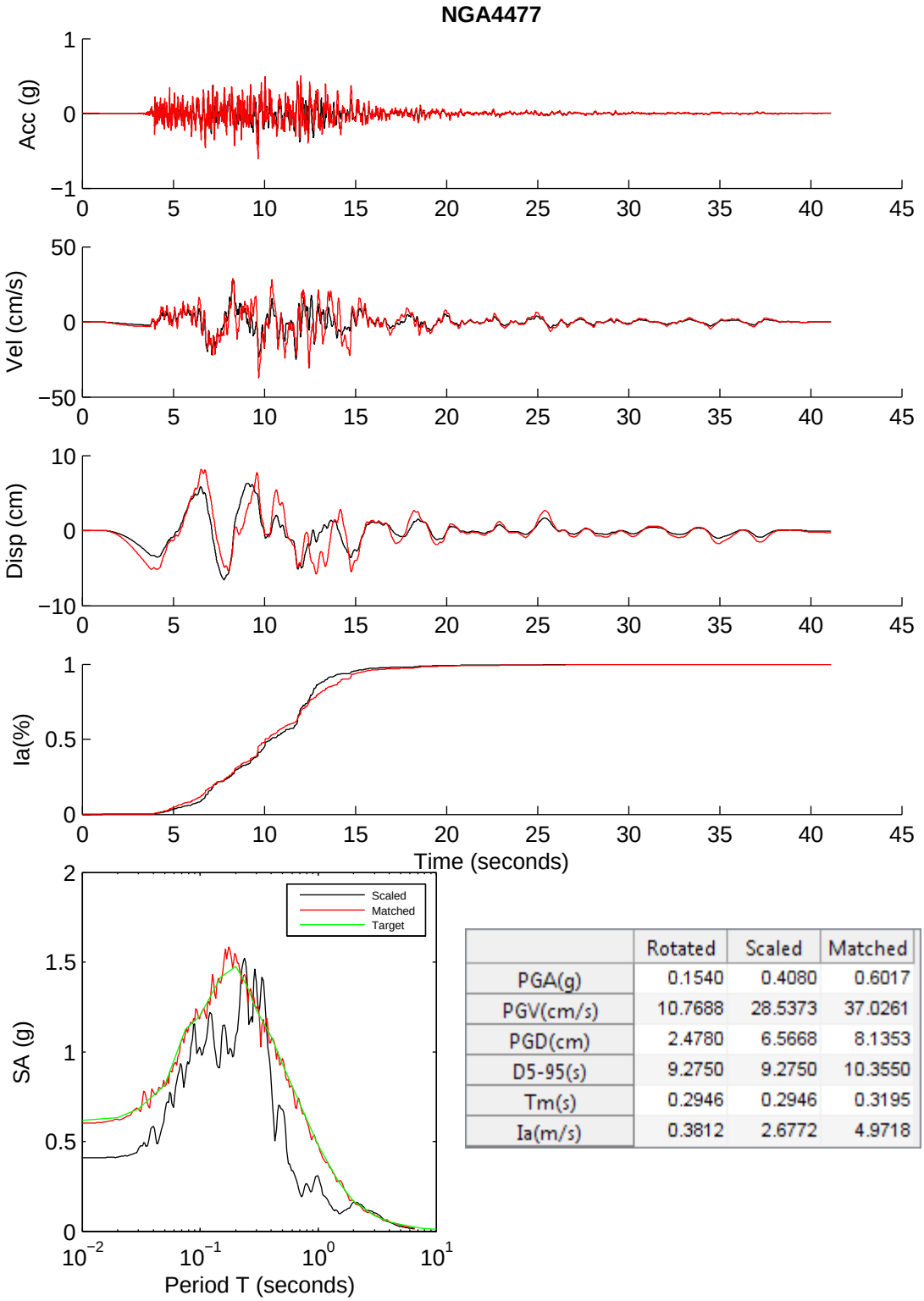

	Rotated	Scaled	Matched
PGA(g)	0.1540	0.4080	0.6017
PGV(cm/s)	10.7688	28.5373	37.0261
PGD(cm)	2.4780	6.5668	8.1353
D5-95(s)	9.2750	9.2750	10.3550
Tm(s)	0.2946	0.2946	0.3195
Ia(m/s)	0.3812	2.6772	4.9718

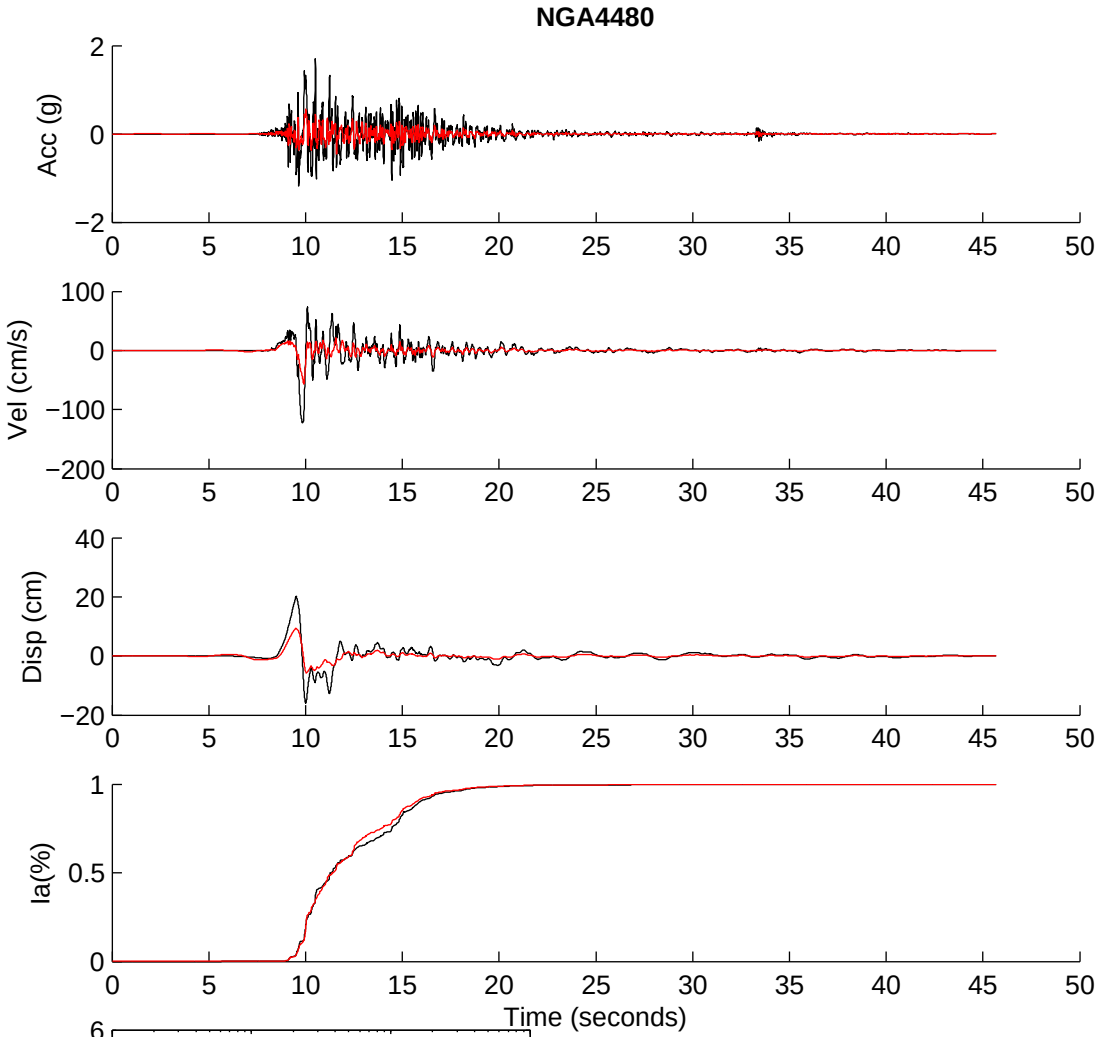

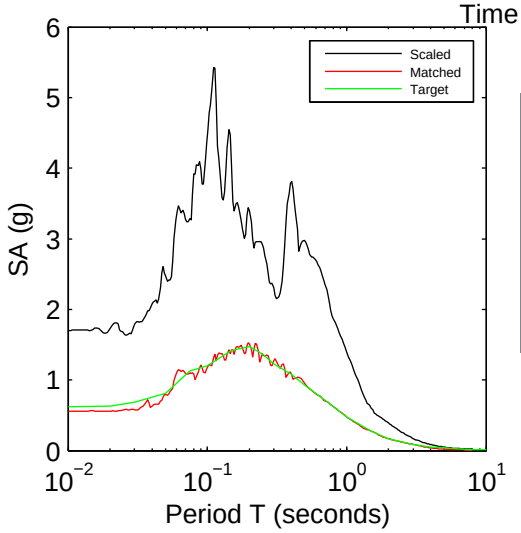

	Rotated	Scaled	Matched
PGA(g)	0.5854	1.7036	0.5569
PGV(cm/s)	42.0104	122.2504	56.4584
PGD(cm)	6.9057	20.0955	9.4214
D5-95(s)	7.5450	7.5450	7.1250
Tm(s)	0.3199	0.3199	0.3112
Ia(m/s)	2.8888	24.4628	3.2623

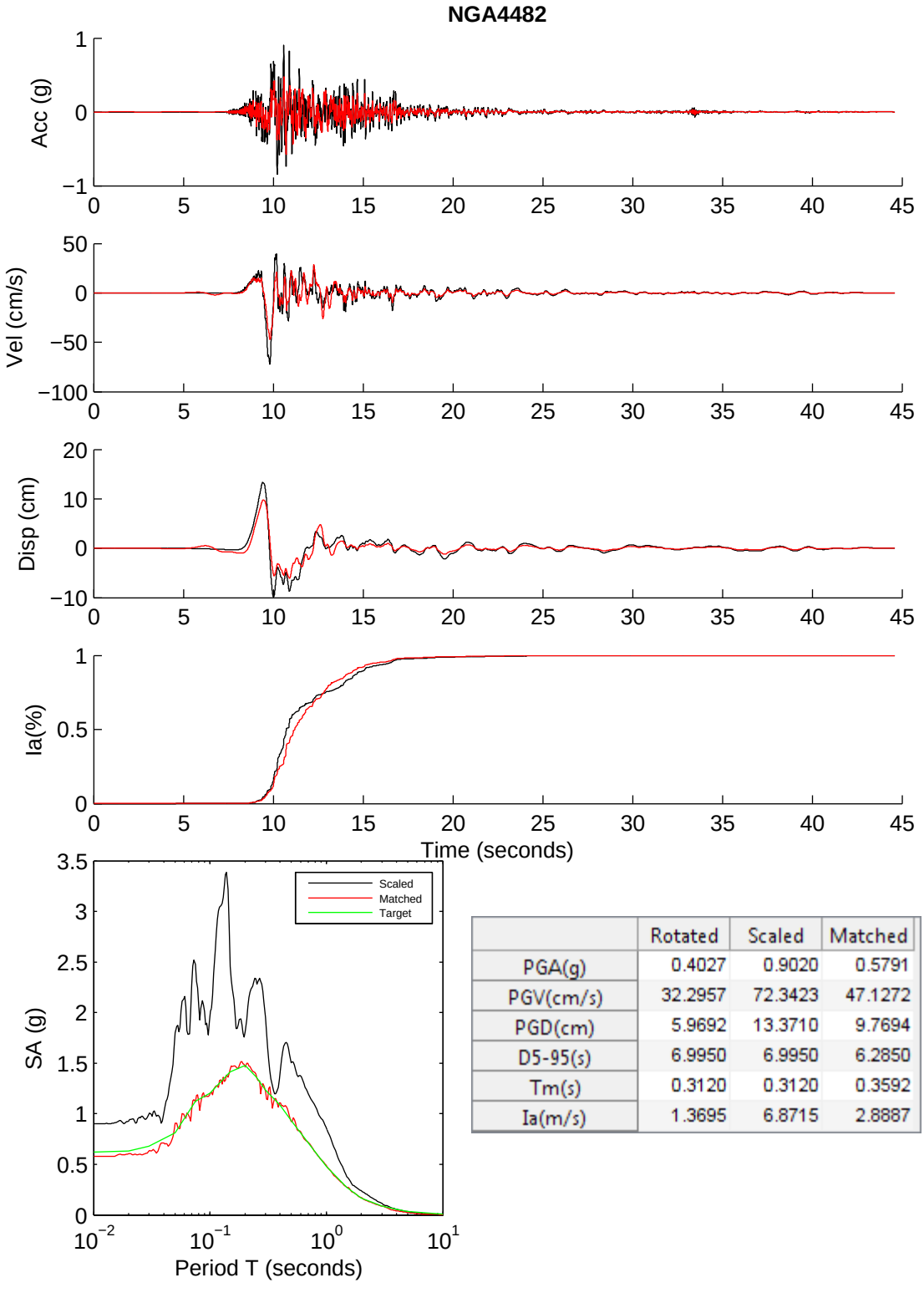

	Rotated	Scaled	Matched
PGA(g)	0.4027	0.9020	0.5791
PGV(cm/s)	32.2957	72.3423	47.1272
PGD(cm)	5.9692	13.3710	9.7694
D5-95(s)	6.9950	6.9950	6.2850
Tm(s)	0.3120	0.3120	0.3592
Ia(m/s)	1.3695	6.8715	2.8887

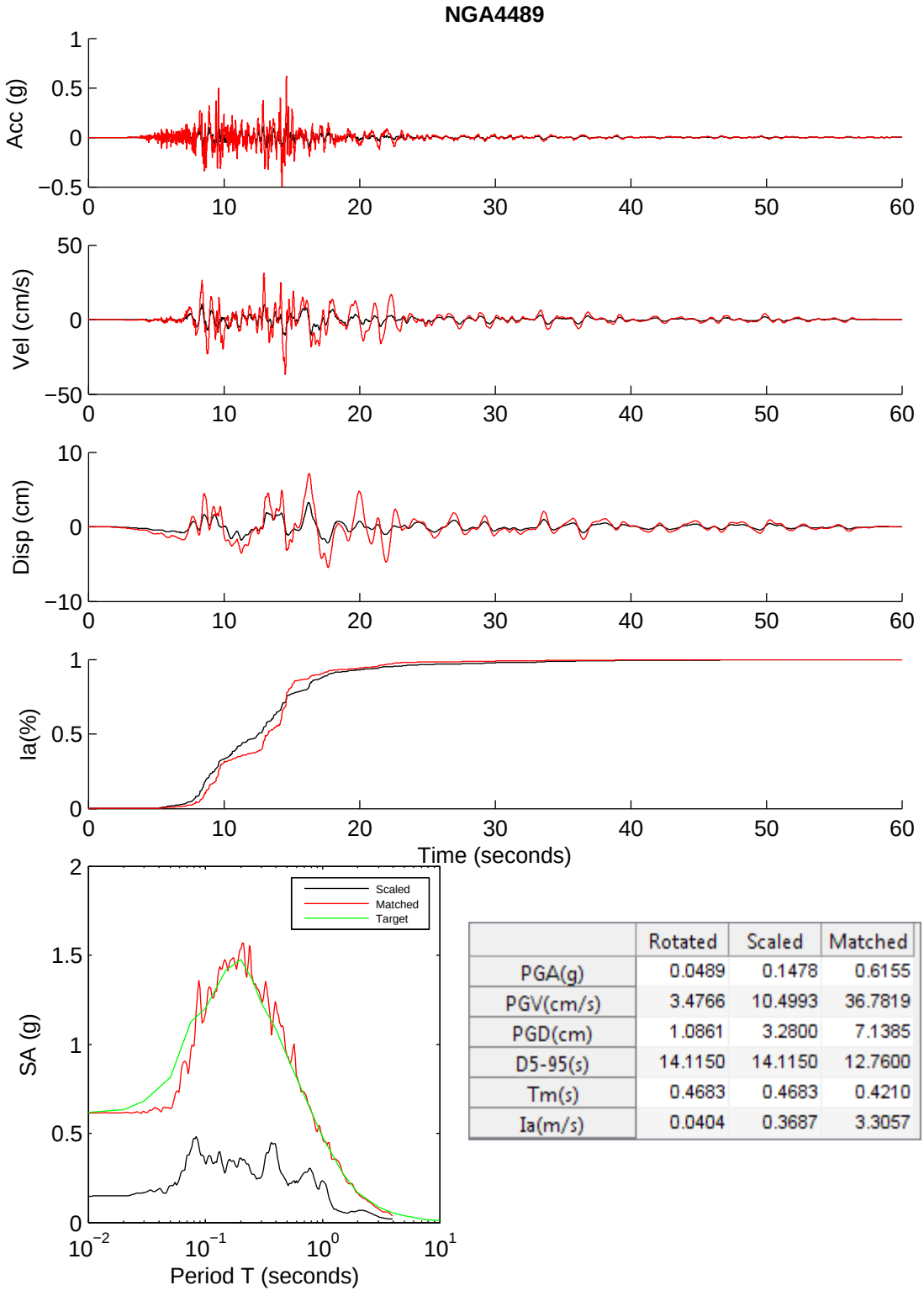

	Rotated	Scaled	Matched
PGA(g)	0.0489	0.1478	0.6155
PGV(cm/s)	3.4766	10.4993	36.7819
PGD(cm)	1.0861	3.2800	7.1385
D5-95(s)	14.1150	14.1150	12.7600
Tm(s)	0.4683	0.4683	0.4210
Ia(m/s)	0.0404	0.3687	3.3057

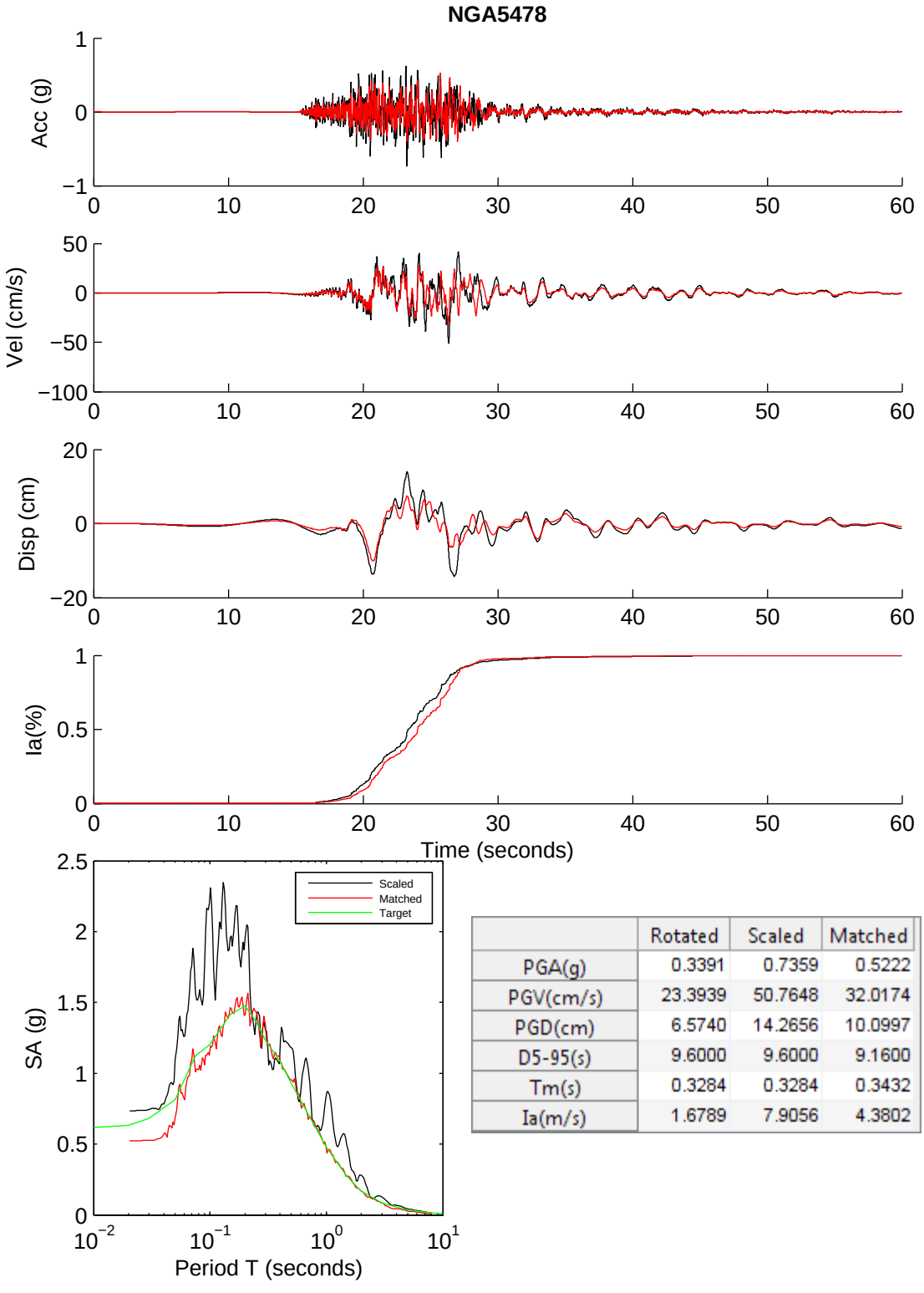

	Rotated	Scaled	Matched
PGA(g)	0.3391	0.7359	0.5222
PGV(cm/s)	23.3939	50.7648	32.0174
PGD(cm)	6.5740	14.2656	10.0997
D5-95(s)	9.6000	9.6000	9.1600
Tm(s)	0.3284	0.3284	0.3432
Ia(m/s)	1.6789	7.9056	4.3802

APPENDIX 3D: SCENARIO ACR3 GROUND MOTION DATA

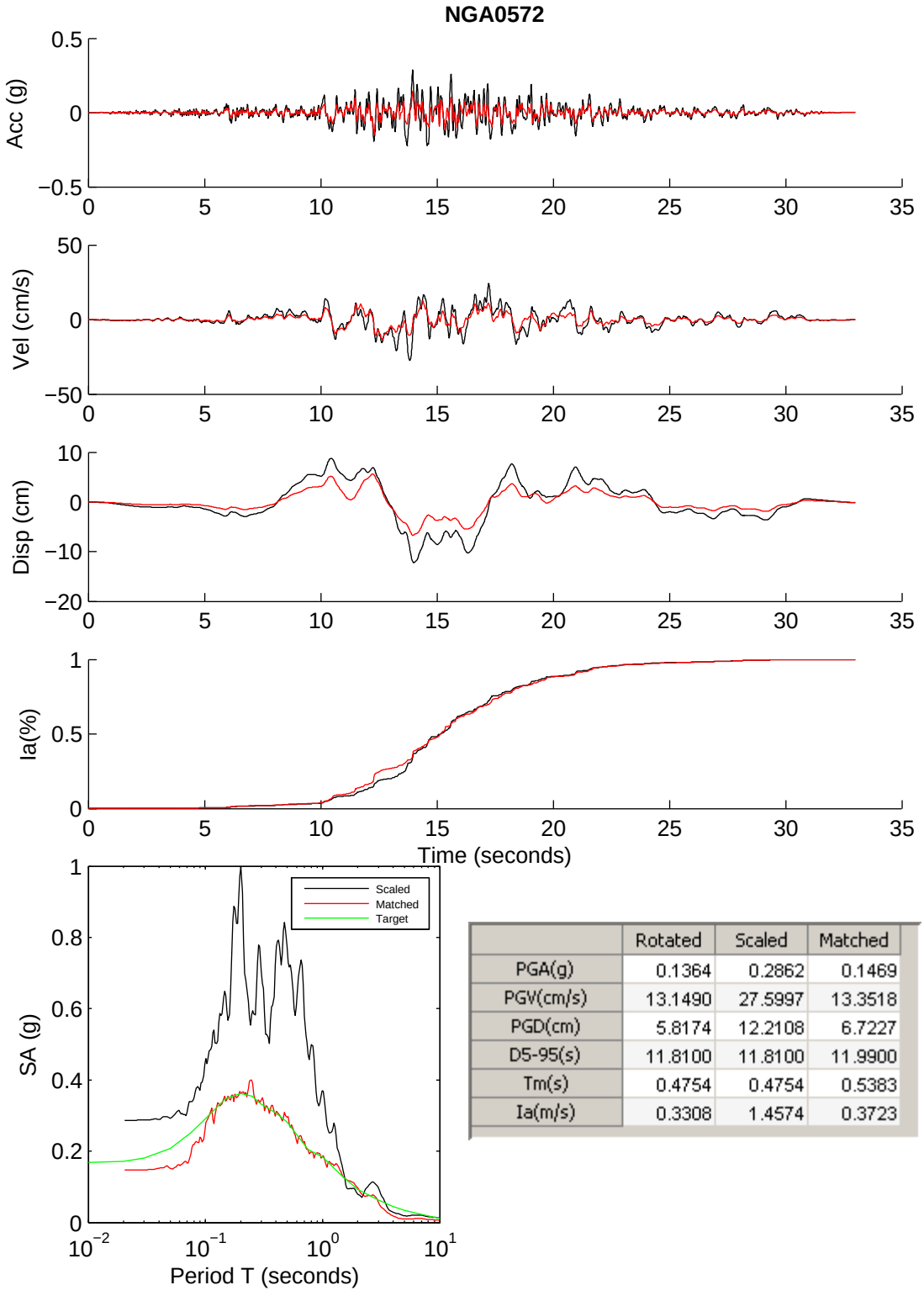

	Rotated	Scaled	Matched
PGA(g)	0.1364	0.2862	0.1469
PGV(cm/s)	13.1490	27.5997	13.3518
PGD(cm)	5.8174	12.2108	6.7227
D5-95(s)	11.8100	11.8100	11.9900
Tm(s)	0.4754	0.4754	0.5383
Ia(m/s)	0.3308	1.4574	0.3723

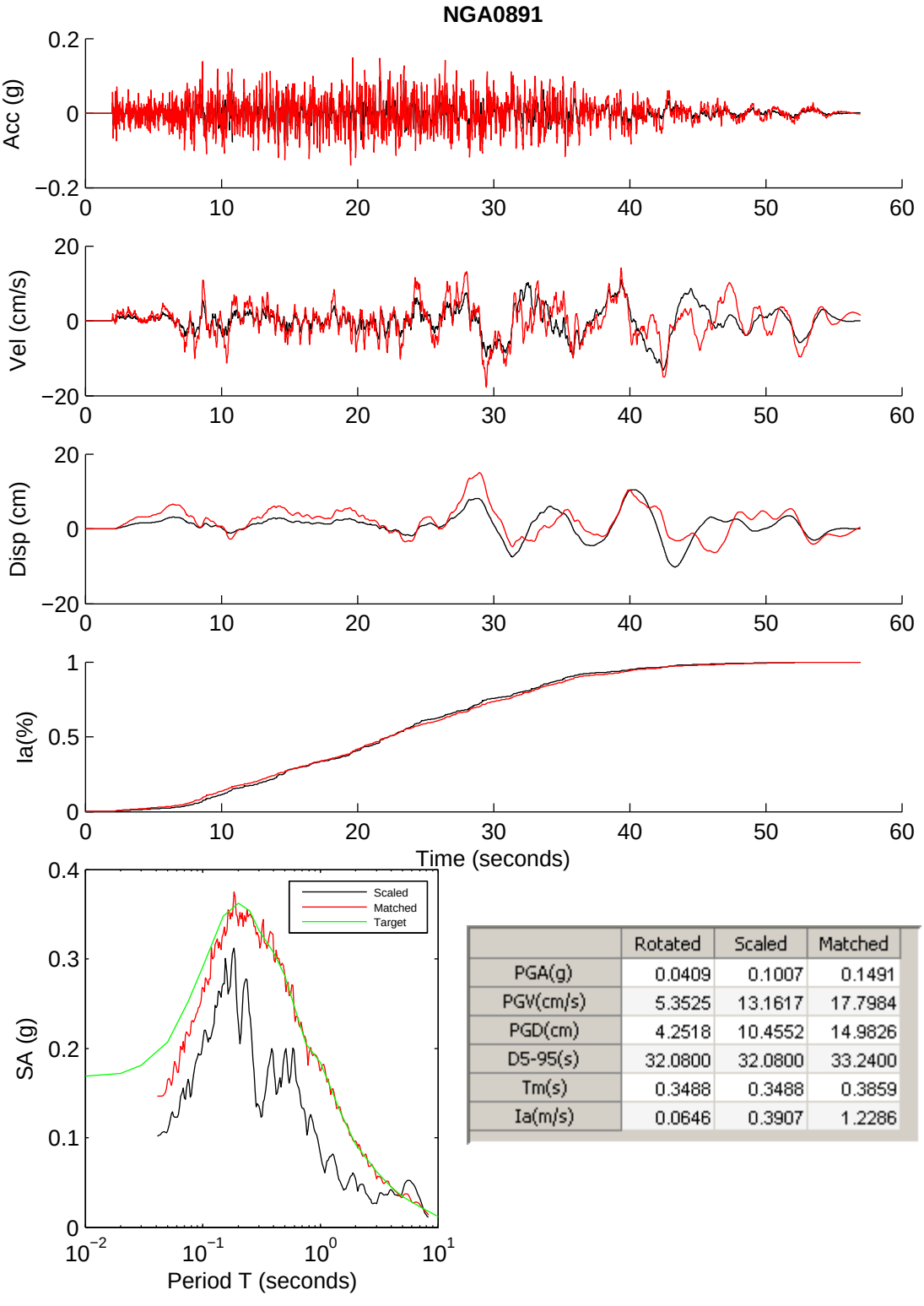

	Rotated	Scaled	Matched
PGA(g)	0.0409	0.1007	0.1491
PGV(cm/s)	5.3525	13.1617	17.7984
PGD(cm)	4.2518	10.4552	14.9826
D5-95(s)	32.0800	32.0800	33.2400
Tm(s)	0.3488	0.3488	0.3859
Ia(m/s)	0.0646	0.3907	1.2286

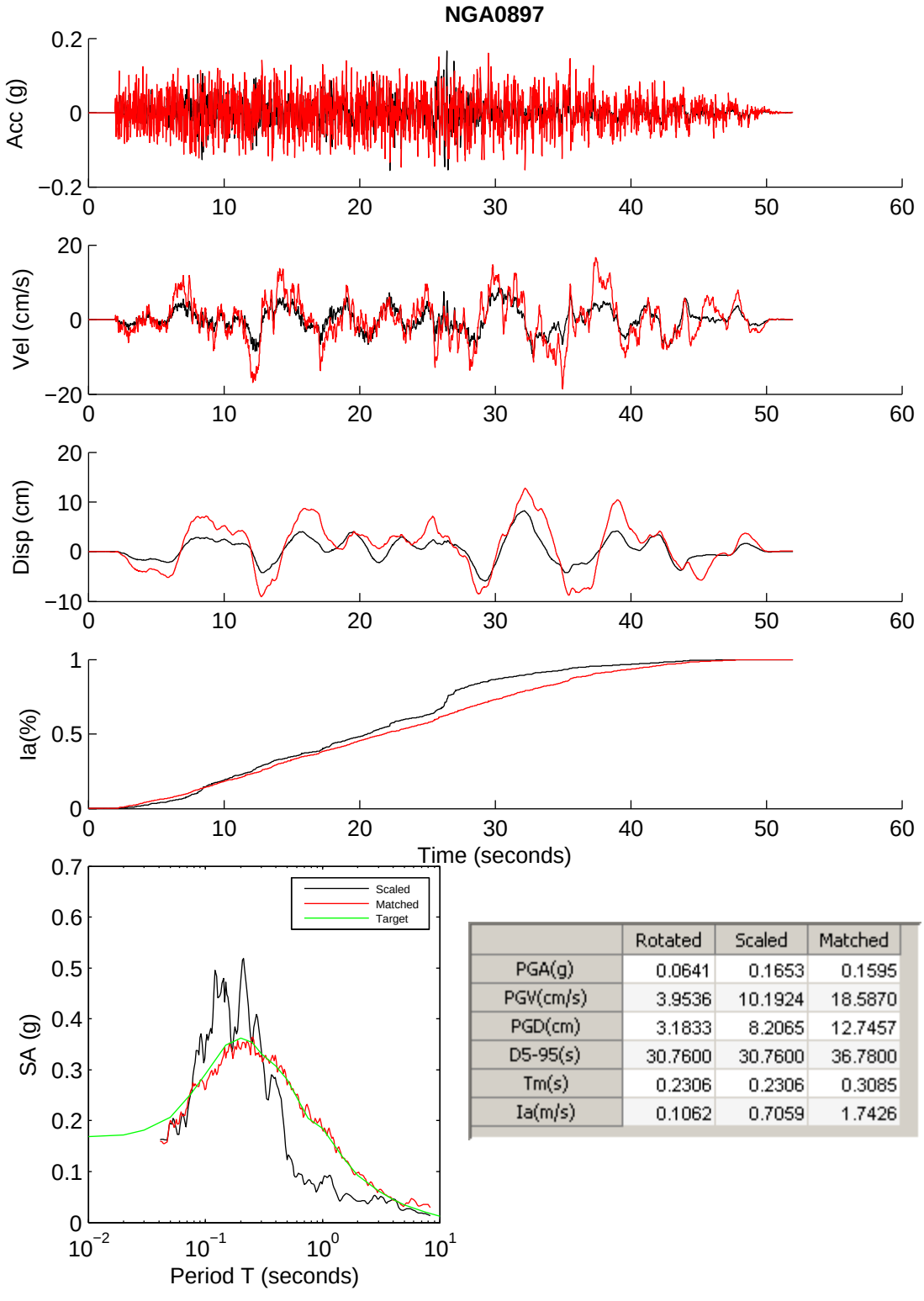

	Rotated	Scaled	Matched
PGA(g)	0.0641	0.1653	0.1595
PGV(cm/s)	3.9536	10.1924	18.5870
PGD(cm)	3.1833	8.2065	12.7457
D5-95(s)	30.7600	30.7600	36.7800
Tm(s)	0.2306	0.2306	0.3085
Ia(m/s)	0.1062	0.7059	1.7426

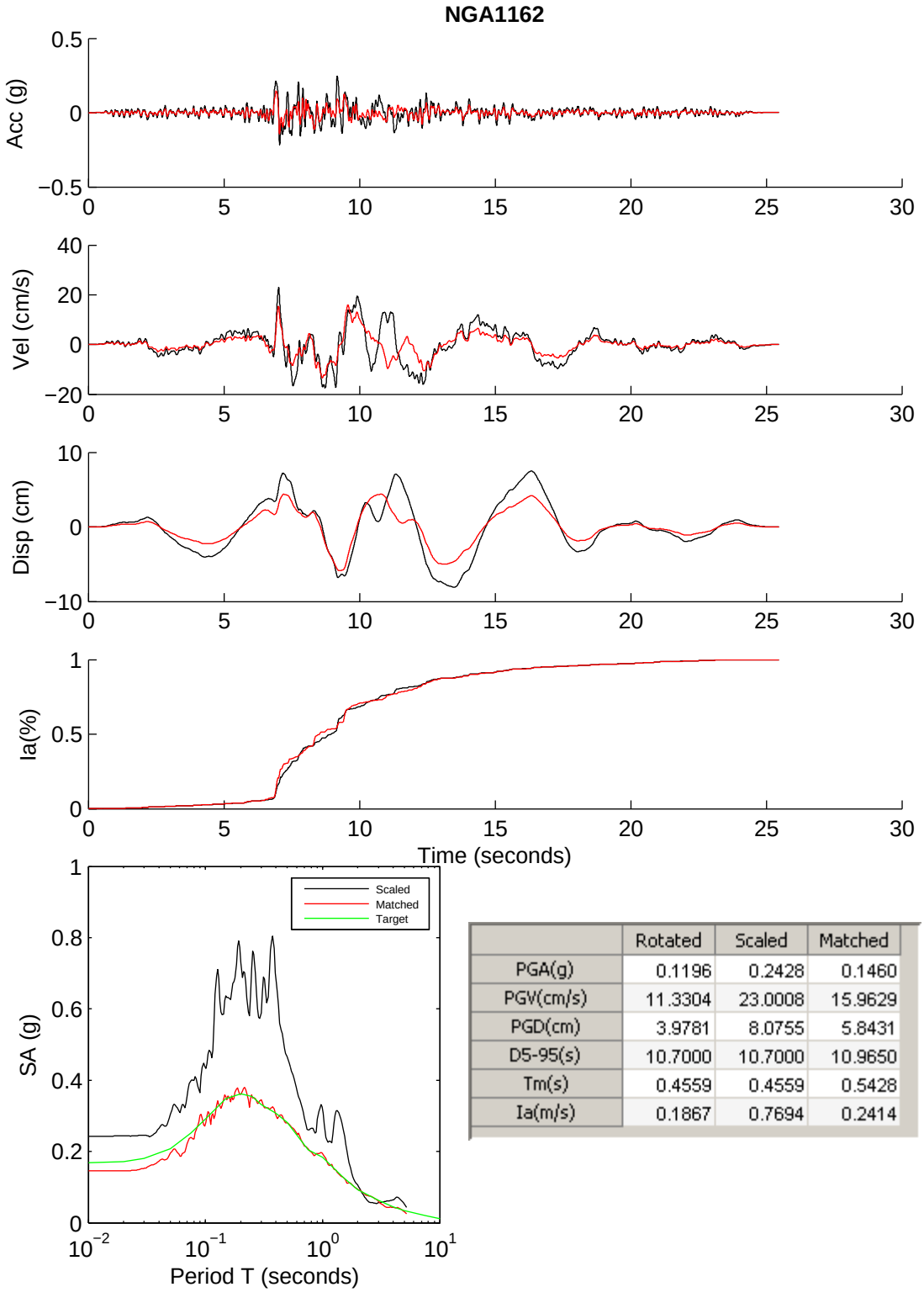

	Rotated	Scaled	Matched
PGA(g)	0.1196	0.2428	0.1460
PGV(cm/s)	11.3304	23.0008	15.9629
PGD(cm)	3.9781	8.0755	5.8431
D5-95(s)	10.7000	10.7000	10.9650
Tm(s)	0.4559	0.4559	0.5428
Ia(m/s)	0.1867	0.7694	0.2414

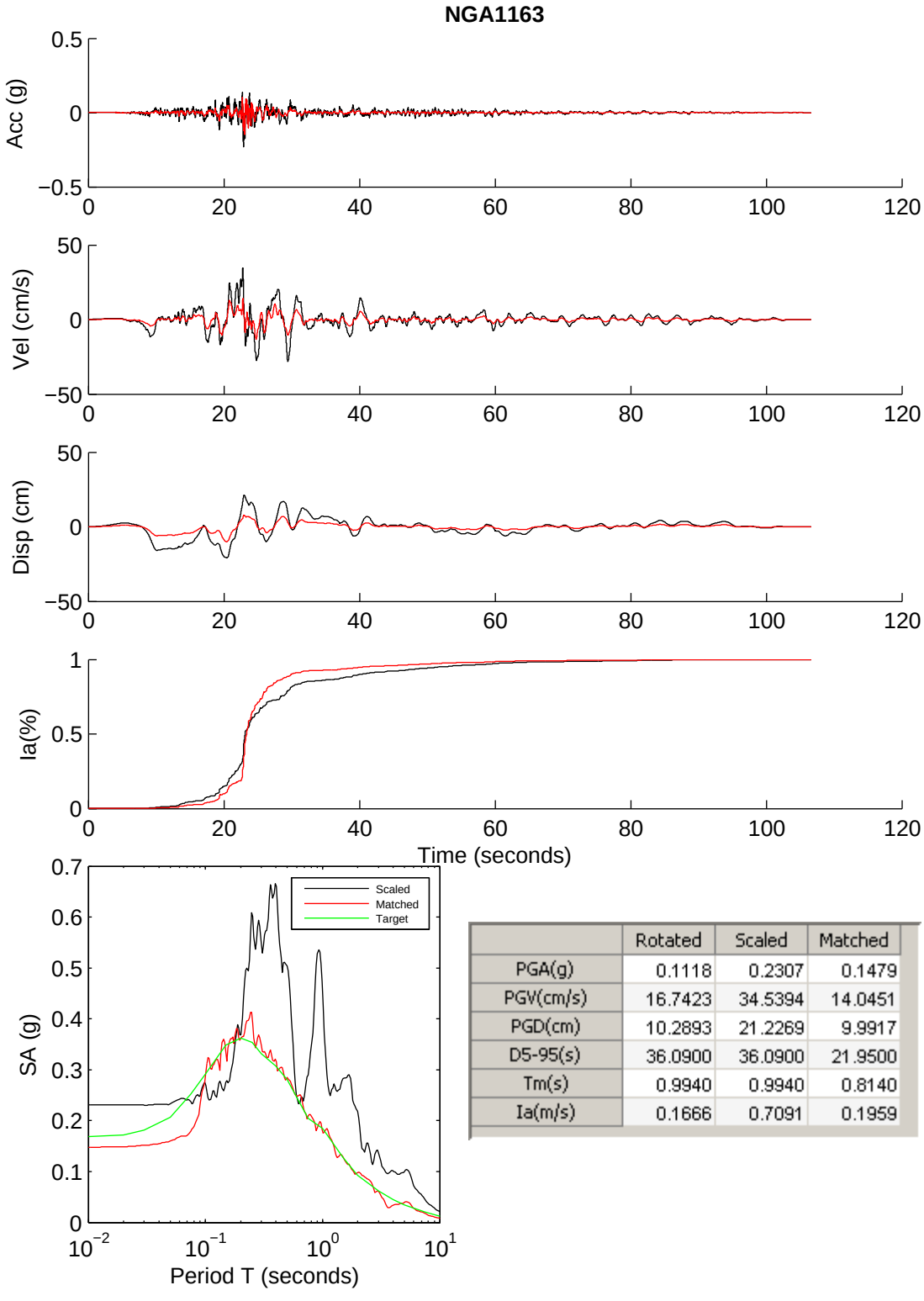

	Rotated	Scaled	Matched
PGA(g)	0.1118	0.2307	0.1479
PGV(cm/s)	16.7423	34.5394	14.0451
PGD(cm)	10.2893	21.2269	9.9917
D5-95(s)	36.0900	36.0900	21.9500
Tm(s)	0.9940	0.9940	0.8140
Ia(m/s)	0.1666	0.7091	0.1959

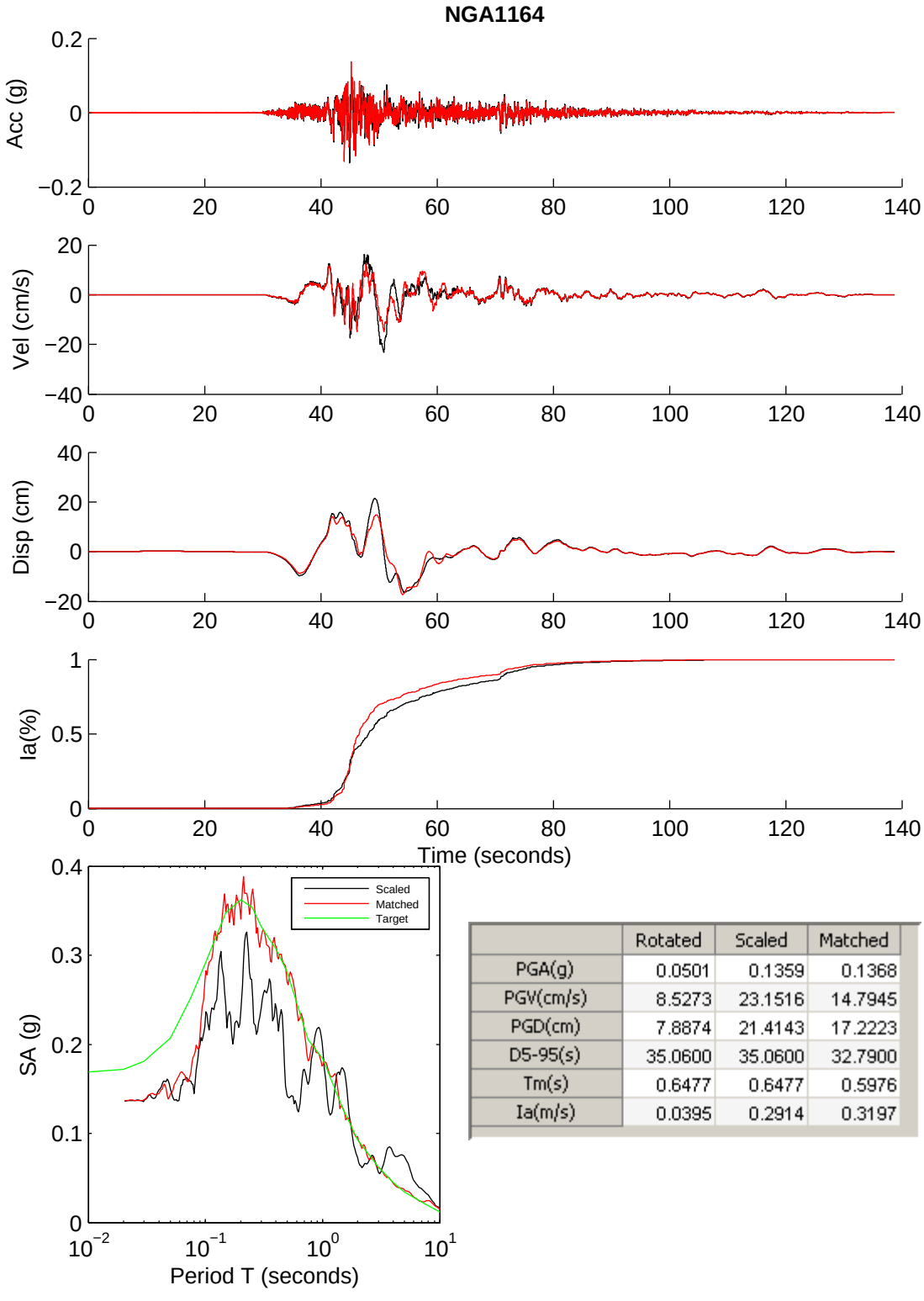

	Rotated	Scaled	Matched
PGA(g)	0.0501	0.1359	0.1368
PGV(cm/s)	8.5273	23.1516	14.7945
PGD(cm)	7.8874	21.4143	17.2223
D5-95(s)	35.0600	35.0600	32.7900
Tm(s)	0.6477	0.6477	0.5976
Ia(m/s)	0.0395	0.2914	0.3197

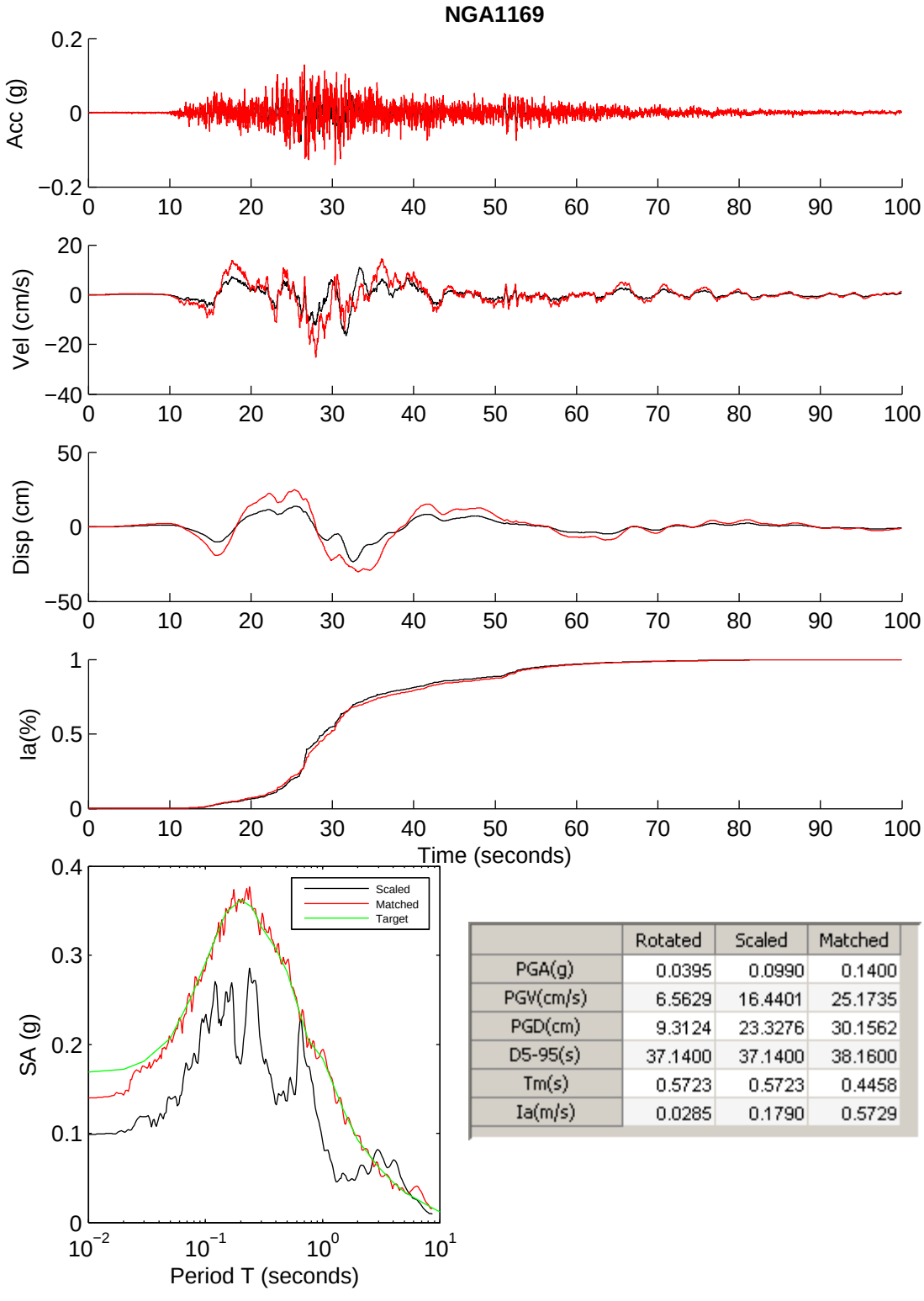

	Rotated	Scaled	Matched
PGA(g)	0.0395	0.0990	0.1400
PGV(cm/s)	6.5629	16.4401	25.1735
PGD(cm)	9.3124	23.3276	30.1562
D5-95(s)	37.1400	37.1400	38.1600
Tm(s)	0.5723	0.5723	0.4458
Ia(m/s)	0.0285	0.1790	0.5729

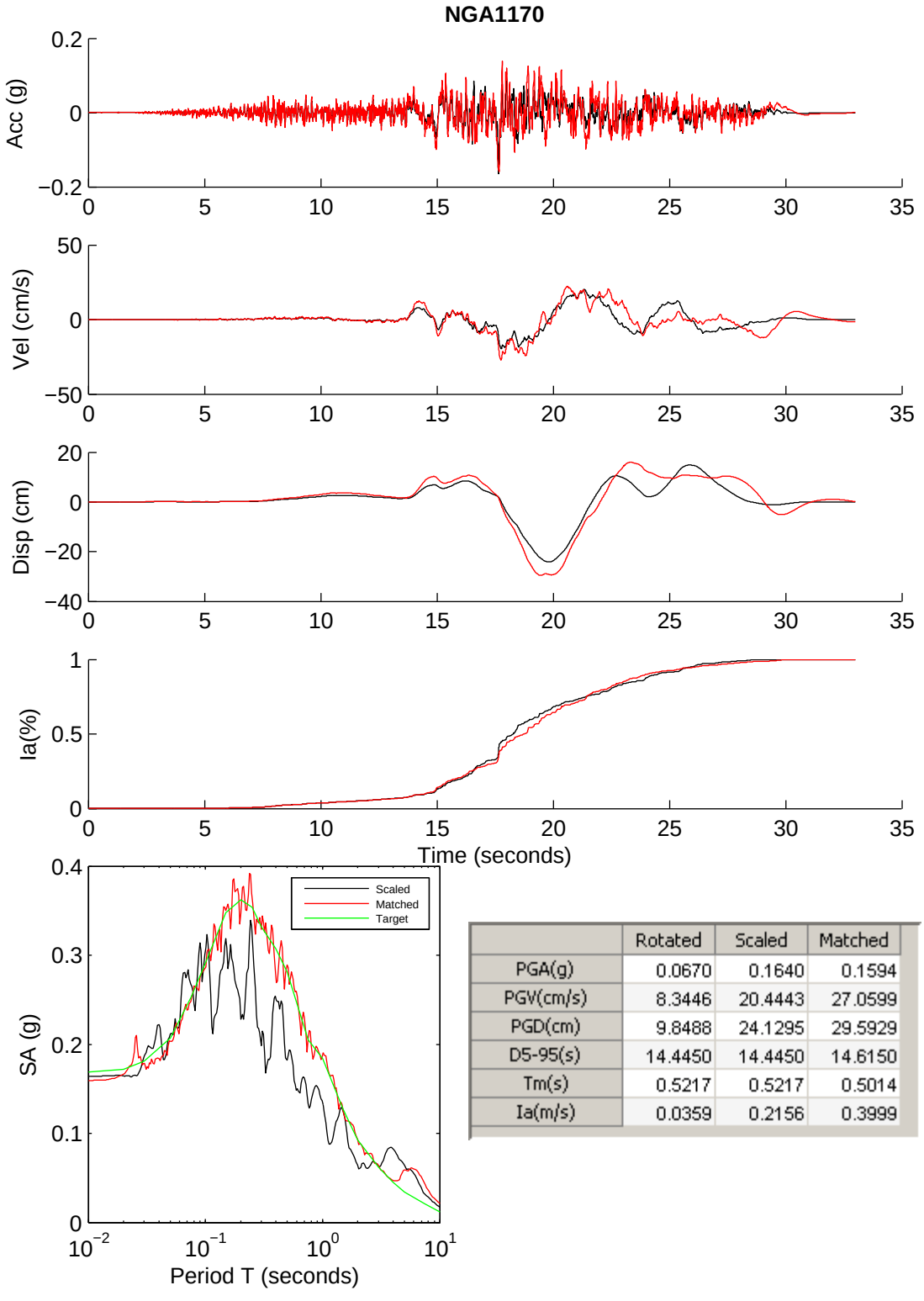

	Rotated	Scaled	Matched
PGA(g)	0.0670	0.1640	0.1594
PGV(cm/s)	8.3446	20.4443	27.0599
PGD(cm)	9.8488	24.1295	29.5929
D5-95(s)	14.4450	14.4450	14.6150
Tm(s)	0.5217	0.5217	0.5014
Ia(m/s)	0.0359	0.2156	0.3999

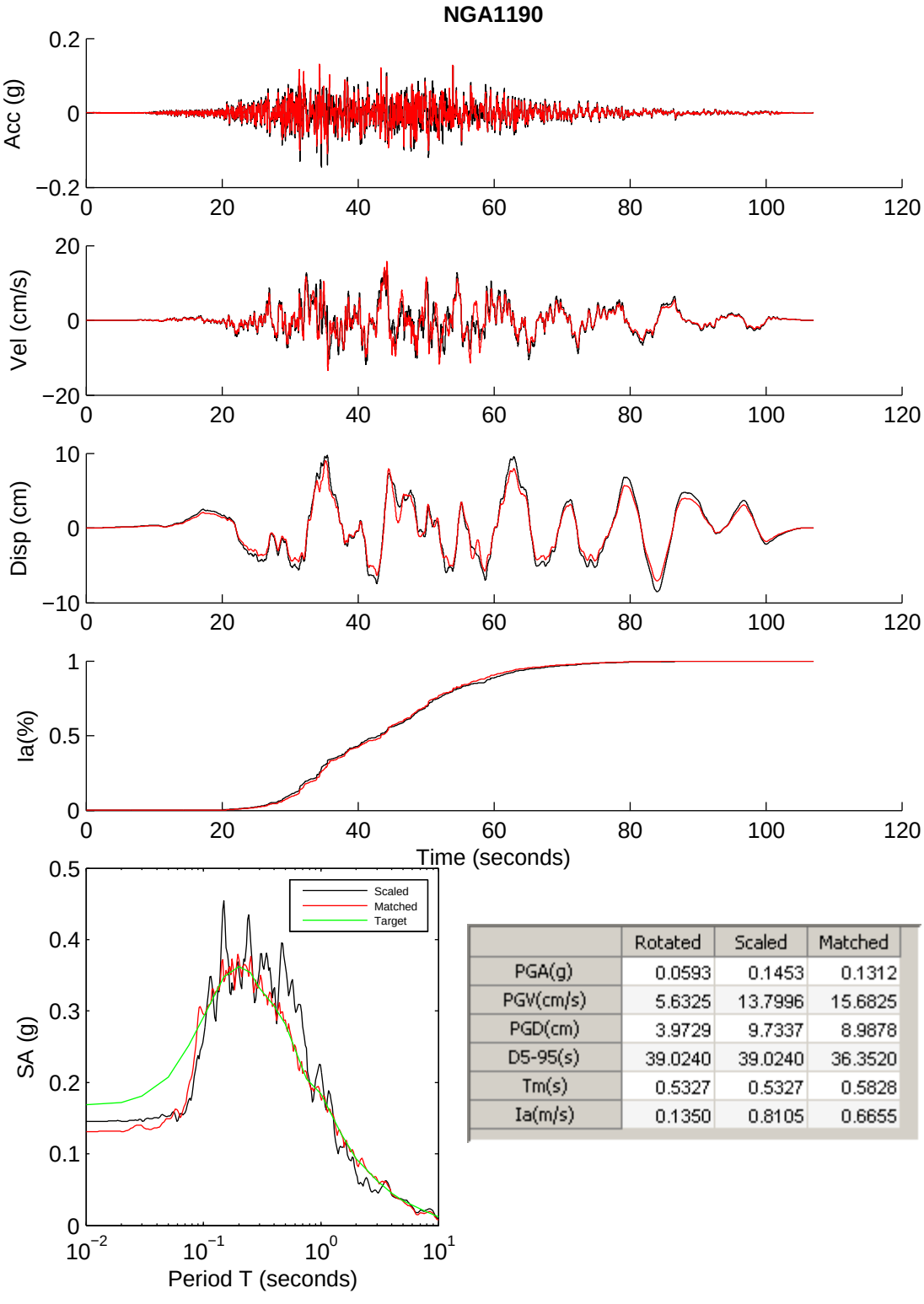

	Rotated	Scaled	Matched
PGA(g)	0.0593	0.1453	0.1312
PGV(cm/s)	5.6325	13.7996	15.6825
PGD(cm)	3.9729	9.7337	8.9878
D5-95(s)	39.0240	39.0240	36.3520
Tm(s)	0.5327	0.5327	0.5828
Ia(m/s)	0.1350	0.8105	0.6655

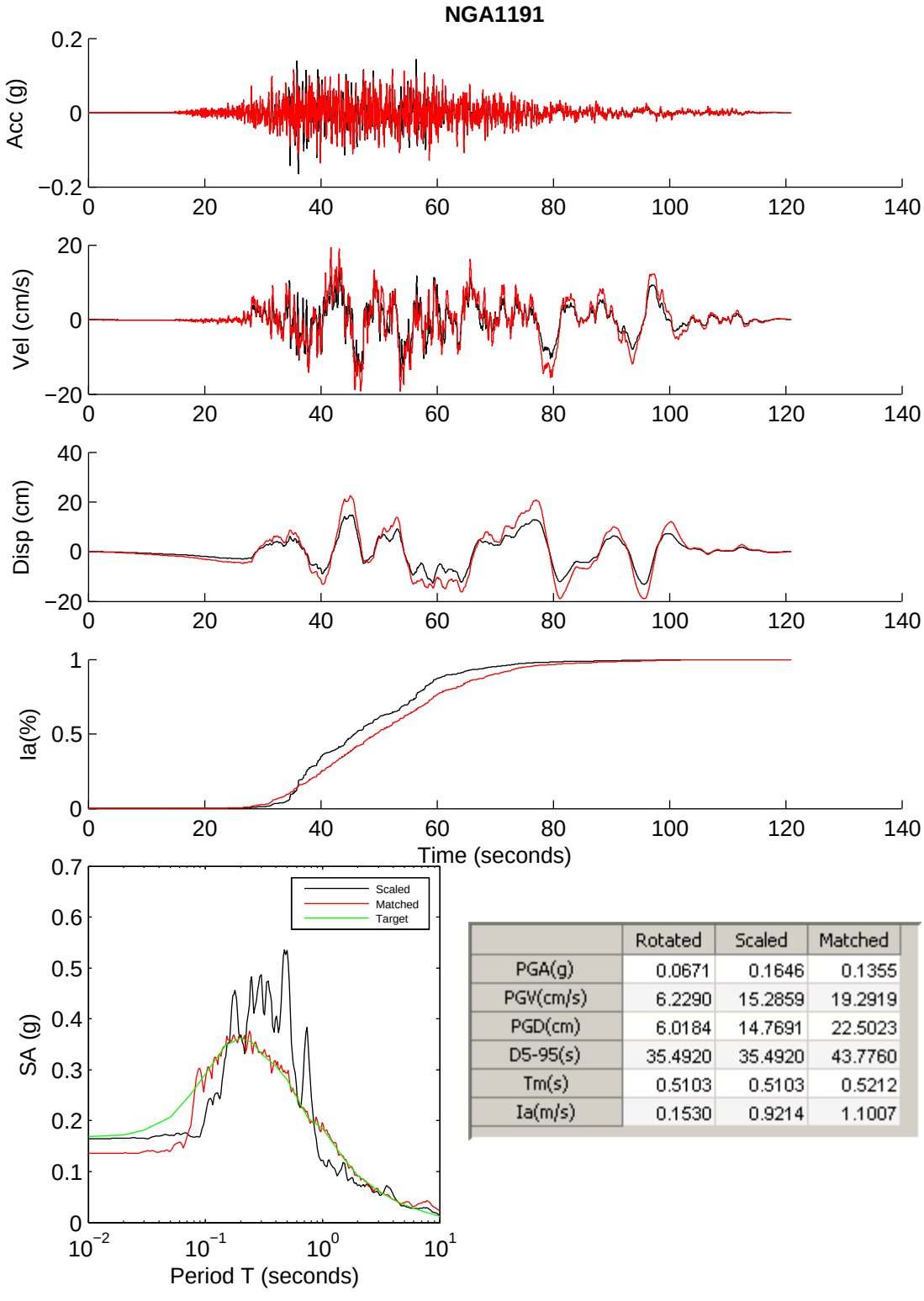

	Rotated	Scaled	Matched
PGA(g)	0.0671	0.1646	0.1355
PGV(cm/s)	6.2290	15.2859	19.2919
PGD(cm)	6.0184	14.7691	22.5023
D5-95(s)	35.4920	35.4920	43.7760
Tm(s)	0.5103	0.5103	0.5212
Ia(m/s)	0.1530	0.9214	1.1007

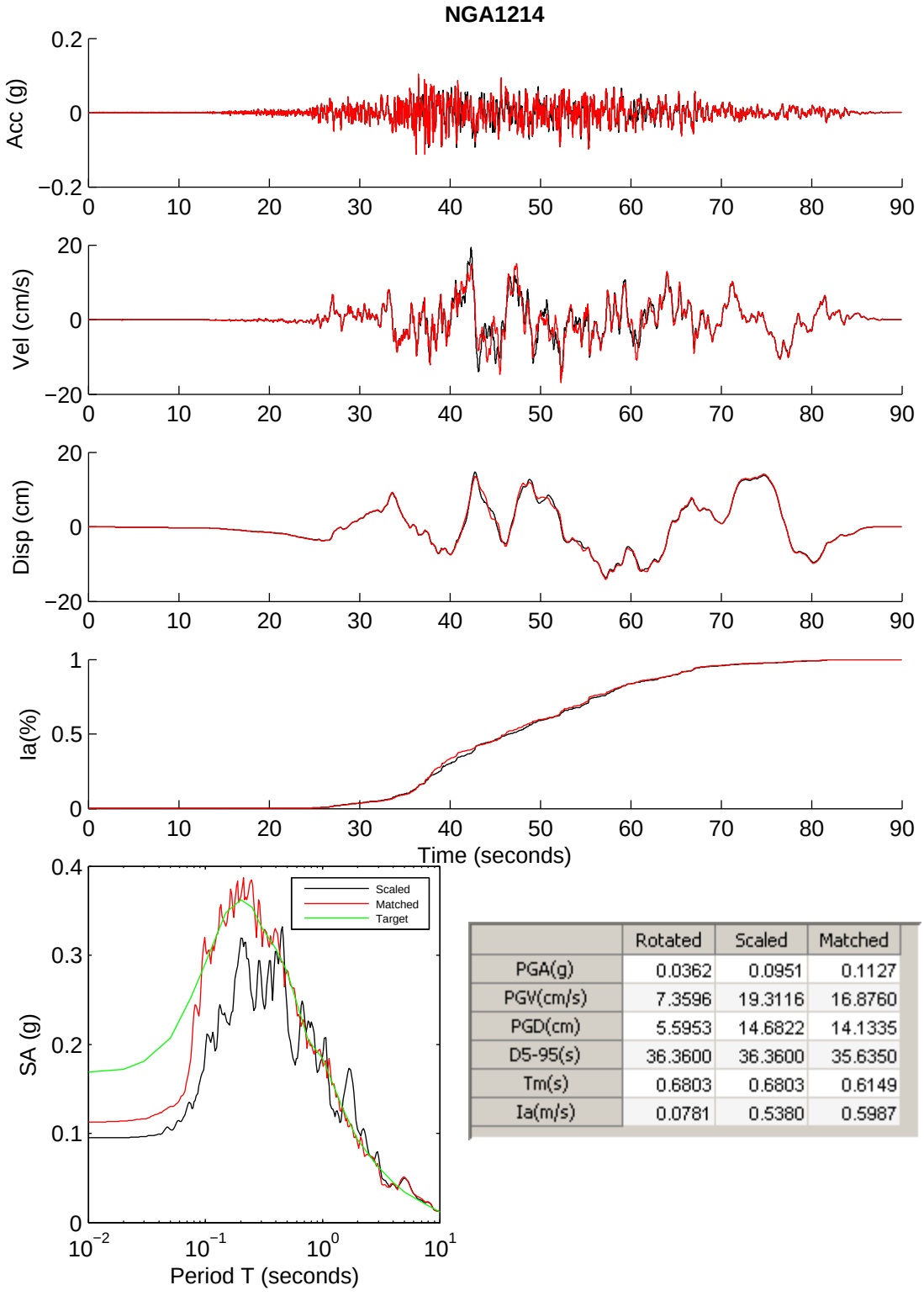

	Rotated	Scaled	Matched
PGA(g)	0.0362	0.0951	0.1127
PGV(cm/s)	7.3596	19.3116	16.8760
PGD(cm)	5.5953	14.6822	14.1335
D5-95(s)	36.3600	36.3600	35.6350
Tm(s)	0.6803	0.6803	0.6149
Ia(m/s)	0.0781	0.5380	0.5987

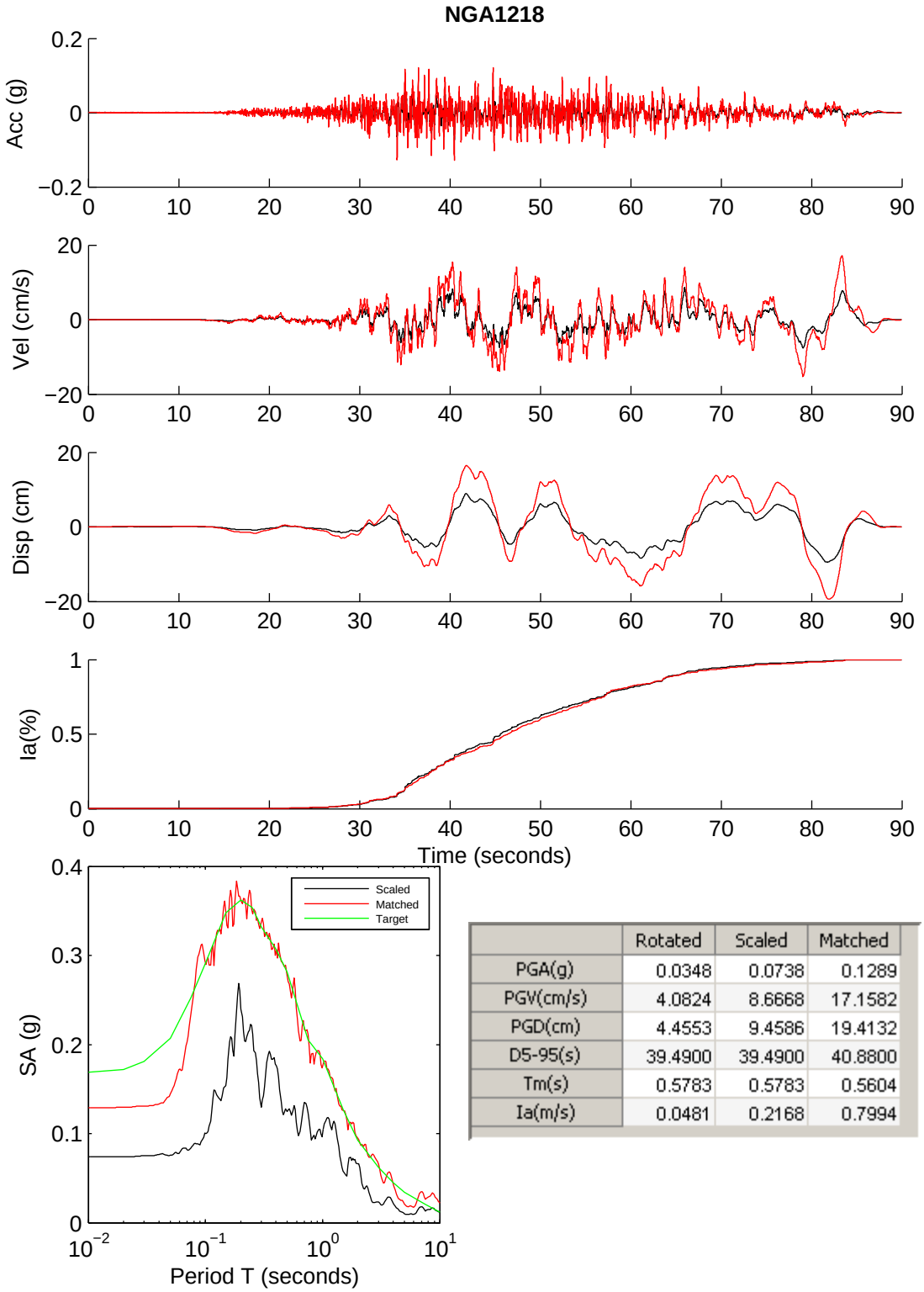

	Rotated	Scaled	Matched
PGA(g)	0.0348	0.0738	0.1289
PGV(cm/s)	4.0824	8.6668	17.1582
PGD(cm)	4.4553	9.4586	19.4132
D5-95(s)	39.4900	39.4900	40.8800
Tm(s)	0.5783	0.5783	0.5604
Ia(m/s)	0.0481	0.2168	0.7994

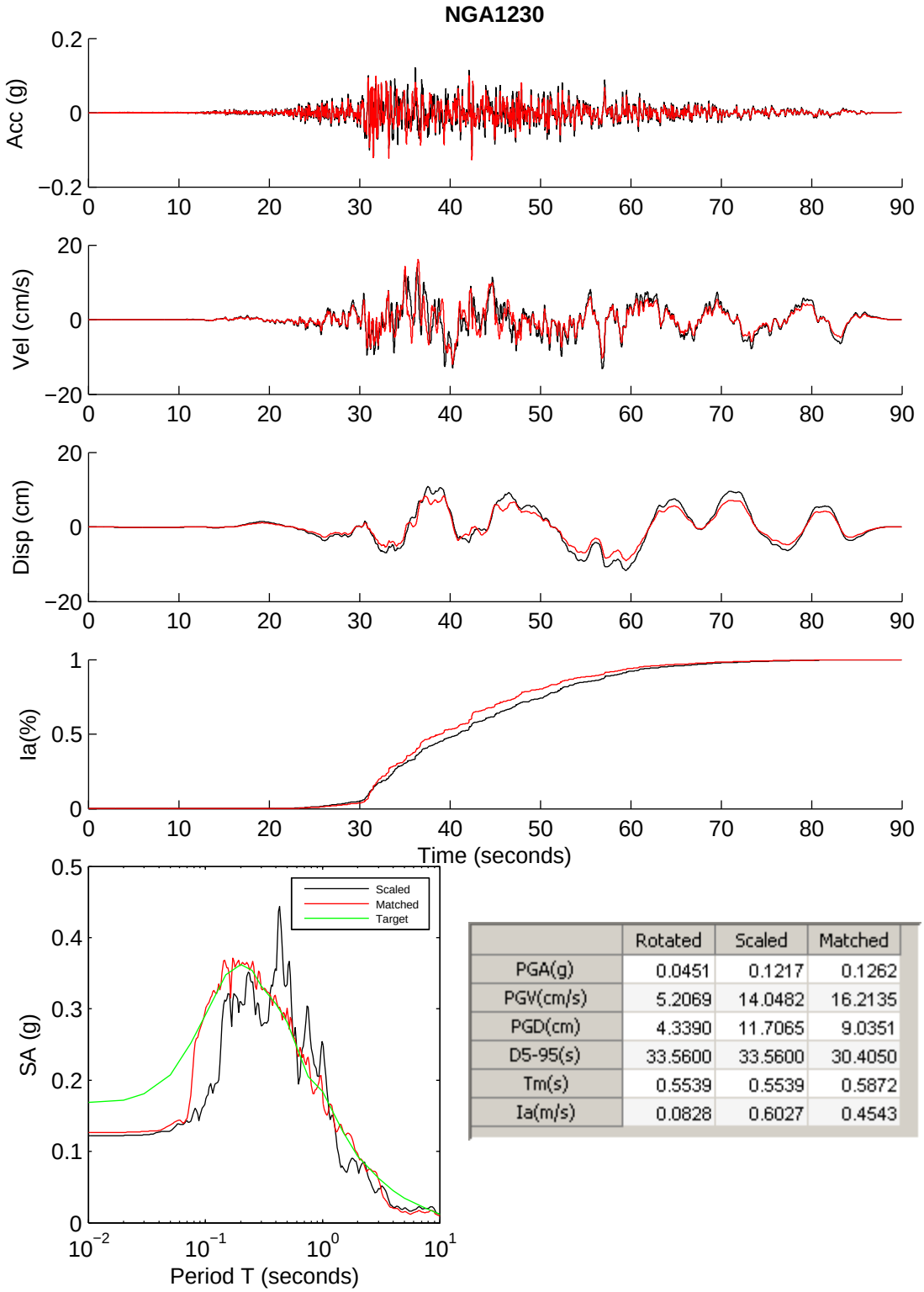

	Rotated	Scaled	Matched
PGA(g)	0.0451	0.1217	0.1262
PGV(cm/s)	5.2069	14.0482	16.2135
PGD(cm)	4.3390	11.7065	9.0351
D5-95(s)	33.5600	33.5600	30.4050
Tm(s)	0.5539	0.5539	0.5872
Ia(m/s)	0.0828	0.6027	0.4543

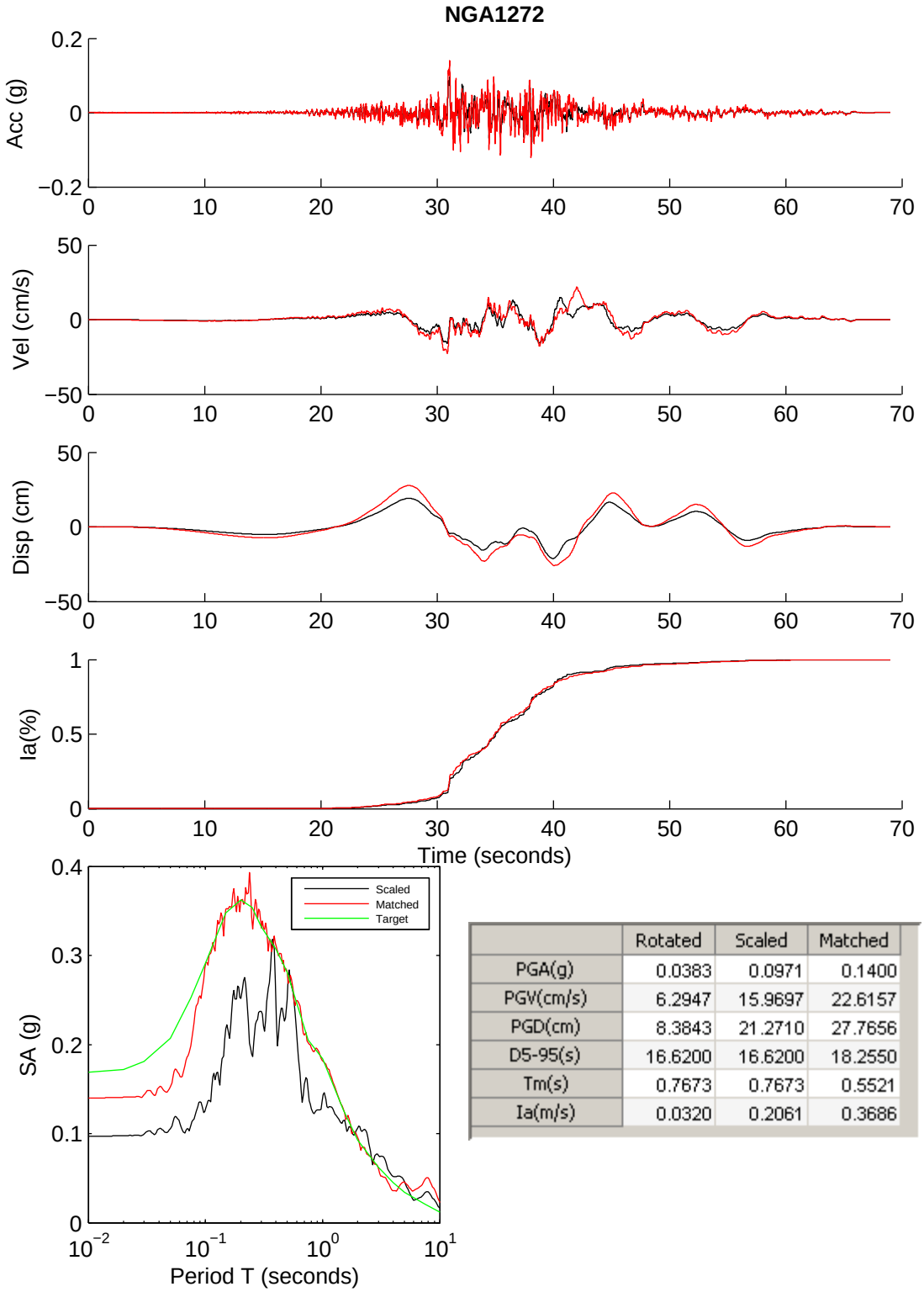

	Rotated	Scaled	Matched
PGA(g)	0.0383	0.0971	0.1400
PGV(cm/s)	6.2947	15.9697	22.6157
PGD(cm)	8.3843	21.2710	27.7656
D5-95(s)	16.6200	16.6200	18.2550
Tm(s)	0.7673	0.7673	0.5521
Ia(m/s)	0.0320	0.2061	0.3686

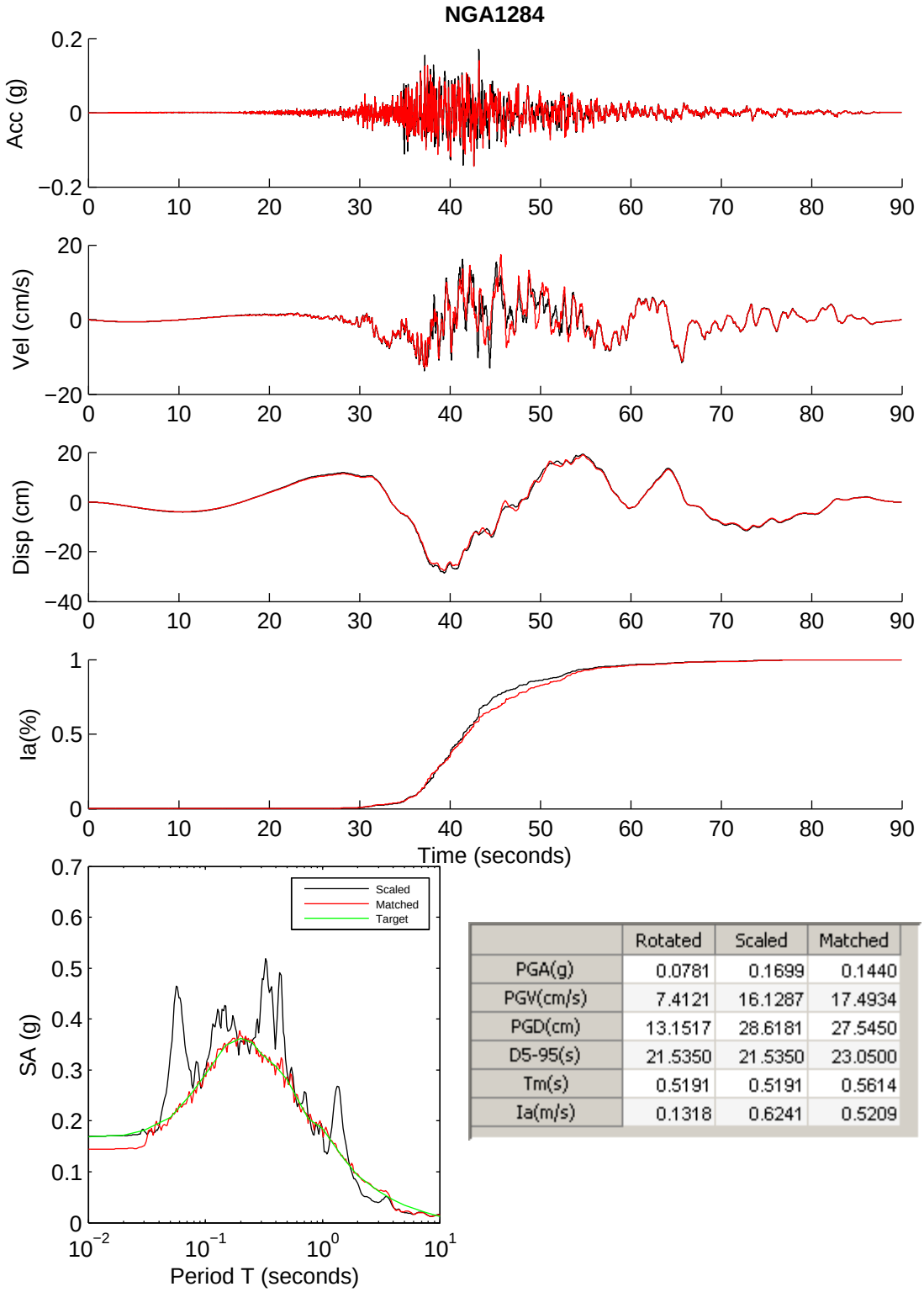

	Rotated	Scaled	Matched
PGA(g)	0.0781	0.1699	0.1440
PGV(cm/s)	7.4121	16.1287	17.4934
PGD(cm)	13.1517	28.6181	27.5450
D5-95(s)	21.5350	21.5350	23.0500
Tm(s)	0.5191	0.5191	0.5614
Ia(m/s)	0.1318	0.6241	0.5209

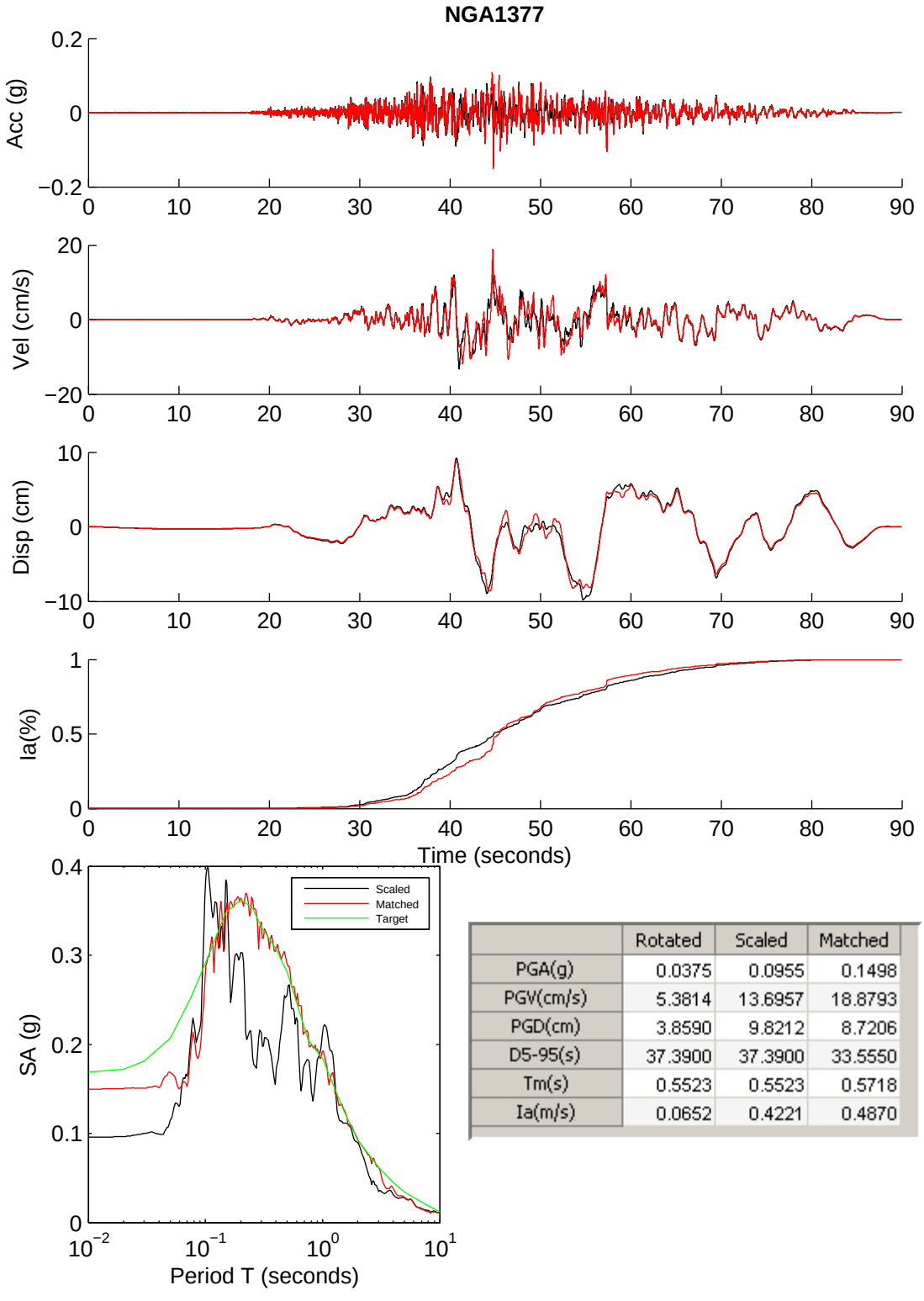

	Rotated	Scaled	Matched
PGA(g)	0.0375	0.0955	0.1498
PGV(cm/s)	5.3814	13.6957	18.8793
PGD(cm)	3.8590	9.8212	8.7206
D5-95(s)	37.3900	37.3900	33.5550
Tm(s)	0.5523	0.5523	0.5718
Ia(m/s)	0.0652	0.4221	0.4870

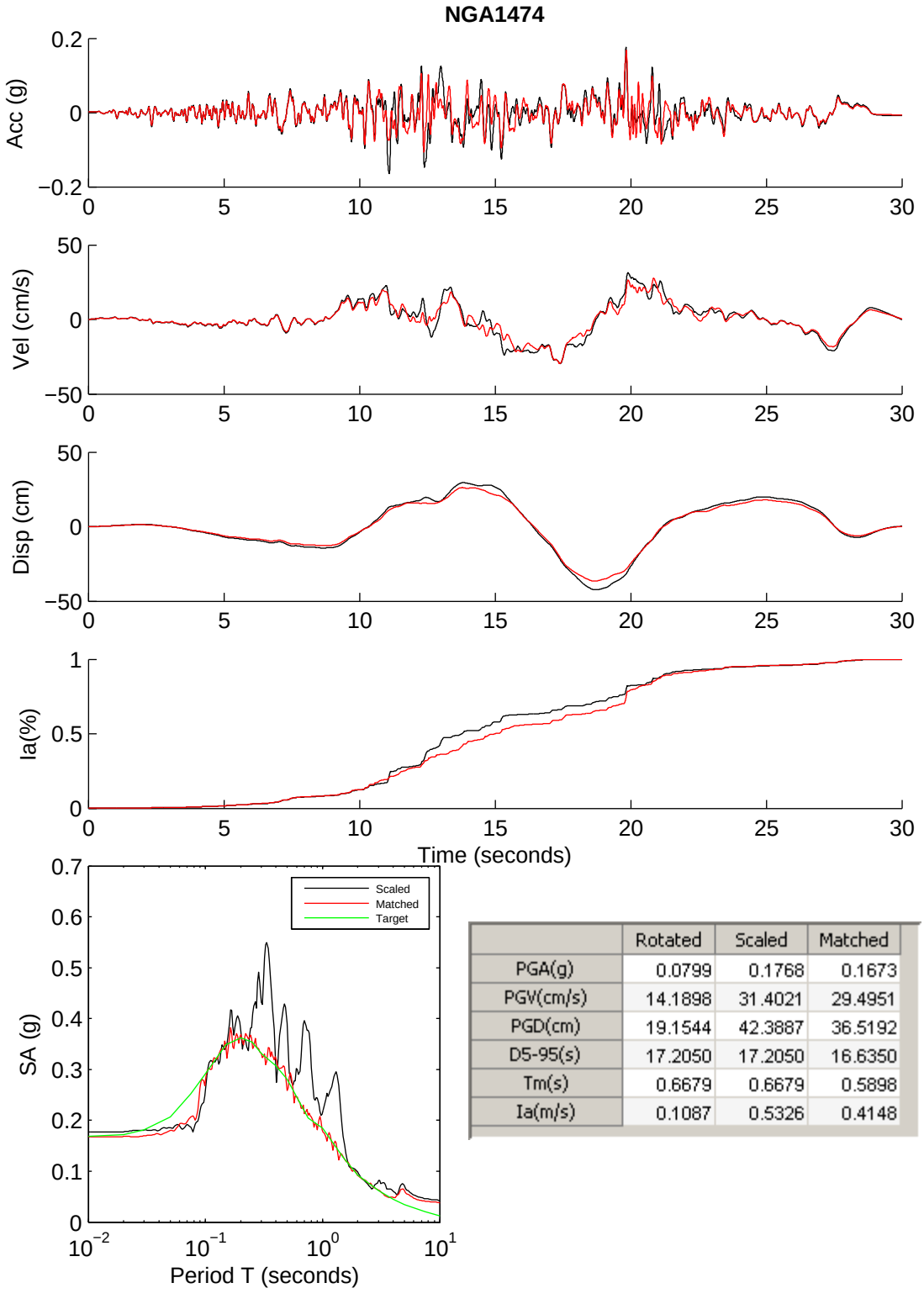

	Rotated	Scaled	Matched
PGA(g)	0.0799	0.1768	0.1673
PGV(cm/s)	14.1898	31.4021	29.4951
PGD(cm)	19.1544	42.3887	36.5192
D5-95(s)	17.2050	17.2050	16.6350
Tm(s)	0.6679	0.6679	0.5898
Ia(m/s)	0.1087	0.5326	0.4148

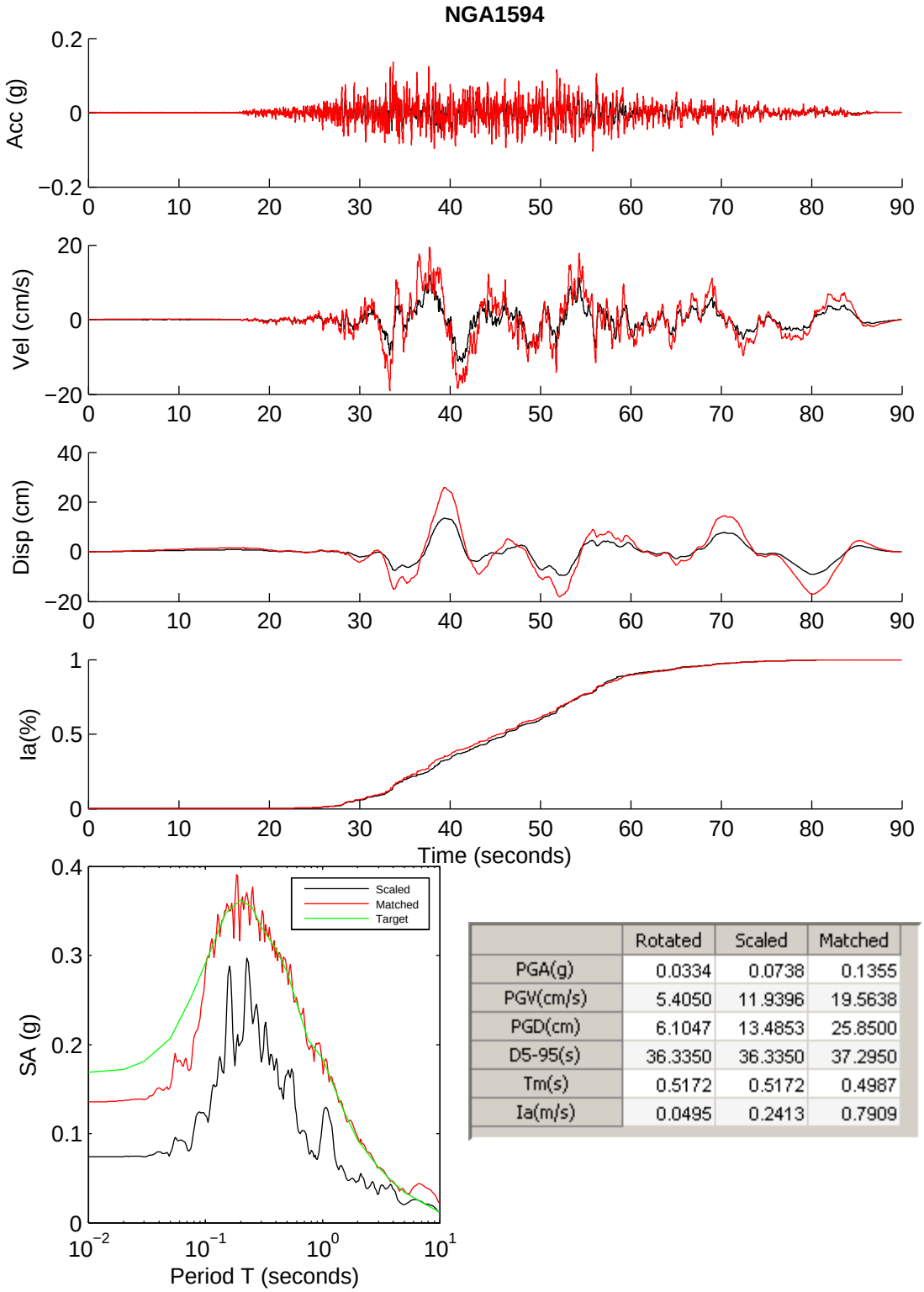

	Rotated	Scaled	Matched
PGA(g)	0.0334	0.0738	0.1355
PGV(cm/s)	5.4050	11.9396	19.5638
PGD(cm)	6.1047	13.4853	25.8500
D5-95(s)	36.3350	36.3350	37.2950
Tm(s)	0.5172	0.5172	0.4987
Ia(m/s)	0.0495	0.2413	0.7909

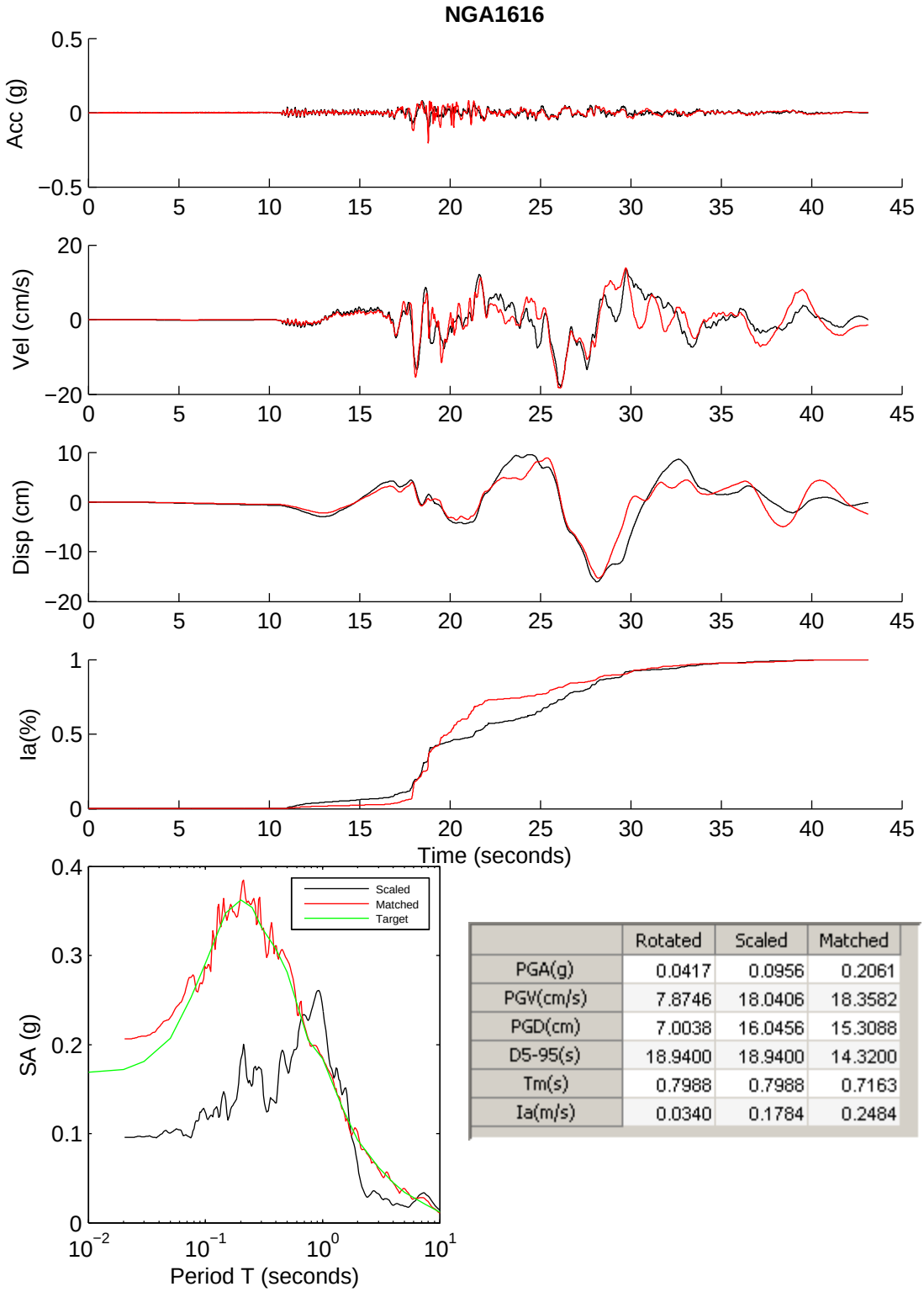

	Rotated	Scaled	Matched
PGA(g)	0.0417	0.0956	0.2061
PGV(cm/s)	7.8746	18.0406	18.3582
PGD(cm)	7.0038	16.0456	15.3088
D5-95(s)	18.9400	18.9400	14.3200
Tm(s)	0.7988	0.7988	0.7163
Ia(m/s)	0.0340	0.1784	0.2484

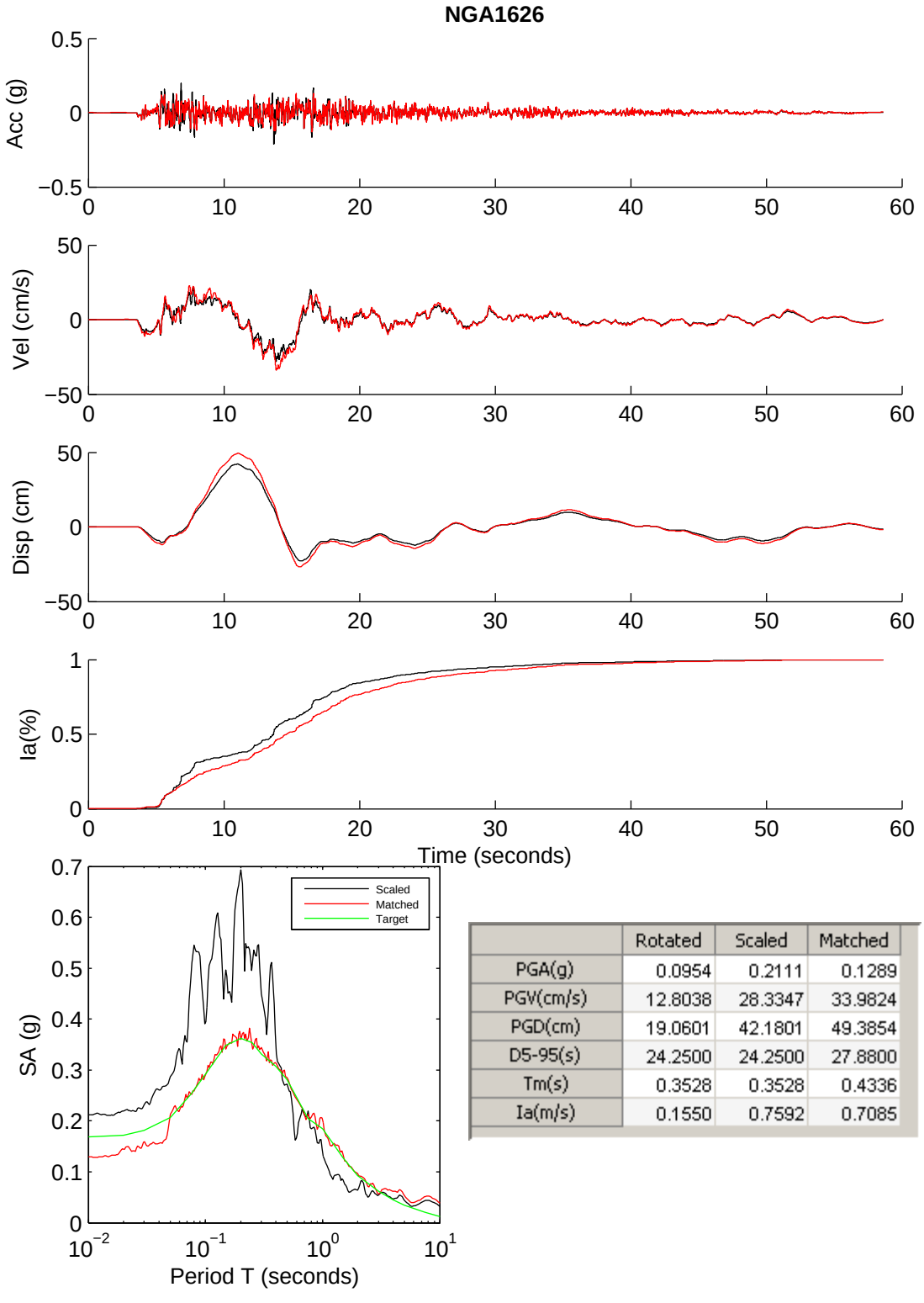

	Rotated	Scaled	Matched
PGA(g)	0.0954	0.2111	0.1289
PGV(cm/s)	12.8038	28.3347	33.9824
PGD(cm)	19.0601	42.1801	49.3854
D5-95(s)	24.2500	24.2500	27.8800
Tm(s)	0.3528	0.3528	0.4336
Ia(m/s)	0.1550	0.7592	0.7085

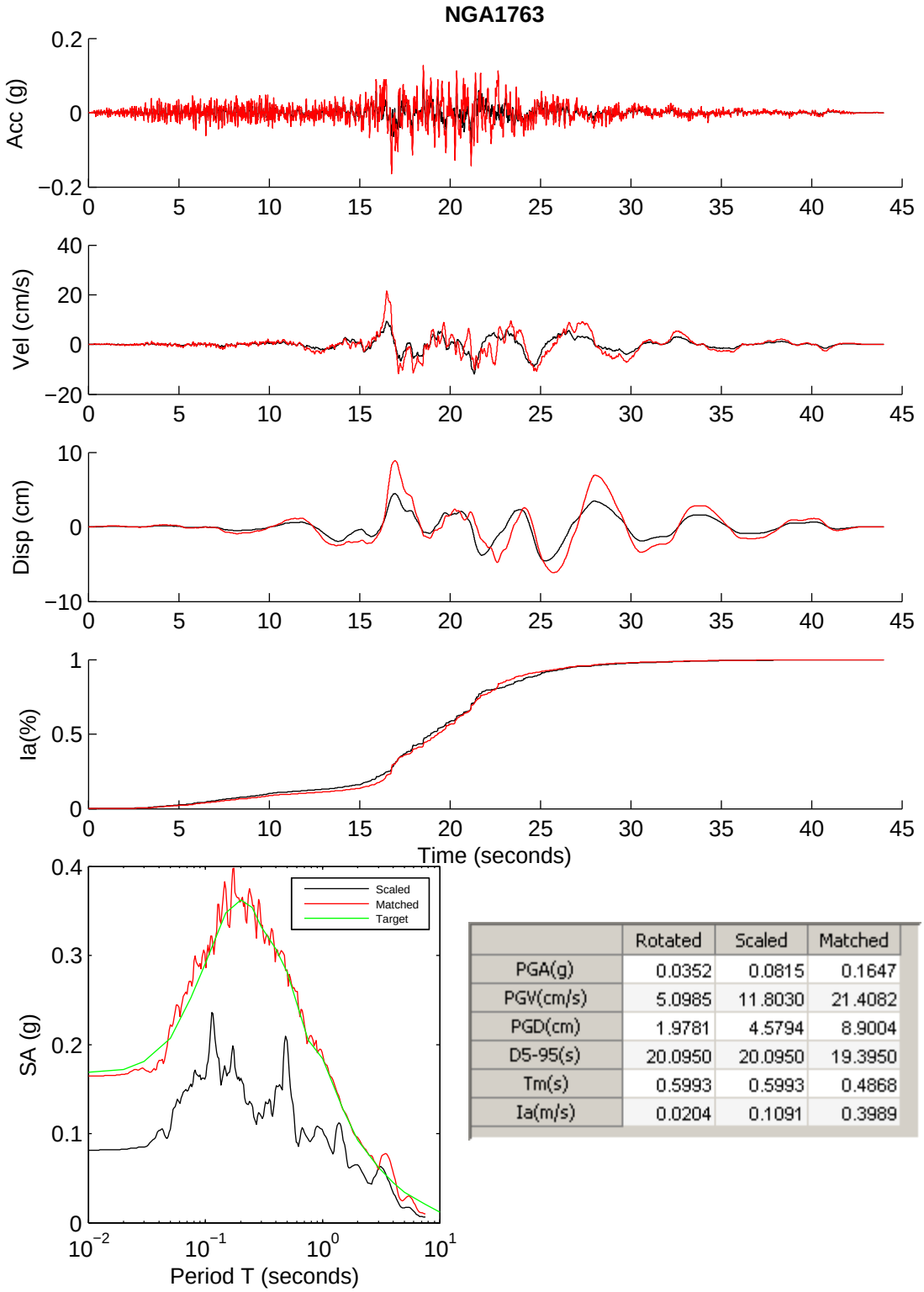

	Rotated	Scaled	Matched
PGA(g)	0.0352	0.0815	0.1647
PGV(cm/s)	5.0985	11.8030	21.4082
PGD(cm)	1.9781	4.5794	8.9004
D5-95(s)	20.0950	20.0950	19.3950
Tm(s)	0.5993	0.5993	0.4868
Ia(m/s)	0.0204	0.1091	0.3989

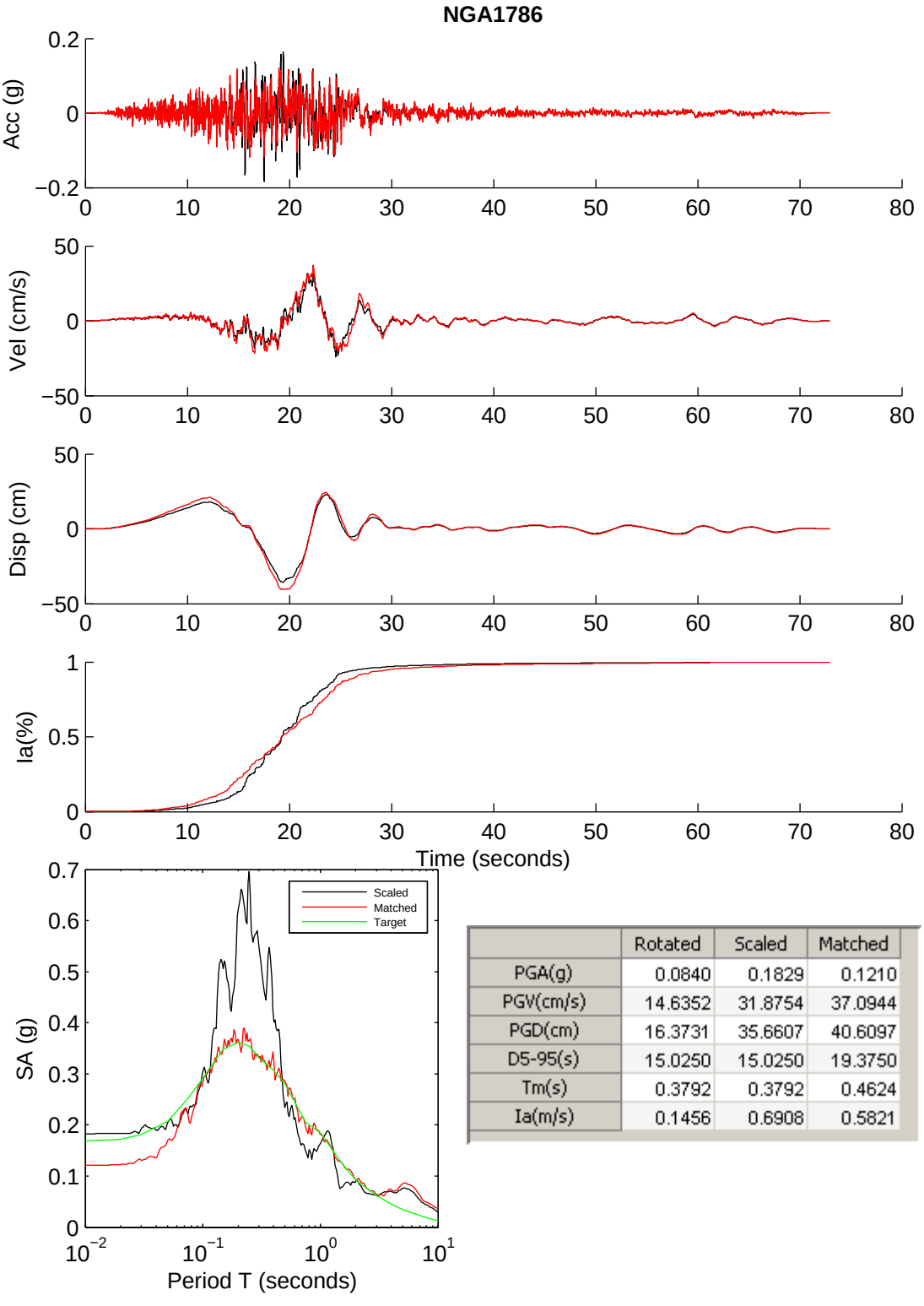

	Rotated	Scaled	Matched
PGA(g)	0.0840	0.1829	0.1210
PGV(cm/s)	14.6352	31.8754	37.0944
PGD(cm)	16.3731	35.6607	40.6097
D5-95(s)	15.0250	15.0250	19.3750
Tm(s)	0.3792	0.3792	0.4624
Ia(m/s)	0.1456	0.6908	0.5821

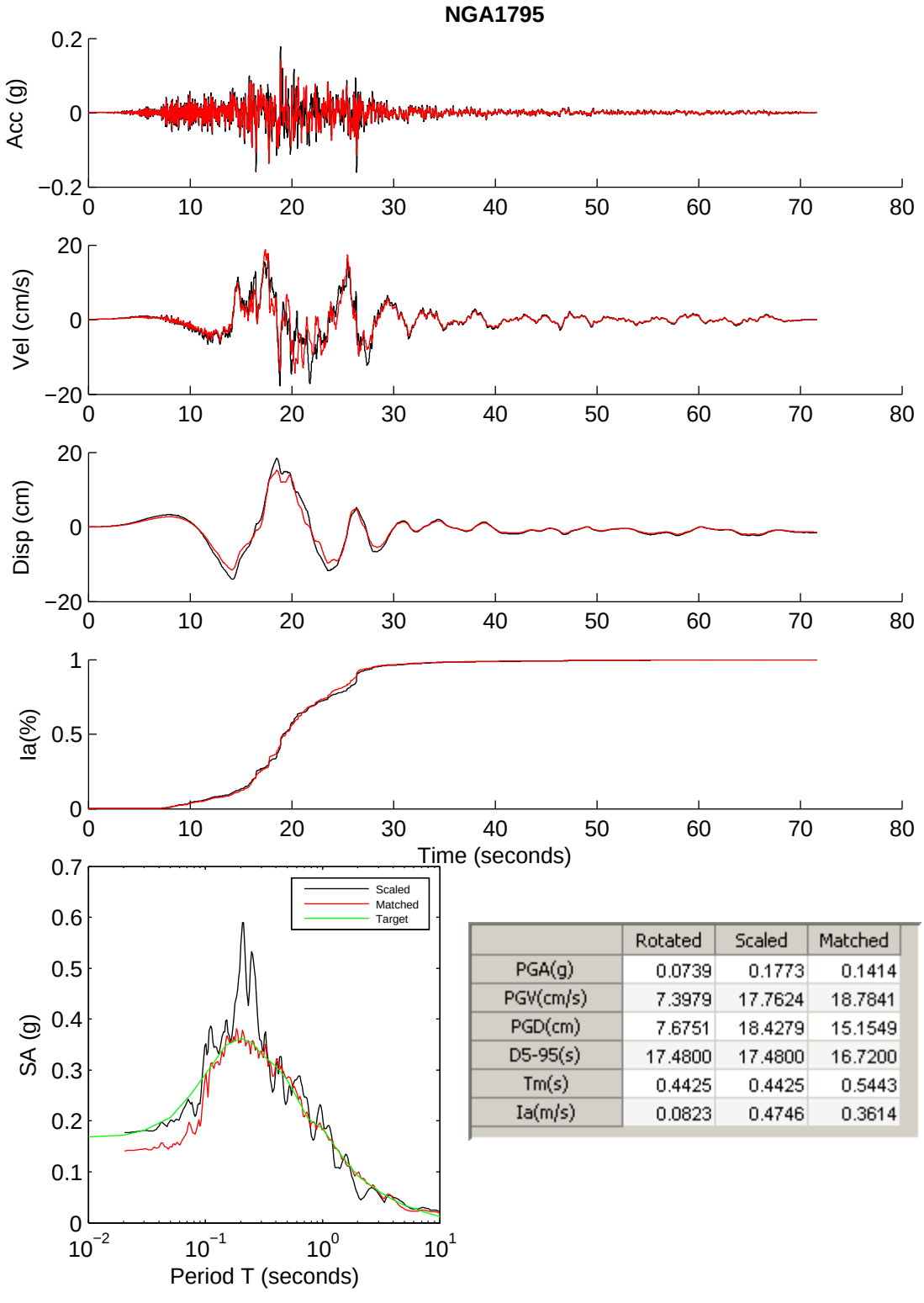

	Rotated	Scaled	Matched
PGA(g)	0.0739	0.1773	0.1414
PGV(cm/s)	7.3979	17.7624	18.7841
PGD(cm)	7.6751	18.4279	15.1549
D5-95(s)	17.4800	17.4800	16.7200
Tm(s)	0.4425	0.4425	0.5443
Ia(m/s)	0.0823	0.4746	0.3614

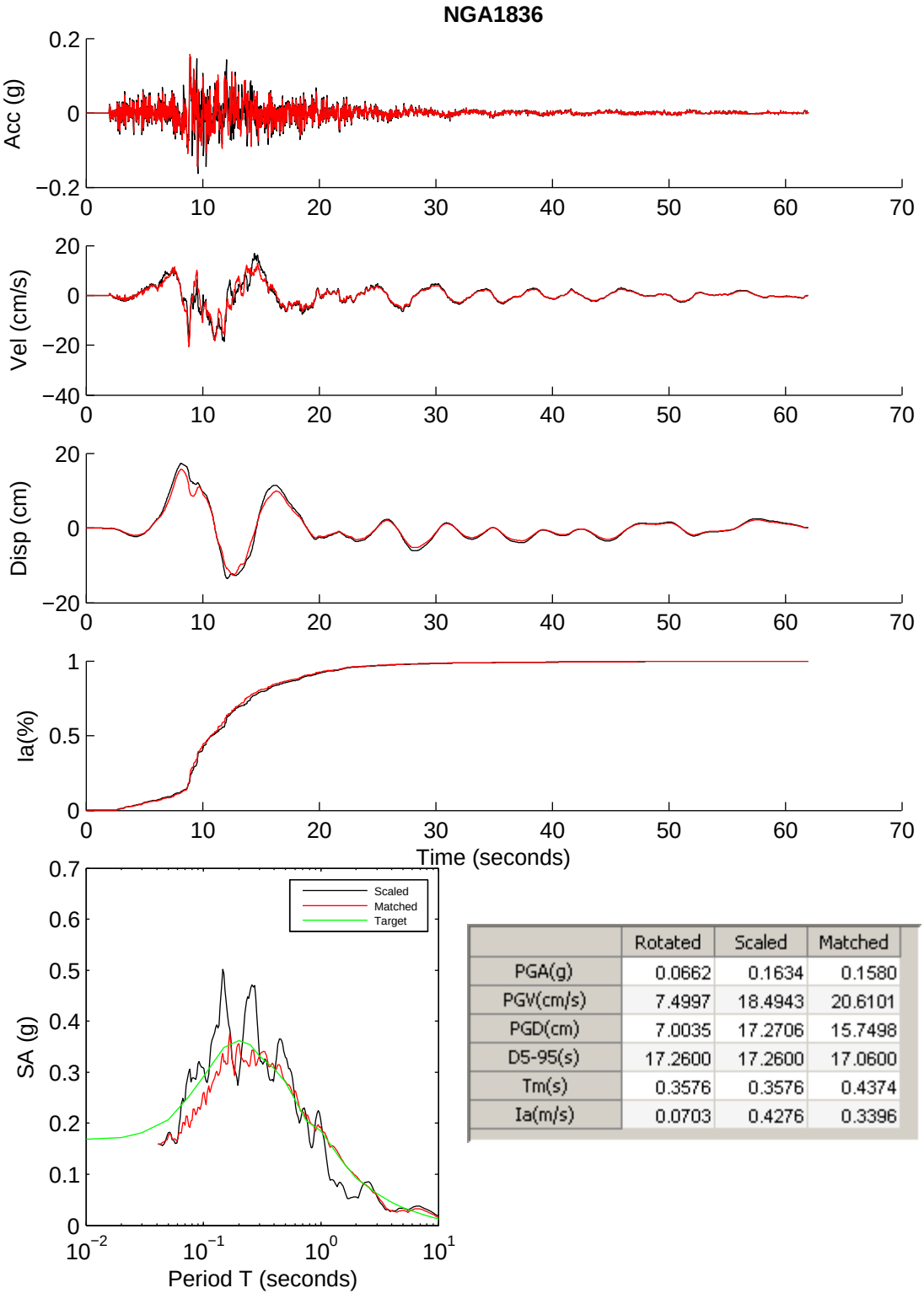

	Rotated	Scaled	Matched
PGA(g)	0.0662	0.1634	0.1580
PGV(cm/s)	7.4997	18.4943	20.6101
PGD(cm)	7.0035	17.2706	15.7498
D5-95(s)	17.2600	17.2600	17.0600
Tm(s)	0.3576	0.3576	0.4374
Ia(m/s)	0.0703	0.4276	0.3396

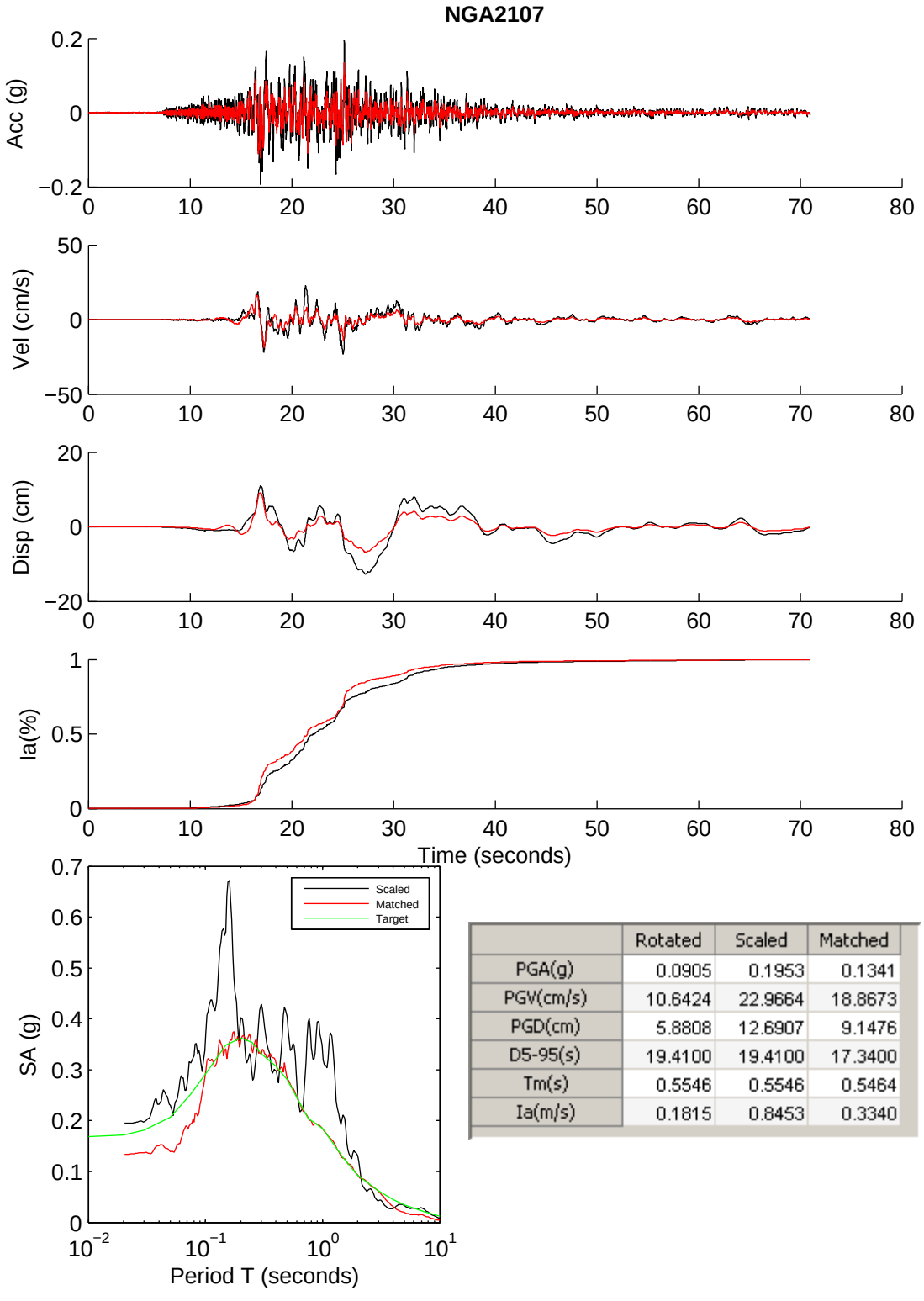

	Rotated	Scaled	Matched
PGA(g)	0.0905	0.1953	0.1341
PGV(cm/s)	10.6424	22.9664	18.8673
PGD(cm)	5.8808	12.6907	9.1476
D5-95(s)	19.4100	19.4100	17.3400
Tm(s)	0.5546	0.5546	0.5464
Ia(m/s)	0.1815	0.8453	0.3340

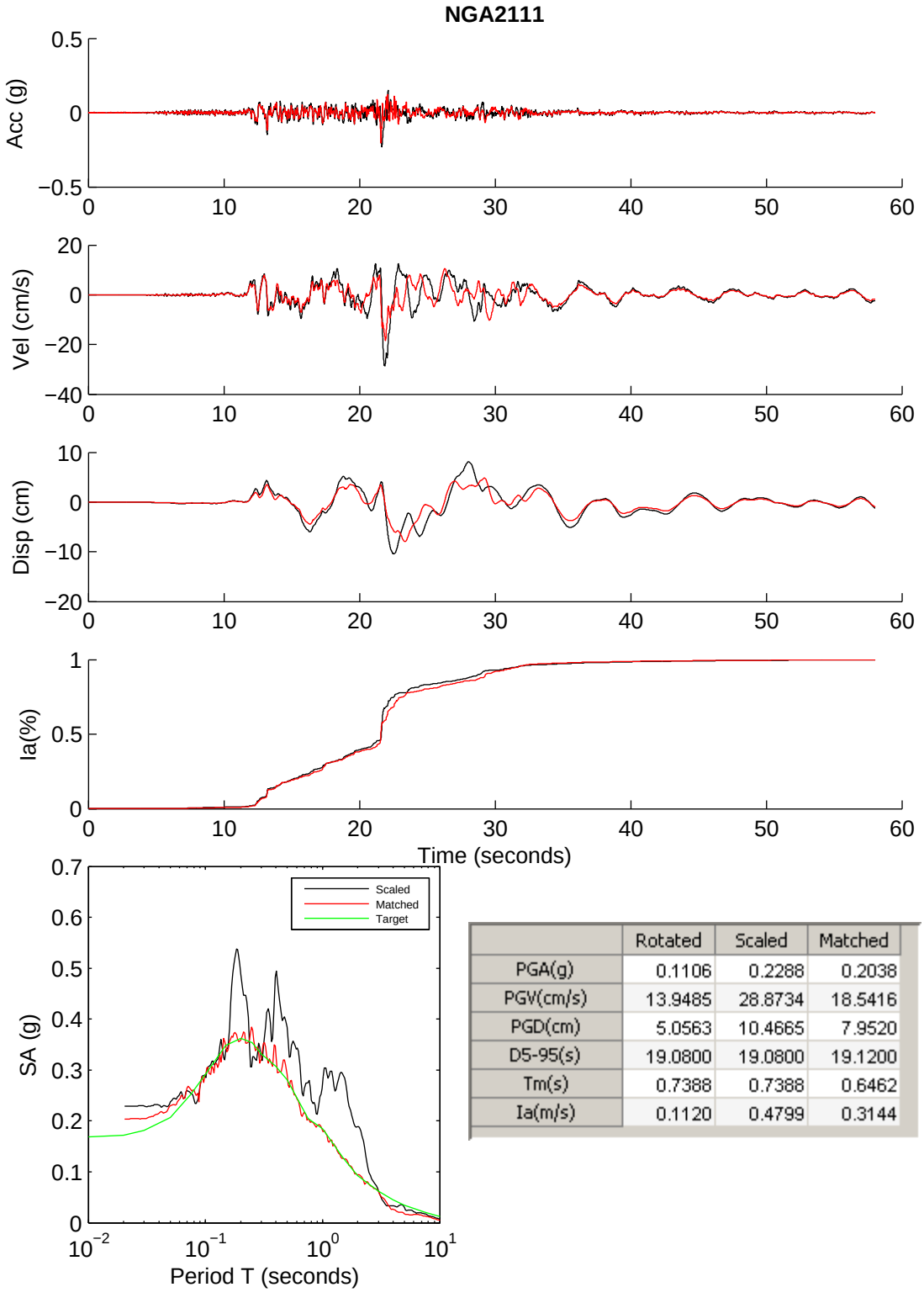

	Rotated	Scaled	Matched
PGA(g)	0.1106	0.2288	0.2038
PGV(cm/s)	13.9485	28.8734	18.5416
PGD(cm)	5.0563	10.4665	7.9520
D5-95(s)	19.0800	19.0800	19.1200
Tm(s)	0.7388	0.7388	0.6462
Ia(m/s)	0.1120	0.4799	0.3144

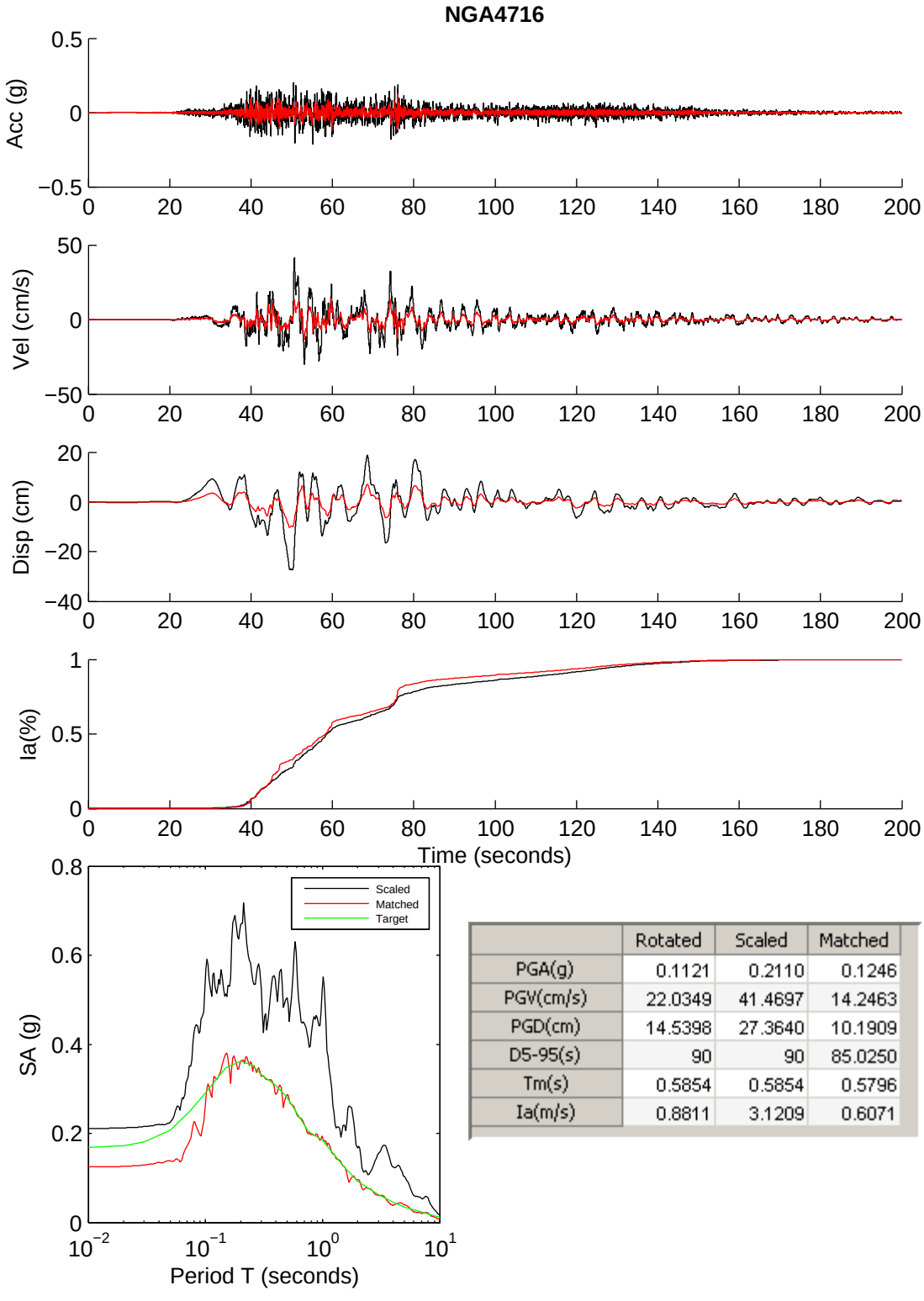

	Rotated	Scaled	Matched
PGA(g)	0.1121	0.2110	0.1246
PGV(cm/s)	22.0349	41.4697	14.2463
PGD(cm)	14.5398	27.3640	10.1909
D5-95(s)	90	90	85.0250
Tm(s)	0.5854	0.5854	0.5796
Ia(m/s)	0.8811	3.1209	0.6071

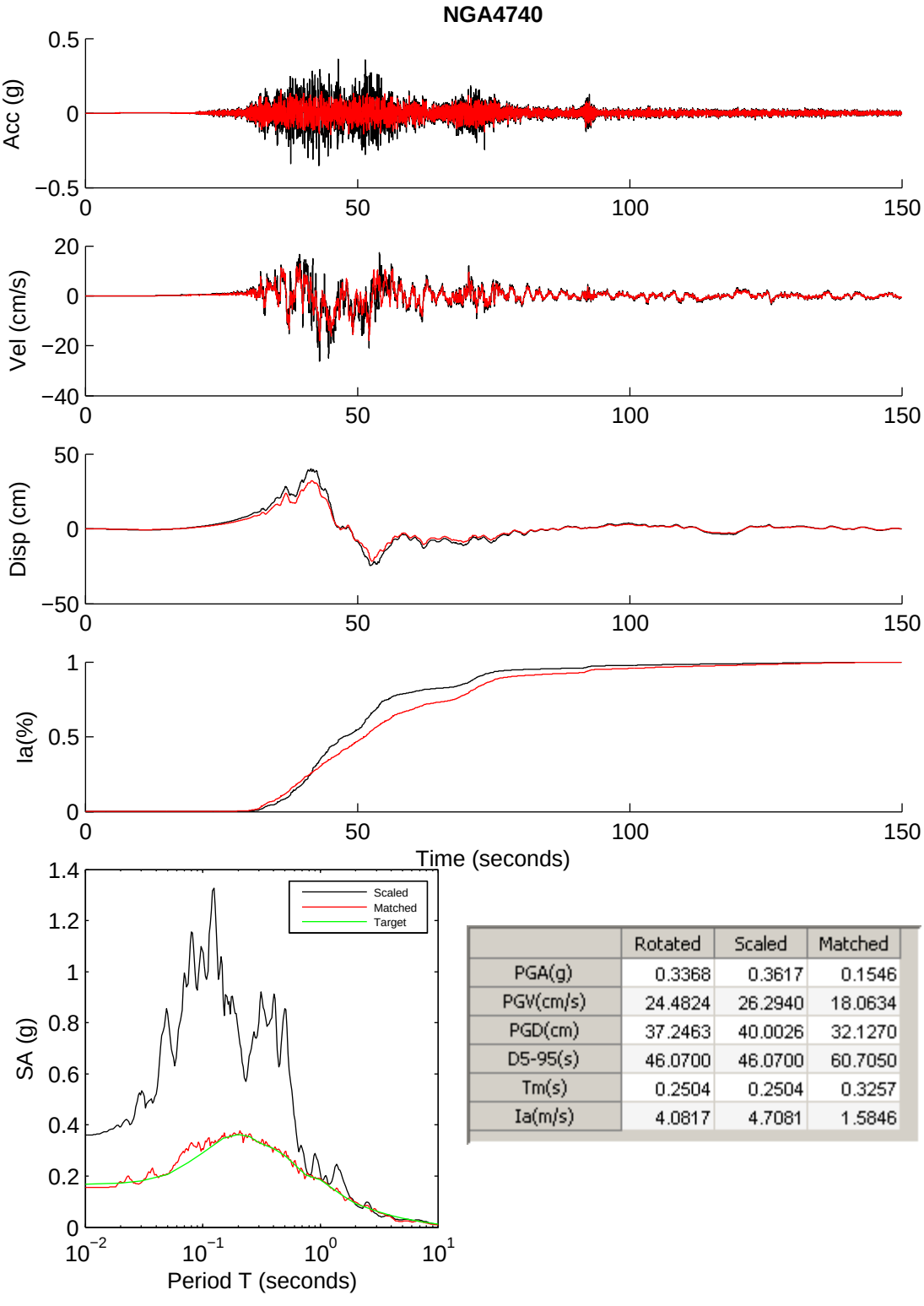

	Rotated	Scaled	Matched
PGA(g)	0.3368	0.3617	0.1546
PGV(cm/s)	24.4824	26.2940	18.0634
PGD(cm)	37.2463	40.0026	32.1270
D5-95(s)	46.0700	46.0700	60.7050
Tm(s)	0.2504	0.2504	0.3257
Ia(m/s)	4.0817	4.7081	1.5846

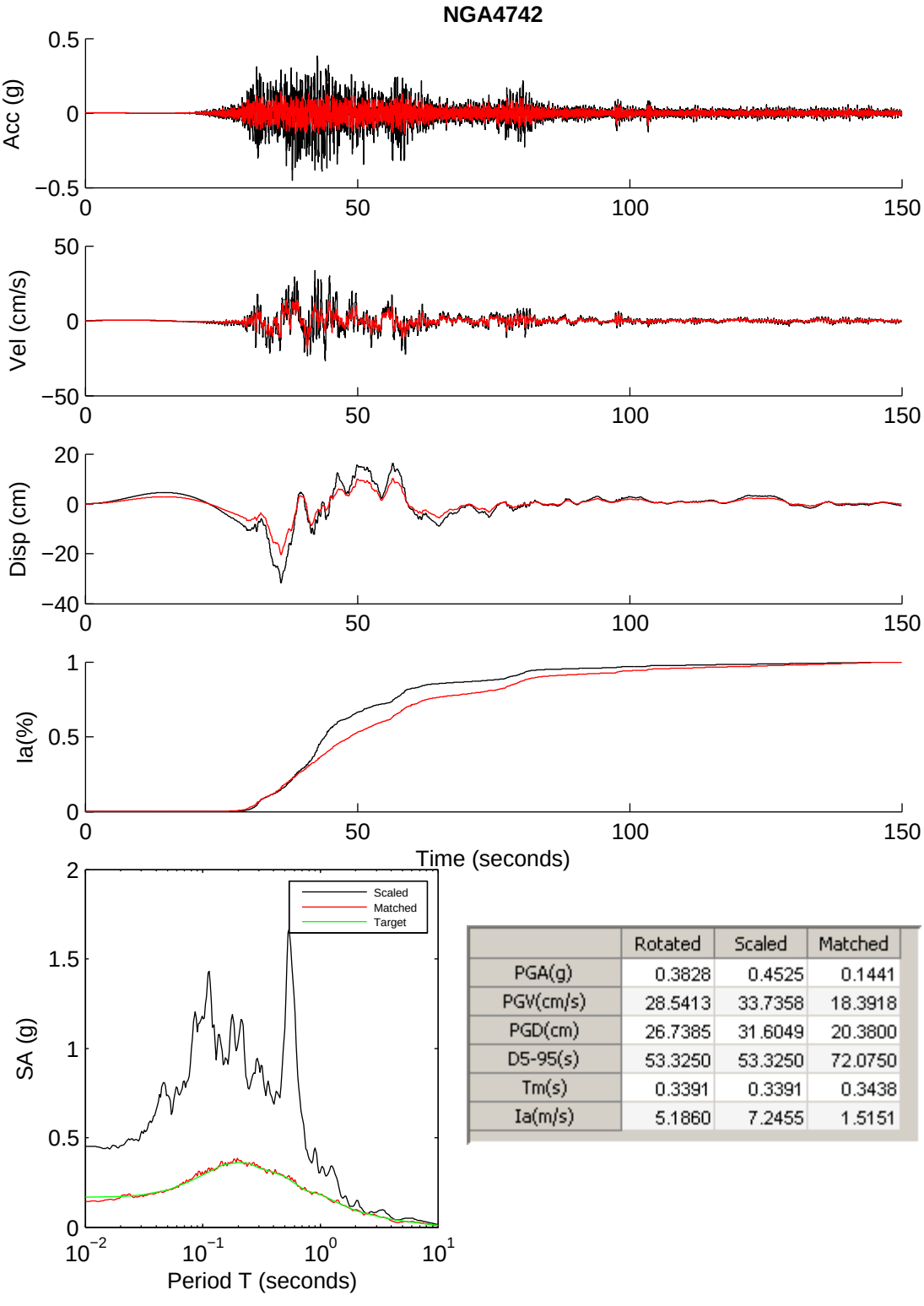

	Rotated	Scaled	Matched
PGA(g)	0.3828	0.4525	0.1441
PGV(cm/s)	28.5413	33.7358	18.3918
PGD(cm)	26.7385	31.6049	20.3800
D5-95(s)	53.3250	53.3250	72.0750
Tm(s)	0.3391	0.3391	0.3438
Ia(m/s)	5.1860	7.2455	1.5151

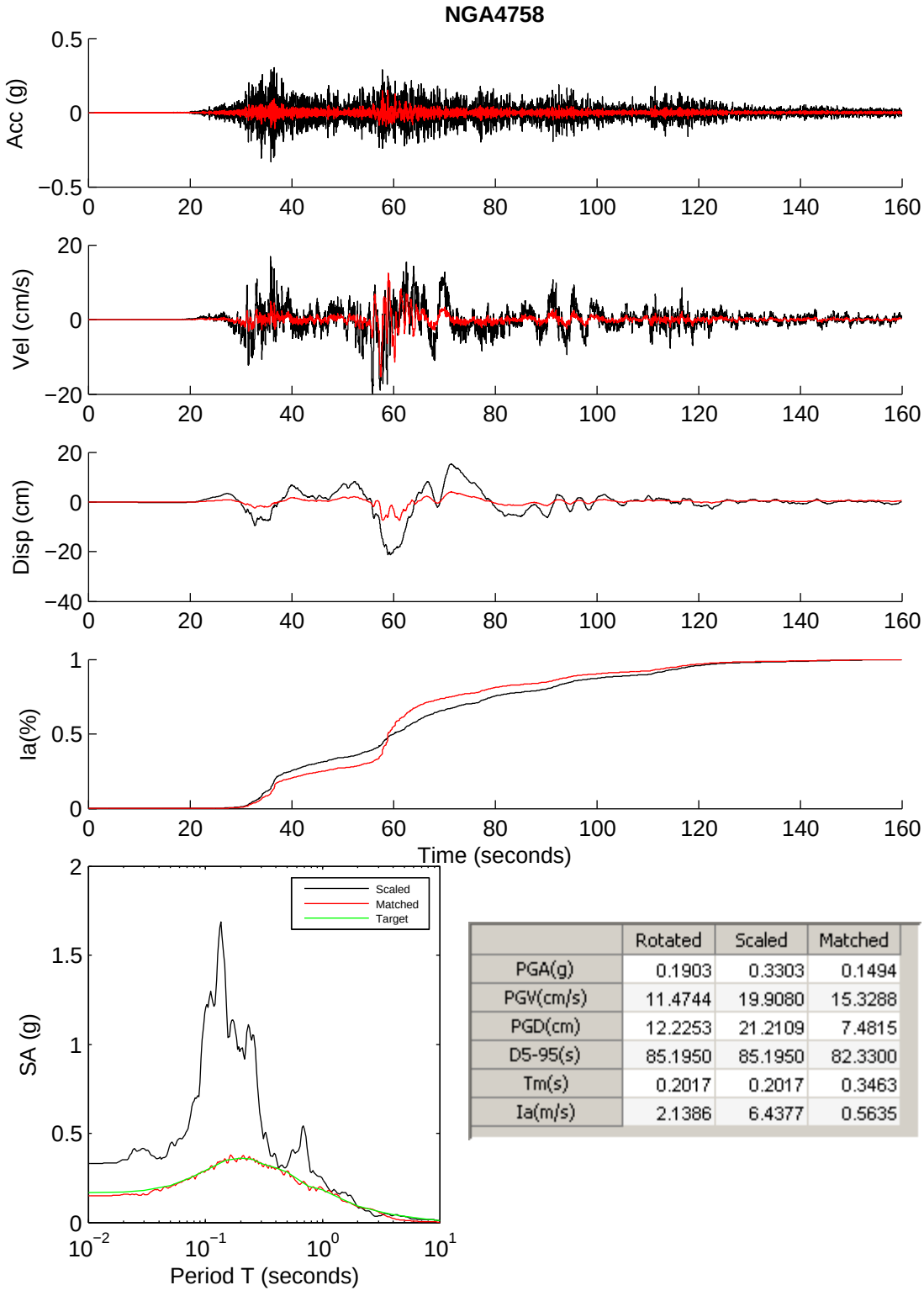

	Rotated	Scaled	Matched
PGA(g)	0.1903	0.3303	0.1494
PGV(cm/s)	11.4744	19.9080	15.3288
PGD(cm)	12.2253	21.2109	7.4815
D5-95(s)	85.1950	85.1950	82.3300
Tm(s)	0.2017	0.2017	0.3463
Ia(m/s)	2.1386	6.4377	0.5635

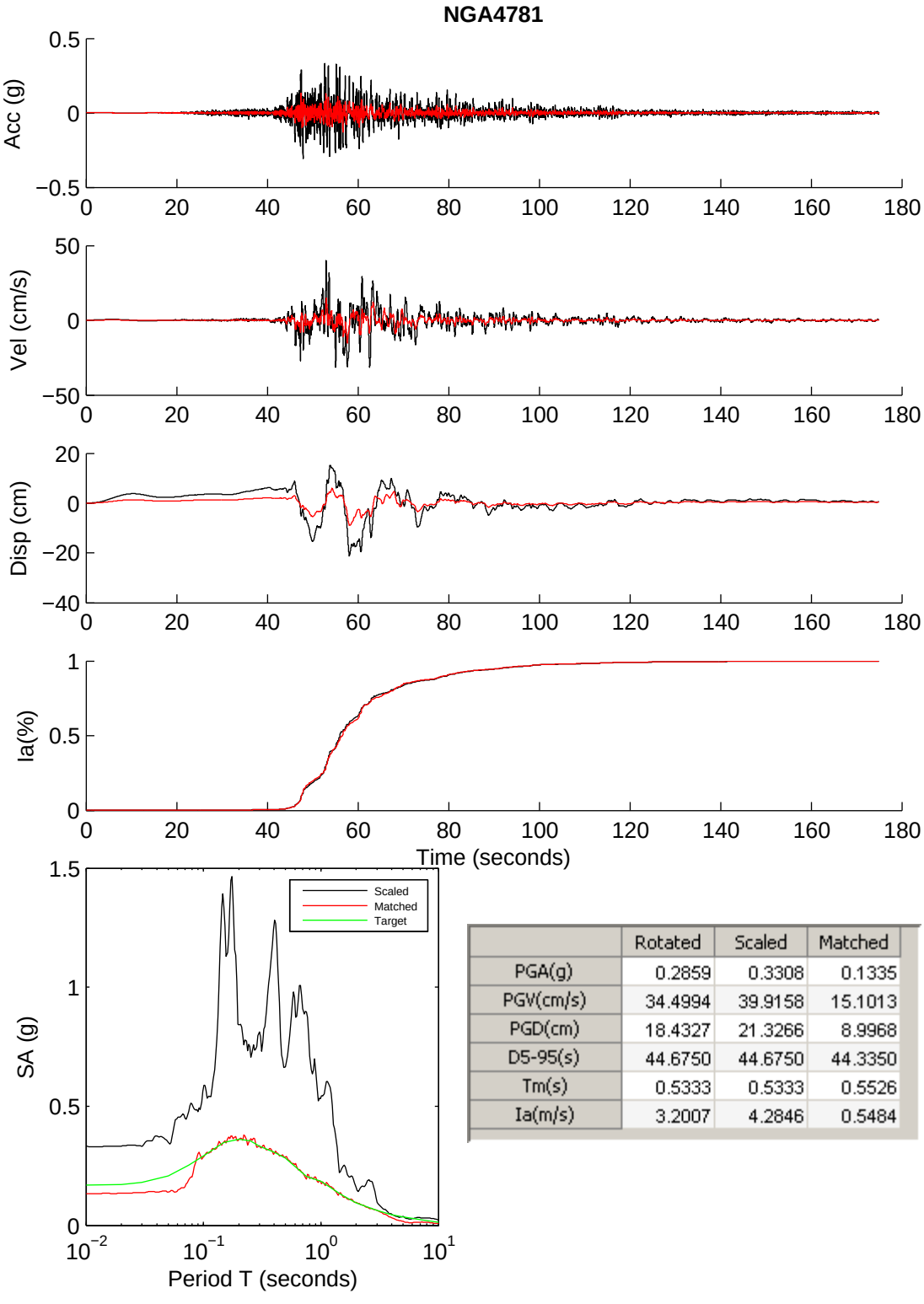

	Rotated	Scaled	Matched
PGA(g)	0.2859	0.3308	0.1335
PGV(cm/s)	34.4994	39.9158	15.1013
PGD(cm)	18.4327	21.3266	8.9968
D5-95(s)	44.6750	44.6750	44.3350
Tm(s)	0.5333	0.5333	0.5526
Ia(m/s)	3.2007	4.2846	0.5484

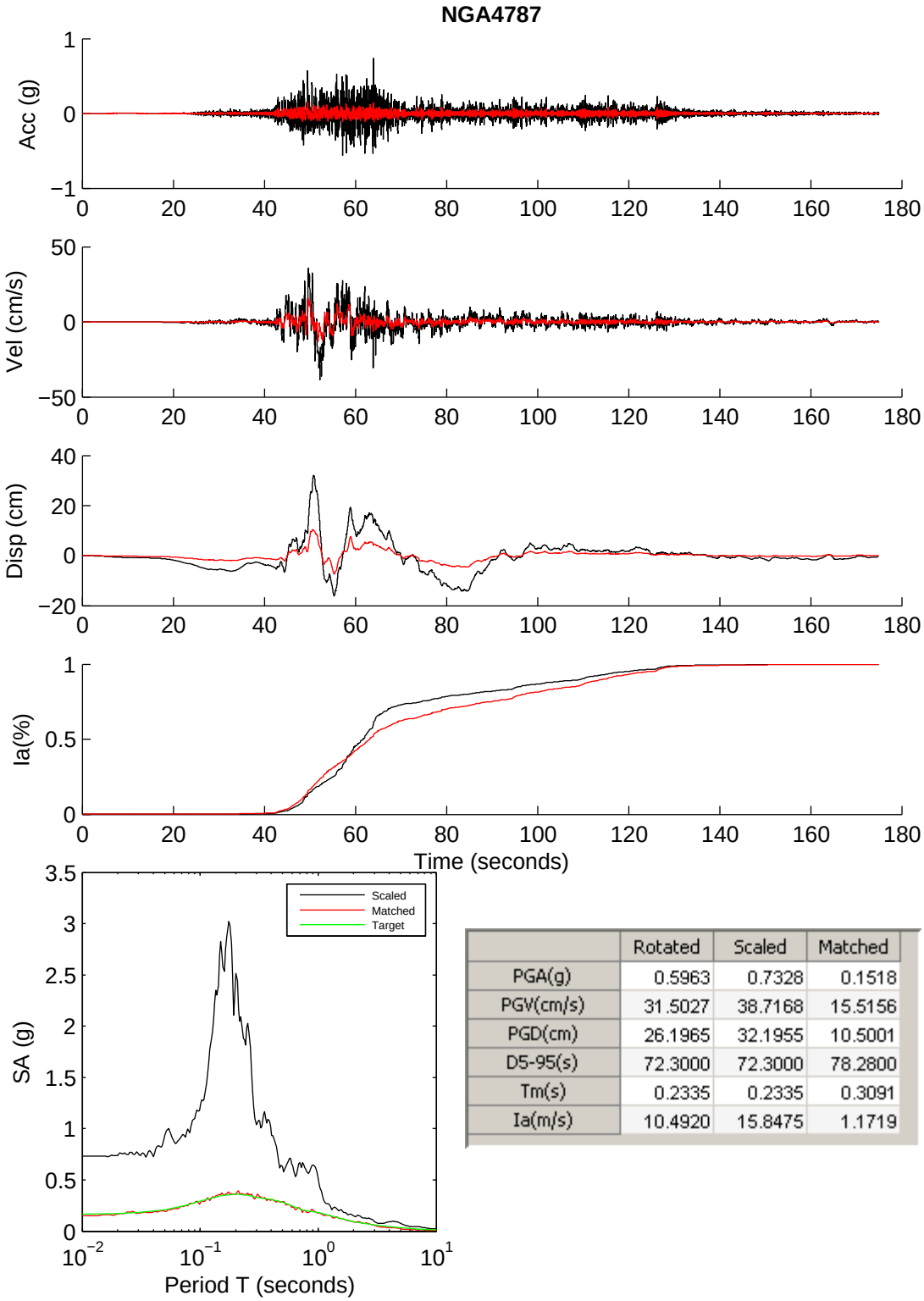

	Rotated	Scaled	Matched
PGA(g)	0.5963	0.7328	0.1518
PGV(cm/s)	31.5027	38.7168	15.5156
PGD(cm)	26.1965	32.1955	10.5001
D5-95(s)	72.3000	72.3000	78.2800
Tm(s)	0.2335	0.2335	0.3091
Ia(m/s)	10.4920	15.8475	1.1719

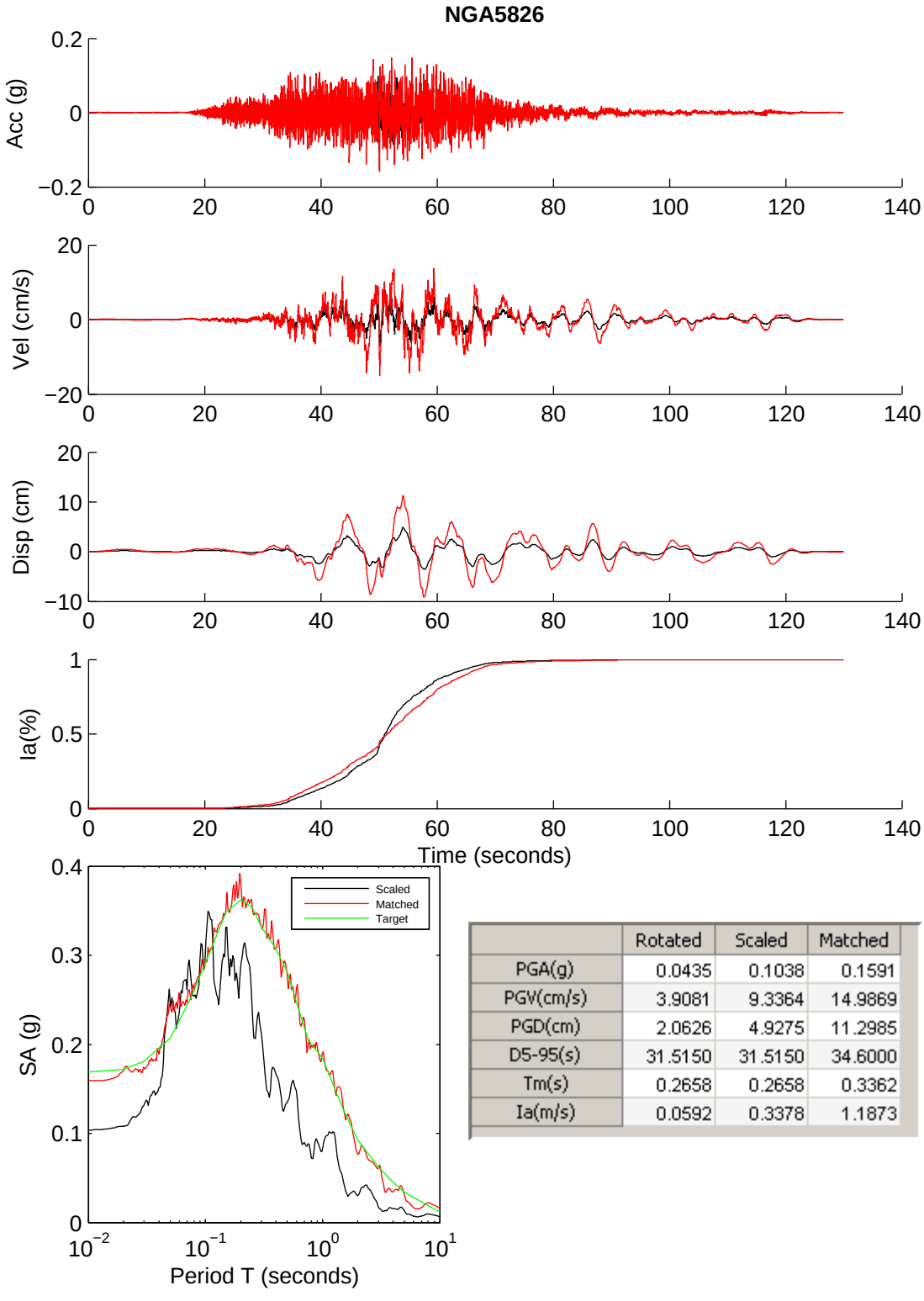

	Rotated	Scaled	Matched
PGA(g)	0.0435	0.1038	0.1591
PGV(cm/s)	3.9081	9.3364	14.9869
PGD(cm)	2.0626	4.9275	11.2985
D5-95(s)	31.5150	31.5150	34.6000
Tm(s)	0.2658	0.2658	0.3362
Ia(m/s)	0.0592	0.3378	1.1873

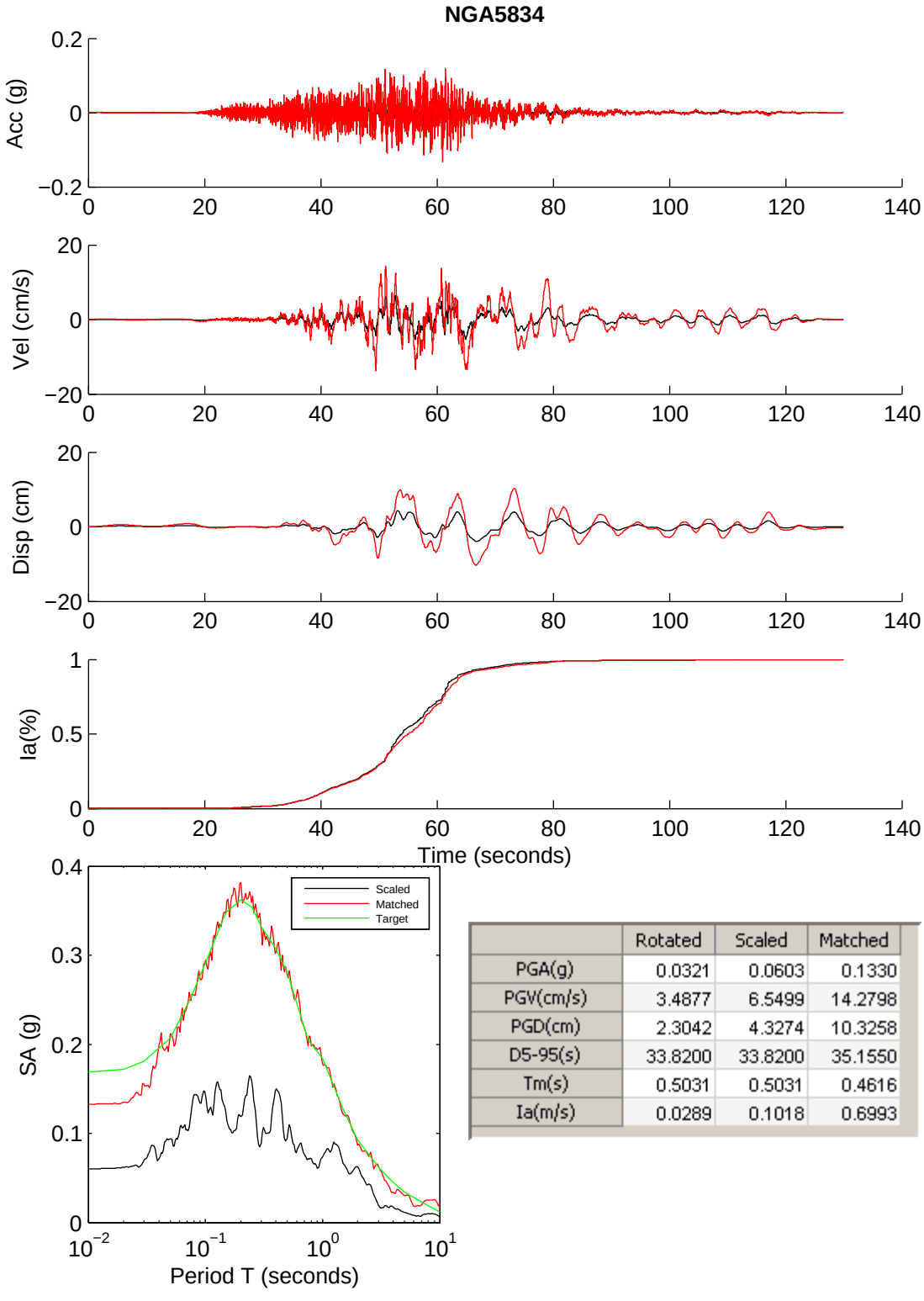

	Rotated	Scaled	Matched
PGA(g)	0.0321	0.0603	0.1330
PGV(cm/s)	3.4877	6.5499	14.2798
PGD(cm)	2.3042	4.3274	10.3258
D5-95(s)	33.8200	33.8200	35.1550
Tm(s)	0.5031	0.5031	0.4616
Ia(m/s)	0.0289	0.1018	0.6993

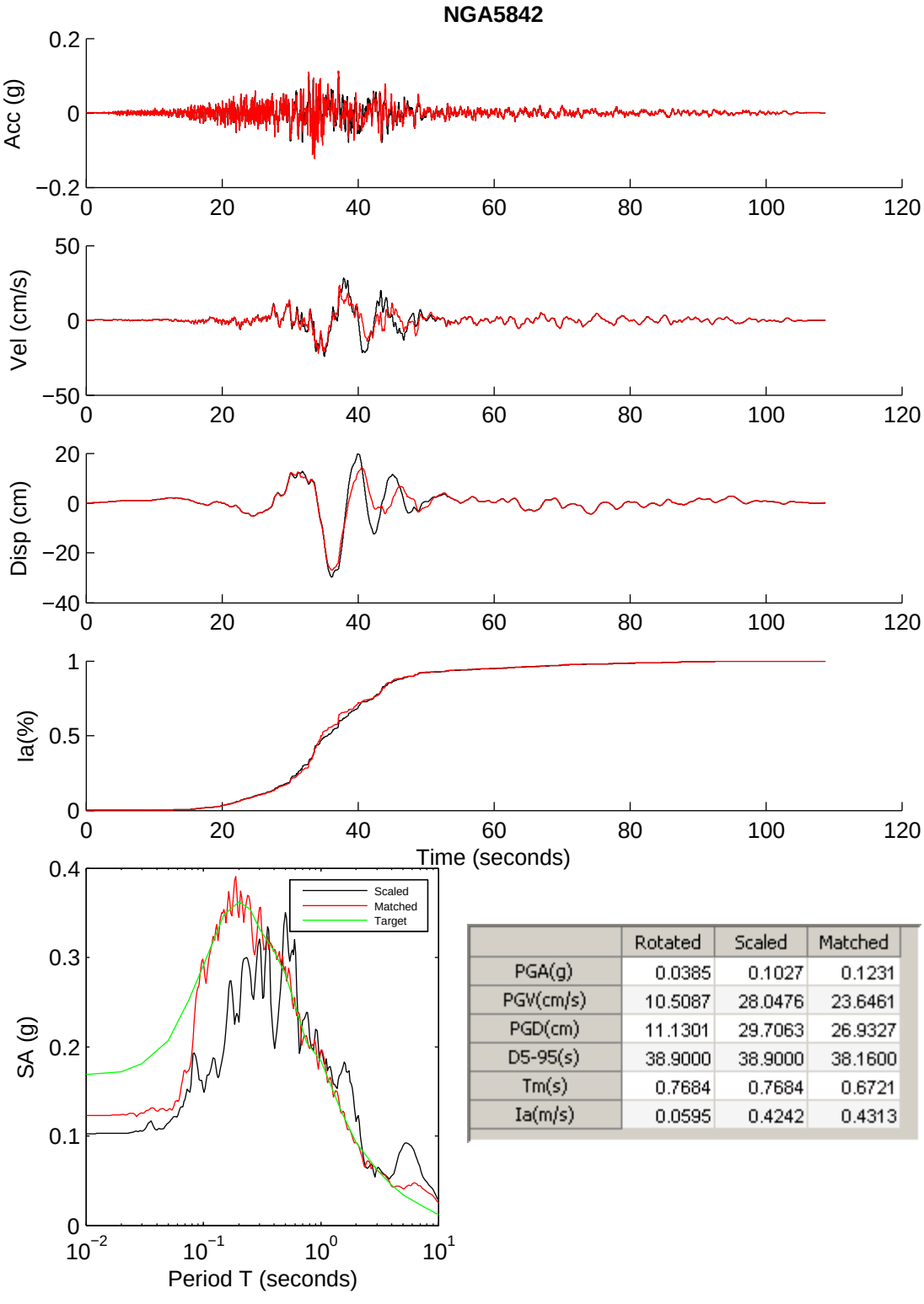

	Rotated	Scaled	Matched
PGA(g)	0.0385	0.1027	0.1231
PGV(cm/s)	10.5087	28.0476	23.6461
PGD(cm)	11.1301	29.7063	26.9327
D5-95(s)	38.9000	38.9000	38.1600
Tm(s)	0.7684	0.7684	0.6721
Ia(m/s)	0.0595	0.4242	0.4313

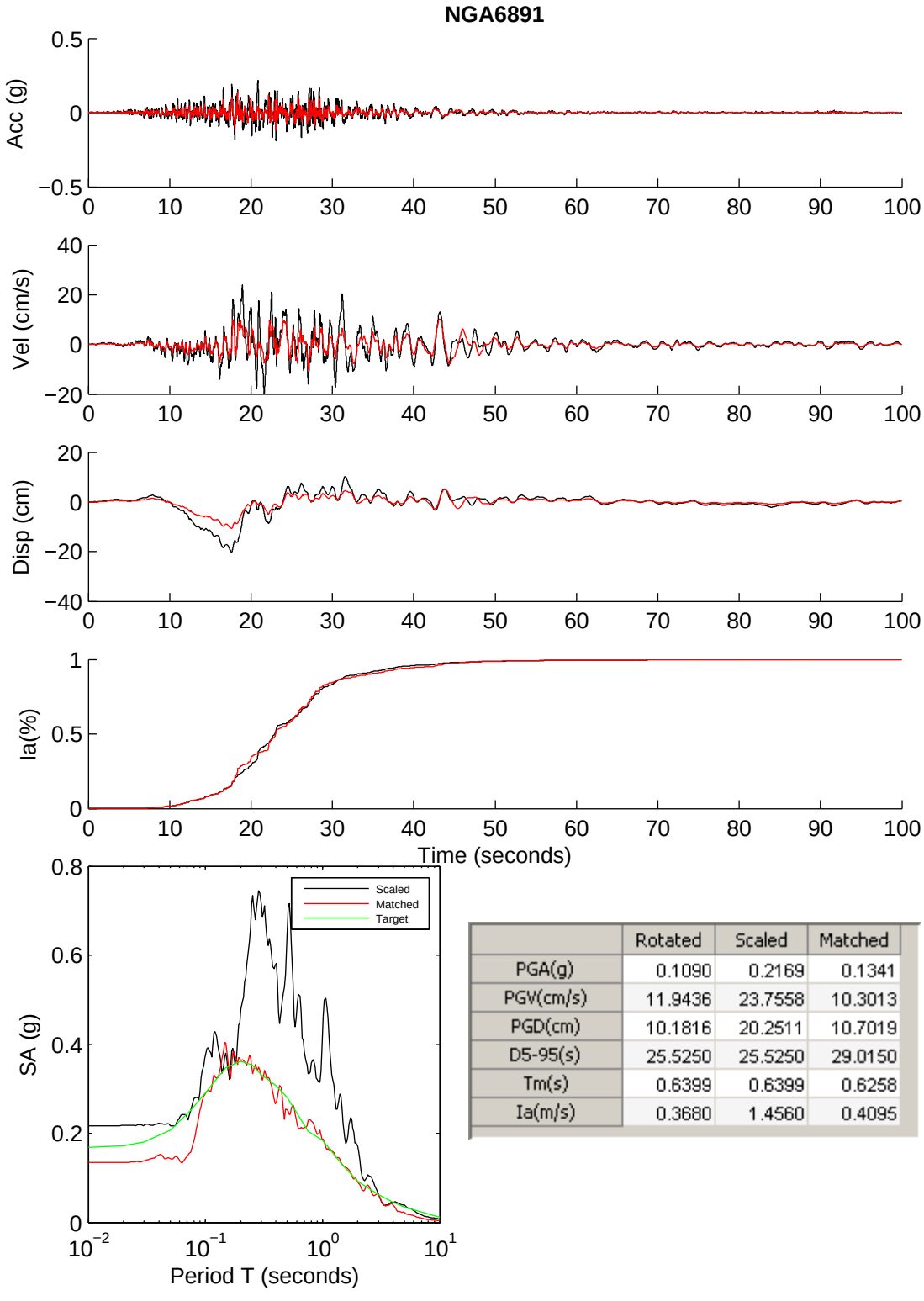

	Rotated	Scaled	Matched
PGA(g)	0.1090	0.2169	0.1341
PGV(cm/s)	11.9436	23.7558	10.3013
PGD(cm)	10.1816	20.2511	10.7019
D5-95(s)	25.5250	25.5250	29.0150
Tm(s)	0.6399	0.6399	0.6258
Ia(m/s)	0.3680	1.4560	0.4095

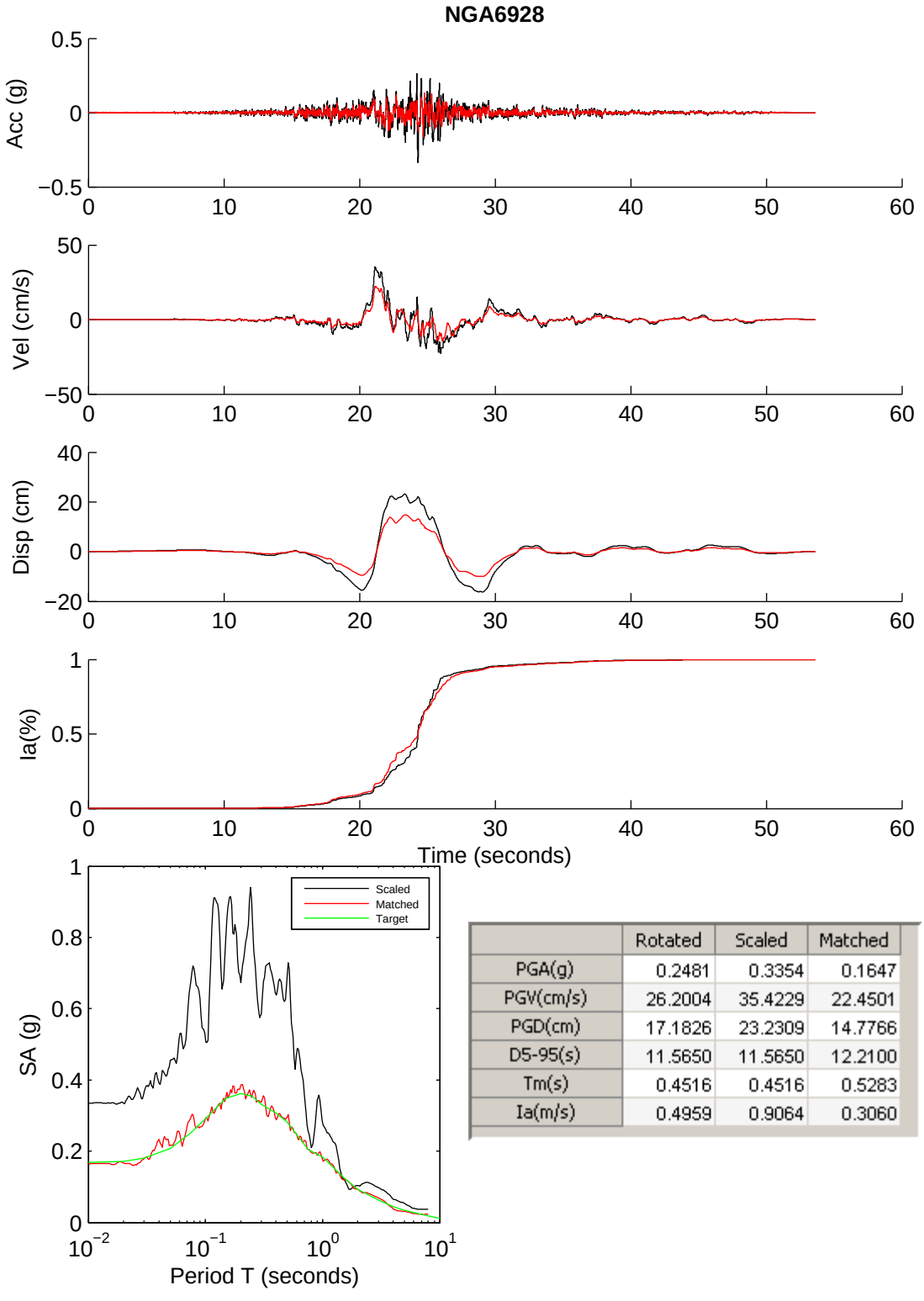

	Rotated	Scaled	Matched
PGA(g)	0.2481	0.3354	0.1647
PGV(cm/s)	26.2004	35.4229	22.4501
PGD(cm)	17.1826	23.2309	14.7766
D5-95(s)	11.5650	11.5650	12.2100
Tm(s)	0.4516	0.4516	0.5283
Ia(m/s)	0.4959	0.9064	0.3060

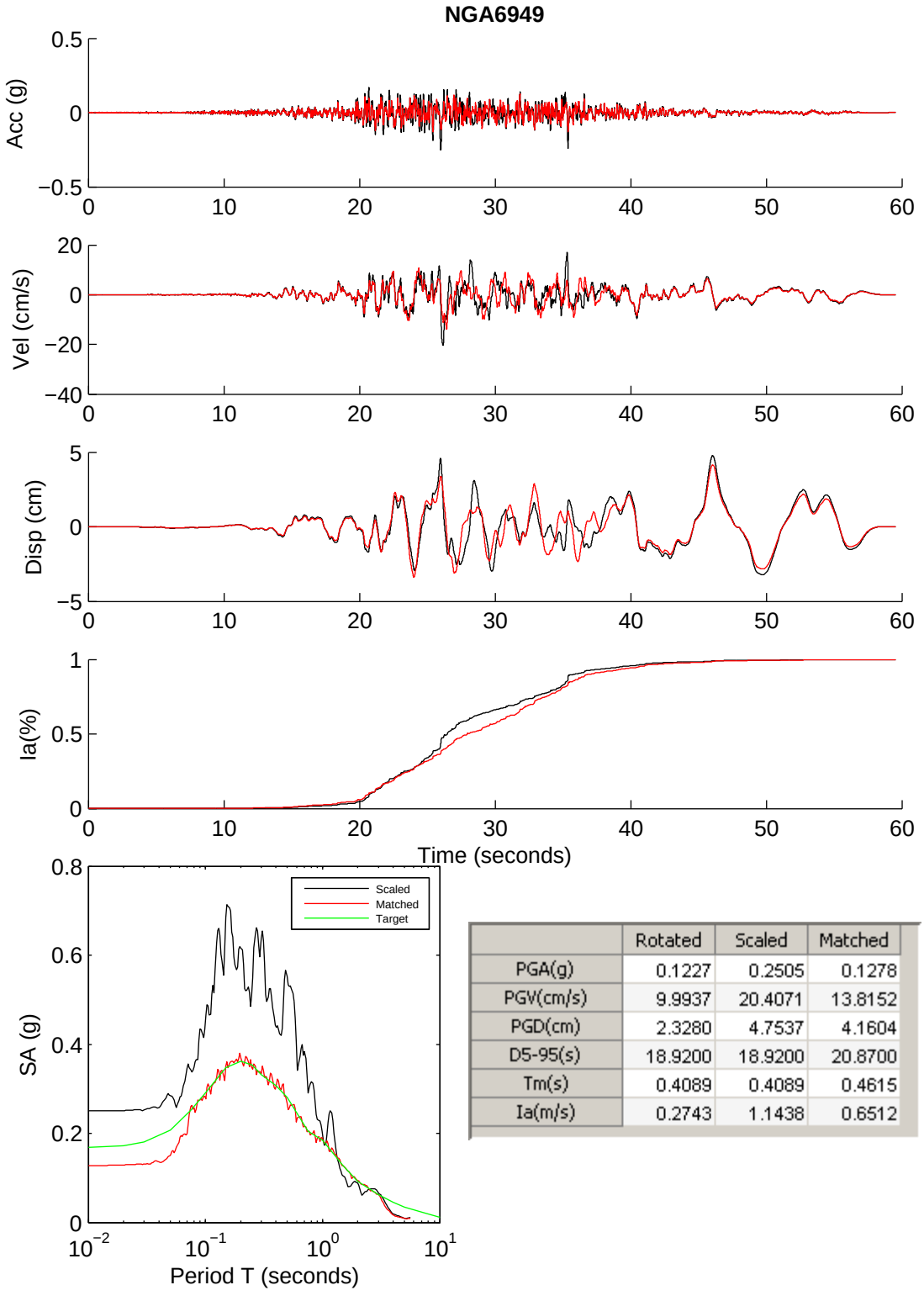

	Rotated	Scaled	Matched
PGA(g)	0.1227	0.2505	0.1278
PGV(cm/s)	9.9937	20.4071	13.8152
PGD(cm)	2.3280	4.7537	4.1604
D5-95(s)	18.9200	18.9200	20.8700
Tm(s)	0.4089	0.4089	0.4615
Ia(m/s)	0.2743	1.1438	0.6512

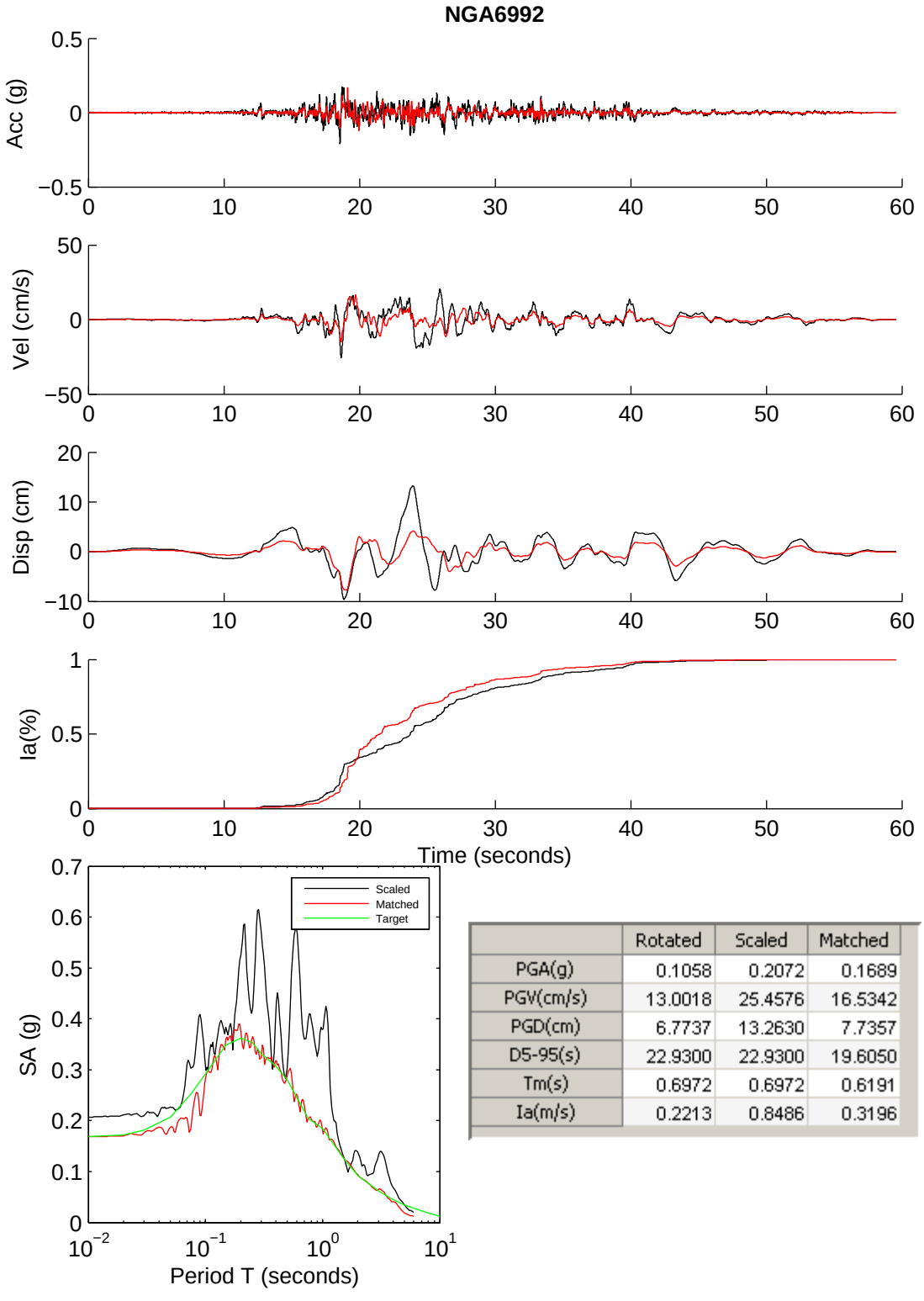

	Rotated	Scaled	Matched
PGA(g)	0.1058	0.2072	0.1689
PGV(cm/s)	13.0018	25.4576	16.5342
PGD(cm)	6.7737	13.2630	7.7357
D5-95(s)	22.9300	22.9300	19.6050
Tm(s)	0.6972	0.6972	0.6191
Ia(m/s)	0.2213	0.8486	0.3196

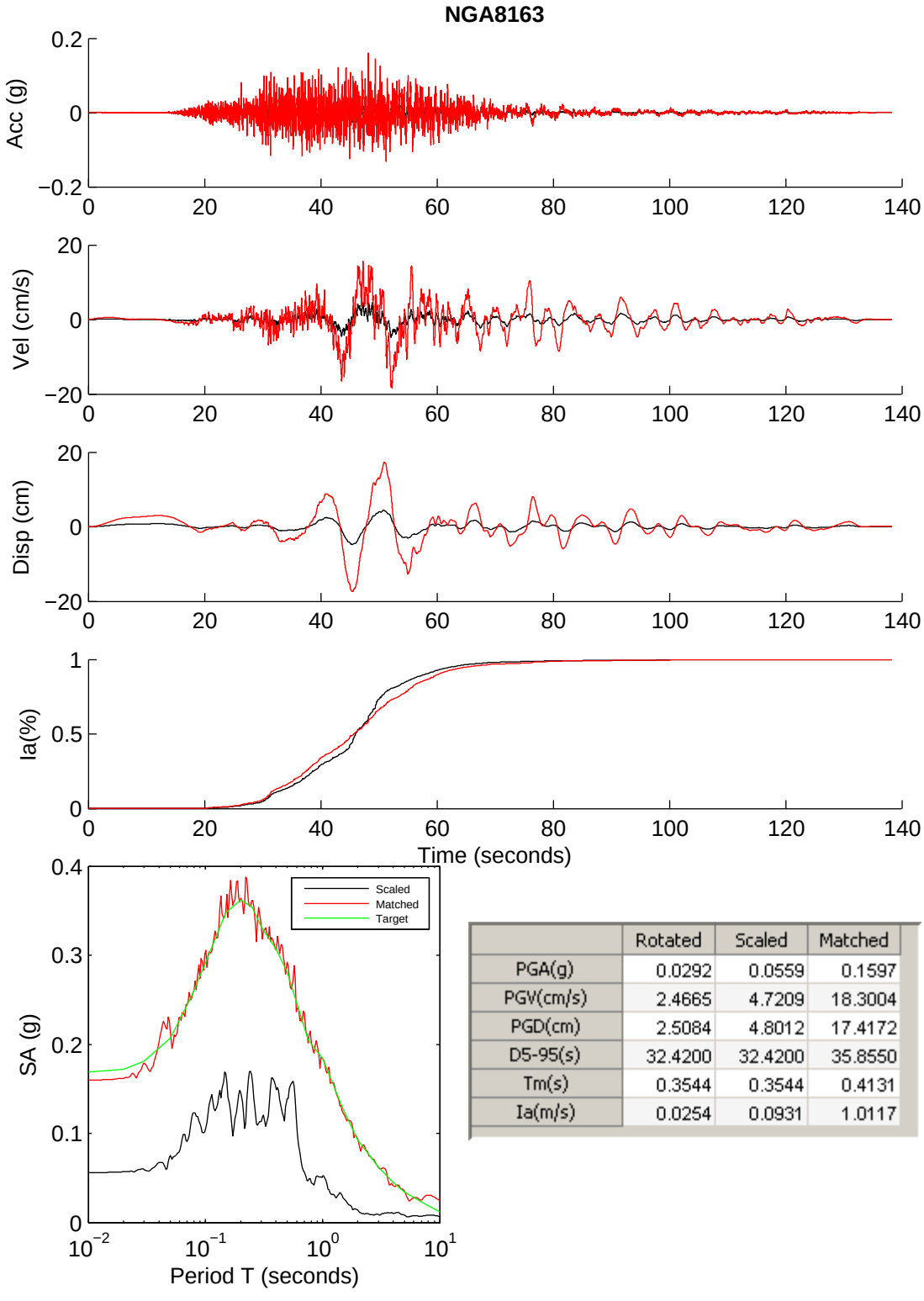

	Rotated	Scaled	Matched
PGA(g)	0.0292	0.0559	0.1597
PGV(cm/s)	2.4665	4.7209	18.3004
PGD(cm)	2.5084	4.8012	17.4172
D5-95(s)	32.4200	32.4200	35.8550
Tm(s)	0.3544	0.3544	0.4131
Ia(m/s)	0.0254	0.0931	1.0117

APPENDIX 3E: SCENARIO SUB GROUND MOTION DATA

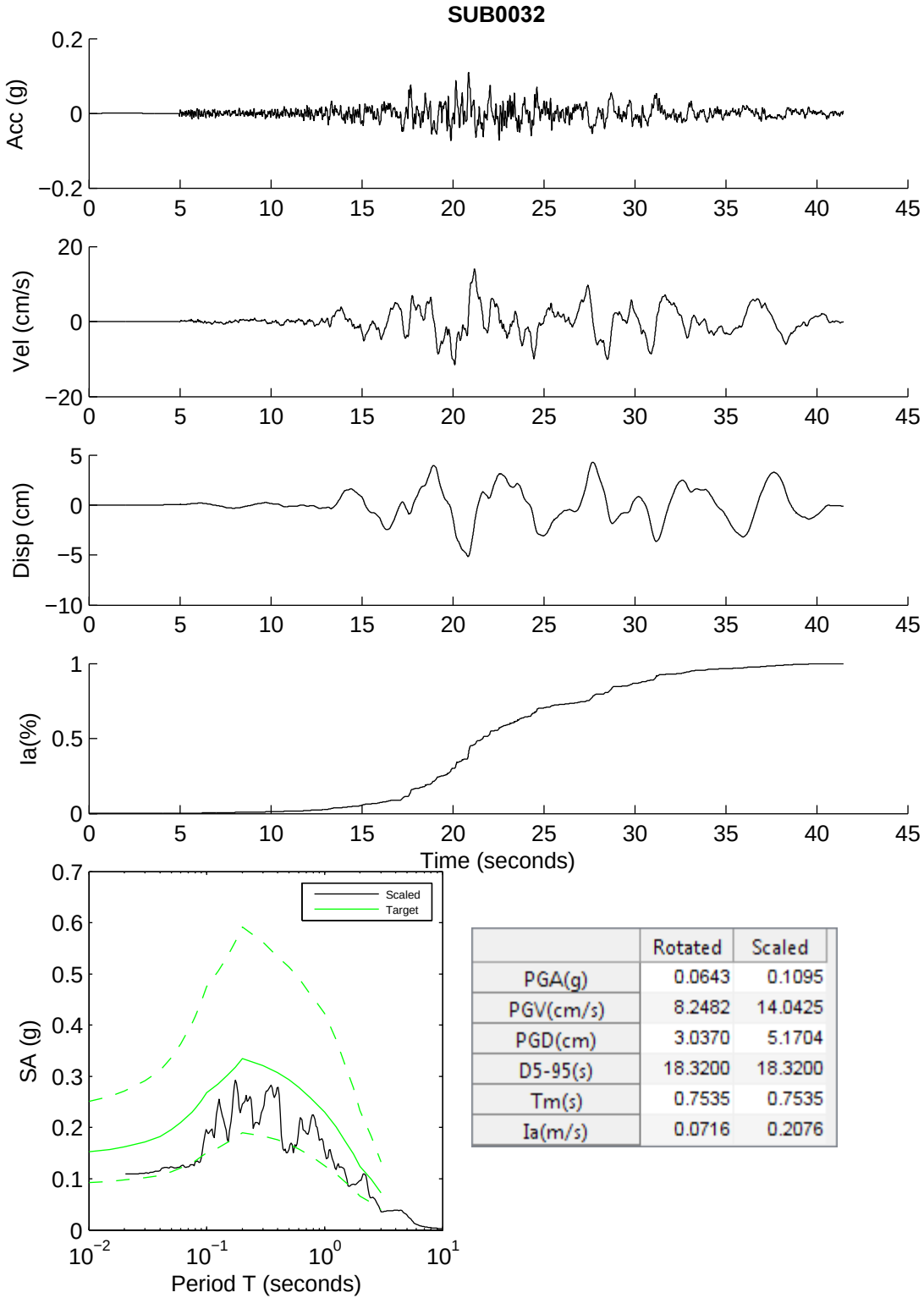

	Rotated	Scaled
PGA(g)	0.0643	0.1095
PGV(cm/s)	8.2482	14.0425
PGD(cm)	3.0370	5.1704
D5-95(s)	18.3200	18.3200
Tm(s)	0.7535	0.7535
Ia(m/s)	0.0716	0.2076

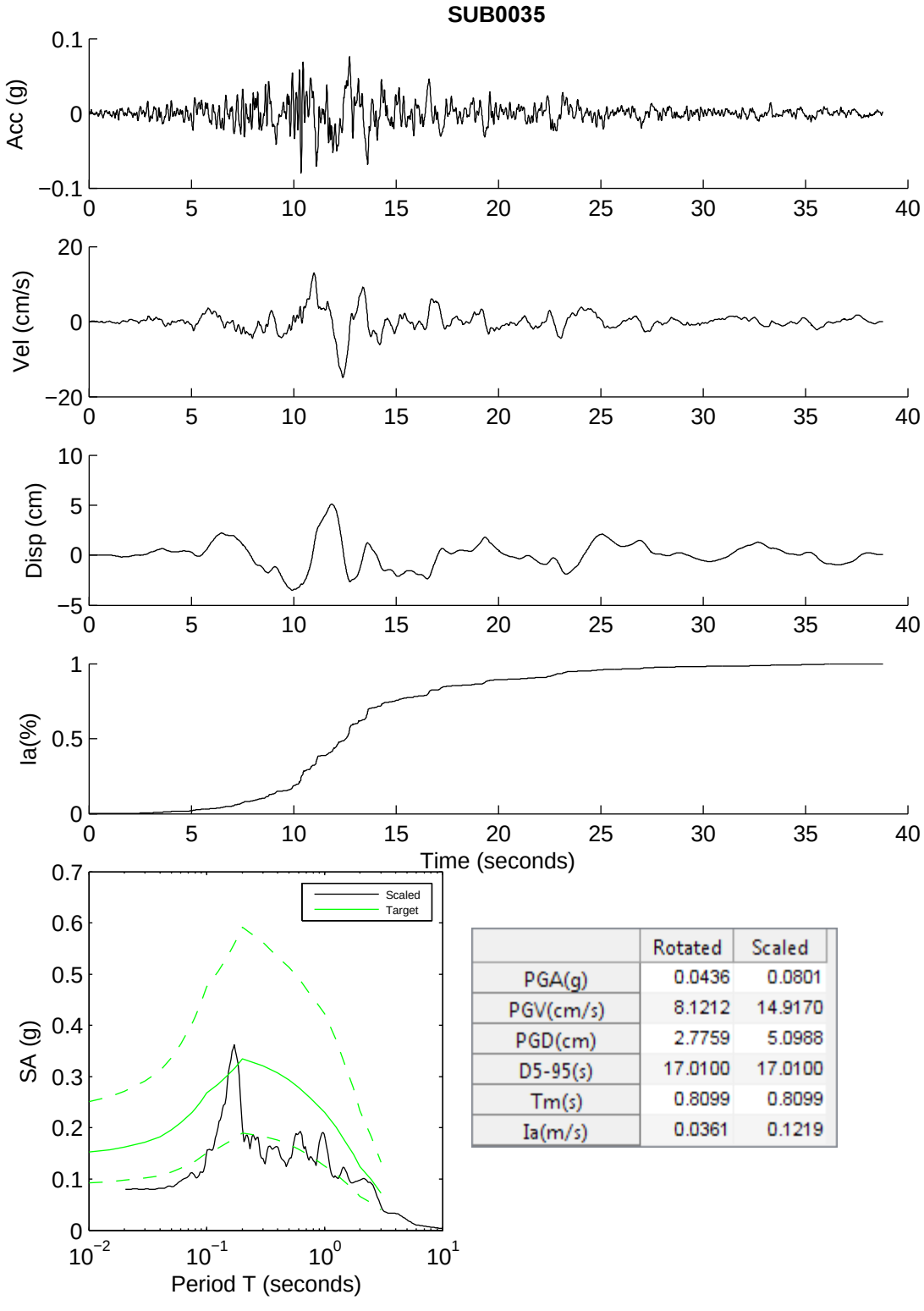

	Rotated	Scaled
PGA(g)	0.0436	0.0801
PGV(cm/s)	8.1212	14.9170
PGD(cm)	2.7759	5.0988
D5-95(s)	17.0100	17.0100
Tm(s)	0.8099	0.8099
Ia(m/s)	0.0361	0.1219

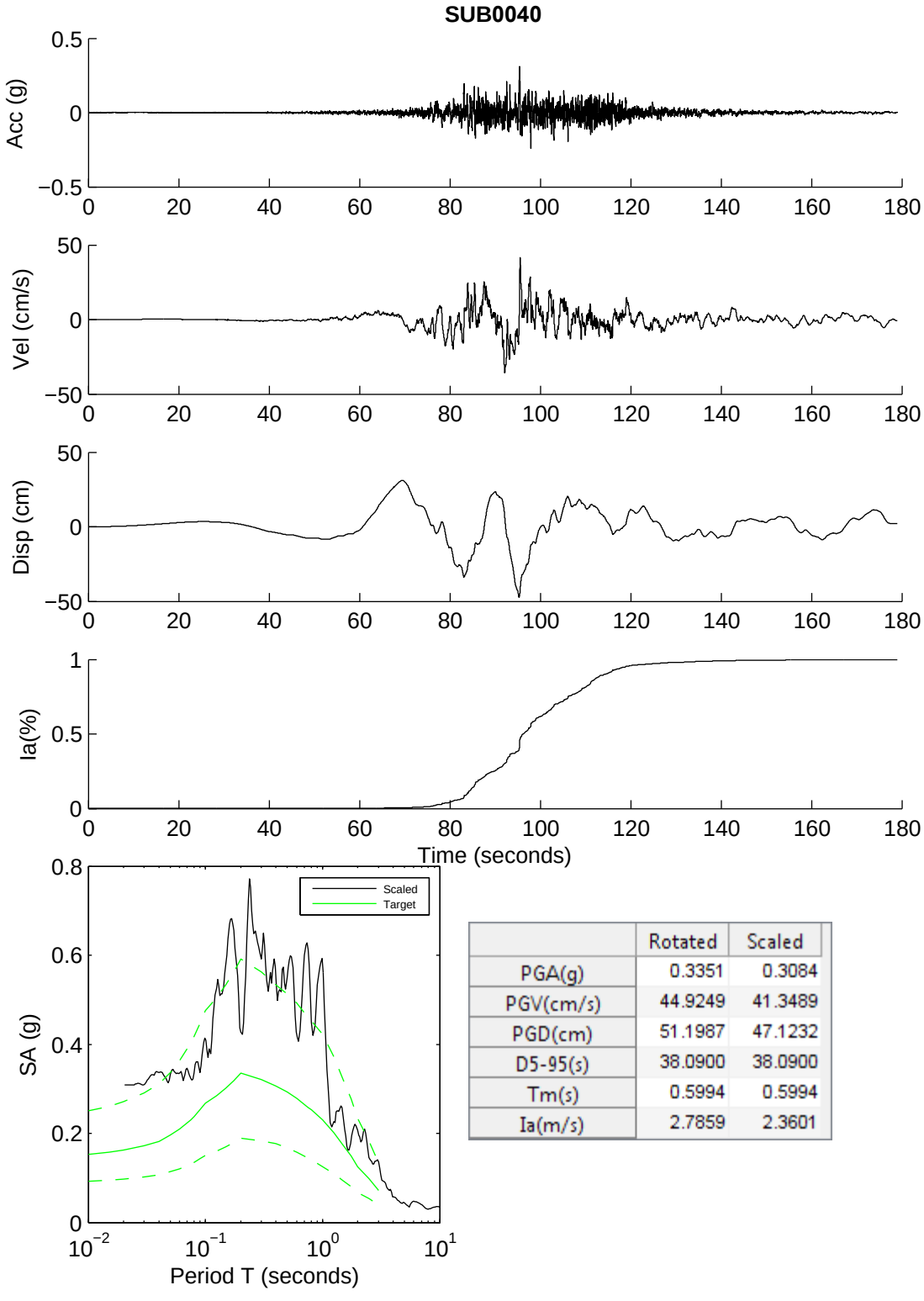

	Rotated	Scaled
PGA(g)	0.3351	0.3084
PGV(cm/s)	44.9249	41.3489
PGD(cm)	51.1987	47.1232
D5-95(s)	38.0900	38.0900
Tm(s)	0.5994	0.5994
Ia(m/s)	2.7859	2.3601

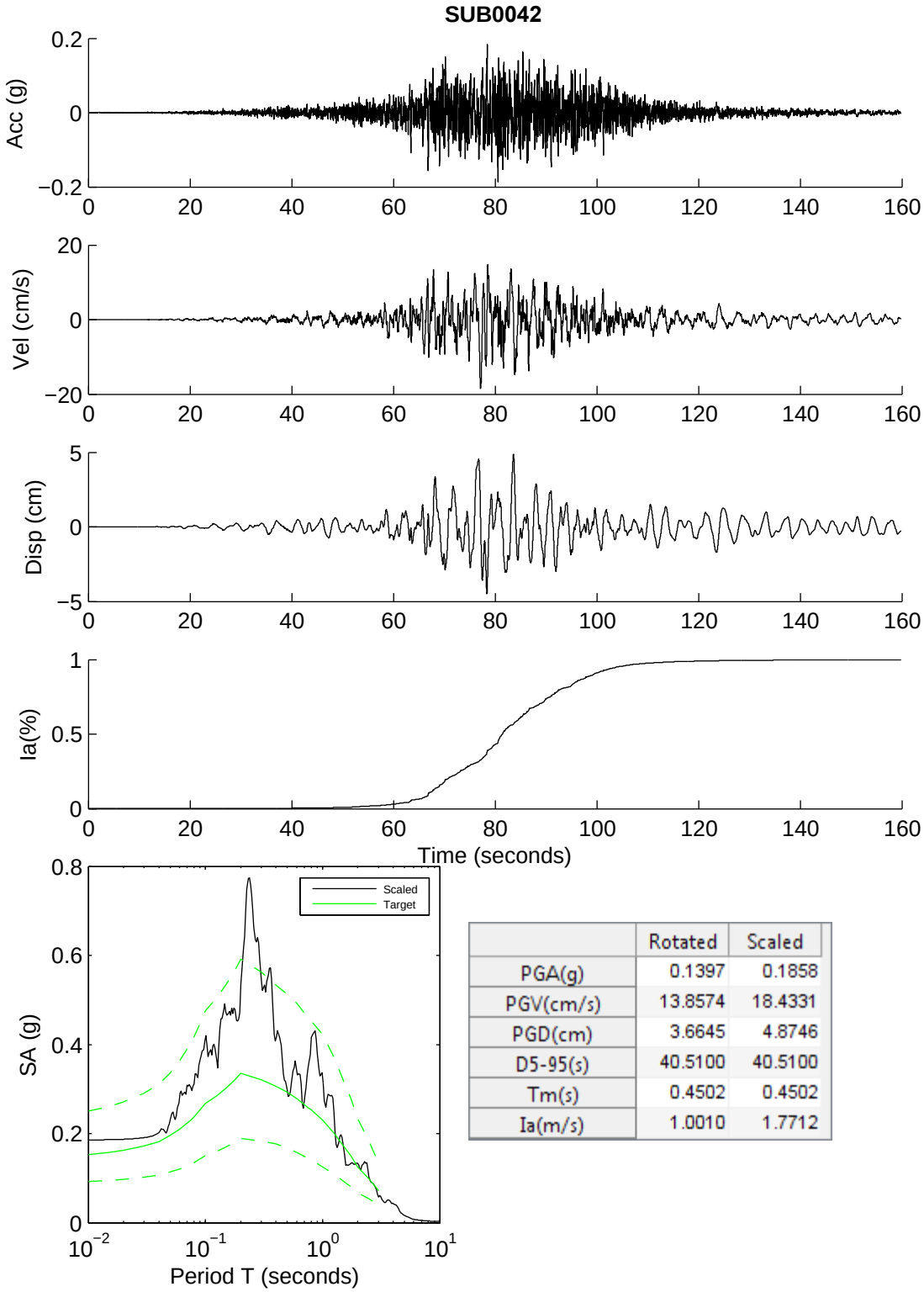

	Rotated	Scaled
PGA(g)	0.1397	0.1858
PGV(cm/s)	13.8574	18.4331
PGD(cm)	3.6645	4.8746
D5-95(s)	40.5100	40.5100
Tm(s)	0.4502	0.4502
Ia(m/s)	1.0010	1.7712

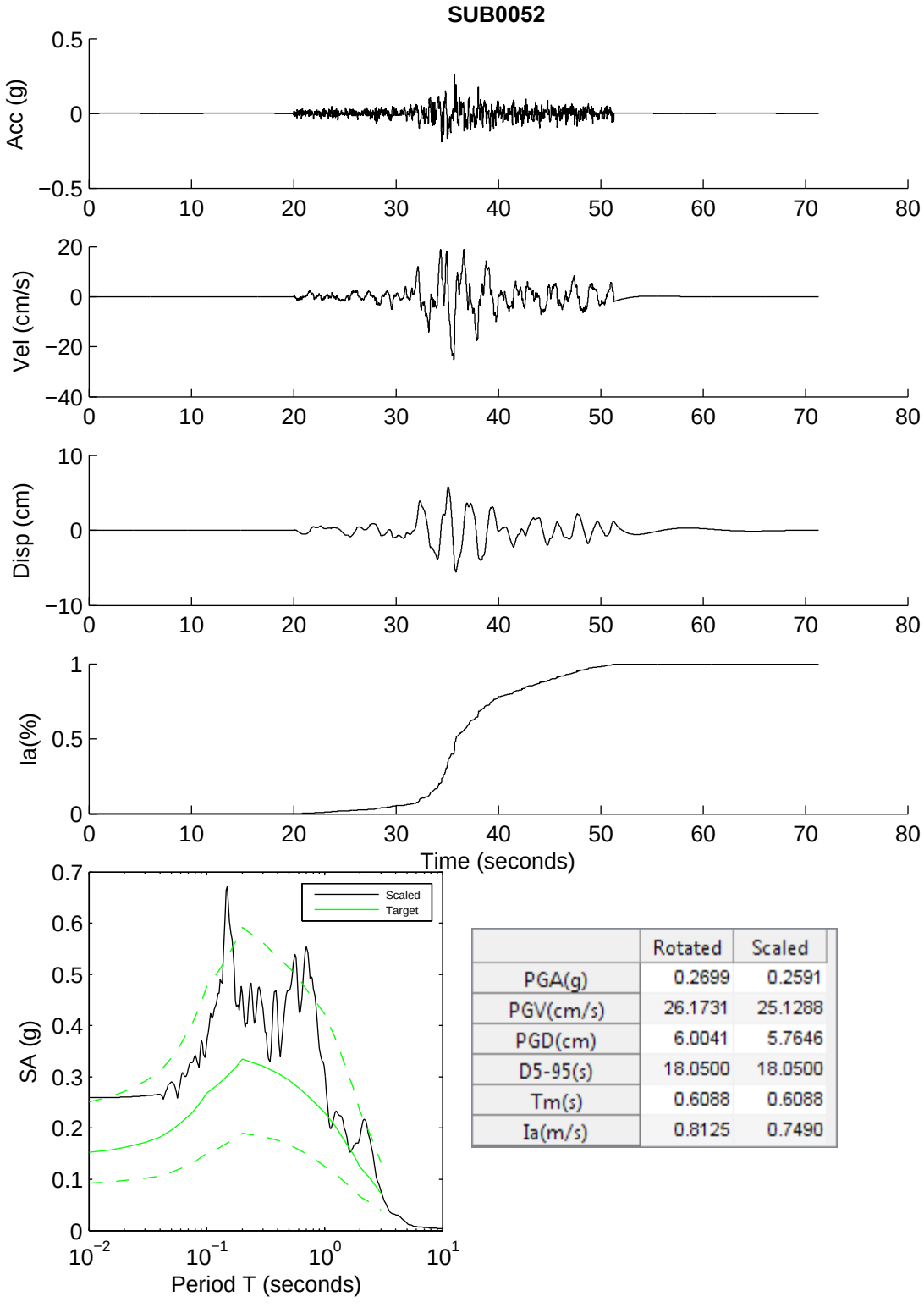

	Rotated	Scaled
PGA(g)	0.2699	0.2591
PGV(cm/s)	26.1731	25.1288
PGD(cm)	6.0041	5.7646
D5-95(s)	18.0500	18.0500
Tm(s)	0.6088	0.6088
Ia(m/s)	0.8125	0.7490

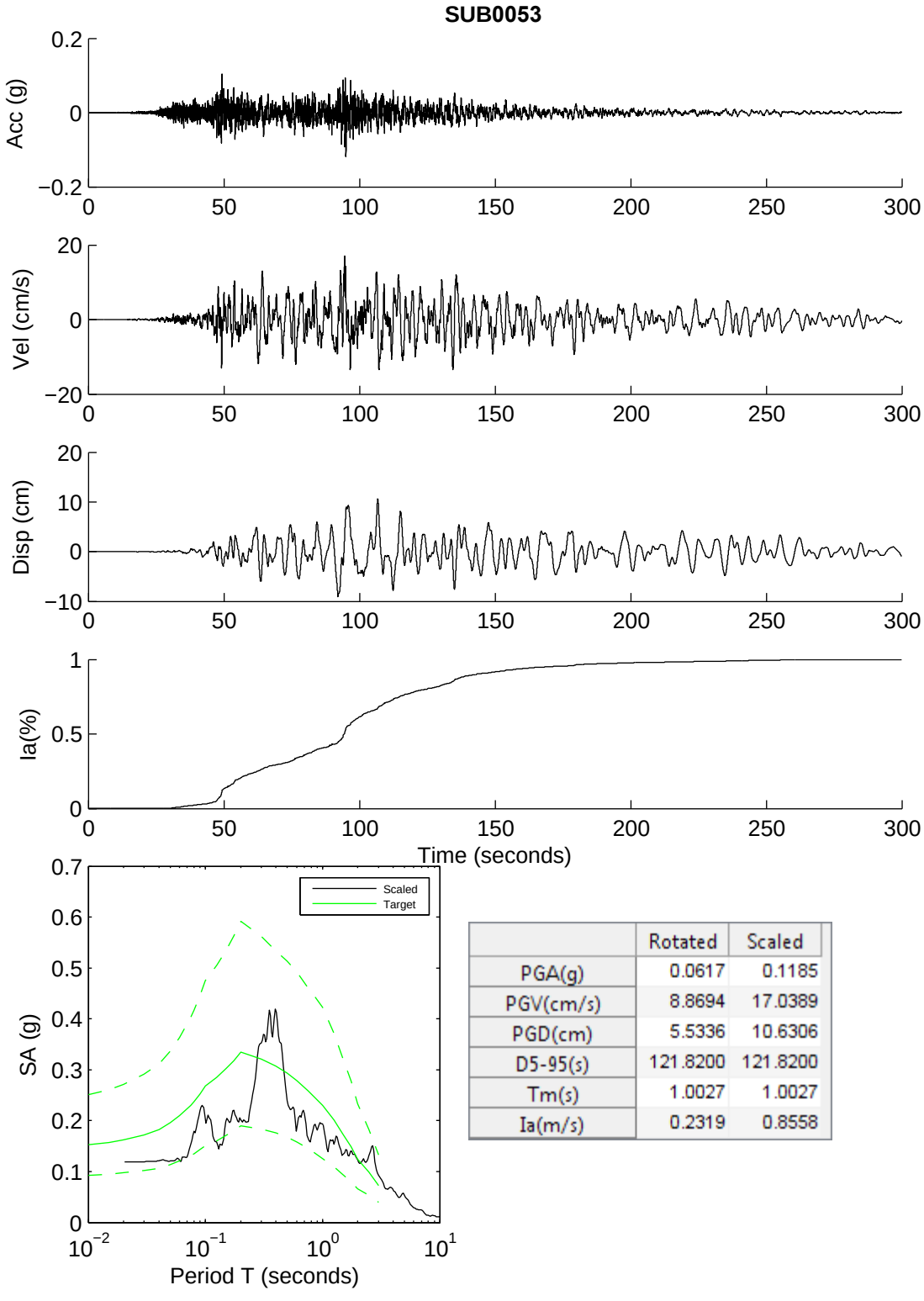

	Rotated	Scaled
PGA(g)	0.0617	0.1185
PGV(cm/s)	8.8694	17.0389
PGD(cm)	5.5336	10.6306
D5-95(s)	121.8200	121.8200
Tm(s)	1.0027	1.0027
Ia(m/s)	0.2319	0.8558

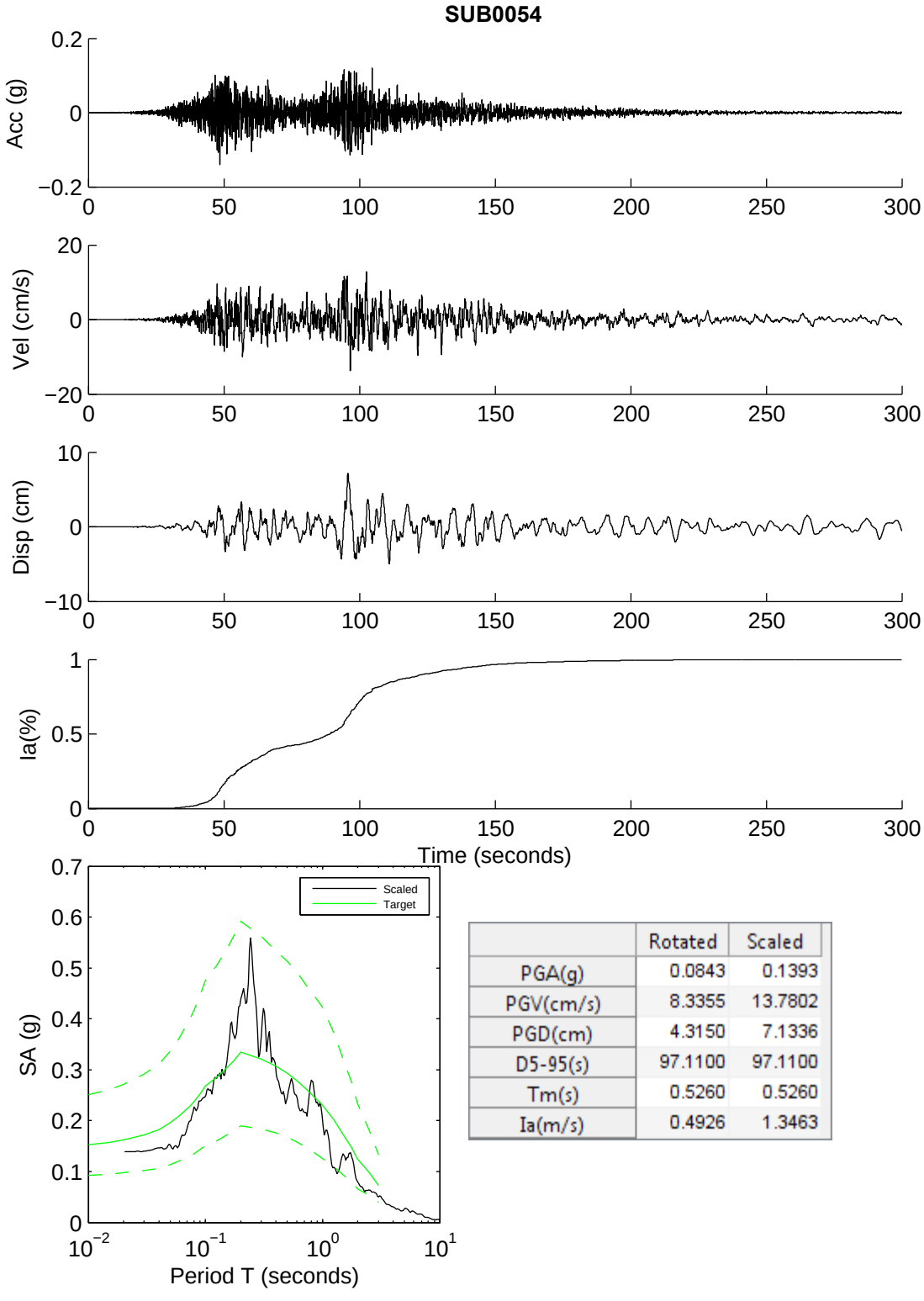

	Rotated	Scaled
PGA(g)	0.0843	0.1393
PGV(cm/s)	8.3355	13.7802
PGD(cm)	4.3150	7.1336
D5-95(s)	97.1100	97.1100
Tm(s)	0.5260	0.5260
Ia(m/s)	0.4926	1.3463

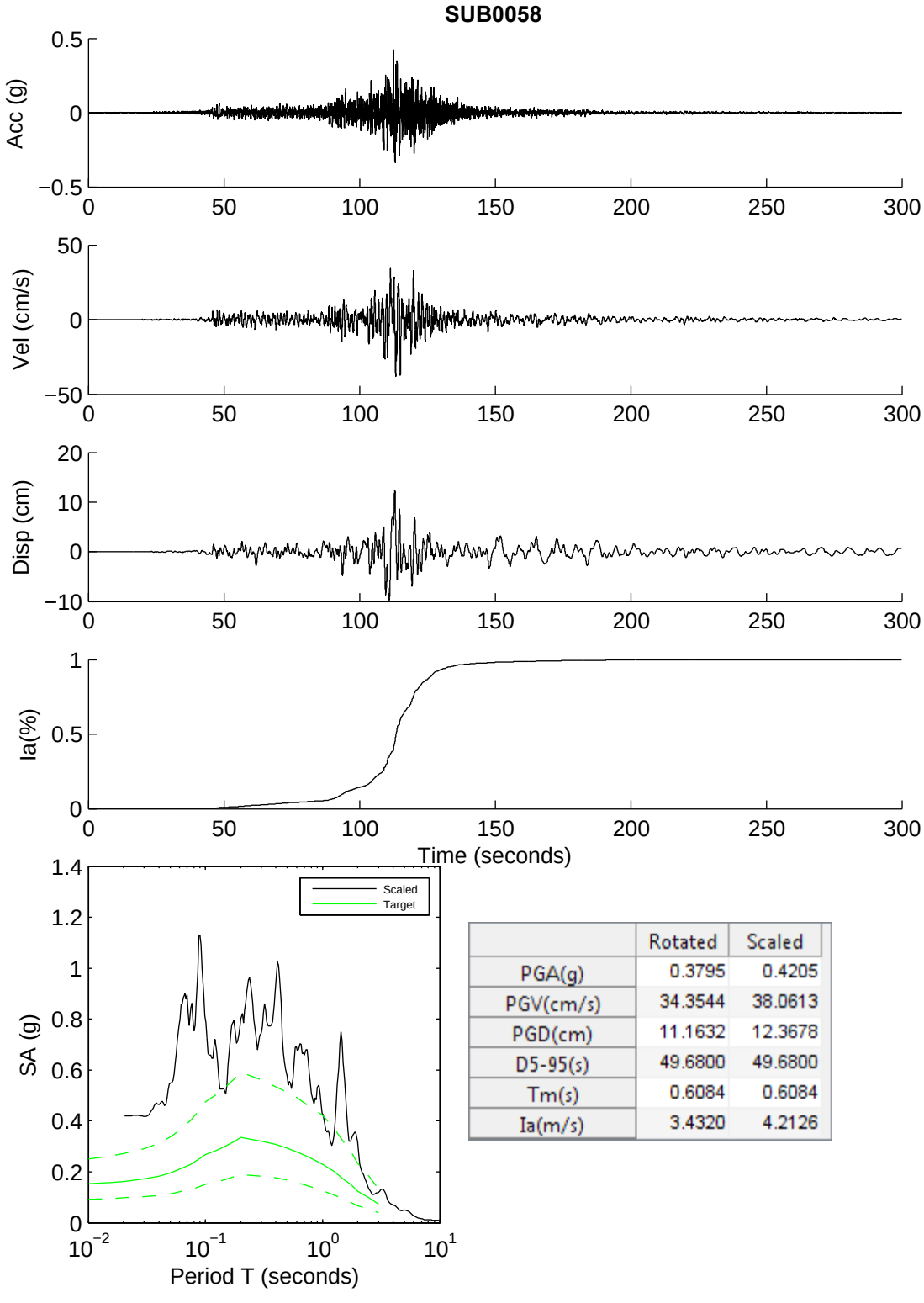

	Rotated	Scaled
PGA(g)	0.3795	0.4205
PGV(cm/s)	34.3544	38.0613
PGD(cm)	11.1632	12.3678
D5-95(s)	49.6800	49.6800
Tm(s)	0.6084	0.6084
Ia(m/s)	3.4320	4.2126

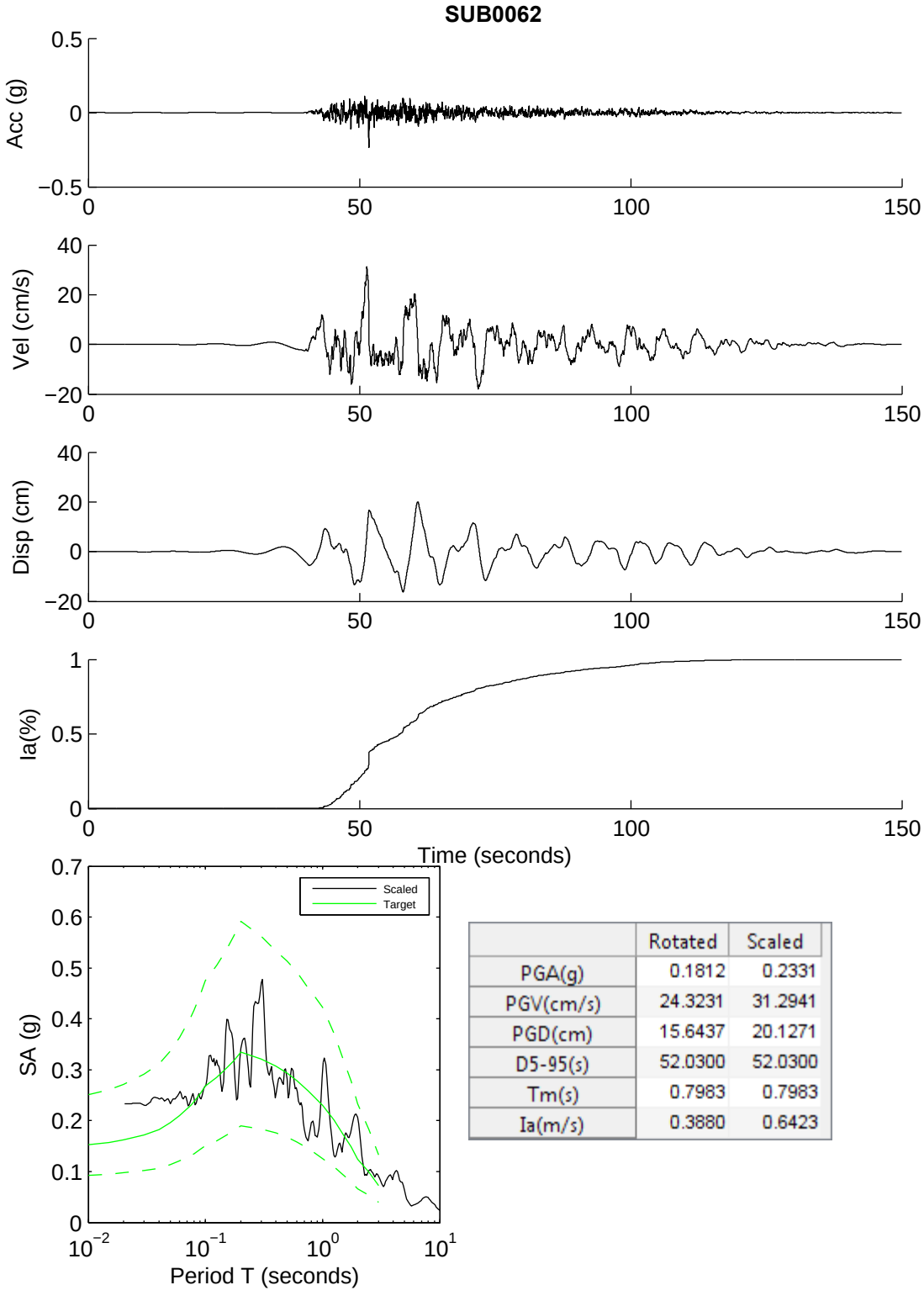

	Rotated	Scaled
PGA(g)	0.1812	0.2331
PGV(cm/s)	24.3231	31.2941
PGD(cm)	15.6437	20.1271
D5-95(s)	52.0300	52.0300
Tm(s)	0.7983	0.7983
Ia(m/s)	0.3880	0.6423

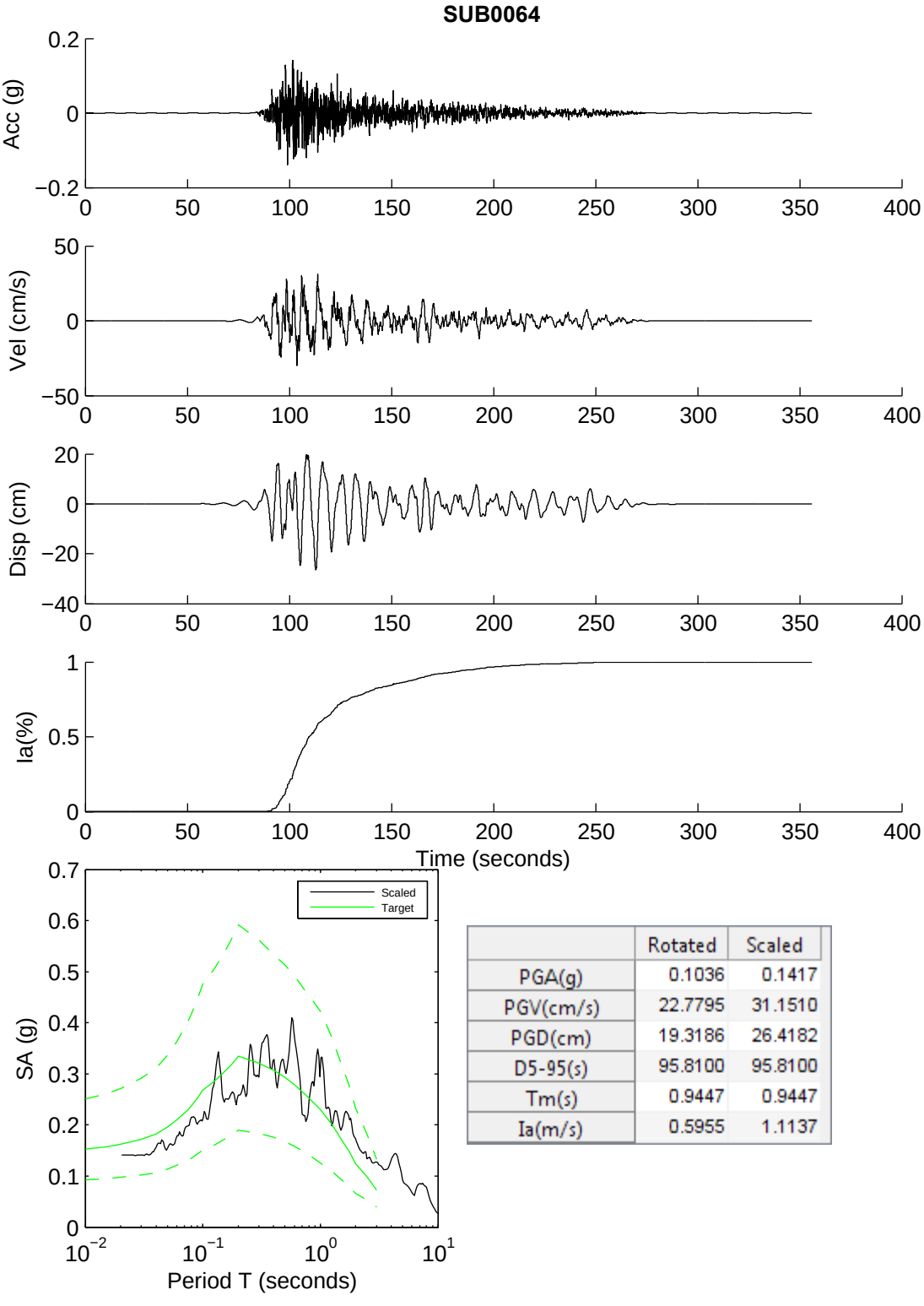

	Rotated	Scaled
PGA(g)	0.1036	0.1417
PGV(cm/s)	22.7795	31.1510
PGD(cm)	19.3186	26.4182
D5-95(s)	95.8100	95.8100
Tm(s)	0.9447	0.9447
Ia(m/s)	0.5955	1.1137

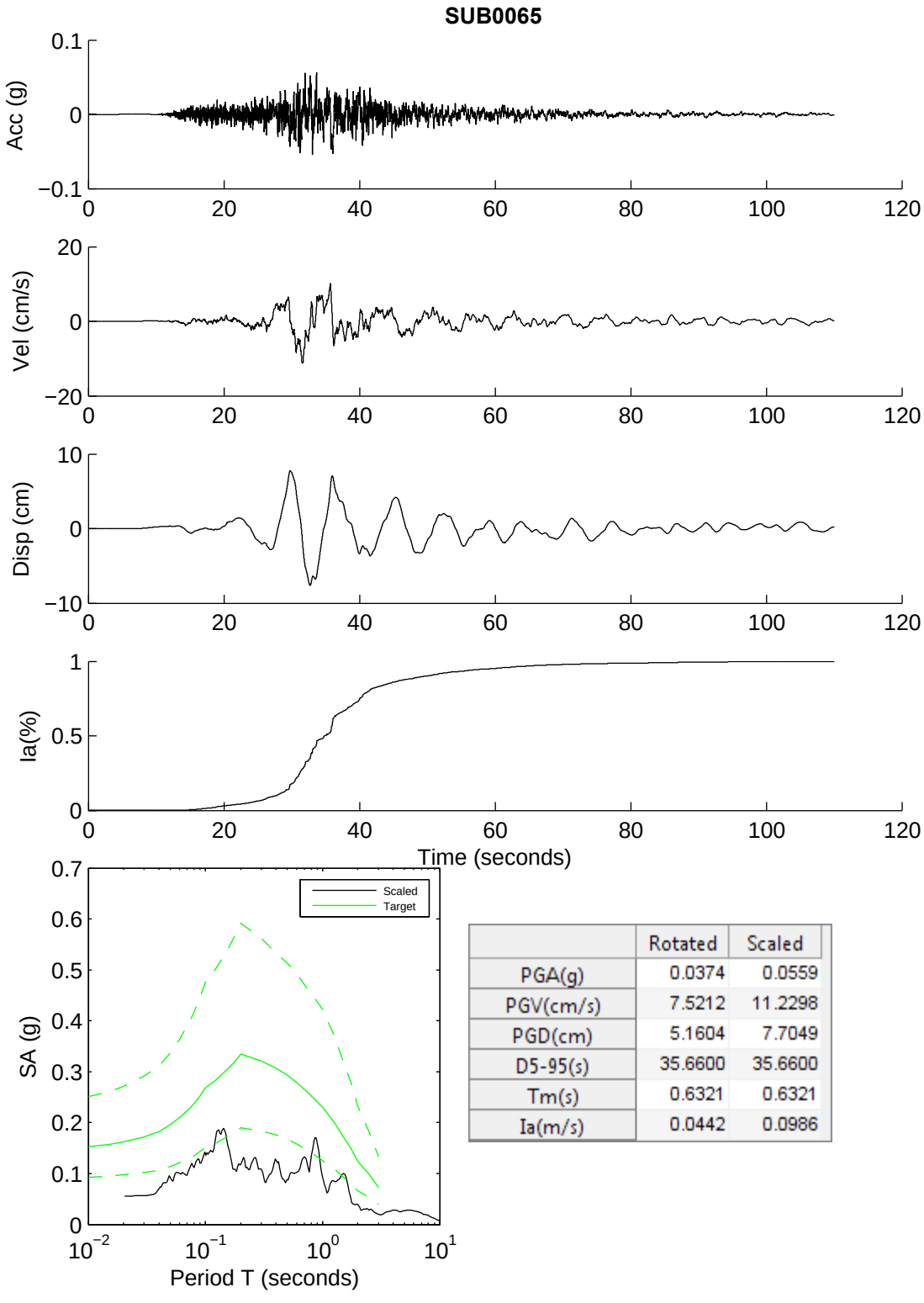

	Rotated	Scaled
PGA(g)	0.0374	0.0559
PGV(cm/s)	7.5212	11.2298
PGD(cm)	5.1604	7.7049
D5-95(s)	35.6600	35.6600
Tm(s)	0.6321	0.6321
Ia(m/s)	0.0442	0.0986

APPENDIX 3F: SCENARIO SCR GROUND MOTION DATA

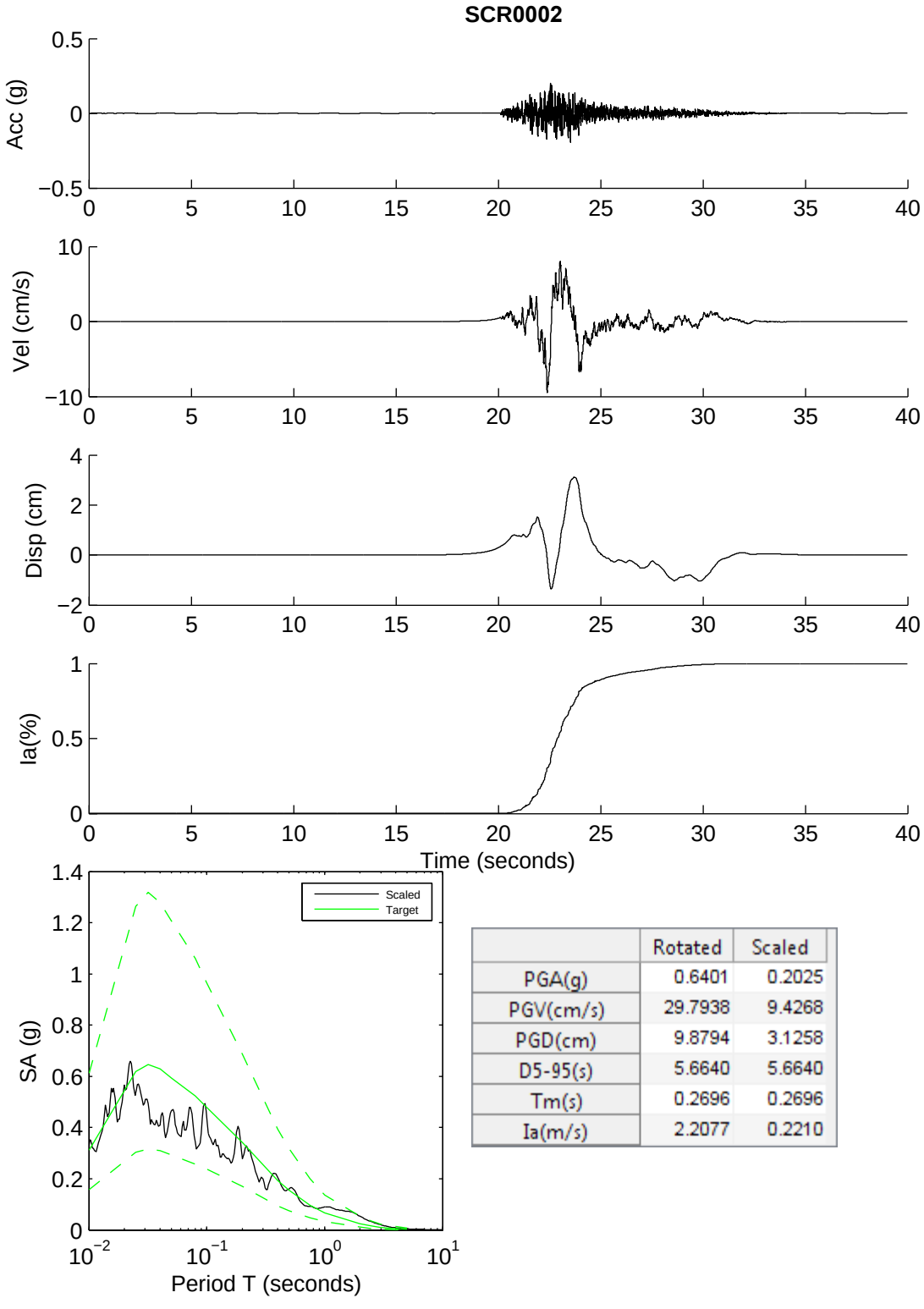

	Rotated	Scaled
PGA(g)	0.6401	0.2025
PGV(cm/s)	29.7938	9.4268
PGD(cm)	9.8794	3.1258
D5-95(s)	5.6640	5.6640
Tm(s)	0.2696	0.2696
Ia(m/s)	2.2077	0.2210

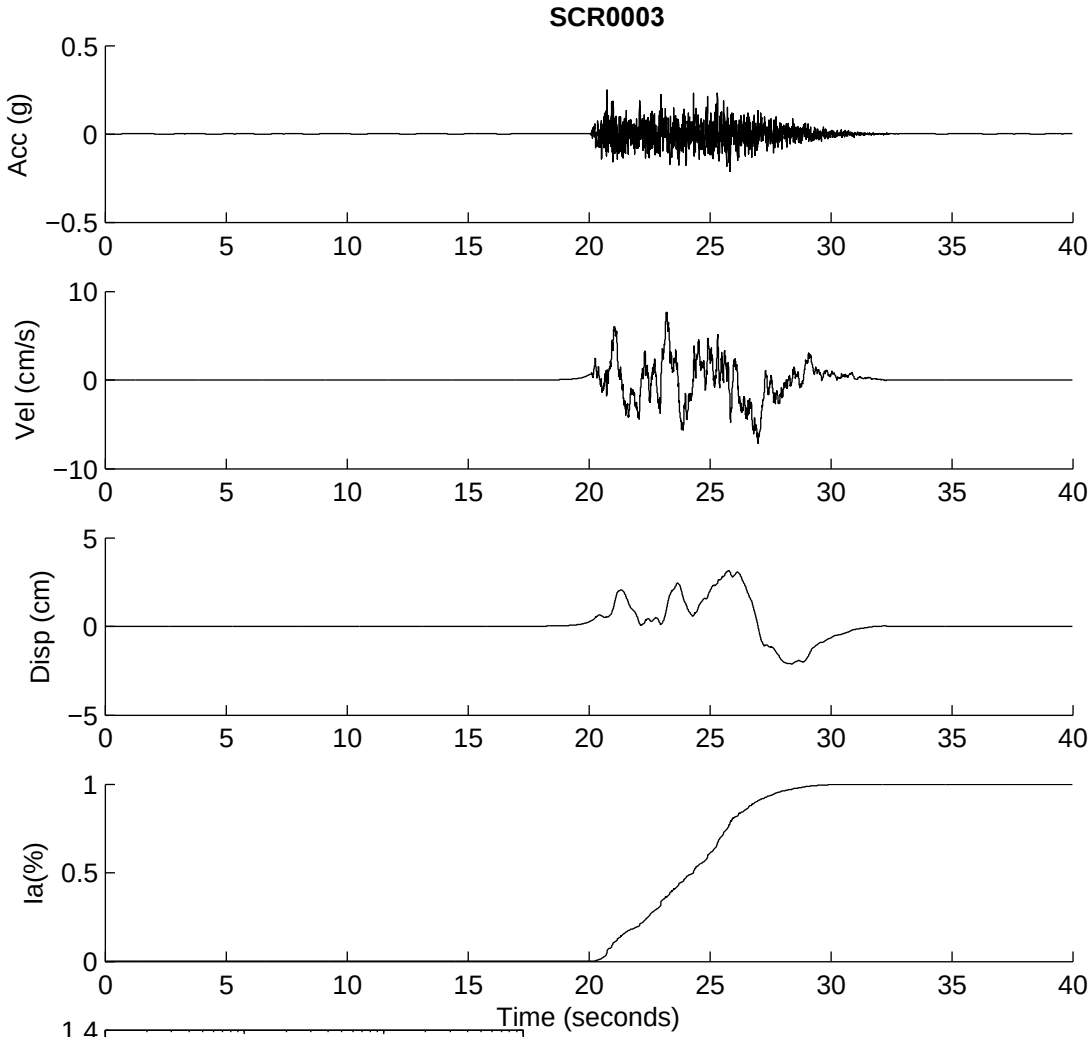

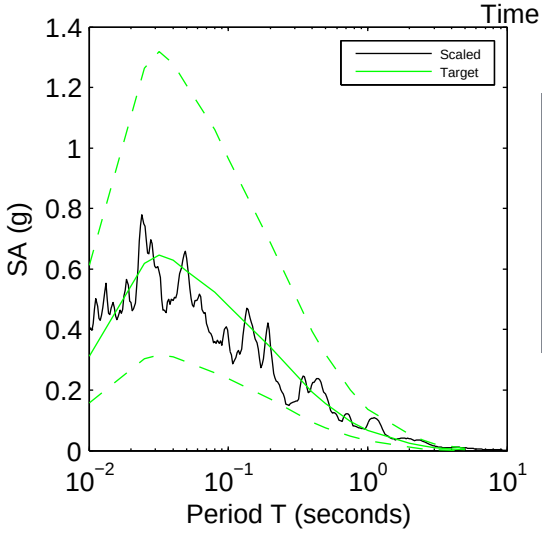

	Rotated	Scaled
PGA(g)	0.7660	0.2487
PGV(cm/s)	23.5294	7.6376
PGD(cm)	9.7358	3.1603
D5-95(s)	6.9840	6.9840
Tm(s)	0.2204	0.2204
Ia(m/s)	3.9919	0.4206

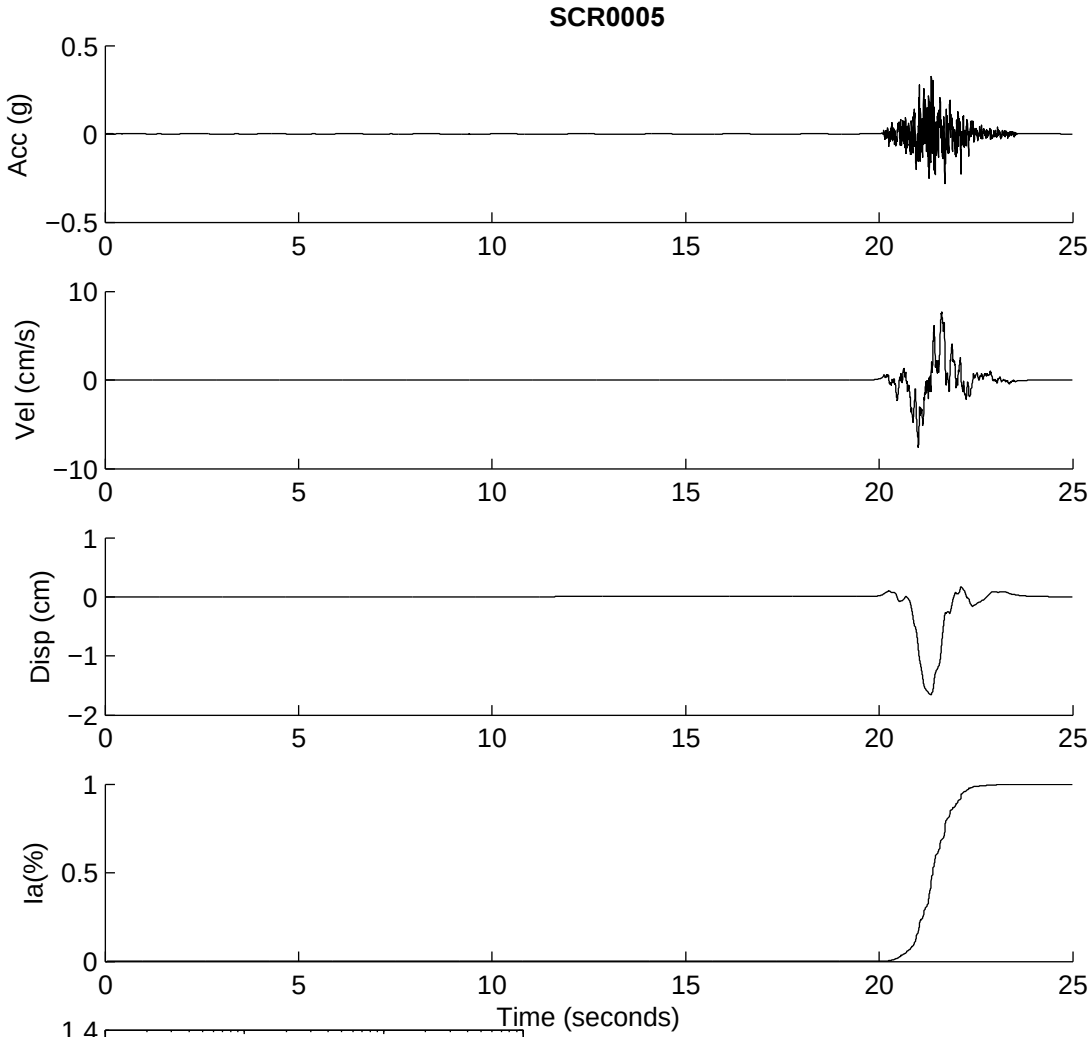

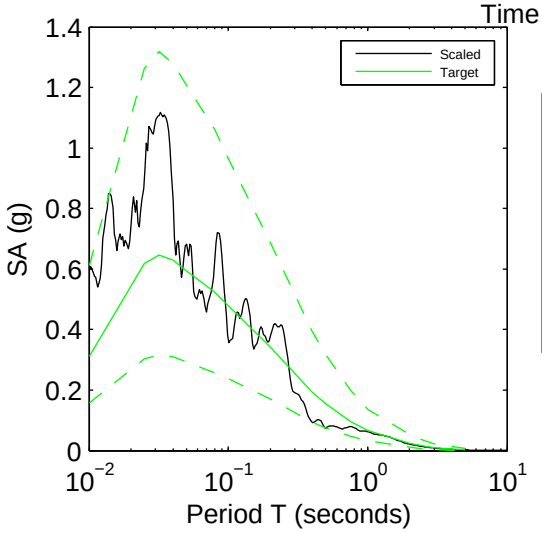

	Rotated	Scaled
PGA(g)	0.4983	0.3290
PGV(cm/s)	11.6198	7.6714
PGD(cm)	2.5095	1.6568
D5-95(s)	1.4740	1.4740
Tm(s)	0.1807	0.1807
Ia(m/s)	0.5192	0.2263

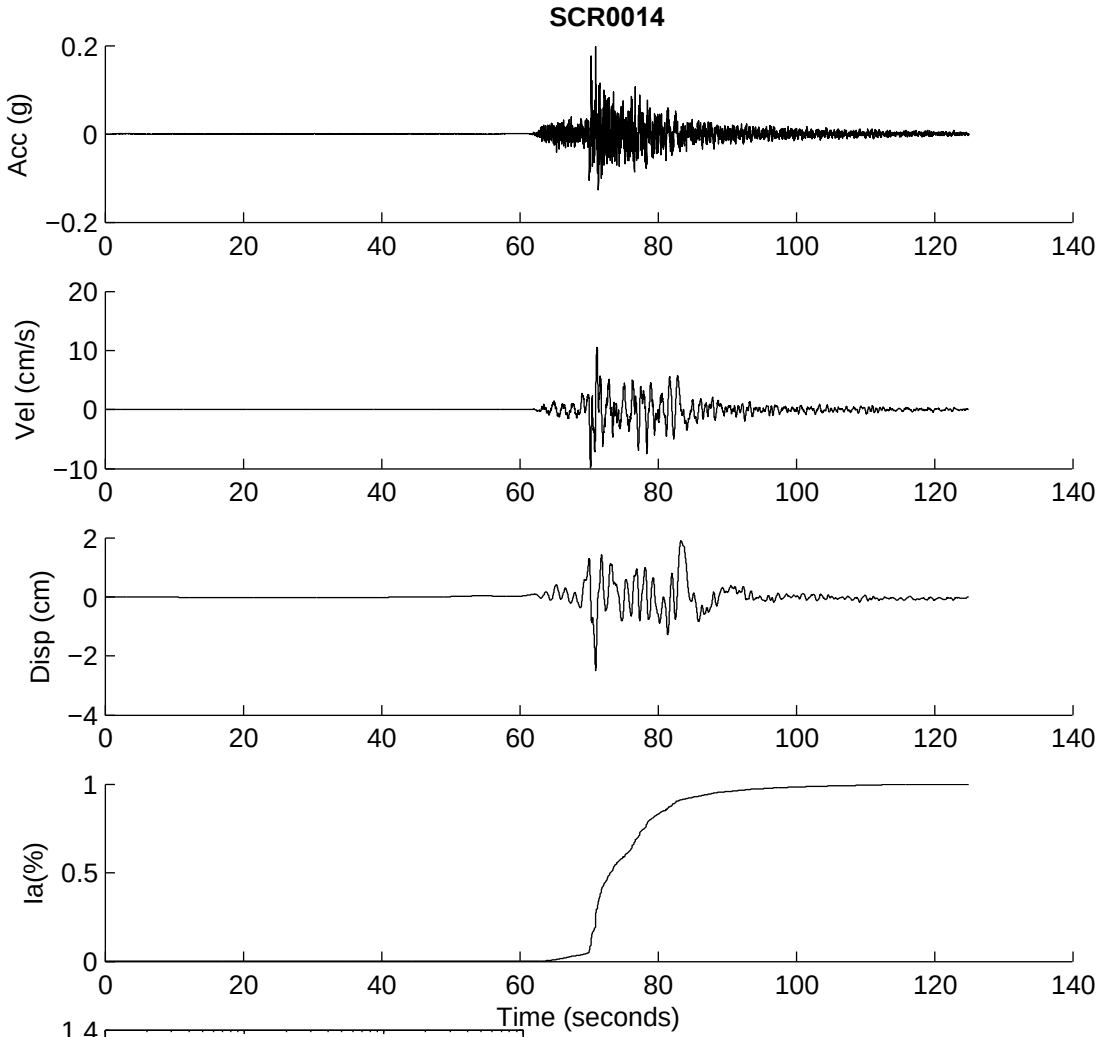

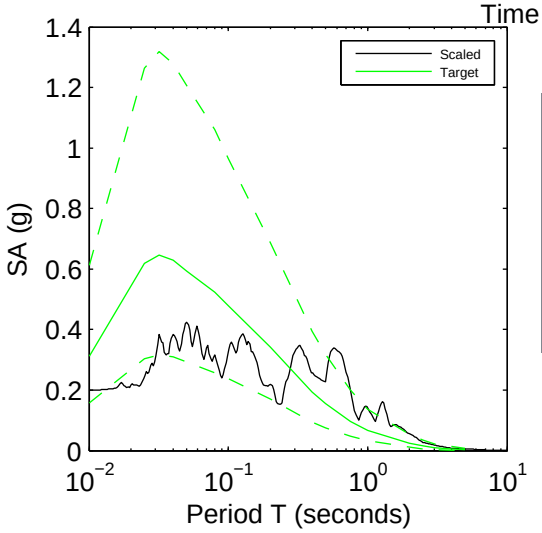

	Rotated	Scaled
PGA(g)	0.1332	0.1980
PGV(cm/s)	7.0630	10.4956
PGD(cm)	1.6771	2.4922
D5-95(s)	18.1200	18.1200
Tm(s)	0.4719	0.4719
Ia(m/s)	0.1327	0.2931

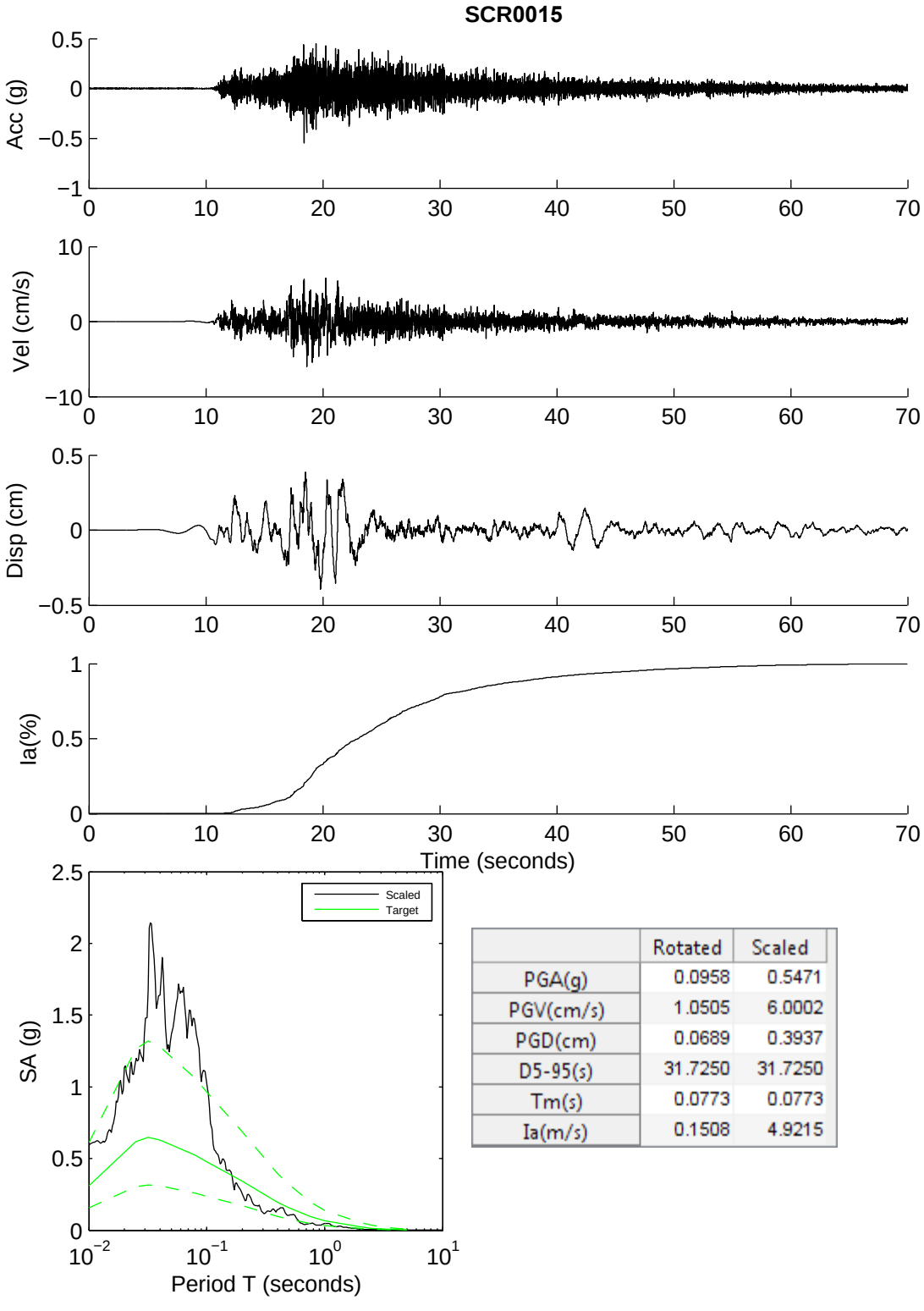

	Rotated	Scaled
PGA(g)	0.0958	0.5471
PGV(cm/s)	1.0505	6.0002
PGD(cm)	0.0689	0.3937
D5-95(s)	31.7250	31.7250
Tm(s)	0.0773	0.0773
Ia(m/s)	0.1508	4.9215

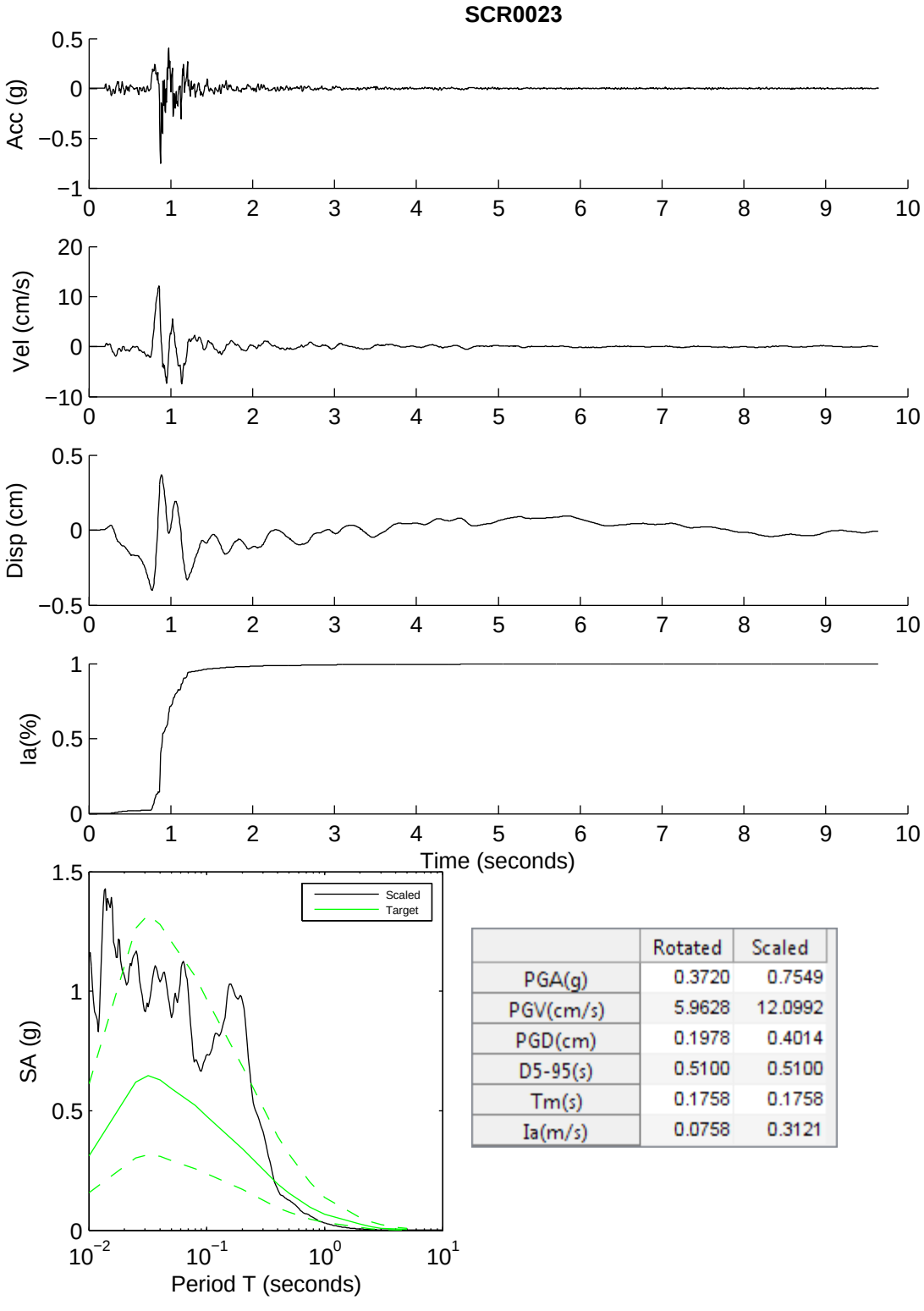

	Rotated	Scaled
PGA(g)	0.3720	0.7549
PGV(cm/s)	5.9628	12.0992
PGD(cm)	0.1978	0.4014
D5-95(s)	0.5100	0.5100
Tm(s)	0.1758	0.1758
Ia(m/s)	0.0758	0.3121

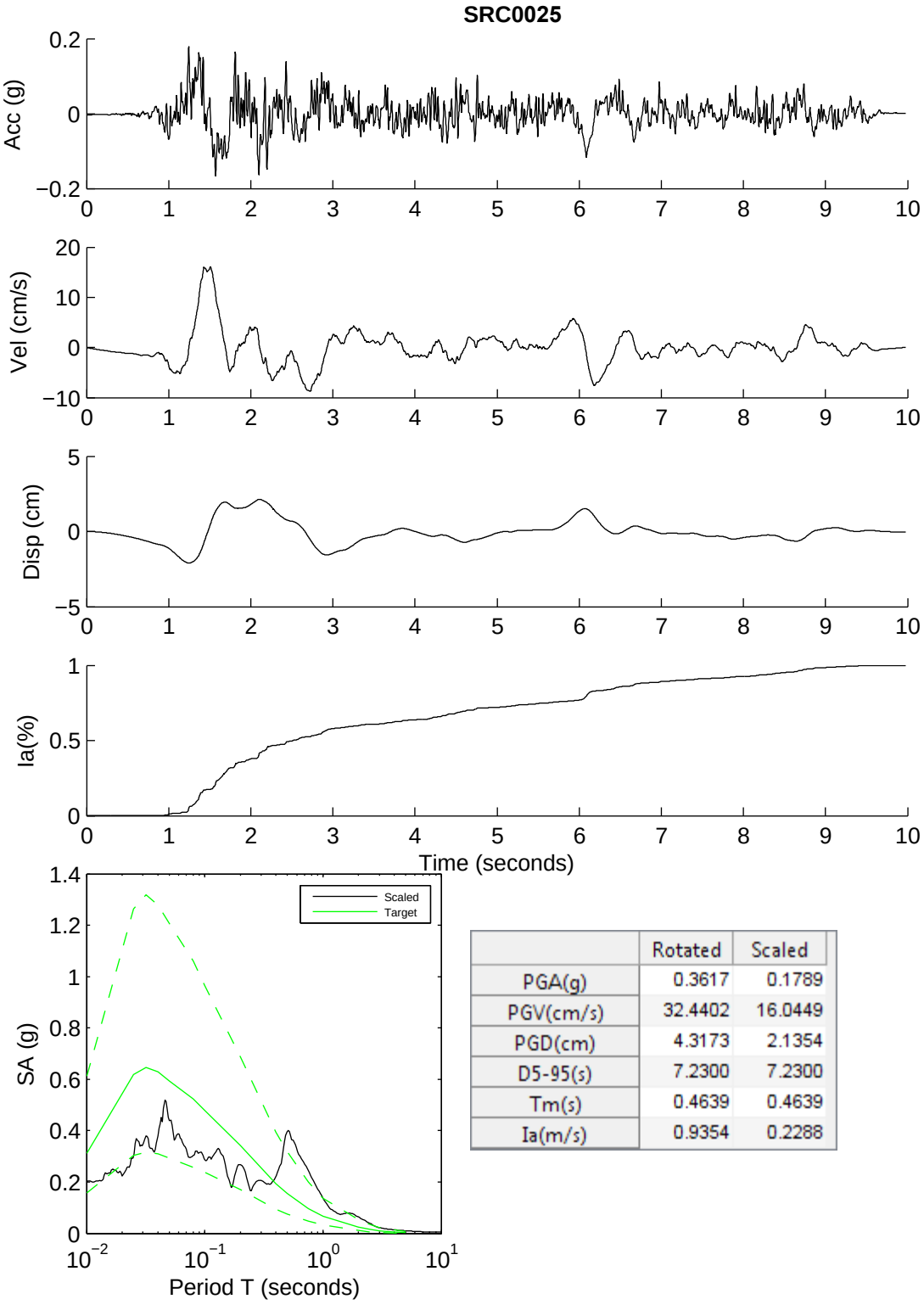

	Rotated	Scaled
PGA(g)	0.3617	0.1789
PGV(cm/s)	32.4402	16.0449
PGD(cm)	4.3173	2.1354
D5-95(s)	7.2300	7.2300
Tm(s)	0.4639	0.4639
Ia(m/s)	0.9354	0.2288

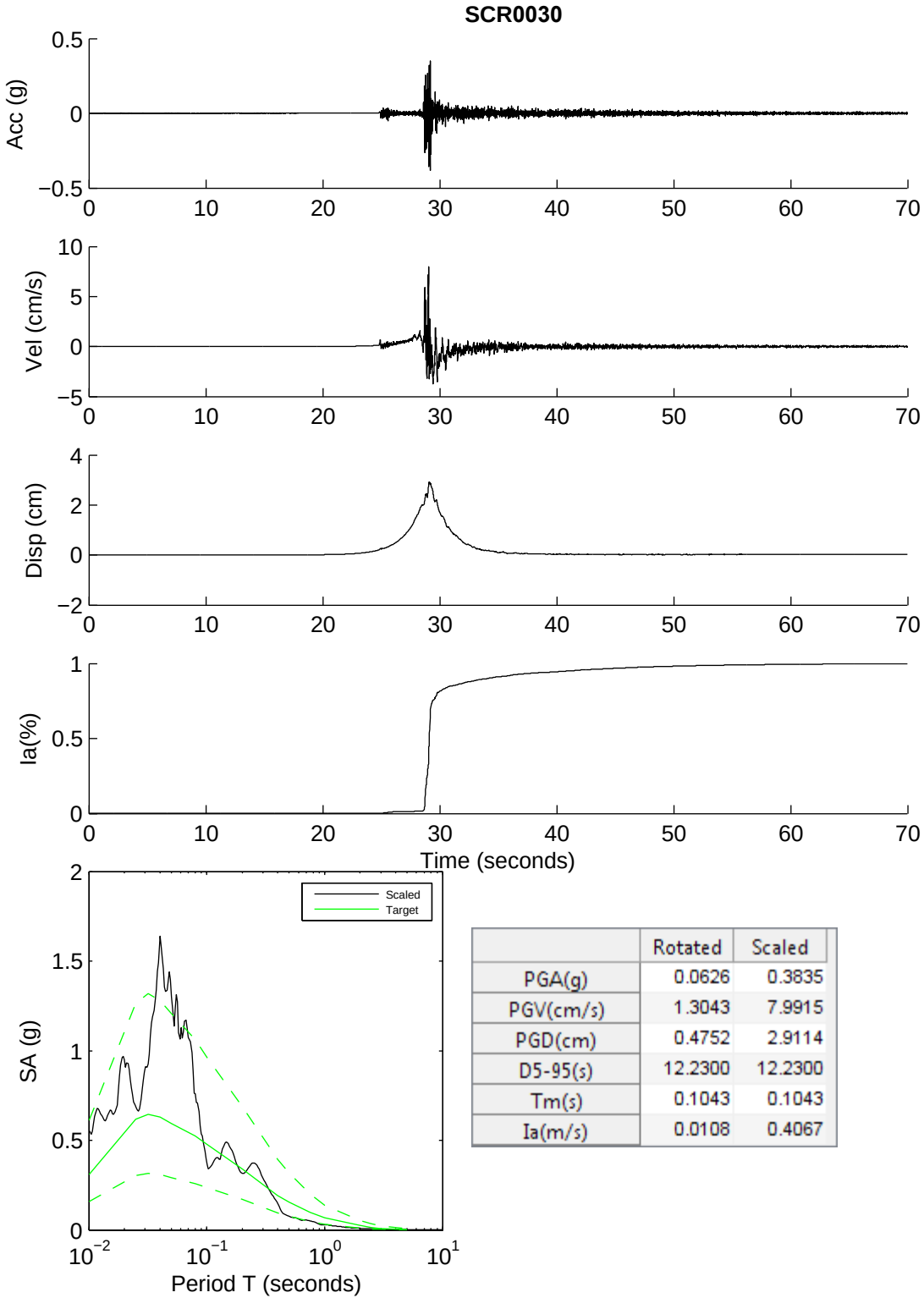

	Rotated	Scaled
PGA(g)	0.0626	0.3835
PGV(cm/s)	1.3043	7.9915
PGD(cm)	0.4752	2.9114
D5-95(s)	12.2300	12.2300
Tm(s)	0.1043	0.1043
Ia(m/s)	0.0108	0.4067

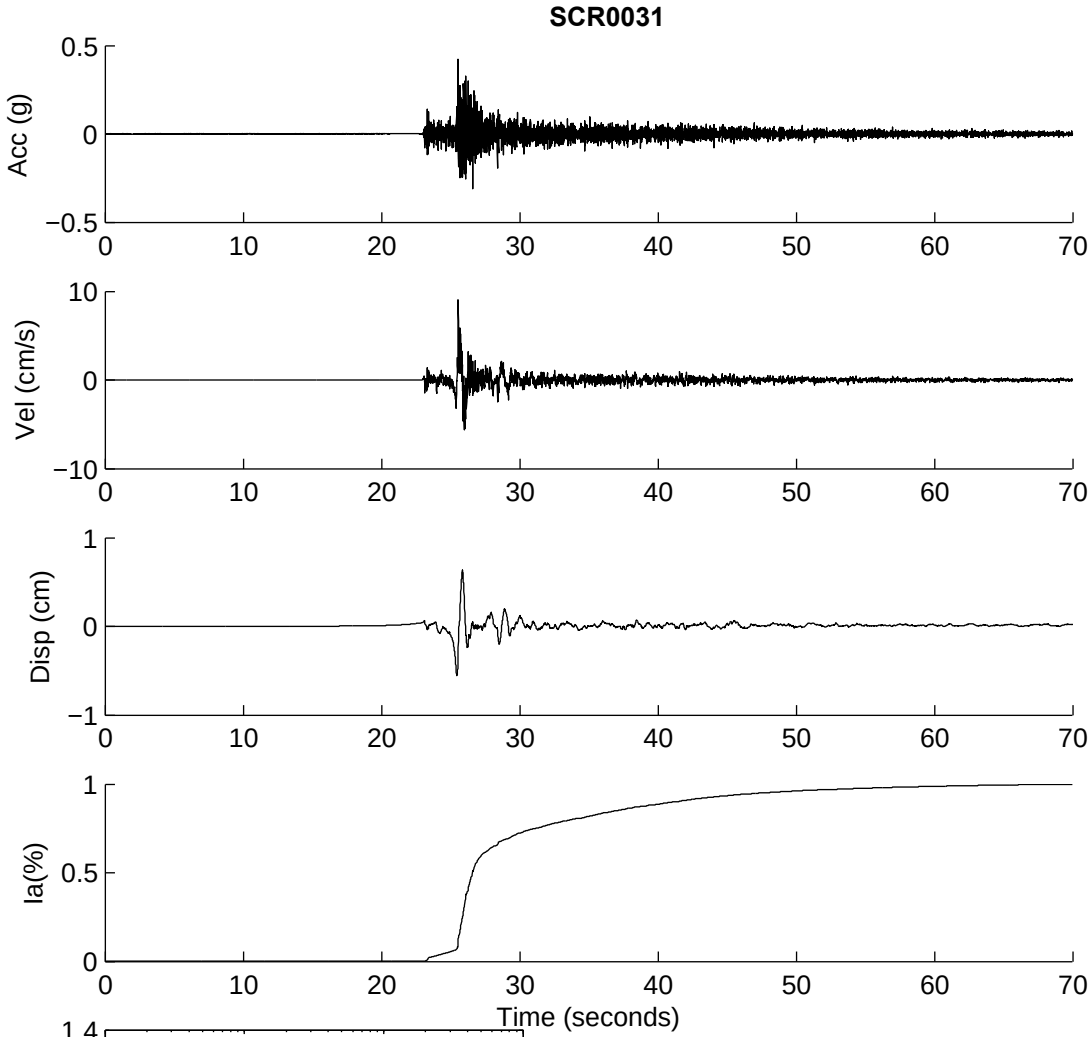

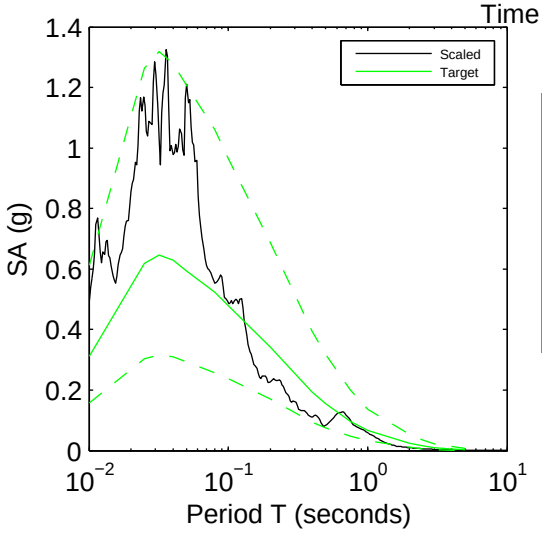

	Rotated	Scaled
PGA(g)	0.0301	0.4206
PGV(cm/s)	0.6482	9.0424
PGD(cm)	0.0455	0.6353
D5-95(s)	22.5200	22.5200
Tm(s)	0.0992	0.0992
Ia(m/s)	0.0048	0.9282

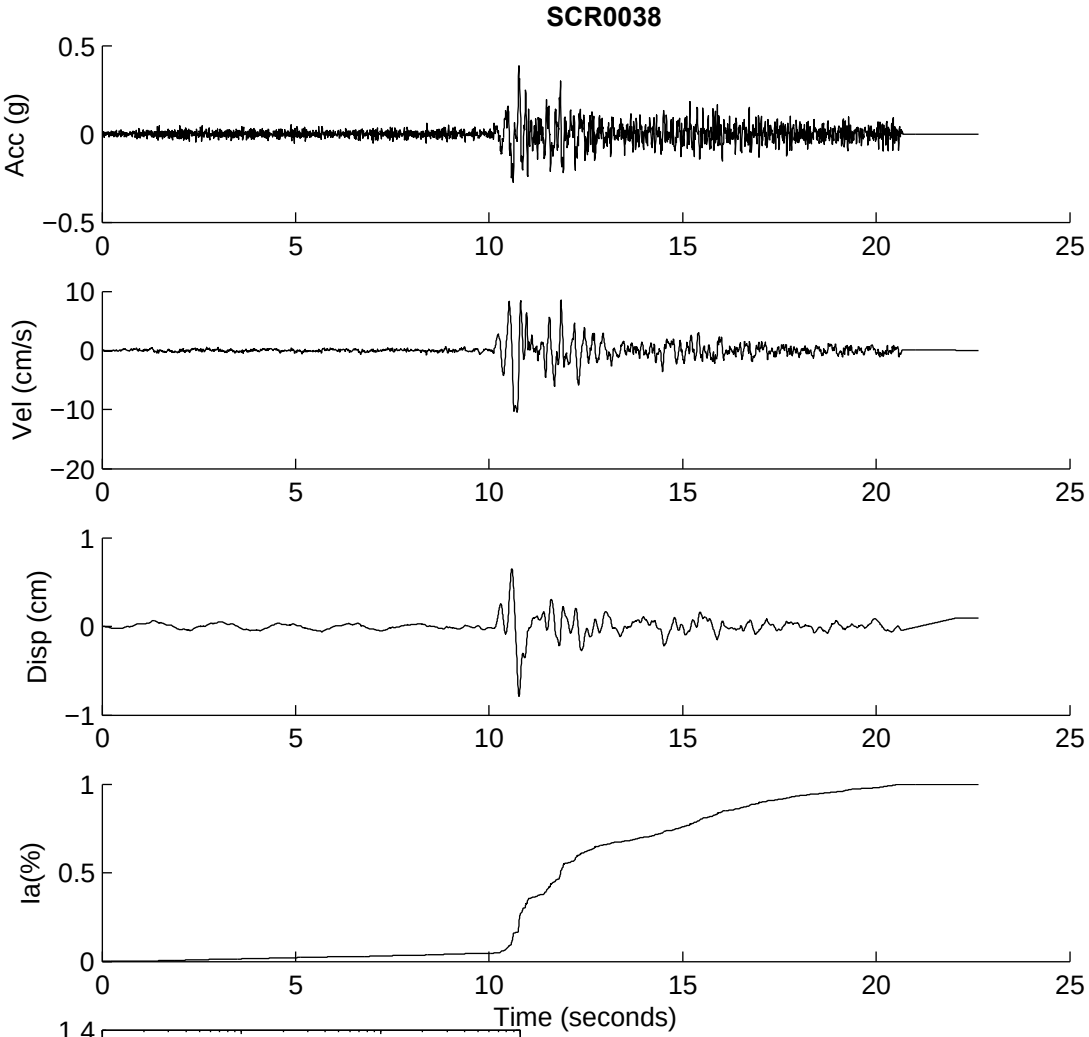

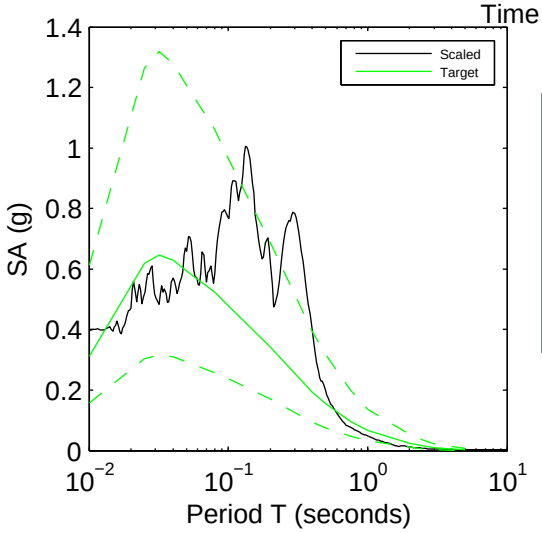

	Rotated	Scaled
PGA(g)	0.1345	0.3867
PGV(cm/s)	3.6037	10.3631
PGD(cm)	0.2743	0.7889
D5-95(s)	8.3650	8.3650
Tm(s)	0.1807	0.1807
Ia(m/s)	0.0910	0.7522

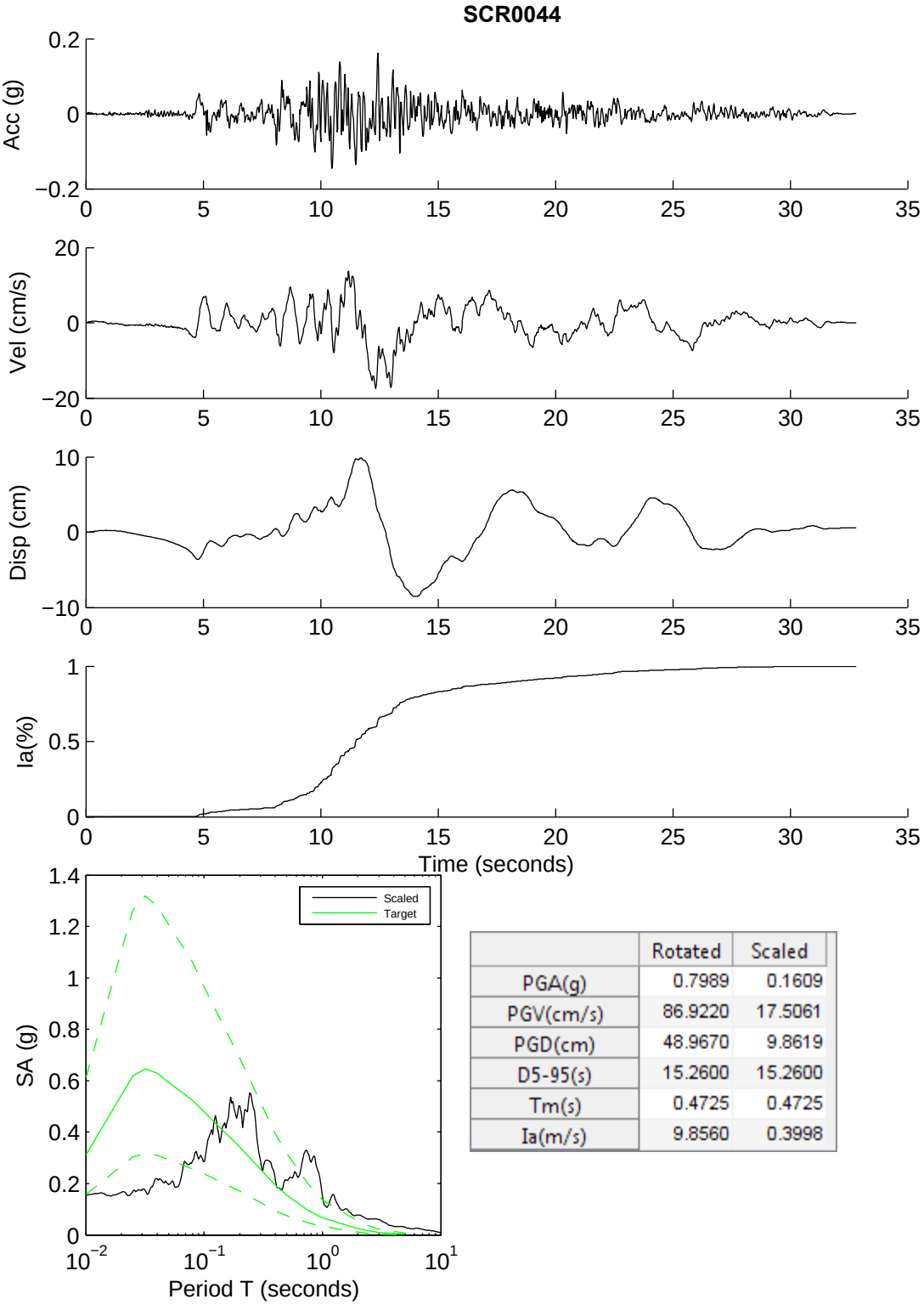

	Rotated	Scaled
PGA(g)	0.7989	0.1609
PGV(cm/s)	86.9220	17.5061
PGD(cm)	48.9670	9.8619
D5-95(s)	15.2600	15.2600
Tm(s)	0.4725	0.4725
Ia(m/s)	9.8560	0.3998

APPENDIX 6A: SELECTED SITE PROPERTIES

Appendix 6A: Selected site properties

The following tables contain the USCS designation, thickness in meters, unit weight (γ) in kN/m^3, shear wave velocity (Vs) in m/s, overconsolidation ratio (OCR), the plasticity index (PI), the adjusted plasticity index to account for age effects (PI ADJ), the geologic age, the dynamic shear strength (τ) in atmospheres, and the small strain shear modulus (G_{max}) in atmospheres for each soil layer by depth. The depth is the depth to the bottom of the soil layer. The two geologic ages are Holocene (H) and Pleistocene (P).

Table 6A.1: Site properties for site Bay Area

Depth (m)	USCS	Thick (m)	γ (kN/m^3)	Vs (m/s)	OCR	PI ADJ	PI	Age	τ_{ff} (atm)	G_{max} (atm)
2	SM-SC	2	18.80	250	1	0	0	H	0.2500	1183.6
2.75	CH	0.75	15.00	82	4	40	40	H	0.1642	101.6
3.5	CH	0.75	15.05	82	3	40	40	H	0.1560	101.9
4.25	CH	0.75	15.10	82	2.5	40	40	H	0.1572	102.3
5	CH	0.75	15.15	82	2	40	40	H	0.1504	102.6
5.75	CH	0.75	15.20	82	1.5	40	40	H	0.1346	103.0
6.5	CH	0.75	15.25	82	1.3	40	40	H	0.1337	103.3
7.25	CH	0.75	15.30	82	1.25	40	40	H	0.1429	103.6
8	CH	0.75	15.35	82	1.2	40	40	H	0.1513	104.0
9.13	CH	1.13	15.30	120	1.15	40	40	H	0.1620	221.9
10.3	CH	1.17	15.35	120	1.15	40	40	H	0.1813	222.7
11.47	CH	1.17	15.40	120	1.15	40	40	H	0.2011	223.4
12.64	CH	1.17	15.45	120	1.15	40	40	H	0.2211	224.1
13.81	CH	1.17	15.50	120	1.15	40	40	H	0.2412	224.8
14.98	CH	1.17	15.55	120	1.15	40	40	H	0.2616	225.6
16.15	CH	1.17	15.60	120	1.15	40	40	H	0.2821	226.3
17.32	CH	1.17	15.65	120	1.15	40	40	H	0.3028	227.0
18.49	CH	1.17	15.70	120	1.15	40	40	H	0.3236	227.7
19.66	CH	1.17	15.75	120	1.15	40	40	H	0.3447	228.5
20.83	CH	1.17	15.80	120	1.15	40	40	H	0.3659	229.2
22	CH	1.17	15.85	120	1.15	40	40	H	0.3873	229.9
23.82	CL	1.82	18	195	2	60	20	P	0.6551	690.6
25.68	CL	1.86	18	195	2	60	20	P	0.7267	690.6
27.54	CL	1.86	18	195	2	60	20	P	0.7990	690.6
29.4	CL	1.86	18	195	2	60	20	P	0.8714	690.6
31.26	CL	1.86	18	195	2	60	20	P	0.9437	690.6
33.12	CL	1.86	18	195	2	60	20	P	1.0161	690.6
34.98	CL	1.86	18	195	2	60	20	P	1.0884	690.6
36.84	CL	1.86	18	195	2	60	20	P	1.1608	690.6
38.7	CL	1.86	18	195	2	60	20	P	1.2332	690.6
40.56	CL	1.86	18	195	2	60	20	P	1.3055	690.6
42.42	CL	1.86	18	195	2	60	20	P	1.3779	690.6
44.28	CL	1.86	18	195	2	60	20	P	1.4502	690.6
46.14	CL	1.86	18	195	2	60	20	P	1.5226	690.6
48	CL	1.86	18	195	2	60	20	P	1.5949	690.6
51.25	CL	3.25	18	330	2	60	20	P	1.6943	1978.0
54.5	CL	3.25	18	330	2	60	20	P	1.8208	1978.0
57.75	CL	3.25	18	330	2	60	20	P	1.9472	1978.0
61	CL	3.25	18	330	2	60	20	P	2.0737	1978.0
64.25	CL	3.25	18	330	2	60	20	P	2.2001	1978.0
67.5	SM-SC	3.25	18	330	1	30	0	P	4.4851	1978.0

70.75	SM-SC	3.25	18	330	1	30	0	P	4.7289	1978.0
74	SM-SC	3.25	18	330	1	30	0	P	4.9726	1978.0
77.25	SM-SC	3.25	18	330	1	30	0	P	5.2164	1978.0
80.5	SM-SC	3.25	18	330	1	30	0	P	5.4602	1978.0
83.75	SM-SC	3.25	18	330	1	30	0	P	5.7040	1978.0
87	CL	3.25	20.3	330	2	60	20	P	3.1028	2226.8
90.25	CL	3.25	20.3	330	2	60	20	P	3.2640	2226.8
93.5	CL	3.25	20.3	330	2	60	20	P	3.4253	2226.8
96.75	CL	3.25	20.3	330	2	60	20	P	3.5866	2226.8
100	CL	3.25	20.3	330	2	60	20	P	3.7479	2226.8
104.375	CL	4.375	20.3	440	2	60	20	P	3.9371	3958.8
108.75	CL	4.375	20.3	440	2	60	20	P	4.1543	3958.8
113.125	CL	4.375	20.3	440	2	60	20	P	4.3714	3958.8
117.5	CL	4.375	20.3	440	2	60	20	P	4.5885	3958.8
121.875	CL	4.375	20.3	440	2	60	20	P	4.8057	3958.8
126.25	CL	4.375	20.3	440	2	60	20	P	5.0228	3958.8
130.625	CL	4.375	20.3	440	2	60	20	P	5.2399	3958.8
135	CL	4.375	20.3	440	2	60	20	P	5.4570	3958.8
139.3	CL	4.3	20.3	477	2	60	20	P	5.6723	4652.6
143.6	CL	4.3	20.3	477	2	60	20	P	5.8857	4652.6
147.9	CL	4.3	20.3	477	2	60	20	P	6.0991	4652.6
152.2	CL	4.3	20.3	477	2	60	20	P	6.3125	4652.6
156.5	CL	4.3	20.3	477	2	60	20	P	6.5259	4652.6
160.8	CL	4.3	20.3	477	2	60	20	P	6.7393	4652.6
165.1	CL	4.3	20.3	477	2	60	20	P	6.9527	4652.6
170	GW	4.9	21	580	1	30	0	P	16.5163	7116.1
175	GW	5	21	580	1	30	0	P	17.1183	7116.1
180	GW	5	21	580	1	30	0	P	17.7264	7116.1
185	SM-SC	5	21	580	1	30	0	P	18.3345	7116.1

Table 6A.2: Site properties for site Bay Area F

Depth (m)	USCS	Thick (m)	γ (kN/m^3)	Vs (m/s)	OCR	PI ADJ	PI	Age	τ_{ff} (atm)	G_{max} (atm)
2	SM-SC	2	18.80	250	1	0	0	H	0.2500	1183.6
2.75	CH	0.75	15.00	82	4	40	40	H	0.1642	101.6
3.5	CH	0.75	15.05	82	3	40	40	H	0.1560	101.9
4.25	CH	0.75	15.10	82	2.5	40	40	H	0.1572	102.3
5	CH	0.75	15.15	82	2	40	40	H	0.1504	102.6
5.75	CH	0.75	15.20	82	1.5	40	40	H	0.1346	103.0
6.5	CH	0.75	15.25	82	1.3	40	40	H	0.1337	103.3
7.25	CH	0.75	15.30	82	1.25	40	40	H	0.1429	103.6
8	CH	0.75	15.35	82	1.2	40	40	H	0.1513	104.0
9.13	CH	1.13	15.30	120	1.15	40	40	H	0.1620	221.9
10.3	CH	1.17	15.35	120	1.15	40	40	H	0.1813	222.7
11.47	CH	1.17	15.40	120	1.15	40	40	H	0.2011	223.4
12.64	CH	1.17	15.45	120	1.15	40	40	H	0.2211	224.1
13.81	CH	1.17	15.50	120	1.15	40	40	H	0.2412	224.8
14.98	CH	1.17	15.55	120	1.15	40	40	H	0.2616	225.6
16.15	CH	1.17	15.60	120	1.15	40	40	H	0.2821	226.3
17.32	CH	1.17	15.65	120	1.15	40	40	H	0.3028	227.0
18.49	CH	1.17	15.70	120	1.15	40	40	H	0.3236	227.7
19.66	CH	1.17	15.75	120	1.15	40	40	H	0.3447	228.5
20.83	CH	1.17	15.80	120	1.15	40	40	H	0.3659	229.2
22	CH	1.17	15.85	120	1.15	40	40	H	0.3873	229.9
23.5	CH	1.5	15.90	150	1.1	40	40	H	0.3975	360.4
25	CH	1.5	15.95	150	1.1	40	40	H	0.4244	361.5
26.5	CH	1.5	16.00	150	1.1	40	40	H	0.4516	362.6
28	CH	1.5	16.05	150	1.1	40	40	H	0.4789	363.8
29.5	CH	1.5	16.10	150	1.1	40	40	H	0.5065	364.9
31	CH	1.5	16.15	150	1.1	40	40	H	0.5343	366.0
32.5	CH	1.5	16.20	150	1.1	40	40	H	0.5623	367.2
34	CH	1.5	16.25	150	1.1	40	40	H	0.5906	368.3
35.5	CH	1.5	16.30	150	1.1	40	40	H	0.6190	369.4
37	CH	1.5	16.35	150	1.1	40	40	H	0.6477	370.6
38.6	CH	1.6	16.40	160	1.1	40	40	H	0.6776	422.9
40.48	CL	1.88	18.03	195	2	60	20	P	1.1546	690.6
42.36	CL	1.88	18.03	195	2	60	20	P	1.2278	690.6
44.24	CL	1.88	18.03	195	2	60	20	P	1.3009	690.6
46.12	CL	1.88	18.03	195	2	60	20	P	1.3740	690.6
48.01	CL	1.89	18.03	195	2	60	20	P	1.4473	690.6
49.9	CL	1.89	18.03	195	2	60	20	P	1.5209	690.6
51.79	CL	1.89	18.03	195	2	60	20	P	1.5944	690.6
55.04	CL	3.25	18.03	330	2	60	20	P	1.6944	1978.0
58.29	CL	3.25	18.03	330	2	60	20	P	1.8208	1978.0

61.54	CL	3.25	18.03	330	2	60	20	P	1.9473	1978.0
64.79	CL	3.25	18.03	330	2	60	20	P	2.0737	1978.0
68.04	CL	3.25	18.03	330	2	60	20	P	2.2002	1978.0
71.29	SM-SC	3.25	18.03	330	1	30	0	P	4.4852	1978.0
74.54	SM-SC	3.25	18.03	330	1	30	0	P	4.7289	1978.0
77.79	SM-SC	3.25	18.03	330	1	30	0	P	4.9727	1978.0
81.04	SM-SC	3.25	18.03	330	1	30	0	P	5.2165	1978.0
84.29	SM-SC	3.25	18.03	330	1	30	0	P	5.4603	1978.0
87.54	SM-SC	3.25	18.03	330	1	30	0	P	5.7040	1978.0
90.79	CL	3.25	20.30	330	2	60	20	P	3.1028	2226.8
94.04	CL	3.25	20.30	330	2	60	20	P	3.2641	2226.8
97.29	CL	3.25	20.30	330	2	60	20	P	3.4254	2226.8
100.54	CL	3.25	20.30	330	2	60	20	P	3.5867	2226.8
103.79	CL	3.25	20.30	330	2	60	20	P	3.7480	2226.8
108.165	CL	4.375	20.30	440	2	60	20	P	3.9372	3958.8
112.54	CL	4.375	20.30	440	2	60	20	P	4.1543	3958.8
116.915	CL	4.375	20.30	440	2	60	20	P	4.3714	3958.8
121.29	CL	4.375	20.30	440	2	60	20	P	4.5886	3958.8
125.665	CL	4.375	20.30	440	2	60	20	P	4.8057	3958.8
130.04	CL	4.375	20.30	440	2	60	20	P	5.0228	3958.8
134.415	CL	4.375	20.30	440	2	60	20	P	5.2399	3958.8
138.79	CL	4.375	20.30	440	2	60	20	P	5.4571	3958.8
143.09	CL	4.3	20.30	477	2	60	20	P	5.6723	4652.6
147.39	CL	4.3	20.30	477	2	60	20	P	5.8857	4652.6
151.69	CL	4.3	20.30	477	2	60	20	P	6.0992	4652.6
155.99	CL	4.3	20.30	477	2	60	20	P	6.3126	4652.6
160.29	CL	4.3	20.30	477	2	60	20	P	6.5260	4652.6
164.59	CL	4.3	20.30	477	2	60	20	P	6.7394	4652.6
168.89	CL	4.3	20.30	477	2	60	20	P	6.9528	4652.6
173.79	GW	4.9	21.00	580	1	30	0	P	16.5164	7116.1
178.79	GW	5	21.00	580	1	30	0	P	17.1184	7116.1
183.79	GW	5	21.00	580	1	30	0	P	17.7265	7116.1
188.79	SM-SC	5	21.00	580	1	30	0	P	18.3346	7116.1

Table 6A.3: Site properties for site Bay Area II and Bay Area II K

Depth (m)	USCS	Thick (m)	γ (kN/m^3)	Vs (m/s)	OCR	PI ADJ	PI	Age	τ_{ff} (atm)	G_{max} (atm)
1.00	SM-SC	1.00	18.00	200.0	1.00	0	0	H	0.2500	725.3
1.25	OH	0.25	10.56	25.0	1.20	200	200	H	0.0553	6.7
1.50	OH	0.25	10.56	25.0	1.20	200	200	H	0.0553	6.7
1.75	OH	0.25	10.56	25.0	1.20	200	200	H	0.0553	6.7
2.00	OH	0.25	10.56	25.0	1.20	200	200	H	0.0553	6.7
2.25	OH	0.25	10.61	27.8	1.10	175	175	H	0.0577	8.2
2.50	OH	0.25	10.61	27.8	1.10	175	175	H	0.0577	8.2
2.75	OH	0.25	10.61	27.8	1.10	175	175	H	0.0577	8.2
3.00	OH	0.25	10.61	27.8	1.10	175	175	H	0.0577	8.2
3.25	OH	0.25	10.65	30.5	1.05	163	163	H	0.0634	10.0
3.50	OH	0.25	10.65	30.5	1.05	163	163	H	0.0634	10.0
3.75	OH	0.25	10.65	30.5	1.05	163	163	H	0.0634	10.0
4.00	OH	0.25	10.65	30.5	1.05	163	163	H	0.0634	10.0
4.33	OH	0.33	10.70	33.3	1.00	156	156	H	0.0691	12.0
4.66	OH	0.33	10.70	33.3	1.00	156	156	H	0.0691	12.0
4.99	OH	0.33	10.70	33.3	1.00	156	156	H	0.0691	12.0
5.33	OH	0.34	10.76	36.0	1.00	153	153	H	0.0749	14.0
5.67	OH	0.34	10.76	36.0	1.00	153	153	H	0.0749	14.0
6.00	OH	0.33	10.76	36.0	1.00	153	153	H	0.0749	14.0
6.33	OH	0.33	10.82	38.8	1.00	152	152	H	0.0806	16.4
6.66	OH	0.33	10.82	38.8	1.00	152	152	H	0.0806	16.4
7.00	OH	0.34	10.82	38.8	1.00	152	152	H	0.0806	16.4
7.33	OH	0.33	10.90	41.5	1.00	151	151	H	0.0863	18.9
7.66	OH	0.33	10.90	41.5	1.00	151	151	H	0.0863	18.9
8.00	OH	0.34	10.90	41.5	1.00	151	151	H	0.0863	18.9
8.33	OH	0.33	10.99	44.3	1.00	150	150	H	0.0920	21.7
8.66	OH	0.33	10.99	44.3	1.00	150	150	H	0.0920	21.7
9.00	OH	0.34	10.99	44.3	1.00	150	150	H	0.0920	21.7
9.33	OH	0.33	11.09	47.0	1.00	150	150	H	0.0977	24.7
9.66	OH	0.33	11.09	47.0	1.00	150	150	H	0.0977	24.7
10.00	OH	0.34	11.09	47.0	1.00	150	150	H	0.0977	24.7
10.50	OH	0.50	11.21	50.0	1.00	150	150	H	0.1040	28.2
11.00	OH	0.50	11.21	50.0	1.00	150	150	H	0.1040	28.2
11.90	CH	0.90	14.18	90.0	1.40	70	70	H	0.2079	115.7
12.90	CH	1.00	14.34	102.0	1.30	60	60	H	0.2235	150.2
14.00	CH	1.10	14.50	114.0	1.25	55	55	H	0.2391	189.8
15.25	CH	1.25	14.68	126.0	1.23	53	53	H	0.2547	234.8
16.75	CH	1.50	15.09	150.0	1.20	50	50	H	0.2703	342.0
18.75	CL	2.00	18.00	200.0	5.00	60	20	P	1.0396	725.3
20.85	CL	2.10	18.10	215.0	2.75	50	13	P	1.1881	842.8
23.00	CL	2.15	18.20	230.0	2.19	47	11	P	1.3366	969.8
25.50	CL	2.50	18.35	252.7	2.02	45	10	P	1.5594	1180.2
28.00	CL	2.50	18.45	270.4	2.00	45	10	P	1.7079	1359.3
31.00	CL	3.00	18.60	300.0	2.00	45	10	P	1.9307	1686.2
32.00	CL	1.00	18.70	320.0	2.00	45	10	P	2.0792	1928.9

Table 6A.4: Site properties for site Bay Area II K S2

Depth (m)	USCS	Thick (m)	γ (kN/m^3)	Vs (m/s)	OCR	PI ADJ	PI	Age	τ_{ff} (atm)	G_{max} (atm)
1.00	SM-SC	1.00	18.00	200.0	1.00	0	0	H	0.2500	725.3
1.25	OH	0.25	10.56	25.0	1.20	200	200	H	0.1106	6.7
1.50	OH	0.25	10.56	25.0	1.20	200	200	H	0.1106	6.7
1.75	OH	0.25	10.56	25.0	1.20	200	200	H	0.1106	6.7
2.00	OH	0.25	10.56	25.0	1.20	200	200	H	0.1106	6.7
2.25	OH	0.25	10.61	27.8	1.10	175	175	H	0.1154	8.2
2.50	OH	0.25	10.61	27.8	1.10	175	175	H	0.1154	8.2
2.75	OH	0.25	10.61	27.8	1.10	175	175	H	0.1154	8.2
3.00	OH	0.25	10.61	27.8	1.10	175	175	H	0.1154	8.2
3.25	OH	0.25	10.65	30.5	1.05	163	163	H	0.1268	10.0
3.50	OH	0.25	10.65	30.5	1.05	163	163	H	0.1268	10.0
3.75	OH	0.25	10.65	30.5	1.05	163	163	H	0.1268	10.0
4.00	OH	0.25	10.65	30.5	1.05	163	163	H	0.1268	10.0
4.33	OH	0.33	10.70	33.3	1.00	156	156	H	0.1383	12.0
4.66	OH	0.33	10.70	33.3	1.00	156	156	H	0.1383	12.0
4.99	OH	0.33	10.70	33.3	1.00	156	156	H	0.1383	12.0
5.33	OH	0.34	10.76	36.0	1.00	153	153	H	0.1497	14.0
5.67	OH	0.34	10.76	36.0	1.00	153	153	H	0.1497	14.0
6.00	OH	0.33	10.76	36.0	1.00	153	153	H	0.1497	14.0
6.33	OH	0.33	10.82	38.8	1.00	152	152	H	0.1611	16.4
6.66	OH	0.33	10.82	38.8	1.00	152	152	H	0.1611	16.4
7.00	OH	0.34	10.82	38.8	1.00	152	152	H	0.1611	16.4
7.33	OH	0.33	10.90	41.5	1.00	151	151	H	0.1726	18.9
7.66	OH	0.33	10.90	41.5	1.00	151	151	H	0.1726	18.9
8.00	OH	0.34	10.90	41.5	1.00	151	151	H	0.1726	18.9
8.33	OH	0.33	10.99	44.3	1.00	150	150	H	0.1840	21.7
8.66	OH	0.33	10.99	44.3	1.00	150	150	H	0.1840	21.7
9.00	OH	0.34	10.99	44.3	1.00	150	150	H	0.1840	21.7
9.33	OH	0.33	11.09	47.0	1.00	150	150	H	0.1954	24.7
9.66	OH	0.33	11.09	47.0	1.00	150	150	H	0.1954	24.7
10.00	OH	0.34	11.09	47.0	1.00	150	150	H	0.1954	24.7
10.50	OH	0.50	11.21	50.0	1.00	150	150	H	0.2079	28.2
11.00	OH	0.50	11.21	50.0	1.00	150	150	H	0.2079	28.2
11.90	CH	0.90	14.18	90.0	1.40	70	70	H	0.4158	115.7
12.90	CH	1.00	14.34	102.0	1.30	60	60	H	0.4470	150.2
14.00	CH	1.10	14.50	114.0	1.25	55	55	H	0.4782	189.8
15.25	CH	1.25	14.68	126.0	1.23	53	53	H	0.5094	234.8
16.75	CH	1.50	15.09	150.0	1.20	50	50	H	0.5406	342.0
18.75	CL	2.00	18.00	200.0	5.00	60	20	P	2.0792	725.3
20.85	CL	2.10	18.10	215.0	2.75	50	13	P	2.3762	842.8
23.00	CL	2.15	18.20	230.0	2.19	47	11	P	2.6732	969.8
25.50	CL	2.50	18.35	252.7	2.02	45	10	P	3.1188	1180.2
28.00	CL	2.50	18.45	270.4	2.00	45	10	P	3.4158	1359.3
31.00	CL	3.00	18.60	300.0	2.00	45	10	P	3.8614	1686.2
32.00	CL	1.00	18.70	320.0	2.00	45	10	P	4.1584	1928.9

Table 6A.5: Site properties for site Bay Area II K S4

Depth (m)	USCS	Thick (m)	γ (kN/m^3)	Vs (m/s)	OCR	PI ADJ	PI	Age	τ_{ff} (atm)	G_{max} (atm)
1.00	SM-SC	1.00	18.00	200.0	1.00	0	0	H	1.0000	725.3
1.25	OH	0.25	10.56	25.0	1.20	200	200	H	0.2211	6.7
1.50	OH	0.25	10.56	25.0	1.20	200	200	H	0.2211	6.7
1.75	OH	0.25	10.56	25.0	1.20	200	200	H	0.2211	6.7
2.00	OH	0.25	10.56	25.0	1.20	200	200	H	0.2211	6.7
2.25	OH	0.25	10.61	27.8	1.10	175	175	H	0.2308	8.2
2.50	OH	0.25	10.61	27.8	1.10	175	175	H	0.2308	8.2
2.75	OH	0.25	10.61	27.8	1.10	175	175	H	0.2308	8.2
3.00	OH	0.25	10.61	27.8	1.10	175	175	H	0.2308	8.2
3.25	OH	0.25	10.65	30.5	1.05	163	163	H	0.2537	10.0
3.50	OH	0.25	10.65	30.5	1.05	163	163	H	0.2537	10.0
3.75	OH	0.25	10.65	30.5	1.05	163	163	H	0.2537	10.0
4.00	OH	0.25	10.65	30.5	1.05	163	163	H	0.2537	10.0
4.33	OH	0.33	10.70	33.3	1.00	156	156	H	0.2765	12.0
4.66	OH	0.33	10.70	33.3	1.00	156	156	H	0.2765	12.0
4.99	OH	0.33	10.70	33.3	1.00	156	156	H	0.2765	12.0
5.33	OH	0.34	10.76	36.0	1.00	153	153	H	0.2994	14.0
5.67	OH	0.34	10.76	36.0	1.00	153	153	H	0.2994	14.0
6.00	OH	0.33	10.76	36.0	1.00	153	153	H	0.2994	14.0
6.33	OH	0.33	10.82	38.8	1.00	152	152	H	0.3223	16.4
6.66	OH	0.33	10.82	38.8	1.00	152	152	H	0.3223	16.4
7.00	OH	0.34	10.82	38.8	1.00	152	152	H	0.3223	16.4
7.33	OH	0.33	10.90	41.5	1.00	151	151	H	0.3451	18.9
7.66	OH	0.33	10.90	41.5	1.00	151	151	H	0.3451	18.9
8.00	OH	0.34	10.90	41.5	1.00	151	151	H	0.3451	18.9
8.33	OH	0.33	10.99	44.3	1.00	150	150	H	0.3680	21.7
8.66	OH	0.33	10.99	44.3	1.00	150	150	H	0.3680	21.7
9.00	OH	0.34	10.99	44.3	1.00	150	150	H	0.3680	21.7
9.33	OH	0.33	11.09	47.0	1.00	150	150	H	0.3909	24.7
9.66	OH	0.33	11.09	47.0	1.00	150	150	H	0.3909	24.7
10.00	OH	0.34	11.09	47.0	1.00	150	150	H	0.3909	24.7
10.50	OH	0.50	11.21	50.0	1.00	150	150	H	0.4158	28.2
11.00	OH	0.50	11.21	50.0	1.00	150	150	H	0.4158	28.2
11.90	CH	0.90	14.18	90.0	1.40	70	70	H	0.8317	115.7
12.90	CH	1.00	14.34	102.0	1.30	60	60	H	0.8940	150.2
14.00	CH	1.10	14.50	114.0	1.25	55	55	H	0.9564	189.8
15.25	CH	1.25	14.68	126.0	1.23	53	53	H	1.0188	234.8
16.75	CH	1.50	15.09	150.0	1.20	50	50	H	1.0812	342.0
18.75	CL	2.00	18.00	200.0	5.00	60	20	P	4.1584	725.3
20.85	CL	2.10	18.10	215.0	2.75	50	13	P	4.7524	842.8
23.00	CL	2.15	18.20	230.0	2.19	47	11	P	5.3465	969.8
25.50	CL	2.50	18.35	252.7	2.02	45	10	P	6.2376	1180.2
28.00	CL	2.50	18.45	270.4	2.00	45	10	P	6.8316	1359.3
31.00	CL	3.00	18.60	300.0	2.00	45	10	P	7.7227	1686.2
32.00	CL	1.00	18.70	320.0	2.00	45	10	P	8.3167	1928.9

Table 6A.6: Site properties for site HAGP

Depth (m)	USCS	Thick (m)	γ (kN/m3)	Vs (m/s)	OCR	PI ADJ	PI	Age	τ_{ff} (atm)	Gmax (atm)
2	SM	2	17.00	200	1	0	0	H	0.2000	685.0
3	CH	1	14.50	100	3	60	60	H	0.0622	146.1
4	CH	1	14.53	100	2	60	60	H	0.0588	146.3
5	CH	1	14.55	100	1.5	60	60	H	0.0579	146.6
6	CH	1	14.58	100	1.5	60	60	H	0.0684	146.9
7	CH	1	14.61	100	1.5	60	60	H	0.0790	147.1
8	CH	1	14.64	100	1.5	60	60	H	0.0896	147.4
9	CH	1	14.66	100	1.5	60	60	H	0.1003	147.7
10	CH	1	14.69	100	1.5	60	60	H	0.1111	148.0
11	CH	1	14.72	100	1.5	60	60	H	0.1219	148.2
12	CH	1	14.74	100	1.5	60	60	H	0.1328	148.5
13	CH	1	14.77	100	1.5	60	60	H	0.1437	148.8
14	CH	1	14.80	108	1.5	60	60	H	0.1547	173.9
15.1	CH	1.1	14.82	117	1.5	59	59	H	0.1663	204.4
16.3	CH	1.2	14.85	126	1.5	58	58	H	0.1791	237.5
17.6	CH	1.3	14.88	135	1.5	57	57	H	0.1931	273.1
19	CH	1.4	14.91	144	1.5	56	56	H	0.2083	311.3
20.5	CH	1.5	14.93	153	1.5	55	55	H	0.2247	352.1
22.1	CH	1.6	14.96	162	1.5	53	53	H	0.2423	395.5
23.8	CH	1.7	14.99	171	1.5	51	51	H	0.2611	441.4
25.6	CH	1.8	15.01	180	1.5	49	49	H	0.2812	490.0
27.4	CH	1.8	15	185	1.5	47	47	H	0.3020	518.5
29.2	CH	1.8	15	190	1.5	45	45	H	0.3229	547.9
31	CH	1.8	15	195	1.5	43	43	H	0.3439	578.2
33	CH	2	15	202	1.5	41	41	H	0.3666	629.3
35	CH	2	15	206	1.5	39	39	H	0.3910	656.8
37	CH	2	15	210	1.5	37	37	H	0.4157	684.9
39	CH	2	16	214	1.5	35	35	H	0.4407	715.0
42.3	SC	3.3	18	330	1	30	0	P	1.9940	1974.5
45.6	SC	3.3	18	330	1	30	0	P	2.2406	1974.5
48.9	SC	3.3	18	330	1	30	0	P	2.4871	1974.5
50	SC	1.1	18	330	1	30	0	P	2.6515	1974.5

Table 6A.7: Site properties for site JSSS

Depth (m)	USCS	Thick (m)	γ (kN/m^3)	Vs (m/s)	OCR	PI ADJ	PI	Age	τ_{ff} (atm)	G_{max} (atm)
2	SC	2	19.00	400	1	0	0	H	0.4400	3062.2
3	CH	1	15.50	175	5	40	40	H	0.2091	478.2
4	CH	1	15.40	144	3	40	40	H	0.1759	321.7
5	CH	1	15.30	120	1.5	40	40	H	0.1218	221.9
6	CH	1	15.20	106	1.3	40	40	H	0.1269	172.0
6.85	CH	0.85	15.10	98	1.3	40	40	H	0.1435	146.1
7.7	CH	0.85	15.00	91	1.3	40	40	H	0.1584	125.1
8.55	CH	0.85	15.00	91	1.3	40	40	H	0.1732	125.1
9.4	MH/CH	0.85	14.90	87	1.3	30	30	H	0.1879	113.6
10.25	MH/CH	0.85	14.80	90	1.3	30	30	H	0.2023	120.8
11.1	MH/CH	0.85	14.70	98	1.3	30	30	H	0.2164	142.2
12.1	MH/CH	1	14.60	106	1.3	30	30	H	0.2314	165.2
13.2	MH/CH	1.1	15.10	111	1.3	30	30	H	0.2492	187.4
14.3	MH/CH	1.1	15.60	113	1.3	30	30	H	0.2696	200.7
15.4	MH/CH	1.1	16.10	120	1.3	30	30	H	0.2919	233.5
16.7	MH/CH	1.3	16.66	133	1.3	30	30	H	0.3184	296.9
18.2	MH/CH	1.5	16.66	160	1.3	30	30	H	0.3506	429.6
20	MH/CH	1.8	16.79	180	1.3	30	30	H	0.3889	547.8
21.66	CH	1.66	16.90	191.486	1.1	25	25	H	0.3759	624.3
23.33	CH	1.67	17.02	194.993	1.1	25	25	H	0.4109	651.8
25	CH	1.67	17.14	198.5	1.1	25	25	H	0.4465	680.1
27	CH	2	17	202.7	1.1	25	25	H	0.4863	715.0
29	CH	2	17	206.9	1.1	25	25	H	0.5305	751.0
31	CH	2	18	211.1	1.1	25	25	H	0.5756	788.1
33	CH	2	18	215.3	1.1	25	25	H	0.6214	826.3
35	CH	2	18	219.5	1.1	25	25	H	0.6681	865.6
37.2	CH	2.2	18	224.12	1.1	25	25	H	0.7181	910.7
39.4	CH	2.2	18	228.74	1.1	25	25	H	0.7693	922.3
41.7	CH	2.3	18	233.57	1.3	25	25	H	0.9373	961.7
44	CH	2.3	18	238.4	1.3	25	25	H	0.9966	1001.9
46.4	CH	2.4	18	243.44	1.3	25	25	H	1.0572	1044.7
48.8	CH	2.4	18	248.48	1.3	25	25	H	1.1191	1088.4
51.3	CH	2.5	18	253.73	1.3	25	25	H	1.1823	1134.9
53.8	CH	2.5	18	258.98	1.3	25	25	H	1.2468	1182.3
56.4	CH	2.6	18	264.44	1.3	25	25	H	1.3125	1232.7
59	CH	2.6	18	269.9	1.3	25	25	H	1.3796	1284.1
61.7	CH	2.7	18	275.57	2.2	75	25	P	2.6467	1338.6
64.4	CH	2.7	18	281.24	2.2	75	25	P	2.7739	1394.3
67.2	CH	2.8	18	287.12	2.2	75	25	P	2.9035	1453.2

70	CH	2.8	18	293	2.2	75	25	P	3.0355	1513.3
72.9	CH	2.9	18	299.09	2.2	75	25	P	3.1761	1640.9
75.8	CH	2.9	18	305.18	2.2	75	25	P	3.3254	1708.4
78.8	CH	3	18	311.48	2.2	75	25	P	3.4717	1720.0
81.8	CH	3	18	317.78	2.2	75	25	P	3.6149	1790.3
84.8	CH	3	18	324.08	2.2	75	25	P	3.7582	1862.0
87.8	CH	3	18	330.38	2.2	75	25	P	3.9014	1935.1
90.9	CH	3.1	18.4	336.89	2.2	75	25	P	4.0546	2103.6
94	CH	3.1	18.4	343.4	2.2	75	25	P	4.2178	2185.7
99	GW	5	19	500	2.2	30	0	P	7.8767	4784.7
104	GW	5	19	500	2.2	30	0	P	8.3762	4784.7
109	GW	5	19	500	2.2	30	0	P	8.8757	4784.7
115	GW	6	19	600	2.2	30	0	P	9.4252	6890.0

Table 6A.8: Site properties for site KIKNET40

Depth (m)	USCS	Thick (m)	γ (kN/m^3)	Vs (m/s)	OCR	PI ADJ	PI	Age	τ_{ff} (atm)	G_{max} (atm)
0.7	CH	0.7	15.50	80	5	40	40	H	0.0300	99.9
1.4	CH	0.7	15.50	80	4	40	40	H	0.0493	99.9
2.1	CH	0.7	15.50	80	3.5	40	40	H	0.0738	99.9
3.1	CH	1	16.50	110	3	40	40	H	0.1002	201.1
4.2	CH	1.1	16.50	110	2	40	40	H	0.1057	201.1
5.3	CH	1.1	16.50	110	1.5	40	40	H	0.1116	201.1
6.4	CH	1.1	16.50	110	1.3	40	40	H	0.1242	201.1
7.5	CH	1.1	16.50	110	1.15	40	40	H	0.1350	201.1
8.6	CH	1.1	16.50	110	1.15	40	40	H	0.1574	201.1
9.7	CH	1.1	16.50	110	1.15	40	40	H	0.1797	201.1
10.8	CH	1.1	16.50	110	1.15	40	40	H	0.2021	201.1
11.9	CH	1.1	16.50	110	1.15	40	40	H	0.2245	201.1
13	CH	1.1	16.50	110	1.15	40	40	H	0.2469	201.1
14.1	CH	1.1	16.50	110	1.15	40	40	H	0.2692	201.1
16	SM	1.9	17.00	200	2	60	20	P	0.4689	685.0
18	SM	2	17.00	200	1.5	60	20	P	0.4252	685.0
20	SM	2	17.00	200	1.3	60	20	P	0.4275	685.0
22	SM	2	17.00	200	1.3	60	20	P	0.4757	685.0
24	SM	2	17.00	200	1.3	60	20	P	0.5239	685.0
26	SM	2	17.00	200	1.3	60	20	P	0.5721	685.0
28	SM	2	17.00	200	1.3	60	20	P	0.6203	685.0
30	SM	2	17	200	1.3	60	20	P	0.6686	685.0
32	SM	2	17	200	1.3	60	20	P	0.7168	685.0
34	SM	2	17	200	1.3	60	20	P	0.7650	685.0
36	SM	2	17	200	1.3	60	20	P	0.8132	685.0
38	SM	2	17	200	1.3	60	20	P	0.8615	685.0
41	SW-SM	3	19	350	1.5	35	10	P	1.2538	2344.5
44.5	SW-SM	3.5	19	350	1.3	35	10	P	1.2383	2344.5
48	SW-SM	3.5	19	350	1.3	35	10	P	1.3677	2344.5
53	ML/MH	5	18	500	3.5	100	30	P	3.3454	4532.9
58	ML/MH	5	18	505	3	100	30	P	3.2789	4624.0
63	ML/MH	5	18	510	2.75	100	30	P	3.3584	4716.0
68	ML/MH	5	18	515	2.5	100	30	P	3.3899	4809.0
73	ML/MH	5	18	520	2.5	100	30	P	3.6679	4902.8
78	ML/MH	5	18	525	2.5	100	30	P	3.9459	4997.5
83	ML/MH	5	18	530	2.5	100	30	P	4.2239	5093.2
88	ML/MH	5	18	530	2.5	100	30	P	4.5019	5093.2
93	ML/MH	5	18	530	2.5	100	30	P	4.7799	5093.2
98	ML/MH	5	18	530	2.5	100	30	P	5.0579	5093.2
103	ML/MH	5	18	530	2.5	100	30	P	5.3359	5093.2

Table 6A.9: Site properties for site KIKNET

Depth (m)	USCS	Thick (m)	γ (kN/m^3)	Vs (m/s)	OCR	PI ADJ	PI	Age	τ_{ff} (atm)	G_{max} (atm)
0.7	CH	0.7	15.50	80	5	80	80	H	0.0300	99.9
1.4	CH	0.7	15.50	80	4	80	80	H	0.0493	99.9
2.1	CH	0.7	15.50	80	3.5	80	80	H	0.0738	99.9
3.1	CH	1	16.50	110	3	80	80	H	0.1002	201.1
4.2	CH	1.1	16.50	110	2	80	80	H	0.1057	201.1
5.3	CH	1.1	16.50	110	1.5	80	80	H	0.1116	201.1
6.4	CH	1.1	16.50	110	1.3	80	80	H	0.1242	201.1
7.5	CH	1.1	16.50	110	1.15	80	80	H	0.1350	201.1
8.6	CH	1.1	16.50	110	1.15	80	80	H	0.1574	201.1
9.7	CH	1.1	16.50	110	1.15	80	80	H	0.1797	201.1
10.8	CH	1.1	16.50	110	1.15	80	80	H	0.2021	201.1
11.9	CH	1.1	16.50	110	1.15	80	80	H	0.2245	201.1
13	CH	1.1	16.50	110	1.15	80	80	H	0.2469	201.1
14.1	CH	1.1	16.50	110	1.15	80	80	H	0.2692	201.1
16	SM	1.9	17.00	200	2	60	20	P	0.4689	685.0
18	SM	2	17.00	200	1.5	60	20	P	0.4252	685.0
20	SM	2	17.00	200	1.3	60	20	P	0.4275	685.0
22	SM	2	17.00	200	1.3	60	20	P	0.4757	685.0
24	SM	2	17.00	200	1.3	60	20	P	0.5239	685.0
26	SM	2	17.00	200	1.3	60	20	P	0.5721	685.0
28	SM	2	17.00	200	1.3	60	20	P	0.6203	685.0
30	SM	2	17	200	1.3	60	20	P	0.6686	685.0
32	SM	2	17	200	1.3	60	20	P	0.7168	685.0
34	SM	2	17	200	1.3	60	20	P	0.7650	685.0
36	SM	2	17	200	1.3	60	20	P	0.8132	685.0
38	SM	2	17	200	1.3	60	20	P	0.8615	685.0
41	SW-SM	3	19	350	1.5	35	10	P	1.2538	2344.5
44.5	SW-SM	3.5	19	350	1.3	35	10	P	1.2383	2344.5
48	SW-SM	3.5	19	350	1.3	35	10	P	1.3677	2344.5
53	ML/MH	5	18	500	3.5	100	30	P	3.3454	4532.9
58	ML/MH	5	18	505	3	100	30	P	3.2789	4624.0
63	ML/MH	5	18	510	2.75	100	30	P	3.3584	4716.0
68	ML/MH	5	18	515	2.5	100	30	P	3.3899	4809.0
73	ML/MH	5	18	520	2.5	100	30	P	3.6679	4902.8
78	ML/MH	5	18	525	2.5	100	30	P	3.9459	4997.5
83	ML/MH	5	18	530	2.5	100	30	P	4.2239	5093.2
88	ML/MH	5	18	530	2.5	100	30	P	4.5019	5093.2
93	ML/MH	5	18	530	2.5	100	30	P	4.7799	5093.2
98	ML/MH	5	18	530	2.5	100	30	P	5.0579	5093.2
103	ML/MH	5	18	530	2.5	100	30	P	5.3359	5093.2

Table 6A.10: Site properties for site KIKNET160

Depth (m)	USCS	Thick (m)	γ (kN/m^3)	Vs (m/s)	OCR	PI ADJ	PI	Age	τ_{ff} (atm)	G_{max} (atm)
0.7	CH	0.7	15.50	80	5	160	160	H	0.0300	99.9
1.4	CH	0.7	15.50	80	4	160	160	H	0.0493	99.9
2.1	CH	0.7	15.50	80	3.5	160	160	H	0.0738	99.9
3.1	CH	1	16.50	110	3	160	160	H	0.1002	201.1
4.2	CH	1.1	16.50	110	2	160	160	H	0.1057	201.1
5.3	CH	1.1	16.50	110	1.5	160	160	H	0.1116	201.1
6.4	CH	1.1	16.50	110	1.3	160	160	H	0.1242	201.1
7.5	CH	1.1	16.50	110	1.15	160	160	H	0.1350	201.1
8.6	CH	1.1	16.50	110	1.15	160	160	H	0.1574	201.1
9.7	CH	1.1	16.50	110	1.15	160	160	H	0.1797	201.1
10.8	CH	1.1	16.50	110	1.15	160	160	H	0.2021	201.1
11.9	CH	1.1	16.50	110	1.15	160	160	H	0.2245	201.1
13	CH	1.1	16.50	110	1.15	160	160	H	0.2469	201.1
14.1	CH	1.1	16.50	110	1.15	160	160	H	0.2692	201.1
16	SM	1.9	17.00	200	2	60	20	P	0.4689	685.0
18	SM	2	17.00	200	1.5	60	20	P	0.4252	685.0
20	SM	2	17.00	200	1.3	60	20	P	0.4275	685.0
22	SM	2	17.00	200	1.3	60	20	P	0.4757	685.0
24	SM	2	17.00	200	1.3	60	20	P	0.5239	685.0
26	SM	2	17.00	200	1.3	60	20	P	0.5721	685.0
28	SM	2	17.00	200	1.3	60	20	P	0.6203	685.0
30	SM	2	17	200	1.3	60	20	P	0.6686	685.0
32	SM	2	17	200	1.3	60	20	P	0.7168	685.0
34	SM	2	17	200	1.3	60	20	P	0.7650	685.0
36	SM	2	17	200	1.3	60	20	P	0.8132	685.0
38	SM	2	17	200	1.3	60	20	P	0.8615	685.0
41	SW-SM	3	19	350	1.5	35	10	P	1.2538	2344.5
44.5	SW-SM	3.5	19	350	1.3	35	10	P	1.2383	2344.5
48	SW-SM	3.5	19	350	1.3	35	10	P	1.3677	2344.5
53	ML/MH	5	18	500	3.5	100	30	P	3.3454	4532.9
58	ML/MH	5	18	505	3	100	30	P	3.2789	4624.0
63	ML/MH	5	18	510	2.75	100	30	P	3.3584	4716.0
68	ML/MH	5	18	515	2.5	100	30	P	3.3899	4809.0
73	ML/MH	5	18	520	2.5	100	30	P	3.6679	4902.8
78	ML/MH	5	18	525	2.5	100	30	P	3.9459	4997.5
83	ML/MH	5	18	530	2.5	100	30	P	4.2239	5093.2
88	ML/MH	5	18	530	2.5	100	30	P	4.5019	5093.2
93	ML/MH	5	18	530	2.5	100	30	P	4.7799	5093.2
98	ML/MH	5	18	530	2.5	100	30	P	5.0579	5093.2
103	ML/MH	5	18	530	2.5	100	30	P	5.3359	5093.2

Table 6A.11: Site properties for site KIKNET S2

Depth (m)	USCS	Thick (m)	γ (kN/m^3)	Vs (m/s)	OCR	PI ADJ	PI	Age	τ_{ff} (atm)	G_{max} (atm)
0.7	CH	0.7	15.50	80	5	80	80	H	0.0600	99.9
1.4	CH	0.7	15.50	80	4	80	80	H	0.0985	99.9
2.1	CH	0.7	15.50	80	3.5	80	80	H	0.1475	99.9
3.1	CH	1	16.50	110	3	80	80	H	0.2003	201.1
4.2	CH	1.1	16.50	110	2	80	80	H	0.2113	201.1
5.3	CH	1.1	16.50	110	1.5	80	80	H	0.2232	201.1
6.4	CH	1.1	16.50	110	1.3	80	80	H	0.2484	201.1
7.5	CH	1.1	16.50	110	1.15	80	80	H	0.2700	201.1
8.6	CH	1.1	16.50	110	1.15	80	80	H	0.3147	201.1
9.7	CH	1.1	16.50	110	1.15	80	80	H	0.3595	201.1
10.8	CH	1.1	16.50	110	1.15	80	80	H	0.4042	201.1
11.9	CH	1.1	16.50	110	1.15	80	80	H	0.4490	201.1
13	CH	1.1	16.50	110	1.15	80	80	H	0.4937	201.1
14.1	CH	1.1	16.50	110	1.15	80	80	H	0.5385	201.1
16	SM	1.9	17.00	200	2	60	20	P	0.9378	685.0
18	SM	2	17.00	200	1.5	60	20	P	0.8505	685.0
20	SM	2	17.00	200	1.3	60	20	P	0.8549	685.0
22	SM	2	17.00	200	1.3	60	20	P	0.9514	685.0
24	SM	2	17.00	200	1.3	60	20	P	1.0478	685.0
26	SM	2	17.00	200	1.3	60	20	P	1.1443	685.0
28	SM	2	17.00	200	1.3	60	20	P	1.2407	685.0
30	SM	2	17	200	1.3	60	20	P	1.3371	685.0
32	SM	2	17	200	1.3	60	20	P	1.4336	685.0
34	SM	2	17	200	1.3	60	20	P	1.5300	685.0
36	SM	2	17	200	1.3	60	20	P	1.6265	685.0
38	SM	2	17	200	1.3	60	20	P	1.7229	685.0
41	SW-SM	3	19	350	1.5	35	10	P	2.5075	2344.5
44.5	SW-SM	3.5	19	350	1.3	35	10	P	2.4766	2344.5
48	SW-SM	3.5	19	350	1.3	35	10	P	2.7354	2344.5
53	ML/MH	5	18	500	3.5	100	30	P	6.6907	4532.9
58	ML/MH	5	18	505	3	100	30	P	6.5578	4624.0
63	ML/MH	5	18	510	2.75	100	30	P	6.7169	4716.0
68	ML/MH	5	18	515	2.5	100	30	P	6.7797	4809.0
73	ML/MH	5	18	520	2.5	100	30	P	7.3357	4902.8
78	ML/MH	5	18	525	2.5	100	30	P	7.8917	4997.5
83	ML/MH	5	18	530	2.5	100	30	P	8.4477	5093.2
88	ML/MH	5	18	530	2.5	100	30	P	9.0037	5093.2
93	ML/MH	5	18	530	2.5	100	30	P	9.5597	5093.2
98	ML/MH	5	18	530	2.5	100	30	P	10.1157	5093.2
103	ML/MH	5	18	530	2.5	100	30	P	10.6717	5093.2

Table 6A.12: Site properties for site KIKNET S4

Depth (m)	USCS	Thick (m)	γ (kN/m^3)	Vs (m/s)	OCR	PI ADJ	PI	Age	τ_{ff} (atm)	G_{max} (atm)
0.7	CH	0.7	15.50	80	5	80	80	H	0.1200	99.9
1.4	CH	0.7	15.50	80	4	80	80	H	0.1970	99.9
2.1	CH	0.7	15.50	80	3.5	80	80	H	0.2951	99.9
3.1	CH	1	16.50	110	3	80	80	H	0.4006	201.1
4.2	CH	1.1	16.50	110	2	80	80	H	0.4227	201.1
5.3	CH	1.1	16.50	110	1.5	80	80	H	0.4465	201.1
6.4	CH	1.1	16.50	110	1.3	80	80	H	0.4969	201.1
7.5	CH	1.1	16.50	110	1.15	80	80	H	0.5400	201.1
8.6	CH	1.1	16.50	110	1.15	80	80	H	0.6295	201.1
9.7	CH	1.1	16.50	110	1.15	80	80	H	0.7190	201.1
10.8	CH	1.1	16.50	110	1.15	80	80	H	0.8084	201.1
11.9	CH	1.1	16.50	110	1.15	80	80	H	0.8979	201.1
13	CH	1.1	16.50	110	1.15	80	80	H	0.9874	201.1
14.1	CH	1.1	16.50	110	1.15	80	80	H	1.0769	201.1
16	SM	1.9	17.00	200	2	60	20	P	1.8757	685.0
18	SM	2	17.00	200	1.5	60	20	P	1.7010	685.0
20	SM	2	17.00	200	1.3	60	20	P	1.7099	685.0
22	SM	2	17.00	200	1.3	60	20	P	1.9027	685.0
24	SM	2	17.00	200	1.3	60	20	P	2.0956	685.0
26	SM	2	17.00	200	1.3	60	20	P	2.2885	685.0
28	SM	2	17.00	200	1.3	60	20	P	2.4814	685.0
30	SM	2	17	200	1.3	60	20	P	2.6743	685.0
32	SM	2	17	200	1.3	60	20	P	2.8672	685.0
34	SM	2	17	200	1.3	60	20	P	3.0601	685.0
36	SM	2	17	200	1.3	60	20	P	3.2529	685.0
38	SM	2	17	200	1.3	60	20	P	3.4458	685.0
41	SW-SM	3	19	350	1.5	35	10	P	5.0150	2344.5
44.5	SW-SM	3.5	19	350	1.3	35	10	P	4.9531	2344.5
48	SW-SM	3.5	19	350	1.3	35	10	P	5.4707	2344.5
53	ML/MH	5	18	500	3.5	100	30	P	13.3814	4532.9
58	ML/MH	5	18	505	3	100	30	P	13.1155	4624.0
63	ML/MH	5	18	510	2.75	100	30	P	13.4337	4716.0
68	ML/MH	5	18	515	2.5	100	30	P	13.5595	4809.0
73	ML/MH	5	18	520	2.5	100	30	P	14.6715	4902.8
78	ML/MH	5	18	525	2.5	100	30	P	15.7835	4997.5
83	ML/MH	5	18	530	2.5	100	30	P	16.8954	5093.2
88	ML/MH	5	18	530	2.5	100	30	P	18.0074	5093.2
93	ML/MH	5	18	530	2.5	100	30	P	19.1194	5093.2
98	ML/MH	5	18	530	2.5	100	30	P	20.2314	5093.2
103	ML/MH	5	18	530	2.5	100	30	P	21.3434	5093.2

Table 6A.13: Site properties for site MRCE1

Depth (m)	USCS	Thick (m)	γ (kN/m^3)	Vs (m/s)	OCR	PI ADJ	PI	Age	τ_{ff} (atm)	G_{max} (atm)
1.5	SM	1.5	17.00	225	1	0	0	H	0.2500	866.9
3	SM	1.5	17.00	155	1	0	0	H	0.2500	411.4
3.85	OH	0.85	15.00	85	4.03	52	52	H	0.4731	109.2
4.7	OH	0.85	15.00	85	2.4	52	52	H	0.3705	109.2
5.55	OH	0.85	15.00	85	2	52	52	H	0.3704	109.2
6.4	OH	0.85	15.00	85	1.87	52	52	H	0.3985	109.2
7.25	OH	0.85	15.00	85	1.87	52	52	H	0.4460	109.2
8.1	OH	0.85	15.00	88	1.6	52	52	H	0.4357	117.9
9	OH	0.9	15.00	92	1.4	52	52	H	0.4303	126.9
9.9	OH	0.9	15.00	95	1.3	52	52	H	0.4432	136.3
10.8	OH	0.9	15.00	98	1.3	52	52	H	0.4808	146.1
11.8	OH	1	15.00	102	1.3	52	52	H	0.5205	156.1
12.8	OH	1	15.00	105	1.3	52	52	H	0.5623	166.5
13.8	OH	1	15.00	108	1.3	52	52	H	0.6041	177.3
14.8	OH	1	15.00	112	1.3	52	52	H	0.6458	188.3
15.8	OH	1	15.00	115	1.35	52	52	H	0.7087	199.7
16.8	OH	1	15.00	118	1.4	52	52	H	0.7740	211.5
17.9	OH	1.1	15.00	122	1.5	52	52	H	0.8671	223.5
19	OH	1.1	15.00	125	1.6	52	52	H	0.9673	235.9
20.5	SP-SM	1.5	18.00	150	1.3	30	0	P	0.8753	408.0
22	SP-SM	1.5	18.00	169	1.3	30	0	P	0.9724	517.9
23.5	ML/CL	1.5	18	176	4.6	75	25	P	1.4970	561.6
25	ML/CL	1.5	18	186	3.3	75	25	P	1.2518	627.3
26.5	ML/CL	1.5	18	196	2.6	75	25	P	1.1205	696.5
28.5	ML/CL	2	18	206	2.2	75	25	P	1.0682	769.4
30.5	ML/CL	2	18	216	2	75	25	P	1.0828	845.9
32.5	ML/CL	2	18	226	2	75	25	P	1.1758	926.1
34.5	ML/CL	2	18	236	2	75	25	P	1.2688	1009.9
36.5	ML/CL	2	18	246	2	75	25	P	1.3618	1097.3
38.5	ML/CL	2	18	256	2	75	25	P	1.4548	1188.3
40.5	ML/CL	2	18	260	2	75	25	P	1.5479	1225.7
42.5	ML/CL	2	18	264	2	75	25	P	1.6409	1263.7
45	ML/CL	2.5	18	268	2	75	25	P	1.7455	1302.3
47.5	ML/CL	2.5	18	272	2	75	25	P	1.8618	1341.5
50	ML/CL	2.5	18	276	2	75	25	P	1.9781	1381.2
52.5	SP-SM	2.5	20	280	1.3	30	0	P	3.3873	1579.5
55	SP-SM	2.5	20	286	1.3	30	0	P	3.6196	1647.9
57.5	SP-SM	2.5	20	292	1.3	30	0	P	3.8519	1717.8
60	SP-SM	2.5	20	298	1.3	30	0	P	4.0843	1789.1

63	CH	3	20	325	2	100	30	C	2.2513	2122.9
66	CH	3	20	330	2	100	30	C	2.3959	2197.7
69	CH	3	20	336	2	100	30	C	2.5405	2270.4
72	CH	3	20	341	2	100	30	C	2.6852	2341.3
75	CH	3	20	346	2	100	30	C	2.8298	2410.5
78	CH	3	20	351	2	100	30	C	2.9744	2478.1
84	SP-SM	6	21	607	1.3	30	0	C	7.6261	7794.0
90	SP-SM	6	21	624	1.3	30	0	C	8.3818	8236.7

Table 6A.14: Site properties for site MRCE2

Depth (m)	USCS	Thick (m)	γ (kN/m^3)	Vs (m/s)	OCR	PI ADJ	PI	Age	τ_{ff} (atm)	G_{max} (atm)
2	SM	2	17.00	350	1	0	0	H	0.2970	2097.7
4	SM	2	17.00	250	1	0	0	H	0.2970	1070.3
4.8	OH	0.8	15.00	80	3	60	60	H	0.2019	96.7
5.6	OH	0.8	15.15	84	2	52.5	52.5	H	0.1659	107.7
6.4	OH	0.8	15.30	88	1.5	45	45	H	0.1481	119.3
7.2	OH	0.8	15.45	92	1.3	37.5	37.5	H	0.1470	131.7
8	OH	0.8	15.60	96	1.3	37.5	37.5	H	0.1623	144.8
9	OH	1	15.80	100	1.25	30	30	H	0.1746	159.2
10	OH	1	16.00	105	1.25	30	30	H	0.1944	177.7
11	OH	1	16.10	110	1.25	30	30	H	0.2147	196.2
12	OH	1	16.20	115	1.25	30	30	H	0.2353	215.8
13	OH	1	16.30	120	1.25	30	30	H	0.2562	236.4
14.2	OH	1.2	16.40	126	1.25	30	30	H	0.2796	262.3
15.4	OH	1.2	16.50	132	1.25	30	30	H	0.3055	289.6
16.6	OH	1.2	16.50	138	1.25	30	30	H	0.3316	316.5
17.8	OH	1.2	16.50	144	1.25	30	30	H	0.3577	344.6
19	OH	1.2	16.50	150	1.25	30	30	H	0.3838	374.0
20.5	OH	1.5	16.50	158	1.25	30	30	H	0.4131	412.3
22	OH	1.5	16.50	165	1.25	30	30	H	0.4458	452.5
25	SM	3	19.00	350	1.5	30	0	P	1.7562	2344.5
30	SM	5	19.00	525	1.5	30	0	P	2.3273	5275.2

APPENDIX 6B: DEEPSOIL INPUT PARAMETERS FOR THE SELECTED SITES

Appendix 6B: DEEPSOIL Input Parameters for the Selected Sites

The following tables contain the DEEPSOIL input parameters of all 15 sites for both the nonlinear total stress and nonlinear effective stress analyses. The first table for each site lists the required inputs for a nonlinear total stress analysis in DEEPSOIL. The total stress parameters are the layer name, thickness in meters, unit weight (γ) in kN/m^3, shear wave velocity (Vs) in m/s, small strain damping (Dmin) in percent, the shear modulus reduction curve parameters (Ref Strain, B, s) and the damping curve parameters (P1, P2, P3). The Reference Stress and parameters b and d are 0 for all layers and all sites. The second table for each site lists the additional parameters necessary to perform a nonlinear effective stress analysis in DEEPSOIL. The value of Ru was 0.95 for all layers and all sites.

Table 6B.1: Input parameters for site Bay Area total stress analysis (Ref Stress = 0.18; b = d = 0 all layers)

Layer	Name	Thick (m)	γ (kN/m3)	Vs (m/s)	Dmin	Ref Strain	B	s	P1	P2	P3
1	SM-SC	2	18.8	250	1.77	0.0228	1.65	0.915	0.67	0.288	3.25
2	CH	0.75	15	82	2.18	0.0946	1.545	0.795	0.746	0.266	2.35
3	CH	0.75	15.05	82	2.09	0.0954	1.56	0.795	0.736	0.252	2.5
4	CH	0.75	15.1	82	2.01	0.0960	1.545	0.795	0.736	0.252	2.505
5	CH	0.75	15.15	82	1.96	0.0968	1.575	0.81	0.744	0.27	2.15
6	CH	0.75	15.2	82	1.92	0.0920	1.56	0.825	0.714	0.252	2.495
7	CH	0.75	15.25	82	1.87	0.0854	1.455	0.825	0.704	0.244	2.75
8	CH	0.75	15.3	82	1.82	0.0986	1.575	0.81	0.724	0.248	2.5
9	CH	0.75	15.35	82	1.77	0.1006	1.56	0.81	0.736	0.258	2.2
10	CH	1.13	15.3	120	1.76	0.0838	1.53	0.93	0.61	0.224	3.25
11	CH	1.17	15.35	120	1.70	0.0874	1.515	0.915	0.618	0.22	3.15
12	CH	1.17	15.4	120	1.65	0.0932	1.545	0.915	0.622	0.224	2.95
13	CH	1.17	15.45	120	1.60	0.0962	1.515	0.9	0.628	0.22	3.05
14	CH	1.17	15.5	120	1.56	0.0996	1.5	0.885	0.638	0.218	2.95
15	CH	1.17	15.55	120	1.52	0.1030	1.5	0.885	0.644	0.224	2.7
16	CH	1.17	15.6	120	1.49	0.1078	1.5	0.87	0.668	0.234	2.35
17	CH	1.17	15.65	120	1.46	0.1126	1.515	0.87	0.682	0.246	2
18	CH	1.17	15.7	120	1.43	0.1132	1.47	0.855	0.658	0.214	2.65
19	CH	1.17	15.75	120	1.40	0.1194	1.5	0.855	0.678	0.234	2.2
20	CH	1.17	15.8	120	1.37	0.1222	1.47	0.84	0.698	0.24	2.05
21	CH	1.17	15.85	120	1.35	0.1256	1.47	0.84	0.704	0.246	1.895
22	CL	1.82	18	195	1.56	0.1450	1.485	1.005	0.598	0.242	2.1
23	CL	1.86	18	195	1.51	0.1528	1.485	0.99	0.584	0.22	2.5
24	CL	1.86	18	195	1.47	0.1604	1.47	0.975	0.6	0.224	2.25
25	CL	1.86	18	195	1.44	0.1640	1.455	0.975	0.602	0.226	2.1
26	CL	1.86	18	195	1.40	0.1844	1.56	0.96	0.588	0.204	2.5
27	CL	1.86	18	195	1.37	0.1908	1.545	0.945	0.602	0.206	2.3
28	CL	1.86	18	195	1.34	0.1976	1.545	0.945	0.606	0.212	2.2
29	CL	1.86	18	195	1.32	0.2020	1.53	0.93	0.594	0.19	2.55
30	CL	1.86	18	195	1.30	0.2108	1.545	0.93	0.598	0.194	2.4
31	CL	1.86	18	195	1.27	0.2146	1.515	0.915	0.622	0.204	2
32	CL	1.86	18	195	1.25	0.2218	1.53	0.915	0.624	0.206	1.85
33	CL	1.86	18	195	1.23	0.2276	1.515	0.9	0.662	0.226	1.35
34	CL	1.86	18	195	1.21	0.2340	1.515	0.9	0.668	0.234	1.3
35	CL	1.86	18	195	1.20	0.2396	1.5	0.885	0.636	0.192	1.75
36	CL	3.25	18	330	1.19	0.1834	1.56	1.11	0.582	0.28	1.95
37	CL	3.25	18	330	1.17	0.1862	1.53	1.11	0.582	0.28	1.9
38	CL	3.25	18	330	1.14	0.1946	1.545	1.095	0.584	0.28	2.2
39	CL	3.25	18	330	1.12	0.2016	1.545	1.08	0.584	0.264	1.9

40	CL	3.25	18	330	1.10	0.2046	1.515	1.065	0.584	0.26	2.2
41	SM-SC	3.25	18	330	0.82	0.1702	1.44	0.825	0.716	0.238	1.45
42	SM-SC	3.25	18	330	0.81	0.1774	1.455	0.825	0.724	0.248	1.35
43	SM-SC	3.25	18	330	0.79	0.2002	1.575	0.825	0.744	0.268	1.15
44	SM-SC	3.25	18	330	0.78	0.2056	1.56	0.81	0.714	0.228	1.5
45	SM-SC	3.25	18	330	0.77	0.2134	1.575	0.81	0.736	0.25	1.25
46	SM-SC	3.25	18	330	0.76	0.2162	1.545	0.795	0.746	0.244	1.2
47	CL	3.25	20.3	330	1.00	0.2376	1.515	1.035	0.584	0.24	2.25
48	CL	3.25	20.3	330	0.98	0.2418	1.5	1.035	0.584	0.24	2.25
49	CL	3.25	20.3	330	0.97	0.2472	1.485	1.02	0.59	0.23	2
50	CL	3.25	20.3	330	0.95	0.2576	1.5	1.005	0.584	0.22	2.4
51	CL	3.25	20.3	330	0.94	0.2614	1.485	1.005	0.584	0.22	2.35
52	CL	4.375	20.3	440	0.93	0.2136	1.515	1.185	0.586	0.32	1.77
53	CL	4.375	20.3	440	0.92	0.2180	1.5	1.17	0.58	0.3	1.55
54	CL	4.375	20.3	440	0.91	0.2214	1.485	1.17	0.58	0.3	1.55
55	CL	4.375	20.3	440	0.89	0.2294	1.5	1.155	0.582	0.3	1.75
56	CL	4.375	20.3	440	0.88	0.2358	1.5	1.14	0.592	0.296	1.5
57	CL	4.375	20.3	440	0.87	0.2368	1.47	1.14	0.59	0.294	1.5
58	CL	4.375	20.3	440	0.86	0.2452	1.485	1.125	0.582	0.28	1.7
59	CL	4.375	20.3	440	0.85	0.2584	1.53	1.11	0.584	0.28	1.95
60	CL	4.3	20.3	477	0.84	0.2386	1.485	1.17	0.58	0.3	1.55
61	CL	4.3	20.3	477	0.83	0.2440	1.485	1.155	0.584	0.3	1.75
62	CL	4.3	20.3	477	0.82	0.2506	1.5	1.155	0.584	0.3	1.745
63	CL	4.3	20.3	477	0.81	0.2540	1.485	1.14	0.586	0.288	1.5
64	CL	4.3	20.3	477	0.81	0.2572	1.47	1.125	0.582	0.28	1.7
65	CL	4.3	20.3	477	0.80	0.2640	1.485	1.125	0.582	0.28	1.7
66	CL	4.3	20.3	477	0.79	0.2794	1.545	1.11	0.584	0.28	1.95
67	GW	4.9	21	580	0.60	0.2566	1.47	0.855	0.684	0.208	1.7
68	GW	5	21	580	0.59	0.2648	1.47	0.84	0.7	0.204	1.5
69	GW	5	21	580	0.58	0.2708	1.47	0.84	0.706	0.212	1.45
70	SM-SC	5	21	580	0.58	0.2758	1.455	0.825	0.678	0.174	2.1

Table 6B.2: Input parameters for site Bay Area effective stress analysis (Max Ru = 0.95 all layers)

Layer	Model	f/s/f	p/r/Dr	F/A/FC	s/B/-	g/C/-	v/D/v	-/g/-	Cv(m2/s)
1	1	1.000	1.000	0.7313377	1.3073	0.0067	1.0000	0.0000	1.63E-01
2	2	0.048	0.425	11.183198	-21.3223	11.2115	-1.0579	0.0246	3.91E-06
3	2	0.054	0.444	11.989503	-23.4457	12.8273	-1.3537	0.0247	3.91E-06
4	2	0.058	0.456	12.530345	-24.8997	13.9698	-1.5827	0.0251	3.91E-06
5	2	0.064	0.471	13.225596	-26.8024	15.5076	-1.9162	0.0252	3.91E-06
6	2	0.072	0.491	14.179158	-29.4716	17.7426	-2.4520	0.0249	3.91E-06
7	2	0.076	0.502	14.678789	-30.8967	18.9715	-2.7719	0.0252	3.91E-06
8	2	0.077	0.505	14.818775	-31.2992	19.3229	-2.8667	0.0259	3.91E-06
9	2	0.079	0.508	14.965894	-31.7237	19.6957	-2.9687	0.0265	3.91E-06
10	2	0.080	0.511	15.12083	-32.1724	20.0919	-3.0790	0.0273	3.91E-06
11	2	0.080	0.511	15.12083	-32.1724	20.0919	-3.0790	0.0284	3.91E-06
12	2	0.080	0.511	15.12083	-32.1724	20.0919	-3.0790	0.0294	3.91E-06
13	2	0.080	0.511	15.12083	-32.1724	20.0919	-3.0790	0.0304	3.91E-06
14	2	0.080	0.511	15.12083	-32.1724	20.0919	-3.0790	0.0313	3.91E-06
15	2	0.080	0.511	15.12083	-32.1724	20.0919	-3.0790	0.0322	3.91E-06
16	2	0.080	0.511	15.12083	-32.1724	20.0919	-3.0790	0.0331	3.91E-06
17	2	0.080	0.511	15.12083	-32.1724	20.0919	-3.0790	0.0339	3.91E-06
18	2	0.080	0.511	15.12083	-32.1724	20.0919	-3.0790	0.0347	3.91E-06
19	2	0.080	0.511	15.12083	-32.1724	20.0919	-3.0790	0.0355	3.91E-06
20	2	0.080	0.511	15.12083	-32.1724	20.0919	-3.0790	0.0362	3.91E-06
21	2	0.080	0.511	15.12083	-32.1724	20.0919	-3.0790	0.0370	3.91E-06
22	2	0.111	0.509	13.225596	-26.8024	15.5076	-1.9162	0.0545	2.70E-05
23	2	0.111	0.509	13.225596	-26.8024	15.5076	-1.9162	0.0565	2.70E-05
24	2	0.111	0.509	13.225596	-26.8024	15.5076	-1.9162	0.0584	2.70E-05
25	2	0.111	0.509	13.225596	-26.8024	15.5076	-1.9162	0.0602	2.70E-05
26	2	0.111	0.509	13.225596	-26.8024	15.5076	-1.9162	0.0619	2.70E-05
27	2	0.111	0.509	13.225596	-26.8024	15.5076	-1.9162	0.0635	2.70E-05
28	2	0.111	0.509	13.225596	-26.8024	15.5076	-1.9162	0.0650	2.70E-05
29	2	0.111	0.509	13.225596	-26.8024	15.5076	-1.9162	0.0665	2.70E-05
30	2	0.111	0.509	13.225596	-26.8024	15.5076	-1.9162	0.0679	2.70E-05
31	2	0.111	0.509	13.225596	-26.8024	15.5076	-1.9162	0.0693	2.70E-05
32	2	0.111	0.509	13.225596	-26.8024	15.5076	-1.9162	0.0706	2.70E-05
33	2	0.111	0.509	13.225596	-26.8024	15.5076	-1.9162	0.0719	2.70E-05
34	2	0.111	0.509	13.225596	-26.8024	15.5076	-1.9162	0.0731	2.70E-05
35	2	0.111	0.509	13.225596	-26.8024	15.5076	-1.9162	0.0743	2.70E-05
36	2	0.111	0.509	13.225596	-26.8024	15.5076	-1.9162	0.0759	2.70E-05
37	2	0.111	0.509	13.225596	-26.8024	15.5076	-1.9162	0.0778	2.70E-05
38	2	0.111	0.509	13.225596	-26.8024	15.5076	-1.9162	0.0796	2.70E-05
39	2	0.111	0.509	13.225596	-26.8024	15.5076	-1.9162	0.0814	2.70E-05

40	2	0.111	0.509	13.225596	-26.8024	15.5076	-1.9162	0.0831	2.70E-05
41	1	1.000	1.000	0.4755852	1.3073	0.0501	1.0000	0.0000	1.63E-01
42	1	1.000	1.000	0.4755852	1.3073	0.0510	1.0000	0.0000	1.63E-01
43	1	1.000	1.000	0.4755852	1.3073	0.0519	1.0000	0.0000	1.63E-01
44	1	1.000	1.000	0.4755852	1.3073	0.0528	1.0000	0.0000	1.63E-01
45	1	1.000	1.000	0.4755852	1.3073	0.0536	1.0000	0.0000	1.63E-01
46	1	1.000	1.000	0.4755852	1.3073	0.0544	1.0000	0.0000	1.63E-01
47	2	0.111	0.509	13.225596	-26.8024	15.5076	-1.9162	0.0937	2.70E-05
48	2	0.111	0.509	13.225596	-26.8024	15.5076	-1.9162	0.0953	2.70E-05
49	2	0.111	0.509	13.225596	-26.8024	15.5076	-1.9162	0.0969	2.70E-05
50	2	0.111	0.509	13.225596	-26.8024	15.5076	-1.9162	0.0985	2.70E-05
51	2	0.111	0.509	13.225596	-26.8024	15.5076	-1.9162	0.1000	2.70E-05
52	2	0.111	0.509	13.225596	-26.8024	15.5076	-1.9162	0.1018	2.70E-05
53	2	0.111	0.509	13.225596	-26.8024	15.5076	-1.9162	0.1037	2.70E-05
54	2	0.111	0.509	13.225596	-26.8024	15.5076	-1.9162	0.1055	2.70E-05
55	2	0.111	0.509	13.225596	-26.8024	15.5076	-1.9162	0.1073	2.70E-05
56	2	0.111	0.509	13.225596	-26.8024	15.5076	-1.9162	0.1091	2.70E-05
57	2	0.111	0.509	13.225596	-26.8024	15.5076	-1.9162	0.1108	2.70E-05
58	2	0.111	0.509	13.225596	-26.8024	15.5076	-1.9162	0.1124	2.70E-05
59	2	0.111	0.509	13.225596	-26.8024	15.5076	-1.9162	0.1140	2.70E-05
60	2	0.111	0.509	13.225596	-26.8024	15.5076	-1.9162	0.1156	2.70E-05
61	2	0.111	0.509	13.225596	-26.8024	15.5076	-1.9162	0.1171	2.70E-05
62	2	0.111	0.509	13.225596	-26.8024	15.5076	-1.9162	0.1185	2.70E-05
63	2	0.111	0.509	13.225596	-26.8024	15.5076	-1.9162	0.1199	2.70E-05
64	2	0.111	0.509	13.225596	-26.8024	15.5076	-1.9162	0.1213	2.70E-05
65	2	0.111	0.509	13.225596	-26.8024	15.5076	-1.9162	0.1227	2.70E-05
66	2	0.111	0.509	13.225596	-26.8024	15.5076	-1.9162	0.1240	2.70E-05
67	1	1.000	1.000	0.1984319	1.0000	0.0742	1.0000	0.0000	1.02E+01
68	1	1.000	1.000	0.1984319	1.0000	0.0751	1.0000	0.0000	1.02E+01
69	1	1.000	1.000	0.1984319	1.0000	0.0760	1.0000	0.0000	1.02E+01
70	1	1.000	1.000	0.1984319	1.3073	0.0769	1.0000	0.0000	1.63E-01

Table 6B.3: Input parameters for site Bay Area F total stress analysis (Ref Stress = 0.18; b = d = 0 all layers)

Layer	Name	Thick (m)	γ (kN/m3)	Vs (m/s)	Dmin	Ref Strain	B	s	P1	P2	P3
1	SM-SC	2	18.8	250	1.77	0.0228	1.65	0.915	0.67	0.288	3.25
2	CH	0.75	15	82	2.18	0.0946	1.545	0.795	0.746	0.266	2.35
3	CH	0.75	15.05	82	2.09	0.0954	1.56	0.795	0.736	0.252	2.5
4	CH	0.75	15.1	82	2.01	0.0960	1.545	0.795	0.736	0.252	2.505
5	CH	0.75	15.15	82	1.96	0.0968	1.575	0.81	0.744	0.27	2.15
6	CH	0.75	15.2	82	1.92	0.0920	1.56	0.825	0.714	0.252	2.495
7	CH	0.75	15.25	82	1.87	0.0854	1.455	0.825	0.704	0.244	2.75
8	CH	0.75	15.3	82	1.82	0.0986	1.575	0.81	0.724	0.248	2.5
9	CH	0.75	15.35	82	1.77	0.1006	1.56	0.81	0.736	0.258	2.2
10	CH	1.13	15.3	120	1.76	0.0838	1.53	0.93	0.61	0.224	3.25
11	CH	1.17	15.35	120	1.70	0.0874	1.515	0.915	0.618	0.22	3.15
12	CH	1.17	15.4	120	1.65	0.0932	1.545	0.915	0.622	0.224	2.95
13	CH	1.17	15.45	120	1.60	0.0962	1.515	0.9	0.628	0.22	3.05
14	CH	1.17	15.5	120	1.56	0.0996	1.5	0.885	0.638	0.218	2.95
15	CH	1.17	15.55	120	1.52	0.1030	1.5	0.885	0.644	0.224	2.7
16	CH	1.17	15.6	120	1.49	0.1078	1.5	0.87	0.668	0.234	2.35
17	CH	1.17	15.65	120	1.46	0.1126	1.515	0.87	0.682	0.246	2
18	CH	1.17	15.7	120	1.43	0.1132	1.47	0.855	0.658	0.214	2.65
19	CH	1.17	15.75	120	1.40	0.1194	1.5	0.855	0.678	0.234	2.2
20	CH	1.17	15.8	120	1.37	0.1222	1.47	0.84	0.698	0.24	2.05
21	CH	1.17	15.85	120	1.35	0.1256	1.47	0.84	0.704	0.246	1.895
22	CH	1.5	15.9	150	1.35	0.1178	1.53	0.915	0.618	0.216	2.8
23	CH	1.5	15.95	150	1.32	0.1236	1.545	0.9	0.642	0.226	2.4
24	CH	1.5	16	150	1.29	0.1258	1.53	0.9	0.644	0.228	2.3
25	CH	1.5	16.05	150	1.27	0.1300	1.515	0.885	0.634	0.208	2.75
26	CH	1.5	16.1	150	1.25	0.1320	1.5	0.885	0.638	0.214	2.65
27	CH	1.5	16.15	150	1.23	0.1376	1.53	0.885	0.638	0.214	2.5
28	CH	1.5	16.2	150	1.21	0.1390	1.5	0.87	0.664	0.224	2.105
29	CH	1.5	16.25	150	1.19	0.1408	1.485	0.87	0.674	0.234	1.9
30	CH	1.5	16.3	150	1.17	0.1450	1.485	0.855	0.688	0.234	1.8
31	CH	1.5	16.35	150	1.16	0.1482	1.485	0.855	0.702	0.246	1.55
32	CH	1.6	16.4	160	1.14	0.1480	1.5	0.87	0.658	0.216	2.1
33	CL	1.86	18	195	1.32	0.2020	1.53	0.93	0.594	0.19	2.55
34	CL	1.86	18	195	1.30	0.2108	1.545	0.93	0.598	0.194	2.4
35	CL	1.86	18	195	1.27	0.2146	1.515	0.915	0.622	0.204	2
36	CL	1.86	18	195	1.25	0.2218	1.53	0.915	0.624	0.206	1.85
37	CL	1.86	18	195	1.23	0.2276	1.515	0.9	0.662	0.226	1.35

38	CL	1.86	18	195	1.21	0.2340	1.515	0.9	0.668	0.234	1.3
39	CL	1.86	18	195	1.20	0.2396	1.5	0.885	0.636	0.192	1.75
40	CL	3.25	18	330	1.19	0.1834	1.56	1.11	0.582	0.28	1.95
41	CL	3.25	18	330	1.17	0.1862	1.53	1.11	0.582	0.28	1.9
42	CL	3.25	18	330	1.14	0.1946	1.545	1.095	0.584	0.28	2.2
43	CL	3.25	18	330	1.12	0.2016	1.545	1.08	0.584	0.264	1.9
44	CL	3.25	18	330	1.10	0.2046	1.515	1.065	0.584	0.26	2.2
45	SM-SC	3.25	18	330	0.82	0.1702	1.44	0.825	0.716	0.238	1.45
46	SM-SC	3.25	18	330	0.81	0.1774	1.455	0.825	0.724	0.248	1.35
47	SM-SC	3.25	18	330	0.79	0.2002	1.575	0.825	0.744	0.268	1.15
48	SM-SC	3.25	18	330	0.78	0.2056	1.56	0.81	0.714	0.228	1.5
49	SM-SC	3.25	18	330	0.77	0.2134	1.575	0.81	0.736	0.25	1.25
50	SM-SC	3.25	18	330	0.76	0.2162	1.545	0.795	0.746	0.244	1.2
51	CL	3.25	20.3	330	1.00	0.2376	1.515	1.035	0.584	0.24	2.25
52	CL	3.25	20.3	330	0.98	0.2418	1.5	1.035	0.584	0.24	2.25
53	CL	3.25	20.3	330	0.97	0.2472	1.485	1.02	0.59	0.23	2
54	CL	3.25	20.3	330	0.95	0.2576	1.5	1.005	0.584	0.22	2.4
55	CL	3.25	20.3	330	0.94	0.2614	1.485	1.005	0.584	0.22	2.35
56	CL	4.375	20.3	440	0.93	0.2136	1.515	1.185	0.586	0.32	1.77
57	CL	4.375	20.3	440	0.92	0.2180	1.5	1.17	0.58	0.3	1.55
58	CL	4.375	20.3	440	0.91	0.2214	1.485	1.17	0.58	0.3	1.55
59	CL	4.375	20.3	440	0.89	0.2294	1.5	1.155	0.582	0.3	1.75
60	CL	4.375	20.3	440	0.88	0.2358	1.5	1.14	0.592	0.296	1.5
61	CL	4.375	20.3	440	0.87	0.2368	1.47	1.14	0.59	0.294	1.5
62	CL	4.375	20.3	440	0.86	0.2452	1.485	1.125	0.582	0.28	1.7
63	CL	4.375	20.3	440	0.85	0.2584	1.53	1.11	0.584	0.28	1.95
64	CL	4.3	20.3	477	0.84	0.2386	1.485	1.17	0.58	0.3	1.55
65	CL	4.3	20.3	477	0.83	0.2440	1.485	1.155	0.584	0.3	1.75
66	CL	4.3	20.3	477	0.82	0.2506	1.5	1.155	0.584	0.3	1.745
67	CL	4.3	20.3	477	0.81	0.2540	1.485	1.14	0.586	0.288	1.5
68	CL	4.3	20.3	477	0.81	0.2572	1.47	1.125	0.582	0.28	1.7
69	CL	4.3	20.3	477	0.80	0.2640	1.485	1.125	0.582	0.28	1.7
70	CL	4.3	20.3	477	0.79	0.2794	1.545	1.11	0.584	0.28	1.95
71	GW	4.9	21	580	0.60	0.2566	1.47	0.855	0.684	0.208	1.7
72	GW	5	21	580	0.59	0.2648	1.47	0.84	0.7	0.204	1.5
73	GW	5	21	580	0.58	0.2708	1.47	0.84	0.706	0.212	1.45
74	SM-SC	5	21	580	0.58	0.2758	1.455	0.825	0.678	0.174	2.1

Table 6B.4: Input parameters for site Bay Area F effective stress analysis (Max Ru = 0.95 all layers)

Layer	Model	f/s/f	p/r/Dr	F/A/FC	s/B/-	g/C/-	v/D/v	-/g/-	$C_v(m^2/s)$
1	1	1.000	1.000	0.7313377	1.3073	0.0067	1.0000	0.0000	1.63E-01
2	2	0.048	0.425	11.183198	-21.3223	11.2115	-1.0579	0.0246	3.91E-06
3	2	0.054	0.444	11.989503	-23.4457	12.8273	-1.3537	0.0247	3.91E-06
4	2	0.058	0.456	12.530345	-24.8997	13.9698	-1.5827	0.0251	3.91E-06
5	2	0.064	0.471	13.225596	-26.8024	15.5076	-1.9162	0.0252	3.91E-06
6	2	0.072	0.491	14.179158	-29.4716	17.7426	-2.4520	0.0249	3.91E-06
7	2	0.076	0.502	14.678789	-30.8967	18.9715	-2.7719	0.0252	3.91E-06
8	2	0.077	0.505	14.818775	-31.2992	19.3229	-2.8667	0.0259	3.91E-06
9	2	0.079	0.508	14.965894	-31.7237	19.6957	-2.9687	0.0265	3.91E-06
10	2	0.080	0.511	15.12083	-32.1724	20.0919	-3.0790	0.0273	3.91E-06
11	2	0.080	0.511	15.12083	-32.1724	20.0919	-3.0790	0.0284	3.91E-06
12	2	0.080	0.511	15.12083	-32.1724	20.0919	-3.0790	0.0294	3.91E-06
13	2	0.080	0.511	15.12083	-32.1724	20.0919	-3.0790	0.0304	3.91E-06
14	2	0.080	0.511	15.12083	-32.1724	20.0919	-3.0790	0.0313	3.91E-06
15	2	0.080	0.511	15.12083	-32.1724	20.0919	-3.0790	0.0322	3.91E-06
16	2	0.080	0.511	15.12083	-32.1724	20.0919	-3.0790	0.0331	3.91E-06
17	2	0.080	0.511	15.12083	-32.1724	20.0919	-3.0790	0.0339	3.91E-06
18	2	0.080	0.511	15.12083	-32.1724	20.0919	-3.0790	0.0347	3.91E-06
19	2	0.080	0.511	15.12083	-32.1724	20.0919	-3.0790	0.0355	3.91E-06
20	2	0.080	0.511	15.12083	-32.1724	20.0919	-3.0790	0.0362	3.91E-06
21	2	0.080	0.511	15.12083	-32.1724	20.0919	-3.0790	0.0370	3.91E-06
22	2	0.082	0.514	15.284368	-32.6478	20.5142	-3.1986	0.0375	3.91E-06
23	2	0.082	0.514	15.284368	-32.6478	20.5142	-3.1986	0.0383	3.91E-06
24	2	0.082	0.514	15.284368	-32.6478	20.5142	-3.1986	0.0392	3.91E-06
25	2	0.082	0.514	15.284368	-32.6478	20.5142	-3.1986	0.0400	3.91E-06
26	2	0.082	0.514	15.284368	-32.6478	20.5142	-3.1986	0.0408	3.91E-06
27	2	0.082	0.514	15.284368	-32.6478	20.5142	-3.1986	0.0415	3.91E-06
28	2	0.082	0.514	15.284368	-32.6478	20.5142	-3.1986	0.0423	3.91E-06
29	2	0.082	0.514	15.284368	-32.6478	20.5142	-3.1986	0.0430	3.91E-06
30	2	0.082	0.514	15.284368	-32.6478	20.5142	-3.1986	0.0437	3.91E-06
31	2	0.082	0.514	15.284368	-32.6478	20.5142	-3.1986	0.0444	3.91E-06
32	2	0.082	0.514	15.284368	-32.6478	20.5142	-3.1986	0.0451	3.91E-06
33	2	0.111	0.509	13.225596	-26.8024	15.5076	-1.9162	0.0664	2.70E-05
34	2	0.111	0.509	13.225596	-26.8024	15.5076	-1.9162	0.0678	2.70E-05
35	2	0.111	0.509	13.225596	-26.8024	15.5076	-1.9162	0.0692	2.70E-05
36	2	0.111	0.509	13.225596	-26.8024	15.5076	-1.9162	0.0705	2.70E-05
37	2	0.111	0.509	13.225596	-26.8024	15.5076	-1.9162	0.0718	2.70E-05
38	2	0.111	0.509	13.225596	-26.8024	15.5076	-1.9162	0.0731	2.70E-05
39	2	0.111	0.509	13.225596	-26.8024	15.5076	-1.9162	0.0743	2.70E-05

40	2	0.111	0.509	13.225596	-26.8024	15.5076	-1.9162	0.0759	2.70E-05
41	2	0.111	0.509	13.225596	-26.8024	15.5076	-1.9162	0.0778	2.70E-05
42	2	0.111	0.509	13.225596	-26.8024	15.5076	-1.9162	0.0796	2.70E-05
43	2	0.111	0.509	13.225596	-26.8024	15.5076	-1.9162	0.0814	2.70E-05
44	2	0.111	0.509	13.225596	-26.8024	15.5076	-1.9162	0.0831	2.70E-05
45	1	1.000	1.000	0.4755852	1.3073	0.0501	1.0000	0.0000	1.63E-01
46	1	1.000	1.000	0.4755852	1.3073	0.0510	1.0000	0.0000	1.63E-01
47	1	1.000	1.000	0.4755852	1.3073	0.0519	1.0000	0.0000	1.63E-01
48	1	1.000	1.000	0.4755852	1.3073	0.0528	1.0000	0.0000	1.63E-01
49	1	1.000	1.000	0.4755852	1.3073	0.0536	1.0000	0.0000	1.63E-01
50	1	1.000	1.000	0.4755852	1.3073	0.0544	1.0000	0.0000	1.63E-01
51	2	0.111	0.509	13.225596	-26.8024	15.5076	-1.9162	0.0937	2.70E-05
52	2	0.111	0.509	13.225596	-26.8024	15.5076	-1.9162	0.0953	2.70E-05
53	2	0.111	0.509	13.225596	-26.8024	15.5076	-1.9162	0.0969	2.70E-05
54	2	0.111	0.509	13.225596	-26.8024	15.5076	-1.9162	0.0985	2.70E-05
55	2	0.111	0.509	13.225596	-26.8024	15.5076	-1.9162	0.1000	2.70E-05
56	2	0.111	0.509	13.225596	-26.8024	15.5076	-1.9162	0.1018	2.70E-05
57	2	0.111	0.509	13.225596	-26.8024	15.5076	-1.9162	0.1037	2.70E-05
58	2	0.111	0.509	13.225596	-26.8024	15.5076	-1.9162	0.1055	2.70E-05
59	2	0.111	0.509	13.225596	-26.8024	15.5076	-1.9162	0.1073	2.70E-05
60	2	0.111	0.509	13.225596	-26.8024	15.5076	-1.9162	0.1091	2.70E-05
61	2	0.111	0.509	13.225596	-26.8024	15.5076	-1.9162	0.1108	2.70E-05
62	2	0.111	0.509	13.225596	-26.8024	15.5076	-1.9162	0.1124	2.70E-05
63	2	0.111	0.509	13.225596	-26.8024	15.5076	-1.9162	0.1140	2.70E-05
64	2	0.111	0.509	13.225596	-26.8024	15.5076	-1.9162	0.1156	2.70E-05
65	2	0.111	0.509	13.225596	-26.8024	15.5076	-1.9162	0.1171	2.70E-05
66	2	0.111	0.509	13.225596	-26.8024	15.5076	-1.9162	0.1185	2.70E-05
67	2	0.111	0.509	13.225596	-26.8024	15.5076	-1.9162	0.1199	2.70E-05
68	2	0.111	0.509	13.225596	-26.8024	15.5076	-1.9162	0.1213	2.70E-05
69	2	0.111	0.509	13.225596	-26.8024	15.5076	-1.9162	0.1227	2.70E-05
70	2	0.111	0.509	13.225596	-26.8024	15.5076	-1.9162	0.1240	2.70E-05
71	1	1.000	1.000	0.1984319	1.0000	0.0742	1.0000	0.0000	1.02E+01
72	1	1.000	1.000	0.1984319	1.0000	0.0751	1.0000	0.0000	1.02E+01
73	1	1.000	1.000	0.1984319	1.0000	0.0760	1.0000	0.0000	1.02E+01
74	1	1.000	1.000	0.1984319	1.3073	0.0769	1.0000	0.0000	1.63E-01

Table 6B.5: Input parameters for site Bay Area II total stress analysis (Ref Stress = 0.18; b = d = 0 all layers)

Layer	Name	Thick (m)	γ (kN/m3)	Vs (m/s)	Dmin	Ref Strain	B	s	P1	P2	P3
1	SM-SC	1	18	200	2.18	0.0160	1.47	0.87	0.714	0.296	3.25
2	OH	0.25	10.56	25	7.45	0.3440	1.485	0.585	0.996	0.38	1.35
3	OH	0.25	10.56	25	7.45	0.3440	1.485	0.585	0.996	0.38	1.35
4	OH	0.25	10.56	25	7.45	0.3440	1.485	0.585	0.996	0.38	1.35
5	OH	0.25	10.56	25	7.45	0.3440	1.485	0.585	0.996	0.38	1.35
6	OH	0.25	10.61	27.8	6.62	0.2814	1.5	0.6	0.996	0.38	1.32
7	OH	0.25	10.61	27.8	6.62	0.2814	1.5	0.6	0.996	0.38	1.32
8	OH	0.25	10.61	27.8	6.62	0.2814	1.5	0.6	0.996	0.38	1.32
9	OH	0.25	10.61	27.8	6.62	0.2814	1.5	0.6	0.996	0.38	1.32
10	OH	0.25	10.65	30.5	6.13	0.2628	1.53	0.615	0.998	0.398	1.3
11	OH	0.25	10.65	30.5	6.13	0.2628	1.53	0.615	0.998	0.398	1.3
12	OH	0.25	10.65	30.5	6.13	0.2628	1.53	0.615	0.998	0.398	1.3
13	OH	0.25	10.65	30.5	6.13	0.2628	1.53	0.615	0.998	0.398	1.3
14	OH	0.33	10.7	33.3	5.86	0.2460	1.545	0.63	0.992	0.398	1.225
15	OH	0.33	10.7	33.3	5.86	0.2460	1.545	0.63	0.992	0.398	1.225
16	OH	0.33	10.7	33.3	5.86	0.2460	1.545	0.63	0.992	0.398	1.225
17	OH	0.34	10.76	36	5.65	0.2422	1.56	0.645	0.962	0.374	1.25
18	OH	0.34	10.76	36	5.65	0.2422	1.56	0.645	0.962	0.374	1.25
19	OH	0.33	10.76	36	5.65	0.2422	1.56	0.645	0.962	0.374	1.25
20	OH	0.33	10.82	38.8	5.51	0.2380	1.59	0.66	0.922	0.338	1.25
21	OH	0.33	10.82	38.8	5.51	0.2380	1.59	0.66	0.922	0.338	1.25
22	OH	0.34	10.82	38.8	5.51	0.2380	1.59	0.66	0.922	0.338	1.25
23	OH	0.33	10.9	41.5	5.36	0.1958	1.425	0.675	0.902	0.326	1.2
24	OH	0.33	10.9	41.5	5.36	0.1958	1.425	0.675	0.902	0.326	1.2
25	OH	0.34	10.9	41.5	5.36	0.1958	1.425	0.675	0.902	0.326	1.2
26	OH	0.33	10.99	44.3	5.23	0.1976	1.455	0.69	0.856	0.29	1.35
27	OH	0.33	10.99	44.3	5.23	0.1976	1.455	0.69	0.856	0.29	1.35
28	OH	0.34	10.99	44.3	5.23	0.1976	1.455	0.69	0.856	0.29	1.35
29	OH	0.33	11.09	47	5.13	0.1958	1.455	0.705	0.856	0.296	1.195
30	OH	0.33	11.09	47	5.13	0.1958	1.455	0.705	0.856	0.296	1.195
31	OH	0.34	11.09	47	5.13	0.1958	1.455	0.705	0.856	0.296	1.195
32	OH	0.5	11.21	50	5.04	0.1956	1.47	0.72	0.852	0.3	1.1
33	OH	0.5	11.21	50	5.04	0.1956	1.47	0.72	0.852	0.3	1.1
34	CH	0.9	14.18	90	2.93	0.1138	1.575	0.795	0.738	0.254	2.2
35	CH	1	14.34	102	2.58	0.1036	1.575	0.81	0.724	0.248	2.345
36	CH	1.1	14.5	114	2.36	0.0922	1.485	0.84	0.706	0.252	2.3
37	CH	1.25	14.68	126	2.22	0.0914	1.485	0.87	0.65	0.222	3.1
38	CH	1.5	15.09	150	2.07	0.0896	1.545	0.93	0.608	0.222	3.25
39	CL	2	18	200	1.95	0.1552	1.545	0.915	0.614	0.208	2.55
40	CL	2.1	18.1	215	1.70	0.1304	1.485	0.885	0.638	0.214	2.55
41	CL	2.15	18.2	230	1.57	0.1286	1.485	0.885	0.636	0.212	2.6
42	CL	2.5	18.35	252.7	1.46	0.1334	1.53	0.9	0.642	0.226	2.25
43	CL	2.5	18.45	270.4	1.39	0.1380	1.53	0.915	0.6	0.198	3.15
44	CL	3	18.6	300	1.33	0.1402	1.53	0.945	0.588	0.202	2.92
45	CL	1	18.7	320	1.29	0.1444	1.545	0.96	0.596	0.218	2.6

Table 6B.6: Input parameters for site Bay Area II effective stress analysis (Max Ru = 0.95 all layers)

Layer	Model	f/s/f	p/r/Dr	F/A/FC	s/B/-	g/C/-	v/D/v	-/g/-	$C_v(m^2/s)$
1	1	1.000	1.000	1.0335	1.3073	0.0051	1.0000	0.0000	1.63E-01
2	2	0.022	0.423	14.9659	-31.7237	19.6957	-2.9687	0.0458	1.63E-07
3	2	0.022	0.423	14.9659	-31.7237	19.6957	-2.9687	0.0462	1.63E-07
4	2	0.022	0.423	14.9659	-31.7237	19.6957	-2.9687	0.0465	1.63E-07
5	2	0.022	0.423	14.9659	-31.7237	19.6957	-2.9687	0.0469	1.63E-07
6	2	0.025	0.435	15.2844	-32.6478	20.5142	-3.1986	0.0412	2.36E-07
7	2	0.025	0.435	15.2844	-32.6478	20.5142	-3.1986	0.0415	2.36E-07
8	2	0.025	0.435	15.2844	-32.6478	20.5142	-3.1986	0.0418	2.36E-07
9	2	0.025	0.435	15.2844	-32.6478	20.5142	-3.1986	0.0421	2.36E-07
10	2	0.027	0.442	15.4574	-33.1529	20.9658	-3.3287	0.0394	2.90E-07
11	2	0.027	0.442	15.4574	-33.1529	20.9658	-3.3287	0.0397	2.90E-07
12	2	0.027	0.442	15.4574	-33.1529	20.9658	-3.3287	0.0400	2.90E-07
13	2	0.027	0.442	15.4574	-33.1529	20.9658	-3.3287	0.0403	2.90E-07
14	2	0.028	0.447	7.6451	-14.7174	6.3800	0.6922	0.0388	3.24E-07
15	2	0.028	0.447	7.6451	-14.7174	6.3800	0.6922	0.0392	3.24E-07
16	2	0.028	0.447	7.6451	-14.7174	6.3800	0.6922	0.0396	3.24E-07
17	2	0.029	0.448	7.6451	-14.7174	6.3800	0.6922	0.0393	3.42E-07
18	2	0.029	0.448	7.6451	-14.7174	6.3800	0.6922	0.0397	3.42E-07
19	2	0.029	0.448	7.6451	-14.7174	6.3800	0.6922	0.0400	3.42E-07
20	2	0.029	0.449	7.6451	-14.7174	6.3800	0.6922	0.0401	3.52E-07
21	2	0.029	0.449	7.6451	-14.7174	6.3800	0.6922	0.0404	3.52E-07
22	2	0.029	0.449	7.6451	-14.7174	6.3800	0.6922	0.0408	3.52E-07
23	2	0.029	0.449	7.6451	-14.7174	6.3800	0.6922	0.0410	3.57E-07
24	2	0.029	0.449	7.6451	-14.7174	6.3800	0.6922	0.0414	3.57E-07
25	2	0.029	0.449	7.6451	-14.7174	6.3800	0.6922	0.0418	3.57E-07
26	2	0.029	0.449	7.6451	-14.7174	6.3800	0.6922	0.0420	3.60E-07
27	2	0.029	0.449	7.6451	-14.7174	6.3800	0.6922	0.0424	3.60E-07
28	2	0.029	0.449	7.6451	-14.7174	6.3800	0.6922	0.0428	3.60E-07
29	2	0.029	0.449	7.6451	-14.7174	6.3800	0.6922	0.0432	3.61E-07
30	2	0.029	0.449	7.6451	-14.7174	6.3800	0.6922	0.0436	3.61E-07
31	2	0.029	0.449	7.6451	-14.7174	6.3800	0.6922	0.0440	3.61E-07
32	2	0.029	0.449	7.6451	-14.7174	6.3800	0.6922	0.0444	3.63E-07
33	2	0.029	0.449	7.6451	-14.7174	6.3800	0.6922	0.0450	3.63E-07
34	2	0.047	0.466	14.4179	-30.1503	18.3248	-2.6013	0.0287	3.04E-06
35	2	0.055	0.479	14.6788	-30.8967	18.9715	-2.7719	0.0272	4.68E-06
36	2	0.060	0.487	14.8188	-31.2992	19.3229	-2.8667	0.0272	5.96E-06
37	2	0.063	0.491	14.8914	-31.5086	19.5065	-2.9167	0.0280	6.79E-06
38	2	0.066	0.495	14.9659	-31.7237	19.6957	-2.9687	0.0288	7.78E-06
39	2	0.076	0.445	10.5953	-19.8086	10.0997	-0.8738	0.0486	1.00E-04
40	2	0.142	0.513	12.2446	-24.1287	13.3604	-1.4586	0.0410	3.72E-04
41	2	0.178	0.540	12.9419	-26.0214	14.8707	-1.7746	0.0405	5.86E-04
42	2	0.191	0.549	13.1884	-26.6996	15.4233	-1.8972	0.0416	6.79E-04
43	2	0.193	0.551	13.2256	-26.8024	15.5076	-1.9162	0.0442	6.94E-04
44	2	0.193	0.551	13.2256	-26.8024	15.5076	-1.9162	0.0469	6.94E-04
45	2	0.193	0.551	13.2256	-26.8024	15.5076	-1.9162	0.0487	6.94E-04

Table 6B.7: Input parameters site Bay Area II K total stress analysis (Ref Stress = 0.18; b = d = 0 all layers)

Layer	Name	Thick (m)	γ (kN/m3)	Vs (m/s)	Dmin	Ref Strain	B	s	P1	P2	P3
1	SM-SC	1	18	200	2.18	0.0160	1.47	0.87	0.714	0.296	3.25
2	OH	0.25	10.56	25	3.52	0.3200	0.315	1.02	0.66	0.4	1.05
3	OH	0.25	10.56	25	3.52	0.3200	0.315	1.02	0.66	0.4	1.05
4	OH	0.25	10.56	25	3.52	0.3200	0.315	1.02	0.66	0.4	1.05
5	OH	0.25	10.56	25	3.52	0.3200	0.315	1.02	0.66	0.4	1.05
6	OH	0.25	10.61	27.8	3.51	0.2710	0.3	1.05	0.656	0.4	1.02
7	OH	0.25	10.61	27.8	3.51	0.2710	0.3	1.05	0.656	0.4	1.02
8	OH	0.25	10.61	27.8	3.51	0.2710	0.3	1.05	0.656	0.4	1.02
9	OH	0.25	10.61	27.8	3.51	0.2710	0.3	1.05	0.656	0.4	1.02
10	OH	0.25	10.65	30.5	3.49	0.2500	0.3	1.05	0.658	0.4	1.05
11	OH	0.25	10.65	30.5	3.49	0.2500	0.3	1.05	0.658	0.4	1.05
12	OH	0.25	10.65	30.5	3.49	0.2500	0.3	1.05	0.658	0.4	1.05
13	OH	0.25	10.65	30.5	3.49	0.2500	0.3	1.05	0.658	0.4	1.05
14	OH	0.33	10.7	33.3	3.48	0.3420	0.45	1.065	0.66	0.4	1
15	OH	0.33	10.7	33.3	3.48	0.3420	0.45	1.065	0.66	0.4	1
16	OH	0.33	10.7	33.3	3.48	0.3420	0.45	1.065	0.66	0.4	1
17	OH	0.34	10.76	36	3.47	0.3444	0.435	1.095	0.638	0.4	1.3
18	OH	0.34	10.76	36	3.47	0.3444	0.435	1.095	0.638	0.4	1.3
19	OH	0.33	10.76	36	3.47	0.3444	0.435	1.095	0.638	0.4	1.3
20	OH	0.33	10.82	38.8	3.45	0.3240	0.435	1.11	0.64	0.4	1.25
21	OH	0.33	10.82	38.8	3.45	0.3240	0.435	1.11	0.64	0.4	1.25
22	OH	0.34	10.82	38.8	3.45	0.3240	0.435	1.11	0.64	0.4	1.25
23	OH	0.33	10.9	41.5	3.43	0.3046	0.435	1.11	0.654	0.4	1.1
24	OH	0.33	10.9	41.5	3.43	0.3046	0.435	1.11	0.654	0.4	1.1
25	OH	0.34	10.9	41.5	3.43	0.3046	0.435	1.11	0.654	0.4	1.1
26	OH	0.33	10.99	44.3	3.41	0.3140	0.48	1.125	0.652	0.4	1.08
27	OH	0.33	10.99	44.3	3.41	0.3140	0.48	1.125	0.652	0.4	1.08
28	OH	0.34	10.99	44.3	3.41	0.3140	0.48	1.125	0.652	0.4	1.08
29	OH	0.33	11.09	47	3.40	0.2980	0.48	1.125	0.658	0.4	1.05
30	OH	0.33	11.09	47	3.40	0.2980	0.48	1.125	0.658	0.4	1.05
31	OH	0.34	11.09	47	3.40	0.2980	0.48	1.125	0.658	0.4	1.05
32	OH	0.5	11.21	50	3.38	0.2760	0.465	1.14	0.656	0.4	1.02
33	OH	0.5	11.21	50	3.38	0.2760	0.465	1.14	0.656	0.4	1.02
34	CH	0.9	14.18	90	2.93	0.1138	1.575	0.795	0.738	0.254	2.2
35	CH	1	14.34	102	2.58	0.1036	1.575	0.81	0.724	0.248	2.345
36	CH	1.1	14.5	114	2.36	0.0922	1.485	0.84	0.706	0.252	2.3
37	CH	1.25	14.68	126	2.22	0.0914	1.485	0.87	0.65	0.222	3.1
38	CH	1.5	15.09	150	2.07	0.0896	1.545	0.93	0.608	0.222	3.25
39	CL	2	18	200	1.95	0.1552	1.545	0.915	0.614	0.208	2.55
40	CL	2.1	18.1	215	1.70	0.1304	1.485	0.885	0.638	0.214	2.55
41	CL	2.15	18.2	230	1.57	0.1286	1.485	0.885	0.636	0.212	2.6
42	CL	2.5	18.35	252.7	1.46	0.1334	1.53	0.9	0.642	0.226	2.25
43	CL	2.5	18.45	270.4	1.39	0.1380	1.53	0.915	0.6	0.198	3.15
44	CL	3	18.6	300	1.33	0.1402	1.53	0.945	0.588	0.202	2.92
45	CL	1	18.7	320	1.29	0.1444	1.545	0.96	0.596	0.218	2.6

Table 6B.8: Input parameters for site Bay Area II K effective stress analysis (Max Ru = 0.95 all layers)

Layer	Model	f/s/f	p/r/Dr	F/A/FC	s/B/-	g/C/-	v/D/v	-/g/-	$C_v(m^2/s)$
1	1	1.000	1.000	1.0335	1.3073	0.0051	1.0000	0.0000	1.63E-01
2	2	0.022	0.423	14.9659	-31.7237	19.6957	-2.9687	0.0458	1.63E-07
3	2	0.022	0.423	14.9659	-31.7237	19.6957	-2.9687	0.0462	1.63E-07
4	2	0.022	0.423	14.9659	-31.7237	19.6957	-2.9687	0.0465	1.63E-07
5	2	0.022	0.423	14.9659	-31.7237	19.6957	-2.9687	0.0469	1.63E-07
6	2	0.025	0.435	15.2844	-32.6478	20.5142	-3.1986	0.0412	2.36E-07
7	2	0.025	0.435	15.2844	-32.6478	20.5142	-3.1986	0.0415	2.36E-07
8	2	0.025	0.435	15.2844	-32.6478	20.5142	-3.1986	0.0418	2.36E-07
9	2	0.025	0.435	15.2844	-32.6478	20.5142	-3.1986	0.0421	2.36E-07
10	2	0.027	0.442	15.4574	-33.1529	20.9658	-3.3287	0.0394	2.90E-07
11	2	0.027	0.442	15.4574	-33.1529	20.9658	-3.3287	0.0397	2.90E-07
12	2	0.027	0.442	15.4574	-33.1529	20.9658	-3.3287	0.0400	2.90E-07
13	2	0.027	0.442	15.4574	-33.1529	20.9658	-3.3287	0.0403	2.90E-07
14	2	0.028	0.447	7.6451	-14.7174	6.3800	0.6922	0.0388	3.24E-07
15	2	0.028	0.447	7.6451	-14.7174	6.3800	0.6922	0.0392	3.24E-07
16	2	0.028	0.447	7.6451	-14.7174	6.3800	0.6922	0.0396	3.24E-07
17	2	0.029	0.448	7.6451	-14.7174	6.3800	0.6922	0.0393	3.42E-07
18	2	0.029	0.448	7.6451	-14.7174	6.3800	0.6922	0.0397	3.42E-07
19	2	0.029	0.448	7.6451	-14.7174	6.3800	0.6922	0.0400	3.42E-07
20	2	0.029	0.449	7.6451	-14.7174	6.3800	0.6922	0.0401	3.52E-07
21	2	0.029	0.449	7.6451	-14.7174	6.3800	0.6922	0.0404	3.52E-07
22	2	0.029	0.449	7.6451	-14.7174	6.3800	0.6922	0.0408	3.52E-07
23	2	0.029	0.449	7.6451	-14.7174	6.3800	0.6922	0.0410	3.57E-07
24	2	0.029	0.449	7.6451	-14.7174	6.3800	0.6922	0.0414	3.57E-07
25	2	0.029	0.449	7.6451	-14.7174	6.3800	0.6922	0.0418	3.57E-07
26	2	0.029	0.449	7.6451	-14.7174	6.3800	0.6922	0.0420	3.60E-07
27	2	0.029	0.449	7.6451	-14.7174	6.3800	0.6922	0.0424	3.60E-07
28	2	0.029	0.449	7.6451	-14.7174	6.3800	0.6922	0.0428	3.60E-07
29	2	0.029	0.449	7.6451	-14.7174	6.3800	0.6922	0.0432	3.61E-07
30	2	0.029	0.449	7.6451	-14.7174	6.3800	0.6922	0.0436	3.61E-07
31	2	0.029	0.449	7.6451	-14.7174	6.3800	0.6922	0.0440	3.61E-07
32	2	0.029	0.449	7.6451	-14.7174	6.3800	0.6922	0.0444	3.63E-07
33	2	0.029	0.449	7.6451	-14.7174	6.3800	0.6922	0.0450	3.63E-07
34	2	0.047	0.466	14.4179	-30.1503	18.3248	-2.6013	0.0287	3.04E-06
35	2	0.055	0.479	14.6788	-30.8967	18.9715	-2.7719	0.0272	4.68E-06
36	2	0.060	0.487	14.8188	-31.2992	19.3229	-2.8667	0.0272	5.96E-06
37	2	0.063	0.491	14.8914	-31.5086	19.5065	-2.9167	0.0280	6.79E-06
38	2	0.066	0.495	14.9659	-31.7237	19.6957	-2.9687	0.0288	7.78E-06
39	2	0.076	0.445	10.5953	-19.8086	10.0997	-0.8738	0.0486	1.00E-04
40	2	0.142	0.513	12.2446	-24.1287	13.3604	-1.4586	0.0410	3.72E-04
41	2	0.178	0.540	12.9419	-26.0214	14.8707	-1.7746	0.0405	5.86E-04
42	2	0.191	0.549	13.1884	-26.6996	15.4233	-1.8972	0.0416	6.79E-04
43	2	0.193	0.551	13.2256	-26.8024	15.5076	-1.9162	0.0442	6.94E-04
44	2	0.193	0.551	13.2256	-26.8024	15.5076	-1.9162	0.0469	6.94E-04
45	2	0.193	0.551	13.2256	-26.8024	15.5076	-1.9162	0.0487	6.94E-04

Table 6B.9: Inputs for site Bay Area II K S2 total stress analysis (Ref Stress = 0.18; b = d = 0 all layers)

Layer	Name	Thick (m)	γ (kN/m3)	Vs (m/s)	Dmin	Ref Strain	B	s	P1	P2	P3
1	SM-SC	1	18	200	2.18	0.0160	1.47	0.87	0.714	0.296	3.25
2	OH	0.25	10.56	25	3.51	0.3140	0.27	0.84	0.758	0.4	0.575
3	OH	0.25	10.56	25	3.51	0.3140	0.27	0.84	0.758	0.4	0.575
4	OH	0.25	10.56	25	3.51	0.3140	0.27	0.84	0.758	0.4	0.575
5	OH	0.25	10.56	25	3.51	0.3140	0.27	0.84	0.758	0.4	0.575
6	OH	0.25	10.61	27.8	3.51	0.3264	0.315	0.855	0.758	0.4	0.57
7	OH	0.25	10.61	27.8	3.51	0.3264	0.315	0.855	0.758	0.4	0.57
8	OH	0.25	10.61	27.8	3.51	0.3264	0.315	0.855	0.758	0.4	0.57
9	OH	0.25	10.61	27.8	3.51	0.3264	0.315	0.855	0.758	0.4	0.57
10	OH	0.25	10.65	30.5	3.49	0.3040	0.315	0.87	0.754	0.4	0.57
11	OH	0.25	10.65	30.5	3.49	0.3040	0.315	0.87	0.754	0.4	0.57
12	OH	0.25	10.65	30.5	3.49	0.3040	0.315	0.87	0.754	0.4	0.57
13	OH	0.25	10.65	30.5	3.49	0.3040	0.315	0.87	0.754	0.4	0.57
14	OH	0.33	10.7	33.3	3.48	0.2766	0.3	0.9	0.736	0.4	0.615
15	OH	0.33	10.7	33.3	3.48	0.2766	0.3	0.9	0.736	0.4	0.615
16	OH	0.33	10.7	33.3	3.48	0.2766	0.3	0.9	0.736	0.4	0.615
17	OH	0.34	10.76	36	3.46	0.2580	0.3	0.9	0.74	0.398	0.615
18	OH	0.34	10.76	36	3.46	0.2580	0.3	0.9	0.74	0.398	0.615
19	OH	0.33	10.76	36	3.46	0.2580	0.3	0.9	0.74	0.398	0.615
20	OH	0.33	10.82	38.8	3.45	0.2438	0.3	0.915	0.738	0.4	0.605
21	OH	0.33	10.82	38.8	3.45	0.2438	0.3	0.915	0.738	0.4	0.605
22	OH	0.34	10.82	38.8	3.45	0.2438	0.3	0.915	0.738	0.4	0.605
23	OH	0.33	10.9	41.5	3.43	0.2298	0.3	0.915	0.74	0.396	0.605
24	OH	0.33	10.9	41.5	3.43	0.2298	0.3	0.915	0.74	0.396	0.605
25	OH	0.34	10.9	41.5	3.43	0.2298	0.3	0.915	0.74	0.396	0.605
26	OH	0.33	10.99	44.3	3.41	0.3320	0.435	0.945	0.716	0.394	0.7
27	OH	0.33	10.99	44.3	3.41	0.3320	0.435	0.945	0.716	0.394	0.7
28	OH	0.34	10.99	44.3	3.41	0.3320	0.435	0.945	0.716	0.394	0.7
29	OH	0.33	11.09	47	3.39	0.3140	0.435	0.945	0.738	0.4	0.58
30	OH	0.33	11.09	47	3.39	0.3140	0.435	0.945	0.738	0.4	0.58
31	OH	0.34	11.09	47	3.39	0.3140	0.435	0.945	0.738	0.4	0.58
32	OH	0.5	11.21	50	3.38	0.2990	0.435	0.96	0.732	0.4	0.59
33	OH	0.5	11.21	50	3.38	0.2990	0.435	0.96	0.732	0.4	0.59
34	CH	0.9	14.18	90	2.85	0.1318	1.425	0.675	0.914	0.348	1.7
35	CH	1	14.34	102	2.51	0.1192	1.455	0.705	0.874	0.33	1.785
36	CH	1.1	14.5	114	2.31	0.1140	1.5	0.735	0.82	0.296	1.9
37	CH	1.25	14.68	126	2.17	0.1152	1.515	0.75	0.796	0.274	1.985
38	CH	1.5	15.09	150	2.03	0.1084	1.56	0.81	0.722	0.246	2.25
39	CL	2	18	200	1.92	0.1956	1.53	0.78	0.736	0.23	1.55
40	CL	2.1	18.1	215	1.66	0.1712	1.53	0.765	0.806	0.292	1.25
41	CL	2.15	18.2	230	1.53	0.1686	1.53	0.765	0.798	0.282	1.3
42	CL	2.5	18.35	252.7	1.43	0.1658	1.53	0.78	0.766	0.264	1.4
43	CL	2.5	18.45	270.4	1.36	0.1770	1.56	0.795	0.762	0.266	1.3
44	CL	3	18.6	300	1.31	0.1802	1.575	0.825	0.746	0.272	1.25
45	CL	1	18.7	320	1.27	0.1674	1.47	0.84	0.7	0.238	1.6

Table 6B.10: Input parameters for site Bay Area II K S2 effective stress analysis (Max Ru = 0.95 all layers)

Layer	Model	f/s/f	p/r/Dr	F/A/FC	s/B/-	g/C/-	v/D/v	-/g/-	$C_v(m^2/s)$
1	1	1.000	1.000	1.0335	1.3073	0.0051	1.0000	0.0000	1.63E-01
2	2	0.022	0.423	14.9659	-31.7237	19.6957	-2.9687	0.0458	1.63E-07
3	2	0.022	0.423	14.9659	-31.7237	19.6957	-2.9687	0.0462	1.63E-07
4	2	0.022	0.423	14.9659	-31.7237	19.6957	-2.9687	0.0465	1.63E-07
5	2	0.022	0.423	14.9659	-31.7237	19.6957	-2.9687	0.0469	1.63E-07
6	2	0.025	0.435	15.2844	-32.6478	20.5142	-3.1986	0.0412	2.36E-07
7	2	0.025	0.435	15.2844	-32.6478	20.5142	-3.1986	0.0415	2.36E-07
8	2	0.025	0.435	15.2844	-32.6478	20.5142	-3.1986	0.0418	2.36E-07
9	2	0.025	0.435	15.2844	-32.6478	20.5142	-3.1986	0.0421	2.36E-07
10	2	0.027	0.442	15.4574	-33.1529	20.9658	-3.3287	0.0394	2.90E-07
11	2	0.027	0.442	15.4574	-33.1529	20.9658	-3.3287	0.0397	2.90E-07
12	2	0.027	0.442	15.4574	-33.1529	20.9658	-3.3287	0.0400	2.90E-07
13	2	0.027	0.442	15.4574	-33.1529	20.9658	-3.3287	0.0403	2.90E-07
14	2	0.028	0.447	7.6451	-14.7174	6.3800	0.6922	0.0388	3.24E-07
15	2	0.028	0.447	7.6451	-14.7174	6.3800	0.6922	0.0392	3.24E-07
16	2	0.028	0.447	7.6451	-14.7174	6.3800	0.6922	0.0396	3.24E-07
17	2	0.029	0.448	7.6451	-14.7174	6.3800	0.6922	0.0393	3.42E-07
18	2	0.029	0.448	7.6451	-14.7174	6.3800	0.6922	0.0397	3.42E-07
19	2	0.029	0.448	7.6451	-14.7174	6.3800	0.6922	0.0400	3.42E-07
20	2	0.029	0.449	7.6451	-14.7174	6.3800	0.6922	0.0401	3.52E-07
21	2	0.029	0.449	7.6451	-14.7174	6.3800	0.6922	0.0404	3.52E-07
22	2	0.029	0.449	7.6451	-14.7174	6.3800	0.6922	0.0408	3.52E-07
23	2	0.029	0.449	7.6451	-14.7174	6.3800	0.6922	0.0410	3.57E-07
24	2	0.029	0.449	7.6451	-14.7174	6.3800	0.6922	0.0414	3.57E-07
25	2	0.029	0.449	7.6451	-14.7174	6.3800	0.6922	0.0418	3.57E-07
26	2	0.029	0.449	7.6451	-14.7174	6.3800	0.6922	0.0420	3.60E-07
27	2	0.029	0.449	7.6451	-14.7174	6.3800	0.6922	0.0424	3.60E-07
28	2	0.029	0.449	7.6451	-14.7174	6.3800	0.6922	0.0428	3.60E-07
29	2	0.029	0.449	7.6451	-14.7174	6.3800	0.6922	0.0432	3.61E-07
30	2	0.029	0.449	7.6451	-14.7174	6.3800	0.6922	0.0436	3.61E-07
31	2	0.029	0.449	7.6451	-14.7174	6.3800	0.6922	0.0440	3.61E-07
32	2	0.029	0.449	7.6451	-14.7174	6.3800	0.6922	0.0444	3.63E-07
33	2	0.029	0.449	7.6451	-14.7174	6.3800	0.6922	0.0450	3.63E-07
34	2	0.047	0.466	14.4179	-30.1503	18.3248	-2.6013	0.0287	3.04E-06
35	2	0.055	0.479	14.6788	-30.8967	18.9715	-2.7719	0.0272	4.68E-06
36	2	0.060	0.487	14.8188	-31.2992	19.3229	-2.8667	0.0272	5.96E-06
37	2	0.063	0.491	14.8914	-31.5086	19.5065	-2.9167	0.0280	6.79E-06
38	2	0.066	0.495	14.9659	-31.7237	19.6957	-2.9687	0.0288	7.78E-06
39	2	0.076	0.445	10.5953	-19.8086	10.0997	-0.8738	0.0486	1.00E-04
40	2	0.142	0.513	12.2446	-24.1287	13.3604	-1.4586	0.0410	3.72E-04
41	2	0.178	0.540	12.9419	-26.0214	14.8707	-1.7746	0.0405	5.86E-04
42	2	0.191	0.549	13.1884	-26.6996	15.4233	-1.8972	0.0416	6.79E-04
43	2	0.193	0.551	13.2256	-26.8024	15.5076	-1.9162	0.0442	6.94E-04
44	2	0.193	0.551	13.2256	-26.8024	15.5076	-1.9162	0.0469	6.94E-04
45	2	0.193	0.551	13.2256	-26.8024	15.5076	-1.9162	0.0487	6.94E-04

Table 6B.11: Inputs for site Bay Area II K S4 total stress analysis (Ref Stress = 0.18; b = d = 0 all layers)

Layer	Name	Thick (m)	γ (kN/m3)	Vs (m/s)	Dmin	Ref Strain	B	s	P1	P2	P3
1	SM-SC	1	18	200	2.18	0.0160	1.47	0.87	0.714	0.296	3.25
2	OH	0.25	10.56	25	3.51	0.3484	0.18	0.72	0.866	0.4	0.555
3	OH	0.25	10.56	25	3.51	0.3484	0.18	0.72	0.866	0.4	0.555
4	OH	0.25	10.56	25	3.51	0.3484	0.18	0.72	0.866	0.4	0.555
5	OH	0.25	10.56	25	3.51	0.3484	0.18	0.72	0.866	0.4	0.555
6	OH	0.25	10.61	27.8	3.50	0.3460	0.24	0.705	0.854	0.4	0.485
7	OH	0.25	10.61	27.8	3.50	0.3460	0.24	0.705	0.854	0.4	0.485
8	OH	0.25	10.61	27.8	3.50	0.3460	0.24	0.705	0.854	0.4	0.485
9	OH	0.25	10.61	27.8	3.50	0.3460	0.24	0.705	0.854	0.4	0.485
10	OH	0.25	10.65	30.5	3.48	0.3482	0.255	0.72	0.84	0.4	0.52
11	OH	0.25	10.65	30.5	3.48	0.3482	0.255	0.72	0.84	0.4	0.52
12	OH	0.25	10.65	30.5	3.48	0.3482	0.255	0.72	0.84	0.4	0.52
13	OH	0.25	10.65	30.5	3.48	0.3482	0.255	0.72	0.84	0.4	0.52
14	OH	0.33	10.7	33.3	3.47	0.3500	0.27	0.735	0.84	0.4	0.49
15	OH	0.33	10.7	33.3	3.47	0.3500	0.27	0.735	0.84	0.4	0.49
16	OH	0.33	10.7	33.3	3.47	0.3500	0.27	0.735	0.84	0.4	0.49
17	OH	0.34	10.76	36	3.46	0.3500	0.285	0.75	0.832	0.4	0.49
18	OH	0.34	10.76	36	3.46	0.3500	0.285	0.75	0.832	0.4	0.49
19	OH	0.33	10.76	36	3.46	0.3500	0.285	0.75	0.832	0.4	0.49
20	OH	0.33	10.82	38.8	3.44	0.3460	0.285	0.78	0.8	0.4	0.6
21	OH	0.33	10.82	38.8	3.44	0.3460	0.285	0.78	0.8	0.4	0.6
22	OH	0.34	10.82	38.8	3.44	0.3460	0.285	0.78	0.8	0.4	0.6
23	OH	0.33	10.9	41.5	3.42	0.3260	0.285	0.78	0.82	0.4	0.535
24	OH	0.33	10.9	41.5	3.42	0.3260	0.285	0.78	0.82	0.4	0.535
25	OH	0.34	10.9	41.5	3.42	0.3260	0.285	0.78	0.82	0.4	0.535
26	OH	0.33	10.99	44.3	3.41	0.3044	0.285	0.795	0.812	0.4	0.525
27	OH	0.33	10.99	44.3	3.41	0.3044	0.285	0.795	0.812	0.4	0.525
28	OH	0.34	10.99	44.3	3.41	0.3044	0.285	0.795	0.812	0.4	0.525
29	OH	0.33	11.09	47	3.39	0.2618	0.285	0.795	0.8	0.396	0.5
30	OH	0.33	11.09	47	3.39	0.2618	0.285	0.795	0.8	0.396	0.5
31	OH	0.34	11.09	47	3.39	0.2618	0.285	0.795	0.8	0.396	0.5
32	OH	0.5	11.21	50	3.38	0.2316	0.285	0.795	0.8	0.392	0.45
33	OH	0.5	11.21	50	3.38	0.2680	0.285	0.81	0.8	0.396	0.55
34	CH	0.9	14.18	90	2.73	0.2002	1.425	0.555	1	0.38	2.65
35	CH	1	14.34	102	2.40	0.1502	1.335	0.585	1	0.4	2.35
36	CH	1.1	14.5	114	2.20	0.1662	1.53	0.615	0.994	0.4	1.845
37	CH	1.25	14.68	126	2.08	0.1640	1.575	0.645	0.97	0.392	1.655
38	CH	1.5	15.09	150	1.96	0.1272	1.44	0.69	0.88	0.316	1.765
39	CL	2	18	200	1.85	0.2992	1.59	0.66	0.946	0.362	0.95
40	CL	2.1	18.1	215	1.59	0.2486	1.56	0.645	0.966	0.384	1.15
41	CL	2.15	18.2	230	1.46	0.2440	1.56	0.645	0.948	0.364	1.25
42	CL	2.5	18.35	252.7	1.36	0.2506	1.59	0.66	0.954	0.38	1.1
43	CL	2.5	18.45	270.4	1.30	0.2116	1.425	0.675	0.898	0.332	1.15
44	CL	3	18.6	300	1.26	0.2142	1.455	0.705	0.856	0.31	1.1
45	CL	1	18.7	320	1.23	0.2212	1.47	0.72	0.864	0.324	0.98

Table 6B.12: Input parameters for site Bay Area II K S4 effective stress analysis (Max Ru = 0.95 all layers)

Layer	Model	f/s/f	p/r/Dr	F/A/FC	s/B/-	g/C/-	v/D/v	-/g/-	$C_v(m^2/s)$
1	1	1.000	1.000	1.0335	1.3073	0.0051	1.0000	0.0000	1.63E-01
2	2	0.022	0.423	14.9659	-31.7237	19.6957	-2.9687	0.0458	1.63E-07
3	2	0.022	0.423	14.9659	-31.7237	19.6957	-2.9687	0.0462	1.63E-07
4	2	0.022	0.423	14.9659	-31.7237	19.6957	-2.9687	0.0465	1.63E-07
5	2	0.022	0.423	14.9659	-31.7237	19.6957	-2.9687	0.0469	1.63E-07
6	2	0.025	0.435	15.2844	-32.6478	20.5142	-3.1986	0.0412	2.36E-07
7	2	0.025	0.435	15.2844	-32.6478	20.5142	-3.1986	0.0415	2.36E-07
8	2	0.025	0.435	15.2844	-32.6478	20.5142	-3.1986	0.0418	2.36E-07
9	2	0.025	0.435	15.2844	-32.6478	20.5142	-3.1986	0.0421	2.36E-07
10	2	0.027	0.442	15.4574	-33.1529	20.9658	-3.3287	0.0394	2.90E-07
11	2	0.027	0.442	15.4574	-33.1529	20.9658	-3.3287	0.0397	2.90E-07
12	2	0.027	0.442	15.4574	-33.1529	20.9658	-3.3287	0.0400	2.90E-07
13	2	0.027	0.442	15.4574	-33.1529	20.9658	-3.3287	0.0403	2.90E-07
14	2	0.028	0.447	7.6451	-14.7174	6.3800	0.6922	0.0388	3.24E-07
15	2	0.028	0.447	7.6451	-14.7174	6.3800	0.6922	0.0392	3.24E-07
16	2	0.028	0.447	7.6451	-14.7174	6.3800	0.6922	0.0396	3.24E-07
17	2	0.029	0.448	7.6451	-14.7174	6.3800	0.6922	0.0393	3.42E-07
18	2	0.029	0.448	7.6451	-14.7174	6.3800	0.6922	0.0397	3.42E-07
19	2	0.029	0.448	7.6451	-14.7174	6.3800	0.6922	0.0400	3.42E-07
20	2	0.029	0.449	7.6451	-14.7174	6.3800	0.6922	0.0401	3.52E-07
21	2	0.029	0.449	7.6451	-14.7174	6.3800	0.6922	0.0404	3.52E-07
22	2	0.029	0.449	7.6451	-14.7174	6.3800	0.6922	0.0408	3.52E-07
23	2	0.029	0.449	7.6451	-14.7174	6.3800	0.6922	0.0410	3.57E-07
24	2	0.029	0.449	7.6451	-14.7174	6.3800	0.6922	0.0414	3.57E-07
25	2	0.029	0.449	7.6451	-14.7174	6.3800	0.6922	0.0418	3.57E-07
26	2	0.029	0.449	7.6451	-14.7174	6.3800	0.6922	0.0420	3.60E-07
27	2	0.029	0.449	7.6451	-14.7174	6.3800	0.6922	0.0424	3.60E-07
28	2	0.029	0.449	7.6451	-14.7174	6.3800	0.6922	0.0428	3.60E-07
29	2	0.029	0.449	7.6451	-14.7174	6.3800	0.6922	0.0432	3.61E-07
30	2	0.029	0.449	7.6451	-14.7174	6.3800	0.6922	0.0436	3.61E-07
31	2	0.029	0.449	7.6451	-14.7174	6.3800	0.6922	0.0440	3.61E-07
32	2	0.029	0.449	7.6451	-14.7174	6.3800	0.6922	0.0444	3.63E-07
33	2	0.029	0.449	7.6451	-14.7174	6.3800	0.6922	0.0450	3.63E-07
34	2	0.047	0.466	14.4179	-30.1503	18.3248	-2.6013	0.0287	3.04E-06
35	2	0.055	0.479	14.6788	-30.8967	18.9715	-2.7719	0.0272	4.68E-06
36	2	0.060	0.487	14.8188	-31.2992	19.3229	-2.8667	0.0272	5.96E-06
37	2	0.063	0.491	14.8914	-31.5086	19.5065	-2.9167	0.0280	6.79E-06
38	2	0.066	0.495	14.9659	-31.7237	19.6957	-2.9687	0.0288	7.78E-06
39	2	0.076	0.445	10.5953	-19.8086	10.0997	-0.8738	0.0486	1.00E-04
40	2	0.142	0.513	12.2446	-24.1287	13.3604	-1.4586	0.0410	3.72E-04
41	2	0.178	0.540	12.9419	-26.0214	14.8707	-1.7746	0.0405	5.86E-04
42	2	0.191	0.549	13.1884	-26.6996	15.4233	-1.8972	0.0416	6.79E-04
43	2	0.193	0.551	13.2256	-26.8024	15.5076	-1.9162	0.0442	6.94E-04
44	2	0.193	0.551	13.2256	-26.8024	15.5076	-1.9162	0.0469	6.94E-04
45	2	0.193	0.551	13.2256	-26.8024	15.5076	-1.9162	0.0487	6.94E-04

Table 6B.13: Input parameters for site HAGP total stress analysis (Ref Stress = 0.18; b = d = 0 for all layers)

Layer	Name	Thick (m)	γ (kN/m3)	Vs (m/s)	Dmin	Ref Strain	B	s	P1	P2	P3
1	SM	2	17	200	1.87	0.0188	1.47	0.9	0.68	0.286	3.25
2	CH	1	14.5	100	3.65	0.0630	1.335	1.005	0.586	0.28	0.45
3	CH	1	14.53	100	3.41	0.0732	1.485	1.02	0.58	0.282	0.45
4	CH	1	14.55	100	3.24	0.0772	1.53	1.035	0.59	0.3	0.45
5	CH	1	14.58	100	3.08	0.0810	1.53	1.035	0.586	0.3	0.45
6	CH	1	14.61	100	2.96	0.0858	1.485	1.005	0.58	0.28	0.45
7	CH	1	14.64	100	2.85	0.0950	1.515	0.99	0.588	0.28	0.45
8	CH	1	14.66	100	2.76	0.0896	1.38	0.99	0.584	0.28	0.45
9	CH	1	14.69	100	2.67	0.1006	1.455	0.975	0.58	0.266	0.45
10	CH	1	14.72	100	2.60	0.1066	1.47	0.975	0.588	0.28	0.45
11	CH	1	14.74	100	2.54	0.1190	1.545	0.96	0.58	0.262	0.45
12	CH	1	14.77	100	2.48	0.1232	1.545	0.945	0.584	0.26	0.45
13	CH	1	14.8	108	2.43	0.1164	1.47	0.975	0.588	0.28	0.45
14	CH	1.1	14.82	117	2.36	0.1072	1.365	0.99	0.584	0.28	0.45
15	CH	1.2	14.85	126	2.30	0.1056	1.35	1.005	0.58	0.28	0.45
16	CH	1.3	14.88	135	2.23	0.1054	1.35	1.02	0.58	0.284	0.45
17	CH	1.4	14.91	144	2.16	0.1064	1.365	1.035	0.588	0.3	0.45
18	CH	1.5	14.93	153	2.10	0.1124	1.515	1.05	0.58	0.3	0.45
19	CH	1.6	14.96	162	2.02	0.1118	1.515	1.05	0.58	0.3	0.45
20	CH	1.7	14.99	171	1.95	0.1130	1.545	1.065	0.58	0.304	0.45
21	CH	1.8	15.01	180	1.87	0.1092	1.515	1.065	0.58	0.304	0.45
22	CH	1.8	15	185	1.80	0.1112	1.545	1.065	0.58	0.306	0.45
23	CH	1.8	15	190	1.74	0.1088	1.515	1.065	0.58	0.306	0.45
24	CH	1.8	15	195	1.68	0.1078	1.5	1.05	0.58	0.3	0.45
25	CH	2	15	202	1.61	0.1092	1.53	1.05	0.58	0.3	0.45
26	CH	2	15	206	1.56	0.1094	1.53	1.05	0.58	0.3	0.45
27	CH	2	15	210	1.50	0.1082	1.515	1.035	0.586	0.3	0.45
28	CH	2	16	214	1.44	0.1040	1.485	1.035	0.586	0.3	0.45
29	SC	3.3	18	330	1.06	0.1144	1.515	0.93	0.624	0.23	2.45
30	SC	3.3	18	330	1.02	0.1202	1.5	0.915	0.616	0.212	2.75
31	SC	3.3	18	330	0.99	0.1314	1.545	0.9	0.64	0.222	2.3
32	SC	1.1	18	330	0.97	0.1304	1.5	0.9	0.646	0.23	2.15

Table 6B. 14: Input parameters for site HAGP effective stress analysis (Max Ru = 0.95 for all layers)

Layer	Model	f/s/f	p/r/Dr	F/A/FC	s/B/-	g/C/-	v/D/v	-/g/-	$C_v(m^2/s)$
1	1	1.000	1.000	1.0335	1.5372	0.0062	1.0000	0.0000	6.12E-02
2	2	0.039	0.424	11.9895	-23.4457	12.8273	-1.3537	0.0286	2.10E-06
3	2	0.046	0.450	13.2256	-26.8024	15.5076	-1.9162	0.0285	2.16E-06
4	2	0.052	0.469	14.1792	-29.4716	17.7426	-2.4520	0.0286	2.22E-06
5	2	0.052	0.469	14.1792	-29.4716	17.7426	-2.4520	0.0304	2.28E-06
6	2	0.052	0.469	14.1792	-29.4716	17.7426	-2.4520	0.0319	2.35E-06
7	2	0.052	0.469	14.1792	-29.4716	17.7426	-2.4520	0.0334	2.42E-06
8	2	0.052	0.469	14.1792	-29.4716	17.7426	-2.4520	0.0347	2.49E-06
9	2	0.052	0.469	14.1792	-29.4716	17.7426	-2.4520	0.0360	2.57E-06
10	2	0.052	0.469	14.1792	-29.4716	17.7426	-2.4520	0.0371	2.64E-06
11	2	0.052	0.469	14.1792	-29.4716	17.7426	-2.4520	0.0383	2.73E-06
12	2	0.052	0.469	14.1792	-29.4716	17.7426	-2.4520	0.0393	2.81E-06
13	2	0.052	0.469	14.1792	-29.4716	17.7426	-2.4520	0.0404	2.90E-06
14	2	0.053	0.470	14.1792	-29.4716	17.7426	-2.4520	0.0409	2.99E-06
15	2	0.053	0.471	14.1792	-29.4716	17.7426	-2.4520	0.0415	3.09E-06
16	2	0.054	0.472	14.1792	-29.4716	17.7426	-2.4520	0.0422	3.19E-06
17	2	0.055	0.473	14.1792	-29.4716	17.7426	-2.4520	0.0428	3.30E-06
18	2	0.056	0.474	14.1792	-29.4716	17.7426	-2.4520	0.0434	3.41E-06
19	2	0.057	0.476	14.1792	-29.4716	17.7426	-2.4520	0.0435	3.52E-06
20	2	0.059	0.478	14.1792	-29.4716	17.7426	-2.4520	0.0436	3.65E-06
21	2	0.061	0.480	14.1792	-29.4716	17.7426	-2.4520	0.0437	3.77E-06
22	2	0.063	0.482	14.1792	-29.4716	17.7426	-2.4520	0.0437	3.91E-06
23	2	0.065	0.485	14.1792	-29.4716	17.7426	-2.4520	0.0435	4.05E-06
24	2	0.068	0.487	14.1792	-29.4716	17.7426	-2.4520	0.0433	4.19E-06
25	2	0.070	0.490	14.1792	-29.4716	17.7426	-2.4520	0.0431	4.35E-06
26	2	0.073	0.493	14.1792	-29.4716	17.7426	-2.4520	0.0429	4.51E-06
27	2	0.076	0.496	14.1792	-29.4716	17.7426	-2.4520	0.0425	4.68E-06
28	2	0.080	0.499	14.1792	-29.4716	17.7426	-2.4520	0.0421	4.86E-06
29	1	1.000	1.000	0.4756	1.5372	0.0377	1.0000	0.0000	6.12E-02
30	1	1.000	1.000	0.4756	1.5372	0.0393	1.0000	0.0000	6.12E-02
31	1	1.000	1.000	0.4756	1.5372	0.0408	1.0000	0.0000	6.12E-02
32	1	1.000	1.000	0.4756	1.5372	0.0417	1.0000	0.0000	6.12E-02

Table 6B.15: Input parameters for site JSSS total stress analysis (Ref Stress = 0.18; b = d = 0 for all layers)

Layer	Name	Thick (m)	γ (kN/m3)	Vs (m/s)	Dmin	Ref Strain	B	s	P1	P2	P3
1	SC	2	19	400	1.78	0.0218	1.65	0.96	0.626	0.272	3.25
2	CH	1	15.5	175	2.18	0.0722	1.485	1.005	0.588	0.248	2.8
3	CH	1	15.4	144	2.07	0.0726	1.485	0.975	0.596	0.238	2.9
4	CH	1	15.3	120	2.02	0.0724	1.56	0.96	0.596	0.232	3.25
5	CH	1	15.2	106	1.94	0.0782	1.56	0.93	0.612	0.23	3.25
6	CH	0.85	15.1	98	1.86	0.0842	1.53	0.885	0.658	0.24	2.6
7	CH	0.85	15	91	1.79	0.0910	1.5	0.84	0.704	0.25	2.25
8	CH	0.85	15	91	1.74	0.0920	1.44	0.825	0.702	0.24	2.6
9	MH/CH	0.85	14.9	87	1.50	0.0958	1.545	0.78	0.762	0.266	2.3
10	MH/CH	0.85	14.8	90	1.47	0.0998	1.56	0.78	0.762	0.266	2.3
11	MH/CH	0.85	14.7	98	1.45	0.0990	1.56	0.795	0.732	0.246	2.55
12	MH/CH	1	14.6	106	1.44	0.1010	1.605	0.825	0.716	0.254	2.35
13	MH/CH	1.1	15.1	111	1.41	0.0930	1.485	0.825	0.696	0.232	2.7
14	MH/CH	1.1	15.6	113	1.38	0.0930	1.47	0.84	0.71	0.258	2.15
15	MH/CH	1.1	16.1	120	1.35	0.0926	1.455	0.855	0.68	0.24	2.52
16	MH/CH	1.3	16.66	133	1.33	0.0948	1.5	0.885	0.656	0.236	2.6
17	MH/CH	1.5	16.66	160	1.30	0.0978	1.59	0.93	0.608	0.22	3.225
18	MH/CH	1.8	16.786	180	1.27	0.0944	1.545	0.96	0.59	0.222	3.25
19	CH	1.66	16.9022	191.5	1.17	0.0802	1.44	0.975	0.592	0.232	2.95
20	CH	1.67	17.0191	195	1.14	0.0862	1.5	0.975	0.59	0.23	2.95
21	CH	1.67	17.136	198.5	1.12	0.0860	1.455	0.975	0.592	0.232	2.9
22	CH	2	17.276	202.7	1.09	0.0904	1.485	0.975	0.592	0.232	2.9
23	CH	2	17.416	206.9	1.06	0.0922	1.47	0.975	0.59	0.228	2.85
24	CH	2	17.556	211.1	1.04	0.0948	1.47	0.975	0.588	0.226	2.85
25	CH	2	17.696	215.3	1.02	0.1058	1.59	0.975	0.59	0.228	2.85
26	CH	2	17.836	219.5	0.99	0.1042	1.53	0.975	0.588	0.226	2.85
27	CH	2.2	18	224.1	0.97	0.1112	1.59	0.975	0.588	0.226	2.85
28	CH	2.2	17.5	228.7	0.95	0.1128	1.56	0.96	0.604	0.23	2.65
29	CH	2.3	17.5	233.6	0.93	0.1194	1.545	0.945	0.594	0.212	3
30	CH	2.3	17.5	238.4	0.91	0.1232	1.56	0.945	0.594	0.212	3
31	CH	2.4	17.5	243.4	0.90	0.1256	1.56	0.945	0.592	0.21	3
32	CH	2.4	17.5	248.5	0.88	0.1280	1.56	0.945	0.59	0.206	3
33	CH	2.5	17.5	253.7	0.87	0.1316	1.575	0.945	0.59	0.206	3
34	CH	2.5	17.5	259	0.86	0.1338	1.575	0.945	0.59	0.206	3
35	CH	2.6	17.5	264.4	0.84	0.1334	1.545	0.945	0.59	0.206	3
36	CH	2.6	17.5	269.9	0.83	0.1378	1.56	0.945	0.59	0.206	3.05
37	CH	2.7	17.5	275.6	1.25	0.2826	1.56	0.975	0.586	0.202	2.2
38	CH	2.7	17.5	281.2	1.23	0.2662	1.455	0.975	0.586	0.202	2.2
39	CH	2.8	17.5	287.1	1.22	0.2738	1.47	0.975	0.586	0.202	2.25

40	CH	2.8	17.5	293	1.20	0.2768	1.47	0.975	0.586	0.202	2.3
41	CH	2.9	18.21	299.1	1.18	0.2776	1.485	0.99	0.596	0.218	1.95
42	CH	2.9	18.21	305.2	1.17	0.2816	1.485	0.99	0.598	0.22	1.95
43	CH	3	17.6	311.5	1.15	0.2876	1.485	0.99	0.596	0.218	1.95
44	CH	3	17.6	317.8	1.14	0.2876	1.47	0.99	0.594	0.214	1.95
45	CH	3	17.6	324.1	1.13	0.2912	1.47	0.99	0.594	0.214	2
46	CH	3	17.6	330.4	1.12	0.2932	1.47	0.99	0.59	0.21	2.05
47	CH	3.1	18.4	336.9	1.10	0.2942	1.485	1.005	0.584	0.22	2.35
48	CH	3.1	18.4	343.4	1.09	0.2966	1.485	1.005	0.584	0.22	2.35
49	GW	5	19	500	0.73	0.1976	1.53	0.93	0.596	0.192	2.5
50	GW	5	19	500	0.72	0.2078	1.545	0.93	0.6	0.198	2.45
51	GW	5	19	500	0.70	0.2132	1.53	0.915	0.62	0.202	2.04
52	GW	6	19	600	0.70	0.1898	1.47	0.975	0.594	0.216	2.3

Table 6B.16: Input parameters for site JSSS effective stress analysis (Max Ru = 0.95 for all layers)

Layer	Model	f/s/f	p/r/Dr	F/A/FC	s/B/-	g/C/-	v/D/v	-/g/-	$C_v(m^2/s)$
1	1	1.000	1.000	0.3530	1.5372	0.0068	1.0000	0.0000	6.12E-02
2	2	0.043	0.412	10.5953	-19.8086	10.0997	-0.8738	0.0264	1.45E-05
3	2	0.054	0.444	11.9895	-23.4457	12.8273	-1.3537	0.0258	1.45E-05
4	2	0.072	0.491	14.1792	-29.4716	17.7426	-2.4520	0.0241	1.45E-05
5	2	0.076	0.502	14.6788	-30.8967	18.9715	-2.7719	0.0248	1.45E-05
6	2	0.076	0.502	14.6788	-30.8967	18.9715	-2.7719	0.0258	1.45E-05
7	2	0.076	0.502	14.6788	-30.8967	18.9715	-2.7719	0.0267	1.45E-05
8	2	0.076	0.502	14.6788	-30.8967	18.9715	-2.7719	0.0276	1.45E-05
9	2	0.096	0.518	14.6788	-30.8967	18.9715	-2.7719	0.0245	3.24E-05
10	2	0.096	0.518	14.6788	-30.8967	18.9715	-2.7719	0.0251	3.24E-05
11	2	0.096	0.518	14.6788	-30.8967	18.9715	-2.7719	0.0257	3.24E-05
12	2	0.096	0.518	14.6788	-30.8967	18.9715	-2.7719	0.0263	3.24E-05
13	2	0.096	0.518	14.6788	-30.8967	18.9715	-2.7719	0.0270	3.24E-05
14	2	0.096	0.518	14.6788	-30.8967	18.9715	-2.7719	0.0277	3.24E-05
15	2	0.096	0.518	14.6788	-30.8967	18.9715	-2.7719	0.0285	3.24E-05
16	2	0.096	0.518	14.6788	-30.8967	18.9715	-2.7719	0.0294	3.24E-05
17	2	0.096	0.518	14.6788	-30.8967	18.9715	-2.7719	0.0304	3.24E-05
18	2	0.096	0.518	14.6788	-30.8967	18.9715	-2.7719	0.0315	3.24E-05
19	2	0.119	0.542	15.2844	-32.6478	20.5142	-3.1986	0.0293	5.38E-05
20	2	0.119	0.542	15.2844	-32.6478	20.5142	-3.1986	0.0302	5.38E-05
21	2	0.119	0.542	15.2844	-32.6478	20.5142	-3.1986	0.0311	5.38E-05
22	2	0.119	0.542	15.2844	-32.6478	20.5142	-3.1986	0.0321	5.38E-05
23	2	0.119	0.542	15.2844	-32.6478	20.5142	-3.1986	0.0331	5.38E-05
24	2	0.119	0.542	15.2844	-32.6478	20.5142	-3.1986	0.0340	5.38E-05
25	2	0.119	0.542	15.2844	-32.6478	20.5142	-3.1986	0.0349	5.38E-05
26	2	0.119	0.542	15.2844	-32.6478	20.5142	-3.1986	0.0358	5.38E-05
27	2	0.119	0.542	15.2844	-32.6478	20.5142	-3.1986	0.0367	5.38E-05
28	2	0.119	0.542	15.2844	-32.6478	20.5142	-3.1986	0.0376	5.38E-05
29	2	0.111	0.529	14.6788	-30.8967	18.9715	-2.7719	0.0394	5.38E-05
30	2	0.111	0.529	14.6788	-30.8967	18.9715	-2.7719	0.0402	5.38E-05
31	2	0.111	0.529	14.6788	-30.8967	18.9715	-2.7719	0.0411	5.38E-05
32	2	0.111	0.529	14.6788	-30.8967	18.9715	-2.7719	0.0419	5.38E-05
33	2	0.111	0.529	14.678789	-30.8967	18.9715	-2.7719	0.0427	5.38E-05
34	2	0.111	0.529	14.6788	-30.8967	18.9715	-2.7719	0.0435	5.38E-05
35	2	0.111	0.529	14.6788	-30.8967	18.9715	-2.7719	0.0443	5.38E-05
36	2	0.111	0.529	14.6788	-30.8967	18.9715	-2.7719	0.0450	5.38E-05
37	2	0.089	0.490	12.9240	-25.9725	14.8311	-1.7659	0.0969	5.38E-05
38	2	0.089	0.490	12.9240	-25.9725	14.8311	-1.7659	0.0985	5.38E-05
39	2	0.089	0.490	12.9240	-25.9725	14.8311	-1.7659	0.1001	5.38E-05

40	2	0.089	0.490	12.9240	-25.9725	14.8311	-1.7659	0.1017	5.38E-05
41	2	0.089	0.490	12.9240	-25.9725	14.8311	-1.7659	0.1033	5.38E-05
42	2	0.089	0.490	12.9240	-25.9725	14.8311	-1.7659	0.1050	5.38E-05
43	2	0.089	0.490	12.9240	-25.9725	14.8311	-1.7659	0.1065	5.38E-05
44	2	0.089	0.490	12.9240	-25.9725	14.8311	-1.7659	0.1080	5.38E-05
45	2	0.089	0.490	12.9240	-25.9725	14.8311	-1.7659	0.1095	5.38E-05
46	2	0.089	0.490	12.9240	-25.9725	14.8311	-1.7659	0.1110	5.38E-05
47	2	0.089	0.490	12.9240	-25.9725	14.8311	-1.7659	0.1125	5.38E-05
48	2	0.089	0.490	12.9240	-25.9725	14.8311	-1.7659	0.1140	5.38E-05
49	1	1.000	1.000	0.2498	1.0000	0.0650	1.0000	0.0000	1.02E+01
50	1	1.000	1.000	0.2498	1.0000	0.0664	1.0000	0.0000	1.02E+01
51	1	1.000	1.000	0.2498	1.0000	0.0677	1.0000	0.0000	1.02E+01
52	1	1.000	1.000	0.1883	1.0000	0.0692	1.0000	0.0000	1.02E+01

Table 6B.17: Input for site KIKNET40 total stress analysis (Ref Stress = 0.18; b = d = 0 for all layers)

Layer	Name	Thick (m)	γ (kN/m3)	Vs (m/s)	Dmin	Ref Strain	B	s	P1	P2	P3
1	CH	0.7	15.5	80	4.27	0.0394	1.65	0.92	0.656	0.268	3.25
2	CH	0.7	15.5	80	3.15	0.0526	1.56	0.90	0.652	0.248	3.25
3	CH	0.7	15.5	80	2.72	0.0622	1.53	0.87	0.666	0.24	3.25
4	CH	1	16.5	110	2.44	0.0654	1.56	0.95	0.612	0.238	3.25
5	CH	1.1	16.5	110	2.22	0.0698	1.59	0.95	0.608	0.234	3.25
6	CH	1.1	16.5	110	2.07	0.0722	1.58	0.95	0.608	0.234	3.25
7	CH	1.1	16.5	110	1.95	0.0778	1.61	0.95	0.604	0.23	3.25
8	CH	1.1	16.5	110	1.86	0.0782	1.53	0.93	0.612	0.226	3.25
9	CH	1.1	16.5	110	1.78	0.0852	1.56	0.93	0.608	0.224	3.25
10	CH	1.1	16.5	110	1.70	0.0910	1.55	0.90	0.628	0.22	3.165
11	CH	1.1	16.5	110	1.65	0.0958	1.55	0.90	0.632	0.226	2.95
12	CH	1.1	16.5	110	1.59	0.0982	1.50	0.89	0.654	0.234	2.55
13	CH	1.1	16.5	110	1.54	0.1058	1.53	0.87	0.682	0.246	2.1
14	CH	1.1	16.5	110	1.50	0.1074	1.49	0.86	0.66	0.218	2.75
15	SM	1.9	17	200	1.72	0.1270	1.52	1.05	0.584	0.26	2.4
16	SM	2	17	200	1.68	0.1242	1.53	1.07	0.586	0.268	2.1
17	SM	2	17	200	1.64	0.1248	1.53	1.07	0.59	0.272	2.05
18	SM	2	17	200	1.59	0.1284	1.50	1.05	0.584	0.26	2.4
19	SM	2	17	200	1.54	0.1374	1.55	1.05	0.584	0.26	2.35
20	SM	2	17	200	1.50	0.1438	1.53	1.02	0.584	0.24	2.5
21	SM	2	17	200	1.47	0.1448	1.49	1.02	0.584	0.24	2.4
22	SM	2	17	200	1.44	0.1536	1.52	1.01	0.598	0.242	2.15
23	SM	2	17	200	1.41	0.1550	1.49	1.01	0.598	0.242	2.1
24	SM	2	17	200	1.38	0.1590	1.47	0.99	0.584	0.22	2.5
25	SM	2	17	200	1.35	0.1650	1.47	0.98	0.6	0.224	2.25
26	SM	2	17	200	1.33	0.1710	1.49	0.98	0.6	0.224	2.2
27	SW-SM	3	19	350	1.04	0.1132	1.58	1.11	0.592	0.296	1.5
28	SW-SM	3.5	19	350	1.02	0.1134	1.58	1.13	0.582	0.3	1.8
29	SW-SM	3.5	19	350	0.99	0.1190	1.55	1.10	0.582	0.28	1.85
30	ML/MH	5	18	500	1.49	0.1736	1.35	1.47	0.58	0.4	0.55
31	ML/MH	5	18	505	1.46	0.1730	1.37	1.49	0.58	0.4	0.55
32	ML/MH	5	18	510	1.43	0.1860	1.52	1.50	0.58	0.4	0.55
33	ML/MH	5	18	515	1.40	0.1872	1.53	1.50	0.58	0.4	0.55
34	ML/MH	5	18	520	1.37	0.1892	1.50	1.49	0.58	0.4	0.55
35	ML/MH	5	18	525	1.34	0.1988	1.50	1.49	0.58	0.4	0.55
36	ML/MH	5	18	530	1.32	0.2070	1.52	1.49	0.58	0.4	0.55
37	ML/MH	5	18	530	1.29	0.2188	1.52	1.47	0.582	0.4	0.55
38	ML/MH	5	18	530	1.27	0.2284	1.49	1.44	0.592	0.4	0.65
39	ML/MH	5	18	530	1.25	0.2496	1.53	1.37	0.608	0.4	1.1
40	ML/MH	5	18	530	1.23	0.2600	1.52	1.32	0.58	0.36	1.5

Table 6B.18: Input parameters for site KIKNET40 effective stress analysis (Max Ru = 0.95 for all layers)

Layer	Model	f/s/f	p/r/Dr	F/A/FC	s/B/-	g/C/-	v/D/v	-/g/-	$C_v(m^2/s)$
1	2	0.043	0.412	10.5953	-19.8086	10.0997	-0.8738	0.0116	1.45E-05
2	2	0.048	0.425	11.1832	-21.3223	11.2115	-1.0579	0.0162	1.45E-05
3	2	0.050	0.434	11.5505	-22.2829	11.9345	-1.1862	0.0188	1.45E-05
4	2	0.054	0.444	11.9895	-23.4457	12.8273	-1.3537	0.0212	1.45E-05
5	2	0.064	0.471	13.2256	-26.8024	15.5076	-1.9162	0.0223	1.45E-05
6	2	0.072	0.491	14.1792	-29.4716	17.7426	-2.4520	0.0233	1.45E-05
7	2	0.076	0.502	14.6788	-30.8967	18.9715	-2.7719	0.0246	1.45E-05
8	2	0.080	0.511	15.1208	-32.1724	20.0919	-3.0790	0.0256	1.45E-05
9	2	0.080	0.511	15.1208	-32.1724	20.0919	-3.0790	0.0270	1.45E-05
10	2	0.080	0.511	15.1208	-32.1724	20.0919	-3.0790	0.0283	1.45E-05
11	2	0.080	0.511	15.1208	-32.1724	20.0919	-3.0790	0.0295	1.45E-05
12	2	0.080	0.511	15.1208	-32.1724	20.0919	-3.0790	0.0306	1.45E-05
13	2	0.080	0.511	15.1208	-32.1724	20.0919	-3.0790	0.0316	1.45E-05
14	2	0.080	0.511	15.1208	-32.1724	20.0919	-3.0790	0.0326	1.45E-05
15	1	1.000	1.000	1.0335	1.5372	0.0485	1.0000	0.0000	1.00E-04
16	1	1.000	1.000	1.0335	1.5372	0.0477	1.0000	0.0000	1.00E-04
17	1	1.000	1.000	1.0335	1.5372	0.0482	1.0000	0.0000	1.00E-04
18	1	1.000	1.000	1.0335	1.5372	0.0501	1.0000	0.0000	1.00E-04
19	1	1.000	1.000	1.0335	1.5372	0.0518	1.0000	0.0000	1.00E-04
20	1	1.000	1.000	1.0335	1.5372	0.0534	1.0000	0.0000	1.00E-04
21	1	1.000	1.000	1.0335	1.5372	0.0549	1.0000	0.0000	1.00E-04
22	1	1.000	1.000	1.0335	1.5372	0.0564	1.0000	0.0000	1.00E-04
23	1	1.000	1.000	1.0335	1.5372	0.0578	1.0000	0.0000	1.00E-04
24	1	1.000	1.000	1.0335	1.5372	0.0591	1.0000	0.0000	1.00E-04
25	1	1.000	1.000	1.0335	1.5372	0.0604	1.0000	0.0000	1.00E-04
26	1	1.000	1.000	1.0335	1.5372	0.0616	1.0000	0.0000	1.00E-04
27	1	1.000	1.000	0.4341	1.3073	0.0473	1.0000	0.0000	6.94E-04
28	1	1.000	1.000	0.4341	1.3073	0.0478	1.0000	0.0000	6.94E-04
29	1	1.000	1.000	0.4341	1.3073	0.0495	1.0000	0.0000	6.94E-04
30	2	0.063	0.448	11.5505	-22.2829	11.9345	-1.1862	0.1297	3.24E-05
31	2	0.068	0.458	11.9895	-23.4457	12.8273	-1.3537	0.1291	3.24E-05
32	2	0.070	0.464	12.2446	-24.1287	13.3604	-1.4586	0.1304	3.24E-05
33	2	0.073	0.471	12.530345	-24.8997	13.9698	-1.5827	0.1311	3.24E-05
34	2	0.073	0.471	12.5303	-24.8997	13.9698	-1.5827	0.1348	3.24E-05
35	2	0.073	0.471	12.5303	-24.8997	13.9698	-1.5827	0.1382	3.24E-05
36	2	0.073	0.471	12.5303	-24.8997	13.9698	-1.5827	0.1416	3.24E-05
37	2	0.073	0.471	12.5303	-24.8997	13.9698	-1.5827	0.1447	3.24E-05
38	2	0.073	0.471	12.5303	-24.8997	13.9698	-1.5827	0.1478	3.24E-05
39	2	0.073	0.471	12.5303	-24.8997	13.9698	-1.5827	0.1507	3.24E-05
40	2	0.073	0.471	12.5303	-24.8997	13.9698	-1.5827	0.1536	3.24E-05

Table 6B.19: Input for site KIKNET total stress analysis (Ref Stress = 0.18; b = d = 0 for all layers)

Layer	Name	Thick (m)	γ (kN/m3)	Vs (m/s)	Dmin	Ref Strain	B	s	P1	P2	P3
1	CH	0.7	15.5	80	5.80	0.0584	1.56	0.96	0.616	0.254	3.25
2	CH	0.7	15.5	80	4.30	0.0806	1.56	0.96	0.608	0.24	3.25
3	CH	0.7	15.5	80	3.73	0.0978	1.56	0.92	0.624	0.222	3.25
4	CH	1	16.5	110	3.34	0.0934	1.52	1.02	0.592	0.256	2.5
5	CH	1.1	16.5	110	3.06	0.0974	1.53	1.02	0.588	0.25	2.5
6	CH	1.1	16.5	110	2.87	0.0984	1.50	1.02	0.59	0.252	2.45
7	CH	1.1	16.5	110	2.71	0.1042	1.52	1.02	0.59	0.252	2.4
8	CH	1.1	16.5	110	2.59	0.1088	1.52	1.01	0.584	0.24	2.8
9	CH	1.1	16.5	110	2.48	0.1154	1.50	0.99	0.592	0.234	2.5
10	CH	1.1	16.5	110	2.39	0.1202	1.47	0.98	0.586	0.22	2.85
11	CH	1.1	16.5	110	2.30	0.1368	1.58	0.96	0.598	0.22	2.55
12	CH	1.1	16.5	110	2.23	0.1406	1.55	0.96	0.6	0.222	2.4
13	CH	1.1	16.5	110	2.17	0.1486	1.52	0.93	0.602	0.204	2.85
14	CH	1.1	16.5	110	2.11	0.1594	1.55	0.92	0.642	0.226	2
15	SM	1.9	17	200	1.72	0.1270	1.52	1.05	0.584	0.26	2.4
16	SM	2	17	200	1.68	0.1242	1.53	1.07	0.586	0.268	2.1
17	SM	2	17	200	1.64	0.1248	1.53	1.07	0.59	0.272	2.05
18	SM	2	17	200	1.59	0.1284	1.50	1.05	0.584	0.26	2.4
19	SM	2	17	200	1.54	0.1374	1.55	1.05	0.584	0.26	2.35
20	SM	2	17	200	1.50	0.1438	1.53	1.02	0.584	0.24	2.5
21	SM	2	17	200	1.47	0.1448	1.49	1.02	0.584	0.24	2.4
22	SM	2	17	200	1.44	0.1536	1.52	1.01	0.598	0.242	2.15
23	SM	2	17	200	1.41	0.1550	1.49	1.01	0.598	0.242	2.1
24	SM	2	17	200	1.38	0.1590	1.47	0.99	0.584	0.22	2.5
25	SM	2	17	200	1.35	0.1650	1.47	0.98	0.6	0.224	2.25
26	SM	2	17	200	1.33	0.1710	1.49	0.98	0.6	0.224	2.2
27	SW-SM	3	19	350	1.04	0.1132	1.58	1.11	0.592	0.296	1.5
28	SW-SM	3.5	19	350	1.02	0.1134	1.58	1.13	0.582	0.3	1.8
29	SW-SM	3.5	19	350	0.99	0.1190	1.55	1.10	0.582	0.28	1.85
30	ML/MH	5	18	500	1.49	0.1736	1.35	1.47	0.58	0.4	0.55
31	ML/MH	5	18	505	1.46	0.1730	1.37	1.49	0.58	0.4	0.55
32	ML/MH	5	18	510	1.43	0.1860	1.52	1.50	0.58	0.4	0.55
33	ML/MH	5	18	515	1.40	0.1872	1.53	1.50	0.58	0.4	0.55
34	ML/MH	5	18	520	1.37	0.1892	1.50	1.49	0.58	0.4	0.55
35	ML/MH	5	18	525	1.34	0.1988	1.50	1.49	0.58	0.4	0.55
36	ML/MH	5	18	530	1.32	0.2070	1.52	1.49	0.58	0.4	0.55
37	ML/MH	5	18	530	1.29	0.2188	1.52	1.47	0.582	0.4	0.55
38	ML/MH	5	18	530	1.27	0.2284	1.49	1.44	0.592	0.4	0.65
39	ML/MH	5	18	530	1.25	0.2496	1.53	1.37	0.608	0.4	1.1
40	ML/MH	5	18	530	1.23	0.2600	1.52	1.32	0.58	0.36	1.5

Table 6B.20: Input parameters for site KIKNET effective stress analysis (Max Ru = 0.95 for all layers)

Layer	Model	f/s/f	p/r/Dr	F/A/FC	s/B/-	g/C/-	v/D/v	-/g/-	$C_v(m^2/s)$
1	2	0.025	0.381	10.5953	-19.8086	10.0997	-0.8738	0.0192	2.10E-06
2	2	0.027	0.393	11.1832	-21.3223	11.2115	-1.0579	0.0266	2.10E-06
3	2	0.029	0.401	11.5505	-22.2829	11.9345	-1.1862	0.0307	2.10E-06
4	2	0.031	0.410	11.9895	-23.4457	12.8273	-1.3537	0.0343	2.10E-06
5	2	0.037	0.435	13.2256	-26.8024	15.5076	-1.9162	0.0354	2.10E-06
6	2	0.041	0.454	14.1792	-29.4716	17.7426	-2.4520	0.0365	2.10E-06
7	2	0.044	0.464	14.6788	-30.8967	18.9715	-2.7719	0.0382	2.10E-06
8	2	0.046	0.472	15.1208	-32.1724	20.0919	-3.0790	0.0395	2.10E-06
9	2	0.046	0.472	15.1208	-32.1724	20.0919	-3.0790	0.0417	2.10E-06
10	2	0.046	0.472	15.1208	-32.1724	20.0919	-3.0790	0.0437	2.10E-06
11	2	0.046	0.472	15.1208	-32.1724	20.0919	-3.0790	0.0455	2.10E-06
12	2	0.046	0.472	15.1208	-32.1724	20.0919	-3.0790	0.0472	2.10E-06
13	2	0.046	0.472	15.1208	-32.1724	20.0919	-3.0790	0.0488	2.10E-06
14	2	0.046	0.472	15.1208	-32.1724	20.0919	-3.0790	0.0503	2.10E-06
15	1	1.000	1.000	1.0335	1.5372	0.0485	1.0000	0.0000	1.00E-04
16	1	1.000	1.000	1.0335	1.5372	0.0477	1.0000	0.0000	1.00E-04
17	1	1.000	1.000	1.0335	1.5372	0.0482	1.0000	0.0000	1.00E-04
18	1	1.000	1.000	1.0335	1.5372	0.0501	1.0000	0.0000	1.00E-04
19	1	1.000	1.000	1.0335	1.5372	0.0518	1.0000	0.0000	1.00E-04
20	1	1.000	1.000	1.0335	1.5372	0.0534	1.0000	0.0000	1.00E-04
21	1	1.000	1.000	1.0335	1.5372	0.0549	1.0000	0.0000	1.00E-04
22	1	1.000	1.000	1.0335	1.5372	0.0564	1.0000	0.0000	1.00E-04
23	1	1.000	1.000	1.0335	1.5372	0.0578	1.0000	0.0000	1.00E-04
24	1	1.000	1.000	1.0335	1.5372	0.0591	1.0000	0.0000	1.00E-04
25	1	1.000	1.000	1.0335	1.5372	0.0604	1.0000	0.0000	1.00E-04
26	1	1.000	1.000	1.0335	1.5372	0.0616	1.0000	0.0000	1.00E-04
27	1	1.000	1.000	0.4341	1.3073	0.0473	1.0000	0.0000	6.94E-04
28	1	1.000	1.000	0.4341	1.3073	0.0478	1.0000	0.0000	6.94E-04
29	1	1.000	1.000	0.4341	1.3073	0.0495	1.0000	0.0000	6.94E-04
30	2	0.063	0.448	11.5505	-22.2829	11.9345	-1.1862	0.1297	3.24E-05
31	2	0.068	0.458	11.9895	-23.4457	12.8273	-1.3537	0.1291	3.24E-05
32	2	0.070	0.464	12.2446	-24.1287	13.3604	-1.4586	0.1304	3.24E-05
33	2	0.073	0.471	12.530345	-24.8997	13.9698	-1.5827	0.1311	3.24E-05
34	2	0.073	0.471	12.5303	-24.8997	13.9698	-1.5827	0.1348	3.24E-05
35	2	0.073	0.471	12.5303	-24.8997	13.9698	-1.5827	0.1382	3.24E-05
36	2	0.073	0.471	12.5303	-24.8997	13.9698	-1.5827	0.1416	3.24E-05
37	2	0.073	0.471	12.5303	-24.8997	13.9698	-1.5827	0.1447	3.24E-05
38	2	0.073	0.471	12.5303	-24.8997	13.9698	-1.5827	0.1478	3.24E-05
39	2	0.073	0.471	12.5303	-24.8997	13.9698	-1.5827	0.1507	3.24E-05
40	2	0.073	0.471	12.5303	-24.8997	13.9698	-1.5827	0.1536	3.24E-05

Table 6B.21: Input for site KIKNET160 total stress analysis (Ref Stress = 0.18; b = d = 0 for all layers)

Layer	Name	Thick (m)	γ (kN/m3)	Vs (m/s)	Dmin	Ref Strain	B	s	P1	P2	P3
1	CH	0.7	15.5	80	8.85	0.0692	1.56	1.25	0.582	0.36	1.225
2	CH	0.7	15.5	80	6.58	0.1182	1.50	1.08	0.584	0.28	2.55
3	CH	0.7	15.5	80	5.73	0.1438	1.53	1.04	0.588	0.25	2.3
4	CH	1	16.5	110	5.12	0.1218	1.52	1.19	0.58	0.32	1.4
5	CH	1.1	16.5	110	4.73	0.1232	1.49	1.17	0.586	0.32	1.52
6	CH	1.1	16.5	110	4.46	0.1344	1.50	1.25	0.592	0.356	1.4
7	CH	1.1	16.5	110	4.23	0.1432	1.55	1.23	0.58	0.34	1.55
8	CH	1.1	16.5	110	4.05	0.1492	1.53	1.20	0.592	0.336	1.45
9	CH	1.1	16.5	110	3.87	0.1612	1.49	1.14	0.582	0.3	1.9
10	CH	1.1	16.5	110	3.73	0.1824	1.55	1.10	0.584	0.28	2.2
11	CH	1.1	16.5	110	3.60	0.1930	1.53	1.07	0.584	0.26	2.25
12	CH	1.1	16.5	110	3.49	0.2038	1.53	1.05	0.59	0.252	1.95
13	CH	1.1	16.5	110	3.40	0.2108	1.50	1.04	0.584	0.24	2.25
14	CH	1.1	16.5	110	3.31	0.2238	1.52	1.02	0.592	0.234	2
15	SM	1.9	17	200	1.72	0.1270	1.52	1.05	0.584	0.26	2.4
16	SM	2	17	200	1.68	0.1242	1.53	1.07	0.586	0.268	2.1
17	SM	2	17	200	1.64	0.1248	1.53	1.07	0.59	0.272	2.05
18	SM	2	17	200	1.59	0.1284	1.50	1.05	0.584	0.26	2.4
19	SM	2	17	200	1.54	0.1374	1.55	1.05	0.584	0.26	2.35
20	SM	2	17	200	1.50	0.1438	1.53	1.02	0.584	0.24	2.5
21	SM	2	17	200	1.47	0.1448	1.49	1.02	0.584	0.24	2.4
22	SM	2	17	200	1.44	0.1536	1.52	1.01	0.598	0.242	2.15
23	SM	2	17	200	1.41	0.1550	1.49	1.01	0.598	0.242	2.1
24	SM	2	17	200	1.38	0.1590	1.47	0.99	0.584	0.22	2.5
25	SM	2	17	200	1.35	0.1650	1.47	0.98	0.6	0.224	2.25
26	SM	2	17	200	1.33	0.1710	1.49	0.98	0.6	0.224	2.2
27	SW-SM	3	19	350	1.04	0.1132	1.58	1.11	0.592	0.296	1.5
28	SW-SM	3.5	19	350	1.02	0.1134	1.58	1.13	0.582	0.3	1.8
29	SW-SM	3.5	19	350	0.99	0.1190	1.55	1.10	0.582	0.28	1.85
30	ML/MH	5	18	500	1.49	0.1736	1.35	1.47	0.58	0.4	0.55
31	ML/MH	5	18	505	1.46	0.1730	1.37	1.49	0.58	0.4	0.55
32	ML/MH	5	18	510	1.43	0.1860	1.52	1.50	0.58	0.4	0.55
33	ML/MH	5	18	515	1.40	0.1872	1.53	1.50	0.58	0.4	0.55
34	ML/MH	5	18	520	1.37	0.1892	1.50	1.49	0.58	0.4	0.55
35	ML/MH	5	18	525	1.34	0.1988	1.50	1.49	0.58	0.4	0.55
36	ML/MH	5	18	530	1.32	0.2070	1.52	1.49	0.58	0.4	0.55
37	ML/MH	5	18	530	1.29	0.2188	1.52	1.47	0.582	0.4	0.55
38	ML/MH	5	18	530	1.27	0.2284	1.49	1.44	0.592	0.4	0.65
39	ML/MH	5	18	530	1.25	0.2496	1.53	1.37	0.608	0.4	1.1
40	ML/MH	5	18	530	1.23	0.2600	1.52	1.32	0.58	0.36	1.5

Table 6B.22: Input parameters for site KIKNET160 effective stress analysis (Max Ru = 0.95 for all layers)

Layer	Model	f/s/f	p/r/Dr	F/A/FC	s/B/-	g/C/-	v/D/v	-/g/-	$C_v(m^2/s)$
1	2	0.014	0.352	10.5953	-19.8086	10.0997	-0.8738	0.0344	3.03E-07
2	2	0.016	0.364	11.1832	-21.3223	11.2115	-1.0579	0.0473	3.03E-07
3	2	0.017	0.371	11.5505	-22.2829	11.9345	-1.1862	0.0544	3.03E-07
4	2	0.018	0.379	11.9895	-23.4457	12.8273	-1.3537	0.0605	3.03E-07
5	2	0.021	0.403	13.2256	-26.8024	15.5076	-1.9162	0.0616	3.03E-07
6	2	0.024	0.420	14.1792	-29.4716	17.7426	-2.4520	0.0629	3.03E-07
7	2	0.025	0.429	14.6788	-30.8967	18.9715	-2.7719	0.0653	3.03E-07
8	2	0.026	0.437	15.1208	-32.1724	20.0919	-3.0790	0.0673	3.03E-07
9	2	0.026	0.437	15.1208	-32.1724	20.0919	-3.0790	0.0710	3.03E-07
10	2	0.026	0.437	15.1208	-32.1724	20.0919	-3.0790	0.0744	3.03E-07
11	2	0.026	0.437	15.1208	-32.1724	20.0919	-3.0790	0.0775	3.03E-07
12	2	0.026	0.437	15.1208	-32.1724	20.0919	-3.0790	0.0804	3.03E-07
13	2	0.026	0.437	15.1208	-32.1724	20.0919	-3.0790	0.0831	3.03E-07
14	2	0.026	0.437	15.1208	-32.1724	20.0919	-3.0790	0.0856	3.03E-07
15	1	1.000	1.000	1.0335	1.5372	0.0485	1.0000	0.0000	1.00E-04
16	1	1.000	1.000	1.0335	1.5372	0.0477	1.0000	0.0000	1.00E-04
17	1	1.000	1.000	1.0335	1.5372	0.0482	1.0000	0.0000	1.00E-04
18	1	1.000	1.000	1.0335	1.5372	0.0501	1.0000	0.0000	1.00E-04
19	1	1.000	1.000	1.0335	1.5372	0.0518	1.0000	0.0000	1.00E-04
20	1	1.000	1.000	1.0335	1.5372	0.0534	1.0000	0.0000	1.00E-04
21	1	1.000	1.000	1.0335	1.5372	0.0549	1.0000	0.0000	1.00E-04
22	1	1.000	1.000	1.0335	1.5372	0.0564	1.0000	0.0000	1.00E-04
23	1	1.000	1.000	1.0335	1.5372	0.0578	1.0000	0.0000	1.00E-04
24	1	1.000	1.000	1.0335	1.5372	0.0591	1.0000	0.0000	1.00E-04
25	1	1.000	1.000	1.0335	1.5372	0.0604	1.0000	0.0000	1.00E-04
26	1	1.000	1.000	1.0335	1.5372	0.0616	1.0000	0.0000	1.00E-04
27	1	1.000	1.000	0.4341	1.3073	0.0473	1.0000	0.0000	6.94E-04
28	1	1.000	1.000	0.4341	1.3073	0.0478	1.0000	0.0000	6.94E-04
29	1	1.000	1.000	0.4341	1.3073	0.0495	1.0000	0.0000	6.94E-04
30	2	0.063	0.448	11.5505	-22.2829	11.9345	-1.1862	0.1297	3.24E-05
31	2	0.068	0.458	11.9895	-23.4457	12.8273	-1.3537	0.1291	3.24E-05
32	2	0.070	0.464	12.2446	-24.1287	13.3604	-1.4586	0.1304	3.24E-05
33	2	0.073	0.471	12.530345	-24.8997	13.9698	-1.5827	0.1311	3.24E-05
34	2	0.073	0.471	12.5303	-24.8997	13.9698	-1.5827	0.1348	3.24E-05
35	2	0.073	0.471	12.5303	-24.8997	13.9698	-1.5827	0.1382	3.24E-05
36	2	0.073	0.471	12.5303	-24.8997	13.9698	-1.5827	0.1416	3.24E-05
37	2	0.073	0.471	12.5303	-24.8997	13.9698	-1.5827	0.1447	3.24E-05
38	2	0.073	0.471	12.5303	-24.8997	13.9698	-1.5827	0.1478	3.24E-05
39	2	0.073	0.471	12.5303	-24.8997	13.9698	-1.5827	0.1507	3.24E-05
40	2	0.073	0.471	12.5303	-24.8997	13.9698	-1.5827	0.1536	3.24E-05

Table 6B.23: Input for site KIKNET S2 total stress analysis (Ref Stress = 0.18; b = d = 0 for all layers)

Layer	Name	Thick (m)	γ (kN/m3)	Vs (m/s)	Dmin	Ref Strain	B	s	P1	P2	P3
1	CH	0.7	15.5	80	5.79	0.0610	1.52	0.90	0.646	0.242	3.25
2	CH	0.7	15.5	80	4.28	0.0892	1.52	0.86	0.668	0.224	3.1
3	CH	0.7	15.5	80	3.70	0.1188	1.59	0.81	0.716	0.234	2.48
4	CH	1	16.5	110	3.32	0.1084	1.52	0.90	0.642	0.226	2.65
5	CH	1.1	16.5	110	3.04	0.1150	1.55	0.90	0.644	0.228	2.55
6	CH	1.1	16.5	110	2.85	0.1178	1.53	0.90	0.644	0.228	2.5
7	CH	1.1	16.5	110	2.70	0.1188	1.50	0.90	0.644	0.228	2.2
8	CH	1.1	16.5	110	2.58	0.1286	1.52	0.89	0.638	0.214	2.65
9	CH	1.1	16.5	110	2.46	0.1398	1.52	0.87	0.676	0.236	1.9
10	CH	1.1	16.5	110	2.36	0.1442	1.47	0.86	0.71	0.258	1.5
11	CH	1.1	16.5	110	2.28	0.1546	1.47	0.84	0.7	0.238	1.65
12	CH	1.1	16.5	110	2.21	0.1630	1.46	0.83	0.724	0.248	1.4
13	CH	1.1	16.5	110	2.15	0.1912	1.58	0.81	0.716	0.23	1.55
14	CH	1.1	16.5	110	2.09	0.1982	1.55	0.80	0.744	0.244	1.32
15	SM	1.9	17	200	1.71	0.1512	1.53	0.92	0.598	0.194	3.05
16	SM	2	17	200	1.67	0.1452	1.53	0.93	0.6	0.202	2.7
17	SM	2	17	200	1.63	0.1482	1.55	0.93	0.6	0.202	2.7
18	SM	2	17	200	1.58	0.1562	1.53	0.92	0.596	0.19	3.1
19	SM	2	17	200	1.53	0.1630	1.53	0.92	0.598	0.194	2.85
20	SM	2	17	200	1.49	0.1690	1.50	0.90	0.64	0.218	2
21	SM	2	17	200	1.45	0.1766	1.50	0.89	0.664	0.228	1.65
22	SM	2	17	200	1.42	0.1804	1.49	0.89	0.68	0.244	1.4
23	SM	2	17	200	1.39	0.1888	1.49	0.87	0.658	0.214	1.75
24	SM	2	17	200	1.36	0.1972	1.49	0.86	0.68	0.22	1.48
25	SM	2	17	200	1.34	0.2014	1.47	0.86	0.696	0.238	1.3
26	SM	2	17	200	1.31	0.2100	1.47	0.84	0.722	0.248	1.1
27	SW-SM	3	19	350	1.03	0.1380	1.53	0.96	0.596	0.218	2.5
28	SW-SM	3.5	19	350	1.01	0.1432	1.56	0.96	0.596	0.218	2.6
29	SW-SM	3.5	19	350	0.98	0.1510	1.56	0.95	0.586	0.2	3.05
30	ML/MH	5	18	500	1.49	0.2982	1.53	1.10	0.584	0.264	2
31	ML/MH	5	18	505	1.46	0.2938	1.55	1.11	0.584	0.28	2.25
32	ML/MH	5	18	510	1.43	0.2956	1.55	1.11	0.584	0.28	2.25
33	ML/MH	5	18	515	1.40	0.2960	1.55	1.11	0.584	0.28	2.3
34	ML/MH	5	18	520	1.37	0.3074	1.55	1.11	0.584	0.28	2.3
35	ML/MH	5	18	525	1.34	0.3172	1.53	1.10	0.584	0.264	2.05
36	ML/MH	5	18	530	1.31	0.3282	1.53	1.08	0.584	0.26	2.35
37	ML/MH	5	18	530	1.29	0.3346	1.52	1.08	0.584	0.26	2.25
38	ML/MH	5	18	530	1.27	0.3166	1.37	1.07	0.586	0.246	2.05
39	ML/MH	5	18	530	1.25	0.3296	1.37	1.05	0.584	0.24	2.35
40	ML/MH	5	18	530	1.23	0.3390	1.37	1.05	0.584	0.24	2.3

Table 6B. 24: Input parameters for site KIKNET S2 effective stress analysis (Max Ru = 0.95 for all layers)

Layer	Model	f/s/f	p/r/Dr	F/A/FC	s/B/-	g/C/-	v/D/v	-/g/-	$C_v(m^2/s)$
1	2	0.025	0.381	10.5953	-19.8086	10.0997	-0.8738	0.0192	2.10E-06
2	2	0.027	0.393	11.1832	-21.3223	11.2115	-1.0579	0.0266	2.10E-06
3	2	0.029	0.401	11.5505	-22.2829	11.9345	-1.1862	0.0307	2.10E-06
4	2	0.031	0.410	11.9895	-23.4457	12.8273	-1.3537	0.0343	2.10E-06
5	2	0.037	0.435	13.2256	-26.8024	15.5076	-1.9162	0.0354	2.10E-06
6	2	0.041	0.454	14.1792	-29.4716	17.7426	-2.4520	0.0365	2.10E-06
7	2	0.044	0.464	14.6788	-30.8967	18.9715	-2.7719	0.0382	2.10E-06
8	2	0.046	0.472	15.1208	-32.1724	20.0919	-3.0790	0.0395	2.10E-06
9	2	0.046	0.472	15.1208	-32.1724	20.0919	-3.0790	0.0417	2.10E-06
10	2	0.046	0.472	15.1208	-32.1724	20.0919	-3.0790	0.0437	2.10E-06
11	2	0.046	0.472	15.1208	-32.1724	20.0919	-3.0790	0.0455	2.10E-06
12	2	0.046	0.472	15.1208	-32.1724	20.0919	-3.0790	0.0472	2.10E-06
13	2	0.046	0.472	15.1208	-32.1724	20.0919	-3.0790	0.0488	2.10E-06
14	2	0.046	0.472	15.1208	-32.1724	20.0919	-3.0790	0.0503	2.10E-06
15	1	1.000	1.000	1.0335	1.5372	0.0485	1.0000	0.0000	1.00E-04
16	1	1.000	1.000	1.0335	1.5372	0.0477	1.0000	0.0000	1.00E-04
17	1	1.000	1.000	1.0335	1.5372	0.0482	1.0000	0.0000	1.00E-04
18	1	1.000	1.000	1.0335	1.5372	0.0501	1.0000	0.0000	1.00E-04
19	1	1.000	1.000	1.0335	1.5372	0.0518	1.0000	0.0000	1.00E-04
20	1	1.000	1.000	1.0335	1.5372	0.0534	1.0000	0.0000	1.00E-04
21	1	1.000	1.000	1.0335	1.5372	0.0549	1.0000	0.0000	1.00E-04
22	1	1.000	1.000	1.0335	1.5372	0.0564	1.0000	0.0000	1.00E-04
23	1	1.000	1.000	1.0335	1.5372	0.0578	1.0000	0.0000	1.00E-04
24	1	1.000	1.000	1.0335	1.5372	0.0591	1.0000	0.0000	1.00E-04
25	1	1.000	1.000	1.0335	1.5372	0.0604	1.0000	0.0000	1.00E-04
26	1	1.000	1.000	1.0335	1.5372	0.0616	1.0000	0.0000	1.00E-04
27	1	1.000	1.000	0.4341	1.3073	0.0473	1.0000	0.0000	6.94E-04
28	1	1.000	1.000	0.4341	1.3073	0.0478	1.0000	0.0000	6.94E-04
29	1	1.000	1.000	0.4341	1.3073	0.0495	1.0000	0.0000	6.94E-04
30	2	0.063	0.448	11.5505	-22.2829	11.9345	-1.1862	0.1297	3.24E-05
31	2	0.068	0.458	11.9895	-23.4457	12.8273	-1.3537	0.1291	3.24E-05
32	2	0.070	0.464	12.2446	-24.1287	13.3604	-1.4586	0.1304	3.24E-05
33	2	0.073	0.471	12.530345	-24.8997	13.9698	-1.5827	0.1311	3.24E-05
34	2	0.073	0.471	12.5303	-24.8997	13.9698	-1.5827	0.1348	3.24E-05
35	2	0.073	0.471	12.5303	-24.8997	13.9698	-1.5827	0.1382	3.24E-05
36	2	0.073	0.471	12.5303	-24.8997	13.9698	-1.5827	0.1416	3.24E-05
37	2	0.073	0.471	12.5303	-24.8997	13.9698	-1.5827	0.1447	3.24E-05
38	2	0.073	0.471	12.5303	-24.8997	13.9698	-1.5827	0.1478	3.24E-05
39	2	0.073	0.471	12.5303	-24.8997	13.9698	-1.5827	0.1507	3.24E-05
40	2	0.073	0.471	12.5303	-24.8997	13.9698	-1.5827	0.1536	3.24E-05

Table 6B.25: Input for site KIKNET S4 total stress analysis (Ref Stress = 0.18; b = d = 0 for all layers)

Layer	Name	Thick (m)	γ (kN/m3)	Vs (m/s)	Dmin	Ref Strain	B	s	P1	P2	P3
1	CH	0.7	15.5	80	5.74	0.0746	1.58	0.80	0.736	0.254	3.065
2	CH	0.7	15.5	80	4.23	0.1066	1.53	0.77	0.774	0.268	2.2
3	CH	0.7	15.5	80	3.64	0.1340	1.44	0.71	0.874	0.316	1.65
4	CH	1	16.5	110	3.28	0.1386	1.55	0.78	0.754	0.248	2.05
5	CH	1.1	16.5	110	3.01	0.1426	1.55	0.78	0.754	0.248	1.9
6	CH	1.1	16.5	110	2.82	0.1486	1.55	0.78	0.76	0.256	1.8
7	CH	1.1	16.5	110	2.66	0.1550	1.55	0.78	0.774	0.274	1.5
8	CH	1.1	16.5	110	2.54	0.1634	1.53	0.77	0.802	0.286	1.3
9	CH	1.1	16.5	110	2.42	0.1762	1.50	0.75	0.802	0.28	1.35
10	CH	1.1	16.5	110	2.32	0.1906	1.49	0.74	0.844	0.31	1.1
11	CH	1.1	16.5	110	2.24	0.2050	1.47	0.72	0.86	0.318	1.075
12	CH	1.1	16.5	110	2.16	0.2192	1.46	0.71	0.882	0.328	0.99
13	CH	1.1	16.5	110	2.10	0.2334	1.44	0.69	0.896	0.332	0.98
14	CH	1.1	16.5	110	2.04	0.2474	1.43	0.68	0.914	0.336	0.93
15	SM	1.9	17	200	1.68	0.1944	1.55	0.80	0.764	0.268	1.22
16	SM	2	17	200	1.65	0.1892	1.58	0.81	0.736	0.252	1.4
17	SM	2	17	200	1.60	0.1914	1.58	0.81	0.736	0.252	1.4
18	SM	2	17	200	1.55	0.2034	1.56	0.80	0.762	0.264	1.2
19	SM	2	17	200	1.50	0.2090	1.53	0.78	0.734	0.228	1.45
20	SM	2	17	200	1.46	0.2220	1.52	0.77	0.778	0.254	1.1
21	SM	2	17	200	1.42	0.2332	1.52	0.77	0.808	0.29	0.94
22	SM	2	17	200	1.39	0.2474	1.52	0.75	0.84	0.306	0.8
23	SM	2	17	200	1.36	0.2524	1.49	0.74	0.8	0.256	1
24	SM	2	17	200	1.33	0.2696	1.50	0.74	0.848	0.308	0.8
25	SM	2	17	200	1.30	0.2736	1.47	0.72	0.856	0.3	0.75
26	SM	2	17	200	1.28	0.2840	1.47	0.72	0.834	0.286	0.85
27	SW-SM	3	19	350	1.01	0.1622	1.47	0.84	0.706	0.246	1.55
28	SW-SM	3.5	19	350	0.99	0.1614	1.46	0.84	0.7	0.238	1.6
29	SW-SM	3.5	19	350	0.95	0.1718	1.46	0.83	0.736	0.258	1.25
30	ML/MH	5	18	500	1.48	0.3458	1.38	0.95	0.606	0.192	1.65
31	ML/MH	5	18	505	1.45	0.3386	1.38	0.95	0.602	0.186	1.7
32	ML/MH	5	18	510	1.42	0.3412	1.38	0.95	0.6	0.182	1.7
33	ML/MH	5	18	515	1.39	0.3442	1.38	0.95	0.602	0.186	1.8
34	ML/MH	5	18	520	1.36	0.3102	1.22	0.95	0.6	0.184	1.7
35	ML/MH	5	18	525	1.33	0.3226	1.22	0.95	0.602	0.186	1.65
36	ML/MH	5	18	530	1.31	0.3356	1.22	0.93	0.588	0.162	2.02
37	ML/MH	5	18	530	1.28	0.3458	1.22	0.93	0.592	0.166	1.76
38	ML/MH	5	18	530	1.26	0.3082	1.05	0.92	0.602	0.162	1.625
39	ML/MH	5	18	530	1.24	0.3160	1.05	0.92	0.618	0.176	1.235
40	ML/MH	5	18	530	1.22	0.3284	1.05	0.90	0.64	0.182	1

Table 6B.26: Input parameters for site KIKNET S4 effective stress analysis (Max Ru = 0.95 for all layers)

Layer	Model	f/s/f	p/r/Dr	F/A/FC	s/B/-	g/C/-	v/D/v	-/g/-	$C_v(m^2/s)$
1	2	0.025	0.381	10.5953	-19.8086	10.0997	-0.8738	0.0192	2.10E-06
2	2	0.027	0.393	11.1832	-21.3223	11.2115	-1.0579	0.0266	2.10E-06
3	2	0.029	0.401	11.5505	-22.2829	11.9345	-1.1862	0.0307	2.10E-06
4	2	0.031	0.410	11.9895	-23.4457	12.8273	-1.3537	0.0343	2.10E-06
5	2	0.037	0.435	13.2256	-26.8024	15.5076	-1.9162	0.0354	2.10E-06
6	2	0.041	0.454	14.1792	-29.4716	17.7426	-2.4520	0.0365	2.10E-06
7	2	0.044	0.464	14.6788	-30.8967	18.9715	-2.7719	0.0382	2.10E-06
8	2	0.046	0.472	15.1208	-32.1724	20.0919	-3.0790	0.0395	2.10E-06
9	2	0.046	0.472	15.1208	-32.1724	20.0919	-3.0790	0.0417	2.10E-06
10	2	0.046	0.472	15.1208	-32.1724	20.0919	-3.0790	0.0437	2.10E-06
11	2	0.046	0.472	15.1208	-32.1724	20.0919	-3.0790	0.0455	2.10E-06
12	2	0.046	0.472	15.1208	-32.1724	20.0919	-3.0790	0.0472	2.10E-06
13	2	0.046	0.472	15.1208	-32.1724	20.0919	-3.0790	0.0488	2.10E-06
14	2	0.046	0.472	15.1208	-32.1724	20.0919	-3.0790	0.0503	2.10E-06
15	1	1.000	1.000	1.0335	1.5372	0.0485	1.0000	0.0000	1.00E-04
16	1	1.000	1.000	1.0335	1.5372	0.0477	1.0000	0.0000	1.00E-04
17	1	1.000	1.000	1.0335	1.5372	0.0482	1.0000	0.0000	1.00E-04
18	1	1.000	1.000	1.0335	1.5372	0.0501	1.0000	0.0000	1.00E-04
19	1	1.000	1.000	1.0335	1.5372	0.0518	1.0000	0.0000	1.00E-04
20	1	1.000	1.000	1.0335	1.5372	0.0534	1.0000	0.0000	1.00E-04
21	1	1.000	1.000	1.0335	1.5372	0.0549	1.0000	0.0000	1.00E-04
22	1	1.000	1.000	1.0335	1.5372	0.0564	1.0000	0.0000	1.00E-04
23	1	1.000	1.000	1.0335	1.5372	0.0578	1.0000	0.0000	1.00E-04
24	1	1.000	1.000	1.0335	1.5372	0.0591	1.0000	0.0000	1.00E-04
25	1	1.000	1.000	1.0335	1.5372	0.0604	1.0000	0.0000	1.00E-04
26	1	1.000	1.000	1.0335	1.5372	0.0616	1.0000	0.0000	1.00E-04
27	1	1.000	1.000	0.4341	1.3073	0.0473	1.0000	0.0000	6.94E-04
28	1	1.000	1.000	0.4341	1.3073	0.0478	1.0000	0.0000	6.94E-04
29	1	1.000	1.000	0.4341	1.3073	0.0495	1.0000	0.0000	6.94E-04
30	2	0.063	0.448	11.5505	-22.2829	11.9345	-1.1862	0.1297	3.24E-05
31	2	0.068	0.458	11.9895	-23.4457	12.8273	-1.3537	0.1291	3.24E-05
32	2	0.070	0.464	12.2446	-24.1287	13.3604	-1.4586	0.1304	3.24E-05
33	2	0.073	0.471	12.530345	-24.8997	13.9698	-1.5827	0.1311	3.24E-05
34	2	0.073	0.471	12.5303	-24.8997	13.9698	-1.5827	0.1348	3.24E-05
35	2	0.073	0.471	12.5303	-24.8997	13.9698	-1.5827	0.1382	3.24E-05
36	2	0.073	0.471	12.5303	-24.8997	13.9698	-1.5827	0.1416	3.24E-05
37	2	0.073	0.471	12.5303	-24.8997	13.9698	-1.5827	0.1447	3.24E-05
38	2	0.073	0.471	12.5303	-24.8997	13.9698	-1.5827	0.1478	3.24E-05
39	2	0.073	0.471	12.5303	-24.8997	13.9698	-1.5827	0.1507	3.24E-05
40	2	0.073	0.471	12.5303	-24.8997	13.9698	-1.5827	0.1536	3.24E-05

Table 6B.27: Input parameters for site MRCE1 total stress analysis (Ref Stress = 0.18; b = d = 0 for all layers)

Layer	Name	Thick (m)	γ (kN/m3)	Vs (m/s)	Dmin	Ref Strain	B	s	P1	P2	P3
1	SM	1.5	17	225	2.01	0.0162	1.365	0.87	0.71	0.288	3.25
2	SM	1.5	17	155	1.42	0.0294	1.545	0.825	0.762	0.32	3.25
3	OH	0.85	15	85	2.22	0.1756	1.59	0.66	0.92	0.354	1.65
4	OH	0.85	15	85	2.19	0.1304	1.455	0.705	0.884	0.348	1.55
5	OH	0.85	15	85	2.12	0.1320	1.455	0.705	0.88	0.342	1.55
6	OH	0.85	15	85	2.03	0.1388	1.44	0.69	0.908	0.356	1.45
7	OH	0.85	15	85	1.95	0.1466	1.41	0.675	0.918	0.358	1.475
8	OH	0.85	15	88	1.92	0.1440	1.425	0.69	0.9	0.346	1.45
9	OH	0.9	15	92	1.89	0.1440	1.455	0.705	0.86	0.316	1.65
10	OH	0.9	15	95	1.85	0.1476	1.47	0.705	0.866	0.312	1.545
11	OH	0.9	15	98	1.81	0.1530	1.47	0.705	0.88	0.324	1.4
12	OH	1	15	102	1.77	0.1576	1.47	0.705	0.866	0.308	1.485
13	OH	1	15	105	1.73	0.1576	1.455	0.705	0.854	0.296	1.49
14	OH	1	15	108	1.70	0.1636	1.485	0.72	0.856	0.318	1.35
15	OH	1	15	112	1.67	0.1658	1.485	0.72	0.846	0.304	1.35
16	OH	1	15	115	1.63	0.1702	1.47	0.72	0.854	0.314	1.275
17	OH	1	15	118	1.60	0.1788	1.455	0.705	0.862	0.302	1.3
18	OH	1.1	15	122	1.56	0.1856	1.455	0.705	0.864	0.308	1.25
19	OH	1.1	15	125	1.53	0.1954	1.455	0.705	0.884	0.33	1.1
20	SP-SM	1.5	18	150	1.23	0.1248	1.515	0.765	0.774	0.268	1.9
21	SP-SM	1.5	18	169	1.20	0.1242	1.545	0.795	0.732	0.244	2.15
22	ML/CL	1.5	18	176	1.67	0.2560	1.485	0.87	0.68	0.224	1.2
23	ML/CL	1.5	18	186	1.66	0.2338	1.53	0.915	0.624	0.204	1.97
24	ML/CL	1.5	18	196	1.65	0.2150	1.545	0.945	0.598	0.2	2.4
25	ML/CL	2	18	206	1.62	0.1900	1.47	0.99	0.584	0.22	2.4
26	ML/CL	2	18	216	1.59	0.1884	1.47	1.005	0.59	0.23	2.15
27	ML/CL	2	18	226	1.55	0.1946	1.5	1.005	0.586	0.224	2.15
28	ML/CL	2	18	236	1.52	0.1998	1.485	1.005	0.584	0.222	2.35
29	ML/CL	2	18	246	1.49	0.2012	1.485	1.02	0.586	0.24	2.555
30	ML/CL	2	18	256	1.46	0.2032	1.485	1.02	0.596	0.24	2
31	ML/CL	2	18	260	1.44	0.2100	1.5	1.02	0.596	0.24	2
32	ML/CL	2	18	264	1.41	0.2144	1.5	1.02	0.596	0.24	2
33	ML/CL	2.5	18	268	1.39	0.2194	1.5	1.02	0.596	0.24	2
34	ML/CL	2.5	18	272	1.36	0.2250	1.5	1.02	0.596	0.24	2
35	ML/CL	2.5	18	276	1.34	0.2292	1.485	1.005	0.584	0.22	2.4
36	SP-SM	2.5	20	280	0.89	0.1622	1.47	0.84	0.714	0.252	1.445
37	SP-SM	2.5	20	286	0.87	0.1678	1.485	0.84	0.714	0.252	1.41
38	SP-SM	2.5	20	292	0.85	0.1700	1.47	0.84	0.716	0.254	1.385
39	SP-SM	2.5	20	298	0.84	0.1758	1.485	0.84	0.716	0.254	1.37

40	CH	3	20	325	1.44	0.2406	1.5	1.2	0.584	0.32	1.8
41	CH	3	20	330	1.41	0.2456	1.5	1.2	0.582	0.32	1.85
42	CH	3	20	336	1.39	0.2518	1.515	1.2	0.582	0.32	1.85
43	CH	3	20	341	1.37	0.2542	1.5	1.2	0.582	0.32	1.85
44	CH	3	20	346	1.35	0.2604	1.515	1.2	0.582	0.32	1.85
45	CH	3	20	351	1.33	0.2644	1.515	1.2	0.582	0.32	1.85
46	SP-SM	6	21	607	0.77	0.1530	1.485	1.02	0.584	0.24	2.4
47	SP-SM	6	21	624	0.74	0.1610	1.515	1.02	0.584	0.24	2.35

Table 6B.28: Input parameters for site MRCE1 effective stress analysis (Max Ru = 0.95 for all layers)

Layer	Model	f/s/f	p/r/Dr	F/A/FC	s/B/-	g/C/-	v/D/v	-/g/-	$C_v(m^2/s)$
1	1	1.000	1.000	0.8611	1.5372	0.0056	1.0000	0.0000	6.12E-02
2	1	1.000	1.000	1.5343	1.5372	0.0082	1.0000	0.0000	6.12E-02
3	2	0.039	0.412	11.1630	-21.2698	11.1724	-1.0512	0.0313	2.10E-06
4	2	0.061	0.445	12.6547	-25.2374	14.2393	-1.6390	0.0296	2.10E-06
5	2	0.069	0.457	13.2256	-26.8024	15.5076	-1.9162	0.0299	2.10E-06
6	2	0.069	0.462	13.4425	-27.4035	16.0031	-2.0298	0.0309	2.10E-06
7	2	0.069	0.462	13.4425	-27.4035	16.0031	-2.0298	0.0321	2.10E-06
8	2	0.069	0.472	13.9594	-28.8506	17.2147	-2.3201	0.0322	2.10E-06
9	2	0.069	0.482	14.4179	-30.1503	18.3248	-2.6013	0.0324	2.10E-06
10	2	0.069	0.487	14.6788	-30.8967	18.9715	-2.7719	0.0329	2.10E-06
11	2	0.069	0.487	14.6788	-30.8967	18.9715	-2.7719	0.0338	2.10E-06
12	2	0.069	0.487	14.6788	-30.8967	18.9715	-2.7719	0.0348	2.10E-06
13	2	0.069	0.487	14.6788	-30.8967	18.9715	-2.7719	0.0357	2.10E-06
14	2	0.070	0.487	14.6788	-30.8967	18.9715	-2.7719	0.0366	2.10E-06
15	2	0.069	0.487	14.6788	-30.8967	18.9715	-2.7719	0.0375	2.10E-06
16	2	0.069	0.484	14.5453	-30.5143	18.6394	-2.6837	0.0386	2.10E-06
17	2	0.069	0.482	14.4179	-30.1503	18.3248	-2.6013	0.0397	2.10E-06
18	2	0.069	0.477	14.1792	-29.4716	17.7426	-2.4520	0.0411	2.10E-06
19	2	0.069	0.472	13.9594	-28.8506	17.2147	-2.3201	0.0425	2.10E-06
20	1	1.000	1.000	1.6143	1.3073	0.0310	1.0000	0.0000	1.63E-01
21	1	1.000	1.000	1.3418	1.3073	0.0322	1.0000	0.0000	1.63E-01
22	2	0.124	0.439	10.8113	-20.3612	10.5016	-0.9385	0.0776	1.45E-05
23	2	0.124	0.461	11.7161	-22.7198	12.2677	-1.2476	0.0736	1.45E-05
24	2	0.124	0.478	12.4120	-24.5795	13.7158	-1.5304	0.0714	1.45E-05
25	2	0.124	0.490	12.9240	-25.9725	14.8311	-1.7659	0.0707	1.45E-05
26	2	0.124	0.497	13.2256	-26.8024	15.5076	-1.9162	0.0713	1.45E-05
27	2	0.124	0.497	13.2256	-26.8024	15.5076	-1.9162	0.0734	1.45E-05
28	2	0.124	0.497	13.2256	-26.8024	15.5076	-1.9162	0.0753	1.45E-05
29	2	0.124	0.497	13.2256	-26.8024	15.5076	-1.9162	0.0772	1.45E-05
30	2	0.124	0.497	13.2256	-26.8024	15.5076	-1.9162	0.0790	1.45E-05
31	2	0.124	0.497	13.2256	-26.8024	15.5076	-1.9162	0.0807	1.45E-05
32	2	0.124	0.497	13.2256	-26.8024	15.5076	-1.9162	0.0824	1.45E-05
33	2	0.124	0.497	13.225596	-26.8024	15.5076	-1.9162	0.0842	1.45E-05
34	2	0.124	0.497	13.2256	-26.8024	15.5076	-1.9162	0.0861	1.45E-05
35	2	0.124	0.497	13.2256	-26.8024	15.5076	-1.9162	0.0879	1.45E-05
36	1	1.000	1.000	0.6135	1.3073	0.0473	1.0000	0.0000	1.63E-01
37	1	1.000	1.000	0.5937	1.3073	0.0484	1.0000	0.0000	1.63E-01
38	1	1.000	1.000	0.5749	1.3073	0.0494	1.0000	0.0000	1.63E-01
39	1	1.000	1.000	0.5570	1.3073	0.0504	1.0000	0.0000	1.63E-01

40	2	0.107	0.486	13.2256	-26.8024	15.5076	-1.9162	0.1218	1.45E-05
41	2	0.107	0.486	13.2256	-26.8024	15.5076	-1.9162	0.1244	1.45E-05
42	2	0.107	0.486	13.2256	-26.8024	15.5076	-1.9162	0.1270	1.45E-05
43	2	0.107	0.486	13.2256	-26.8024	15.5076	-1.9162	0.1295	1.45E-05
44	2	0.107	0.486	13.2256	-26.8024	15.5076	-1.9162	0.1319	1.45E-05
45	2	0.107	0.486	13.2256	-26.8024	15.5076	-1.9162	0.1342	1.45E-05
46	1	1.000	1.000	0.1849	1.3073	0.0583	1.0000	0.0000	1.63E-01
47	1	1.000	1.000	0.1772	1.3073	0.0602	1.0000	0.0000	1.63E-01

Table 6B.29: Input parameters for site MRCE2 total stress analysis (Ref Stress = 0.18; b = d = 0 for all layers)

Layer	Name	Thick (m)	γ (kN/m3)	Vs (m/s)	Dmin	Ref Strain	B	s	P1	P2	P3
1	SM	2	17	350	1.91	0.0182	1.485	0.945	0.648	0.29	3.25
2	SM	2	17	250	1.37	0.0294	1.575	0.915	0.664	0.28	3.25
3	OH	0.8	15	80	0.74	0.1382	1.545	0.795	0.618	0.222	1.55
4	OH	0.8	15.15	84	0.68	0.1032	1.44	0.825	0.594	0.216	1.8
5	OH	0.8	15.3	88	0.63	0.0932	1.485	0.84	0.586	0.22	2.13
6	OH	0.8	15.45	92	0.57	0.0822	1.47	0.855	0.59	0.23	1.8
7	OH	0.8	15.6	96	0.55	0.0840	1.455	0.855	0.586	0.226	1.85
8	OH	1	15.8	100	0.49	0.0784	1.455	0.84	0.584	0.22	2.3
9	OH	1	16	105	0.48	0.0834	1.5	0.855	0.588	0.228	1.85
10	OH	1	16.1	110	0.46	0.0826	1.455	0.855	0.586	0.226	1.85
11	OH	1	16.2	115	0.45	0.0882	1.5	0.855	0.584	0.222	1.85
12	OH	1	16.3	120	0.44	0.0888	1.485	0.87	0.602	0.248	1.5
13	OH	1.2	16.4	126	0.43	0.0912	1.485	0.87	0.594	0.238	1.55
14	OH	1.2	16.5	132	0.42	0.0924	1.485	0.885	0.582	0.24	1.7
15	OH	1.2	16.5	138	0.41	0.0962	1.5	0.885	0.584	0.24	1.7
16	OH	1.2	16.5	144	0.40	0.0978	1.5	0.885	0.584	0.24	1.7
17	OH	1.2	16.5	150	0.40	0.1014	1.53	0.9	0.586	0.246	1.4
18	OH	1.5	16.5	158	0.39	0.1022	1.515	0.9	0.584	0.244	1.45
19	OH	1.5	16.5	165	0.38	0.1048	1.53	0.915	0.586	0.26	1.56
20	SM	3	19	350	1.16	0.1070	1.575	0.975	0.588	0.226	2.9
21	SM	5	19	525	1.10	0.0902	1.515	1.11	0.586	0.3	1.86

Table 6B.30: Input parameters for site MRCE2 effective stress analysis (Max Ru = 0.95 for all layers)

Layer	Model	f/s/f	p/r/Dr	F/A/FC	s/B/-	g/C/-	v/D/v	-/g/-	$C_v(m^2/s)$
1	1	1.000	1.000	0.4341	1.5372	0.0062	1.0000	0.0000	6.12E-02
2	1	1.000	1.000	0.7313	1.5372	0.0091	1.0000	0.0000	6.12E-02
3	2	0.039	0.424	11.9895	-23.4457	12.8273	-1.3537	0.0354	1.61E-06
4	2	0.062	0.457	13.2256	-26.8024	15.5076	-1.9162	0.0309	2.04E-06
5	2	0.077	0.485	14.1792	-29.4716	17.7426	-2.4520	0.0276	2.64E-06
6	2	0.089	0.505	14.6788	-30.8967	18.9715	-2.7719	0.0252	3.52E-06
7	2	0.089	0.505	14.6788	-30.8967	18.9715	-2.7719	0.0260	4.86E-06
8	2	0.107	0.521	14.8188	-31.2992	19.3229	-2.8667	0.0240	6.97E-06
9	2	0.107	0.521	14.8188	-31.2992	19.3229	-2.8667	0.0249	6.97E-06
10	2	0.107	0.521	14.8188	-31.2992	19.3229	-2.8667	0.0257	6.97E-06
11	2	0.107	0.521	14.8188	-31.2992	19.3229	-2.8667	0.0266	6.97E-06
12	2	0.107	0.521	14.8188	-31.2992	19.3229	-2.8667	0.0274	6.97E-06
13	2	0.107	0.521	14.8188	-31.2992	19.3229	-2.8667	0.0282	6.97E-06
14	2	0.109	0.521	14.8188	-31.2992	19.3229	-2.8667	0.0291	6.97E-06
15	2	0.107	0.521	14.8188	-31.2992	19.3229	-2.8667	0.0300	6.97E-06
16	2	0.107	0.521	14.8188	-31.2992	19.3229	-2.8667	0.0308	6.97E-06
17	2	0.107	0.521	14.8188	-31.2992	19.3229	-2.8667	0.0315	6.97E-06
18	2	0.107	0.521	14.8188	-31.2992	19.3229	-2.8667	0.0323	6.97E-06
19	2	0.107	0.521	14.8188	-31.2992	19.3229	-2.8667	0.0332	6.97E-06
20	1	1.000	1.000	0.4341	1.5372	0.0357	1.0000	0.0000	6.12E-02
21	1	1.000	1.000	0.2316	1.5372	0.0385	1.0000	0.0000	6.12E-02

APPENDIX 7A: EFFECT OF GROUND MOTION – COMPARING SCENARIOS FOR A GIVEN SITE

Appendix 7A: Effect of Ground Motion - Comparing Scenarios for a Given Site

This appendix shows comparing the results of the effective stress site response analyses for all sites. There are three figures per site. The first figure compares scenarios 12ACR3, 25ACR3, 50ACR3, 100ACR3, 200ACR3, and 400ACR3, the second figure compares scenarios ACR1, ACR2, ACR2M, 100ACR3, and ACR3M, and the third figure compares scenarios 100ACR, SUB, and SCR. The scenarios were grouped in this fashion to investigate the effect of ground motion intensity, near fault effects and scaling versus spectral matching, and the effect of tectonic region, respectively. All curves are the mean values of the parameter for effective stress analyses and the given scenario and site.

Each figure contains six plots. The top left plot is the calculated response spectra for each scenario at the surface of the given site. The top right plot gives the spectral amplification ratio versus period, where Amp(T) is the calculated surface response spectra divided by the input rock response spectra at each period. The bottom four plots on each page show, from left to right, the maximum shear strain, shear stress ratio, pore pressure ratio, and PGA with depth, where the shear stress ratio and pore pressure ratio are the shear stress and pore pressure divided by the vertical effective stress. The dotted horizontal lines in the bottom four plots define the boundary between different soil types. The USCS soil designation for each layer is given in the plot with shear strain. This makes it easier to visualize the soil column while interpreting the results. The red dotted line in the maximum shear stress ratio plot is the shear strength ratio of the soil profile, where the shear strength ratio is the shear strength divided by the vertical effective stress.

Figures 7A.46 through 7A.60 compare the spectral ratio (Sa(T) / PGA) calculated at the surface for each site. The plots in the top row show scenarios 12ACR3, 25ACR3, 50ACR3, 100ACR3, 200ACR3, and 400ACR3, the plots in the middle row show scenarios ACR1, ACR2, ACR2M, 100ACR3, and ACR3M, and the plots in the bottom row show scenarios 100ACR3, SUB, and SCR. The left column is plotted in semi-log space and the right column is plotted arithmetically. Both plots also show the spectral ratios given by Seed et al (1997) for their soil class E, which is analogous to NEHRP F sites.

Figure 7A.1: Scenario comparison for effective stress analysis and site Bay Area − Intensity

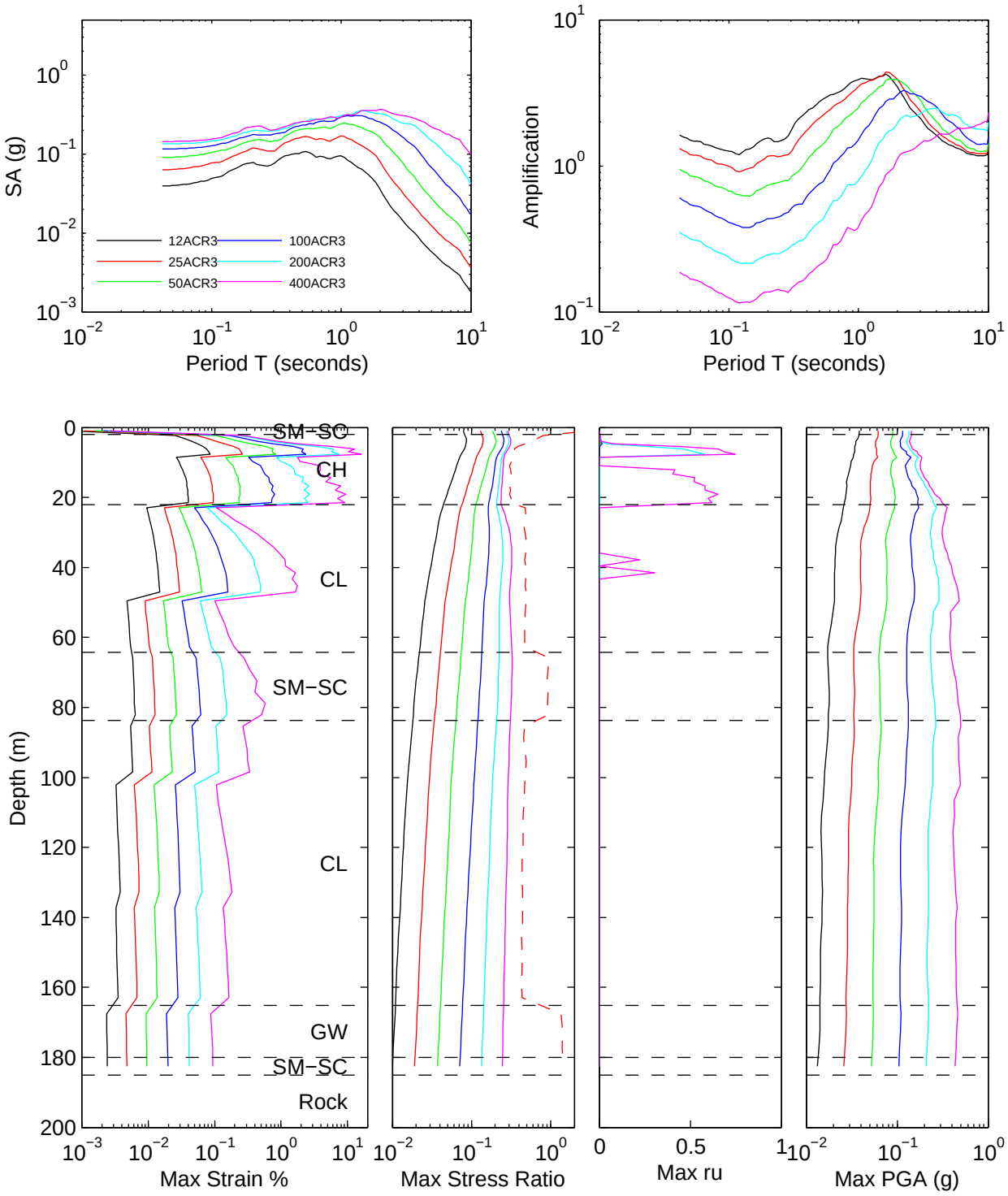

Figure 7A.2: Scenario comparison for effective stress analysis and site Bay Area − Near fault and Scaled vs Matched

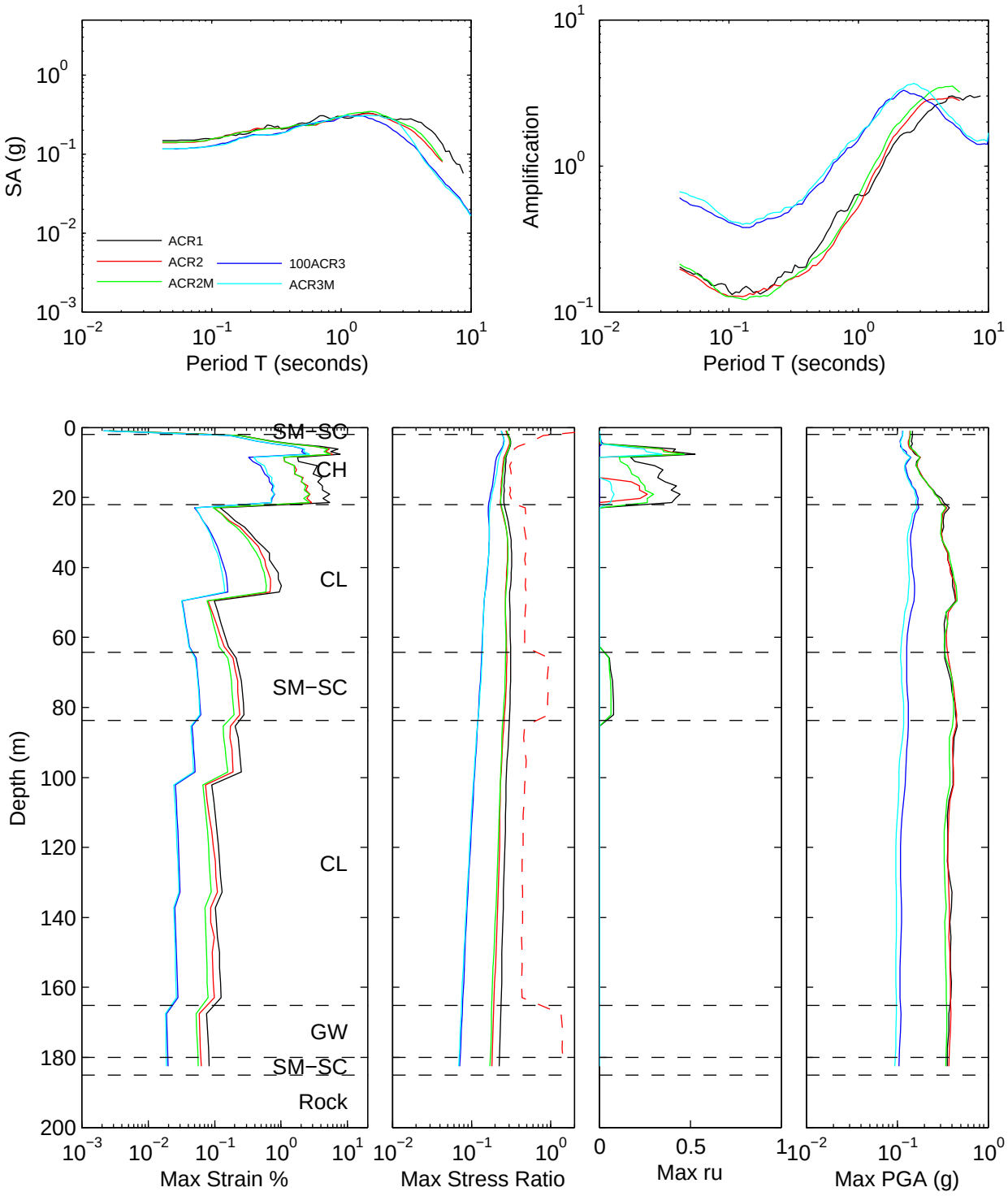

Figure 7A.3: Scenario comparison for effective stress analysis and site Bay Area − Tectonic Region

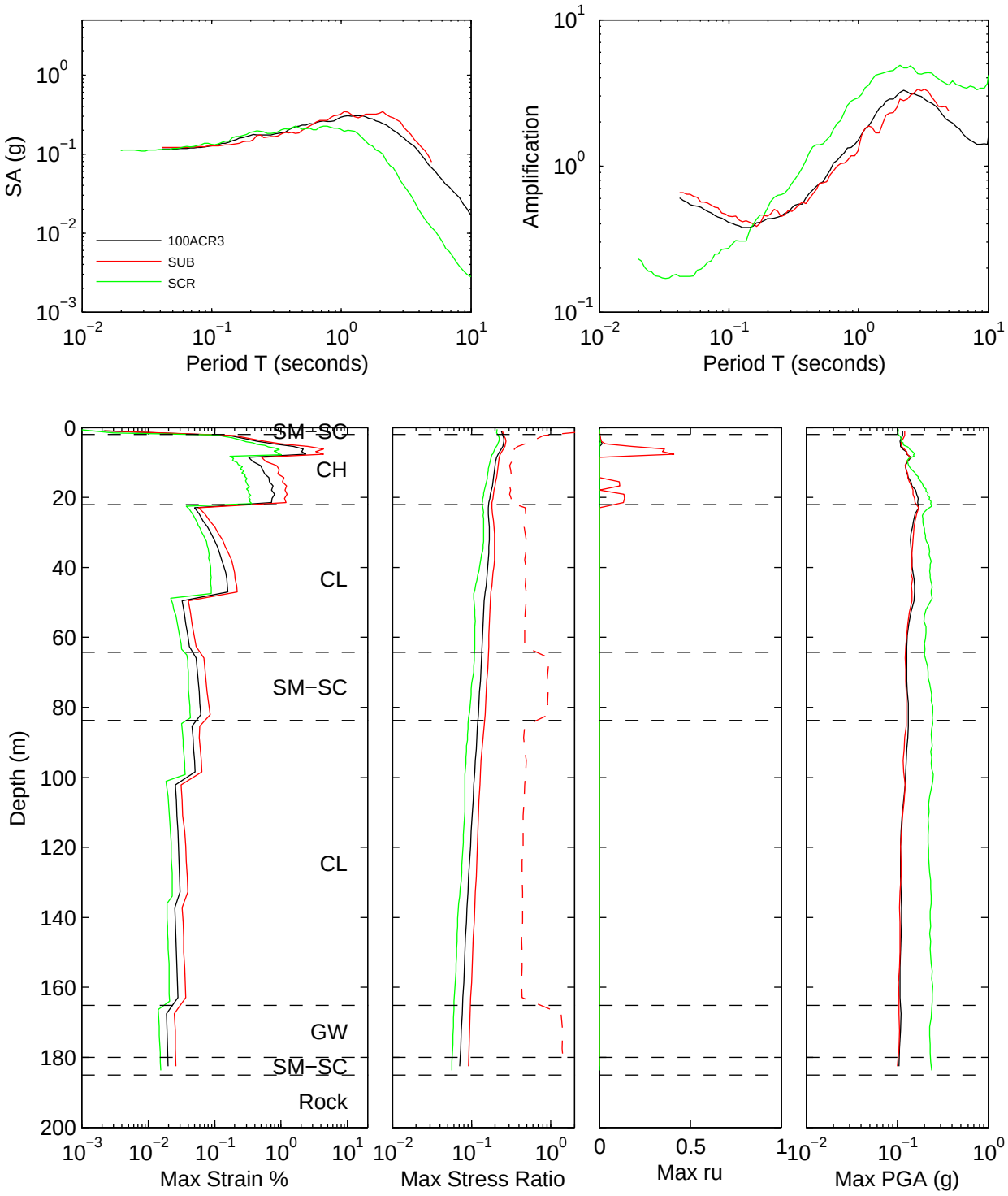

Figure 7A.4: Scenario comparison for effective stress analysis and site Bay Area F − Intensity

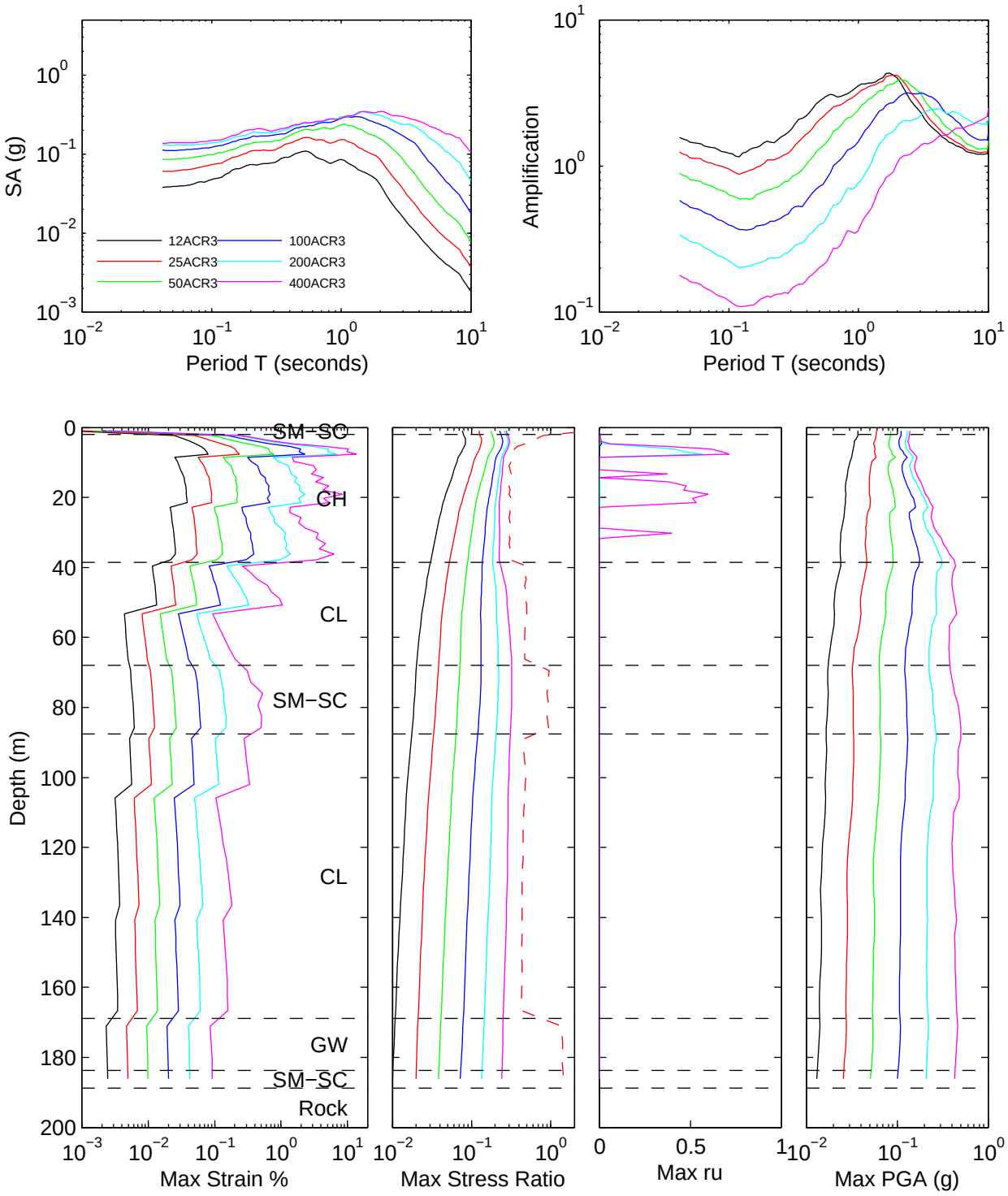

Figure 7A.5: Scenario comparison for effective stress analysis and site Bay Area F − Near fault and Scaled vs Matched

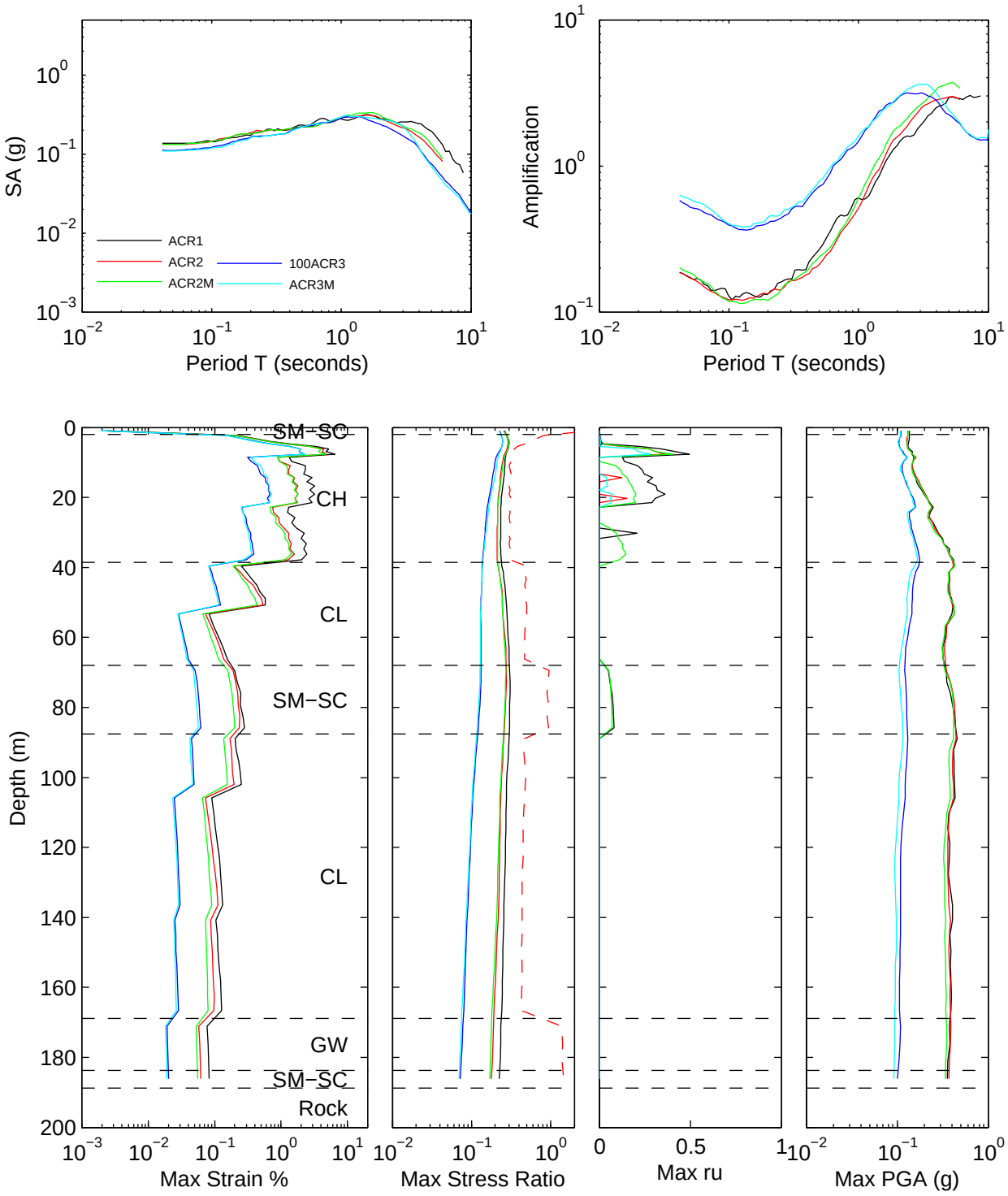

Figure 7A.6: Scenario comparison for effective stress analysis and site Bay Area F − Tectonic Region

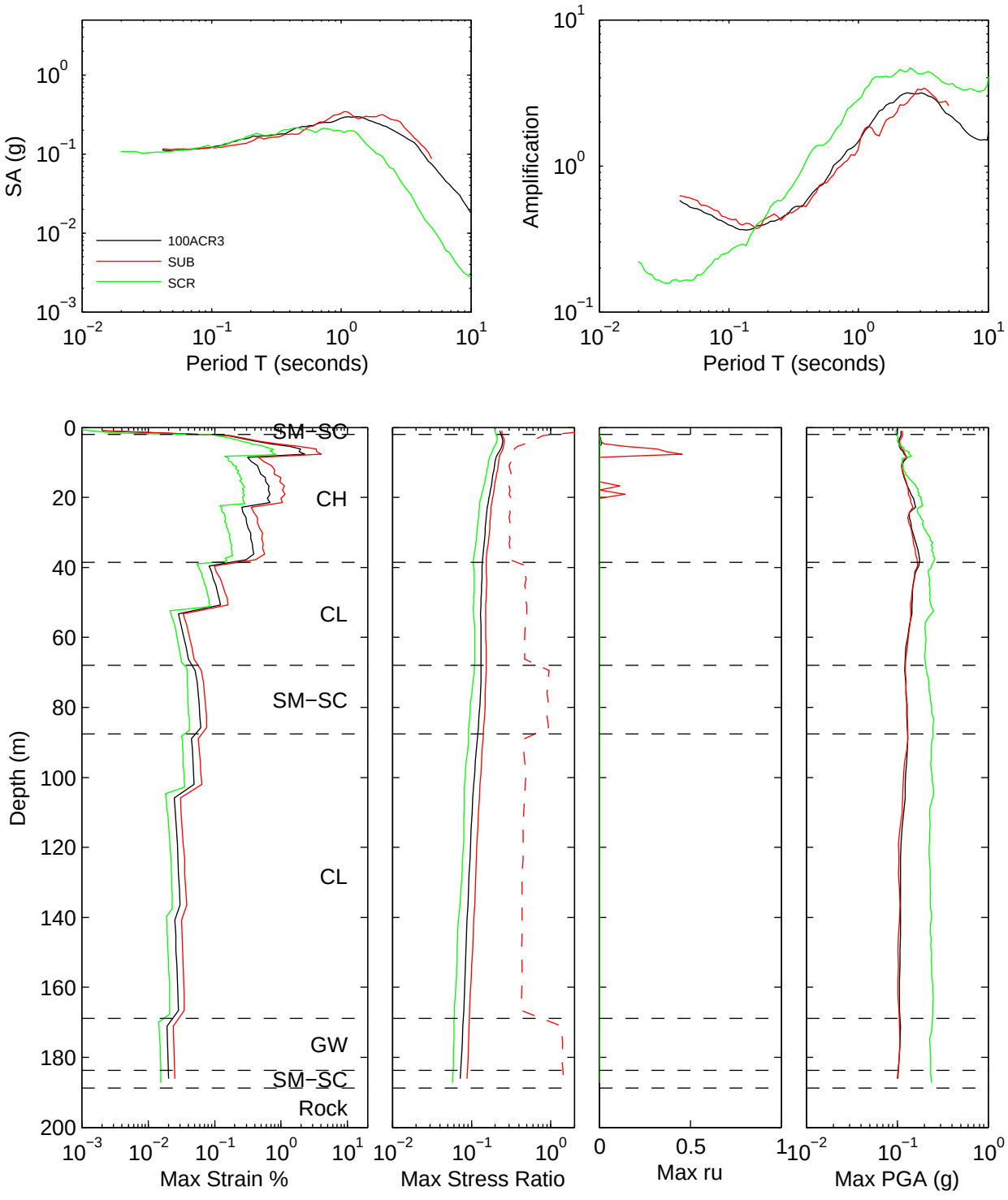

Figure 7A.7: Scenario comparison for effective stress analysis and site Bay Area II − Intensity

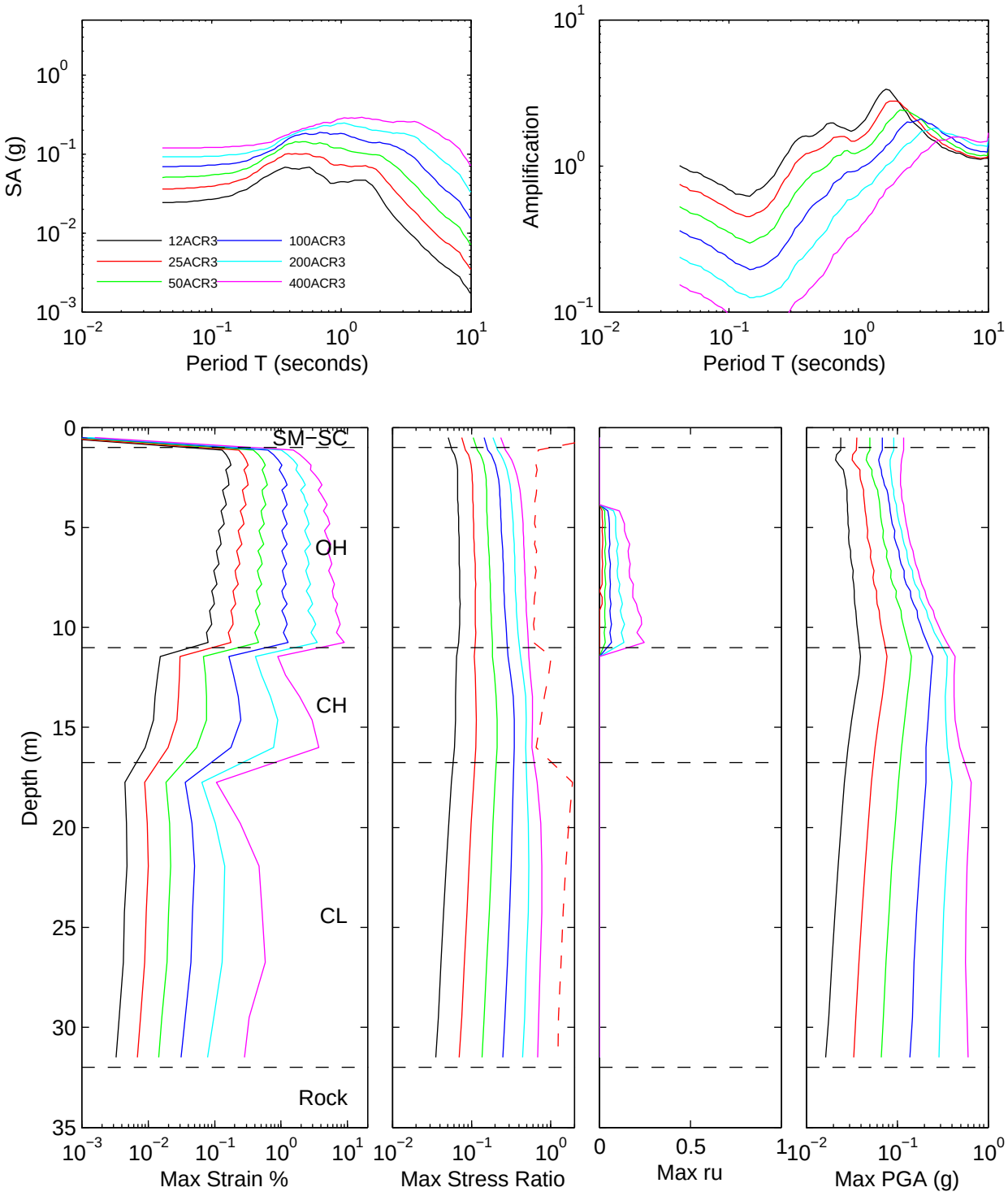

Figure 7A.8: Scenario comparison for effective stress analysis and site Bay Area II − Near fault and Scaled vs Matched

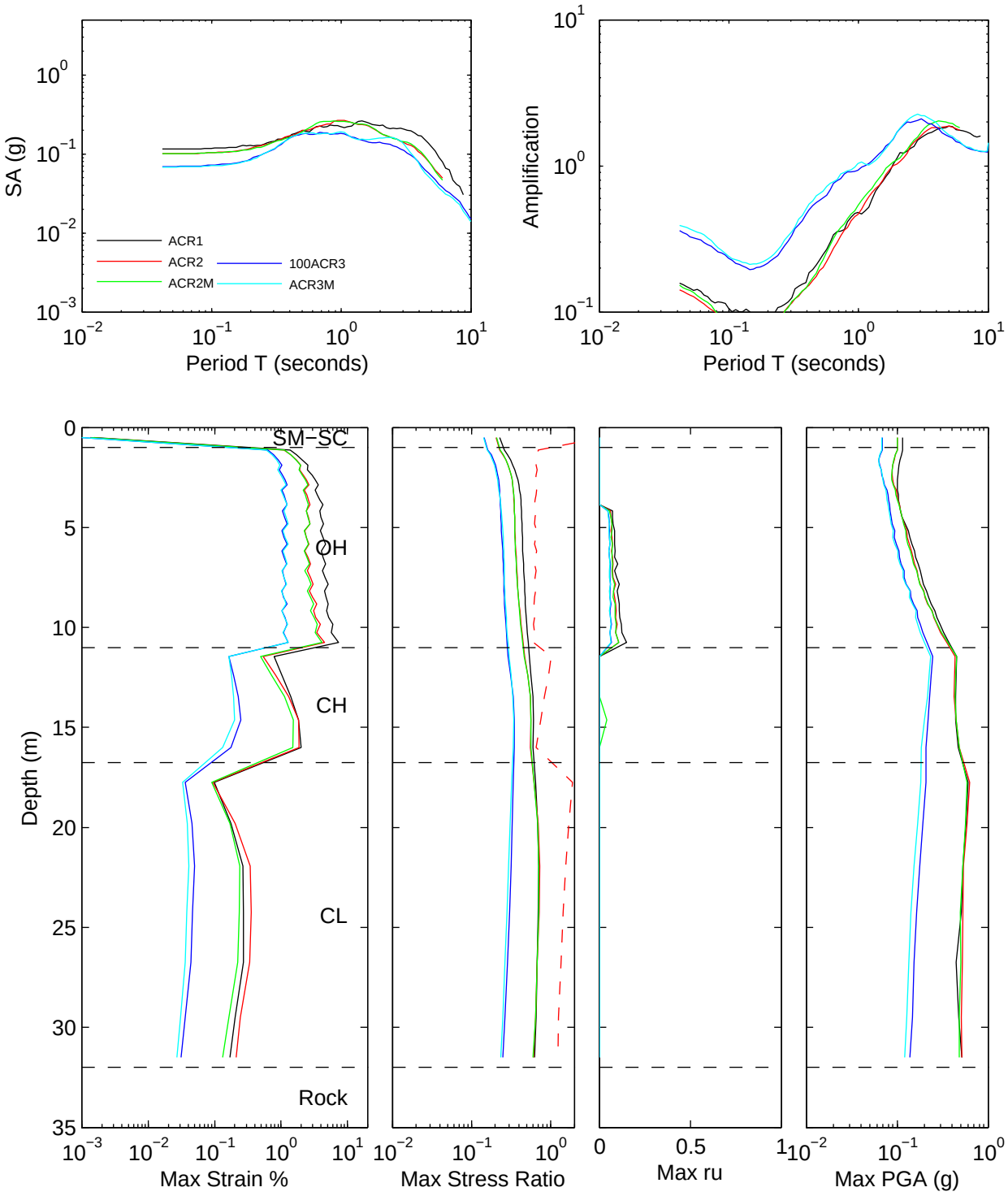

Figure 7A.9: Scenario comparison for effective stress analysis and site Bay Area II − Tectonic Region

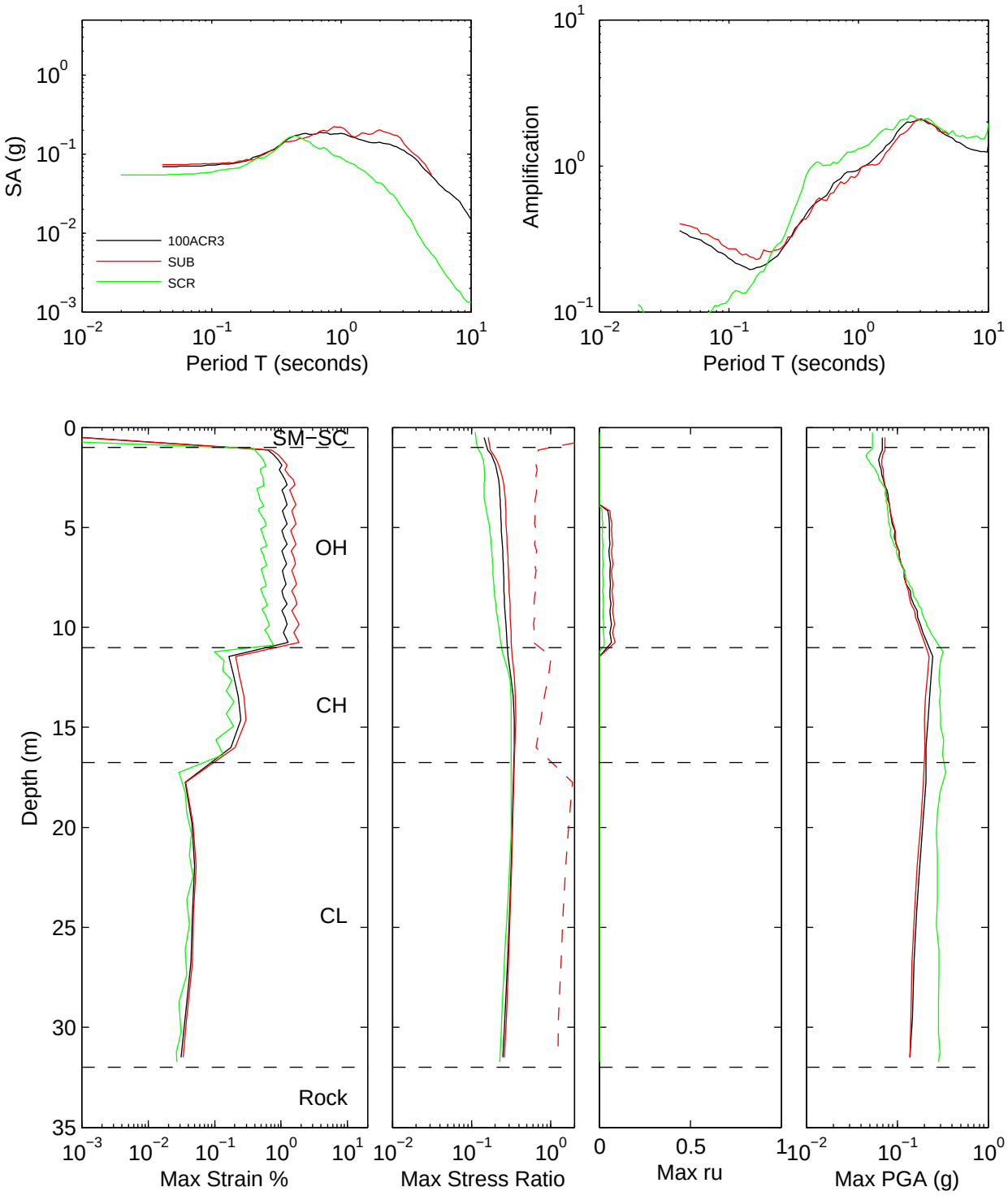

Figure 7A.10: Scenario comparison for effective stress analysis and site Bay Area II K − Intensity

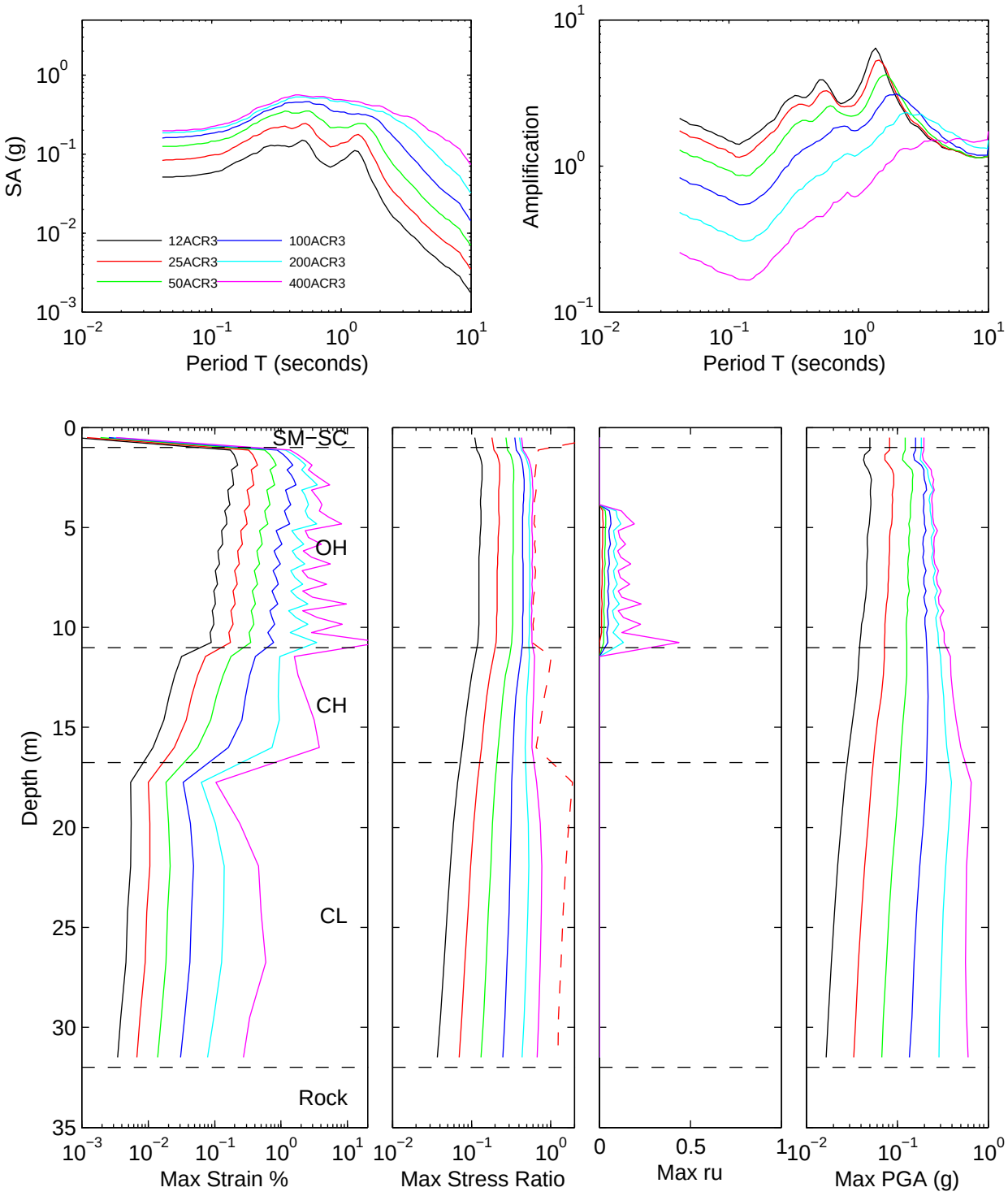

Figure 7A.11: Scenario comparison for effective stress analysis and site Bay Area II K − Near fault and Scaled vs Matched

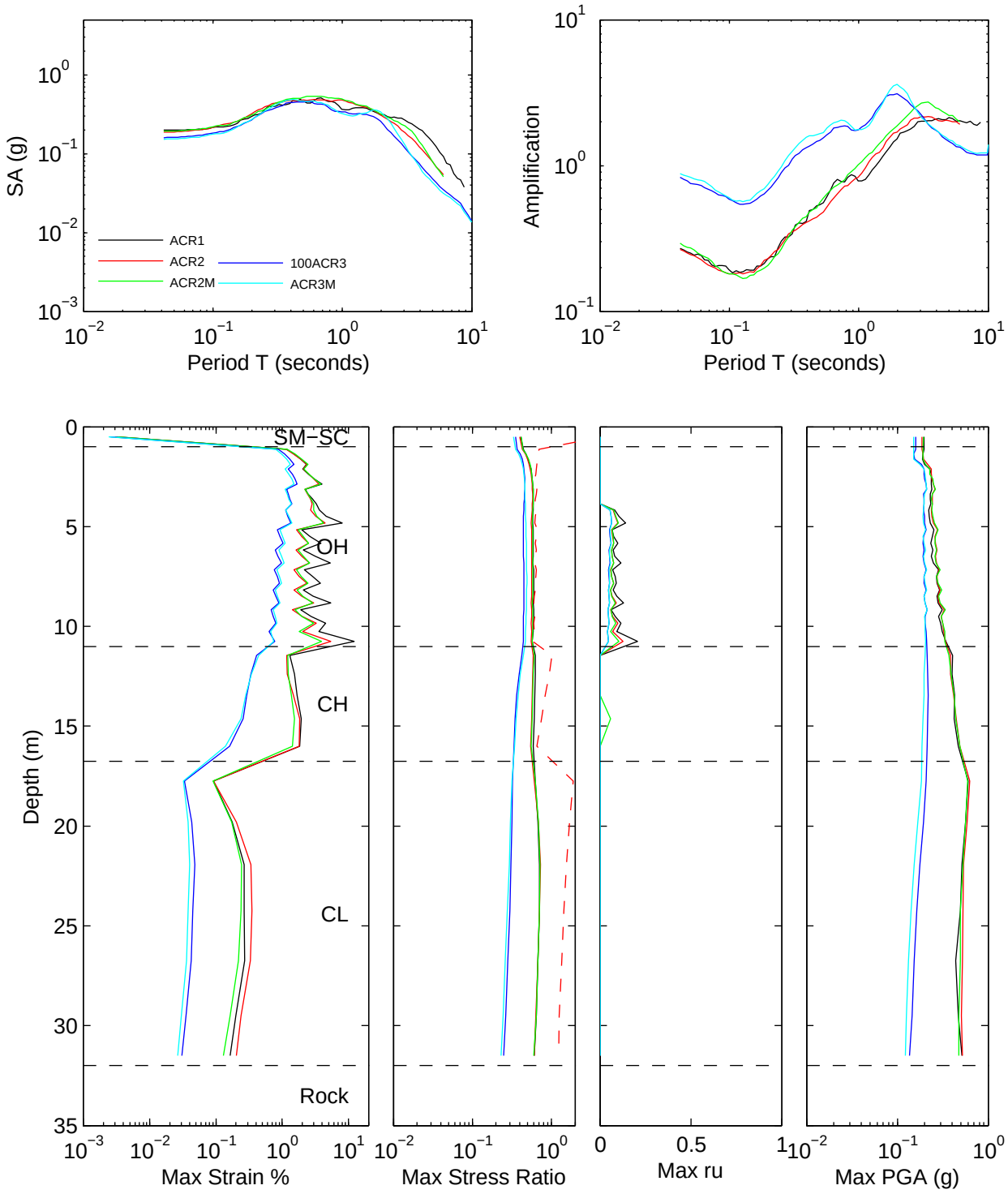

Figure 7A.12: Scenario comparison for effective stress analysis and site Bay Area II K − Tectonic Region

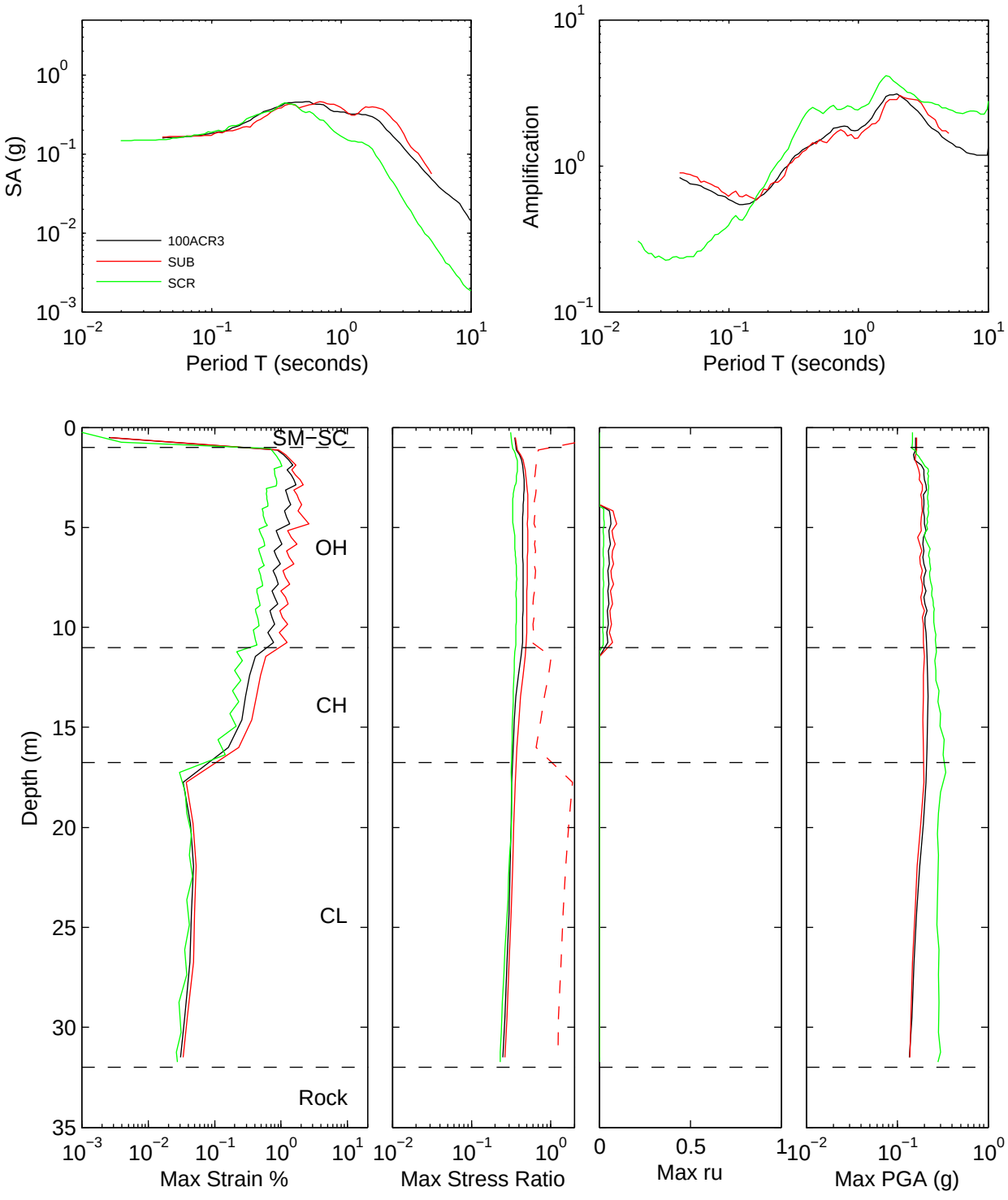

Figure 7A.13: Scenario comparison for effective stress analysis and site Bay Area II K S2 − Intensity

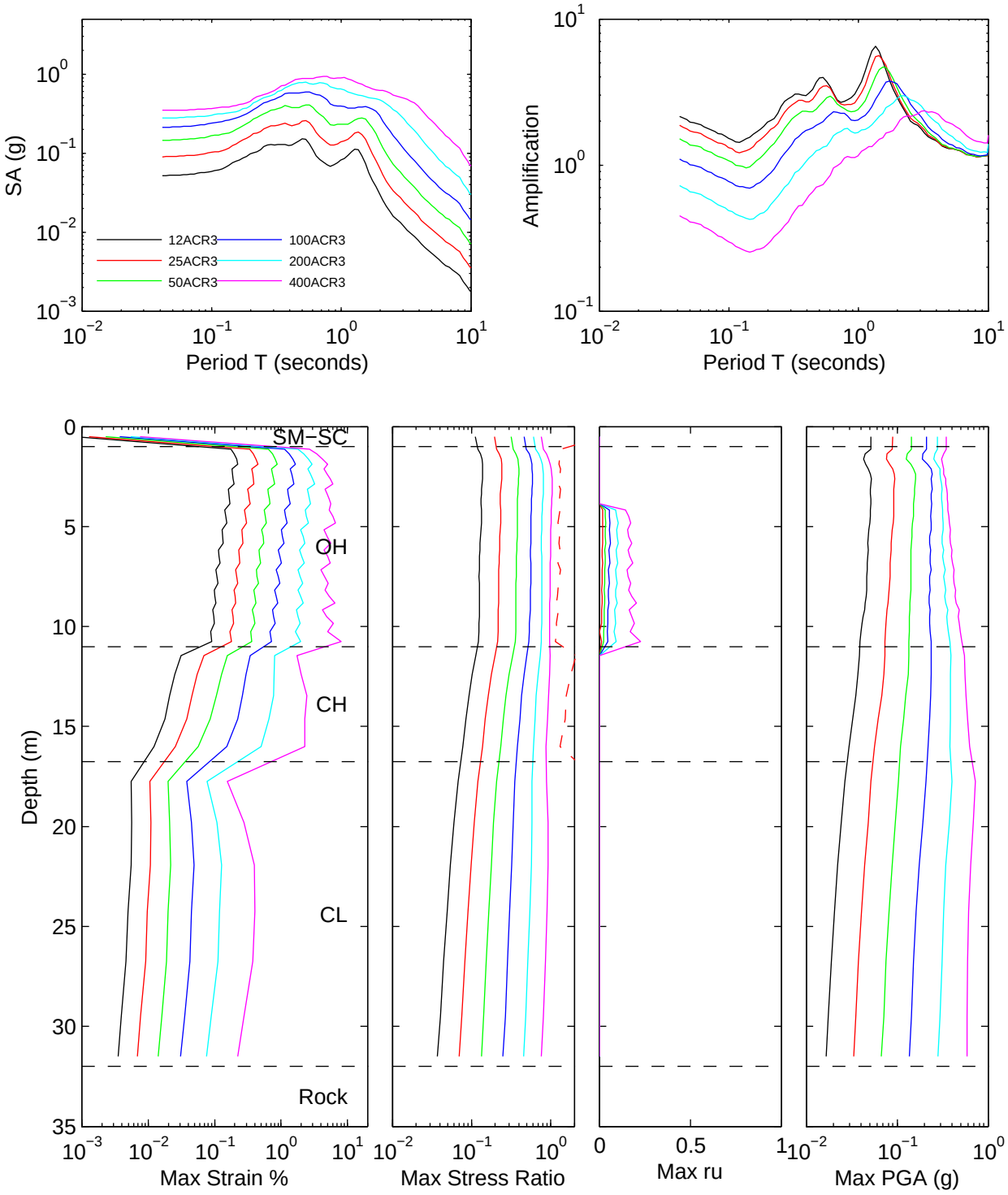

igure 7A.14: Scenario comparison for effective stress analysis and site Bay Area II K S2 − Near fault and Scaled vs Matche

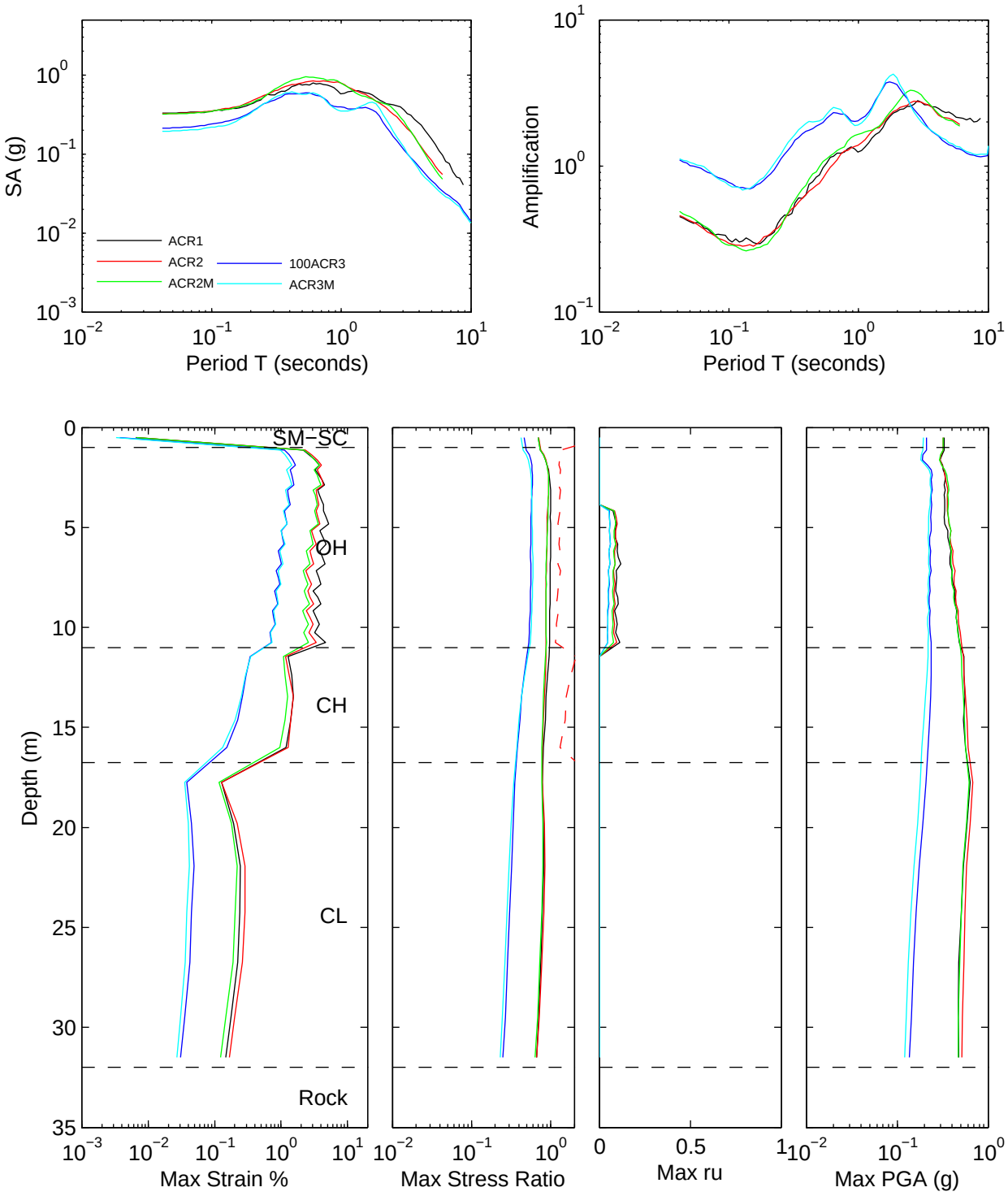

Figure 7A.15: Scenario comparison for effective stress analysis and site Bay Area II K S2 − Tectonic Region

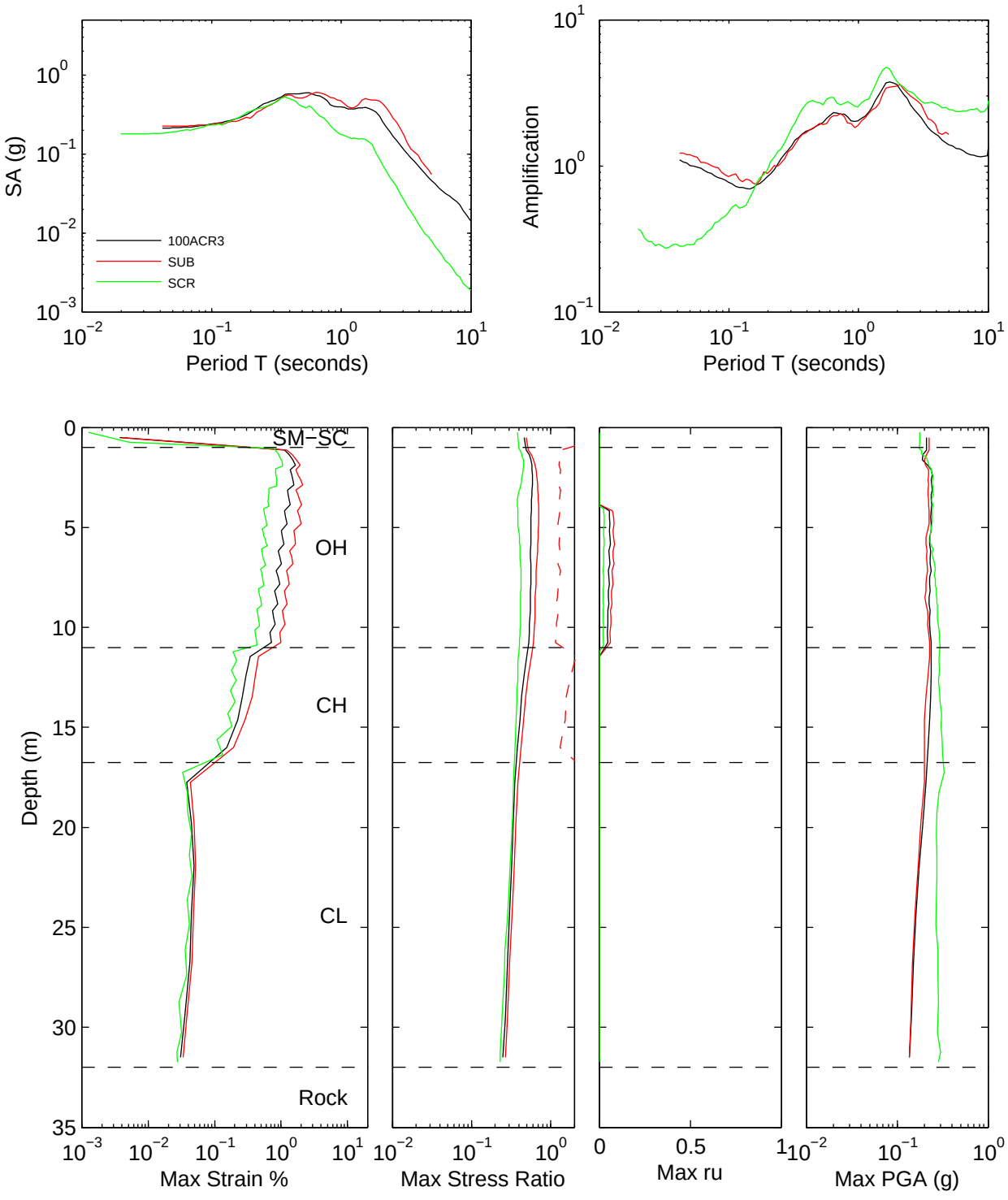

Figure 7A.16: Scenario comparison for effective stress analysis and site Bay Area II K S4 − Intensity

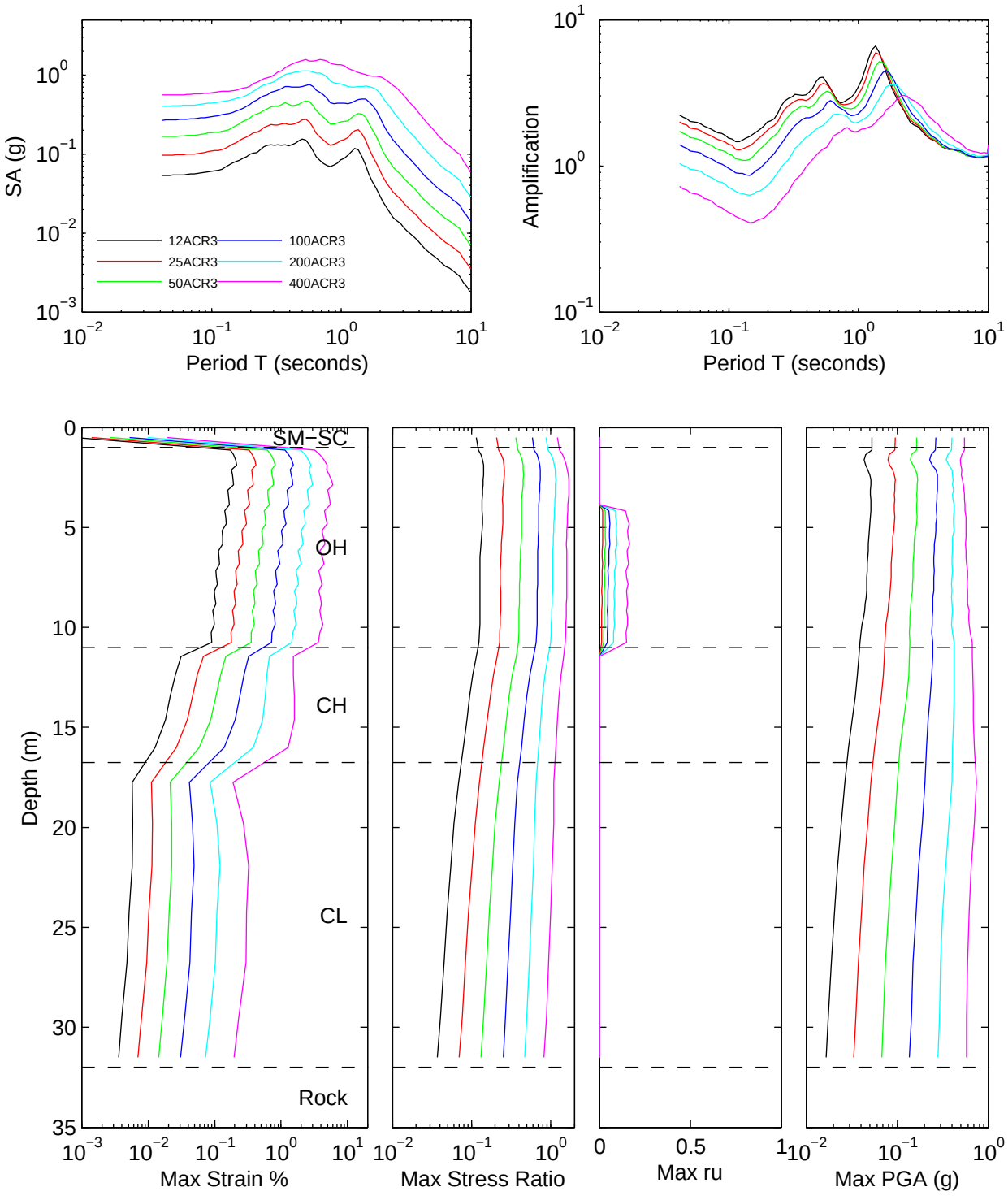

igure 7A.17: Scenario comparison for effective stress analysis and site Bay Area II K S4 − Near fault and Scaled vs Matche

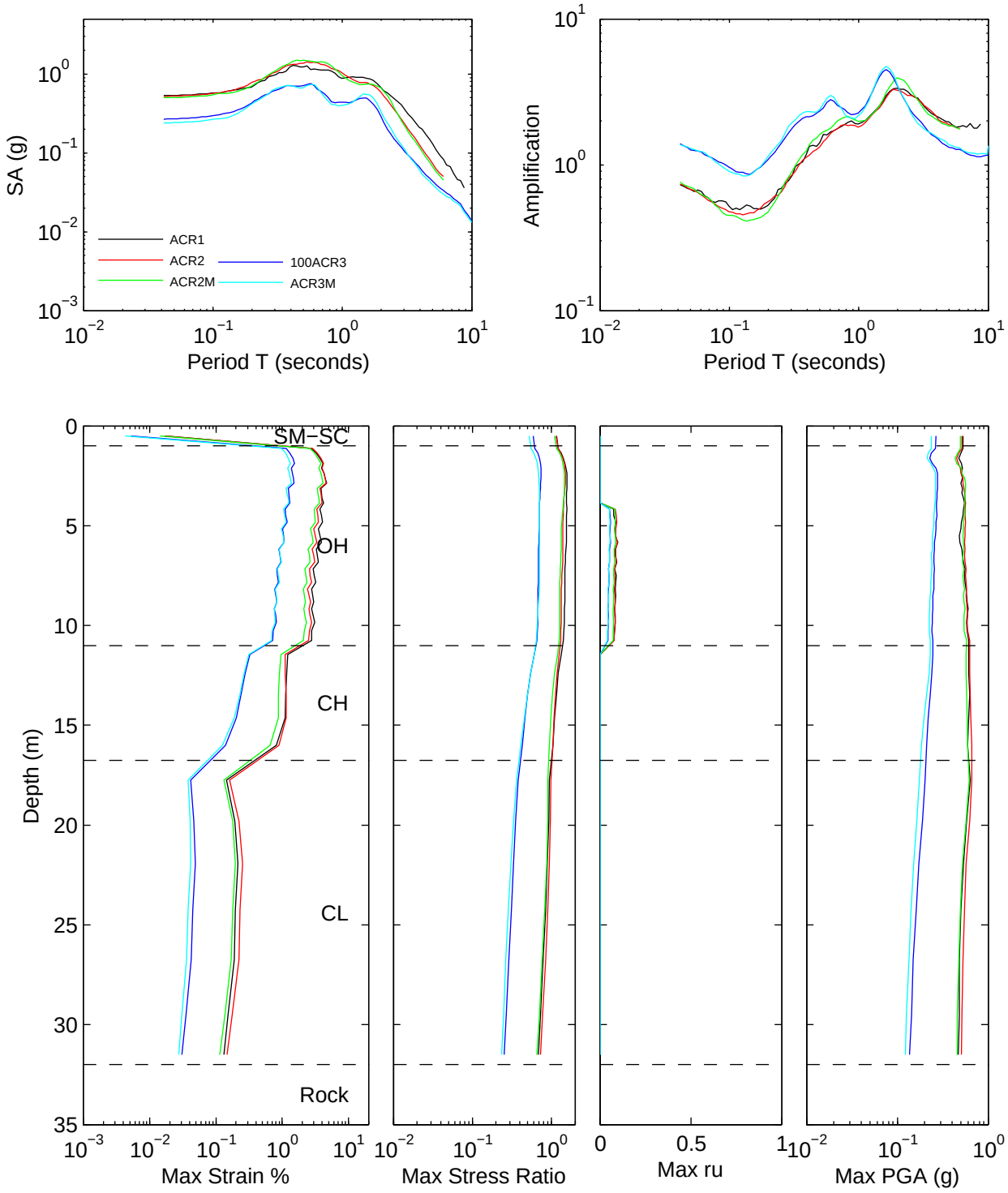

Figure 7A.18: Scenario comparison for effective stress analysis and site Bay Area II K S4 − Tectonic Region

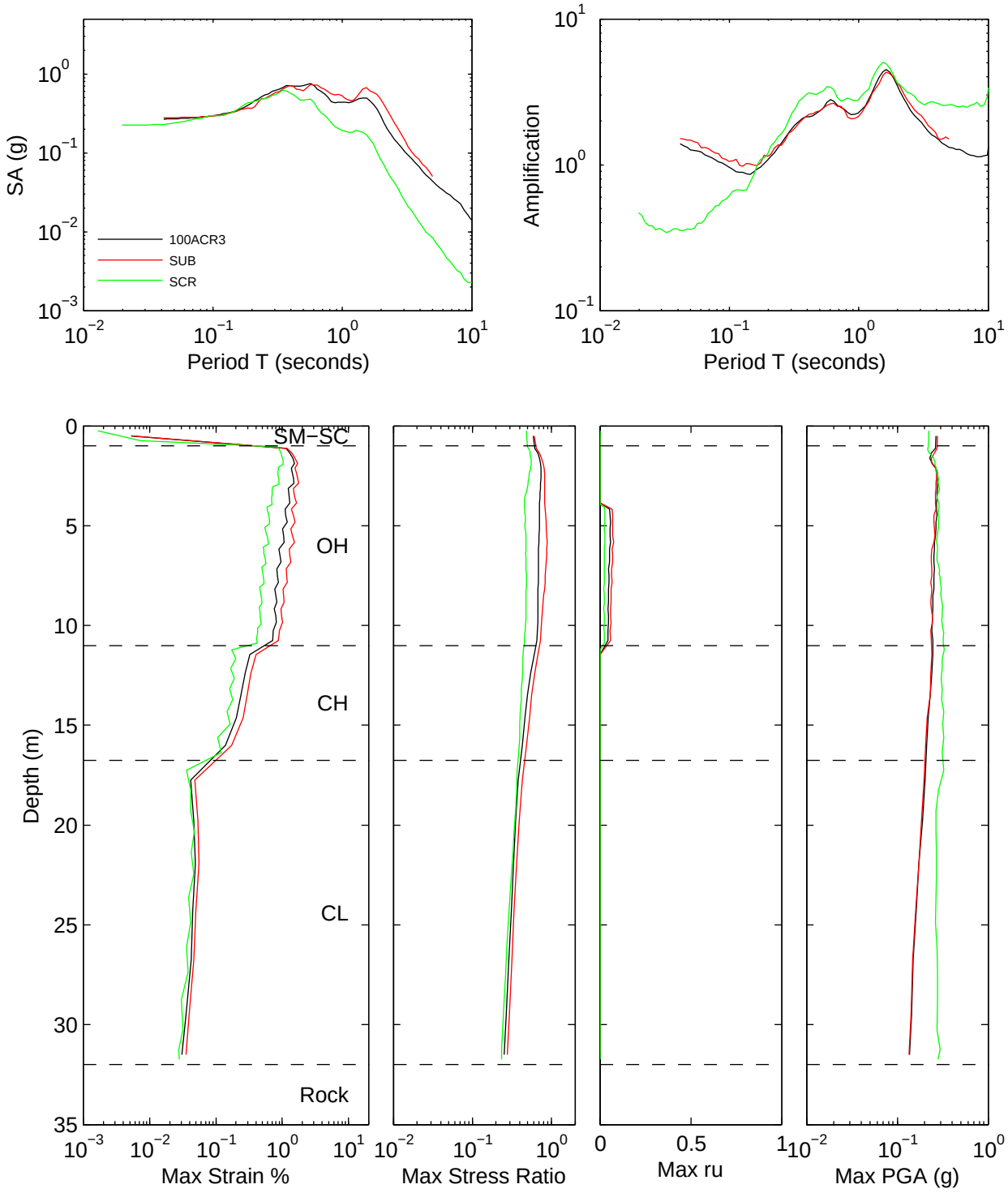

Figure 7A.19: Scenario comparison for effective stress analysis and site HAGP − Intensity

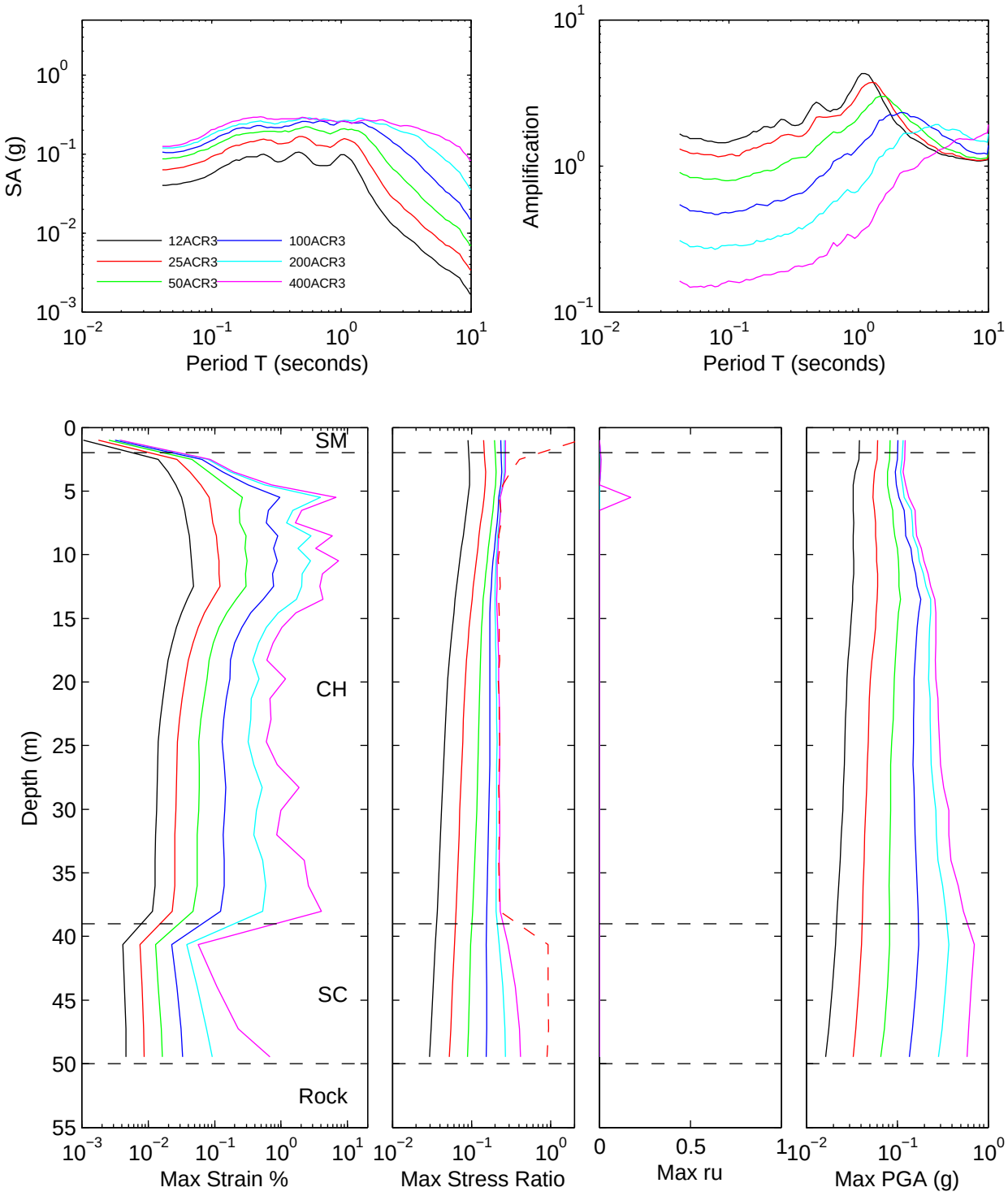

Figure 7A.20: Scenario comparison for effective stress analysis and site HAGP − Near fault and Scaled vs Matched

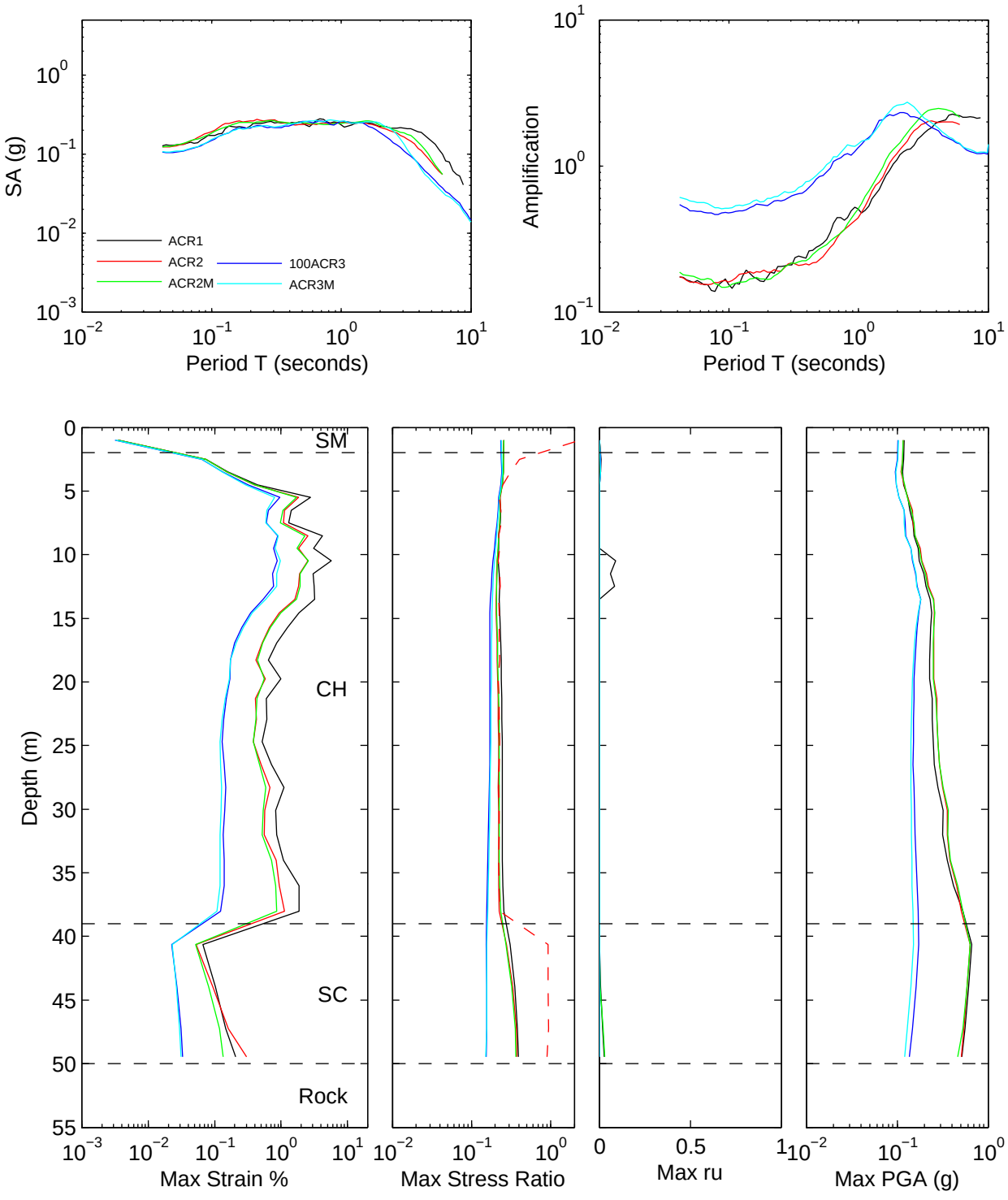

Figure 7A.21: Scenario comparison for effective stress analysis and site HAGP − Tectonic Region

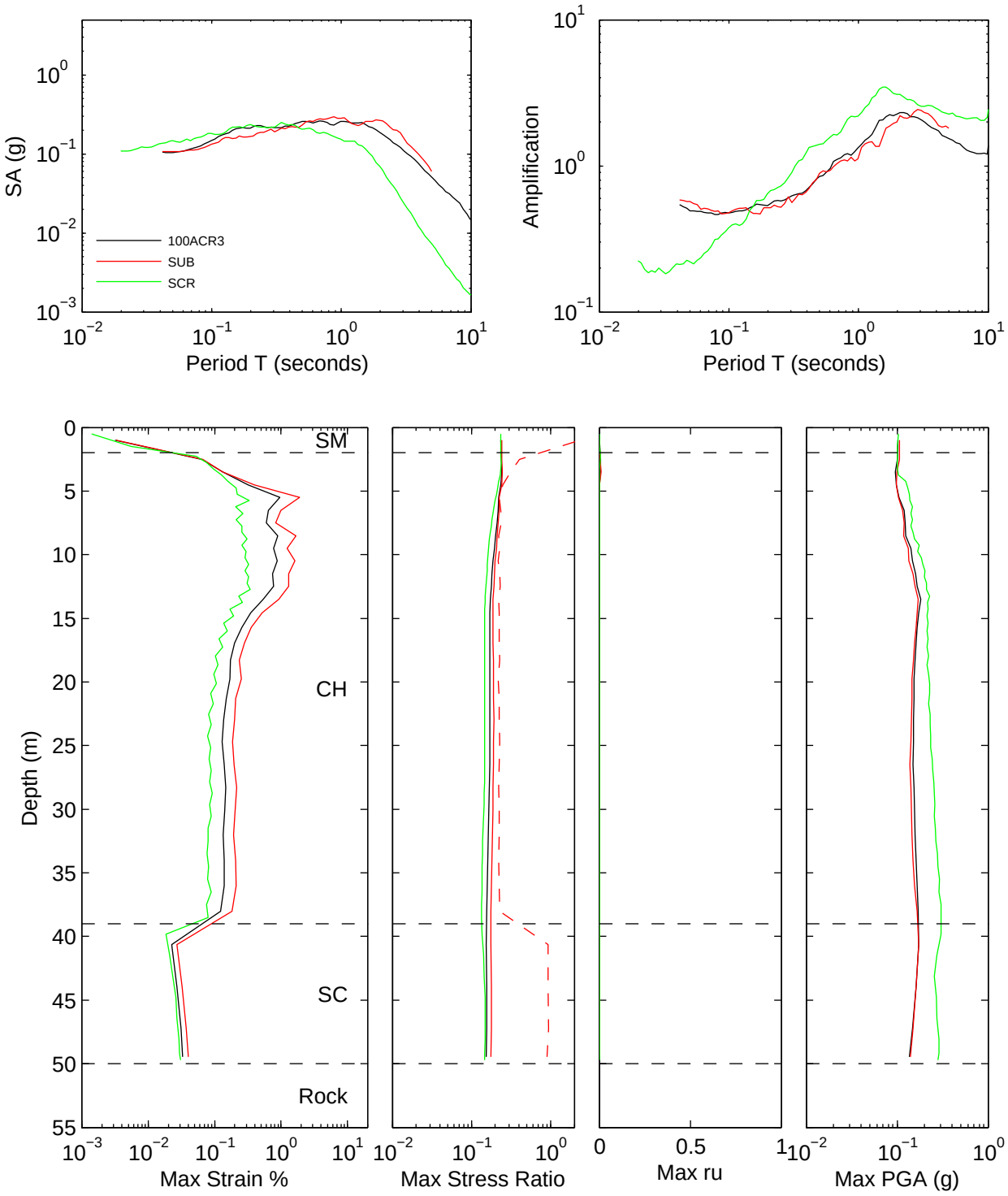

Figure 7A.22: Scenario comparison for effective stress analysis and site JSSS − Intensity

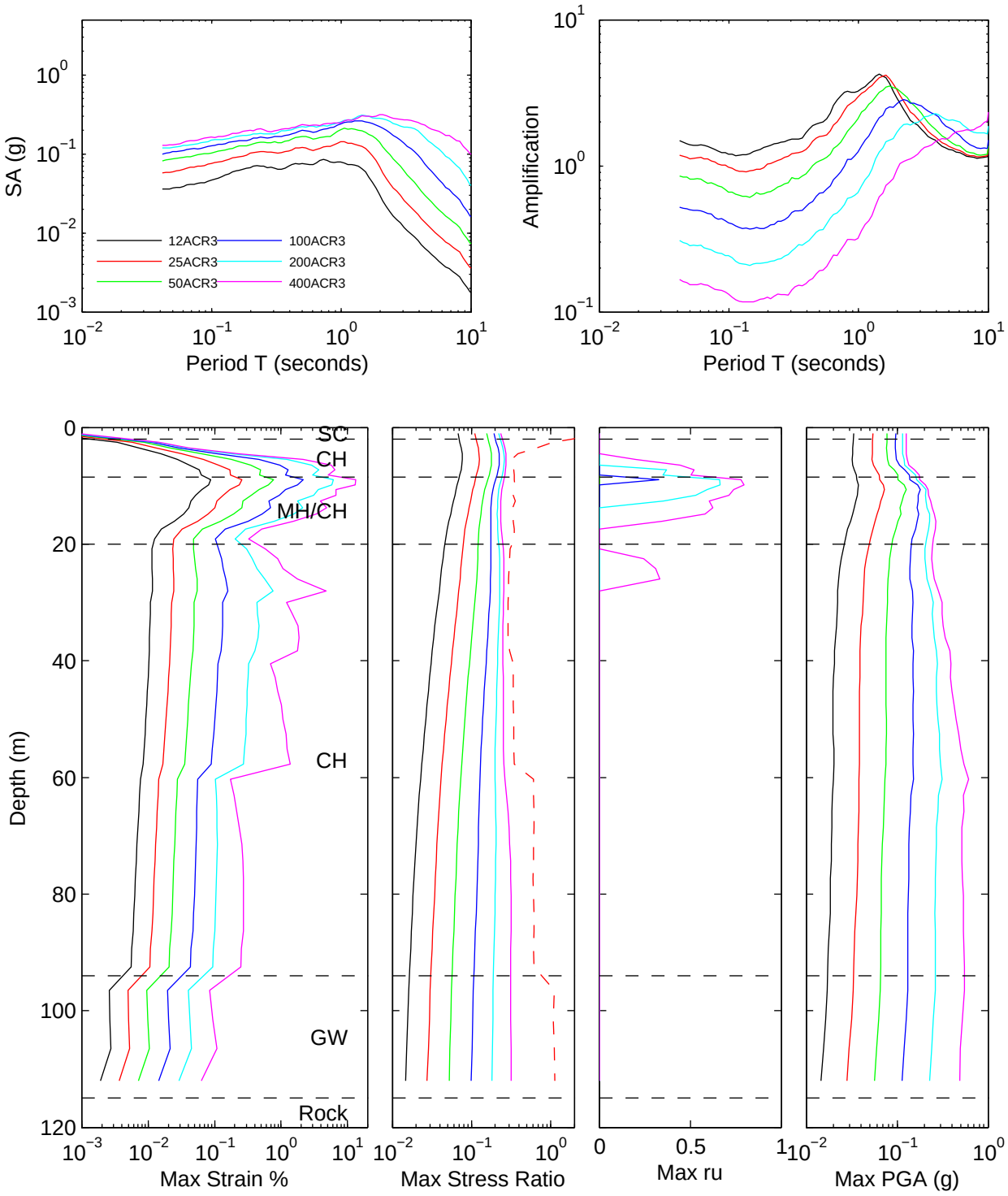

Figure 7A.23: Scenario comparison for effective stress analysis and site JSSS − Near fault and Scaled vs Matched

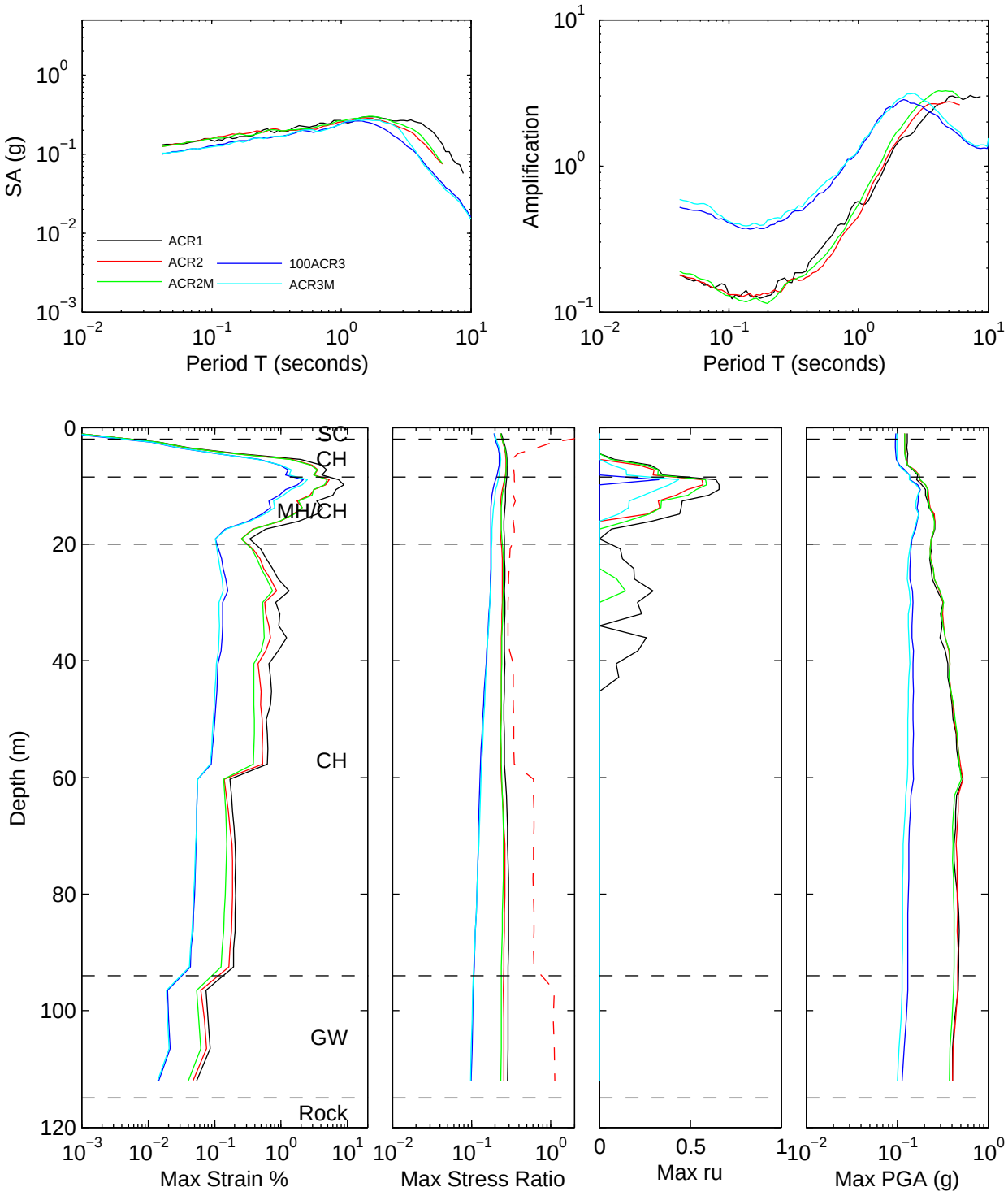

Figure 7A.24: Scenario comparison for effective stress analysis and site JSSS − Tectonic Region

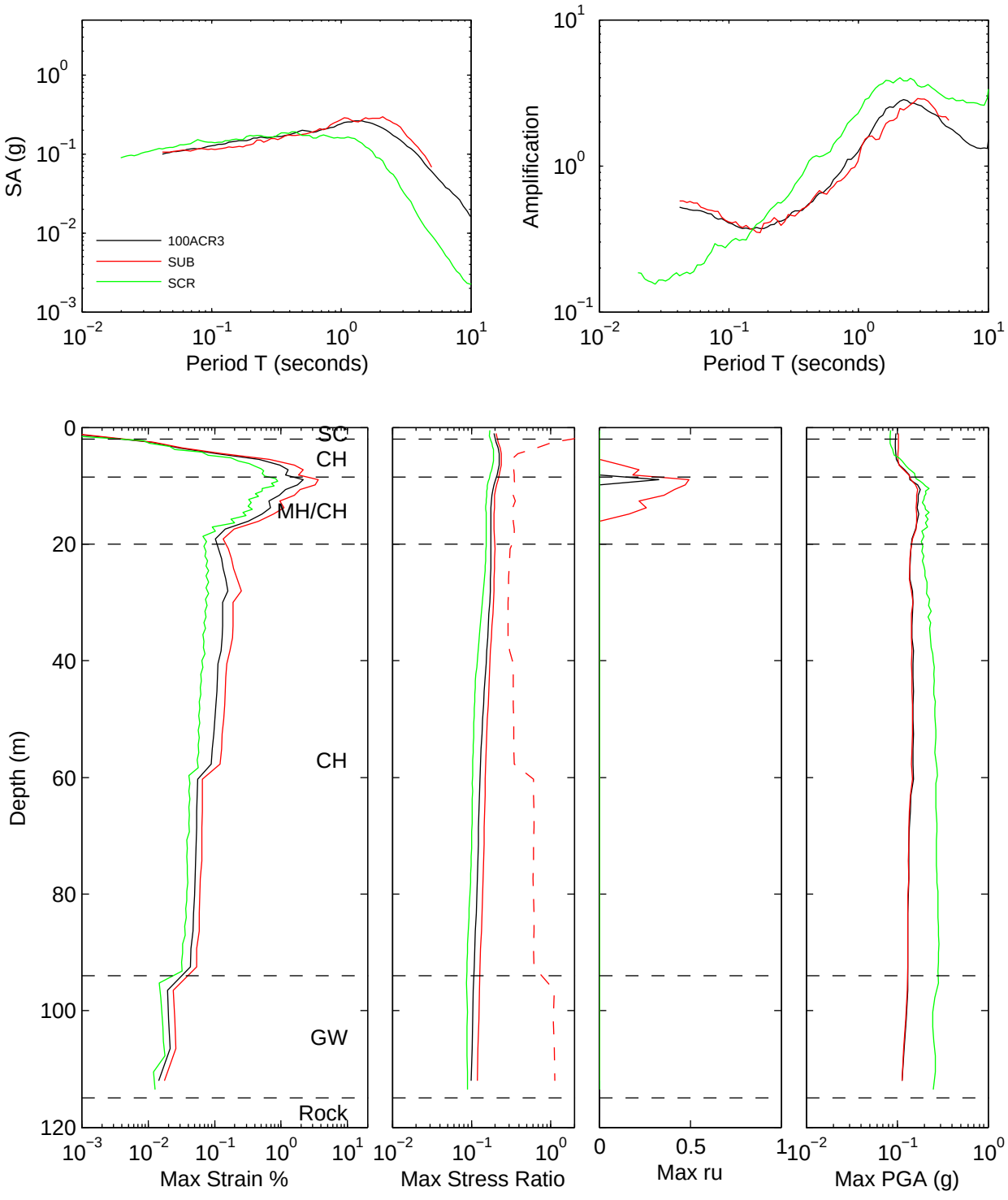

Figure 7A.25: Scenario comparison for effective stress analysis and site KIKNET − Intensity

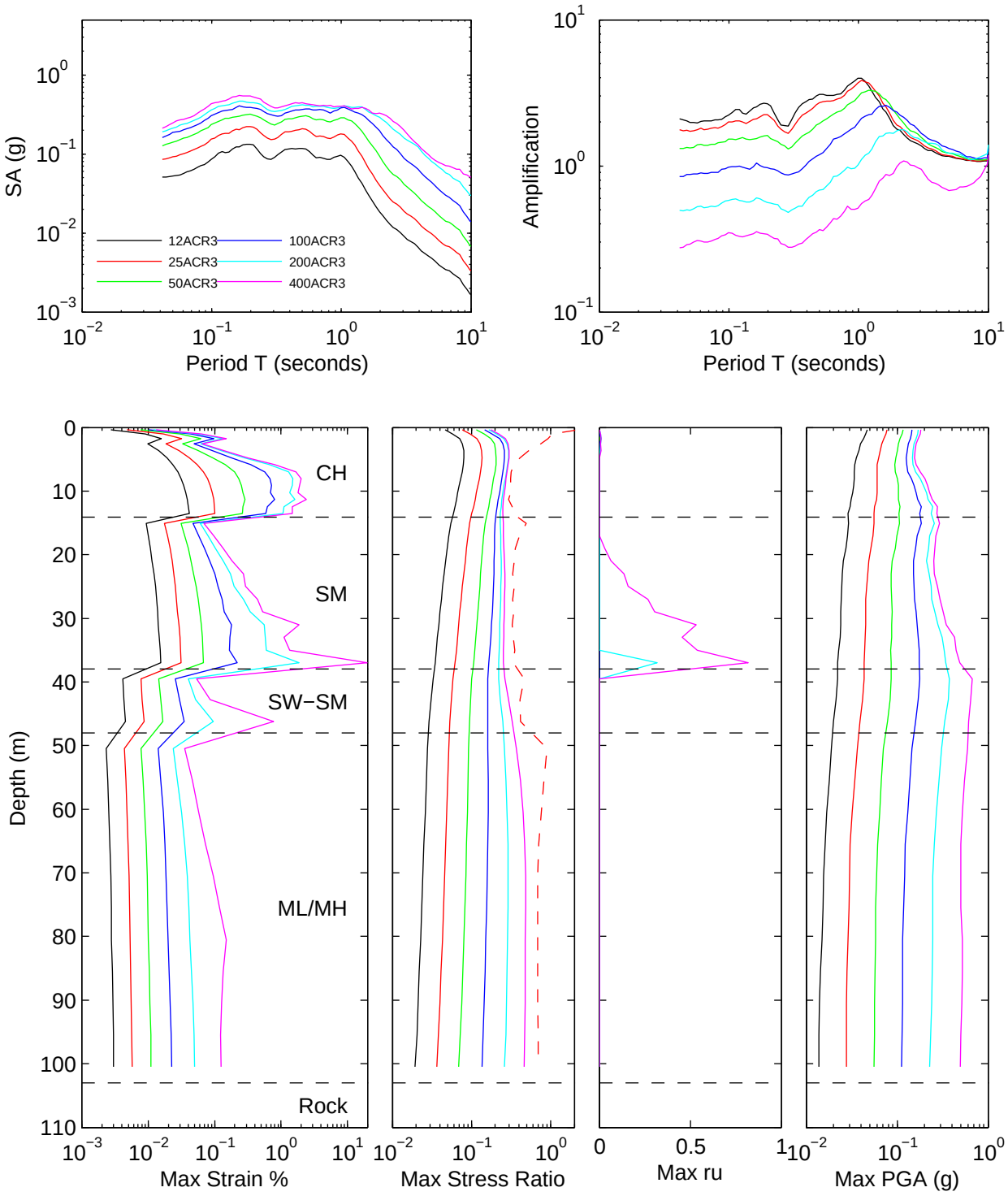

Figure 7A.26: Scenario comparison for effective stress analysis and site KIKNET − Near fault and Scaled vs Matched

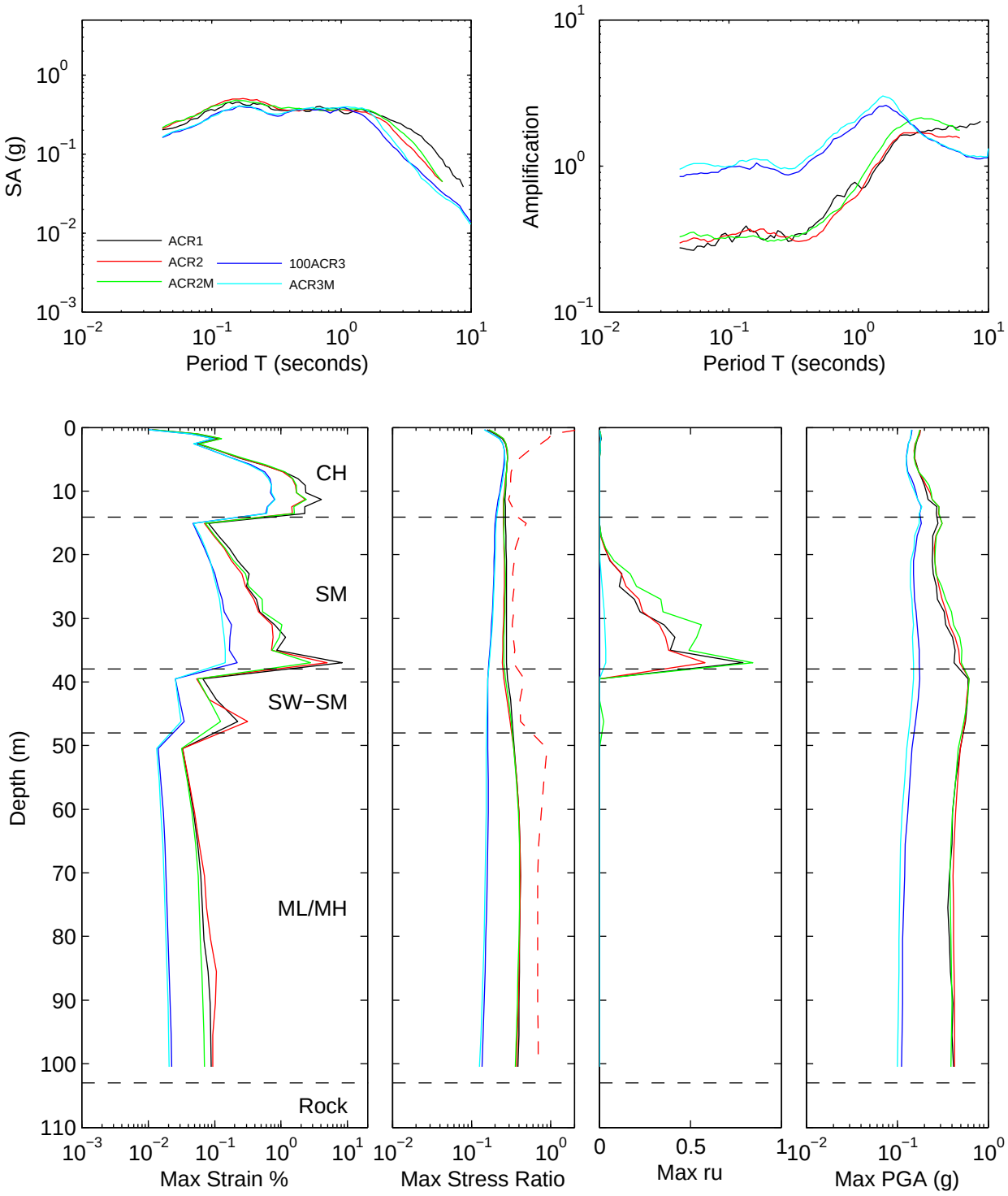

Figure 7A.27: Scenario comparison for effective stress analysis and site KIKNET − Tectonic Region

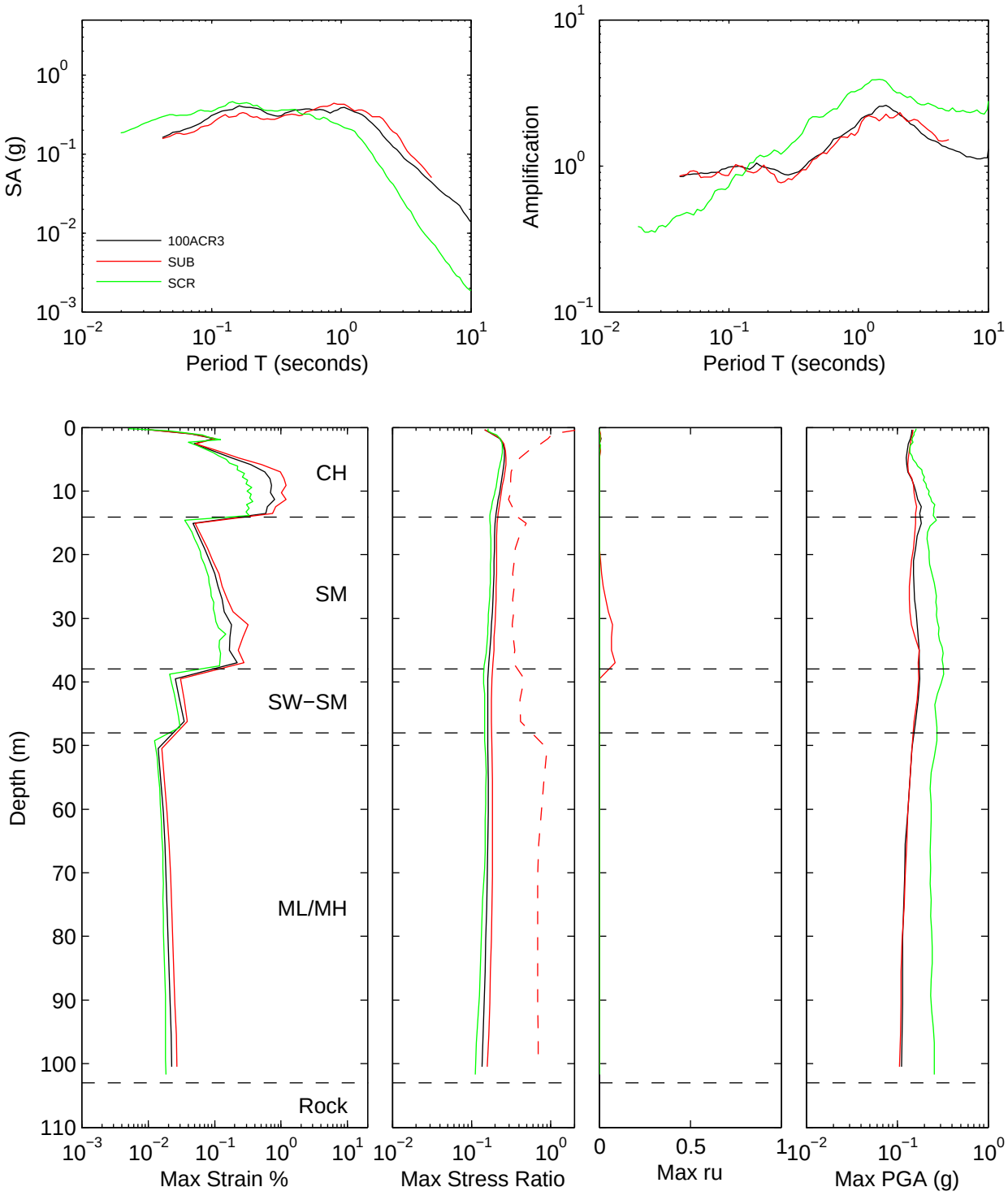

Figure 7A.28: Scenario comparison for effective stress analysis and site KIKNET S2 − Intensity

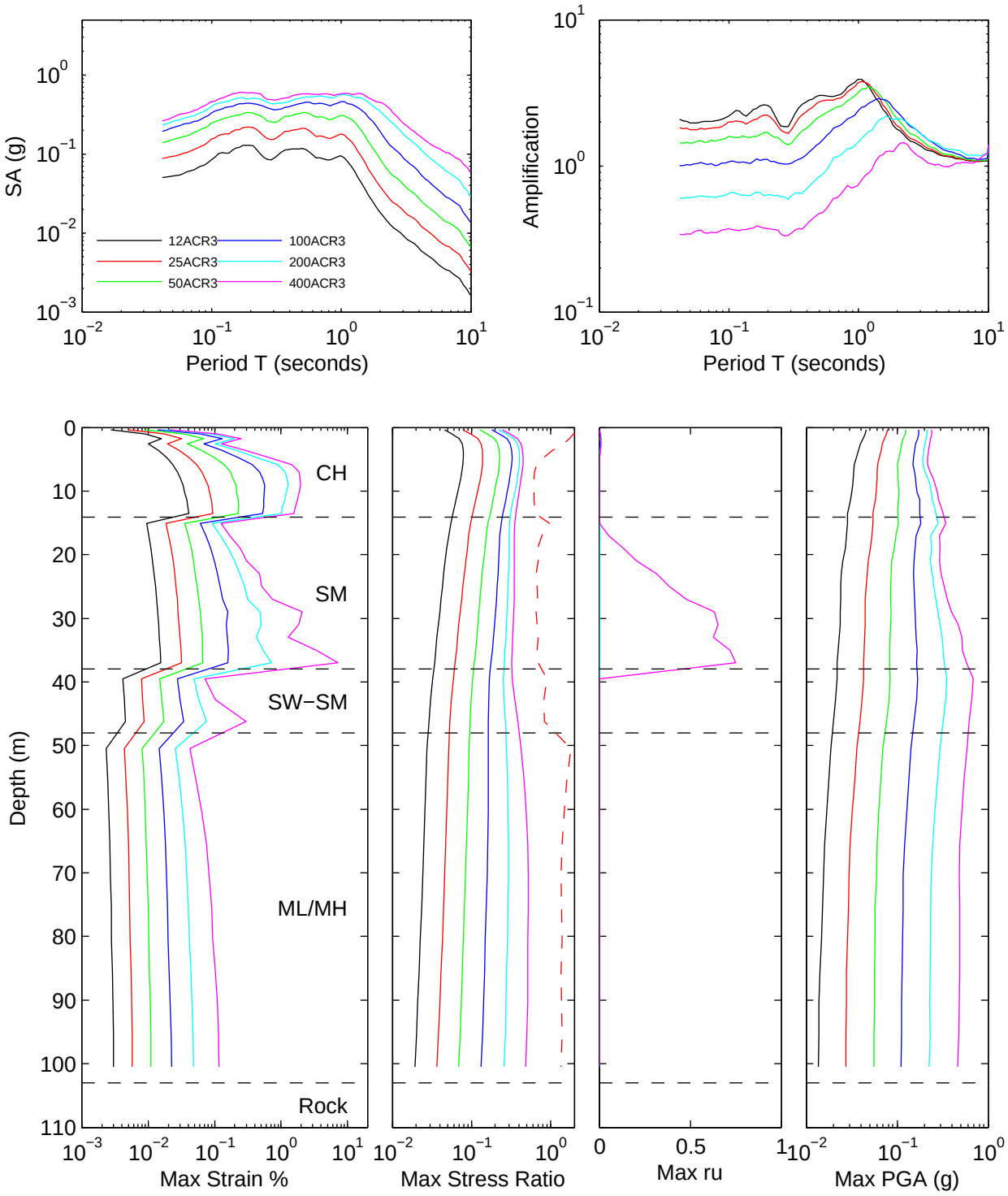

Figure 7A.29: Scenario comparison for effective stress analysis and site KIKNET S2 − Near fault and Scaled vs Matched

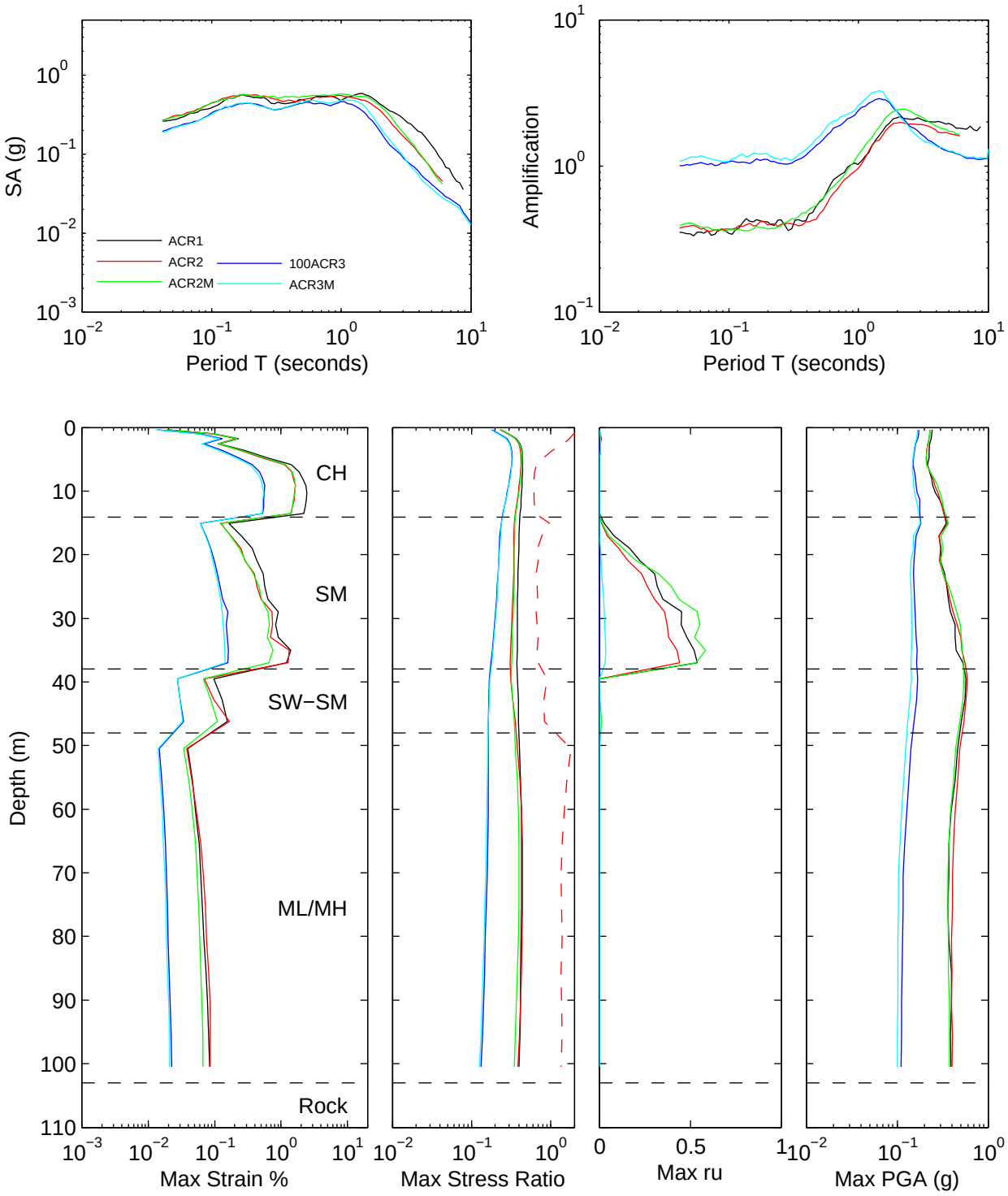

Figure 7A.30: Scenario comparison for effective stress analysis and site KIKNET S2 − Tectonic Region

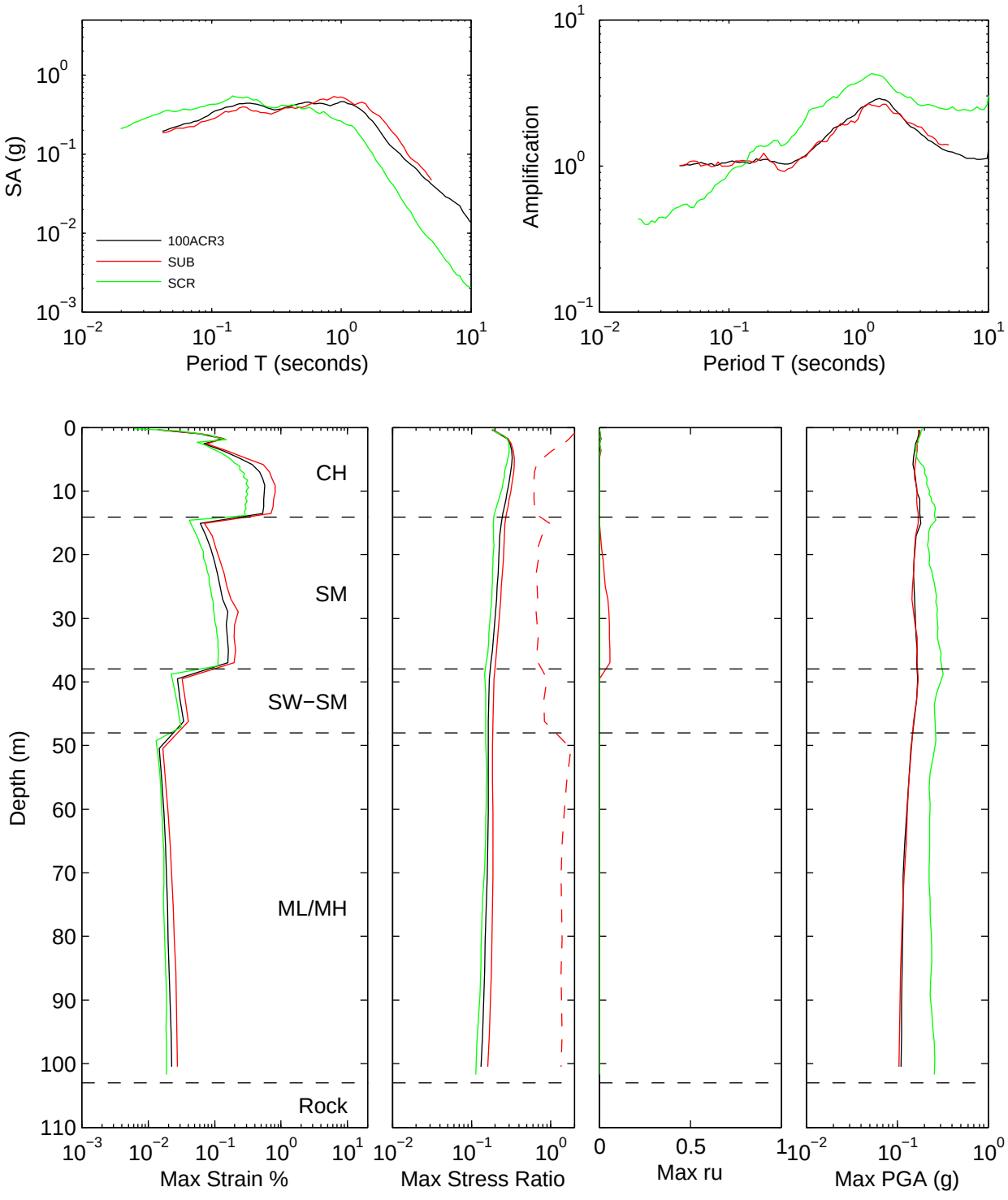

Figure 7A.31: Scenario comparison for effective stress analysis and site KIKNET S4 − Intensity

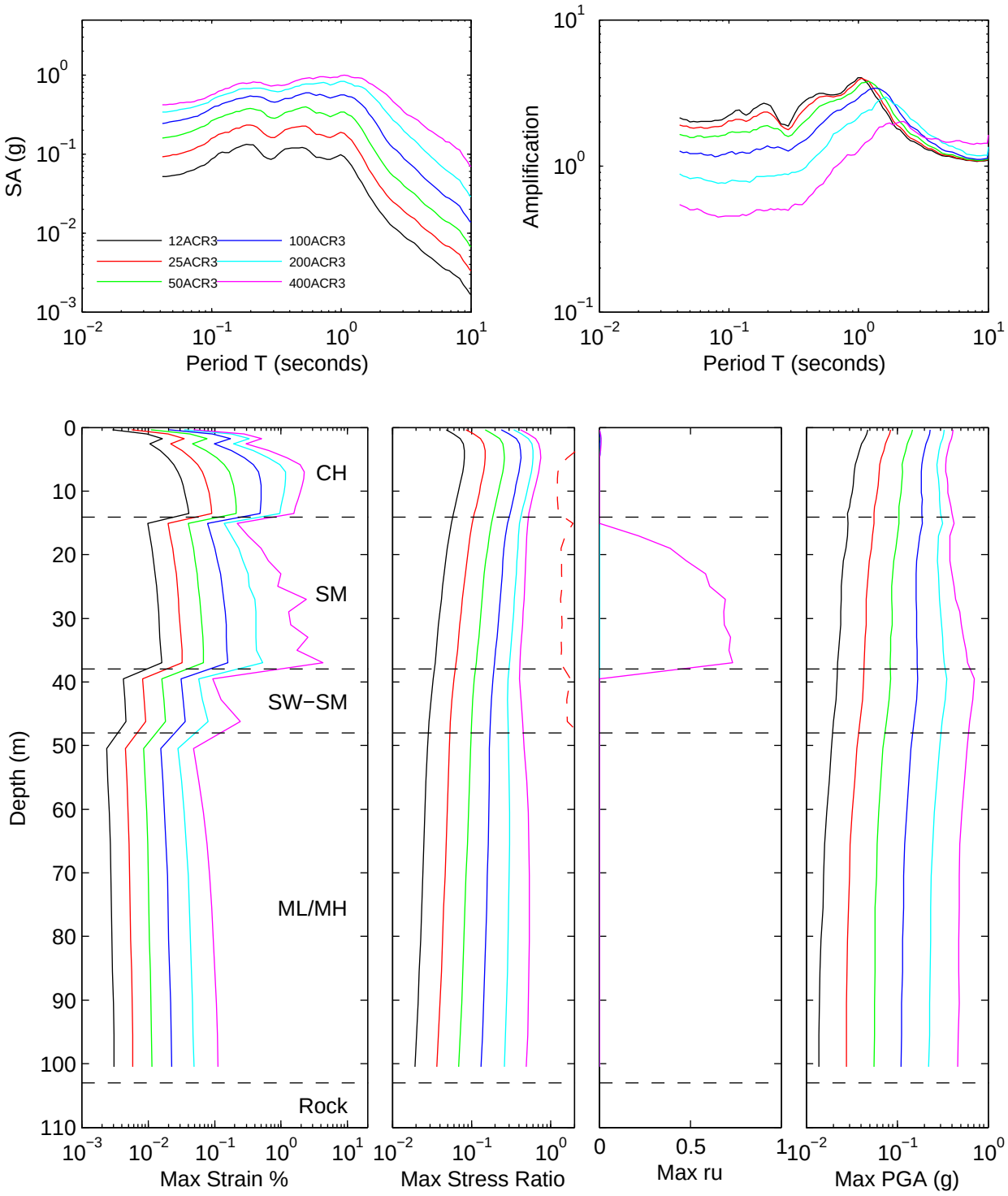

Figure 7A.32: Scenario comparison for effective stress analysis and site KIKNET S4 − Near fault and Scaled vs Matched

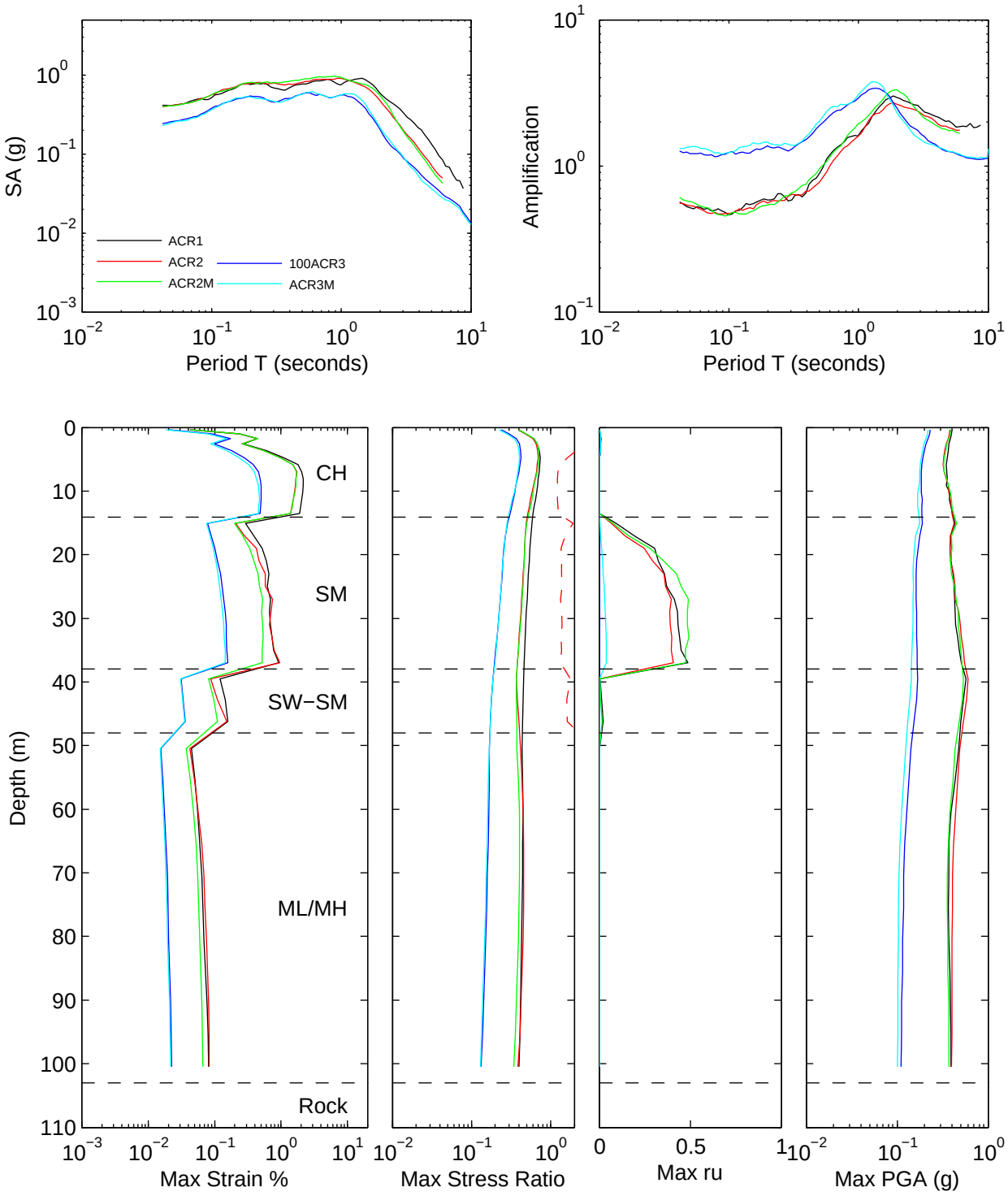

Figure 7A.33: Scenario comparison for effective stress analysis and site KIKNET S4 − Tectonic Region

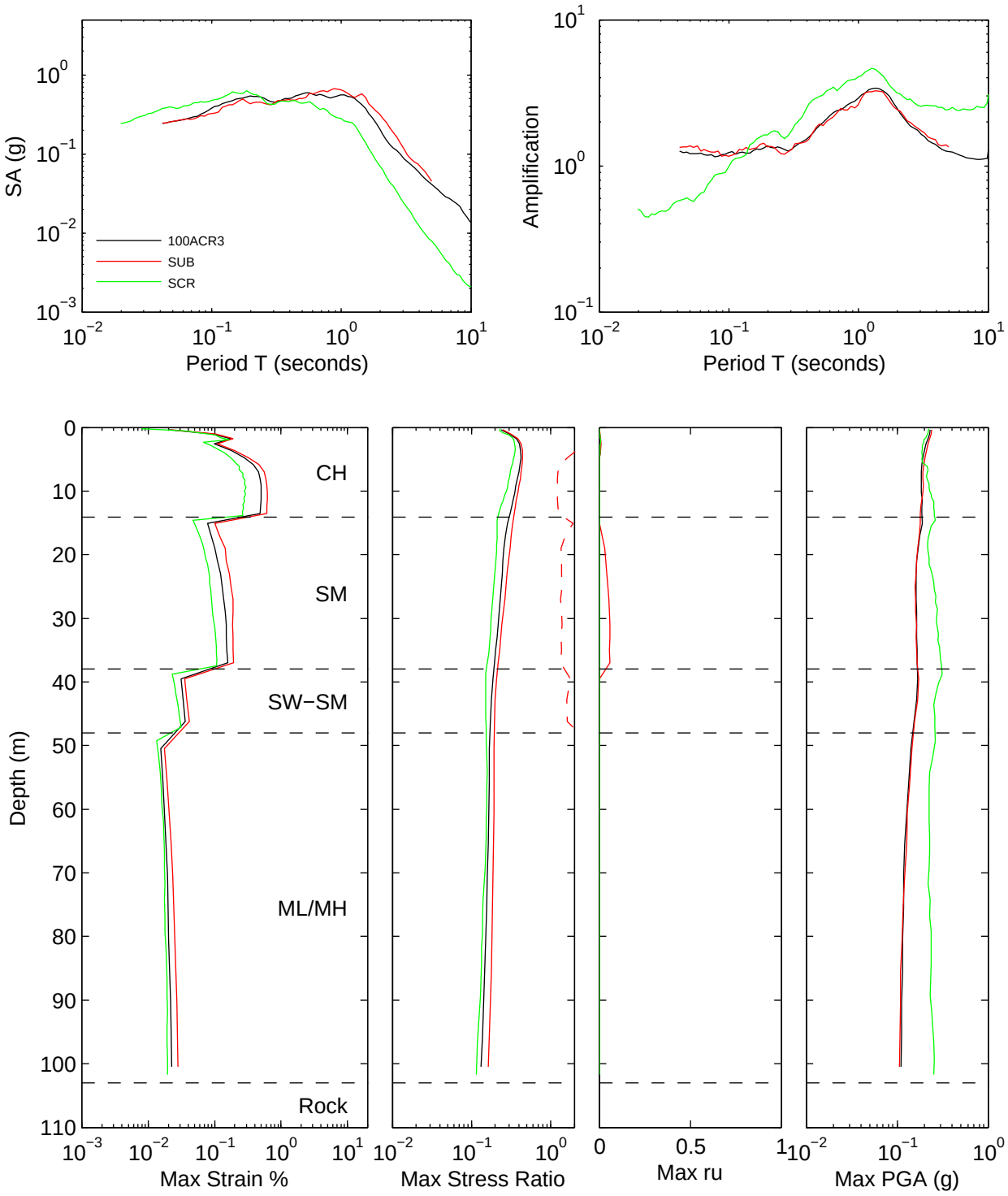

Figure 7A.34: Scenario comparison for effective stress analysis and site KIKNET40 − Intensity

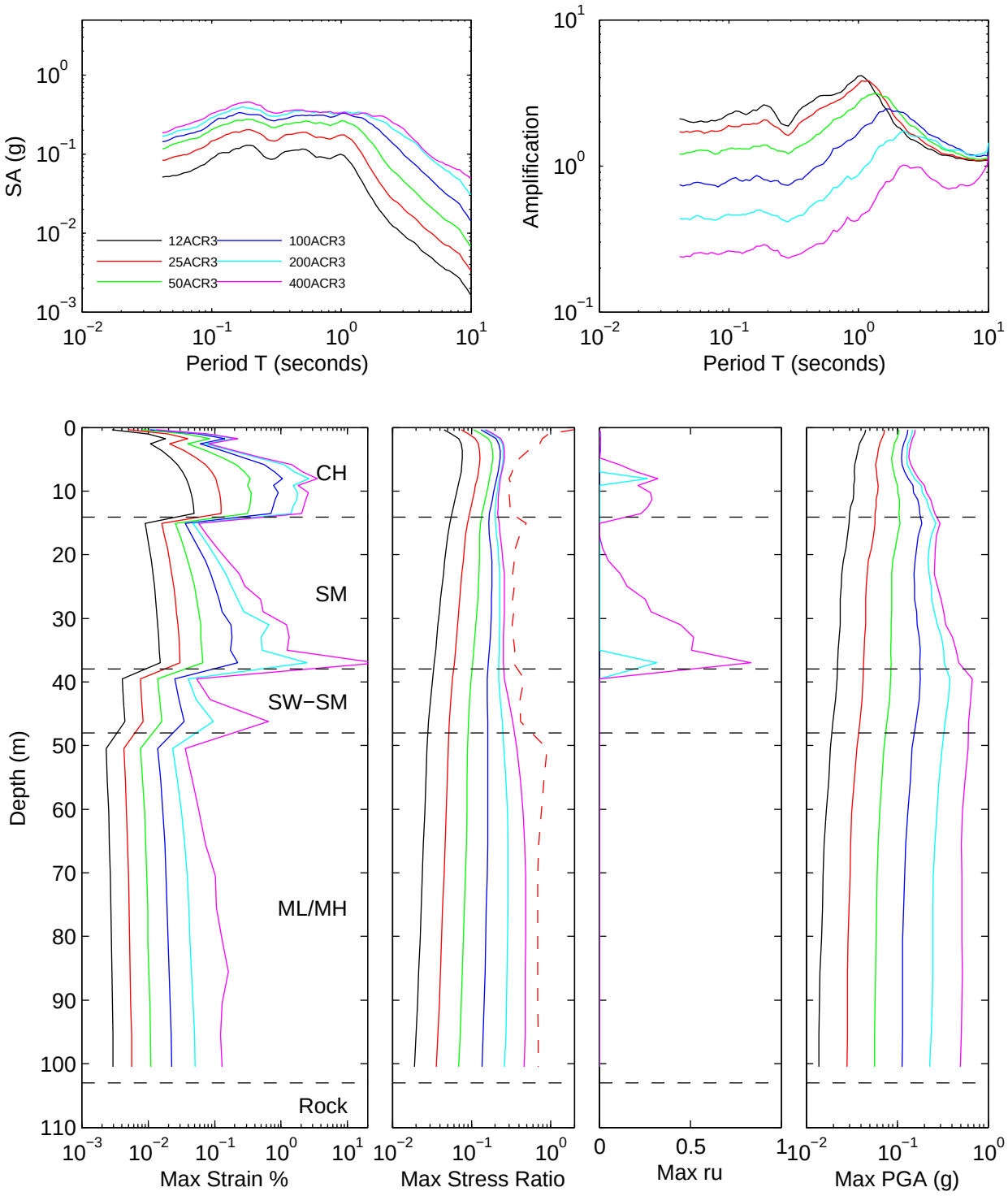

Figure 7A.35: Scenario comparison for effective stress analysis and site KIKNET40 − Near fault and Scaled vs Matched

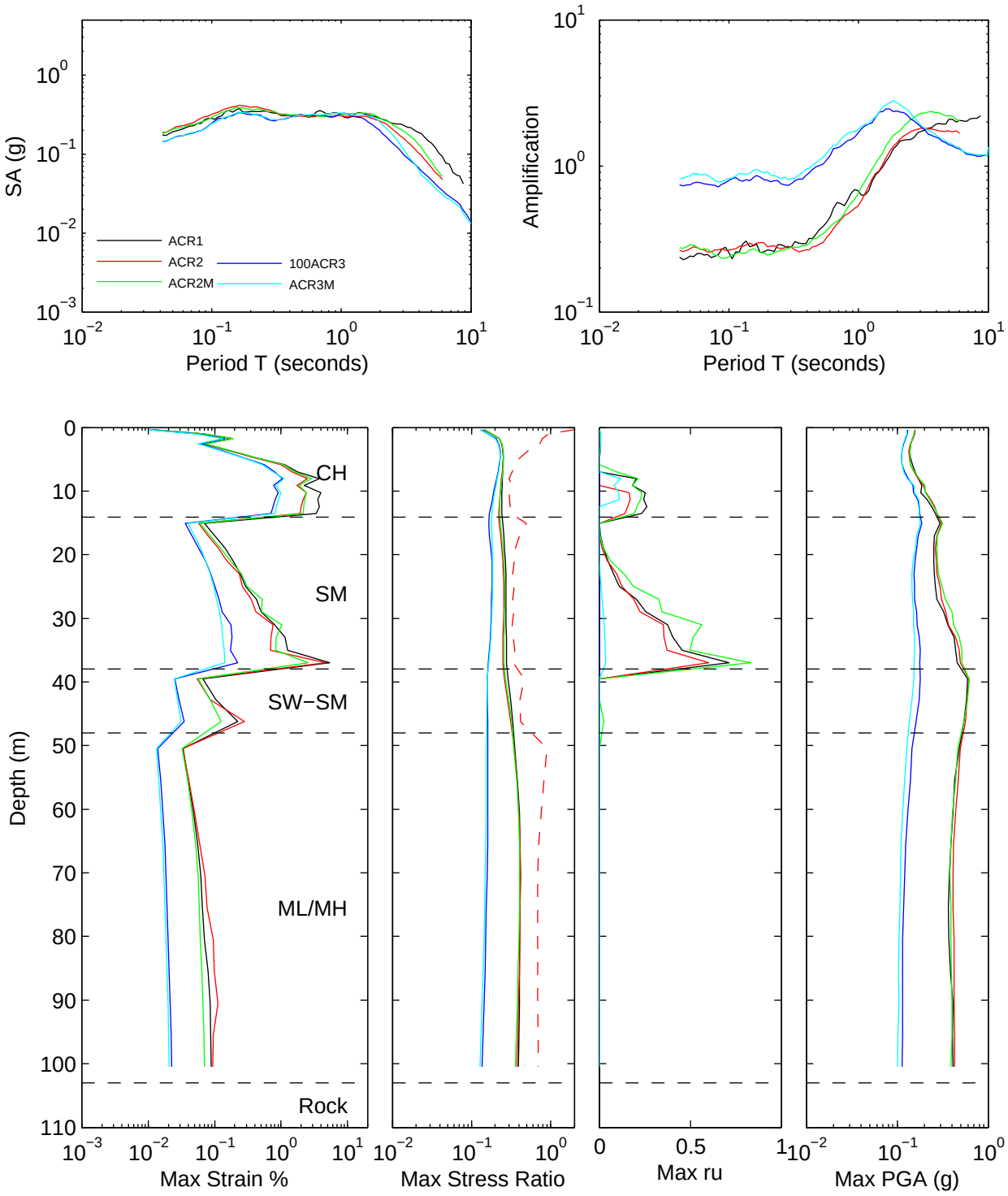

Figure 7A.36: Scenario comparison for effective stress analysis and site KIKNET40 − Tectonic Region

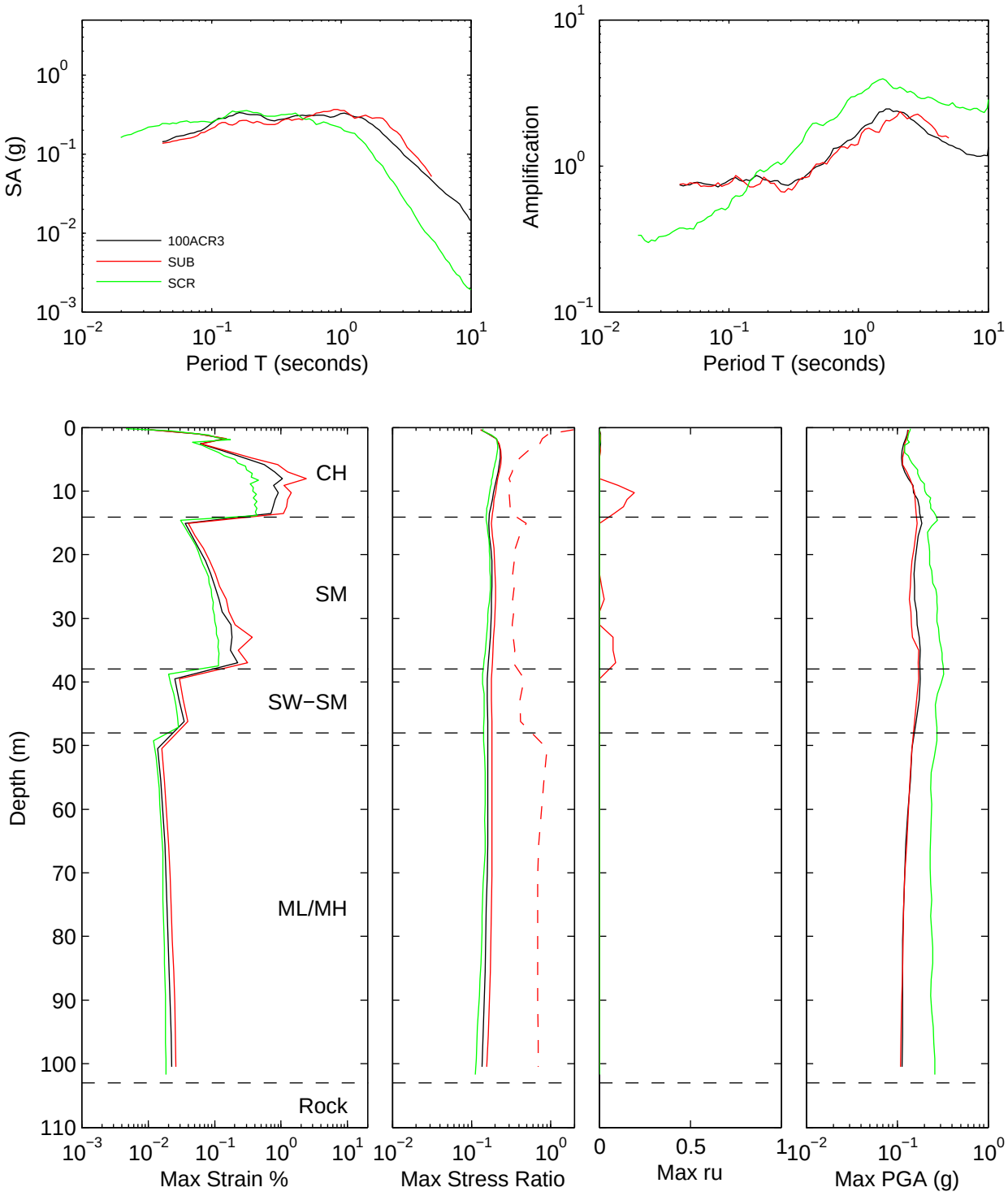

Figure 7A.37: Scenario comparison for effective stress analysis and site KIKNET160 − Intensity

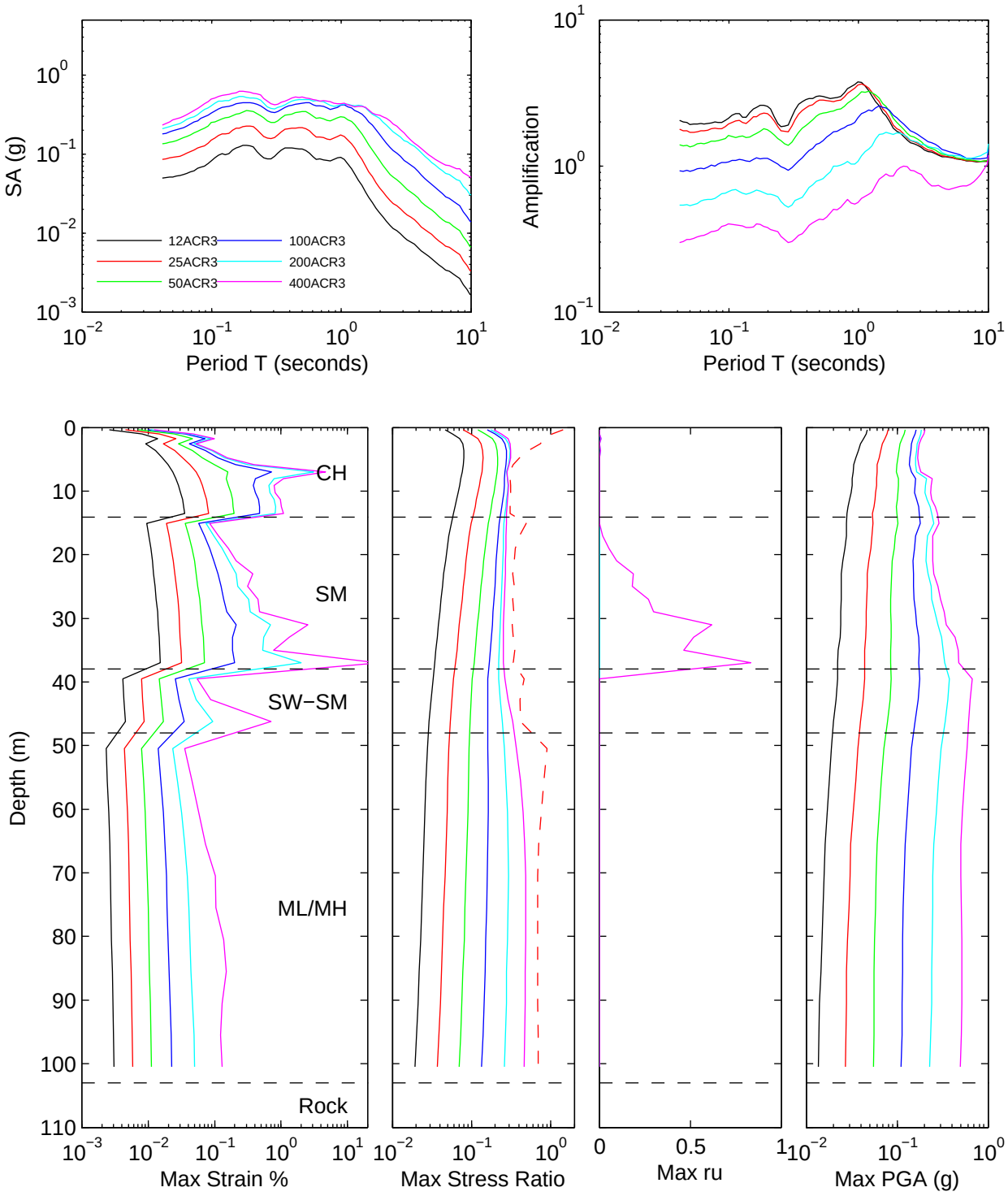

Figure 7A.38: Scenario comparison for effective stress analysis and site KIKNET160 − Near fault and Scaled vs Matched

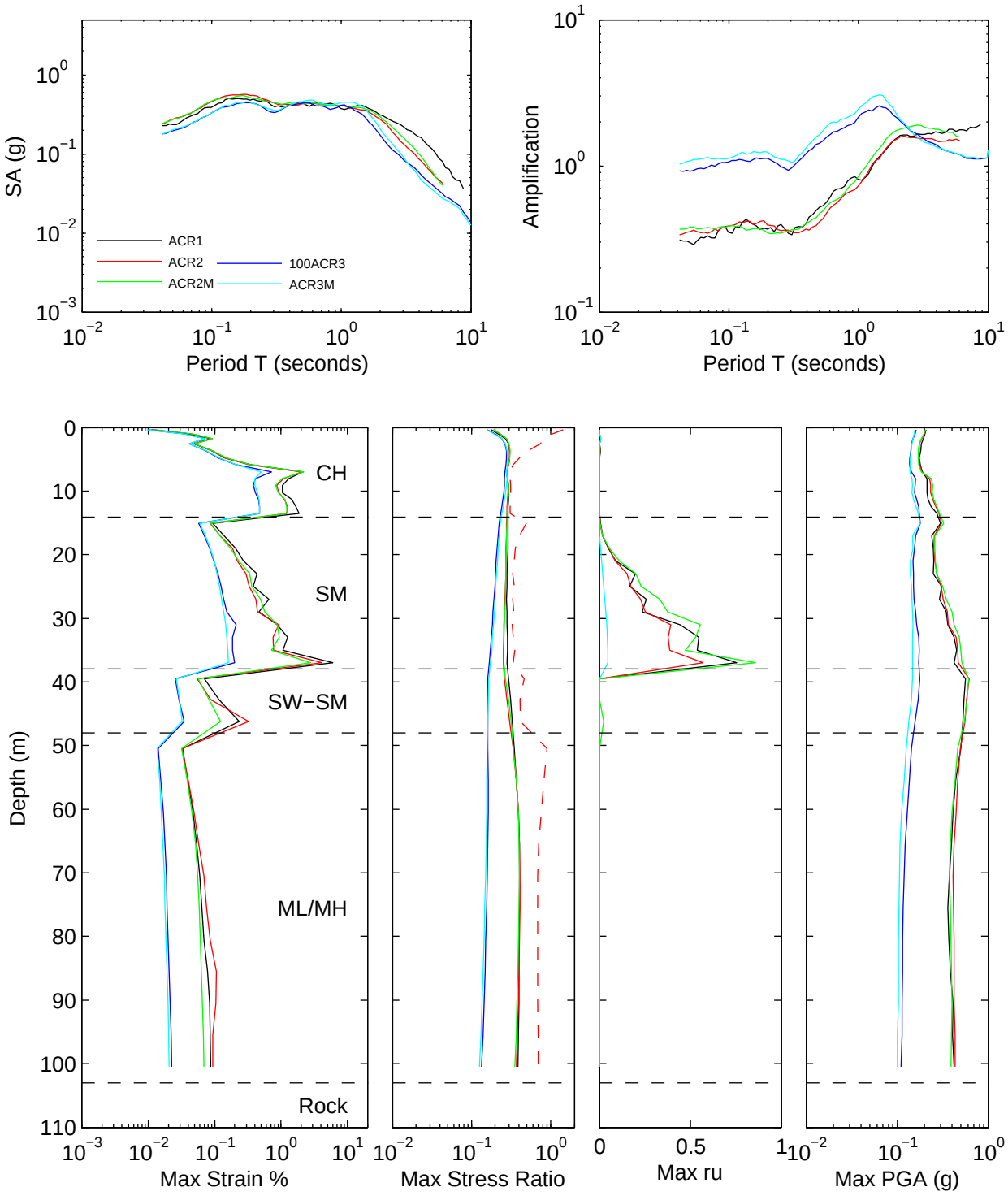

Figure 7A.39: Scenario comparison for effective stress analysis and site KIKNET160 − Tectonic Region

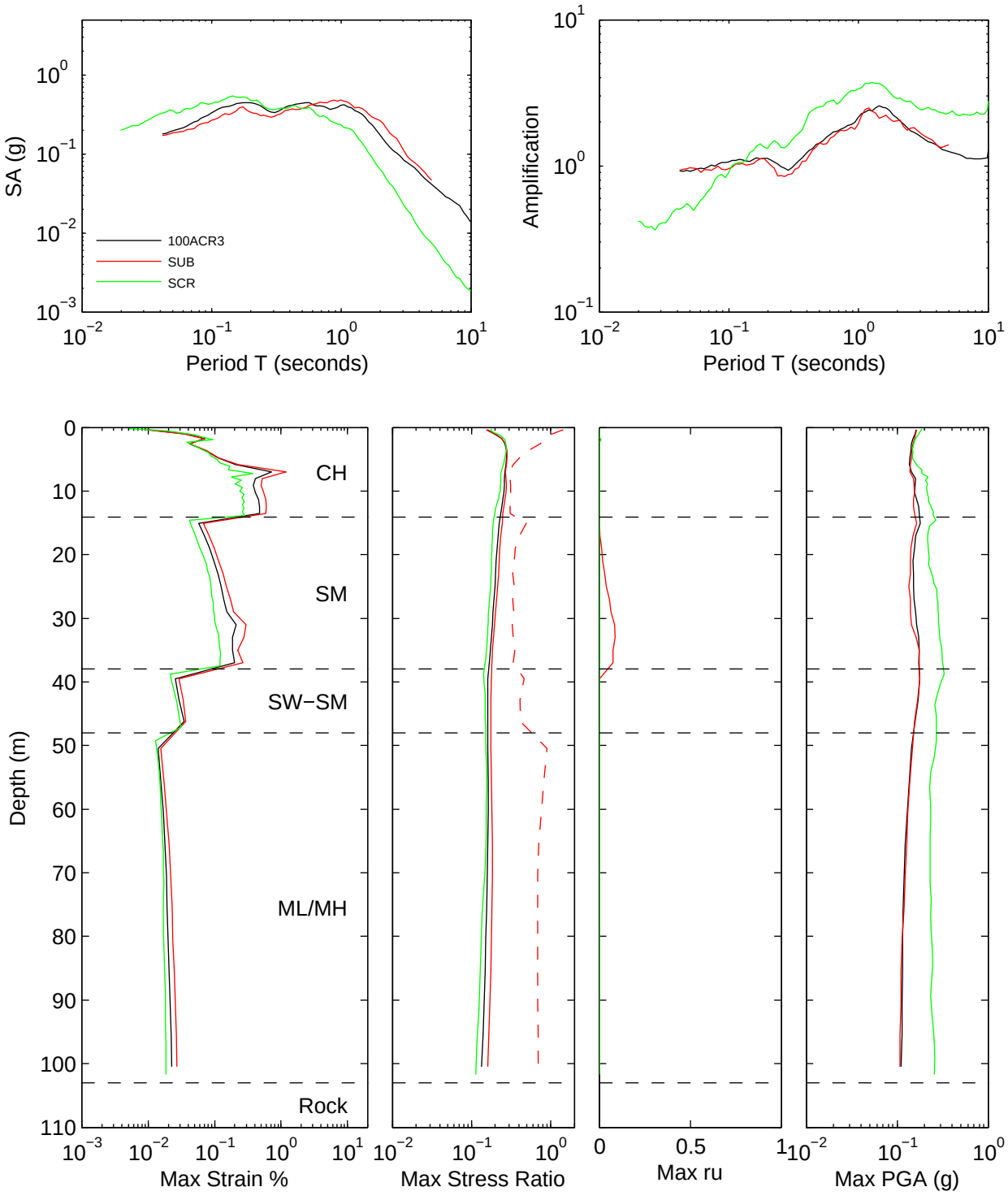

Figure 7A.40: Scenario comparison for effective stress analysis and site MRCE1 − Intensity

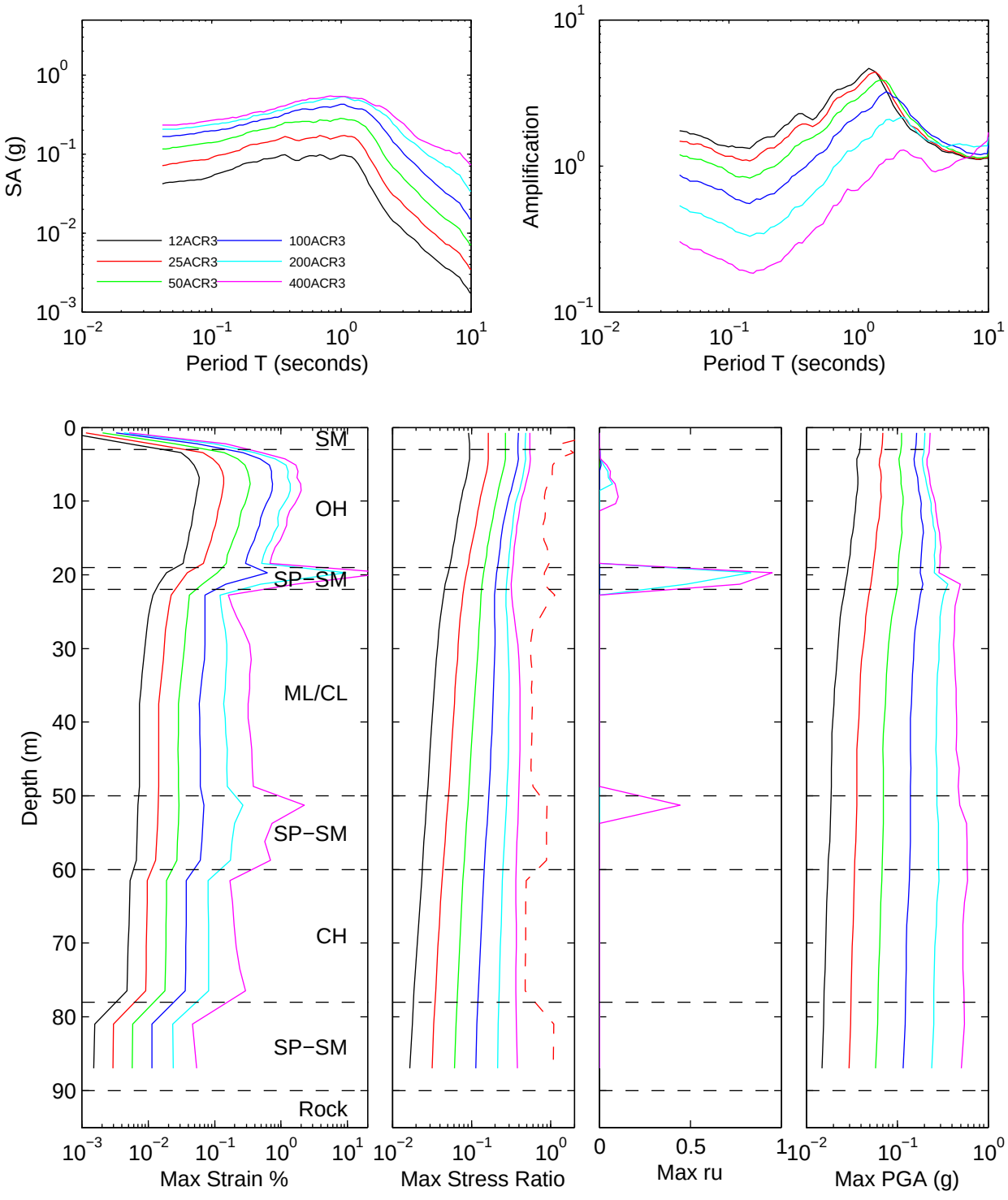

Figure 7A.41: Scenario comparison for effective stress analysis and site MRCE1 − Near fault and Scaled vs Matched

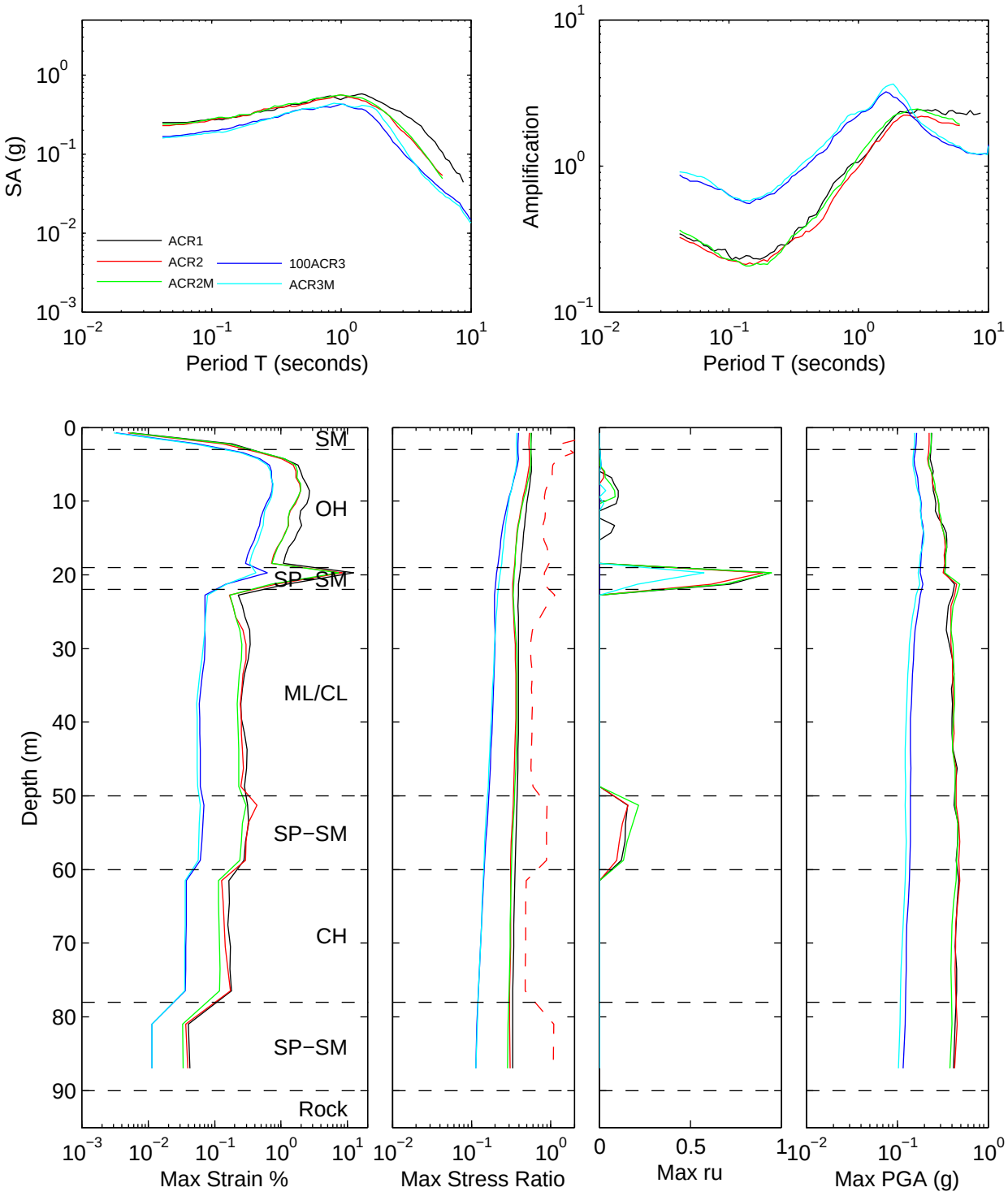

Figure 7A.42: Scenario comparison for effective stress analysis and site MRCE1 − Tectonic Region

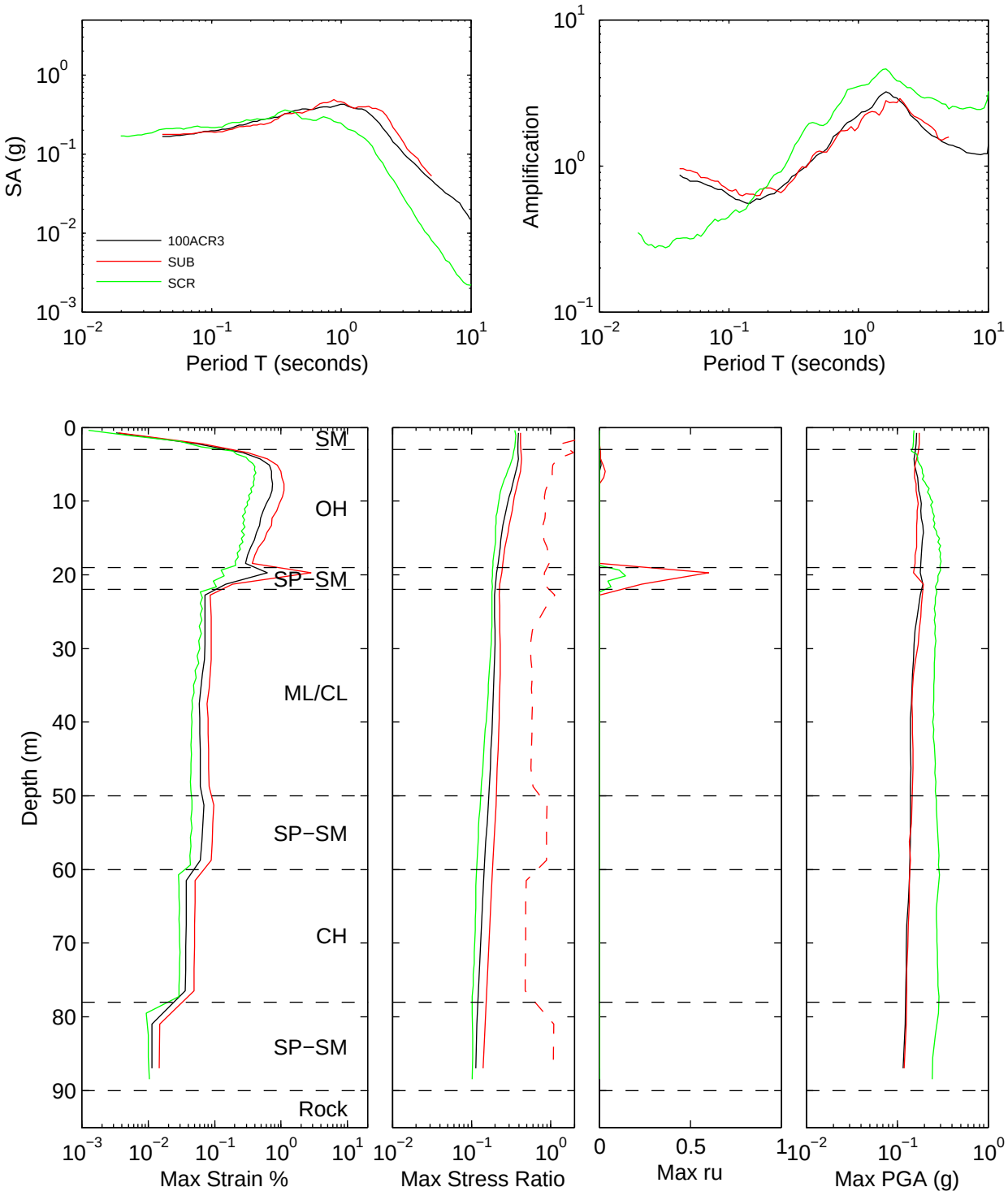

Figure 7A.43: Scenario comparison for effective stress analysis and site MRCE2 − Intensity

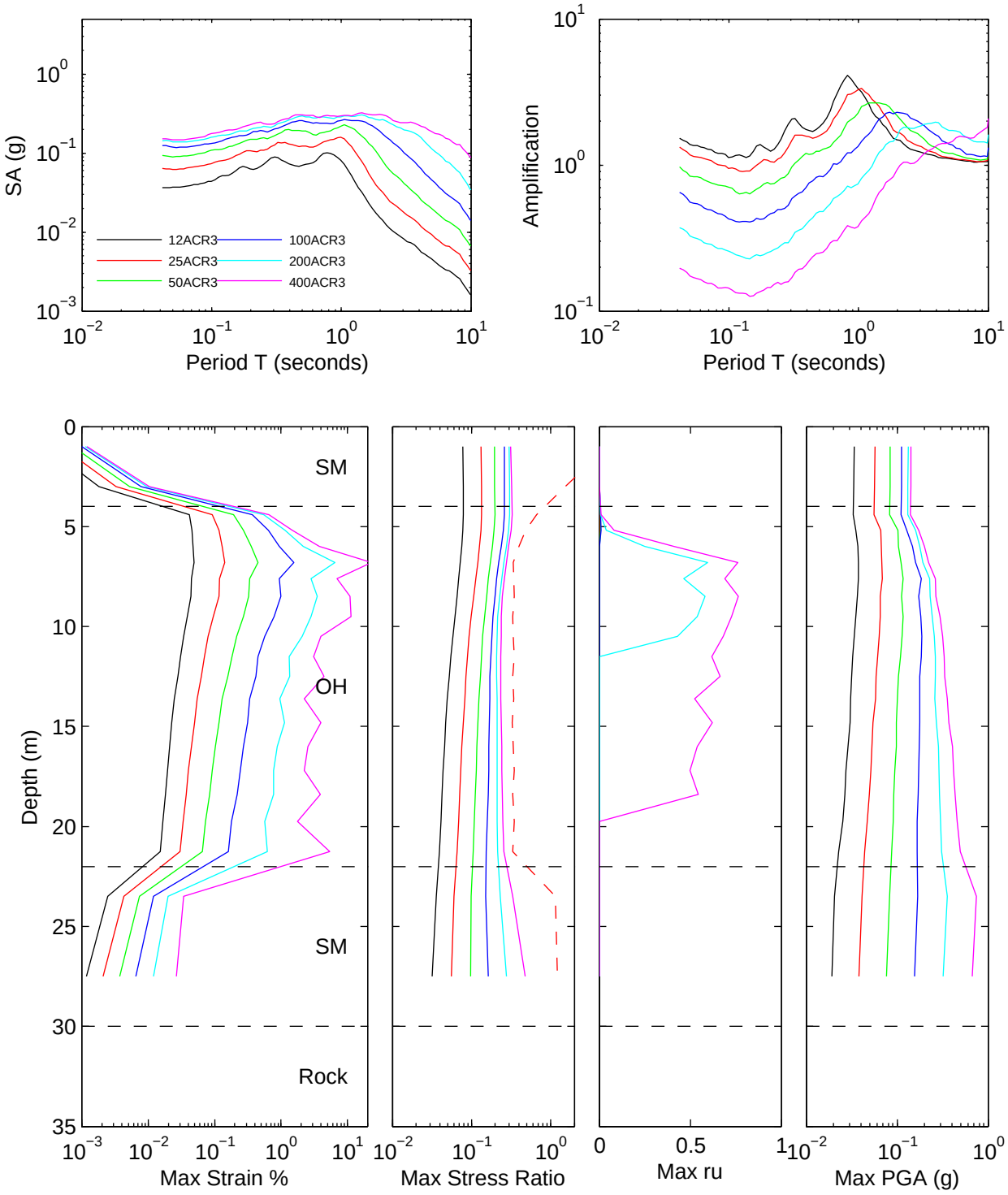

Figure 7A.44: Scenario comparison for effective stress analysis and site MRCE2 − Near fault and Scaled vs Matched

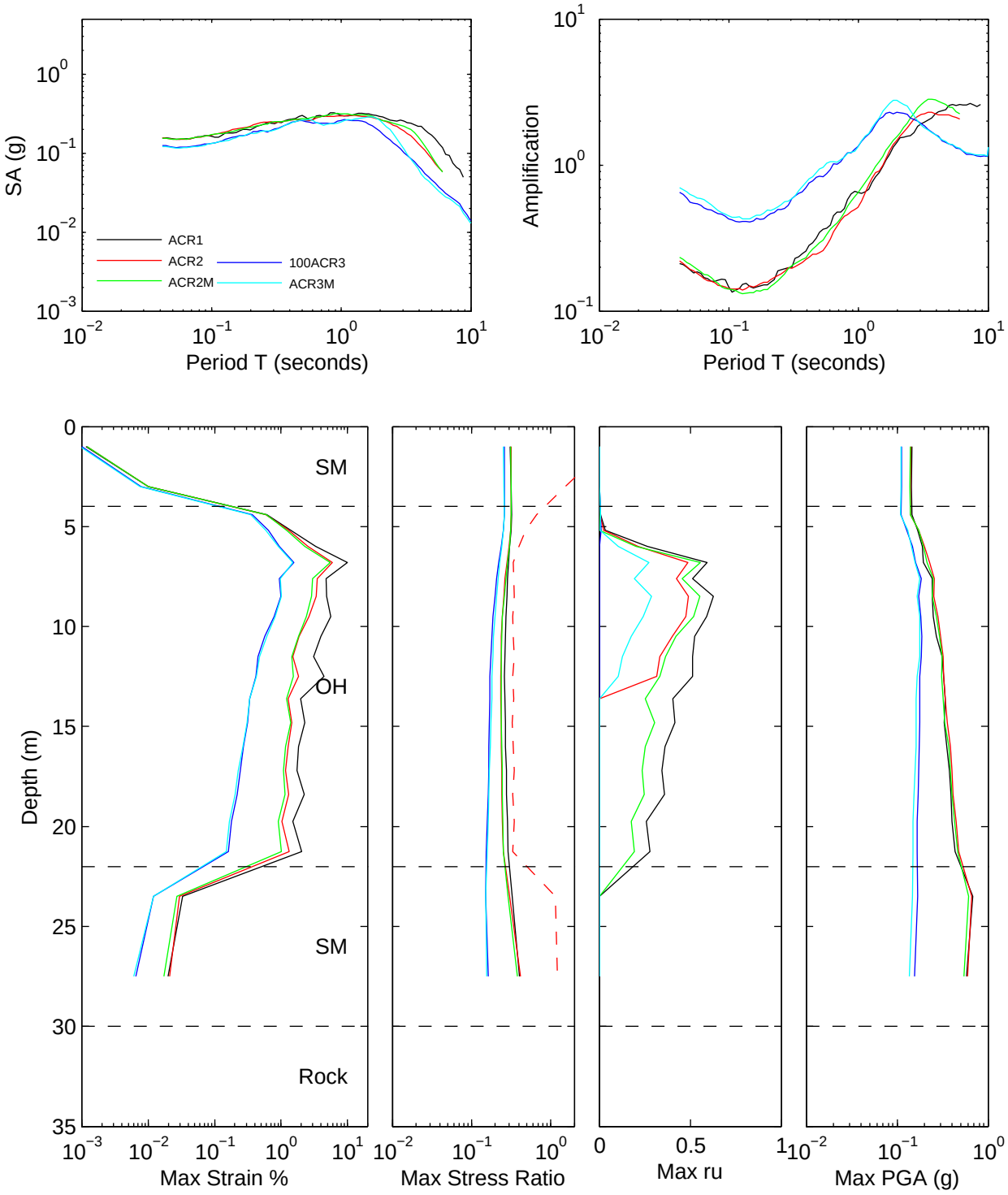

Figure 7A.45: Scenario comparison for effective stress analysis and site MRCE2 − Tectonic Region

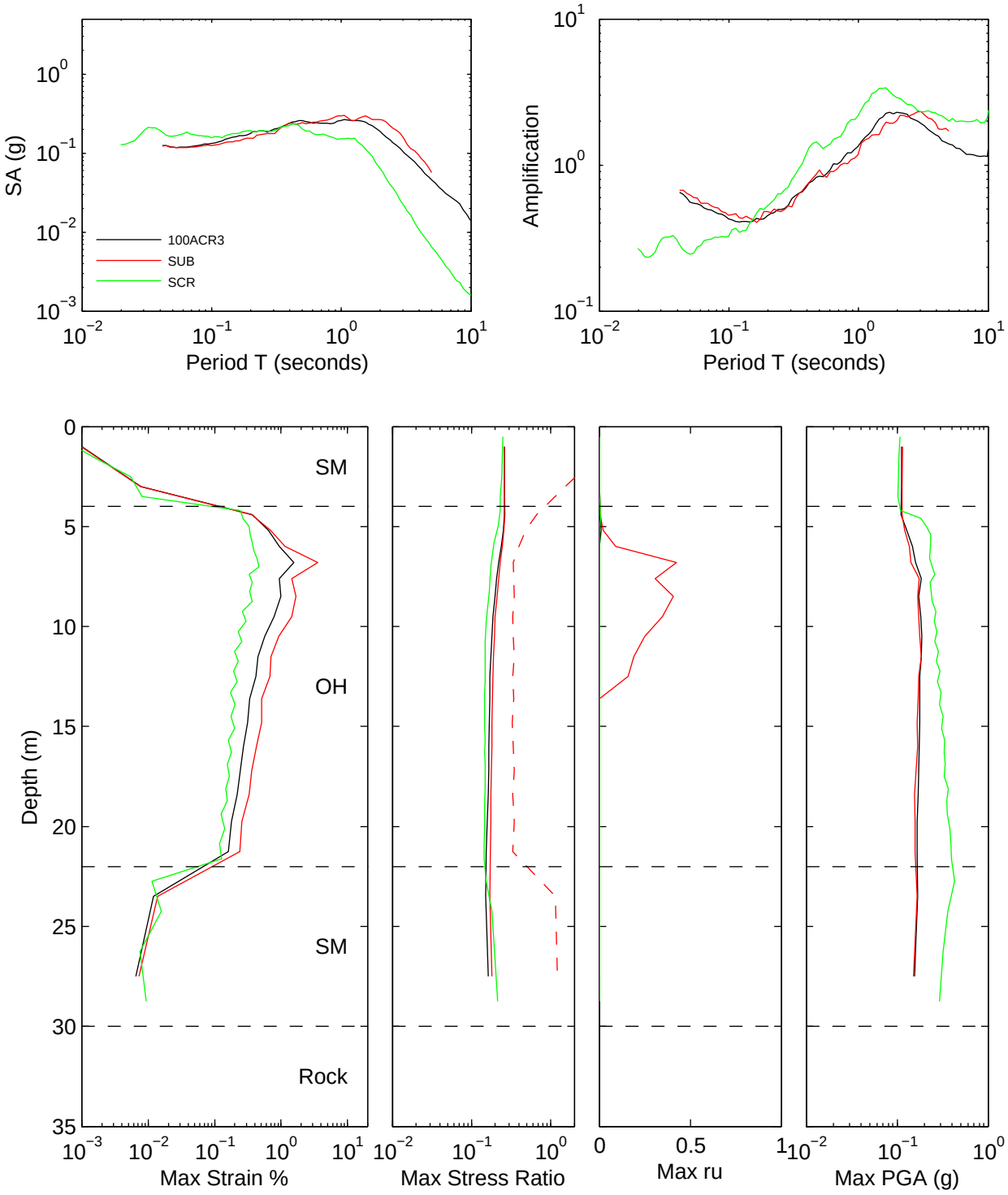

Figure 7A.46: Comparison of response spectra shape for site Bay Area and effective stress analyses

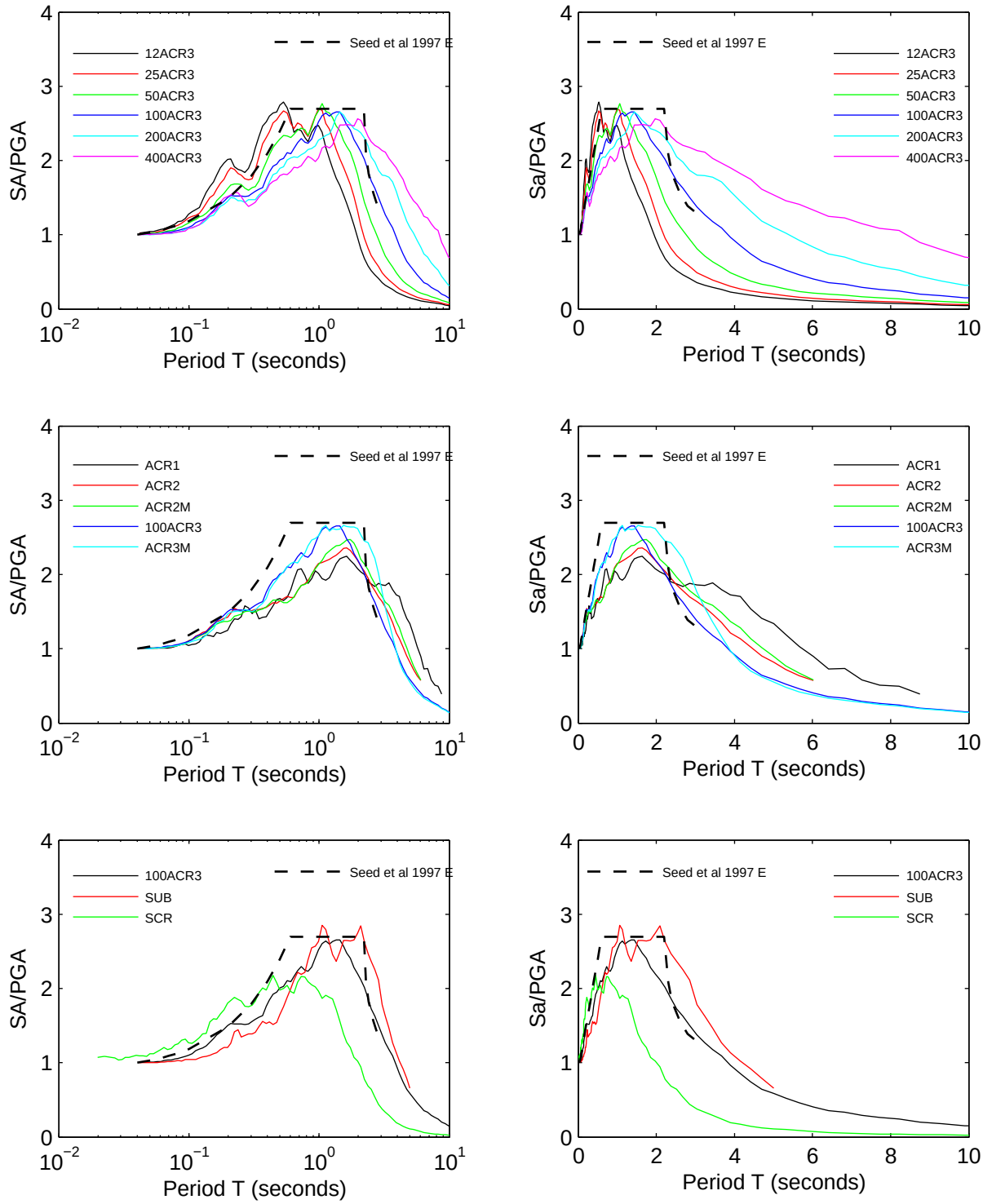

Figure 7A.47: Comparison of response spectra shape for site Bay Area F and effective stress analyses

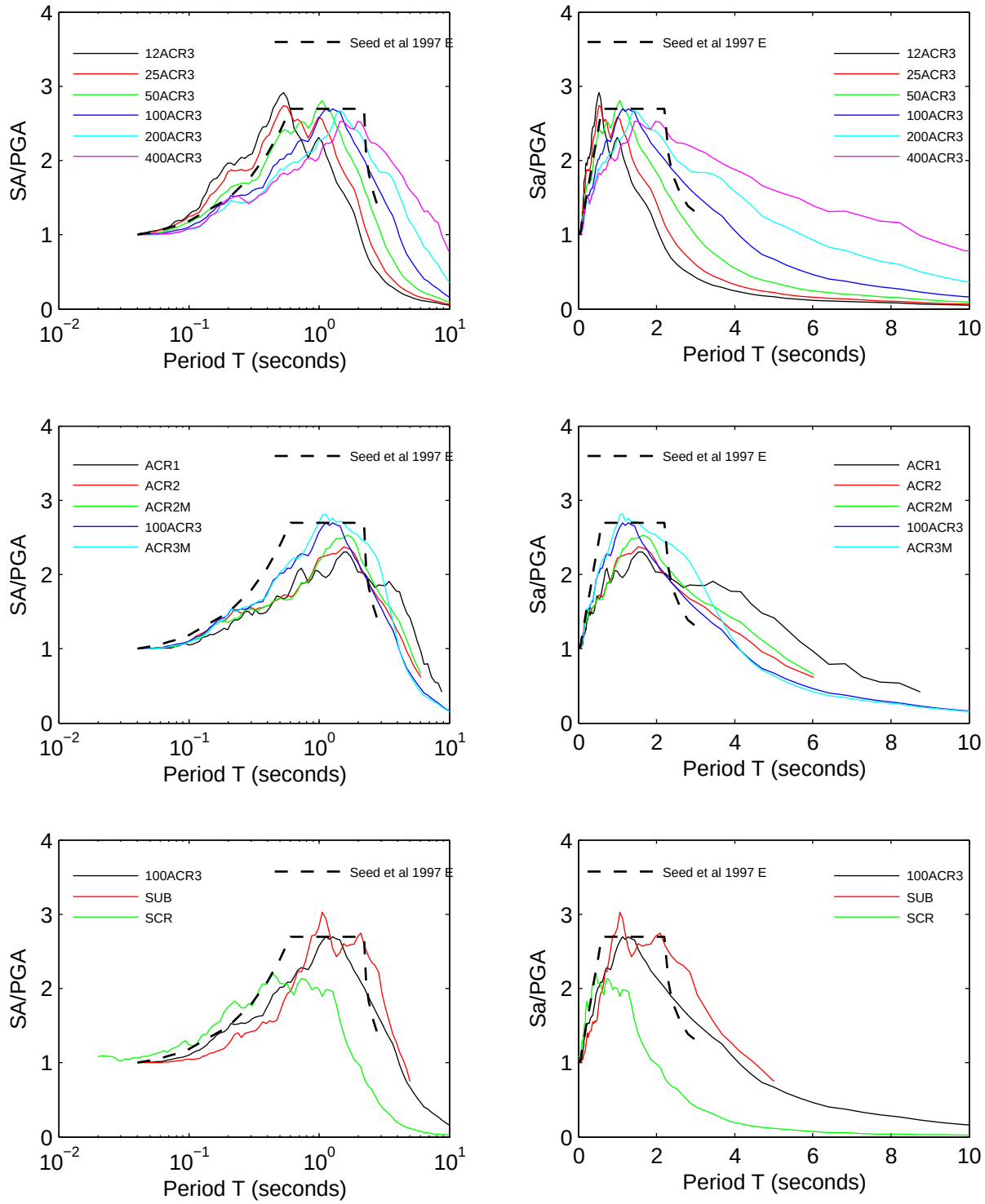

Figure 7A.48: Comparison of response spectra shape for site Bay Area II and effective stress analyses

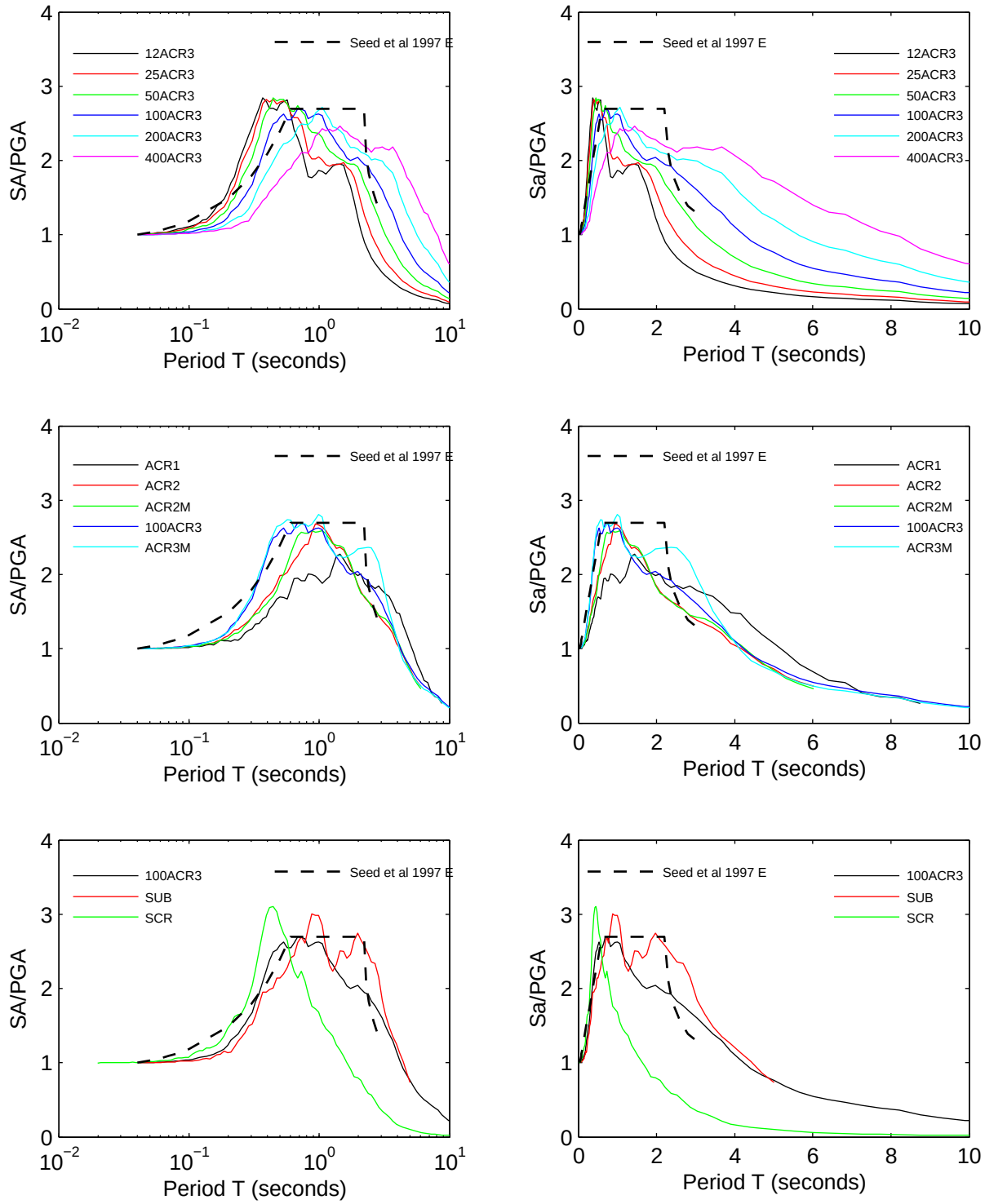

Figure 7A.49: Comparison of response spectra shape for site Bay Area II K and effective stress analyses

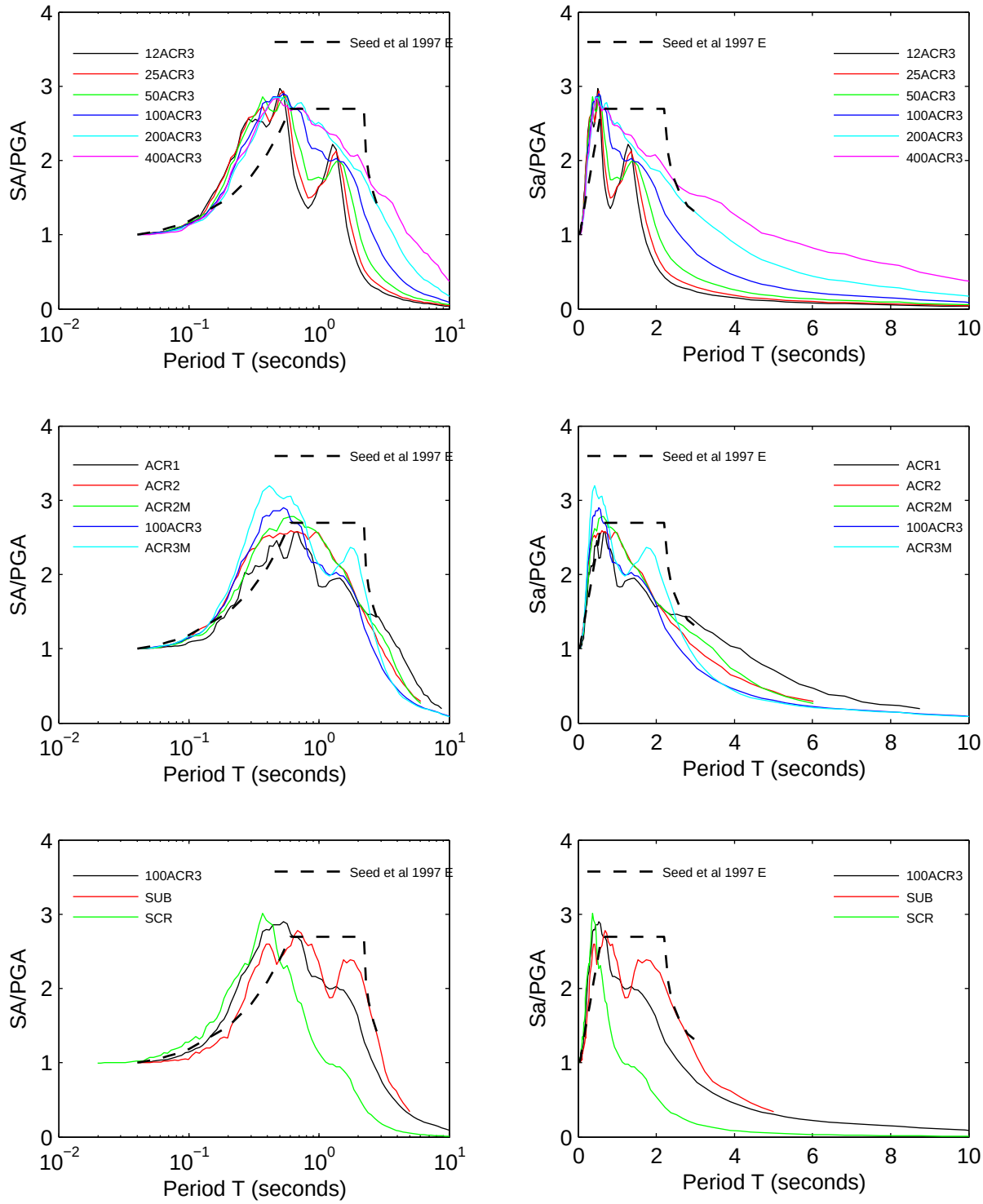

Figure 7A.50: Comparison of response spectra shape for site Bay Area II K S2 and effective stress analyses

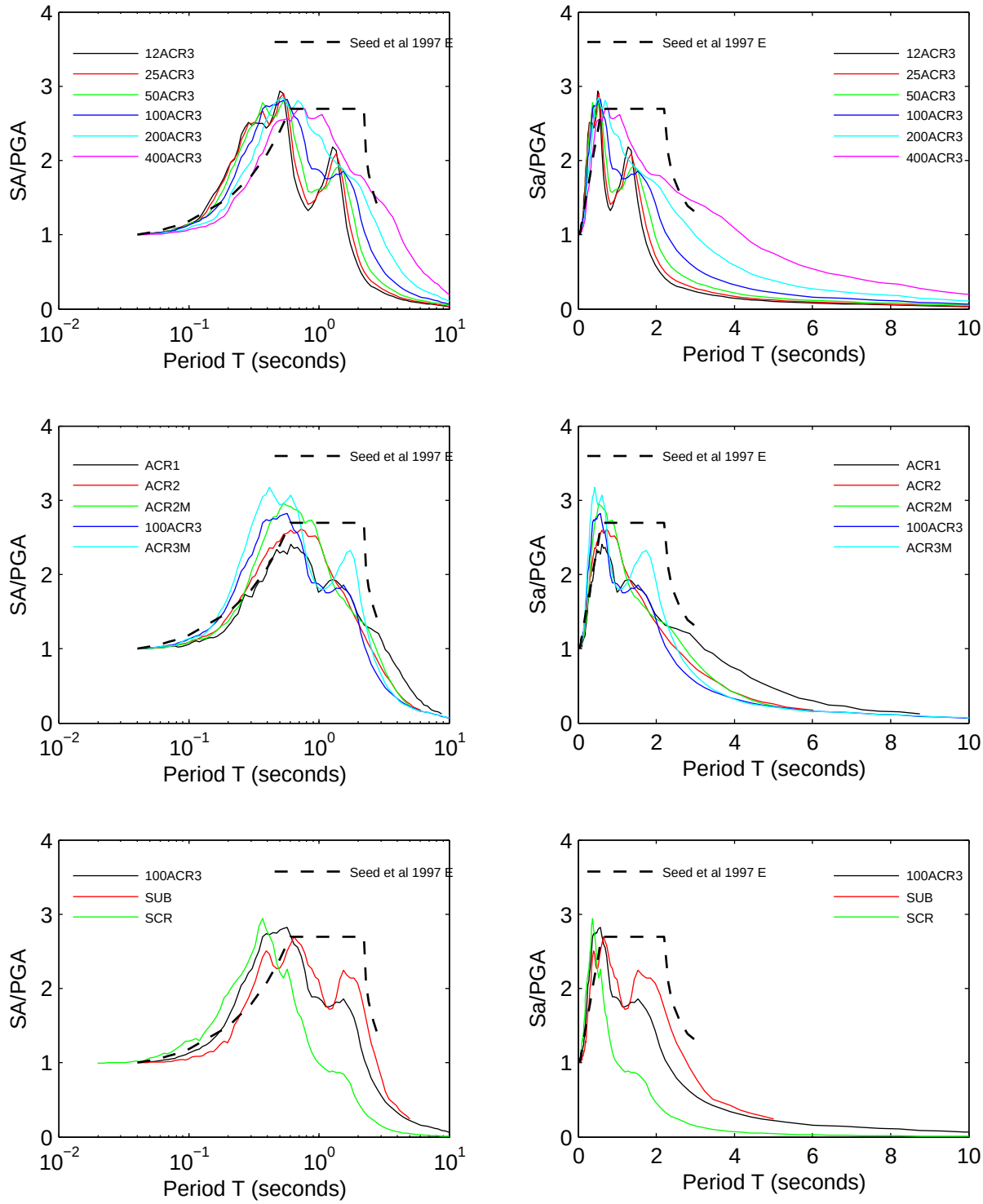

Figure 7A.51: Comparison of response spectra shape for site Bay Area II K S4 and effective stress analyses

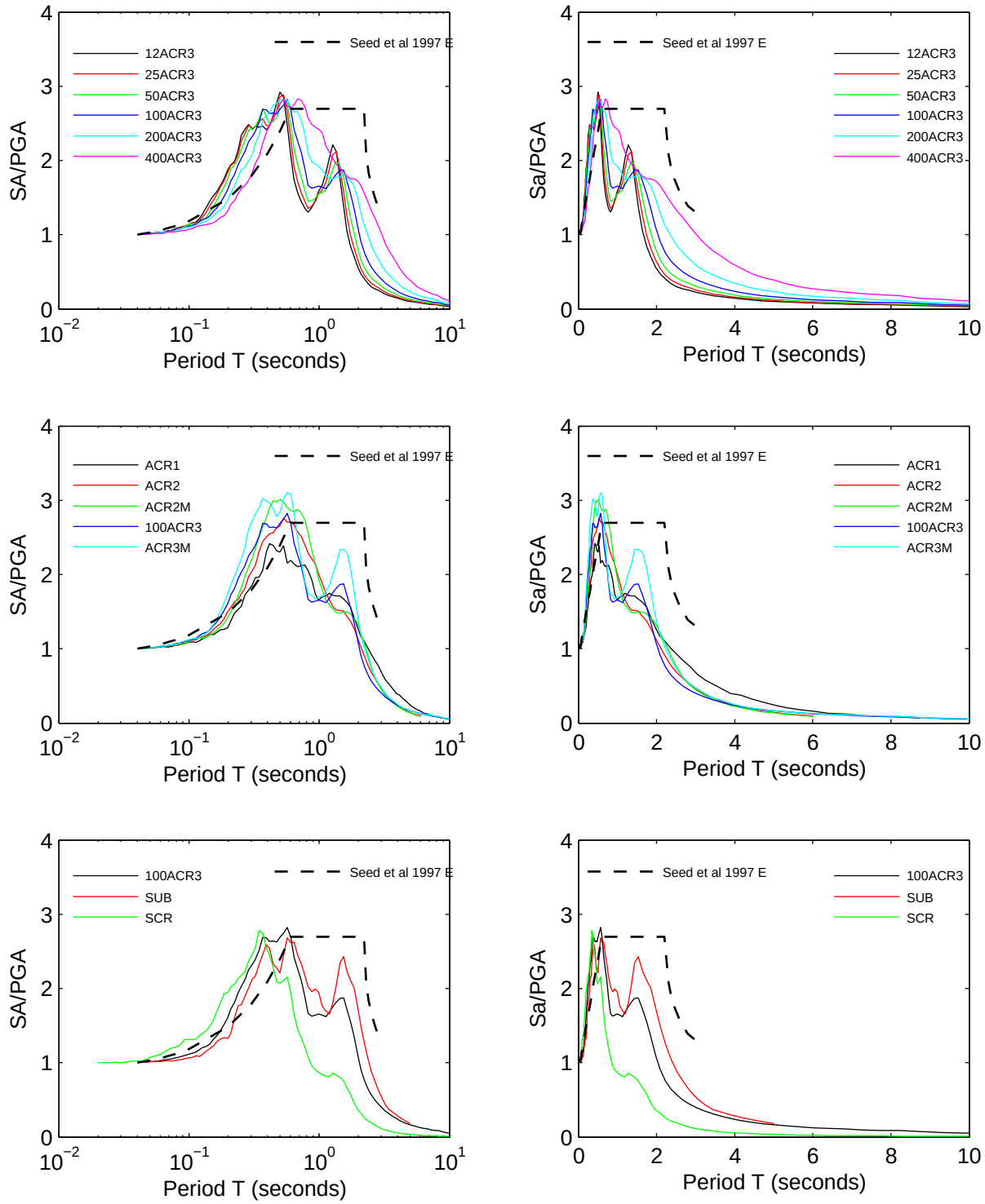

Figure 7A.52: Comparison of response spectra shape for site HAGP and effective stress analyses

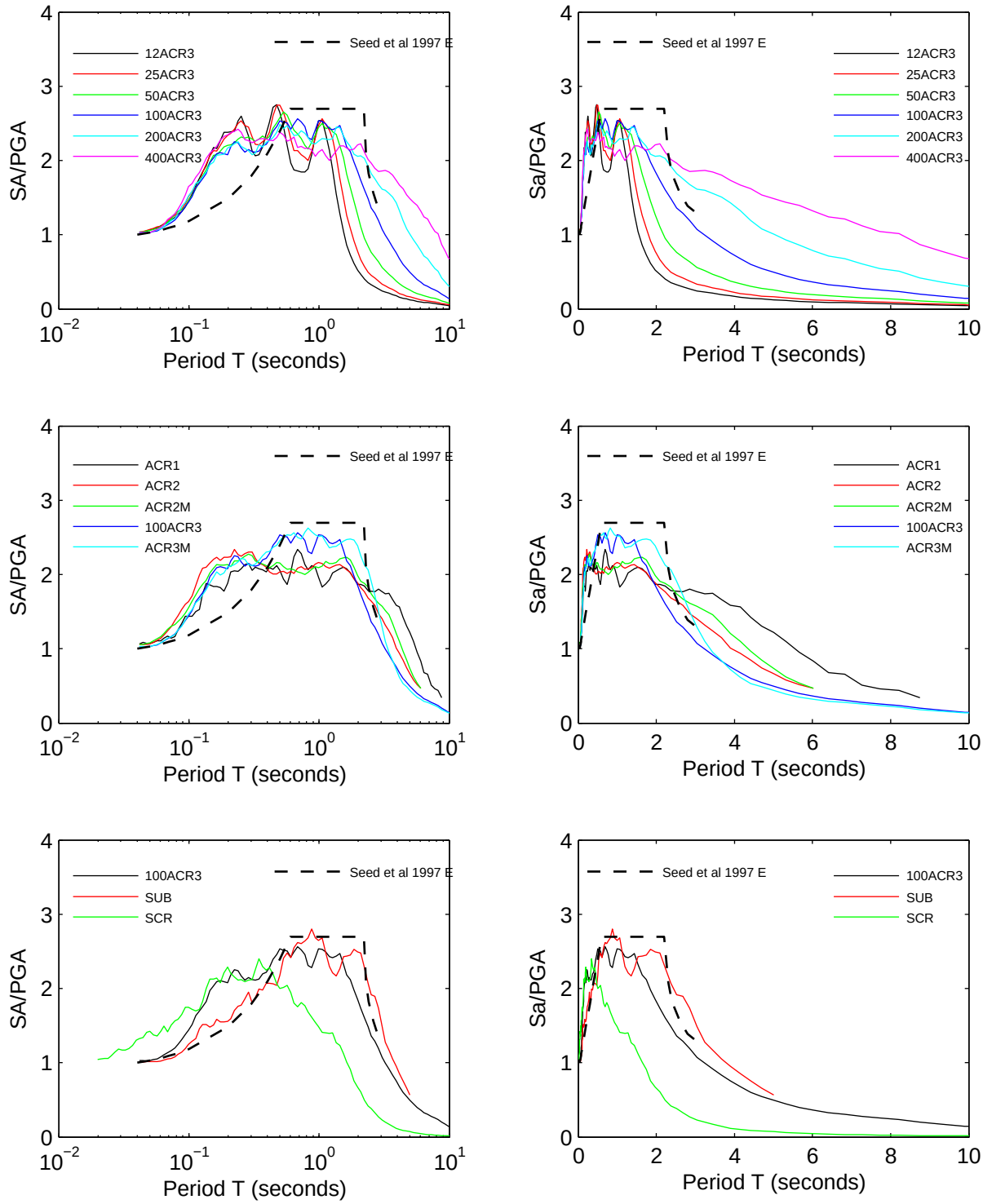

Figure 7A.53: Comparison of response spectra shape for site JSSS and effective stress analyses

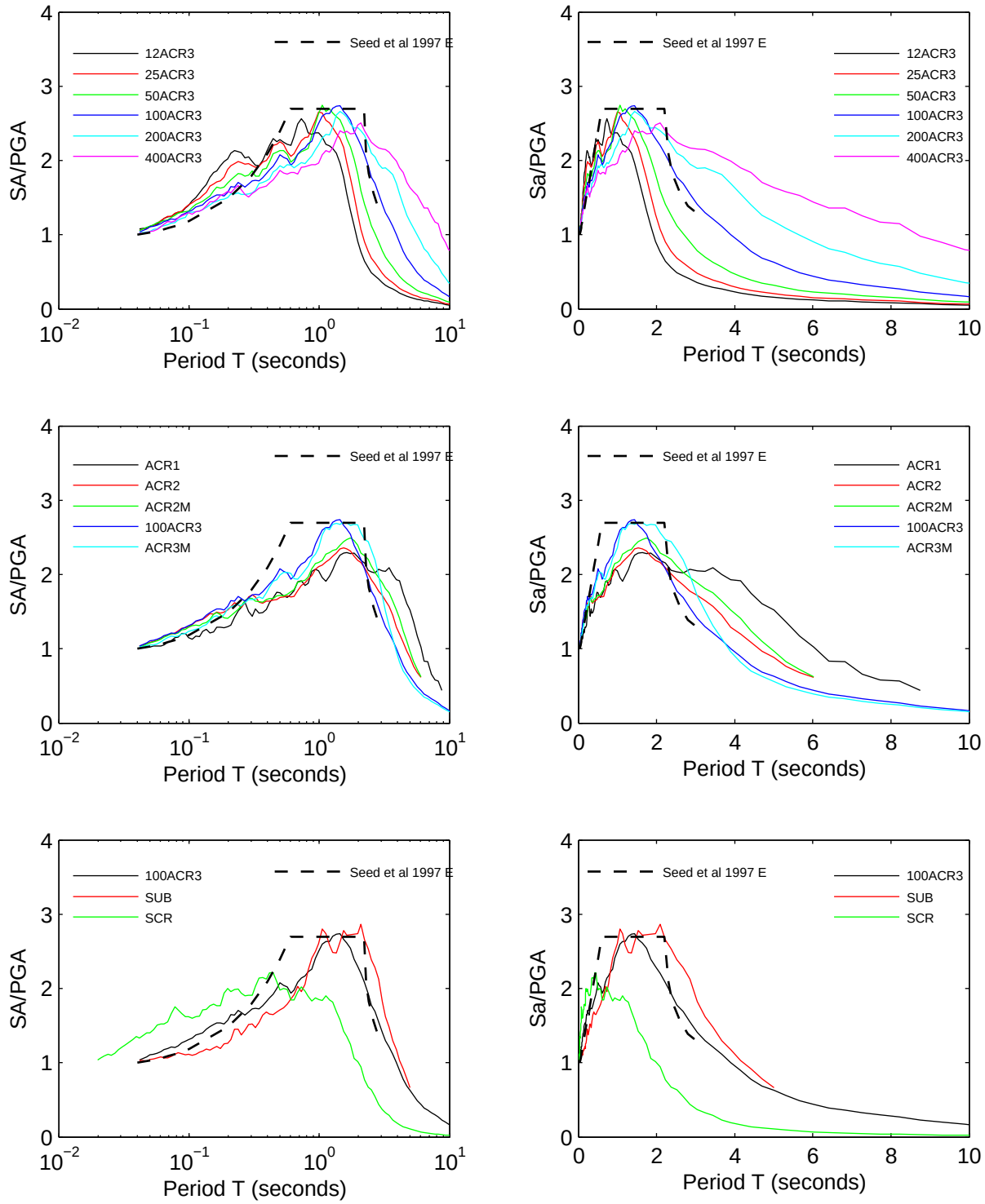

Figure 7A.54: Comparison of response spectra shape for site KIKNET and effective stress analyses

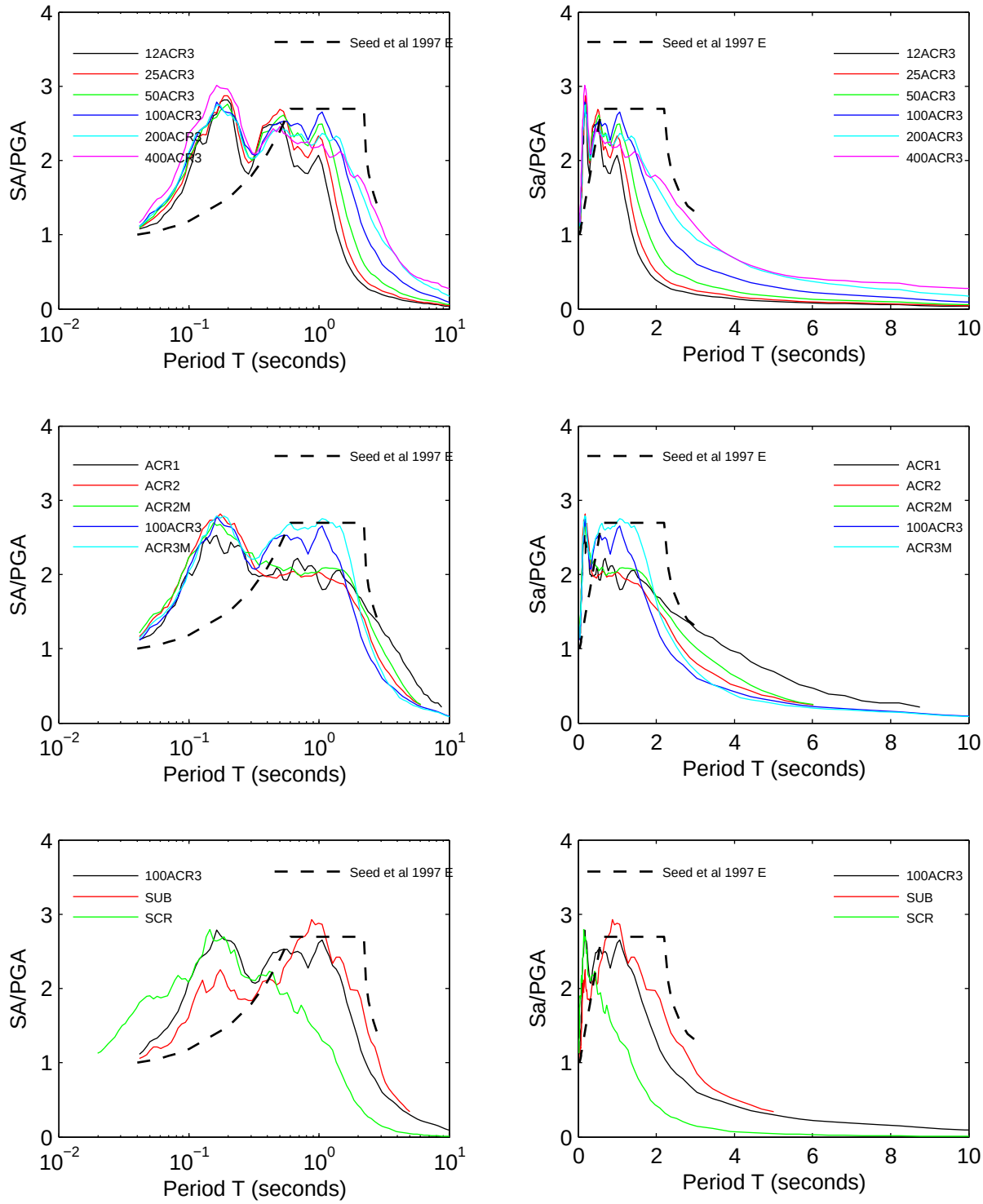

Figure 7A.55: Comparison of response spectra shape for site KIKNET S2 and effective stress analyses

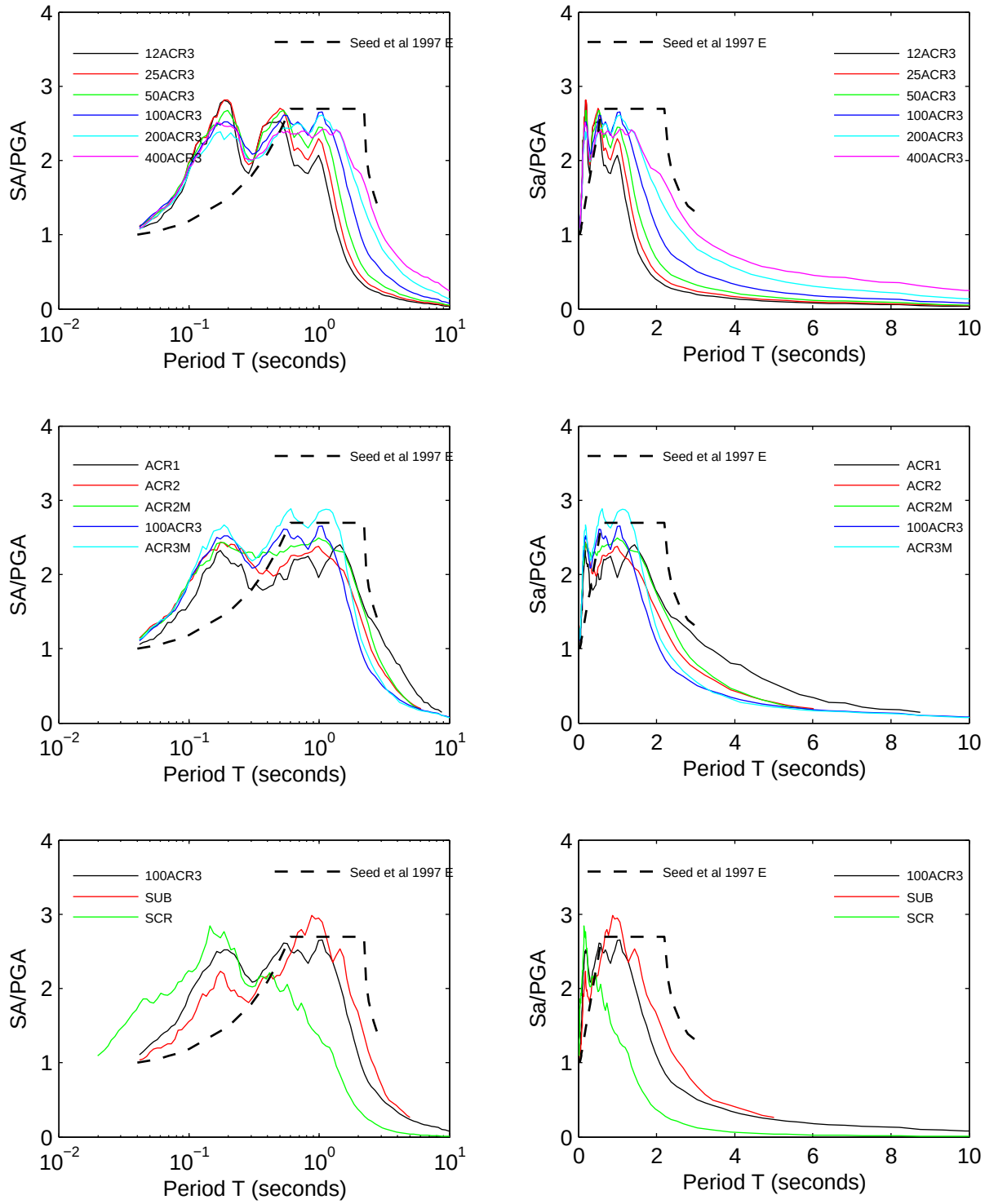

Figure 7A.56: Comparison of response spectra shape for site KIKNET S4 and effective stress analyses

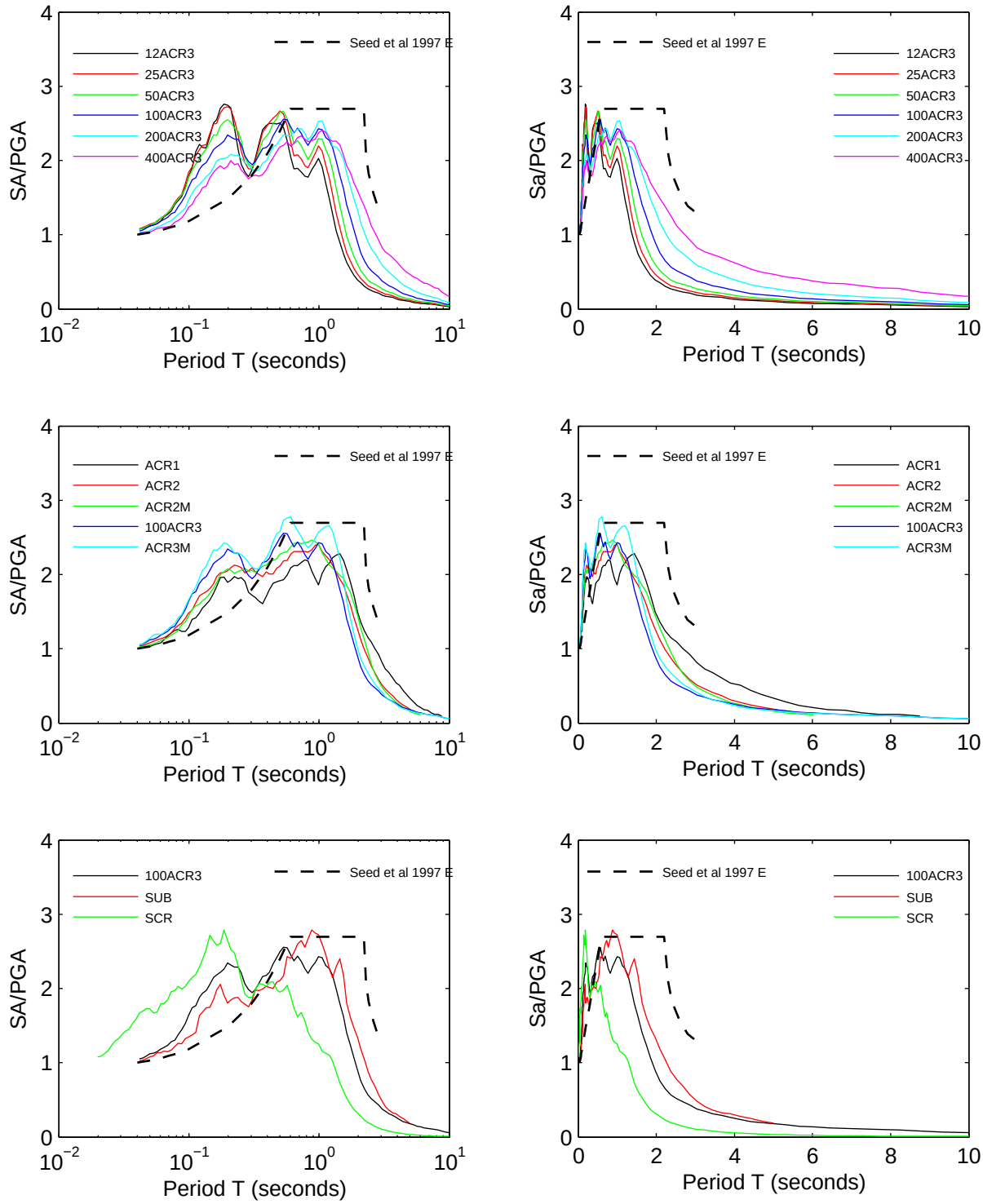

Figure 7A.57: Comparison of response spectra shape for site KIKNET40 and effective stress analyses

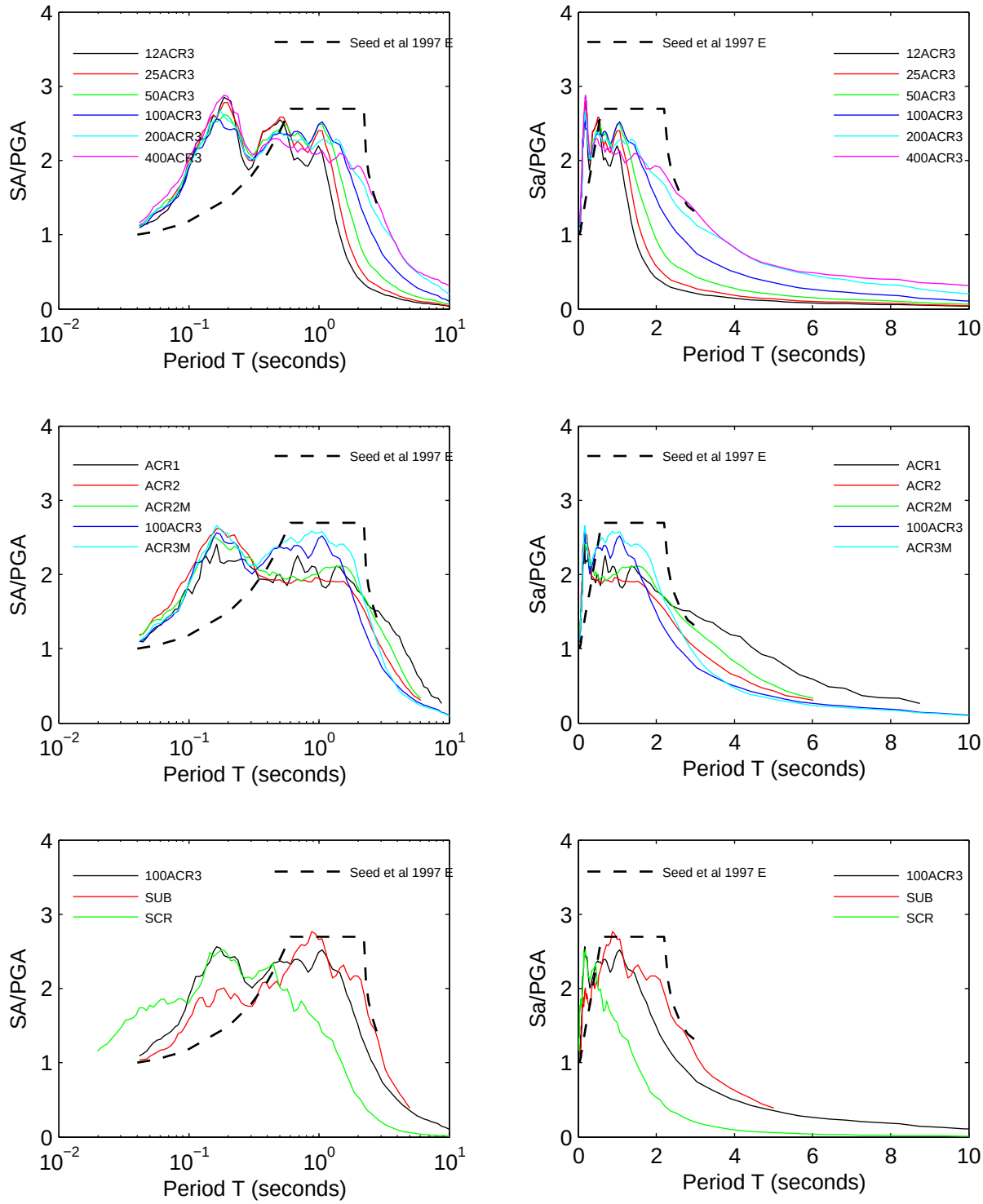

Figure 7A.58: Comparison of response spectra shape for site KIKNET160 and effective stress analyses

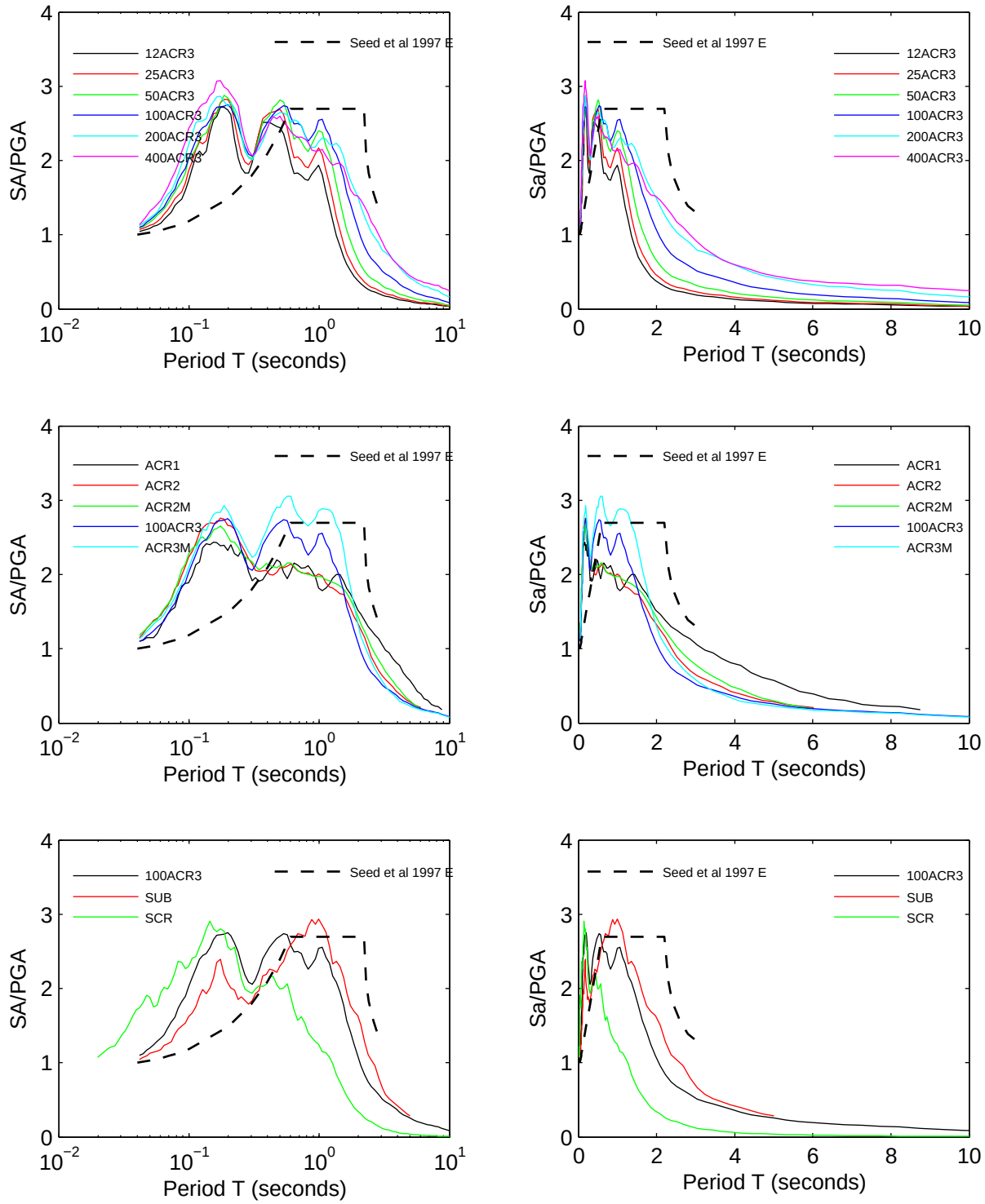

Figure 7A.59: Comparison of response spectra shape for site MRCE1 and effective stress analyses

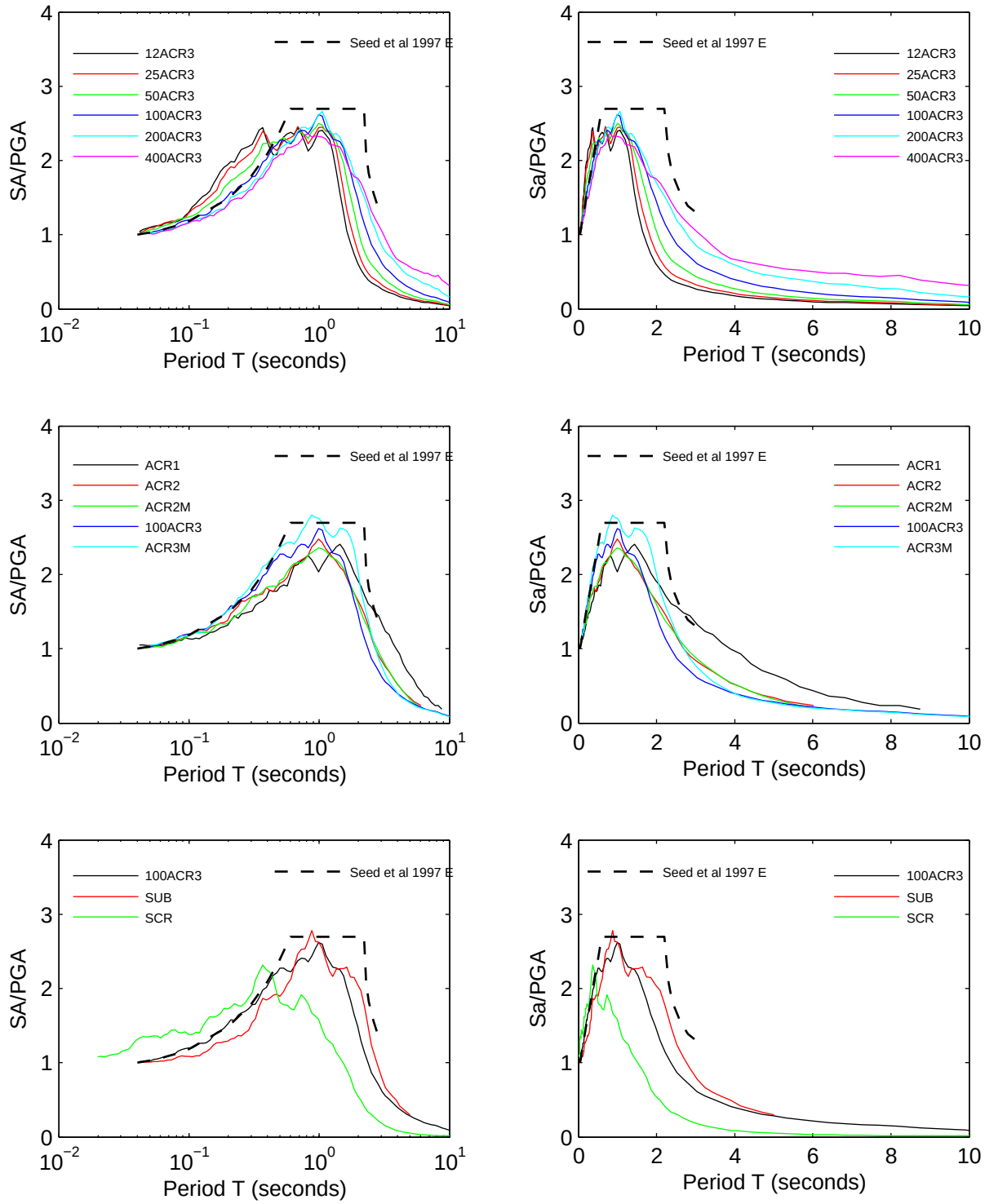

Figure 7A.60: Comparison of response spectra shape for site MRCE2 and effective stress analyses

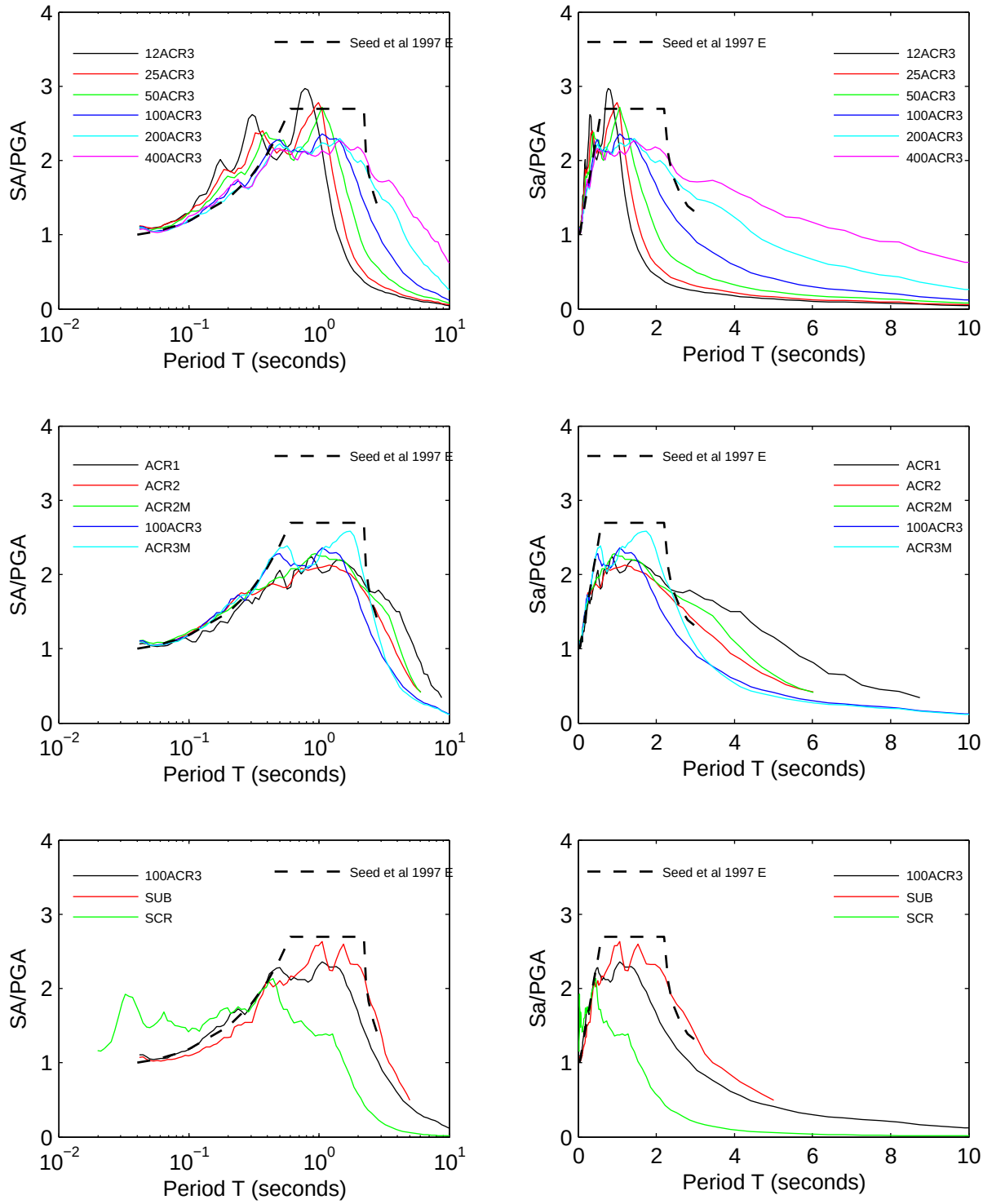

APPENDIX 7B: EFFECT OF SITE – COMPARING SITES FOR A GIVEN GROUND MOTION SCENARIO

Appendix 7B: Effect of Site - Comparing Sites for a Given Ground Motion Scenario

Appendix 7B contains figures comparing results of the effective stress site response analyses by strength, MRD curves, and elastic site period for response spectrum and amplification ratios. To examine the effect of strength the sites Bay Area II K, Bay Area II K S2, and Bay Area II K S4 are compared, and the sites KIKNET, KIKNET S2, and KIKNET S4 are compared. The results of these sites are shown because the only difference between them is their soil strengths. In other words, only the shear modulus reduction and damping curves at large strains are changed, all of the other parameters such as shear wave velocity, unit weight, soil types etc. remain the same.

The soil MRD curves are investigated by plotting site Bay Area II against Bay Area II K, and sites KIKNET40, KIKNET, and KIKNET160 together. The results of these sites are shown because the only difference between them is shear modulus reduction and damping curves at small and medium strains. All of the other parameters such as shear wave velocity, unit weight, soil strength etc. remain the same.

The effect of the elastic site periods (T_s) is investigated by comparing sites MRCE2, HAGP, KIKNET, Bay Area II K, MRCE1, JSSS, Bay Area, and Bay Area F. Unlike the sites shown to investigate the effects of soil strength and shear modulus reduction curves, these sites do not have all other parameters in common. Each site has a different soil shear strength, different shear wave velocity profiles etc., in addition to having different elastic site periods.

Figures 7B.13 through 7B.36 look at the effect of soil strength, MRD curves, and elastic site period on the spectral shape (Sa(T) / PGA) and soil properties with depth. Each figure contains six plots. The top left plot is the spectral shape in semi-logarithmic space, and the top right plot shows the spectral shape in arithmetic space. The bottom four plots on each page show, from left to right, the maximum shear strain, shear stress ratio, pore pressure ratio, and PGA with depth, where the shear stress ratio and pore pressure ratio are the shear stress and pore pressure divided by the vertical effective stress. The dotted horizontal lines in the bottom four plots define the boundary between different soil types. The USCS soil designation for each layer is given in the plot with shear strain. This makes it easier to visualize the soil column while interpreting the results.

Figure 7B.1: Comparison of the effect of site strength on the response spectra for scenarios 1−6

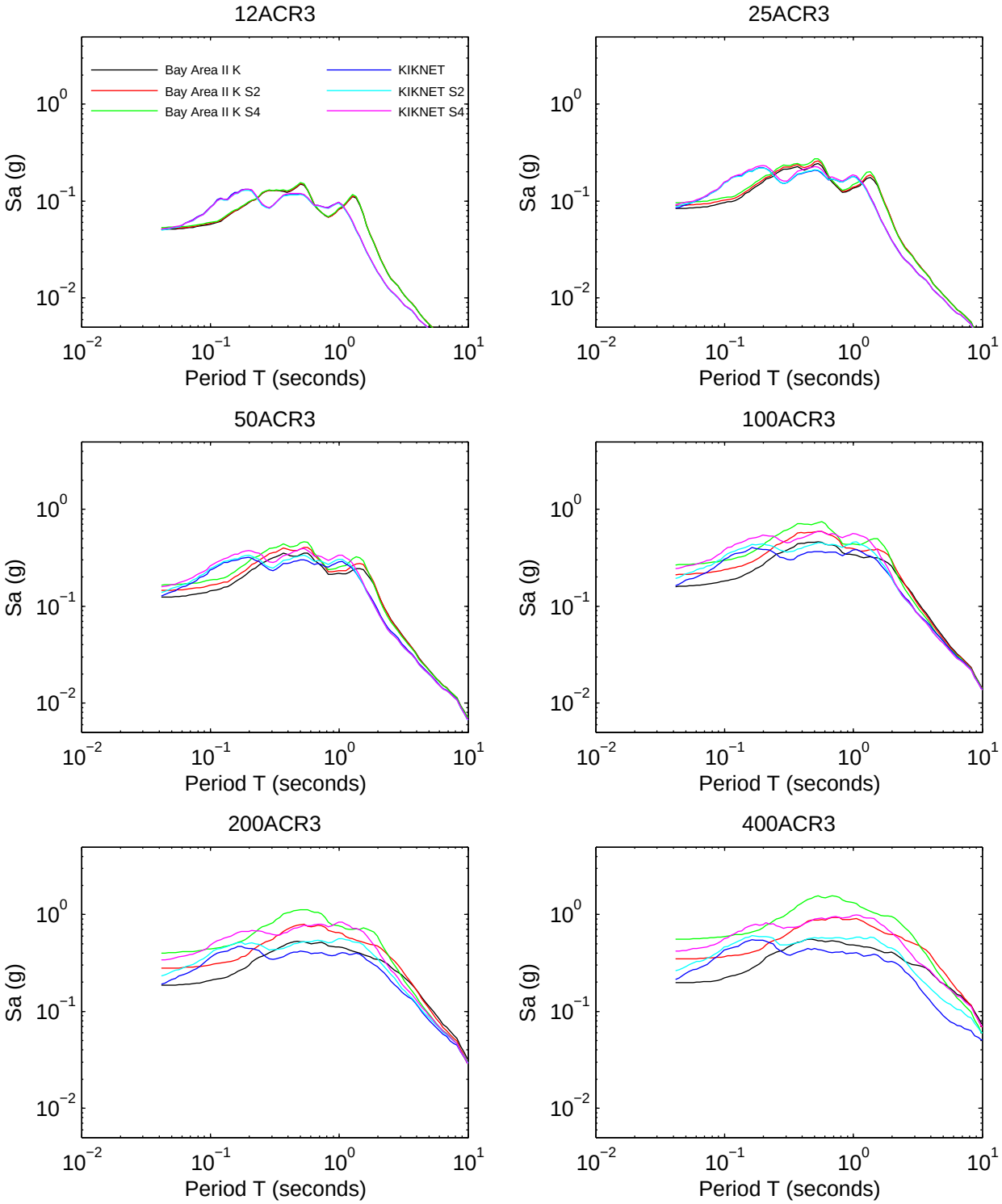

Figure 7B.2: Comparison of the effect of site strength on the response spectra for scenarios 7−12

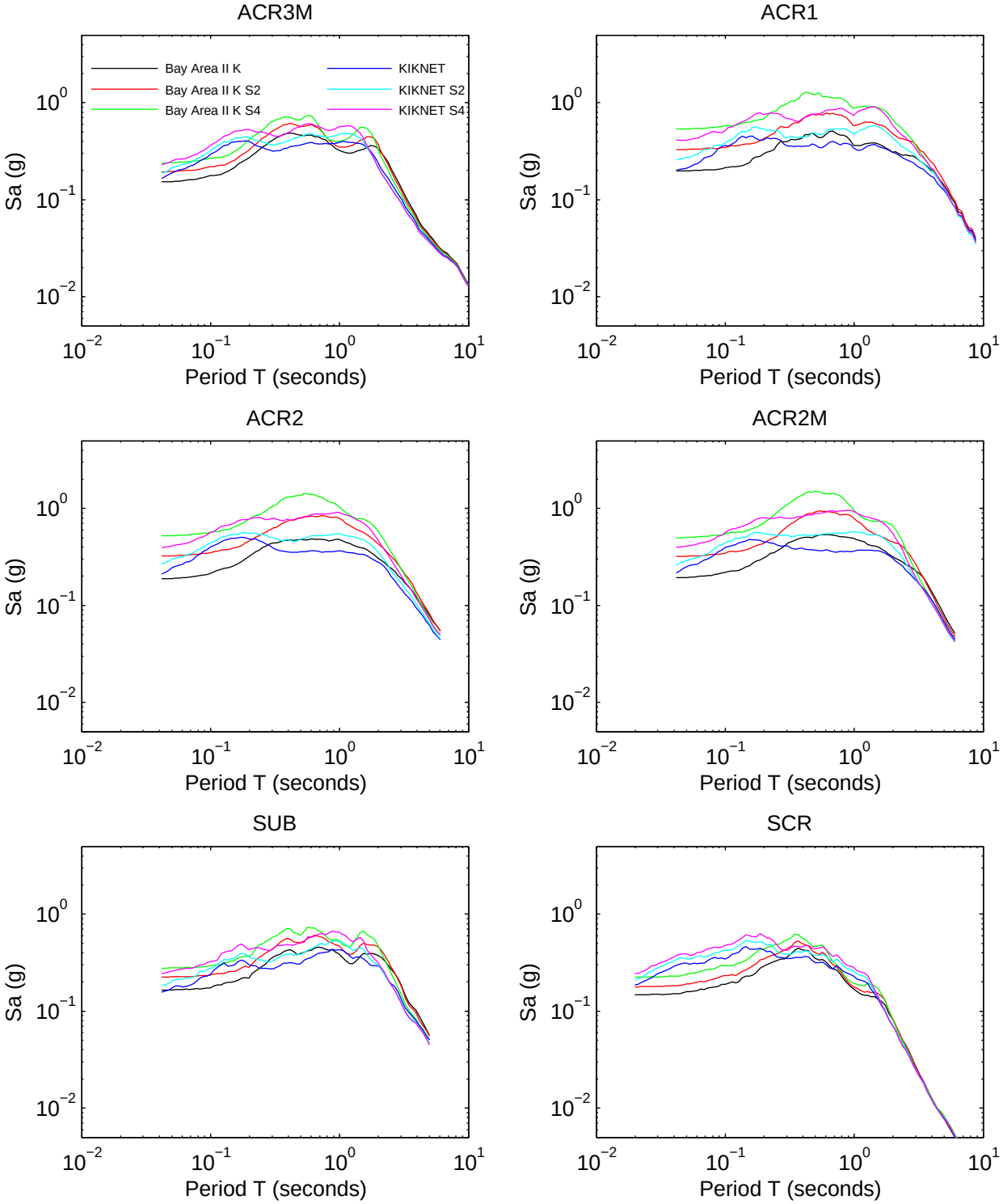

Figure 7B.3: Comparison of the effect of site strength on the amplification for scenarios 1−6

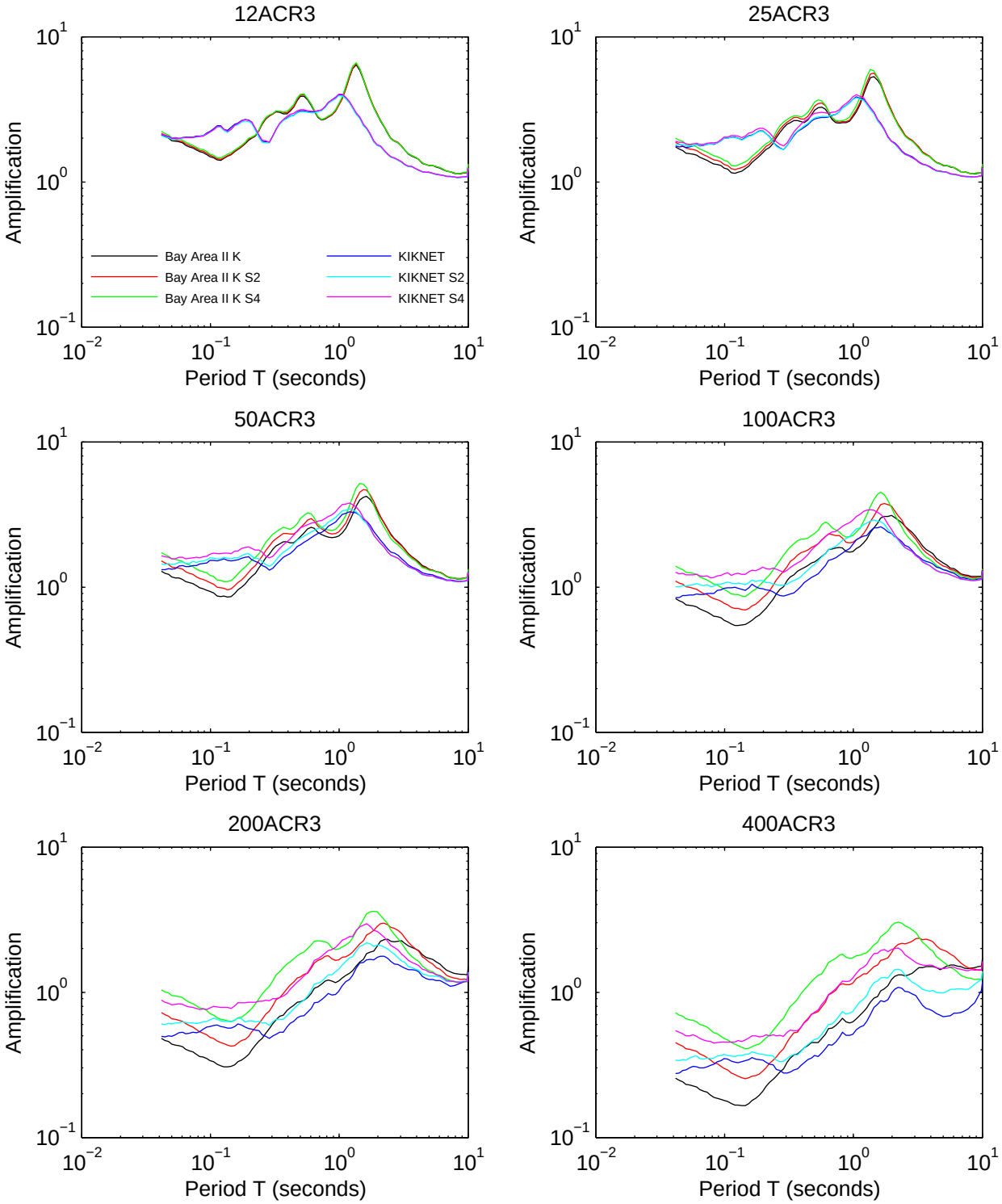

Figure 7B.4: Comparison of the effect of site strength on the amplification for scenarios 7−12

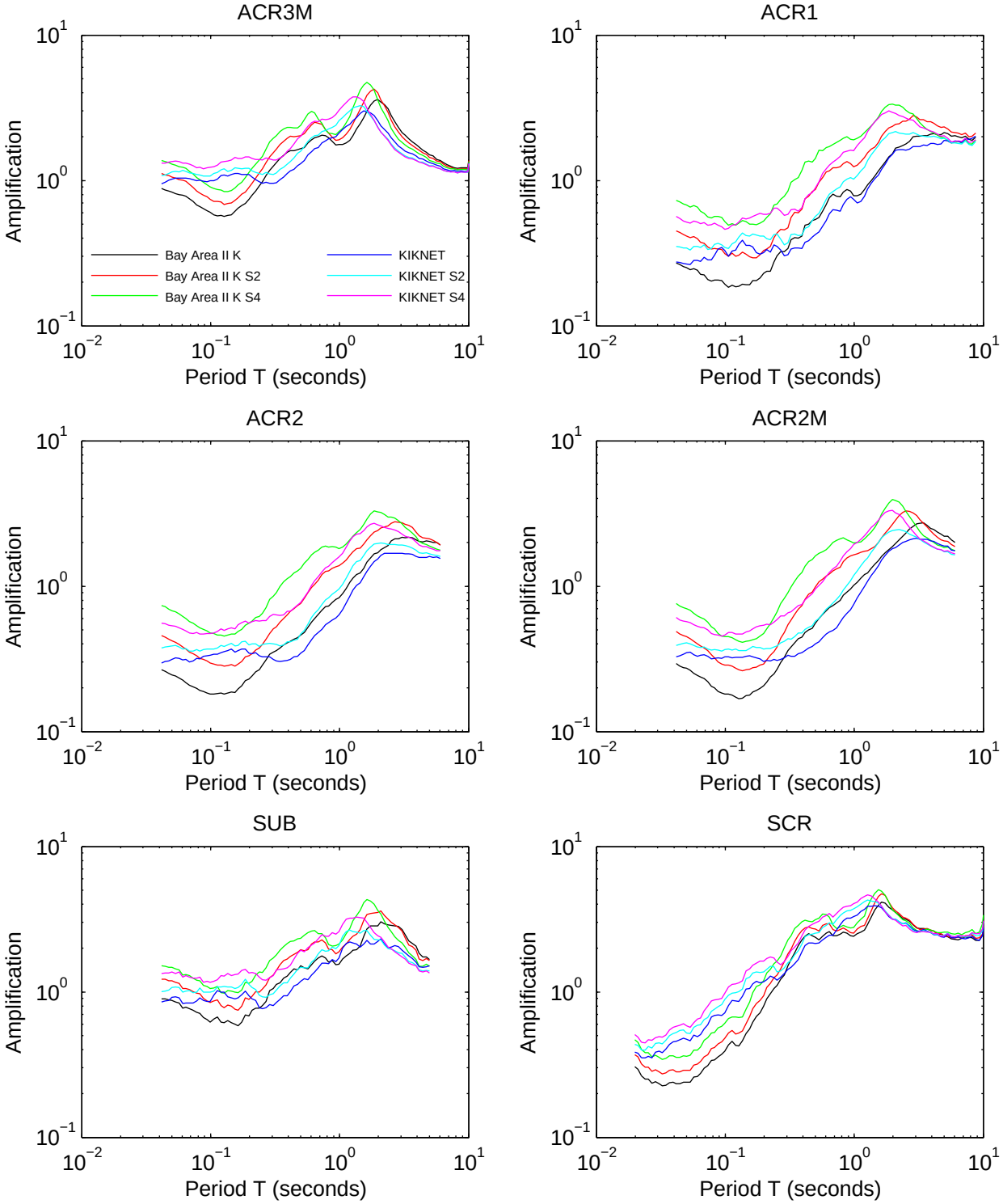

Figure 7B.5: Comparison of the effect of site stiffness on the response spectra for scenarios 1−6

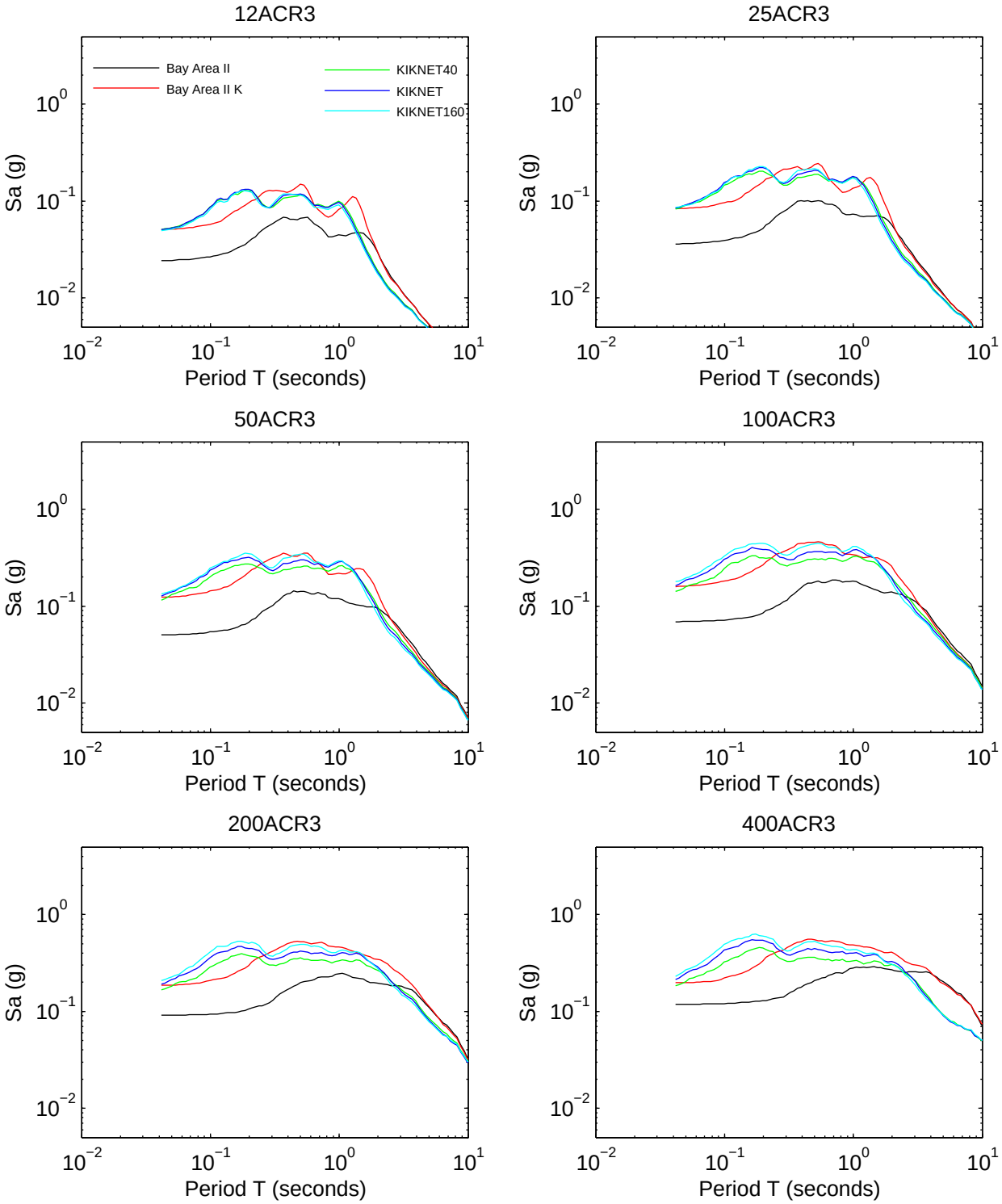

Figure 7B.6: Comparison of the effect of site stiffness on the response spectra for scenarios 7−12

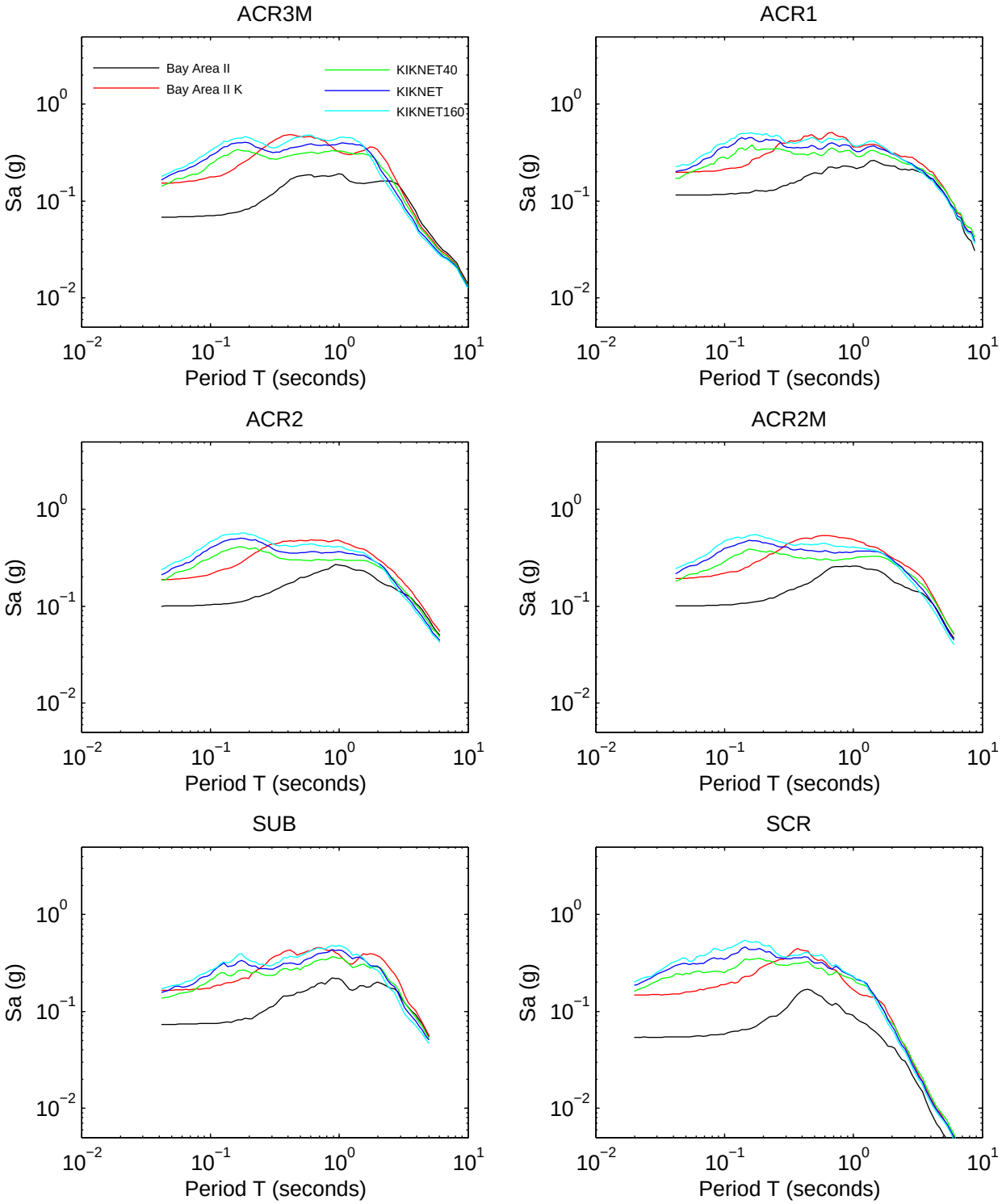

Figure 7B.7: Comparison of the effect of site stiffness on the amplification for scenarios 1−6

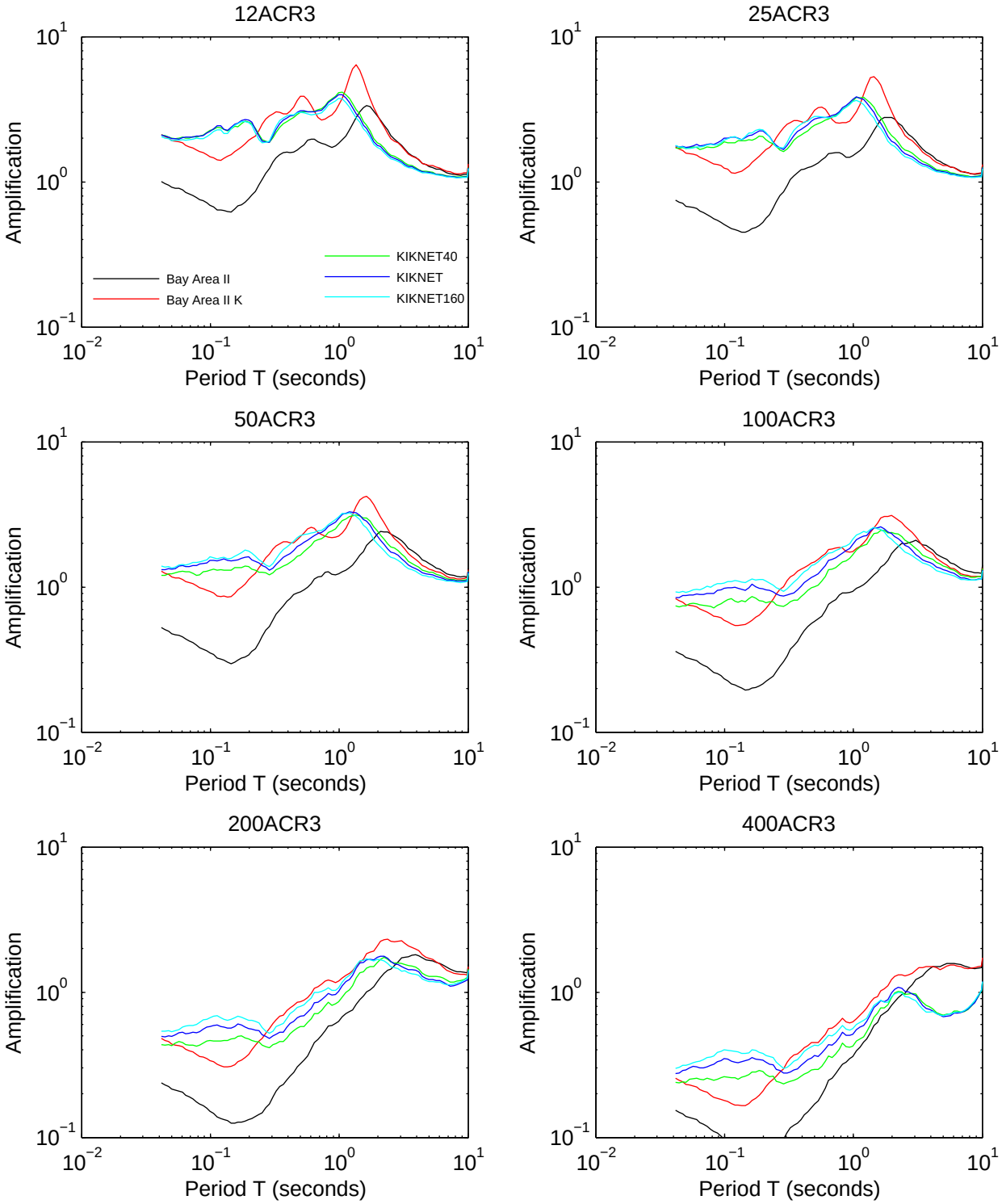

Figure 7B.8: Comparison of the effect of site stiffness on the amplification for scenarios 7−12

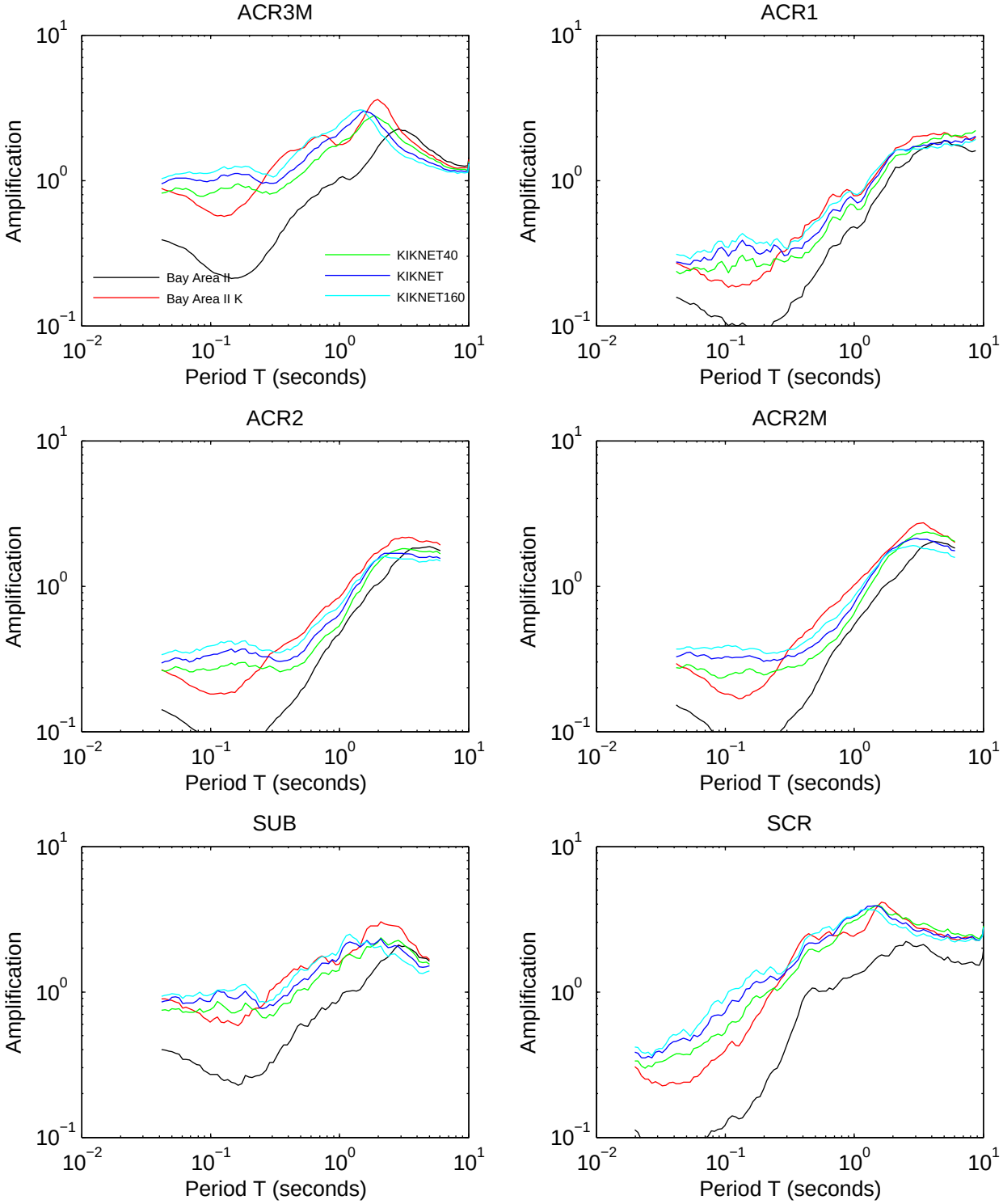

Figure 7B.9: Comparison of the effect of site elastic site period on the response spectra for scenarios 1−6

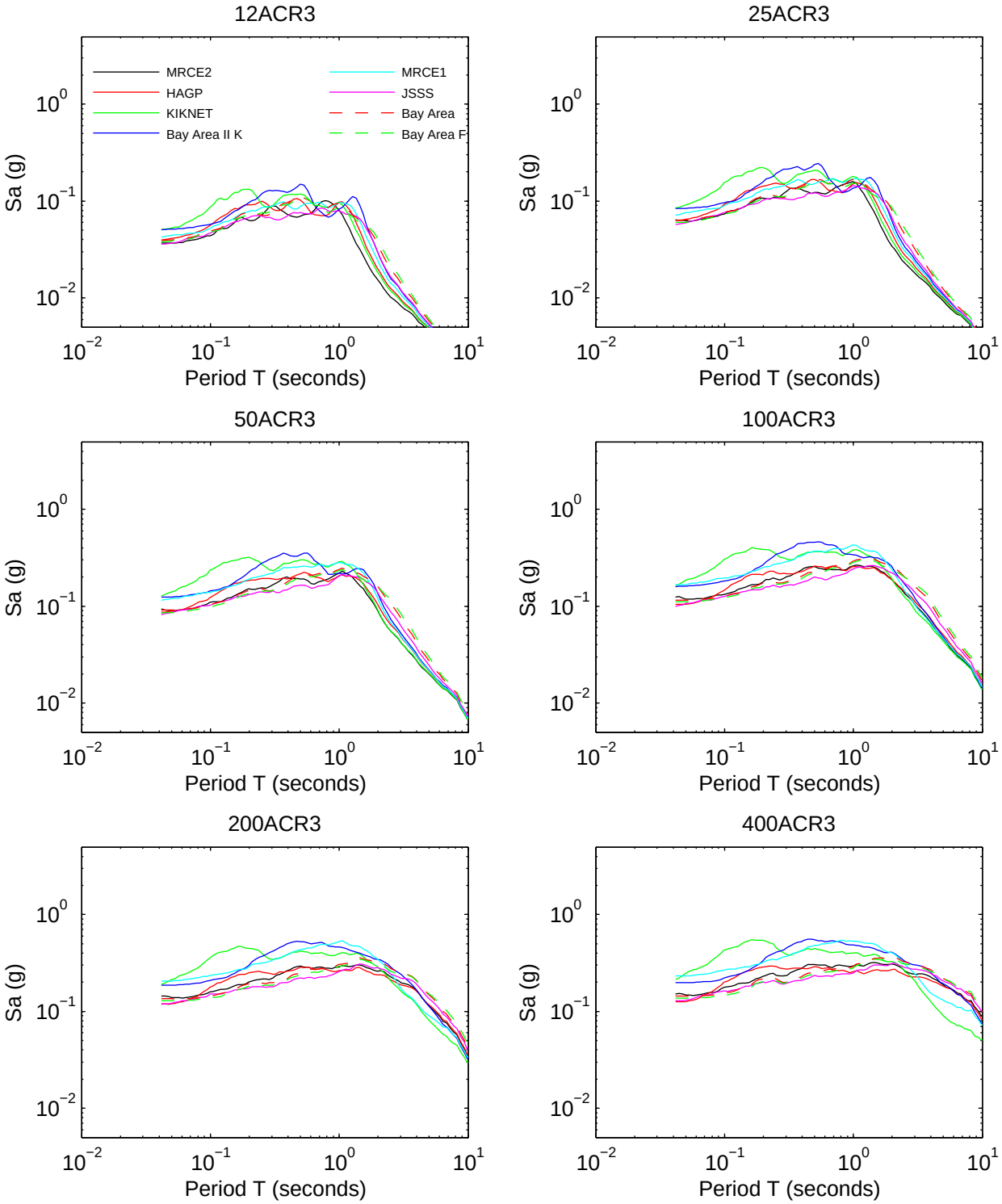

Figure 7B.10: Comparison of the effect of site elastic site period on the response spectra for scenarios 7−12

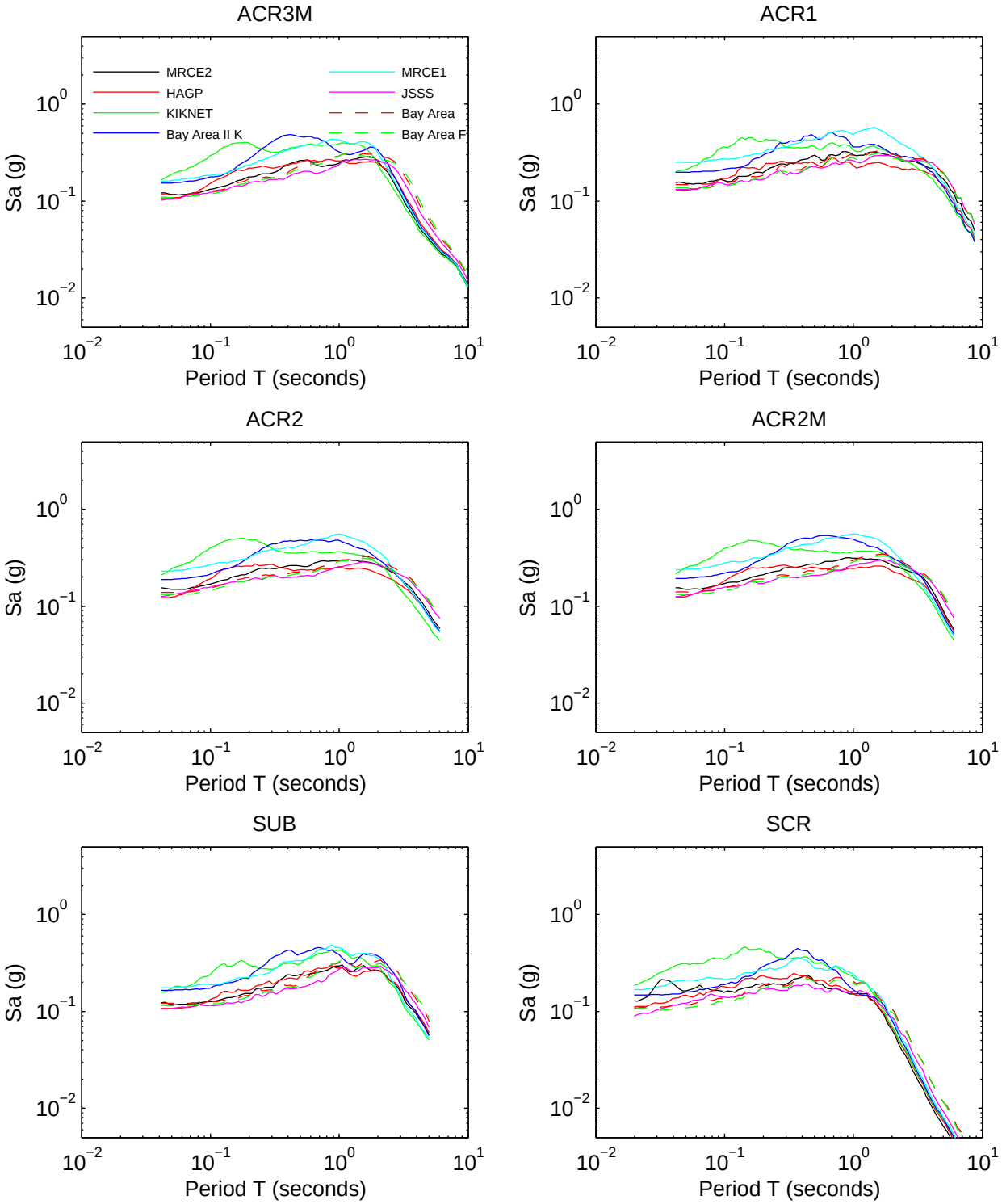

Figure 7B.11: Comparison of the effect of site elastic site period on the amplification for scenarios 1−6

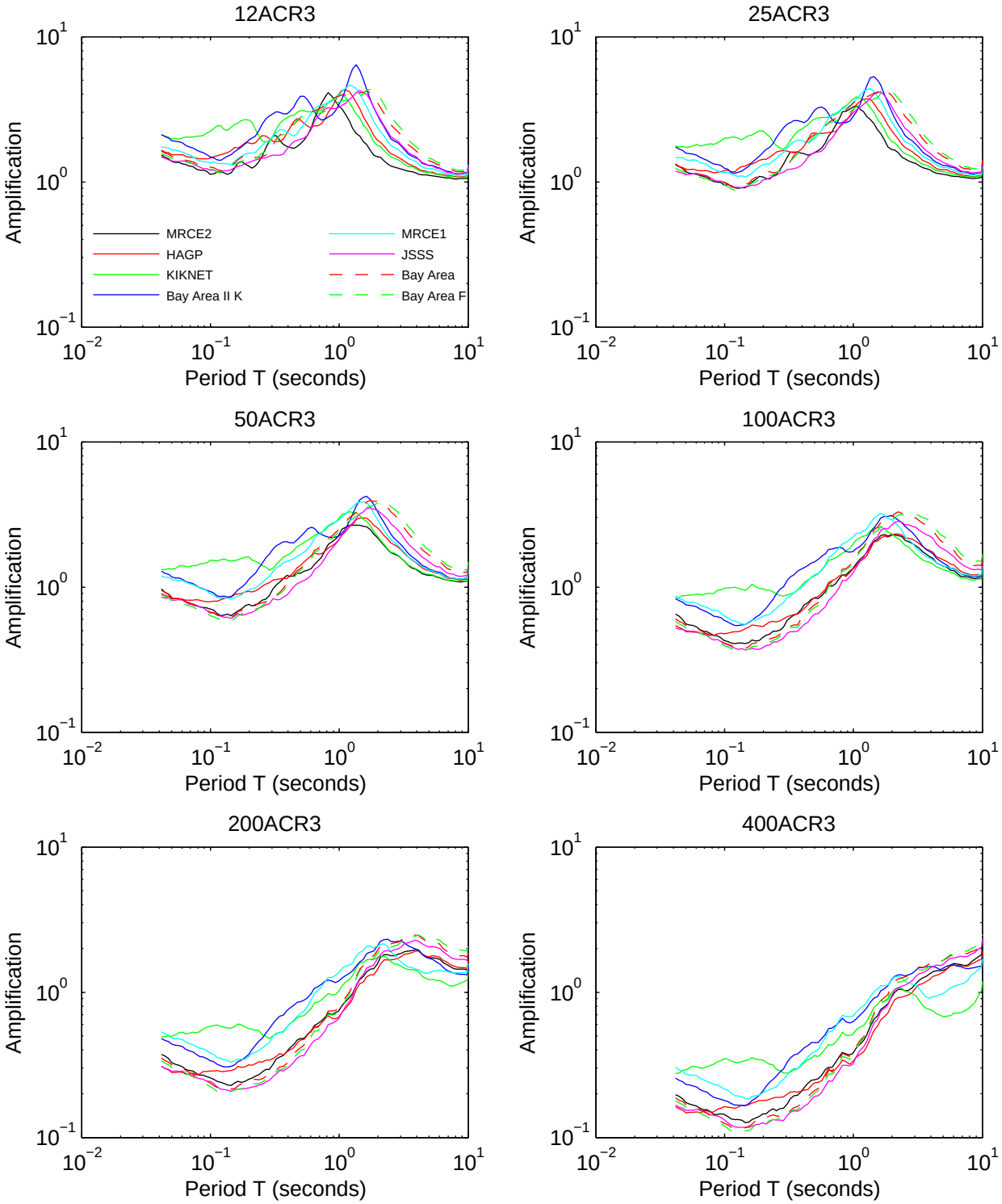

Figure 7B.12: Comparison of the effect of site elastic site period on the amplification for scenarios 7−12

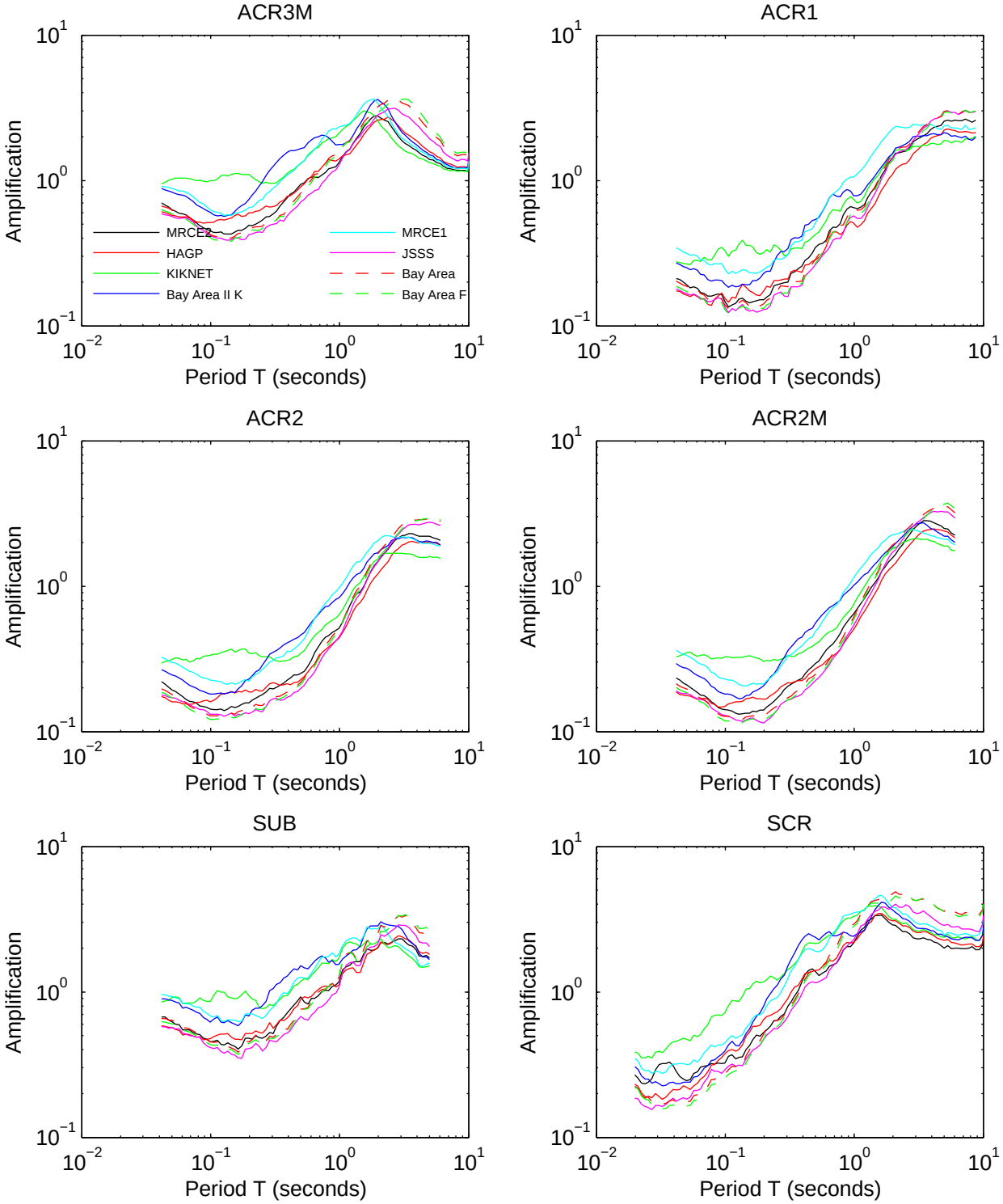

Figure 7B.13: Compare soil strength and MRD curves for KIKNET sites for scenario 12ACR3

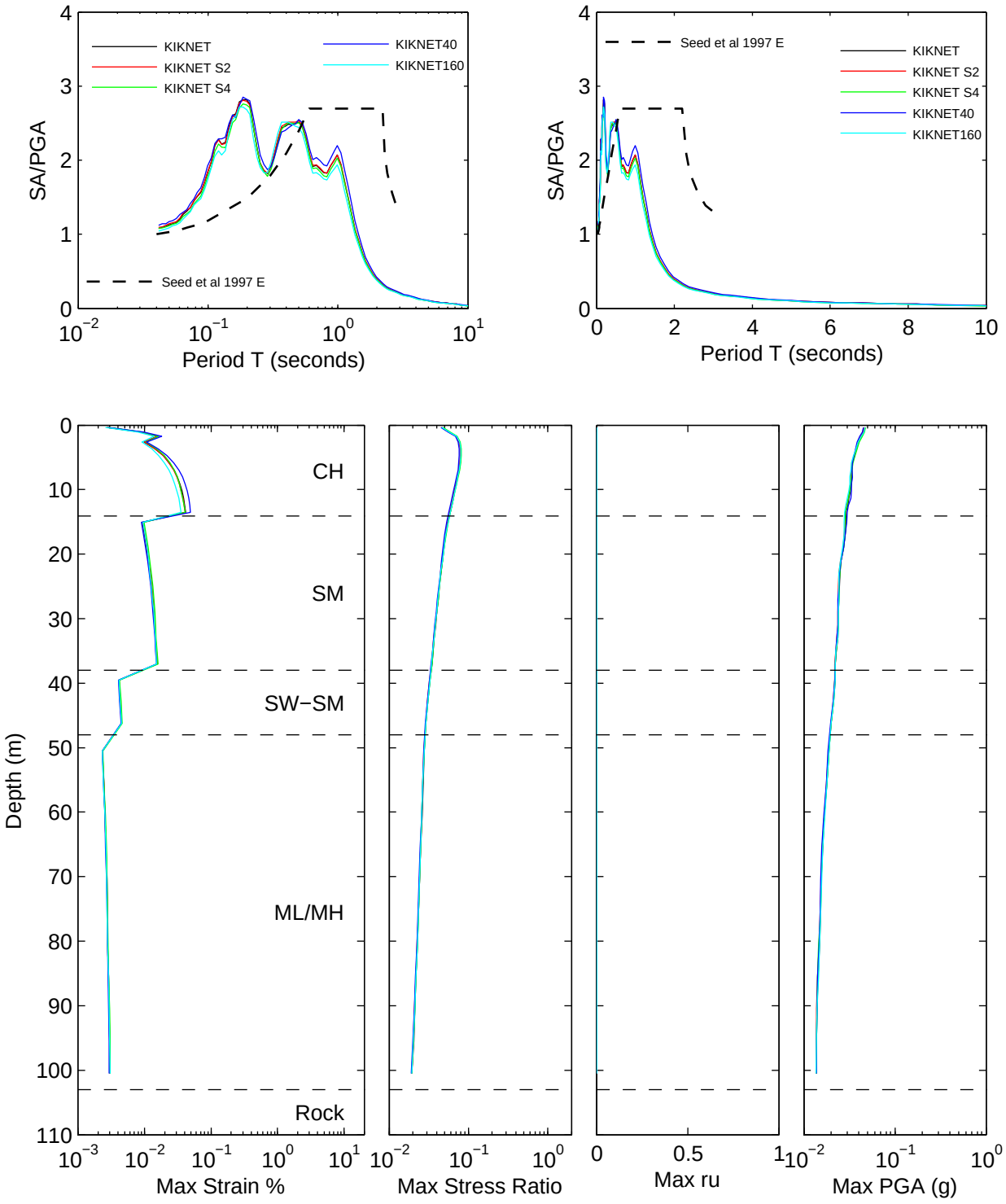

Figure 7B.14: Compare soil strength and MRD curves for KIKNET sites for scenario 25ACR3

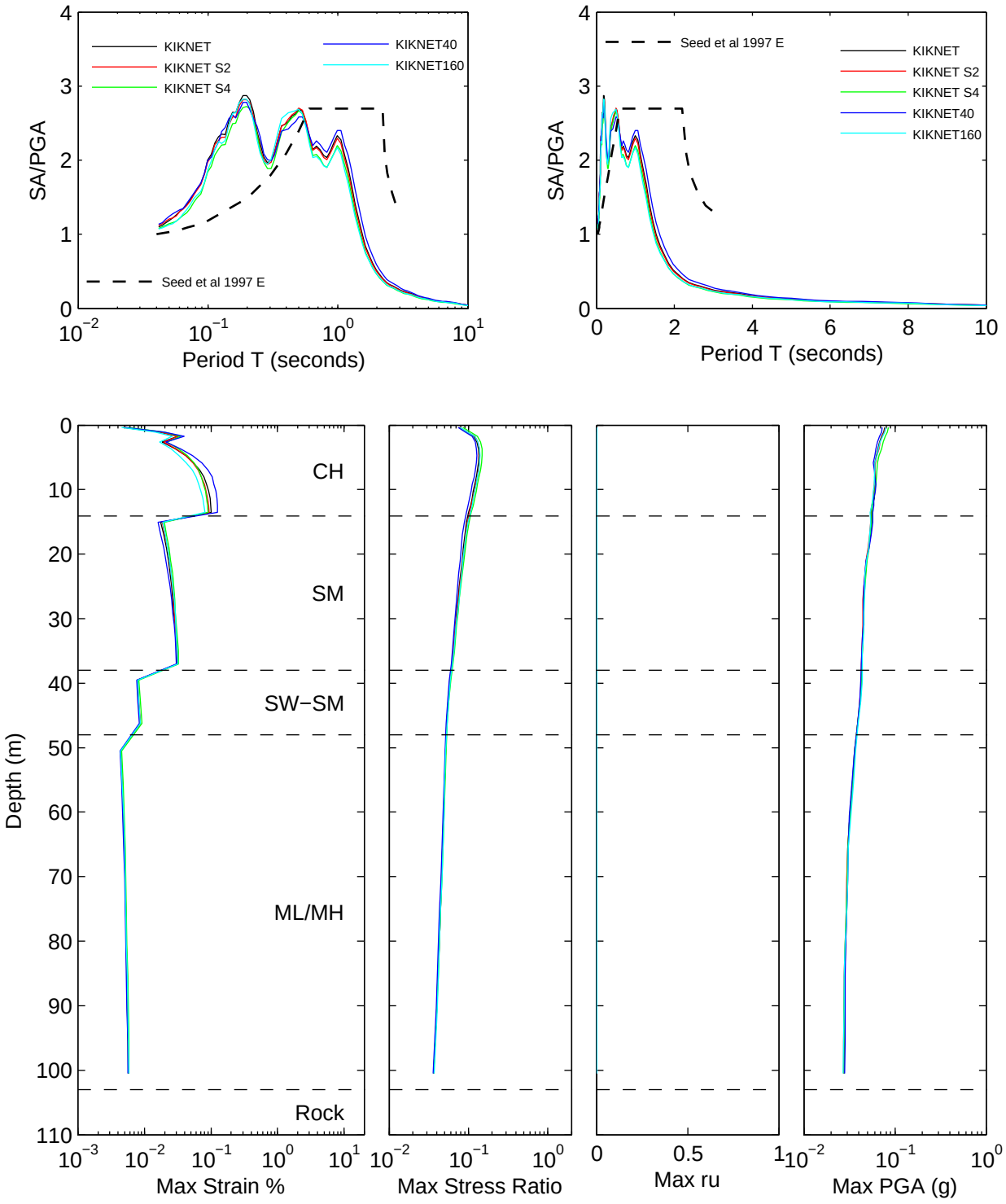

Figure 7B.15: Compare soil strength and MRD curves for KIKNET sites for scenario 50ACR3

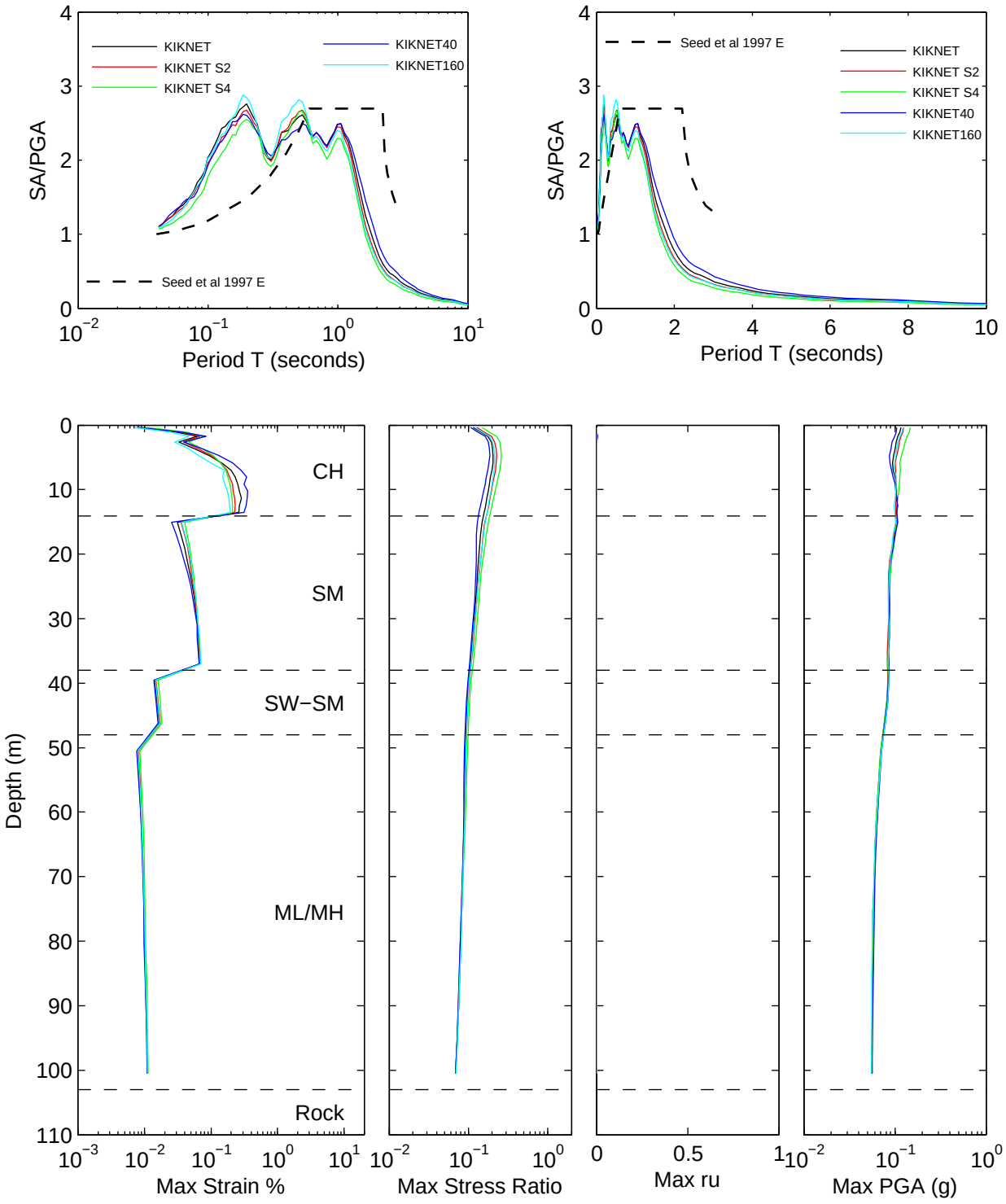

Figure 7B.16: Compare soil strength and MRD curves for KIKNET sites for scenario 100ACR3

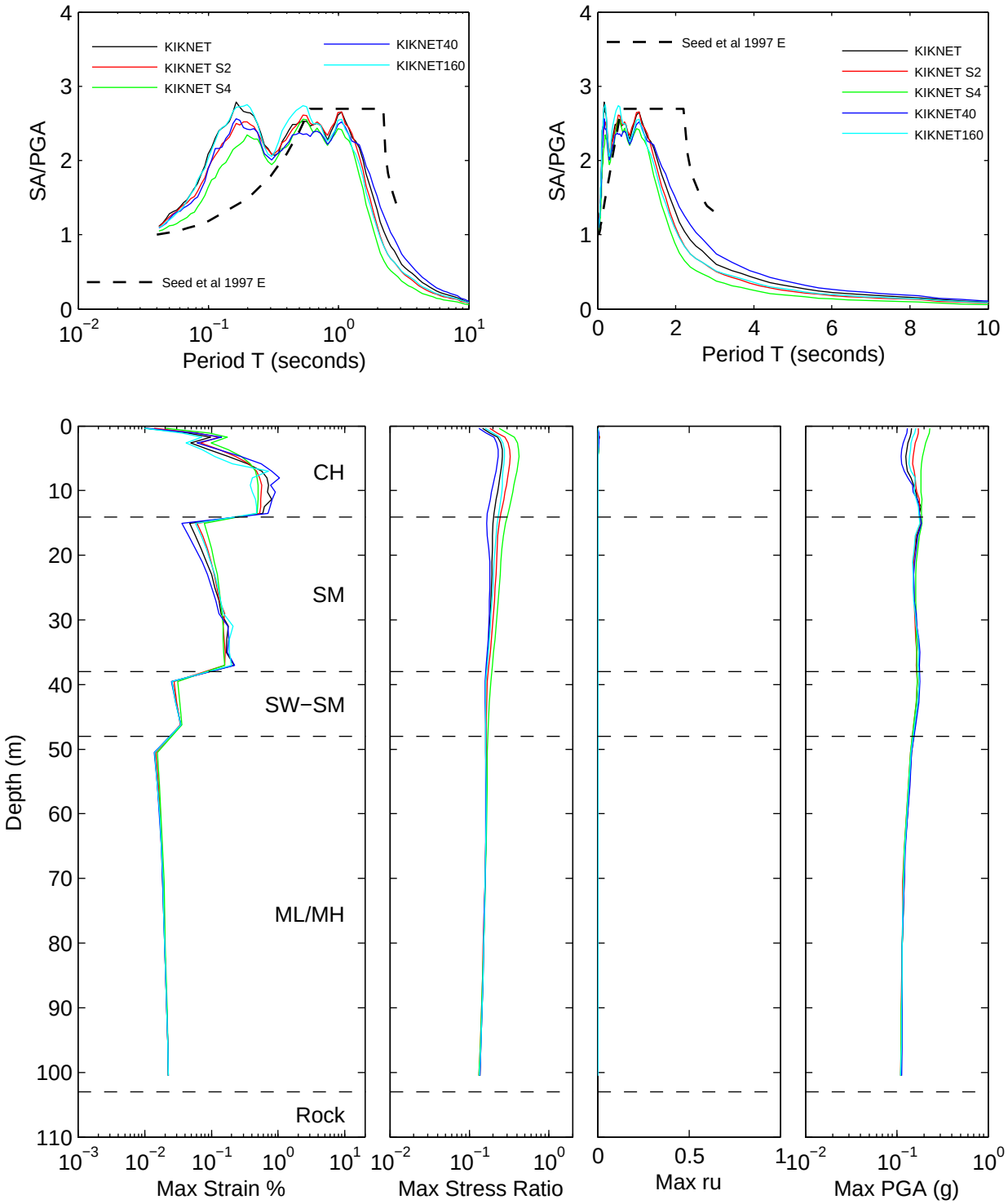

Figure 7B.17: Compare soil strength and MRD curves for KIKNET sites for scenario 200ACR3

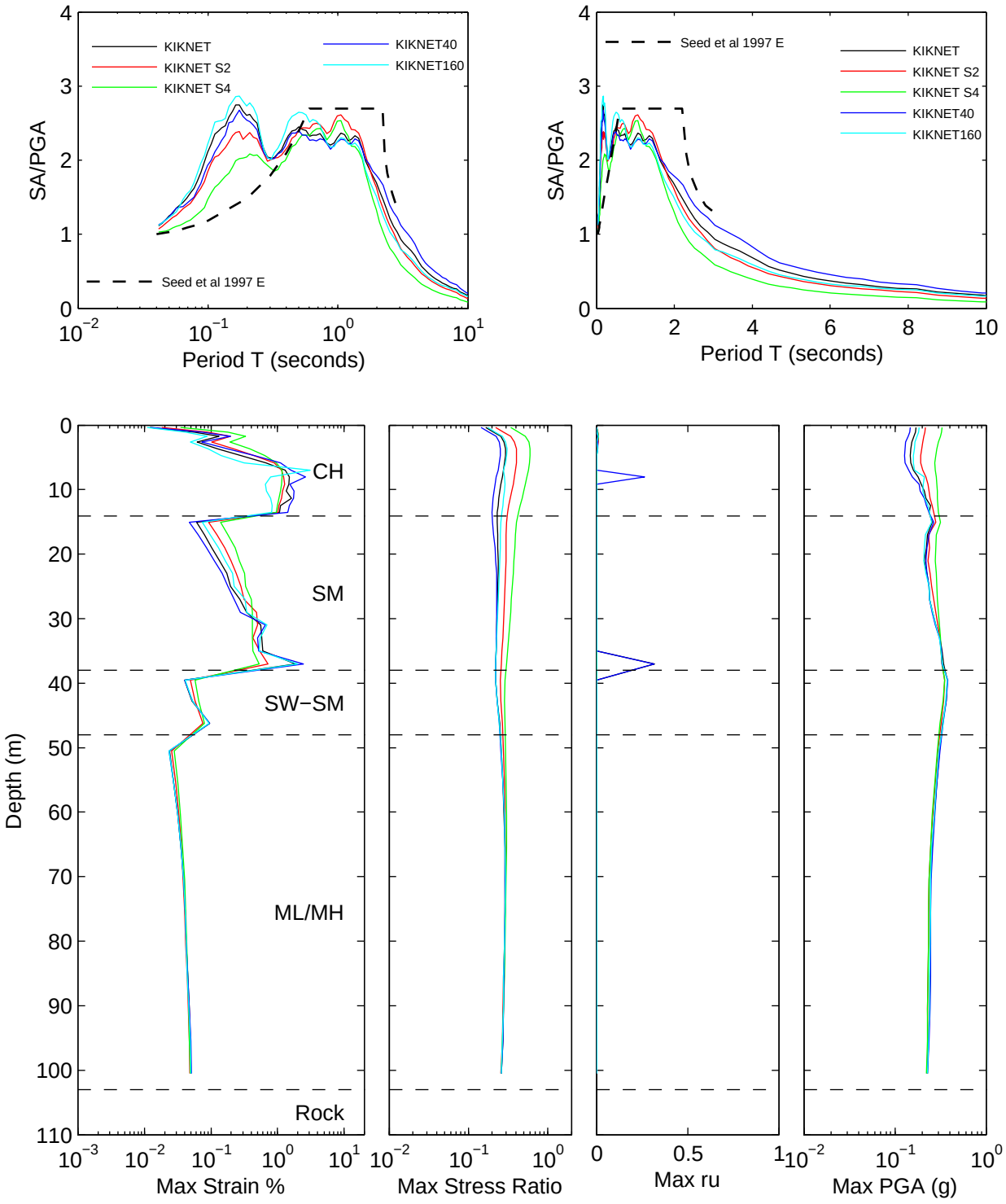

Figure 7B.18: Compare soil strength and MRD curves for KIKNET sites for scenario 400ACR3

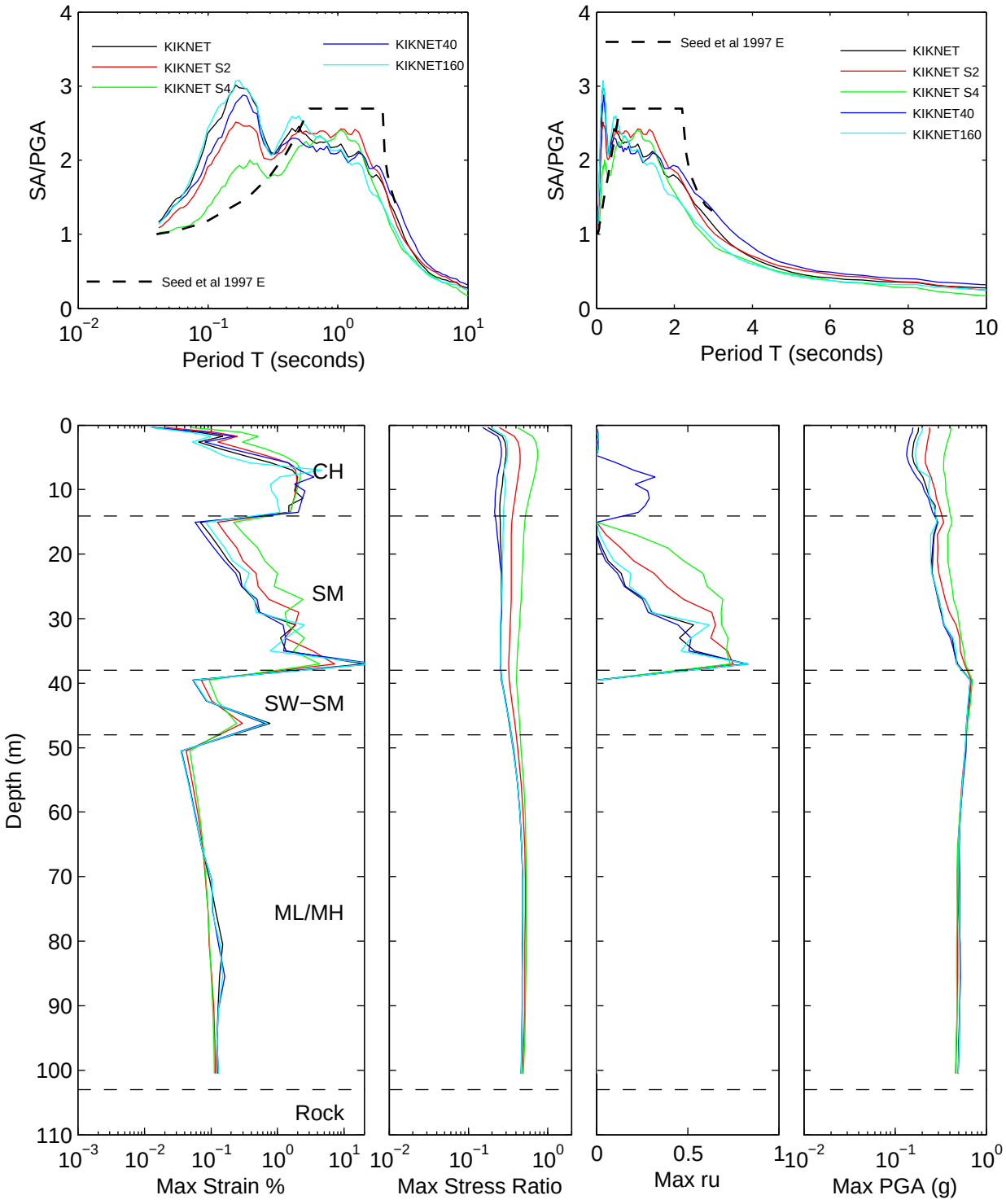

Figure 7B.19: Compare soil strength and MRD curves for KIKNET sites for scenario ACR3M

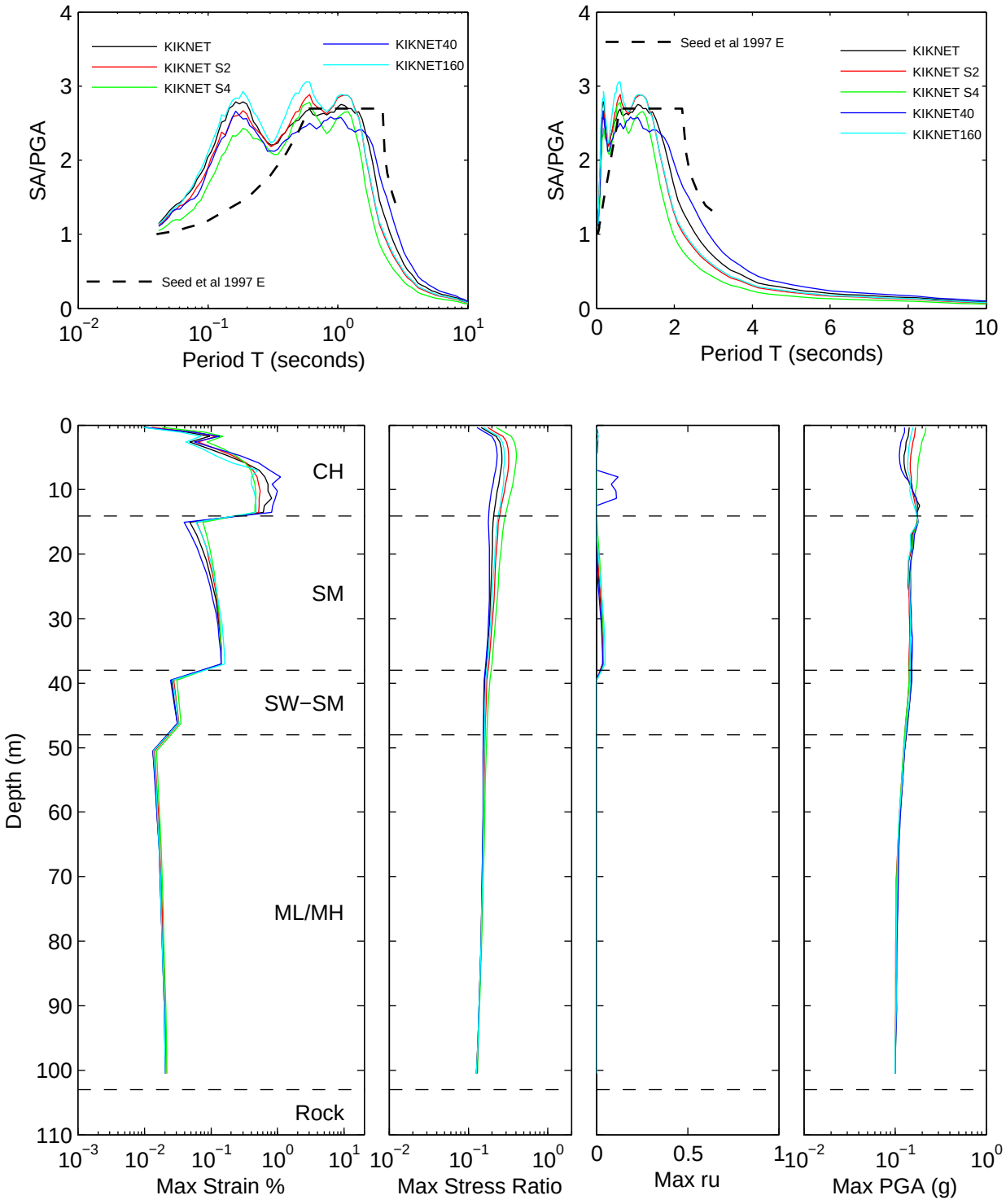

Figure 7B.20: Compare soil strength and MRD curves for KIKNET sites for scenario ACR1

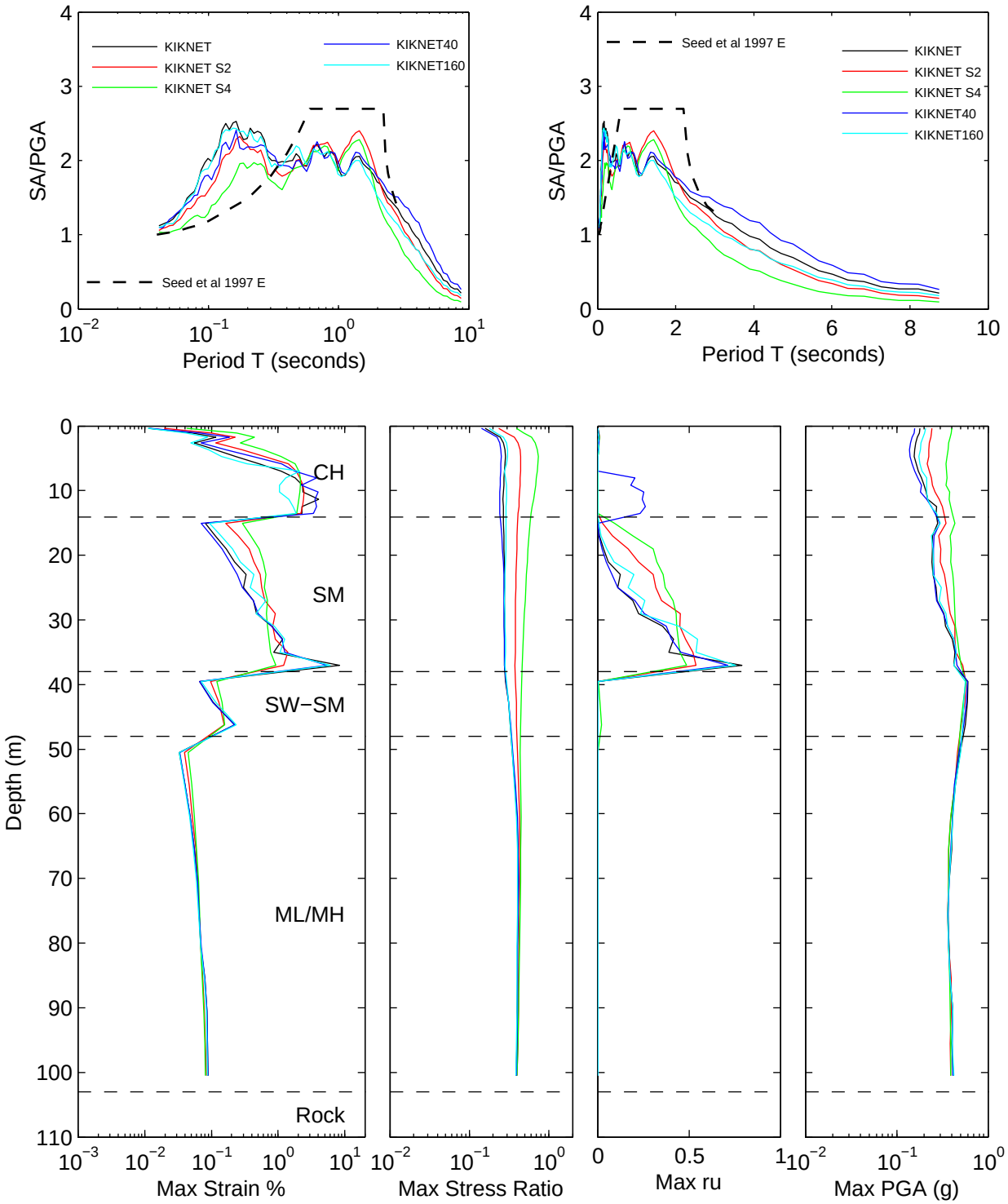

Figure 7B.21: Compare soil strength and MRD curves for KIKNET sites for scenario ACR2

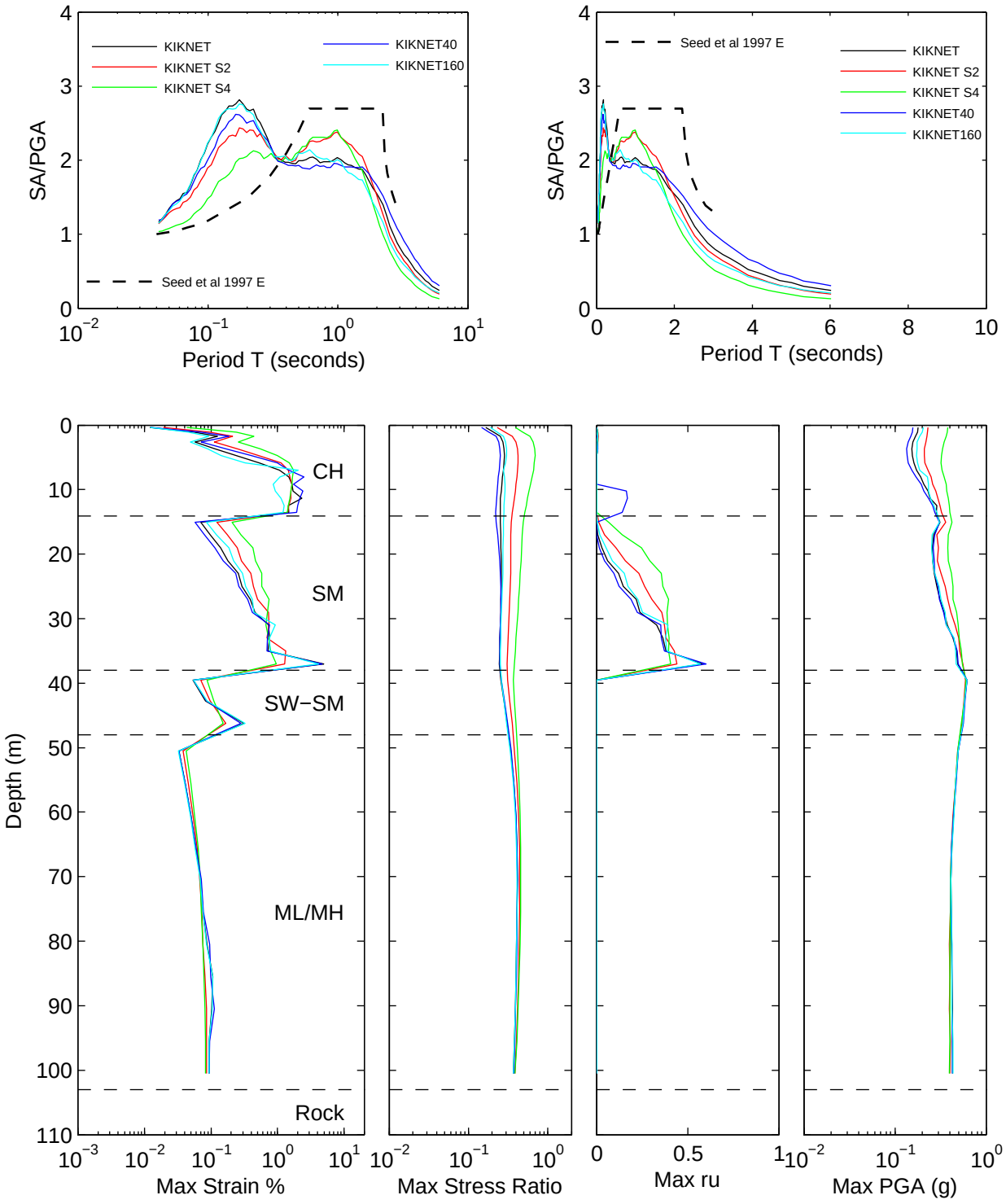

Figure 7B.22: Compare soil strength and MRD curves for KIKNET sites for scenario ACR2M

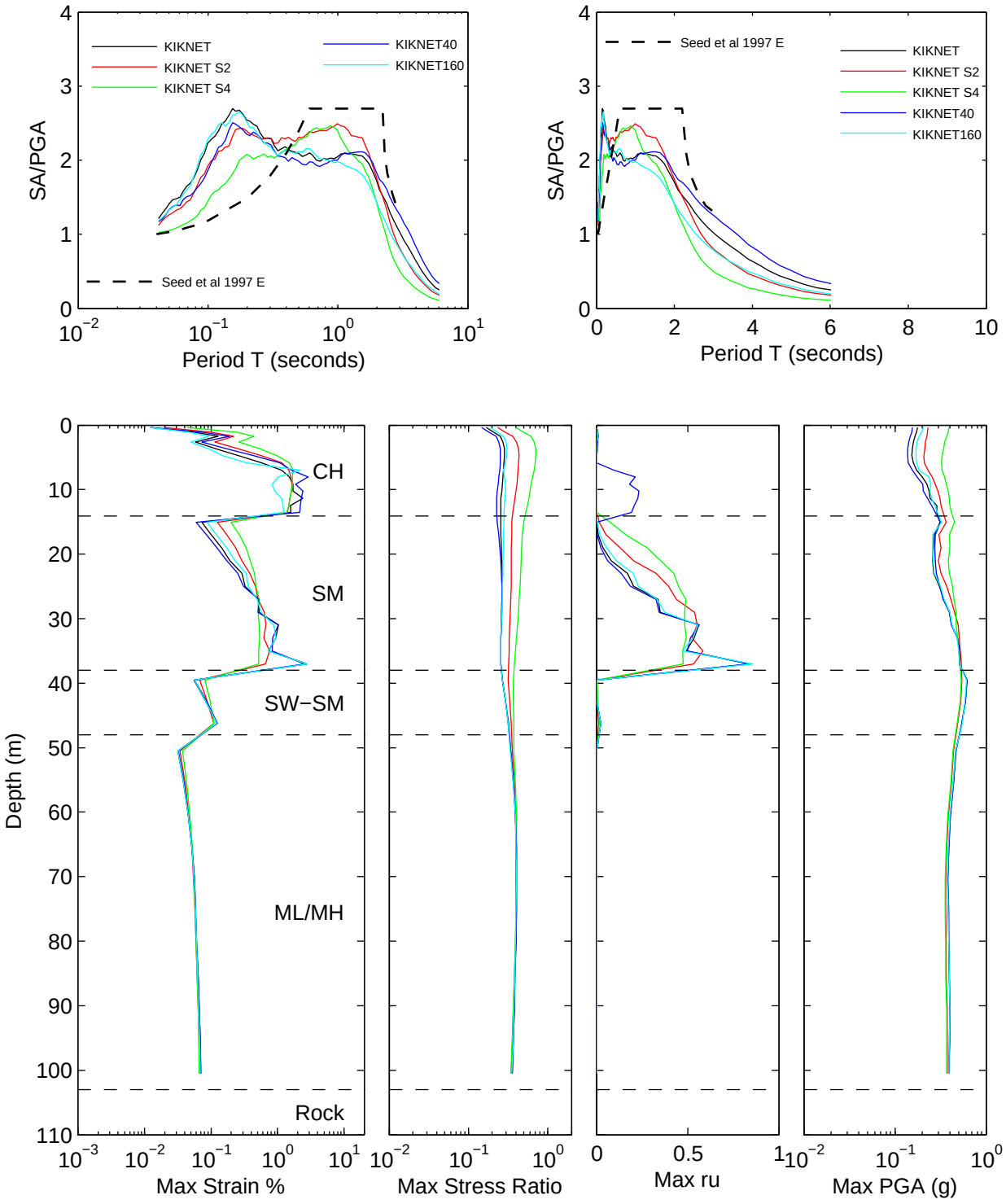

Figure 7B.23: Compare soil strength and MRD curves for KIKNET sites for scenario SUB

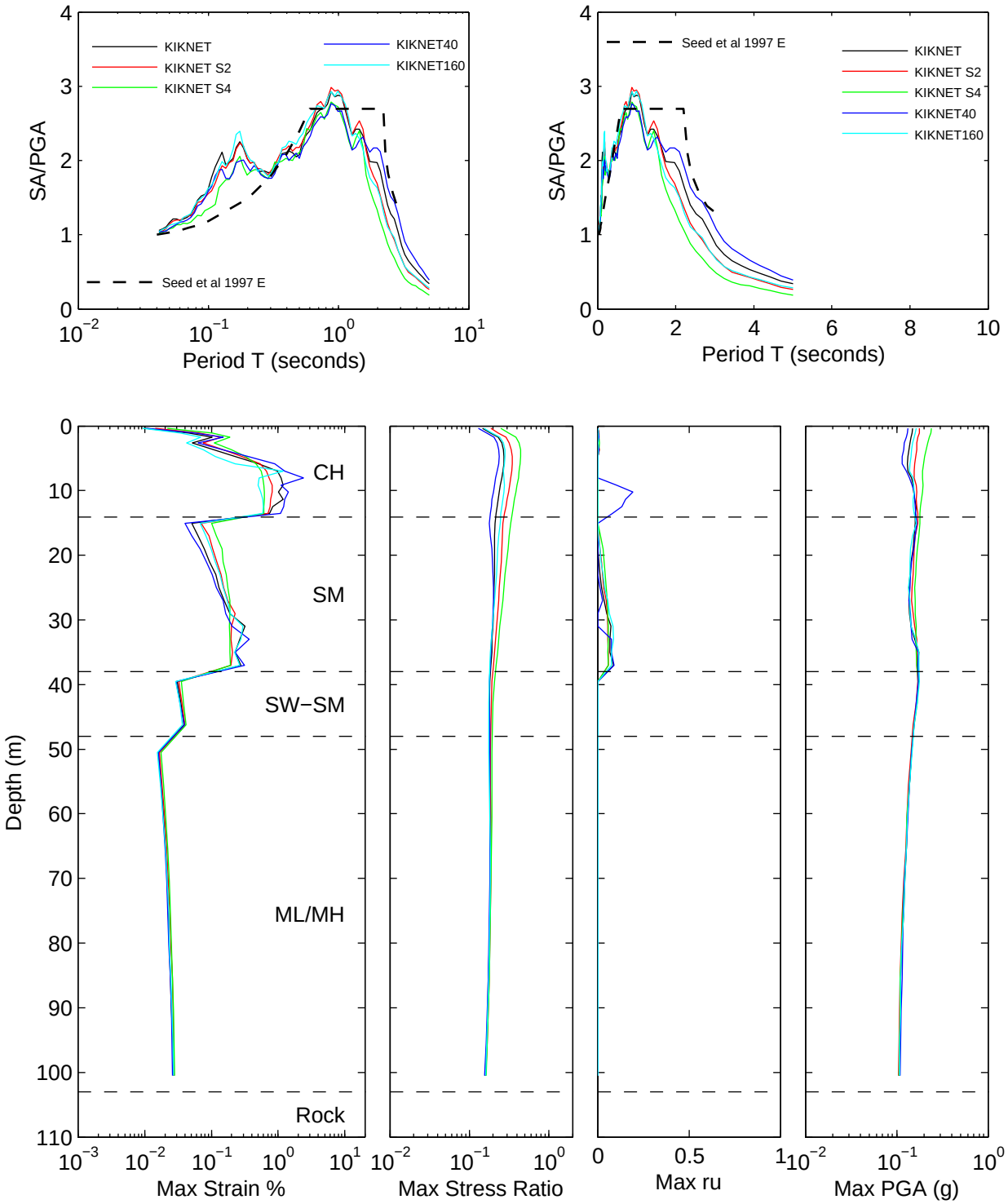

Figure 7B.24: Compare soil strength and MRD curves for KIKNET sites for scenario SCR

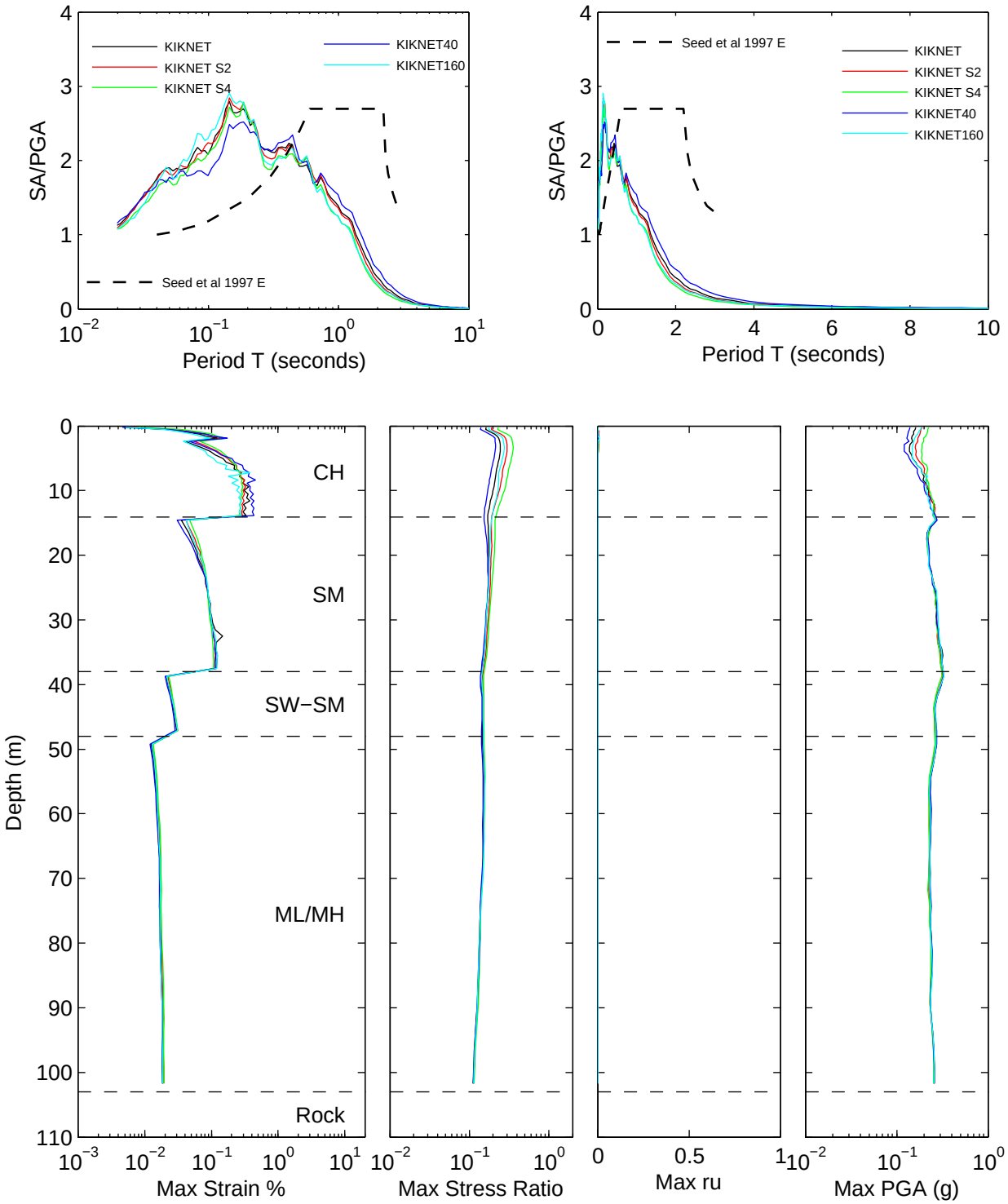

Figure 7B.25: Compare soil strength and MRD curves for Bay Area II sites for scenario 12ACR3

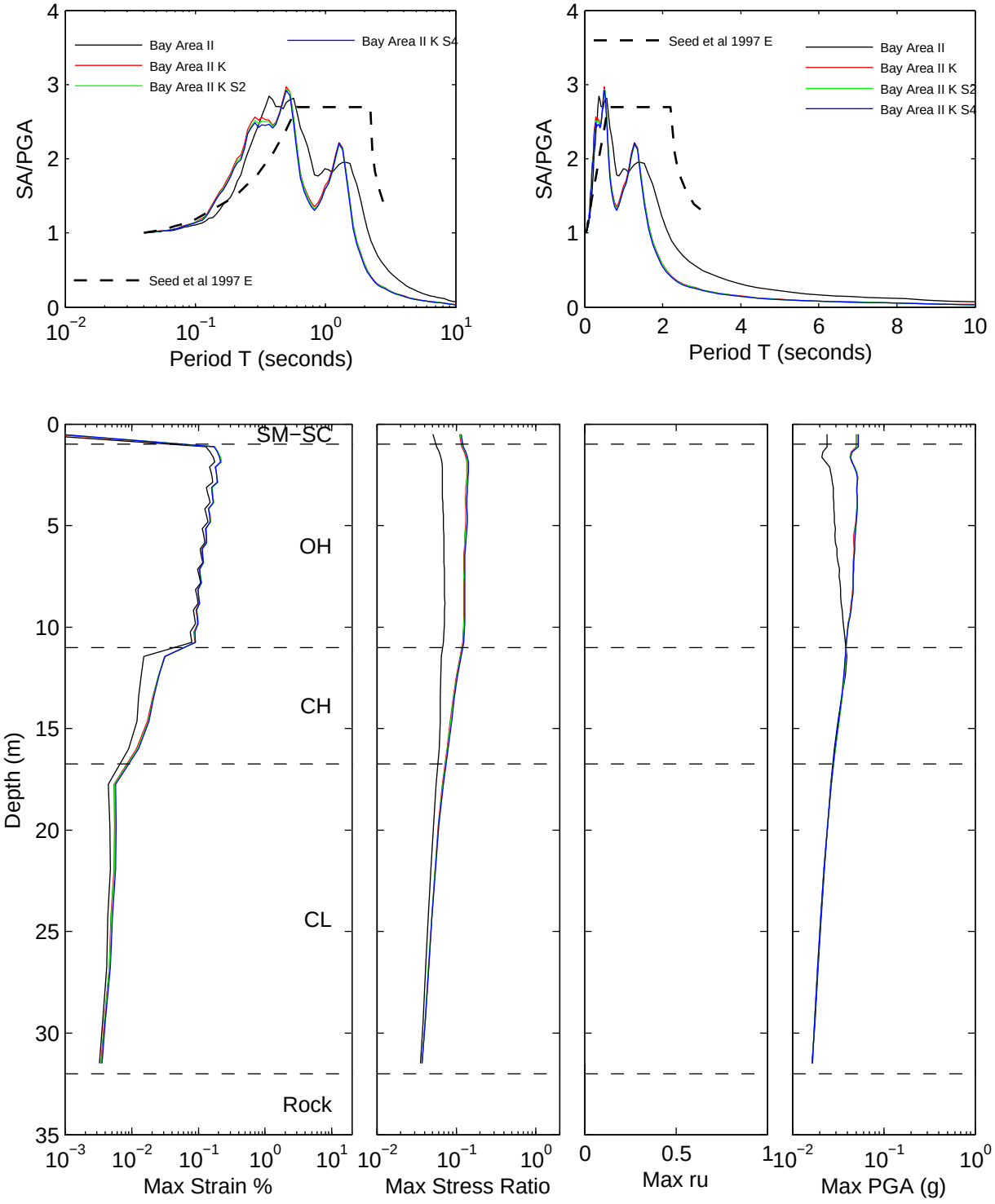

Figure 7B.26: Compare soil strength and MRD curves for Bay Area II sites for scenario 25ACR3

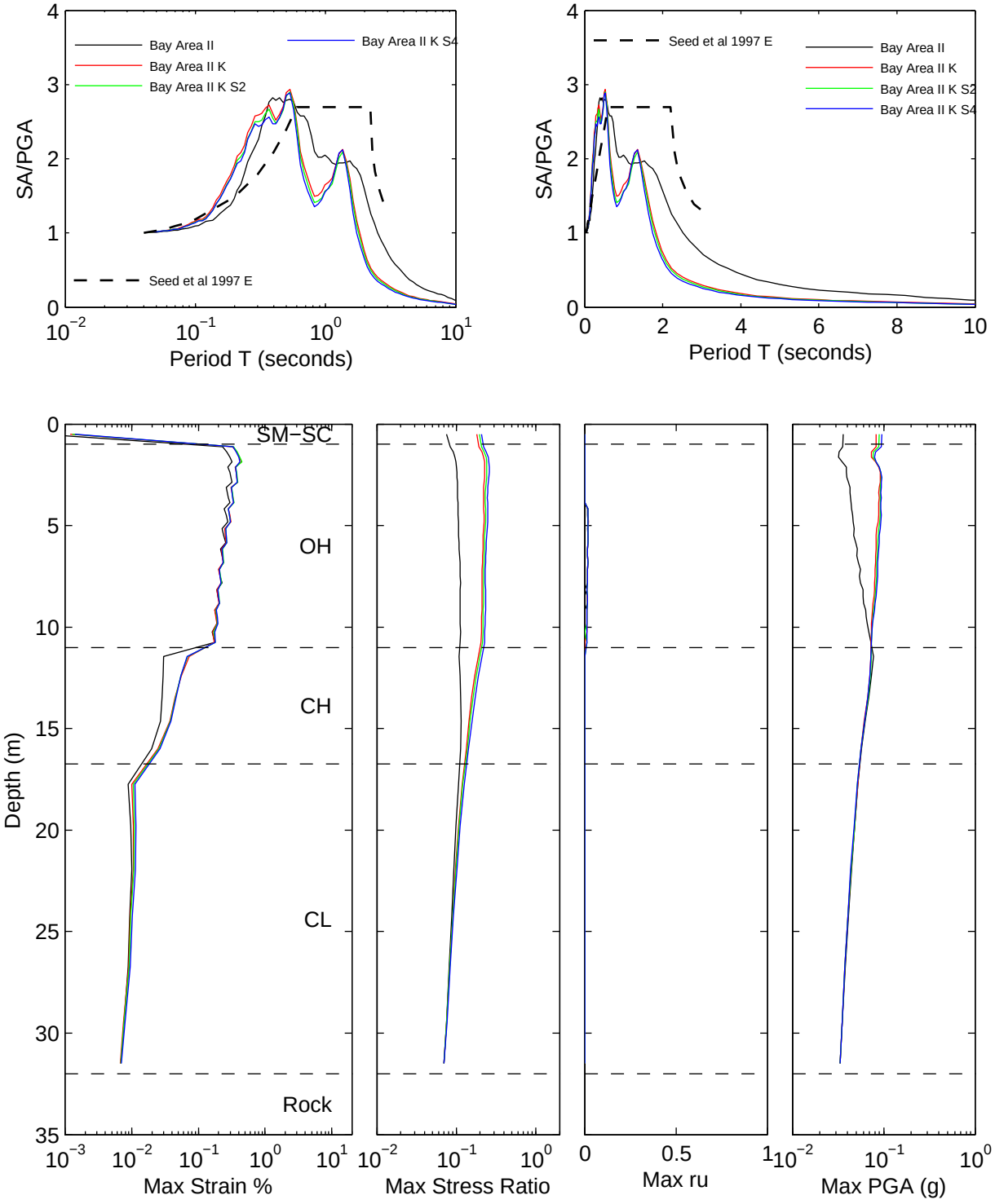

Figure 7B.27: Compare soil strength and MRD curves for Bay Area II sites for scenario 50ACR3

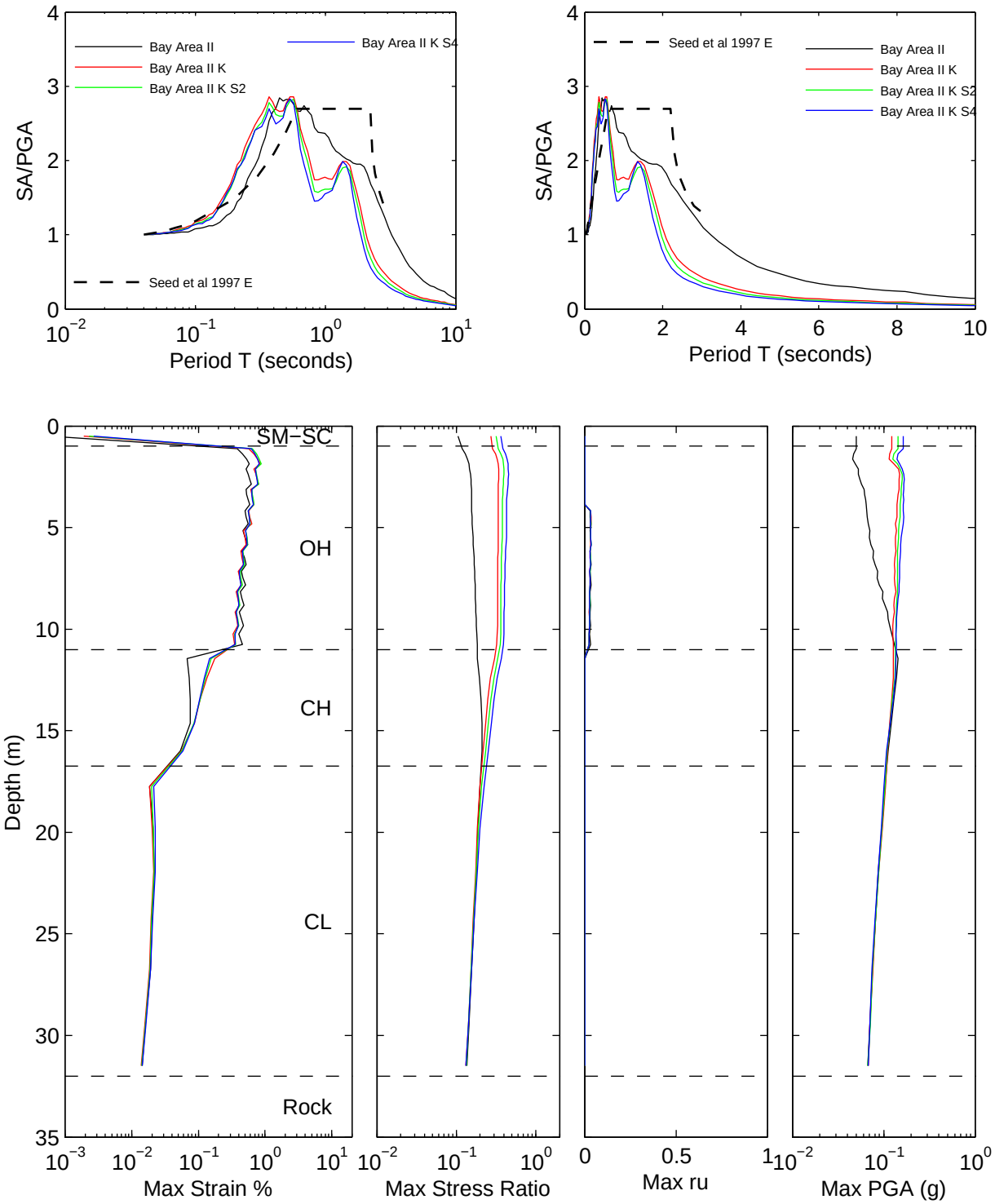

Figure 7B.28: Compare soil strength and MRD curves for Bay Area II sites for scenario 100ACR3

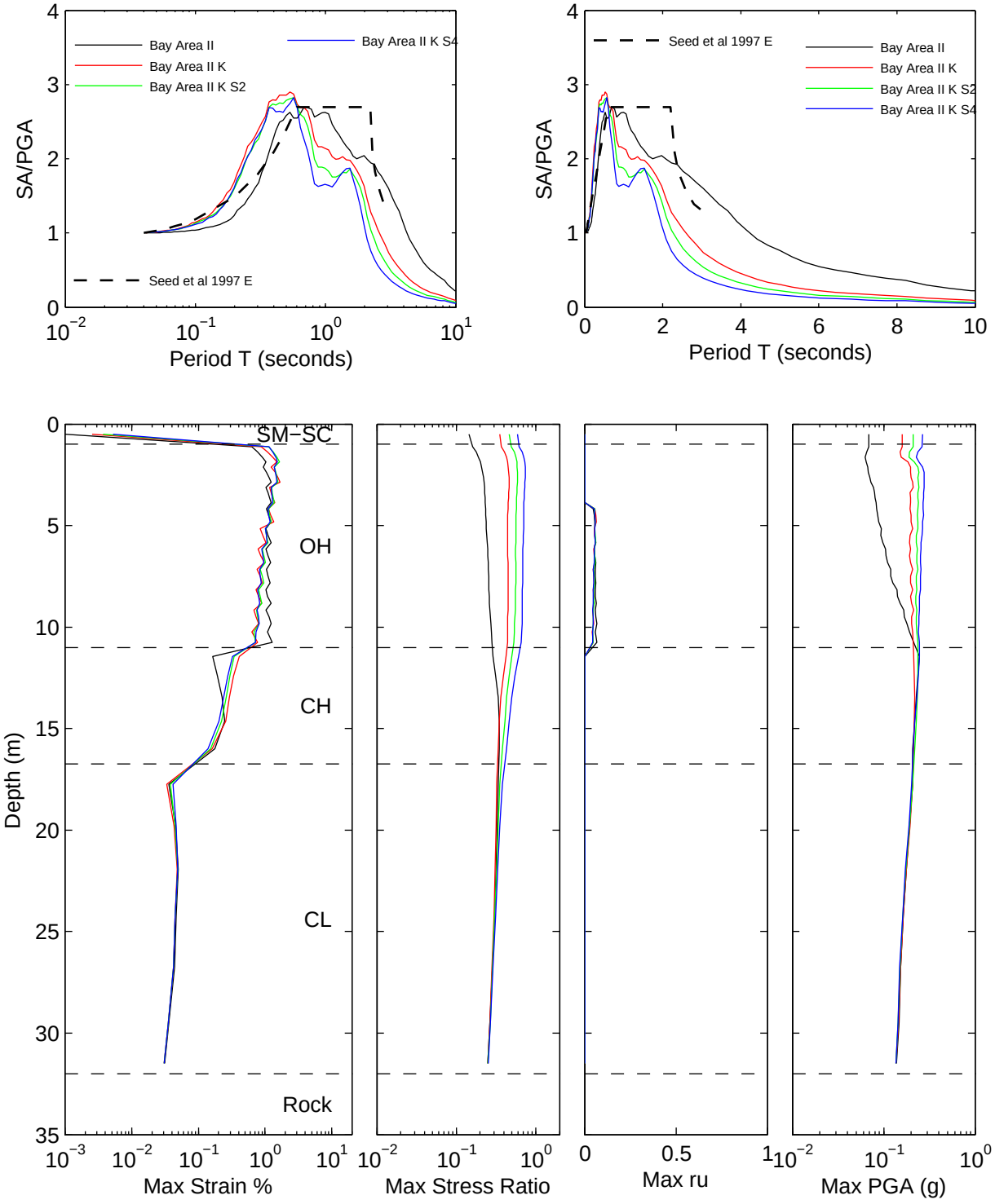

Figure 7B.29: Compare soil strength and MRD curves for Bay Area II sites for scenario 200ACR3

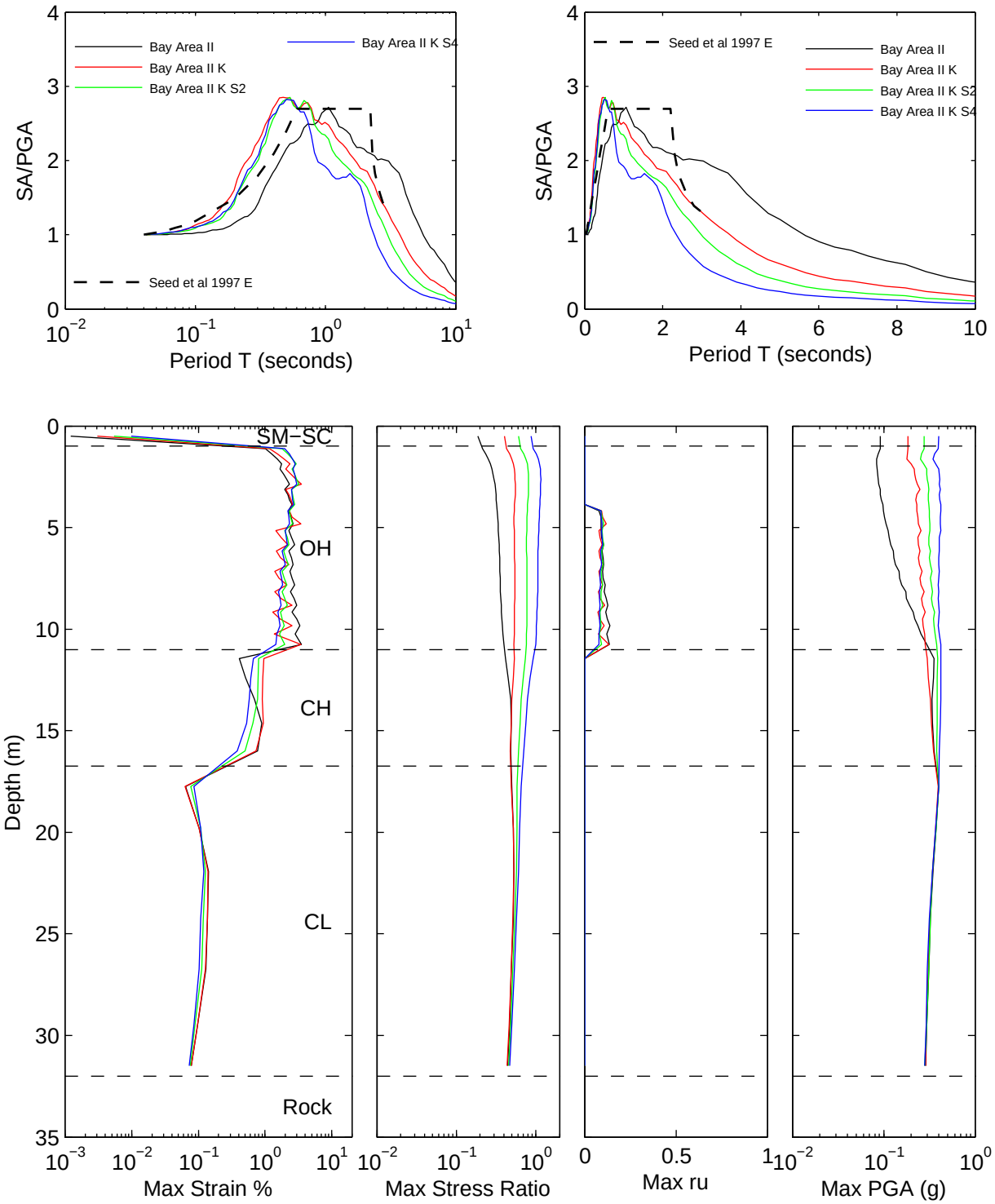

Figure 7B.30: Compare soil strength and MRD curves for Bay Area II sites for scenario 400ACR3

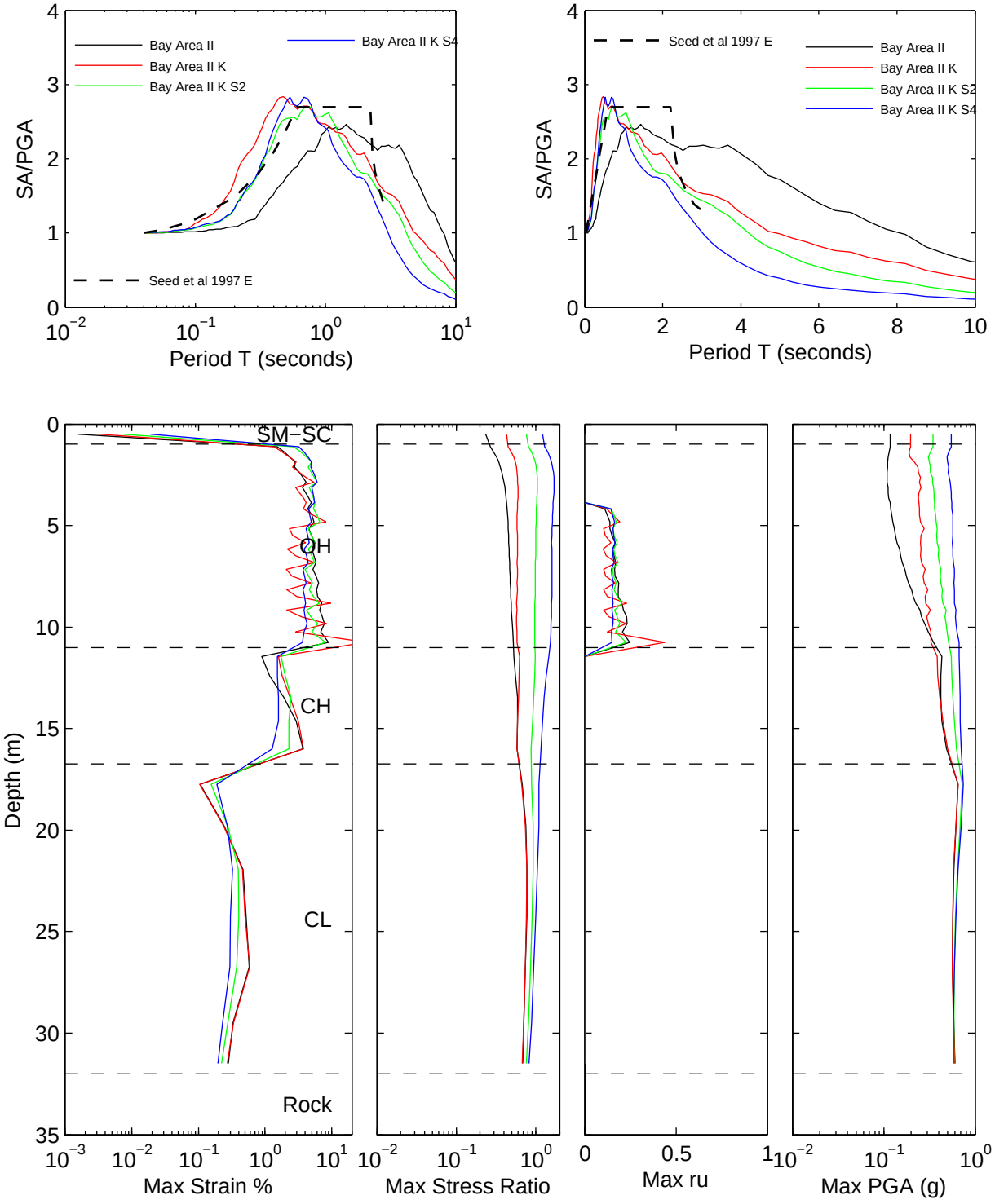

Figure 7B.31: Compare soil strength and MRD curves for Bay Area II sites for scenario ACR3M

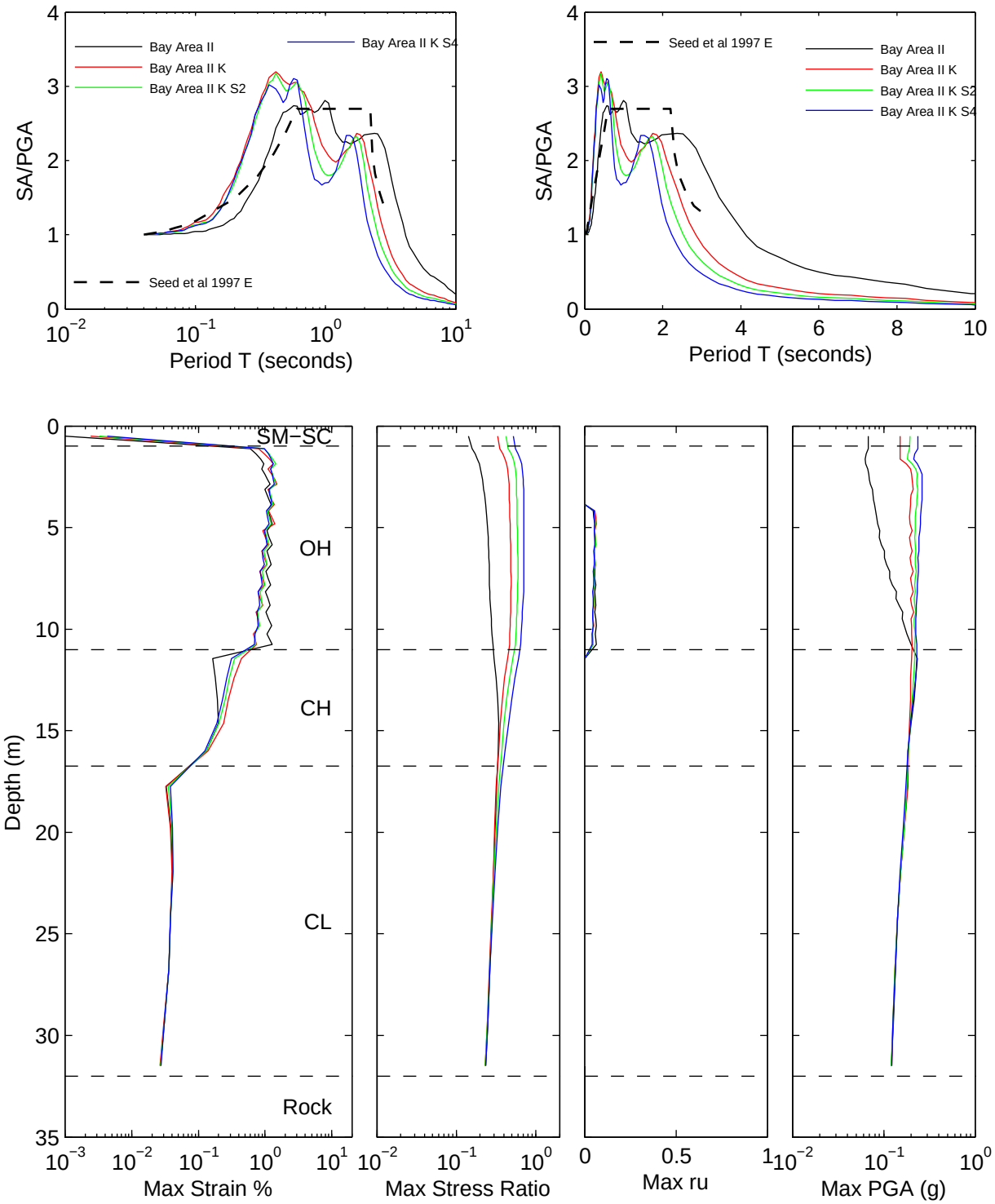

Figure 7B.32: Compare soil strength and MRD curves for Bay Area II sites for scenario ACR1

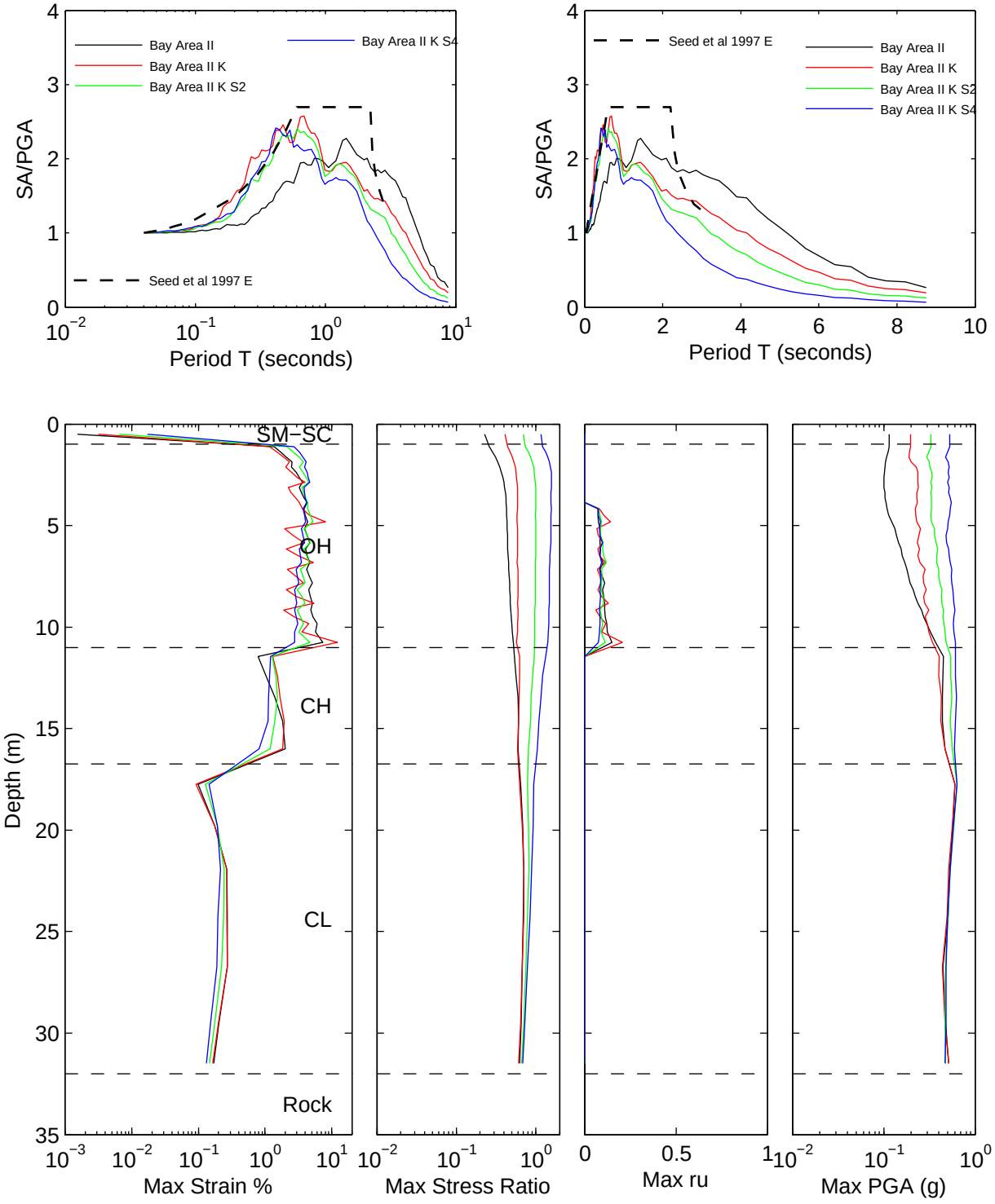

Figure 7B.33: Compare soil strength and MRD curves for Bay Area II sites for scenario ACR2

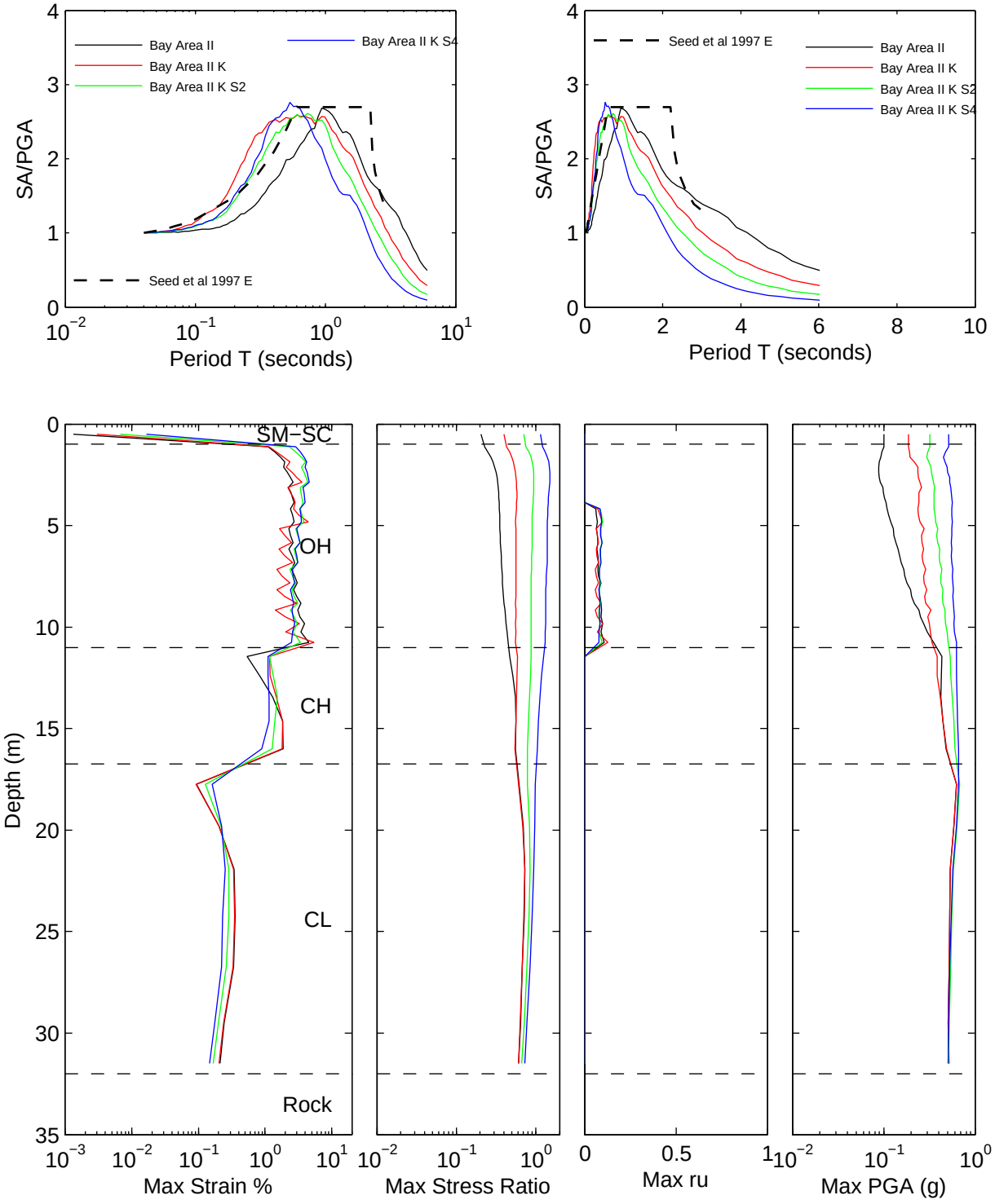

Figure 7B.34: Compare soil strength and MRD curves for Bay Area II sites for scenario ACR2M

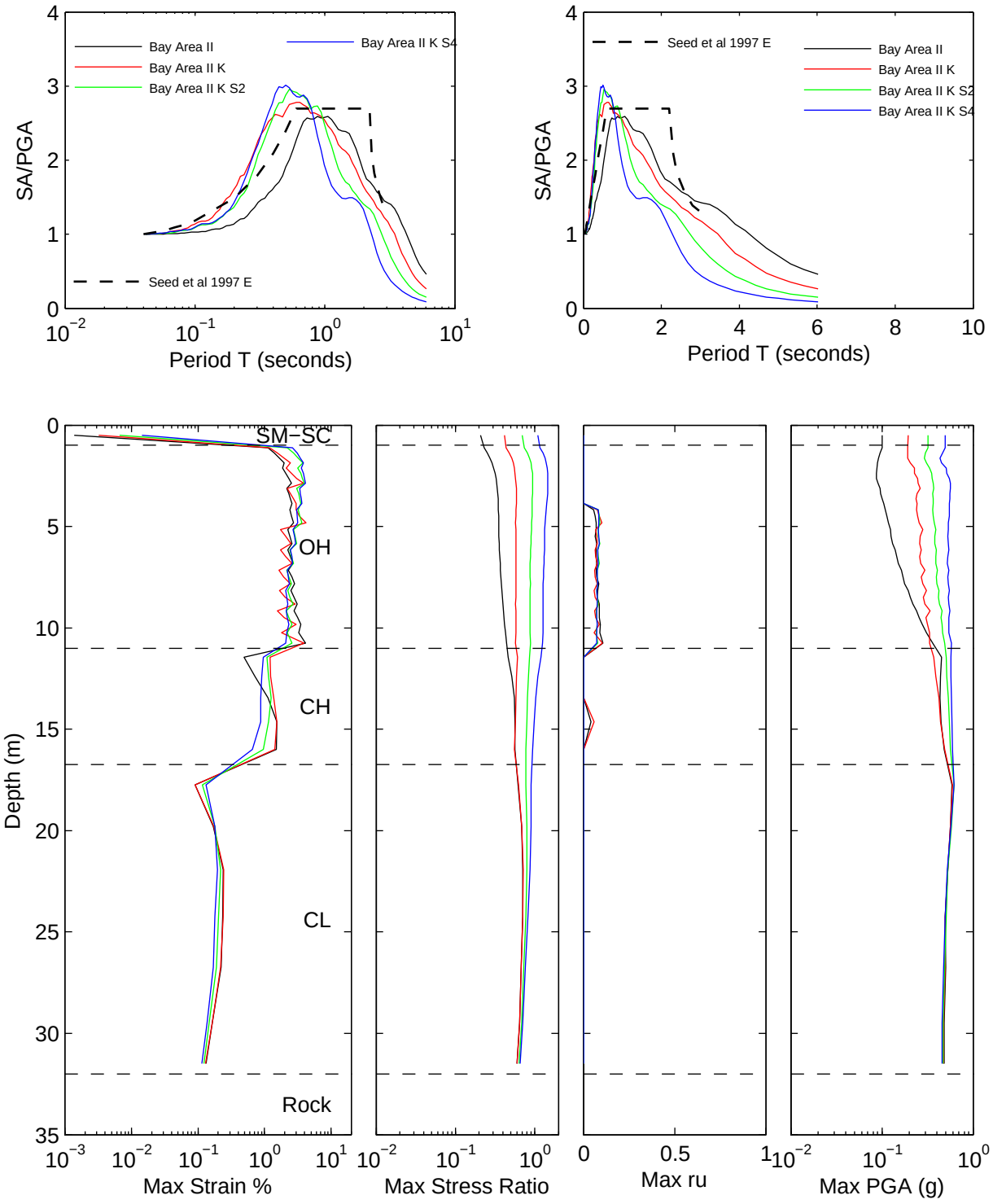

Figure 7B.35: Compare soil strength and MRD curves for Bay Area II sites for scenario SUB

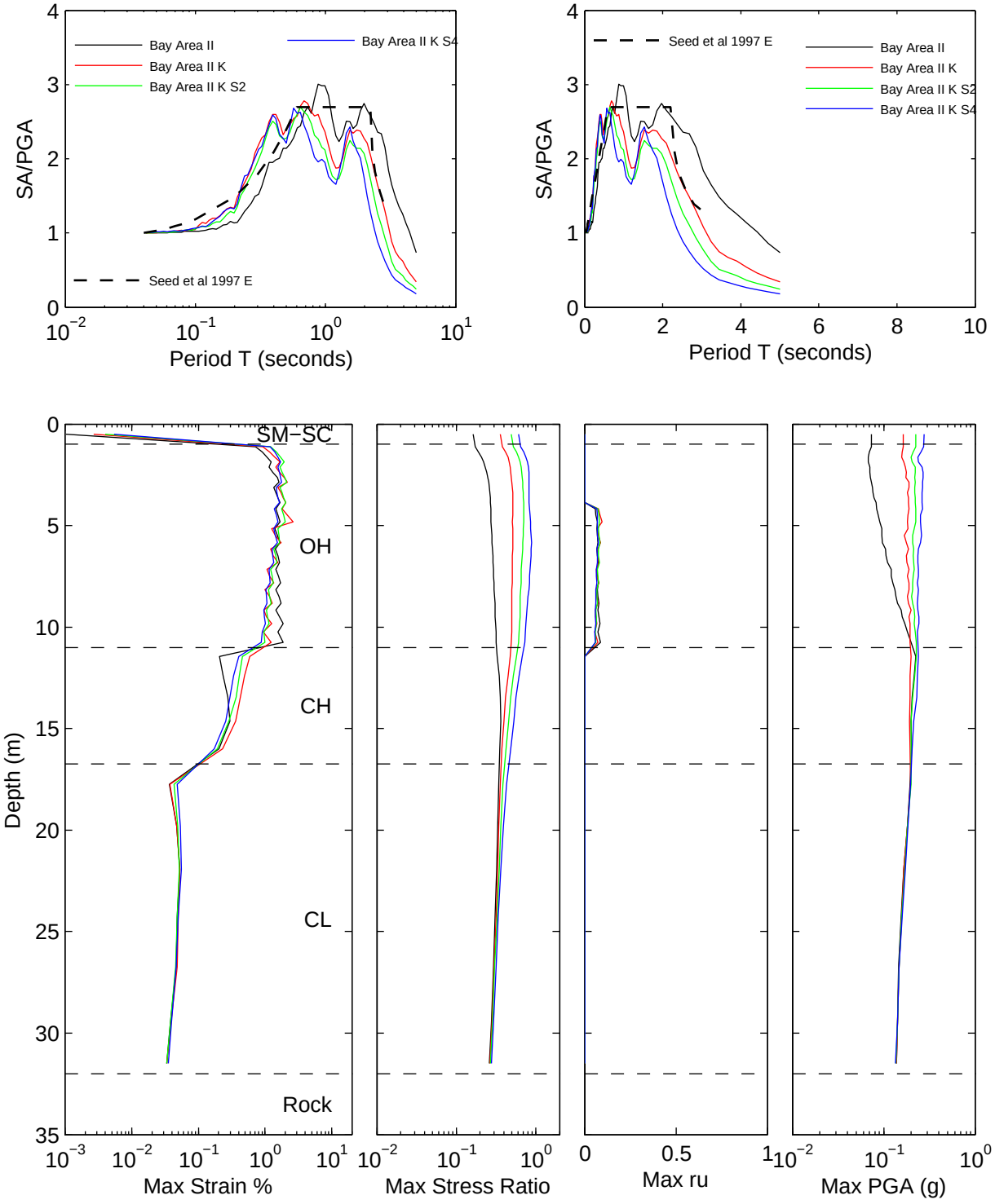

Figure 7B.36: Compare soil strength and MRD curves for Bay Area II sites for scenario SCR

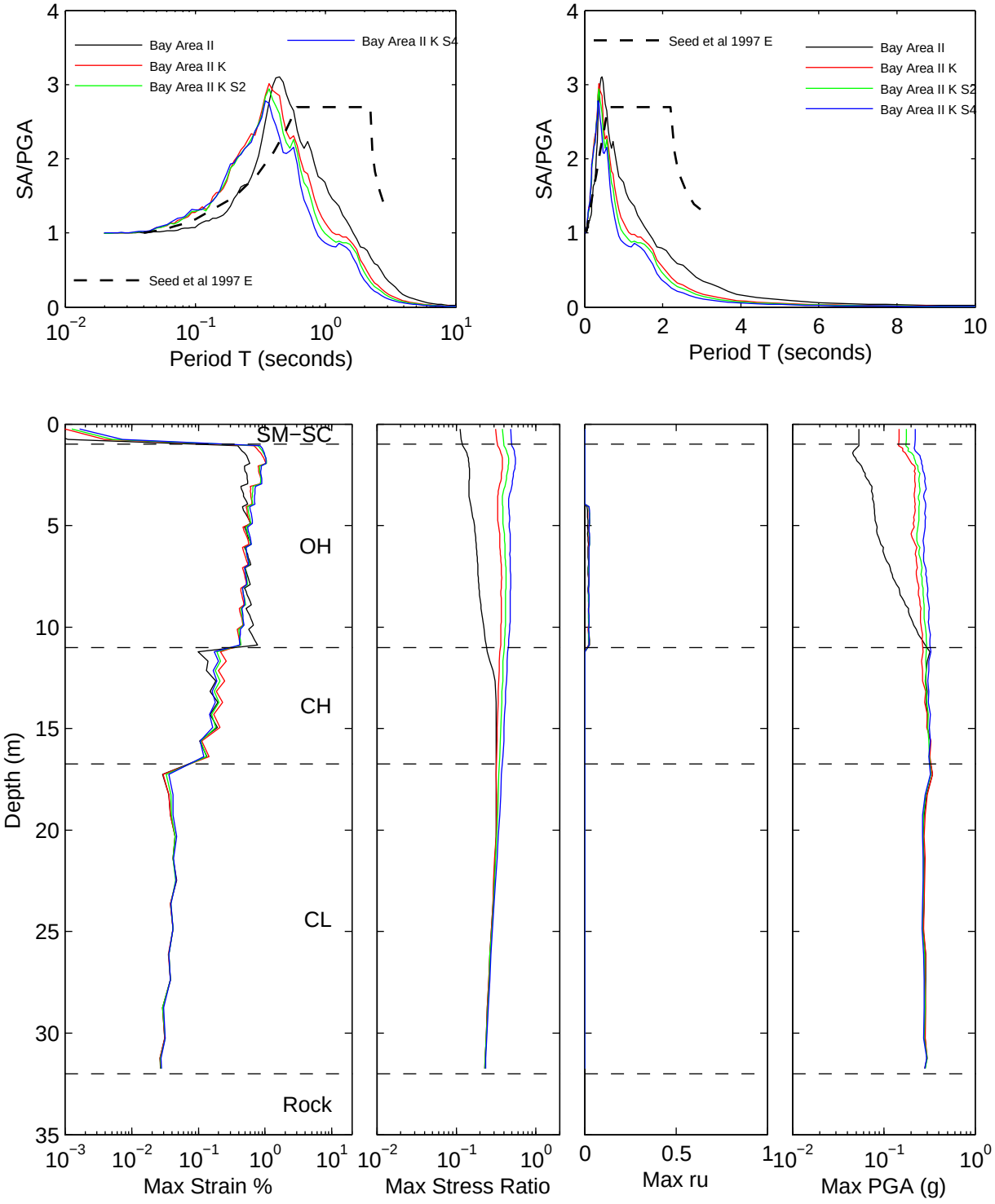

APPENDIX 7C: EFFECT OF ANALYSIS TYPE – COMPARING EQUIVALENT LINEAR, NONLINEAR TOTAL STRESS, AND NONLINEAR EFFECTIVE STRESS ANLAYSES

Appendix 7C: Effect of Analysis Type - Comparing Equivalent Linear, Nonlinear Total Stress, and Nonlinear Effective Stress Analyses

Site response analyses were conducted in this study using equivalent linear, nonlinear total stress and nonlinear effective stress analyses for the seven base case sites. Appendix 7C shows the response spectra, amplification, and spectral shape calculated using equivalent linear, nonlinear total stress, and nonlinear effective stress site response analyses for site all 7 sites where these three analysis methods were used. Each figure contains 12 plots, where each plot corresponds to a scenario. All curves are the mean values for a given site and scenario.

Figure 7C.1: Analysis type comparison of MRCE2 response spectra

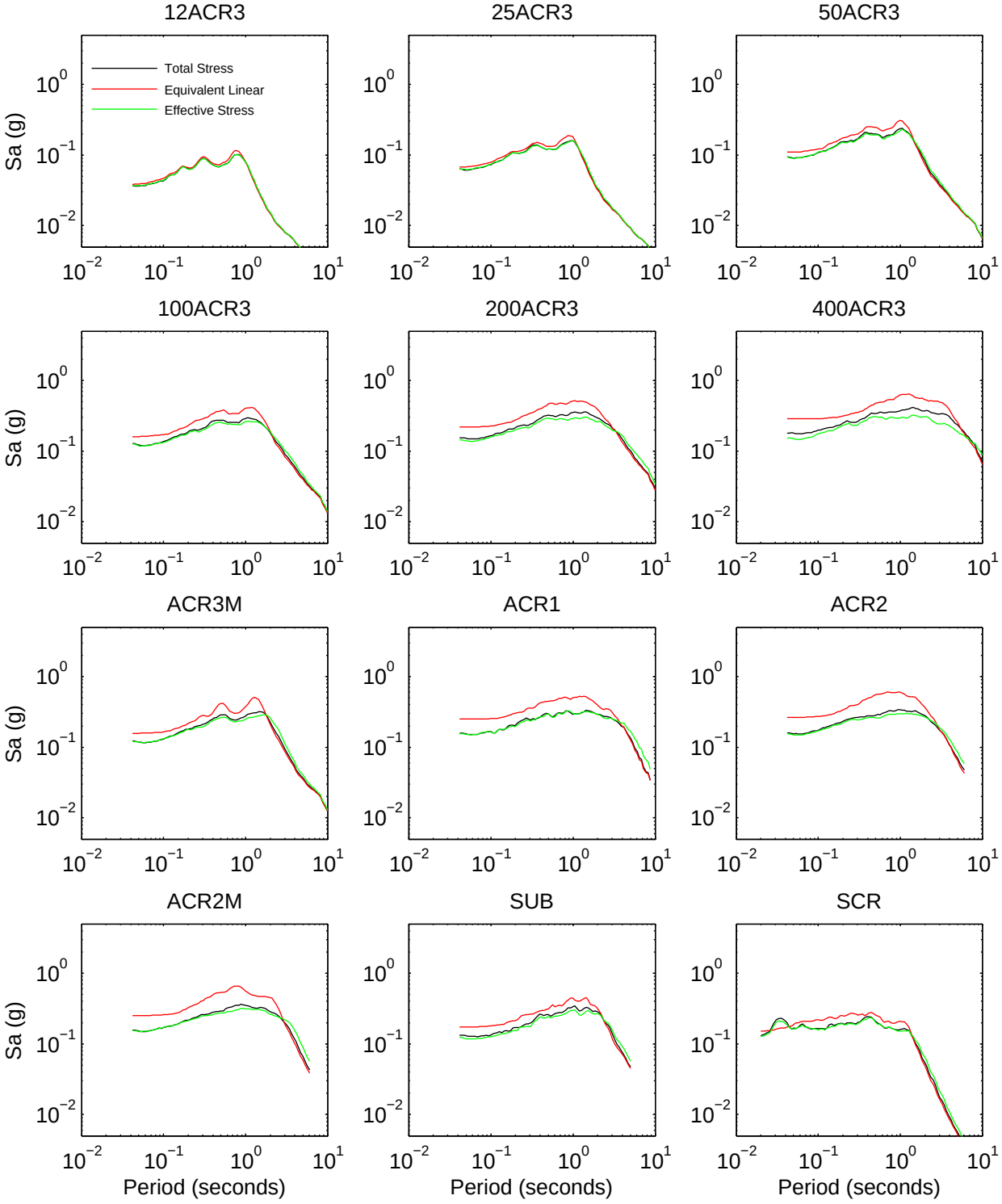

Figure 7C.2: Analysis type comparison of MRCE2 amplification

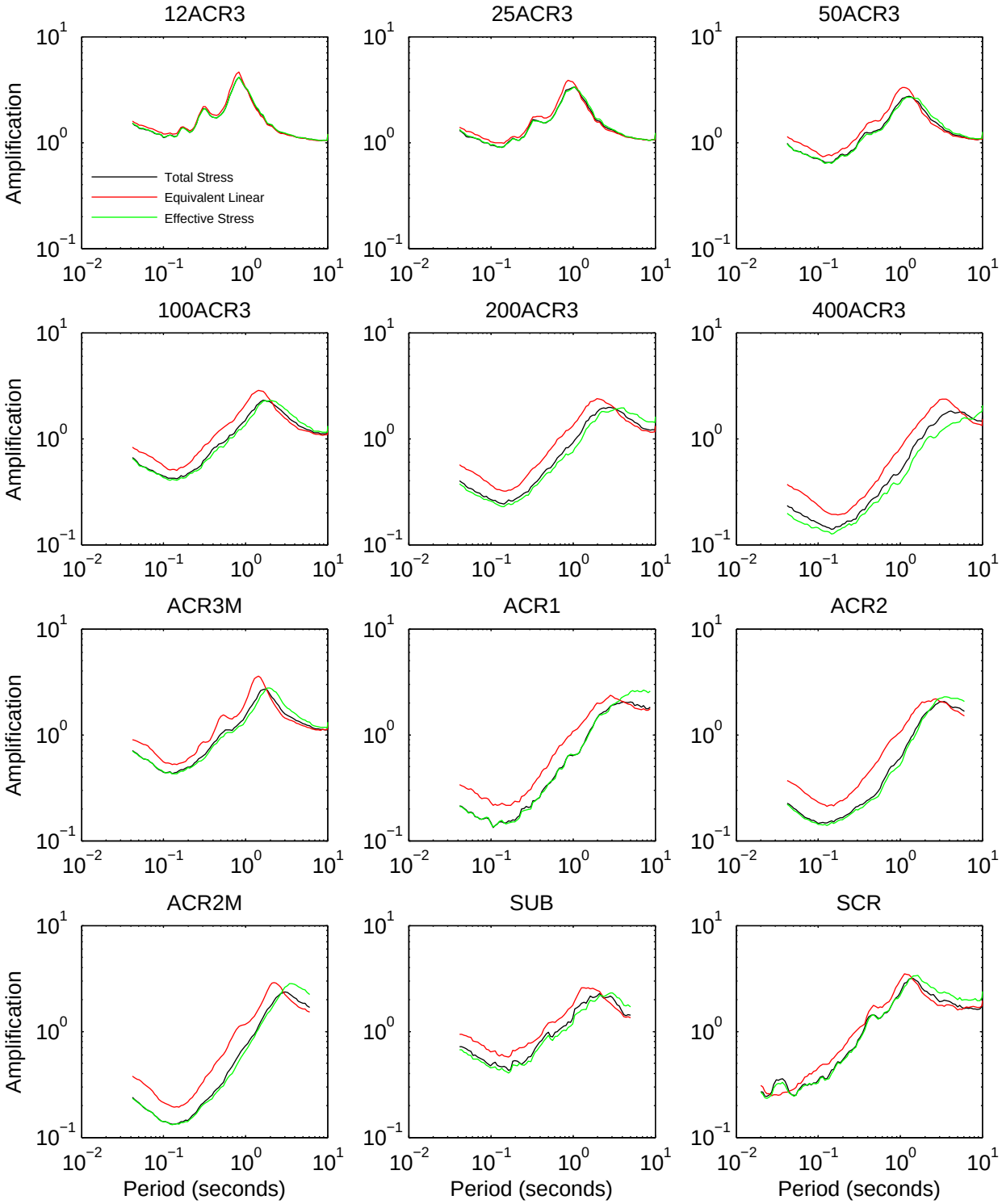

Figure 7C.3: Analysis type comparison of MRCE2 spectral shape

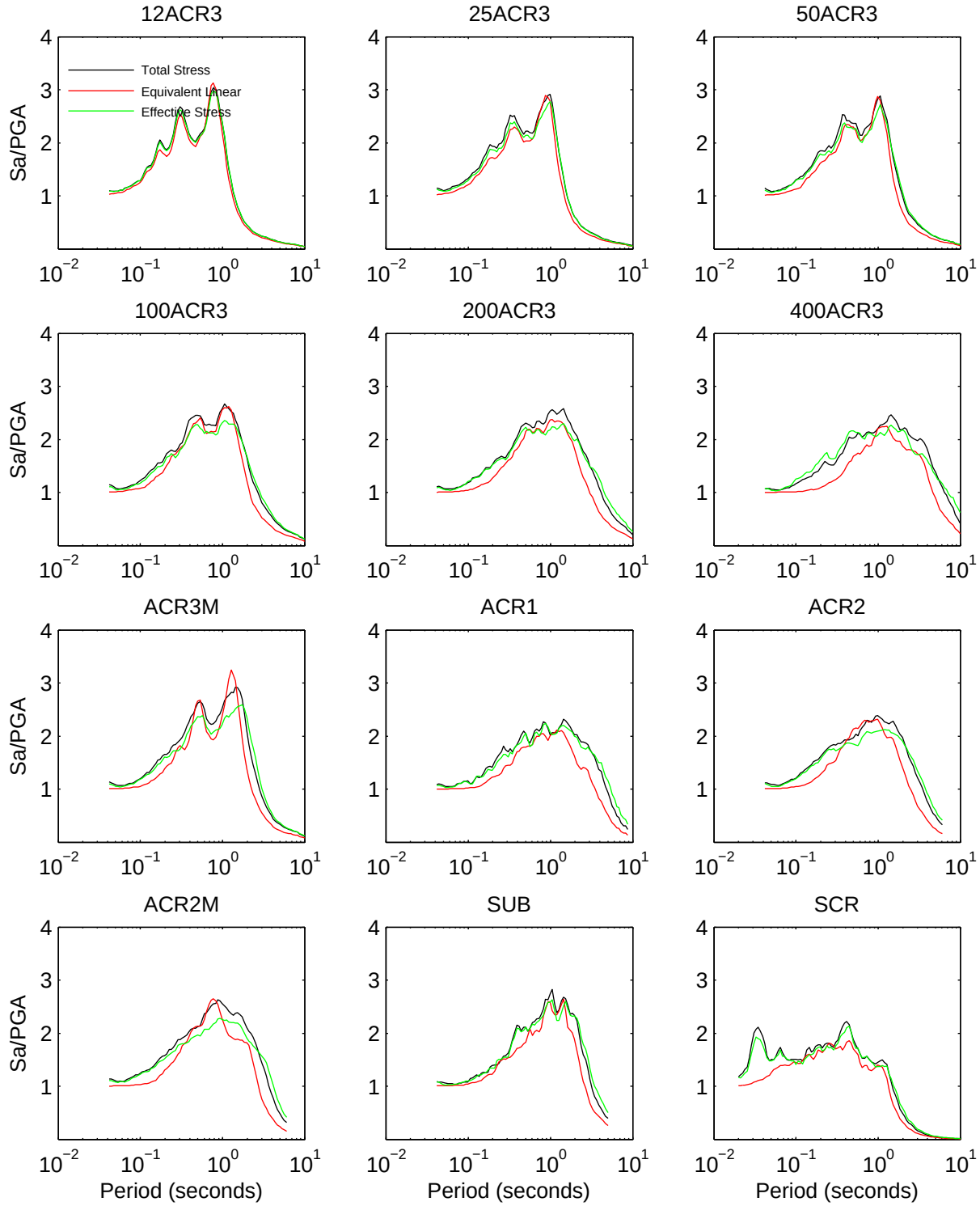

Figure 7C.4: Analysis type comparison of HAGP response spectra

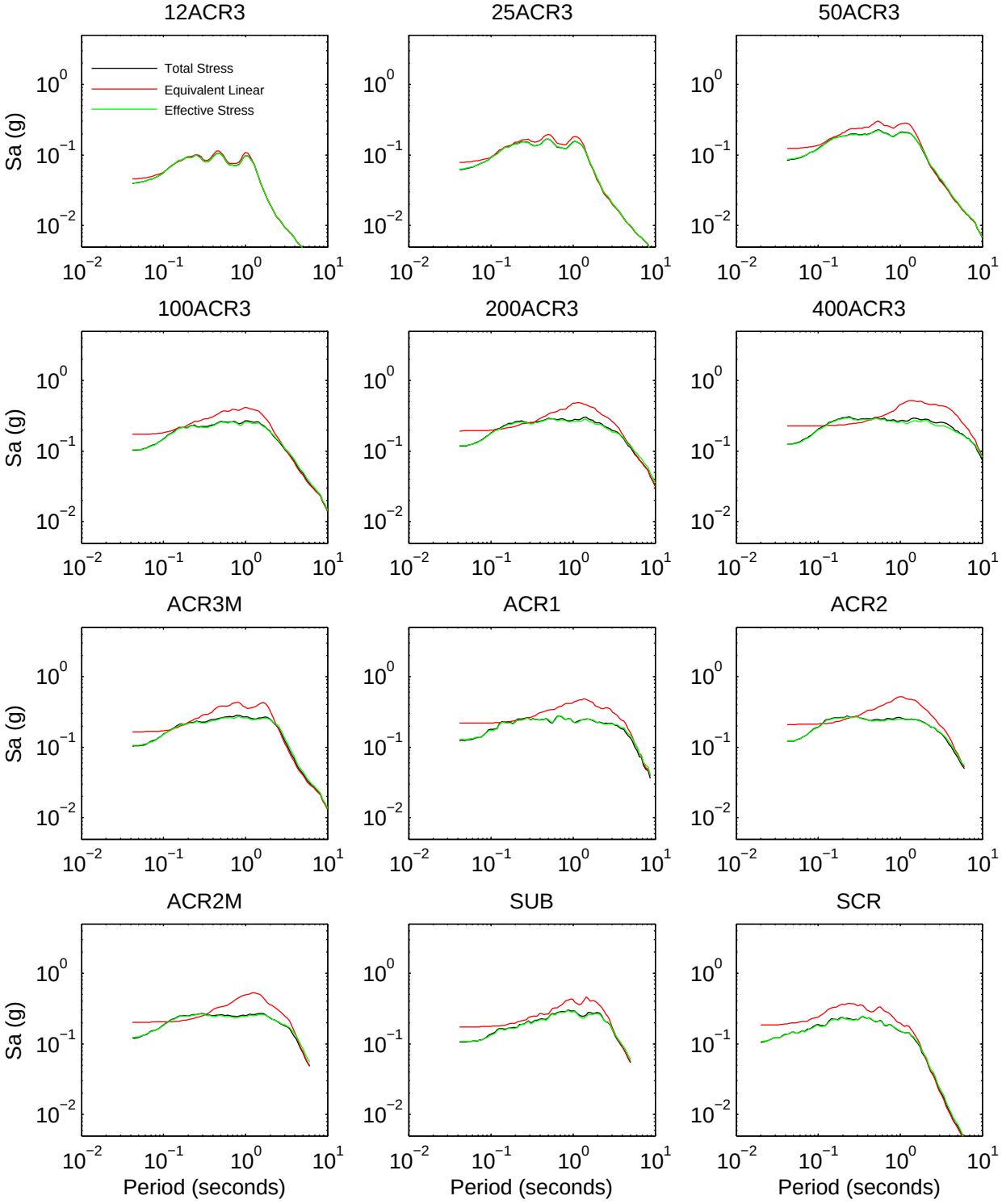

Figure 7C.5: Analysis type comparison of HAGP amplification

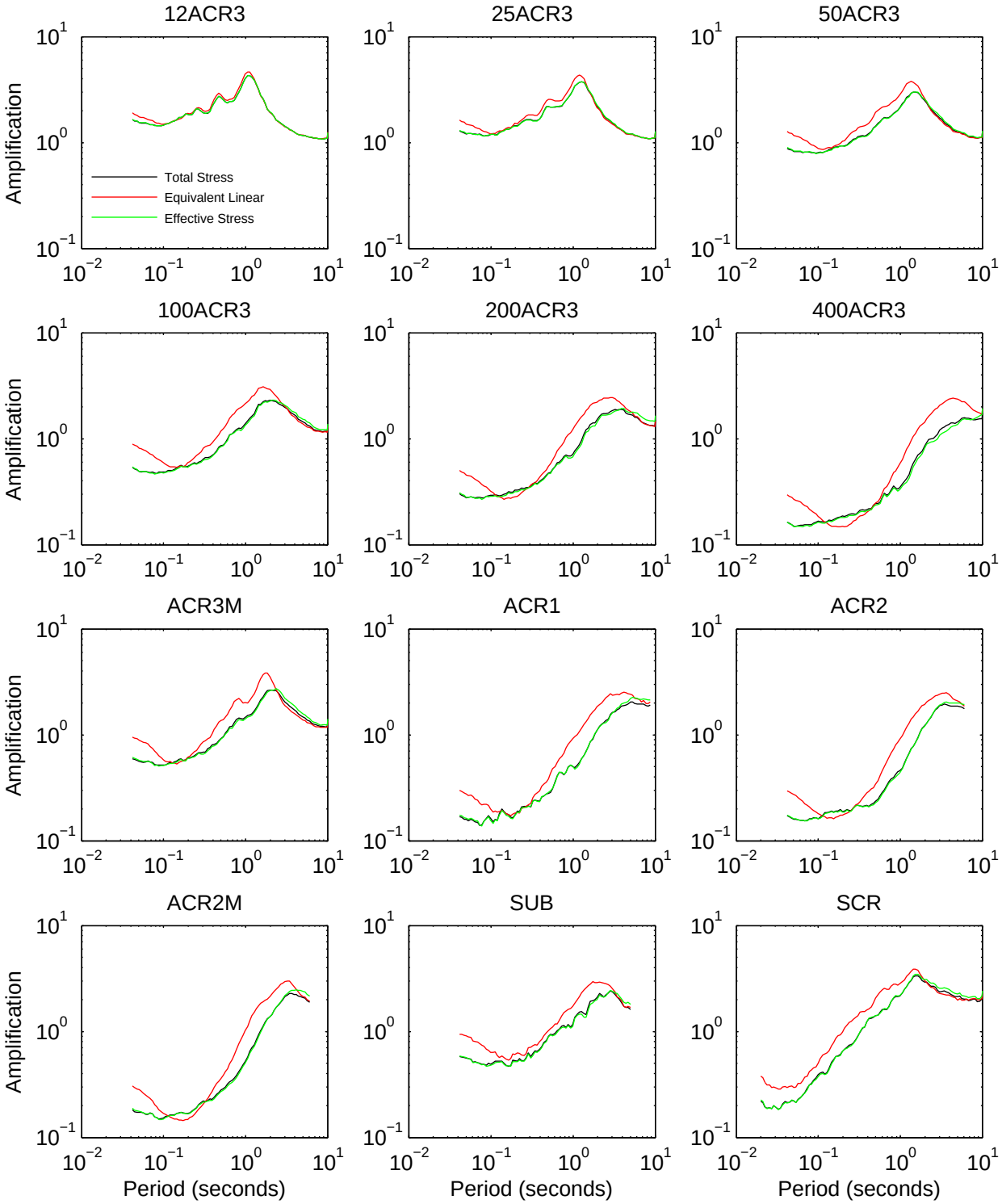

Figure 7C.6: Analysis type comparison of HAGP spectral shape

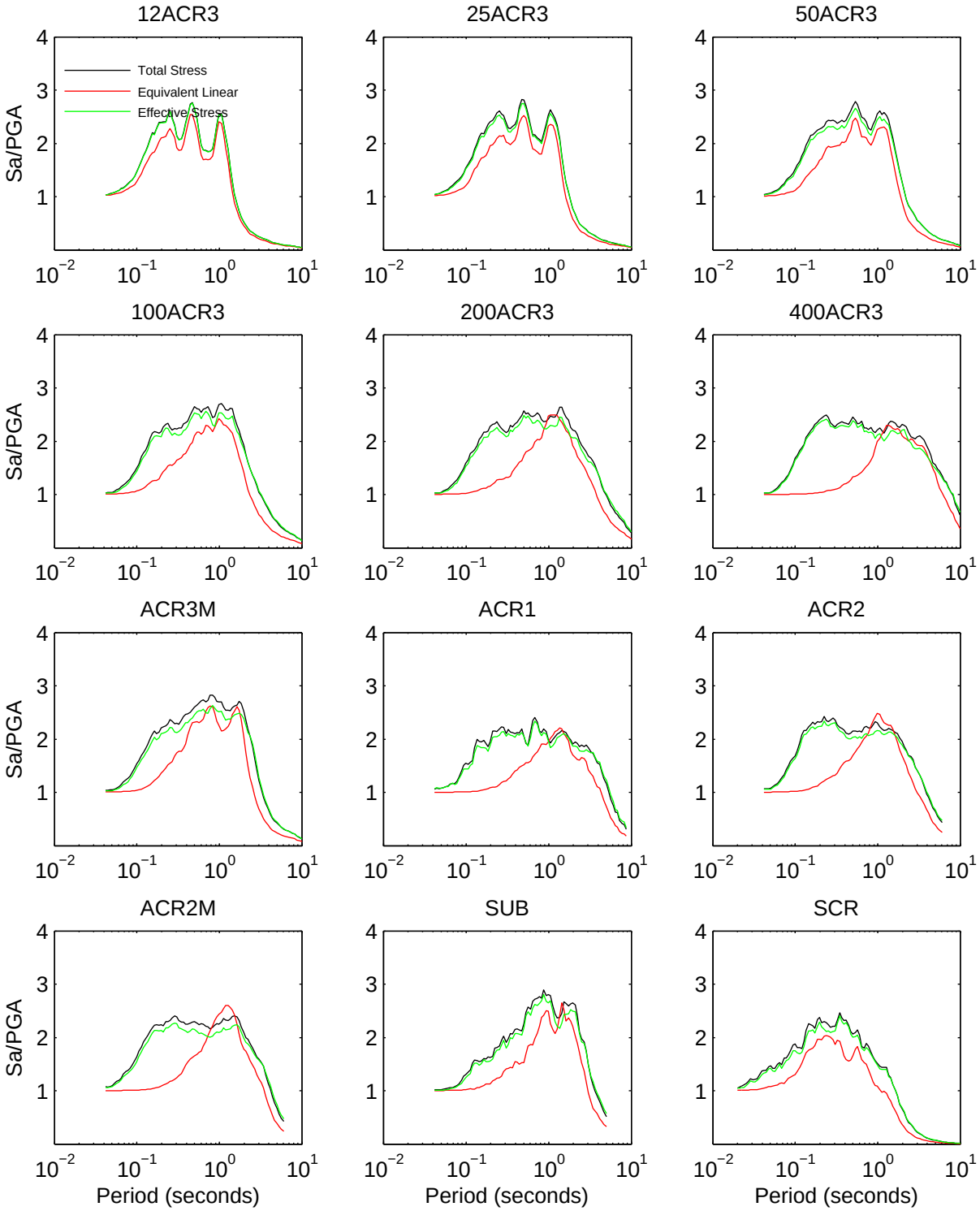

Figure 7C.7: Analysis type comparison of KIKNET response spectra

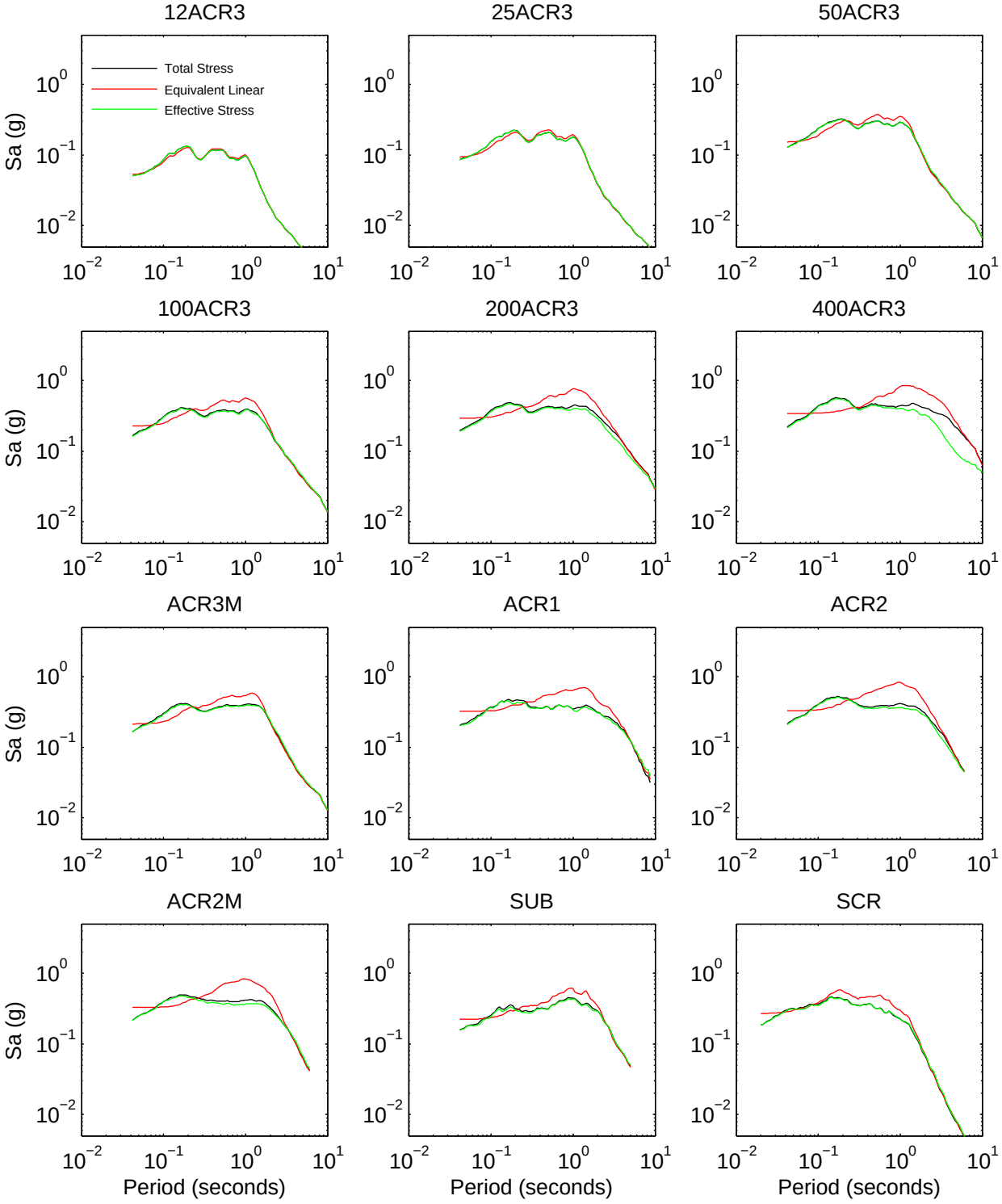

Figure 7C.8: Analysis type comparison of KIKNET amplification

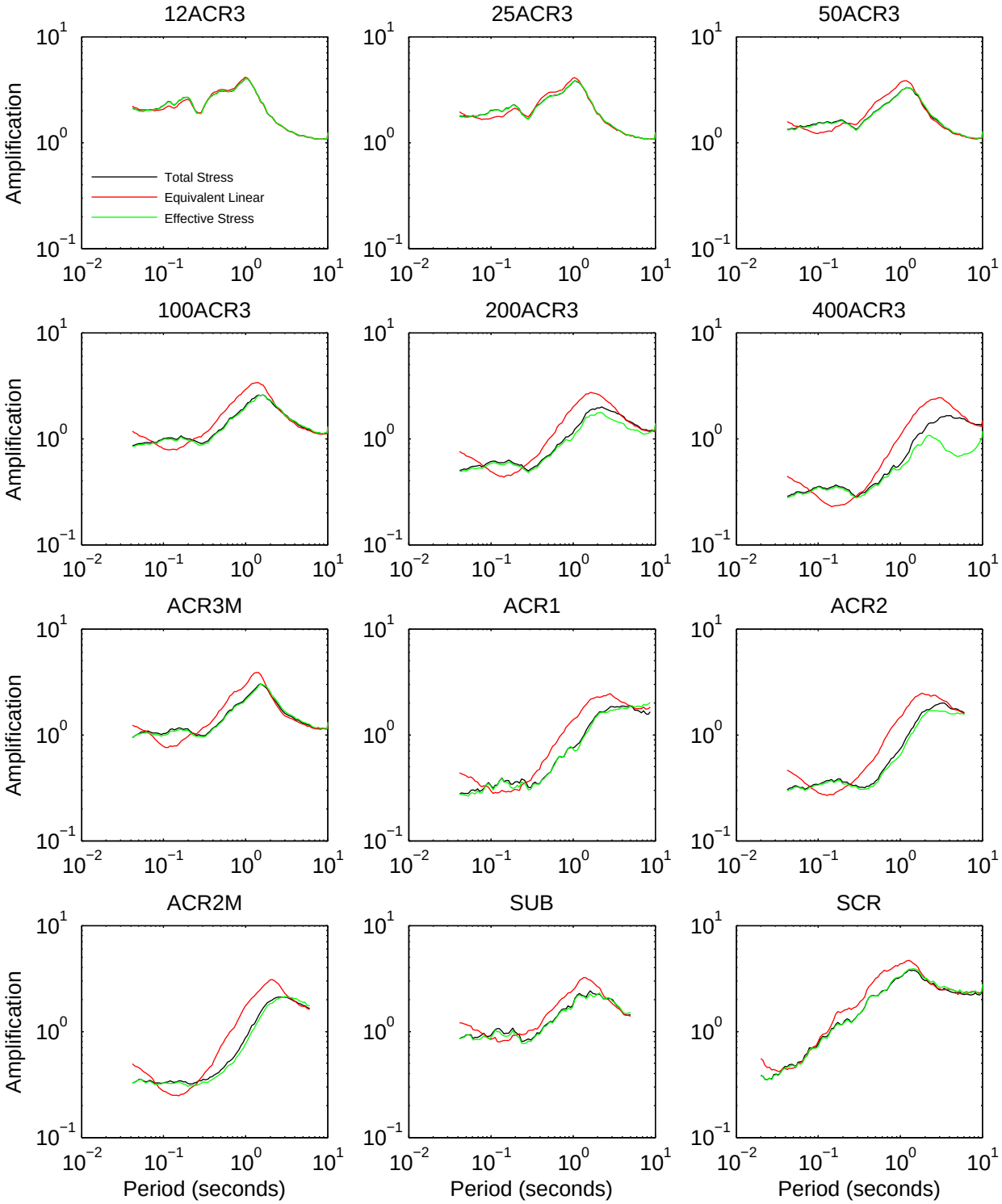

Figure 7C.9: Analysis type comparison of KIKNET spectral shape

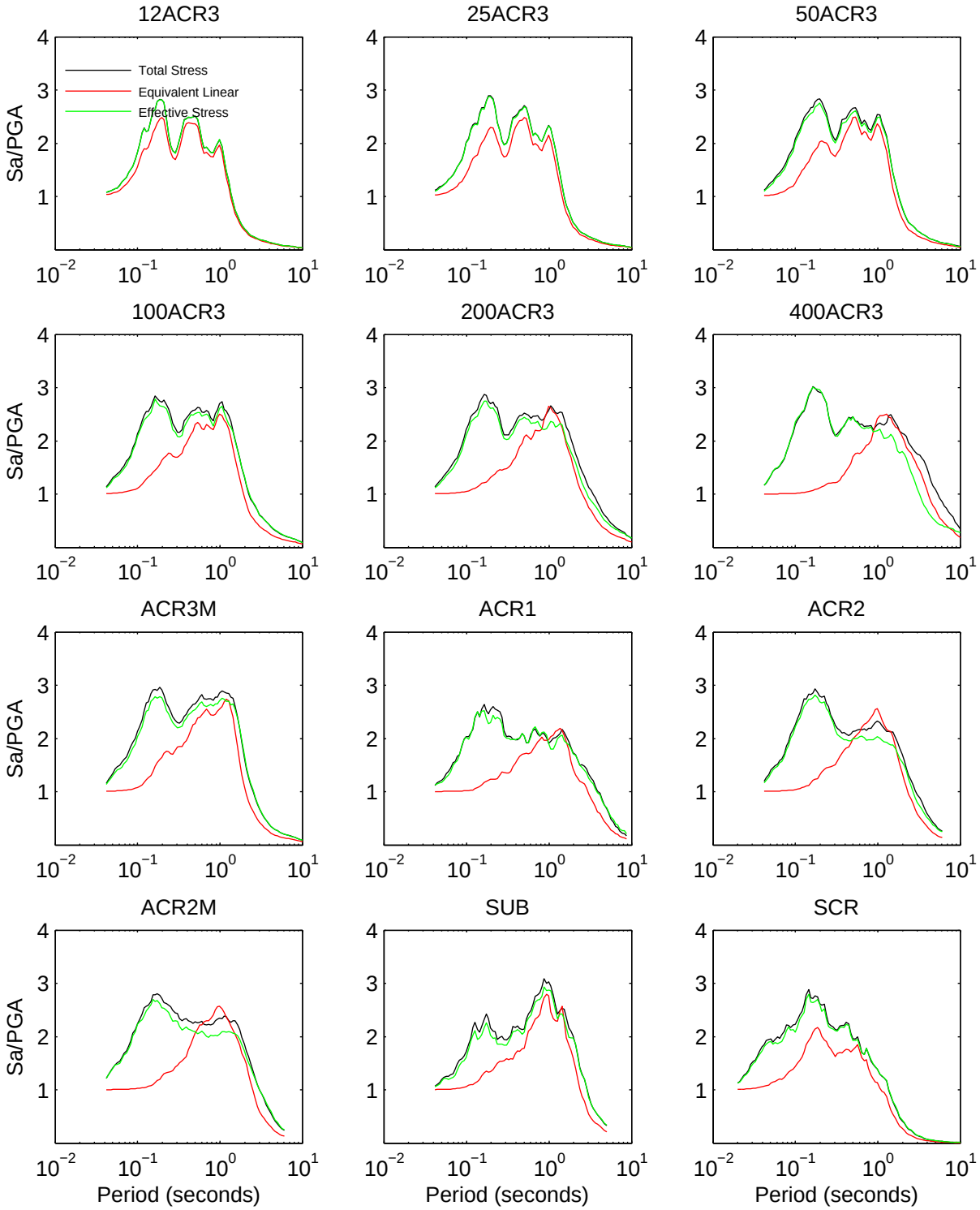

Figure 7C.10: Analysis type comparison of Bay Area II response spectra

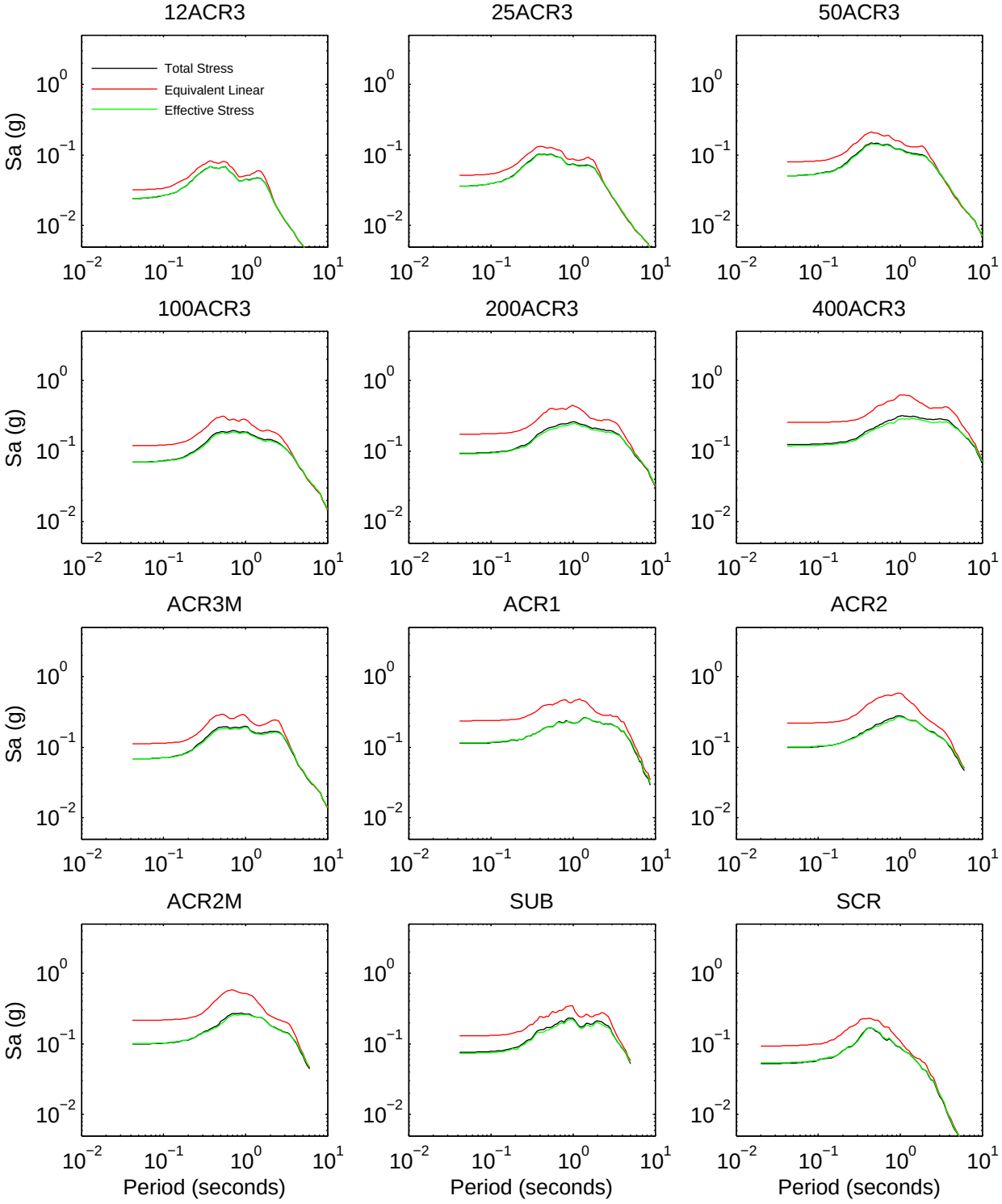

Figure 7C.11: Analysis type comparison of Bay Area II amplification

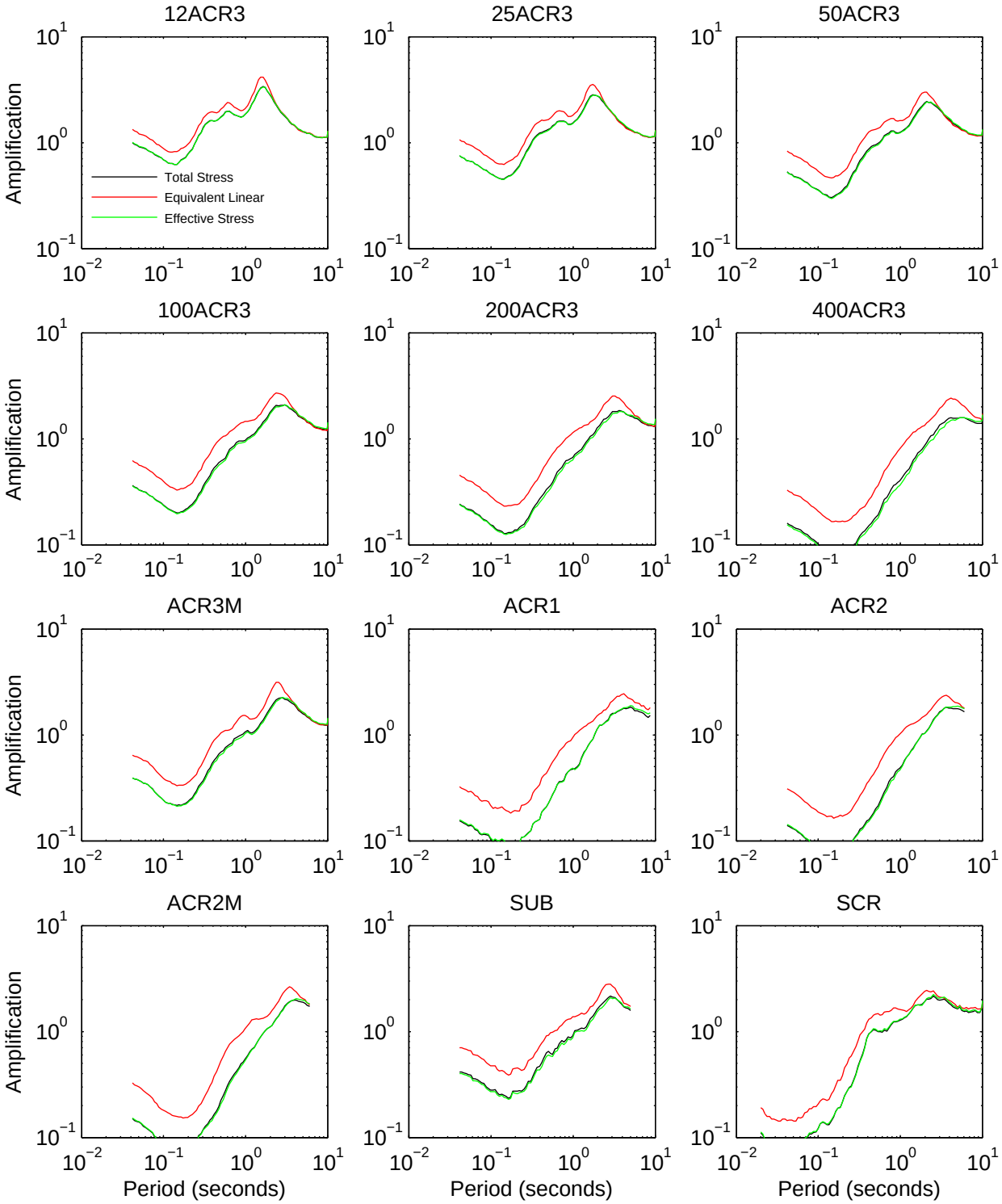

Figure 7C.12: Analysis type comparison of Bay Area II spectral shape

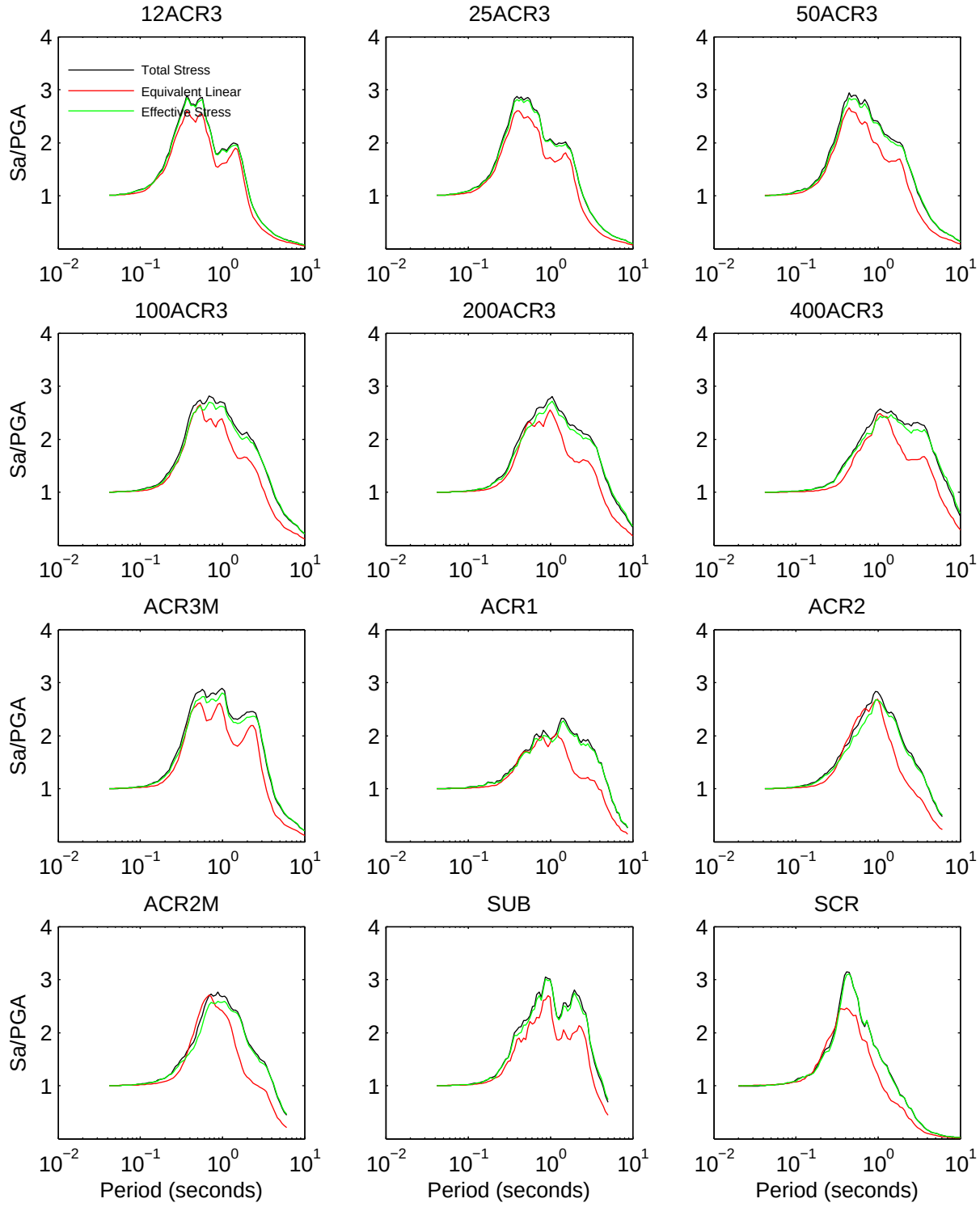

Figure 7C.13: Analysis type comparison of MRCE1 response spectra

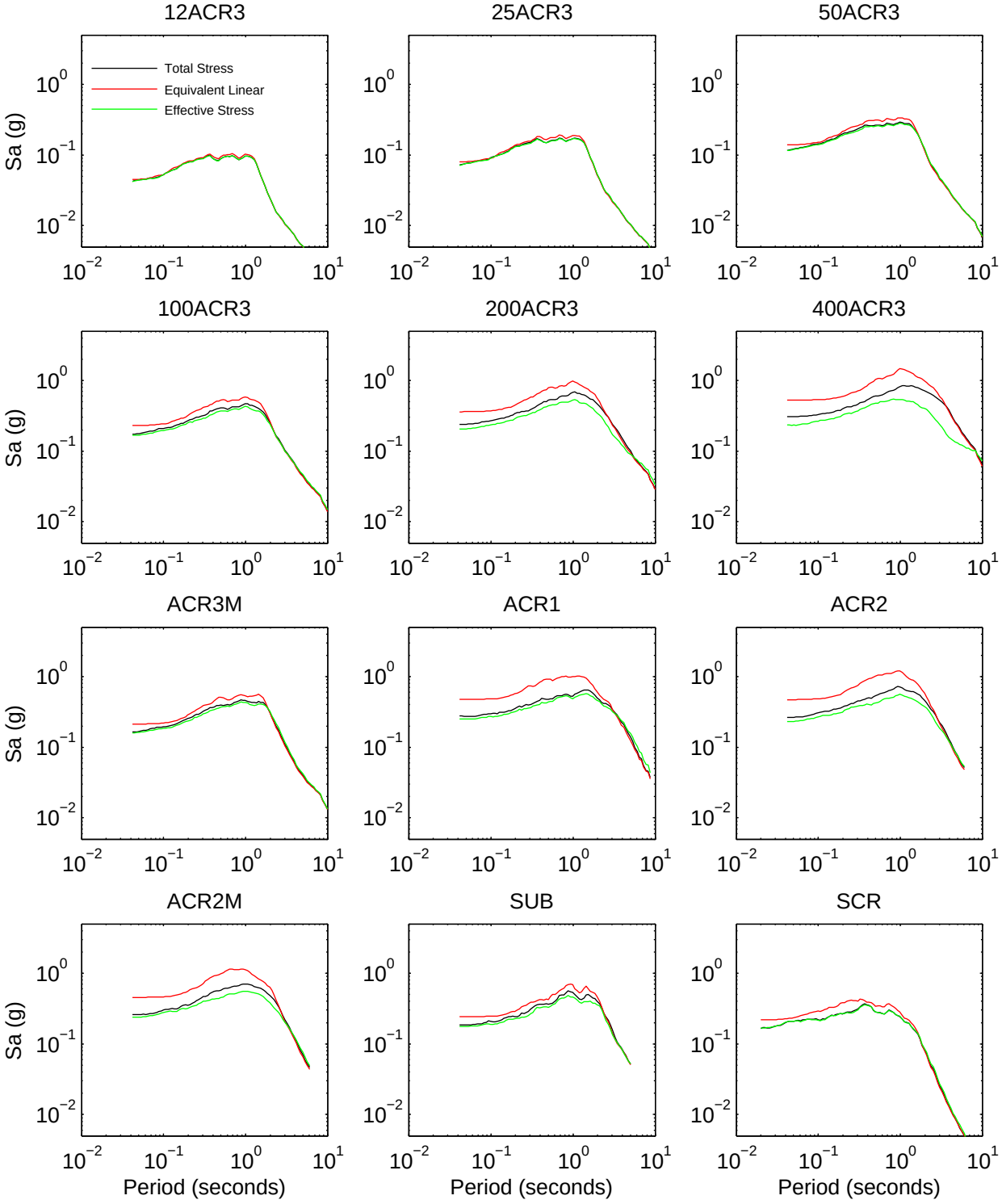

Figure 7C.14: Analysis type comparison of MRCE1 amplification

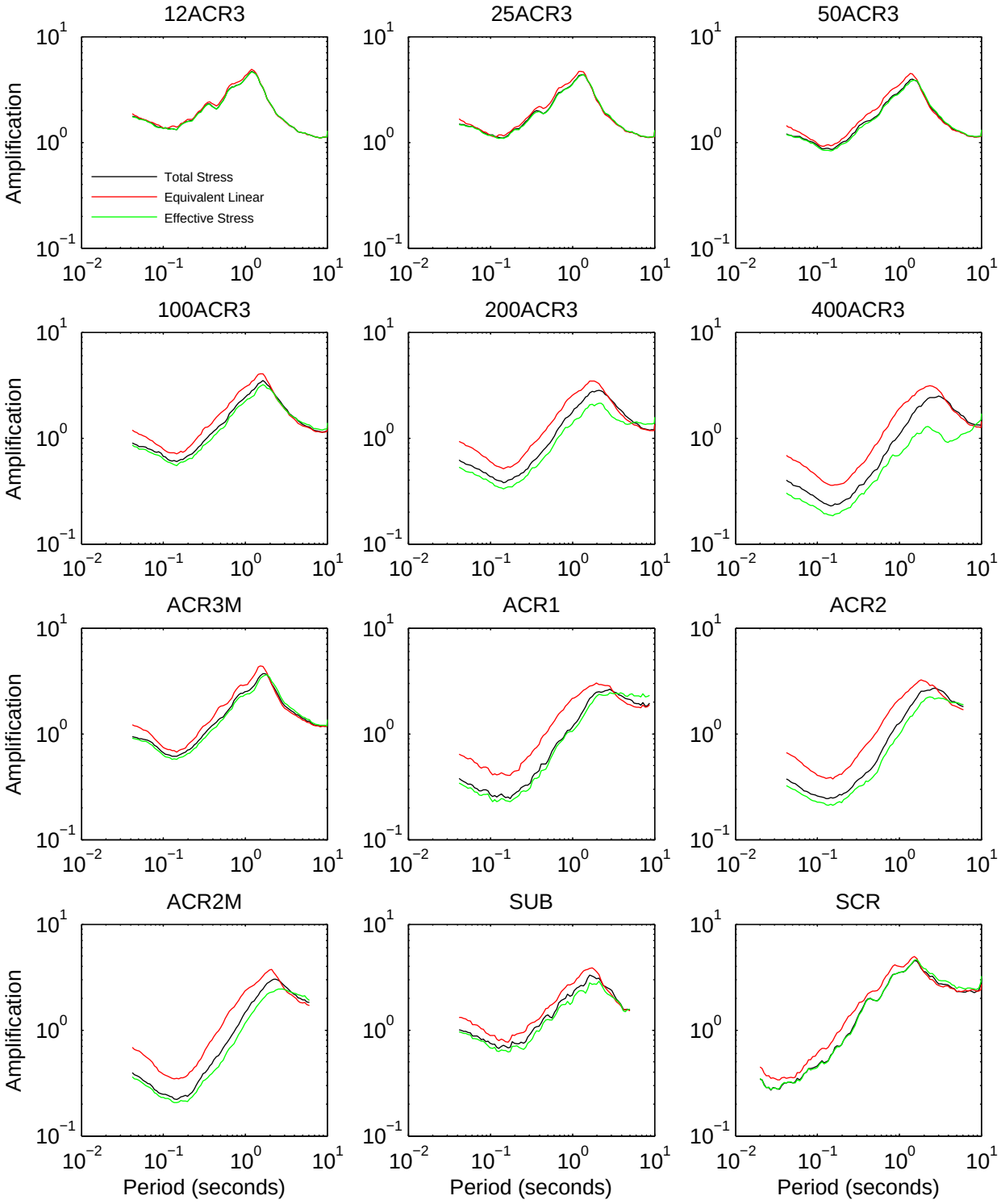

Figure 7C.15: Analysis type comparison of MRCE1 spectral shape

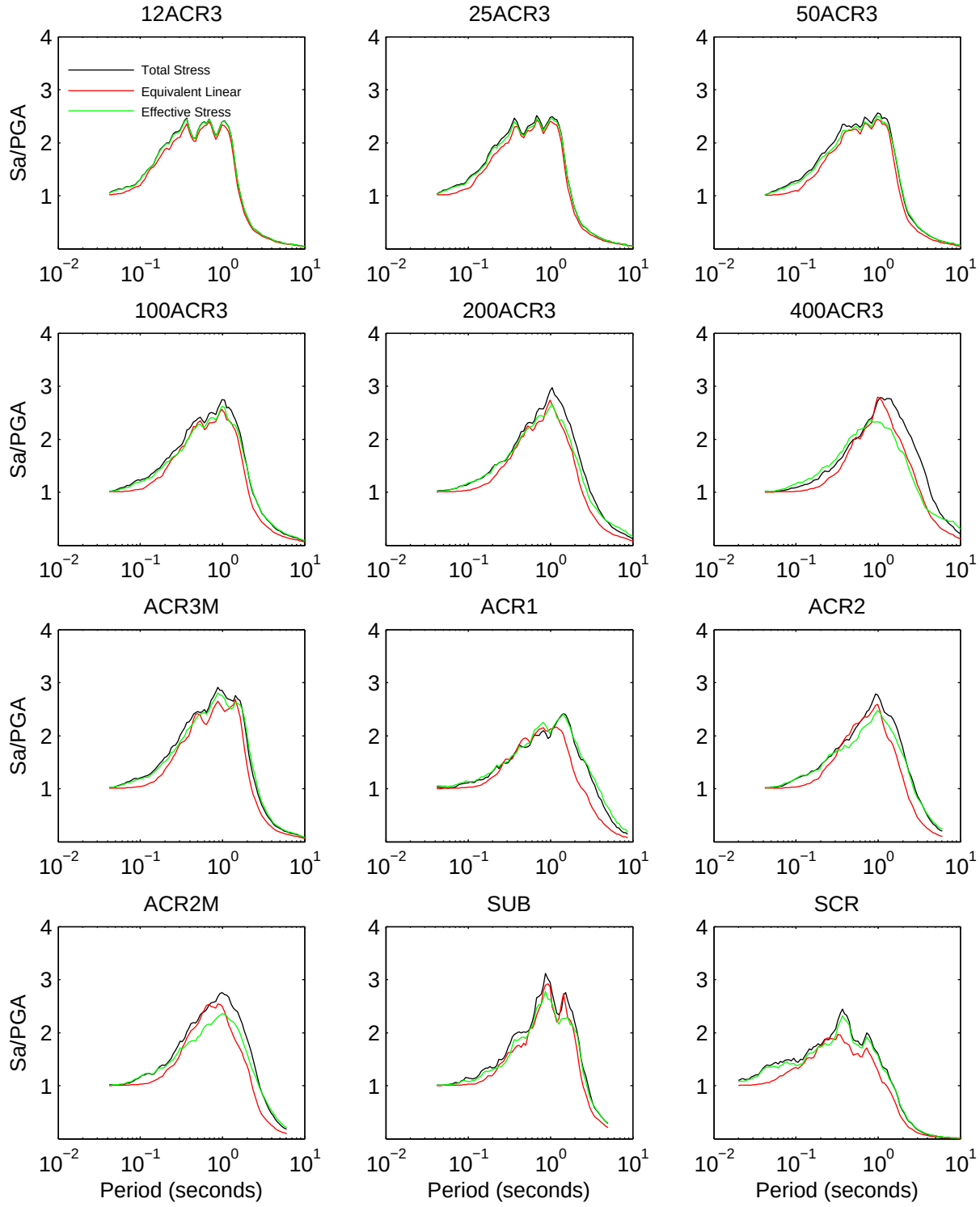

Figure 7C.16: Analysis type comparison of JSSS response spectra

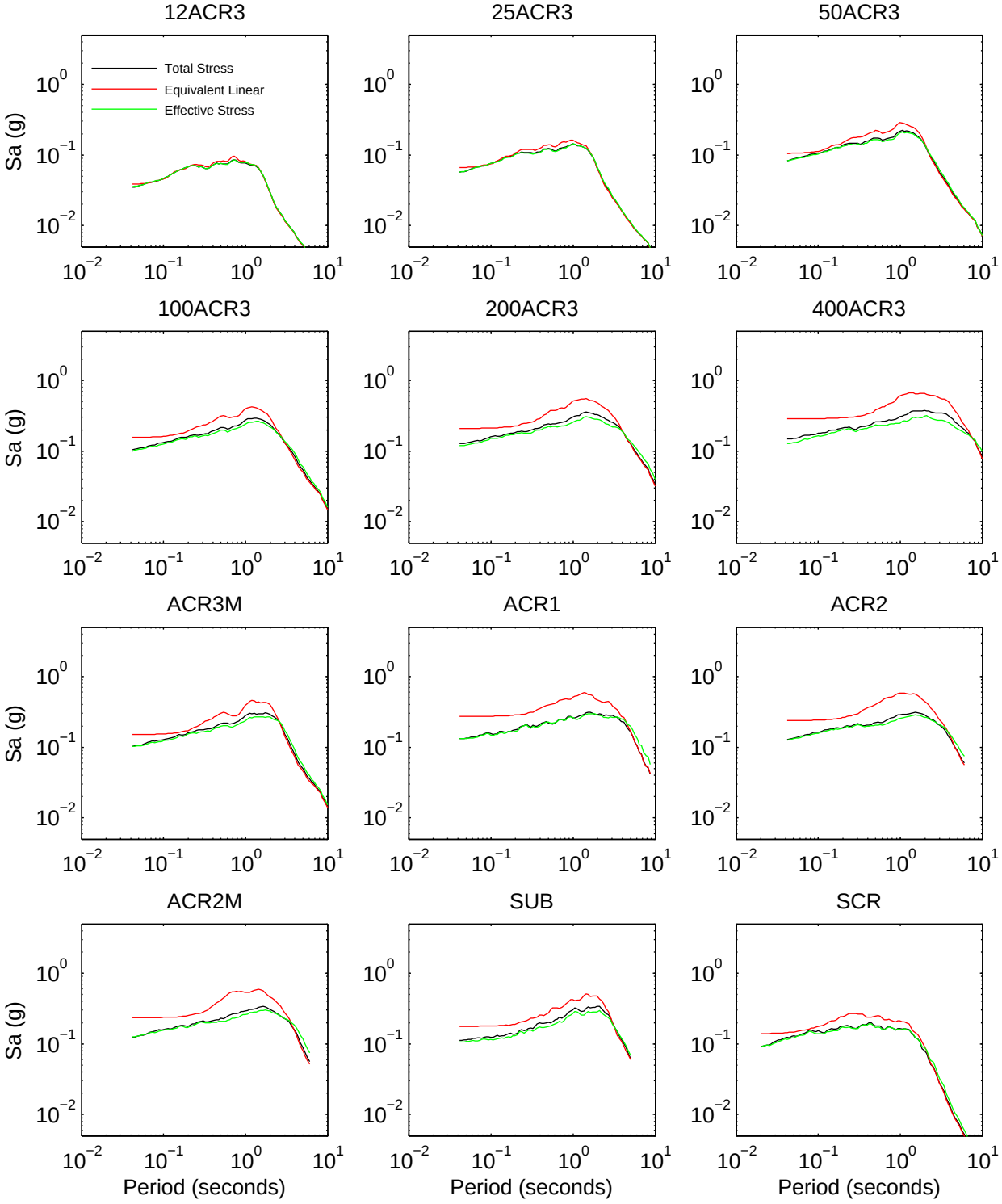

Figure 7C.17: Analysis type comparison of JSSS amplification

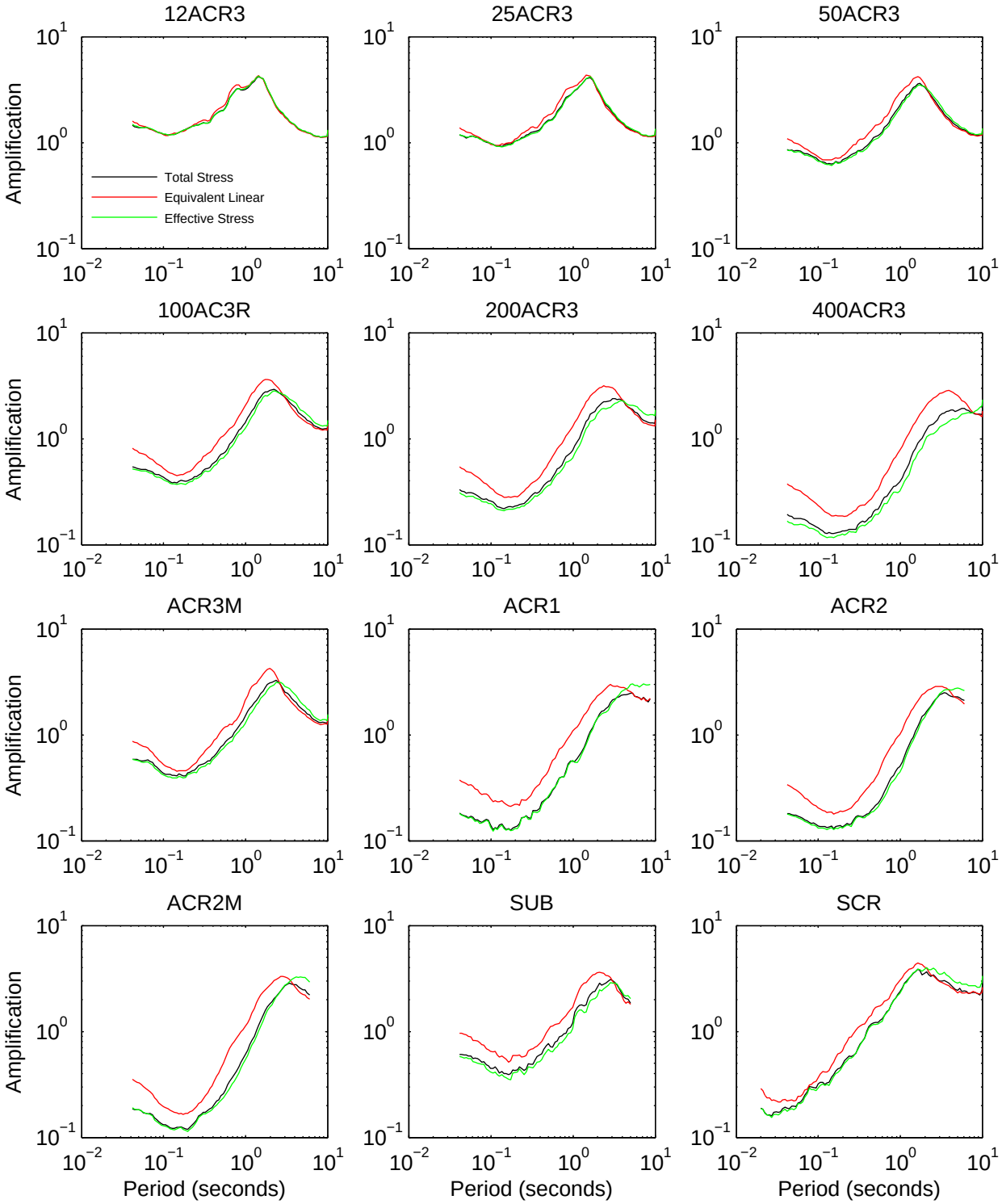

Figure 7C.18: Analysis type comparison of JSSS spectral shape

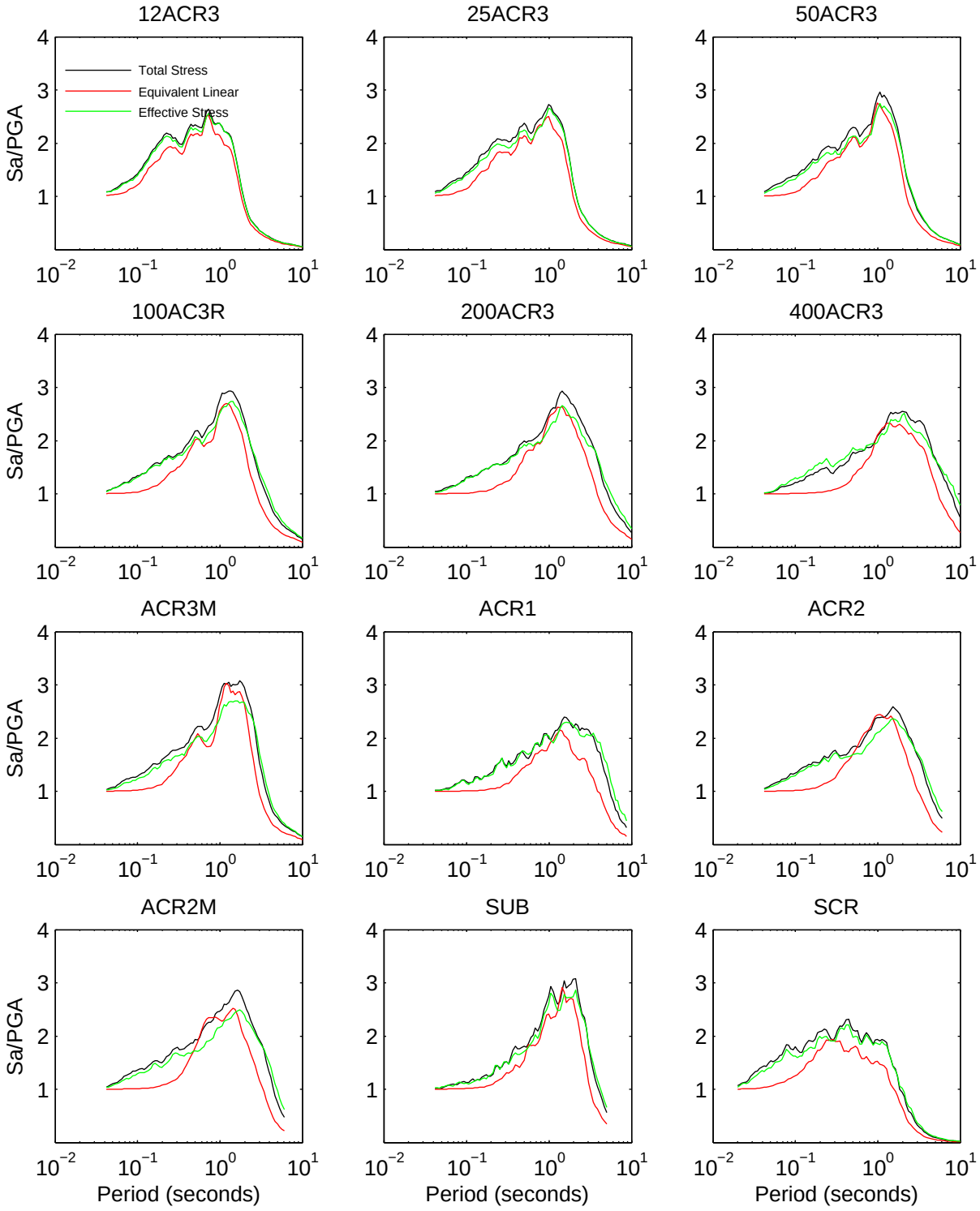

Figure 7C.19: Analysis type comparison of Bay Area response spectra

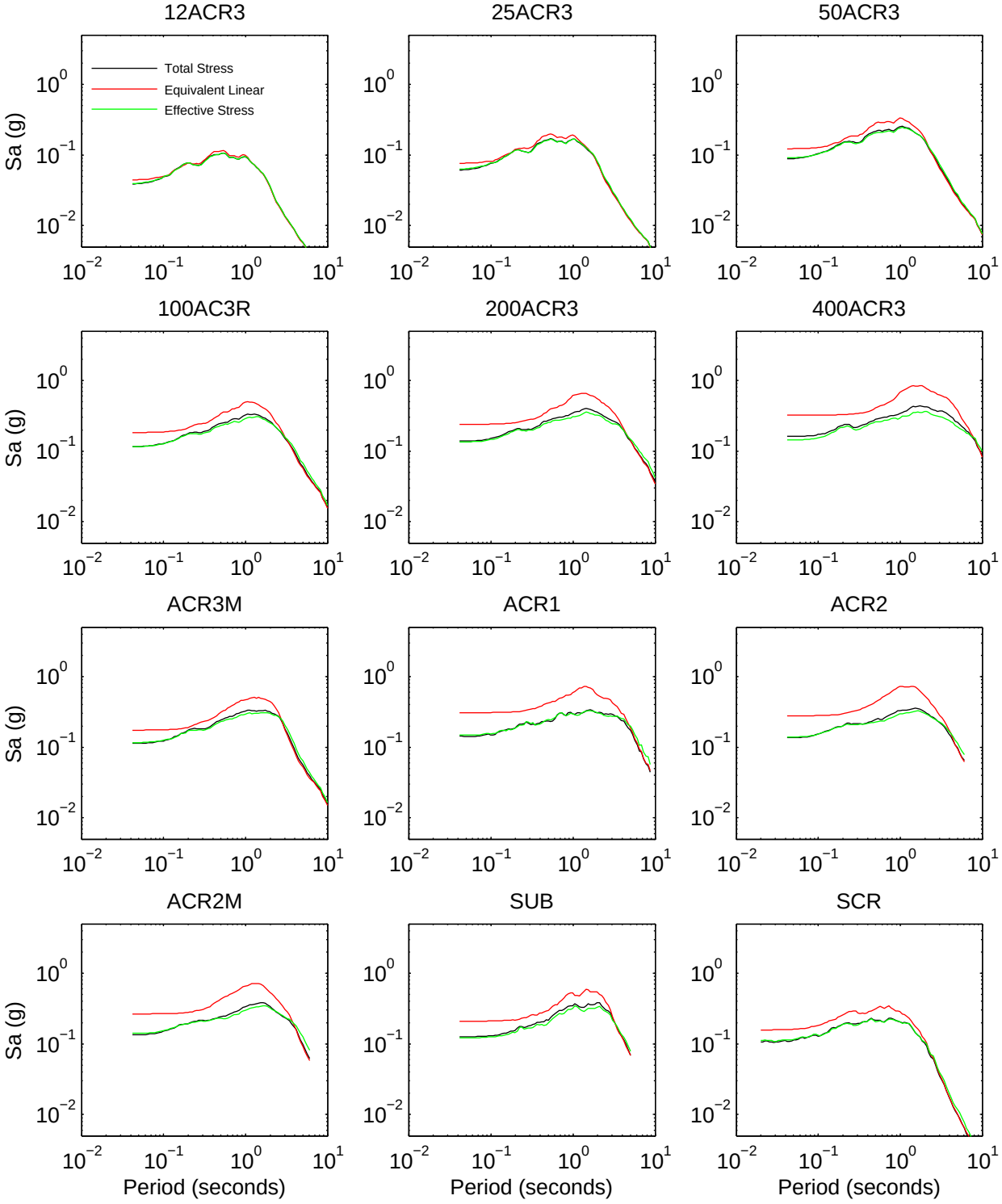

Figure 7C.20: Analysis type comparison of Bay Area amplification

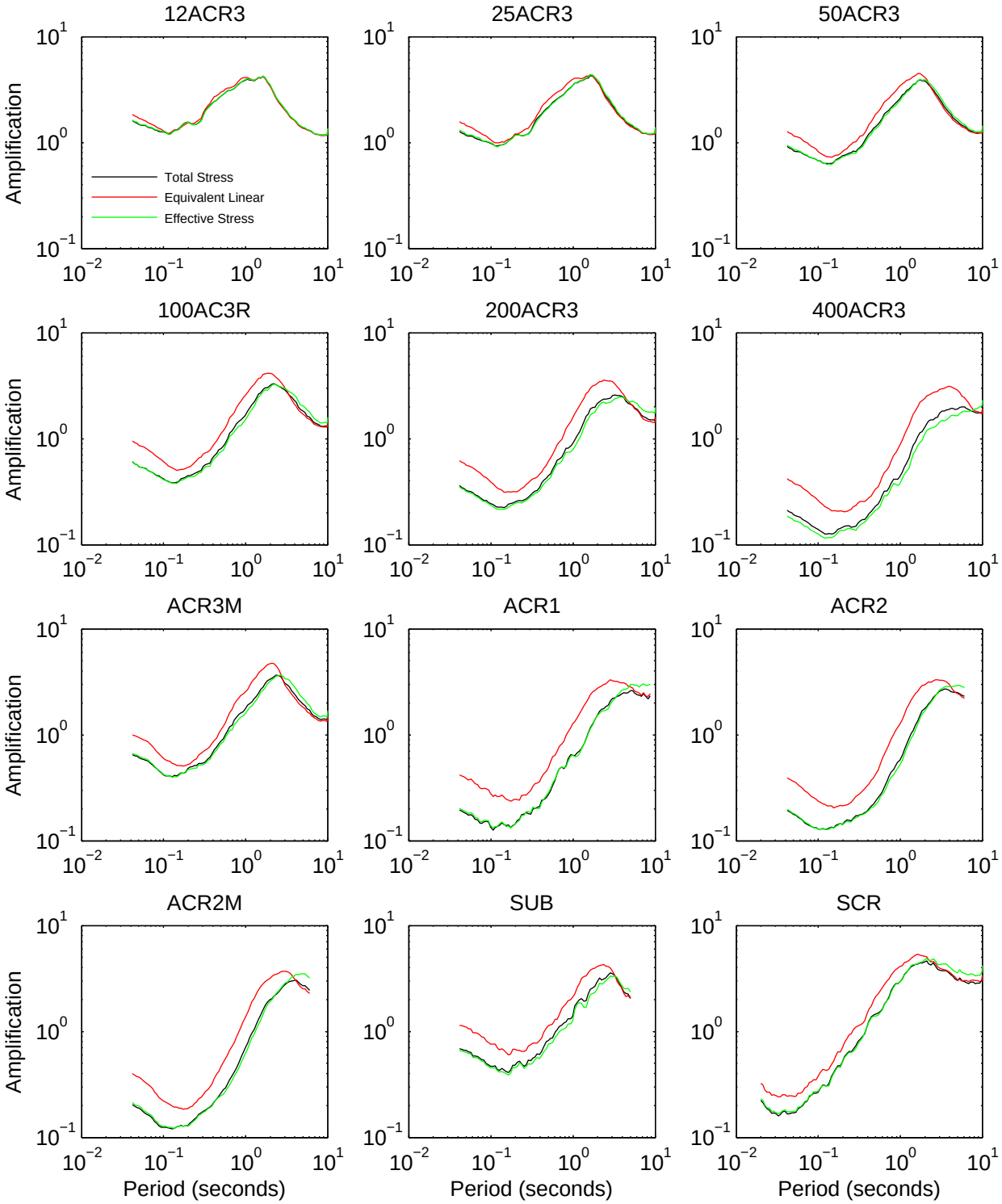

Figure 7C.21: Analysis type comparison of Bay Area spectral shape

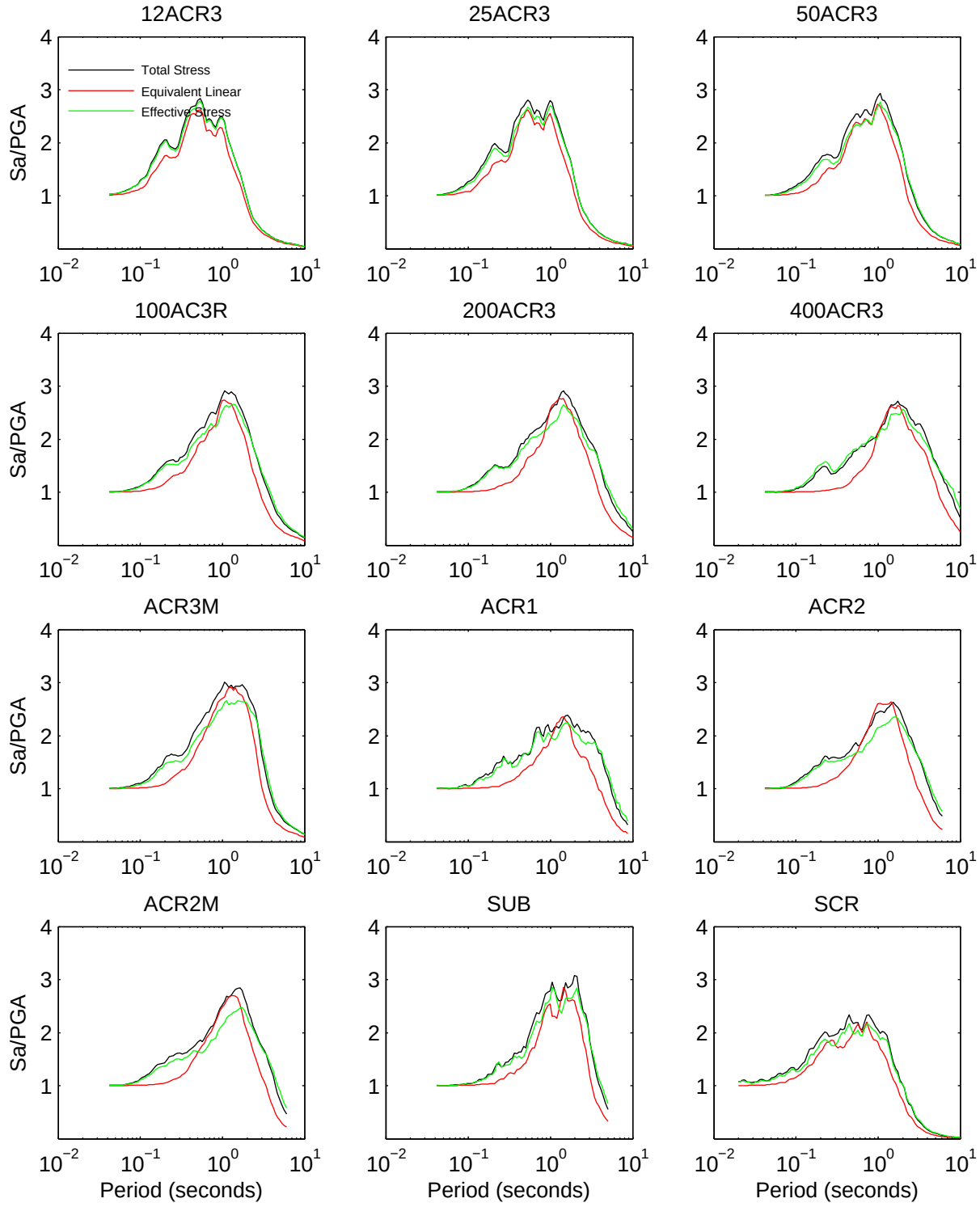

APPENDIX 7D: STANDARD DEVIATION OF THE SITE RESPONSE ANALYSES

Appendix 7D: Standard Deviation of the Site Response Analyses

Appendix 7D contains plots of the standard deviation calculated from the results of the site response analyses. Figures 7D.1 through 7D.15 show the response spectrum standard deviation and the amplification standard deviation for the given site and scenario. Figures 7D.16 through 7D.27 show the effects of soil strength, MRD curves, and elastic site period on the response spectrum standard deviation and the amplification standard deviation. Figure 7D.28 through 7D.41 compare the response spectrum standard deviation and the amplification standard deviation calculated from equivalent linear, nonlinear total stress, and nonlinear effective stress analyses. Each figure corresponds to one site and has 12 plots, which each correspond to a different scenario.

Figure 7D.1: Response spectra and amplification standard deviation for site Bay Area

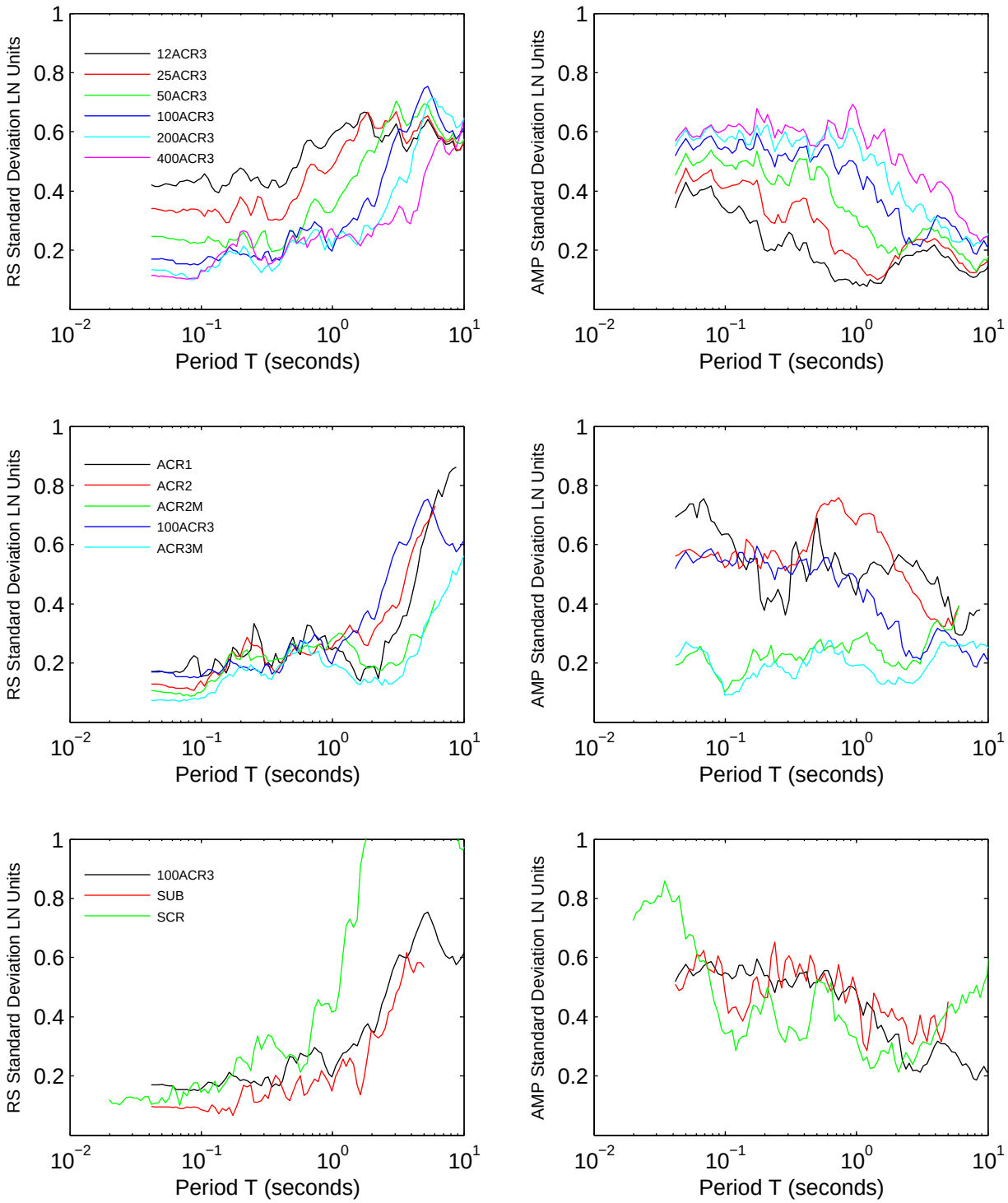

Figure 7D.2: Response spectra and amplification standard deviation for site Bay Area F

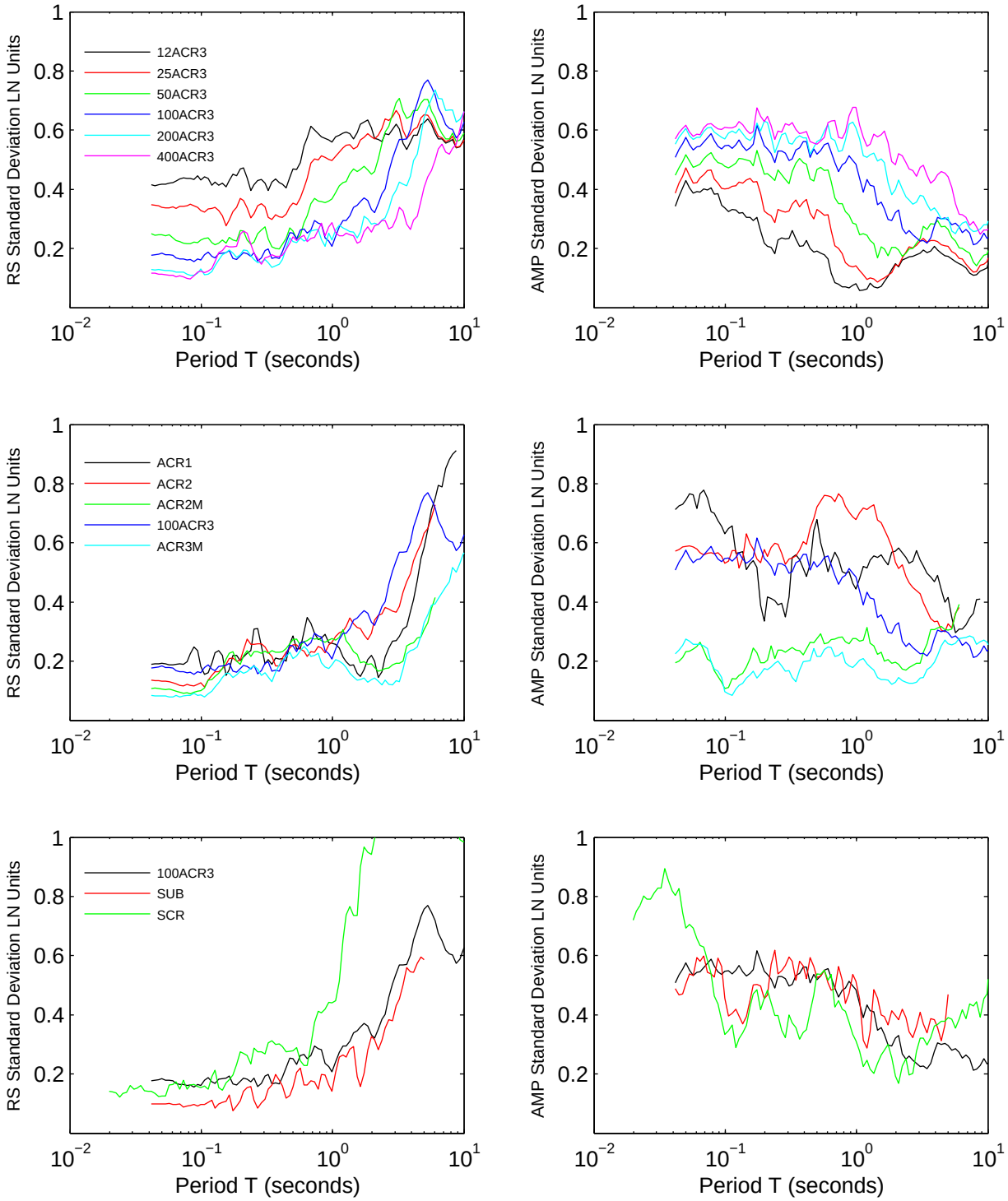

Figure 7D.3: Response spectra and amplification standard deviation for site Bay Area II

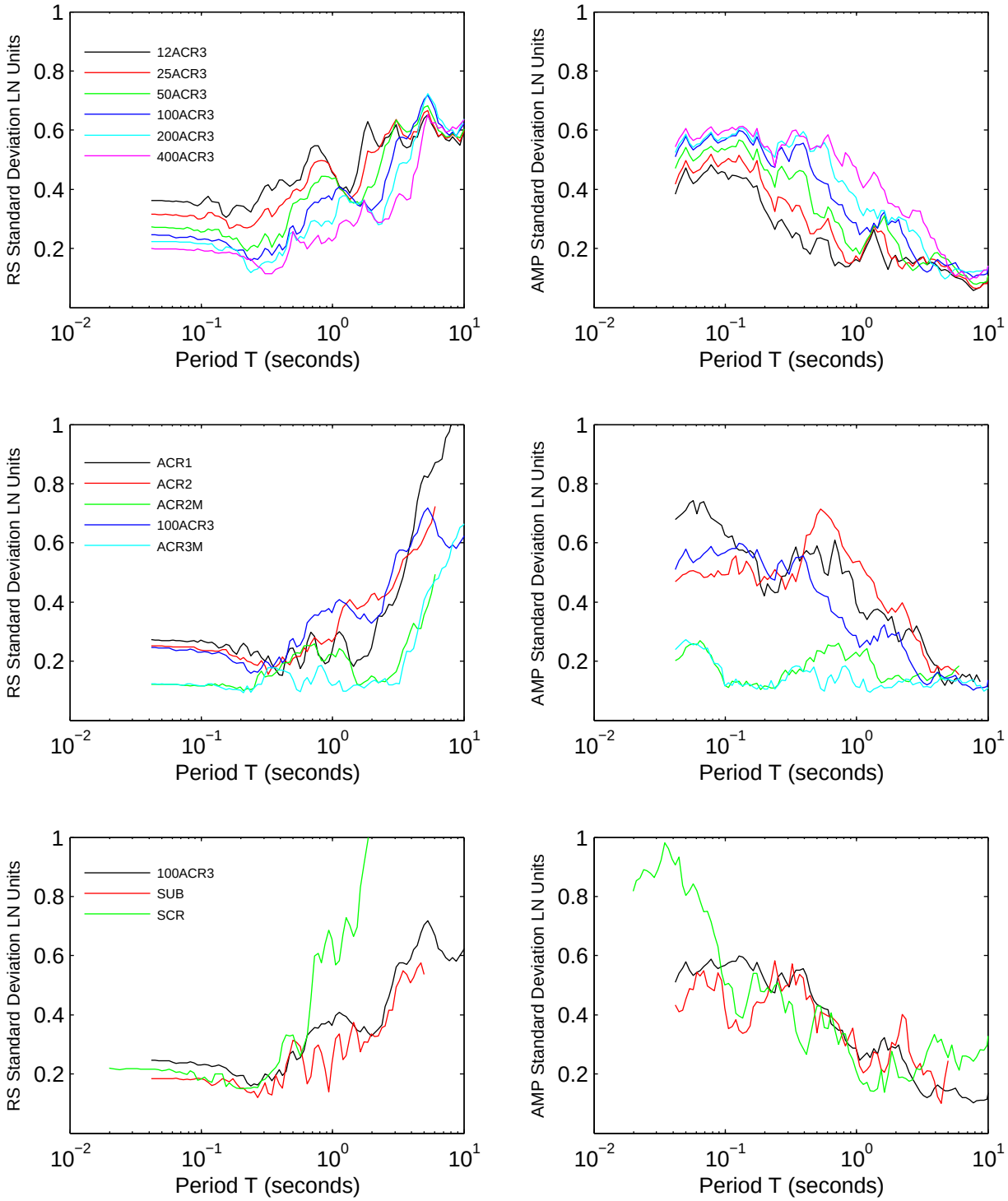

Figure 7D.4: Response spectra and amplification standard deviation for site Bay Area II K

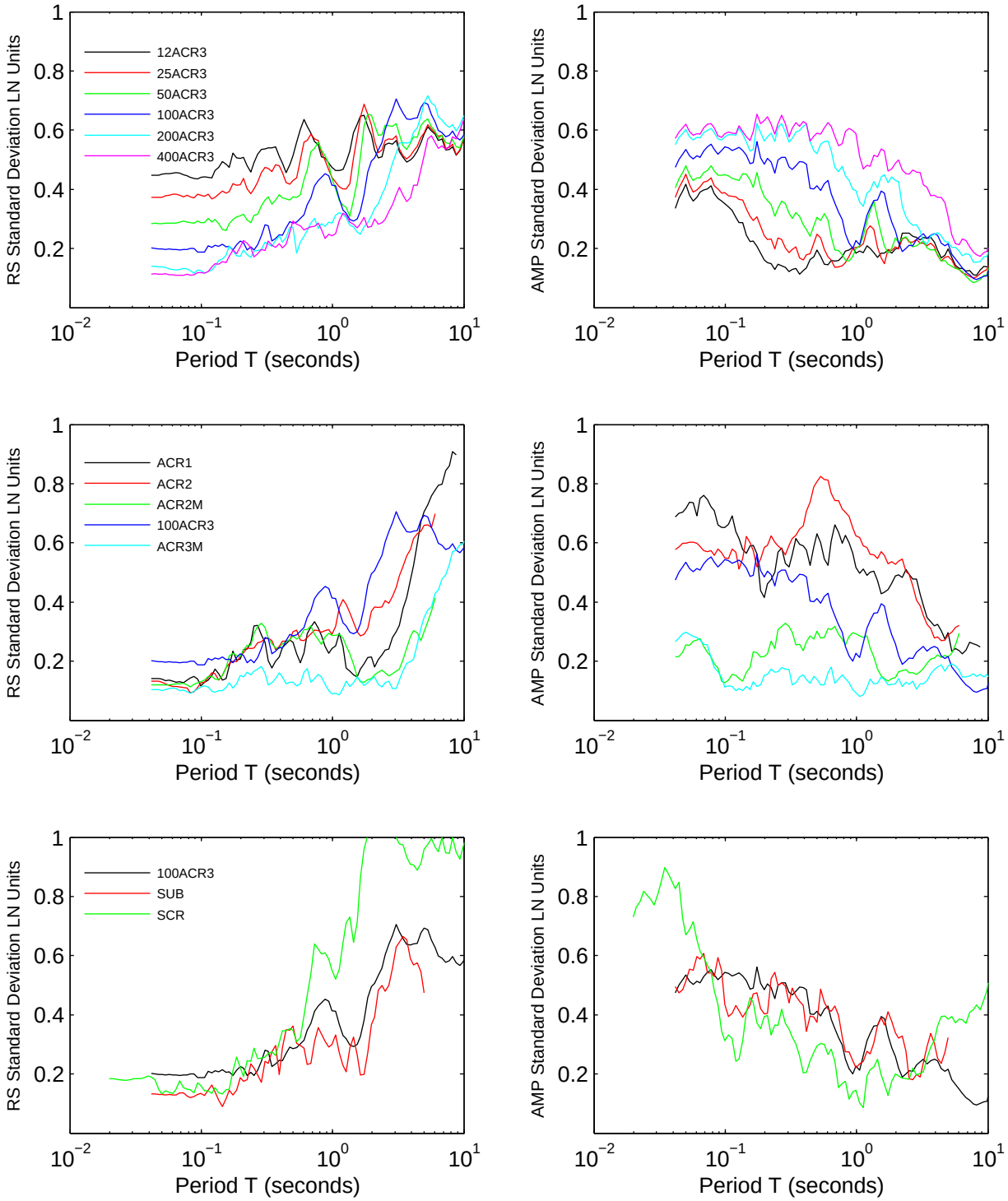

Figure 7D.5: Response spectra and amplification standard deviation for site Bay Area II K S2

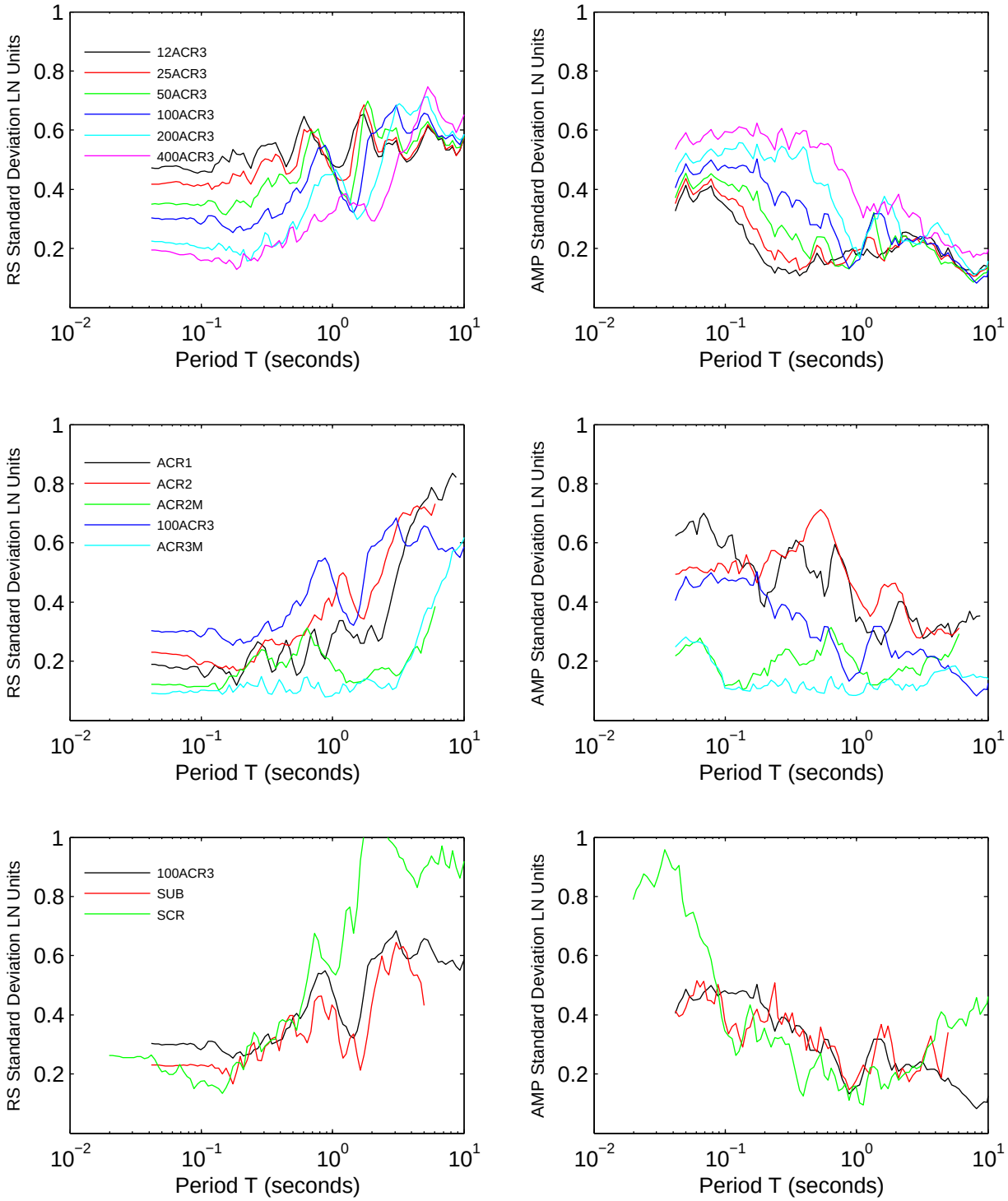

Figure 7D.6: Response spectra and amplification standard deviation for site Bay Area II K S4

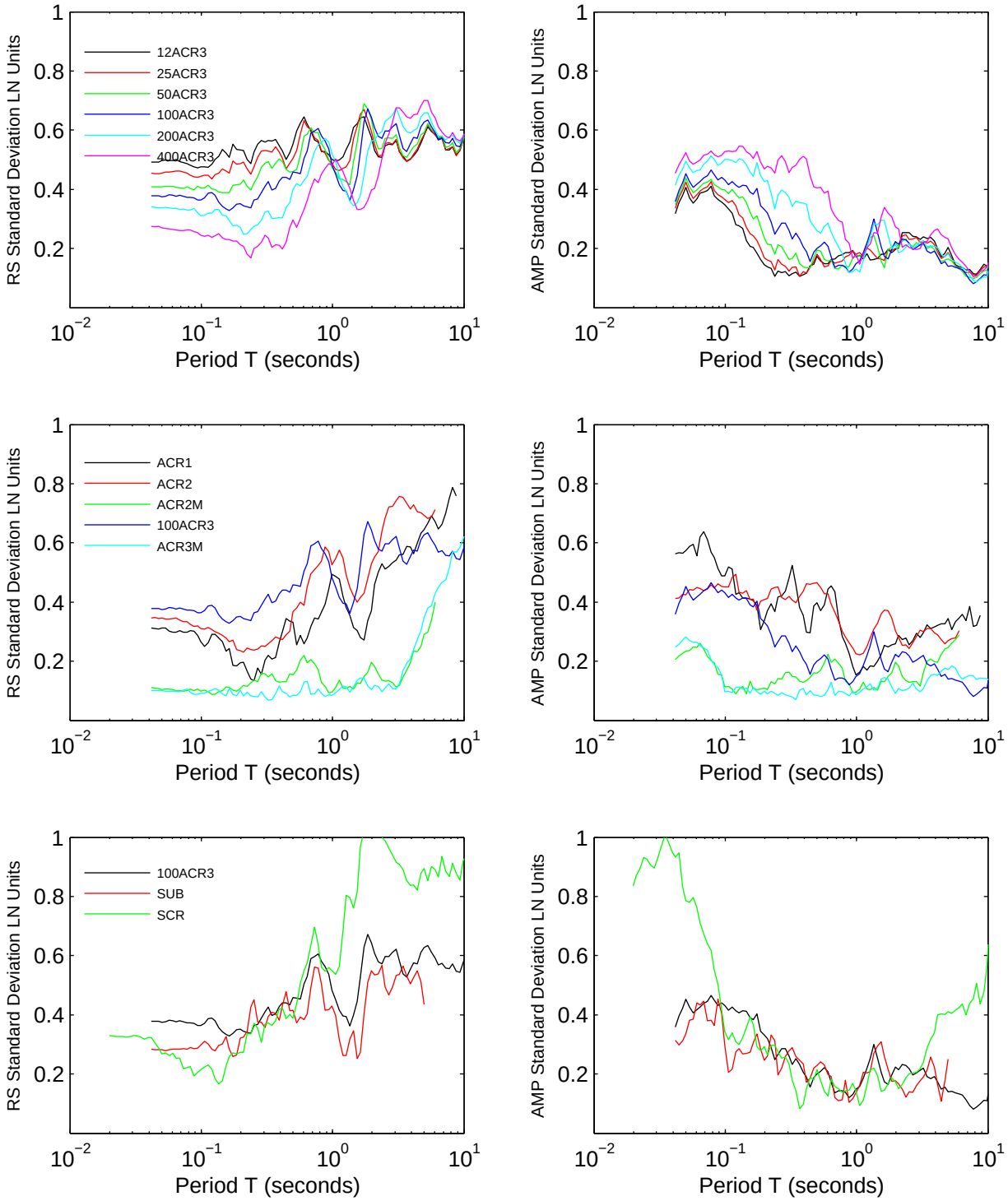

Figure 7D.7: Response spectra and amplification standard deviation for site HAGP

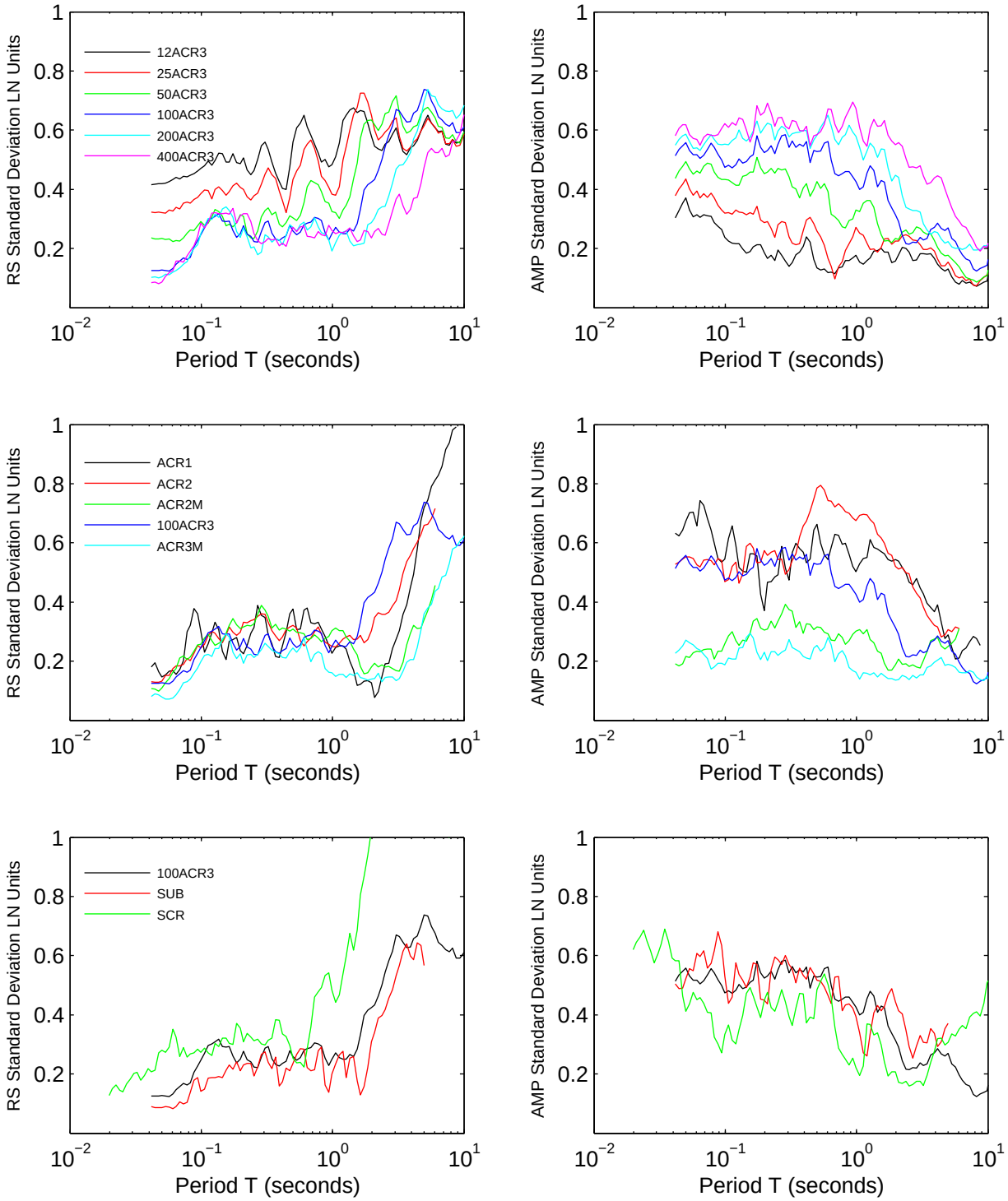

Figure 7D.8: Response spectra and amplification standard deviation for site JSSS

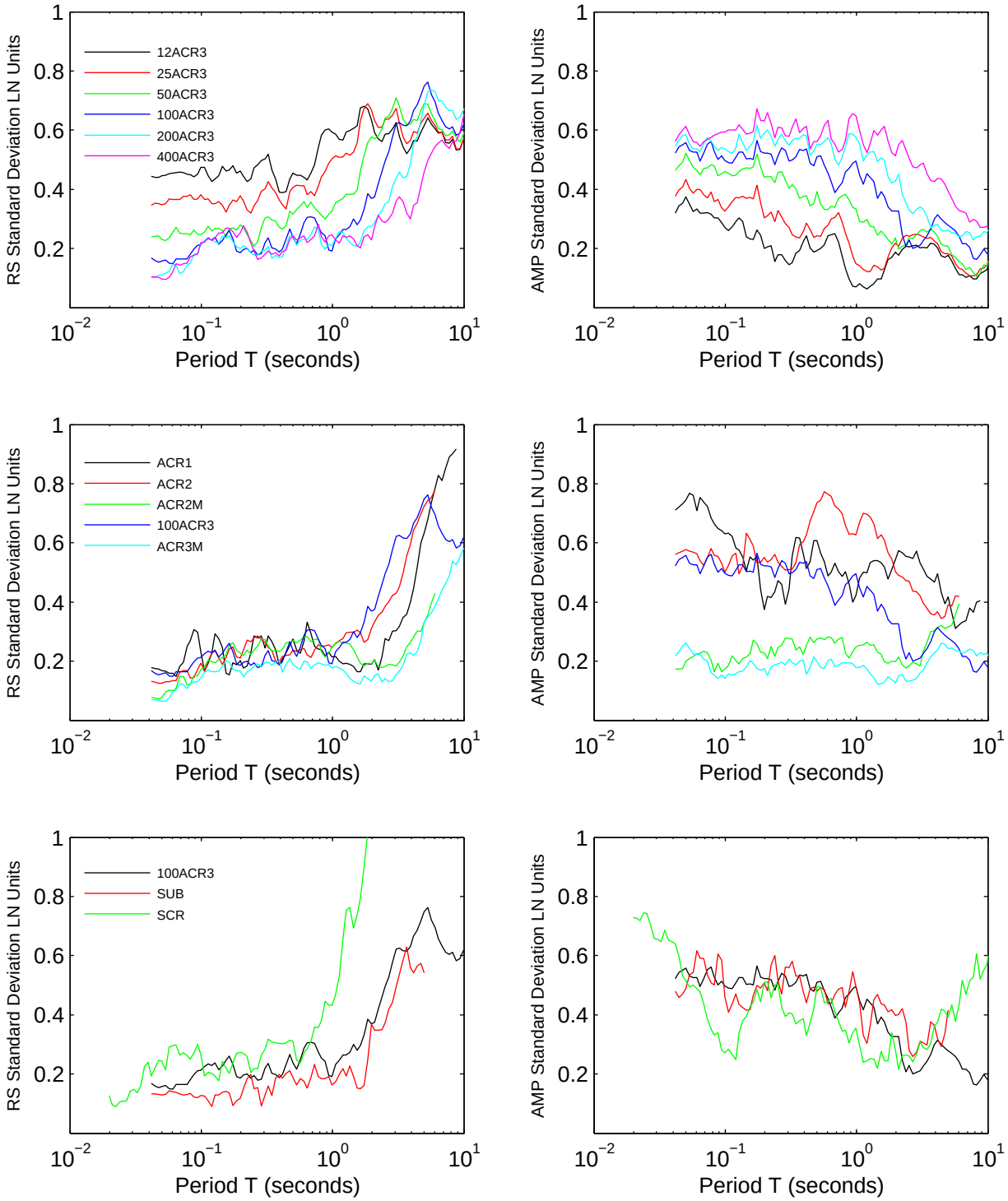

Figure 7D.9: Response spectra and amplification standard deviation for site KIKNET

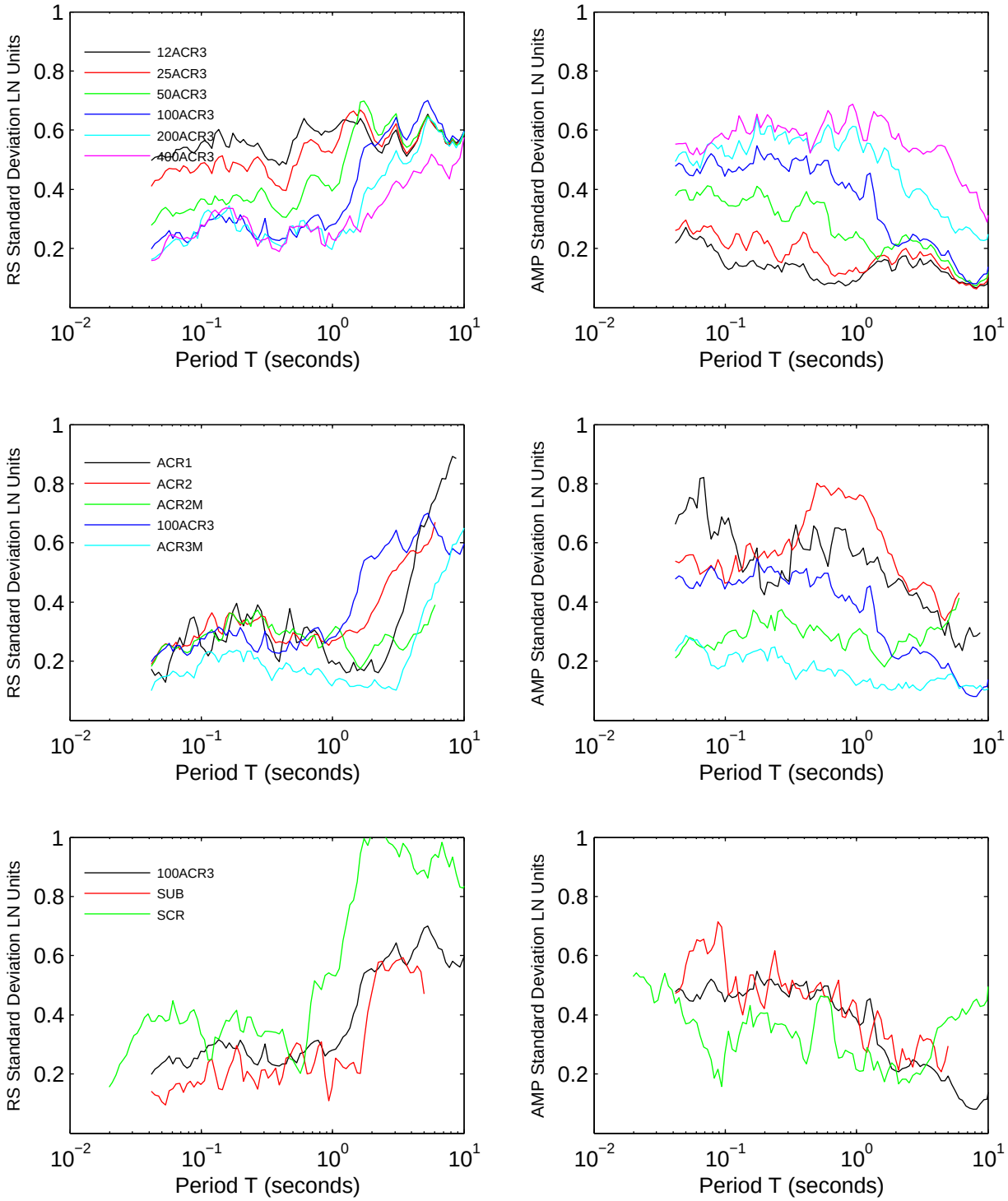

Figure 7D.10: Response spectra and amplification standard deviation for site KIKNET S2

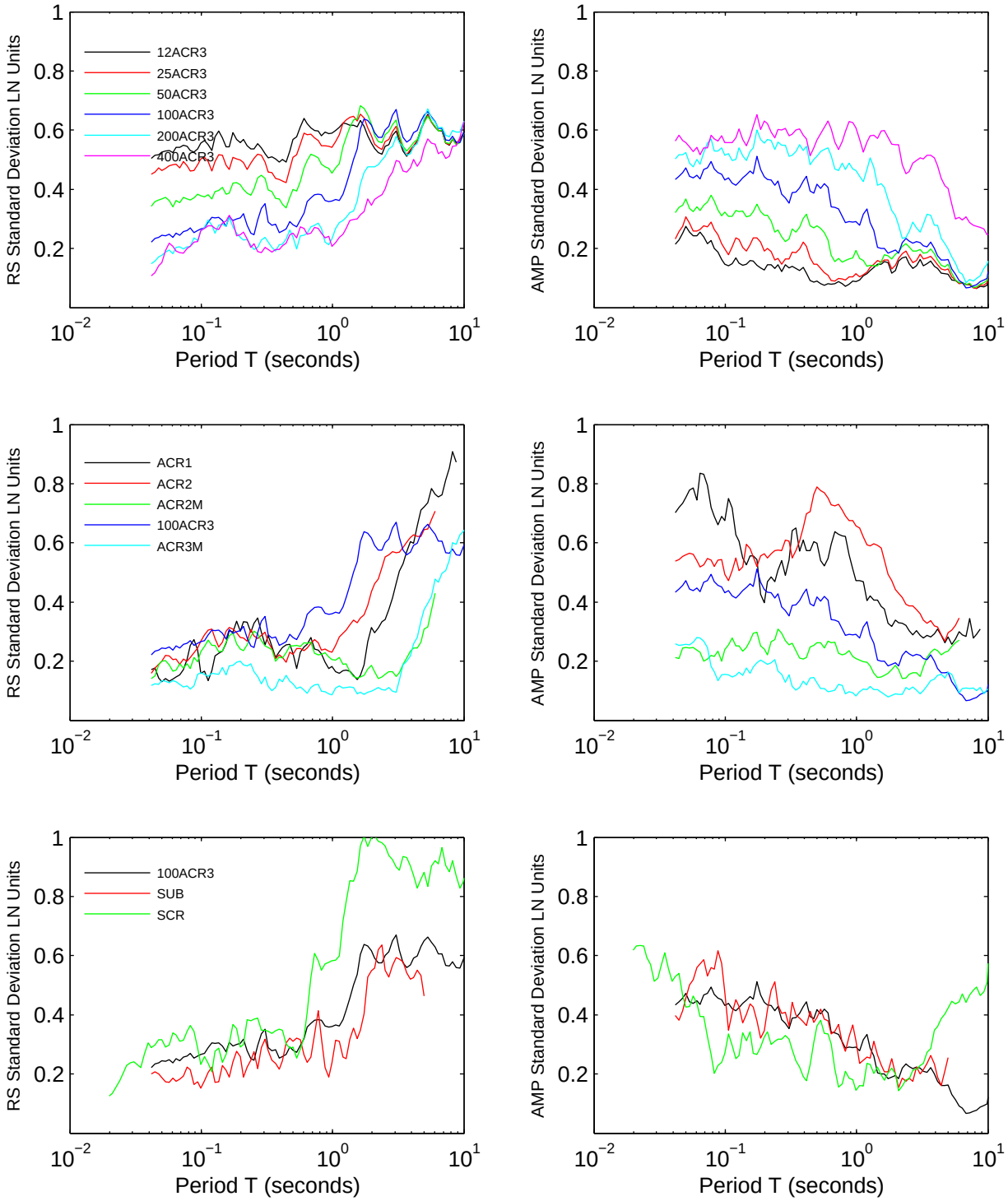

Figure 7D.11: Response spectra and amplification standard deviation for site KIKNET S4

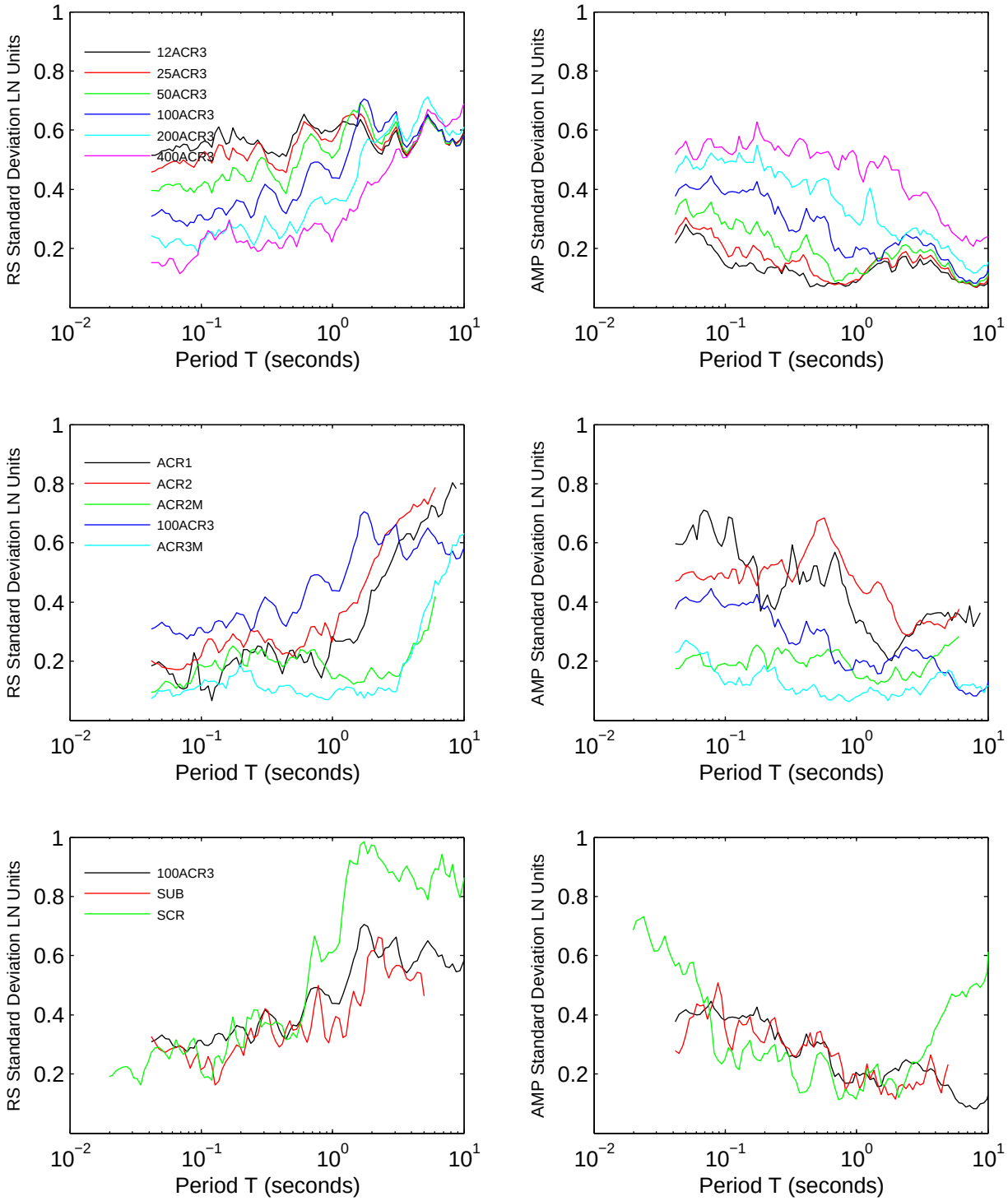

Figure 7D.12: Response spectra and amplification standard deviation for site KIKNET40

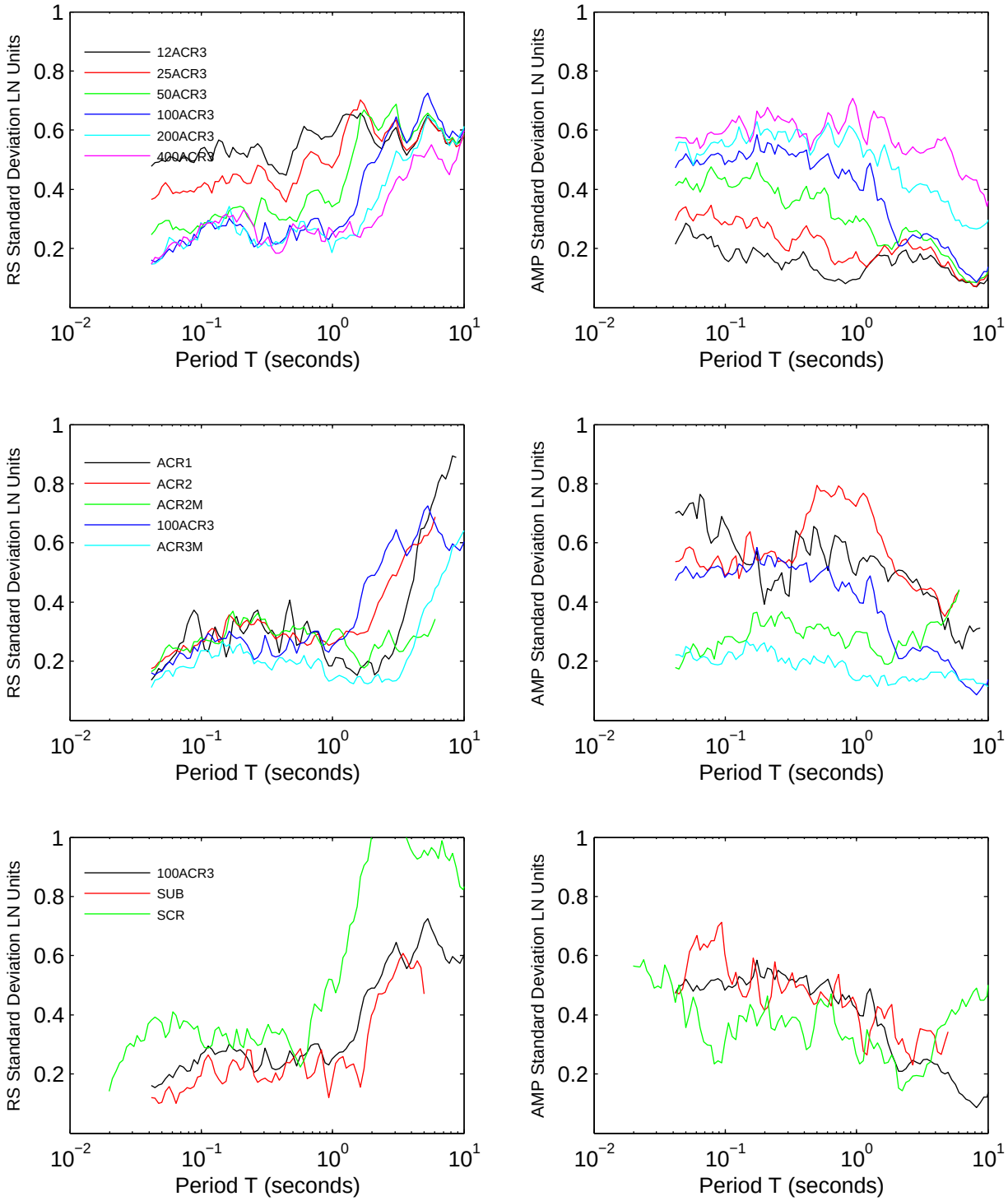

Figure 7D.13: Response spectra and amplification standard deviation for site KIKNET160

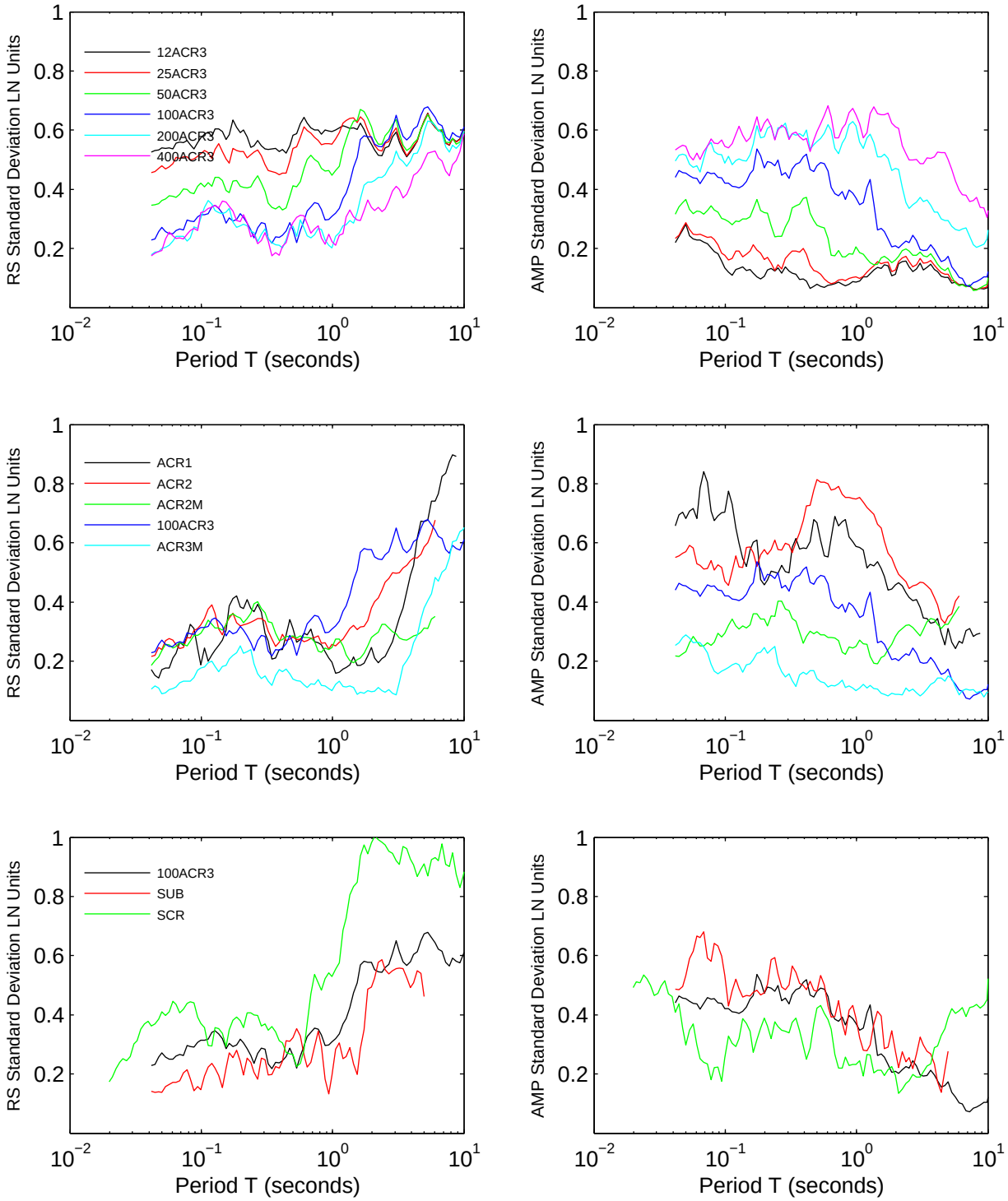

Figure 7D.14: Response spectra and amplification standard deviation for site MRCE1

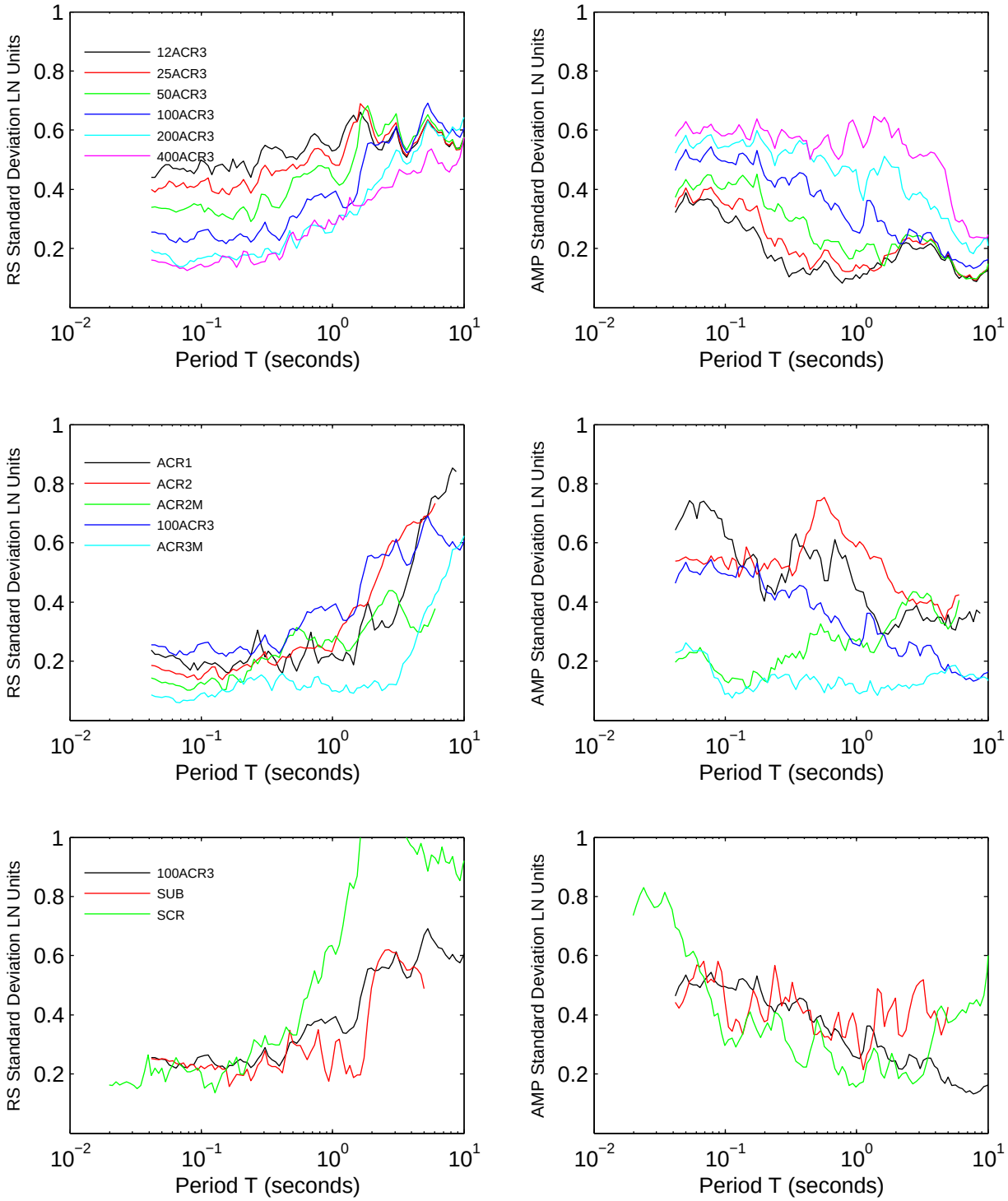

Figure 7D.15: Response spectra and amplification standard deviation for site MRCE2

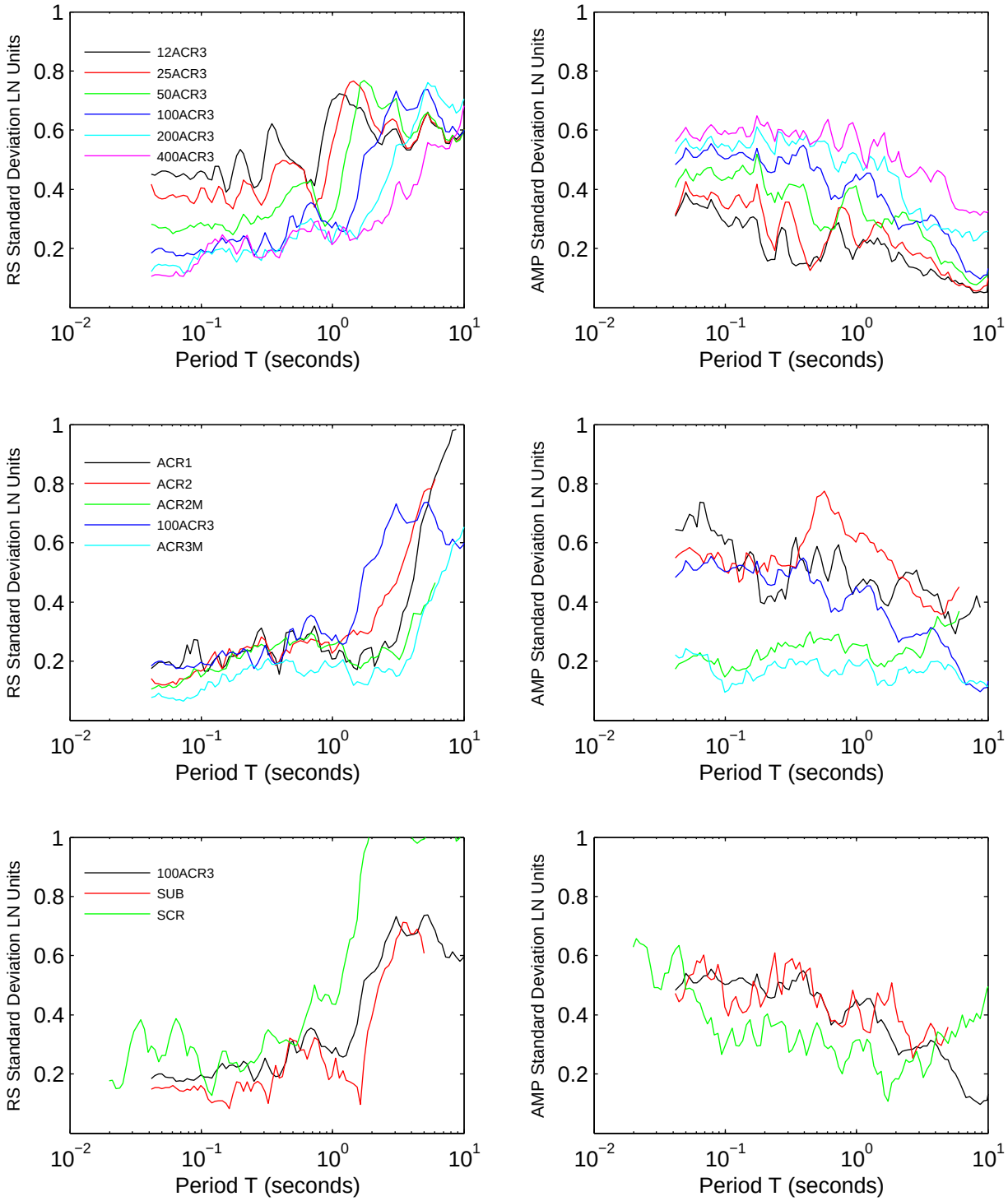

Figure 7D.16: Effect of strength on the standard deviation of response spectra for scenarios 1−6

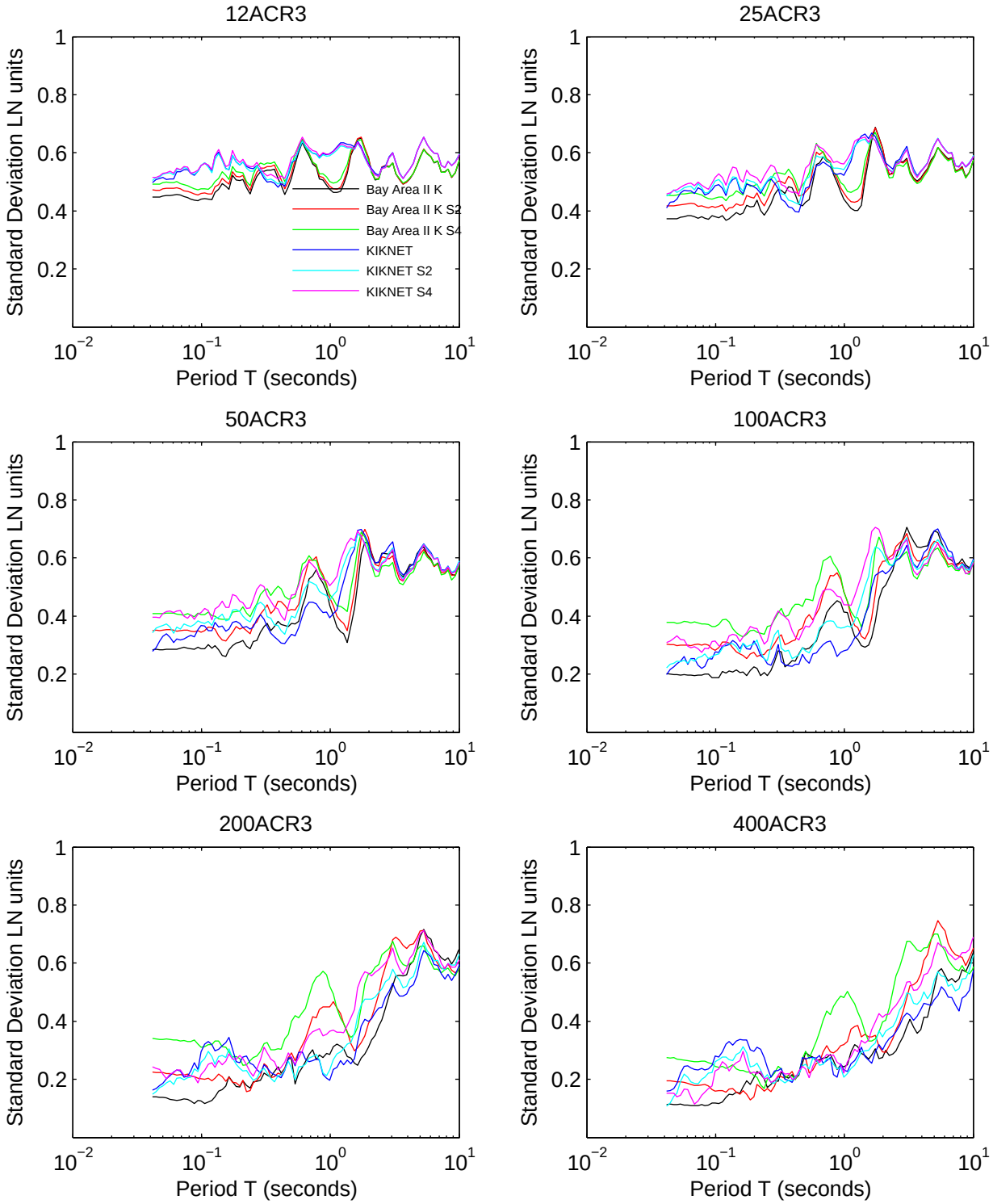

Figure 7D.17: Effect of strength on the standard deviation of response spectra for scenarios 7−12

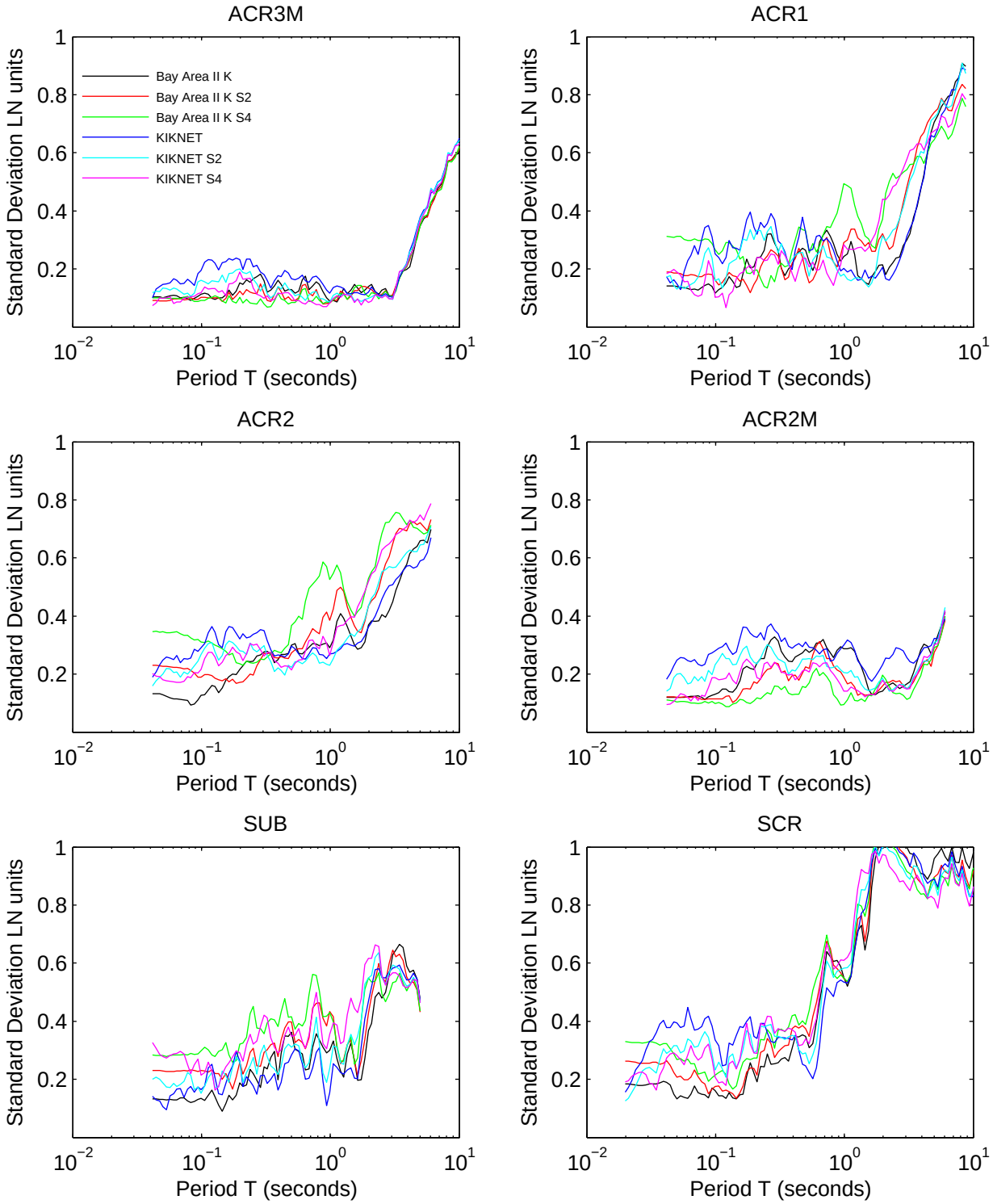

Figure 7D.18: Effect of strength on the standard deviation of amplification for scenarios 1−6

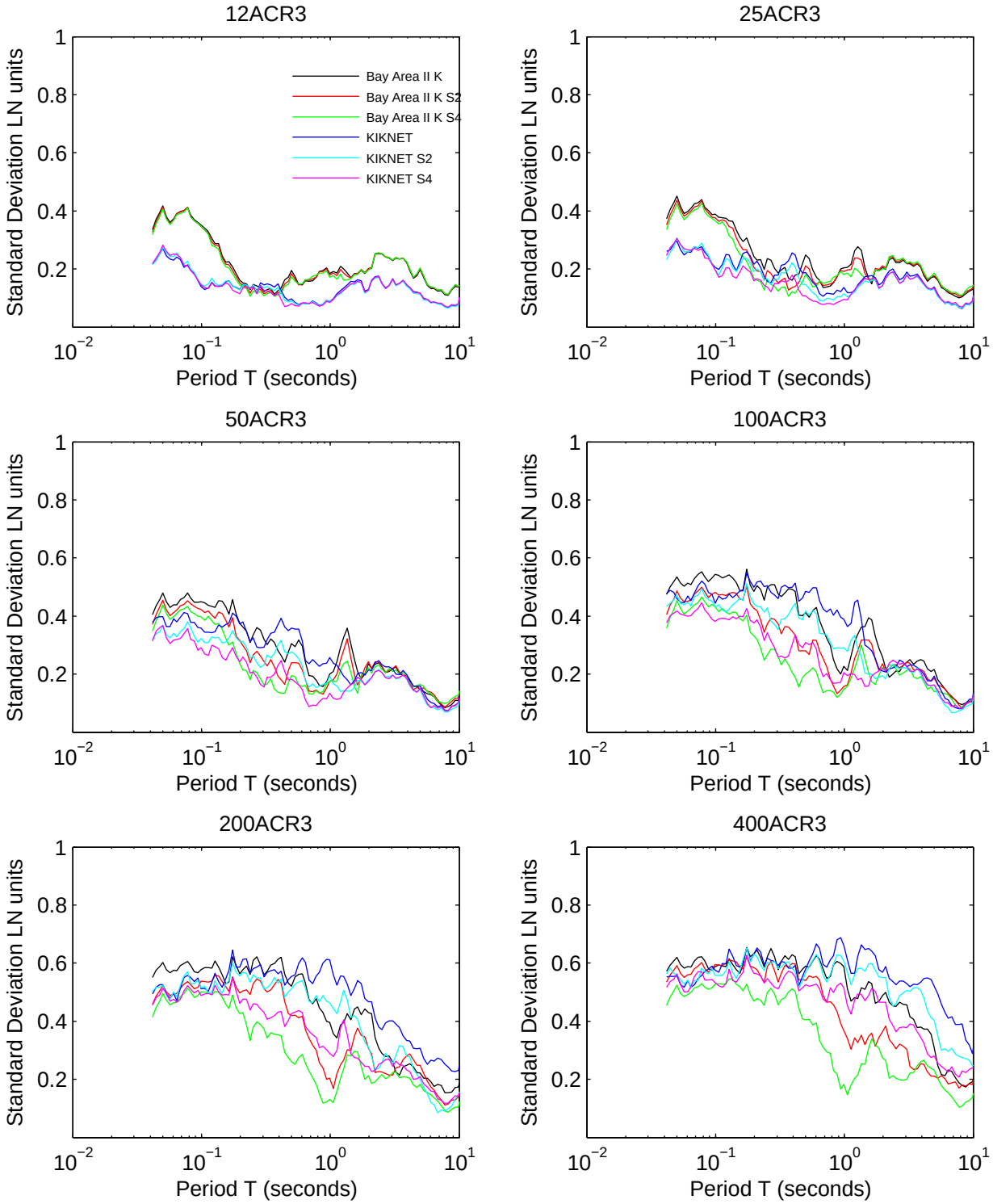

Figure 7D.19: Effect of strength on the standard deviation of amplification for scenarios 7−12

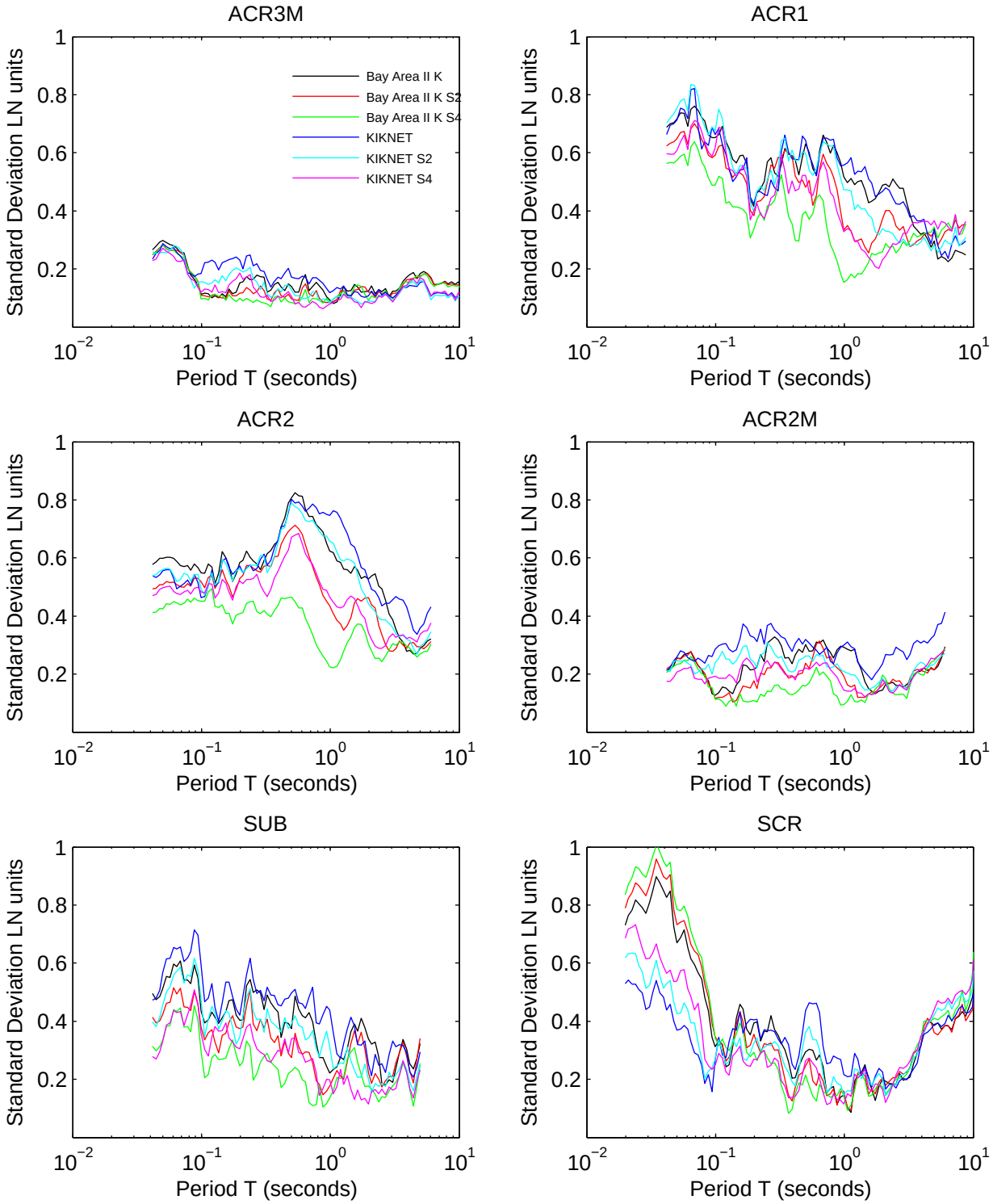

Figure 7D.20: Effect of MRD on the standard deviation of response spectra for scenarios 1−6

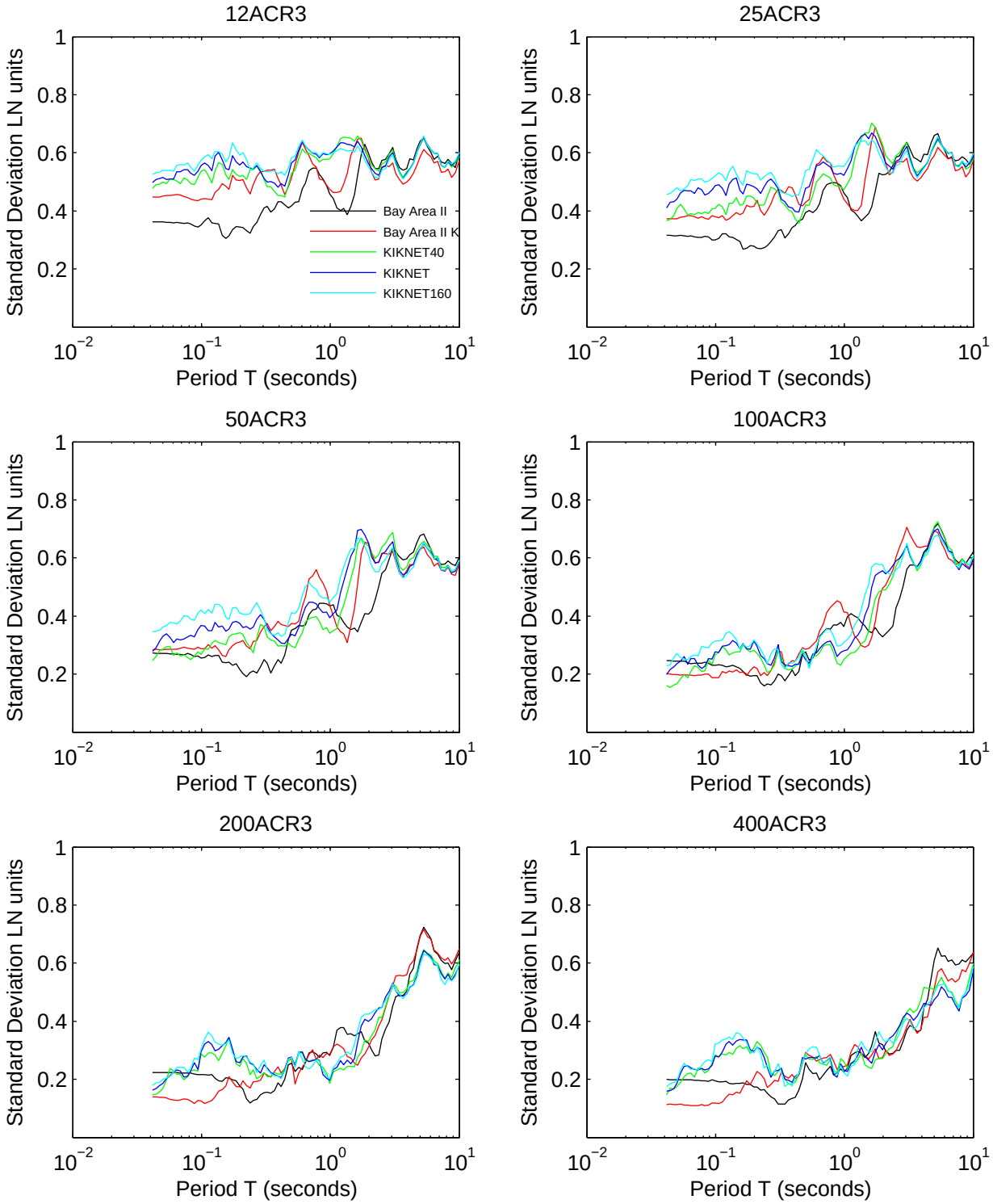

Figure 7D.21: Effect of MRD on the standard deviation of response spectra for scenarios 7−12

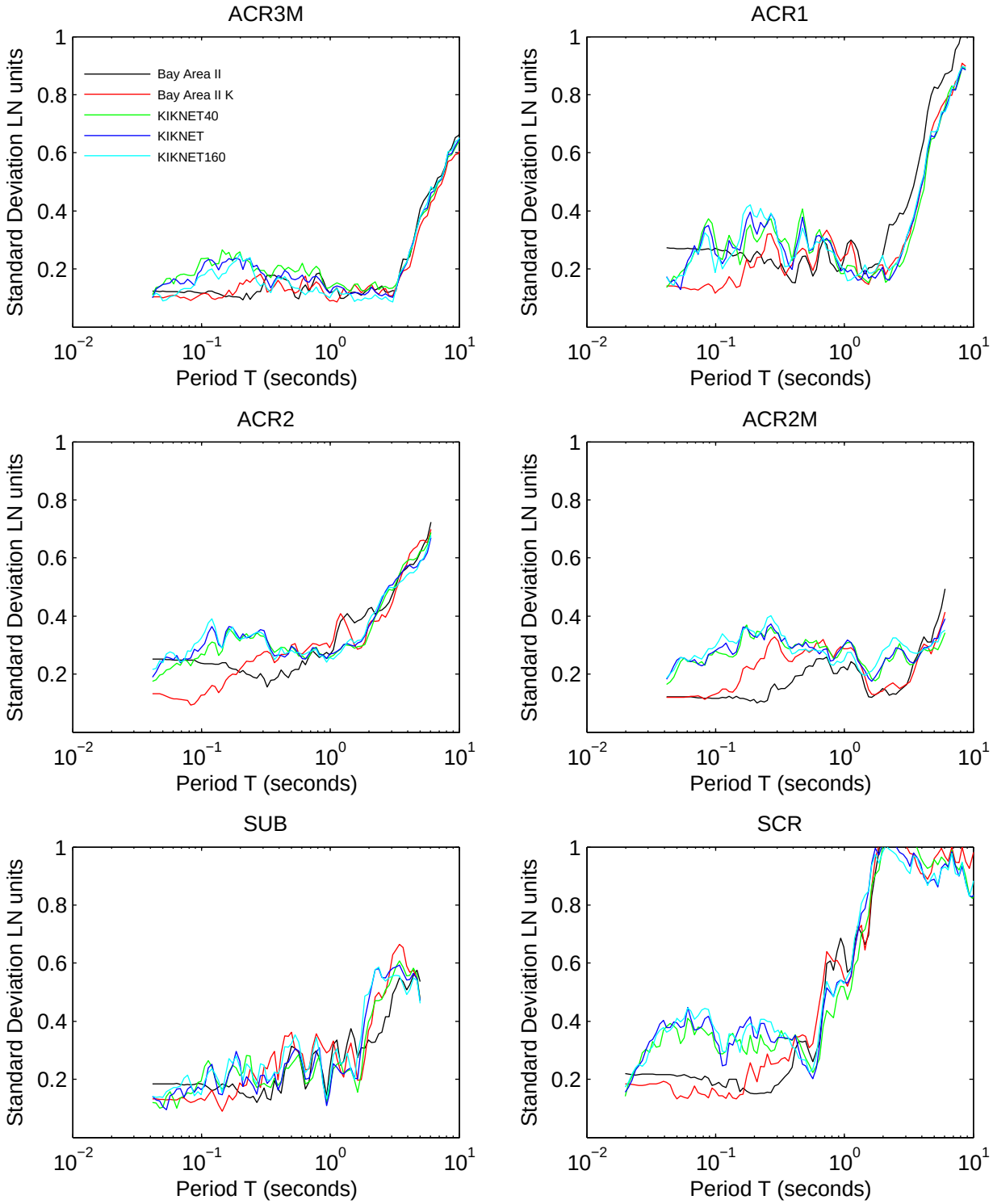

Figure 7D.22: Effect of MRD on the standard deviation of amplification for scenarios 1−6

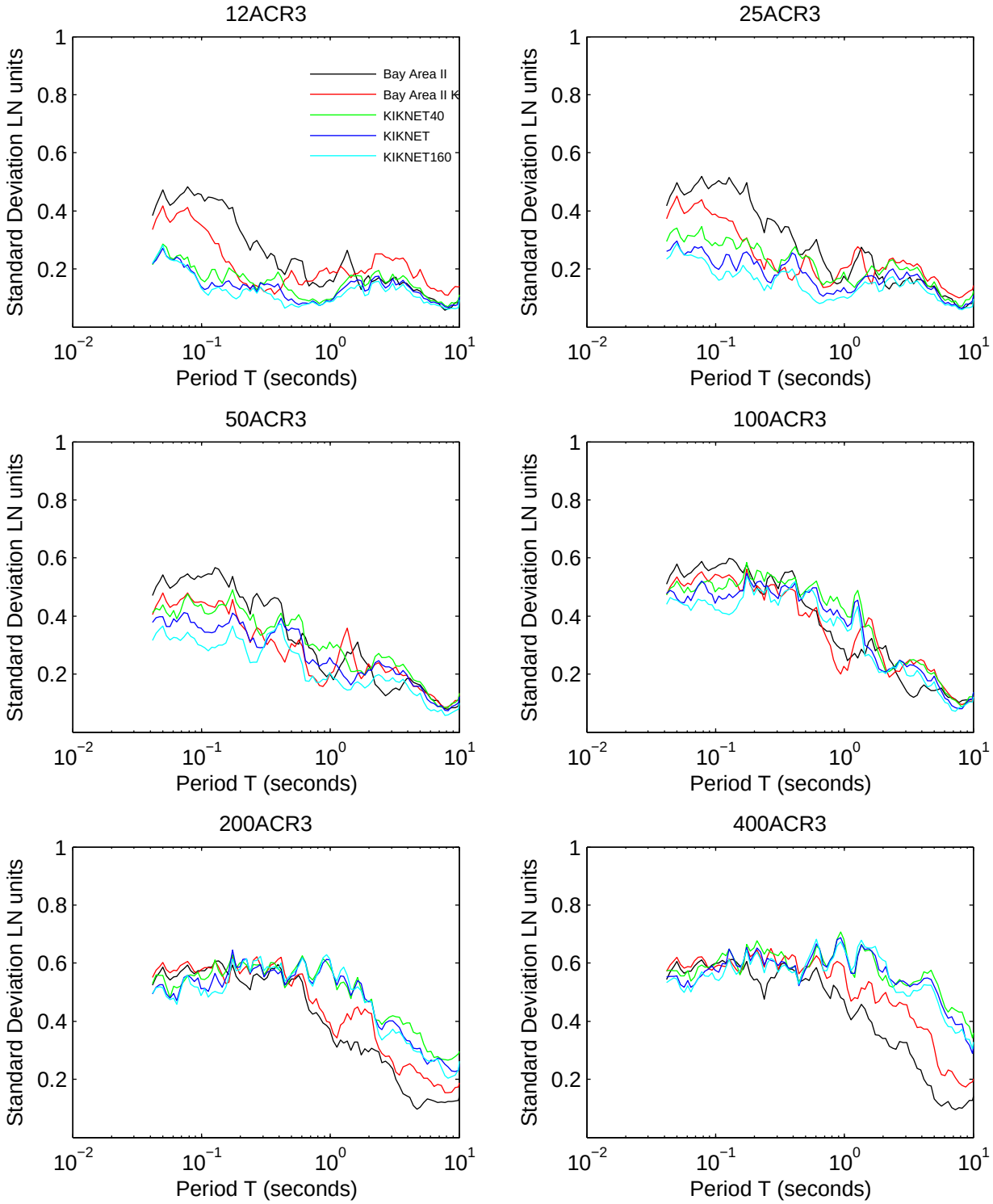

Figure 7D.23: Effect of MRD on the standard deviation of amplification for scenarios 7−12

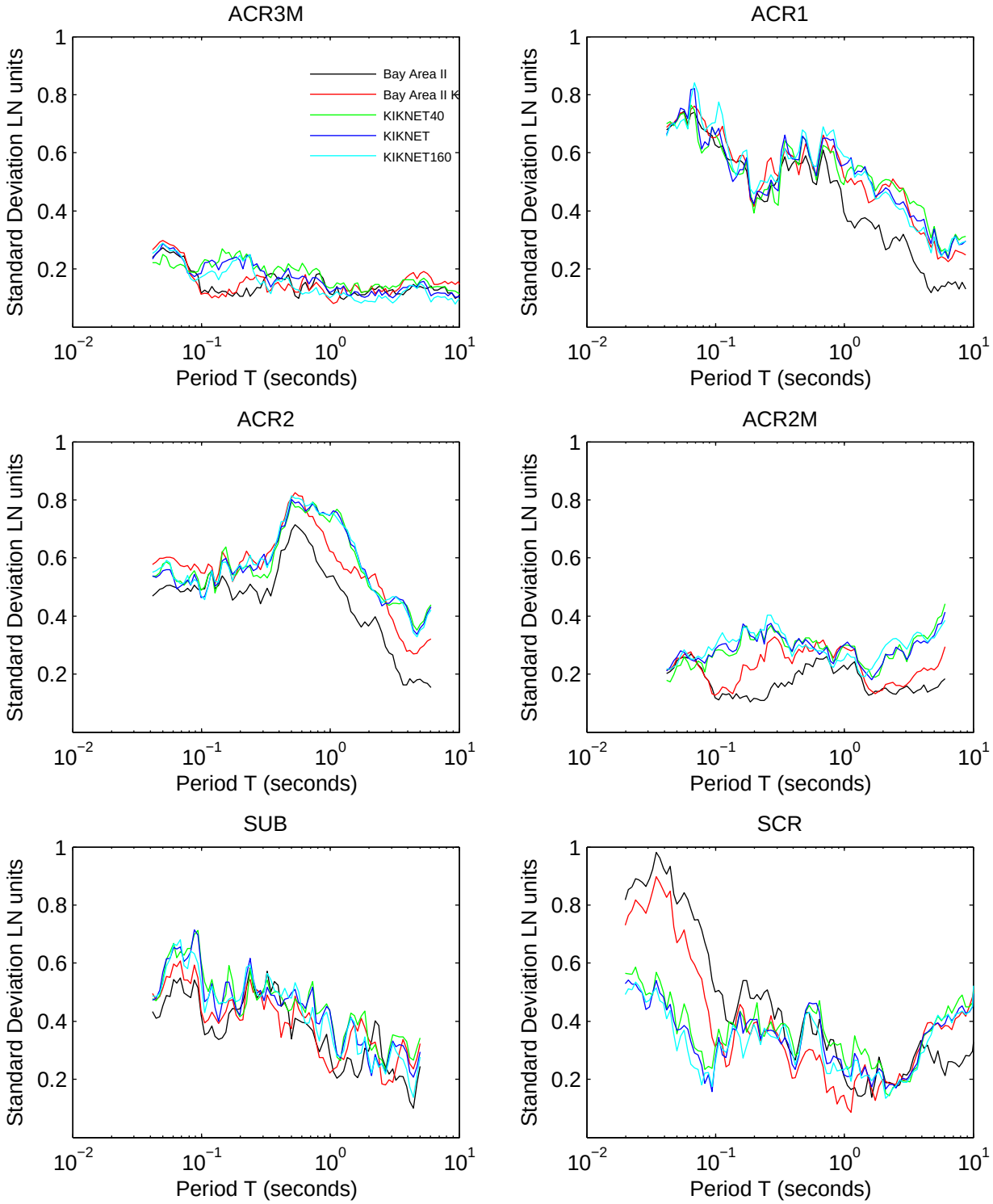

Figure 7D.24: Effect of elastic site period on the standard deviation of response spectra for scenarios 1−6

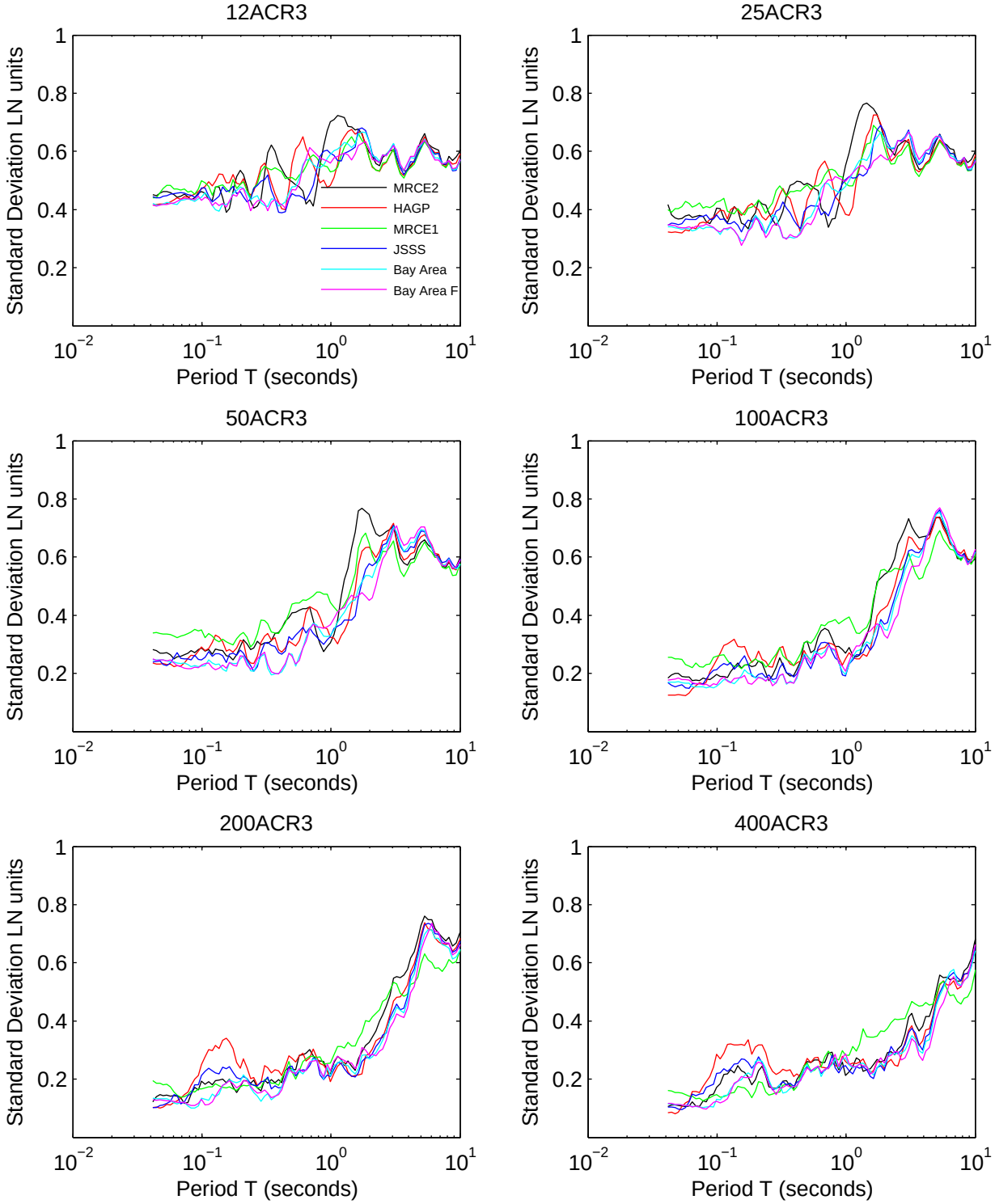

Figure 7D.25: Effect of elastic site period on the standard deviation of response spectra for scenarios 7−12

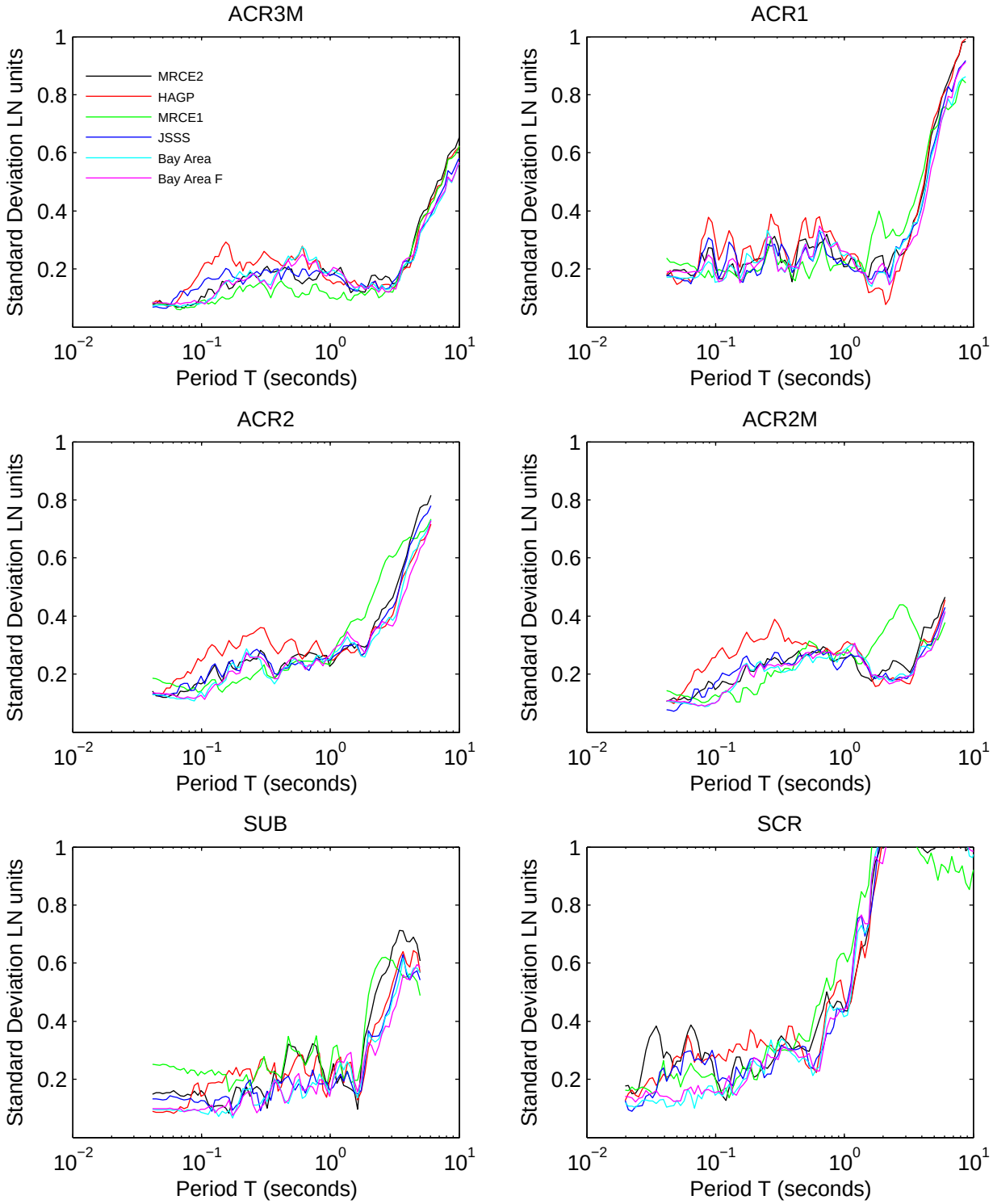

Figure 7D.26: Effect of elastic site period on the standard deviation of amplification for scenarios 1−6

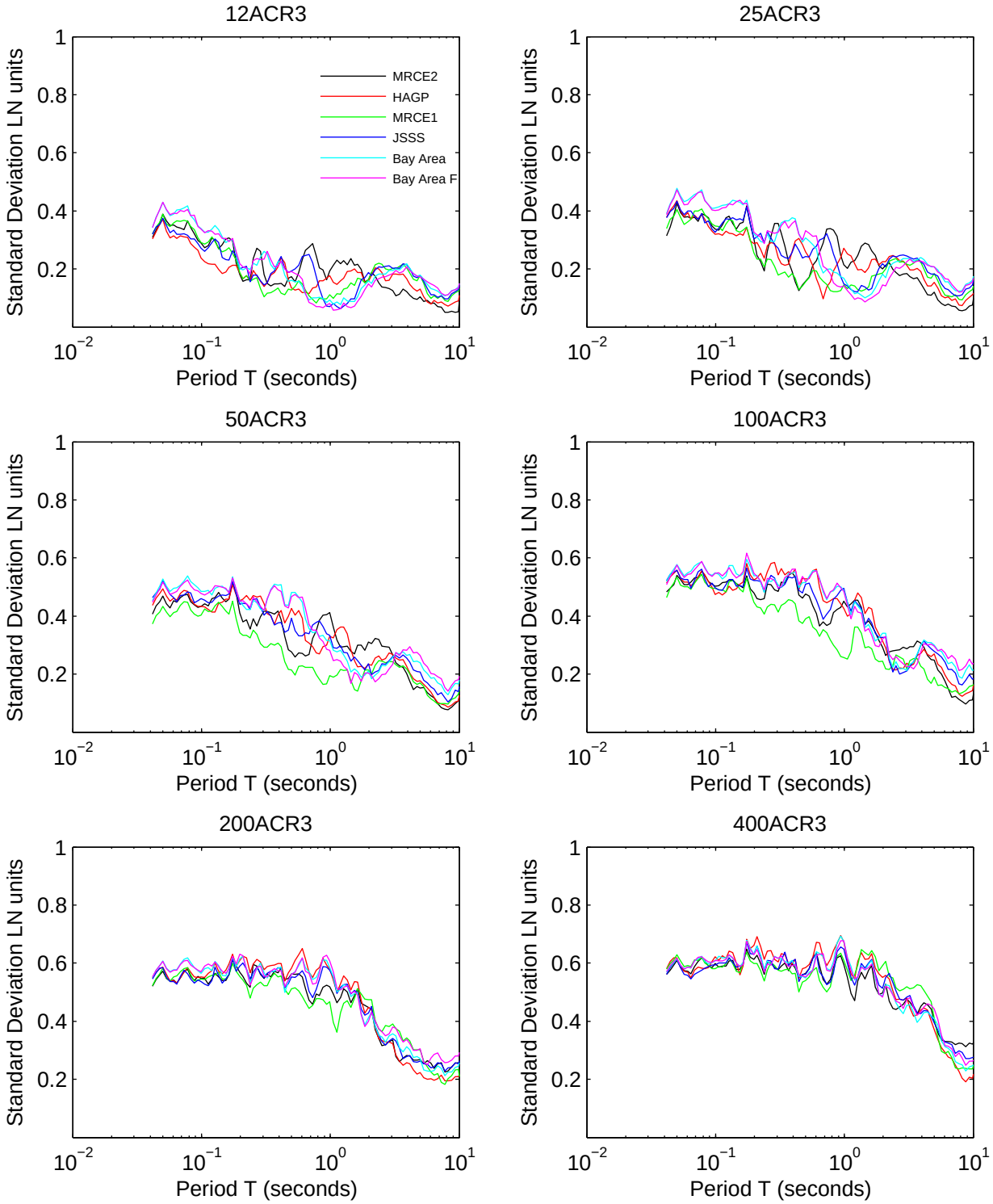

Figure 7D.27: Effect of elastic site period on the standard deviation of amplification for scenarios 7−12

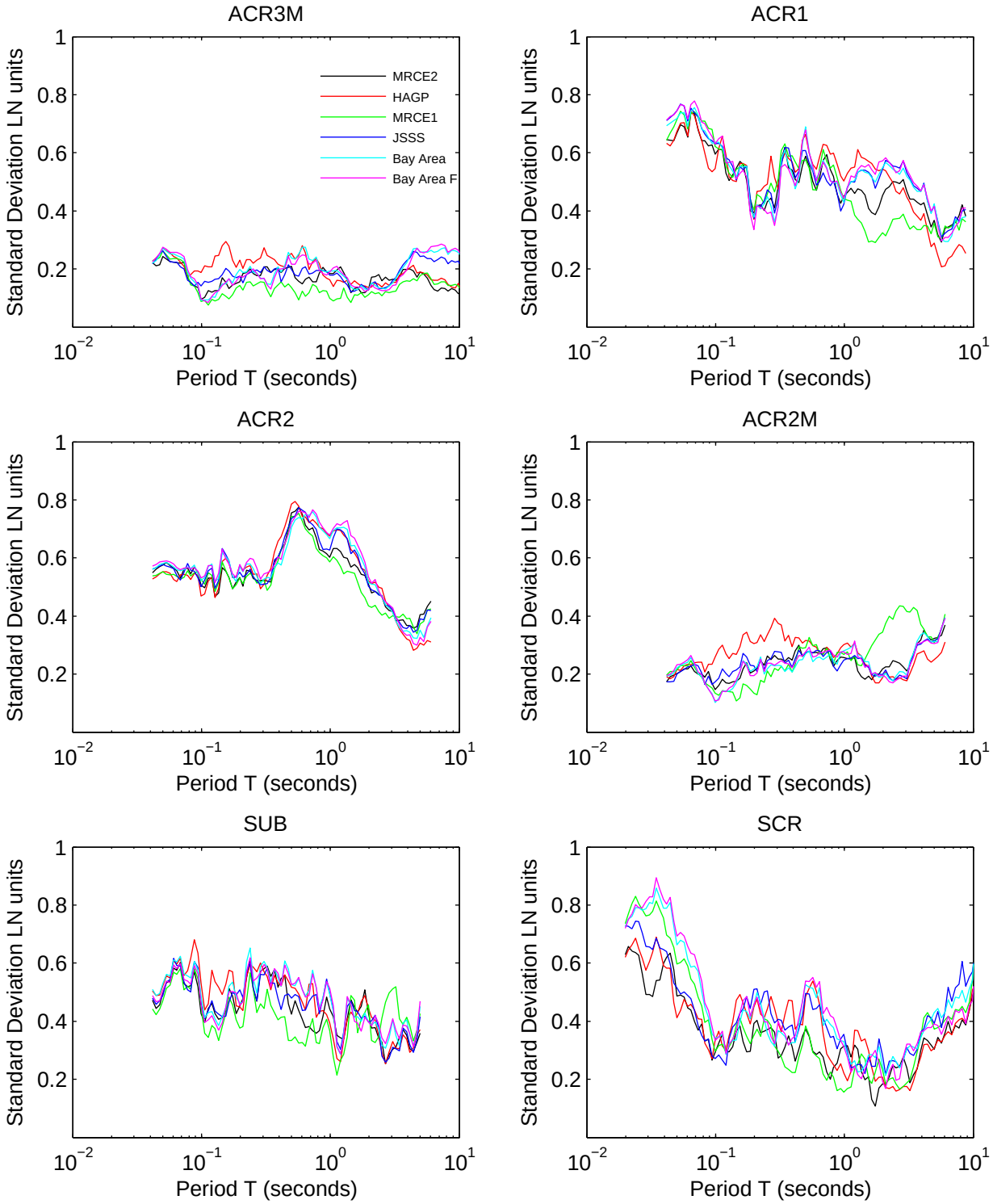

Figure 7D.28: Effect of analysis type on the standard deviation of response spectra for site MRCE2

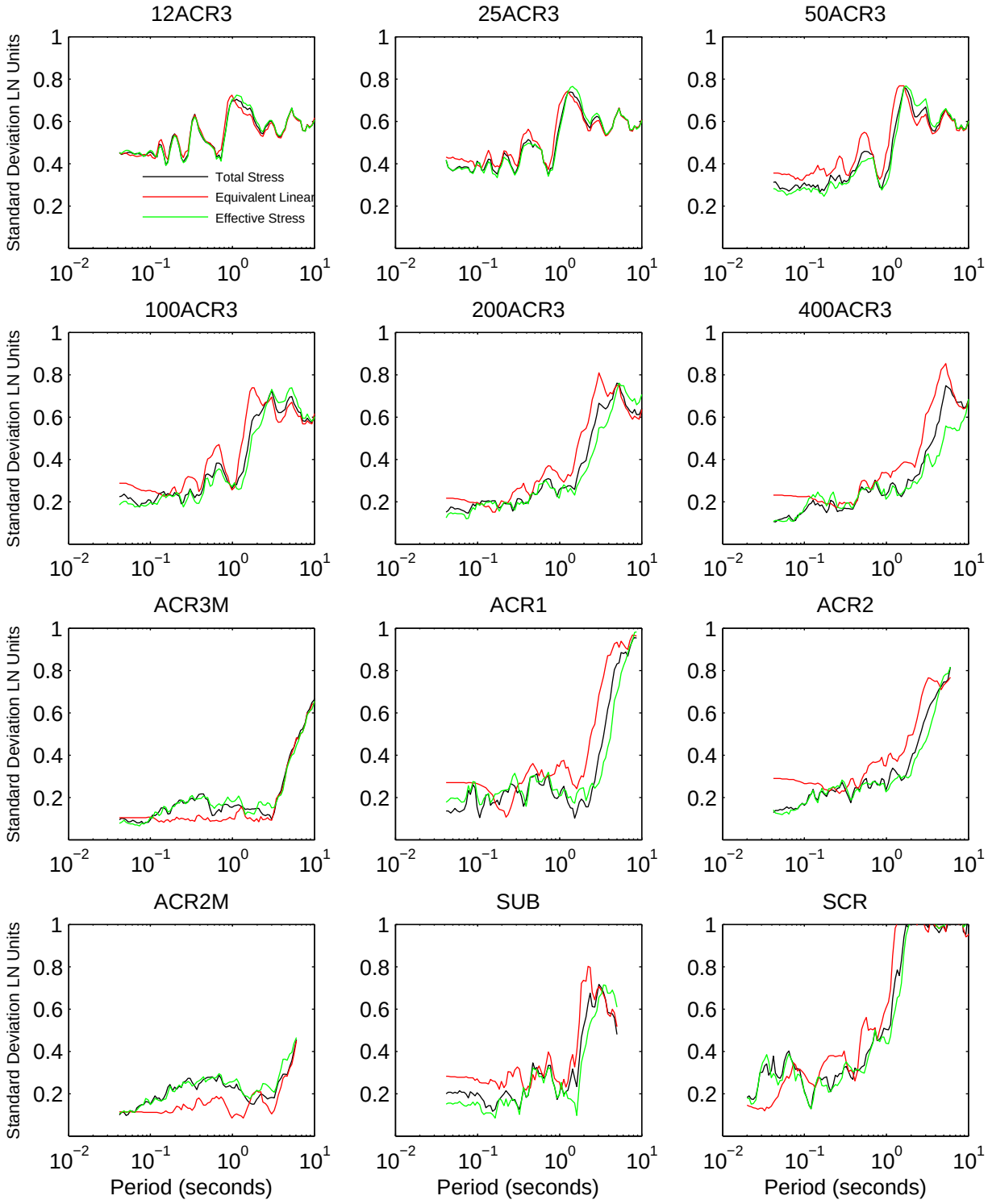

Figure 7D.29: Effect of analysis type on the standard deviation of amplification for site MRCE2

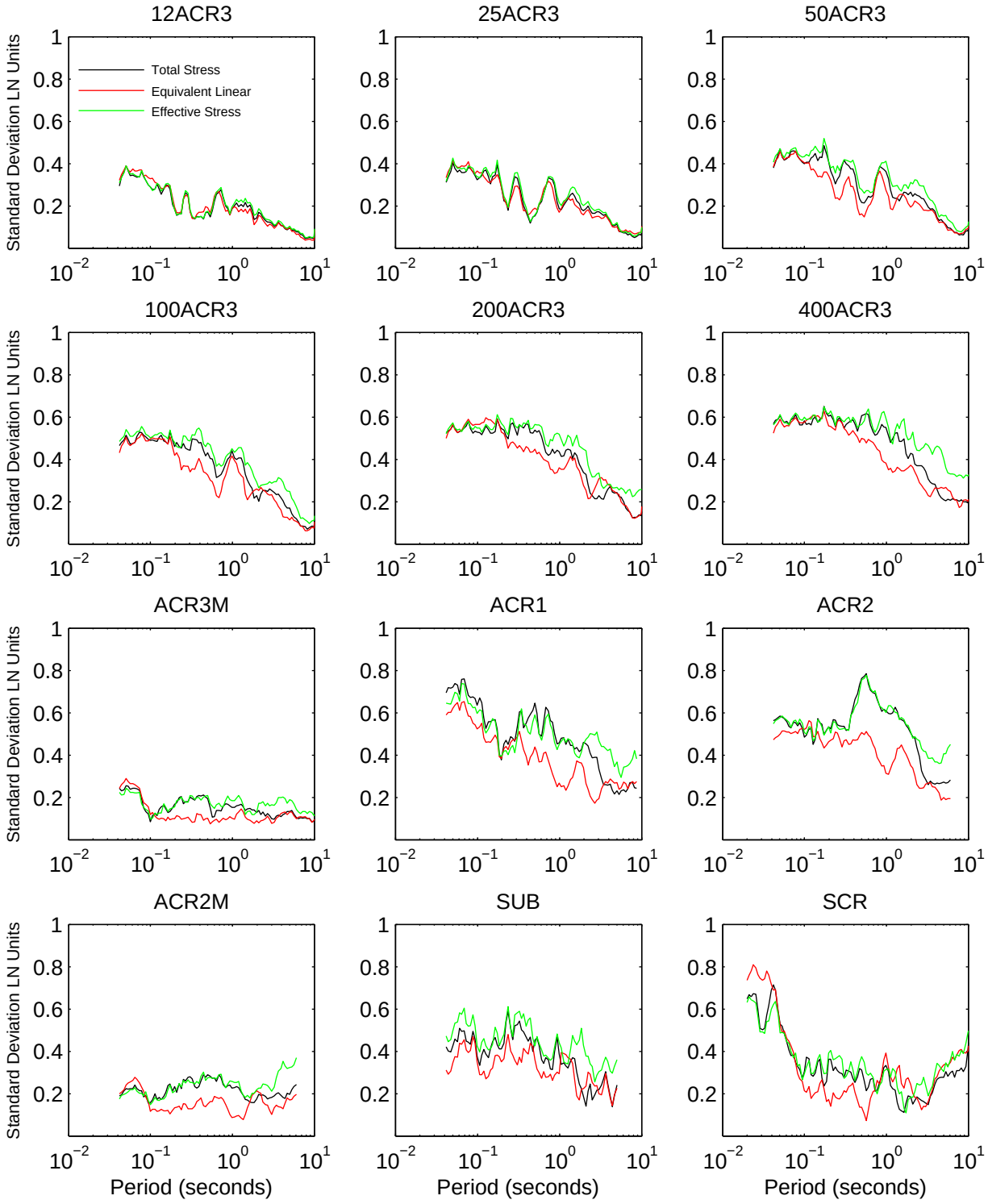

Figure 7D.30: Effect of analysis type on the standard deviation of response spectra for site HAGP

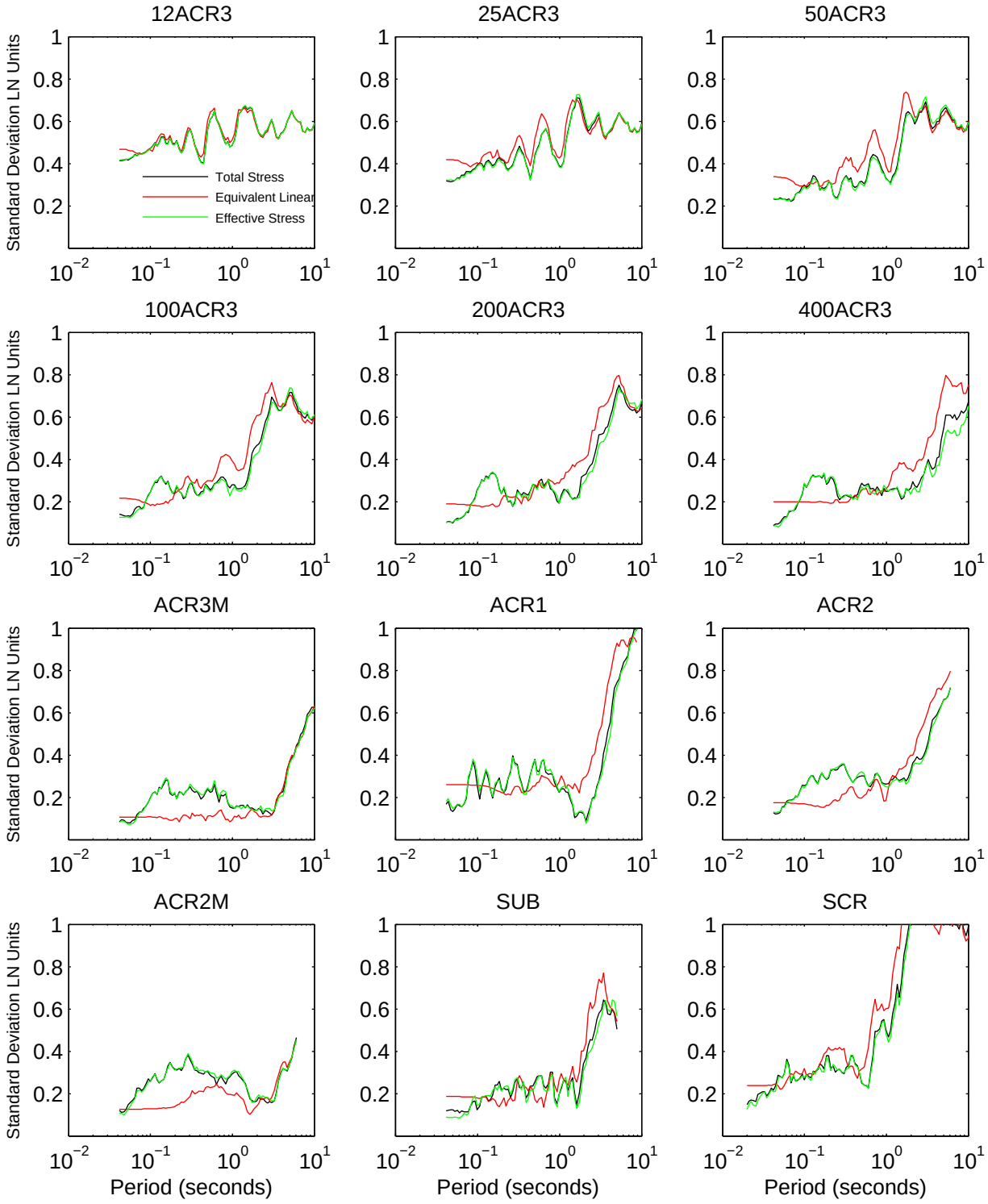

Figure 7D.31: Effect of analysis type on the standard deviation of amplification for site HAGP

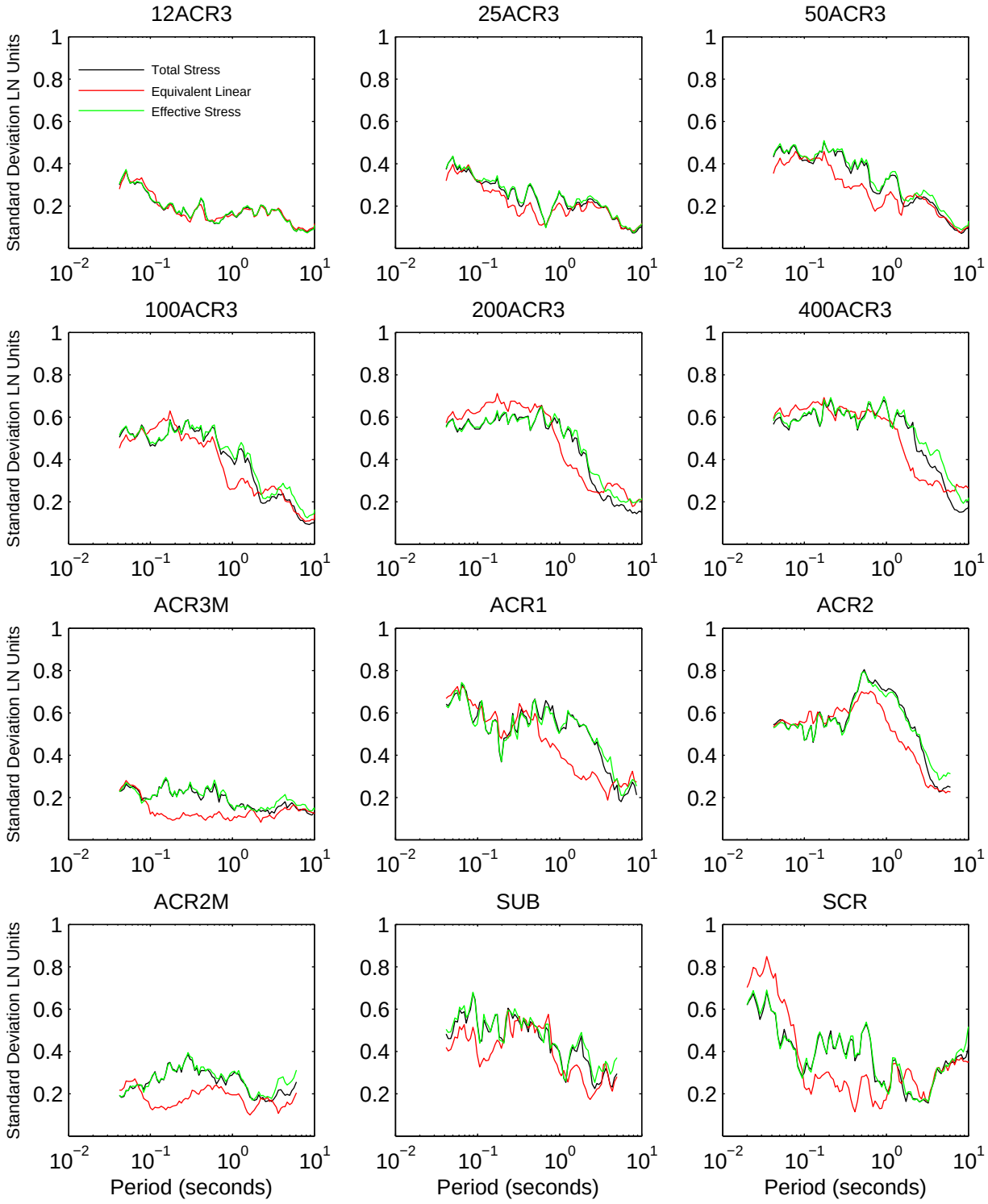

Figure 7D.32: Effect of analysis type on the standard deviation of response spectra for site KIKNET

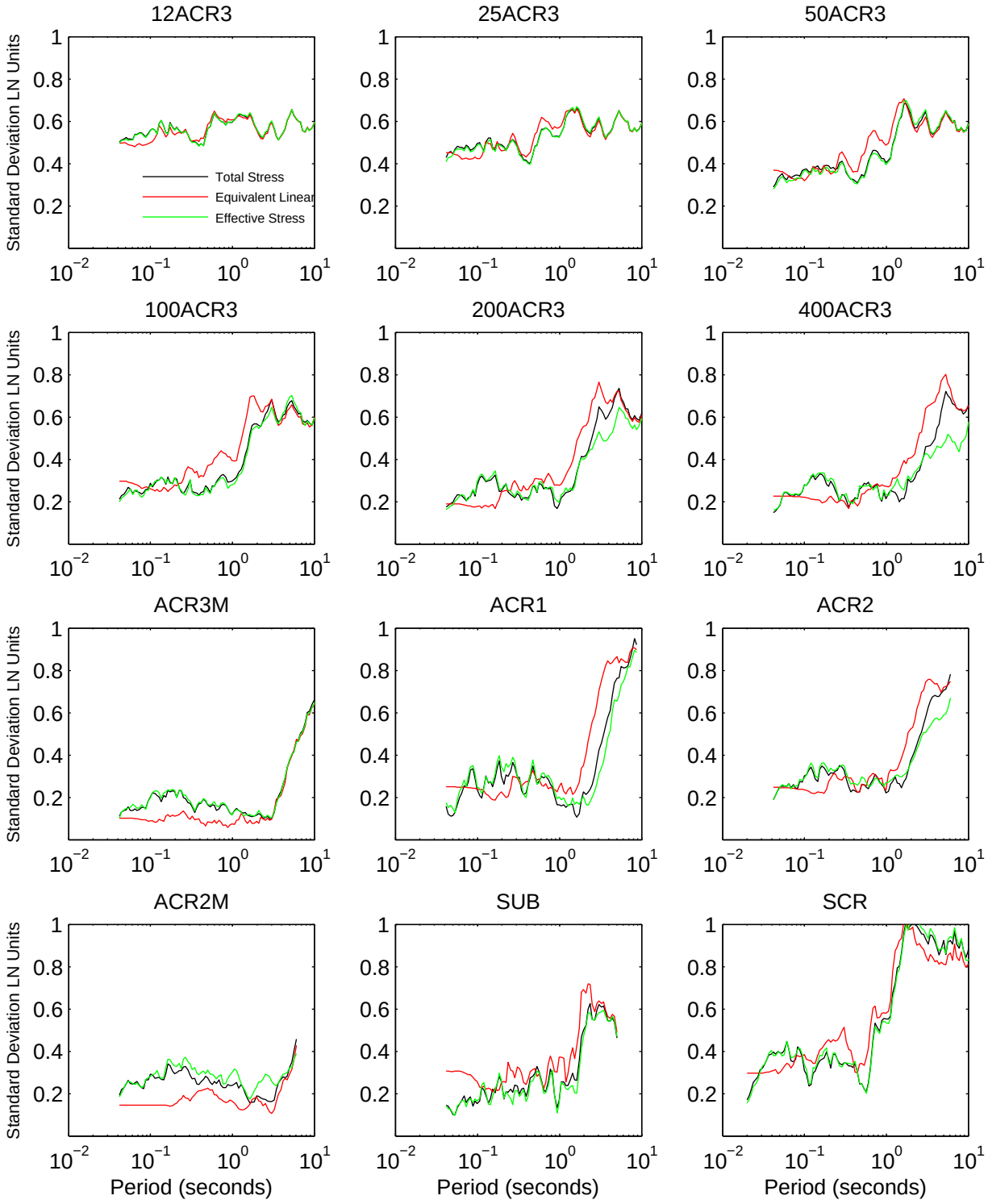

Figure 7D.33: Effect of analysis type on the standard deviation of amplification for site KIKNET

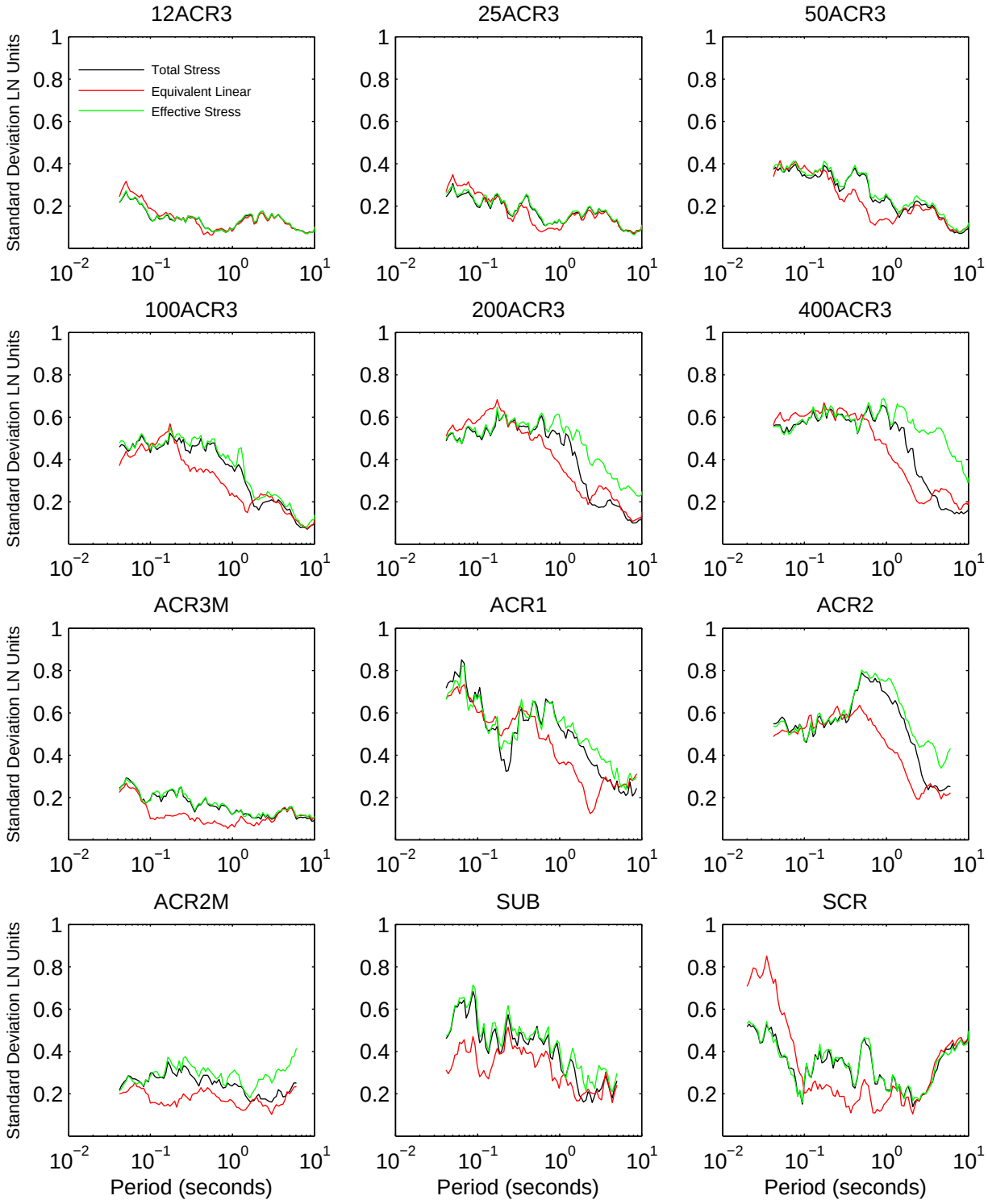

Figure 7D.34: Effect of analysis type on the standard deviation of response spectra for site Bay Area II

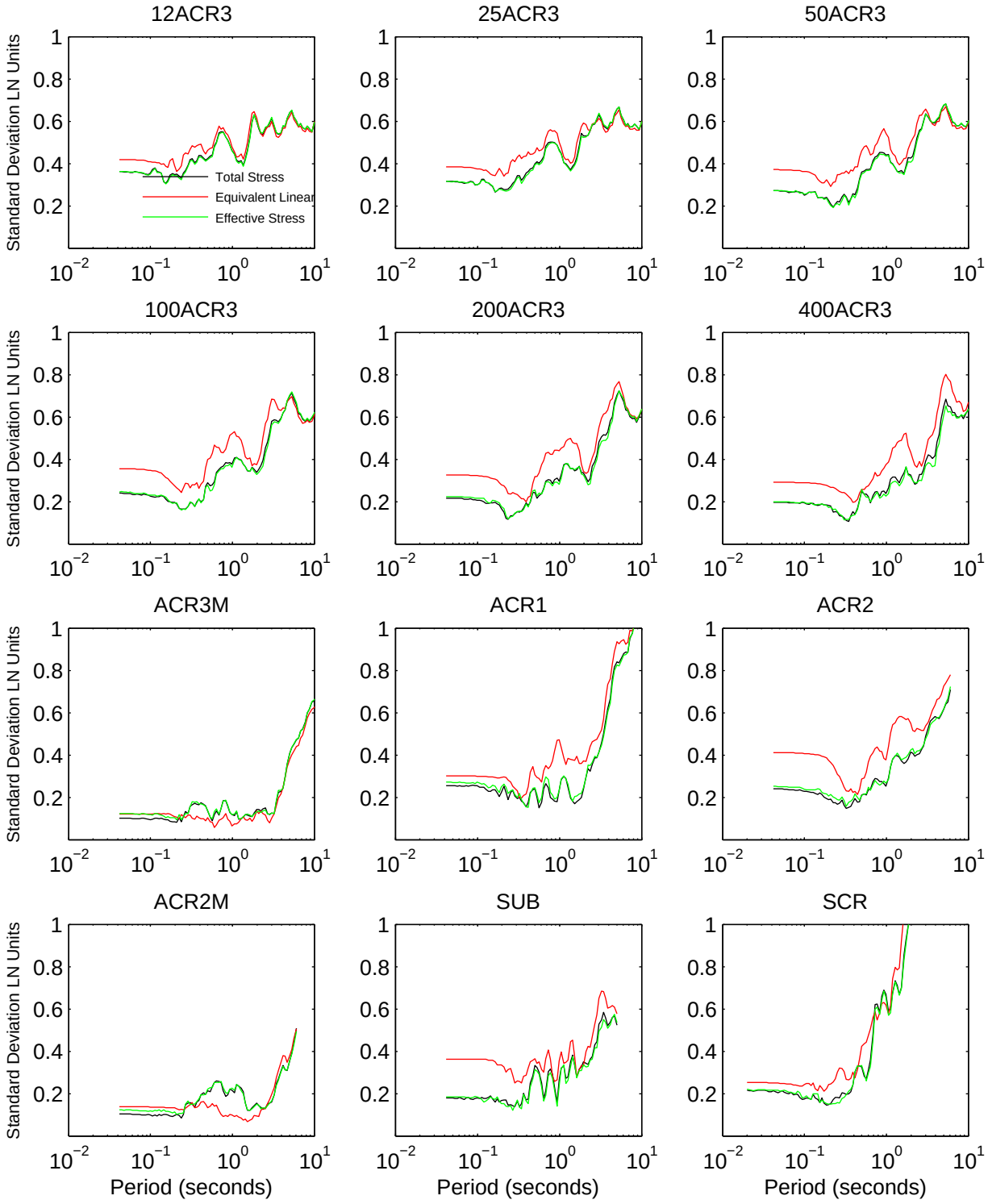

Figure 7D.35: Effect of analysis type on the standard deviation of amplification for site Bay Area II

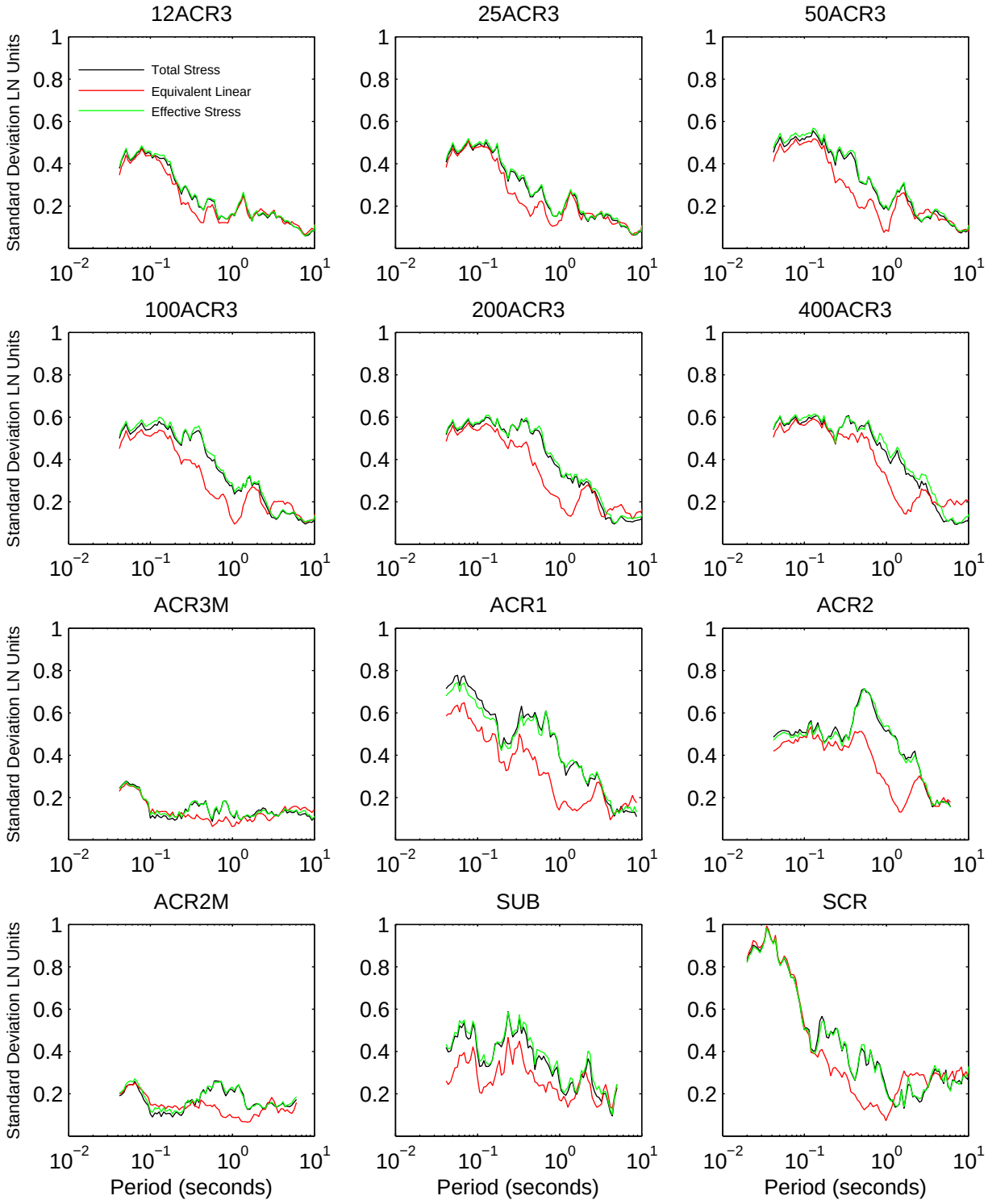

Figure 7D.36: Effect of analysis type on the standard deviation of response spectra for site MRCE1

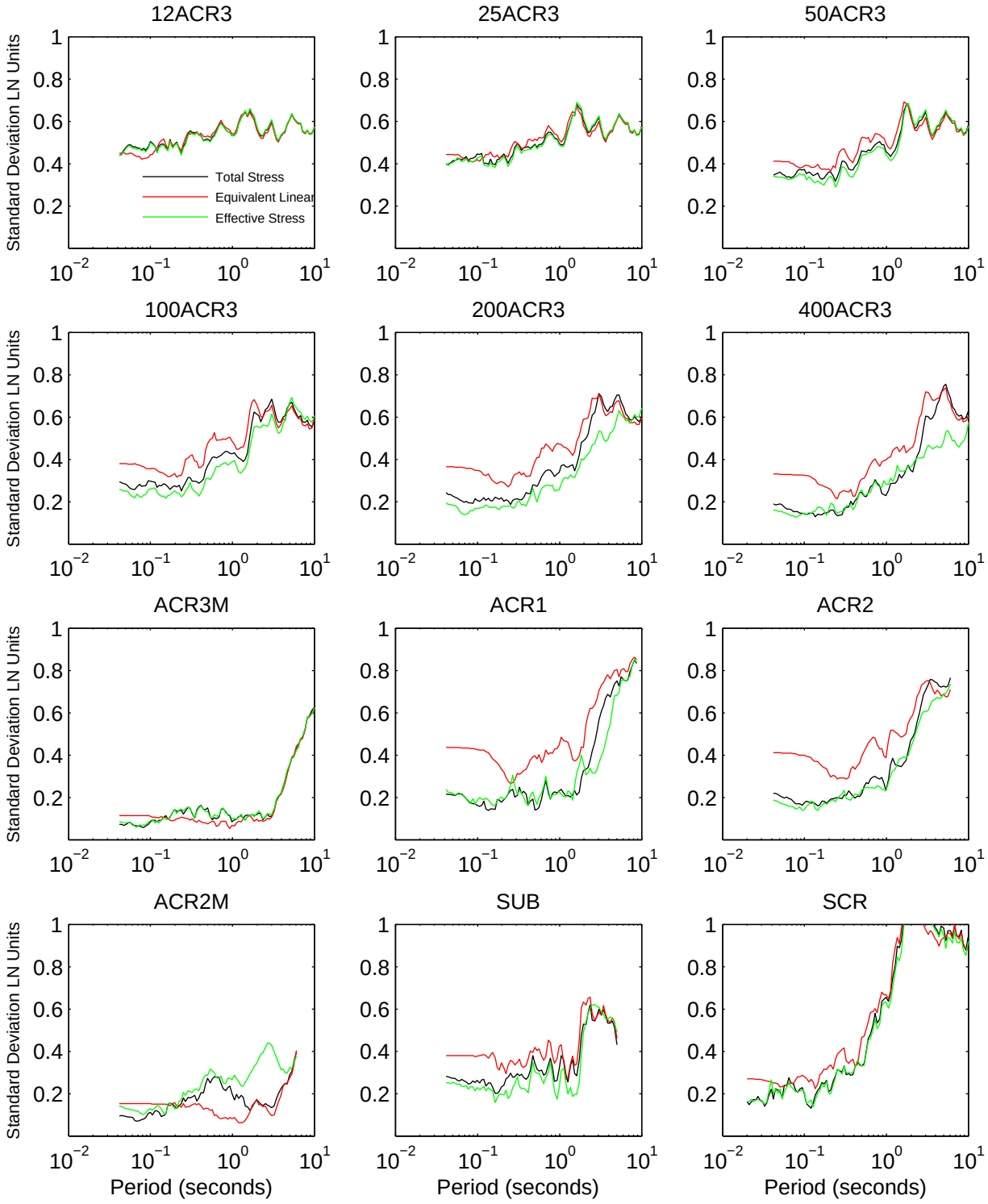

Figure 7D.37: Effect of analysis type on the standard deviation of amplification for site MRCE1

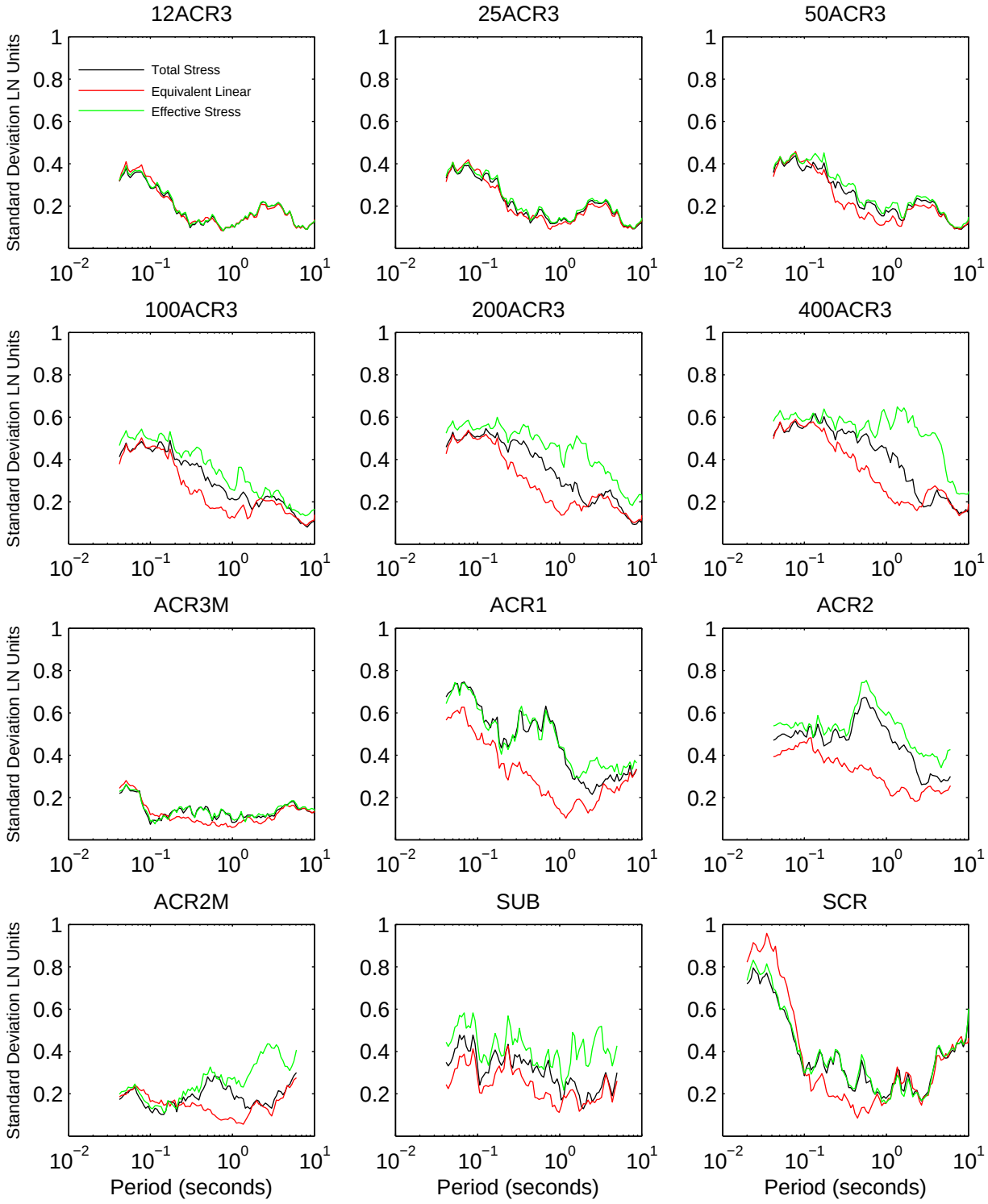

Figure 7D.38: Effect of analysis type on the standard deviation of response spectra for site JSSS

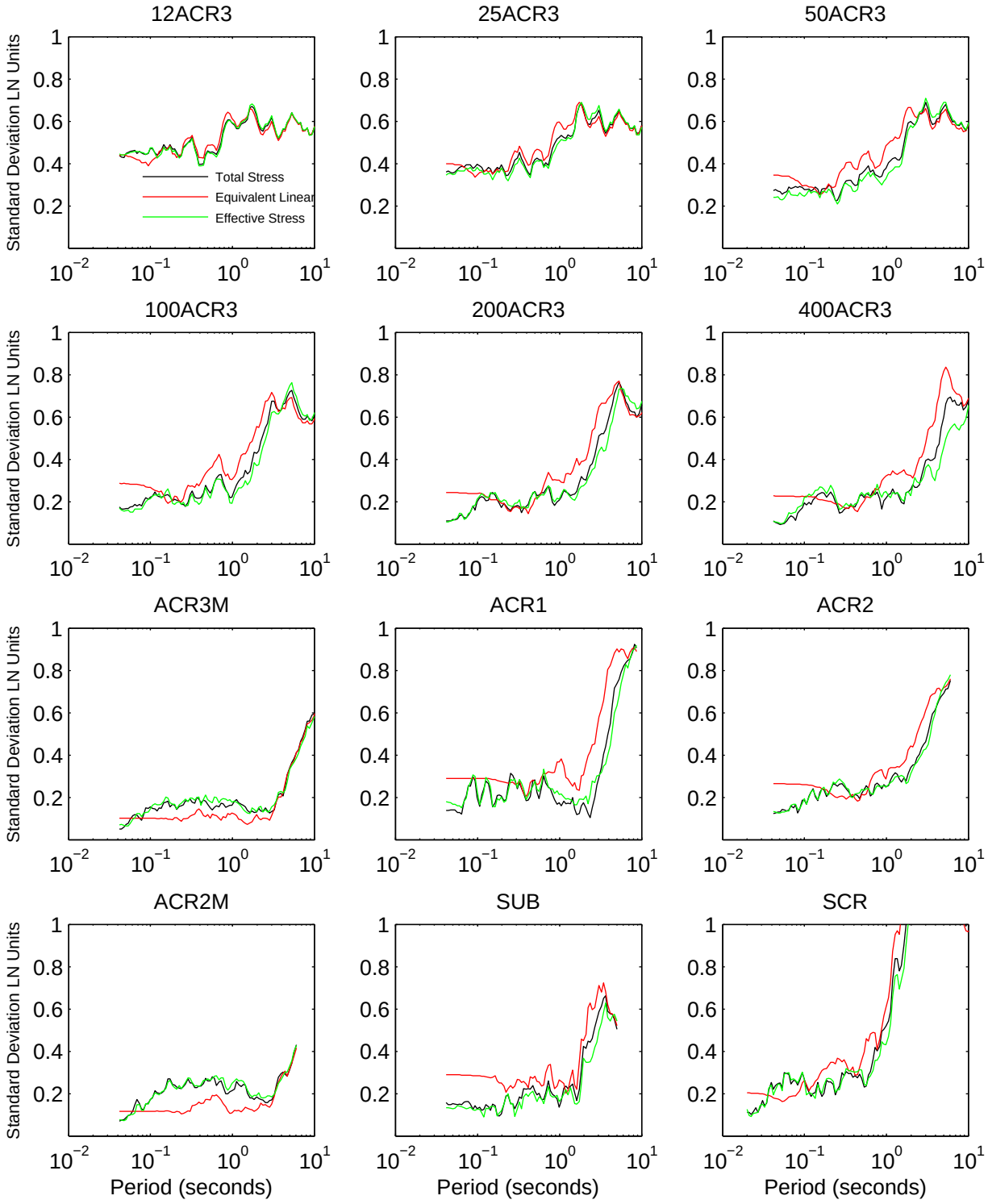

Figure 7D.39: Effect of analysis type on the standard deviation of amplification for site JSSS

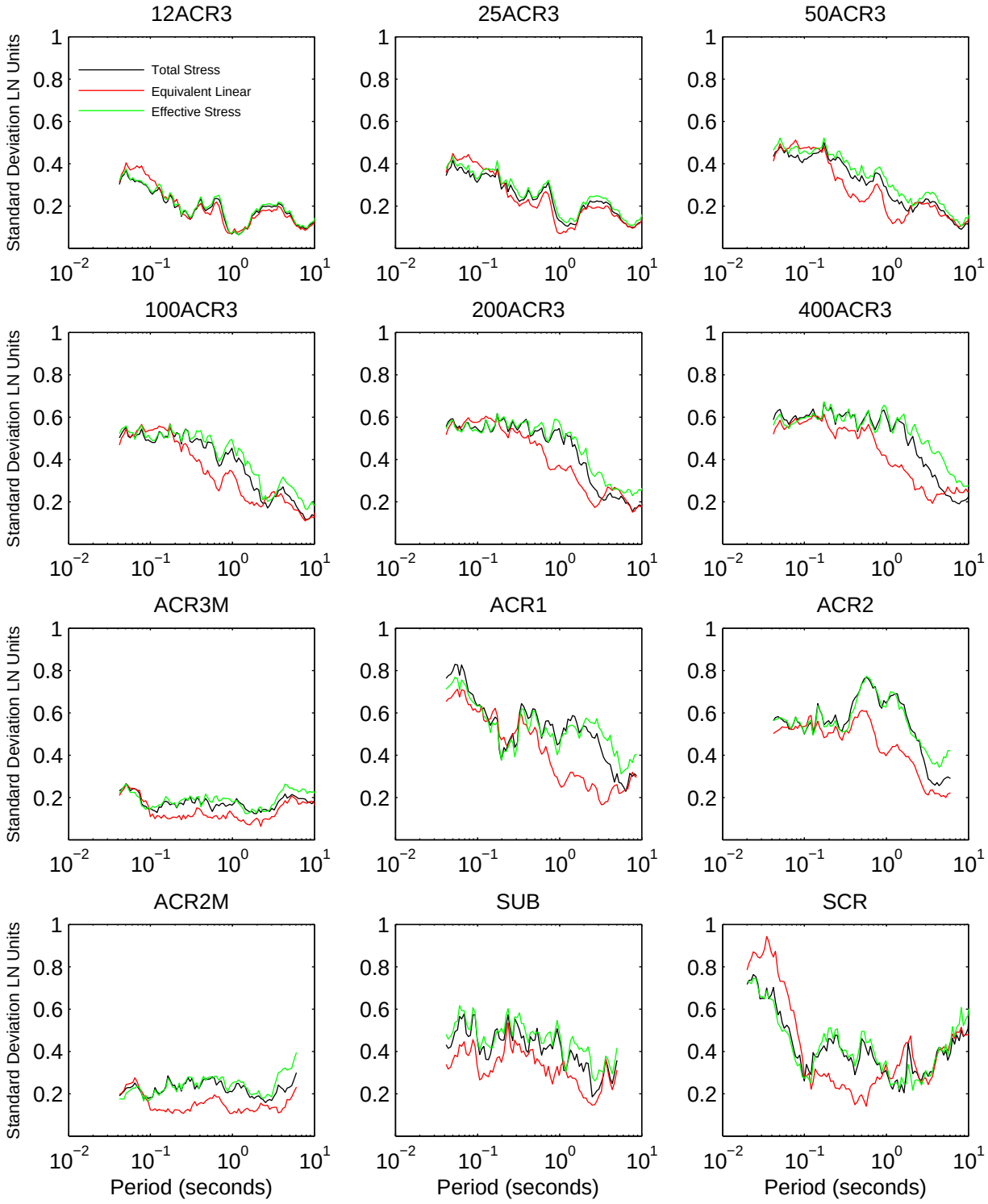

Figure 7D.40: Effect of analysis type on the standard deviation of response spectra for site Bay Area

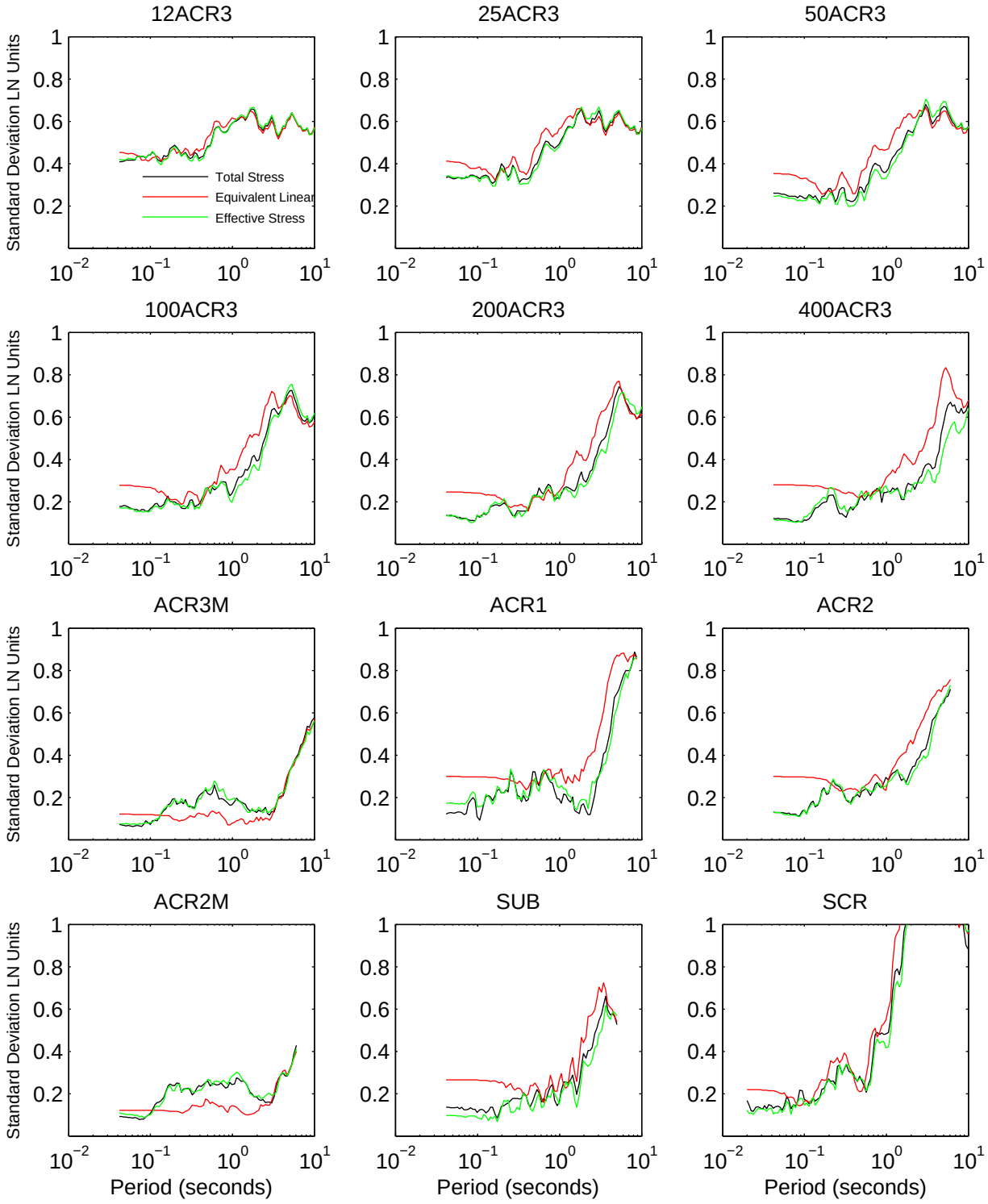

Figure 7D.41: Effect of analysis type on the standard deviation of amplification for site Bay Area

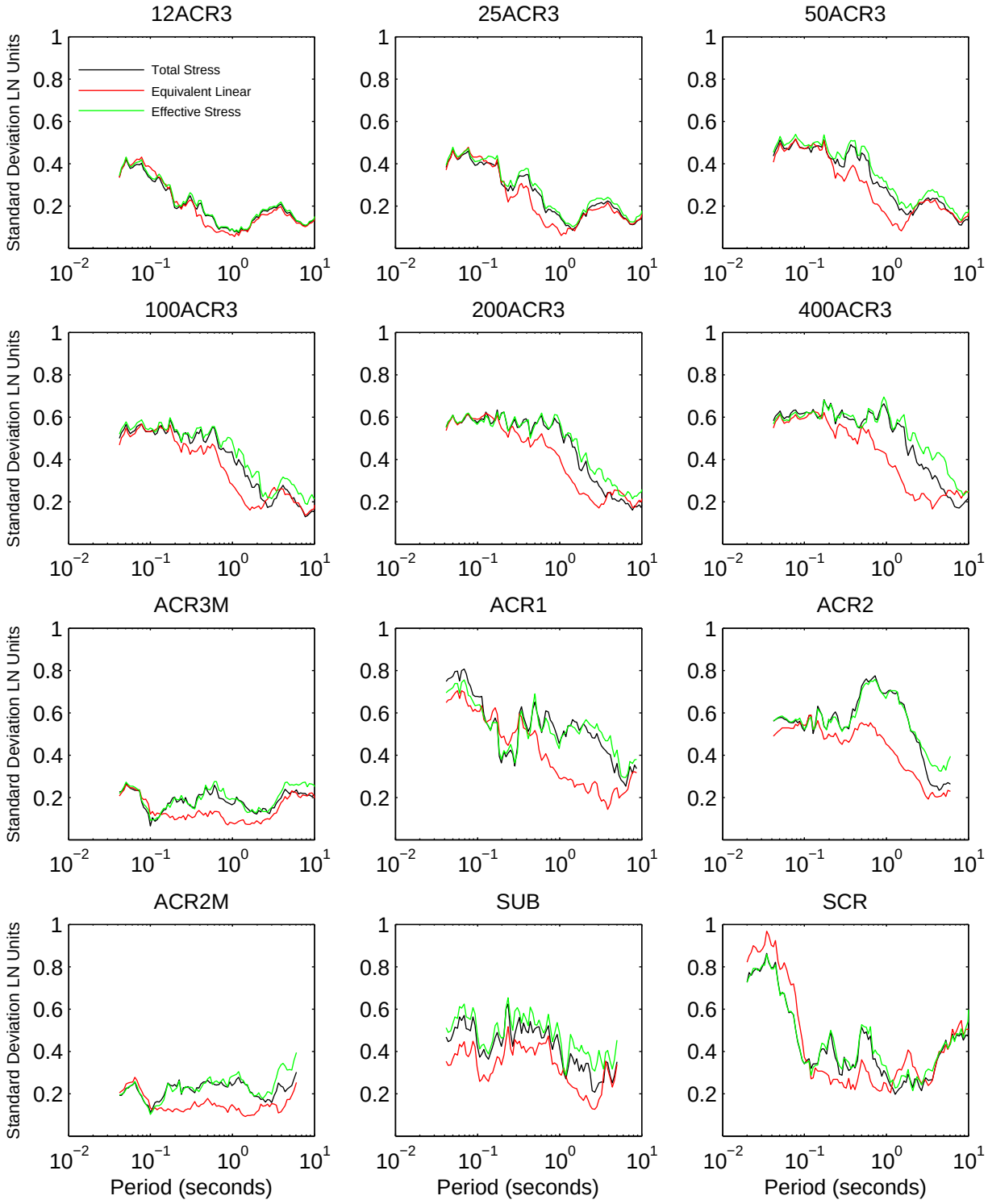

APPENDIX 7E: COMPARISON WITH IMPLIED NGA WEST 2 SITE AMPLIFICATION FACTORS Fa AND Fv

Appendix 7E: Comparison with Implied NGA West 2 Site Amplification Factors Fa and Fv

Appendix 7E compares amplification factors Fa and Fv calculated from the nonlinear effective stress site response analyses conducted in this investigation and those implied by the NGA West 2 GMPEs for NEHRP E sites as calculated by Stewart and Seyhan (2013). The NGA West 2 GMPEs did not calculate values of Fa or Fv, the values compared here are the Fa and Fv values calculated by Stewart and Seyhan (2013) using the NGA West 2 GMPEs.

Figures 7E.1 through 7E.12 show Fa and Fv values for scenariosACR3M, ACR1, ACR2, ACR2M, SUB, and SCR individually. Figures 7E.13 and 7E.14 show Fa and Fv values for 12ACR3, 25ACR3, 50ACR3, 100ACR3, 200ACR3, and 400ACR3 in the same plots. There are six plots per figure, where the top left plot in each figure compares the results from sites Bay Area II K, Bay Area II K S2, and Bay Area II K S4 (soil strength), the top right plot compares the sites KIKNET, KIKNET S2, and KIKNET S4 (soil strength), the middle left plot compares sites Bay Area II and Bay Area II K (soil MRD curves), the middle right plot compares sites KIKNET40, KIKNET, and KIKNET160 (soil MRD curves), the bottom left plot compares sites MRCE2, HAGP, KIKNET, and Bay Area II K (elastic site period), and the bottom right plot compares sites MRCE1, JSSS, Bay Area, and Bay Area F (elastic site period). The individual points show the results of one ground motion for nonlinear effective stress analysis and the given site, scenario, and amplification factor.

Figure 7E.1: Comparison of amplification factor Fa for scenario ACR3M

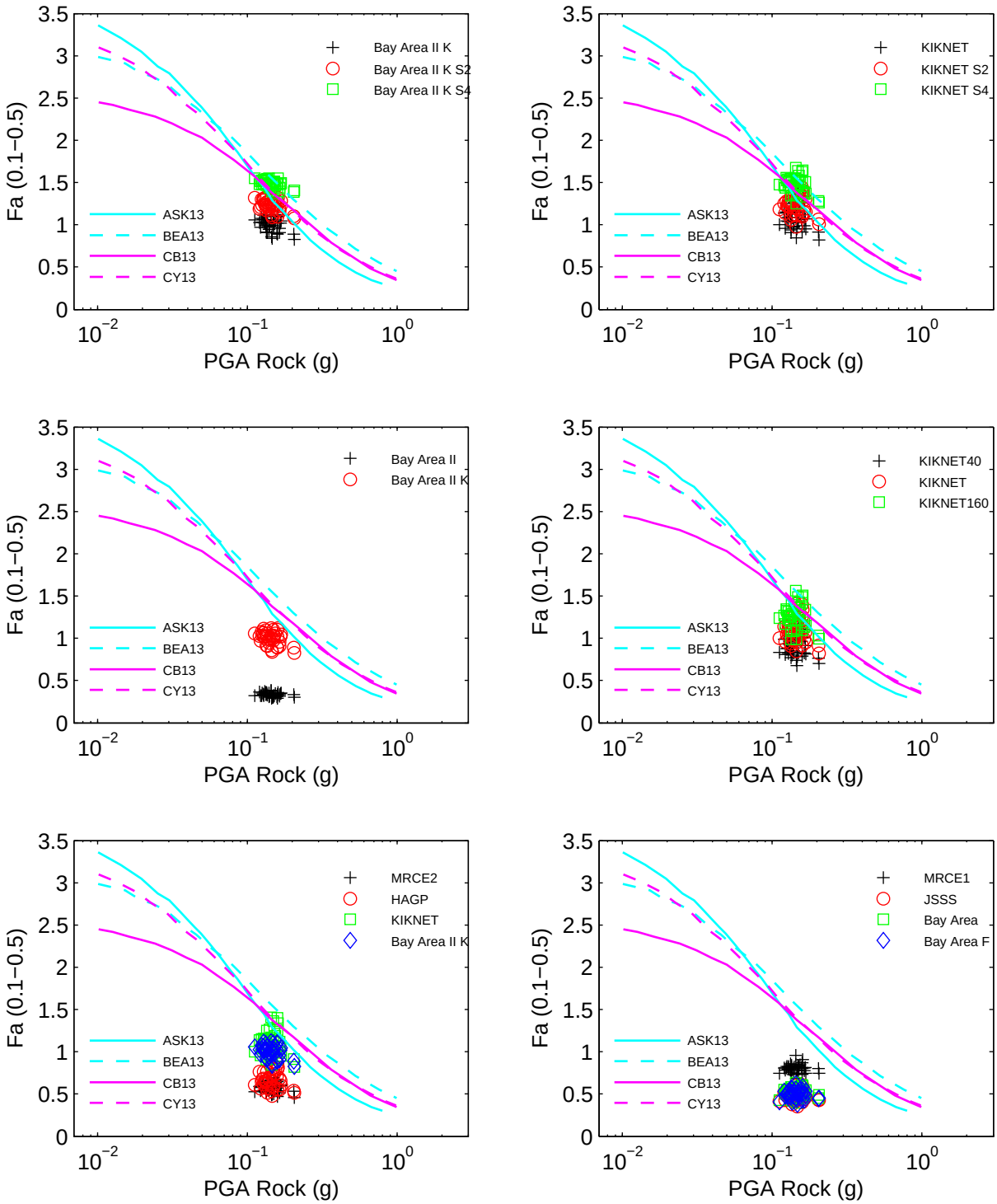

Figure 7E.2: Comparison of amplification factor Fv for scenario ACR3M

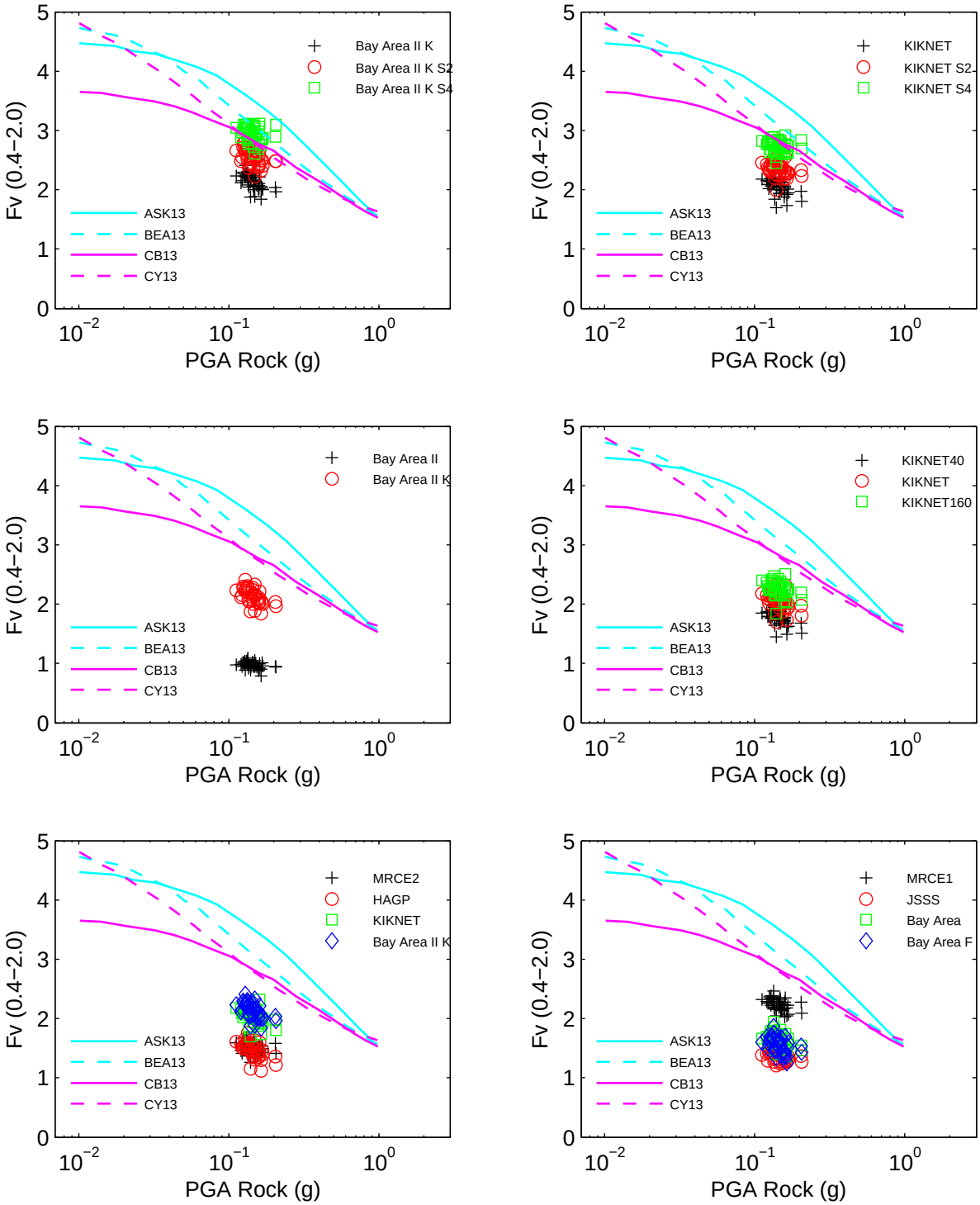

Figure 7E.3: Comparison of amplification factor Fa for scenario ACR1

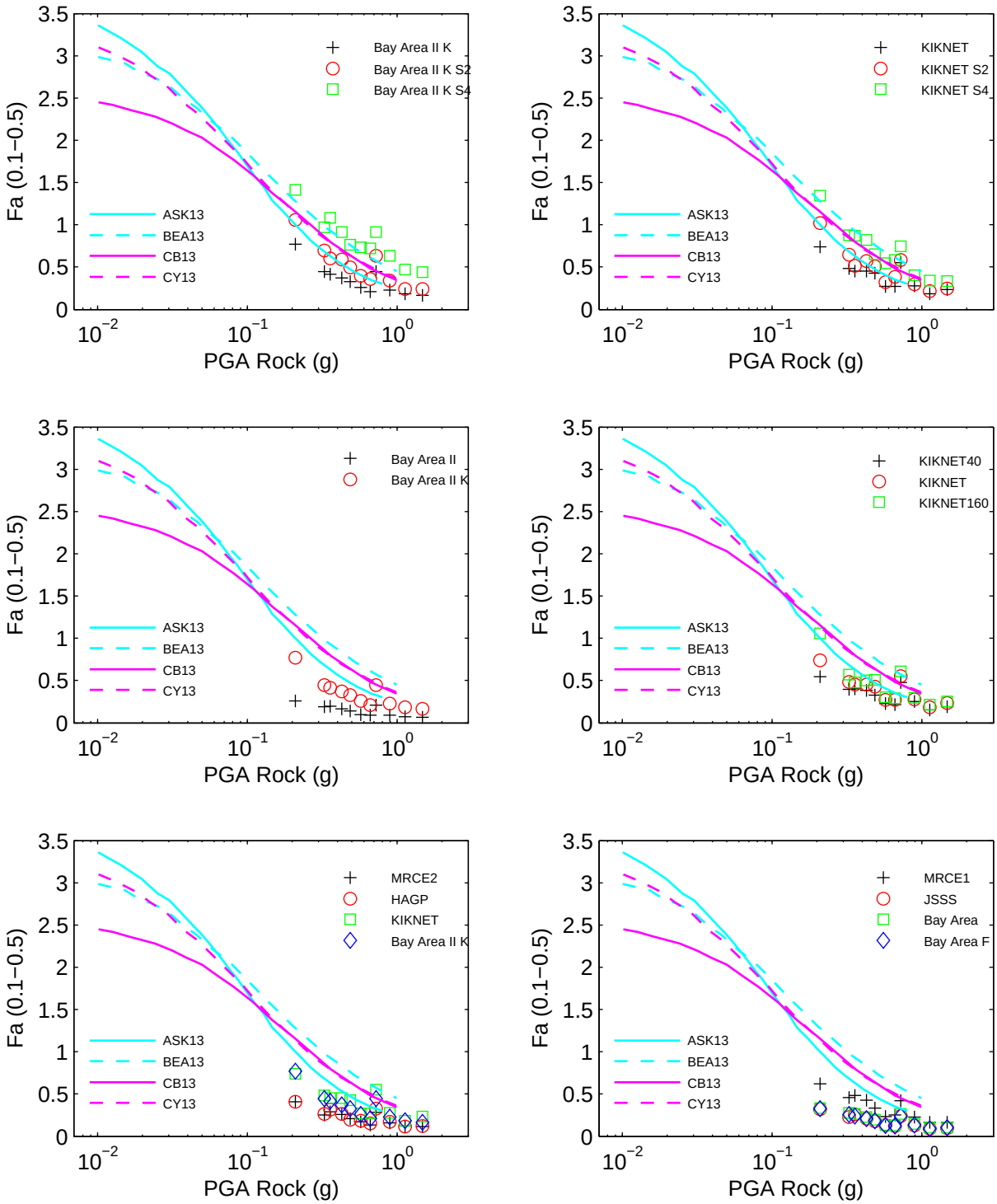

Figure 7E.4: Comparison of amplification factor Fv for scenario ACR1

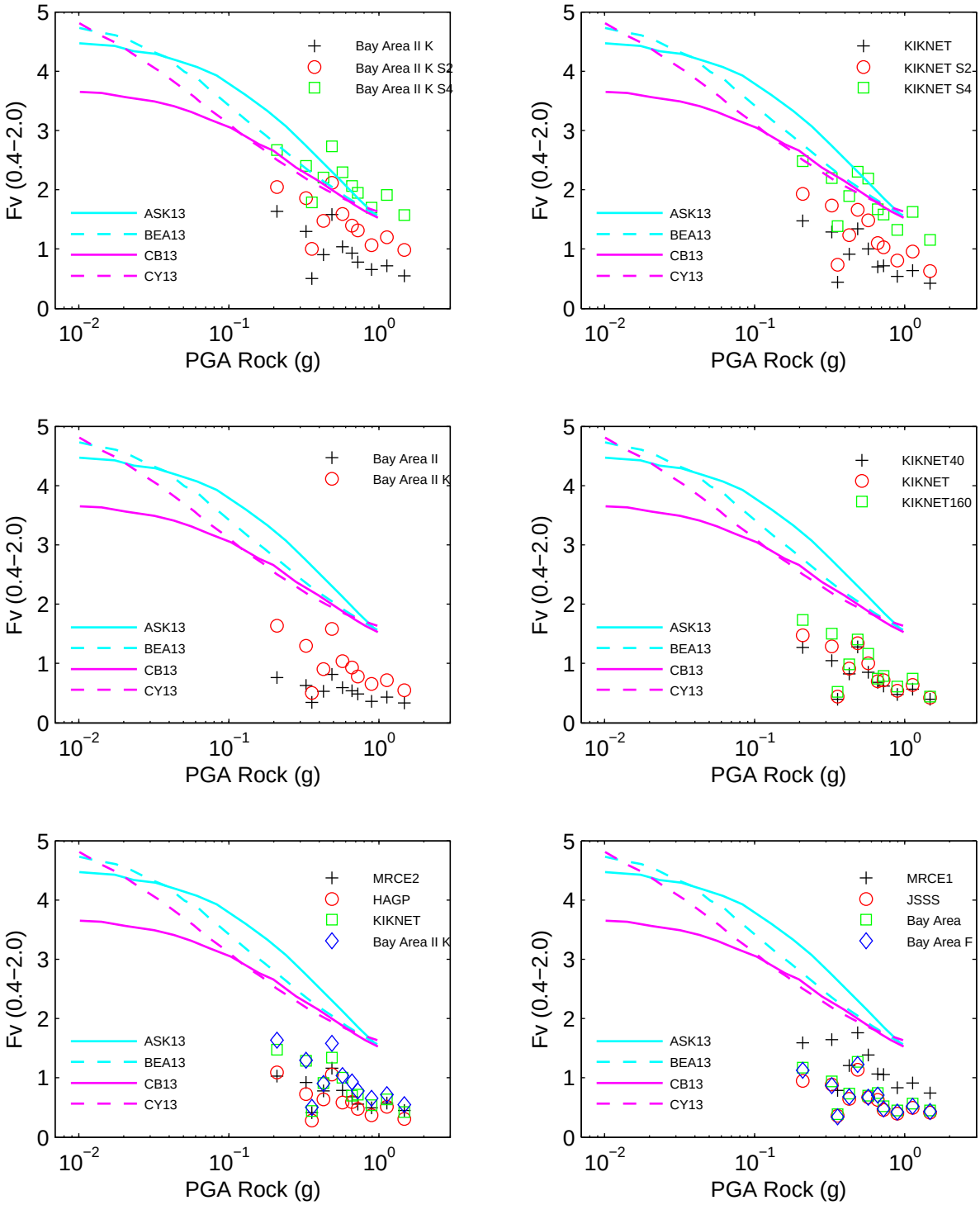

Figure 7E.5: Comparison of amplification factor Fa for scenario ACR2

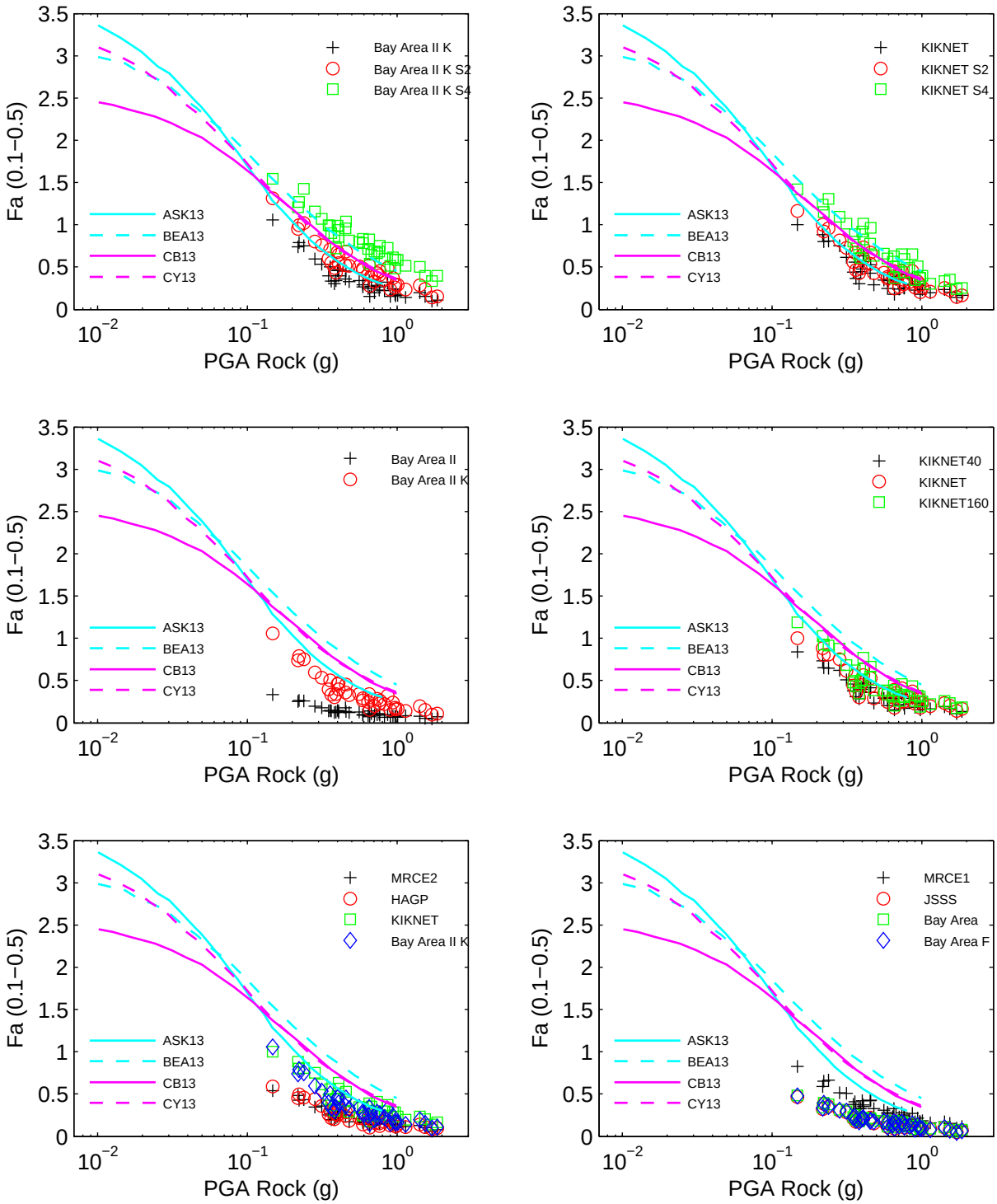

Figure 7E.6: Comparison of amplification factor Fv for scenario ACR2

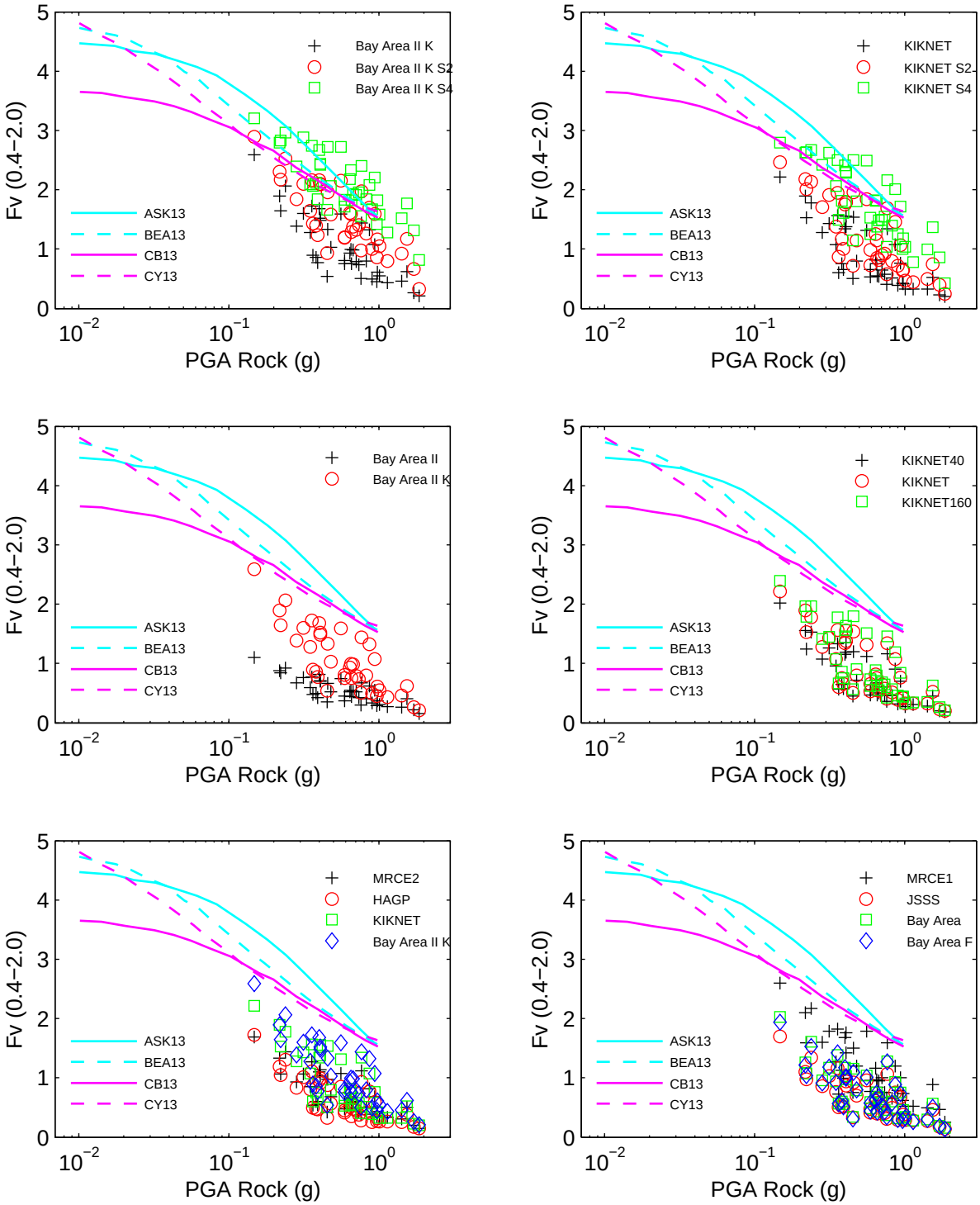

Figure 7E.7: Comparison of amplification factor Fa for scenario ACR2M

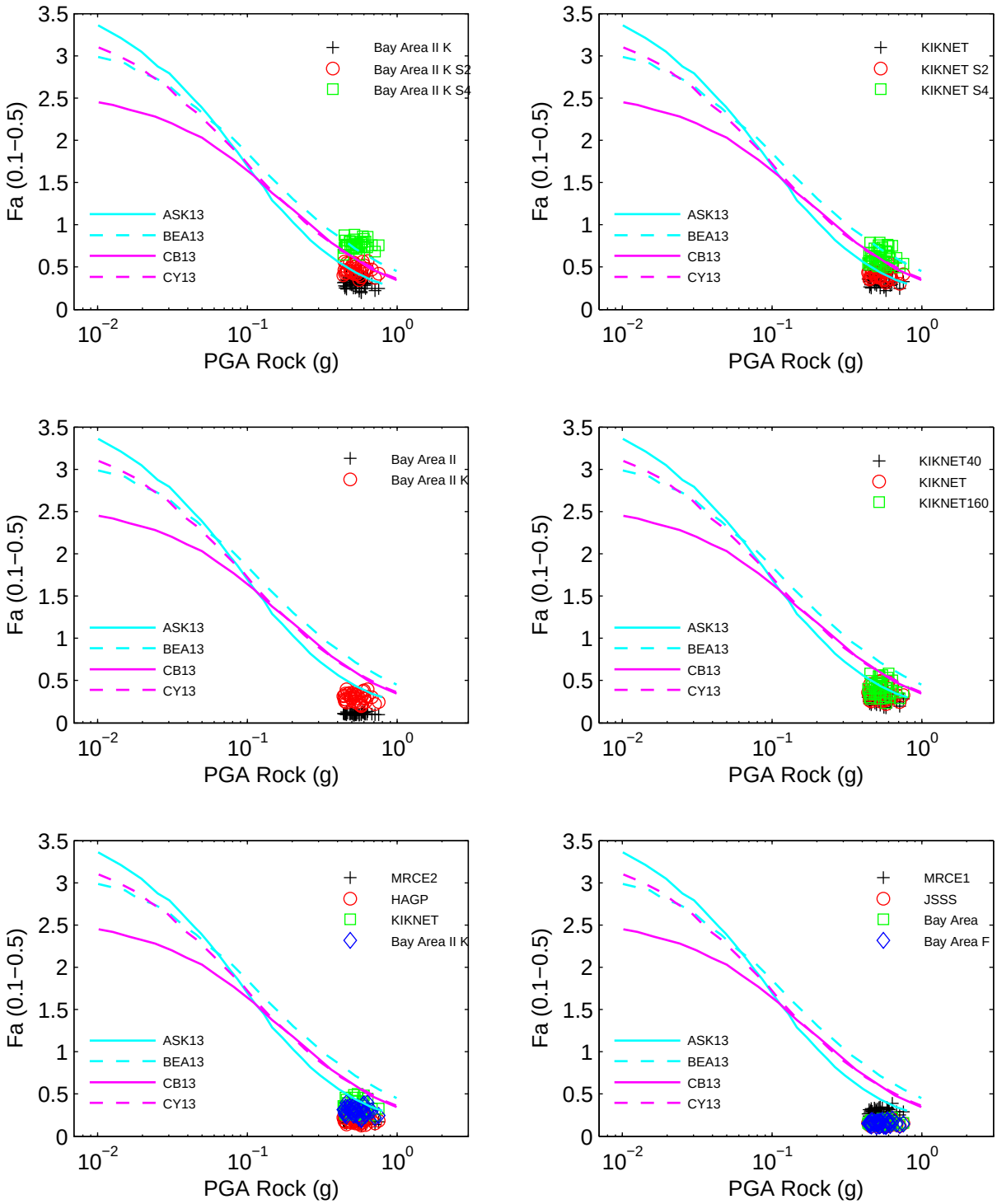

Figure 7E.8: Comparison of amplification factor Fv for scenario ACR2M

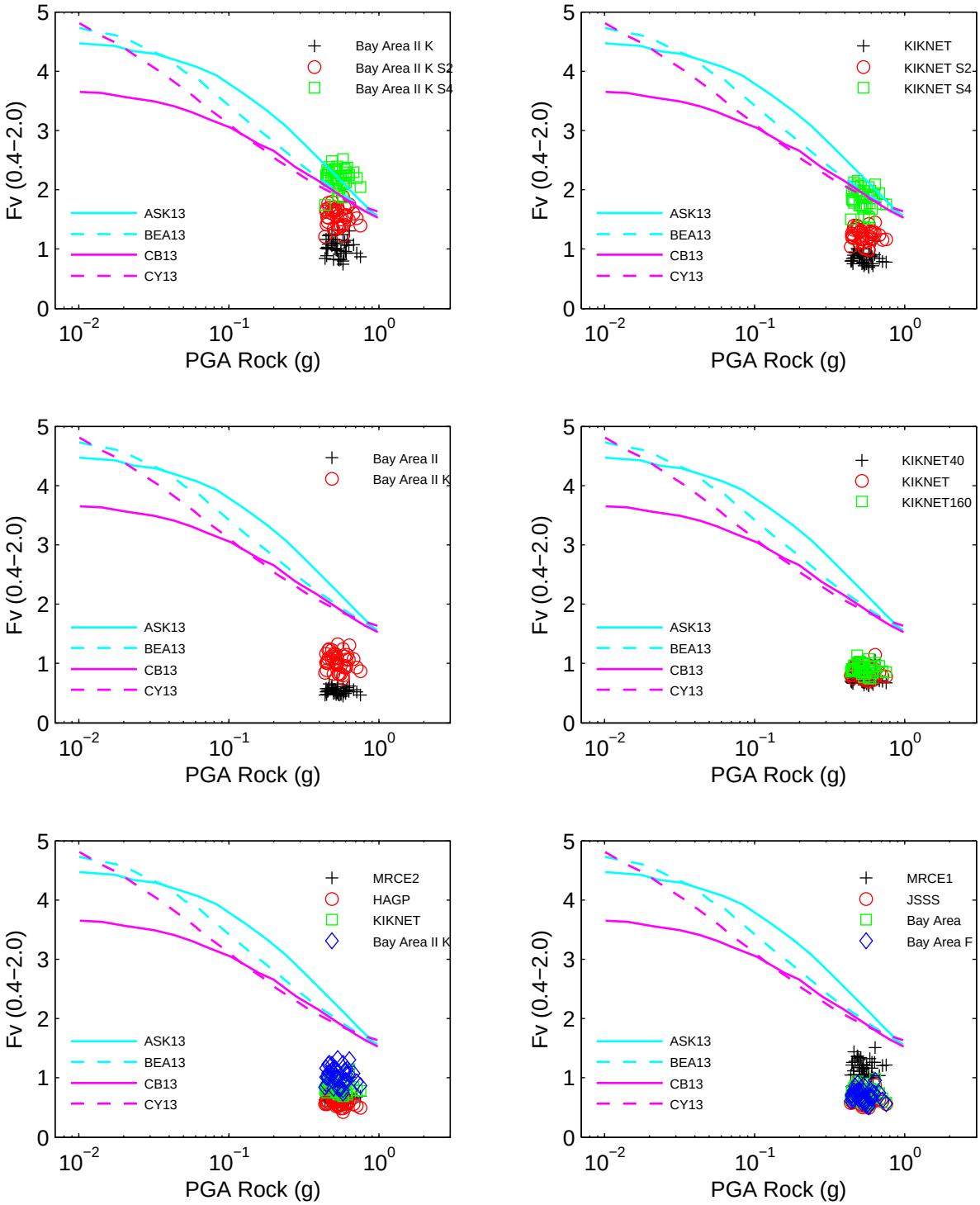

Figure 7E.9: Comparison of amplification factor Fa for scenario SUB

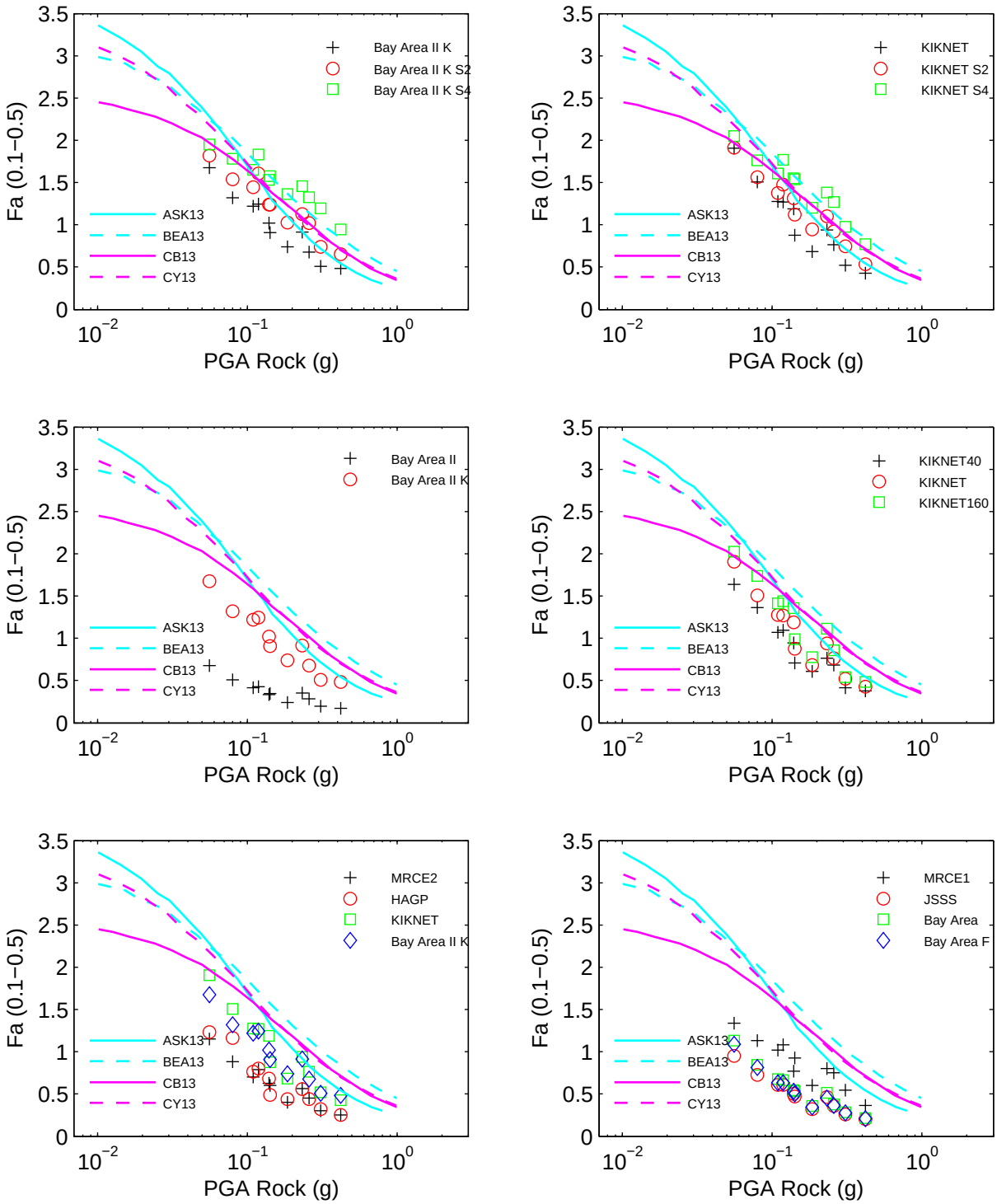

Figure 7E.10: Comparison of amplification factor Fv for scenario SUB

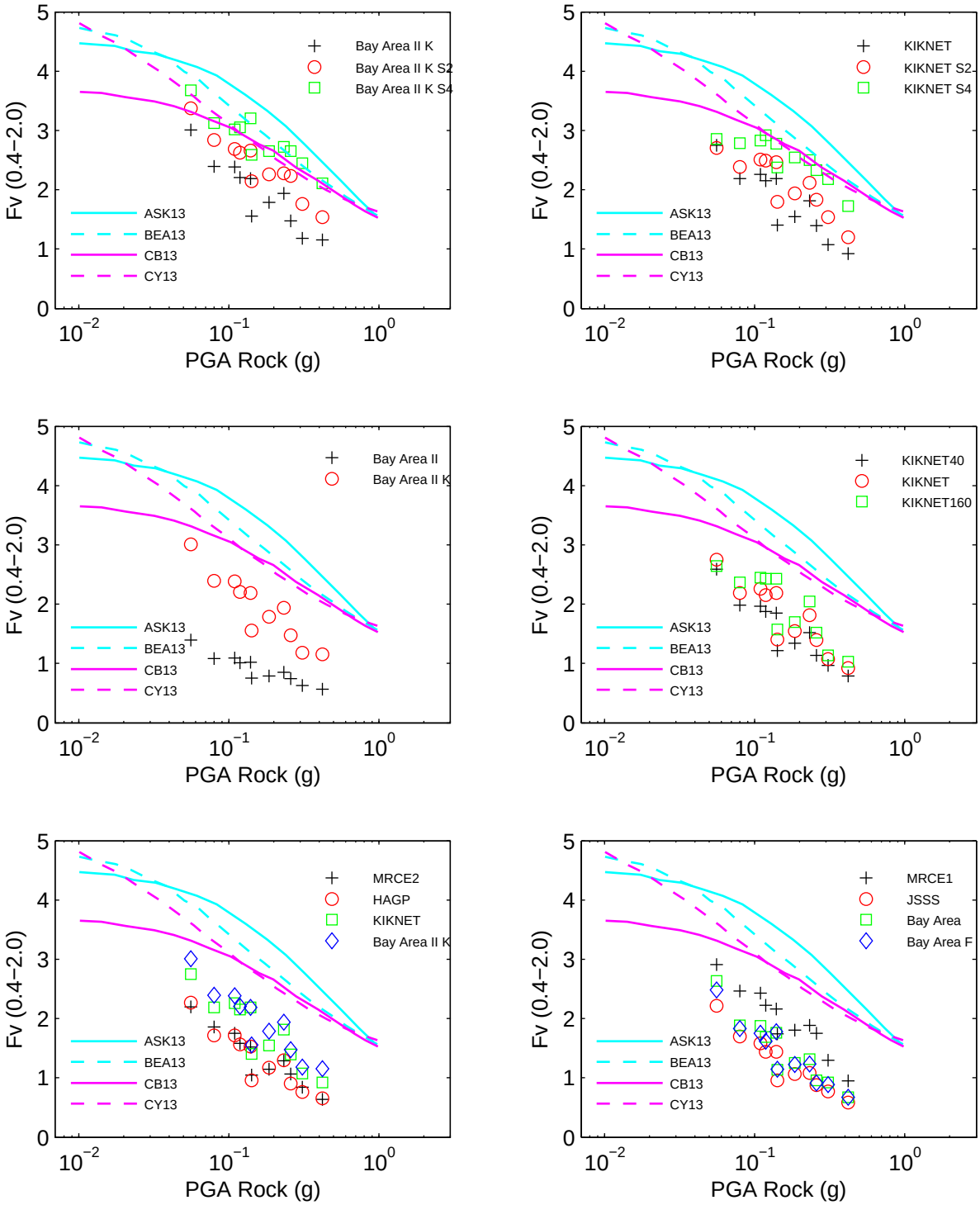

Figure 7E.11: Comparison of amplification factor Fa for scenario SCR

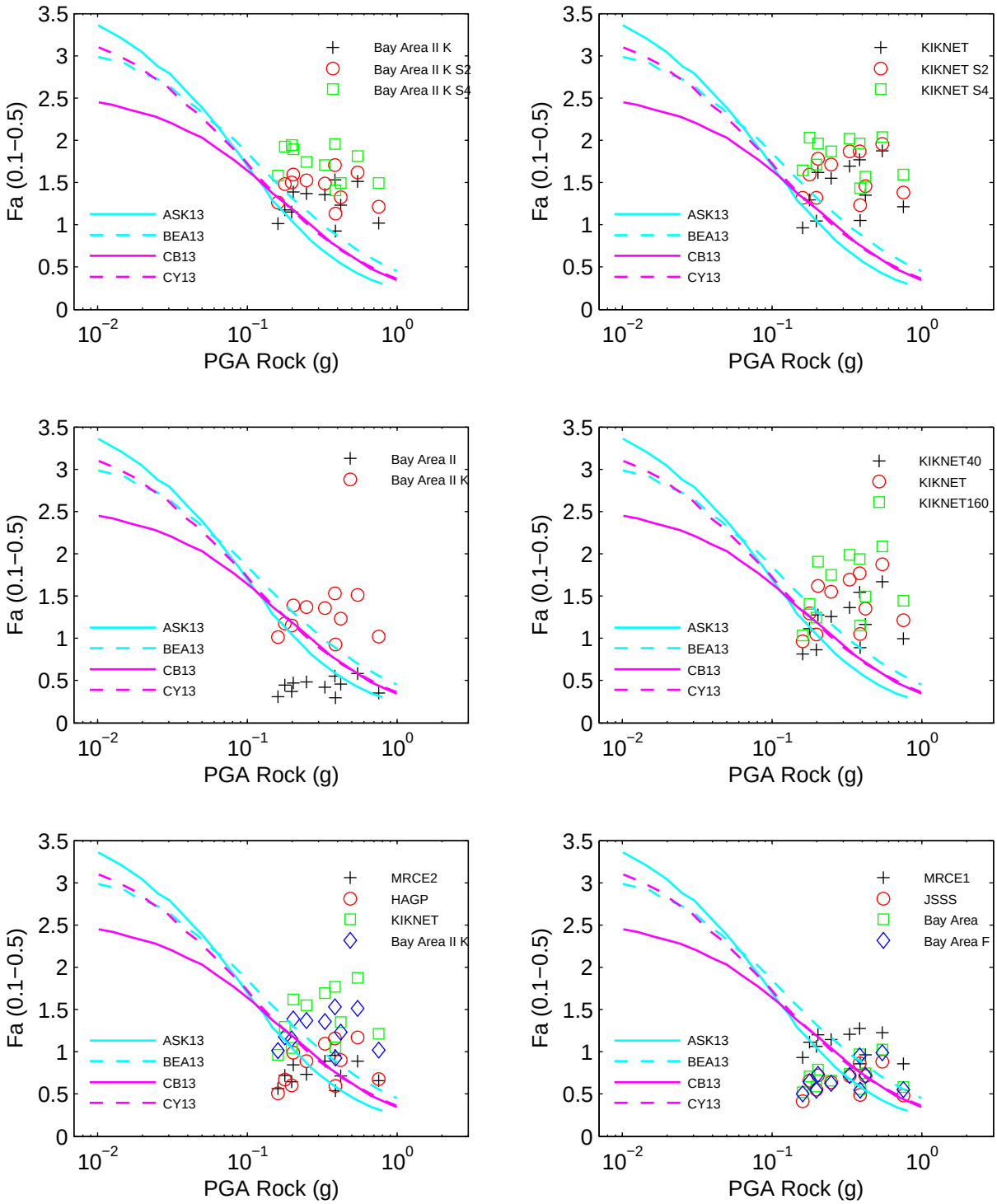

Figure 7E.12: Comparison of amplification factor Fv for scenario SCR

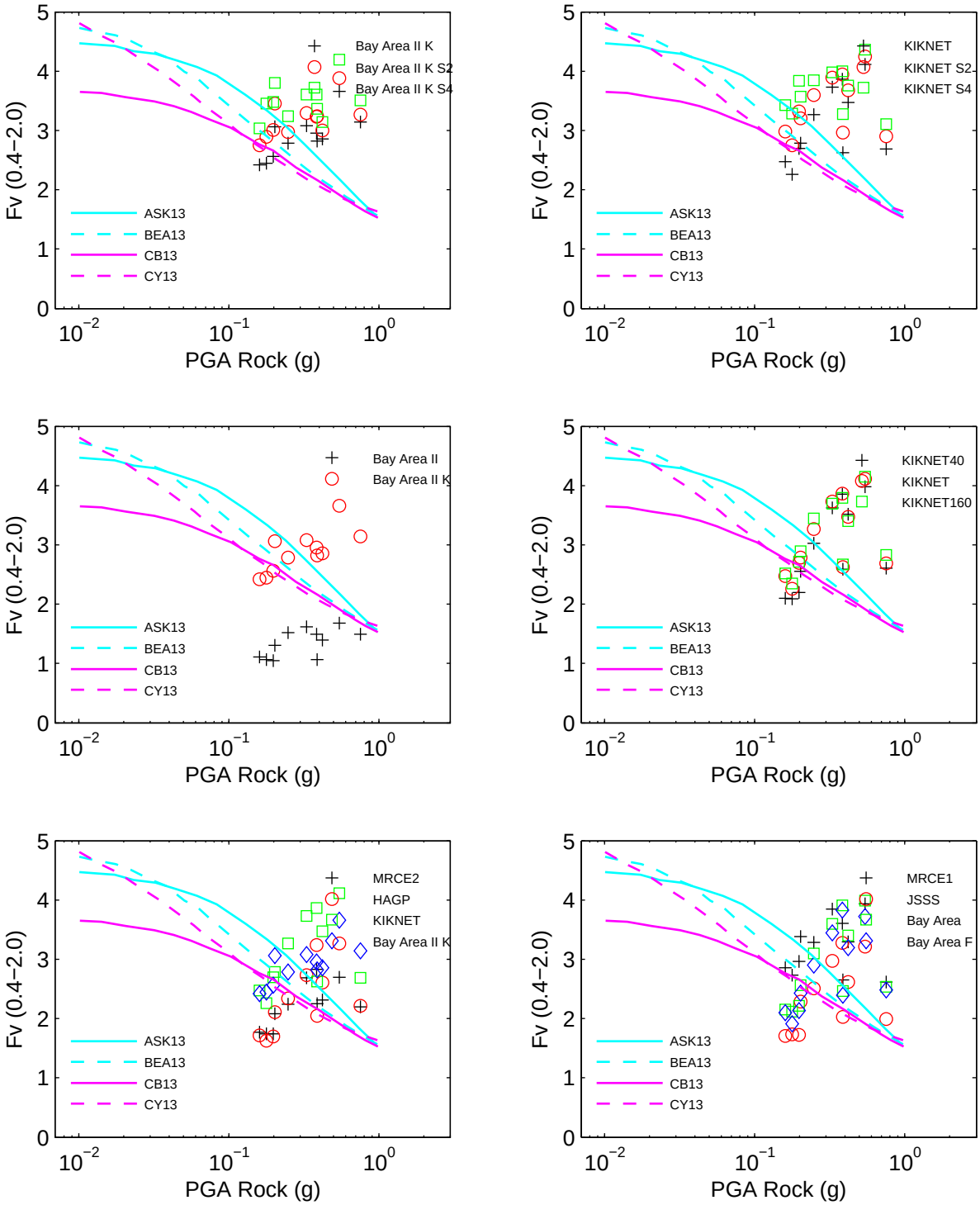

Figure 7E.13: Comparison of amplification factor Fa for scenarios 1−6

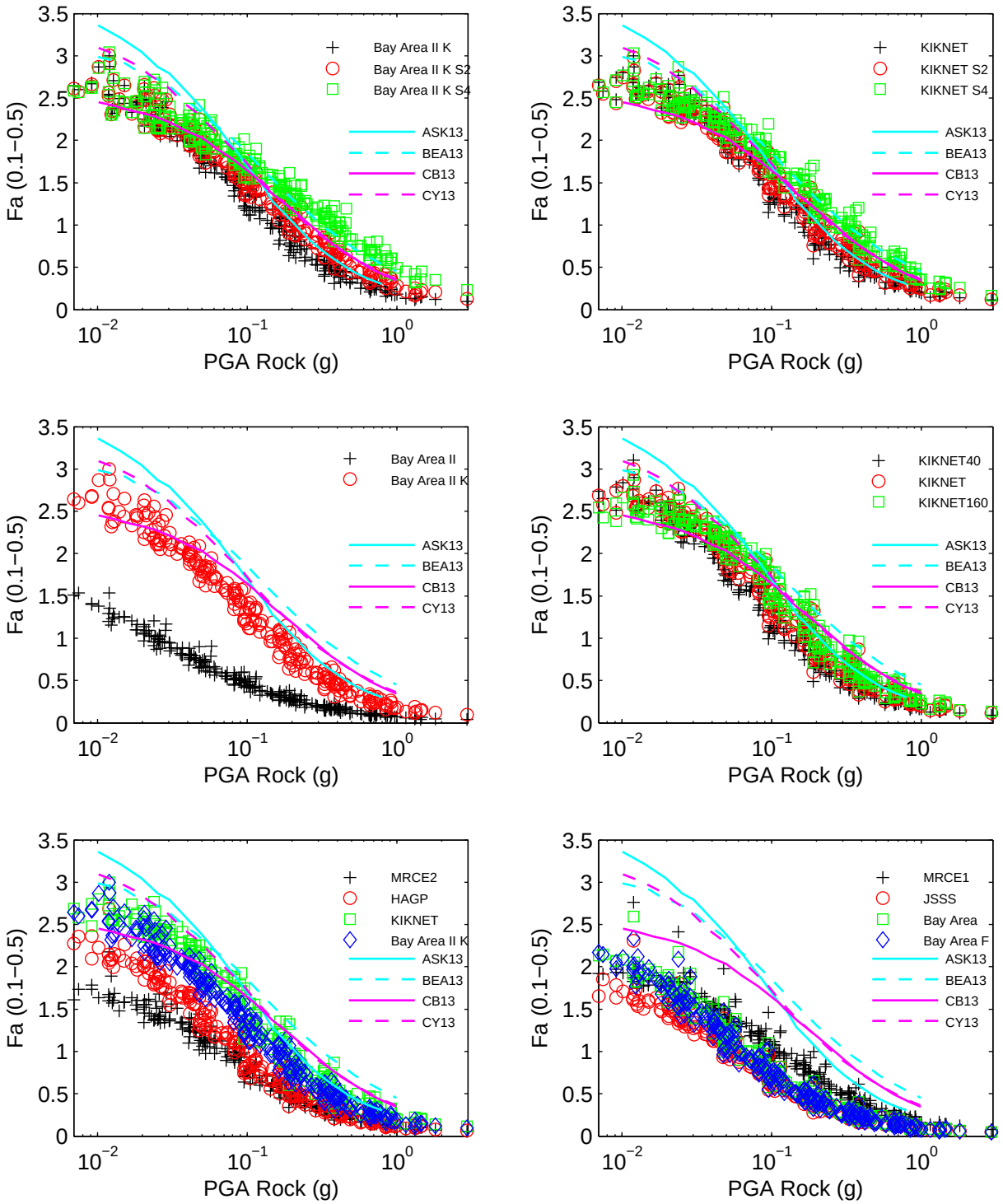

Figure 7E.14: Comparison of amplification factor Fv for scenarios 1−6

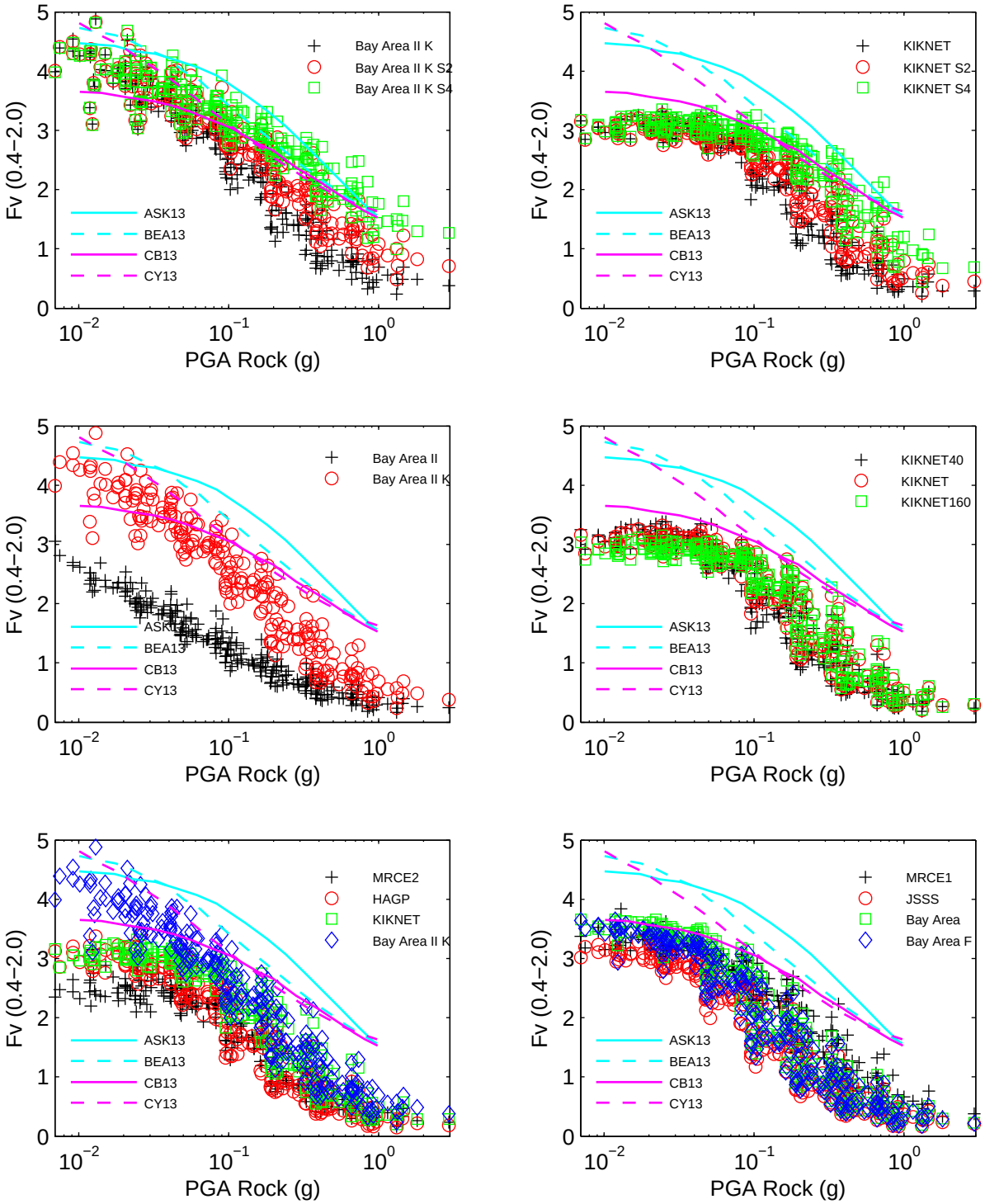

APPENDIX 7F: RESULTS OF OTHER GROUND MOTION PARAMETERS

Appendix 7F: Results of Other Ground Motion Parameters

Appendix 7F compares amplification ratios of PGA, PGV, T_m, $D_{5\text{-}95}$, and I_a versus the input rock PGA. There are six plots per figure, with one parameter per plot. The plot in the upper left of each page shows the amplification of PGA, the plot in the upper right shows PGV amplification, the middle left plot shows PGD amplification, the middle right shows $D_{5\text{-}95}$ amplification, the lower left plot presents T_m amplification, and the lower right plot in each figure shows the amplification of I_a versus PGA rock. Each plot in all three figures shows results from scenarios 12ACR3, 25ACR3, 50ACR3, 100ACR3, 200ACR3, and 400ACR3. Figures 7F.1 through 7F.9 explore simultaneously the effects of soil strength, soil MRD curves, elastic site period, ground motion intensity, near fault effects and scaling versus matched scenarios, and tectonic region. Figure 7F.10 through 7F.16 show the effects of analysis type on ground motion parameters.

Figure 7F.1: Comparison of scenario intensity and site strength

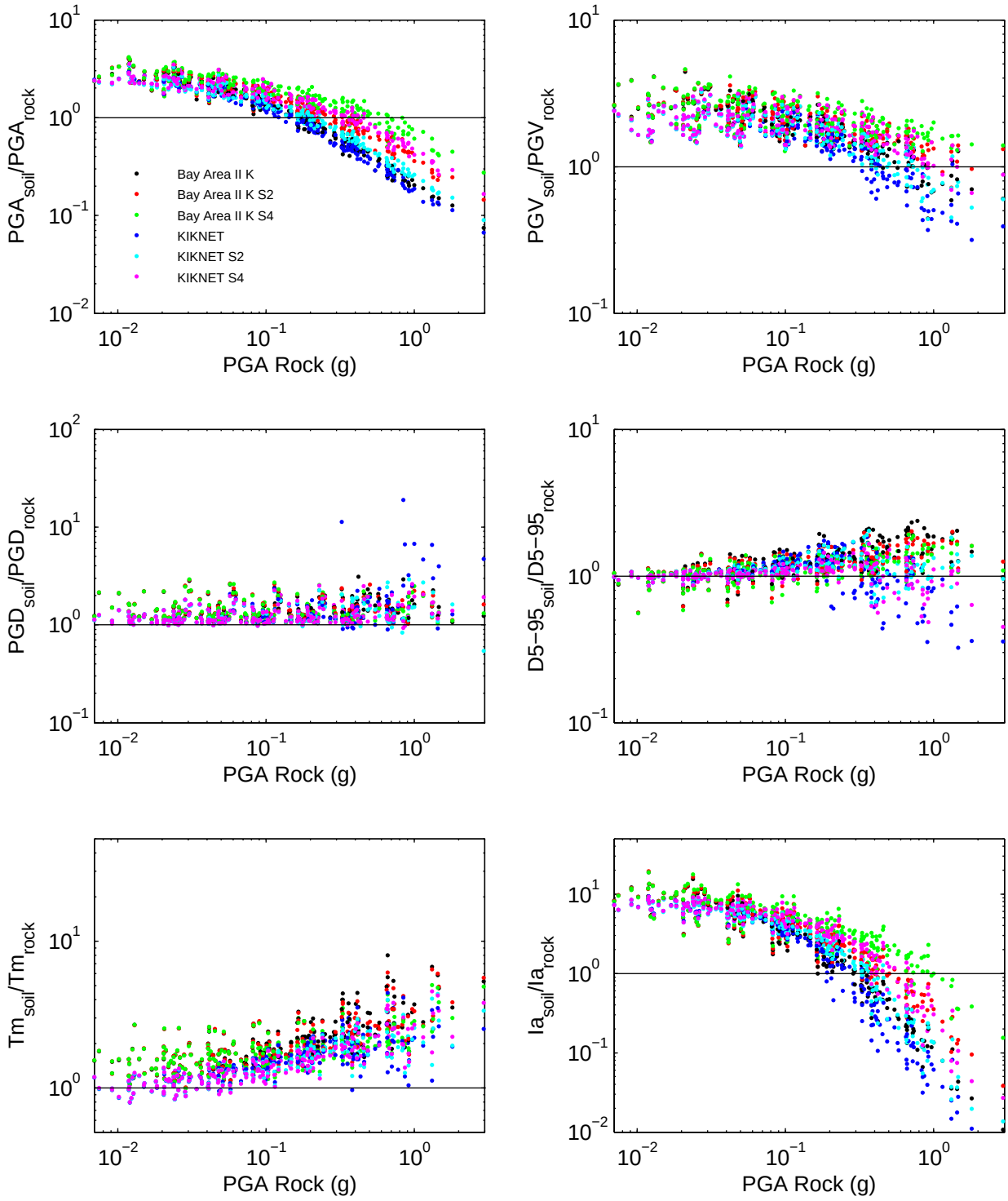

Figure 7F.2: Comparison of scenario intensity and site MRD curves

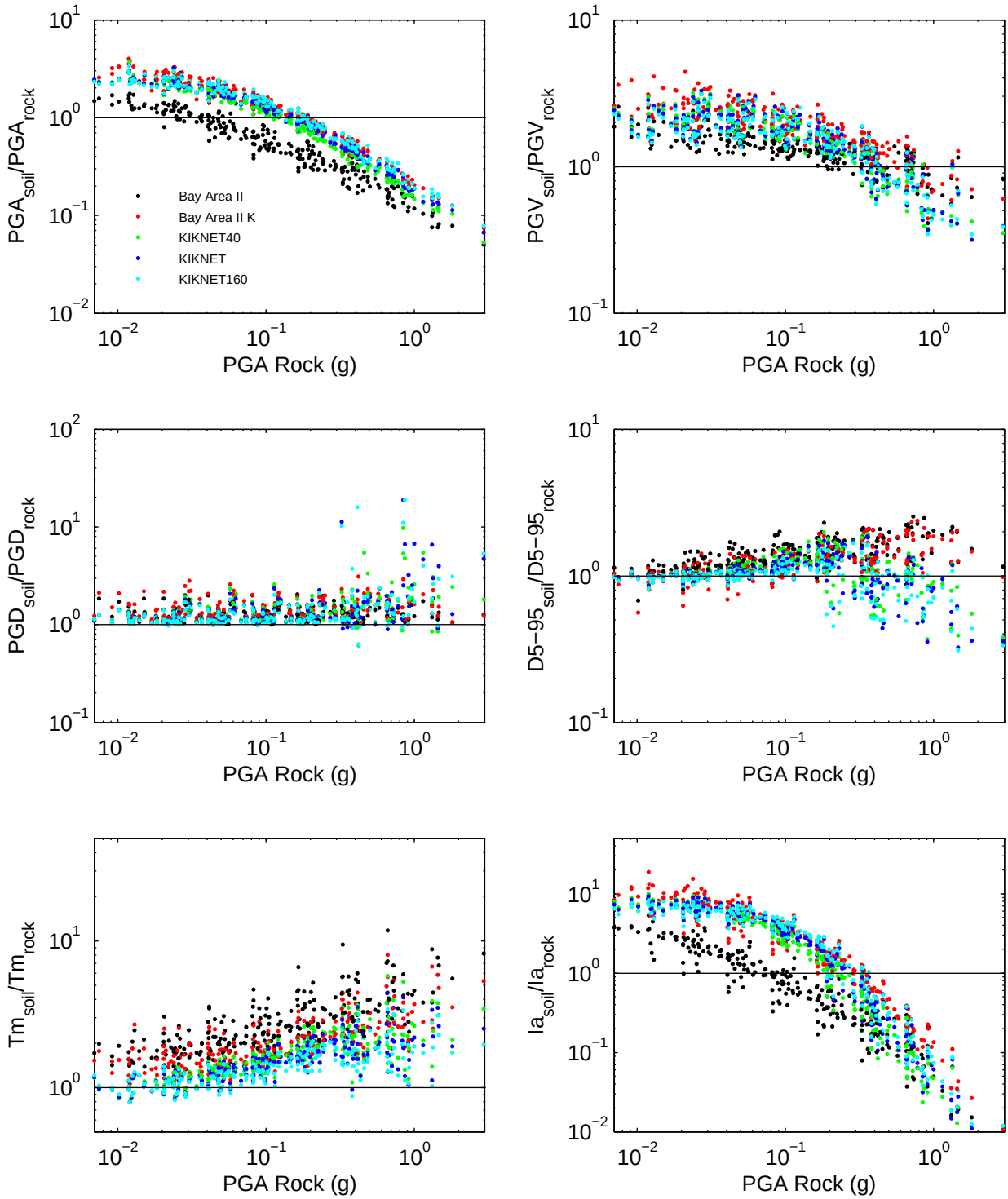

Figure 7F.3: Comparison of scenario intensity and site elastic period

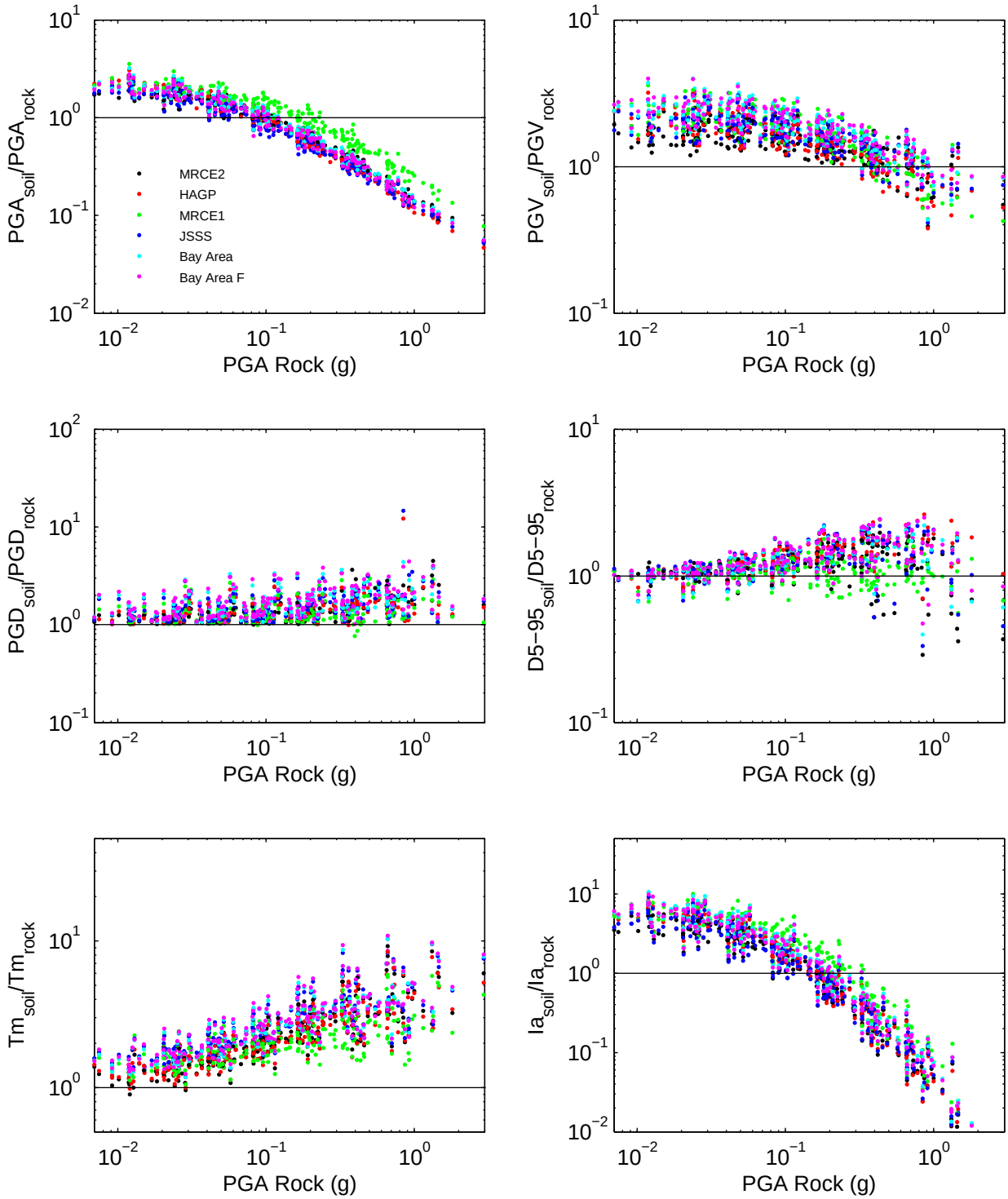

Figure 7F.4: Comparison of scenario near fault and scaled vs matched and site strength

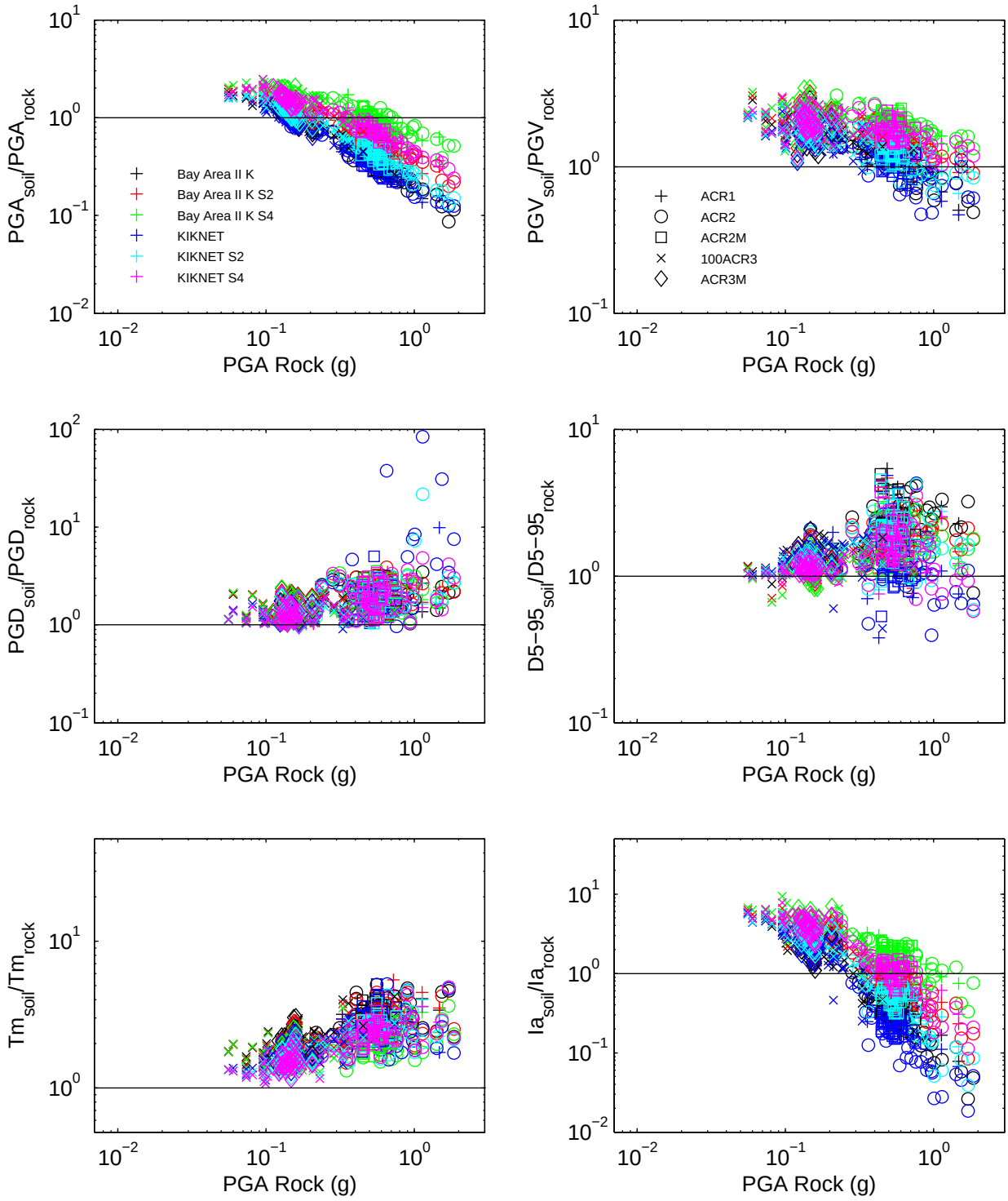

Figure 7F.5: Comparison of scenario near fault and scaled vs matched and site MRD curves

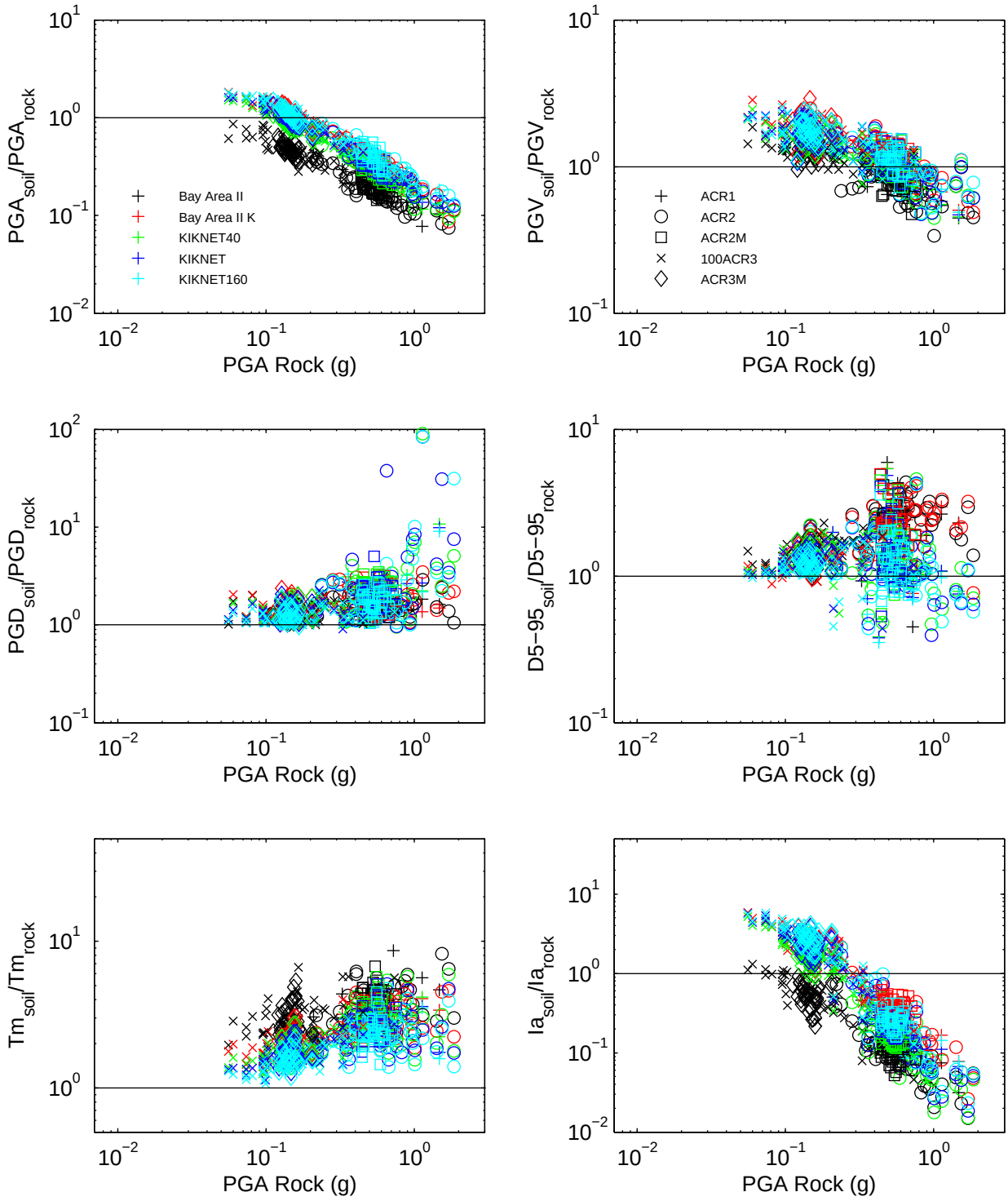

Figure 7F.6: Comparison of scenario near fault and scaled vs matched and site elastic period

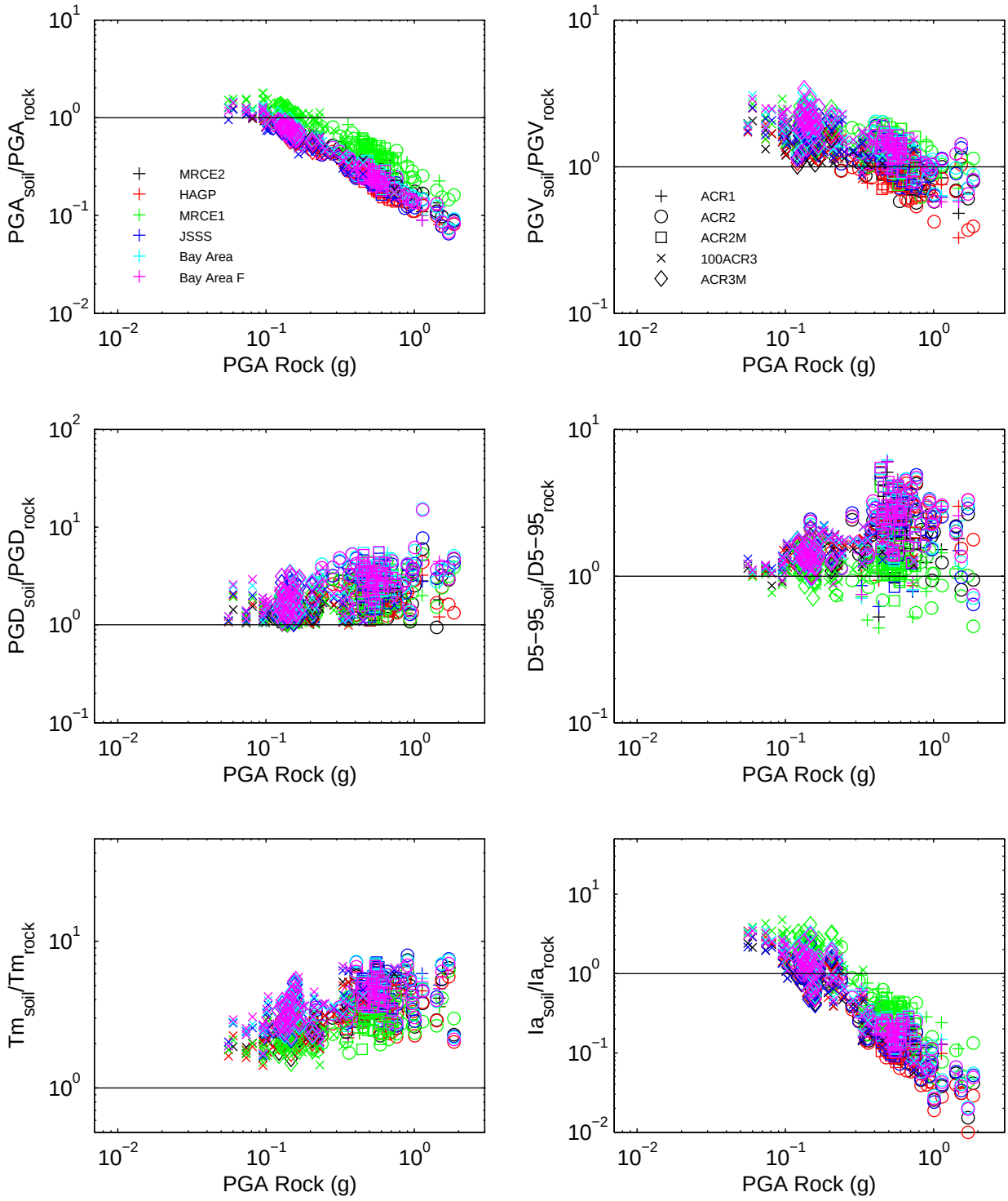

Figure 7F.7: Comparison of scenario tectonic region and site strength

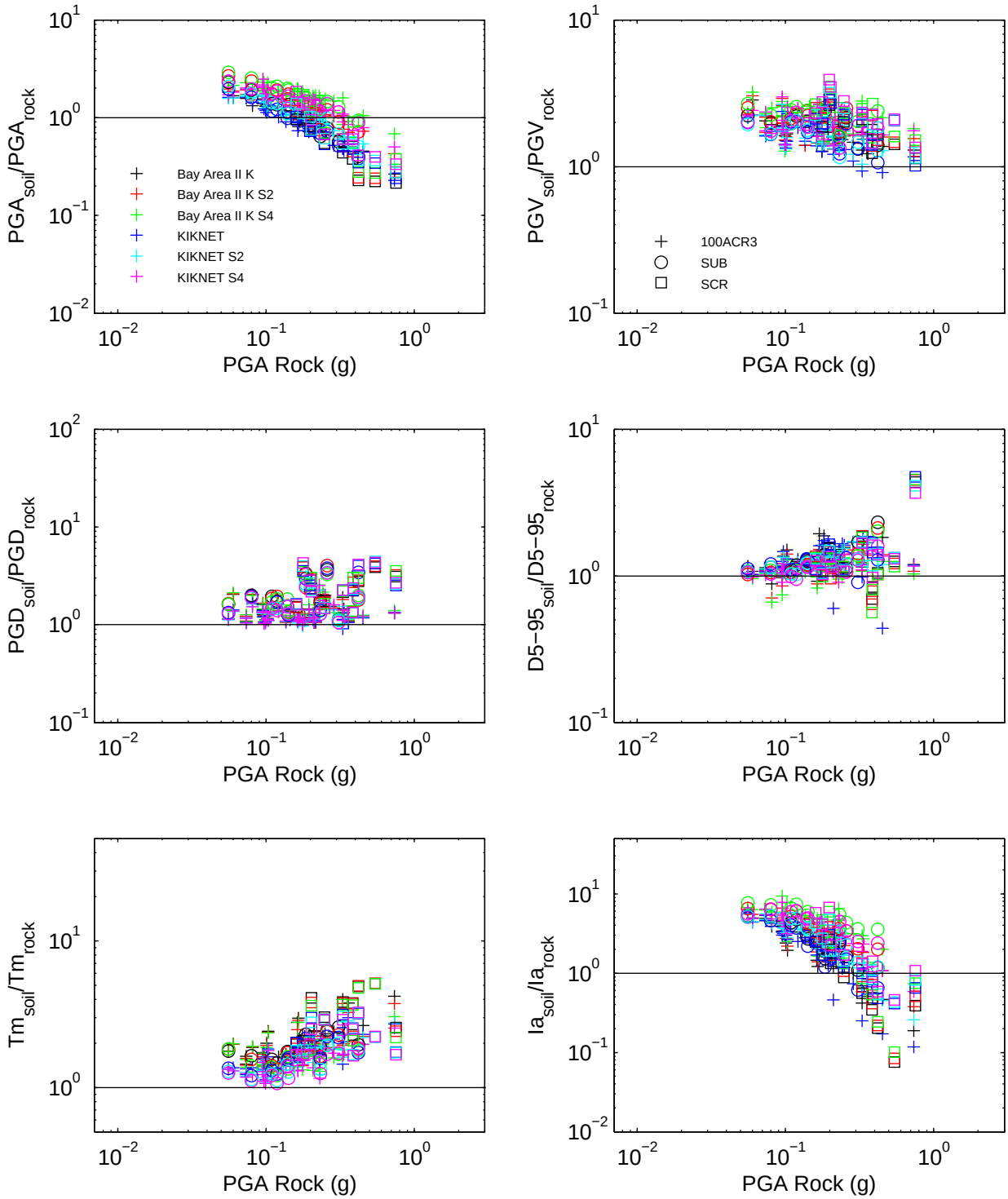

Figure 7F.8: Comparison of scenario tectonic region and site MRD curves

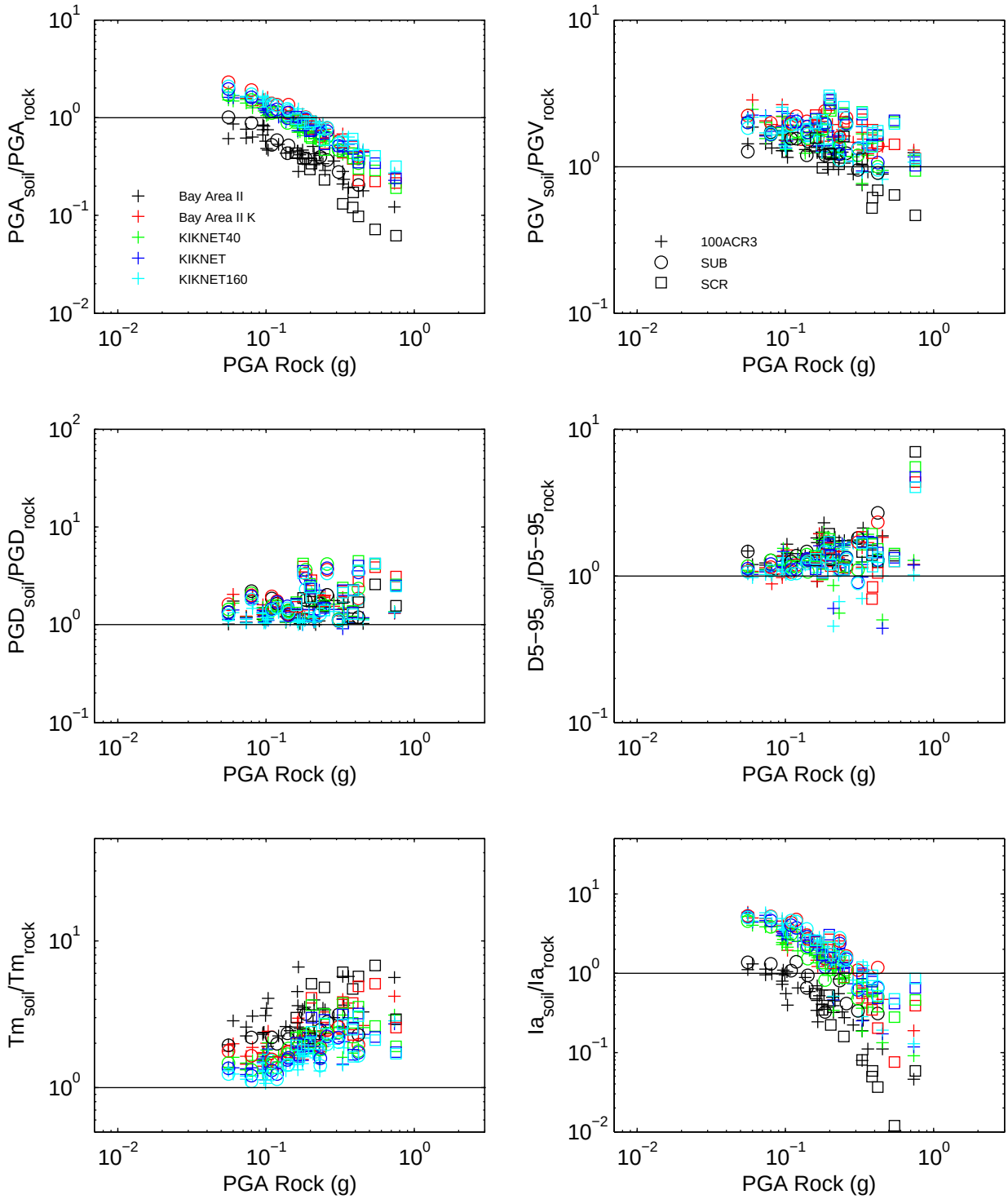

Figure 7F.9: Comparison of scenario tectonic region and site elastic period

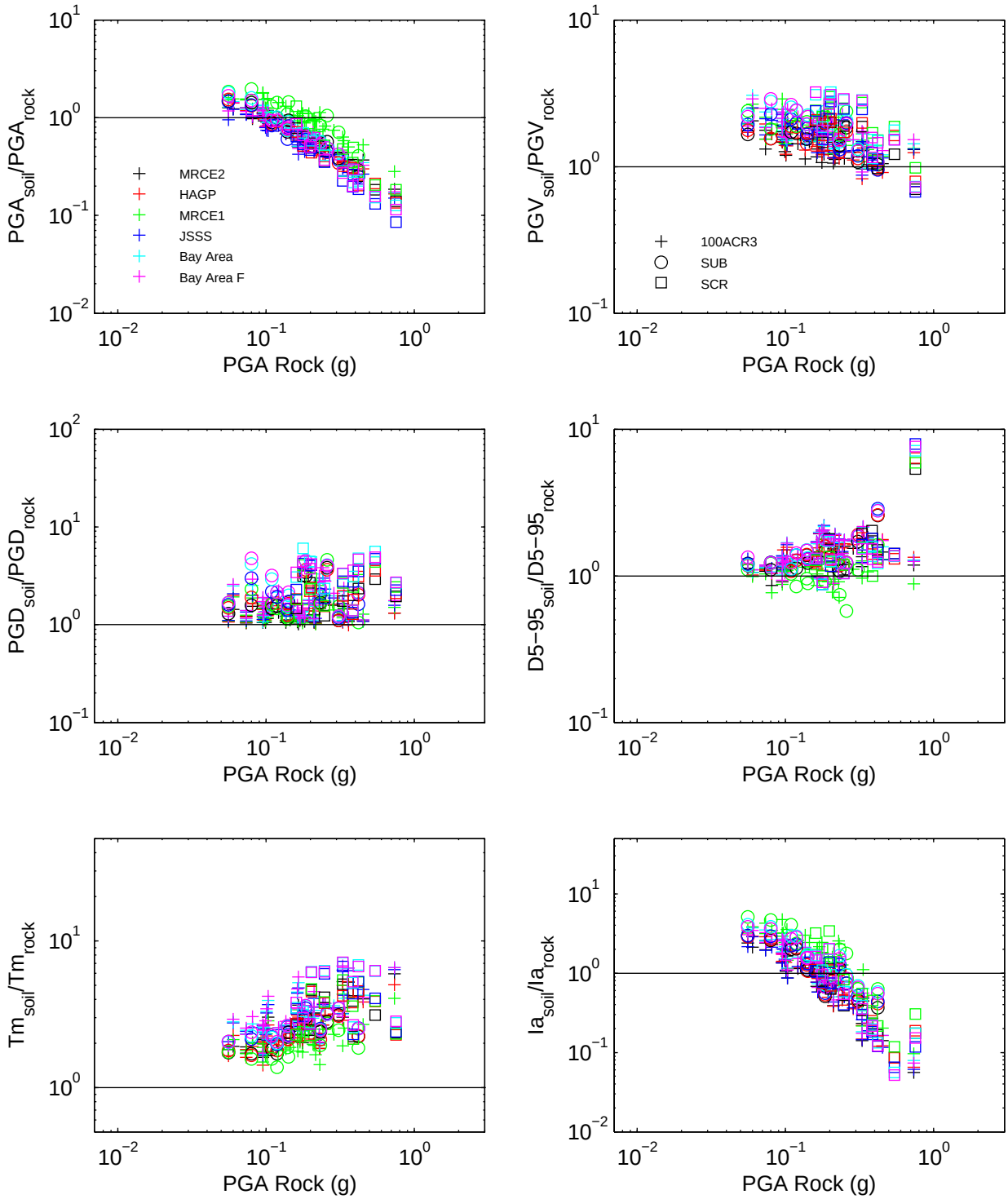

Figure 7F.10: Comparison of analysis type and scenarios 1−6 for site MRCE2

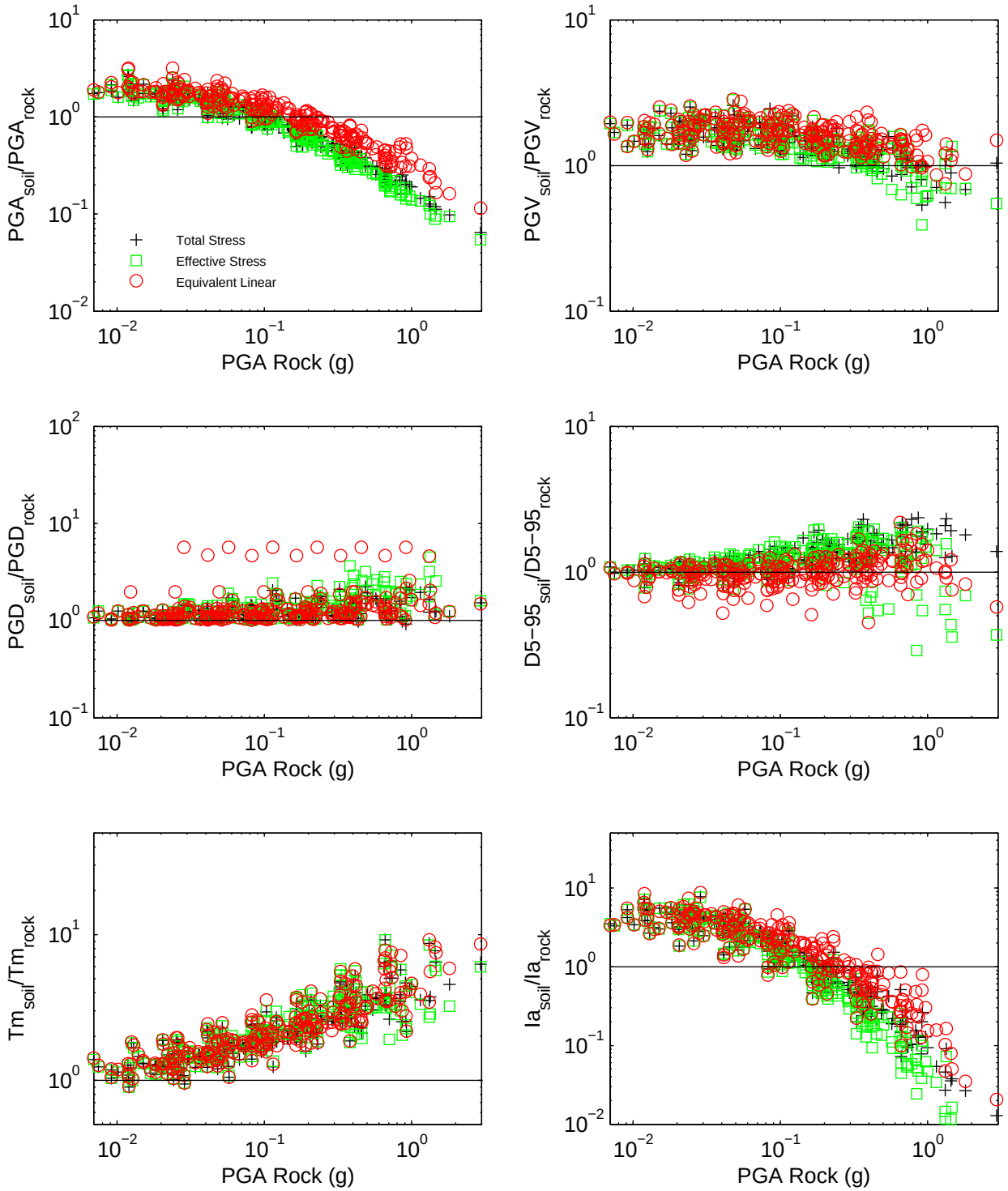

Figure 7F.11: Comparison of analysis type and scenarios 1−6 for site HAGP

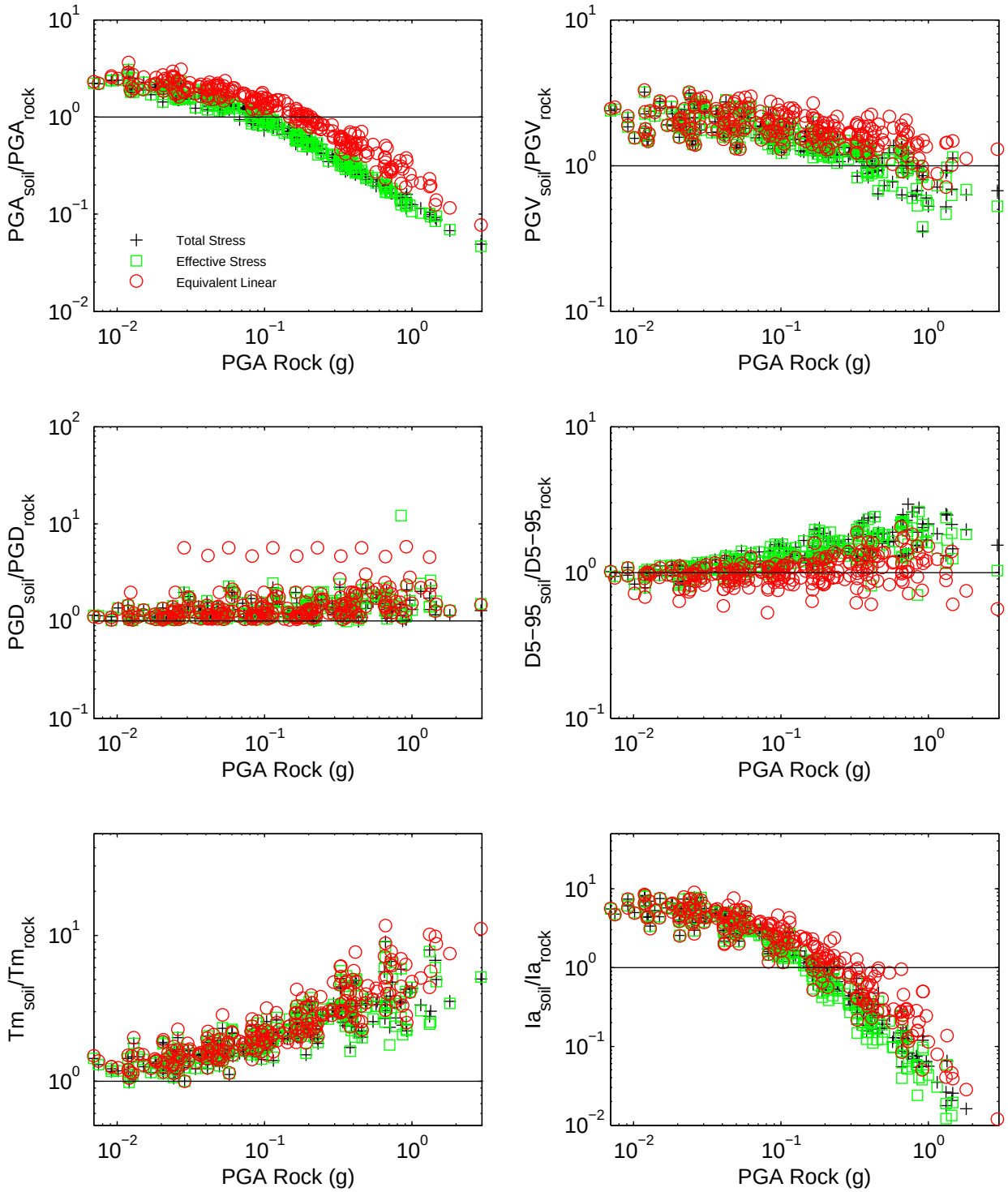

Figure 7F.12: Comparison of analysis type and scenarios 1−6 for site KIKNET

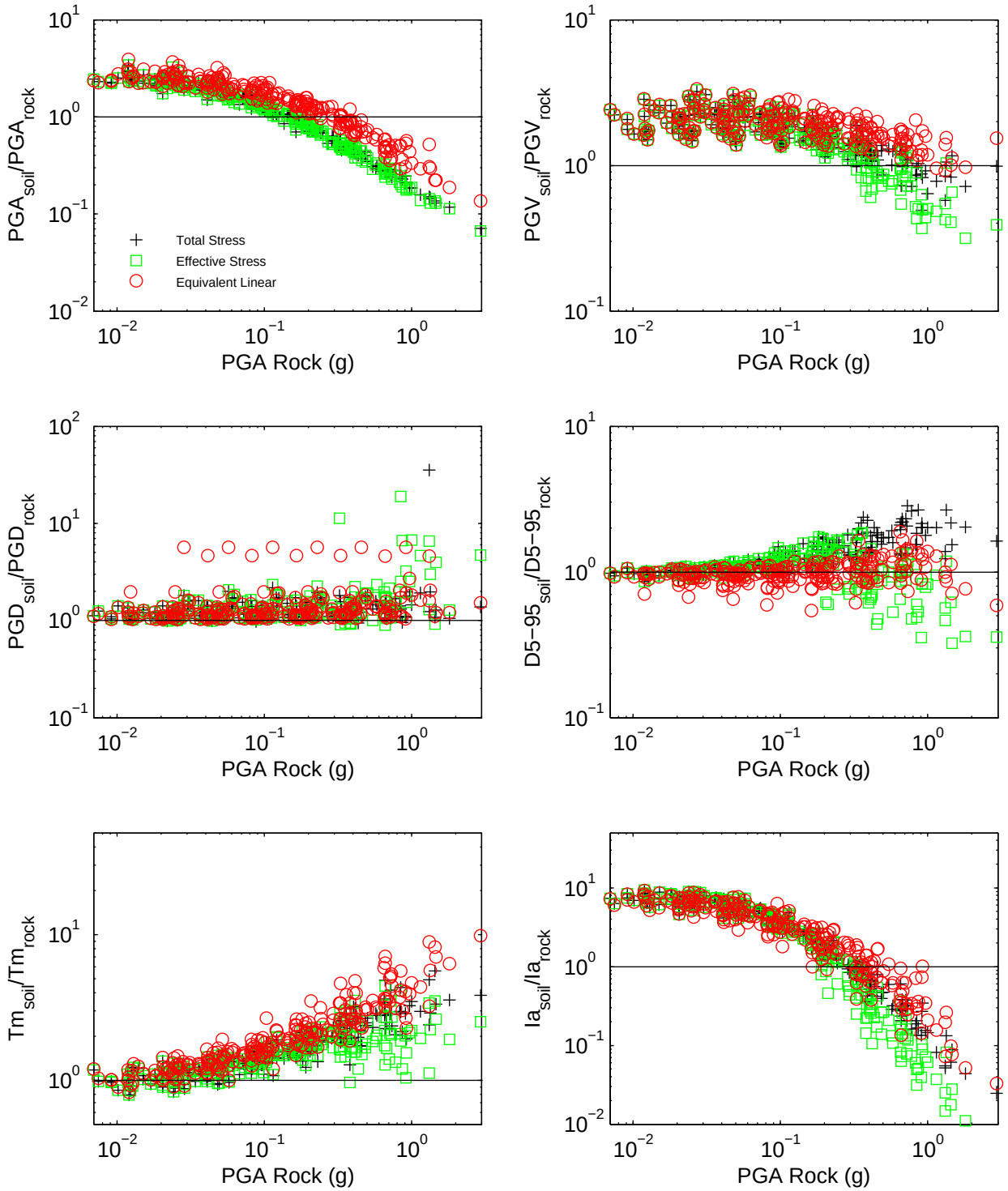

Figure 7F.13: Comparison of analysis type and scenarios 1−6 for site Bay Area II

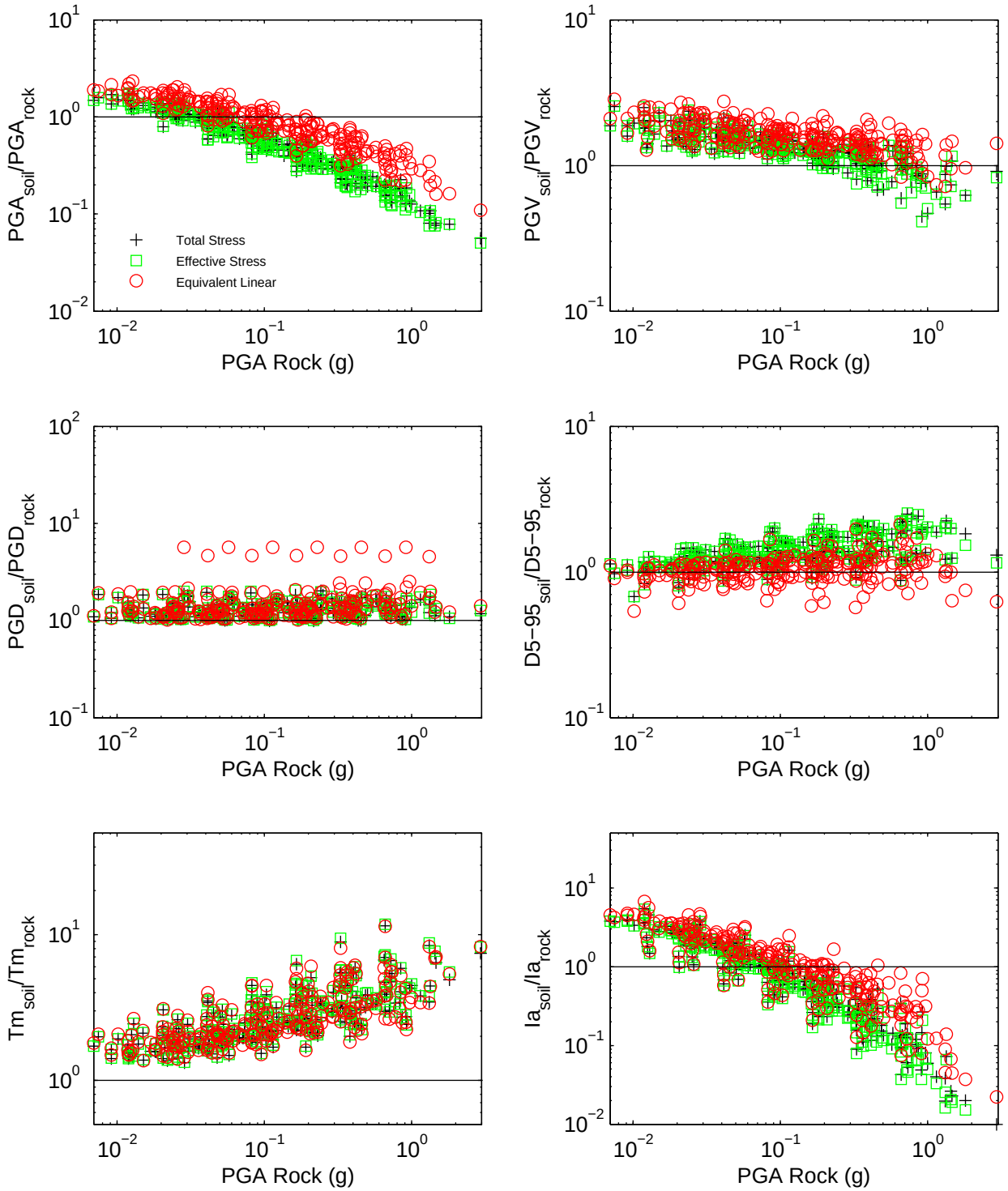

Figure 7F.14: Comparison of analysis type and scenarios 1−6 for site MRCE1

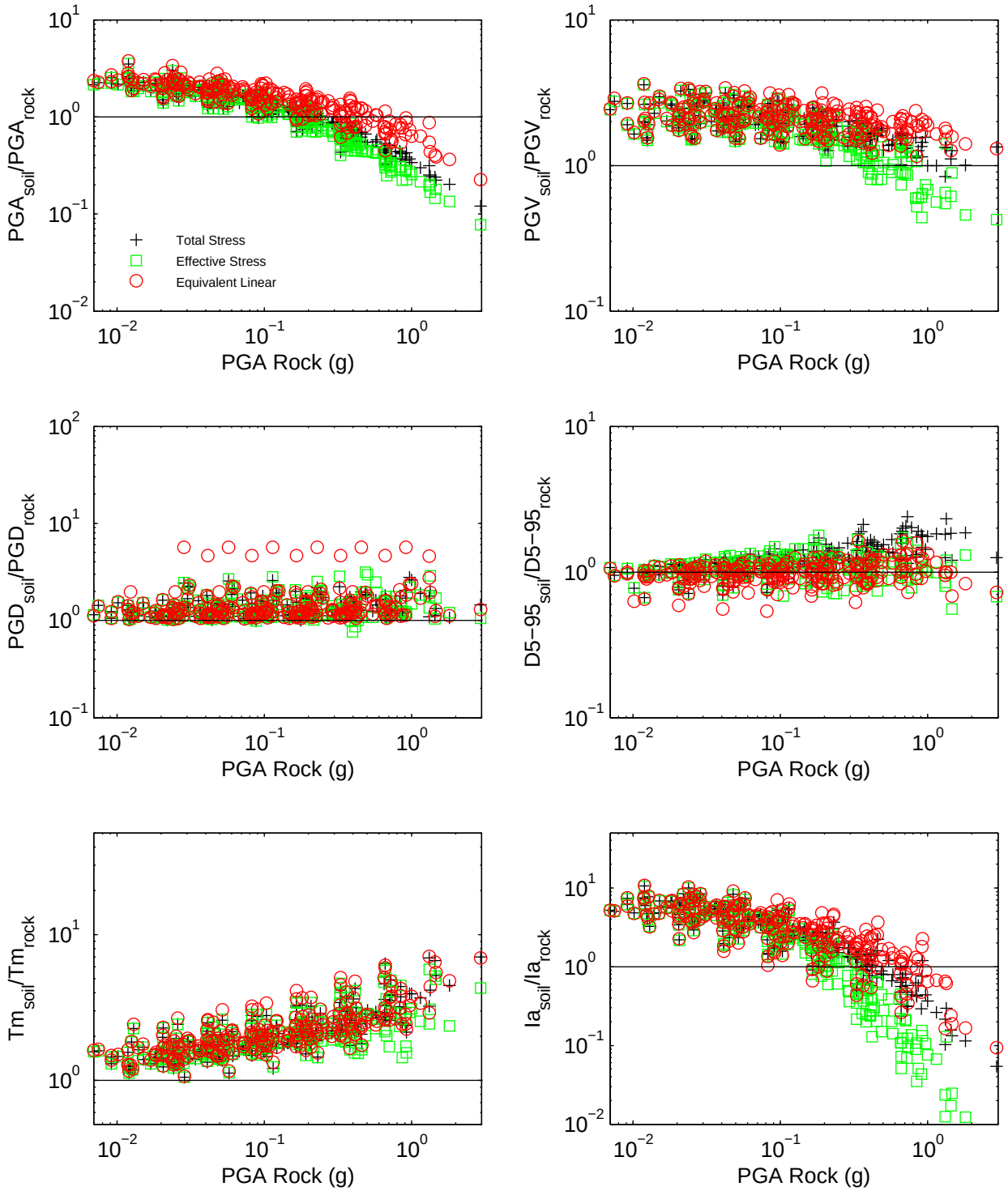

Figure 7F.15: Comparison of analysis type and scenarios 1−6 for site JSSS

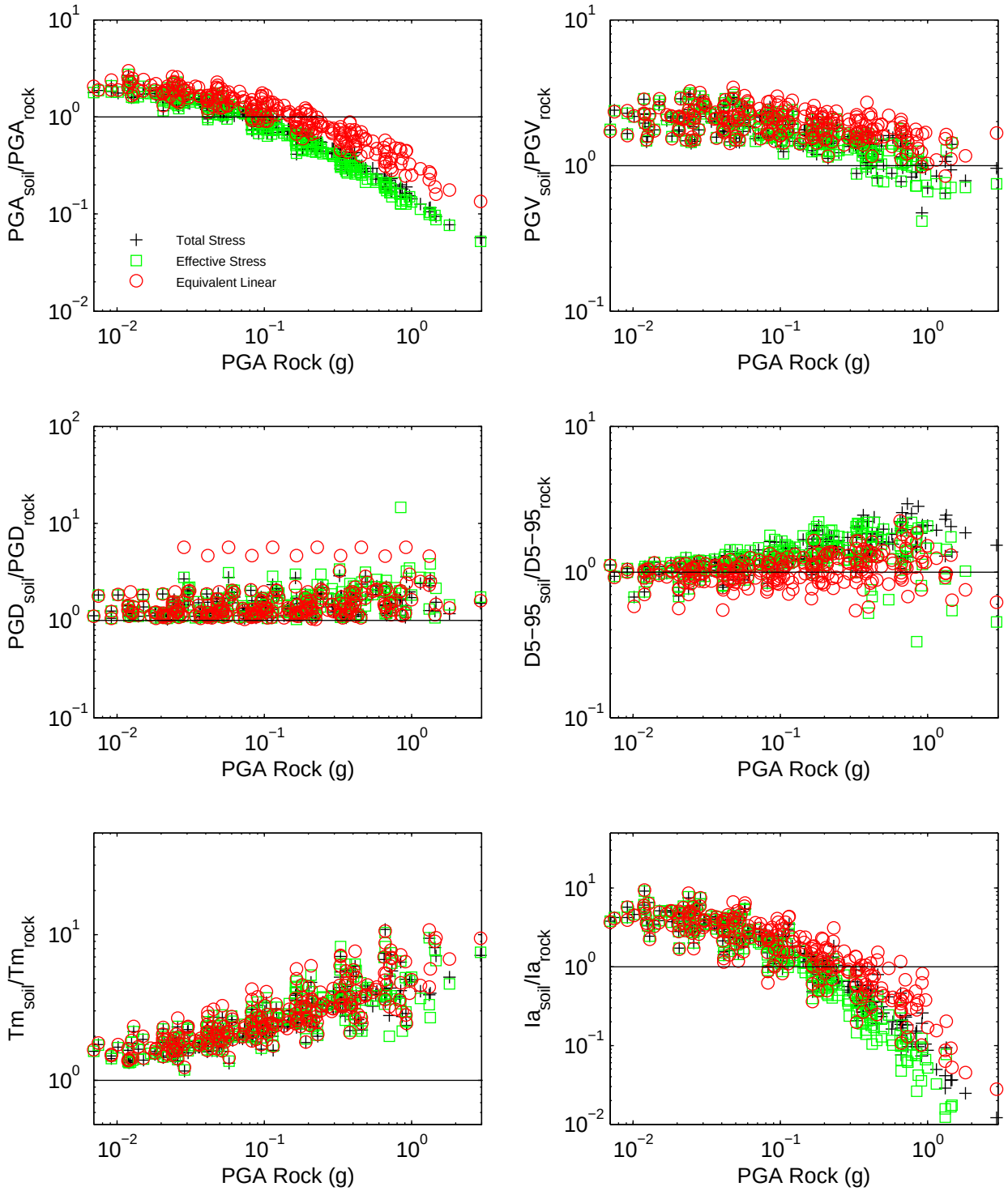

Figure 7F.16: Comparison of analysis type and scenarios 1−6 for site Bay Area

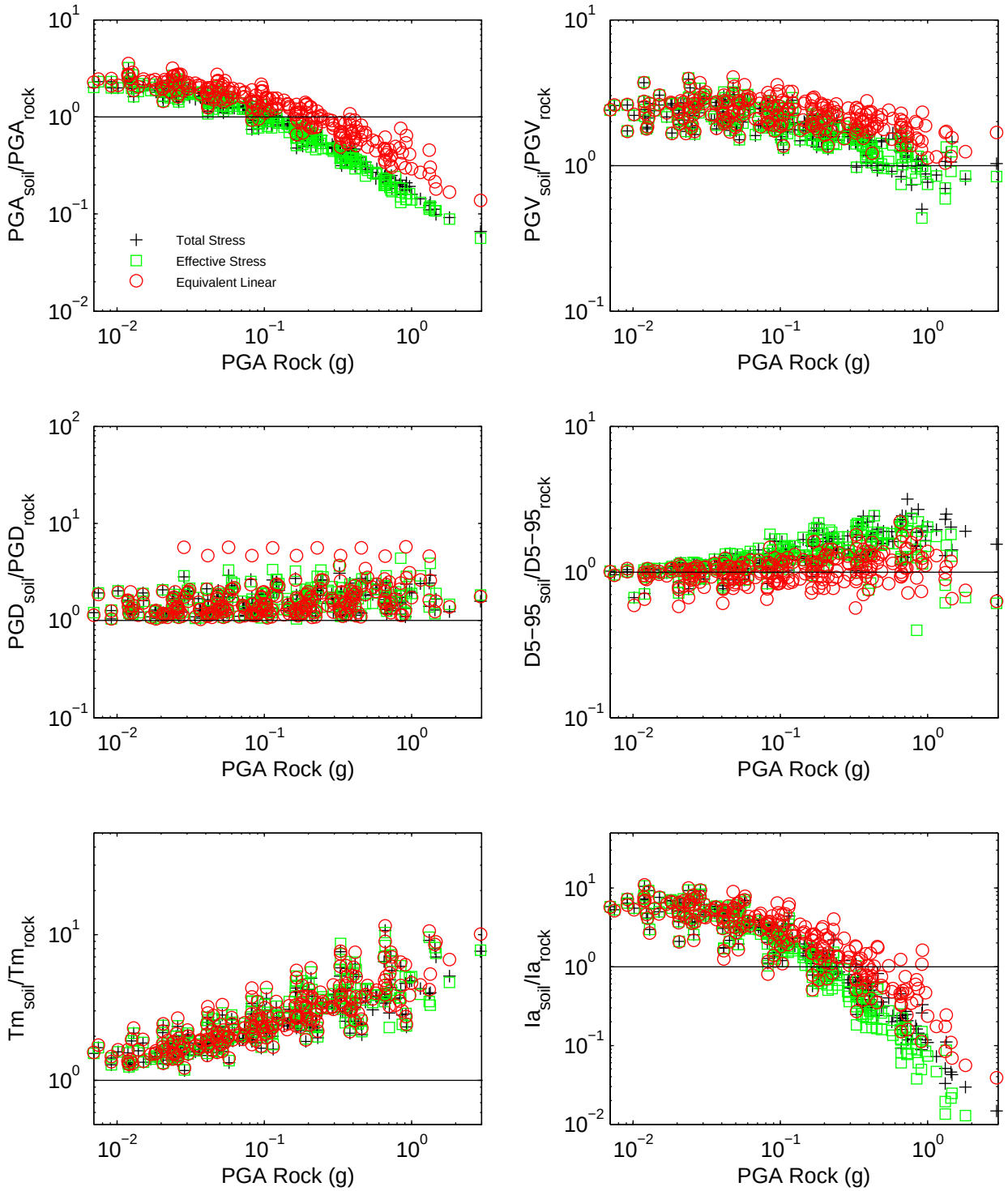

APPENDIX 8A: RESULTS OF THE SIMPLIFIED PROCEDURE

Appendix 8A: Results of the Simplified Procedure

Appendix 8A contains figures that compare the response spectra calculated from the site response analyses (solid lines) with the response spectra predicted from the simplified method (dashed lines) for all scenarios and sites. The top two plots in each figure show the response spectra in loglog space and the middle two plots show the response spectra in semi-logarithmic space. The bottom two plots show the residuals versus period.

Figure 8A.1: Bay Area Results

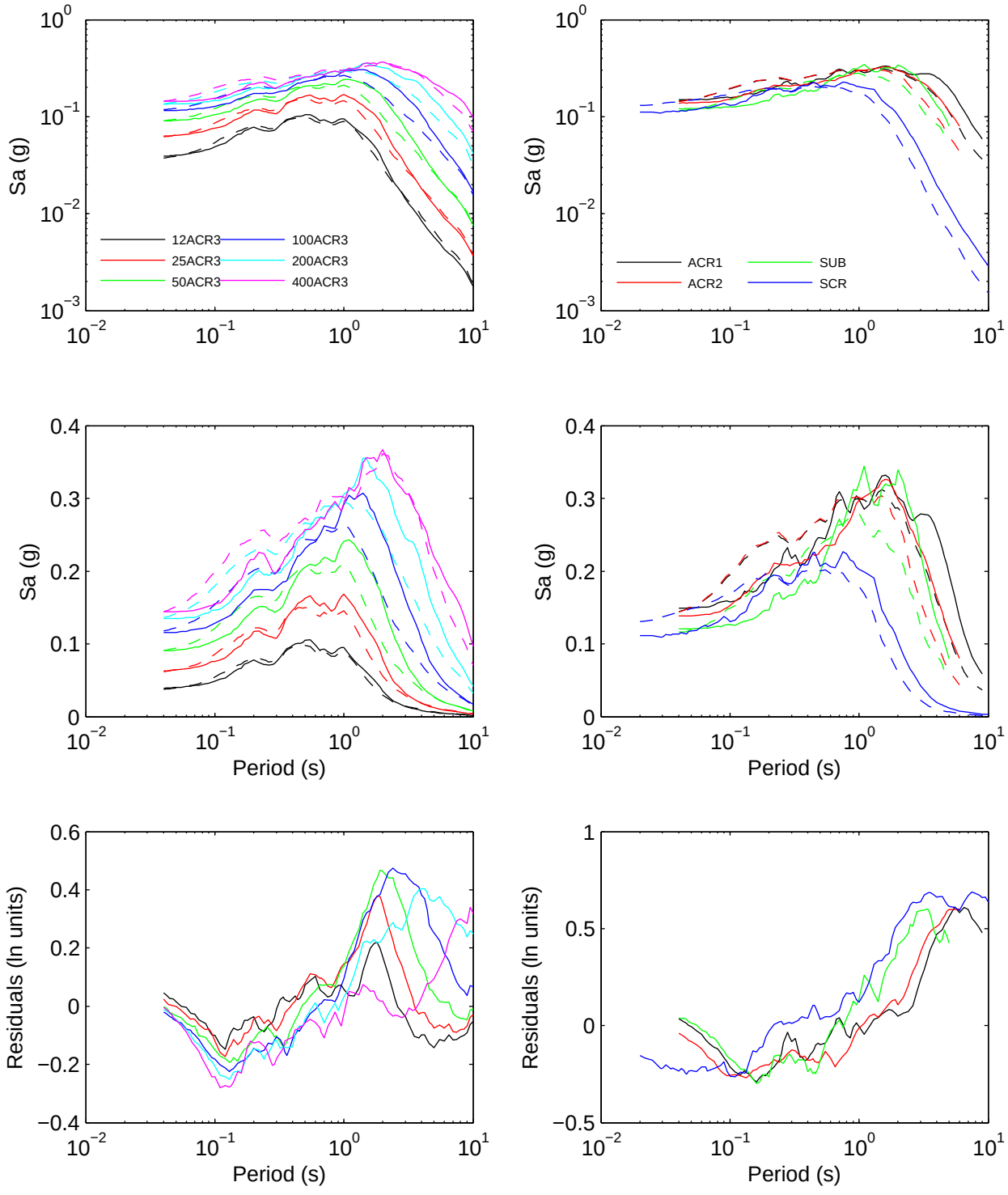

Figure 8A.2: Bay Area F Results

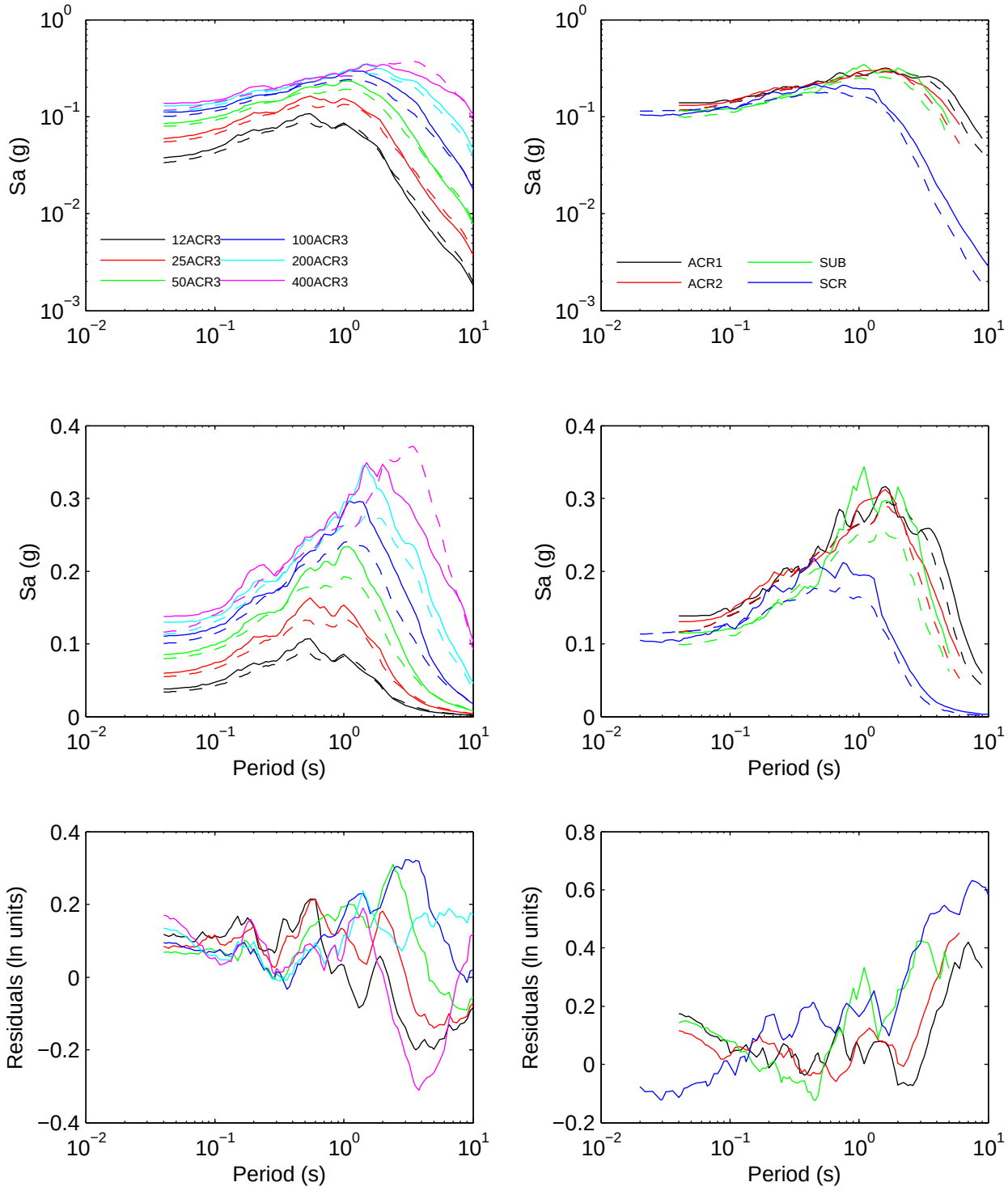

Figure 8A.3: Bay Area II Results

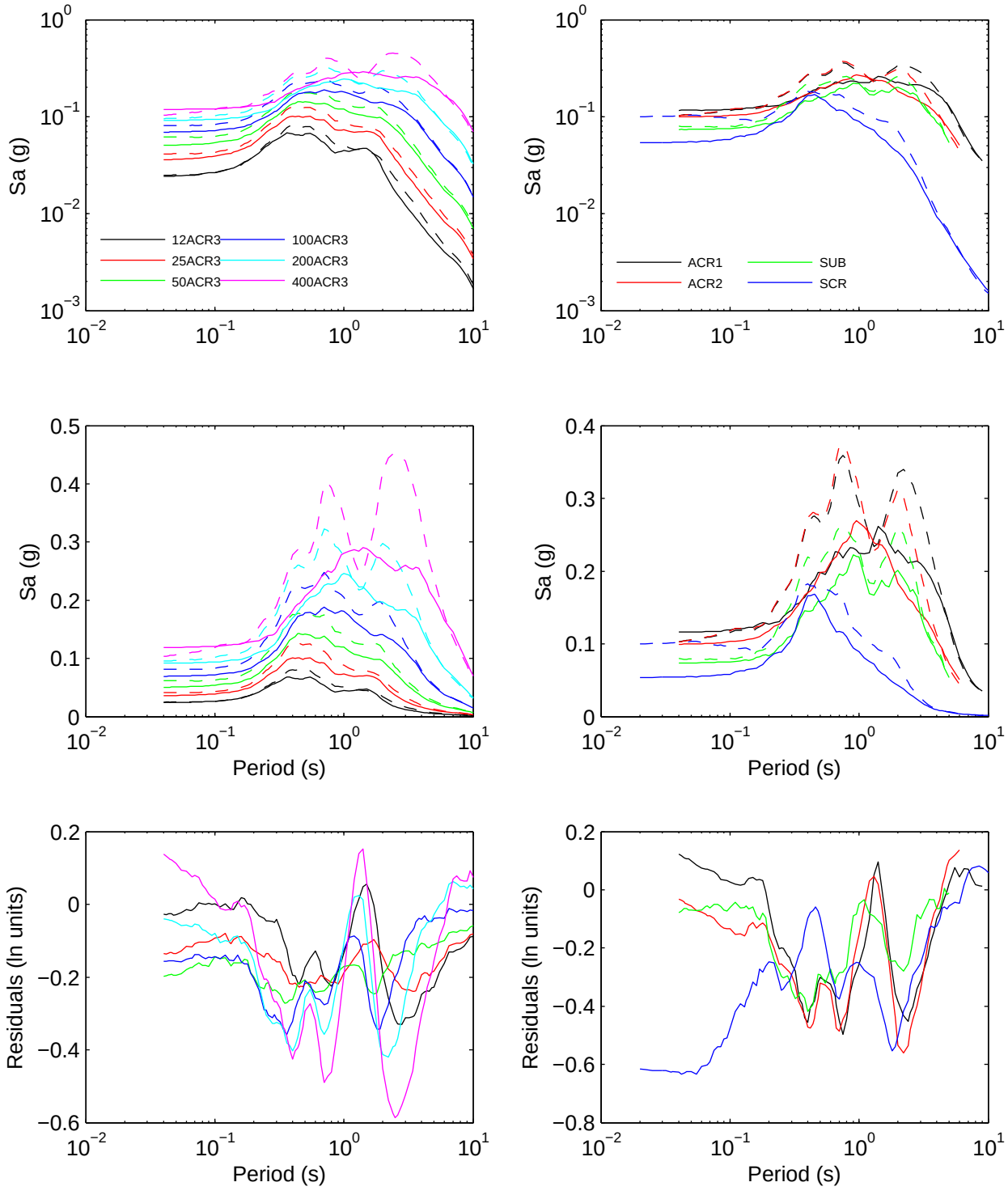

Figure 8A.4: Bay Area II K Results

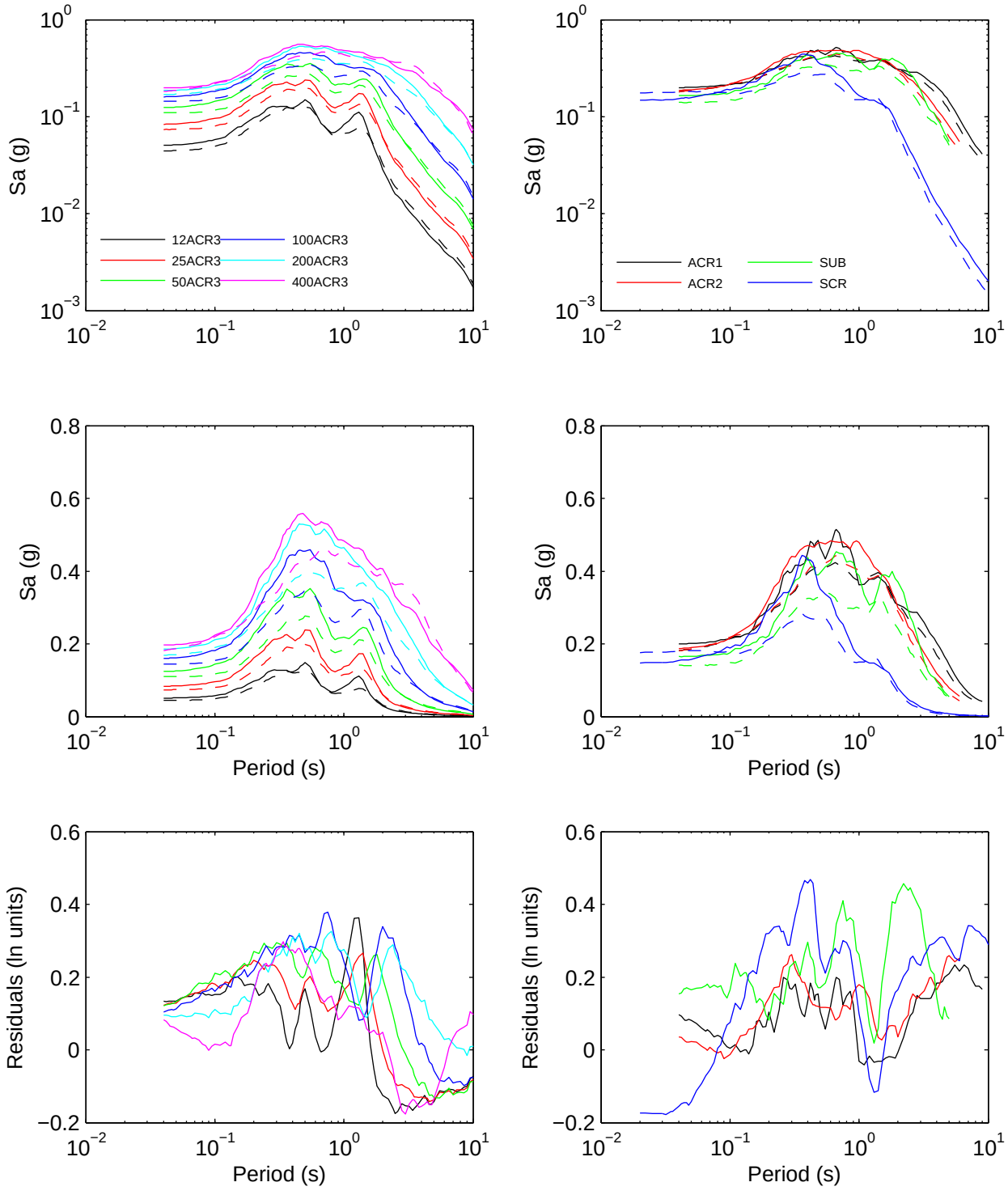

Figure 8A.5: Bay Area II K S2 Results

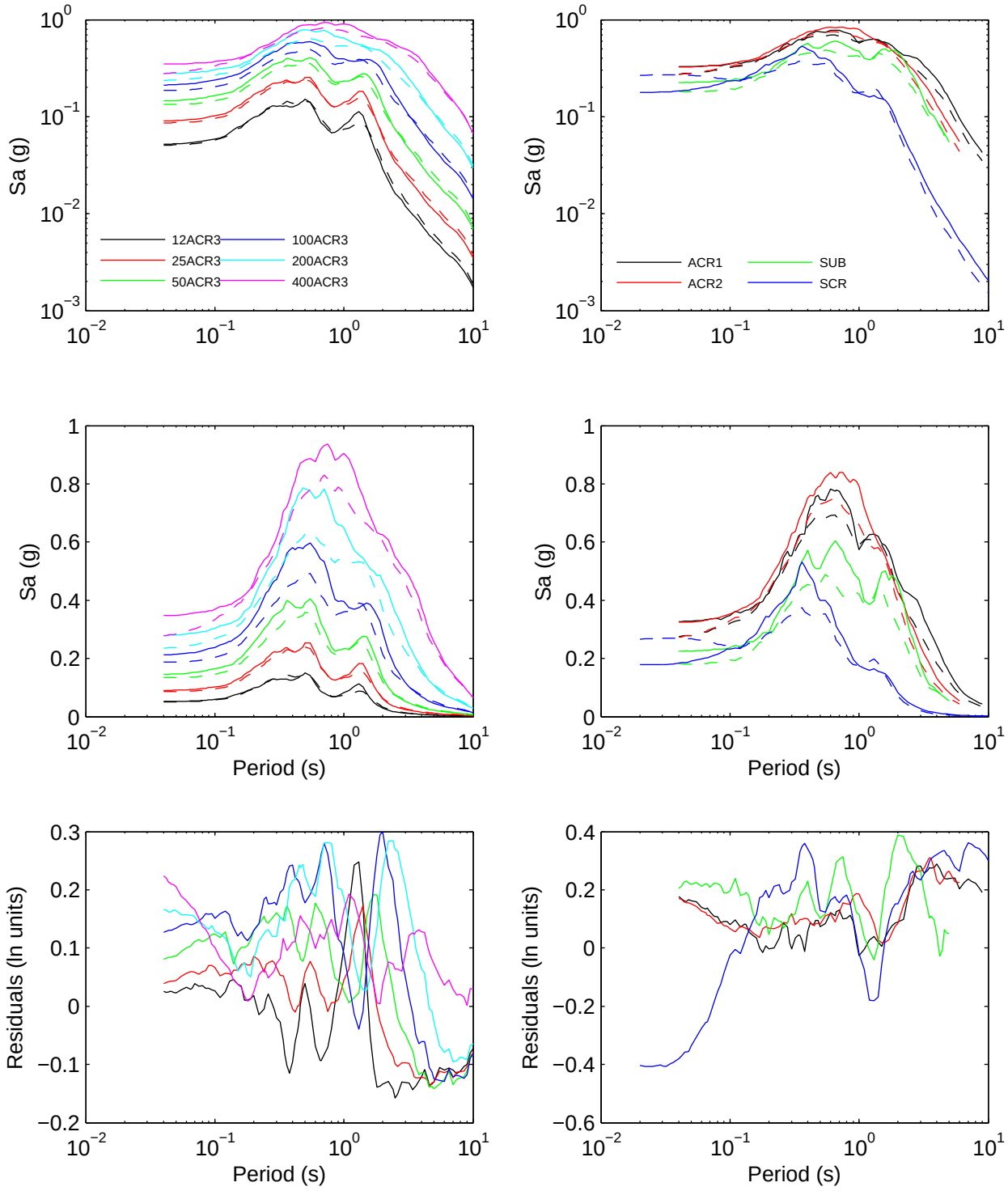

Figure 8A.6: Bay Area II K S4 Results

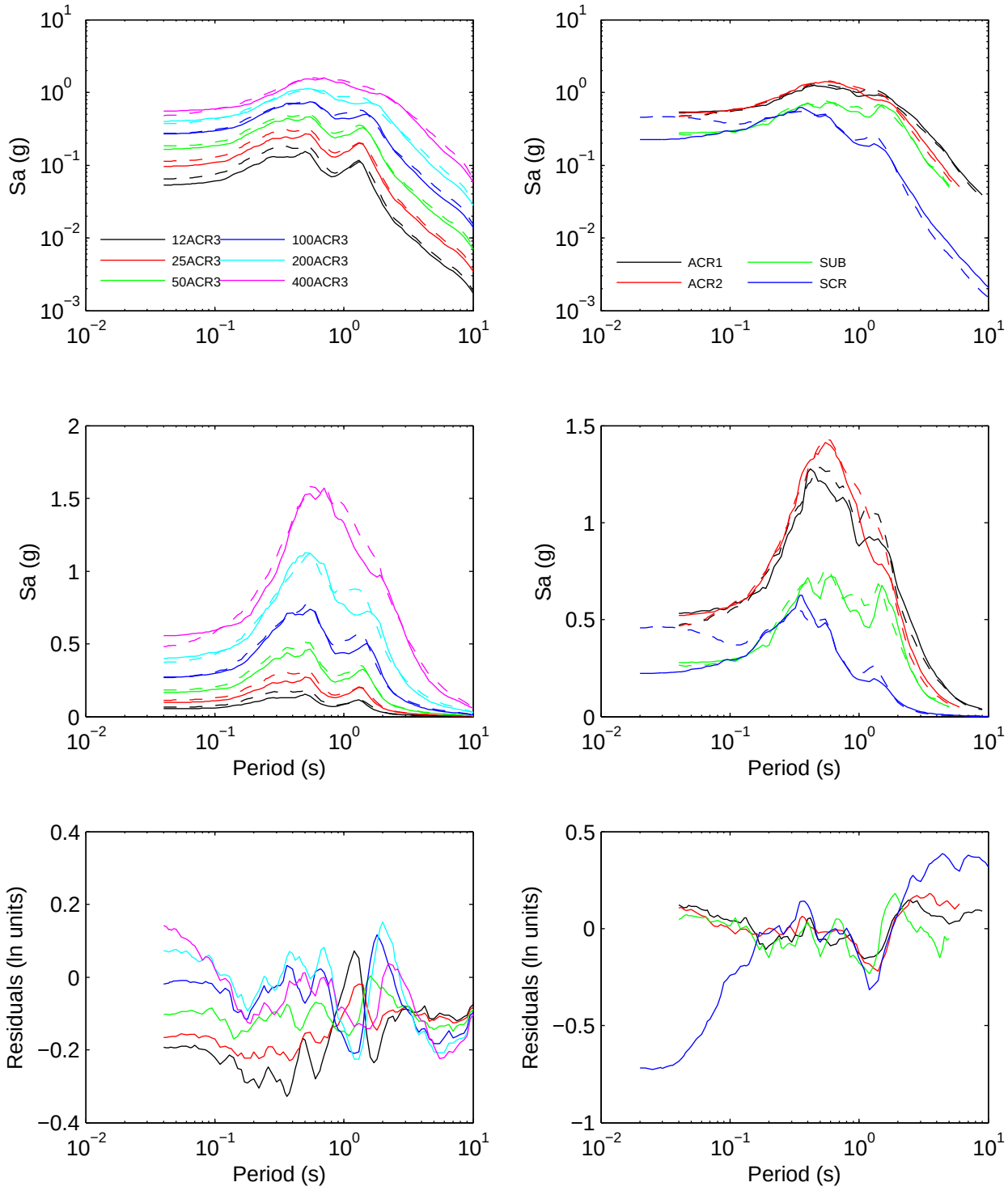

Figure 8A.7: HAGP Results

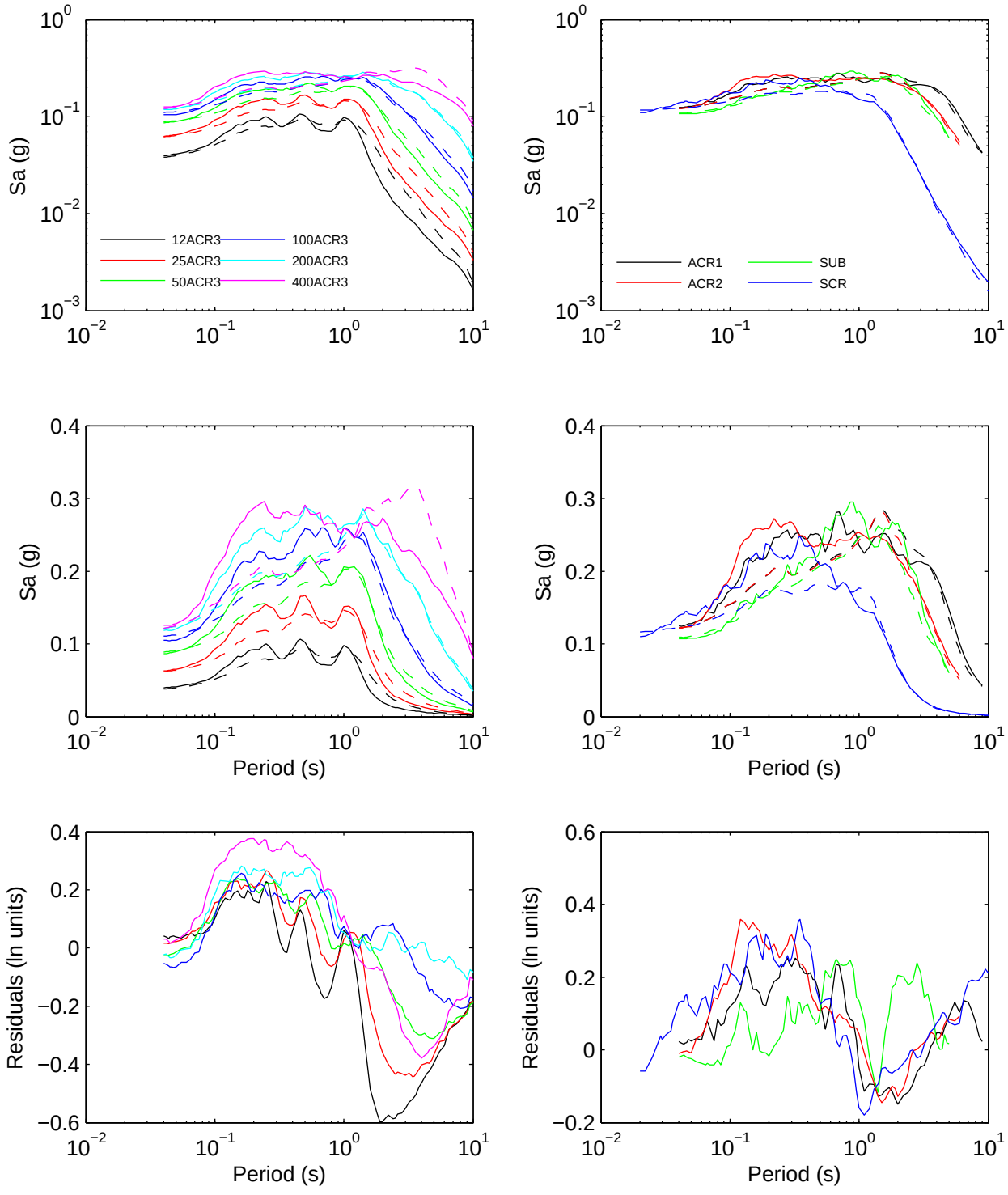

Figure 8A.8: JSSS Results

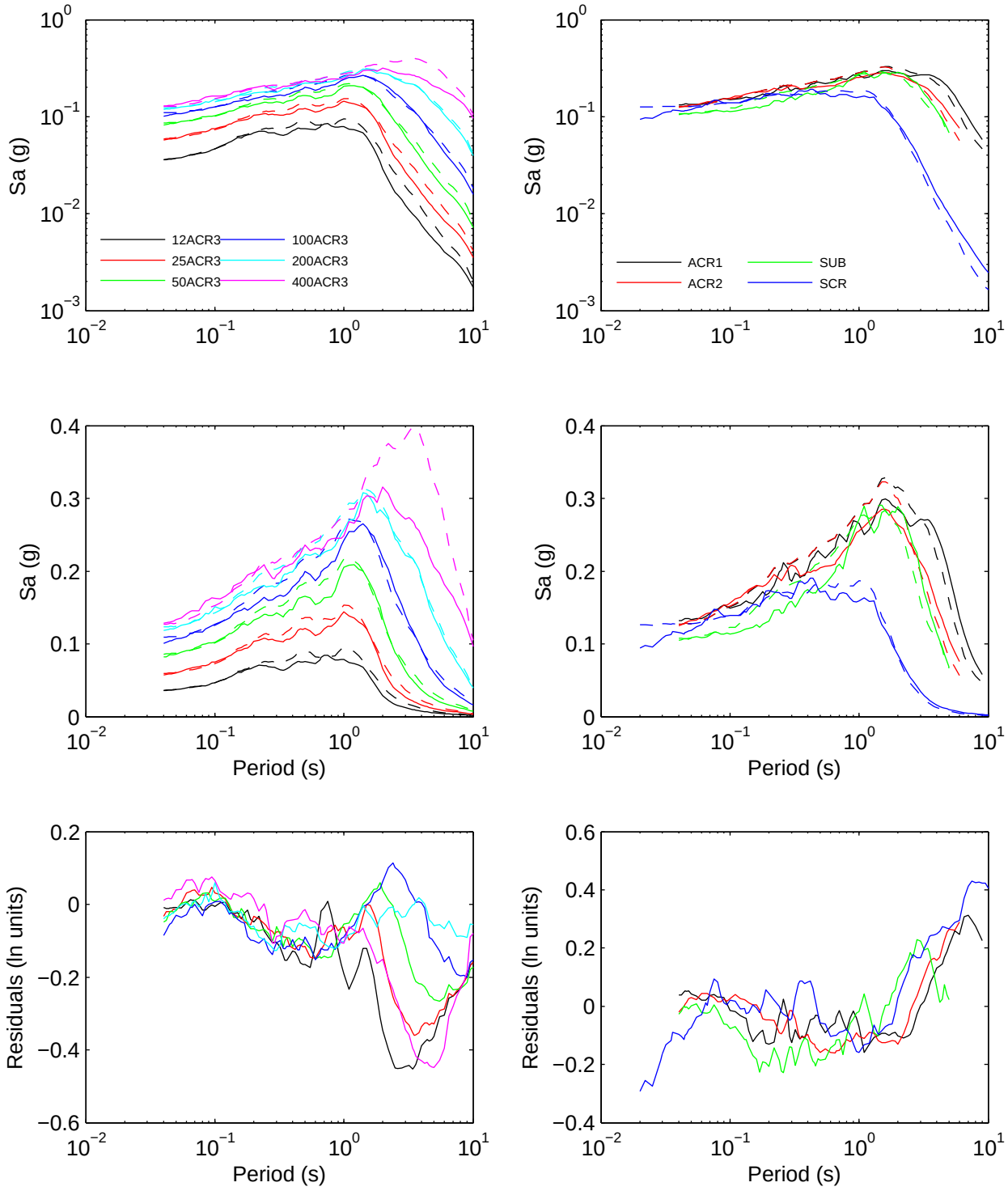

Figure 8A.12: KIKNET40 Results

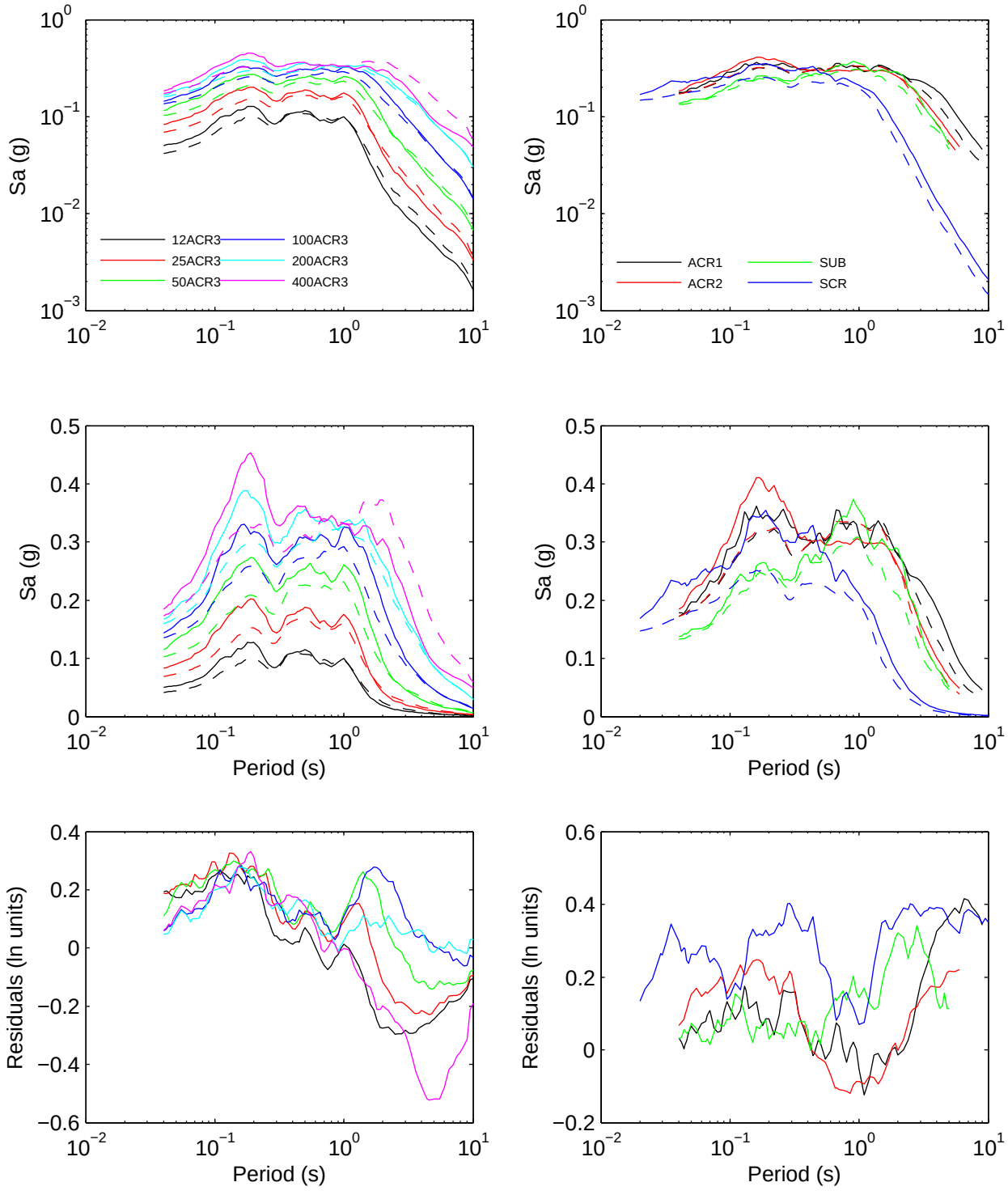

Figure 8A.9: KIKNET Results

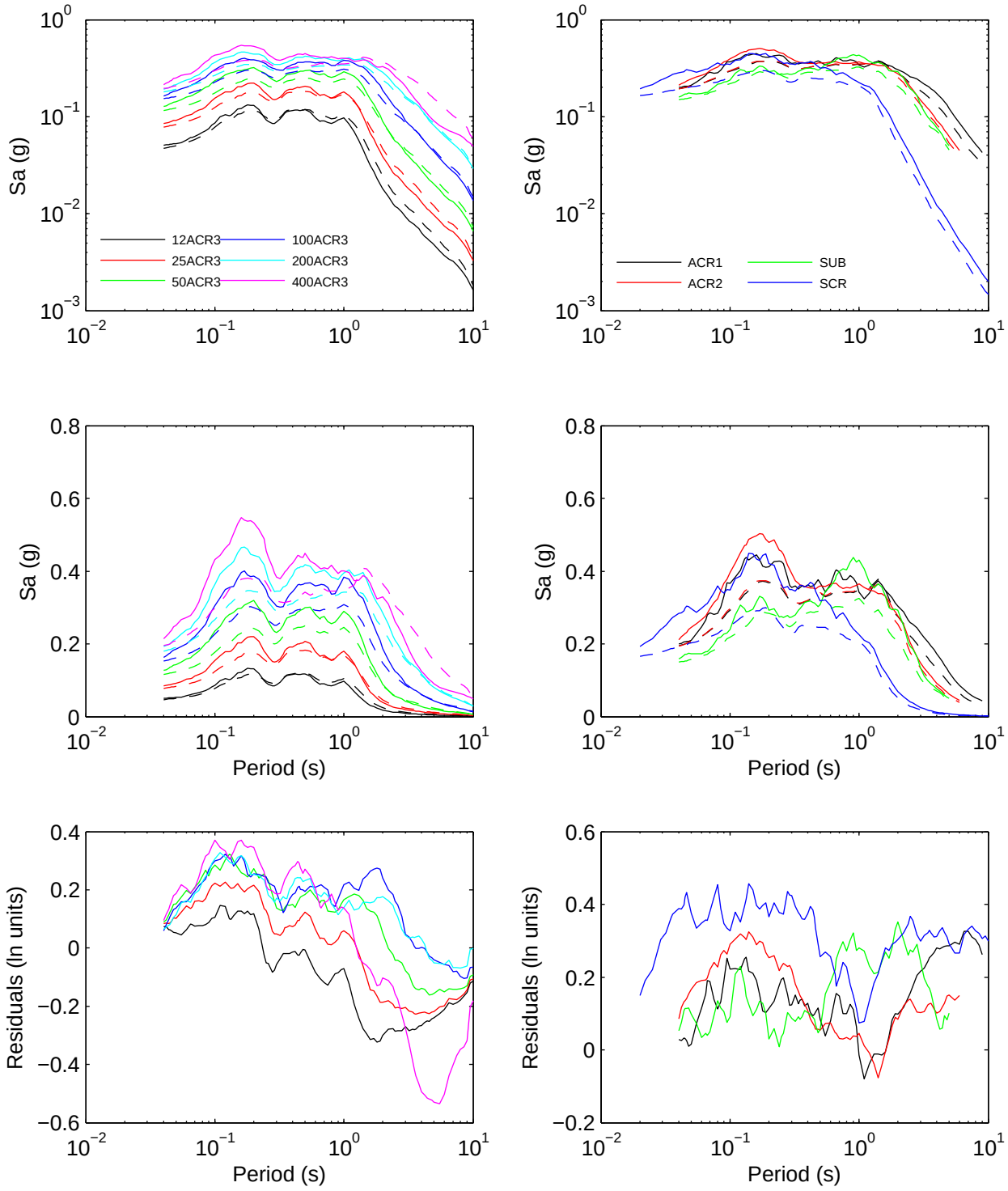

Figure 8A.13: KIKNET160 Results

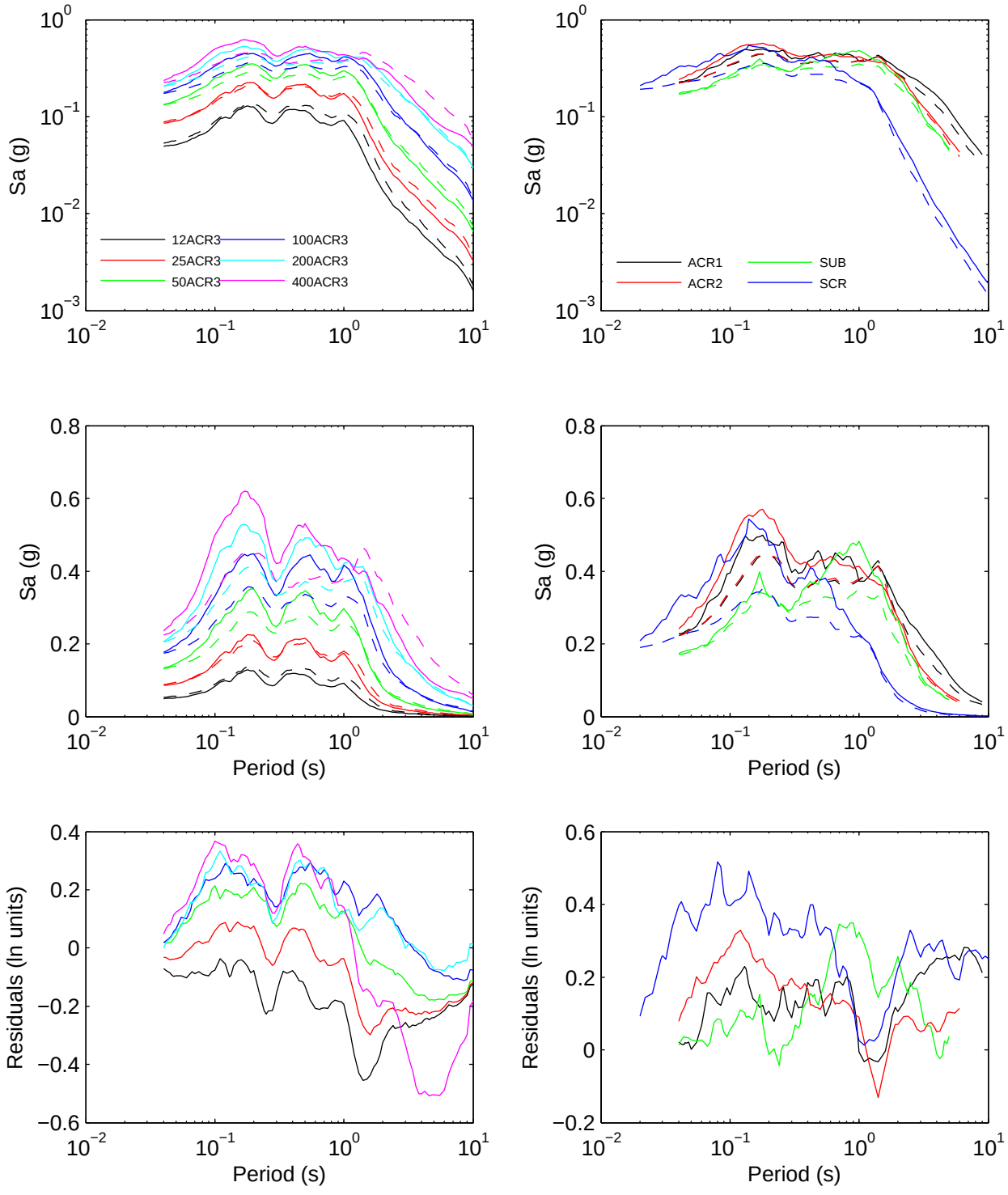

Figure 8A.10: KIKNET S2 Results

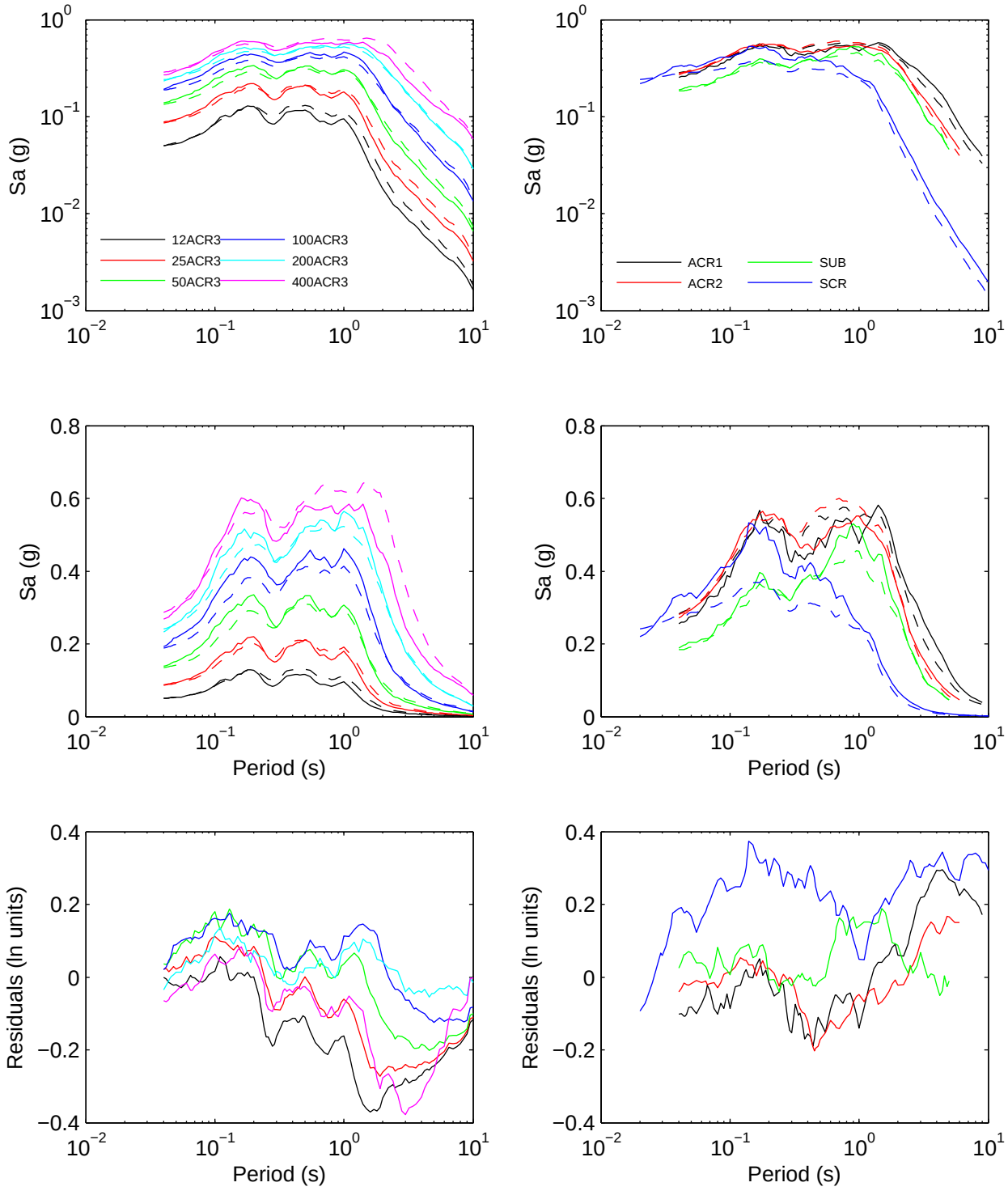

Figure 8A.11: KIKNET S4 Results

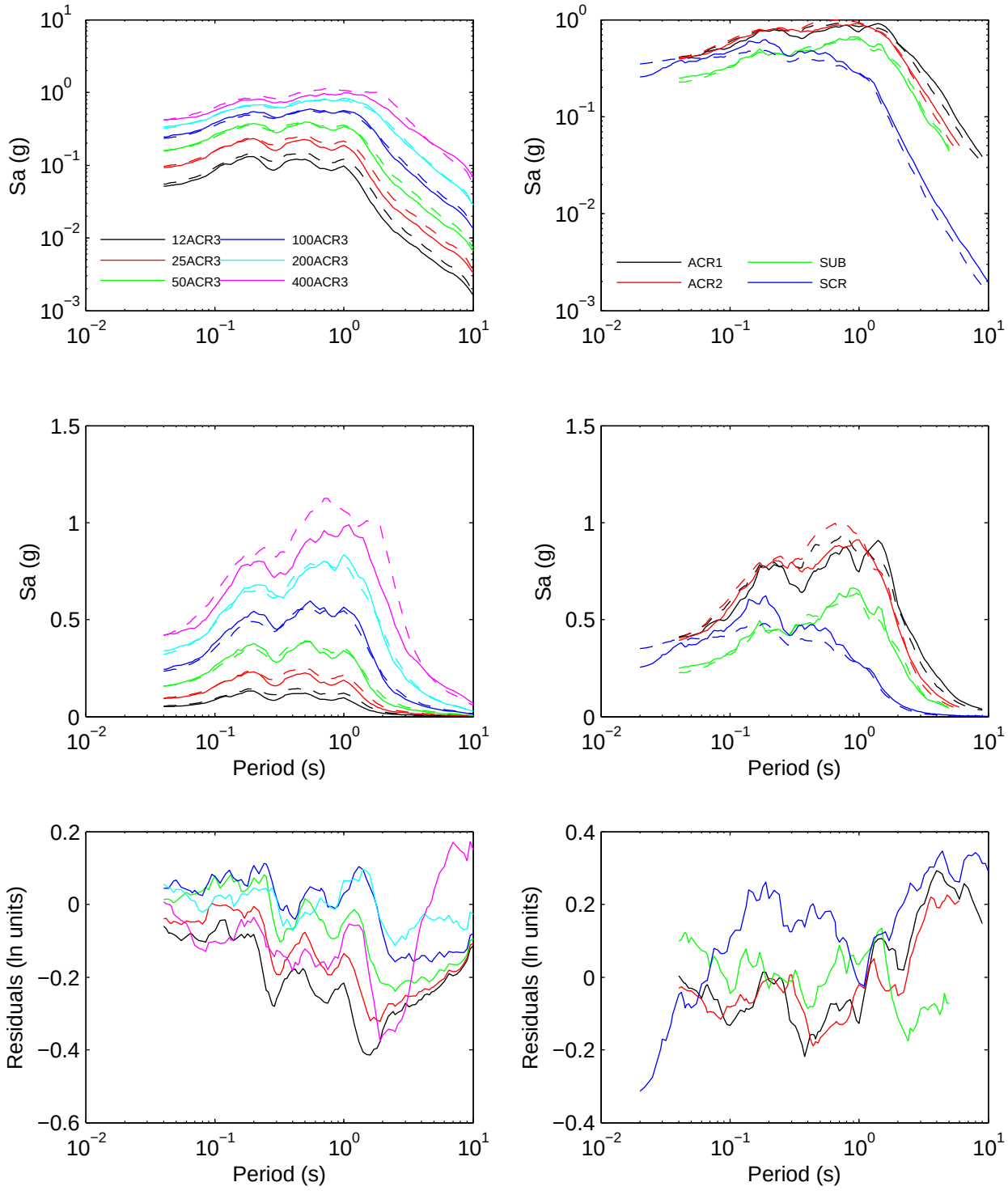

Figure 8A.14: MRCE1 Results

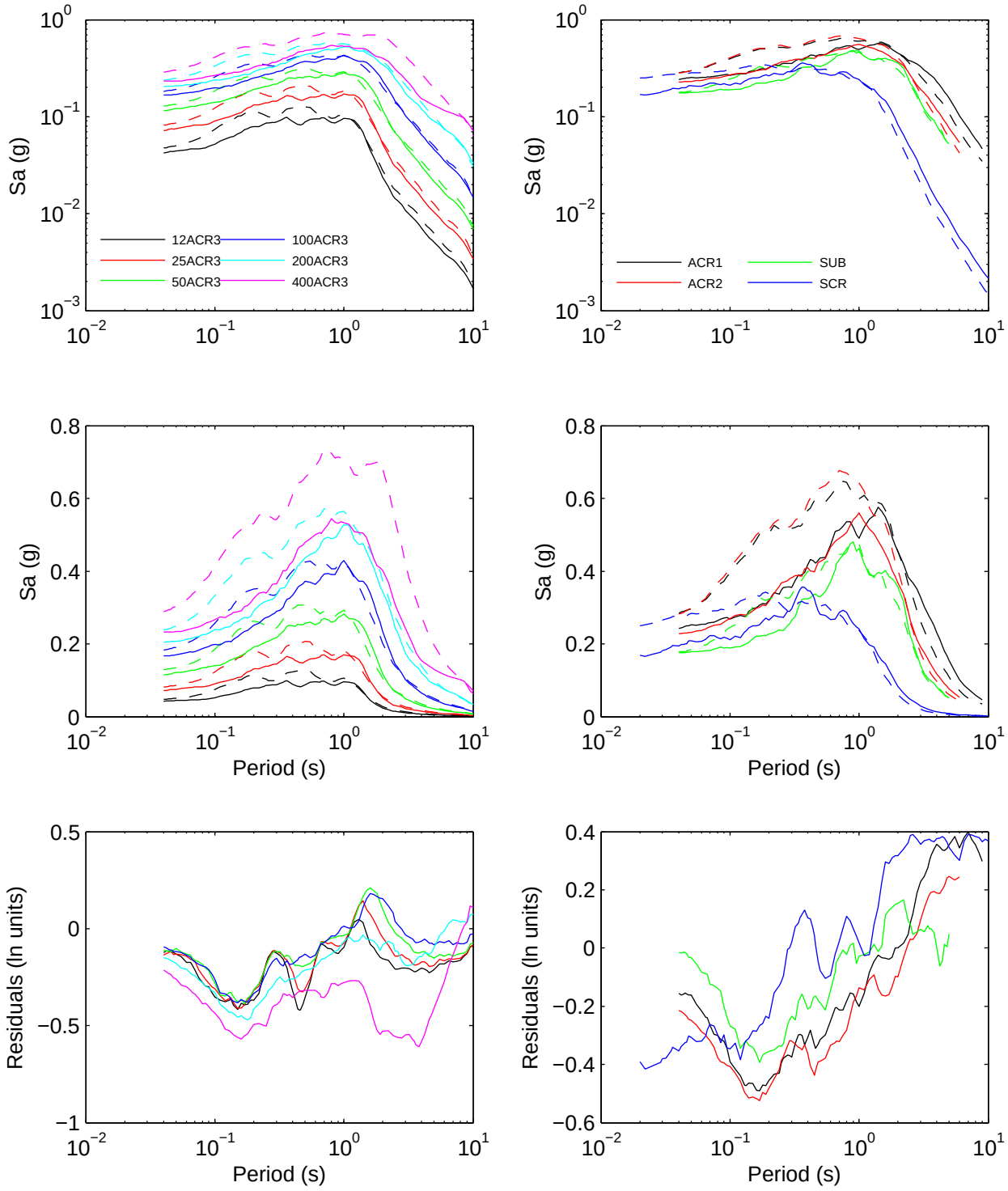

Figure 8A.15: MRCE2 Results

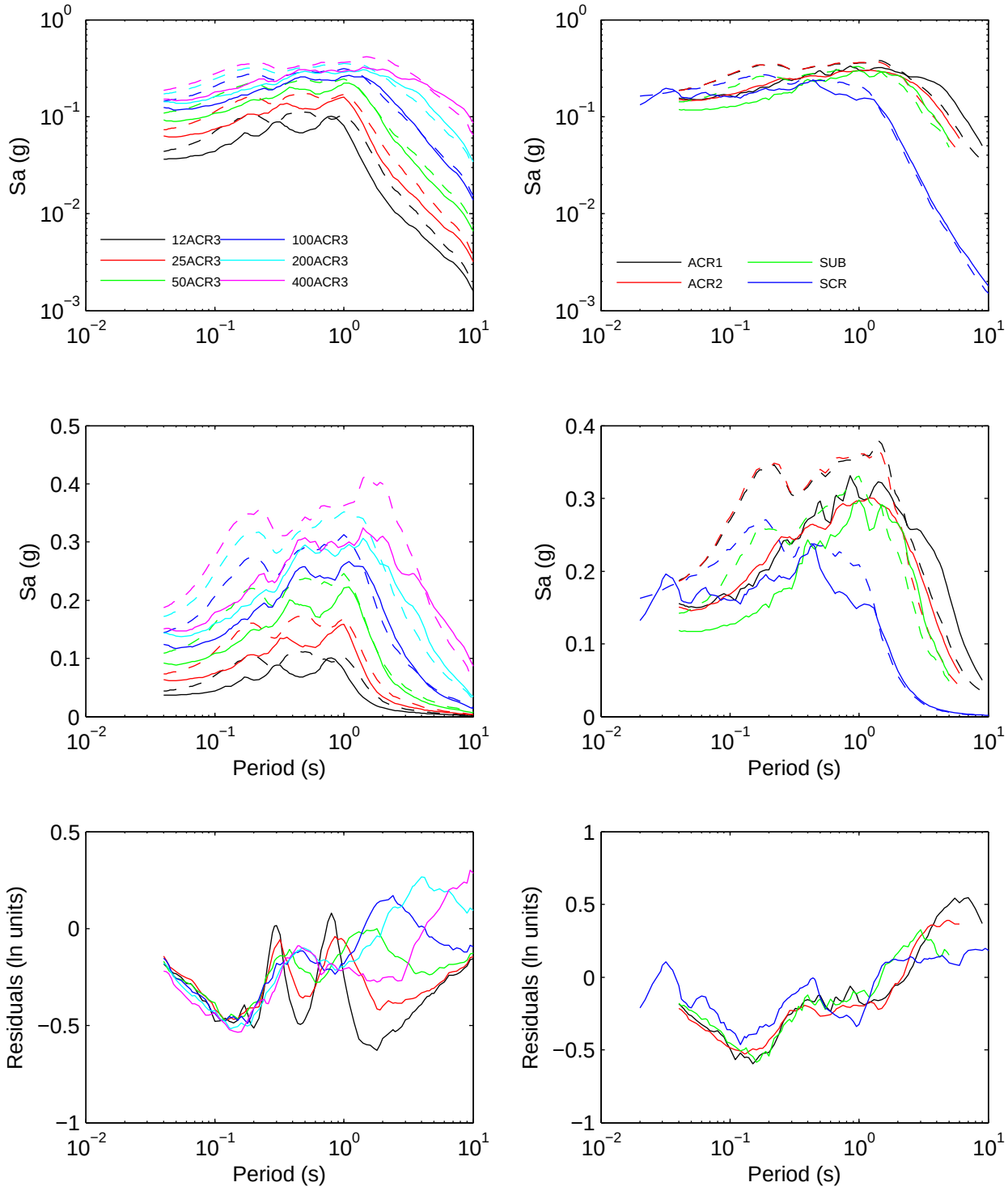

APPENDIX 8B: VALIDATION DATASET AND RESULTS

Appendix 8B: Validation Dataset and Results

Appendix 8B contains information on the dataset and results of the validation procedure. Figures 8B.1 through 8B.8 show the ground motions used in the validation dataset. Figures 8B.9 through 8B.11 show the site properties of the three validation sites. Tables 8B.1 through 8B.6 list the DEEPSOIL input parameters for the three validation sites. Figures 8B.12 through 8B.14 compare the response spectra calculated from the validation site response analyses (solid lines) with the response spectra predicted from the simplified method (dashed lines) for all validation scenarios and sites. The top two plots in each figure show the response spectra in loglog space and the middle two plots show the response spectra in semi-logarithmic space. The bottom two plots show the residuals versus period.

Figure 8B.1: NGA1070 ground motion data

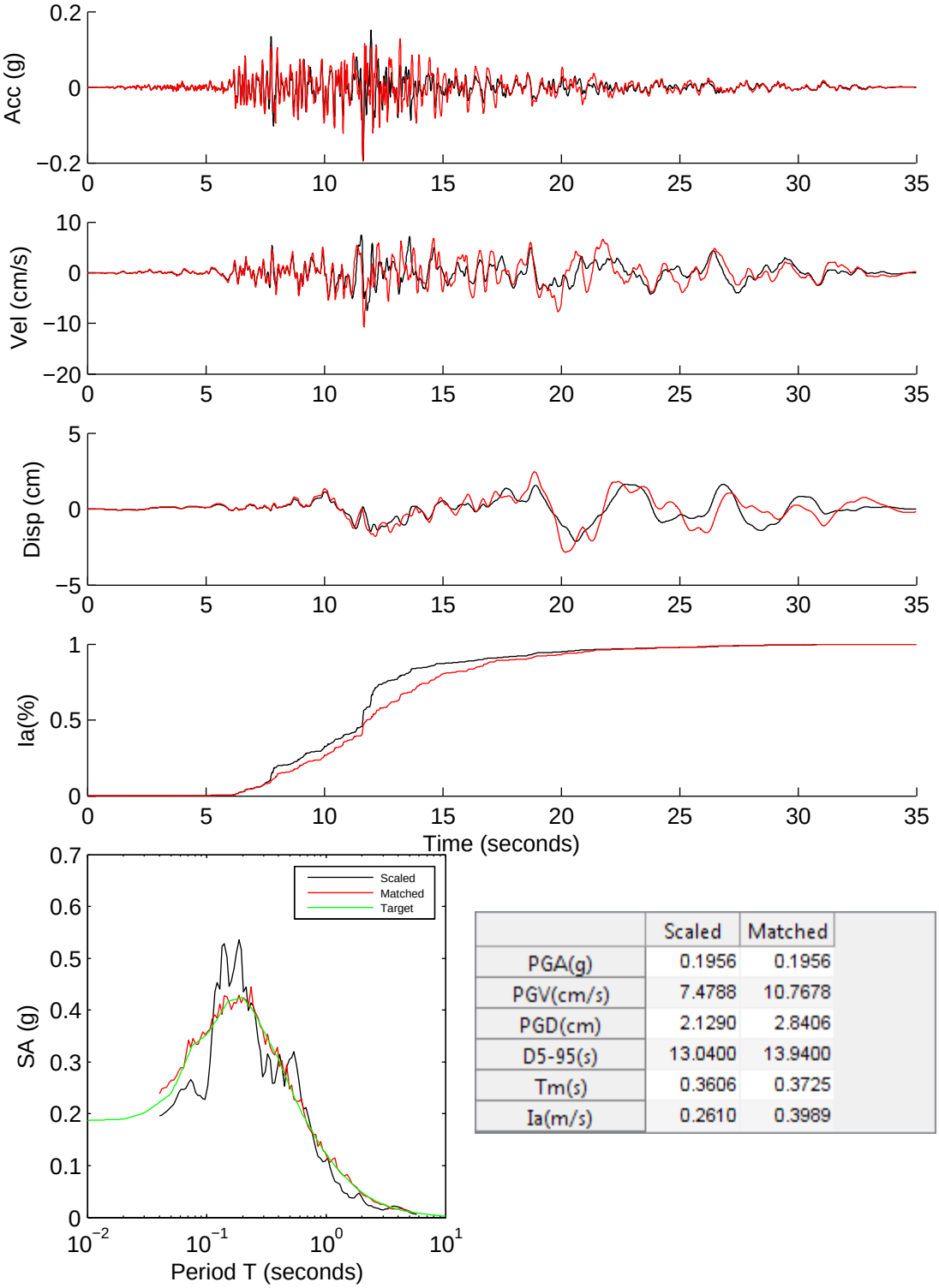

	Scaled	Matched
PGA(g)	0.1956	0.1956
PGV(cm/s)	7.4788	10.7678
PGD(cm)	2.1290	2.8406
D5-95(s)	13.0400	13.9400
Tm(s)	0.3606	0.3725
Ia(m/s)	0.2610	0.3989

Figure 8B.2: NGA1184 ground motion data

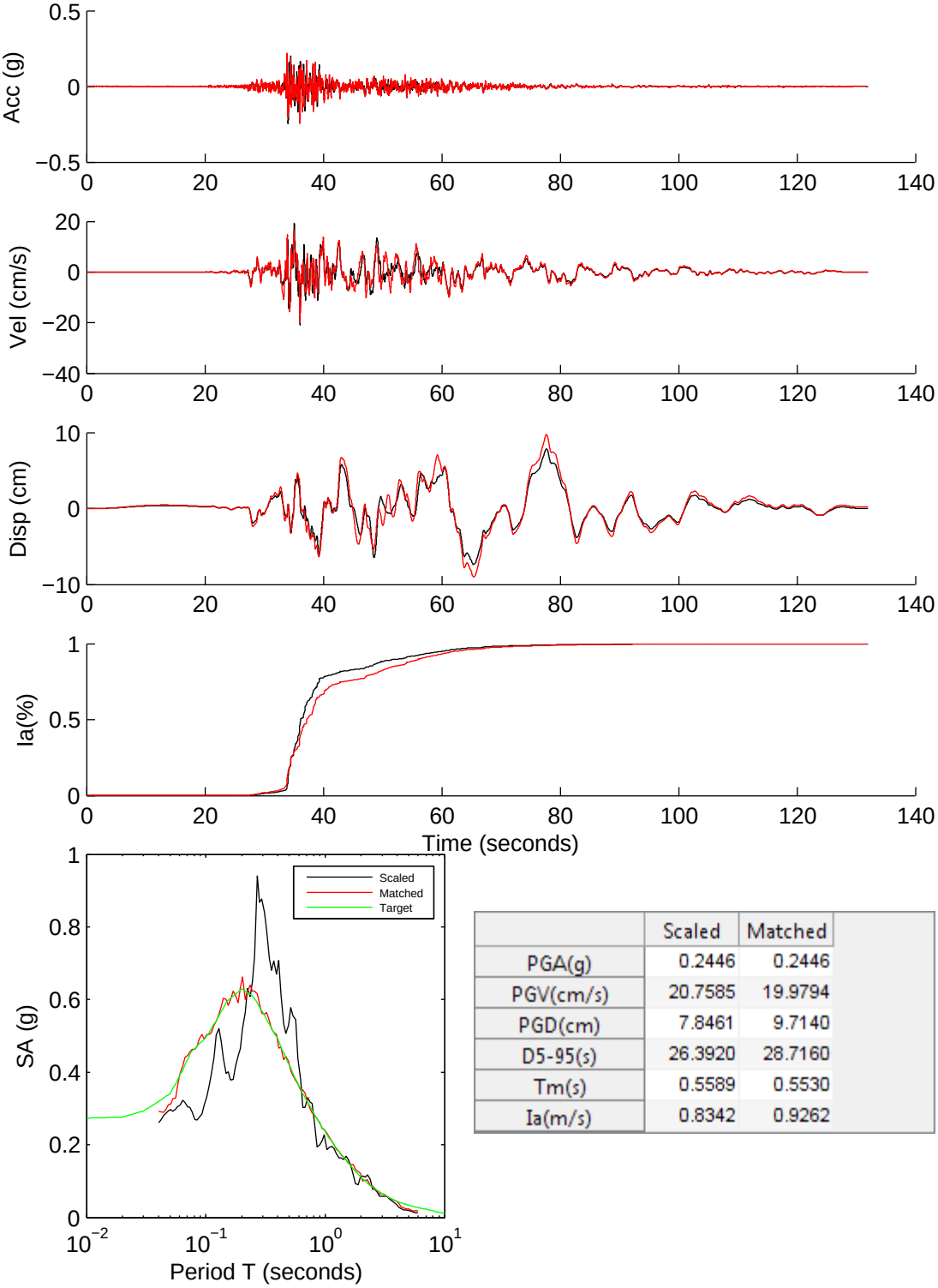

	Scaled	Matched
PGA(g)	0.2446	0.2446
PGV(cm/s)	20.7585	19.9794
PGD(cm)	7.8461	9.7140
D5-95(s)	26.3920	28.7160
Tm(s)	0.5589	0.5530
Ia(m/s)	0.8342	0.9262

Figure 8B.3: NGA1521 ground motion data

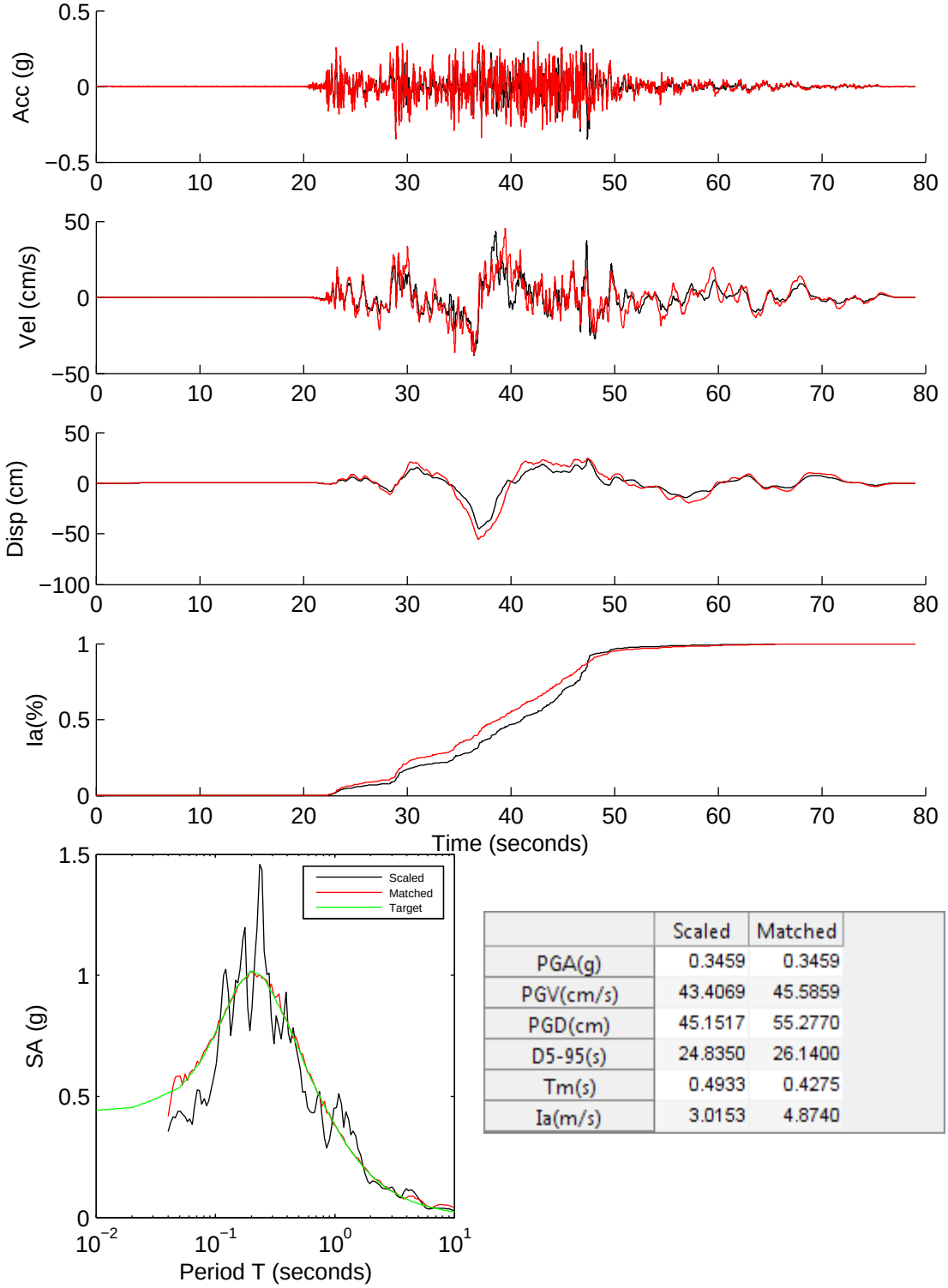

	Scaled	Matched
PGA(g)	0.3459	0.3459
PGV(cm/s)	43.4069	45.5859
PGD(cm)	45.1517	55.2770
D5-95(s)	24.8350	26.1400
Tm(s)	0.4933	0.4275
Ia(m/s)	3.0153	4.8740

Figure 8B.4: NGA2150 ground motion data

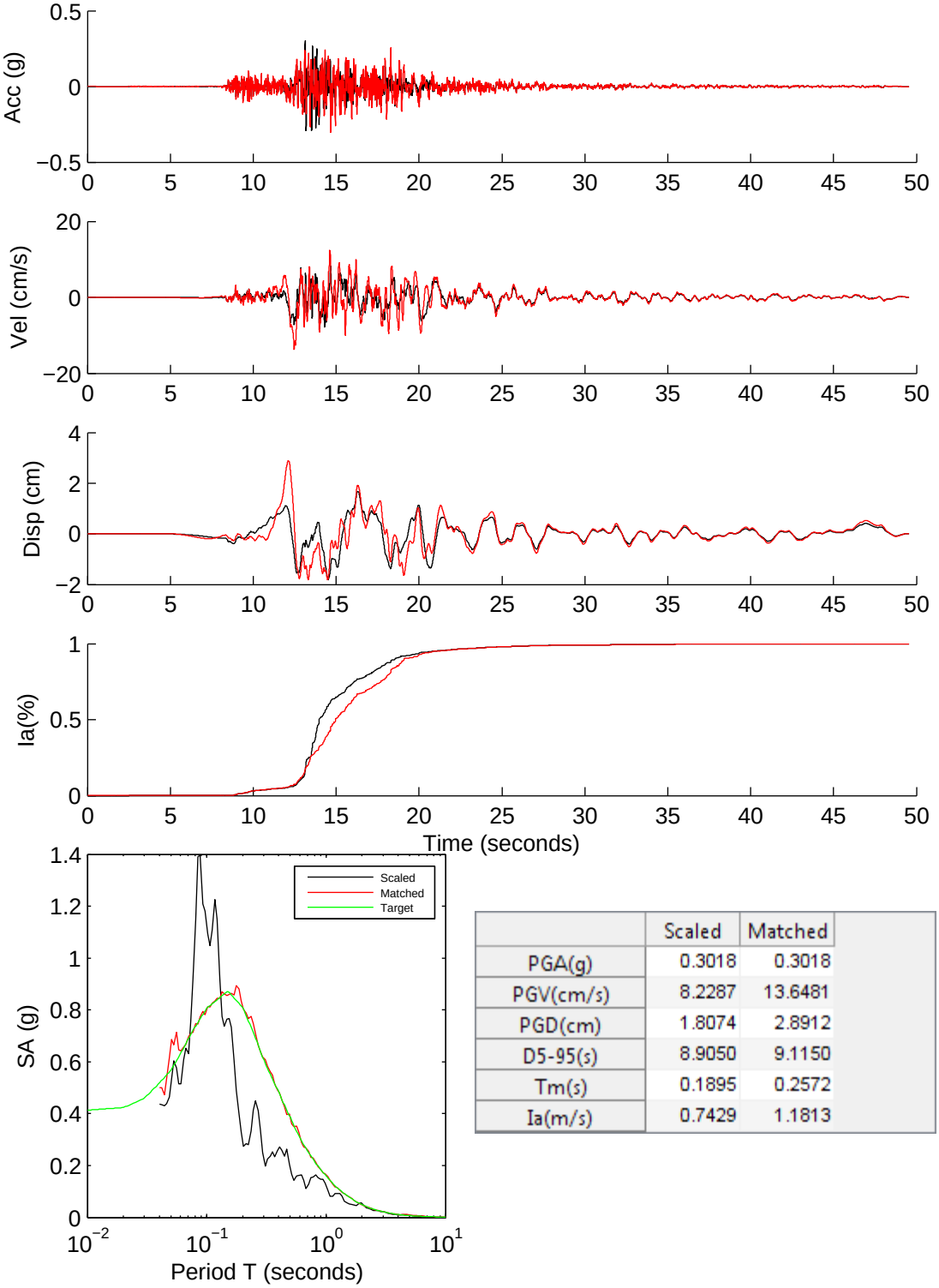

	Scaled	Matched
PGA(g)	0.3018	0.3018
PGV(cm/s)	8.2287	13.6481
PGD(cm)	1.8074	2.8912
D5-95(s)	8.9050	9.1150
Tm(s)	0.1895	0.2572
Ia(m/s)	0.7429	1.1813

Figure 8B.5: SCR0021 ground motion data

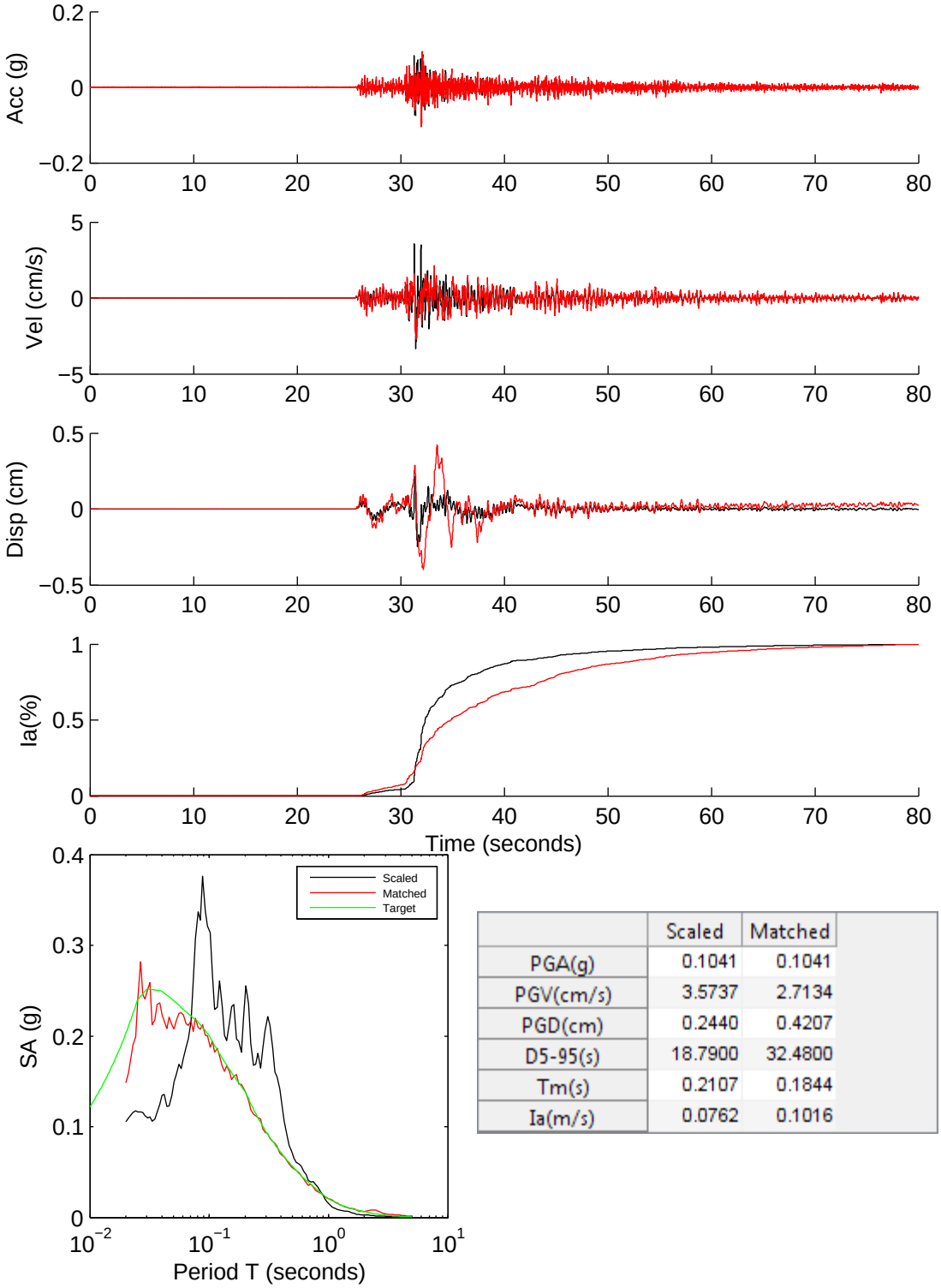

	Scaled	Matched
PGA(g)	0.1041	0.1041
PGV(cm/s)	3.5737	2.7134
PGD(cm)	0.2440	0.4207
D5-95(s)	18.7900	32.4800
Tm(s)	0.2107	0.1844
Ia(m/s)	0.0762	0.1016

Figure 8B.6: SCR0026 ground motion data

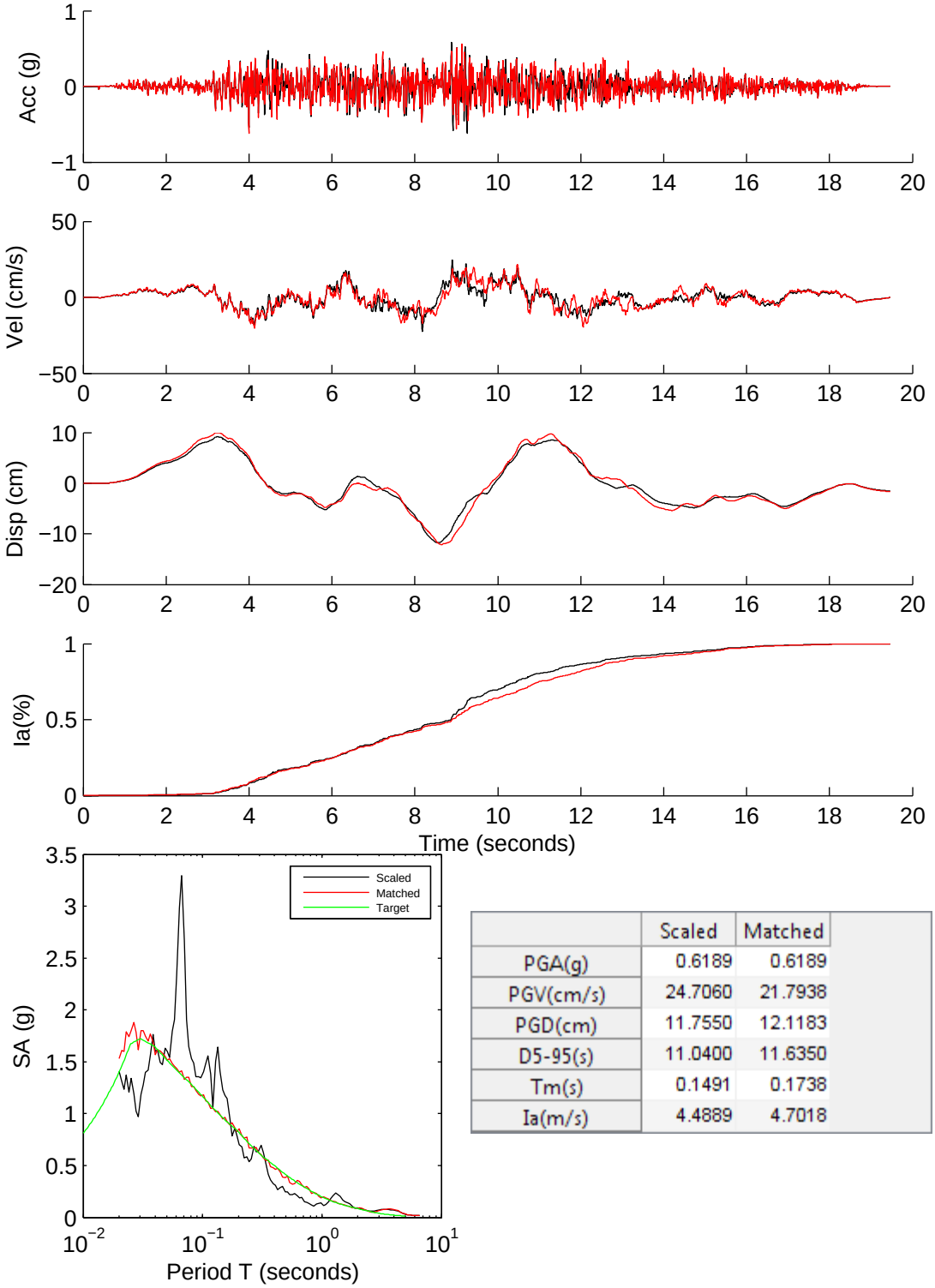

	Scaled	Matched
PGA(g)	0.6189	0.6189
PGV(cm/s)	24.7060	21.7938
PGD(cm)	11.7550	12.1183
D5-95(s)	11.0400	11.6350
Tm(s)	0.1491	0.1738
Ia(m/s)	4.4889	4.7018

Figure 8B.7: SUB0039 ground motion data

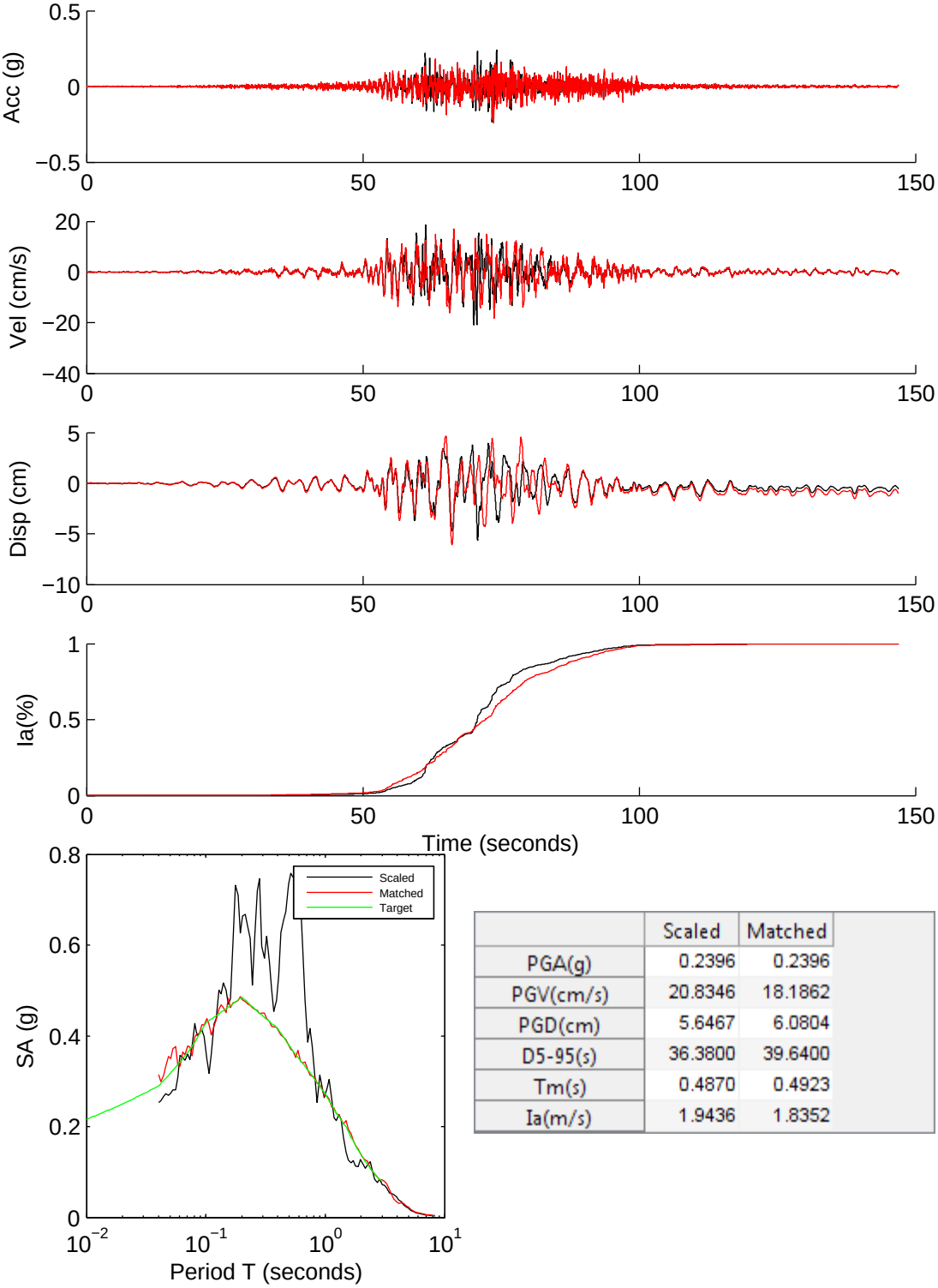

	Scaled	Matched
PGA(g)	0.2396	0.2396
PGV(cm/s)	20.8346	18.1862
PGD(cm)	5.6467	6.0804
D5-95(s)	36.3800	39.6400
Tm(s)	0.4870	0.4923
Ia(m/s)	1.9436	1.8352

Figure 8B.8: SUB0059 ground motion data

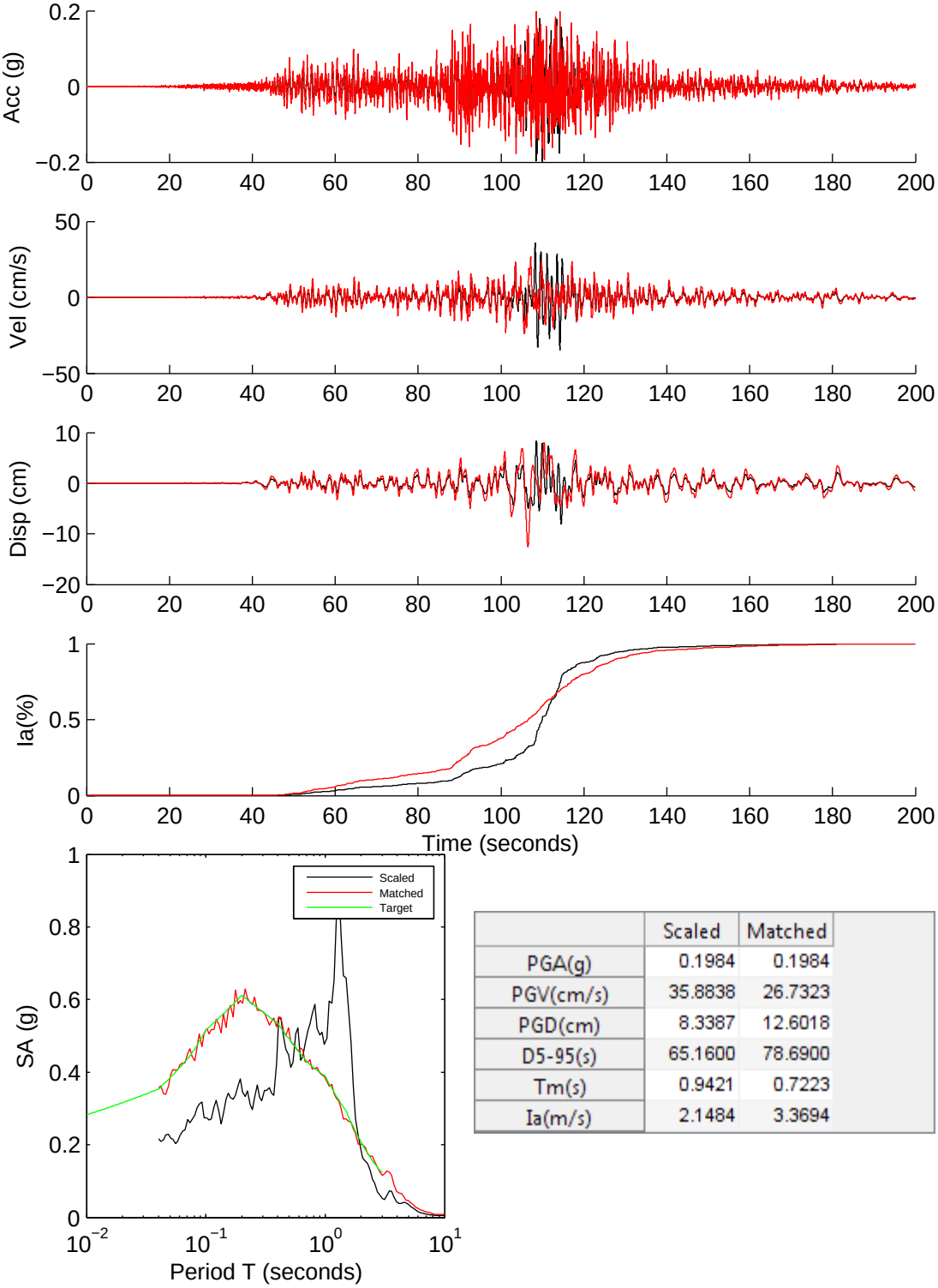

	Scaled	Matched
PGA(g)	0.1984	0.1984
PGV(cm/s)	35.8838	26.7323
PGD(cm)	8.3387	12.6018
D5-95(s)	65.1600	78.6900
Tm(s)	0.9421	0.7223
Ia(m/s)	2.1484	3.3694

Figure 8B.9: Validation site 1 profile

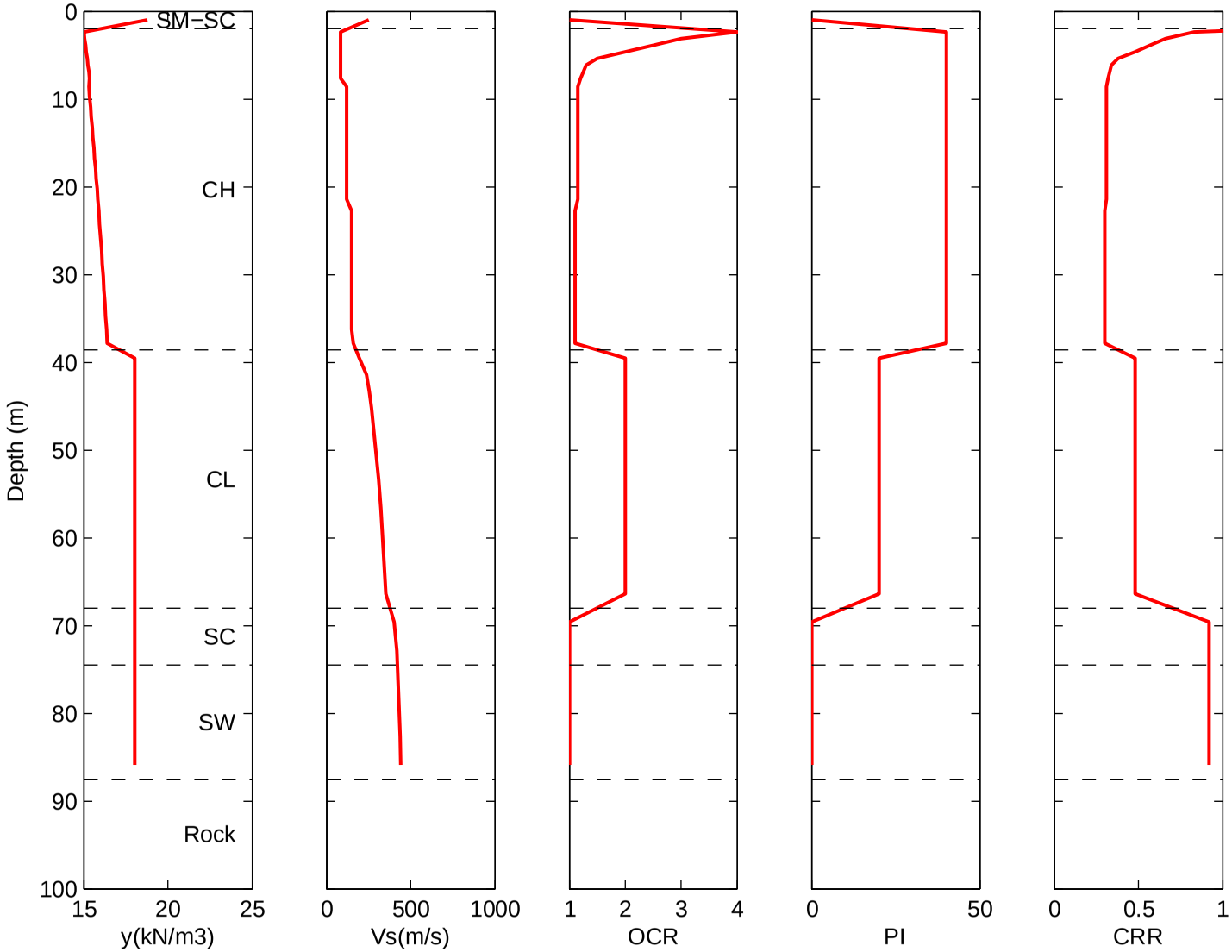

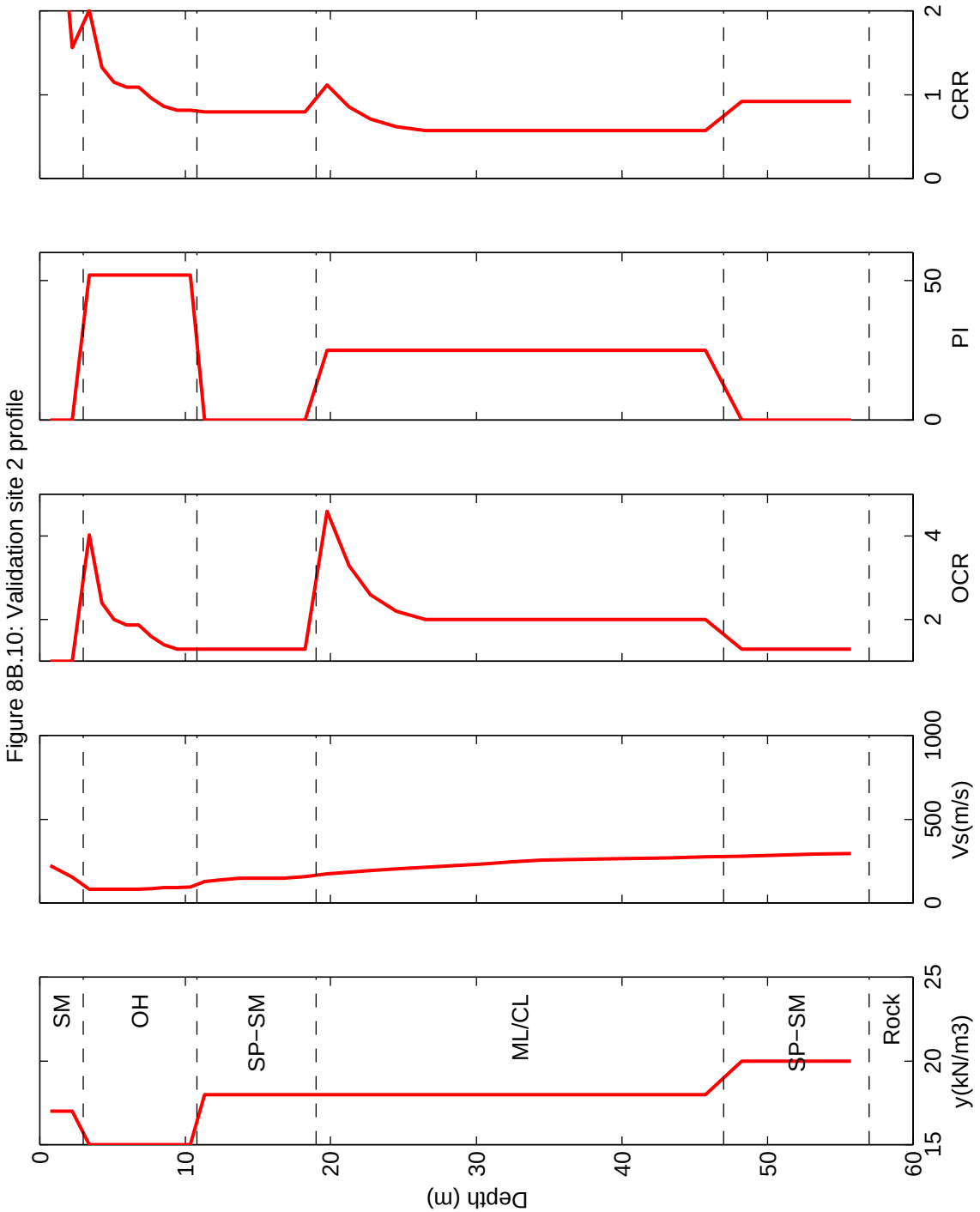

Figure 8B.10: Validation site 2 profile

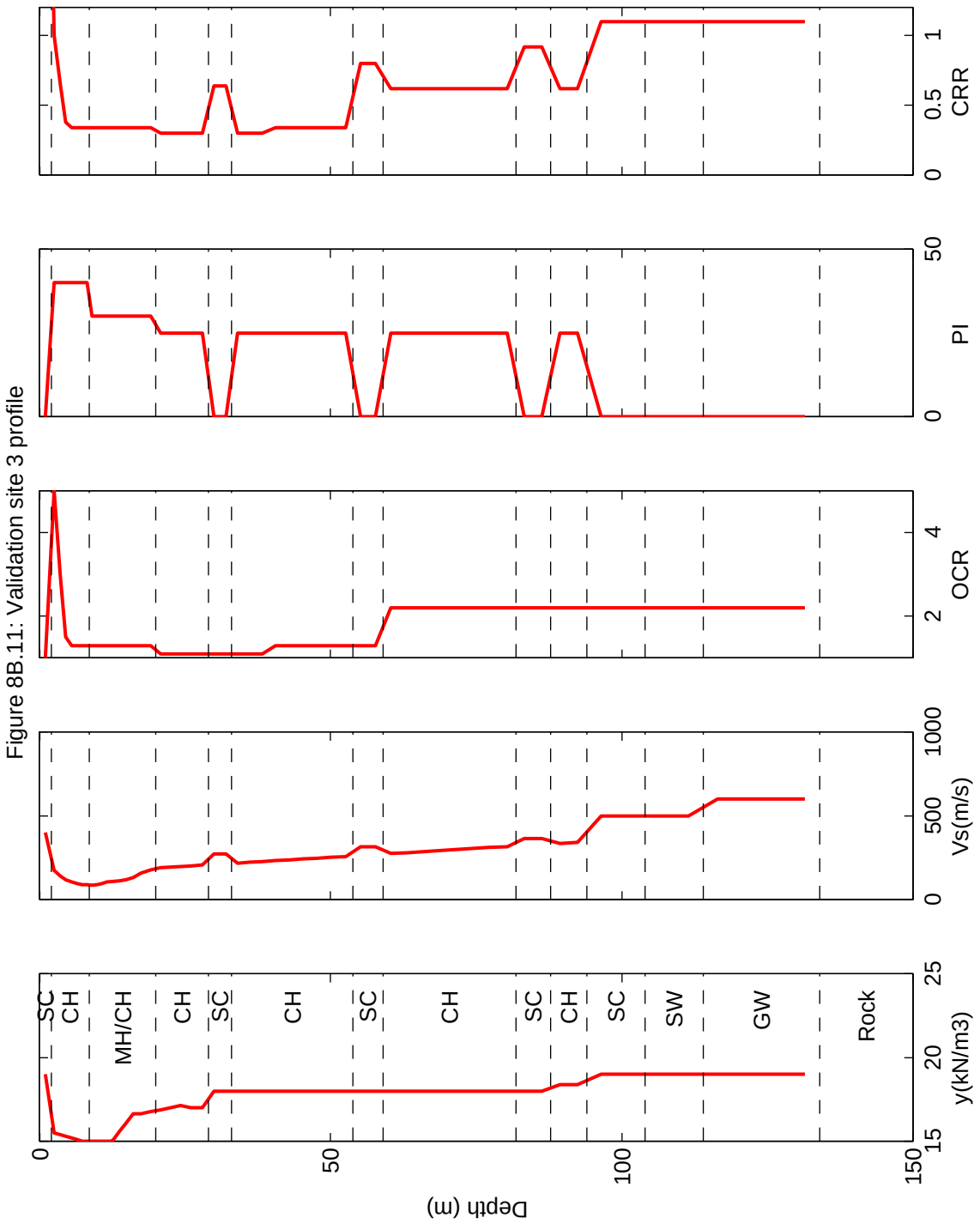

Figure 8B.11: Validation site 3 profile

Table 8B.1: DEEPSOIL total stress input parameters for validation site 1 (Ref Stress = 0.18; b = d = 0)

Layer	Name	Thick (m)	γ (kN/m3)	Vs (m/s)	Dmin	Ref Strain	B	s	P1	P2	P3
1	SM-SC	2	18.8	250	1.77	0.0228	1.65	0.915	0.670	0.288	3.25
2	CH	0.75	15	82	2.18	0.0946	1.55	0.795	0.746	0.266	2.35
3	CH	0.75	15.05	82	2.09	0.0954	1.56	0.795	0.736	0.252	2.50
4	CH	0.75	15.1	82	2.01	0.0960	1.55	0.795	0.736	0.252	2.51
5	CH	0.75	15.15	82	1.96	0.0968	1.58	0.810	0.744	0.270	2.15
6	CH	0.75	15.2	82	1.92	0.0920	1.56	0.825	0.714	0.252	2.50
7	CH	0.75	15.25	82	1.87	0.0854	1.46	0.825	0.704	0.244	2.75
8	CH	0.75	15.3	82	1.82	0.0986	1.58	0.810	0.724	0.248	2.50
9	CH	0.75	15.35	82	1.77	0.1006	1.56	0.810	0.736	0.258	2.20
10	CH	1.13	15.3	120	1.76	0.0838	1.53	0.930	0.610	0.224	3.25
11	CH	1.17	15.35	120	1.70	0.0874	1.52	0.915	0.618	0.220	3.15
12	CH	1.17	15.4	120	1.65	0.0932	1.55	0.915	0.622	0.224	2.95
13	CH	1.17	15.45	120	1.60	0.0962	1.52	0.900	0.628	0.220	3.05
14	CH	1.17	15.5	120	1.56	0.0996	1.50	0.885	0.638	0.218	2.95
15	CH	1.17	15.55	120	1.52	0.1030	1.50	0.885	0.644	0.224	2.70
16	CH	1.17	15.6	120	1.49	0.1078	1.50	0.870	0.668	0.234	2.35
17	CH	1.17	15.65	120	1.46	0.1126	1.52	0.870	0.682	0.246	2.00
18	CH	1.17	15.7	120	1.43	0.1132	1.47	0.855	0.658	0.214	2.65
19	CH	1.17	15.75	120	1.40	0.1194	1.50	0.855	0.678	0.234	2.20
20	CH	1.17	15.8	120	1.37	0.1222	1.47	0.840	0.698	0.240	2.05
21	CH	1.17	15.85	120	1.35	0.1256	1.47	0.840	0.704	0.246	1.90
22	CH	1.5	15.9	150	1.35	0.1178	1.53	0.915	0.618	0.216	2.80
23	CH	1.5	15.95	150	1.32	0.1236	1.55	0.900	0.642	0.226	2.40
24	CH	1.5	16	150	1.29	0.1258	1.53	0.900	0.644	0.228	2.30
25	CH	1.5	16.05	150	1.27	0.1300	1.52	0.885	0.634	0.208	2.75
26	CH	1.5	16.1	150	1.25	0.1320	1.50	0.885	0.638	0.214	2.65
27	CH	1.5	16.15	150	1.23	0.1376	1.53	0.885	0.638	0.214	2.50
28	CH	1.5	16.2	150	1.21	0.1390	1.50	0.870	0.664	0.224	2.11
29	CH	1.5	16.25	150	1.19	0.1408	1.49	0.870	0.674	0.234	1.90
30	CH	1.5	16.3	150	1.17	0.1450	1.49	0.855	0.688	0.234	1.80
31	CH	1.5	16.35	150	1.16	0.1482	1.49	0.855	0.702	0.246	1.55
32	CH	1.6	16.4	160	1.14	0.1480	1.50	0.870	0.658	0.216	2.10
33	CL	1.86	18	195	1.32	0.1934	1.56	0.975	0.630	0.256	1.40
34	CL	1.86	18	236	1.30	0.1770	1.50	1.020	0.596	0.258	1.35
35	CL	1.86	18	253	1.28	0.1752	1.50	1.035	0.590	0.264	1.25
36	CL	1.86	18	266	1.26	0.1810	1.52	1.035	0.590	0.264	1.20
37	CL	1.86	18	277	1.24	0.1766	1.50	1.050	0.692	0.376	0.70
38	CL	1.86	18	287	1.22	0.1836	1.53	1.050	0.704	0.388	0.65
39	CL	1.91	18	296	1.21	0.1854	1.52	1.050	0.704	0.390	0.65
40	CL	3.2	18	309	1.19	0.1884	1.52	1.065	0.582	0.260	2.55
41	CL	3.25	18	321	1.16	0.1970	1.53	1.065	0.582	0.260	2.55
42	CL	3.25	18	333	1.14	0.1992	1.53	1.065	0.584	0.260	2.40
43	CL	3.25	18	343	1.12	0.2016	1.55	1.080	0.584	0.264	1.90
44	CL	3.25	18	352	1.10	0.2046	1.52	1.065	0.584	0.260	2.20
45	SC	3.25	18	400	0.83	0.1572	1.52	0.900	0.688	0.286	1.15
46	SC	3.25	18	418	0.82	0.1628	1.53	0.900	0.708	0.306	1.00
47	SW	3.25	18	425	0.81	0.1620	1.50	0.900	0.728	0.328	0.89
48	SW	3.25	18	431	0.80	0.1660	1.50	0.885	0.668	0.260	1.20
49	SW	3.25	18	436	0.78	0.1696	1.53	0.900	0.772	0.376	0.70
50	SW	3.25	18	440	0.77	0.1712	1.52	0.900	0.792	0.398	0.65

Table 8B.2: DEEPSOIL effective stress input parameters for validation site 1 (Max Ru = 0.95 for all layers)

Layer	Model	f/s/f	p/r/Dr	F/A/FC	s/B/-	g/C/-	v/D/v	-/g/-	$C_v(m^2/s)$
1	1	1.000	1.000	0.73	1.31	10.000	1.000	0.000	1.63E-01
2	2	0.048	0.425	11.18	-21.32	11.211	-1.058	0.025	3.91E-06
3	2	0.054	0.444	11.99	-23.45	12.827	-1.354	0.025	3.91E-06
4	2	0.058	0.456	12.53	-24.90	13.970	-1.583	0.025	3.91E-06
5	2	0.064	0.471	13.23	-26.80	15.508	-1.916	0.025	3.91E-06
6	2	0.072	0.491	14.18	-29.47	17.743	-2.452	0.025	3.91E-06
7	2	0.076	0.502	14.68	-30.90	18.972	-2.772	0.025	3.91E-06
8	2	0.077	0.505	14.82	-31.30	19.323	-2.867	0.026	3.91E-06
9	2	0.079	0.508	14.97	-31.72	19.696	-2.969	0.027	3.91E-06
10	2	0.080	0.511	15.12	-32.17	20.092	-3.079	0.027	3.91E-06
11	2	0.080	0.511	15.12	-32.17	20.092	-3.079	0.028	3.91E-06
12	2	0.080	0.511	15.12	-32.17	20.092	-3.079	0.029	3.91E-06
13	2	0.080	0.511	15.12	-32.17	20.092	-3.079	0.030	3.91E-06
14	2	0.080	0.511	15.12	-32.17	20.092	-3.079	0.031	3.91E-06
15	2	0.080	0.511	15.12	-32.17	20.092	-3.079	0.032	3.91E-06
16	2	0.080	0.511	15.12	-32.17	20.092	-3.079	0.033	3.91E-06
17	2	0.080	0.511	15.12	-32.17	20.092	-3.079	0.034	3.91E-06
18	2	0.080	0.511	15.12	-32.17	20.092	-3.079	0.035	3.91E-06
19	2	0.080	0.511	15.12	-32.17	20.092	-3.079	0.035	3.91E-06
20	2	0.080	0.511	15.12	-32.17	20.092	-3.079	0.036	3.91E-06
21	2	0.080	0.511	15.12	-32.17	20.092	-3.079	0.037	3.91E-06
22	2	0.082	0.514	15.28	-32.65	20.514	-3.199	0.037	3.91E-06
23	2	0.082	0.514	15.28	-32.65	20.514	-3.199	0.038	3.91E-06
24	2	0.082	0.514	15.28	-32.65	20.514	-3.199	0.039	3.91E-06
25	2	0.082	0.514	15.28	-32.65	20.514	-3.199	0.040	3.91E-06
26	2	0.082	0.514	15.28	-32.65	20.514	-3.199	0.041	3.91E-06
27	2	0.082	0.514	15.28	-32.65	20.514	-3.199	0.042	3.91E-06
28	2	0.082	0.514	15.28	-32.65	20.514	-3.199	0.042	3.91E-06
29	2	0.082	0.514	15.28	-32.65	20.514	-3.199	0.043	3.91E-06
30	2	0.082	0.514	15.28	-32.65	20.514	-3.199	0.044	3.91E-06
31	2	0.082	0.514	15.28	-32.65	20.514	-3.199	0.044	3.91E-06
32	2	0.082	0.514	15.28	-32.65	20.514	-3.199	0.045	3.91E-06
33	2	0.111	0.509	13.23	-26.80	15.508	-1.916	0.066	2.70E-05
34	2	0.111	0.509	13.23	-26.80	15.508	-1.916	0.068	2.70E-05
35	2	0.111	0.509	13.23	-26.80	15.508	-1.916	0.069	2.70E-05
36	2	0.111	0.509	13.23	-26.80	15.508	-1.916	0.071	2.70E-05
37	2	0.111	0.509	13.23	-26.80	15.508	-1.916	0.072	2.70E-05
38	2	0.111	0.509	13.23	-26.80	15.508	-1.916	0.073	2.70E-05
39	2	0.111	0.509	13.23	-26.80	15.508	-1.916	0.074	2.70E-05
40	2	0.111	0.509	13.23	-26.80	15.508	-1.916	0.076	2.70E-05
41	2	0.111	0.509	13.23	-26.80	15.508	-1.916	0.078	2.70E-05
42	2	0.111	0.509	13.23	-26.80	15.508	-1.916	0.080	2.70E-05
43	2	0.111	0.509	13.23	-26.80	15.508	-1.916	0.081	2.70E-05
44	2	0.111	0.509	13.23	-26.80	15.508	-1.916	0.083	2.70E-05
45	1	1.000	1.000	0.35	1.31	0.050	1.000	0.000	1.63E-01
46	1	1.000	1.000	0.33	1.31	0.051	1.000	0.000	1.63E-01
47	1	1.000	1.000	0.32	1.31	0.052	1.000	0.000	1.63E-01
48	1	1.000	1.000	0.31	1.31	0.053	1.000	0.000	1.63E-01
49	1	1.000	1.000	0.31	1.31	0.054	1.000	0.000	1.63E-01
50	1	1.000	1.000	0.30	1.31	0.054	1.000	0.000	1.63E-01

Table 8B.3: DEEPSOIL total stress input parameters for validation site 2 (Ref Stress = 0.18; b = d = 0)

Layer	Name	Thick (m)	γ (kN/m3)	Vs (m/s)	Dmin	Ref Strain	B	s	P1	P2	P3
1	SM	1.5	17	225	2.01	0.0162	1.37	0.870	0.710	0.288	3.25
2	SM	1.5	17	155	1.42	0.0294	1.55	0.825	0.762	0.320	3.25
3	OH	0.85	15	85	2.22	0.1756	1.59	0.660	0.920	0.354	1.65
4	OH	0.85	15	85	2.19	0.1304	1.46	0.705	0.884	0.348	1.55
5	OH	0.85	15	85	2.12	0.1320	1.46	0.705	0.880	0.342	1.55
6	OH	0.85	15	85	2.03	0.1388	1.44	0.690	0.908	0.356	1.45
7	OH	0.85	15	85	1.95	0.1466	1.41	0.675	0.918	0.358	1.48
8	OH	0.85	15	88.33	1.92	0.1440	1.43	0.690	0.900	0.346	1.45
9	OH	0.9	15	91.66	1.89	0.1440	1.46	0.705	0.860	0.316	1.65
10	OH	0.9	15	94.99	1.85	0.1476	1.47	0.705	0.866	0.312	1.55
11	OH	0.9	15	98.32	1.81	0.1530	1.47	0.705	0.880	0.324	1.40
12	SP-SM	1.1	18	130	1.43	0.1020	1.55	0.780	0.758	0.260	2.25
13	SP-SM	1.1	18	140	1.39	0.1076	1.58	0.795	0.738	0.254	2.35
14	SP-SM	1.5	18	150	1.33	0.1100	1.55	0.795	0.734	0.248	2.40
15	SP-SM	1.5	18	150	1.28	0.1164	1.52	0.780	0.766	0.266	2.01
16	SP-SM	1.5	18	150	1.22	0.1272	1.53	0.765	0.800	0.284	1.65
17	SP-SM	1.5	18	160	1.20	0.1266	1.53	0.780	0.764	0.264	1.81
18	ML/CL	1.5	18	176	1.67	0.2560	1.49	0.870	0.680	0.224	1.20
19	ML/CL	1.5	18	186	1.66	0.2338	1.53	0.915	0.624	0.204	1.97
20	ML/CL	1.5	18	196	1.65	0.2150	1.55	0.945	0.598	0.200	2.40
21	ML/CL	2	18	206	1.62	0.1900	1.47	0.990	0.584	0.220	2.40
22	ML/CL	2	18	216	1.59	0.1884	1.47	1.005	0.590	0.230	2.15
23	ML/CL	2	18	226	1.55	0.1946	1.50	1.005	0.586	0.224	2.15
24	ML/CL	2	18	236	1.52	0.1998	1.49	1.005	0.584	0.222	2.35
25	ML/CL	2	18	246	1.49	0.2012	1.49	1.020	0.586	0.240	2.56
26	ML/CL	2	18	256	1.46	0.2032	1.49	1.020	0.596	0.240	2.00
27	ML/CL	2	18	260	1.44	0.2100	1.50	1.020	0.596	0.240	2.00
28	ML/CL	2	18	264	1.41	0.2144	1.50	1.020	0.596	0.240	2.00
29	ML/CL	2.5	18	268	1.39	0.2194	1.50	1.020	0.596	0.240	2.00
30	ML/CL	2.5	18	272	1.36	0.2250	1.50	1.020	0.596	0.240	2.00
31	ML/CL	2.5	18	276	1.34	0.2292	1.49	1.005	0.584	0.220	2.40
32	SP-SM	2.5	20	280	0.89	0.1622	1.47	0.840	0.714	0.252	1.45
33	SP-SM	2.5	20	286	0.87	0.1678	1.49	0.840	0.714	0.252	1.41
34	SP-SM	2.5	20	292	0.85	0.1700	1.47	0.840	0.716	0.254	1.39
35	SP-SM	2.5	20	298	0.84	0.1758	1.49	0.840	0.716	0.254	1.37

Table 8B.4: DEEPSOIL effective stress input parameters for validation site 2 (Max Ru = 0.95 for all layers)

Layer	Model	f/s/f	p/r/Dr	F/A/FC	s/B/-	g/C/-	v/D/v	-/g/-	$C_v(m^2/s)$
1	1	1.000	1.000	0.86	1.54	10.000	1.000	0.000	6.12E-02
2	1	1.000	1.000	1.53	1.54	10.000	1.000	0.000	6.12E-02
3	2	0.039	0.412	11.16	-21.27	11.172	-1.051	0.031	2.10E-06
4	2	0.061	0.445	12.65	-25.24	14.239	-1.639	0.030	2.10E-06
5	2	0.069	0.457	13.23	-26.80	15.508	-1.916	0.030	2.10E-06
6	2	0.069	0.462	13.44	-27.40	16.003	-2.030	0.031	2.10E-06
7	2	0.069	0.462	13.44	-27.40	16.003	-2.030	0.032	2.10E-06
8	2	0.069	0.472	13.96	-28.85	17.215	-2.320	0.032	2.10E-06
9	2	0.069	0.482	14.42	-30.15	18.325	-2.601	0.032	2.10E-06
10	2	0.069	0.487	14.68	-30.90	18.972	-2.772	0.033	2.10E-06
11	2	0.069	0.487	14.68	-30.90	18.972	-2.772	0.034	2.10E-06
12	1	1.000	1.000	2.02	1.31	0.026	1.000	0.000	1.63E-01
13	1	1.000	1.000	1.80	1.31	0.027	1.000	0.000	1.63E-01
14	1	1.000	1.000	1.61	1.31	0.028	1.000	0.000	1.63E-01
15	1	1.000	1.000	1.61	1.31	0.030	1.000	0.000	1.63E-01
16	1	1.000	1.000	1.61	1.31	0.031	1.000	0.000	1.63E-01
17	1	1.000	1.000	1.46	1.31	0.032	1.000	0.000	1.63E-01
18	2	0.124	0.439	10.81	-20.36	10.502	-0.939	0.078	1.45E-05
19	2	0.124	0.461	11.72	-22.72	12.268	-1.248	0.074	1.45E-05
20	2	0.124	0.478	12.41	-24.58	13.716	-1.530	0.071	1.45E-05
21	2	0.124	0.490	12.92	-25.97	14.831	-1.766	0.071	1.45E-05
22	2	0.124	0.497	13.23	-26.80	15.508	-1.916	0.071	1.45E-05
23	2	0.124	0.497	13.23	-26.80	15.508	-1.916	0.073	1.45E-05
24	2	0.124	0.497	13.23	-26.80	15.508	-1.916	0.075	1.45E-05
25	2	0.124	0.497	13.23	-26.80	15.508	-1.916	0.077	1.45E-05
26	2	0.124	0.497	13.23	-26.80	15.508	-1.916	0.079	1.45E-05
27	2	0.124	0.497	13.23	-26.80	15.508	-1.916	0.081	1.45E-05
28	2	0.124	0.497	13.23	-26.80	15.508	-1.916	0.082	1.45E-05
29	2	0.124	0.497	13.23	-26.80	15.508	-1.916	0.084	1.45E-05
30	2	0.124	0.497	13.23	-26.80	15.508	-1.916	0.086	1.45E-05
31	2	0.124	0.497	13.23	-26.80	15.508	-1.916	0.088	1.45E-05
32	1	1.000	1.000	0.61	1.31	0.047	1.000	0.000	1.63E-01
33	1	1.000	1.000	0.59	1.31	0.048	1.000	0.000	1.63E-01
34	1	1.000	1.000	0.57	1.31	0.049	1.000	0.000	1.63E-01
35	1	1.000	1.000	0.56	1.31	0.050	1.000	0.000	1.63E-01

Table 8B.5: DEEPSOIL total stress input parameters for validation site 3 (Ref Stress = 0.18; b = d = 0)

Layer	Name	Thick (m)	γ (kN/m3)	Vs (m/s)	Dmin	Ref Strain	B	s	P1	P2	P3
1	SC	2	19	400	1.78	0.0218	1.65	0.960	0.626	0.272	3.25
2	CH	1	15.5	175	2.18	0.0722	1.49	1.005	0.588	0.248	2.80
3	CH	1	15.4	144	2.07	0.0726	1.49	0.975	0.596	0.238	2.90
4	CH	1	15.3	120	2.02	0.0724	1.56	0.960	0.596	0.232	3.25
5	CH	1	15.2	106	1.94	0.0782	1.56	0.930	0.612	0.230	3.25
6	CH	0.85	15.1	98	1.86	0.0842	1.53	0.885	0.658	0.240	2.60
7	CH	0.85	15	91	1.79	0.0910	1.50	0.840	0.704	0.250	2.25
8	CH	0.85	15	91	1.74	0.0920	1.44	0.825	0.702	0.240	2.60
9	MH/CH	0.85	14.9	87	1.50	0.0958	1.55	0.780	0.762	0.266	2.30
10	MH/CH	0.85	14.8	90	1.47	0.0998	1.56	0.780	0.762	0.266	2.30
11	MH/CH	0.85	14.7	98	1.45	0.0990	1.56	0.795	0.732	0.246	2.55
12	MH/CH	1	14.6	106	1.44	0.1010	1.61	0.825	0.716	0.254	2.35
13	MH/CH	1.1	15.1	111	1.41	0.0930	1.49	0.825	0.696	0.232	2.70
14	MH/CH	1.1	15.6	113	1.38	0.0930	1.47	0.840	0.710	0.258	2.15
15	MH/CH	1.1	16.1	120	1.35	0.0926	1.46	0.855	0.680	0.240	2.52
16	MH/CH	1.3	16.66	133	1.33	0.0948	1.50	0.885	0.656	0.236	2.60
17	MH/CH	1.5	16.66	160	1.30	0.0978	1.59	0.930	0.608	0.220	3.23
18	MH/CH	1.8	16.786	180	1.27	0.0944	1.55	0.960	0.590	0.222	3.25
19	CH	1.66	16.9022	19	1.17	0.0802	1.44	0.975	0.592	0.232	2.95
20	CH	1.67	17.0191	195	1.14	0.0862	1.50	0.975	0.590	0.230	2.95
21	CH	1.67	17.136	199	1.12	0.0860	1.46	0.975	0.592	0.232	2.90
22	CH	2	17.276	203	1.09	0.0904	1.49	0.975	0.592	0.232	2.90
23	CH	2	17.416	207	1.06	0.0922	1.47	0.975	0.590	0.228	2.85
24	SC	2	17.556	275	0.70	0.0644	1.49	0.855	0.682	0.246	3.00
25	SC	2	17.696	275	0.68	0.0696	1.52	0.840	0.688	0.242	3.25
26	CH	2	17.836	220	0.99	0.1042	1.53	0.975	0.588	0.226	2.85
27	CH	2.2	18	224	0.97	0.1112	1.59	0.975	0.588	0.226	2.85
28	CH	2.2	17.5	229	0.95	0.1128	1.56	0.960	0.604	0.230	2.65
29	CH	2.3	17.5	234	0.93	0.1194	1.55	0.945	0.594	0.212	3.00
30	CH	2.3	17.5	238	0.91	0.1232	1.56	0.945	0.594	0.212	3.00
31	CH	2.4	17.5	243	0.90	0.1256	1.56	0.945	0.592	0.210	3.00
32	CH	2.4	17.5	248	0.88	0.1280	1.56	0.945	0.590	0.206	3.00
33	CH	2.5	17.5	254	0.87	0.1316	1.58	0.945	0.590	0.206	3.00
34	CH	2.5	17.5	259	0.86	0.1338	1.58	0.945	0.590	0.206	3.00
35	SC	2.6	17.5	315	0.54	0.0992	1.56	0.780	0.764	0.268	2.20
36	SC	2.6	17.5	315	0.53	0.1012	1.55	0.780	0.784	0.290	1.95
37	CH	2.7	17.5	276	1.25	0.2826	1.56	0.975	0.586	0.202	2.20
38	CH	2.7	17.5	281	1.23	0.2662	1.46	0.975	0.586	0.202	2.20
39	CH	2.8	17.5	287	1.22	0.2738	1.47	0.975	0.586	0.202	2.25
40	CH	2.8	17.5	293	1.20	0.2768	1.47	0.975	0.586	0.202	2.30
41	CH	2.9	18.21	299	1.18	0.2776	1.49	0.990	0.596	0.218	1.95
42	CH	2.9	18.21	305	1.17	0.2816	1.49	0.990	0.598	0.220	1.95
43	CH	3	17.6	311	1.15	0.2876	1.49	0.990	0.596	0.218	1.95
44	CH	3	17.6	318	1.14	0.2876	1.47	0.990	0.594	0.214	1.95
45	SC	3	17.6	365	0.76	0.2042	1.47	0.855	0.682	0.222	1.47
46	SC	3	17.6	365	0.75	0.2110	1.49	0.855	0.694	0.234	1.32
47	CH	3.1	18.4	337	1.10	0.2942	1.49	1.005	0.584	0.220	2.35
48	CH	3.1	18.4	343	1.09	0.2966	1.49	1.005	0.584	0.220	2.35
49	SC	5	19	500	0.73	0.1976	1.53	0.930	0.596	0.192	2.50
50	SC	5	19	500	0.72	0.2078	1.55	0.930	0.600	0.198	2.45
51	SW	5	19	500	0.70	0.2132	1.53	0.915	0.620	0.202	2.04

52	SW	5	19	500	0.69	0.2122	1.52	0.930	0.608	0.200	3.25
53	GW	5	19	600	0.69	0.1886	1.47	0.990	0.584	0.220	2.25
54	GW	5	19	600	0.68	0.2118	1.56	0.960	0.586	0.200	2.64
55	GW	5	19	600	0.67	0.2150	1.55	0.960	0.586	0.200	2.55
56	GW	5	19	600	0.66	0.2218	1.55	0.945	0.598	0.200	2.40

Table 8B.6: DEEPSOIL effective stress input parameters for validation site 3 (Max Ru = 0.95 for all layers)

Layer	Model	f/s/f	p/r/Dr	F/A/FC	s/B/-	g/C/-	v/D/v	-/g/-	$C_v(m^2/s)$
1	1	1.000	1.000	0.35	1.54	10.000	1.000	0.000	6.12E-02
2	2	0.043	0.412	10.60	-19.81	10.100	-0.874	0.026	1.45E-05
3	2	0.054	0.444	11.99	-23.45	12.827	-1.354	0.026	1.45E-05
4	2	0.072	0.491	14.18	-29.47	17.743	-2.452	0.024	1.45E-05
5	2	0.076	0.502	14.68	-30.90	18.972	-2.772	0.025	1.45E-05
6	2	0.076	0.502	14.68	-30.90	18.972	-2.772	0.026	1.45E-05
7	2	0.076	0.502	14.68	-30.90	18.972	-2.772	0.027	1.45E-05
8	2	0.076	0.502	14.68	-30.90	18.972	-2.772	0.028	1.45E-05
9	2	0.096	0.518	14.68	-30.90	18.972	-2.772	0.024	3.24E-05
10	2	0.096	0.518	14.68	-30.90	18.972	-2.772	0.025	3.24E-05
11	2	0.096	0.518	14.68	-30.90	18.972	-2.772	0.026	3.24E-05
12	2	0.096	0.518	14.68	-30.90	18.972	-2.772	0.026	3.24E-05
13	2	0.096	0.518	14.68	-30.90	18.972	-2.772	0.027	3.24E-05
14	2	0.096	0.518	14.68	-30.90	18.972	-2.772	0.028	3.24E-05
15	2	0.096	0.518	14.68	-30.90	18.972	-2.772	0.029	3.24E-05
16	2	0.096	0.518	14.68	-30.90	18.972	-2.772	0.029	3.24E-05
17	2	0.096	0.518	14.68	-30.90	18.972	-2.772	0.030	3.24E-05
18	2	0.096	0.518	14.68	-30.90	18.972	-2.772	0.032	3.24E-05
19	2	0.119	0.542	15.28	-32.65	20.514	-3.199	0.029	5.38E-05
20	2	0.119	0.542	15.28	-32.65	20.514	-3.199	0.030	5.38E-05
21	2	0.119	0.542	15.28	-32.65	20.514	-3.199	0.031	5.38E-05
22	2	0.119	0.542	15.28	-32.65	20.514	-3.199	0.032	5.38E-05
23	2	0.119	0.542	15.28	-32.65	20.514	-3.199	0.033	5.38E-05
24	1	1.000	1.000	0.63	1.54	0.020	1.000	0.000	6.12E-02
25	1	1.000	1.000	0.63	1.54	0.020	1.000	0.000	6.12E-02
26	2	0.119	0.542	15.28	-32.65	20.514	-3.199	0.036	5.38E-05
27	2	0.119	0.542	15.28	-32.65	20.514	-3.199	0.037	5.38E-05
28	2	0.119	0.542	15.28	-32.65	20.514	-3.199	0.038	5.38E-05
29	2	0.111	0.529	14.68	-30.90	18.972	-2.772	0.039	5.38E-05
30	2	0.111	0.529	14.68	-30.90	18.972	-2.772	0.040	5.38E-05
31	2	0.111	0.529	14.68	-30.90	18.972	-2.772	0.041	5.38E-05
32	2	0.111	0.529	14.68	-30.90	18.972	-2.772	0.042	5.38E-05
33	2	0.111	0.529	14.68	-30.90	18.972	-2.772	0.043	5.38E-05
34	2	0.111	0.529	14.68	-30.90	18.972	-2.772	0.043	5.38E-05
35	1	1.000	1.000	0.51	1.54	0.025	1.000	0.000	6.12E-02
36	1	1.000	1.000	0.51	1.54	0.025	1.000	0.000	6.12E-02
37	2	0.089	0.490	12.92	-25.97	14.831	-1.766	0.097	5.38E-05
38	2	0.089	0.490	12.92	-25.97	14.831	-1.766	0.099	5.38E-05
39	2	0.089	0.490	12.92	-25.97	14.831	-1.766	0.100	5.38E-05
40	2	0.089	0.490	12.92	-25.97	14.831	-1.766	0.102	5.38E-05
41	2	0.089	0.490	12.92	-25.97	14.831	-1.766	0.103	5.38E-05
42	2	0.089	0.490	12.92	-25.97	14.831	-1.766	0.105	5.38E-05
43	2	0.089	0.490	12.92	-25.97	14.831	-1.766	0.107	5.38E-05
44	2	0.089	0.490	12.92	-25.97	14.831	-1.766	0.108	5.38E-05
45	1	1.000	1.000	0.41	1.54	0.061	1.000	0.000	6.12E-02
46	1	1.000	1.000	0.41	1.54	0.062	1.000	0.000	6.12E-02
47	2	0.089	0.490	12.92	-25.97	14.831	-1.766	0.112	5.38E-05
48	2	0.089	0.490	12.92	-25.97	14.831	-1.766	0.114	5.38E-05
49	1	1.000	1.000	0.25	1.54	0.065	1.000	0.000	6.12E-02
50	1	1.000	1.000	0.25	1.54	0.066	1.000	0.000	6.12E-02
51	1	1.000	1.000	0.25	1.00	0.068	1.000	0.000	1.02E+00

52	1	1.000	1.000	0.25	1.00	0.069	1.000	0.000	1.02E+00
53	1	1.000	1.000	0.19	1.00	0.070	1.000	0.000	1.02E+01
54	1	1.000	1.000	0.19	1.00	0.072	1.000	0.000	1.02E+01
55	1	1.000	1.000	0.19	1.00	0.073	1.000	0.000	1.02E+01
56	1	1.000	1.000	0.19	1.00	0.074	1.000	0.000	1.02E+01

Figure 8B.12: Validation site 1 Results

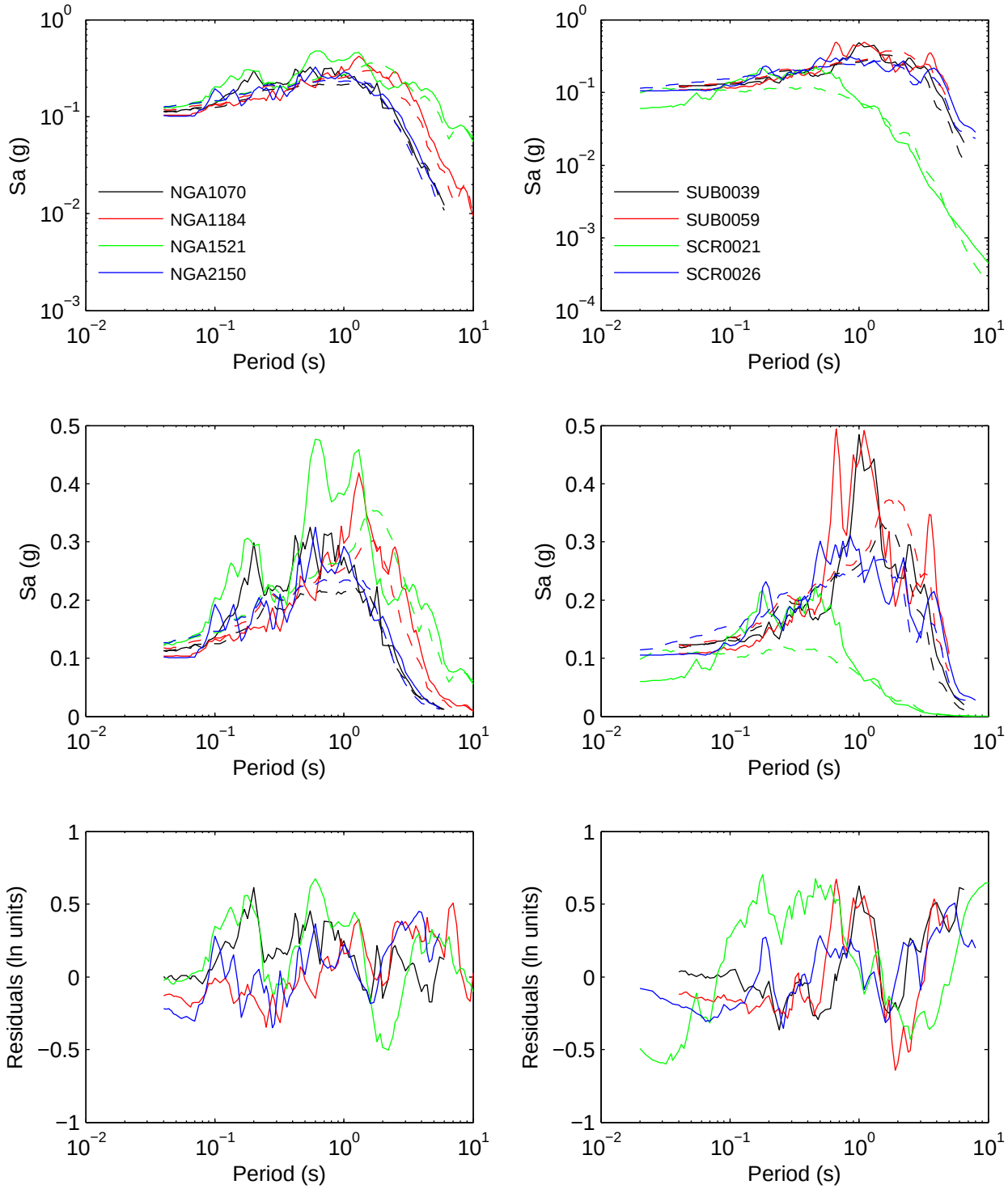

Figure 8B.13: Validation site 2 Results

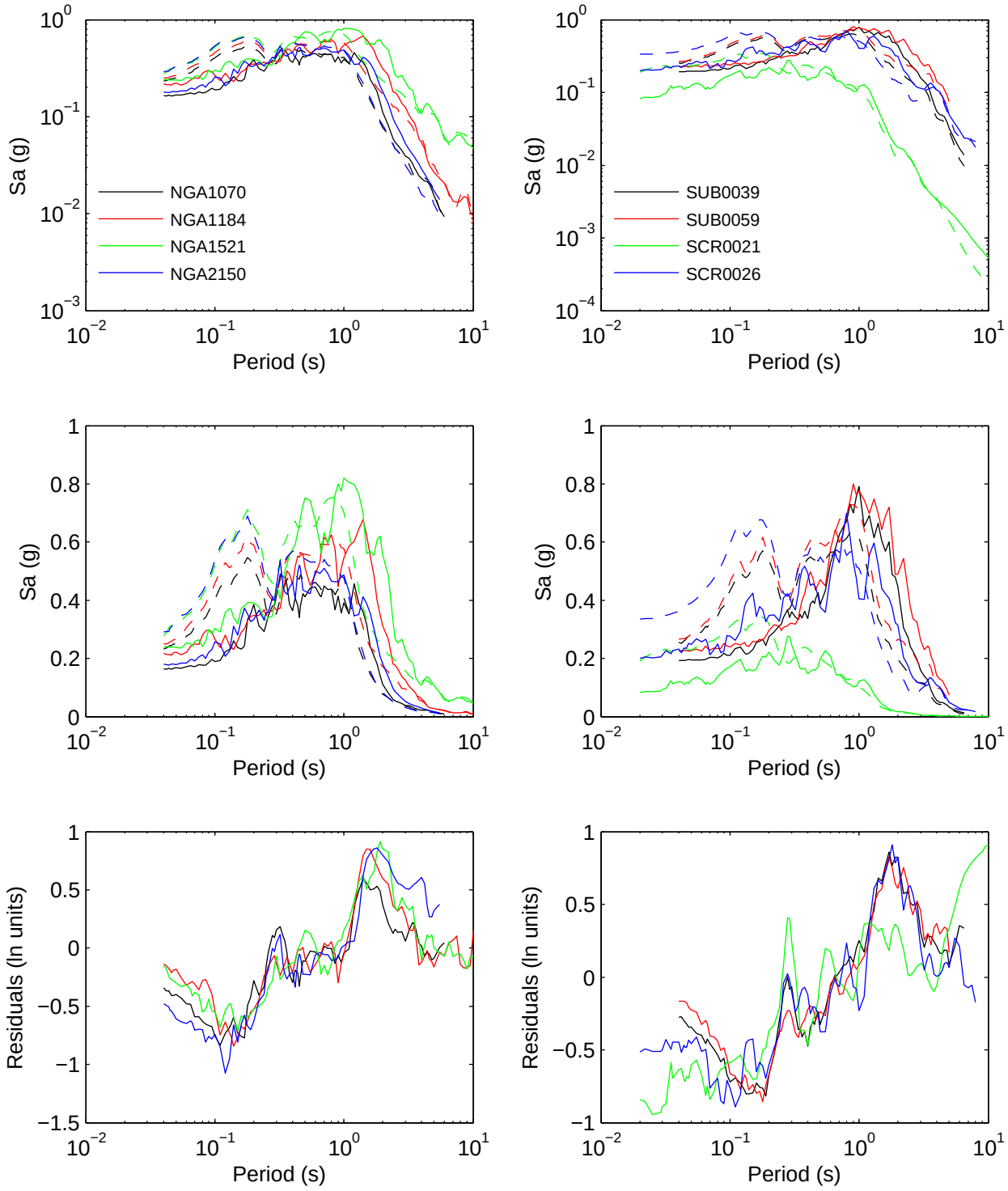

Figure 8B.14: Validation site 3 Results